RIKEN Accelerator Progress Report

2022

vol. 56

理化学研究所　仁科加速器科学研究センター
RIKEN Nishina Center for Accelerator-Based Science

RIKEN Accelerator Progress Report 2022

vol. **56**

理化学研究所　仁科加速器科学研究センター
RIKEN Nishina Center for Accelerator-Based Science
Wako, Saitama, 351-0198 JAPAN

RIKEN Accelerator Progress Report 2022 Vol. 56

This is an unabridged version of the 56th volume of RIKEN Accelerator Progress Report (hereinafter referred to as APR), the official annual report of the Nishina Center for Accelerator-Based Science.

A PDF version of APR can be downloaded from our website.
http://www.nishina.riken.jp/researcher/APR/index_e.html

Published by
RIKEN Nishina Center for Accelerator-Based Science
2-1 Hirosawa, Wako-shi, Saitama 351-0198 JAPAN

Director of RIKEN Nishina Center for Acclerator-Based Science
Hiroyoshi Sakurai

Contact
progress@ml.riken.jp

RIKEN Nishina Center for Accelerator-Based Science, December 2023

PREFACE

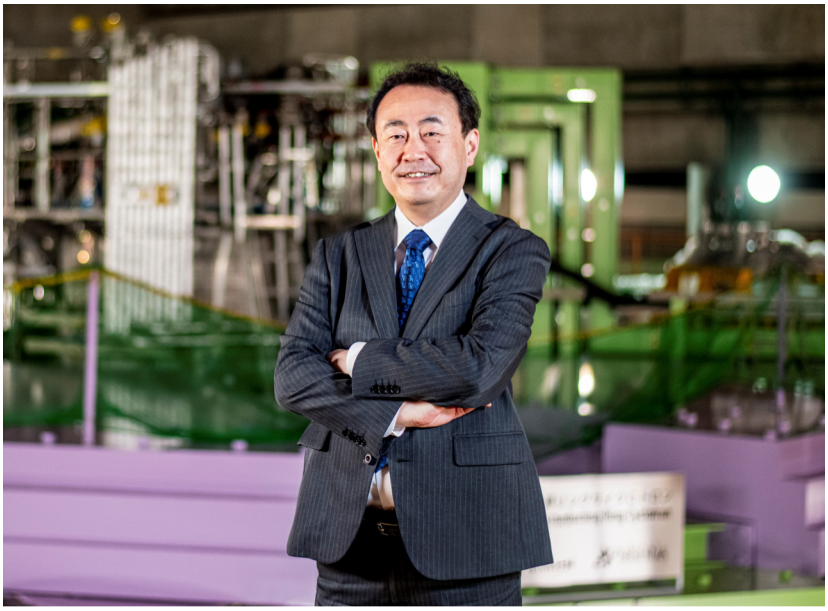

The RIKEN Accelerator Progress Report is the annual report of all the research activities conducted at the RIKEN Nishina Center for Accelerator-Based Science (RNC). This volume (No. 56) covers the activities conducted during the Japanese fiscal year 2022 (i.e., April 2022 to March 2023).

With restrictions on social activity due to the coronavirus pandemic being gradually eased last year, we have been able to reconnect with friends and families in person for the first time since the spring of 2020. The same was true research-wise, with many researchers from abroad visiting to RIKEN to participate in the experiments scheduled at the end of the year. At the end of October 2022, "The Yoshio Nishina Memorial Event" was successfully held in person as well. With the attendance of guests related to or have connection with Dr. Nishina who came all the way to Wako, the event turned out to be a great opportunity to spark interest not just among the participants but to a wider community about Dr. Nishina's achievements and the Nishina Center's latest initiatives and research activities.

One of the messages that we wanted to communicate through "The Nishina Yoshio Memorial Laboratory" is the "Copenhagen Spirit" that took hold in the research field pioneered by Dr. Nishina. The Spirit is still very much alive in Japan, and I think the main reason is because it matches the philosophy of "Yaoyorozu no kami (eight million gods)," a traditional Japanese belief that says god exists in everything. Because individual's ideas and curiosity are the base of science and technology, each one can be called a Creator. Every social activity should acknowledge and embrace differences in one's sensibility and heighten each other's originality. It is my wish that we will contribute to realizing a peaceful society where individuals can shine, an endeavor to be achieved when the essence and role of science and technology are fully incorporated into society while not repeating the mistakes made about 80 years ago.

95 years later, since the first cyclotron built by Dr. Yoshio Nishina, the superconducting ring cyclotron (SRC) was registered in the Guinness World Records in April 2022, as the highest energy beam cyclotron which achieves 82,400 MeV of a uranium beam. The SRC was constructed with advanced technology from Japanese industries and completed in 2006. Since then, the uranium beam has been utilized in more than 100 publications. The other beams also have made a significant contribution to the development of the low energy nuclear physics.

Yasuki Akiba has been appointed as the Director of RHIC Physics Research Group to conduct the sPHENIX program at RHIC as of April 2022. Tetsuya Ohnishi has succeeded, as the Director of Instrumentation Development Group as of October 2022. Yoshihide Higurashi has been appointed as the Team Leader of RILAC Team as of October 2022.

In March 2023, an event celebrating three decades of collaboration between RAL and RIKEN was organized. The RIKEN-RAL Muon Facility was concluded at the end of March. The muon programs have produced over 500 publications, including muon-catalyzed fusion, condensed matter physics and chemistry and battery materials, and have made new departures in international collaborations, involving South-East Asian countries such as Indonesia, Malaysia, and Thailand. A new partnership between ISIS RNC has been established since April 2023 to encourage collaboration in areas of accelerator-based sciences.

Many outstanding research results were obtained at RNC last year. Twelve press releases were disseminated in FY2022. Selected strides made in 2022 have been compiled in the "Highlights of the Year" section in this volume, which show successful multi-disciplinary activities of RNC for science, technology, and innovation. One of the highlights was the successful observation of four neutron states by using a different method to observe the phenomenon already observed few years ago. This research achievement has been chosen by the Institute of Physics as one of the "Top 10 Breakthroughs of the Year for 2022." The discovery of ^{39}Na was featured by the YouTube program of "Periodic Table of Videos." The first mass measurement with Rare-RI Ring was published to give an impact to the *r*-

process path. Reduction of chiral condensate was found through precise observation of pionic atomic states.

Members of RNC received various awards. Kimiko Sekiguchi received the "42nd Saruhashi Prize" and Pieter Doornenbal received the "Friedrich Wilhelm Bessel Research Award." The members of the Beam Mutagenesis Group were also awarded. Tomoko Abe received the "10th Wada Memorial Award," Tomoko Abe, Yusuke Kazama, and Tomoya Hirano received the "Japanese Society of Breeding Award," and Tomoko Abe, Hiroyuki Ichida, and Ryohei Morita received the "Japanese Society of Crop Science Best Paper Award." The "Young Presentation Award by the Beam Physics Study Group" was presented to Yasuyuki Morita. Yusuke Kazawa was awarded the "Atomic Energy Society of Japan Data Division Encouragement Award." Kai Kikuchi and Rurie Mizuno were presented the "29th International Conference on Low Temperature Physics Poster Award" and "Outstanding Presentation Award," respectively. The "2022 RIKEN Awards" included the "EIHO Award" presented to Hiromitsu Haba, "BAIHO Award" presented to Takashi Abe and Takaharu Otsuka, Yoshitaka Yamaguchi and Makiko Nio, and "OHBU Award" presented to Yudai Shigekawa and Yasushi Abe.

Hiroyoshi Sakurai
Director
RIKEN Nishina Center for Accelerator-Based Science

C O N T E N T S

Ⅱ. RESEARCH ACTIVITIES I (Nuclear, Particle and Astro-Physics)

1. Nuclear Physics

2. Nuclear Physics (Theory)

3. Nuclear Data

4. Hadron Physics

5. Hadron Physics (Theory)

6. Particle Physics

7. Astrophysics and Astro-Graciology

8. Accelerator

9. Instrumentation

4. Radiation Chemistry and Biology

Ⅳ. OPERATION RECORDS

Ⅴ. EVENTS

Ⅶ. APPENDICES

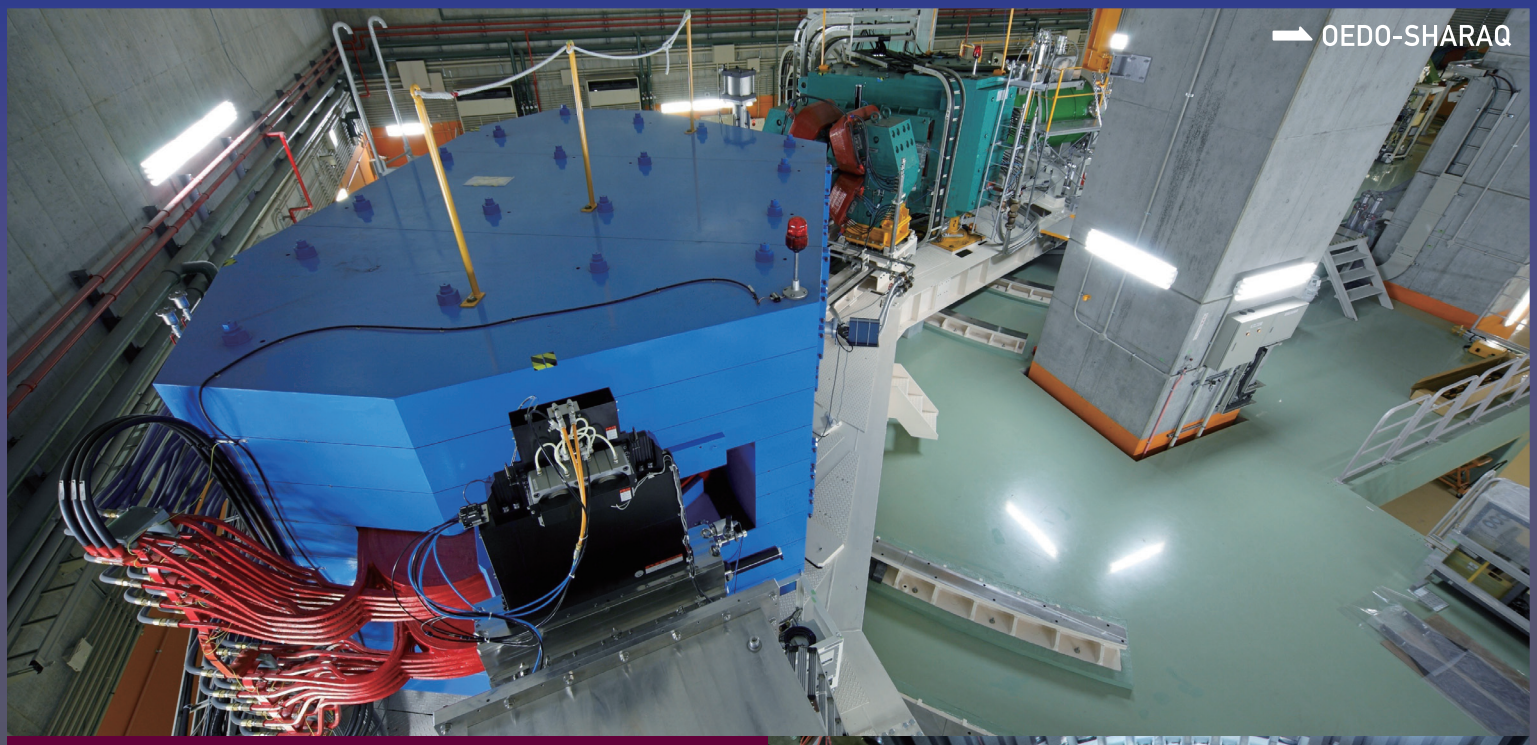

ACCELERATOR PROGRESS REPORT
FEATURE ARTICLE

NUCLEAR MASSES WEIGH HEAVILY WITH US

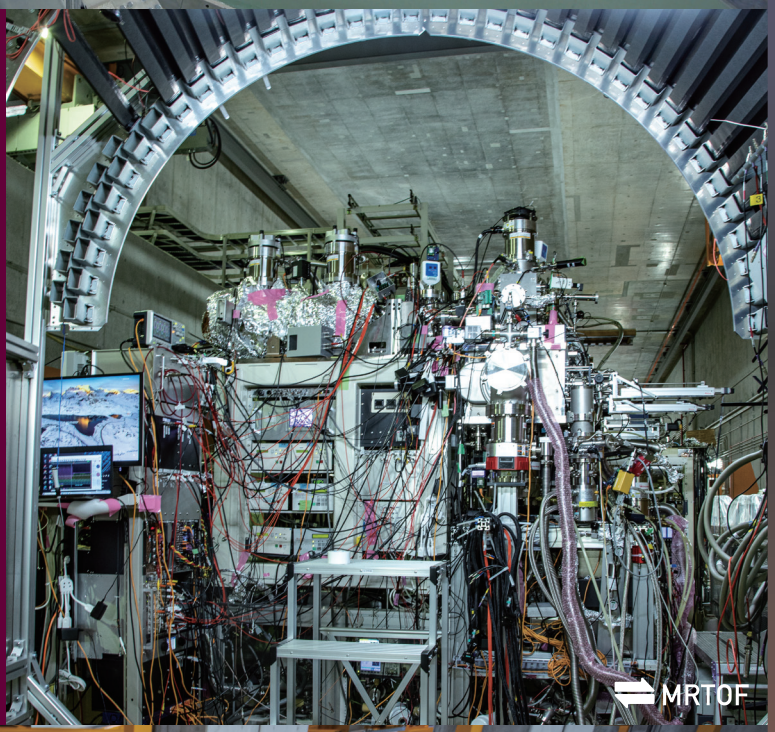

Nuclear masses weigh heavily with us

As a self-organizing quantum system, the nucleus makes every effort to reduce its mass. As a natural consequence, the nuclear mass contains all the information on mechanisms that stabilize the nucleus. These mechanisms can be traced back using the nuclear mass data.

In 1919, Francis William Aston performed the first successful mass measurement and discovered many isotopes using his mass spectrograph. At that time, the mass resolution was approximately 1%. The subsequent century has witnessed incredible developments in techniques used for measuring nuclear masses. The most established and famous techniques of precision mass measurements are the Penning trap method and the Schottky method using a storage ring.

Unfortunately, neither of the methods can be applied to mass measurements of rare nuclei produced at the RI Beam Factory (RIBF). This is solely because of their short lifetimes of $\gg$1 s. In the long measurement time (>1 s) of the Penning trap and the Schottky methods, the short-lived nuclei decay to their daughters, which prevents us from measuring their masses. The main physics cases in nuclear mass measurements at RIBF involve the magicity and the r-process nucleosynthesis, both of which require a mass precision of 100 keV, or δm/m $\sim 10^{-6}$. Since the statics expected for rare nuclei are as small as $\sim 10^2$, a mass resolving power of 10^5 or better is mandatory in their studies.

The unprecedentedly fast mass-measurement technique with a mass resolving power as high as $m/\Delta m > 10^5$ has been highly desired, but accomplishing it is a big challenge for nuclear physicists.

Scientists at RIKEN, KEK, and CNS have tackled this problem and have recently succeeded in measuring masses of rare nuclei: The first one is the TOF-$B\rho$ mass measurement using the long OEDO beamline coupled with the SHARAQ spectrometer. The measurement combining a flight length of 105 m (one path) and the high-resolution magnetic system with a controlled correction of higher-order aberrations enables an extremely short measurement time of 0.0005 ms with a reasonable resolving power of $>10^4$ and a high efficiency of $\sim$100%.

The second is an isochronous mass measurement using the Rare RI Ring (R3). R3 is the world's first cyclotron-type storage ring with an individual injection capability. The setup leads to a 0.7-ms measurement time with a resolving power $> 3 \times 10^5$.

The third is the multireflection time-of-flight (MRTOF) mass spectrograph combined with a gas catcher system. This versatile and "portable" device can be placed at any beamline to accept a wide variety of nuclei, whose masses are measured in several tens of ms (including the time needed to stop the ions) with a high resolving power of 10^6.

The combined use of the abovementioned three techniques with different characteristics, shown in Fig. 1, opens a broad spectrum of research opportunities at RIBF.

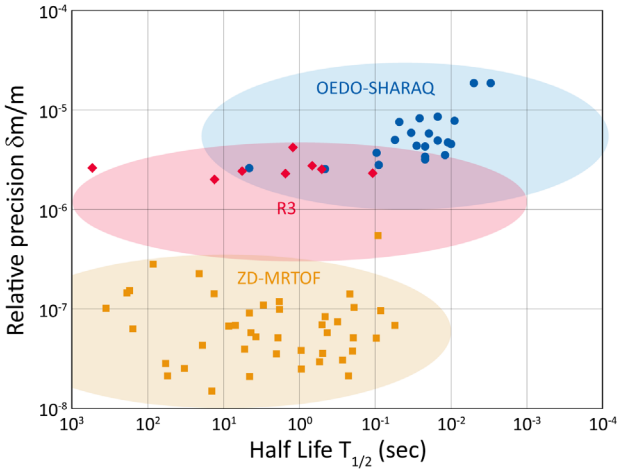

Fig. 1. Mass precision and nuclear half-life regions covered by the three mass measurement methods.

TOF-$B\rho$ mass measurement using OEDO-SHARAQ

The OEDO-SHARAQ system, initiated collaboratively by CNS, the University, of Tokyo and RIKEN Nishina Center is promoting the program of direct mass measurements of radioactive nuclei far from the β stability line. In 2009, the OEDO-SHARAQ program started with the installation of the SHARAQ spectrometer[1] and a dispersion-matched High-Resolution beamline[2] (renamed by OEDO beamline in 2017) into the downstream of the BigRIPS separator[3] at the RIBF facility.

Atomic masses of very short-lived nuclei have been determined so far by various time-of-flight (TOF) methods. In our system, the TOF magnetic-rigidity (TOF-$B\rho$) method, developed at GANIL,[4] has been adopted, and further sophistication in its ion optics and detector performance has been implemented for the measurements. The principle of mass determination using the TOF-$B\rho$ method can be simply expressed by the following relation:

$$\frac{m}{q} = \frac{B\rho}{c}\sqrt{\left(\frac{ct}{L}\right)^2 - 1}, \quad (1)$$

where m, q, c, t, and L are the nuclear mass, atomic

charge, speed of light in vacuum, TOF, and the flight-path length, respectively. This relation corresponds to the Lorentz force in a magnetic field, and indicates that the mass-to-charge ratio (m/q) is determined by TOF as long as the flight-path length and the magnet field of the beamline are fixed. However, because the flight-path length is indeed dependent on the incident condition of the short-lived nuclei, we perform an event-by-event correction of the flight-path length using the trajectory information obtained at the starting and final foci of the beamline. The essential point that has led to the success of our direct mass measurement program has been the high-resolution performance of the system.

The detector setup for the mass measurements is shown in Fig. 2. The CVD diamond detectors were installed at F3 and S2 to measure the TOF. The CVD diamond detector was developed at CNS to achieve high-resolution timing and high-rate capability.[5] The low-pressure multiwire drift chambers (LP-MWDCs)[6] were used for beam tracking at F3 and S2, and provided beam-trajectory information that is mandatory for accurate corrections of the flight-path lengths. A delay-line parallel-plate avalanche counter (DL-PPAC) installed at S0 measured the $B\rho$ values of the beam particles. The m/q values of the individual short-lived nuclei were determined based on the combination of these measured quantities on an event-by-event basis. Additionally, a silicon solid-state detector (SSD) was used to identify the atomic numbers. The delayed γ-ray detection system was placed at the end of the beamline to search for the unknown isomeric states in the radioactive nuclei.

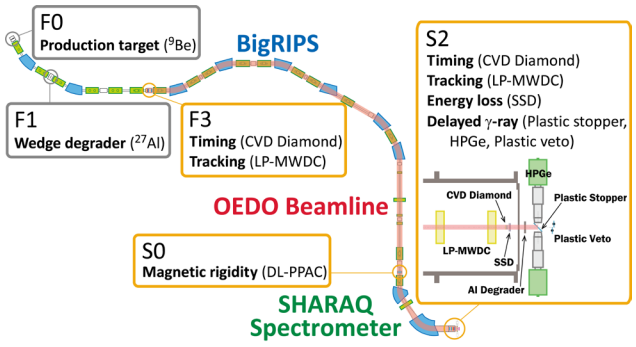

Fig. 2. Experimental detector setup in the OEDO-SHARAQ system for the direct mass measurements.

An advantage of the SHARAQ mass measurements is its accessibility to very short-lived isotopes, whose lifetimes are less than 1 ms, with its high transmission efficiency, because the TOF of the system is as short as ~500 ns. With this capability, the system is expected to enable the measurement of nuclear masses on the dripline.

We have successfully measured the atomic masses of very neutron-rich Ca and Ti isotopes towards the dripline by a single setting of the BigRIPS separator and the SHARAQ spectrometer. These new masses are covered with the region connecting the emergence of magicities at $N = 32$ and 34 and the island-of-inversion at $N = 40$. The work has clearly exhibited the sudden emergence of magicity in ^{54}Ca.[7] Moreover, the results for Ti isotopes reveal an onset of the Jahn-Teller stability around ^{62}Ti,[8] indicating shell quenching at $N = 40$ based on the comparison with the theoretical mass predictions.[9]

These experiments have demonstrated that our experimental technique has capabilities to efficiently pin down the mass irregularities and provide essential information on its onset mechanism based on mass evolution. Recently, the first TOF-$B\rho$ mass measurements after the construction of the OEDO system were performed to access the mass region of two-proton radioactivity.[10] The TOF-$B\rho$ method excels in extending the mass data toward the nuclear drip lines. We will extend our challenge toward the ^{78}Ni and ^{100}Sn regions in the near future.

Isochronous mass measurement with the rare RI ring

In the decade after the R3 was built, we have successfully conducted its commissioning using a primary beam, validation of the mass measurement method using unstable nuclei with known masses, and precise mass measurements. Recently, the mass of ^{123}Pd, one of the nuclei near the second peak of the r-process, was successfully determined.[11] The impact of the measured mass on the heavy element synthesis was investigated by inputting the new mass value into the r-process network simulations from which its effect on the probability of neutron capture and neutron emission after beta decay were evaluated. The compositions observed in the solar system can be reproduced with the new mass value.

Figure 3 illustrates the mass measurement scheme of the R3. The mass measurements for such nuclei have been achieved by our bold move to connect a cyclotron and a storage ring, which have been known to be essentially incompatible, taking the advantage of the "long" fragment separator. The key point of this scheme is to know, prior to injection, that the nucleus of interest is produced in the first section of the BigRIPS and to inject it into R3. The masses are then determined event-by-event by performing isochronous mass spectrometry (IMS).[12,13]

In RIBF, various unstable nuclei are produced by the in-flight fission of the uranium beam or the projectile fragmentation of heavy-ion beams such as xenon, krypton, *etc.* Their extremely low production rate makes the timing of production completely random.

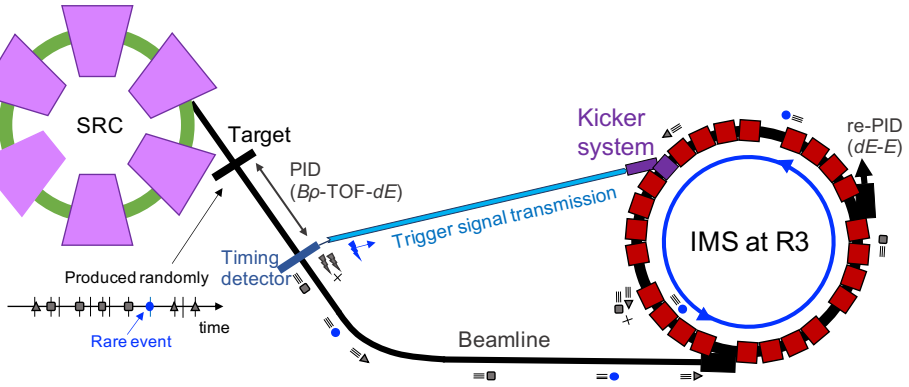

Fig. 3. Conceptual design and method for measuring the mass of short-lived rare nuclei using R3.

The species of the produced nuclei can be identified on an event-by-event basis using the $B\rho$-TOF-dE method in the F0–F3 section of BigRIPS.[14] Subsequently, the identified isotope passes though the timing detector placed at F3. Using the timing and energy-loss information from the detector, the signal to trigger the R3 kicker system is generated only for the isotopes of interest. Synchronization of the kicker excitation to the arrival of the isotope beam is the key technology enabling the unique combination of a cyclotron and a storage ring. It should also be noted that the RF signal from the accelerator is utilized to efficiently reduce the trigger rate by filtering the signals corresponding to unnecessary events. Using this setup, we have realized the isotope-selectable self-triggered injection, called the individual injection, for the first time.

The injected isotope is circulated in R3 for certain turns (typically ∼2000) and extracted after ∼1 ms. The revolution time is obtained by dividing the flight-time between injection and extraction by the number of turns. Further, the extracted events are identified once again for verification (re-PID). The ratio of the revolution times of the nucleus of interest to a reference nucleus, whose mass is well known, is use to accurately determine the mass. It should be noted here that isochronism of R3 holds only for a single isotope, the reference nucleus in many cases and the revolution time of the nucleus of interest has momentum dependence. Thus a small correction is introduced using the velocity, β, or $B\rho$ determined by the measurements prior to injection.

The main factor crucial for the precision of the derived mass is the degree of isochronism, including the magnetic field fluctuation. Isochronism is defined by the spread of the revolution time, dT/T, in the acceptance of the ring. A standard deviation of $dT/T \sim 2.8 \times 10^{-6}$ for a high degree of isochronism has been achieved at R3 for the full momentum acceptance ($dp/p \sim \pm 0.3\%$). This leads to a high mass resolving power of 3.5×10^6. We have established a scheme that can determine masses of the order of 10^{-6} with a measurement time of less than 1 ms. Further efforts are ongoing to increase the mass resolving power and injection efficiency by upgrading the kicker system,[15,16] and by fine-tuning the ion optics. In the near future, it is expected to be able to derive the masses of nuclei in a region that can only be achieved with the R3, *i.e.*, the nuclei having half-lives of <10 ms, and extremely rare that one can be extracted in a day.

MRTOF mass measurement

Three multi-reflection time-of-flight mass spectrographs (MRTOF-MS) are in operation at RIBF. One of them is called ZD-MRTOF, which is located behind the ZeroDegree spectrometer (ZDS), combined with an RF-carpet-type cryogenic He gas catcher (RFGC)[17,18] in the SLOWRI project (Fig. 4). The fast (>100 MeV/nucleon) RIs provided from BigRIPS are stopped in the He gas and extracted as slow (<10 eV) RI ions from the RFGC using RF ion carpets. They are then guided into an ion trap, accumulated, cooled, and injected into the mass spectrograph (Fig. 5).[19] The ions are reflected back and forth between the ion mirrors typically for 600 revolutions corresponding to ≈10 ms at a maximum kinetic energy of 2.5 keV. Currently, the maximum mass resolving power has reached to 10^6.

Since the location of the ZD-MRTOF is just in front of the beam dump of ZDS, mass measurements have been conducted symbiotically by re-using the RIs from other experiments carried out upstream without extra costs. For example, during the in-beam γ-ray experiments (HiCARI campaign) in winter 2020, more than 70 masses on RIs were measured with the ZD-MRTOF system (Fig. 6). Among them, three isotope masses have been measured for the first time and mass uncertainties of 11 isotope have been significantly improved from the previous ones.

For Ti and V isotopes, the nonexistence of the $N = 34$ empirical two neutron shell-gaps has been revealed experimentally with the new precision achieved by our equipment.[20]

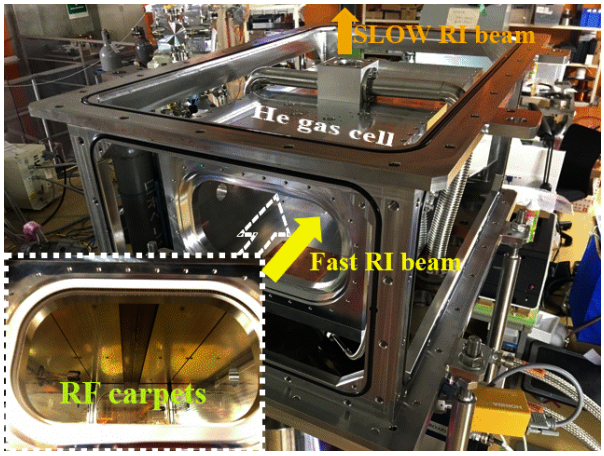

Fig. 4. Photographs of an RF-carpet-type He gas catcher (RFGC) behind ZDS of BigRIPS.

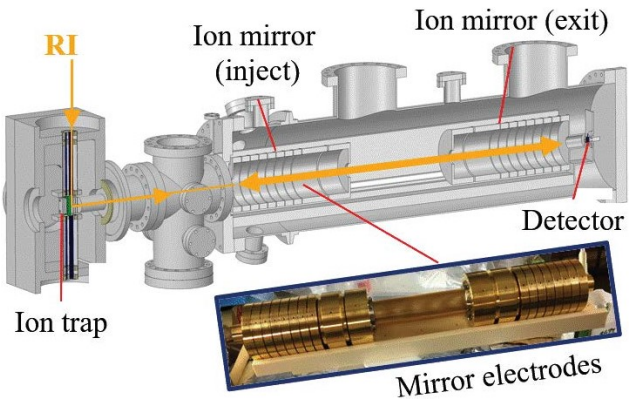

Fig. 5. Schematic view of MRTOF-MS (top) and a photograph of the ion mirrors behind ZDS of BigRIPS (bottom).

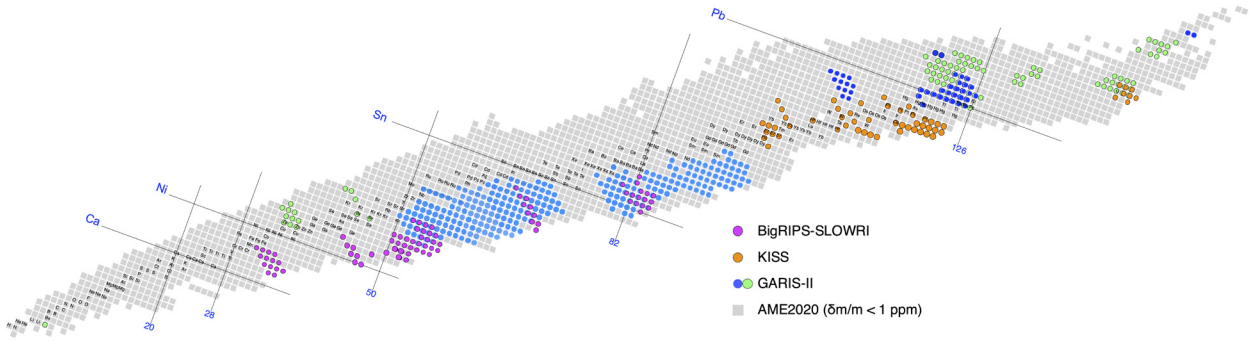

Fig. 6. Nuclear mass measurements performed with the three MRTOF-MS.

The second MRTOF is located downstream of the beamline at the KEK isotope separation system (KISS), which employs a mass spectrograph and a particle identification detector for laser spectroscopy. In-gas-cell laser resonant ionization spectroscopies for Os and Pt isotopes have been conducted with the KISS-MRTOF.[21,22] In addition, a new isotope of ^{241}U has also been discovered by a precise mass measurement using KISS-MRTOF.[23]

The third MRTOF, SHE-Mass, is located behind GARIS-II at E6. It has been used for mass measurements of super-heavy nuclei such as ^{257}Db.[24] In addition, a 9 MBq ^{252}Cf fission source has been installed just in front of the He gas catcher. Even off-line, mass measurements on the fission fragments have continued and several first mass measurements have been performed.[25]

We have a plan to increase this versatile and portable instrumentation at RIBF; an MRTOF-MS is being installed behind GARIS-III, and a plan is underway to install an MRTOF-MS with a large He gas catcher behind SD4 at BigRIPS, which will lead to more opportunities to study unexplored nuclear species.

References

1) T. Uesaka *et al.*, Prog. Theor. Exp. Phys. **2012**, 03C007 (2012).
2) S. Michimasa *et al.*, Nucl. Instrum. Methods Phys. Res. B **317**, 305 (2013).
3) T. Kubo, Nucl. Instrum. Methods Phys. Res. B **204**, 97 (2003).
4) N. Orr *et al.*, Phys. Lett. B **258**, 29 (1991).
5) S. Michimasa *et al.*, Proc. Sci. **INPC2016**, 106 (2017).
6) H. Miya *et al.*, Nucl. Instrum. Methods Phys. Res. B **317**, 701 (2013).
7) S. Michimasa *et al.*, Phys. Rev. Lett. **121**, 022506 (2018).
8) S. Michimasa *et al.*, Phys. Rev. Lett. **125**, 122501 (2020).
9) N.-N. Ma *et al.*, Chin. Phys. C **43**, 044105 (2019).
10) S. Hanai *et al.*, in this report.
11) H. F. Li *et al.*, Phys. Rev. Lett. **128**, 152701 (2022).
12) H. Wollnik, Nucl. Instrum. Methods Phys. Res. A **258**, 289 (1987).
13) J. Trotscher *et al.*, Nucl. Instrum. Methods Phys. Res. B **70**, 455 (1992).
14) N. Fukuda *et al.*, Nucl. Instrum. Methods Phys. Res. B **317**, 323 (2013).
15) Y. Yamaguchi *et al.*, RIKEN Accel. Prog. Rep. **54**, 100 (2021).
16) Y. Yamaguchi *et al.*, in this report.

17) A. Takamine *et al.*, in this report.
18) J. M. Yap *et al.*, in this report.
19) M. Rosenbush *et al.*, in this report; Nucl. Instrum. Methods Phys. Res. A **1047**, 167824 (2023).
20) S. Iimura *et al.*, in this report; Phys. Rev. Lett. **130**, 012501 (2023).
21) H. Choi *et al.*, Phys. Rev. C **102**, 034309 (2020).
22) Y. Hirayama *et al.*, Phys. Rev. C **106**, 034326 (2022).
23) T. Niwase *et al.*, in this report; Phys. Lett. **130**, 132502 (2023).
24) P. Schury *et al.*, Phys. Rev. C **104**, L021304 (2021).
25) S. Kimura *et al.*, RIKEN Accel. Prog. Rep. **55**, 8 (2022).

I. HIGHLIGHTS OF THE YEAR

<< Selection process of highlights >>

Highlights are selected by a two-step process. In the first step, a referee who reviews a manuscript decides whether she/he would recommend it as one of the highlights.
Members of the editorial board then make additional recommendations if they think an important contribution has not been recommended by the referee.

The second step involves the editor-in-chief proposing a list of highlights based on the recommendation given above to the editorial board. After discussing the scientific merits and uniqueness of the manuscripts from viewpoints of experts/non-experts, the editorial board makes the final decision.

Discovery of ^{39}Na†

D. S. Ahn,[*1] J. Amano,[*3] H. Baba,[*1] N. Fukuda,[*1] H. Geissel,[*5] N. Inabe,[*1] S. Ishikawa,[*4] N. Iwasa,[*4] T. Komatsubara,[*1] T. Kubo,[*1] K. Kusaka,[*1] D. J. Morrissey,[*6] T. Nakamura,[*2] M. Ohtake,[*1] H. Otsu,[*1] T. Sakakibara,[*4] H. Sato,[*1] B. M. Sherrill,[*6] Y. Shimizu,[*1] T. Sumikama,[*1] H. Suzuki,[*1] H. Takeda,[*1] O. B. Tarasov,[*6] H. Ueno,[*1] Y. Yanagisawa,[*1] and K. Yoshida[*1]

The location of the neutron dripline provides a key benchmark for advanced nuclear models and theories. It reflects the details of the underlying nuclear structure and interactions, which include the evolution of the nuclear shell property and associated nuclear deformation. Thus, locating the neutron dripline experimentally provides a significant key to understanding the nuclear structure under extremely neutron-rich conditions.

In our previous study,[1] we searched for the new isotopes ^{32,33}F, ^{35,36}Ne, and ^{38,39}Na to investigate the neutron dripline at fluorine (atomic number $Z = 9$), neon ($Z = 10$), and sodium ($Z = 11$). No events were recorded for ^{32,33}F, ^{35,36}Ne, and ^{38}Na and only one event was recorded for ^{39}Na. This enabled us to determine the neutron dripline for fluorine and neon to be ^{31}F and ^{34}Ne, respectively, nearly 20 y after ^{24}O was confirmed as the dripline nucleus of oxygen ($Z = 8$).

In this study,[2] we conducted a new experiment dedicated to searching specifically for ^{39}Na to establish that it is particle-bound. The new isotope ^{39}Na has the mass number $A = 3Z + 6$, located beyond the previously known most neutron-rich isotope ^{37}Na, which was discovered 20 y ago;[3] see Fig. 1. It is a strong candidate to be the dripline nucleus of sodium, and establishing its existence provides a significant extension of the neutron dripline and a benchmark for nuclear structure calculations as well as nuclear mass models. It should be noted that ^{39}Na has the neutron number $N = 28$, which is normally a magic number.

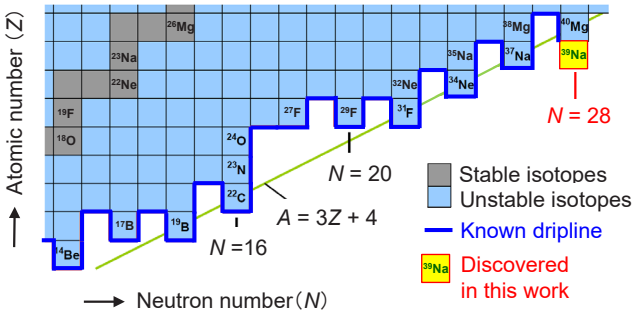

Fig. 1. Section of the nuclear chart indicating the location of the ^{39}Na isotope discovered in this study.

The search was conducted at the RIKEN RIBF using projectile fragmentation of an intense ^{48}Ca beam at 345 MeV/nucleon on a 20-mm-thick beryllium target. The projectile fragments including ^{39}Na were separated and identified in flight by the large-acceptance two-stage fragment separator BigRIPS.[4,5] The intensity of the ^{48}Ca beam was as high as ∼540 particle nA.

The particle identification was made at the second stage of the BigRIPS separator, relying on the combination of time of flight (TOF), magnetic rigidity ($B\rho$), and energy loss (ΔE) measurements, from which the Z and A/Z values were deduced for each fragment. The TOF was measured between two thin plastic scintillators installed at the intermediate and final foci of the second stage. The value of ΔE was measured using a stack of six identical silicon semiconductor detectors installed at the final focus. The value of $B\rho$ was determined from a position measurement at the intermediate focus using the plastic scintillator that also measured the TOF. The separator setting was tuned for the optimal transmission of ^{39}Na. The production of ^{36}Ne was also revisited with another separator setting tuned for that of ^{36}Ne to improve the confidence level that ^{34}Ne is the dripline nucleus of neon.

After extensive running, we observed nine events for ^{39}Na and clearly established that the ^{39}Na nucleus is particle-bound. Furthermore, no events were observed for ^{35,36}Ne, which is consistent with their particle instability established in our previous work. The measurement enabled us to significantly improve the confidence level and hence firmly determine that ^{34}Ne is the dripline nucleus.

The particle stability of ^{39}Na, established by the present discovery, suggests the occurrence of nuclear deformation in ^{39}Na, as it induces more stability to the nuclear binding. ^{39}Na could be particle-bound as its ground state is deformed, suggesting the loss of the $N = 28$ magicity at sodium. This interpretation is supported by the recent state-of-the-art large-scale shell model calculation with *ab initio* effective *NN* interactions,[6] which reproduces the stability of ^{39}Na as well as the neutron dripline at fluorine and neon. The calculation reveals that the quadrupole deformation plays a key role in nuclear binding in this region and thus in determining the location of the neutron dripline.

† Condensed from the article in Phys. Rev. Lett. **129**, 212502 (2022)

*1 RIKEN Nishina Center
*2 Department of Physics, Tokyo Institute of Technology
*3 Department of Physics, Rikkyo University
*4 Department of Physics, Tohoku University
*5 GSI Helmholtzzentrum für Schwerionenforschung GmbH
*6 National Superconducting Cyclotron Laboratory, Michigan State University

References
1) D. S. Ahn *et al.*, Phys. Rev. Lett. **123**, 212501 (2019).
2) D. S. Ahn *et al.*, Phys. Rev. Lett. **129**, 212502 (2022).
3) M. Notani *et al.*, Phys. Lett. B **542**, 49 (2002).
4) T. Kubo, Nucl. Instrum. Methods Phys. Res. Sect. B **204**, 97 (2003).
5) T. Kubo *et al.*, Prog. Theor. Exp. Phys. **2012**, 03C003 (2012).
6) N. Tsunoda *et al.*, Nature **587**, 66 (2020).

Study of the $N = 32$ and $N = 34$ shell gap for Ti and V by the first high-precision multireflection time-of-flight mass measurements at BigRIPS-SLOWRI†

S. Iimura,[*1,*2,*3,*4] M. Rosenbusch,[*3] A. Takamine,[*1] Y. Tsunoda,[*5] M. Wada,[*3] S. Chen,[*6] D. S. Hou,[*7] W. Xian,[*6] H. Ishiyama,[*1] S. Yan,[*8] P. Schury,[*3] H. Crawford,[*9] P. Doornenbal,[*1] Y. Hirayama,[*3] Y. Ito,[*10] S. Kimura,[*1] T. Koiwai,[*11,*1] T. M. Kojima,[*1] H. Koura,[*10] J. Lee,[*6] J. Liu,[*6,*7] S. Michimasa,[*12] H. Miyatake,[*3] J. Y. Moon,[*13] S. Naimi,[*1] S. Nishimura,[*1] T. Niwase,[*3,*1,*14] A. Odahara,[*2] T. Otsuka,[*11,*1,*10] S. Paschalis,[*15] M. Petri,[*15] N. Shimizu,[*5] T. Sonoda,[*1] D. Suzuki,[*1] Y. X. Watanabe,[*3] K. Wimmer,[*11,*16,*1] and H. Wollnik[*17]

Masses of neutron-rich isotopes with $N \geq 32$ between Ca and Ni have recently been studied intensely as valuable probes of the complex nuclear structure. For Ca isotopes, a pronounced reduction of tensor-interaction effects[1] due to the decrease of proton valence particles occupying the $\pi f_{7/2}$ orbits has been confirmed by the discovery of two new magic neutron numbers, *i.e.*, $N = 32$ and $N = 34$. In the Ti isotope chain, a shell gap at $N = 32$ had been confirmed, and the collective behavior due to a $\nu g_{9/2}$ level intrusion was found in the region close to $N = 40$ in several studies.[2–4] As for the $N = 34$ shell gap, previous mass measurements have suggested the existence of a pronounced shell gap with moderate uncertainties.[5,6] However, a new study has revealed the vanishing of the magicity.

The experiment was performed at RIKEN RI Beam Factory (RIBF), which is operated by an international collaboration team primarily from RIKEN Nishina Center and KEK Wako Nuclear Science Center. Radioactive isotopes (RIs) have been produced by the fragmentation of a 345 MeV/nucleon Zn beam with a Be target and delivered to the ZD MRTOF system[7] for the first time as part of the SLOWRI project. The new setup has been located downstream of the ZeroDegree spectrometer following the BigRIPS separator.

During the first commission, the masses of 15 neutron-rich nuclei have been measured with high precision and accuracy. Among the results, the mass precisions of ^{55}Sc, ^{56,58}Ti, and $^{56–59}$V have been significantly improved to the order of 10 keV or below. The newly determined masses of ^{58}Ti and ^{59}V were found to deviate from previously measured values, where—especially for ^{58}Ti—an increased binding energy has been measured. Figure 1 shows the newly determined two-neutron shell gap of $N = 34$ isotones (red line) deduced directly from masses. Literature values suggested an enhancement of the gap with Ti and V, whereas there is no gap found in this study, indicating that the $N = 34$ shell gap is a unique feature of Ca.

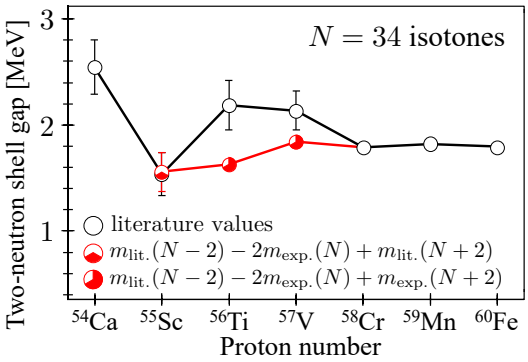

Fig. 1. Two-neutron shell gaps for $N = 34$ isotones including the new mass data. Data are from AME2020 with recent measurements (black open circles) and our experimental values (partly filled red circles).

In order to understand the observed results, we performed new Monte Carlo shell model calculations using the A3DA-m Hamiltonian[8] and compared the results with conventional shell model calculations, which exclude the higher ($\nu g_{9/2}$, $\nu d_{5/2}$) orbits. The comparison indicates that the reduction of the shell gap in Ti is related to partial occupation of the higher orbitals for the outer two valence neutrons at $N = 34$.

† Condensed from the article in Phys. Rev. Lett. **130**, 012501 (2023)

*1 RIKEN Nishina Center
*2 Department of Physics, Osaka University
*3 Wako Nuclear Science Center (WNSC), IPNS, KEK
*4 Department of Physics, Rikkyo University
*5 Center for Computational Sciences, University of Tsukuba
*6 Department of Physics, University of Hong Kong
*7 Institute of Modern Physics, Chinese Academy of Sciences
*8 IAESPC, Jinan University
*9 Nuclear Structure Group, Lawrence Berkeley National Laboratory
*10 Advanced Science Research Center, Japan Atomic Energy Agency
*11 Department of Physics, University of Tokyo
*12 Center for Nuclear Study, University of Tokyo
*13 Rare Isotope Science Project, Institute for Basic Science
*14 Department of Physics, Kyushu University
*15 School of Physics, University of York
*16 GSI Helmholtzzentrum für Schwerionenforschung GmbH
*17 New Mexico State University

References

1) T. Otsuka *et al.*, Rev. Mod. Phys. **92**, 015002 (2020).
2) K. Wimmer *et al.*, Phys. Lett. B **792**, 16 (2019).
3) M. Cortés *et al.*, Phys. Lett. B **800**, 135071 (2020).
4) E. Leistenschneider *et al.*, Phys. Rev. Lett. **120**, 062503 (2018).
5) Z. Meisel *et al.*, Phys. Rev. C **101**, 052801(R) (2020).
6) S. Michimasa *et al.*, Phys. Rev. Lett. **125**, 122501 (2020).
7) M. Rosenbusch *et al.*, Nucl. Instrum. Methods Phys. Res. A **1047**, 167824 (2023).
8) Y. Tsunoda *et al.*, Phys. Rev. C **89**, 031301(R) (2014).

Charge-changing cross sections for $^{42–51}$Ca and effect of charged-particle evaporation induced by neutron removal reactions†

M. Tanaka,[*1,*2] M. Takechi,[*3] A. Homma,[*3] A. Prochazka,[*4] M. Fukuda,[*2] D. Nishimura,[*5,*1] T. Suzuki,[*6] T. Moriguchi,[*7,*1] D. S. Ahn,[*1] A. Aimaganbetov,[*8,*9] M. Amano,[*7] H. Arakawa,[*6] S. Bagchi,[*4,*10,*11,*12] K. H. Behr,[*4] N. Burtebayev,[*8,*13] K. Chikaato,[*3] H. Du,[*2] T. Fujii,[*6] N. Fukuda,[*1] H. Geissel,[*4] T. Hori,[*2] S. Hoshino,[*3] R. Igosawa,[*6] A. Ikeda,[*3] N. Inabe,[*1] K. Inomata,[*6] K. Itahashi,[*1] T. Izumikawa,[*14] D. Kamioka,[*7] N. Kanda,[*3] I. Kato,[*6] I. Kenzhina,[*8,*13] Z. Korkulu,[*15,*1] Y. Kuk,[*8,*9] K. Kusaka,[*1] K. Matsuta,[*2] M. Mihara,[*2] E. Miyata,[*3] D. Nagae,[*1,*16] S. Nakamura,[*2] M. Nassurlla,[*8,*13] K. Nishimuro,[*6] K. Nishizuka,[*3] K. Ohnishi,[*2] M. Ohtake,[*1] T. Ohtsubo,[*3] S. Omika,[*6] H. J. Ong,[*17,*1] A. Ozawa,[*7,*1] H. Sakurai,[*1,*18] C. Scheidenberger,[*4] Y. Shimizu,[*1] T. Sugihara,[*2] T. Sumikama,[*1] H. Suzuki,[*1] S. Suzuki,[*7] H. Takeda,[*1] Y. Tanaka,[*2] Y. K. Tanaka,[*4] I. Tanihata,[*17,*19] T. Wada,[*3] K. Wakayama,[*6] S. Yagi,[*2] T. Yamaguchi,[*6] R. Yanagihara,[*2] Y. Yanagisawa,[*1] K. Yoshida,[*1] and T. K. Zholdybayev[*8,*13]

The point-proton radius r_p of an atomic nucleus is generally determined by optical isotope shift and muonic X-ray measurements. However, these experimental methods are limited to certain elements. Alternatively, "alternative methods, particularly for unstable nuclei, have been proposed to overcome this limitation, such as electron scattering using SCRIT at RIBF."[1] A charge-changing cross-section σ_{CC} is one of the possible quantities to extract the r_p of unstable nuclei. Recently, the σ_{CC} measurement has been utilized to extract the r_p of light-mass nuclei.[2,3] However, some σ_{CC} data for medium-mass nuclides around Ca deviate from the Glauber-like models adopted in previous studies.[4]

To clarify the relationship between σ_{CC} and r_p, σ_{CC} on ^{12}C for $^{42–51}$Ca at around 280 MeV/nucleon was measured at RIBF. The present data are shown in Fig. 1. For comparison, the Glauber-like calculation adopted in previous studies[2–4] was performed using the existing r_p value[4] as an input. The calculated values ($\tilde{\sigma}_{CC}$: black dashed line), which reflect the trend of experimental r_p,[5] show a significant discrepancy from the experimental values of stable nuclei around ^{42}Ca.

This discrepancy was found to correlate with the proton separation energy. From this figure, the cross-section of the charged-particle evaporation induced by the neutron removal, σ_{evap}, was introduced based on the abrasion-ablation scheme in addition to $\tilde{\sigma}_{CC}$. The calculated values of $\tilde{\sigma}_{CC} + \sigma_{evap}$ (solid red line) reproduced well in the experimental data. This calculation also systematically explained the existing σ_{CC} data for other isotopic chains from C to Fe with a standard deviation of 1.6%.

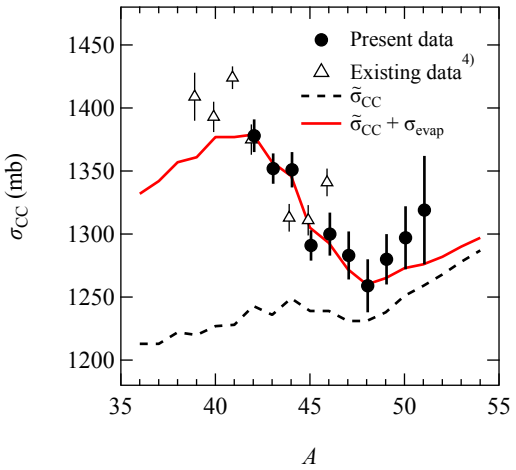

Fig. 1. Mass number (A) dependence of σ_{CC} for Ca isotopes on ^{12}C at 280 MeV/nucleon.

Figure 1 also shows that the effect of σ_{evap} becomes negligibly small in the neutron-rich region. It was found that a 1% accuracy of σ_{CC} has the potential to determine r_p with 0.9% accuracy in neutron-rich Ca isotopes ($A \geq 51$).

References
1) T. Tsukada *et al.*, Phys. Rev. Lett. **118**, 262501 (2017).
2) T. Yamaguchi *et al.*, Phys. Rev. Lett. **107**, 032502 (2011).
3) S. Bagchi *et al.*, Phys. Lett. B **790**, 251 (2019).
4) S. Yamaki *et al.*, Nucl. Instrum. Methods Phys. Res. B **317**, 774 (2013).
5) R. F. Garcia Ruiz *et al.*, Nat. Phys. **12**, 594 (2016).

† Condensed from the article in Phys. Rev. C **106**, 014617 (2022)

*1 RIKEN Nishina Center
*2 Department of Physics, Osaka University
*3 Department of Physics, Niigata University
*4 GSI Helmholtzzentrum für Schwerionenforschung GmbH
*5 Department of Physics, Tokyo City University
*6 Department of Physics, Saitama University
*7 Department of Physics, University of Tsukuba
*8 Institute of Nuclear Physics
*9 L. N. Gumilyov Eurasian National University
*10 Astronomy and Physics Department, Saint Mary's University
*11 Jutus Liebig University
*12 Indian Institute of Technology (Indian School of Mines) Dhanbad
*13 Al-Farabi Kazakh National University
*14 Institute for Research Promotion, Niigata University
*15 Center for Exotic Nuclear Studies, Institute for Basic Science
*16 RCSHE, Kyushu University
*17 Research Center for Nuclear Physics (RCNP), Osaka University
*18 Department of Physics, University of Tokyo
*19 School of Physics and Nuclear Energy Engineering, Beihang University

Probing optimal reaction energy for synthesis of element 119 from ^{51}V+^{248}Cm reaction with quasielastic barrier distribution measurement†

M. Tanaka,[*1,*2,*3] P. Brionnet,[*3] M. Du,[*4] J. Ezold,[*4] K. Felker,[*4] B. J. P. Gall,[*5] S. Go,[*1,*2,*3] R. K. Grzywacz,[*4,*6] H. Haba,[*3] K. Hagino,[*7] S. Hogle,[*4] S. Ishizawa,[*3,*8] D. Kaji,[*3] S. Kimura,[*3] T. T. King,[*6] Y. Komori,[*3] R. K. Lemon,[*3,*9] M. G. Leonard,[*3,*9] K. Morimoto,[*3] K. Morita,[*1,*2,*3] D. Nagae,[*1,*2,*3] N. Naito,[*3,*10] T. Niwase,[*1,*3] B. C. Rasco,[*4] J. B. Roberto,[*4] K. P. Rykaczewski,[*4] S. Sakaguchi,[*1,*2,*3] H. Sakai,[*3] Y. Shigekawa,[*3] D. W. Stracener,[*4] S. VanCleve,[*4] Y. Wang,[*3] K. Washiyama,[*2] and T. Yokokita[*3]

At RIKEN, there is a search for element 119 using a ^{51}V + ^{248}Cm hot fusion reaction. The optimal reaction energy of this reaction system is unknown owing to wide variations in theoretical predictions. A method has been developed to estimate the optimal energy from the quasielastic (QE) barrier distribution.[1)] In this study, the QE barrier distribution of the ^{51}V + ^{248}Cm reaction was measured using the gas-filled recoil ion separator GARIS-III at the recently upgraded facility, SRILAC,[2)] and the optimal reaction energy for synthesizing element 119 from the ^{51}V + ^{248}Cm reaction was estimated.

The experimental excitation function of the QE backscattering cross section $\sigma_{\rm QE}$ relative to the Rutherford cross section $\sigma_{\rm Ruth.}$, denoted as $R(E)$, for the ^{51}V + ^{248}Cm reaction is shown in Fig. 1(a) with the single- and coupled-channel calculations. Figure 1(b) shows the barrier distribution, $D(E)$, derived from the energy derivative of Fig. 1. Both the experimental trends of $R(E)$ and $D(E)$ are explained by the coupled-channel calculation, indicating a significant effect of the rotational excitation of the deformed ^{248}Cm.

Aiming to estimate the optimal energy for element-119 synthesis, the average Coulomb barrier height, B_0, for the ^{51}V + ^{248}Cm reaction was derived from the present data to be 225.6(2) MeV (closed arrow in Fig. 1). The side-collision energy, $B_{\rm side}$, which is considered to be favorable for forming a compound nucleus, was also determined to be 233.0(2) MeV (open arrow) by considering the deformation of ^{248}Cm. By evaluating the relation between $B_{\rm side}$ and the optimal energy for maximizing the evaporation-residue cross section in the ^{48}Ca + ^{248}Cm system, the optimal energy for the ^{248}Cm(^{51}V, 3;4n)$^{296;295}$119 reaction was estimated to be 234.8 ± 1.8 MeV. Using this deduced reaction energy, an experiment for the synthesis of element 119 at RIKEN is currently underway.

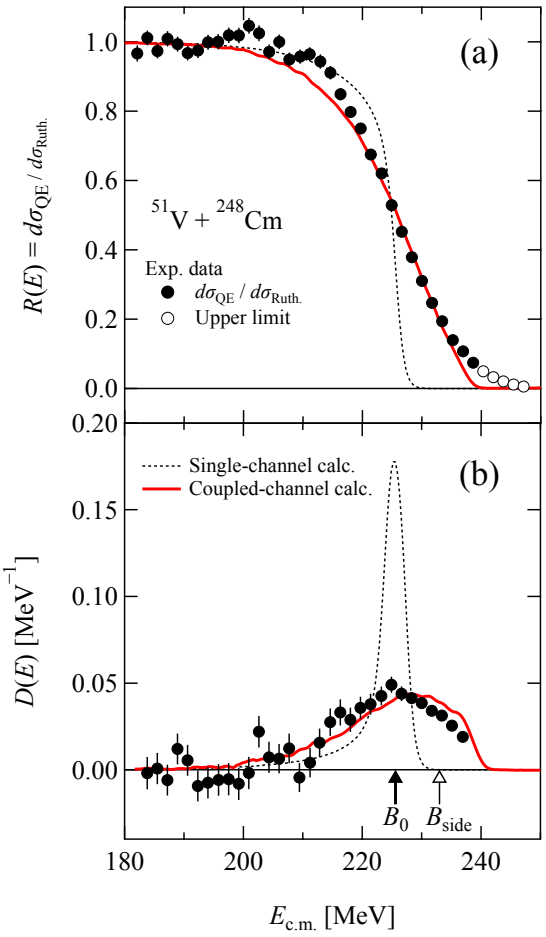

Fig. 1. (a) $R(E)$ and (b) $D(E)$ as a function of the center-of-mass energy $E_{\rm c.m.}$. The dashed and solid lines represent the single- and coupled-channel calculations, respectively.

† Condensed from the article in J. Phys. Soc. Jpn. **91**, 084201 (2022)

*1 Department of Physics, Kyushu University
*2 Research Center for Superheavy Elements, Kyushu University
*3 RIKEN Nishina Center
*4 Oak Ridge National Laboratory
*5 IPHC, CNRS, Université de Strasbourg
*6 Department of Physics and Astronomy, University of Tennessee
*7 Department of Physics, Kyoto University
*8 Graduate School of Science and Engineering, Yamagata University
*9 Department of Nuclear Physics and Accelerator Applications, Australian National University
*10 Graduate School for Science, Kyushu University

References

1) T. Tanaka *et al.*, Phys. Rev. Lett. **124**, 052502 (2020).
2) H. Sakai *et al.*, Eur. Phys. J. A **58**, 238 (2022).

β-delayed one and two neutron emission probabilities south-east of ^{132}Sn and the odd-even distribution of the r-process abundances†

V. H. Phong,[*1,*2] S. Nishimura,[*1] G. Lorusso,[*1,*3,*4] T. Davinson,[*5] A. Estrade,[*6] O. Hall,[*5] T. Kawano,[*7] J. Liu,[*1,*8] F. Montes,[*9] N. Nishimura,[*1,*10] R. Grzywacz,[*11] K. P. Rykaczewski,[*12] J. Agramunt,[*13] D. S. Ahn,[*1,*14] A. Algora,[*13,*25] J. M. Allmond,[*12] H. Baba,[*1] S. Bae,[*14] N. T. Brewer,[*11,*12] C. G. Bruno,[*5] R. Caballero-Folch,[*15] F. Calviño,[*16] P. J. Coleman-Smith,[*17] G. Cortes,[*16] I. Dillmann,[*15,*18] C. Domingo-Pardo,[*13] A. Fijalkowska,[*19] N. Fukuda,[*1] S. Go,[*1] C. J. Griffin,[*5] J. Ha,[*1,*20] L. J. Harkness-Brennan,[*21] T. Isobe,[*1] D. Kahl,[*5,*22] L. H. Khiem,[*23,*24] G. G. Kiss,[*1,*25] A. Korgul,[*19] S. Kubono,[*1] M. Labiche,[*17] I. Lazarus,[*17] J. Liang,[*26] Z. Liu,[*27,*28] K. Matsui,[*1,*29] K. Miernik,[*19] B. Moon,[*14] A. I. Morales,[*13] P. Morrall,[*17] N. Nepal,[*6] R. D. Page,[*21] M. Piersa-Siłkowska,[*19] V. F. E. Pucknell,[*17] B. C. Rasco,[*12] B. Rubio,[*13] H. Sakurai,[*1,*29] Y. Shimizu,[*1] D. W. Stracener,[*12] T. Sumikama,[*1] H. Suzuki,[*1] J. L. Tain,[*13] H. Takeda,[*1] A. Tarifeño-Saldivia,[*13,*16] A. Tolosa-Delgado,[*13] M. Wolińska-Cichocka,[*30] P. J. Woods,[*5] and R. Yokoyama[*11,*31]

The nucleosynthesis of elements around the second r-process abundance peak has attracted considerable interest recently, with metal-poor star observations of elemental and isotopic abundances[1,2] providing important clues on the sensitivity of the peak to the r-process environments. To connect such observations to the astrophysical models and ultimately derive the r-process conditions, knowledge of the nuclear properties of the second r-process peak radioactive progenitors is essential.

After r-process freezeout, final r-process abundances of the second peak originate from a network of competing reactions including the neutron capture, photodisintegration, fission contribution and β-delayed neutron emission. The latter has been the main focus of our experiment carried out within the BRIKEN project[3] at RIBF, where β-delayed one and two neutron emission probabilities (P_{1n} and P_{2n}) of neutron-rich nuclei south-east of ^{132}Sn have been measured. The systematic of the measured P_{1n} and P_{2n} values, shown in Fig. 1, highlighted the nuclear shell effects around doubly-magic ^{132}Sn. Our results also provided important benchmarks for the recent macroscopic-microscopic and self-consistent global model, including the statistical treatment of neutron and γ emission.[4,5] Direct impacts of the measured P_{1n} and P_{2n} on the odd-even staggering of the final r-process abundance around the second r-process peak were demonstrated. The observed odd-mass isotopic fractions of Ba in metal-poor stars[2] were found to be better reproduced by using our data.

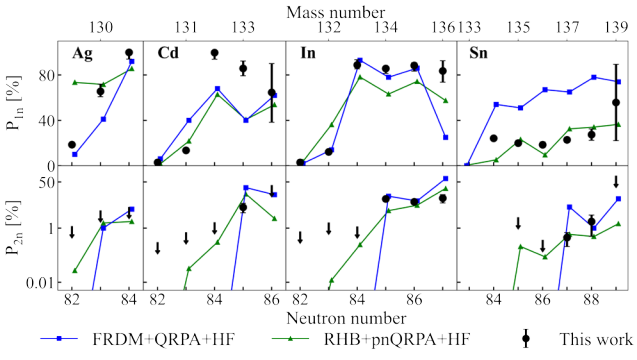

Fig. 1. Systematics of measured P_{1n} (top panels) and P_{2n} compared with theoretical calculations.[4,5]

† Condensed from the article in Phys. Rev. Lett. **129**, 172701 (2022)

*1 RIKEN Nishina Center
*2 Vietnam National University, Hanoi
*3 National Physical Laboratory, Teddington
*4 Department of Physics, University of Surrey
*5 School of Physics and Astronomy, University of Edinburgh
*6 Department of Physics, Central Michigan University
*7 Theoretical Division, Los Alamos National Laboratory
*8 Department of Physics, University of Hong Kong
*9 National Superconducting Cyclotron Laboratory
*10 Astrophysical Big-Bang Laboratory
*11 University of Tennessee, Knoxville
*12 Physics Division, Oak Ridge National Laboratory
*13 Instituto de Física Corpuscular, CSIC-University of Valencia
*14 Center for Exotic Nuclear Studies, Institute for Basic Science
*15 TRIUMF, Vancouver
*16 Universitat Politecnica de Catalunyan
*17 STFC Daresbury Laboratory
*18 Department of Physics and Astronomy, University of Victoria
*19 Faculty of Physics, University of Warsaw
*20 Department of Physics and Astronomy, Seoul National University
*21 Department of Physics, University of Liverpool
*22 Extreme Light Infrastructure – Nuclear Physics, Horia Hulubei National Institute for R&D in Physics and Nuclear Engineering
*23 Institute of Physics, VAST
*24 Graduate University of Science and Technology, VAST
*25 Institute for Nuclear Research (ATOMKI)
*26 Department of Physics and Astronomy, McMaster University
*27 Institute of Modern Physics, Chinese Academy of Sciences
*28 School of Nuclear Science and Technology, University of Chinese Academy of Sciences
*29 Department of Physics, University of Tokyo
*30 Heavy Ion Laboratory, University of Warsaw
*31 Center for Nuclear Study, University of Tokyo

References

1) I. U. Roederer *et al.*, Astrophys. J. Suppl. Ser. **260**, 27 (2022).
2) C. Wenyuan *et al.*, Astrophys. J. **854**, 131 (2018).
3) I. Dillmann *et al.*, Nucl. Phys. News **28**, 28 (2018).
4) T. Kawano *et al.*, Phys. Rev. C **78**, 054601 (2008).
5) F. Minato *et al.*, Phys. Rev. C **104**, 044321 (2021).

Various nuclear structures in ^{140}Xe studied by β decay of ground and isomeric states in ^{140}I†

A. Yagi,[*1,*2] A. Odahara,[*1] H. Nishibata,[*1,*2,*3] R. Lozeva,[*4,*5] C. -B. Moon,[*6,*7] S. Nishimura,[*2] K. Yoshida,[*8] and N. Yoshinaga[*9] for the EURICA Collaboration

Nuclear-shape transition with the increase of neutron and/or proton numbers is one of the most important subjects to disentangle competition between single-particle and collective structures in the finite quantum many-body system. The neutron-rich $N = 86$ isotope ^{140}Xe, located northeast of a doubly-magic nucleus ^{132}Sn, was investigated by β-γ spectroscopy, as one of experiments in the Euroball RIKEN Cluster Array (EURICA) project.[1,2)]

Neutron-rich Sb, Te, I, Xe, and Cs isotopes with $A \sim 140$ were produced by in-flight fission of a 345-MeV/nucleon ^{238}U beam with an average intensity of 5 particle nA. These isotopes were transported based on in-flight separation technique by using BigRIPS separator and ZeroDegree spectrometer[3)] up to the last focal plane (F11) with setting magnetic rigidity ($B\rho$) for ^{142}Te^{52+}. The isotopes were implanted into a position sensitive active stopper, Wide-range Active Silicon Strip Stopper Array for Beta and Ion detection (WAS3ABi), which consists of five double-sided Si strip detectors (DSSSDs). In addition, the WAS3ABi was used as a β counter. Parent β-decaying nuclei were identified by position correlation of the implanted fragments with information of particle identification (PI) and the detected β rays in WAS3ABi. Gamma rays emitted after the β decay were detected by a γ-ray detector array, EURICA, which consists of twelve cluster-type high-purity Ge detectors with seven crystals. To study the β decay of ^{140}I in this work, two data sets with PI of hydrogen-like ^{140}I^{52+} and fully stripped ^{140}Te^{52+} were analyzed. Namely, the parent nucleus ^{140}I was produced by two different reactions of (i) direct in-flight fission at primary target and (ii) β decay of ^{140}Te inside WAS3ABi. Relative intensity of γ ray was obtained by using γ-ray photo-peak efficiency, which was simulated using the Geant4 code for the EURICA Ge array with distribution of the ^{140}I and ^{140}Te particles on five DSSSD detectors in WAS3ABi.

Two β-decay isomers in ^{140}I are newly found in the study of two different β decays of ^{140}I (^{140}I $\rightarrow$ ^{140}Xe) and ^{140}Te (^{140}Te $\rightarrow$ ^{140}I $\rightarrow$ ^{140}Xe). Half-lives of the β decays of the ground state (g.s.), low-spin isomer (LSI), and high-spin isomer (HSI) are determined to be 0.38(2), 0.91(5), and 0.47(4) sec, respectively, by the analysis of time-difference (implanted particle and β-decay event) spectra gated by the γ rays in ^{140}Xe. Decay schemes of the β decay of the HSI and of the mixed β decays of the g.s. and the LSI in ^{140}I to ^{140}Xe are constructed using the information on γ-ray coincidence relation and γ-ray intensity.

Nuclear structures of the low-lying states in ^{140}Xe are compared between the experimental results and two theoretical calculations based on the large-scale shell model and the deformed Skyrme Hartree-Fock-Bogoliubov (HFB) plus deformed quasiparticle-random-phase approximation (QRPA), as shown in Fig. 1. Low-lying states can be classified into (a) g.s. band, (b) (quasi-)γ-band, and (c) octupole collective states. Possible candidates for the (quasi-)γ-band members of 2^+ and 4^+ and the octupole collective 1^- state are proposed in ^{140}Xe. This work demonstrates that in the low-lying states of ^{140}Xe, coexistence of nuclear structures, such as vibrational nature with prolate collectivity, large-γ collectivity (γ softness), and octupole-vibrational nature, could appear due to four valence protons and four valence neutrons being coupled to the doubly-magic nucleus ^{132}Sn.

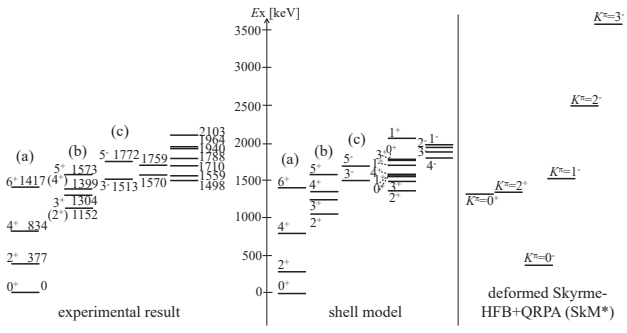

Fig. 1. Experimental low-lying states are compared to those calculated in the shell model and the deformed Skyrme-HFB + QRPA (SkM*).

† Condensed from the article in Phys. Rev. C **105**, 044325 (2022)

*1 Department of Physics, Osaka University
*2 RIKEN Nishina Center
*3 Department of Physics, Kyushu University
*4 IPHC, CNRS, IN2P3 and University of Strasbourg
*5 Université Paris-Saclay, IJCLab, CNRS/IN2P3
*6 Department of Display Engineering, Hoseo University
*7 Center for Exotic Nuclear Studies, Institute for Basic Science
*8 Department of Physics, Kyoto University
*9 Department of Physics, Saitama University

References

1) S. Nishimura, Prog. Theor. Exp. Phys. **2012**, 03C006 (2012).
2) P. -A. Söderström *et al.*, Nucl. Instrum. Methods Phys. Res. B **317**, 649 (2013).
3) T. Kubo *et al.*, Prog. Theor. Exp. Phys. **2012**, 03C003 (2012).

Observation of a correlated free four-neutron system†

M. Duer,[*1] T. Aumann,[*1,*2,*3] R. Gernhäuser,[*4] V. Panin,[*2,*5] S. Paschalis,[*1,*6] D. M. Rossi,[*1] N. L. Achouri,[*7] D. Ahn,[*5] H. Baba,[*5] C. A. Bertulani,[*8] M. Böhmer,[*4] K. Boretzky,[*2] C. Caesar,[*1,*2,*5] N. Chiga,[*5] A. Corsi,[*9] D. Cortina-Gil,[*10] C. A. Douma,[*11] F. Dufter,[*4] Z. Elekes,[*12] J. Feng,[*13] B. Fernández-Domínguez,[*10] U. Forsberg,[*6] N. Fukuda,[*5] I. Gasparic,[*1,*5,*14] Z. Ge,[*5] J. M. Gheller,[*9] J. Gibelin,[*7] A. Gillibert,[*9] K. I. Hahn,[*15,*16] Z. Halász,[*12] M. N. Harakeh,[*11] A. Hirayama,[*17] M. Holl,[*1] N. Inabe,[*5] T. Isobe,[*5] J. Kahlbow,[*1] N. Kalantar-Nayestanaki,[*11] D. Kim,[*16] S. Kim,[*1,*16] T. Kobayashi,[*18] Y. Kondo,[*17] D. Körper,[*2] P. Koseoglou,[*1] Y. Kubota,[*5] I. Kuti,[*12] P. J. Li,[*19] C. Lehr,[*1] S. Lindberg,[*20] Y. Liu,[*13] F. M. Marqués,[*7] S. Masuoka,[*21] S. Masuoka,[*21] M. Matsumoto,[*17] J. Mayer,[*22] K. Miki,[*1,*18] B. Monteagudo,[*7] T. Nakamura,[*17] T. Nilsson,[*20] A. Obertelli,[*1,*9] N. A. Orr,[*7] H. Otsu,[*5] S. Y. Park,[*15,*16] M. Parlog,[*7] P. M. Potlog,[*23] S. Reichert,[*4] A. Revel,[*7,*9,*24] A. T. Saito,[*17] M. Sasano,[*5] H. Scheit,[*1] F. Schindler,[*1] S. Shimoura,[*21] H. Simon,[*2] L. Stuhl,[*16,*21] H. Suzuki,[*5] D. Symochko,[*1] H. Takeda,[*5] J. Tanaka,[*1,*5] Y. Togano,[*17] T. Tomai,[*17] H. T. Törnqvist,[*1,*2] J. Tscheuschner,[*1] T. Uesaka,[*5] V. Wagner,[*1] H. Yamada,[*17] B. Yang,[*13] L. Yang,[*21] Z. H. Yang,[*5] M. Yasuda,[*17] K. Yoneda,[*5] L. Zanetti,[*1] J. Zenihiro,[*5,*25] and M. V. Zhukov[*20]

The high impact potential of multi-neutron systems has led to many experimental searches for such isolated systems starting in the early 60 s, with in particular, the four-neutron system. Till date, only a few indications of its existence have been found.[1)]

This study used the quasi-elastic knockout reaction ^{8}He$(p, p\alpha)$ at maximum momentum transfer, removing the α-core from ^{8}He as fast as possible, to ensure a recoil-less production of the $4n$ as spectators.

The experiment was conducted at SAMURAI, where a 156 MeV/nucleon ^{8}He beam was transported to a liquid-hydrogen target. From the combined selection of charged particles in the reaction, the energy spectrum of the $4n$ system was reconstructed via the missing-mass method, as shown in Fig. 1. Two components are observed: a pronounced peak at low energy which experimentally has a resonance-like structure, and a wide distribution at higher energies attributed to a non-resonant continuum response.[2)] As the non-resonant part cannot explain the sharp low-energy peak, the energy and width of the resonance-like structure was determined assuming a Breit-Wigner shape as $E_{\mathrm{r}} = 2.37 \pm 0.58$ MeV and $\Gamma = 1.75 \pm 0.40$ MeV, respectively, with a striking significance level.

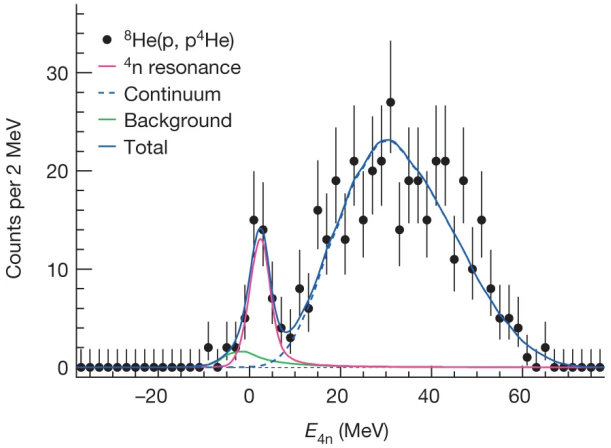

Fig. 1. Missing-mass spectrum of the $4n$ system.

From theoretical perspective there is no consensus among the different studies. While some predict a low-energy resonance,[3)] others exclude this possibility[4)] and even predict that a low-energy structure can appear as a consequence of neutron's final-state interaction, and the reaction mechanism.[5)] Whether our observation is attributed to a tetra-neutron correlation or other correlations between the neutrons in the final state, needs to be clarified by ab initio theories accounting fully for the continuum. Next-generation experiments, foreseen at SAMURAI, using different reaction mechanisms and detecting the four neutrons in coincidence will shed light on the properties of the four-neutron system and the origin of the low-energy peak.

† Condensed from the article in Nature **606**, 678 (2022)
*1 Institut für Kernphysik, Technische Universität Darmstadt
*2 GSI Helmholtzzentrum für Schwerionenforschung GmbH
*3 Helmholtz Forschungsakademie Hessen für FAIR
*4 Physik Department, Technische Universität München
*5 RIKEN Nishina Center
*6 Department of Physics, University of York
*7 Laboratoire de Physique Corpusculaire de Caen
*8 Department of Physics, Texas A&M University
*9 IRFU, CEA, Université Paris-Saclay
*10 Molecular and Nuclear Physics, USC
*11 Faculty of Science and Engineering, University of Groningen
*12 Hungarian Academy of Sciences, Eötvös Loránd Research Network
*13 Department of Physics, Peking University
*14 Division of Experimental Physics, Rudjer Bošković Institute
*15 Department of Physics, Ewha Womans University
*16 Korea Basic Science Institute
*17 Department of Physics, Tokyo Institute of Technology
*18 Department of Physics, Tohoku University
*19 Department of Physics, University of Hong Kong
*20 Department of Physics, Chalmers University of Technology
*21 Center for Nuclear Study, University of Tokyo
*22 Institut für Kernphysik, Universität zu Köln
*23 Department of Physics, Institute of Space Sciences
*24 GANIL, CEA Caen
*25 Department of Physics, Kyoto University

References
1) F. M. Marqués *et al.*, Eur. Phys. J. A **57**, 105 (2021).
2) L. V. Grigorenko *et al.*, Eur. Phys. J. A **19**, 187 (2004).
3) S. Gandolfi *et al.*, Phys. Rev. Lett. **118**, 232501 (2017).
4) E. Hiyama *et al.*, Phys. Rev. C **93**, 044004 (2016).
5) R. Lazauskas *et al.*, arXiv:2207.07575.

Isoscaling in central Sn + Sn collisions at 270 MeV/nucleon†

J. W. Lee,[*1] M. B. Tsang,[*2,*3] C. Y. Tsang,[*2,*3] R. Wang,[*2] J. Barney,[*2,*3] J. Estee,[*2,*3] T. Isobe,[*4] M. Kaneko,[*4,*5] M. Kurata-Nishimura,[*4] W. G. Lynch,[*2,*3] T. Murakami,[*4,*5] A. Ono,[*6] S. R. Souza,[*7,*8] D. S. Ahn,[*4] L. Atar,[*9,*10] T. Aumann,[*9,*10] H. Baba,[*4] K. Boretzky,[*10] J. Brzychczyk,[*11] G. Cerizza,[*2] N. Chiga,[*4] N. Fukuda,[*4] I. Gasparic,[*12,*4,*9] B. Hong,[*1] A. Horvat,[*9,*10] K. Ieki,[*13] N. Ikeno,[*14] N. Inabe,[*4] G. Jhang,[*2] Y. J. Kim,[*15] T. Kobayashi,[*6,*4] Y. Kondo,[*16,*4] P. Lasko,[*17] H. S. Lee,[*15] Y. Leifels,[*10] J. Łukasik,[*17] J. Manfredi,[*2,*3] A. B. McIntosh,[*18] P. Morfouace,[*2] T. Nakamura,[*16,*4] N. Nakatsuka,[*4,*5] S. Nishimura,[*4] H. Otsu,[*4] P. Pawłowski,[*17] K. Pelczar,[*11] D. Rossi,[*9] H. Sakurai,[*4] C. Santamaria,[*2] H. Sato,[*4] H. Scheit,[*9] R. Shane,[*2] Y. Shimizu,[*4] H. Simon,[*10] A. Snoch,[*19] A. Sochocka,[*11] T. Sumikama,[*4] H. Suzuki,[*4] D. Suzuki,[*4] H. Takeda,[*4] S. Tangwancharoen,[*2] Y. Togano,[*13,*4] Z. G. Xiao,[*20] S. J. Yennello,[*18,*21] and Y. Zhang[*20]

Experimental study on the early stage of heavy-ion collision is challenging as excited fragments produced from the collision decay into lighter particles before they are detected. The nuclear isoscaling phenomenon is a useful tool as the ratio of yields from two different reactions is weakly affected by the fragment de-excitation process.[1)]

Rare isotope Tin beams ^{132}Sn and ^{108}Sn were produced from RIBF and impinged onto the isotopically enriched Tin targets. Hydrogen and helium isotopes were detected in SπRIT time projection chamber[2)] placed inside the SAMRURAI dipole magnet.[3)] Particles were identified from the magnetic rigidity and mean energy loss.[4)] Most central events with impact parameter $b <$ 1.5 fm and mid rapidity range $y_0 = 0$–0.4 are chosen for this analysis.

The yield ratios between two systems $R_{21} = \mathrm{Y}(^{132}\mathrm{Sn} + {}^{124}\mathrm{Sn})/\mathrm{Y}(^{108}\mathrm{Sn} + {}^{112}\mathrm{Sn})$ as a function of p_T/A are shown in Fig. 1. Given that the collision systems are thermally equilibrated, R_{21} follow the isoscaling law $R_{21} = C\exp(\alpha N + \beta Z)$ where α and β are the fit parameters. Empirically, α and β have similar values with opposite signs, therefore, particles with the same $(N-Z)$ value show similar R_{21} values. Figure 1 show isoscaling effect for $p_\mathrm{T} < 280$ MeV/c (left side of vertical dashed line). In this region, the isoscaling fit gives $\alpha = 0.29$ and $\beta = -0.23$ (inner panel of Fig. 1). On the other hand, the triton and helium R_{21} values breakdown above this limit, and the isoscaling phenomenon vanishes. This suggests that high p_T/A particles come from the non-equilibrated environment.

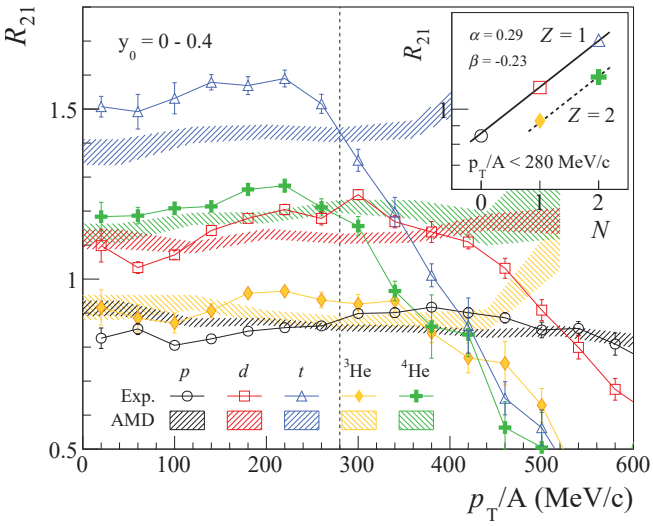

Fig. 1. The yield ratio R_{21} between two systems ^{132}Sn + ^{124}Sn and ^{108}Sn + ^{112}Sn. Experimental data (markers) are compared with AMD (shaded area). Inner panel: Isoscaling fit for $p_\mathrm{T}/A < 280$ MeV/c.

The antisymmetrized molecular dynamics (AMD) model[5,6)] is employed with Skyrme SLy4 effective interaction and symmetry energy slope parameter $L =$ 46 MeV. The AMD result qualitatively explains isoscaling for $p_\mathrm{T}/A < 280$ even though AMD is a dynamical model. However, AMD underestimate triton R_{21} and do not reproduce breakdown of R_{21}.

† Condensed from the article in Eur. Phys. J. A **58**, 201 (2022)

*1 Department of Physics, Korea University
*2 Facility for Rare Isotope Beams, Michigan State University
*3 Department of Physics, Michigan State University
*4 RIKEN Nishina Center
*5 Department of Physics, Kyoto University
*6 Department of Physics, Tohoku University
*7 Instituto de Física, Universidade Federal do Rio de Janeiro
*8 Departamento de Engenharia Nuclear, Universidade Federal de Minas Gerais
*9 Institut für Kernphysik, Technische Universität Darmstadt
*10 GSI Helmholtzzentrum für Schwerionenforschung GmbH
*11 Faculty of Physics, Jagiellonian University
*12 Division of Experimental Physics, Rudjer Boskovic Institute
*13 Department of Physics, Rikkyo University
*14 Department of Life and Environmental Agricultural Sciences, Tottori University
*15 Rare Isotope Science Project, Institute for Basic Science
*16 Department of Physics, Tokyo Institute of Technology
*17 Institute of Nuclear Physics PAN
*18 Cyclotron Institute, Texas A&M University
*19 Nikhef National Institute for Subatomic Physics
*20 Department of Physics, Tsinghua University
*21 Department of Chemistry, Texas A&M University

References

1) M. B. Tsang *et al.*, Phys. Rev. C **64**, 054615 (2001).
2) J. Barney *et al.*, Rev. Sci. Instrum. **92**, 063302 (2021).
3) H. Otsu *et al.*, Nucl. Instrum. Methods Phys. Res. B **376**, 175 (2016).
4) J. W. Lee *et al.*, Nucl. Instrum. Methods Phys. Res. A **965**, 163840 (2020).
5) A. Ono, Prog. Part. Nucl. Phys. **105**, 139 (2019).
6) M. Kaneko *et al.*, Phys. Lett. B **822**, 136681 (2021).

Breakup of proton halo nucleus ^{8}B at near-barrier energies†

L. Yang,[*1,*2] C. J. Lin,[*1,*3] H. Yamaguchi,[*2,*4] A. M. Moro,[*5,*6] N. R. Ma,[*1] D. X. Wang,[*1] K. J. Cook,[*7,*8] M. Mazzocco,[*9,*10] P. W. Wen,[*1] S. Hayakawa,[*2] J. S. Wang,[*11] Y. Y. Yang,[*12] G. L. Zhang,[*13] Z. Huang,[*13] A. Inoue,[*14] H. M. Jia,[*1] D. Kahl,[*15] A. Kim,[*16] M. S. Kwag,[*17] M. La Commara,[*18] G. M. Gu,[*17] S. Okamoto,[*19] C. Parascandolo,[*20] D. Pierroutsakou,[*20] H. Shimizu,[*2] H. H. Sun,[*1] M. L. Wang,[*13] F. Yang,[*1] and F. P. Zhong[*1,*3]

As recognized since the very first measurements in the mid-1980s,[1] the most neutron-rich unstable isotope of lithium, ^{11}Li, was reported to present an unexpected halo-type structure. After this experimental discovery in ^{11}Li, several other nuclear systems with neutron halo structures were reported. On the proton-rich side, ^{8}B is one of the few cases whose ground state presents the proton halo.[2] The large extent of the nuclear matter distribution and the very low threshold of the breakup channel strongly impact the reaction mechanism, particularly at energies around the Coulomb barrier, where couplings to the breakup continuums are expected to be particularly significant. Consequently, the detailed knowledge of the breakup mechanism is critical for an understanding of the reaction dynamics of halo nuclear systems.

The breakup mechanism of the proton halo nuclei is rather complicated. The dynamic Coulomb polarization effect[3] may produce a hindrance to both the proton transfer and breakup processes,[4] which results in the rather elusive character of proton halo systems. To obtain a comprehensive understanding of the breakup process, the coincident measurement of the breakup fragments is the inevitable course. However, it is a significant challenge for incident energies close to the Coulomb barrier, as it is not easy to carry out a coincidence measurement among the breakup fragments as was done at higher energies owing to the much reduced kinematic focusing. It becomes worse owing to the very low beam intensities of proton halo nuclei.

To address this long-standing challenge, we performed the complete kinematics measurement of ^{8}B + ^{120}Sn at two energies around the barrier.[5] Owing to the highly efficient silicon detector array, the correlation of the breakup fragments, ^{7}Be and proton, is derived for the first time. As an example, the relative energy spectra ($E_{\rm rel}$) is presented in Fig. 1. The correlations can be explained by the state-of-the-art continuum discretized coupled channel calculations. The results indicate that ^{8}B presents distinctive reaction dynamics: the dominance of the elastic breakup. This breakup occurs primarily through short-lived continuum states and almost exhausts the ^{7}Be yield. The correlation reveals that the prompt breakup mechanism dominates, occurring predominantly on the outgoing trajectory. We also report that, as a large environment, the continuum of ^{8}B breakup may not significantly impact elastic scattering and complete fusion.

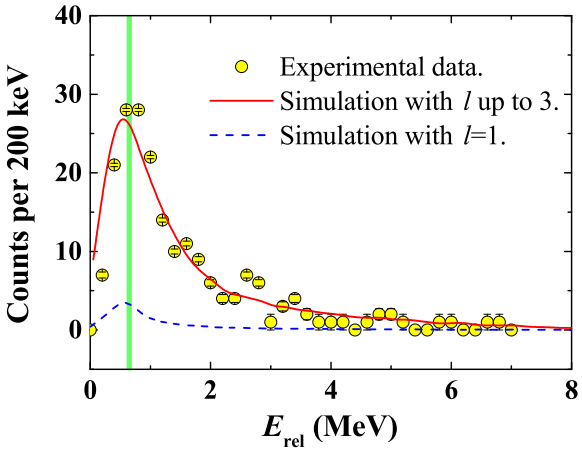

Fig. 1. Measured $E_{\rm rel}$ distribution (circles) for the breakup fragment at 38.7 MeV. The vertical line indicates the expected location of the peak from the first 1^{+} resonance of ^{8}B. The solid and dashed curves denote the simulated distributions of $E_{\rm rel}$ with the orbital angular momentum up to $l = 3$ and the $l = 1$ (1^{+}) state, respectively.

† Condensed from the article in Nat. Commun. **13**, 7193 (2022)

*1 Department of Nuclear Physics, China Institute of Atomic Energy
*2 Center for Nuclear Study, University of Tokyo
*3 College of Physics and Technology & Guangxi Key Laboratory of Nuclear Physics and Technology, Guangxi Normal University
*4 National Astronomical Observatory of Japan
*5 Departamento de FAMN, Universidad de Sevilla
*6 Instituto Interuniversitario Carlos I de Física Teórica y Computacional (iC1)
*7 Department of Physics, Tokyo Institute of Technology
*8 Facility for Rare Isotope Beams, Michigan State University
*9 Dipartimento di Fisica e Astronomia, Universita di Padova
*10 Istituto Nazionale di Fisica Nucleare-Sezione di Padova
*11 School of Science, Huzhou University
*12 Institute of Modern Physics, Chinese Academy of Sciences
*13 School of Physics, Beihang University
*14 Research Center for Nuclear Physics, Osaka University
*15 Extreme Light Infrastructure—Nuclear Physics, Horia Hulubei National Institute for R&D in Physics and Nuclear Engineering (IFIN-HH)
*16 Center for Extreme Nuclear Matters, Korea University
*17 Department of Physics, Sungkyunkwan University
*18 Department of Pharmacy, University Federico II
*19 Department of Physics, Kyoto University
*20 Istituto Nazionale di Fisica Nucleare-Sezione di Napoli

References

1) I. Tanihata *et al.*, Phys. Rev. Lett. **55**, 2676 (1985).
2) G. A. Korolev *et al.*, Phys. Lett. B **780**, 200 (2018).
3) M. Ito *et al.*, Nucl. Phys. A **787**, 267 (2007).
4) Y. Kucuk *et al.*, Phys. Rev. C **86**, 034601 (2012).
5) L. Yang *et al.*, Nat. Commun. **13**, 7193 (2022).

Discovery of new isotope ^{241}U and systematical mass measurement of neutron-rich Pa-Pu nuclei with KISS-MRTOF system

T. Niwase,[*1] Y. X. Watanabe,[*1] Y. Hirayama,[*1] M. Mukai,[*2] P. Schury,[*1] A. N. Andreyev,[*3] T. Hashimoto,[*4] S. Iimura,[*5] H. Ishiyama,[*2] Y. Ito,[*6] S. C. Jeong,[*1] D. Kaji,[*2] S. Kimura,[*2] H. Miyatake,[*1] K. Morimoto,[*2] J. -Y. Moon,[*4] M. Oyaizu,[*1] M. Rosenbusch,[*1] A. Taniguchi,[*7] and M. Wada[*1]

We previously operated the KEK Isotope Separation System (KISS)[1,2] for nuclear spectroscopy of neutron-rich nuclei around $N = 126$ and beyond. We explore neutron-rich uranium regions with a recently developed multi-reflection time-of-flight mass spectrograph (MRTOF-MS).[3] In this manuscript, we report the first systematic mass measurements of neutron-rich Pa-Pu isotopes produced as projectile-like fragments (PLF) via several multi-nucleon transfer (MNT) channels of the ^{238}U + ^{198}Pt reaction at the KISS facility.

The experimental setup of KISS facility is described elsewhere.[1,2] A rotating ^{198}Pt (enriched to 91.63%) target with a thickness of 12.5 mg/cm^2 was bombarded by a primary beam of ^{238}U (10.75 MeV/nucleon), which was provided by the RIKEN Ring Cyclotron with typical intensity of approximately 30 particle nA. The isotopes of interest were produced as PLFs in the MNT reactions, with their masses and velocities being close to those of the primary beam particle. Moreover, they were scattered around the grazing angle. The energy of reaction products were attenuated using a 40-μm Ti energy degrader to maximize the yield stopping in a doughnut-shaped gas cell filled with 65-kPa argon gas.

We successfully performed the high-precision direct mass measurement of 19 neutron-rich Pa-Pu nuclides (Fig. 1) and discovered a new uranium isotope ^{241}U.[4] Figure 2(a) shows the TOF spectrum at 1001 laps in the MRTOF with resonant laser wavelength for the new isotope ^{241}U. Figure 2(b) shows the TOF spectrum at 600 laps with resonant wavelength for ^{241}Np. The comparison of the spectra in Figs. 2(a) and (b) indicates the identification of the new isotope ^{241}U.

This study was demonstrated to explore the neutron-rich actinide region using MNT reaction via KISS and MRTOF setup. We plan to use further heavier/symmetric projectile and target combinations such as ^{238}U+^{238}U/^{248}Cm, which is promising for reaching more exotic nuclei to understand both astrophysically relevant processes and the evolution of nuclear structure at $N = 152$ and beyond.

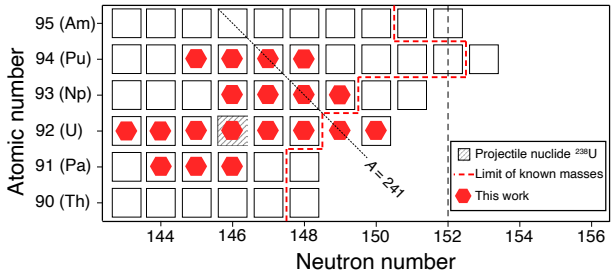

Fig. 1. Part of nuclear chart of the neutron-rich actinide region. Red dashed line indicates the mass known line, and red hexagon symbols denote the measured data in this work.

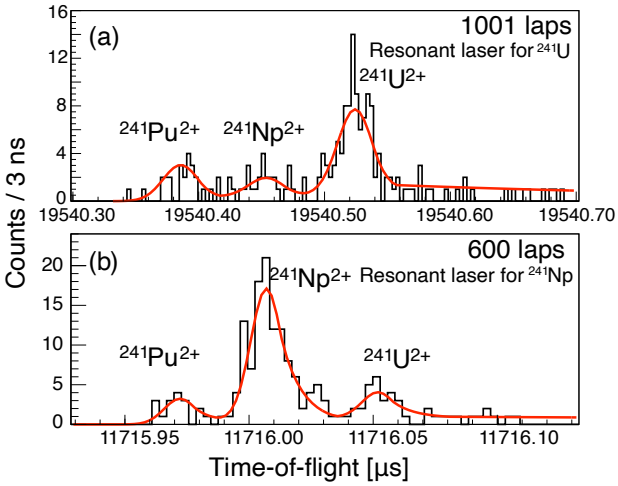

Fig. 2. TOF spectra with the solid red lines denoting the fitting curves. (a) $A/q = 120.5$ region after 1001 laps in the MRTOF-MS with resonant wavelength for the new isotope ^{241}U. (b) $A/q = 120.5$ region after 600 laps with resonance for ^{241}Np. The absolute TOF values were different between (a) and (b) owing to the difference in the number of laps.

*1 Wako Nuclear Science Center (WNSC), IPNS, KEK
*2 RIKEN Nishina Center
*3 School of Physics, Engineering and Technology, University of York
*4 Institute for Basic Science
*5 Department of Physics, Rikkyo University
*6 Advanced Science Research Center, Japan Atomic Energy Agency
*7 Institute for Integrated Radiation and Nuclear Science, Kyoto University

References

1) Y. Hirayama *et al.*, Nucl. Instrum. Methods Phys. Res. B **353**, 4 (2015).
2) Y. Hirayama *et al.*, Nucl. Instrum. Methods Phys. Res. B **412**, 11 (2017).
3) J. Y. Moon *et al.*, RIKEN Accel. Prog. Rep. **52**, 138 (2018).
4) T. Niwase *et al.*, Phys. Rev. Lett. **130**, 132502 (2023).

α-cluster structure of ^{12}C from first principles†

T. Abe,[*1] T. Otsuka,[*2,*1,*3] T. Yoshida,[*4,*5] Y. Tsunoda,[*4] N. Shimizu,[*4] N. Itagaki,[*6] Y. Utsuno,[*3,*4] J. P. Vary,[*7] P. Maris,[*7] and H. Ueno[*1]

The ^{12}C nucleus is of particular importance in stellar nucleosynthesis. It is produced by triple-α reactions through the second 0^+ state (Hoyle state). However, the properties of the Hoyle state are not fully understood. The Hoyle state is still being studied actively from both sides of experiments and theories. On the theoretical side, *ab initio* approaches for low-energy nuclear structure calculations have been advanced rapidly in recent years, owing to recent computational and methodological developments. Here, we report the low-lying structure of ^{12}C studied by the *ab initio* calculations in the no-core Monte Carlo shell model (MCSM).[1)]

Figure 1 shows the no-core MCSM results compared to the experiments. The calculations were carried out in the basis space of $N_{\rm shell} = 7$ with the harmonic-oscillator energy of $\hbar\omega = 20$ MeV. The Daejeon16 NN interaction[2)] was adopted. In Fig. 1, the excitation energies and transition strengths ($B(E2)$, $M(E0)$) for the ground (0_1^+) and two low-lying (2_1^+, 0_2^+) states are indicated. For the 2_1^+ state, the Q-moment is also depicted in the unit of e fm^2. As seen in Fig. 1, the no-core MCSM calculations ("th" in the figure) provide a reasonable agreement with the experimental values ("exp" in the figure). It is remarkable that the *ab initio* calculations for the low-lying states of the twelve-body system can reproduce the experimental data.

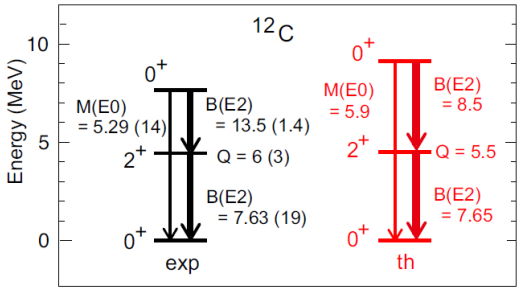

Fig. 1. ^{12}C excitation spectra and the $B(E2)$ ($M(E0)$) values in the unit of e^2 fm^4 (e fm^2) compared to experiments. For more details, see Ref. 1).

The density in the body-fixed frame (intrinsic density) is closely related to the structure of atomic nuclei. It is, however, still difficult to observe the intrinsic density experimentally. Thus, the theoretical approaches are indispensable to investigate the intrinsic density of atomic nuclei. Figure 2 displays the density distributions of the ground (0_1^+) and Hoyle (0_2^+) states in comparison with the α-particle (^{4}He) density. For the ground state, three α-like clusters are closely lying one another, being closer to the quantum liquid (*i.e.*, normal nuclear matter). The Hoyle state appears rather clearly separated three α-like clusters compared to the ground state. It is noteworthy that *ab initio* calculations in the twelve-body system exhibit three-α-like cluster structure of ^{12}C without any *a priori* assumptions of α particles.

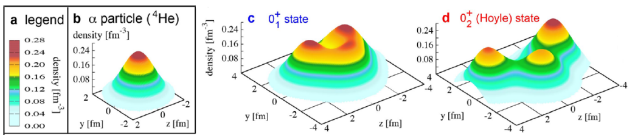

Fig. 2. (a) Color code of density. (b) Density of the ground state of the α-particle. (c) Density of the ground state of ^{12}C. (d) Density of the Hoyle state of ^{12}C. See the details in Ref. 1).

From the T-plot analysis,[3)] it is found that the ground state is composed of the quantum liquid (normal nuclear matter) with ∼94% probability and the α-like clusters with ∼6% probability, while the Hoyle state comprises the quantum liquid with ∼33% probability and the α-like clusters with ∼61% probability. Therefore, the structure of ^{12}C can be viewed as a crossover of the quantum liquid and clustering in terms of the critical phenomena in quantum many-bod systems. Note that this feature obtained by the T-plot analysis is verified by the hierarchical cluster analysis with dendrogram, that is one of the techniques employed in the machine learning.

Now, we can describe the low-lying structure (static property) of ^{12}C. From future perspective, we would like to apply the no-core MCSM wave functions obtained here to the calculations for triple-α reactions (dynamics) so that we can fully understand the process of the ^{12}C production in stars from first principles.

† Condensed from the article in Nat. Commun. **13**, 2234 (2022)

*1 RIKEN Nishina Center
*2 Department of Physics, University of Tokyo
*3 Advanced Science Research Center, Japan Atomic Energy Agency
*4 Center for Nuclear Study, University of Tokyo
*5 Research Organization for Information Science and Technology
*6 Yukawa Institute for Theoretical Physics, Kyoto University
*7 Department of Physics and Astronomy, Iowa State University

References

1) T. Otsuka *et al.*, Nat. Commun. **13**, 2234 (2022).
2) A. M. Shirokov *et al.*, Phys. Lett. B **761**, 87 (2016).
3) Y. Tsunoda *et al.*, Phys. Rev. C **89**, 031301(R) (2014).

Isovector density and isospin impurity in ^{40}Ca†

H. Sagawa,[*1,*2] S. Yoshida,[*3] T. Naito,[*4,*1] T. Uesaka,[*5] J. Zenihiro,[*6] J. Tanaka,[*1] and T. Suzuki[*7]

Experimental charge densities have been studied by electron scattering experiments since the 1950s. Proton densities can be extracted from charge densities removing the proton finite-size effect. It has been shown in Ref. 1) that proton elastic scattering is quite useful to extract the neutron density from the angular distributions of cross sections and analyzing powers of polarized proton beams.

Charge symmetry breaking (CSB) and charge independence breaking (CIB) forces have been discussed in the context of isospin impurity effect on the superallowed Fermi decays. The quantitative information of isospin symmetry breaking (ISB) forces has been recently examined to calculate the binding energies of isodoublet and isotriplet nuclei and also the excitation energies of isobaric analogue states (IAS). This study introduces the Skyrme-type ISB interactions and study their effect on the IV density in ^{40}Ca.

The isovector density defined as the difference between neutron and proton densities as $\rho_{\rm IV} = \rho_n - \rho_p$ is plotted with a factor of $4\pi r^2$ (Fig. 1). The theoretical predictions of the isovector density are qualitatively different from the experimental results: the experimental result of the isovector density exhibits a peak at $r \sim 3.2$ fm, whereas the Hatree-Fock (HF) model with SAMi-J27 interaction predicts a peak at $r \sim 2.5$ fm with positive values (neutron excess) in the interior and negative values on the surface.

A strong correlation between the maximum of IV density and isospin impurity was reported in Ref. 2) with the correlation coefficient $r = 0.992$. The isospin impurity can be extracted from the peak height of the IV density when the proton and neutron densities are available experimentally. The experimental peak height of the IV density is 0.208 ± 0.066 fm^{-1} in Fig. 1. Then, the isospin impurity is then extracted from the correlation plot as

$$\varepsilon^2 = (0.928 \pm 0.586)\,\%. \qquad (1)$$

This central value is about 50% larger than the value of RPA calculations without the ISB forces. From this value of the isospin impurity, the strength of CSB interaction s_0 is further obtained as $s_0 = -(8.80 \pm 16.0)$ MeV fm^3.

In summary, we studied the IV density of ^{40}Ca using the mean-field and particle-vibration coupling (PVC) models. We adopted the Skyrme SAMi-J model as the mean-field model. We observed a significant difference between the experimental and calculated IS densities in the interior part and also dilute density region of ^{40}Ca. This difference implies the modification of density distribution owing to the reduced occupation probabilities of single-particle states near the Fermi surface, which may be caused by many-body correlations beyond the mean-field model.

It was shown in Ref. 2) that the magnitude of the IV density significantly changes owing to the CSB interaction, whereas the CIB interaction exhibits no appreciable effect. It is found that the CSB interaction exhibits a strong linear correlation with the maximum of IV density and isospin impurity. Thus, the magnitude of IV density helps experimentally to determine the isospin impurity and the magnitude of CSB interaction. This characteristic of the IV density appears in general in $N = Z$ nuclei, ^{40}Ca, ^{80}Zr, and ^{100}Sn. The measurements of the IV density is desired to obtain the experimental information of the isospin impurity and the CSB interaction.

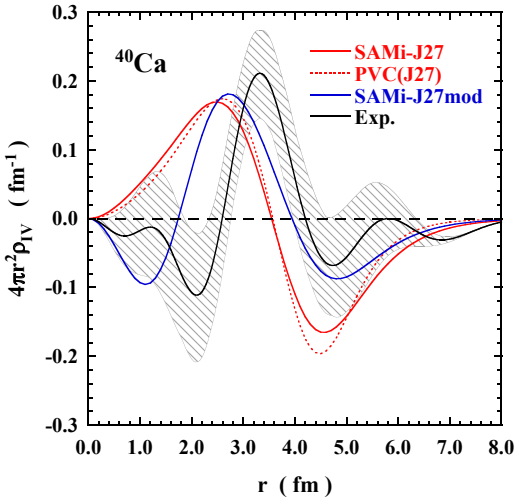

Fig. 1. IV densities multiplied by a factor of $4\pi r^2$ of ^{40}Ca calculated by the HF, modified HF and PVC models as well as the experimental IV density. The red (blue) solid and dashed curves denote the HF (modified HF) and PVC densities with SAMi-J27 (SAMi-J27mod) model, respectively. The occupation probabilities near the Fermi surface are optimized to fit the IS density in the case of modified HF. The experimental data are denoted with a black solid curve considering the experimental uncertainty depicted by the shaded area.

† Condensed from the article in Phys. Lett. B **829**, 137072 (2022)

*1 RIKEN Nishina Center
*2 Center for Mathematical Sciences, University of Aizu
*3 Science Research Center, Hosei University
*4 Department of Physics, University of Tokyo
*5 RIKEN Cluster for Pioneering Research
*6 Department of Physics, Kyoto University
*7 Department of Physics, Nihon University

References

1) H. Sakaguchi *et al.*, Prog. Part. Nucl. Phys. **97**, 1 (2017).
2) H. Sagawa *et al.*, Phys. Lett. B **829**, 137072 (2022).

Large amplitude collective motion in ^{44}S†

Y. Suzuki,[*1] W. Horiuchi,[*2,*3,*4,*5] and M. Kimura[*5]

It is well known that neutron-rich $N \simeq 28$ nuclei exhibit strong quadrupole collectivity.[1,2] Using antisymmetrized molecular dynamics (AMD), we have discovered many interesting features such as triaxial deformation and shape coexistence in ^{42}Si and neighboring nuclei.[3,4] Herein, we report the large-amplitude collective motion (LACM) in ^{44}S.

Figure 1 shows the comparison between the energy curves and collective amplitudes of ^{40}Mg and ^{44}S. ^{40}Mg possesses the prolately-deformed energy minimum and the collective amplitude of the ground state is localized around it, whereas the 0_2^+ state is localized in the oblately-deformed region. Thus, ^{40}Mg depicts the coexistence of the prolate and oblate rigid rotors. In contrast, ^{44}S exhibits a significantly different structure: The energy curve is extremely flat as a function of γ and the collective amplitudes of the ground, and the 0_2^+ states demonstrate broad and non-localized distributions, which imply that ^{44}S possesses no rigid shape due to the LACM.

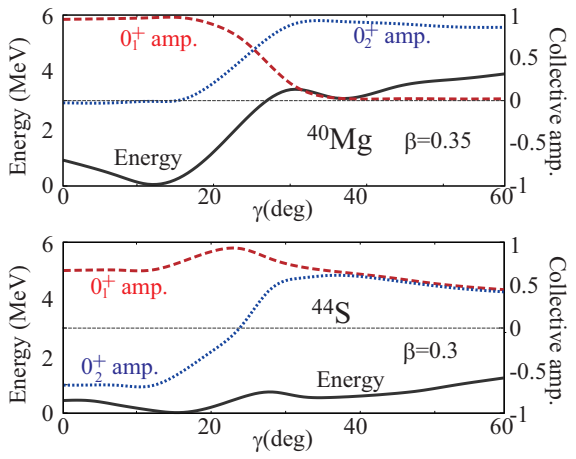

Fig. 1. Energy curves and collective amplitudes of the 0_1^+ and 0_2^+ states as functions of the quadrupole deformation parameter γ. The values of quadrupole parameter β are set to 0.35 and 0.30 for ^{40}Mg and ^{44}S, respectively.

A general question is as follows: Based on which type of physical quantity, can we distinguish rigid-rotor and LACM? The monopole transition is the solution to this question. The monopole transition strength (Table 1) is strongly hindered in ^{40}Mg, whereas it is non-negligible in ^{44}S.[5] This feature can be explained using a two-configuration mixing model.[6] ^{40}Mg possesses prolate ground state and oblate 0_2^+ state; hence, the monopole matrix element is given as $\langle \text{obl.}|\mathcal{M}|\text{pro.}\rangle$, where $|\text{pro.}\rangle$ and $|\text{obl.}\rangle$ denote the prolate and oblate configurations, respectively, and $\mathcal{M}$ denotes the transition operator (1p1h operator). This matrix element vanishes because single-particle configurations of $|\text{pro.}\rangle$ and $|\text{obl.}\rangle$ differ by 2p2h. This is the reason why the transition is strongly hindered in ^{40}Mg.

Table 1. Electric ($E0$) and isoscalar ($IS0$) monopole transition strengths in Weisskopf unit (Wu).

	^{40}Mg	^{44}S (calc.)	^{44}S (expt.)[5]
$B(E0; 0_1^+ \to 0_2^+)$	0.0	0.04	0.022(2)
$B(IS0; 0_1^+ \to 0_2^+)$	0.0	0.38	

Owing to LACM, we approximate ^{44}S as a mixture of prolate and oblate shapes with equal amplitudes,

$$|0_1^+\rangle = (|\text{pro.}\rangle + |\text{obl.}\rangle)/\sqrt{2}, \quad (1)$$

$$|0_2^+\rangle = (|\text{pro.}\rangle - |\text{obl.}\rangle)/\sqrt{2}. \quad (2)$$

In this case, the transition matrix read

$$\langle 0_2^+|\mathcal{M}|0_1^+\rangle = \frac{1}{2}\{\langle \text{pro.}|\mathcal{M}|\text{pro.}\rangle - \langle \text{obl.}|\mathcal{M}|\text{obl.}\rangle\} \quad (3)$$

Thus, the transition matrix is proportional to the difference in the squared-radii of the prolate and oblate shapes. Consequently, ^{44}S possesses non-negligible monopole transition strength. Using the single AMD wave functions with prolate and oblate deformation and Eq. (3), we obtain $B(E0) = 0.05$ Wu and $B(IS0) = 0.4$ Wu, which are close to the results of the full model space calculation listed in Table 1.

Thus, there is an interesting relationship between the monopole transition and LACM. In ^{40}Mg, the prolate and oblate rotors coexist, and the monopole transition is hindered as they do not mix with each other. In ^{44}S, there is a considerable mixture of prolate and oblate shapes due to LACM. This leads to the non-negligible monopole transition, which is roughly proportional to the difference in the squared-radii of the two shapes.

† Condensed from the article in Phys. Rev. C **104**, 024327 (2021) and Prog. Theor. Exp. Phys. **2022**, 063D02 (2022)

*1 Research Center for Nuclear Physics, Osaka University
*2 Department of Physics, Osaka Metropolitan University
*3 Nambu Yoichiro Institute of Theoretical and Experimental Physics (NITEP), Osaka Metropolitan University
*4 Department of Physics, Hokkaido University
*5 RIKEN Nishina Center

References

1) O. Sorlin *et al.*, Prog. Part. Nucl. Phys. **61**, 602 (2008).
2) S. Takeuchi *et al.*, Phys. Rev. Lett. **109**, 182501 (2012).
3) Y. Suzuki *et al.*, Phys. Rev. C **104**, 024327 (2021).
4) Y. Suzuki *et al.*, Prog. Theor. Exp. Phys. **2022**, 063D02 (2022).
5) S. Grévy *et al.*, Eur. Phys. J. A **25**, 111 (2005).
6) S. Shimoura *et al.*, Phys. Lett. B **654**, 87 (2007).

Measurement of flavor asymmetry of light-quark sea in the proton with Drell-Yan dimuon production in $p+p$ and $p+d$ collisions at 120 GeV†

K. Nakano,[*1,*2] Y. Goto,[*2] Y. Miyachi,[*3] K. Nagai,[*4] S. Sawada,[*2,*5] and T.-A. Shibata[*2,*6]
for the E906/SeaQuest Collaboration

Evidence for a flavor asymmetry between the $\bar{u}$ and $\bar{d}$ quark distributions in the proton has been found in deep-inelastic scattering and Drell-Yan experiments.[1,2] The asymmetry observed in the E866 experiment[3] suggested a drop of the $\bar{d}(x)/\bar{u}(x)$ ratio in the $x > 0.15$ region, where x means the fraction of nucleon momentum carried by partons. Here, we report results from the SeaQuest experiment, with improved statistical precision, for the flavor asymmetry in the large x region up to $x = 0.45$.

The SeaQuest experiment detects $\mu^+\mu^-$ pairs (dimuons) produced in the Drell-Yan process.[4] The differential cross section at leading order is given by:

$$\frac{d^2\sigma}{dx_1 dx_2} = \frac{4\pi\alpha^2}{9x_1x_2s} \times \sum_{i\in u,d,s,\ldots} e_i^2 \left[q_i^A(x_1)\,\bar{q}_i^B(x_2) + \bar{q}_i^A(x_1)\,q_i^B(x_2)\right], \quad (1)$$

where α is the fine-structure constant, e_i is the charge of a quark with flavor i, and $q_i^{A,B}(x_{1,2})$ are the quark distribution functions in hadrons A and B for quarks carrying a momentum fraction x_1 and x_2, respectively. SeaQuest utilized the 120-GeV proton beam at Fermilab for hadron A and liquid hydrogen and deuterium targets for hadron B. The cross-section ratio of the two targets has a direct sensitivity to $\bar{d}(x)/\bar{u}(x)$ as

$$\frac{\sigma^{pd}}{2\sigma^{pp}} \approx \frac{1}{2}\left[1 + \frac{\bar{d}(x_2)}{\bar{u}(x_2)}\right]. \quad (2)$$

The data that SeaQuest recorded between June 2014 and July 2015 were analyzed.

The result of $\sigma^{pd}/2\sigma^{pp}$ using the "Intensity-Extrapolation" (IE) method was reported in Refs. 5) and 6). We developed another method of extracting $\sigma^{pd}/2\sigma^{pp}$, called "Mass-Fit" (MF) method, in order to confirm that the systematic uncertainty of the IE method has been properly evaluated. The results of $\sigma^{pd}/2\sigma^{pp}$ using the two methods are shown in Fig. 1. They are in excellent agreement.

The ratio of $\bar{d}(x)/\bar{u}(x)$ was derived from $\sigma^{pd}/2\sigma^{pp}$ and reported in Refs. 5) and 6). Using $\bar{d}(x)/\bar{u}(x)$ as input, we can determine the difference, $\bar{d}(x) - \bar{u}(x)$. It provides a direct measure of the contribution from non-perturbative processes, since perturbative processes should cancel out in $\bar{d}(x) - \bar{u}(x)$. Figure 2 shows $\bar{d}(x) - \bar{u}(x)$ at $Q^2 = 25.5$ GeV^2 over the region $0.13 < x < 0.45$. For comparison, experimental data and theoretical calculations are overlaid. The SeaQuest data have better uncertainty than the existing data, and are in good agreement with the two calculations.

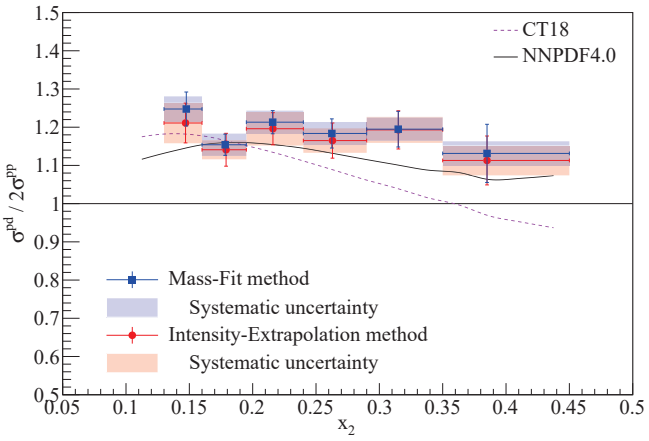

Fig. 1. The cross section ratio versus x_2 obtained with the two extraction methods.

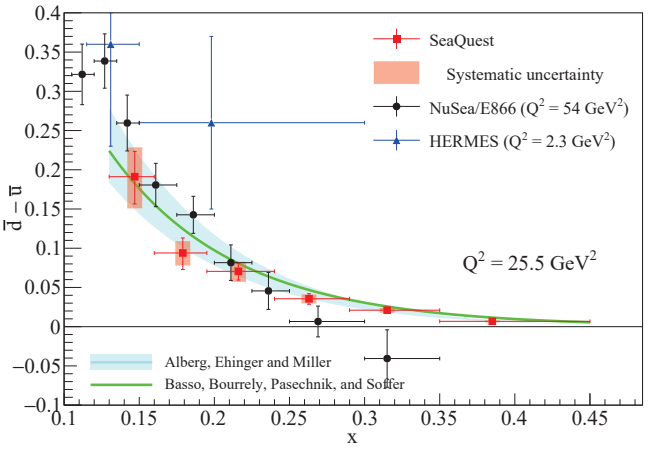

Fig. 2. Result of $\bar{d}(x) - \bar{u}(x)$.

References
1) P. Amaudruz *et al.*, Phys. Rev. Lett. **66**, 2712 (1991).
2) A. Baldit *et al.*, Phys. Lett. B **332**, 244 (1994).
3) R. S. Towell *et al.*, Phys. Rev. D **64**, 052002 (2001).
4) S. D. Drell *et al.*, Phys. Rev. Lett. **25**, 316 (1970).
5) J. Dove *et al.*, Nature **590**, 561 (2021).
6) Y. Goto *et al.*, RIKEN Accel. Prog. Rep. **55**, S16 (2022).

† Condensed from the article in arXiv:2212.12160 (2022)

*1 Department of Physics, University of Virginia
*2 RIKEN Nishina Center
*3 Faculty of Science, Yamagata University
*4 High Energy Nuclear Physics, Los Alamos National Lab
*5 Wako Nuclear Science Center (WNSC), IPNS, KEK
*6 College of Science and Technology, Nihon University

Energy measurement of beam from SRC for GUINNESS WORLD RECORDS^{TM} registration

H. Okuno,[*1] N. Fukuda,[*1] H. Haba,[*1] H. Hasebe,[*1] Y. Higurashi,[*1] H. Imao,[*1] H. Otsu,[*1] H. Sakurai,[*1] Y. Shimizu,[*1] T. Sumikama,[*1] D. Suzuki,[*1] H. Suzuki,[*1] H. Takeda,[*1] K. Yoshida,[*1] and M. Yoshimoto[*1]

The SRC (Superconducting Ring Cyclotron) was registered into GUINNESS WORLD RECORDS^{TM} as the highest beam energy cyclotron on April 11 2022.[1)] The energy of the beam from the SRC was measured mainly using BigRIPS prior to the registration. The acceleration of ^{238}U up to 345 MeV/nucleon was chosen to maximize the energy of the extracted beam.

The energy E_T of the beam extracted from the SRC is expressed as

$$E_T = \sqrt{(M_0c^2)^2 + (pc)^2} - M_0c^2 \quad (1)$$

$$pc = Q \times ecB\rho \quad (2)$$

$$M \sim M_0/M_{amu} \quad (3)$$

where M_0, M, M_{amu}, p, c, Q, e, and $B\rho$ express the rest ion mass, mass number, unified atomic mass unit, momentum, speed of light, charge state, elementary charge, and magnetic rigidity, respectively. Therefore, M, Q, and $B\rho$ must be measured or defined. Z is also required to be defined in the measurement.

Firstly we must show that the accelerated particle is ^{238}U ($Z = 92$, $M = 238$). Mass spectra were measured in the ion source plasma used in the RIBF accelerator complex. Measurements were taken at 2 kV and 22 kV extraction voltages. M/Q was calibrated using the two peaks of $m/q = 1$ and $m/q = 2$ at 22 kV. The obtained data show that the mass of the heaviest element in the source is approximately 236. The only nuclei that are stable in nature at these mass numbers are ^{232}Th or ^{238}U. The color of the sample in the ion source was dark brown, a typical color of UO_2, while the color of ThO_2 is white. From these reasons, it can be deduced that the Z and M of the accelerated ion beam are 92 and 238, respectively. The accelerated ion, therefore, is ^{238}U.

Secondly, the beam energy is roughly measured. This measurement helps us to define charge state of the accelerated beam in the succeeding measurement. A target of Be is placed at F0 in BigRIPS, and the energy of the particles in full strip ($Q = Z = 92$) is measured. Three target thicknesses are prepared: 0.5 mm, 1 mm, and 2 mm. The obtained data are plotted as shown in Fig. 1 together with linear regression. When the thickness of the target is zero, the approximation indicates the beam's original energy. Because the energy loss is not proportional to the thickness of the target, it is a little off from the correct answer but is still accurate enough to identify Q in the next process.

Thirdly, magnetic rigidity $B\rho$ of the accelerated beam is measured through the BigRIPS without the target. Because the charge is still undetermined, the blue dots in Fig. 2 show that the energy can jump from one value to another under a constant $B\rho$ condition. In contrast, from the results obtained previously, we know that the energy is approximately around the orange line, so thus we determined Q to be 86. We deduced the extracted energy of 82400 MeV by combining the measured $B\rho$ value with $Q = 86$.

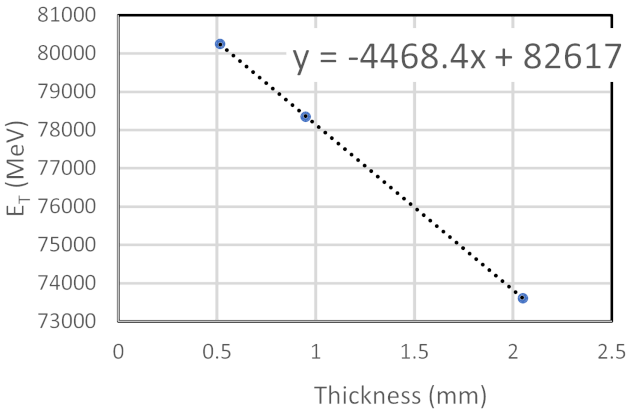

Fig. 1. Energy of $^{238}U^{92+}$ versus the target thickness with linear regression.

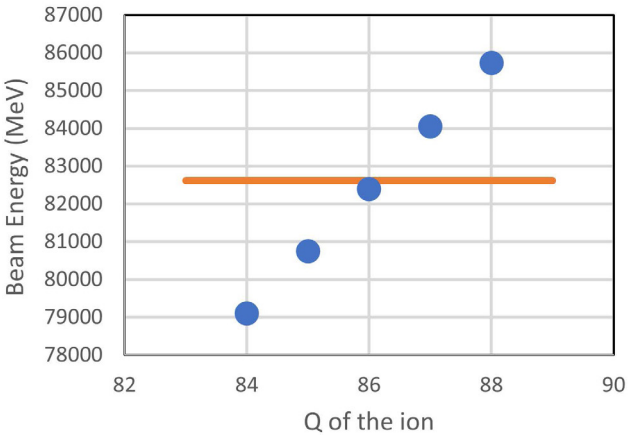

Fig. 2. Beam energy converted from the measured $B\rho$ as a function of assumed Q values of the accelerated ion.

Reference

1) https://www.guinnessworldrecords.com/world-records/675272-highest-beam-energy-cyclotron.

*1 RIKEN Nishina Center

Development of new ionization chamber specialized for high Z beam (II)

M. Yoshimoto,[*1] N. Fukuda,[*1] R. Matsumura,[*1] D. Nishimura,[*2] H. Otsu,[*1] Y. Shimizu,[*1] T. Sumikama,[*1] H. Suzuki,[*1] H. Takahashi,[*2] H. Takeda,[*1] J. Tanaka,[*1] and K. Yoshida[*1]

Ionization chambers (ICs) are detectors used to determine the energy deposit (ΔE) of the ions with sufficient accuracy to distinguish the atomic number (Z) in the BigRIPS separator and ZeroDegree spectrometer. A new IC has been developed to improve the Z resolution of heavy ions with $Z > 80$ and the energy of 200–300 MeV/nucleon,[1)] for which experimental proposals are on the rise. The difficulty in Z determination is because of the change in the charge state,[2)] which is more pronounced for higher Z beams. To overcome this effect, previous studies suggested the replacement of the commonly used P-10 with a gas with a smaller or larger Z.[1,3)]

We conducted machine studies (MS-EXP21-10, -11) on the gas dependence of the IC at RIKEN RIBF. The IC setup has been described in a previous study.[1)] We used three gas species, P-10 gas (Ar 90% + CH_4 10%), methane gas (CH_4 100%) with a smaller cross section of the charge state changing, and xenon-based gas (Xe 70% + CH_4 30%) with a larger cross section of the charge state changing. The ICs with these gases were operated at 620 Torr in the F7 vacuum chamber.

The ΔE in the IC was measured with $^{238}U^{90+,91+}$ ions at 344 MeV/nucleon. Figure 1 shows the ΔE distributions for the three gas species. The shape for the CH_4 gas differed significantly between 90+ and 91+. The lowest energy peak corresponds to 90+ passing through the IC without charge state changing and the second-lowest peak corresponds to 91+.

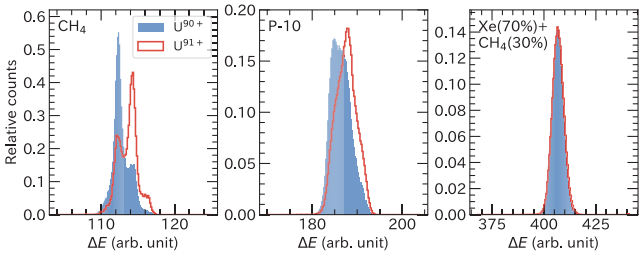

Fig. 1. Energy deposit (ΔE) distributions of the IC in methane, P-10, and xenon-based gases irradiated with 344 MeV/nucleon $^{238}U^{90+}$ (blue area) and $^{238}U^{91+}$ (red line).

The shape difference for the P-10 gas was smaller than that for the CH_4 gas. However, the mean fitted with a normal distribution changed by 0.56% depending on the charge states. When multiple charge states are transmitted, the mean shift adversely affects particle identification (PID). The energy resolution of 90+ and 91+ was 1.1%, which was worse than the 0.7% energy resolution required to achieve the 3σ separation at $Z = 92$ from $Z = 91$ isotopes. In contrast to the CH_4 and P-10 gases, the xenon-based gas yielded almost identical shapes for 90+ and 91+. The difference between the means was only 0.03%. This is because a charge-state equilibrium was reached immediately after the injection into the IC. The energy resolution was obtained to be 0.69%, which is sufficient for the 3σ separation in Z. Hence, the xenon-based gas was demonstrated to be suitable for the IC specialized for high Z beams.

We injected the high-Z secondary beam at approximately $A/Q = 2.5$ into the xenon-based gas IC. The secondary beam was produced from the 345 MeV/nucleon ^{238}U primary beam impinging on a 4 mm-thick Be target. The magnetic rigidity of the first dipole was 6.3 Tm and no degraders were used in the separator. The PID was performed using the TOF-$B\rho$-ΔE method, as shown in Fig. 2. Further, the beam energy at F7 was typically 264 MeV/nucleon at $Z = 80-92$. Although the blobs for He-like and H-like ions are dense, the different ion species were well separated and identified. The averaged Z resolution of $Z = 81-91$ was 0.34 (1σ). The resolution is approximately twice better than that by the P-10 gas IC.[4)]

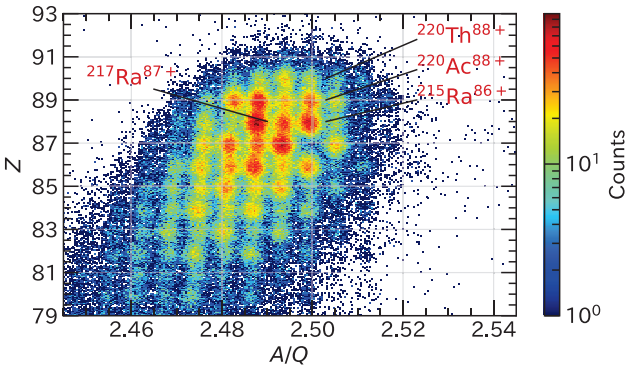

Fig. 2. PID plot of Z versus A/Q obtained with the xenon-based gas IC. The typical energy is 264 MeV/nucleon.

In conclusion, the xenon-based gas IC achieved the 3σ separation in Z, and rendered the PID for the secondary beams with $Z > 80$ at approximately 260 MeV/nucleon practical for all experimental groups.

*1 RIKEN Nishina Center
*2 Department of Natural Sciences, Tokyo City University

References

1) M. Yoshimoto *et al.*, RIKEN Accel. Prog. Rep. **55**, 70 (2022).
2) H. Weick *et al.*, Phys. Rev. Lett. **85**, 2725 (2000).
3) T. Sumikama *et al.*, in this report.
4) N. Fukuda *et al.*, RIKEN Accel. Prog. Rep. **54**, 81 (2021).

Atomic-number identification of heavy RI beams using the energy loss in a Xe-based gas

T. Sumikama,[*1] N. Fukuda,[*1] and M. Yoshimoto[*1]

Radioactive isotope (RI) beams produced at RIBF are tagged event-by-event with the atomic number Z and mass-to-charge ratio A/Q determined using beam-line detectors. For heavy RI beams, particle identification (PID) becomes difficult owing to the change in Q inside the beam-line detectors because Z is determined from the energy loss depending on Q^2. Blobs in the PID plot were clearly visible for the ^{208}Rn case[1)] but not for the ^{220}Th case.[2)] The relative Z resolutions were 0.45% and 0.69% (1σ) for the 185-MeV/nucleon ^{208}Rn beam and 315-MeV/nucleon ^{220}Th beam, respectively. The worse resolution was considered to be due to the energy-loss straggling caused by charge-state fluctuation in the gas of the ionization chamber. The difference between these two cases indicates the impact of the energy dependence of the charge-state fluctuation.

In this paper, the difference in the Z resolutions is discussed in regards to the energy dependence of the cross section of the change in Q in the gas using the GLOBAL code.[3)] Figure 1 shows the energy dependence of the partial mean free path length L, given a change in $Z-Q$ from 1 to 2 or from 2 to 1. The energy dependence of L is mainly for the electron-pickup reaction. In the ^{208}Rn case, the mean value of the equilibrium charge-state distribution $\langle Q\rangle$ is 84.5 at 185 MeV/nucleon. Since $\langle Q\rangle$ is a decimal, the charge state must change multiple times in the ionization chamber to make the effective Q in a single event closer to 84.5. L ($Z-Q=1\rightarrow2$) is roughly 1/2 of the effective length of the ionization chamber, as indicated by the dotted line in Fig. 1. Thus, even if $Z-Q$ changes from 2 to 1, it could be back. In contrast, L ($Z-Q=1\rightarrow2$) is longer than the effective length at 315 MeV/nucleon. $Z-Q$ might not change to 2 once it becomes 1. This is mainly the nature of Ar gas, which accounts for 90% of the P10 gas. Figure 1 also shows L of a Xe-based mixed gas (Xe 90% + CH_4 10%). The gas pressure was determined so that the energy deposit at 300 MeV/nucleon is same as that of the P10 gas. Even at 300 MeV/nucleon, L is shorter than that of P10 at 185 MeV/nucleon, indicating a better Z resolution.

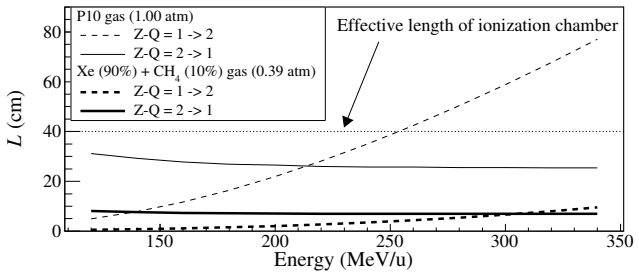

Fig. 1. Partial mean free path length of the change in the charge state in the ionization chamber as a function of the energy of the ^{208}Rn beam.

The energy loss in the ionization chamber was simulated by using the energy-loss code ATIMA[4)] and GLOBAL. The fluctuation in Q was taken into account by the Monte Carlo method. The Z resolution of the 180-MeV/nucleon $^{210}_{85}$At beam was simulated to be 0.46%, which is consistent with the experimental value of 0.45%. Figure 2 shows the energy deposit of the 300-MeV/nucleon ^{208}Rn and ^{206}Ac beams into the effective region of the ionization chamber. The Z resolution is improved from 0.60% for the P10 gas to 0.39% for the Xe-based gas. This result is consistent with the discussion of Fig. 1.

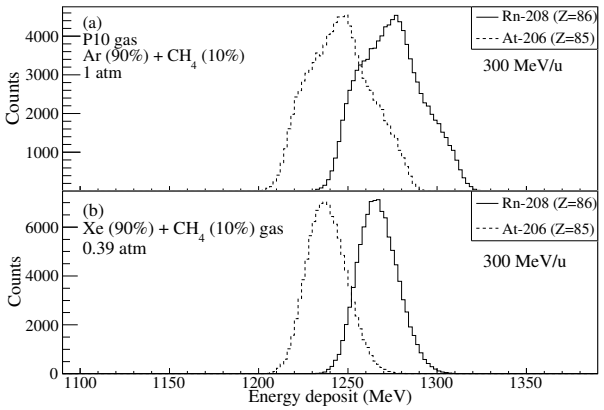

Fig. 2. Monte Carlo simulation of the energy deposit in the ionization chamber. Half of the energy-loss straggling in ATIMA was applied for the energy deposit.[5)]

An experimental study of PID using a Xe-based gas was already conducted, and a good Z resolution was obtained.[6,7)]

References

1) T. Sumikama *et al.*, Nucl. Instrum. Methods Phys. Res. B **463**, 237 (2020).
2) N. Fukuda *et al.*, RIKEN Accel. Prog. Rep. **54**, 81 (2021).
3) C. Scheidenberger *et al.*, Nucl. Instrum. Methods Phys. Res. B **142**, 441 (1998).
4) `https://web-docs.gsi.de/~weick/atima/`.
5) Y. Sato *et al.*, RIKEN Accel. Prog. Rep. **46**, 159 (2013).
6) M. Yoshimoto *et al.*, 19th Int. Conf. on Electromagnetic Isotope Separators and Related Topics (EMIS XIX), Daejeon, South Korea, Oct. 3–7, 2022.
7) M. Yoshimoto *et al.*, in this report.

*1 RIKEN Nishina Center

Improved transmission of OEDO

T. Chillery,[*1] S. Michimasa,[*1] N. Imai,[*1] D. Suzuki,[*2] M. Dozono,[*2,*3] N. Fukuda,[*2] T. Haginouchi,[*2,*4] S. Hanai,[*1] S. Hayakawa,[*1] Y. Hijikata,[*2,*3] J. W. Hwang,[*5] S. Ishio,[*2,*4] N. Iwasa,[*2,*4] K. Kawata,[*1] R. Kojima,[*1] K. Kusaka,[*2] J. Li,[*1] M. Ohtake,[*2] K. Okawa,[*1] T. Saito,[*5] Y. Shimizu,[*2] T. Sumikama,[*2] H. Suzuki,[*2] H. Takeda,[*2] H. Tanaka,[*2,*6] T. Teranishi,[*2,*6] Y. Togano,[*2] Y. Yanagisawa,[*2] R. Yokoyama,[*1] K. Yoshida,[*2] and M. Yoshitomo[*2]

The optimized energy degrading optics (OEDO) system[1] was installed at RIBF in 2017. The principle aim of OEDO is to decelerate and focus medium-heavy radioactive ion beams provided by BigRIPS from approximately 200 to 15–50 MeV/nucleon. The system was commissioned in the day 0 campaign by studying transfer reactions on ^{77}Se, ^{93}Zr, and ^{107}Pd. During this, the transmission from F3 decreased from 61% at FE9 to 18% at S0, despite the effective focusing effort of the RF-Deflector (RFD) at FE10. This poor transmission was attributed to the small bore radius of the quadrupole magnet, *i.e.* QE19, located at FE11, and thus, during 2021, the OEDO beamline was reconfigured. The QE20 (STQ18) magnet was installed upstream of FE11 (FE12), and the QE19 magnet was entirely removed from the beamline. The impact to OEDO's low-energy focusing capabilities was tested in April 2022 during the machine study "MS22-1" followed by the SHARAQ18 experiment[2] measuring ^{130}Sn$(d,p)^{131}$Sn. This report summarises the new low-energy optics of the OEDO beamline, including the improved transmission.

The ion-optical transport code COSY-Infinity (v 9.0) was used to simulate the beam transport through the updated F3–S1 beamline. The beam trajectories in X and Y planes are shown in Fig. 1. Compared with the previous beam trajectories,[1] the new magnet setup between the RFD and S0[a] should enable higher transmission to the secondary target. In addition, the QE20 magnet placed downstream of the RFD enables the fine tuning of the parallel beam condition, which was not possible in the previous configuration.

COSY matrix elements for the new OEDO transport were incorporated into the CNS-developed Monte Carlo simulation code. The simulation used the measured condition at F3 from MS22-1 and included beamline materials, the opening of the beam pipes, and the RFD. The simulated spot size at S0 was $X(Y) = \pm 5$ (10) mm, within the target radius of 25 mm. The estimated F3–S0 transmission was 97% till third-order aberrations.

Following optics tuning in April 2022, the measured ^{130}Sn beam spot at S0 is shown in Fig. 2. The beam was

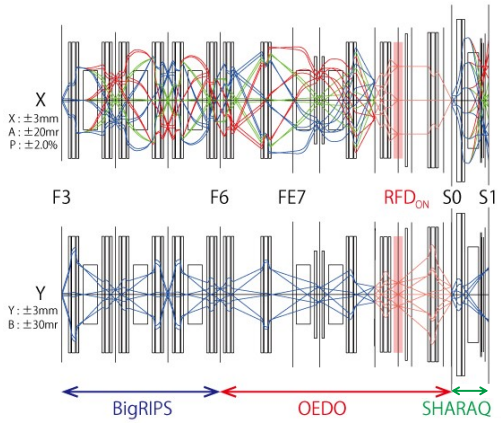

Fig. 1. COSY-calculated beam trajectories in the X and Y planes between F3 and S1 for low energy tuning in OEDO.

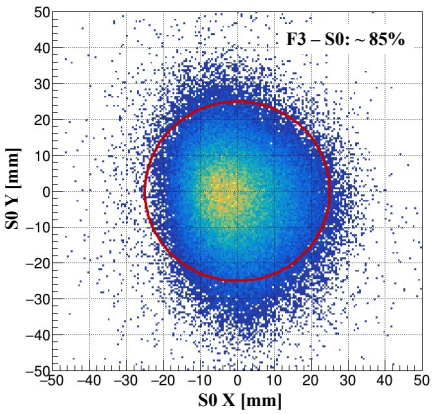

Fig. 2. ^{130}Sn Beam focus at S0. Red circle represents the CD_2 target's radius of 25 mm.

centred at $X(Y) = -2(-1)$ mm with a spot size of ± 8 (12) mm, within the CD_2 target's radius of 25 mm. The beam energy was degraded to 23.3 ± 1.1 MeV/nucleon at S0. The measured F3–S0 transmission of 85% is lower than the calculated value of 97%; however, it still improves OEDO's transmission by a factor of 4.7 over the previous condition.[1] Following this improved transmission of low-energy beam, we performed the OEDO experiment[2] to measure ^{130}Sn$(d,p)^{131}$Sn.

*1 Center for Nuclear Study, University of Tokyo
*2 RIKEN Nishina Center
*3 Department of Physics, Kyoto University
*4 Department of Physics, Tohoku University
*5 CENS, Institute for Basic Science
*6 Department of Physics, Kyushu University

a) S0 focal plane = target position in the TINA silicon-detector array, as used in the ^{130}Sn experiment.

References

1) S. Michimasa *et al.*, Prog. Theor. Exp. Phys. **2019** 043D01 (2019).
2) N. Imai *et al.*, in this report.

Operation test of kicker system with new PFN capacitors

Y. Yamaguchi,[*1] T. Ohnishi,[*1] G. Hudson-Chang,[*1,*2] M. Kanda,[*3] Y. Koizumi,[*3] D. Nagae,[*1,*4] K. Okubo,[*3] K. Sasaki,[*3] N. Shinozaki,[*3] A. Yano,[*5] A. Ozawa,[*1,*5] T. Yamaguchi,[*1,*3,*5] and M. Wakasugi[*1,*6]

In the rare-RI ring (R3) facility, the kicker system is a key device for injecting and extracting particles one-by-one. Recently, we have succeeded in magnetic field flattening during injection duration and extending the extraction duration, thereby improving the experimental efficiency.[1] However, the ceramic capacitors used in the pulse forming network (PFN) of the kicker power supply were broken several times due to insulation breakdown after 1 day of operation with a charging voltage of 45 kV to 55 kV in the 2021 mass measurement experiments.[2,3] This failure, which interferes with the execution of the experiment, must be repaired quickly. We report the progress of the repair work.

The PFN, consisting of sixteen capacitor and inductor sections, forms a high-voltage unit together with a thyratron and other components.[4] The high-voltage unit is installed in a tank filled with insulating oil. The capacitor HP40-H132-00 we have used so far is made by the former AVX corporation (Kyocera AVX now). It has a three-layer structure and is insulated with molded resin. The outer diameter is 38 mm, the length is 47 mm, the rated voltage is 80 kV, and the capacitance is 375 pF.

A failure analysis was performed by Kyocera. The central part of the three-layer structure was found to be particularly damaged (see Fig. 1(b)). The damage was so severe that it is difficult to pinpoint the cause, but the following are possible causes: 1) due to the part of dielectric layer is slightly weak, 2) due to the stacked element structure, the central element overheated, and then the increase in dielectric loss and further overheating caused an electron avalanche, or 3) due to electric field concentration on the washer between the elements. Thus, it is thought that the stacked elements structure could not withstand our use of the repetition of the high-voltage charging within 200 μs and the instantaneous discharging by thyratron. Then we decided to replace it with a single-layer structure capacitor, a commercially available product with proven track record.

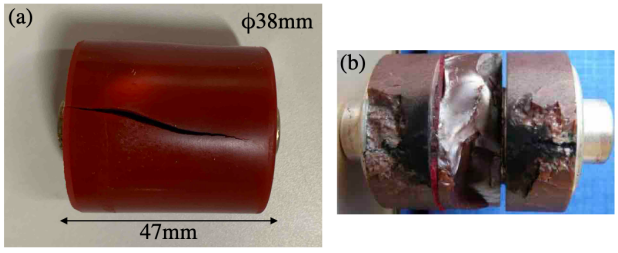

Fig. 1. (a) shows broken AVX capacitor, and (b) shows internal damage revealed by Kyocera.

Figure 2(a) shows a new capacitor FHV-10AN made by TDK corporation. The outer diameter is 38 mm, the length is 33 mm, the rated voltage is 50 kV, and the capacitance is 700 pF. Two TDK capacitors are connected in series to make almost the same capacitance as the AVX one. Figure 2(b) indicates the output currents when operated at a charging voltage of 55 kV. It can be seen that the waveform (blue-line) obtained with TDK capacitors is almost the same as that (black-line) obtained with AVX capacitors.

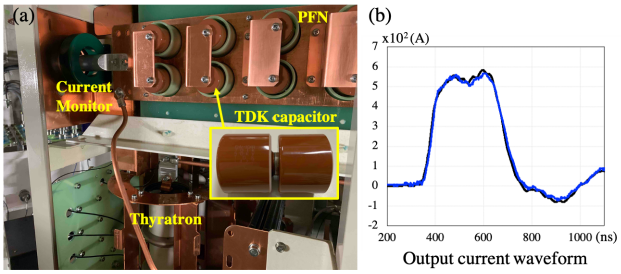

Fig. 2. (a) shows installed new capacitors. (b) indicates output signals from current monitor (details in text).

There are eight high-voltage units in total. Currently, the two high-voltage units for one twin-type kicker magnet have been replaced with TDK capacitors. Recently, we conducted 5-days continuous operation test for all units with a charging voltage of around 50 kV. As a result, five of the six units with AVX capacitors failed again. On the other hand, the two units with TDK capacitors had no problems. We concluded that the use of TDK capacitors would solve the above three concerns and enable stable continuous operation. Therefore, the remaining six high-voltage units will also be replaced with new capacitors soon.

*1 RIKEN Nishina Center
*2 Department of Physics, University of Surrey
*3 Department of Physics, Saitama University
*4 Laboratory for Zero-Carbon Energy, Tokyo Institute of Technology
*5 Institute of Physics, University of Tsukuba
*6 Institute for Chemical Research, Kyoto University

References

1) Y. Yamaguchi *et al.*, RIKEN Accel. Prog. Rep. **54**, 100 (2021).
2) A. Ozawa *et al.*, RIKEN Accel. Prog. Rep. **55**, 13 (2022).
3) S. Naimi *et al.*, RIKEN Accel. Prog. Rep. **55**, 14 (2022).
4) Y. Yamaguchi *et al.*, Phys. Scr. **T166**, 014056 (2015).

Design of radiation shield for RI production beam line

A. Akashio,[*1] K. Tanaka,[*1] N. Shigyo,[*1,*2] K. Sugihara,[*1,*2,*3] and H. Haba[*1]

A radiation shield for a target of new radioactive isotope (RI) production beamline at the large irradiation room in the Linac building was designed. Figure 1 shows the schematic of the shield. A 7.18 MeV/nucleon helium-4 beam is irradiated from upward to downward on a bismuth target. In this study, the conceptual structure of the radiation shield for the side direction from the target was designed using the radiation transport code PHITS.[1)] The size of the shield was limited to less than 2 m because the new RI production beam line will be installed at the small space in the large irradiation room. In addition, the requested shield weight was less than 10 ton owing to the load capacity of the floor. Although the PHITS calculation is not well studied in this helium-4 beam energy region, the benchmark has already been obtained via measurement of the neutron yield with the same beam condition.[2)]

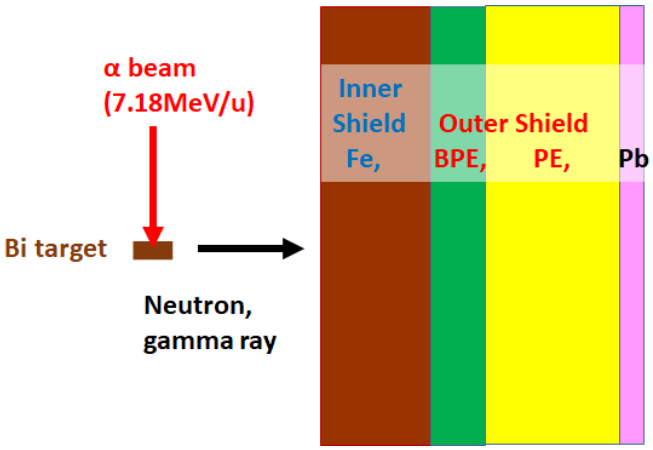

Fig. 1. Schematic of the radiation shield.

The radiation dose around the target is 3×10^8 μSv/h at the beam intensity of 100 particle μA. This study aimed to reduce the neutron and γ-ray dose rate below 10 μSv/h on the surface of the shield. A simple shield composed of one substance is not effective when neutrons and γ rays in wide range energies are mixed. The maximum energy of neutrons from the target is about approximately 15 MeV. In general, polyethylene (PE) or water, a hydrogen-rich material, is effective in shielding neutrons up to several MeV. For the higher energy neutron, iron or other heavy metal material is applied as an inner shield to reduce the neutron energy by inelastic scattering. Subsequently PE is applied as an outer shield to reduce the neutron dose rate. In addition, the secondary γ ray generated in the shield is absorbed in the heavy material such as lead set outside PE as shown in Fig. 1.

Figure 2 shows position distribution of the neutron and γ-ray radiation dose rate calculated by PHITS. Although the tungsten-inner shield was also assumed, iron was selected considering the cost and weight. The iron thickness was optimized to realize the minimum thickness of the shield satisfying the requested neutron dose rate at the shield surface. Despite the 30-cm-thick iron and 50-cm-thick PE successfully reducing the neutron dose rate, the γ-ray dose was still serious. The main component was a 2.2 MeV secondary γ ray attributed to the reactions between neutrons and proton included in the outer PE shield as shown at black-dashed line in Fig. 2. Therefore, additional heavy weight lead shield outside PE is necessary to reduce the γ ray. To render the lead thickness thinner, reduction of low-energy neutron entering to outer PE shield was considered. PE with 10% B_2O_3 (BPE) was installed between the iron and the PE to apply $^{10}B(n,\alpha)$ reaction. Red lines in Fig. 2 show the effect of 10 cm BPE. The generated γ ray is reduced down to 1/8 by BPE shield at the border between inner and outer shield. Although the 50 cm thick BPE was also evaluated as an alternative to the PE, 10 cm BPE was sufficient because low energy neutron from iron-inner shield was absorbed by the first 10 cm of BPE. Owing to the boron effect, the thickness of the lead was successfully reduced approximately 5 cm. Owing to the design, the shield of iron 30 cm thick, BPE of 10 cm, PE of 40 cm, and lead of 7 cm satisfied the requirement of 10 μSv/h on the surface against 100 particle μA helium-4 beam.

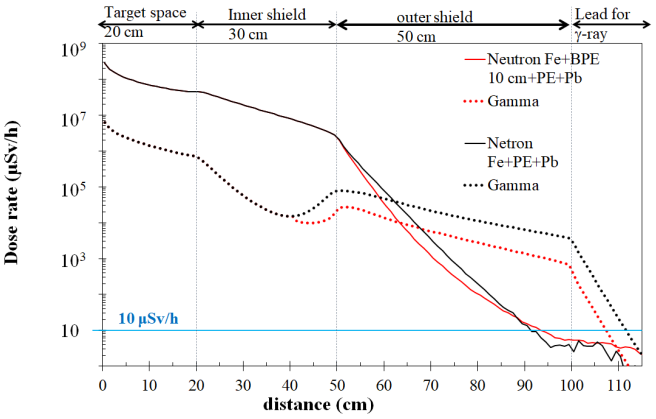

Fig. 2. Radiation dose distribution calculated with PHITS. The assumed helium-4 beam intensity was 100 particle μA.

*1 RIKEN Nishina Center
*2 Department of Applied Quantum Physics and Nuclear Engineering, Kyushu University
*3 High Energy Accelerator Research Organization (KEK)

References
1) T. Sato *et al.*, J. Nucl. Sci. Tech. **55**, 684 (2018).
2) K. Sugihara *et al.*, Nucl. Instrum. Methods Phys. Res. B **470**, 15 (2020).

Amorphous to polycrystalline phase transition in La_2O_3 films grown on a silicon substrate forming Si-doped La_2O_3 films†

S. R. Lee,[*1] A. Kim,[*2,*3] S. Choi,[*2,*3] T. Ikeda,[*4] T. Kobayashi,[*5] T. Isoshima,[*6] S. Cho,[*7] and Y. Kim[*1,*8]

Currently, the semiconducting industry is heavily reliant on Si-based electronic devices. SiO_2 has been used as a principal dielectric in Si-based industry owing to its good film properties and stability in the complementary metal-oxide-semiconductor (CMOS) process. However, its low dielectric constant has raised issues of low performance of device and large leakage current with decreasing gate thickness, channel length, *etc.* Consequently, extensive efforts have been made to find alternative dielectrics with high-permittivity (κ) on Si as a replacement for SiO_2. One of important conditions for high-κ dielectric is that the dielectric layer should not result in the formation of silicide or SiO_2 interfacial layer between silicon wafer and dielectric layer. Intriguingly, it has been shown that upon the deposition of La_2O_3 is deposited on Si, La silicate is formed rather than a SiO_2 interfacial layer.[1)]

In this study, we used a pulsed laser deposition (PLD) method to obtain a high-quality La_2O_3 film on a Si substrate. Using a high-resolution transmission electron microscope (HRTEM) it was observed that approximately 10 nm thick amorphous La_2O_3 layer was initially formed on Si. Subsequently, and then a polycrystalline La_2O_3 layer was formed on top of the amorphous La_2O_3 layer, as Fig. 1(a), which is attributed to Ostwald's step rule, this is a metastable state formation prior to the formation of a stable state of a material. HRTEM images also suggested that no interfacial oxide layer was formed between La_2O_3 and Si. Furthermore, through an in-depth study using Rutherford backscattering (RBS), performed at the RIKEN Pelletron accelerator facility, it was further confirmed that La-Silicate interfacial layer is extremely reduced, as Fig. 1(b). Rather, the results of X-ray photoelectron spectroscopy atomic depth profile analysis, using Ar^+ ion beam sputtering, indicated the presence of La-silicate present over the entire La_2O_3 film, as Fig. 1(c). This suggests that Si diffuses through whole thick La_2O_3 films, thereby forming Si-doped La_2O_3 films. Our study suggests that employment of advanced growth technique may improve the status of high-κ gate oxide of La_2O_3 gate oxide in CMOS industry.

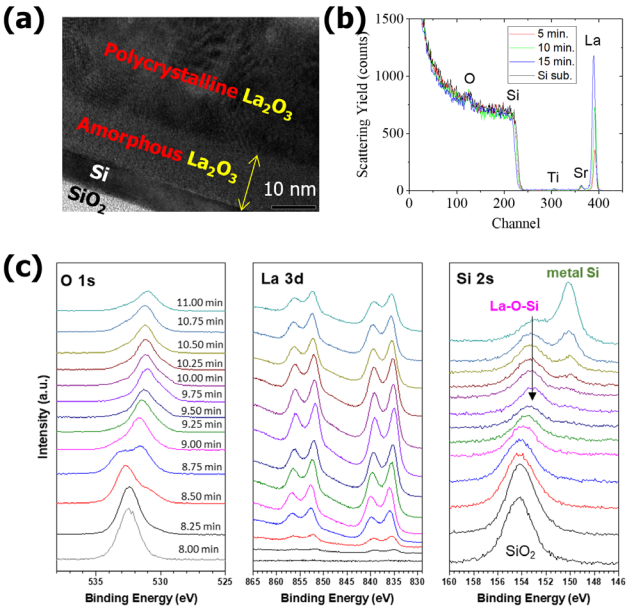

Fig. 1. (a) Transmission electron microscope image of polycrystalline/amorphous La_2O_3 films, (b) Rutherford backscattering, and (c) X-ray photoelectron spectroscopy atomic depth profile of La_2O_3/Si.

Reference

1) T. Kawanago *et al.*, Proc. 41st European Solid State Device Research Conf., Helsinki, Finland, 2011-4, p. 67.

† Condensed from the article in Phys. Status Solidi A **219**, 2200318 (2022)

*1 Surface and Interface Science Laboratory, RIKEN
*2 Interdisciplinery Materials Measurement Institute, Korea Research Institute of Standards and Science
*3 Department of Nano Science, University of Science and Technology
*4 RIKEN Nishina Center
*5 Neutron Beam Technology Team, RIKEN
*6 RIKEN Cluster for Pioneering Research
*7 Division of Physical Metrology, Korea Research Institute of Standards and Science
*8 Department of Applied Chemistry, University of Tokyo

Proton hyperpolarization relay from nanocrystals to liquid water†

N. Matsumoto,[*1] K. Nishimura,[*1] N. Kimizuka,[*1] Y. Nishiyama,[*2] K. Tateishi,[*3,*4] T. Uesaka,[*3,*4] and N. Yanai[*1,*4,*5]

While nuclear magnetic resonance (NMR) spectroscopy is indispensable over a wide range of fields from chemistry to medicine, it suffers from inherently poor sensitivity due to low nuclear spin polarization. Dynamic nuclear polarization (DNP), in which the electron spin polarization is transferred to the nuclear spins, is one of the most promising methods to improve the sensitivity of NMR. Water is an extremely attractive and ubiquitous target material because hyperpolarized water can lead to highly sensitive NMR of proteins and biomolecules.[1] Here, we report the nuclear spin hyperpolarization of bulk liquid water achieved via a novel strategy called "hyperpolarization relay," in which the photogenerated transient electron spin polarization is transferred to the nuclear spins within nanocrystals, and then transferred to the nuclear spins of liquid water (Fig. 1).

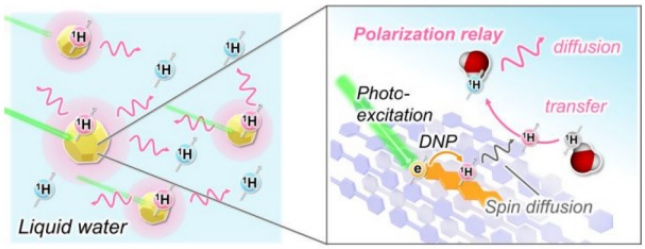

Fig. 1. Schematic of "hyperpolarization relay" from nanocrystals to bulk liquid water.

We prepared organic nanocrystals of 5,12-diazatetracene (DAT)-doped *p*-terphenyl (Fig. 2(a))[2] using the reprecipitation method,[3] that can be hyperpolarized at room temperature by DNP based on photoexcited triplet state (triplet-DNP).[4] The size of nanocrystals was characterized by dynamic light scattering (DLS) measurements. Nanocrystals of three sizes were fabricated and referred to as NC_{390}, NC_{270}, and NC_{170}, respectively. The number represents the average diameter of the nanocrystal. The nanocrystals were mixed with water of 10% H_2O in D_2O with a weight ratio of NC: water = 1 : 4 for the triplet-DNP experiments.

In the ^{1}H NMR spectrum for the mixture of NC_{170} and water at thermal equilibrium, only a sharp peak from water was observed (Figs. 2(b) and 2(c)). After a triplet-DNP sequence for 120 s, the intensity of the water-derived sharp peak clearly increased in addition to the enhanced nanocrystal-derived broad peak. The

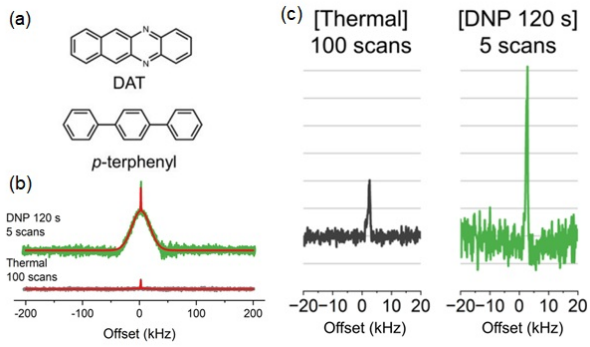

Fig. 2. (a) Chemical structures of DAT (5,12-diazatetracene) and *p*-terphenyl. (b) ^{1}H NMR spectra of the mixture of NC_{170} and water at thermal equilibrium (black) and after triplet-DNP for 120 s (green). (c) Enlarged ^{1}H NMR spectra before (black) and after triplet-DNP for 120 s (green) after subtracting the fitted spectra of NC_{170}.

enhancement factor of nanocrystals and water was estimated as 104 ± 10 and 2.4 ± 0.3 times, respectively. The transfer of proton spin polarization from the nanocrystal surface to water was indicated by the size dependence of the nanocrystals. As the nanocrystal size increased from 170 nm to 270 nm and 390 nm, the enhancement of water polarization decreased from 2.4 ± 0.3 to 1.5 ± 0.2 and 1.2 ± 0.1 times. This trend supports that the polarization transfer occurs at the interface between the nanocrystals and water.

To better understand the nanocrystal-to-water polarization transfer mechanism, the polarization buildup was simulated using Solomon equations. Interestingly, a negative cross relaxation rate constant was obtained, which often occurs in macromolecules or viscous liquids. This implies that the water dynamics are slowed at the surface of nanocrystals. A possible scenario is that polarization is transferred from the nanocrystals to the surface-bound water and that the surface-bound water exchanges with the bulk water, resulting in the enhanced polarization of the bulk water.

In conclusion, we demonstrated the polarization relay that first transfers the polarization from photoexcited triplet electron spins to proton spins within the nanocrystals, and then transfers the polarization to proton spins of water on the nanocrystal surface. This will lead to the realization of a continuous hyperpolarized water supply system that will revolutionize life science and drug discovery.

† Condensed from the article in J. Am. Chem. Soc. **144**, 18023 (2022)

*1 Department of Applied Chemistry, Kyushu University
*2 RIKEN-JEOL Collaboration Center, RIKEN
*3 RIKEN Nishina Center
*4 Spin-Isospin Laboratory, CPR, RIKEN
*5 PRESTO and FOREST, JST

References

1) T. Harris *et al.*, J. Phys. Chem. B **118**, 3281 (2014).
2) H. Kouno *et al.*, J. Phys. Chem. Lett. **10**, 2208 (2019).
3) H. R. Chung *et al.*, J. Cryst. Growth **294**, 459 (2006).
4) K. Nishimura *et al.*, Chem. Commun. **56**, 7217 (2020).

Estimation of the on-site Coulomb potential in La_2CuO_4: A μSR and DFT Study

M. R. Ramadhan[*1,*2] and I. Watanabe[*1,*2]

Since its discovery in the late 1980s, high-temperature superconducting cuprates are known to have a rich variety of physics and have attracted interest from researchers worldwide. There are open questions on exotic electronic states that need to be investigated, such as pseudogaps, stripes of spins and holes, and charge-ordered states. These properties are usually described on the basis of the strong on-site Coulomb potential, U, and the covalent states of the Cu $3d$ orbitals with the surrounding O $2p$ orbitals. To understand more about these properties, La_2CuO_4 (LCO) can be used as the ideal candidate material. LCO is the parent compound of high-Tc superconducting is classified as a Mott insulator, and has strong covalent states between the Cu $3d$ and O $2p$ orbitals. These interactions produce antiferromagnetic insulating behavior due to the existence of the on-site Coulomb potential energy (U). The value of U of this system has been thoroughly investigated but still has large ambiguities in the range of 3–10 eV, raising uncertainties in the discussion of the electronic states in high-Tc superconducting cuprates.

Our group has been developing a technique to estimate the value of U by combining the muon spin rotation (μSR) and density functional theory (DFT) and including U as an adjustable parameter (DFT + U). From an experimental perspective, a muon is a sensitive local magnetic probe that can be used to observe the ordered state of LCO. Our group has shown that an implanted muon has three frequency components using the high-statistic μSR ,as shown in Fig. 1. These three frequency components can be translated into three internal fields of 426.7(1), 109.2(4), and 1251.6(3) G.[1)] From a theoretical perspective, we develop a method to obtain a more precise muon position by utilizing DFT + U. From calculations, we show that there are three possible positions at which a muon can reside. As discussed in the previous APR report, we expand the calculation further by considering the local effect of an implanted muon from both the crystal and spin structures of supercell LCO.[2,3)] After that, we also consider the zero-point vibration motion (ZPVM) of an implanted muon inside the structure by calculating the distribution of the muon position as a quantum particle.[4)] Both of these considerations can be utilized to calculate the internal field by using the following equation:

$$\sum_{i,j} \frac{1}{|\vec{r}_i - \vec{r}_j|^3} \left[3\vec{\rho}_i \left(\vec{r}_i - \vec{r}_j\right) \frac{\left(\vec{r}_i - \vec{r}_j\right)}{|\vec{r}_i - \vec{r}_j|^2} - \vec{\rho} \right] |\psi_j|^2 . \quad (1)$$

Here, $\vec{\rho}_i$ denotes the vector data for the spin grids and

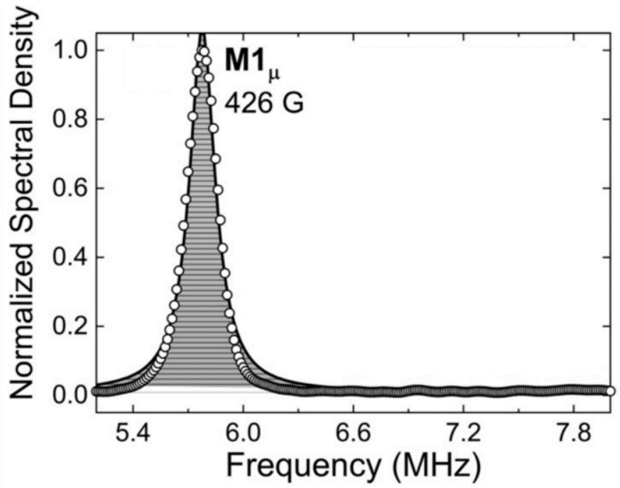

Fig. 1. Fourier transfrom spectrum from the high-statistic μSR experiment.

$\vec{r}_i - \vec{r}_j$ denotes the relative distance between Cu-spin grids with a density of $\vec{\rho}_i$ and the muon distribution grids ψ_j. Then, we sum all grid components obtained from our DFT calculations to estimate the internal field at each muon, a sphere with a radius of 50 Å. After obtaining the internal fields for each fields muon position, we optimize U by comparing the calculated internal fields with the experimental internal fields:

$$\Delta H_{M_i} = \left(H_{DFT}^{M_i} - H_{\mu SR}^{M_i} \right), \ |i = 1, 2, 3|, \quad (2)$$

and sum all ΔH_{M_i} for each U with the fitting errors of the internal fields, σ_i, as follows:

$$\sum_i \frac{\Delta H_{M_i}^2}{\sigma_i^2}, \quad |i = 1, 2, 3|. \quad (3)$$

By applying the Gaussian function, we obtain optimized U of 4.87(4) eV. By using this optimized U, we observe that the difference between the calculated and experimental internal fields for the M1, M2, and M3 positions are 3.4 (≈1%) , 38.2 (≈40%), and 97.9 (≈8%) G respectively.[1)]

*1 Department of Physics, Universitas Indonesia
*2 RIKEN Nishina Center

References

1) M. R. Ramadhan *et al.*, Phys. Rev. Res. **4**, 033044 (2022).
2) M. R. Ramadhan *et al.*, RIKEN Accel. Prog. Rep. **51**, 197 (2017).
3) M. R. Ramadhan *et al.*, RIKEN Accel. Prog. Rep. **52**, 173 (2018).
4) M. R. Ramadhan *et al.*, RIKEN Accel. Prog. Rep. **53**, 150 (2019).

Comparison of basis sets for DFT calculation of guanine nucleobase

W. N. Zaharim,[*1,*2] S. Sulaiman,[*1,*2] H. Rozak,[*1,*3] and I. Watanabe[*1,*2]

Deoxyribonucleic acid (DNA) consists of two polynucleotide chains twisted around each other in the form of a double helix. DNA is formed using sequences of four nitrogenous bases (guanine, adenine, cytosine and thymine). Several reports showed that μSR is an experimental technique that can be used to study the properties of organic systems.[1–3] The interpretation and analysis of the μSR results are often complemented and enhanced through computational studies.[4–7]

Two possible muon stopping sites have been reported for each nitrogenous base.[4] In guanine nucleobase, muon is likely to attach itself to the carbon atom (C8). The DFT cluster framework using hybrid functional was used in this study.[8–11] In this study, B3LYP were used in combination with 6 different standard set of Gaussian basis function; (1) 6-31+G, (2) 6-31+G(d), (3) 6-31+G(d,p), (4) 6-31++G, (5) 6-31++G(d), (6) 6-31++G(d,p). The question of how the functional and the basis set is chosen will affect the optimized geometry and electronic structure calculated is therefore becoming the motivation of this study.

Figure 1 shows the total energy of the optimized structure calculated using different basis sets. 6-31+G and 6-31++G produce an optimized structure with the highest energy compared to the other basis sets. The difference in energies between the basis set that uses a diffuse function to all atoms and diffuse function to all atoms except hydrogen is only 0.01 eV. A huge difference in total energy is observed when polarization function is used in the basis set. Total energy produces by using a basis set that includes polarization function is reduced by approximately ∼5 eV. Polarization function gives more room for the atom to get away from each other to minimize the electron-electron repulsion thus reduces the total energy of the system.

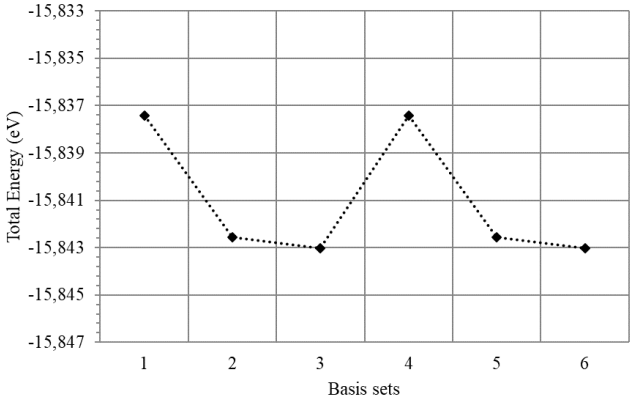

Fig. 1. The total energy of the optimized structure using different basis sets.

The estimated isotropic interaction values calculated using different basis sets were summarized in Fig. 2. 6-31++G basis set produces the lowest isotropic interaction value. This is due to the diffuse function used in the atomic orbital calculation for all atoms including muon. The diffuse function allows the electron to move far away from the nucleus which may affect the isotropic interaction value. As the electron moves far away from the nucleus the isotropic interaction decreases. In particular, among all basis sets, high hyperfine frequency was produced when using 6-31+G(d,p). This value is 13.18% lower than the experimental value obtained by Hubbard *et al.*[4] and it is the closest to the experimental value.

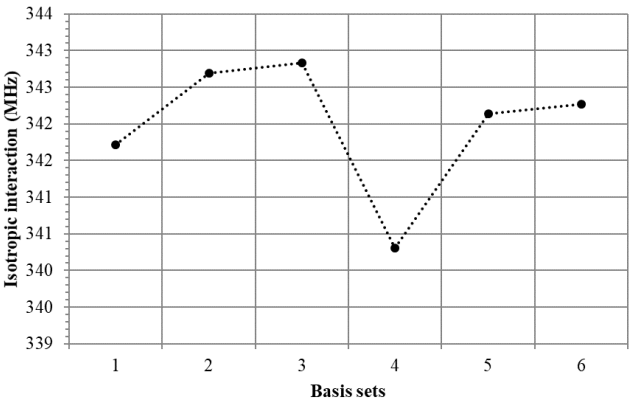

Fig. 2. Isotropic interaction values obtained using different basis sets.

The DFT cluster method was applied to study the effects of different basis sets on the electronic structure and properties of guanine nucleobase. The basis set with polarization function should be utilized for applications where the total energy is crucial and the diffuse function can be excluded to all atoms in a calculation that considers the isotropic interaction between the muon and atoms at the trapping location. By considering both total energy and muon hyperfine interaction, 6-31+G(d,p) basis set is the best one to use for guanine nucleobase molecules.

*1 RIKEN Nishina Center
*2 Computational Physics Laboratory, School of Distance Education, Universiti Sains Malaysia
*3 Graduate School of Engineering and Science, Shibaura Institute of Technology

References

1) K. Nagamine *et al.*, J. Condens. Matter Phys. **16**, S4797 (2004).
2) K. Nagamine *et al.*, Physica B **404**, 953 (2009).
3) E. Torikai *et al.*, Physica B **374**, 441 (2006).

4) P. L. Hubbard *et al.*, J. Phys. Chem. **108**, 9302 (2004).
5) P. L. Hubbard *et al.*, Physica B **374**, 437 (2006).
6) R. Scheicher *et al.*, HFI/NQI 2004, (Springer, 2005), p. 53.
7) R. Scheicher *et al.*, Physica B **374**, 448 (2006).
8) W. N. Zaharim *et al.*, J. Phys. Soc. Jpn. **90**, 044301 (2021).
9) W. N. Zaharim *et al.*, Acta. Chem. Scand. Omega **6**, 40 (2021).
10) W. N. Zaharim *et al.*, J. Phys. Soc. Jpn. **91**, 094301 (2022).
11) A. Jamaludin *et al.*, J. Phys. Soc. Jpn. **91**, 024301 (2022).

Relative formation probabilities for fluoride and oxyfluoride anions of U, Np, Pu and Am in accelerator mass spectrometry measurements at VERA†

A. Wiederin,[*1,*2] M. Kern,[*1,*2] K. Hain,[*1] M. Martschini,[*1] A. Sakaguchi,[*3,*4] P. Steier,[*1] A. Yokoyama,[*3,*5] and R. Golser[*1]

Atomic anions of actinides are not formed efficiently in a Cs sputter ion source, so they must be extracted as molecular anions for AMS measurements.[1] Fluoride anions were introduced as an alternative to the oxide anions previously established for this purpose.[2] Some potential benefits of fluoride extraction of actinides have already been reported: Fluorine is monoisotopic, fluoride anions have the potential for increased ionization yields in low cesium flux ion sources,[2] could reduce the hydride background[2] and show some degree of elemental selectivity.[3] Furthermore, fluoride and oxyfluoride molecular anions could also be of use in isobar separation techniques such as Ion Laser InterAction Mass Spectrometry (ILIAMS)[4] or the Isobar Separator for Anions (ISA).[5] The efficiency with which an anion species is formed in the sputter process is determined by the electron affinity of the corresponding neutral atom or molecule.[1] The stability of an anion against photodetachment in systems like ILIAMS is in turn also related to this electron affinity.

Developing such isobar separation methods in the actinide range could open up new possibilities for the study of actinides in the environment, such as new potential isotopic spikes for normalization or an extended multi-actinide analysis with simplified chemistry from a single AMS sample.

Based on estimates of the releases from nuclear tests and reprocessing plants, ^{237}Np is thought to be the second most abundant anthropogenic actinide in the environment.[6] ^{237}Np exhibits conservative behavior in natural waters as it mainly exists in the highly soluble $Np(V)O_2^+$ form under oxidizing conditions[7] and has a long half-life ($T_{1/2} = 2.1 \times 10^6$ y). These two properties could turn ^{237}Np into a valuable tool for tracking environmental processes such as water mass transport.[8,9] The main obstacle to establishing ^{237}Np as an environmental tracer is the lack of an isotopic spike material for a matrix independent and reliable normalization of ^{237}Np measurements by mass spectrometric methods.

For this purpose, ^{236}Np was produced via the ^{232}Th(^{7}Li, $3n$)^{236}Np reaction at the RIKEN Nishina Center. In addition to the desired ^{236g}Np, isobaric contamination can arise either from ^{236}U produced by neutron capture on ^{235}U impurities in the irradiation target, or from the decay of metastable ^{236m}Np to ^{236}U or ^{236}Pu, so further analysis of the mass 236 fraction was required.

The relative formation probabilities of AnF_5^-, AnF_4O^-, $AnF_3O_2^-$, AnF_4^-, AnF_3O^- and $AnF_2O_2^-$, with An representing the actinides U, Np, Pu or Am, have been investigated. The AnF_4^-/AnF_5^- ratios of these actinides have been shown to be element-specific within each measurement, with an order of magnitude separating the AnF_4^-/AnF_5^- ratios from one actinide element to the next. The magnitude factor is robust and reproducible. Based on these findings, the AnF_4^-/AnF_5^- ratio serves as an elemental fingerprint. A significant amount of isobaric interference would shift this ratio relative to the reference ratio for the actinide of interest as determined on calibration samples in the same measurement. The prospective neptunium spike material provided a first application for this kind of isobar analysis, and the tentative first results are compatible with a successful production and chemical separation of ^{236}Np.

Choosing the tetrafluoride system molecular anions for the extraction of Np and U suppresses the interfering isobar $^{236}UF_4^-$ by an order of magnitude compared to $^{236}NpF_4^-$ in the ion source. The large number of (oxy) fluoride anions of various actinides greatly enhances the possibility of finding suitable molecular ion systems for isobar separation using methods such as element-selective photodetachment in ILIAMS.

References
1) R. Middleton, Nucl. Instrum. Methods Phys. Res. **122**, 35 (1974).
2) X. L. Zhao *et al.*, Nucl. Instrum. Methods Phys. Res. B **510**, 10 (2022).
3) X. L. Zhao *et al.*, Nucl. Instrum. Methods Phys. Res. B **294**, 356 (2013).
4) M. Martschini *et al.*, Nucl. Instrum. Methods Phys. Res. B **456**, 213 (2019).
5) J. Eliades *et al.*, Nucl. Instrum. Methods Phys. Res. B **268**, 839 (2010).
6) J. M. Kelley *et al.*, Sci. Total Environ. **237-238**, 483 (1999).
7) W. L. Keeney-Kennicutt *et al.*, Mar. Chem. **15**, 133 (1984).
8) P. Lindahl *et al.*, J. Environ. Radioact. **82**, 285 (2005).
9) M. Lopez-Lora *et al.*, Sci. Total Environ. **708**, 135222 (2020).

† Condensed from the article in Nucl. Instrum. Methods Phys. Res. B **528**, 40 (2022)

*1 Faculty of Physics, Isotope Physics, University of Vienna
*2 Vienna Doctoral School of Physics, University of Vienna
*3 RIKEN Nishina Center
*4 Faculty of Pure and Applied Sciences, University of Tsukuba
*5 Institute of Science and Engineering, Kanazawa University

Extraction of $^{229}Th^{3+,2+}$ using RF carpet gas cell and observation of internal conversion process of ^{229m}Th

Y. Shigekawa,[*1] A. Yamaguchi,[*2,*3] K. Tokoi,[*4] N. Sato,[*1] M. Wada,[*5] and H. Haba[*1]

The first excited state of the ^{229}Th nucleus, ^{229m}Th, has an excitation energy of ∼8.3 eV,[1,2] which may lead to variations in the decay modes (internal conversion (IC), electronic bridge (EB) transitions, and γ-ray emission) depending on the chemical environment. To observe the EB transitions and γ-ray emission of ^{229m}Th, we are aiming to trap ^{229m}Th ions such as $^{229m}Th^{3+}$, $^{229m}Th^{2+}$, $^{229m}Th^{+}$, and ^{229m}Th molecular ions in an ion trap.[3] We previously developed a radiofrequency (RF) carpet gas cell and extracted ^{220}Rn ions emitted from an ^{224}Ra source.[3] In this study, we fabricated an ion trap and then extracted and trapped ^{229}Th ions produced from a ^{233}U source. Moreover, we confirmed the existence of the IC decay of ^{229m}Th using ^{229}Th ion bunches created by the ion trap, which was reported only by the Munich group.[4,5]

We fabricated a quadrupole ion trap having three segments (Trap 1, 2, and 3), and it was connected between the quadrupole ion guide (QPIG) and the quadrupole mass separator (QMS), as shown in Fig. 1. Gasses can be introduced into the ion-trap region for changing the chemical state of ^{229m}Th ions. Trap 1 has four T-shaped electrodes called LINAC rods,[6] which make axial gradient to rapidly move ions downstream in the presence of gas.

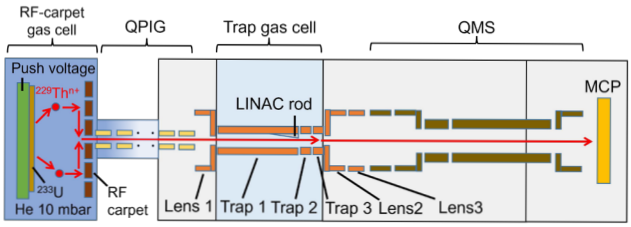

Fig. 1. Schematic view of the ion trap connected with the RF-carpet gas cell and the QMS.

We placed a ^{233}U source (diameter 90 mm, 596(10) kBq) inside the RF-carpet gas cell. The gas cell was first evacuated to less than 1×10^{-7} Pa by a getter pump, and then filled with purified He gas of 10 mbar. ^{229}Th ions recoiling out of the ^{233}U source were decelerated by the gas and transported by DC and RF voltages to the ion trap. First, we continuously extracted ions by operating the ion trap as an ion guide and detected them with a multichannel plate detector (MCP). As shown in Fig. 2, we successfully

*1 RIKEN Nishina Center
*2 Quantum Metrology Laboratory, RIKEN
*3 PRESTO, Japan Science and Technology Agency
*4 Graduate School of Science, Osaka University
*5 Wako Nuclear Science Center, IPNS, KEK

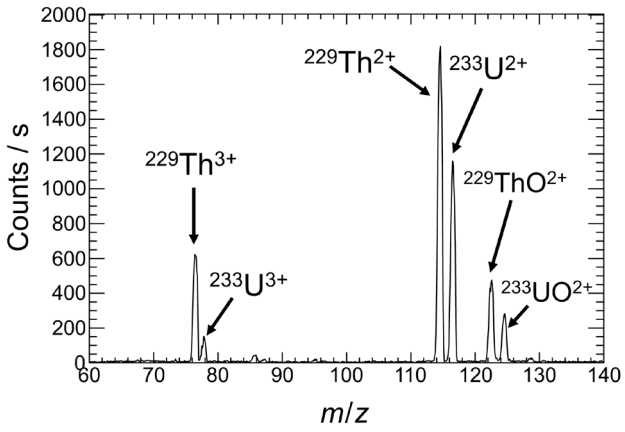

Fig. 2. Mass spectrum of ions extracted to the MCP.

extracted $^{229}Th^{3+}$ and $^{229}Th^{2+}$ using the RF-carpet gas cell, having simpler electronics and a smaller chamber size than the RF-funnel gas cell developed by the Munich group.[4]

We made short ion bunches using the ion trap for observing the IC electrons of ^{229m}Th. First, the ions were trapped in Trap 3 by applying +10 V to Lens 2 (Fig. 1) at a He pressure of 0.5 Pa. They were collisionally cooled for 20 ms and then extracted downstream by switching the voltage of Lens 2 to −35 V. Each ion bunch had ∼270 $^{229g,m}Th^{3+}$ (∼5 $^{229m}Th^{3+}$), and ∼80 $^{233}U^{3+}$ ions. The ion bunches were repeatedly extracted to the MCP by two different MCP surface voltages of −2000 and −50 V to detect only ions and both ions and IC electrons, respectively. Figure 3 shows the time traces of the MCP counts. For $^{229}Th^{3+}$, the decay curve for −50 V is clearly different from that for −2000 V, while no such difference is observed for $^{233}U^{3+}$. The shapes of ion bunches at

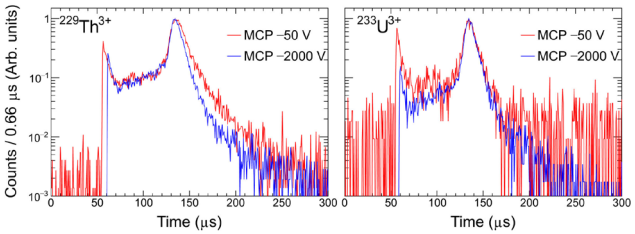

Fig. 3. MCP counts as a function of the time at MCP surface voltages of −50 V (red) and −2000 V (blue) for $^{229}Th^{3+}$ (left) and $^{233}U^{3+}$ (right). The plots are arranged so that the peak tops at 134 μs are matched to each other.

−2000 and −50 V should be the same as observed for $^{233}U^{3+}$. Hence, the decay curve having longer lifetime for $^{229}Th^{3+}$ at −50 V corresponds to IC electrons of ^{229m}Th, which were emitted after the neutralization of $^{229m}Th^{3+}$ on the MCP surface.[4] The preliminary value of the IC-decay half-life is 8(1) μs, which is consistent with the previous study (7(1) μs[5]). Hence, we successfully confirmed the existence of the IC decay of ^{229m}Th.[4,5] We will introduce some reactive gasses into the ion trap to make various chemical species of ^{229m}Th to observe the EB transitions.

References
1) B. Seiferle *et al.*, Nature **573**, 243 (2019).
2) A. Yamaguchi *et al.*, Phys. Rev. Lett. **123**, 222501 (2019).
3) Y. Shigekawa *et al.*, RIKEN Accel. Prog. Rep. **55**, 127 (2022).
4) L. von der Wense *et al.*, Nature **533**, 47 (2016).
5) B. Seiferle *et al.*, Phys. Rev. Lett. **118**, 042501 (2017).
6) A. Loboda *et al.*, Eur. J. Mass Spectrom. **6**, 531 (2000).

Innovative targeted alpha therapy for prostate cancer: preclinical evaluation of [^{211}At]PSMA5†

T. Watabe,[*1,*2] K. Kaneda-Nakashima,[*2,*3] Y. Shirakami,[*2] Y. Kadonaga,[*1,*2] K. Ooe,[*2] Y. Wang,[*4] H. Haba,[*4] A. Toyoshima,[*2] J. Cardinale,[*5] F. Giesel,[*5] N. Tomiyama,[*2] and K. Fukase[*2,*3]

Prostate cancer is currently the most prevalent cancer among men (92,021 new cases/year in Japan). After surgery and radiation therapy, hormone therapy is performed for recurrent lesions. However, the prognosis is poor if the hormone therapy becomes resistant with multiple metastases.

In recent years, prostate-specific membrane antigen (PSMA), which is a membrane marker expressed in prostate cancer, has received significant attention. PSMA is expressed in more than 90% of prostate cancers.[1] Targeted α-therapy (TAT) for PSMA is a promising treatment for metastatic castration-resistant prostate cancer (CRPC).[2] Astatine is an α-emitter (half-life $T_{1/2}$ = 7.2 h) that can be produced by a 30 MeV cyclotron. In this study, we evaluated the treatment effect of ^{211}At-labeled PSMA compounds in mouse xenograft models.

^{211}At was procured from RIKEN via the short-lived RI supply platform. Upon procurement, dry distillation was used to separate and purify ^{211}At. ^{211}At-labeled PSMA1, PSMA5, and PSMA6 were synthesized by the substitution reaction of ^{211}At with the dihydroxyboryl groups.[3]

Tumor xenograft models were established by subcutaneous transplantation of human prostate cancer cells (LNCaP) in NOD/SCID mice.[4] [^{211}At]PSMA1, [^{211}At]PSMA5, or [^{211}At]PSMA6 was administered to LNCaP xenograft mice to evaluate biodistribution at 3 and 24 h. The treatment effect was evaluated by administering [^{211}At]PSMA1 (0.40 ± 0.07 MBq), [^{211}At]PSMA5 (0.39 ± 0.03 MBq), or saline. Histopathological evaluation was performed for the at-risk organs at three and six weeks after administration.

All the animal experiments were performed in compliance with the guidelines of the Institute of Experimental Animal Sciences. The protocol was approved by the Animal Care and Use Committee of the Osaka University Graduate School of Medicine.

[^{211}At]PSMA5 resulted in higher tumor retention compared to [^{211}At]PSMA1 and [^{211}At]PSMA6 (30.6 ± 17.8, 12.4±4.8, and 19.1±4.5%ID/g at 3 h versus 40.7± 2.6, 8.7±3.5, and 18.1±2.2%ID/g at 24 h, respectively), whereas kidney excretion was superior in [^{211}At]PSMA1 compared to [^{211}At]PSMA5 and [^{211}At]PSMA6. The administration of [^{211}At]PSMA5 had an excellent treatment effect on tumor growth. [^{211}At]PSMA1 also showed a substantial treatment effect; however, the tumor size was relatively more prominent than in the case of [^{211}At]PSMA5. In the histopathological evaluation, regenerated tubules were detected in the kidneys at three and six weeks after administering [^{211}At]PSMA5. No abnormality was found in the histology of the thyroid.

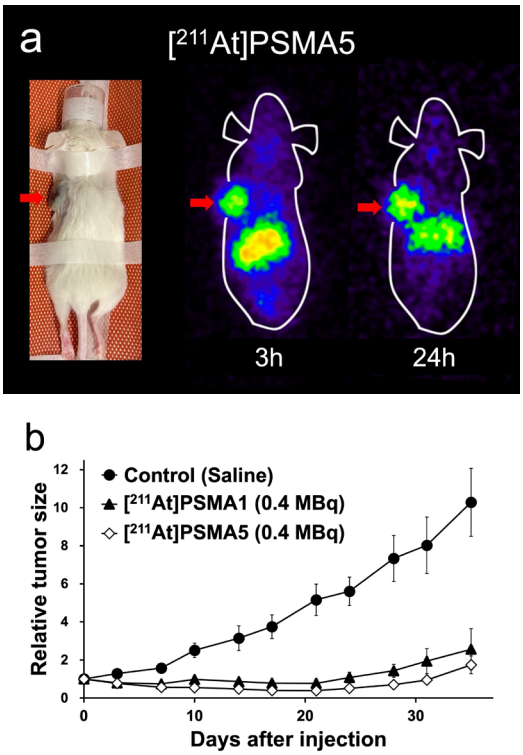

Fig. 1. (a) Planar images of [^{211}At]PSMA5 in LNCaP xenograft mice. High uptake was observed in the xenografts (arrows). (b) Change in the tumor size after administering [^{211}At]PSMA1 (0.4 MBq, n = 5), [^{211}At]PSMA5 (0.4 MBq, n = 12), or control (saline, n = 10).

TAT using [^{211}At]PSMA5 resulted in excellent tumor growth suppression with minimal side effects in the normal organs. [^{211}At]PSMA5 should be considered as a new possible TAT for metastatic CRPC. An investigator-initiated clinical trial will start at the Osaka University after tox studies.

References
1) T. Watabe *et al.*, Ann. Nucl. Med. **35**, 523 (2021).
2) C. Kratochwil *et al.*, J. Nucl. Med. **57**, 1941 (2016).
3) Y. Shirakami *et al.*, Sci. Rep. **11**, 12982 (2021).
4) F. Soeda *et al.*, J. Nucl. Med. **60**, 1594 (2019).

† Condensed from the article in Eur. J. Nucl. Med. Mol. Imaging. **50**, 849 (2023)

*1 Graduate School of Medicine, Osaka University
*2 Institute for Radiation Sciences, Osaka University
*3 Graduate School of Science, Osaka University
*4 RIKEN Nishina Center
*5 University Hospital Dusseldorf

Prevention of radionuclide-induced antibody denaturation maintains active targeting and maximizes antitumor efficacy in ^{211}At-radioimmunotherapy†

H. Takashima,[*1,*2] K. Ohnuki,[*3] S. Manabe,[*2,*4,*5,*6] Y. Koga,[*1,*7] R. Tsumura,[*1] T. Anzai,[*1] Y. Wang,[*2] X. Yin,[*2] N. Sato,[*2] Y. Shigekawa,[*2] A. Nambu,[*2] S. Usuda,[*2] H. Haba,[*2] H. Fujii,[*3] and M. Yasunaga[*1]

Selective tumor accumulation of alpha emitters with high linear energy transfer and a short particle range in tissue results in potent antitumor efficacy without serious toxicity. Thus, there is a growing interest in developing novel target alpha therapies. Astatine-211 (^{211}At) is a promising alpha emitter that is applicable to cancer treatment.

In the preparation process of radioactive antibodies, caution should be exercised in the radionuclide-induced chemical reaction causing antibody denaturation. We demonstrated that reactive oxygen species (ROS) generated from ^{211}At-induced radiolysis of water denature astatinated antibodies.[1)] The radionuclide-induced antibody denaturation disrupts binding activity and attenuates *in vivo* antitumor effect. In contrast, sodium ascorbate (SA), a free radical scavenger, successfully quenches ROS and prevents denaturation, resulting in the maintenance of binding activity and antitumor effect.[2)] Although we revealed the influence of radiochemical reaction on ^{211}At-labeled antibody as described above, several questions remain. First, it is unclear whether ^{211}At-induced denaturation affects the pharmacokinetics of radioactive antibodies, such as half-life in blood circulation, distribution to normal organs, and tumor accumulation via active targeting and passive targeting, which are based on antigen-antibody reaction and enhanced permeability and retention effect, respectively.[3)] In addition, the protective effects of SA on the pharmacokinetics have not been clarified.

In this study, using an ^{211}At-labeled anti-human epidermal growth factor receptor 2 (HER2) antibody stabilized with SA, a denatured radioactive anti-HER2 antibody, and an ^{211}At-labeled nontargeted control antibody (anti-CD20 antibody) stabilized with SA, we compared their residence time in blood circulation, distribution to normal organs, tumor accumulation, and antitumor effect in a xenograft model with high expression of HER2.

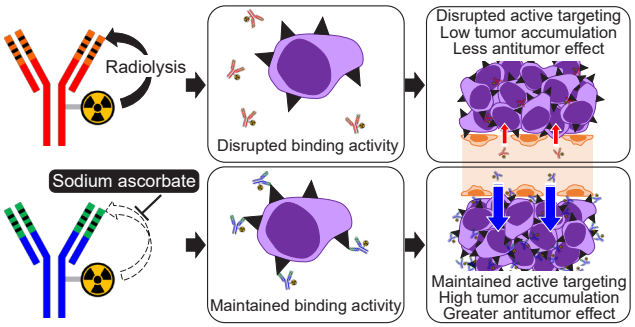

Fig. 1. Graphical abstract of this study.

In sodium dodecyl sulfate-polyacrylamide gel electrophoresis analysis, we confirmed that ^{211}At denatured radioactive anti-HER2 and anti-CD20 antibodies under no protection, and SA successfully stabilized the radioactive antibodies. The binding activity of the denatured radioactive anti-HER2 antibody was consistently disrupted, whereas the binding activity of the stabilized immunoconjugate was comparable to the naked antibody. Similarly, the cytocidal effect of the denatured radioactive anti-HER2 antibody on HER2-positive cancer cells was attenuated more than the stabilized radioactive antibody.

There is no difference in blood circulation time as well as distribution to normal organs between the groups administered ^{211}At-labeled anti-HER2 antibody under SA protection and the denatured radioactive anti-HER2 antibody in *ex vivo* biodistribution study. These findings suggest that ^{211}At-induced antibody denaturation may not affect tumor accumulation via passive targeting. However, single-photon emission computed tomography and *ex vivo* biodistribution studies demonstrated that tumor accumulation of ^{211}At-labeled anti-HER2 antibody stabilized with SA was significantly higher than that of the denatured radioactive anti-HER2 antibody and ^{211}At-labeled nontargeted control antibody under SA protection. In a xenograft model with high expression of HER2, the stabilized radioactive anti-HER2 antibody consistently outperformed the denature immunoconjugate and the radioactive nontargeted control antibody. ^{211}At-induced antibody denaturation hampers

† Condensed from the article in Mol. Pharm. **20**, 1156 (2023)

*1 Developmental Therapeutics, Exploratory Oncology Research & Clinical Trial Center (EPOC), National Cancer Center
*2 RIKEN Nishina Center
*3 Division of Functional Imaging, EPOC, National Cancer Center
*4 Laboratory of Functional Molecule Chemistry, Pharmaceutical Department and Institute of Medicinal Chemistry, Hoshi University
*5 Research Center for Pharmaceutical Development, Tohoku University
*6 Glycometabolic Biochemistry Laboratory, RIKEN
*7 Department of Strategic Programs, EPOC, National Cancer Center

tumor accumulation via active targeting, attenuating antitumor efficacy, whereas SA successfully maintains tumor targeting and antitumor activity. In alpha-radioimmunotherapy, active targeting significantly increases tumor accumulation of ^{211}At.

In conclusion, SA-dependent protection that maintains tumor targeting and *in vivo* antitumor effect will facilitate the clinical application of ^{211}At-radioimmunotherapy.

References

1) S. Manabe *et al.*, ACS Omega **6**, 14887 (2021).
2) H. Takashima *et al.*, Cancer Sci. **112**, 1975 (2021).
3) Y. Matsumura *et al.*, Cancer Res. **46**, 6387 (1986).

Identification of a sex determining gene in a dioecious plant *Silene latifolia*†

Y. Kazama,[*1,*2] M. Kitoh,[*1] T. Kobayashi,[*1] K. Ishii,[*2,*3] M. Krasovec,[*4,*5] Y. Yasui,[*6] T. Abe,[*2] S. Kawano,[*7] and D. A. Filatov[*4]

Silene latifolia is a dioecious flowering plant with XY-type sex chromosomes belonging to the Caryophyllaceae family. Since its discovery in 1923 as one of the first species with sex chromosomes discovered in higher plants, it has been used for studies of sex chromosome evolution and sex-determining mechanisms in plants.[1,2] Two sex-determining genes have been postulated to be present on the Y chromosome: the male-promoting gene (SPF) and the female-suppressor gene (GSF). However, the Y chromosome is 1arge (approx. 660 Mb) and most of it comprises a non-recombining region and occupied by repetitive sequences, which has prevented genome sequence assembly and rendered the identification of sex-determining genes difficult.

We irradiated *S. latifolia* with heavy-ion beams to obtain several hermaphroditic (GSF-deficient) and asexual (SPF-deficient) mutants, and mapped the shared deleted regions of mutants as two sex-determining regions, respectively.[3] Genome sequencing and RNA-seq were performed on two of the hermaphroditic mutants with small deletion sizes. Sequences were then compared between male, female, and mutants. Consequently, we found three genes that were present and expressed only in males. One gene was commonly deleted in both of the 11 hermaphroditic mutants and females, which was identified as a candidate gene for *GSF*. Further, a Blast search revealed that this gene was highly homologous to the Arabidopsis *CLV3* gene, which regulates the size of the shoot apical meristems (SAMs) and flower bud primordia.[4]

clv3 mutants exhibited increased carpel size, while transgenic plants with overexpression of *CLV3* showed suppressed carpel development, suggesting that this gene is a promising candidate for the GSF. Furthermore, in addition to the Y copy (*GSFY*), we found its X-lined gametolog (*GSFX*). RT-PCR results showed that both *GSFY* and *GSFX* were expressed in the shoot apical meristems and young flower buds. The translation product of *CLV3* is known to act as a peptide with 12 amino acid residues in the final product. Therefore, we compared the amino acid residue sequences of GSFY and GSFX peptides and found that the sixth glycine residue in GSFX was mutated to an alanine residue. As this mutation is the same as that of the Arabidopsis *clv3-1/clv3-5* mutant (CLV3m), *GSFX* was considered to be a loss-of-function type. When these peptides were artificially synthesized and treated to the SAMs of *S. latifolia*. GSFY was found to be active in suppressing SAM size, similar to CLV3, where GSFX and CLV3m were inactive. Next, when *GSFY* was introduced into *Arabidopsis thaliana*, a hermaphroditic plant, the carpel development was inhibited. However, introduction of *GSFX* did not inhibit development of the carpel. Furthermore, treatment of flower buds of *S. latifolia* with the GSFY peptide also inhibited the development of the pistils. These results indicate that *GSFY*, a homolog of the *CLV3* gene, is a likely candidate of the sex-determining gene that suppresses gynoecium development in *S. latifolia*, and that *GSFX* on the X chromosome is dysfunctional.

We have previously shown that, in contrast to *GSFY, SlWUS1*, which is considered to function in enlarging the carpels, is present on the X chromosome but not on the Y chromosome in *S. latifolia*.[5] This suggests that the function of the X chromosome functions is to promote female development. In fact, there is a report in the old literature that the creation of XXXXY pentaploid chromosomes cause the carpels to enlarge and produce hermaphroditic flowers.[6] The manner in which the Y chromosome acquired the dominant *GSFY* during the evolution of sex chromosomes has been the greatest mystery; however, this system, wherein the X chromosome enlarges the carpels and the Y chromosome reduces its size, can successfully explain the emergence of the dominant GSFY (Fig. 1).

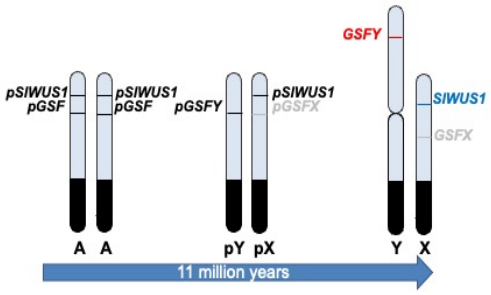

Fig. 1. Model for the evolution of *S. latifolia* sex chromosomes with *GSFX* dysfunction and loss of *SlWUS1* in the Y chromosome.

† Condensed from the article in Mol. Biol. Evol. **39**, msac195 (2022)
*1 Department of Bioscience and Biotechnology, Fukui Prefectural University
*2 RIKEN Nishina Center
*3 National Institutes for Quantum Science and Technology (NIRS)
*4 Department of Biology, Oxford University
*5 CNRS, Sorbonne University
*6 Graduate School of Agriculture, Kyoto University
*7 Graduate School of Frontier Sciences, University of Tokyo

References

1) E. Kejnovsky *et al.*, Cytogenet. Genome Res. **129**, 250 (2010).
2) D. Charlesworth, Genetics **210**, 1143 (2018).
3) Y. Kazama *et al.*, Sci. Rep. **6**, 18917 (2016).
4) J. C. Fletcher *et al.*, Science **283**, 1911 (1999).
5) Y. Kazama *et al.*, G3 (Bethesda) **2**, 1269 (2012).
6) H. E. Warmke, Am. J. Bot. **33**, 648 (1946).

Screening for high-growth mutants in sporophytes of *Undaria pinnatifida* using heavy-ion beam irradiation†

Y. Sato,[*1,*2] T. Hirano,[*1,*3] Y. Hayashi,[*1] N. Fukunishi,[*1] S. Kawano,[*4] and T. Abe[*1]

Undaria pinnatifida (Wakame) is primarily cultivated as a food resource on Japan's Sanriku coast, but production yield is declining due to environmental changes and a decrease in the number of producers. To meet domestic market demand, excellent strains that improve productivity per producer must be developed. Until now, there have been no results of mutation breeding using heavy ion beams in brown macroalgae. Our previous study developed a technique for producing mutants in the gametophyte from zoospores obtained by irradiance of heavy-ion beams on the sporophylls.[1)] However, this method limits the time for obtaining mature sporophylls. Therefore, in this study, gametophytes and young sporophytes of this alga were irradiated with a heavy-ion beam, and the subsequent culture was conducted using a tank system (CFCS)[2)] to select elite cultivars without aquaculture on the sea.

The mother plant for the irradiation was collected from Hirota Bay, Iwate Prefecture. According to the method described in previous studies,[1,2)] the zoospores were induced and cultured to gametophytes and sporophytes. Gametophytes, and sporophytes were irradiated with C ions (135 MeV/nucleon, LET, 30.0 keV/μm) at a dose of 0.5–25 Gy or Ar ions (95 MeV/nucleon LET, 284 keV/μm) at a dose of 0.2–10 Gy. The sporophytes obtained from these ions irradiated gametophytes, and the irradiated sporophytes were cultivated in a 7 L plastic tank for about two weeks and then transferred to a CFCS for cultivation. UV-sterilized seawater was used throughout the cultivation. The seawater temperature and light intensity were set at 10°C and 100 μmol photons m^{-2} s^{-1}, respectively. On the 100th day after the start of cultivation, mutant candidates (M_1) were selected based on a total length of 100 cm or more and an individual weight of 40 g or more. Cultivation was continued until sporophylls were formed and zoospores could be collected. The sporophytes obtained by crossing male and female gametophytes derived from the individual zoospore were cultured for 20 days, and the total length was measured. Subsequently, the culture of M_2 was continued, and those with a weight twice that of the non-irradiated group, at 100 days after germination, were selected as excellent mutant candidates (M_2). M_2 was then cultured until sporophylls were formed, released zoospores, and obtained gametophytes.

The survival rate of irradiated individuals varied depending on the irradiated generation, ions, and dose. The decreasing rate was more pronounced in the sporophyte than in the gametophyte at higher doses. Although the survival rates of female gametophytes irradiated with heavy-ion beams with C and Ar ions decreased with increasing dose, those of male gametophytes did not decrease after both irradiations. These differences in sensitivity to ions may be influenced by differences in haploid and diploid stages or differences in tissue structure.

In the M_1 generation, 18 individuals were selected from 210 sporophytes obtained from irradiated gametophytes, and 30 were selected from 297 irradiated sporophytes. As a result of cultivating the sporophyte obtained by self-crossing of these 48 individuals and confirming their growth, a total of four lines was obtained for particularly large individuals compared to others; 3 lines [1302G-R68 (C ions, 5 Gy), 1302G-B60 (Ar ions, 0.2 Gy), 1302G-W40 (Ar ions, 2.5 Gy)] from M_1 candidate of irradiated gametophytes, and one line [1302S-R40 (C ions, 2 Gy)] from the M_1 candidate of the irradiated sporophyte (Fig. 1). Among these four lines, the weight of the largest individuals on the 100th day of cultivation was two to three times that of the non-irradiated group, so they were selected as M_2 individuals. In addition, a sensory test was conducted after cutting off a part of the blade and boiling it; the taste and texture of M_2 candidates did not differ from those of the non-irradiated individuals. As a result of cultivating the next-generation sporophytes from the gametophytes obtained from M_2, all four lines showed earlier growth in size than non-irradiated individuals, similar to the M_2 generation. These lines are stored as M_3, confirming the fixation of the mutation. In the future, these high-growth mutants can be used for food production and biomass utilization, including feed and fertilizer.

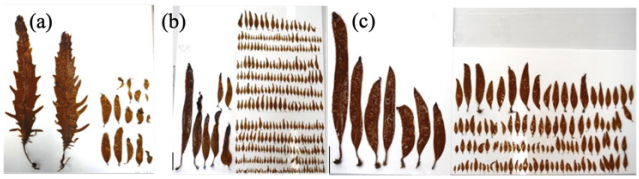

Fig. 1. Sporophytes in selected M_2 lines (3 lines out of total 4 lines) containing high-growth mutants 100 days after germination. (a): 1302G-B60 line, (b): 1302G-W40 line, (c) 1302S-R40 line. Bars = 10 cm.

† Condensed from the article in Cytologia **86**, 291 (2021)
*1 RIKEN Nishina Center
*2 Riken Food Co., Ltd.
*3 Faculty of Agriculture, University Miyazaki
*4 Future Center, Tokyo University

References

1) T. Hirano *et al.*, Phycological Res. **68**, 63 (2020).
2) Y. Sato *et al.*, J. Appl. Phycol. **29**, 1683 (2017).

Radio-fluorogenic nanoclay gel dosimeters with reduced linear energy transfer dependence for carbon-ion beam radiotherapy†

T. Maeyama,[*1,*2] A. Mochizuki,[*1] K. Yoshida,[*1] N. Fukunishi,[*2] K. L. Ishikawa,[*3] and S. Fukuda[*4]

The complex therapeutic dose distributions associated with new heavy-ion irradiation techniques require the development of 3D dosimeters; however, the precise measurement of dose distributions when using high linear energy transfer (LET) radiation remains a challenge. Specifically, the dosimeter sensitivity is typically decreased, and signal saturation occurs as a result of recombination reactions induced by high-density ionization and excitation. Thus, heavy-ion beam dosimetry necessitates a sensitivity correction for the LET being used. Consequently, we reported a magnetic resonance imaging-based 3D chemical gel ion-beam dosimeter for high LET irradiation that does not require the correction.[1)] However, several hundred Gy is required to perform measurements.

For improving the sensitivity, we examined the development of a new gel dosimeter based on fluorometry, which is the most sensitive detection method for radiation-induced products. Gel dosimeters comprise of a radiation-sensitive compound, a gelling agent, and water. In the case of low LET radiation, several types of radio-fluorogenic gel dosimeters have been reported to date, and we have prepared highly sensitive nanoclay radio-fluorogenic gel (NC-RFG)[2,3)] dosimeters from dihydrorhodamine 123 (DHR123) and nano-sized clay. The non-fluorescent DHR123 was oxidized to fluorescent rhodamine 123 (RD123) via exposure to ionizing radiation. The spatial information that describes the absorbed dose distribution was retained in the nanoclay gel matrix. Consequently, scanning spatial dosimetry can be performed using a fluorescent gel such as this because the fluorescence intensity increases linearly with increasing absorbed dose.

In the NC-RFG using DHR123, the dose-response or sensitivity of this gel dosimeters decreases with increasing LET, because RD123 is produced by oxidation reactions, primarily with OH radicals. Therefore, this study developed a method for reducing the effect of LET on NC-RFG dosimeters. Through the use of a new and optimal Fe^{3+} catalyst together with pyridine (Py) as a dispersant, more than 20 samples of NC-RFG with different preparation conditions were investigated. They were irradiated with 135 and 290 MeV/nucleon $^{12}C^{6+}$ ions accelerated by the RIKEN Ring Cyclotron and the Heavy Ion Medical Accelerator in Chiba, respectively. In this paper, only the preparation conditions after optimization are presented.

The prepared NC-RFG was deaerated with 1 mM Fe^{3+}, 100 mM Py, 100 μM DHR123, and 2 wt% Clay. The dose response of fluorescence intensity (I_{FL}) of irradiated samples was obtained via a fluorescence gel scanner. Figure 1(a) shows the IFL distributions obtained from the Fe^{3+}-Py-DHR123 NC-RFG using a 290 MeV/nucleon $^{12}C^{6+}$ ion beam for various entrance surface doses (ESDs). The distributions in (b) were determined by subtracting the pre-exposure distribution and dividing by the ESD. These plots demonstrate good agreement with one another, and the correlation coefficient (R^2) of I_{FL} versus dose was greater than 0.995 even near the Bragg peak, as shown in (c). Figure 1(d) presents a comparison of the relative δI_{FL}/ESD and absorbed dose distributions as evaluated through a standard method of dosimetry using an ionization camber (IC). These data confirm that the relative δI_{FL}/ESD distribution closely matched the dose distribution. Although the LET value increased to 266 eV/nm at the Bragg peak, the sensitivity was almost constant.[4)]

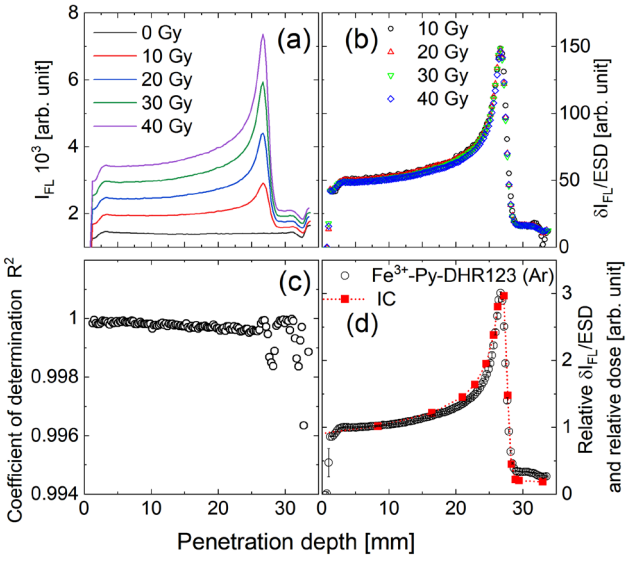

Fig. 1. Radiological properties of NC-RFG after irradiation with a carbon-ion beam ($^{12}C^{6+}$ 290 MeV/nucleon).[4)]

NC-RFG resulted in a significant reduction in the unwanted effect of the LET. The promotion of Fenton-like reactions decomposed H_2O_2 (the main product of the high-LET ion radiolysis of water) and thus en-

† Condensed from the article in Med. Phys. **50**, 1073 (2023)

*1 Department of Chemistry, Kitasato University
*2 RIKEN Nishina Center
*3 Department of Nuclear Engineering and Management, University of Tokyo
*4 QST Hospital, National Institutes for Quantum Science and Technology

hanced the oxidation reaction of DHR123. For the first time, this proposed dosimeter allows an evaluation of the depth dose profile when using a carbon-ion beam at a typical therapeutic dose level of several Gy without the need to perform sensitivity corrections based on LET.[4)]

References

1) T. Maeyama *et al.*, J. Phys. Chem. B **121**, 4238 (2017).
2) T. Maeyama *et al.*, Sens. Actuators A Phys. **298**, 111435 (2019).
3) T. Maeyama *et al.*, J. Photochem. Photobiol. A **418**, 113423 (2021).
4) T. Maeyama *et al.*, Med. Phys. **50**, 1073 (2023).

Variability in the net ecosystem productivity (NEP) of seaweed farms†

Y. Sato,[*1,*2] G. N. Nishihara,[*3] A. Tanaka,[*4] and D. F. C. Belleza[*3]

The critical role of vegetated ecosystems in carbon sequestration has attracted substantial interest across various disciplines. With growing evidence of the potential of macroalgae ecosystems to capture carbon, there is burgeoning interest in applying newfound knowledge of carbon capture rates to better understand this potential for carbon sequestration. Seaweed farms are expected to play a significant role in carbon capture; advocates for expanding seaweed farms are increasing in many countries.

In general, seaweed farms are expected to be highly productive, although whether they are autotrophic or heterotrophic ecosystems and hence their potential as exporters of carbon is under debate. All in all, we present our investigation on three seaweed farms, two *Undaria pinnatifida* (Wakame) farms in northern Japan (Matsushima Bay and Hirota Bay) and one *Cladosiphon okamuranus* (Mozuku) farm in southern Japan (Bise Point). In addition, data were collected from two natural seaweed ecosystems (Arikawa Bay and Omura Bay) and one degraded seaweed ecosystem (Tainoura Bay) in Nagasaki Prefecture. We examined the frequency of autotrophic days and compared potential carbon capture rates from these six geographic locations across Japan.

We estimated potential carbon capture rates by calculating the net ecosystem productivity (NEP) from continuous recordings of dissolved oxygen concentrations under natural environmental conditions. Water temperature and dissolved oxygen concentrations were recorded with dataloggers at a rate of one sample every ten minutes. In the natural and degraded ecosystems, one datalogger was placed directly above the sediment, another 50 cm above the sediment, and a third 50 cm below the water surface (*i.e.*, a total of three instruments and a mean depth of 3 m for Omura Bay, 5 m for Arikawa Bay, and 8 m for Tainoura Bay). The dataloggers at the seaweed aquaculture farms were placed on the cultivation ropes and 1 m (Bise Point) and 2 m (Hirota Bay and Matsushima Bay) below the cultivation ropes (*i.e.*, a total of two instruments). The instruments were placed so that the majority of the biomass of the seaweed was between the data loggers. Recordings were carried out for four to twenty days before the instruments were retrieved for maintenance and data offloading. Calculations of productivity were based on the ensemble mean of the dissolved oxygen time series recorded by the dataloggers to account for vertical heterogeneity. The gross ecosystem production (GEP) rates and ecosystem respiration (ER) rates were estimated from the diurnal fluctuations of the dissolved oxygen concentration with the open-water method (*e.g.*, Hinode *et al.*, 2020). Briefly, the NEP rate can be defined as NEP = GEP + ER.

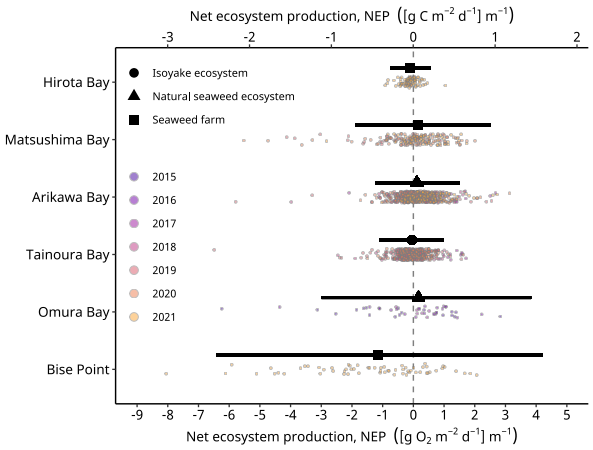

Fig. 1. Observed (colored points) and conditional mean of the net ecosystem production (black symbols) rates of the study sites. The black horizontal lines indicate the 95% highest density credible interval of the predicted values. Hirota Bay and Matsushima Bay are Wakame farms, Bise Point is Mozuku farm, Arikawa Bay and Omura Bay are sites of the natural Sargassum spp. ecosystem, and Tainoura Bay is a site where a seaweed ecosystem has degraded. The net ecosystem production in O_2 and C are calculated assuming a 1 to 1 molar ratio.

The NEP rates for the natural ecosystems in Arikawa Bay and Omura Bay were equivalent to 0.043 and 0.054 [g C m^{-2} d^{-1}] m^{-1}, respectively (Fig. 1). Consering for the degraded ecosystem in Tainoura Bay, it was -0.01 [g C m^{-2} d^{-1}] m^{-1}. We noticed that the Wakame farm in Matsushima Bay experiences autotrophy more often than natural ecosystems, although autotrophy of the Wakame farm in Hirota Bay and Mozuku farm at Bise Point was less frequently observed. Nevertheless, up to 14.1 g C m^{-2} (0.110 g C m^{-2} d^{-1}) was captured by the production of Wakame and 3.6 g C m^{-2} (0.034 g C m^{-2} d^{-1}) was captured by Mozuku, and the total yield of carbon captured during 2021 production season for these farms was 43,385 kg C. Seaweed farms are still highly valuable for their contribution to the livelihood of coastal communities and have lesser detrimental impact on the environment than other forms of aquaculture (*e.g.*, Visch *et al.*, 2020). We believe that the potential for carbon capture will not be homogenous across species and location, and that more studies on carbon flux at organismal and ecosystem scales remain to be conducted.

† Condensed from the article in Front. Mar. Sci. **9**, 861932 (2022)
*1 RIKEN Nishina Center
*2 Riken Food Co., Ltd.
*3 Organization of Marine Science Technology, Nagasaki University
*4 Faculty of Science, University of Ryukyus

References

1) K. Hinode *et al.*, Phycol. Res. **68**, 298 (2020).
2) W. Visch *et al.*, J. Appl. Phycol. **32**, 3199 (2020).

II. RESEARCH ACTIVITIES I
(Nuclear, Particle and Astro-Physics)

1. Nuclear Physics

RI beam production at BigRIPS in 2022

H. Suzuki,[*1] N. Fukuda,[*1] H. Takeda,[*1] Y. Shimizu,[*1] M. Yoshimoto,[*1] Y. Togano,[*1] N. Inabe,[*1] K. Kusaka,[*1] M. Ohtake,[*1] Y. Yanagisawa,[*1] H. Sato,[*1] K. Yoshida,[*1] and N. Fukunishi[*1]

Here, the radioactive-isotope (RI) beams produced at the BigRIPS fragment separator[1] in 2022 are presented. The experimental programs involving the use of BigRIPS during this year and the RI beams produced for each experiment are summarized in Table 1.

In the spring beamtime, a ^{238}U-beam campaign was conducted, followed by another with a ^{78}Kr beam. The ^{238}U-beam campaign was divided into two parts: a series of director's Discretionary Allocation (DA) programs with low-intensity (∼10 particle nA) primary beams, and experimental programs with full-intensity (∼70 particle nA) beams.

The first part of the ^{238}U-beam campaign began in March. The performance of a newly developed ionization chamber (IC) specialized in heavy-mass beams with a Xe-based gas was examined with the primary beam, energy-degraded ^{238}U beams, a ^{210}Rn^{84+}-centered cocktail beam, and an $A/Q = 2.5$ setting beam with wide range of atomic number $Z = 30$–90.[2] Then, a production test of a ^{237}Np beam was performed for the DA to investigate the energy dependence of its production cross section. The energy of the ^{238}U beams for this DA was degraded via the use of degraders located at T11 in the primary beamline, not at F1 or F5. For the next DA in the search for unusual nuclear pathways in nuclear synthesis, 300- and 70-MeV/nucleon ^{238}U beams were supplied. Subsequently, ^{225}Ac-centerd cocktail beams were produced for their production cross-section measurement. These beams were also supplied for the following DA of PALIS. Thereafter, the IC test with P10 and CH_4 gases were performed[2] with the same beams as in the previous IC test. Energy measurement of the ^{238}U primary beam was conducted using the primary and energy-degraded ^{238}U beams. This DA was performed for an application of SRC as the world's highest-beam-energy cyclotron as per the Guinness Book of Records. For the final DA, ^{99}Tc was produced for the measurement of its transmutation cross section.

The second part of the ^{238}U-beam campaign began in April, 1.5 days after the accelerator tunning. First, a ^{79}Ni-centered cocktail beam was supplied for multi-reflection time-of-flight mass spectrometer (MRTOF-MS) experiment at F11. Subsequently, a Machine Study (MS) and an experiment for the nucleosynthesis in r-process were conducted using OEDO with ^{124}Sn, ^{130}Te, and ^{130}Sn beams whose energies were adjusted to be 180 MeV/nucleon in BigRIPS. A ^{202}Re-centered cocktail beam was produced for the second MRTOF-MS experiment to measure the mass in vicinity of the neutron magic number $N = 126$ region. A tertiary spin-aligned ^{99}Zr beam at F7 was produced from the secondary ^{100}Zr beam impinging on a wedge-shaped Al target at F5 for an experiment to measure the quadrupole moment of an isomeric state of ^{99}Zr. Finally, a MS for production cross-section measurements was conducted with ^{132}Sn-, ^{138}Te-, ^{144}Xe-, ^{150}Ba-, and ^{154}Ce-centered cocktail beams.[3] In addition, an auto-PID system was tested with the ^{132}Sn setting in this MS.[4]

The ^{78}Kr-beam campaign began in May. An OEDO experiment to study vp-process nucleosynthesis was conducted with ^{56}Ni and ^{58}Ni beams. During changes of the magnet configurations and detector setups in OEDO, two MSs were performed. The first MS was for a development of automatic ion-optics tuning in the primary beam line with low-intensity primary beam. The second one was for production cross-section measurements with ^{64}As-, ^{39}Ca-, ^{37}Ca-, and ^{35}Ca-centered cocktail beams.[5] Subsequently, mass measurements around the proton-drip line using SHARAQ were performed with ^{50}Fe-, ^{46}Fe-, and ^{23}Si-centered cocktail beams.

During the autumn beam time, the ^{70}Zn campaign was conducted from December following the repair of the large helium refrigerator in BigRIPS. During the BigRIPS tuning, the performance of a new DAQ system with Mesytec MDPP-16 module for germanium-detectors array for isomer tagging was examined with a ^{52}Ca-centered cocktail beam.[6] Then, a ^{50}Ca beam was produced for an OEDO experiment, wherein the single-particle structure of ^{51}Ca was studied. During this experiment, a severe problem occurred on the SRC cyclotron caused the beam time to stop. Consequently, the other scheduled experiment was postponed.

RI beam production at BigRIPS from the start of the operation in March 2007 is summarized in our database[7] available at `https://ribeam.riken.jp/`.

*1 RIKEN Nishina Center

References
1) T. Kubo, Nucl. Instrum. Methods Phys. Res. B **204**, 97 (2003).
2) M. Yoshimoto *et al.*, in this report.
3) Y. Shimizu *et al.*, in this report.
4) Y. Shimizu *et al.*, in this report.
5) H. Suzuki *et al.*, in this report.
6) H. Takeda *et al.*, in this report.
7) Y. Shimizu *et al.*, Nucl. Instrum. Methods Phys. Res. B **463**, 158 (2020).

Table 1. List of experimental programs with RI beams produced at the BigRIPS separator in 2022.

Primary beam (Period)	Proposal No.	Spokesperson	Course	RI beams
^{238}U 345 MeV/nucleon (Mar. 21 – May 31)	MS-EXP21-10	M. Yoshimoto	BigRIPS	primary, energy-degraded ^{238}U, A/Q=2.5, ^{210}Rn^{84+}
	DA21-03-01	H. Otsu	F12	^{237}Np
	DA21-05-01	D. Suzuki	F12	300, 70-MeV/nucleon ^{238}U
	DA21-08-01	T. Sumikama	BigRIPS	^{225}Ac
	DA21-07-01	T. Sonoda	PALIS	^{225}Ac
	MS-EXP21-11	M. Yoshimoto	BigRIPS	primary, energy-degraded ^{238}U, A/Q=2.5, ^{210}Rn^{84+}
	DA21-09-01	H. Okuno	BigRIPS	primary, energy-degraded ^{238}U
	DA21-04-02	H. Otsu	ZeroDegree	^{99}Tc
^{238}U 345 MeV/nucleon (Apr. 2 – Apr. 20)	NP2012-RIBF202-03	M. Rosenbusch	ZeroDegree	^{79}Ni
	NP1912-SHARAQ18-01	N. Imai	SHARAQ	^{124}Sn, ^{130}Te, ^{130}Sn
	MS-EXP22-01	N. Imai	SHARAQ	^{124}Sn, ^{130}Te, ^{130}Sn
	NP2012-RIBF199-03	M. Wada	ZeroDegree	^{202}Re
	NP1912-RIBF175-01	Y. Ichikawa	ZeroDegree	^{100}Zr→^{99}Zr
	MS-EXP22-04	Y. Shimizu	BigRIPS	^{132}Sn, ^{138}Te, ^{144}Xe, ^{150}Ba, ^{154}Ce
^{78}Kr 345 MeV/nucleon (May 16 – Jun. 3)	NP1912-SHARAQ19-01	D. Suzuki	SHARAQ	^{56}Ni, ^{58}Ni
	MS-EXP22-03	T. Nishi	BigRIPS	primary
	MS-EXP22-02	H. Suzuki	BigRIPS	^{64}As, ^{39}Ca, ^{37}Ca, ^{35}Ca
	NP1812-SHARAQ13-01	S. Michimasa	SHARAQ	^{50}Fe, ^{46}Fe, ^{23}Si
^{70}Zn 345 MeV/nucleon (Dec. 5 – Dec. 11)	NP1812-SHARAQ12R1-01	K. Wimmer	SHARAQ	^{50}Ca

Production cross-section measurements for very-neutron-deficient Ca and As isotopes produced from a ^{78}Kr beam at 345 MeV/nucleon by BigRIPS separator

H. Suzuki,[*1] N. Fukuda,[*1] H. Takeda,[*1] Y. Shimizu,[*1] M. Yoshimoto,[*1] Y. Togano,[*1] T. Sumikama,[*1] K. Kusaka,[*1] and K. Yoshida[*1]

We performed production cross-section measurements using a ^{78}Kr primary beam for the neutron-deficient region around $_{20}$Ca and $_{33}$As isotopes, whose cross sections were not measured in previous ^{78}Kr campaigns in 2015 or 2019. The radioactive isotopes (RIs) were produced by the projectile fragmentation of the 400-particle nA primary beam at 345 MeV/nucleon impinging on a 5-mm-thick Be target in the BigRIPS separator. Particle identification based on the TOF-$B\rho$-ΔE method[1] was performed in the second stage of BigRIPS.

The production cross sections were deduced from the measured production rates at the F7 focal plane and their transmission efficiencies in the separator, which were simulated with the LISE^{++} codes.[2] In the simulation, the momentum distribution was represented by an assymetrical Gaussian distribution instead of the default distribution, *i.e.*, Universal parameterization,[3] which is a combination of a Gaussian distribution in high momentum side and an exponential tail in low momentum side. In the asymmetric Gaussian distribution, the Fermi momentum σ_0 and asymmetry coefficient α[2] were set to be 134.1 MeV/c and 9% (preliminary), respectively, obtained from fitting results of the experimental momentum distribution.

Figure 1 shows the production cross sections of RIs obtained in this study (colored symbols) and the previous measurements (black symbols) under the assumption that their lifetimes are long enough compared to the TOF values through the separator (∼460 ns). The cross sections vary smoothly and exhibit natural behavior, except for ^{68}Br. The apparent small cross-section of ^{68}Br could be caused by a decay loss in the separator due to its very short lifetime. K. Wimmer *et al.*[4] reported a lifetime of 45–57 ns for ^{68}Br produced from neighboring RI beams by secondary fragmentation reaction under the assumption of a systematic cross section of ^{68}Br. Assumming this lifetime value, the cross section of ^{68}Br from ^{78}Kr beam is estimated to be $\sim 10^{-5}$ mb and is on the systematics of the neighboring nuclei. The solid, dashed, and dotted lines show the cross sections predicted by semi-empirical formulae FRACS1.1,[5] EPAX3.1a,[6] and EPAX2.15.[7] Overall, FRACS1.1 provides better agreement with the measured cross sections than the other formulae; however, around the very-neutron-deficient region, the discrepancy between the measured and predicted cross sections becomes larger. A detailed analysis is currently in progress.

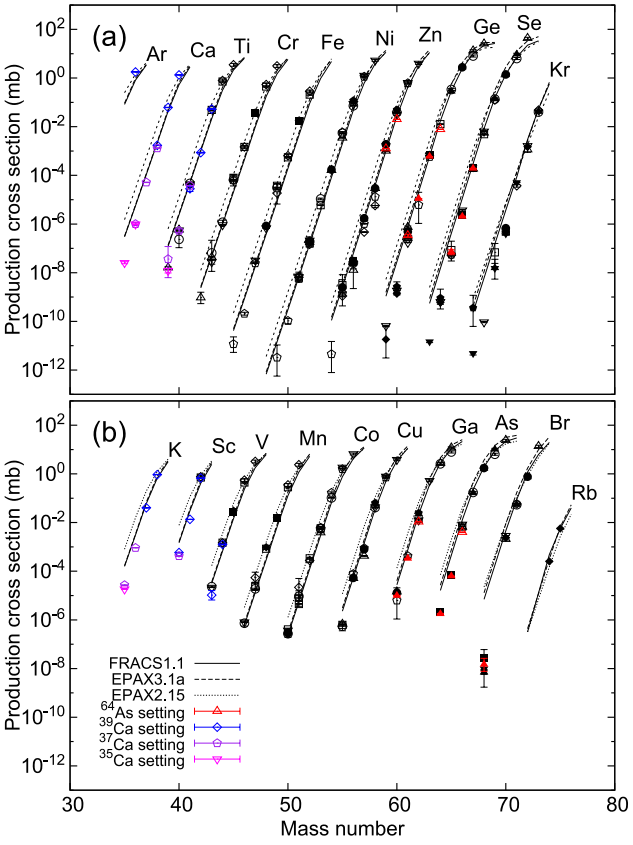

Fig. 1. (Preliminary) Measured production cross sections of RIs produced in the ^{78}Kr + Be reaction at 345 MeV/nucleon with semi-empirical cross-section formulae: (a) results for even-Z isotopes; (b) results for odd-Z isotopes.

References
1) N. Fukuda *et al.*, Nucl. Instrum. Methods Phys. Res. B **317**, 323 (2013).
2) O. B. Tarasov *et al.*, LISE^{++} site, Michigan State University, `https://lise.nscl.msu.edu`.
3) O. B. Tarasov, Nucl. Phys. A **734**, 536 (2004).
4) K. Wimmer *et al.*, Phys. Lett. B **795**, 266 (2019).
5) B. Mei, Phys. Rev. C **95**, 034608 (2017).
6) K. Sümmerer, Phys. Rev. C **86**, 014601 (2012).
7) K. Sümmerer *et al.*, Phys. Rev. C **61**, 034607 (2000).

*1 RIKEN Nishina Center

Production cross-section measurements of neutron-rich nuclei in the northeast region of ^{132}Sn by the in-flight fission of a ^{238}U beam at 345 MeV/nucleon

Y. Shimizu,[*1] N. Fukuda,[*1] H. Takeda,[*1] H. Suzuki,[*1] M. Yoshimoto,[*1] Y. Togano,[*1] N. Inabe,[*1] K. Kusaka,[*1] M. Ohtake,[*1] Y. Yanagisawa,[*1] and K. Yoshida[*1]

The systematic trends of production cross-sections are essential to predict not only the production rates of rare isotopes but also their purities and total rates. We measured the production cross-sections in the neutron-rich region with the atomic numbers Z = 49–57, located northeast of ^{132}Sn in the nuclear chart. The fission fragments produced via in-flight fission of a ^{238}U beam were separated and identified in flight using the BigRIPS separator. We ran four different separator settings, used with ^{132}Sn, ^{138}Te, ^{144}Xe, and ^{150}Ba as central particles. The particle identification (PID) was performed using the TOF-$B\rho$-ΔE method.[1] Figure 1 shows the PID plot summed over the four different separator settings.

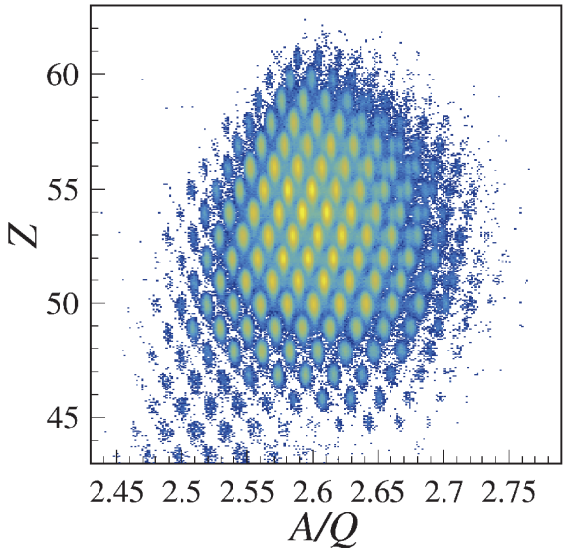

Fig. 1. PID plot for fission fragments produced in the ^{238}U+Be reaction at 345 MeV/nucleon.

Figure 2 shows the production cross-sections for each isotope as a function of mass number in this work (filled symbols) and the previous experiments[3–5] (open symbols). The measured production cross sections were derived from the measured production rates and transmission efficiencies in the BigRIPS separator, which were based on the LISE^{++} simulations.[2] The systematic uncertainty of the cross-sections is estimated to be ∼40%. The error is dominated by the uncertainties of the primary beam intensity and the transmission efficiency. Our results are in good agreement with previous ones. The blue solid lines show the cross-sections predicted using the LISE^{++} abrasion fission (AF) model.[2] The measured cross-sections have plateaued as the mass number decreases, and the AF model predictions reproduce those in this region fairly well. On the other hand, the AF model predictions underestimate the measured cross-sections in the very neutron-rich region.

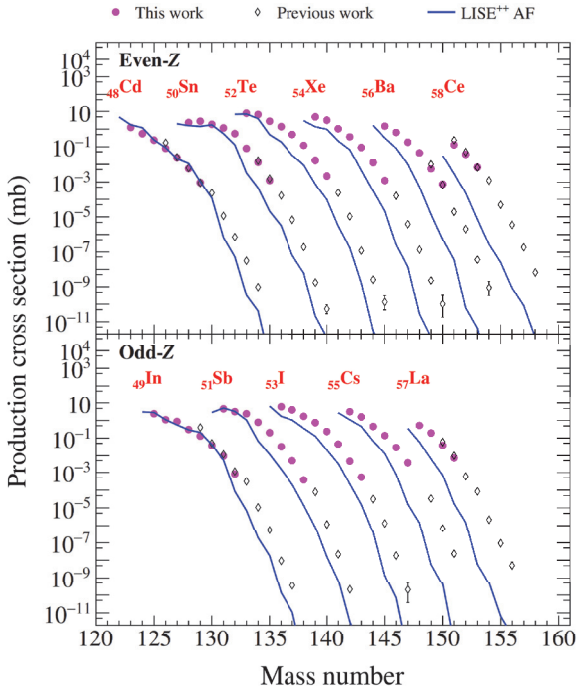

Fig. 2. Production cross-sections for each isotope from ^{238}U+Be reaction at 345 MeV/nucleon. The filled and open symbols represent the production cross-sections of this work and previous experiments,[3–5] respectively. The blue solid lines show the cross-sections predicted by the LISE^{++} AF model.[2]

Detailed analysis is currently in progress.

*1 RIKEN Nishina Center

References
1) N. Fukuda *et al.*, Nucl. Instrum. Methods Phys. Res. B **317**, 323 (2013).
2) O. B. Tarasov *et al.*, Nucl. Instrum. Methods Phys. Res. B **266**, 4657 (2013).
3) T. Ohnishi *et al.*, J. Phys. Soc. Jpn. **79**, 073201 (2010).
4) Y. Shimizu *et al.*, J. Phys. Soc. Jpn. **87**, 014203 (2018).
5) N. Fukuda *et al.*, J. Phys. Soc. Jpn. **87**, 014202 (2018).

Production of ^{237}Np from ^{238}U beam at BigRIPS

C. Fukushima,[*1,*2] R. Matsumura,[*2,*3] D. Nishimura,[*1,*2] H. Otsu,[*2] H. Wang,[*4] H. Baba,[*2] N. Fukuda,[*2] T. Isobe,[*2] K. Kokubun,[*5,*2] M. Kurata-Nishimura,[*2] S. Meigo,[*6] T. Nishi,[*2] H. Sakurai,[*2] M. Sasano,[*2] H. Sato,[*2] Y. Shimizu,[*2] T. Sumikama,[*2] H. Suzuki,[*2] H. Takahashi,[*1] H. Takeda,[*2] J. Tanaka,[*2] Y. Togano,[*2] K. Yoshida,[*2] and M. Yoshimoto[*2]

A variety of unstable nuclear beams with atomic numbers (Z) up to 92 can be produced by the projectile fragmentation and in-flight fission from high-intensity U beams at RIBF. Recently, it was found that $^{234-238}$Np can be created by a proton pickup reaction on 1 GeV/nucleon ^{238}U beam.[1] Owing to the recent developments of the high-Z beams at BigRIPS,[2,3] energy dependence of the proton pickup reaction on ^{238}U can be obtained at RIBF. Thus, we conducted an experiment to determine the energy dependence of the production cross section of ^{237}Np. A test of the production of Np isotopes was performed by using the BigRIPS spectrometer at RIBF in March 2022.

Secondary beams around $Z = 90$ were produced by a ^{238}U beam with energies of 345 and 250 MeV/nucleon[4] impinging on a 1-mm-thick ^{9}Be production target at F0 in BigRIPS. To reduce ambiguity of production cross section, no degraders for separation were inserted in the F1/F5 dispersive focal planes. The particle identification (PID) of the secondary beam was performed using the TOF-$B\rho$-ΔE method.[5] Plastic scintillators at F3 and F7, and parallel-plate avalanche counters (PPACs) at F3, F5, and F7 were installed, respectively. As no materials were installed at F1, charge states of ions were unchanged between F0 and F3. The configuration of the BigRIPS was optimized for the production of a ^{237}Np beam, with magnetic rigidity $B\rho$ values at D1, D2, D3-D4, and D5-D6 set to optimized for fully-stripped, fully-stripped, H-like, and He-like ^{237}Np ions, respectively. Further, newly developed ionization chamber (IC) with xenon-based gas was utilized at F7 for better separation of Z at high-Z region.[6]

Figure 1 shows a PID plot of Z vs. A/Q, with typical relative A/Q and Z resolutions of 0.057% and 0.43% in 1σ, respectively. Calibrations of A/Q and Z were conducted using primary beams of ^{238}U$^{90+,91+}$ that had passed through the 1-mm-thick Be target. Even with the new IC, the blobs, corresponding to nuclides of incoming beam, are not clearly separated. To validate the production of the ^{237}Np^{91+}, a two-dimensional (2D) Gaussian fitting approach was conducted in accordance with the distribution patterns of neighboring ions of ^{234}U^{90+}, ^{235}U^{90+}, and ^{232}Pa^{89+}. Figure 2(a) shows the experimental data and the fitted distribution by the 2D Gaussian function in color lego and red mesh, respectively. By subtracting the fitted distribution from the experimental data, the residuals were deduced and are presented in Fig. 2(b). As evident the blob of ^{237}Np^{91+} at $Z = 93$ and $A/Q = 2.604$. As shown in Fig. 2(b), it was found that ^{237}Np^{91+} can be counted up with contaminated U/Pa isotopes using the 2D Gaussian fitting technique. In the future, we plan to determine the production cross section by examining the beam amount and transport efficiency. We are also planning to analyze the data of 250 MeV/nucleon to discuss the energy dependence of the production cross section.

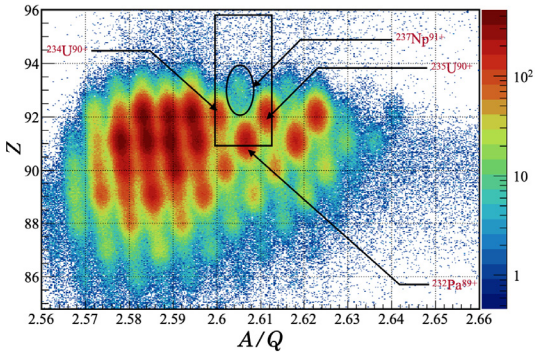

Fig. 1. Particle identification plot of Z vs. A/Q for fragments produced in the 345-MeV/nucleon ^{238}U. The box region around ^{237}Np^{91+} was used for the two-dimensional fitting approach (see Fig. 2).

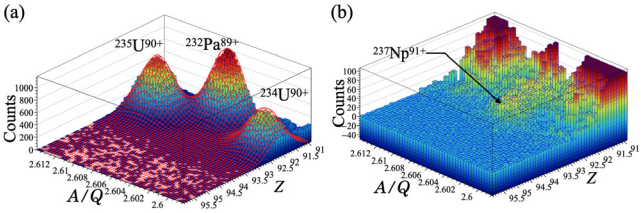

Fig. 2. (a) 3D-lego plots of PID around ^{237}Np^{91+} in the box region of Fig. 1. (b) Residual by subtracting the fitted distribution from the experimental data.

*1 Department of Natural Sciences, Tokyo City University
*2 RIKEN Nishina Center
*3 Department of Physics, Saitama University
*4 RIKEN HENP Laboratory
*5 Department of Physics, University of Tokyo
*6 Japan Atomic Energy Agency

References
1) E. Casarejos *et al.*, Phys. Rev. C **74**, 044612 (2006).
2) T. Sumikama *et al.*, Nucl. Instrum. Methods Phys. Res. B **463**, 237 (2020).
3) N. Fukuda *et al.*, RIKEN Accel. Prog. Rep. **54**, 81 (2021).
4) H. Otsu *et al.*, in this report.
5) N. Fukuda *et al.*, Nucl. Instrum. Methods Phys. Res. B **317**, 323 (2013).
6) M. Yoshimoto *et al.*, in this report.

Search for the double Gamow-Teller giant resonance using double charge exchange reaction

A. Sakaue,[*1] T. Uesaka,[*2] and K. Yako[*1] for the RIBF-141R1 Collaboration

The double Gamow-Teller (DGT) transition is the nuclear process where the spin and isospin are changed twice by a $(\sigma\tau)^2$ operator, where σ and τ are the spin and isospin operators, respectively. It is theoretically predicted that there is a giant resonance which occupies most of the whole DGT transition strength in a high-excitation energy region.[1] This resonance, called the DGT giant resonance (DGTGR), remains undiscovered experimentally. The observable of the DGTGR such as the strength or the width will provide information about the two-phonon excitations with spin-dependent correlations. In addition, it is suggested that such observables will give a constraint to the nuclear matrix element of neutrinoless double β decay, which has a large ambiguity in the current theoretical calculation.[2]

We observe DGTGR using the double charge exchange reaction (^{12}C, ^{12}Be(0_2^+)) at RIBF. We employ an experimental method developed in the pionic atoms spectroscopy[3] using a part of BigRIPS, from the F0 focal plane to the F5 focal plane, as a spectrometer. A reaction target at F0 is bombarded with the primary beam of ^{12}C and the (^{12}C, ^{12}Be(0_2^+)) reaction is induced. The momentum of the ejected particle is obtained by measuring the position at F5 and thus the excitation energy of the residual nucleus of F0 is deduced. To select events with spin-flip mode, ^{12}Be is transported to the stopper of ^{9}Be at F8 and delayed γ rays deriving from ^{12}Be(0_2^+) are detected by DALI2; ^{12}Be(0_2^+) decays into the ground state by emitting an electron-positron pair with the lifetime of 331 ± 12 ns.[4]

We successfully detected the delayed-γ rays from ^{12}Be(0_2^+) for the ^{48}Ca target at F0 in the experiment conducted at RIBF in May 2021 using this method for the first time.[5] The signal-to-background ratio is estimated to approximately 5 : 1 for the events with photons of 500 ± 100 keV detected in DALI2. It is improved from the one of the pilot experiment performed at RCNP, approximately 1 : 1.[6]

The preliminary spectrum of the position at F5 for the measurement of the ^{48}Ca target is shown in Fig. 1. Here the event selection is such that the timing of the photon is between 20 ns and 700 ns after from the timing of prompt γ-rays, and the energy is in the region of 510 ± 100 keV. Each color corresponds to the scattering angle of ^{12}Be at F0 target in the laboratory system, which is reconstructed from the position and the angle measured at F5, within 0.0–0.3° (blue line, blue hatched), 0.3–0.6° (red line, green hatched), and 0.6–0.9° (black line, black hatched). In this spectrum, the kinematical position aberration with the scattering angle is corrected for. The preliminarily calibrated energy of ^{48}Ti is shown below the figure. The energy resolution and the angular resolution was evaluated as 1.6 MeV and 0.17°, respectively. The main background is an accidental coincidence of ^{12}Be and γ rays from room backgrounds. The amount of the background is estimated to about 5% with the event selection by the gate of DALI2 described above. This background is subtracted by assuming that its energy spectrum is same as events that are not gated by DALI2. In the region of the position from -10 mm to 0 mm, which corresponds to about from 23 to 30 MeV in the excitation energy where the DGTGR is expected to be observed[2], there seem to be enhancements at -2 mm and -8 mm especially in the forward angle, though statistics are limited. The structure around -20 mm, on the other hand, is likely due to the events of the ^{12}C(^{12}C, ^{12}Be)^{12}O$_{\text{g.s.}}$ reaction from the graphene sheet attached to the ^{48}Ca target.

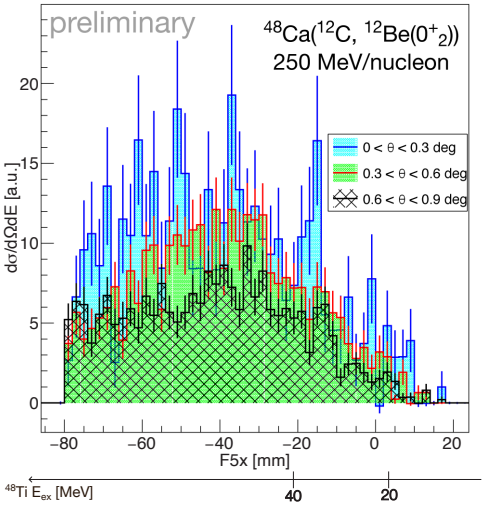

Fig. 1. Preliminary result of position measured at F5. Line and hatching colors correspond to selected regions of scattering angles: 0–0.3° (blue line, blue hatched), 0.3–0.6° (red line, green hatched), and 0.6–0.9° (black line, blacked hatched).

In order to interpret the structure, we are now working on the comparison of the angular distribution with the calculated ones.

References
1) N. Auerbach *et al.*, Annu. Phys. **192**, 77 (1989).
2) N. Shimizu *et al.*, Phys. Rev. Lett. **120**, 142502 (2018).
3) T. Nishi *et al.*, Nucl. Instrum. Method Phys. Res. B **317**, 290 (2013).
4) S. Shimoura *et al.*, Phys. Lett. B **654**, 87 (2007).
5) A. Sakaue *et al.*, RIKEN Accel. Prog. Rep. **55**, 9 (2022).
6) M. Takaki *et al.*, CNS Annu. Rep. 2016, CNS-REP-**96**, 3 (2018).

*1 Center for Nuclear Study, University of Tokyo
*2 RIKEN Nishina Center

Retracted on February 1, 2024

RIKEN Accel. Prog. Rep. 56 (2023)

Development of dispersion matching optics in OEDO beamline

S. Hanai,[*1] S. Michimasa,[*1] T. Chillery,[*1] S. Ota,[*1] N. Imai,[*1] S. Shimoura,[*1] N. Fukuda,[*2] Y. Hijikata,[*3,*2] K. Kameya,[*4,*2] S. Kitayama,[*4,*2] K. Kishimoto,[*5,*2] K. Kusaka,[*2] J. Li,[*1] Y. Maeda,[*6,*2] Y. Maruta,[*4,*2] T. Matsui,[*4,*2] K. Miki,[*4,*2] D. Nagae,[*2] H. Nishibata,[*5,*2] D. Nishimura,[*7,*1,*2] M. Sasano,[*2] Y. Shimizu,[*2] S. Sugawara,[*2] T. Sumikama,[*2] H. Suzuki,[*2] H. Takahashi,[*7] H. Takeda,[*2] T. Uesaka,[*2] R. Urayama,[*4,*2] T. Wakasa,[*5] K. Yako,[*1] Y. Yamaguchi,[*2] Y. Yanagisawa,[*2] N. Yokota,[*5,*2] C. Yonemura,[*5,*2] and K. Yoshida[*2]

The Optimized Energy Degrading Optics (OEDO) beamline provides potential opportunities to perform nuclear physics experiments with spatially and achromatically well-focused low-energy RI beams[1] or high momentum resolution by selecting a suitable ion transportation method. High-quality low-energy RI beam production has been achieved.[2] Recently, several beamline magnets in the OEDO beamline were rearranged aiming at the realizing a high momentum resolution. To conduct nuclear spectroscopy with a resolution greater than the energy width of the incident beam, lateral and angular momentum dispersion matching techniques are essential. Figure 1 shows a designed dispersion matching ion optics from BigRIPS F3 to SHARAQ S2 foci through the OEDO beamline. The S0 intermediate focus, where a target will be inserted in a future experiment, has the largest momentum dispersion in the beamline of 14.7 m, and this momentum dispersion vanishes at the final focus, S2. We report here a study showing dispersion matching optics of the OEDO beamline.

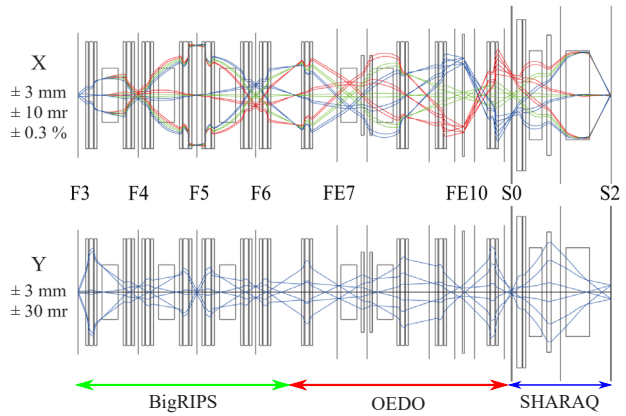

Fig. 1. Trajectories of ion beam with dispersion matching setting in BigRIPS-OEDO-SHARAQ beamline. Trajectories are calculated from first-order matrix elements.

We performed the study using an 82 MeV/nucleon triton beam produced by the BigRIPS separator from the 200 MeV/nucleon ^{4}He primary beam. Position detectors, a parallel-plate avalanche counter and a low-pressure multiwire drift chamber, were placed at the foci from F3 to S2, to measure the transfer matrix elements at each focal plane. We verified the consistency of the measured matrix elements by comparison with ion optics calculation results.

By evaluating the matrix elements, the momentum dispersion at S0 was deduced as 16.3 m, which corresponds to a dispersion of 0.025 mm/% and satisfies the lateral dispersion matching condition with the SHARAQ spectrometer. Figure 2(a) shows that there is no correlation between the horizontal position (momentum dispersion) at S0 and that at S2 and therefore, the condition of momentum dispersion matching is fulfilled. Figure 2(b) shows the correlation between the horizontal position (momentum dispersion) at S0 and the horizontal angle at S2, which suggests that angular dispersion matching is efficiently satisfied. We conclude that angular momentum dispersion matching is also achieved at S2.

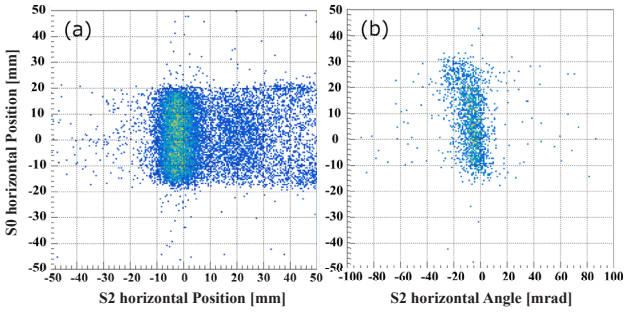

Fig. 2. (a) Correlation between S0 and S2 horizontal positions. (b) Correlation between S0 horizontal position and S2 horizontal angle. (a|δ) term is approximately 0.4 mrad/%.

Consequently, we achieved dispersion matching ion transportation through the OEDO beamline. Using this ion-optical mode, we plan to conduct an approved experimental program of direct mass measurements of very rare RI nuclei.

*1 Center for Nuclear Study, University of Tokyo
*2 RIKEN Nishina Center
*3 Department of Physics, Kyoto University
*4 Department of Physics, Tohoku University
*5 Department of Physics, Kyushu University
*6 Faculty of Engineering, University of Miyazaki
*7 Department of Natural Sciences, Tokyo City University

References

1) S. Michimasa *et al.*, Prog. Theor. Exp. Phys. **2019**, 043D01 (2019).
2) S. Michimasa *et al.*, CNS Annu. Rep. 2018, CNS, REP-98-35 (2020).

Single-particle states in *fp-shell* nuclei through ^{50}Ca$(d,p)^{51}$Ca transfer reaction

C. Ferrera,[*1] K. Wimmer,[*2,*3] D. Suzuki,[*3] N. Imai,[*4] M. Armstrong,[*5] T. Chillery,[*4] Y. Cho,[*6] M. Dozono,[*3,*7] F. Endo,[*8,*3] S. Escrig,[*1] N. Fukuda,[*3] T. Haginouchi,[*3,*8] S. Hanai,[*4] S. Hayakawa,[*4] Y. Hijikata,[*3,*7] J. W. Hwang,[*6] S. Ishio,[*3,*8] A. Jungclaus,[*1] A. Kasagi,[*9,*10] K. Kawata,[*4] N. Kitamura,[*4] R. Kojima,[*4] J. Li,[*4] S. Masuoka,[*4] S. Michimasa,[*4] B. Moon,[*6] K. Okawa,[*4] S. Ota,[*4,*11] T. Saito,[*4] H. Sakurai,[*3] Y. Shimizu,[*3] S. Shimoura,[*3,*4] Y. Son,[*6] T. Sumikama,[*3] H. Suzuki,[*3] H. Takeda,[*3] Y. Togano,[*3] J. Vesic,[*12] K. Yako,[*4] R. Yokoyama,[*4] K. Yoshida,[*3] and M. Yoshimoto[*3]

Neutron-rich Ca isotopes towards neutron number $N = 34$ are pivotal for exploring the evolution of the fp-shell orbitals. Beyond the $N = 28$ shell gap in ^{48}Ca, new magic numbers at $N = 32$ and 34 were established through spectroscopy of low-lying states and mass measurements. Most recently, the spatial extension of the $1f_{7/2}$ and $2p_{3/2}$ neutron orbitals was determined via a one-neutron knockout reaction from ^{52}Ca.[1] However, the single-particle $2p_{1/2}$ and $1f_{5/2}$ orbitals defining the shell gaps at $N = 32, 34$ remain to be established experimentally. The one-neutron transfer reaction is an experimental method well-suited to study low-spin single-particle orbitals. The cross section of this reaction gives access to the spectroscopic factors, while the angular distribution of the reaction products allows for deduction of the angular momentum transfer.

In December 2022, the SHARAQ12 experiment was performed at RIKEN, aiming to study the single-particle structure of ^{51}Ca via the (d,p) transfer reaction using an energy-degraded secondary ^{50}Ca beam. The beam was produced at BigRIPS from a primary ^{70}Zn beam at an energy of 345 MeV/nucleon fragmented on a Be target. For the energy degrading procedure, the ^{50}Ca beam was conducted to the OEDO[2] beamline, where a combination of an angle-tunable wedge-shaped degrader and an additional aluminum flat-plate degrader placed at FE9 successfully reduced the beam energy to approximately 15 MeV/nucleon, which improves the momentum matching of the reaction compared to the typical beam energies at RIBF. Particle identification based on the ToF-$B\rho$ method showed excellent isotope separation, is shown in Fig. 1, where the ^{50}Ca beam can be clearly identified. Therefore, the use of the Radio-Frequency Deflector (RFD) of OEDO was not required. The secondary target of CD_2 (260 μg/cm^2) was placed at the SHARAQ spectrometer reaction chamber with the purpose of inducing one-neutron transfer reactions. The recoiling protons were measured with the detector setup TINA2,[3] consisting of a box of four TTT double-sided silicon strip detectors backed by CsI crystals and a backward annular YY1-type silicon strip detector array with CsI crystals behind. The array was placed at laboratory backward direction covering θ_{lab} = 95–165 deg (solid angle 35% of 4π) which is the angular range most sensitive to the angular momentum transfer of the reaction. The excitation energy of states populated will be determined from the measured missing mass of the reaction. Heavy ^{51}Ca ejectiles were measured by the QQD spectrometer equipped with a set of Strip-Readout PPAC detectors and an ionization chamber, so background coming from fusion reactions can be suppressed via charge identification. The analysis of excitation energies and angular distributions is ongoing.

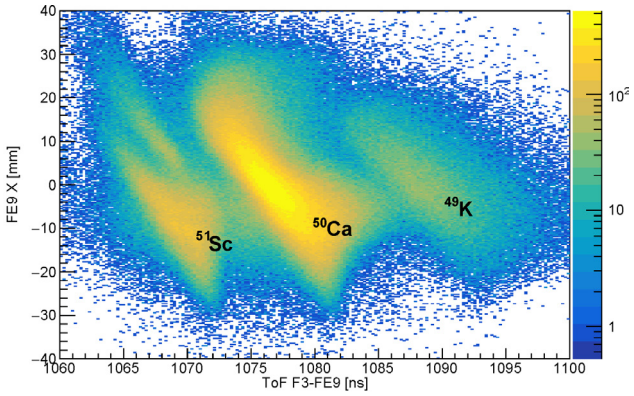

Fig. 1. Particle identification in OEDO with horizontal position at FE9 and corrected time-of-flight between F3 and FE9.

*1 Instituto de Estructura de la Materia, CSIC
*2 GSI Helmholtzzentrum für Schwerionenforschung GmbH
*3 RIKEN Nishina Center
*4 Center for Nuclear Study, University of Tokyo
*5 Institute of Nuclear Physics, University of Cologne
*6 CENS Institute for Basic Science
*7 Department of Physics, Kyoto University
*8 Department of Physics, Tohoku University
*9 Department of Physics, Gifu University
*10 RIKEN Cluster for Pioneering Research
*11 Research Center for Nuclear Physics, Osaka University
*12 Department of Low and Medium Energy Physics, Jožef Stefan Institute

References

1) M. Enciu *et al.*, Phys. Rev. Lett. **129**, 262501 (2022).
2) S. Michimasa *et al.*, Prog. Theor. Exp. Phys. **2019**, 043D01 (2019).
3) P. Schrock *et al.*, RIKEN Accel. Prog. Rep. **51**, 20 (2018).

Study of νp-process nucleosynthesis at OEDO

D. Suzuki,[*1] B. Mauss,[*2] N. Imai,[*3] S. Michimasa,[*3] D. Beaumel,[*4,*1] K. Y. Chae,[*5] S. Cherubini,[*6] T. Chillery,[*3] M. Dozono,[*7,*1] M. Egeta,[*8,*1] F. Endo,[*8,*1] N. Fukuda,[*1] T. Haginouchi,[*8,*1] S. Hanai,[*3] S. Hayakawa,[*3] Y. Hijikata,[*7,*1] J. W. Hwang,[*9] S. Ishio,[*8,*1] N. Iwasa,[*8,*1] S. Kawase,[*10,*1] K. Kawata,[*3] R. Kojima,[*3] S. Kubono,[*1] M. La Cognata,[*6] J. Li,[*3] N. Nishimura,[*1] K. Okawa,[*3] M. Oishi,[*10,*1] H. J. Ong,[*11,*1,*12] S. Ota,[*12] S. Palmerini,[*13,*14] R. Pizzone,[*6] T. Saito,[*3] H. Sakurai,[*1] S. Shimoura,[*3,*1] Y. Shimizu,[*1] T. Sumikama,[*1] H. Suzuki,[*1] H. Takeda,[*1] H. Tanaka,[*15,*1] M. Tanaka,[*1] X. Tang,[*12] T. Teranishi,[*15,*1] Y. Togano,[*1] A. Tunimo,[*6] Y. Wang,[*16] K. Yako,[*3] K. Yahiro,[*7,*1] H. Yamaguchi,[*3] R. Yokoyama,[*3] K. Yoshida,[*1] R. Yoshida,[*7,*1] and M. Yoshimoto[*1]

Neutron-deficient stable isotopes, referred to as p-nuclei, are known to be produced by p process nucleosynthesis. However, certain lighter p-nuclei, *e.g.* Mo and Ru, are significantly underproduced in the present astrophysical scenario. The νp process[1] ascribes their origin to core-collapse supernovae, wherein the availability of neutrons aids the flow to bypass the waiting point ^{56}Ni on the synthesis path. The neutron capture cross section of ^{56}Ni, howeve, remains experimentally unknown because both the neutron and ^{56}Ni are short-lived. To evaluate the cross sections, we applied the surrogate method[2] to the (d, p) reaction by using an energy-degraded ^{56}Ni beam at OEDO.

The experiment was performed at the OEDO beam line of RIBF. The secondary beam was produced by the projectile fragmentation reaction of a ^{78}Kr beam at 345 MeV/nucleon and purified by the BigRIPS fragment separator. The total beam intensity at F3 was measured to be about 500 kpps (particles per second) with a purity of about 30% for ^{56}Ni. The impurities included ^{55}Co (50%) and ^{54}Fe (10%), both isotones of ^{56}Ni with $N = 28$. The energy of ^{56}Ni transmitted from BigRIPS to OEDO was about 113 MeV/nucleon. The beam energy was degraded at FE9 by an angle-tunable wedge-shaped degrader (3 mm in central thickness) together with a flat degrader (0.3 mm in thickness),[3] both made of aluminum. The angle of the former was set to 4 mrad to obtain a desired beam energy. The beam energy of ^{56}Ni was estimated to be 15.1(10) MeV/nucleon based on the time of flight measurement from FE9 to FE12. The RF deflector at FE10 was operated at 100 kV to reduce the spot size of ^{56}Ni. The phase shift of RF was optimized to increase the transmission through the target frame aperture of 50 mm in diameter (Fig. 1). The transmission from F3 to FE12 was about 75% with a total rate of 370 kpps at FE12. CD_2 targets of 285 and 644 μg/cm^2, provided by INFN, were set at S0 about 1 m downstream of FE12. The incident position and angle of the secondary beam were deduced by a pair of SR-PPACs[4] in the vacuum chamber of FE12. The recoiling protons were detected by the silicon and CsI detectors array TiNA.[5] Missing mass spectra are deduced from the scattering angle and total kinetic energy measured by TiNA. The scattered particles were transmitted to a QQD spectrometer at zero degrees for the particle identification, which facillitated the determination of the decay channels. The spectrometer was equipped with a pair of SR-PPACs followed by an ionization chamber with CF_4 gas at 100 Torr. The transmission through the spectrometer was roughly 50%.

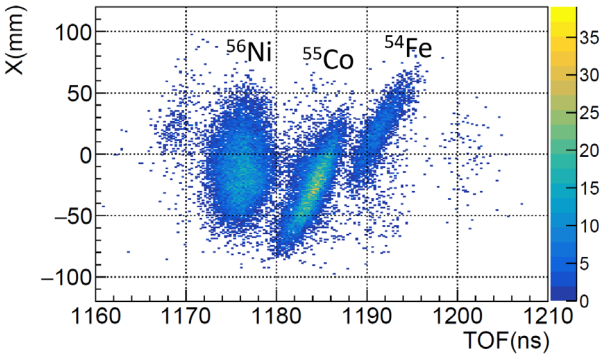

Fig. 1. Horizontal position at S0 vs. TOF from F3 to FE9 of the secondary beam with the optimal RF settings.

The data analysis is underway. The current focus is directed towards the beam tracking detectors.

*1 RIKEN Nishina Center
*2 CEA-DAM
*3 Center for Nuclear Study, University of Tokyo
*4 IJClab, IN2P3, CNRS
*5 Department of Physics, Sungkyunkwan Unviversity
*6 INFN Laboratori Nazionali del Sud
*7 Department of Physics, Kyoto University
*8 Department of Physics, Tohoku University
*9 CENS, Institute for Basic Science
*10 IGSES, Kyushu University
*11 Institute of Modern Physics, Chinese Academy of Sciences
*12 Research Center for Nuclear Physics, Osaka University
*13 INFN Sezione di Perugia
*14 Department of Physics, University of Perugia
*15 Department of Physics, Kyushu University
*16 Department of Physics, Tsinghua University

References

1) C. Fröhlich *et al.*, Phys. Rev. Lett. **96**, 142502 (2006).
2) N. Imai *et al.*, submitted to Phys. Lett. B.
3) J. W. Hwang *et al.*, RIKEN Accel. Prog. Rep. **53**, 16 (2020).
4) S. Hanai, Master thesis, University of Tokyo (2021).
5) B. Mauss *et al.*, RIKEN Accel. Prog. Rep. **54**, 114 (2021).

Study of ^{130}Sn(d,p) reaction in inverse kinematics for r-process nucleosynthesis

N. Imai,[*1] S. Michimasa,[*1] T. Chillery,[*1] D. Suzuki,[*2] D. S. Ahn,[*3] A. Chae,[*4] S. Cherubini,[*5] M. La Cognata,[*6] M. Dozono,[*7,*2] M. Egeta,[*8,*2] F. Endo,[*8,*2] N. Fukuda,[*2] T. Haginouchi,[*8,*2] S. Hanai,[*1] S. Hayakawa,[*1] J. W. Hwang,[*3] Y. Hijikata,[*2,*7] S. Ishio,[*8,*2] N. Iwasa,[*8,*2] K. Kawata,[*1] S. Kubono,[*2] R. Kojima,[*1] L. Lamia,[*5] J. Li,[*1] N. Nishimura,[*2] K. Okawa,[*1] H. J. Ong,[*9,*10,*2] S. Ota,[*10] S. Palmerini,[*11] R. G. Pizzone,[*6] T. Saito,[*1] Y. Shimizu,[*2] S. Shimoura,[*1,*2] T. Sumikama,[*2] H. Suzuki,[*2] H. Takeda,[*2] A. Tumino,[*12,*6] X. Tang,[*9] H. Tanaka,[*13,*2] M. Tanaka,[*2] T. Teranishi,[*13,*2] Y. Togano,[*2] R. Yokoyama,[*1] R. Yoshida,[*6,*2] K. Yoshida,[*2] M. Yoshitomo,[*2] Y. Wang,[*14] and Z. Xiao[*14]

The r-process nucleosynthesis is a major origin of heavy elements beyond iron. Because of rich neutrons in explosive astrophysical conditions, neutron-rich radioactive isotopes (RIs) are involved in the r-process. Though the scenario of the r-process was proposed more than fifty years ago, the astrophysical sites of the r-process are still one of the biggest problems in physics. Nucleosynthesis simulations require precise nuclear-physics inputs such as β decay rates, masses of the nuclei, and neutron capture rates, which can constrain the astrophysical conditions. However, as the neutron targets are not available yet, it is impossible to measure the capture cross sections and related rates directly. In the case of the compound neutron-capture rates, since there are significant uncertainties in the level density of the unbound state and the γ emission probability from the highly excited state, the cross sections differ by more than one order of the magnitude even in the statistical model calculations.

We have evaluated the neutron capture reaction rate on ^{79}Se with the surrogate reaction of ^{79}Se(d,p) in inverse kinematics, where the γ emission probabilities in the unbound states of ^{80}Se have been determined by measuring the residual nuclei without detecting the γ rays.[1)] The present study aims to determine the neutron capture rate on ^{130}Sn via (d,p) reaction with a ^{130}Sn beam. In addition, to evaluate the systematic error of the method, (d,p) reactions on ^{130}Te and ^{124}Sn were also measured.

The experiment was conducted at the OEDO beamline at RIBF. The cocktail beam including ^{130}Sn was produced by the in-flight fission of ^{238}U at 345 MeV/nucleon. The energy of the beam from F3 to FE9 was chosen to be around 170 MeV/nucleon. RI beams were identified by the $B\rho$-TOF method. Figure 1 shows the particle identification (PID) map of the secondary beam, demonstrating that ^{130}Sn beam is well separated from the other isotopes. Thanks to the new optics developed in the MS22-1 and described elsewhere in this volume, the transmission between F3 and FE9 was improved to be 85% for the beam with the F1 momentum slit of ±0.5%. The energy of the cocktail beam was further degraded to 20 MeV/nucleon by a combination of the angle-tunable degrader and a flat degrader.

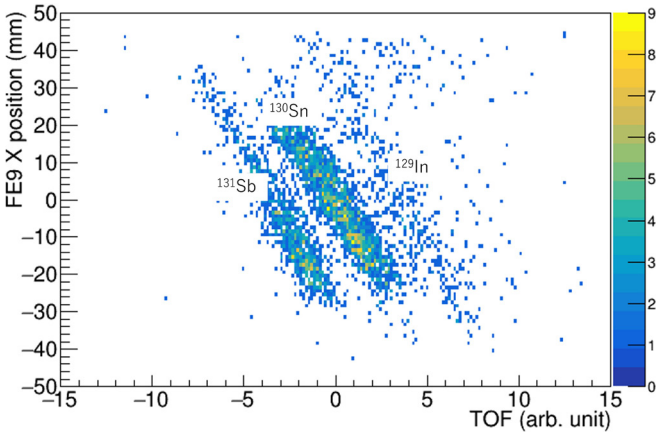

Fig. 1. PID map of the secondary beams at FE9. See the text for details.

The ^{130}Sn beam of around 150 kcps was focused on the secondary target of 287 μg/cm^2-thick deuterated polyethylene. The recoil protons were detected by the TiNA2 array which was composed of four TTT double-sided square-shape Si detectors, six YY1 single-sided sector-shape Si detectors, and sixteen CsI(Tl) detectors. The four CsI(Tl) were placed behind each TTT to measure the ΔE-E correlation of the charged particles. The outgoing residual nuclei were momentum-analyzed by the D1 magnet of the SHARAQ spectrometer. Two SR-PPACs and an ionization chamber were installed at the final focal plane to identify the residual nuclei. Analysis of the data is on going.

*1 Center for Nuclear Study, University of Tokyo
*2 RIKEN Nishina Center
*3 CENS, Institute for Basic Science
*4 Department of Physics, Sonkyunkwan University
*5 Department of Physics and Astronomy, University of Catania
*6 INFN, LNS
*7 Department of Physics, Kyoto University
*8 Department of Physics, Tohoku University
*9 Nuclear Physics Div. Institute of Modern Physics
*10 Research Center for Nuclear Physics, Osaka University
*11 INFN sezione di Perugia
*12 Faculty of Engineering and Architecture, Kore University of Enna
*13 Department of Physics, Kyushu University
*14 Department of Physics, Tsinghua University

Reference

1) N. Imai *et al.*, submitted to Phys. Lett. B.

Toward the mass measurement of neutron-rich nuclei in the vicinity of $N = 126$ isotones with SLOWRI/ZD-MRTOF

H. Ishiyama,[*1] M. Wada,[*3] A. Takamine,[*1] M. Rosenbusch,[*3] J. M. Yap,[*1,*6] V. H. Phong,[*1] S. Nishimura,[*1] S. Iimura,[*1,*2] D. Hou,[*4,*3,*5] S. Chen,[*3,*6] J. Liu,[*4] W. Xian,[*3,*6] S. Yan,[*7,*3] P. Schury,[*3] S. Kimura,[*1] T. Niwase,[*1,*3] Y. Ito,[*9] T. Sonoda,[*1] T. M. Kojima,[*1] Y. X. Watanabe,[*3] Y. Hirayama,[*3] H. Miyatake,[*3] S. Naimi,[*1] S. Michimasa,[*10] A. Odahara,[*2] and S. Kubono[*1,*10]

Despite the first observation of an r-process production site (GW170817) in 2017, confirming neutron-star mergers as probably the most important site, many open questions remain to understand r-process nucleosynthesis fully. A major unanswered question is whether neutron star merger r-process products alone can explain the observed large scatter of Eu/Fe and other r-process elements at [Fe/H] < 3 metalicites.[1] The shape and position of the 3rd peak on r-process element abundances would serve as an anchor point to confirm the reproducibility of the element abundances in the reaction network calculations when investigating an astrophysical site for r-process nucleosynthesis. However, there is no experimental data for nuclear physics inputs such as masses, half-lives, and neutron branching ratios in the vicinity of $N = 126$ waiting point nuclei, which critically affect the formation of the 3rd peak.[2] Therefore, direct mass measurement of neutron-rich nuclei in the vicinity of $N = 126$ waiting point nuclei, which are considered to be the progenitors for the 3rd peak formation, is strongly desired.

RIBF199 experiment was performed to measure the masses of these nuclides with MRTOF in combination with an RF carpet type He gas cell (RFGC) of SLOWRI installed at F11 of BigRIPS (ZD-MRTOF).[3] No neutron-rich nuclei in this region were observed with ZD-MRTOF during the beam time. There are two possible reasons why we could not observe any RIs. One possible reason was the 'low' extraction efficiency from the RFGC. Unfortunately, the ion guide was found to be defective. Therefore, the RFGC chamber was opened, and the ion guide replaced just before the beamtime. We had no sufficient baking time to suppress contaminant molecules which reduces the extraction efficiency due to various molecular formations of RI atoms. After our beamtime, the RFGC was long baked for about 10 days. Then, the extraction efficiency was examined using a ^{248}Cm fission source installed inside the RFGC. The extraction efficiencies after stopping inside RFGC for the fission fragments such as Tc and Mo have been recovered to be roughly 10%.

The second and most important reason is that yields on RIs of interest provided by BigRIPS were too low. Figure 1 shows the intensities of RIs measured in this region using BigRIPS/ZDS detectors. As shown in Fig. 1, almost measured intensities for RIs of interest are 10^{-2} pps or less, roughly two orders of magnitude lower than expected values estimated with LISE++. The production yield from uranium beam fragmentation seems insufficient to measure the masses in this region, even if the extraction efficiency is recovered.

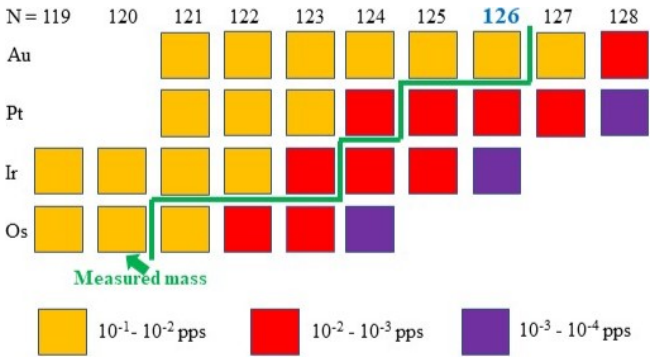

Fig. 1. Measured yields for RIs of interest at F11. The production reaction is ^{238}U + ^{9}Be with the beam energy of 345 MeV/nucleon and the intensity of 70 particle nA.

We are currently considering using lead beam fragmentation to produce RIs in this region. In the southwest part of $N = 126$ down to $Z = 70$, higher production cross-sections are expected to be obtained with ^{208}Pb beam than with ^{238}U beam.[4] A Letter of Intent was submitted to NP-PAC 2022 to request the development of a Pb beam at RIBF, and the PAC "enthusiastically endorsed" it. We hope to continue the experiment with the Pb beam.

*1 RIKEN Nishina Center
*2 Department of Physics, Osaka University
*3 Wako Nuclear Science Center (WNSC), IPNS, KEK
*4 Institute of Modern Physics, Chinese Academy of Science
*5 School of Nuclear Science and Technology, Lanzhou University
*6 Department of Physics, University of Hong Kong
*7 Institute of Mass Spectrometer and Atmospheric Environment, Jinan University
*8 Department of Physics, Kyushu University
*9 Advances Science Research Center, Japan Atomic Energy Agency
*10 Center for Nuclear Study, University of Tokyo

References

1) J. J. Cowan *et al.*, Rev. Mod. Phys. **93**, 015002 (2021).
2) M. R. Mumpower *et al.*, Prog. Part. Nucl. Phys. **86**, 86 (2016).
3) M. Rosecbusch *et al.*, Nucl. Instrum. Methods Phys. Res. A **1047**, 167824 (2023).
4) T. Kurtukian-Nieto *et al.*, Phys. Rev. C **89**, 024616 (2014).

Q-moment measurement of isomeric state of ^{99}Zr using spin-aligned beam

Y. Shinohara,[*1,*2] Y. Ichikawa,[*1,*2] S. Go,[*2] H. Nishibata,[*1,*2] S. Ando,[*1,*2] K. Asahi,[*2] H. Baba,[*2] N. Fukuda,[*2] G. Georgiev,[*2,*3] A. Gladkov,[*2] K. Imamura,[*2] K. Kishimoto,[*1,*2] R. Lozeva,[*2,*3] M. Mukai,[*2] M. Niikura,[*2] Nurhafiza M. Nor,[*2,*4] A. Odahara,[*2,*4] Y. Shimizu,[*2] M. Si,[*2,*3] K. Stoychev,[*3] H. Suzuki,[*2] M. Tajima,[*2] A. Takamine,[*2] H. Takeda,[*2] S. Takeshige,[*2,*5] M. Tanaka,[*2] Y. Togano,[*2] H. Ueno,[*2] T. Wakasa,[*1,*2] W. Yamashita,[*1,*2] H. Yamazaki,[*2] M. Yoshimoto,[*2] and J. M. Daugas[*2,*6]

The ^{99}Zr nucleus with a neutron number $N = 59$ is located at the border of a region where a sudden onset of ground-state deformation occurs for Zr isotopes between $N = 58$ and 60.[1)] This change has been described as a quantum phase transition (QPT) with the neutron number as a control parameter. The ^{99}Zr nucleus closest to the critical point of the QPT has an isomer (^{99m}Zr) with a spin parity of $7/2^+$ at 252 keV. A recent measurement of its magnetic moment showed a surprising result. Namely, the $7/2^+$ state is not of single-particle-like nature but rather collective.[2)] To confirm this collectivity directly, measurement of the quardupole (Q) moment of the same isomer was conducted.

The experiment was conducted at BigRIPS at RIBF in April 2022. The two-step fragmentation scheme with the momentum-dispersion matching technique[3,4)] was employed to produce a highly spin-aligned beam of ^{99}Zr. First, ^{100}Zn was produced by a fission reaction of a 345-MeV/nucleon ^{238}U beam on a ^{9}Be target with a thickness of 1.29 g/cm^2. The secondary ^{100}Zr beam was impinged to a second target of wedge-shaped aluminum with a mean thickness of 0.810 g/cm^2 and a wedge angle of 2.65 mrad, placed at the momentum-dispersive focal plane F5. The ^{99}Zr nuclei, including those in isomeric state ^{99m}Zr, were produced through one-neutron removal from ^{100}Zr. The tertiary ^{99}Zr beam was subsequently transported to F7 while matching the momentum dispersion of ^{99}Zr in F5–F7 to that of ^{100}Zr in F3–F5. F7 slits with a width of ±10 mm were used to extract the region around the center of the momentum distribution for ^{99}Zr.

Prior to the Q-moment measurement, the magnitude of spin alignment realized in ^{99m}Zr was checked by the time-differential perturbed angular distribution (TDPAD) methods. The TDPAD apparatus, placed at F8, consisted of a dipole magnet, Cu crystal stopper, Ge detectors, and plastic scintillator. The dipole magnet provided a static magnetic field of $B_0 = 0.200$ T. ^{99m}Zr was implanted into the Cu stopper, and γ rays were detected with four Ge detectors placed on a plane perpendicular to B_0 at angles of ±45 and ±135 degrees with respect to the beam axis. A plastic scintillator with a thickness of 0.1 mm was placed upstream of the stopper to provide the time-zero trigger.

The $R(t)$ ratio, which represents the change of the γ ray's anisotropy synchronized with the spin precession, associated with the 130-keV γ ray deexciting ^{99m}Zr was obtained, as shown in Fig. 1. Preliminarily, the magnitude of spin alignment realized in this measurement was found to be approximately 10%.

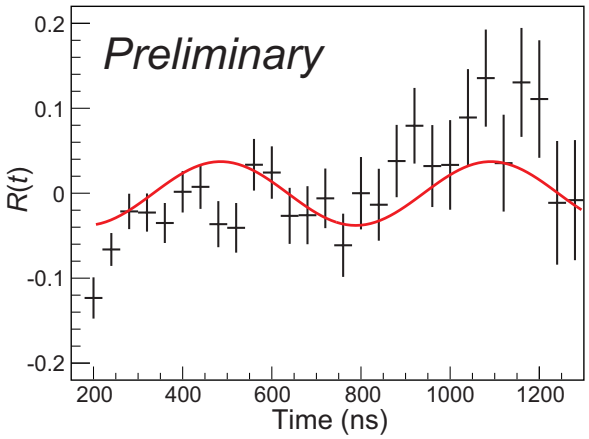

Fig. 1. $R(t)$ ratio associated with the 130-keV γ ray deexciting ^{99m}Zr under a static magnetic field. The magnitude of spin alignment was deduced from the amplitude of the ocscillation.

For the Q moment measurement, the interaction between the Q moment and electric-field gradient in a single crystal of zyrconium metal was used to apply the TDPAD method. The zyrconium crystal was set so that the crystal axis was perpendicular to both the beam axis and detector plane. The ^{99}Zr beam collimated to 10 mm ϕ was implanted into the stopper crystal. Three Ge detectors were arranged at angles of 0 and ±90 degrees with respect to the beam axis. Data analysis on the Q-moment measurement is in progress.

*1 Department of Physics, Kyushu University
*2 RIKEN Nishina Center
*3 IJCLab, CNRS/IN2P3, Université Paris-Saclay
*4 Department of Physics, Osaka University
*5 Department of Physics, Rikkyo University
*6 Institut Laue-Langevin

References

1) P. Campbell *et al.*, Phys. Rev. Lett. **89**, 082501 (2002).
2) F. Boulay *et al.*, Phys. Rev. Lett. **124**, 112501 (2020).
3) Y. Ichikawa *et al.*, Nat. Phys. **8**, 918 (2012).
4) Y. Ichikawa *et al.*, Nat. Phys. **15**, 321 (2019).

In-beam γ-ray spectroscopy of exotic ^{79}Cu with HiCARI

M. Kaci,[*1] S. Franchoo,[*1] R. Taniuchi,[*3,*2] D. Suzuki,[*2] N. Aoi,[*4,*2] H. Baba,[*2] F. Browne,[*2] C. M. Campbell,[*5] S. Chen,[*3,*6] R. Crane,[*3,*2] H. L. Crawford,[*5] H. De Witte,[*7,*2] P. Doornenbal,[*2] C. Fransen,[*8] N. Fukuda,[*2] H. Hess,[*8,*2] E. Ideguchi,[*4,*2] S. Iwazaki,[*4,*2] J. Kim,[*9] A. Kohda,[*4,*2] T. Koike,[*10,*2] T. Koiwai,[*11,*2] B. Mauss,[*2] R. Mizuno,[*11,*2] B. Moon,[*2] M. Niikura,[*11,*2] D. Nishimura,[*12,*2] T. Parry,[*13,*2] M. Petri,[*3] P. Reiter,[*8] H. Sakurai,[*11,*2] Y. Shimizu,[*2] H. Suzuki,[*2] H. Takahashi,[*12,*2] H. Takeda,[*2] S. Thiel,[*8] K. Wimmer,[*14,*2] Y. Yamamoto,[*4,*2] and M. Yoshimoto[*2] for the RIBF 181 Collaboration

^{78}Ni is an emblematic nucleus for the study of nuclear structure far from stability. Although it is expected to have a doubly magic character for proton ($Z = 28$) and neutron ($N = 50$) shells, theoretical and experimental studies around this region hint to a weakening of this magicity, with possible shape coexistence phenomena associated with shell quenching in proton and neutron gaps.[1] To address these questions, the RIBF181 experiment aiming at the in-beam γ-ray spectroscopy of nuclei in the vicinity of ^{78}Ni was conducted at RIKEN for 7 days in April 2021. In this report, we focus on the analysis of the spectroscopy of ^{79}Cu, which contains one proton above the core of ^{78}Ni.

A wide range of exotic isotopes including ^{80}Zn were produced after the induced in-flight fission of a primary beam of ^{238}U at 345 MeV/nucleon and 90-particle nA on a 4-mm-thick primary beryllium target. These nuclei were sent through the BigRIPS separator onto a secondary 6.8-mm-thick beryllium target, in which knock-out reactions took place. The outgoing fragments including ^{79}Cu were subsequently identified in the ZeroDegree spectrometer. The emitted γ-rays were detected by the HiCARI germanium array[2] placed around the secondary target. To carry out event-by-event particle identification (PID) of the beam nuclei, we used the combination of the ToF-$B\rho$-ΔE and two-fold $B\rho$ methods in both the BigRIPS and ZeroDegree spectrometers to obtain the atomic number (Z) and mass-to-charge ratio (A/Q). To reduce the number of contaminating events, we applied conditions in correlations within different detectors. The removed events include the δ-electrons in the parallel-plate avalanche counters (PPACs), the changing charge states, and the pile-up events in the plastic scintillators and ionization chambers. The combination of these cuts reduced the total number of events during PID in BigRIPS by 11%.

To enhance the A/Q resolution, we applied optical corrections up to the third order using a multidimensional fit to eliminate the dependencies of the A/Q values on the position and angular variables at different focal planes. This resolution improved from 0.11% to 0.08% in BigRIPS for ^{80}Zn isotopes and from 0.22% to 0.15% in ZeroDegree for ^{79}Cu isotopes.

The cores and segments of the 10 available germanium clusters (4 Miniballs, 4 Clovers, P3, and Quad) were calibrated in energy with sources of ^{60}Co, ^{152}Eu, ^{133}Ba, and ^{88}Y. A preliminary Doppler correction of the γ-ray energy for the ^{80}Zn(^{9}Be, X)^{79}Cu channel was applied. Figure 1 shows the spectrum of the Miniballs and Clovers. This was produced using the photogrammetry positions of the detectors and a fixed velocity at the target center. The latter was estimated using the mean values of the measured velocity distributions in BigRIPS and ZeroDegree and LISE++ simulations to correct for the energy loss in the intermediate materials upstream and downstream from the target. In this γ-spectrum, the 656 keV transition[3] from the first ($3/2^-$) excited state to the ($5/2^-$) ground state can already be confirmed. We foresee to optimize the Doppler correction by using an event-by-event velocity and apply γ-γ coincidences to find the remaining transitions and reconstruct the resulting level scheme.

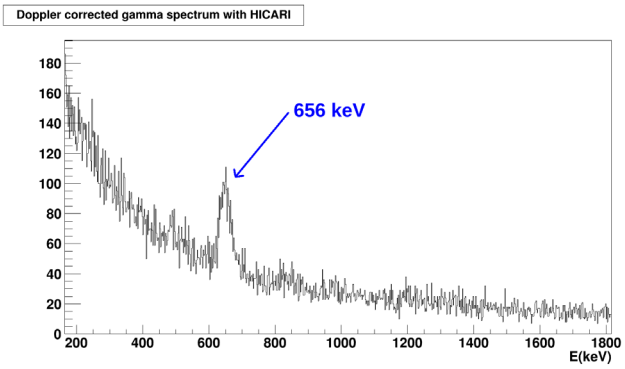

Fig. 1. Preliminary Doppler corrected γ spectrum of ^{79}Cu.

*1 Laboratoire Irène Joliot Curie, Université Paris Saclay
*2 RIKEN Nishina Center
*3 School of Physics, Electronics and Technology, University of York
*4 Research Center for Nuclear Physics, Osaka University
*5 Nuclear Science Division, Lawrence Berkeley National Laboratory
*6 Department of Physics, University of Hong Kong
*7 Instituut voor Kern- en Stralingsfysica, KU Leuven
*8 Institut für Kernphysik, Universität zu Köln
*9 Department of Physics, Korea University
*10 Department of Physics, Tohoku University
*11 Department of Physics, University of Tokyo
*12 Department of Natural Sciences, Tokyo City University
*13 Department of Physics, University of Surrey
*14 IEM-CSIC

References

1) R. Taniuchi *et al.*, Nature **569**, 53 (2019).
2) K. Wimmer *et al.*, RIKEN Accel. Prog. Rep. **54**, S27 (2021).
3) L. Olivier *et al.*, Phys. Rev. Lett. **119**, 192501 (2017).

Barrier distribution measurement of the ^{51}V + ^{159}Tb system

P. Brionnet,[*1] M. Forge,[*2,*1] T. Fukatsu,[*3] H. Haba,[*1] D. Kaji,[*1] S. Kimura,[*1] K. Morimoto,[*1] Y. Michimoto,[*3,*1] T. Niwase,[*4,*1] S. Sakaguchi,[*3,*1] H. Sakai,[*1] M. Tanaka,[*1] and Y. Yamanouchi[*3] for the nSHE Collaboration

With the discovery of elements up to oganesson (Z = 118), all reactions based on the ^{48}Ca beam leading to a new element have already been performed. The next step forward to produce new element Z = 119 and beyond needs to rely on ^{50}Ti, ^{51}V, or ^{54}Cr beam on trans-actinium targets. However, in the super heavy mass region, the reactions using these beams have only been studied on spherical targets (^{208}Pb and ^{209}Bi). Thus, very little information regarding the reaction parameters on deform targets is currently available with these beams. Most of the information used by the predictions is extrapolated from the ^{48}Ca results. Systematic studies of reaction using these beams on deform targets are thus needed to improve the predictive power of the different models.

One of these important parameters is the beam energy selected for the search for new elements. The search of the element Z = 119 is currently ongoing at RIKEN using the ^{51}V + ^{248}Cm reaction. The optimal beam energy was selected by studying the barrier distribution of this reaction.[1)] We decided to begin the systematic measurement of the same parameters extracted in Refs. 1) and 2) with lighter deformed targets, starting with the ^{159}Tb. The relation between the maximum cross-section of production and the QuasiElastic (QE) barrier distribution is directly linked to the reaction dynamics.

The ^{51}V^{13+} beam was provided by the newly upgraded SRILAC accelerator.[3)] Similarly to the reports,[1,2)] we used the GARIS-III separator to transport the QE backscattering. These events correspond to the recoil of target-like events at 180° (or a beam-like event at 0°). Using the information from our detector array located at the end of GARIS-III,[3)] we can use the time-of-flight telescope to select the target-like recoil nuclei. Then, by using the dose estimated through elastic scattering of the ^{51}V beam onto the ^{159}Tb at the target position, we can extract the barrier distribution as shown in Fig. 1 (bottom panel). The top panel represents the reflection probability $R(E)$, which is the normalized ratio of target-like events detected at the focal plane to the number of elastic scatterings detected at the target position. The bottom panel represents the barrier distribution $D(E)$ defined as:

$$D(E) \equiv -dR/dE$$

The average barrier height is defined at the 0.5 crossing

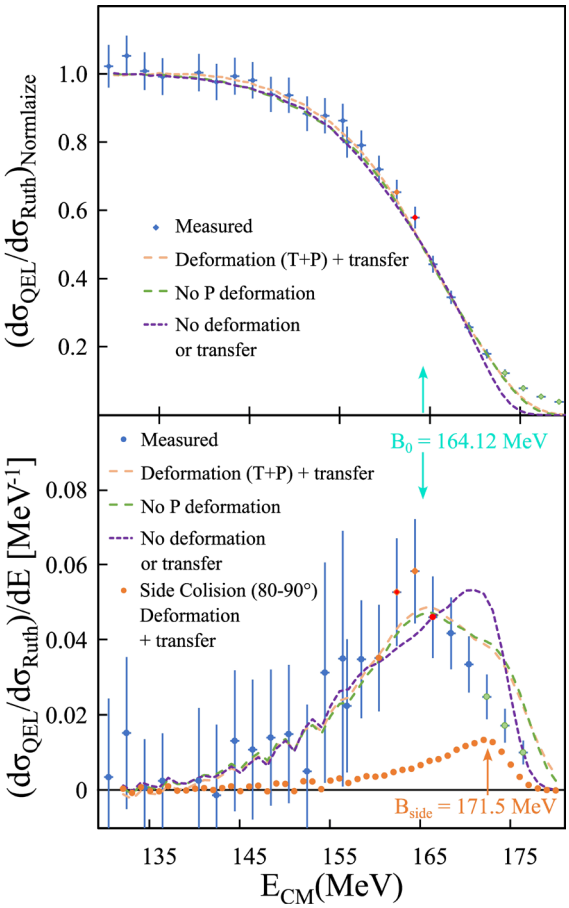

Fig. 1. Reflection probability (top panel) and barrier distribution (bottom panel) of the ^{51}V+^{159}Tb reaction. The points (blue, red/orange, and green) are the measured data and the several curves CCFULL calculations[4)] with different input parameters.

in the $R(E)$ distribution. It is determined as 164.12 ± 0.3 MeV (blue arrow in Fig. 1). This value is related to the maximum of the cross-section of production in the case of reaction on spherical targets. However, in the case of the deformed targets, the side collision energy is more important, as has been pointed out.[1,2)]

This side collision corresponds to the collision of the projectile and target at a 90° angle in a compact configuration. In order to extract this side collision energy, we need to perform the Coupled Channels calculation (CCFULL[4)]).

The dashed orange line in Fig. 1 represents the optimized CCFULL calculations,[4)] and the orange dots represent the contribution of the side collision to the

*1 RIKEN Nishina Center
*2 IPHC Strasbourg
*3 Department of Physics, Kyushu University
*4 Wako Nuclear Science Center (WNSC), IPNS, KEK

overall barrier distribution. We optimized the parameters of the CCFULL calculation to reproduce both the reflection probability and the barrier distribution. We can then extract from these calculations the side collision energy as 171.5 ± 0.5 MeV (orange dot and arrow in Fig. 1 bottom panel). These results will be compared and correlated with the precise excitation function we simultaneously measured for this reaction.[5)]

References

1) M. Tanaka *et al.*, J. Phys. Soc. Jpn. **91**, 084201 (2022).
2) T. Tanaka *et al.*, Phys. Rev. Lett. **124**, 052502 (2020).
3) H. Sakai *et al.*, Eur. Phys. J. A **58**, 238 (2022).
4) K. Hagino *et al.*, Comput. Phys. Commun. **123**, 143 (1999).
5) P. Brionnet, in this report.

Excitation functions for the ^{51}V + ^{159}Tb fusion evaporation reaction

P. Brionnet,[*1] M. Forge,[*2,*1] T. Fukatsu,[*3] H. Haba,[*1] D. Kaji,[*1] K. Morimoto,[*1] Y. Michimoto,[*3,*1] T. Niwase,[*4,*1] S. Sakaguchi,[*3,*1] H. Sakai,[*1] and Y. Yamanouchi[*3,*1] for the nSHE Collaboration

Syntheses of elements from flerovium ($Z = 114$) till oganesson ($Z = 118$) were made using the hot-fusion reactions with ^{48}Ca beams on actinide targets. To synthesize the elements beyond $Z = 118$, reactions with either ^{50}Ti, ^{51}V, or ^{54}Cr beam on actinide targets are necessary. However, these beams have, so far, only been used on spherical targets around ^{208}Pb. Thus, any information regarding the reaction mechanisms using these beams on actinide targets will provide valuable information for the success of current and future searches for new elements. Unfortunately, the direct systematic study of reaction mechanisms on actinides target is unrealistic due to the too-small fusion-evaporation cross-sections (pb–fb range). Thus, the use of a lighter surrogate system based on deformed targets with similar deformation characteristics around lanthanide nuclei may give insight and valuable information regarding reaction mechanisms with ^{50}Ti, ^{51}V, or ^{54}Cr beams, especially regarding the side collision effect.[1,2] The reaction of ^{51}V beam on ^{159}Tb target presents much higher production rates (μb range) while being an excellent surrogate reaction. Indeed, the ^{159}Tb deformation parameters ($\beta_2 = 0.271$, $\beta_4 = 0.066$) are similar to the one of the ^{248}Cm ($\beta_2 = 0.286$, $\beta_4 = 0.039$) that is currently used in the search for the new element $Z = 119$ at RIKEN.

This similarity in deformation parameters allows for the study of the side collision effect using ^{51}V beam on deformed target. Has it been pointed out in Refs. 1) and 2). this side collision effect is involved in the relation between the barrier distribution and the maximum production cross-section of production for the super heavy elements. This relation also shows surprising differences between spherical and deformed targets as indicated in Refs. 1) and 2). Furthermore, these relations were derived using beams lighter than ^{48}Ca and never had been directly extracted for ^{50}Ti, ^{51}V, or ^{54}Cr beams.

The ^{51}V + ^{159}Tb $\rightarrow$ ^{210}Ra* reaction was selected as the first test surrogate reaction, measuring a wide range of excitation energies from 32 to 66 MeV. The barrier distribution was also measured separately and reported elsewhere.[3]

The GARIS-III separator was set to transport the Evaporation Residue (ER) nuclei to the focal plane detector array.[4] The ^{51}V^{13+} beam was provided by the newly upgraded SRILAC accelerator.[4] The experiment used a rotating target of metallic ^{159}Tb with an average density of 365 ± 16 μg/cm^2 and beam intensities ranging from 152 particle nA to 345 particle nA. The ER nuclei were implanted into a Double-sided Strip Silicon Detector[4] that was also used for the detection of the subsequent α-decays.

The identification of reaction channels was only based on the known α-decay energies and branching ratios, without any timing selection. The overall fit of the α-spectrum accumulated over 24 hours at each energy was used to extract the individual yield of ERs produced. Considering the transmission and detection efficiency, the cross section of various exit channels was extracted from those yields. Figure 1 shows the measured cross section of the xn, pxn, and αxn exit channels for the ^{51}V + ^{159}Tb $\rightarrow$ ^{210}Ra* reaction.

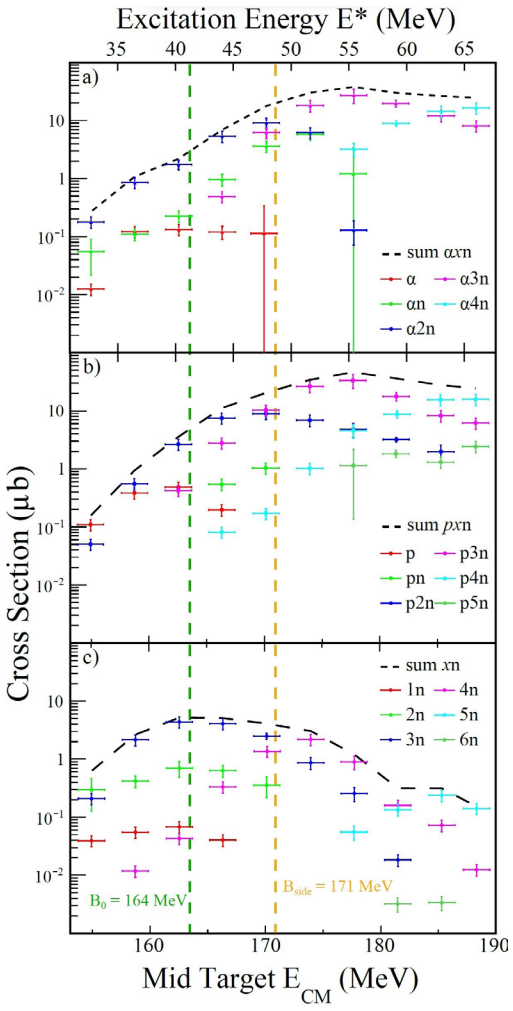

Fig. 1. Excitation function of the reaction ^{51}V + ^{159}Tb: (a) αxn exit channel, (b) pxn exit channel, (c) xn exit channel.

*1 RIKEN Nishina Center
*2 IPHC Strasbourg
*3 Department of Physics, Kyushu University
*4 Wako Nuclear Science Center (WNSC), IPNS, KEK

The maximum cross-sections are the $p3n$ with 33.1 ± 8.9 μb, followed by the $\alpha 3n$ at 27.2 ± 7.3 μb and then the $3n$ at 4.4 ± 0.9 μb. The increase of the charged particle exit channel has been observed in this lower mass region but are not yet well reproduced by models. Discussions with the team of M. Kowal in Poland are ongoing to reproduce this behavior and our data based on their model.[5] It also seems that the side collision effect is not as present as expected for the xn exit channel and is under discussion with K. Hagino.[6]

References

1) M. Tanaka *et al.*, J. Phys. Soc. Jpn. **91**, 084201 (2022).
2) T. Tanaka *et al.*, Phys. Rev. Lett. **124**, 052502 (2020).
3) P. Brionnet *et al.*, in this report.
4) H. Sakai *et al.*, Eur. Phys. J. A **58**, 238 (2022).
5) T. Cap *et al.*, Eur. Phys. J. A **58**, 231 (2022).
6) K. Hagino *et al.*, Comput. Phys. Commun. **123**, 143 (1999).

Analysis of proton elastic scattering from ^{132}Sn and ^{48}Ca at 300 MeV/nucleon in inverse kinematics

T. Harada,[*1,*2] J. Zenihiro,[*3,*2] Y. Matsuda,[*4,*2] S. Terashima,[*5] H. Sakaguchi,[*6] N. Aoi,[*6,*2] H. Baba,[*2] M. Dozono,[*7,*2] F. Endo,[*8,*2] S. Enyo,[*3] Y. Fujikawa,[*3] S. Hanai,[*7] S. Hayakawa,[*7] Y. Hijikata,[*3,*2] J. W. Hwang,[*7] N. Imai,[*7] K. Inaba,[*3] S. Ishida,[*4] T. Isobe,[*2] T. Kawabata,[*9,*2] S. Kiyotake,[*10] A. Kohda,[*6,*2] H. Kurosawa,[*4] R. Kojima,[*7] R. Maeda,[*4] Y. Maeda,[*10] S. Y. Matsumoto,[*3] R. Matsumura,[*1,*2] B. Mauss,[*2] S. Michimasa,[*7] T. Murakami,[*3,*2] D. Nishimura,[*11,*2] T. Nishimura,[*10] K. Nosaka,[*4] S. Ota,[*7] K. Sakanashi,[*3] H. Shimizu,[*7] D. Suzuki,[*2] J. Tanaka,[*2] R. Tsunoda,[*7] T. Uesaka,[*2] and K. Yamamoto[*4]

In this report, we show progress of analysis of proton elastic scattering from ^{132}Sn at 300 MeV/nucleon in inverse kinematics. Previously, we already reported the experimental conditions. We also showed the analyses of the particle identifications of the RI beams, and the excitation energy spectra, and the angular distribution of the elastic scattering yields of ^{132}Sn.[1,2] We have discussed particle identification for beam particles, the excitation energy and of the angular distribution of ^{132}Sn.[1–3] In order to obtain the absolute value of elastic scattering cross-section of ^{132}Sn, it is necessary to determine the target thickness. As calibration data to determine it, it was necessary to analyze ^{48}Ca data obtained in the same environment as the ^{132}Sn measurement. ^{48}Ca is a stable nucleus and, like ^{132}Sn, a double magic number nucleus. The elastic scattering differential cross section of ^{48}Ca has already been measured with high accuracy at RCNP. We assume that the target thickness can be determined by comparing the cross-section obtained in the analysis with the data already obtained at RCNP. Herein, we report on the analysis of ^{48}Ca. We performed measurement of proton elastic scattering from ^{48}Ca in inverse kinematics at 300 MeV/nucleon at F12 area. The total beam rate was up to 300 kcps, and purity of ^{48}Ca was 15%. By using missing mass spectroscopy, the excitation energy distribution of ^{48}Ca was deduced from the measured recoil proton kinetic energy and scattering angle information. We identified elastic events of ^{48}Ca as shown in Fig. 2. Figure 2 shows the excitation energy spectrum of the proton scattering from ^{48}Ca in the recoil angle 77°–80°. The excitation energy resolution (in r.m.s.) of 900 keV was achieved at a scattering angle of 77–80 degrees. Although the resolution is 1.5 times worse than that for ^{132}Sn, we could separate the excited state and the elastic scattering as shown in Fig. 2. The main excited state energy are 3.8 MeV (J^π) or 4.5 MeV (J^π). We will deduce the elastic scattering differential cross section of ^{48}Ca by selecting elastic scattering from information on the excitation energy distribution. We plan to determine the target thickness by comparing the differential cross section obtained by analysis data and the data already obtained at RCNP. Using the determined target thickness, we plan to determine the differential cross section of ^{132}Sn for the first time in the world.

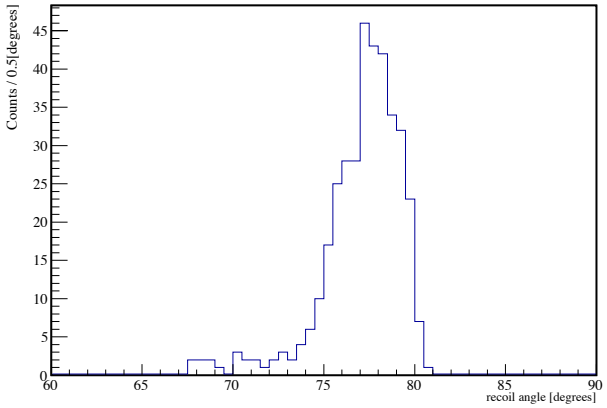

Fig. 1. Angular distribution spectrum for selected elastic scattering events using NaI(TI) calorimeters.

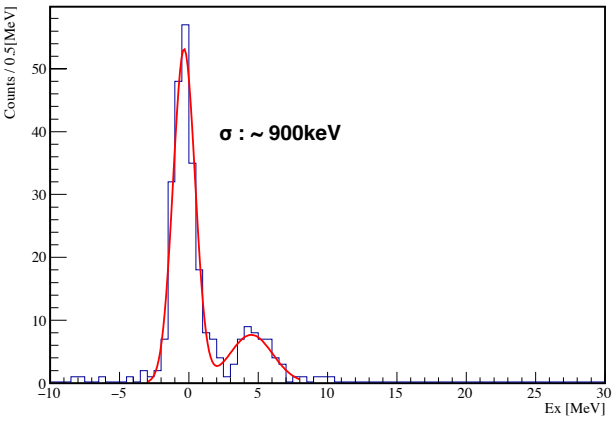

Fig. 2. Excitation energy spectrum of ^{48}Ca at recoil angles in the range of 77°–80°.

*1 Department of Physics, Toho University
*2 RIKEN Nishina Center
*3 Department of Physics, Kyoto University
*4 Cyclotron and Radioisotope Center, Tohoku University
*5 School of Physics, Beihang University
*6 Research Center for Nuclear Physics, Osaka University
*7 Center for Nuclear Study, University of Tokyo
*8 Department of Physics, Tohoku University
*9 Department of Physics, Osaka University
*10 Department of Applied Physics, Miyazaki University
*11 Department of Natural Sciences, Tokyo City University

References

1) J. Zenihiro *et al.*, RIKEN Accel. Prog. Rep. **53**, 44 (2019).
2) T. Harada *et al.*, RIKEN Accel. Prog. Rep. **54**, 18 (2020).
3) T. Harada *et al.*, RIKEN Accel. Prog. Rep. **55**, 23 (2021).

The result of electron scattering with Xe isotopes at SCRIT electron scattering facility

H. Wauke,[*1] D. Abe,[*1] Y. Abe,[*2] A. Enokizono,[*2] R. Danjo,[*1] T. Goke,[*1] Y. Honda,[*1,*2] Y. Ishikura,[*1] Y. Itou,[*3] K. Kurita,[*4] H. Ohnishi,[*2] C. Legris,[*1] Y. Maehara,[*3] Y. Nagano,[*5] R. Obara,[*1] R. Ogawara,[*3] T. Suda,[*1,*2] K. Tsukada,[*2,*3] M. Watanabe,[*2] M. Wakasugi,[*2,*3] and S. Yoshida[*3]

Self-Confining Radioactive Ion Target (SCRIT) electron scattering facility[1] was constructed to perform electron scattering experiments for short-lived unstable nuclei. SCRIT is a unique technique to achieve a luminosity of 10^{27} cm^{-2}s^{-1} via the trapping of a few target ion that is, 10^8 particles/pulse, along the electron beam.

We have started a series of measurements of isotope ($Z = 50$) and isotone ($N = 82$) dependence of nuclear charge density distribution. These studies use the nuclei of Xe isotopes (^{138,136,134,132,130,128,126,124}Xe) and $N = 82$ isotones (^{138}Ba,[2] ^{137}Cs,[3] ^{136}Xe, ^{132}Sn) including the ^{132}Sn and ^{137}Cs, unstable nuclei. The Xe isotope has the second most stable nuclei after Sn; however, no electron scattering data is available, except for ^{132}Xe,[4] which was measured at the SCRIT facility. These isotope and isotone dependencies should provide invaluable information for theoretical development.[5,6]

In 2022 July, we conducted the electron scattering experiment using ^{136,134,132,130}Xe targets. The Xe target was ionized with FEBIAD-type ion source by injecting natural Xe gas directly into the ionization chamber inside the ERIS.[7] The ionized Xe was mass-separated by a bending magnet installed after ERIS. After cooling and stacking inside the FRAC,[8] almost 10^8 of mass-specific Xe ions/pules were transported to the SCRIT system at a frequency of 1 Hz. Experiments with ^{136}Xe were performed at both 150 and 250 MeV, whereas the experiments with ^{134,132,130}Xe were only performed at 150 MeV. Further, the beam current was 250 mA at the beginning of the data acquisition and reduced to 150 mA at the end. Figure 1 shows the yield distributions of ^{136}Xe with momentum transfer following acceptance corrections. The solid lines represent the calculated ones using the theoretical charge density distribution of ^{136}Xe[5] using the phase shift calculation code DREPHA.[9] The total experimental time and average luminosity of each experiment is presented in Table 1. Average luminosities were measured by a luminosity monitor.

The ^{124}Xe, which is scheduled to be launched soon, has a smaller abundance ratio than other Xe, thus, we have upgraded ERIS and have already achieved a production rate similar to that of ^{136}Xe. From 2023, we will conduct experiments on the remaining Xe and proceed with further analysis.

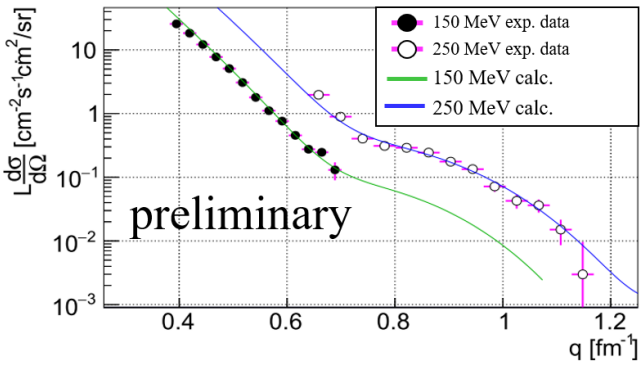

Fig. 1. Yield distributions of ^{136}Xe with momentum transfer following acceptance corrections. Filled and opened circles indicate preliminary results from this study. The solid lines are the phase-shift calculated values obtained using a theoretically calculated charge-density distribution of ^{136}Xe.[5]

Table 1. Experimental situation.

Nuclei	Beam Energy [MeV]	Total Exp. time [s]	Lumi. ave [$\times 10^{27}$ cm^{-2}s^{-1}]
^{136}Xe	150	1.94×10^5	1.55
^{136}Xe	250	4.28×10^5	2.08
^{134}Xe	150	1.18×10^5	1.66
^{132}Xe	150	0.90×10^5	1.69
^{130}Xe	150	1.29×10^5	1.33
total		9.59×10^5	

*1 Research Center for Electron Photon Science, Tohoku University
*2 RIKEN Nishina Center
*3 Institute for Chemical Research, Kyoto University
*4 Department of Physics, Rikkyo University
*5 Faculty of Science, Yamagata University

References

1) M. Wakasugi *et al.*, Phys. Rev. Lett. **100**, 164801 (2008).
2) K. Tsukada *et al.*, RIKEN Accel. Prog. Rep. **55**, 24 (2021).
3) K. Tsukada *et al.*, Phy. Rev. Lett. **131**, 092502 (2023)
4) K. Tsukada *et al.*, Phys. Rev. Lett. **118**, 262501 (2017).
5) T. Liang *et al.*, Phys. Rev. C **98**, 044310 (2018).
6) X. Roca-Maza *et al.*, Phys. Rev. C **87**, 014304 (2013).
7) T. Ohnishi *et al.*, Nucl. Instrum. Methods Phys. Res. B **317**, 357 (2013).
8) M. Wakasugi *et al.*, Rev. Sci. Instrum. **89**, 095107 (2018).
9) B. Drepher, A phase-shift calculation code for elastic electron scattering (private communication with J. Friedrich).

Beta-delayed proton emission in the decay of ^{71}Kr

A. Vitéz-Sveiczer,[*1,*2,*3] A. Algora,[*1,*2] G. Kiss,[*2,*4] B. Rubio,[*1] A. Morales,[*1] P. Sarriguren,[*5] P. Van Isacker,[*6] G. de Angelis,[*7] F. Recchia,[*8,*9] S. Nishimura,[*4] J. Agramunt,[*1] V. Guadilla,[*1] A. Montaner-Pizá,[*1] S. Orrigo,[*1] Á. Horváth,[*10] D. Napoli,[*7] S. Lenzi,[*8,*9] A. Boso,[*8,*9] V. Phong,[*4,*11] J. Wu,[*4] P. Söderström,[*4] T. Sumikama,[*4] H. Suzuki,[*4] H. Takeda,[*4] D. Ahn,[*4] H. Baba,[*4] P. Doornebal,[*4] N. Fukuda,[*4] N. Inabe,[*4] T. Isobe,[*4] T. Kubo,[*4] S. Kubono,[*4] H. Sakurai,[*4] Y. Shimizu,[*4] C. Sidong,[*4] B. Blank,[*12] P. Ascher,[*12] M. Gerbaux,[*12] T. Goigoux,[*12] J. Giovinazzo,[*12] S. Grévy,[*12] T. Kurtukián Nieto,[*12] C. Magron,[*12] W. Gelletly,[1,*13] Z. Dombrádi,[*2] Y. Fujita,[*14,*15] M. Tanaka,[*15,*4] P. Aguilera,[*16] F. Molina,[*16] J. Eberth,[*17] F. Diel,[*17] D. Lubos,[*18] C. Borcea,[*19] E. Ganioglu,[*20] D. Nishimura,[*21] H. Oikawa,[*22] Y. Takei,[*22] S. Yagi,[*22] W. Korten,[*23] G. de France,[*6] P. Davies,[*24] J. Liu,[*25] J. Lee,[*25] T. Lokotko,[*25] I. Kojouharov,[*26] N. Kurz,[*26] H. Shaffner,[*26] and A. Petrovici[*19]

We present preliminary results of our study of β-delayed proton emission detected in the β-decay of ^{71}Kr. These results were obtained in the framework of the experiment NP1112-RIBF93. In our experiment a 40 particle nA ^{78}Kr primary beam provided by RI Beam Factory (RIBF) impinged on a 5-mm thick Be target to produce 9.8 million ^{71}Kr implants—after optimization to separate ^{71}Kr secondary beams—in the WAS3ABi active stopper.[1)] The WAS3ABi detector was surrounded by the EURICA γ-ray spectrometer.[2)]

Beta-delayed protons were distinguished from β-particles in the same way as in our earlier work on ^{70}Kr, using an energy threshold of 1400 keV measured in WAS3ABi,[3)] resulting in the deposited energy spectrum shown in Fig. 1. The number of protons was divided by the number of implants in order to calculate the β-delayed proton emission probability $\varepsilon_p = 2.49(10)\%$ in agreement with the value of $\varepsilon_p^{lit} = 3.1(4)\%$ found in the literature.[4)] In our analysis the dead time of the detector system was also accounted for, while a 100% detection efficiency was assumed for single protons.

A half-life value of $T_{1/2} = 94.1(4)$ ms was derived from the time correlations between protons and implants using an exponential fit shown in Fig. 2, in agreement with the results obtained from implant-β time correlations ($T_{1/2} = 94.5(2)$ ms) and from the decay curve of β-delayed γ-transitions in the daughter nucleus ($T_{1/2} = 95.5(24)$ ms).

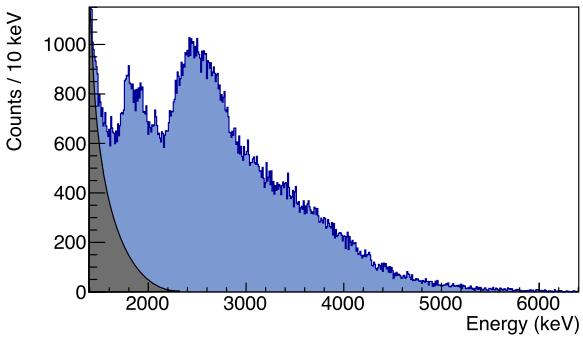

Fig. 1. Intensity distribution as a function of the deposited energy of the β-delayed proton events in the DSSSD. The high energy tail of β-particles was extrapolated by an exponential function, shown in grey.

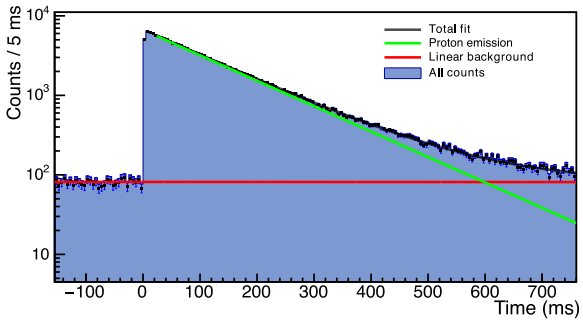

Fig. 2. Time correlations between β-delayed proton events and ^{71}Kr implants. The total fit represents an exponential function plus a linear background.

The theoretical interpretation of the experimental data is ongoing.

*1 Instituto de Fisica Corpuscular
*2 Institute for Nuclear Research (Atomki)
*3 PhD School of Physics, University of Debrecen
*4 RIKEN Nishina Center
*5 Instituto de Estructura de la Materia
*6 Grand Accélérateur National d'Ions Lourds
*7 INFN, Laboratori Nazionali di Legnaro
*8 INFN, Sezione di Padova
*9 Dipartimento di Fisica dell Universitá degli Studi di Padova
*10 Department of Physics, Eötvös Loránd University
*11 Faculty of Physics, VNU Hanoi University of Science
*12 Centre d Etudes Nucléaires de Bordeaux-Gradignan
*13 Department of Physics, University of Surrey
*14 Research Center for Nuclear Physics, Osaka University
*15 Department of Physics, Osaka University
*16 Comisión Chilena de Energía Nuclear
*17 Institute of Nuclear Physics, University of Cologne
*18 Physik Department E12, Technische Universität München
*19 National Institute for Physics, Horia Hulubei National Institute for R&D in Physics and Nuclear Engineering
*20 Department of Physics, Istanbul University
*21 Department of Natural Sciences, Tokyo City University
*22 Department of Physics, Tokyo University of Science
*23 CEA Saclay, IRFU, Gif-sur-Yvette
*24 Department of Physics, University of York
*25 Department of Physics, University of Hong Kong
*26 GSI Helmholtzzentrum für Schwerionenforschung GmbH

References

1) S. Nishimura, Prog. Theor. Exp. Phys. **2012**, 03C006 (2012).
2) P. -A. Söderström *et al.*, Nucl. Instrum. Methods Phys. Res. B **317**, 649 (2013).
3) A. Vitéz-Sveiczer *et al.*, Phys. Lett. B **830**, 137123 (2022).
4) S. Waniganeththi *et al.*, Phys. Rev. C **106**, 044317 (2022).

Isomeric state studies using the DTAS detector

J. A. Victoria,[*1] V. Vegas,[*1] A. Algora,[*1,*2] B. Rubio,[*1] J. L. Tain,[*1] A. Tolosa,[*1] J. Agramunt,[*1] E. Nacher,[*1] S. E. A. Orrigo,[*1] V. Guadilla,[*3] G. Kiss,[*2] D. Sohler,[*2] I. Kuti,[*2] T. Davinson,[*4] O. B. Hall,[*4] D. M. Kahl,[*4] C. G. Bruno,[*4] C. J. Appleton,[*4] P. J. Woods,[*4] S. Nishimura,[*5] N. Fukuda,[*5] H. Suzuki,[*5] D. S. Ahn,[*5] H. Baba,[*5] Y. Shimizu,[*5] H. Takeda,[*5] D. Nishimura,[*5] T. Isobe,[*5] M. Kaneko,[*5] S. Kubono,[*5] H. Sakurai,[*5] H. Shimizu,[*5] T. Sumikama,[*5] P. Doornenbal,[*5] M. L. Cortes,[*6] Zs. Podolyak,[*7] W. Gelletly,[*7] E. Ganioglu,[*8] Y. Fujita,[*9] F. Molina,[*10] J. Liu,[*11] J. Lee,[*11] K. P. Rykaczewski,[*12] M. Wolinska-Cichocka,[*13] M. Labiche,[*14] C. J. Griffin,[*15] S. Bae,[*16] J. Ha,[*16] and Y. Litvinov[*17]

In this contribution we present preliminary work aimed to assess the capabilities of the DTAS detector to study isomeric states. They are of particular interest, since they can provide information about nuclear structure. They are also relevant in the analysis of total absorption data, since they may break the continuity of emitted gamma-ray cascades from high lying states populated in beta decay. This contribution is related to experiment NP1612-RIBF147,[1)] which focuses on the study of the beta decay of ^{100}Sn and neighbouring nuclei using the DTAS modular total absorption spectrometer[2)] and the AIDA implantation detector.

In the study, we developed analysis tools to look for nuclei with unknown isomeric states in the vicinity of ^{100}Sn using DTAS in combination with the in-flight radioactive ion beam separator BigRIPS. This setup allows one to study the gamma rays of a particular isomeric decay, looking for time correlations between ions identified in BigRIPS and the associated gamma cascade detected in DTAS, taking advantage of its high efficiency. In our analysis two dimensional spectra were generated where in one axis we have the time difference between the time of correlated gamma events detected in DTAS modules and the ion implantation time provided by BigRIPS and on the other axis we have the energy detected by the DTAS individual modules. Isomeric states should be seen in this figure as gamma transitions (or levels) vanishing as time differences increase. The very high efficiency of the DTAS detector to gamma cascades can be an asset in this context.

To test the viability of the procedure we have studied the ^{98}Cd case, which has a high production rate in our experiment and has well known isomeric states. The gamma cascade data obtained with the DTAS detector from the de-excitation of ^{98}Cd isomeric decay populated in the fragmentation reaction can be compared with data obtained previously from high resolution experiments using germanium detectors.[3)]

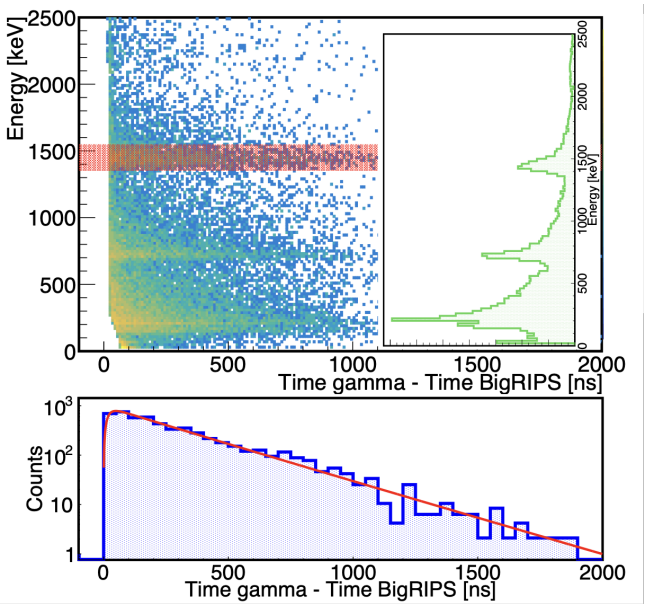

Fig. 1. Top: 2D figure corresponding to a ^{98}Cd gamma cascade detected in DTAS and its energy projection. Bottom: Fit of the the time projection of a gate around the ∼1400 keV energy peak marked in the upper panel.

The comparison between the half-lives from the literature[3,4)] and the results from our preliminary analysis shows the validity of the method. In the analysis of the lower states, feeding from above is taking into account.

Level	Literature[3,4)]	Present Work
12^+	224(5) ns	216(7) ns
8^+	154(16) ns	150(3) ns
6^+	13(2) ns	11(1) ns

In the next step we plan to systematically look for isomers produced in our experiment.

*1 IFIC, CSIC-Univ. Valencia
*2 Institute for Nuclear Research (ATOMKI)
*3 SUBATECH
*4 School of Physics and Astronomy, University of Edinburgh
*5 RIKEN Nishina Center
*6 INFN-Legnaro
*7 Department of Physics, Surrey University
*8 Department of Physics, University of Istanbul
*9 Osaka University
*10 CCHEN
*11 Department of Physics, University of Hong Kong
*12 Oak Ridge National Laboratory
*13 Heavy Ion Laboratory, Warsaw University
*14 STFC Daresbury Laboratory
*15 Physical Sciences Division, TRIUMF
*16 Department of Physics and Astronomy, Seoul National University
*17 GSI Helmholtzzentrum für Schwerionenforschung GmbH

References

1) A. Algora *et al.*, RIKEN Accel. Prog. Rep. **53**, 30 (2019).
2) J. L. Tain *et al.*, Nucl. Instrum. Methods Phys. Res. A **803**, 36 (2015).
3) J. Park *et al.*, Phys. Rev. C **96**, 044311 (2017).
4) J. Chen *et al.*, Nucl. Data Sheets **164**, 1 (2020).

Progress on the analysis of P_n-values relevant for the formation of the r-process rare-earth peak

M. Pallàs,[*1] A. Tarifeño-Saldivia,[*2,*1] G. G. Kiss,[*3] J. L. Tain,[*2] A. Tolosa-Delgado,[*4,*2] A. Vitéz-Sveiczer,[*3,*5] F. Calviño,[*1] J. Agramunt,[*2] A. Algora,[*2] N. T. Brewer,[*8,*6] R. Caballero-Folch,[*9] T. Davinson,[*10] I. Dillmann,[*9,*11] A. Estrade,[*12] N. Fukuda,[*7] R. K. Grzywacz,[*8,*6] O. Hall,[*10] N. Mont-Geli,[*1] A. I. Morales,[*2] A. Navarro,[*1] N. Nepal,[*7] S. Nishimura,[*7] B. C. Rasco,[*8,*6] K. P. Rykaczewski,[*6] T. N. Szegedi,[*3] V. Phong,[*7] R. Yokoyama,[*13] M. Wolińska-Cichocka,[*14] and P. J. Woods[*10] for the BRIKEN Collaboration[*15]

Rapid neutron capture (the r-process) produces nearly half of the nuclei heavier than iron in explosive stellar scenarios. Above the mass number $A = 100$, there are two main peaks in the r-process solar-system abundances, are located at $A \sim 130$ and $A \sim 195$. Located between them, the Rare-Earth Peak (REP) is a tiny but definite peak at mass number $A \sim 160$ that results from the freeze-out during the last stages of neutron exposure. According to theoretical models and sensitivity studies, half-lives ($T_{1/2}$) and β-delayed neutron emission probabilities (P_{xn}) of neutron-rich nucleus, in the mass region $A \sim 160$ for $55 \leq Z \leq 64$ are critical for the formation of the REP.[1,2] As a part of the BRIKEN collaboration, the NP1612-RIBF148 experiment measured half-lives and β-delayed from Ba to Gd ($Z = 56$–64). In 2018, an experimental run centered on ^{165}Pm was conducted using a total of 5 days of beamtime. The results for Pm to Gd ($Z = 61$–64) species are already published.[3] The data analysis for Ba to Nd ($Z = 56$–60) species using the method proposed in[4] is presented in this report.

The NP1612-RIBF148 experimental setup consisted of the Advanced Implantation Detector Array (AIDA)[5] and the BRIKEN neutron counter.[6] The neutron counter was placed surrounding AIDA to detect the β-delayed neutrons offering a nominal value for the efficiency of 68.6% up to 1 MeV.

In Fig. 1, the preliminary results for the P_{1n} values are compared with evaluated nuclear data from the ENSDF and some theoretical predictions.[7–9] Preliminary reports include 14 new P_{1n} values ($^{151–152}$Ba, $^{151–153}$La, $^{154–156}$Ce, $^{155–158}$Pr, and $^{159–160}$Nd). Two other P_{1n} values ($^{149–150}$La) were also remeasured, obtaining consistent results with previous measurements. Our data supports the overall trend for all P_{1n} predictions when compared to theoretical models. The pn-RQRPA + HFM model[9] best replicates the experimental data and provides good agreement for the majority of the isotopes.

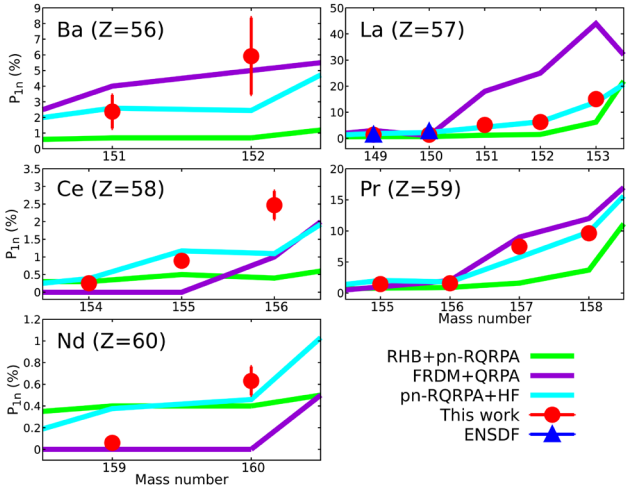

Fig. 1. Preliminary P_{1n} values derived in this work (red dot) compared with previous measurements (blue triangle) and theoretical calculations.[7–9]

*1 Institut de Tècniques Energètiques (INTE), Universitat Politècnica de Catalunya (UPC)
*2 Instituto de Física Corpuscular (IFIC), CSIC-UV
*3 Institute for Nuclear Research (ATOMKI)
*4 Department of Physics, University of Jyväskylä
*5 Doctoral School of Physics, University of Debrecen
*6 Physics Division, Oak Ridge National Laboratory
*7 RIKEN Nishina Center
*8 Department of Physics and Astronomy, University of Tennessee
*9 TRIUMF, Vancouver
*10 School of Physics and Astronomy, University of Edinburgh
*11 Department of Physics and Astronomy, University of Victoria
*12 Department of Physics and Science of Advanced Materials Program, Central Michigan University
*13 Center for Nuclear Study, University of Tokyo
*14 Heavy Ion Laboratory, University of Warsaw
*15 www.wiki.ed.ac.uk/display/BRIKEN/Home

References

1) A. Arcones *et al.*, Phys. Rev. C **83**, 045809 (2011).
2) M. R. Mumpower *et al.*, Phys. Rev. C **85**, 045801 (2012).
3) G. G. Kiss *et al.*, Astrophys. J. **936**, 107 (2022).
4) C. J. Griffin *et al.*, Jap. Phys. Soc. Conf. Proc. **14**, 020622 (2017).
5) A. Tarifeño-Saldivia *et al.*, J. Instrum. **12**, P04006 (2017).
6) A. Tolosa-Delgado *et al.*, Nucl. Instrum. Methods Phys. Res. A **925**, 133 (2019).
7) P. Möller *et al.*, At. Data Nucl. Data Tables **125**, 1 (2019).
8) T. Marketin *et al.*, Phys. Rev. C **93**, 025805 (2016).
9) F. Minato *et al.*, Phys. Rev. C **104**, 044321 (2021).

The study of the core-excited component in ^{11}Li

Y. Li,[*1,*2] Z. Yang,[*3] Y. Kubota,[*1] and T. Uesaka[*1] for the SAMURAI18 Collaboration

^{11}Li is one of the most well-known drip-line nuclei in nuclear physics. The discovery of a spatially extended structure of neutrons in ^{11}Li, which is now widely known as "halo" structure, opened the very active field of research with unstable nuclear beams.[1] ^{11}Li has the Borromean nature, generally considered as a 3-body system of ^{9}Li plus 2 well-decoupled valence neutrons. However, recent theoretical studies pointed out that contribution of the excited ^{9}Li core could also be significant[2,3] in the ground state of ^{11}Li. But no experiment has hitherto succeeded in providing a direct information about the excited-core in ^{11}Li.

The SAMURAI18 experiment performed at the Radioactive Isotope Beam Factory (RIBF) in RIKEN employed the quasi-free (p, pn) reaction. Kubota *et al.*[4] reported the dineutron correlation localized radially on the ^{11}Li surface with the data of the $^{11}\mathrm{Li}(p,pn)^{9}\mathrm{Li}(g.s)+n$ channel. The core-excited component associated with bound excited states of ^{9}Li ($J^{\pi}=1/2^{-}$, $E_x=2.69$ MeV) was also studied from coincident gamma-ray measurement and no significant contribution of this component was observed, which can be attributed to the spin-parity constraints.[5] Thus, it can be expected that the core-excited component in ^{11}Li that we are interested in should be associated with a ^{9}Li excited state with $J^{\pi}=3/2^{-}$ and with a higher excitation energy above the $^{8}\mathrm{Li}+n$ breakup threshold. By looking into the $^{8}\mathrm{Li}+2n$ channel of the SAMURAI18 experiment, we will be able to probe the ^{9}Li*(unbound) + n component in ^{11}Li.

Secondary ^{11}Li beams ($\sim 1\times10^{5}$ pps, ~246 MeV/nucleon) were produced from the fragmentation of ^{48}Ca beam at 345 MeV/nucleon and selected by the BigRIPS fragment separator. They were then tracked onto the 150-mm-thick MINOS target using two multiwire drift chambers. After a (p, pn) reaction, the target proton and one of the neutron of ^{11}Li were scattered to large polar angles. The recoil particle detector (RPD) was composed of a multiwire drift chamber and a plastic scintillator hodoscope. The neutron detector array WINDS was installed to measure the scattering angle and the time of flight of the knockout neutron. The beam-like residues—the charged fragment ^{8}Li and two neutrons—were analyzed by the SAMURAI spectrometer and the neutron detector array NEBULA, respectively. Single incoming neutron could induce signals in multiple detectors of NEBULA, a phenomenon commonly called cross-talk. The time-space-separation cuts and the causality cuts of velocity were applied to eliminate these fake two-neutron events.[6]

The relative energy spectrum of ^{10}Li is reconstructed from coincident $^{8}\mathrm{Li}+n+n$ events using the invariant-mass method and is presented in Fig. 1. Two resonance-like structures are observed at $E_{\mathrm{rel}}\sim0.3$ MeV and at $E_{\mathrm{rel}}\sim1.6$ MeV. The spectrum can be well fitted using a sum of an Is-wave virtual state for the first peak and a p-wave resonance for the second peak. Figure 2 shows the Dalitz plot of the relative energy of the subsystem $^{8}\mathrm{Li}+n$ (E_{fn}) versus that of $^{8}\mathrm{Li}+n+n$ (E_{rel}). The correlation pattern in the E_{rel} range of 1.3–1.7 MeV is consistent with the sequential two-neutron emission via an intermediate ^{9}Li resonant state with $E_{\mathrm{fn}}\sim0.3$ MeV, and

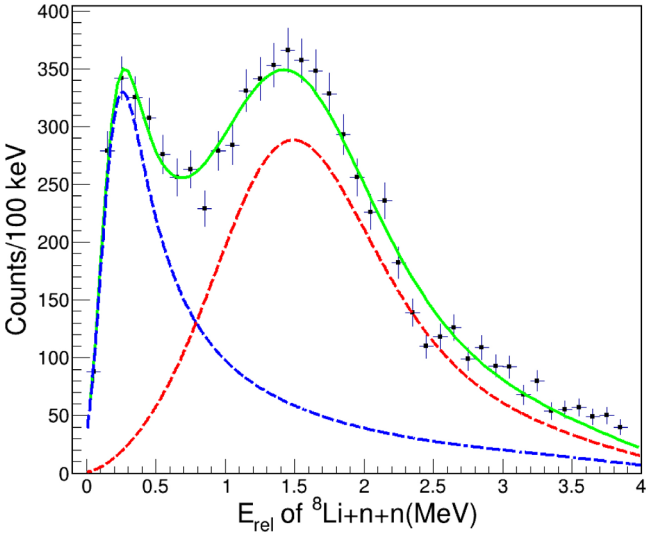

Fig. 1. Relative energy spectrum for $^{8}\mathrm{Li}+2n$. The blue dashed line, red dashed line and the green line represent the the s-wave virtual state fit, p-wave resonance fit and sum of these two components, respectively.

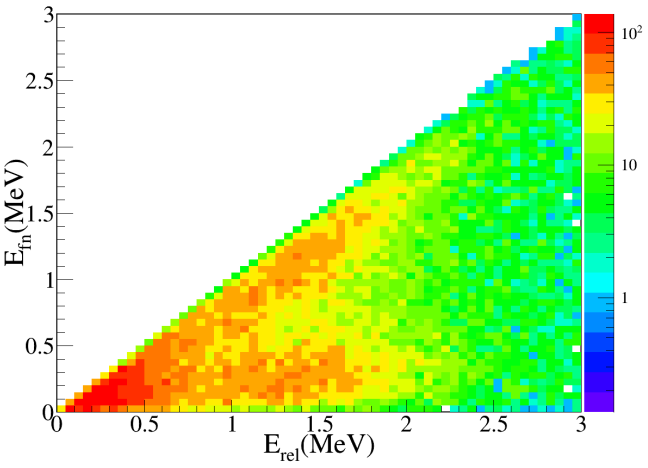

Fig. 2. Dalitz plot of the relative energy. The horizontal axis represents the relative energy of $^{8}\mathrm{Li}+n+n$ (E_{rel}) and vertical axis represents the relative energy of $^{8}\mathrm{Li}+n$ (E_{fn}).

*1 Spin isospin Laboratory, RIKEN
*2 Institute of Modern Physics, Chinese Academy of Sciences
*3 School of Physics, Peking University

this component should thus be assigned to the excited-core configuration in the ground state of ^{11}Li. For the next step, we will analyze the momentum distribution of the knockout neutron to determine its single-particle orbital occupation. By combining with the theoretical calculation that is now in progress we will be able to pin down the excited-core component in ^{11}Li.

References

1) I. Tanihata *et al.*, Phys. Rev. Lett. **55**, 2676 (1985).
2) G. Potel *et al.*, Phys. Rev. Lett. **105**, 172502 (2010).
3) Y. Kikuchi *et al.*, Phys. Rev. C **87**, 034606 (2013).
4) Y. Kubota *et al.*, Phys. Rev. Lett. **125**, 252501 (2020).
5) Y. Kubota, Ph.D Thesis, University of Tokyo (2016).
6) Y. Kondo *et al.*, Nucl. Instrum. Methods Phys. Res. B **463**, 173 (2020).

Observation of ^{9}Li + d decay channel in ^{11}Li(p, n) reaction

L. Stuhl,[*1,*2,*3] M. Sasano,[*3] J. Gao,[*3,*4] Y. Hirai,[*5] K. Yako,[*2] T. Wakasa,[*5] D. S. Ahn,[*3] H. Baba,[*3] A. I. Chilug,[*6,*3] S. Franchoo,[*7] Y. Fujino,[*8] J. Gibelin,[*9] I. S. Hahn,[*1,*10] Z. Halász,[*11] T. Harada,[*12,*3] M. N. Harakeh,[*13,*14] D. Inomoto,[*5] T. Isobe,[*3] H. Kasahara,[*5] D. Kim,[*1,*15] G. G. Kiss,[*11] T. Kobayashi,[*16,*3] Y. Kondo,[*17,*3] Z. Korkulu,[*1,*3] S. Koyama,[*18,*3] Y. Kubota,[*3] A. Kurihara,[*17] H. N. Liu,[*19] M. Matsumoto,[*17] S. Michimasa,[*2] H. Miki,[*17,*3] M. Miwa,[*20] T. Motobayashi,[*3] T. Nakamura,[*17,*3] M. Nishimura,[*3] H. Otsu,[*3] V. Panin,[*3] S. Park,[*10] A. T. Saito,[*17,*3] H. Sakai,[*3] H. Sato,[*3] T. Shimada,[*17] Y. Shimizu,[*3] S. Shimoura,[*2] A. Spiridon,[*6] I. C. Stefanescu,[*6] X. Sun,[*3,*4] Y. L. Sun,[*19] H. Suzuki,[*3] E. Takada,[*21] Y. Togano,[*8,*3] T. Tomai,[*17,*3] L. Trache,[*6] D. Tudor,[*6,*3] T. Uesaka,[*3] H. Yamada,[*17] M. Yasuda,[*17] K. Yoneda,[*3] K. Yoshida,[*3] J. Zenihiro,[*3] and N. Zhang[*22,*2]

In the SAMURAI30 experiment, we studied the Gamow-Teller (GT) giant resonance in the drip-line nucleus ^{11}Li at 181 MeV/nucleon utilizing the missing-mass technique.[1] The ^{11}Li nucleus is the showcase of a two-neutron halo system, with its very extended matter distribution related to the small energy necessary to remove the neutrons. The charge-exchange (p, n) reactions in inverse kinematics are efficient tools to extract the B(GT) strengths of unstable isotopes up to high excitation energies without the Q-value limitation.[2] In our previous study, we demonstrated that accurate information about isovector spin-flip giant resonances can be obtained for unstable nuclei using this probe.[3] The setup of the PANDORA low-energy neutron time-of-flight counter[4] and SAMURAI magnetic spectrometer[5] as well as a thick liquid hydrogen target, facilitate the performance of measurements with high luminosity.

The β decay of ^{11}Li is complex. The large mass difference between ^{11}Li and its daughter ^{11}Be (Q = 20.6 MeV) implies that several decay channels to the bound and unbound states in ^{11}Be are open. In the latter cases, the daughter breaks into fragments, and the emission of one, two, and three neutrons, α particles and ^{6}He, tritons, and deuterons has been observed in several β-decay studies.[6,7] In our previous reports[8] on the preliminary results on GT giant resonance, the observation of these different decay channels was confirmed. Among them, the most interesting decay mode is ^{9}Li + d. This channel is related to the possibility that in halo nuclei, the core and halo particles could decay, more or less independently, into different channels.[9]

We observed a strong transition at approximately 19 MeV in the excitation energy spectrum of ^{11}Be. The angular distribution in center-of-mass angle of the observed state indicates a strong forward peaking nature, which suggests the GT transition, as depicted in Fig. 1, in agreement with previous β-decay studies.

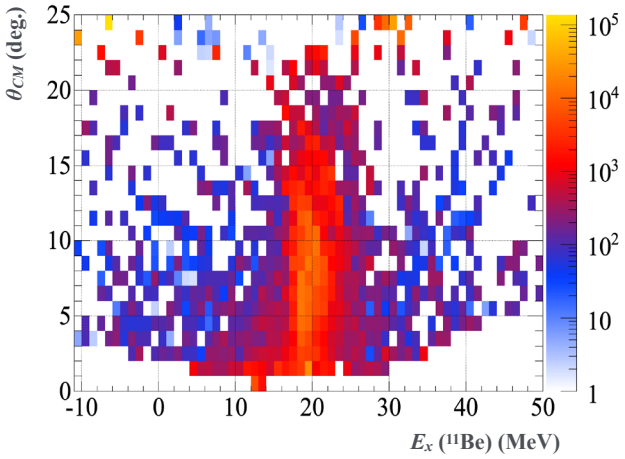

Fig. 1. Angular distribution, in the 0°–25° center-of-mass angular range, of the strong peak observed in the excitation energy spectrum of the daughter nucleus ^{11}Be for the ^{9}Li + d decay mode.

*1 Center for Exotic Nuclear Studies, Institute for Basic Science
*2 Center for Nuclear Study, University of Tokyo
*3 RIKEN Nishina Center
*4 School of Physics, Peking University
*5 Department of Physics, Kyushu University
*6 Horia Hulubei National Institute for R&D in Physics and Nuclear Engineering
*7 Institute de Physique Nucléaire, University Paris-Saclay
*8 Department of Physics, Rikkyo University
*9 Nuclear Physics Labratory LPC CAEN
*10 Department of Physics, Ewha Womans University
*11 Institute for Nuclear Research (ATOMKI)
*12 Department of Physics, Toho University
*13 Department of Physics, University of Groningen
*14 GSI Helmholtzzentrum für Schwerionenforschung
*15 Department of Physics, Korea University
*16 Department of Physics, Tohoku University
*17 Department of Physics, Tokyo Institute of Technology
*18 Department of Physics, University of Tokyo
*19 Département Physique Nucl., CEA, University Paris-Saclay
*20 Department of Physics, Saitama University
*21 National Institute of Radiological Sciences (NIRS)
*22 Institute of Modern Physics, Chinese Academy of Sciences

References

1) M. Sasano *et al.*, Phys. Rev. Lett. **107**, 202501 (2011).
2) T. N. Taddeucci *et al.*, Nucl. Phys. A **469**, 125 (1987).
3) J. Yasuda *et al.*, Phys. Rev. Lett. **121**, 132501 (2018).
4) L. Stuhl *et al.*, Nucl. Instrum. Methods Phys. Res. A **866**, 164 (2017).
5) T. Kobayashi *et al.*, Nucl. Instrum. Methods Phys. Res. B **317**, 294 (2013).
6) R. Raabe *et al.*, Phys. Rev. Lett. **101**, 212501 (2008).
7) I. Mukha *et al.*, Nucl. Phys. A **616**, 201 (1997).
8) L. Stuhl *et al.*, RIKEN Accel. Prog. Rep. **53**, 38 (2019).
9) T. Nilsson *et al.*, Hyperfine Interact. **129**, 67 (2000).

SAMURAI18: comprehensive study of ^{11}Li

Y. Kubota,[*1,*2] A. Corsi,[*3] Z. H. Yang,[*4] P. André,[*3] Y. Li,[*2,*5] M. Miwa,[*6] Y. L. Sun,[*7] and T. Uesaka[*1,*2]
for the SAMURAI18 Collaboration

Since the discovery of the neutron halo, ^{11}Li has been one of the most attractive neutron drip-line nuclei. It is known as a Borromean nucleus, described as a three-body system with two weakly bound valance neutrons around a ^{9}Li core nucleus, with none of the two-body subsystems (^{10}Li or ^{2}n) having bound states. A hypothetical bound state of two neutrons, known as the *dineutron*,[1] is thought to be closely related to its existence.

The quasi-free knockout reaction in inverse kinematics was employed in this study to reveal the two-neutron correlation in ^{11}Li without breaking quantum coherence.[2] By introducing the liquid hydrogen target system MINOS[3] to the RIKEN RIBF, an unprecedentedly high luminosity has been realized. The dedicated (p, pn) setup combined with the SAMURAI spectrometer[4] allowed kinematically "too" complete measurement resulting in high reliability.

By knocking out a valence neutron, the unbound ^{10}Li was produced, and the decay channel of $^{9}\mathrm{Li}+n$ was investigated. The known low-lying structures of s-wave virtual state and p-wave resonances were identified, and the resonance parameters were significantly improved. Furthermore, an exceptionally narrow resonance with a width of 0.7 MeV at a relative energy of 5.5 MeV was newly found and identified as a d-wave resonance by the multipole decomposition analysis. Recently, the analysis of the decay channel of $^{8}\mathrm{Li}+2n$ has revealed an interesting structure that provides insight into the ^{9}Li core excitation in the ground state of the ^{11}Li.[5]

The in-nucleus momentum k of the knockout neutron is reconstructed from the measured momentum of the recoil proton and the knockout neutron. This value is used as a measure of the radial position of the dineutron as well as to define the correlation angle θ_{nf}, which is the measure of the dineutron strength. The relationship between θ_{nf} and k reveals that the dineutron is localized at the surface of ^{11}Li and changes its shape in other region, such as near the center of the nucleus and in the tail of the halo.[6] The same analysis has been carried out for ^{14}Be and ^{17}B, and the universality of the dineutron is becoming apparent.[7]

Only dineutron in the ground state can be studied with one neutron knockout. In order to overcome this limitation, the proton knockout from ^{12}Be was used to produce the excited ^{11}Li. The decay mode of the $^{9}\mathrm{Li}+2n$ channel was investigated through the energy sharing between the two-body subsystems and it was found that in most cases ^{11}Li decays through ^{10}Li, *i.e.*, emitting the two neutrons sequentially.[8]

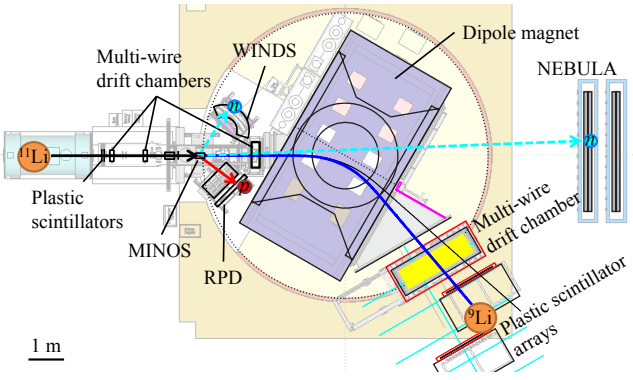

Fig. 1. Schematic of the setup.

From the interest of the tensor force, the formation of deuteron clusters in ^{11}Li was investigated using the deuteron knockout reaction. Since deuterons are weakly bound systems, approximately half dissociates during the knockout process. However, choosing the appropriate kinematics can distinguish deuteron-originated protons and protons from proton knockout. The deuteron spectroscopic factor could be obtained by comparing it with the distorted-wave impulse approximation (DWIA) calculation, though it contains large systematic uncertainties.[9]

The proton knockout channel was also investigated for the ^{10}He spectroscopy. A three-body correlation analysis showed convincing result on the long-debated ground state of ^{10}He.[10]

In summary, ^{11}Li was comprehensively studied using the quasi-free knockout reaction. In addition to two-neutron correlation in the ground and excited states, the structure of unbound subsystems and the formation of deuteron clusters were investigated.

*1 RIKEN Cluster for Pioneering Research
*2 RIKEN Nishina Center
*3 Département de Physique Nucléaire, IRFU, CEA, Université Paris-Saclay
*4 Department of Physics, Peking University
*5 Institute of Modern Physics, Chinese Academy of Sciences
*6 Department of Physics, Saitama University
*7 Institut für Kernphysik, Technische Universität Darmstadt

References

1) A. B. Migdal, Soviet J. Nucl. Phys. **16**, 238 (1973).
2) Y. Kikuchi *et al.*, Prog. Theor. Exp. Phys. **2016**, 103D03 (2016).
3) A. Obertelli *et al.*, Eur. Phys. J. A **50**, 8 (2014).
4) T. Kobayashi *et al.*, Nucl. Instrum. Methods Phys. Res. B **317**, 294 (2013).
5) Y. Li, SAMURAI International Workshop (2022).
6) Y. Kubota *et al.*, Phys. Rev. Lett. **125**, 252501 (2020).
7) A. Corsi *et al.*, Phys. Lett. B **840**, 137875 (2023).
8) P. André, Direct Reactions with Exotic Beams (2022).
9) M. Miwa, Direct Reactions with Exotic Beams (2018).
10) Y. L. Sun, Direct Reactions with Exotic Beams (2022).

Analysis of ^{48}Cr(p,n) reaction in inverse kinematics

M. Sasano,[*1] J. Gao,[*1,*3] L. Stuhl,[*9,*22] Y. Hirai,[*4] T. Wakasa,[*4] D. S. Ahn,[*1] J. K. Ahn,[*13] H. Baba,[*1] K. Chae,[*20] A. Chilug,[*5,*1] K. Cook,[*15] Y. Fujino,[*7] N. Fukuda,[*1] B. Gao,[*19] S. Goto,[*4] I. S. Hahn,[*8,*22] Y. Hamano,[*4] Z. Halász,[*9] T. Harada,[*10,*1] S. Hong,[*20] S. Huang,[*1,*3] N. Inabe,[*1] D. Inomoto,[*4] T. Isobe,[*1] H. Kasahara,[*4] D. Kim,[*8] T. Kobayashi,[*14,*1] Y. Kondo,[*15,*1] Z. Korkulu,[*1] A. Krasznahorkai,[*9] H. Miki,[*15] K. Miki,[*14,*1] S. Mitsumoto,[*4] M. Miwa,[*18,*1] T. Motobayashi,[*1] T. Nakamura,[*15,*1] M. Nishimura,[*1] H. Oshiro,[*4] H. Otsu,[*1] V. Panin,[*1] S. Sakaguchi,[*4,*1] D. Sakai,[*14] H. Sakai,[*1] S. Sakaki,[*4] H. Sato,[*1] T. Shimada,[*15] Y. Shimizu,[*1] B. Sun,[*21] X. Sun,[*1,*3] H. Suzuki,[*1] J. Tanaka,[*1] Y. Togano,[*7,*1] T. Tomai,[*15,*1] T. Uesaka,[*1] Y. Utsuki,[*14] H. Wang,[*15,*1] X. Xu,[*19] K. Yako,[*2] A. Yasuda,[*15] K. Yoneda,[*1] K. Yoshida,[*1] Y. Yoshitome,[*15] and J. Zenihiro[*1]

In this paper, we report on the progress in the data analysis of the SAMURAI11 experiment performed at the RI Beam Factory (RIBF) of RIKEN Nishina Center in spring, 2019. This experiment was conducted to measure the (p,n) reaction on $N=Z$ unstable nuclei, namely, ^{48}Cr and ^{64}Ge. Previously, in Refs. 1) and 2), we reported on the experimental setup and the particle identification (PID) analysis of the reaction residues with the SAMURAI spectrometer,[3] respectively. In Ref. 4), we reported on the observation of a kinetic curve in the recoil-neutron data produced in the ^{48}Cr$(p,n)^{48}$Mn reaction, under the condition that the reaction residues ^{47}Cr were selected through PID analysis.

Figure 1 shows a plot of neutron kinetic energy vs. neutron scattering angle in the laboratory frame for those events in which the reaction residues ^{46}V were selected through PID analysis. The ^{46}V residues were populated through the two-proton decay from the ^{48}Mn. There was no clear locus along the calculated kinetic curves in ^{48}Mn, above the two-proton separation energy at 6.828 MeV. The plot contains events due to the background in a low neutron-kinetic-energy region below 500 keV.

A further analysis is ongoing to substract the background. We are working on the background evaluation by using the reaction channels where the (p,n) reaction does not occur, following the method utilized in a prior study.[5]

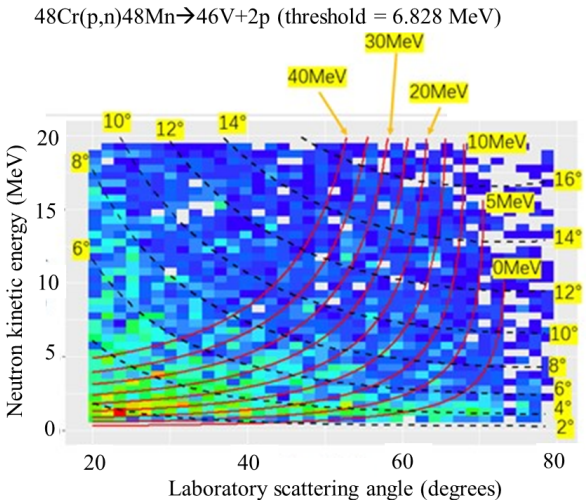

Fig. 1. A two-dimensional plot of neutron kinetic energy vs. neutron scattering angle in the laboratory frame. The reaction residues ^{46}V were selected through the PID analysis. The solid and dashed curves represent calculated kinetic curves for excitation energies and scattering angles in the center-of-mass system of the ^{48}Cr(p,n) reaction, respectively.

We are grateful to the RIKEN accelerator staff and CNS, University of Tokyo, for their continuous efforts to accomplish this stable beam acceleration.

References

1) M. Sasano *et al.*, RIKEN Accel. Prog. Rep. **53**, 40 (2019).
2) J. Gao *et al.*, RIKEN Accel. Prog. Rep. **54**, 14 (2020).
3) T. Kobayashi *et al.*, Nucl. Instrum. Methods Phys. Res. B **317**, 294 (2013).
4) M. Sasano *et al.*, RIKEN Accel. Prog. Rep. **55**, 22 (2022).
5) M. Sasano *et al.*, Phys. Rev. C **86**, 034324 (2012).

*1 RIKEN Nishina Center
*2 Center for Nuclear Study, University of Tokyo
*3 School of Physics, Peking University
*4 Department of Physics, Kyushu University
*5 Horia Hulubei National Institute for R&D in Physics and Nuclear Engineering
*7 Department of Physics, Rikkyo University
*8 Department of Physics, Ewha Womans University
*9 Institute for Nuclear Research (ATOMKI)
*10 Department of Physics, Toho University
*11 KVI - CART, University of Groningen
*12 GSI Helmholtzzentrum für Schwerionenforschung GmbH
*13 Department of Physics, Korea University
*14 Department of Physics, Tohoku University
*15 Department of Physics, Tokyo Institute of Technology
*16 Department of Physics, University of Tokyo
*18 Department of Physics, Saitama University
*19 Institute of Modern Physics, Chinese Academy of Sciences
*20 Department of Physics, Sungkyunkwan University
*21 School of Physics and Nuclear Engineering, Beihang University
*22 Center for Exotic Nuclear Studies, Institute for Basic Science

^{26}Si + α resonant scattering measurement to study ^{26}Si$(\alpha, p)^{29}$P reaction rate

M. J. Kim,[*1] K. Y. Chae,[*1] K. Okawa,[*2] S. Hayakawa,[*2] S. Adachi,[*3] S. M. Cha,[*4] T. Chillery,[*2] N. N. Duy,[*1] T. Furuno,[*3] G. M. Gu,[*1] S. Hanai,[*2] N. Imai,[*2] D. Kahl,[*5] T. Kawabata,[*3,*6] C. H. Kim,[*1] D. Kim,[*4] S. H. Kim,[*1] S. Kubono,[*6] M. S. Kwag,[*1] J. Li,[*2] N. R. Ma,[*2] S. Michimasa,[*2] K. Sakanashi,[*3] H. Shimizu,[*2] O. Sirbu,[*5] N. K. Uyen,[*1] H. Yamaguchi,[*2] R. Yokoyama,[*2] and Q. Zhang[*2]

An X-ray burst can be characterized by a sudden and intense release of X-ray radiation from a compact stellar object such as a neutron star. A total energy release of approximately $10^{39–40}$ ergs can be achieved per burst in just a few seconds. It is believed that the proton-rich nuclei up to the Sn-Sb-Te region can be synthesized during the burst. To better understand the X-ray bursts, studying the ^{26}Si$(\alpha, p)^{29}$P reaction is essential since ^{26}Si is considered to be one of the waiting points in the nucleosynthesis.

A sensitivity study, which identifies the important nuclear reaction rates that affect the X-ray light curves or ash composition, suggests that the ^{26}Si$(\alpha, p)^{29}$P is one of the impactful reactions to the light curve of the X-ray burst.[1)] Despite its importance, the study of ^{26}Si$(\alpha, p)^{29}$P is less understood experimentally. Thus we have performed a ^{26}Si + α experiment to measure the ^{26}Si$(\alpha, p)^{29}$P reaction directly and the resonant scattering to investigate resonances in ^{30}S, which can be populated in the ^{26}Si$(\alpha, p)^{29}$P reaction as intermediate states. The result on the ^{26}Si + α resonant scattering is described in this report.

The ^{26}Si + α resonant scattering was measured at the Center for Nuclear Study Radioactive Ion Beam Separator (CRIB)[2)] of the University of Tokyo. The radioactive ^{26}Si beam was produced at E = 2.14 MeV/nucleon through the ^{3}He$(^{24}$Mg$, n)^{26}$Si reaction by impinging ^{24}Mg at E = 7.56 MeV/nucleon on a cryogenic ^{3}He gas target.[3)] The ^{26}Si beam was separated and purified by combining the magnetic analysis and velocity selection with a double achromatic system and a Wien filter. Two PPACs were located at the upstream of the reaction target for the event-by-event monitoring of beam position and time-of-flight. The typical ^{26}Si beam intensity was 2.8×10^4 pps, and the beam purity was ∼16%. The ^{26}Si beam was impinged on the ^{4}He gas target with a pressure of 250 Torr. The reaction target was kept at room temperature. The thick target method is adopted for the experiment to scan a wide excitation energy range in ^{30}S.

The light charged particles were measured by silicon detector telescopes. Using four layers of silicon detectors ($\Delta E1$, $\Delta E2$, $E1$, and $E2$ layer), each species of charged particles could be easily identified. The $\Delta E1$ and $\Delta E2$ detectors are segmented into 16 strips providing the horizontal and vertical position information, respectively. The $E1$ and $E2$ detectors are pad type silicon detectors. The scattering angle was obtained based on the position information. To obtain the excitation function of ^{26}Si$(\alpha, \alpha)^{26}$Si reaction, the α energies were converted to the center-of-mass energy by considering the kinematics of the reaction and the energy loss of particles in the gas target. Figure 1 shows the excitation function obtained at $\theta_{C.M.}$ = 174°. Fitting the experimental excitation function with the theoretical R-matrix calculations, we will extract resonance parameters of levels in the ^{30}S, such as excitation energy, spin, parity, and α partial width, to constrain the ^{26}Si$(\alpha, p)^{29}$P reaction rate.

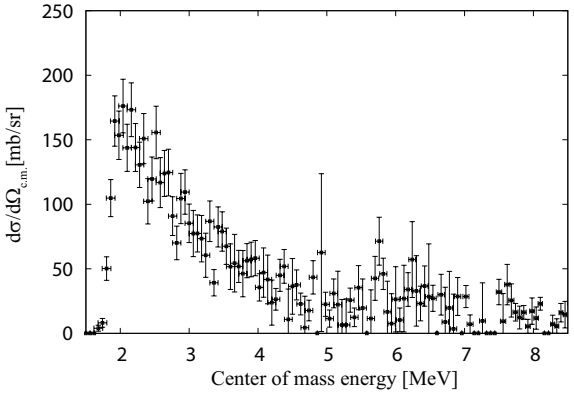

Fig. 1. Excitation function of ^{26}Si + α elastic scattering at $\theta_{c.m.}$ = 174°

References

1) R. H. Cyburt *et al.*, Astrophys. J. **55**, 830 (2016).
2) Y. Yanagisawa *et al.*, Nucl. Instrum. Methods Phys. Res. A, **539**, 74 (2005).
3) H. Yamaguchi *et al.*, Nucl. Instrum. Methods Phys. Res. A **589**, 150 (2008).

*1 Department of Physics, Sungkyunkwan University
*2 Center for Nuclear Study, University of Tokyo
*3 Department of Physics, Osaka University
*4 Center for Exotic Nuclear Studies, Institute for Basic Science (IBS)
*5 Extreme Light Infrastructure Nuclear Physics (ELI-NP)
*6 RIKEN Nishina Center

Yield investigation of neutron-rich W isotopes produced by multi-nucleon transfer reactions of ^{136}Xe + ^{nat}Ir

M. Mukai,[*1,*2] Y. Hirayama,[*3] Y. X. Watanabe,[*3] P. Schury,[*3] A. Andreyev,[*4] S. C. Jeong,[*3] H. Miyatake,[*3] T. Niwase,[*3] M. Reponen,[*5] M. Rosenbusch,[*3] H. Ueno,[*2] and M. Wada[*3]

Nuclear charge radius is a quantity sensitive to changes in nuclear structure, such as shape transition, shell closure, and proton-neutron pairing. The nuclei around Z = 72–78 are known as transitional nuclei, which exhibit a multitude of nuclear shapes depending on the neutron and proton numbers.[1] In the W isotopic chain, nuclear shape evolution has been investigated up to ^{190}W in terms of the properties of the first 2^+, 4^+ excited states[2] and K-isomers[3] via γ-ray spectroscopy using relativistic ions produced in fragmentation reactions. However, laser spectroscopic data obtained using low-energy isotope separator on-line (ISOL) beams are lacking, especially in the neutron-rich side of this nuclear region,[4] due to the refractory nature of these elements. Thus, to investigate the ground state shape evolution with the help of theoretical calculations, we are planning to study the change in nuclear mean-square charge radii of neutron-rich ^{188,190}W via in-gas-cell laser ionization spectroscopy[5] at KISS.[6] As a preliminary effort, we report the measured extraction yields of $^{188–190}$W isotopes at KISS.

The KISS facility at which we conducted the measurement is an argon-gas-cell-based laser ion source combined with an ISOL, designed to produce otherwise difficult-to-access nuclides by multi-nucleon transfer (MNT) reactions. Neutron-rich W isotopes were produced in MNT reactions using an ^{136}Xe beam (30 particle nA, 10.75 MeV/nucleon) impinging upon a ^{nat}Ir (22.7 mg/cm^2) target. The target-like fragments were stopped and neutralized in a gas cell pressurized to 75 kPa with purified Ar gas. The neutralized W atoms were transported by gas flow and ionized by element-selective laser resonance ionization at the gas cell exit. The W atoms were resonantly excited by laser irradiation at λ_1 = 260.7165 nm ($5d^46s^2\ ^5\mathrm{D}_0 \rightarrow J$ = 1°),[7] followed by non-resonant excitation to continuum states by laser irradiation at λ_2 = 308 nm from an XeCl laser. The post-accelerated ions (E = 20 keV/q) were mass separated using a dipole magnet with a mass resolving power of $m/\Delta m$∼900. After being thermalized in a gas cell cooler-buncher[8] (GCCB), the ions were analyzed in a multi-reflection time-of-flight (MRTOF) mass spectrograph for isobaric identification and ion counting. At a typical mass resolving power of $m/\Delta m$∼500,000,[9] the overall efficiency of MRTOF+GCCB was 2%.

Figure 1 shows time-of-flight spectra for A/q = 95 ions measured with (black) and without (red) resonant laser excitation of ^{190}W. An enhancement of ^{190}W ion counts accompanying resonant laser irradiation can be clearly observed. In addition to laser ionized ^{190}W, we observed intense isobaric contaminants consisting of ^{190}Re, ^{190}Os, ^{190}Ir, ^{190}Pt, and ^{190}Au, which are produced with much higher yields than the more neutron-rich ^{190}W; whether they are non-resonantly ionized alongside the ^{190}W or the result of a non-neutralized fraction in the argon gas remains uncertain. The recent improvements in MRTOF performance[9] at KISS allowed for the successful counting of ^{190}W^{2+} ions in spite of these intense isobaric contaminants. A similar situation was encountered in measurements of ^{188,189}W. The measured extraction yields of ^{188,189,190}W were 65, 5.6, and 1.6 pps, respectively. These yields are sufficient to perform future in-gas-cell laser ionization spectroscopy.

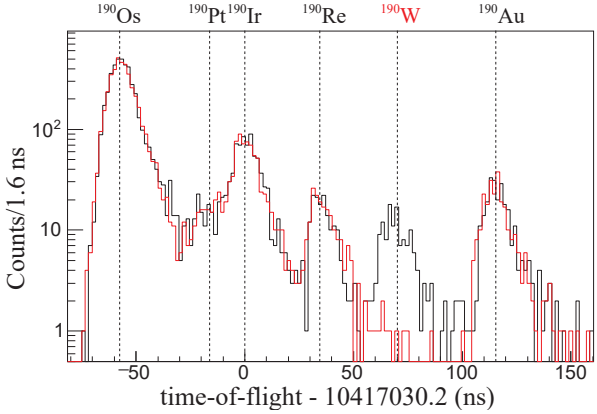

Fig. 1. Measured time-of-flight spectra with resonant excitation laser ON (black) and OFF (red) for ^{190}W.

*1 RIKEN Nishina Center
*2 Graduate School of Engineering, Nagoya University
*3 Wako Nuclear Science Center (WNSC), IPNS, KEK
*4 School of Physics, Engineering and Technology, University of York
*5 Department of Physics, University of Jyväskylä

References
1) R. F. Casten, Nucl. Phys. A **443**, 1 (1985).
2) N. Alkhomashi *et al.*, Phys. Rev. C **80**, 064308 (2009).
3) G. J. Lane *et al.*, Phys. Rev. C **82**, 051304(R) (2010).
4) P. Campbell *et al.*, Prog. Part. Nucl. Phys. **86**, 127 (2016).
5) M. Mukai *et al.*, Phys. Rev. C **102**, 054307 (2020).
6) Y. Hirayama *et al.*, Nucl. Instrum. Methods Phys. Res. B **412**, 11 (2017).
7) NIST Atomic Spectra Database, `https://physics.nist.gov/asd`.
8) Y. Ito *et al.*, JPS Conf. Proc. **6**, 030112 (2015).
9) P. Schury *et al.*, in this report.

First application of mass measurements with the Rare-RI ring reveals the solar r-process abundance trend at $A = 122$ and $A = 123$†

H. F. Li,[*1] S. Naimi,[*2] T. M. Sprouse,[*3] M. R. Mumpower,[*3] Y. Abe,[*2] Y. Yamaguchi,[*2] D. Nagae,[*2] F. Suzaki,[*3] M. Wakasugi,[*2] H. Arakawa,[*4] W. B. Dou,[*4] D. Hamakawa,[*4] S. Hosoi,[*4] Y. Inada,[*4] D. Kajiki,[*4] T. Kobayashi,[*4] M. Sakaue,[*4] Y. Yokoda,[*4] T. Yamaguchi,[*4] R. Kagesawa,[*5] D. Kamioka,[*5] T. Moriguchi,[*5] M. Mukai,[*5] A. Ozawa,[*5] S. Ota,[*6] N. Kitamura,[*6] S. Masuoka,[*6] S. Michimasa,[*6] H. Baba,[*2] N. Fukuda,[*2] Y. Shimizu,[*2] H. Suzuki,[*2] H. Takeda,[*2] D. S. Ahn,[*2] M. Wang,[*1] C. Y. Fu,[*1] Q. Wang,[*1] S. Suzuki,[*1] Z. Ge,[*1] Y. A. Litvinov,[*7] G. Lorusso,[*8,*9] P. M. Walker,[*9] Zs. Podolyak,[*9] and T. Uesaka[*2]

The rapid neutron capture process (r-process) is responsible for synthesizing about half of the elements beyond iron up to bismuth, as well as all of the thorium and uranium. Masses of the neutron-rich nuclides are essential input parameters for the r-process simulation. However, most of the nuclides involved in the r-process can not be produced in the laboratory. Usually, the masses predicted by the theoretical mass models are used. Not only does measuring the mass of exotic nuclei provide dependable experimental data for r-process calculations, but it also plays a crucial role in improving mass models.

The Rare-RI Ring at RIBF is a newly commissioned cyclotron-like storage ring mass spectrometer.[1] We performed the mass measurement experiment for the exotic nuclei on the southwest of the ^{132}Sn with R3. In this experiment, five $N = 77$ isotones, ^{127}Sn, ^{126}In, ^{125}Cd, ^{124}Ag, ^{123}Pd, were produced by the in-flight fission of ^{238}U beam, selected by the BigRIPS and finally injected into the R3. Details of the experiment can be found in the previous report.[2] Masses of ^{126}In, ^{125}Cd, and ^{123}Pd were measured whereby the mass uncertainty of ^{123}Pd was improved.

We investigate the impact of the new mass value of ^{123}Pd on the solar r-process abundances in the r-process by employing the Portable Routines for Integrated nucleoSynthesis Modeling reaction network.[3] Reaction network calculations of 20 trajectories with a specific entropy 40 k_B/baryon, expansion timescale τ = 20 ms and varying electron fraction Y_e from 0.15 to 0.35 in steps of 0.01 are performed. The $A = 122$ to $A = 123$ abundance ratio for each trajectory with the new mass result is calculated and compared with the baseline model in which the mass value of the ^{123}Pd is taken from FRDM2012,[4] as shown in Fig. 1. We find that the abundance ratio of each trajectory in the baseline model is smaller than the solar ratio, making it impossible to reproduce the observed feature with any combination of trajectories. However, when the newly measured ^{123}Pd mass was used, the ratio is sufficiently varied across the range of trajectories. This variability makes it possible to use suitable linear combinations of trajectories to reproduce the observed ratio. The increase in the abundance ratio is attributed to changes in calculated nuclear properties resulting from the newly measured ^{123}Pd mass. The neutron capture cross section for ^{122}Pd decreases by a factor of 2.6 and for ^{123}Pd increases by a factor of 2.2, while the probability for the β-delayed neutron emission of ^{123}Rh increases by 14% with the updated mass. This results in the material pileup along the $A = 122$ isobar relative to the baseline.

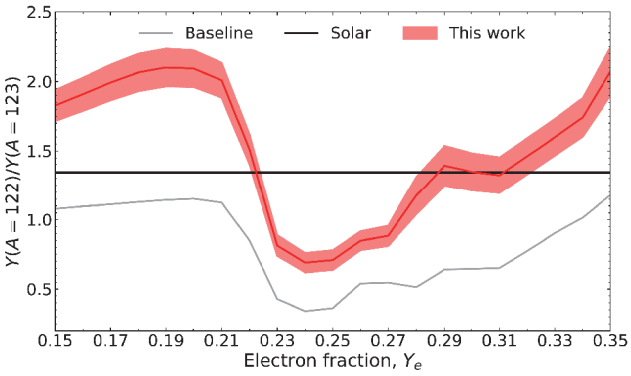

Fig. 1. Ratio of the $A = 122$ to $A = 123$ isotopic abundances as a function of electron fraction for the baseline model (gray line) and if our new mass measurement (red line) and its uncertainty (red band) are included. The horizontal black line indicates the value of the same ratio in the solar r-process residuals of Ref. 5).

† Condensed from the article in Phys. Rev. Lett. **128**, 153001 (2022)

*1 Institute of Modern Physics, Chinese Academy of Sciences
*2 RIKEN Nishina Center
*3 Theoretical Division, Los Alamos National Laboratory
*4 Department of Physics, Saitama University
*5 Institute of Physics, University of Tsukuba
*6 Center for Nuclear Study, University of Tokyo
*7 GSI Helmholtzzentrum für Schwerionenforschung GmbH
*8 National Physical Laboratory
*9 Department of Physics, University of Surrey

References

1) S. Naimi *et al.*, Eur. Phys. J. A **59**, 90 (2023).
2) S. Naimi *et al.*, RIKEN Accel. Prog. Rep. **52**, 102 (2019).
3) T. M. Sprouse *et al.*, Phys. Rev. C **101**, 055803 (2019).
4) P. Möller *et al.*, At. Data Nucl. Data Tables **109**, 1 (2016).
5) M. Arnould *et al.*, Phys. Rep. **450**, 97 (2017).

Direct determination of the atomic mass of ^{189}W

M. Mukai,[*1,*2] Y. Hirayama,[*3] P. Schury,[*3] Y. X. Watanabe,[*3] S. C. Jeong,[*3] H. Miyatake,[*3] T. Niwase,[*3] M. Rosenbusch,[*3] H. Ueno,[*1] and M. Wada[*3]

We measured the atomic mass of ^{189}W in an experiment to investigate the yields of $^{188-190}$W[1)] produced in multi-nucleon transfer (MNT) reactions for future laser ionization spectroscopy at the KEK Isotope Separation System (KISS).[2)] The mass of $^{189}_{74}$W has previously been determined from Q_β[3)] and via Schottky mass spectroscopy at ESR,[4)] but both were excluded from the Atomic Mass Evaluation (AME2020)[5)] based on deviations from the trends of the mass surface, making a complementary mass evaluation highly desirable. We have produced ^{189}W at KISS in MNT reactions of ^{136}Xe + ^{nat}Ir and used the multi-reflection time-of-flight mass spectrograph (MRTOF-MS) for ion counting, isobaric identification, and atomic mass determination. A detailed description of the experiment is given in Ref. 1).

The identification of ^{189}W was achieved by confirming that the relative intensity of the ^{189}W TOF spectral peak reduced significantly when the resonant excitation laser was turned off. After correcting for TOF drift, *e.g.*, from thermal expansion of the MRTOF-MS, the mass resolving power was $m/\Delta m$∼500,000.[6)] Figure 1 provides the drift-corrected sum total measured spectrum for ions with mass-to-charge ratio A/q = 189/2 with and without laser ionization applied. Least squares fitting of the spectrum was performed to determine the TOF values of extracted isobars. The TOF for each ion species was determined using a Gaussian-exponential hybrid function with exponential tails on one side. The shape parameters were determined from a high-statistics TOF spectrum of the elastic particle ^{191}Ir^{2+} and scaled based on A/q. From the evaluated peak positions (t and $t_{\rm ref}$), the mass value (m) was calculated using

$$m = \frac{q}{q_{\rm ref}} m_{\rm ref} \left(\frac{t - t_0}{t_{\rm ref} - t_0} \right)^2 \quad (1)$$

where t_0 is constant offset, while $m_{\rm ref}$, $q_{\rm ref}$, and $t_{\rm ref}$ are the mass, charge, and TOF of a reference ion, respectively. The t_0 term was determined from Eq. (1) based on the results of high-statistics measurements of ^{85}Rb and ^{190}Os, which have well-known atomic masses. To limit mass-dependent systematic errors, nearly isobaric ^{190}Os^{2+} was used as a reference ion along with ^{85}Rb in a double-referencing scheme.[7)] Among the observed A/q = 189/2 ions, ^{189}Os has a long-lived isomer ($E_{\rm ex}$ = 30.82(2) keV, $T_{1/2}$ = 5.8(1) h),[8)] which can be extracted from the KISS gas cell but cannot be resolved by the MRTOF-MS. Due to the minimal TOF difference between ^{189g}Os^{2+} and ^{189m}Os^{2+}, a single peak was fitted, and the evaluated mass represents the weighted average of the two states.

Figure 2 shows the differences between our measured mass values and the AME2020 evaluation. Our measured mass values of ^{189}Re, ^{189}Os, ^{189}Ir, and ^{189}Pt are in good agreement with the evaluated values. Our measured mass for ^{189}W is within the AME2020 error band and is also consistent with the previously reported values in Refs. 3) and 4). This provides some confirmation of the validity of the previous data.

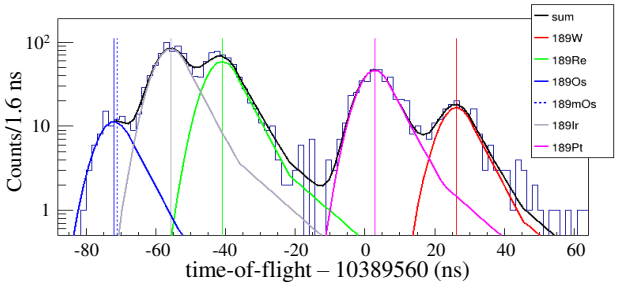

Fig. 1. Measured TOF spectra of A/q = 189/2 ions. The colored curves show the best fitting curves to the data. Solid vertical lines show the fitted TOF position of each isobar.

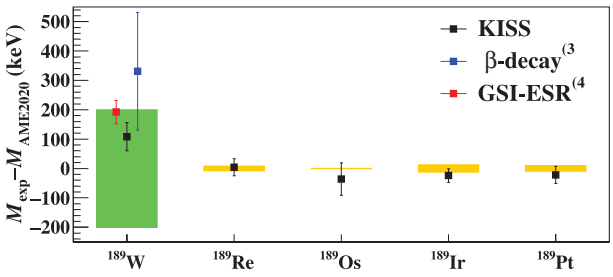

Fig. 2. Differences between our measured mass values and AME2020 evaluation. The AME2020 error bands are represented by yellow and green stripes.

*1 RIKEN Nishina Center
*2 Graduate School of Engineering, Nagoya University
*3 Wako Nuclear Science Center (WNSC), IPNS, KEK

References
1) M. Mukai *et al.*, in this report.
2) Y. Hirayama *et al.*, Nucl. Instrum. Methods Phys. Res. B **412**, 11 (2017).
3) P. Kauranen *et al.*, J. Inorg. Nucl. Chem. **27**, 1451 (1965).
4) D. Shubina *et al.*, Phys. Rev. C **88**, 024310 (2013).
5) W. J. Huang *et al.*, Chin. Phys. C **45**, 030002 (2021).
6) P. Schury *et al.*, in this report.
7) P. Schury *et al.*, Phys. Rev. C **95**, 011305(R) (2017).
8) T. D. Johnson *et al.*, Nucl. Data Sheets **142**, 1 (2017).

2. Nuclear Physics (Theory)

Spatial correlation of a particle-hole pair with a repulsive isovector interaction†

K. Hagino*1 and H. Sagawa*2,*3

It has been well recognized that the pairing correlation among valence neutrons plays a decisive role in the structure of weakly bound nuclei. In particular, there have been several theoretical studies of a strong dineutron correlation, in which two neutrons attract each other and show a large probability of a two-body wave function with a small correlation angle in the coordinate space. A strong signature of the dineutron correlation has also been experimentally observed in several weakly bound nuclei such as ^{11}Li, ^{6}He, and ^{19}B.

It would be an interesting question to ask what happens to the spatial correlation when the interaction is repulsive rather than attractive. Besides the trivial Coulomb repulsion between protons, a well-known repulsive interaction in nuclear physics is the isovector particle-hole (p-h) interaction, which plays an important role in generating collective giant dipole resonances (GDRs). In this paper, we pursue the correlation induced by the repulsive interaction, studying nuclei with one neutron particle and one proton hole on top of a doubly magic nucleus, such as ^{56}Co ($=$ ^{56}Ni$+n-p$) and ^{40}K ($=$ ^{40}Ca$+n-p$). To construct the density distribution for the p-h state, we perform the Hartree-Fock (HF) plus Tamm-Dancoff approximation (TDA) with Skyrme-type interactions.

The spatial distribution for the proton hole in the two-dimensional (z, x) plane is shown in Fig. 1(a) for the 4^+ state in ^{56}Co with the azimuthal angular momentum component $M = 0$. The reference neutron ($2p_{3/2}$ particle state) is placed at $(z, x) = (3.7, 0.0)$ fm. The upper panel shows the unperturbed case with the $(1f_{7/2})_p^{-1}$ wave function. As expected, the hole wave function $(1f_{7/2})_p^{-1}$ has two symmetric peaks at the positions opposite to the center of the core nucleus. The correlated hole density, in which the p-h repulsive interaction is active, is shown in Fig. 1(b). One can see a strong repulsive correlation, where the component close to the reference neutron-particle state is largely hindered. This is analogous to the Coulomb hole observed in many-electron systems and is completely opposite to the dineutron configuration, in which the two valence neutrons mainly remain on the same side of the two-dimensional plane with a small relative distance, that is, a small correlation angle.

In Ref. 1), as an outcome of the repulsive correlation

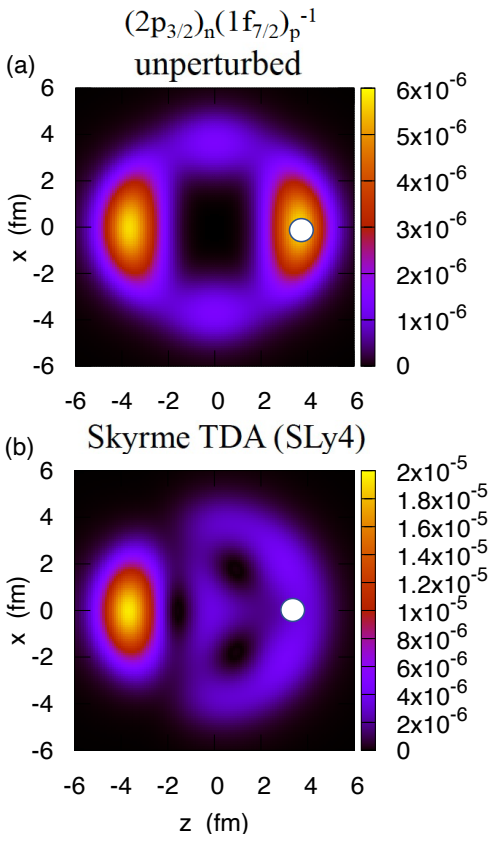

Fig. 1. Uncorrelated (upper panel) and correlated (lower panel) proton-hole distributions in the two-dimensional (z, x) plane for the 4^+ state in ^{56}Co when the neutron-particle is located at $(z, x) = (3.7, 0.0)$ fm indicated by a white circle. The azimuthal angular momentum component is set to be $M = 0$.

of an isovector p-h pair, a suppression of a ground-state-to-ground-state deuteron transfer reaction, *e.g.*, ^{54}Fe(^{3}He, p)^{56}Co, was pointed out. Note that the two proton holes in ^{54}Fe prefer the spatial configuration in which the two holes are close to each other. If one of those proton holes is filled in via deuteron transfer, the neutron in the deuteron and the other proton hole would be located close to each other. This would correspond to an excited state of ^{56}Co; thus, the transfer to the ground state of ^{56}Co would be largely suppressed. It would be interesting future work to estimate the transfer cross sections with the coupled-reaction-channel method or second-order distorted wave Born approximation.

Reference

1) G. F. Bertsch, Phys. Lett. B **25**, 62 (1967).

† Condensed from the article in Phys. Rev. C **106**, 034313 (2022)

*1 Department of Physics, Kyoto University
*2 RIKEN Nishina Center
*3 Center for Mathematics and Physics, University of Aizu

Momentum-space structure of dineutron in ^{11}Li†

M. Yamagami *1

A recent knockout-reaction experiment for the Borromean nucleus ^{11}Li measured the mean correlation angle between the momenta of emitted neutrons n_1 and n_2 in the reaction channel $^{11}\mathrm{Li}(p,pn_1)^{10}\mathrm{Li}^* \to {}^9\mathrm{Li} + n_2$.[1] The dependence on the missing momentum k of n_1 is considered to reflect the spatial structure of dineutron.

Here, the reflection of the spatial structure of dineutron to the mean opening angle between the momenta $\mathbf{k}_1$ and $\mathbf{k}_2$ of the valence neutrons at the ground state of ^{11}Li is discussed. Further, the similarities with the mean correlation angle are highlighted.

A three-body model calculation is performed in the momentum space using a finite-range n–n interaction, which reproduces the two-neutron ($2n$) separation energy and the matter radius of ^{11}Li. Further, the $2n$ density, $\rho_2(k_1,k_2,\theta_k)$, is calculated using $k_1 = |\mathbf{k}_1|$, $k_2 = |\mathbf{k}_2|$, and the opening angle between $\mathbf{k}_1$ and $\mathbf{k}_2$, θ_k. Figure 1(a) shows $\rho_2(k_1,k_2,\theta_k)$ as a function of both $k_1 = k_2 = k_n$ and θ_k. Figure 1(b) shows the $2n$ density in real space via the Fourier transformation, $\rho_2(r_1,r_2,\theta_r)$, using the radial coordinates, $r_1 = r_2 = r$, and opening angle, θ_r.

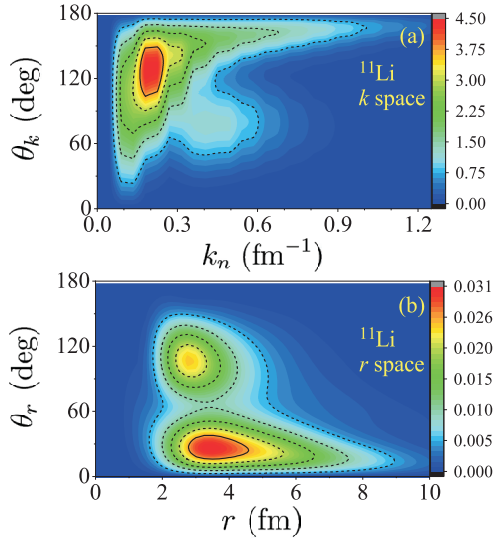

Fig. 1. (a) $2n$ density for ^{11}Li as functions of $k_1 = k_2 = k_n$ and the opening angle θ_k. It is weighted with a factor of $8\pi^2 k_n^4 \sin\theta_k$. (b) Same as (a) but $2n$ density in real space as functions of $r_1 = r_2 = r$ and the opening angle θ_r. It is weighted with a factor of $8\pi^2 r^4 \sin\theta_r$.

The dineutron configuration is obtained at the low-momentum of $(k_n,\theta_k) = (0.18\ \mathrm{fm}^{-1}, 128°)$. It is accompanied by the broad angular distribution, and the long k_n-tail indicates the strong dineutron correlation (the high n–n relative momentum).

The mean opening angle $\langle\theta_k\rangle$ is defined as a function of $k_1 = k_n$ as follows

$$\cos\langle\theta_k\rangle \equiv \left[\int_0^{k_{\mathrm{cut}}} k_2^2 dk_2 \int_0^{\pi} 2\pi \sin\theta_k d\theta_k \times \rho_2(k_n,k_2,\theta_k)\cos\theta_k\right]/\rho_k(k_n), \quad (1)$$

where $\rho_k(k_n)$ is the one-neutron density distribution. Figure 2(a) shows $\langle\theta_k\rangle$ using the cutoff momenta of $k_{\mathrm{cut}} = \infty$ (no cutoff) and $k_{\mathrm{cut}} = k_{\mathrm{surf}} = 0.62$ fm^{-1}.

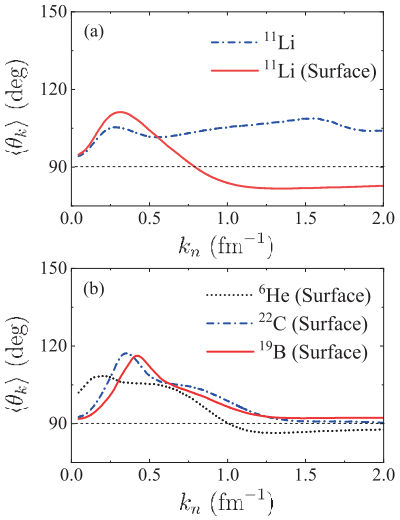

Fig. 2. (a) Mean opening angle $\langle\theta_k\rangle$ as a function of $k_1 = k_n$ for ^{11}Li. "Surface" indicates the cutoff of $k_{\mathrm{cut}} = k_{\mathrm{surf}}$. (b) Same as (a) but for ^{6}He, ^{22}C, and ^{19}B.

$\langle\theta_k\rangle$ (no cutoff) exhibits a peak at $k_n = 0.27$ fm^{-1}; however, it gradually increases above $k_n \approx 0.5$ fm^{-1}.

k_{surf} characterizes the low-momentum halo region by $k_1, k_2 < k_{\mathrm{surf}}$. $\langle\theta_k\rangle$ using $k_{\mathrm{cut}} = k_{\mathrm{surf}}$ exhibits a peak at $k_n = 0.31$ fm^{-1} and a plateau of $\langle\theta_k\rangle \approx 82°$ above $k_n \approx 1.0$ fm^{-1}. These features are consistent with the observed k dependence of the mean correlation angle (the peak at $k \approx 0.3$ fm^{-1} and the plateau of approximately 87° above $k \approx 0.9$ fm^{-1}),[1] which is considered to reflect the $2n$ correlations in the surface region.[2]

In conclusion, the manner in which the mean opening angle reflects the $2n$ density in ^{11}Li was discussed. For $\langle\theta_k\rangle$, the importance of the surface effect and the similarities with the mean correlation angle in the knockout reaction were highlighted. The same conclusion was obtained for ^{6}He, ^{22}C, and ^{19}B (see Fig. 2(b)), wherein the measurement of the momentum dependence of the angular correlations between the halo neutrons can provide useful information on dineutron correlations at low density.

† Condensed from the article in Phys. Rev. C **106**, 044316 (2022)
*1 Department of Computer Science and Engineering, University of Aizu

References

1) Y. Kubota *et al.*, Phys. Rev. Lett. **125**, 252501 (2020).
2) J. Casal *et al.*, Phys. Rev. C **104**, 024618 (2021).

He cluster formation in light neutron-rich nuclei†

H. Motoki,[*1] S. Shin,[*1] Y. Suzuki,[*2] Q. Zhao,[*3] B. Zhou,[*4] and M. Kimura[*5]

Recently, a negative correlation between the neutron number and ^{4}He cluster formation probability on the nuclear surface was experimentally reported for Sn isotopes.[1)] A similar trend was theoretically observed for C isotopes.[2)] However, this trend contradicts to the previous expectation; ^{4}He clustering develops toward the neutron drip-line of Be and B isotopes.[3)] To understand these ambiguous results, we have quantitatively evaluated the ^{4}He cluster formation probability based on the antisymmetrized molecular dynamics (AMD).

Figure 1 shows the calculated intrinsic proton density distributions of the ground states.[4)] Except for ^{11}B, the distributions exhibit two peaks, indicating the formation of He + He and He + He clusters in Be and B isotopes, respectively. The development of clusters can be estimated from the distance between the clusters (distance between two peaks), which is shown in the lower panel of Fig. 1. It suggests a gradual growth of clusters toward the drip line, which is qualitatively consistent with the previous expectation.[3)]

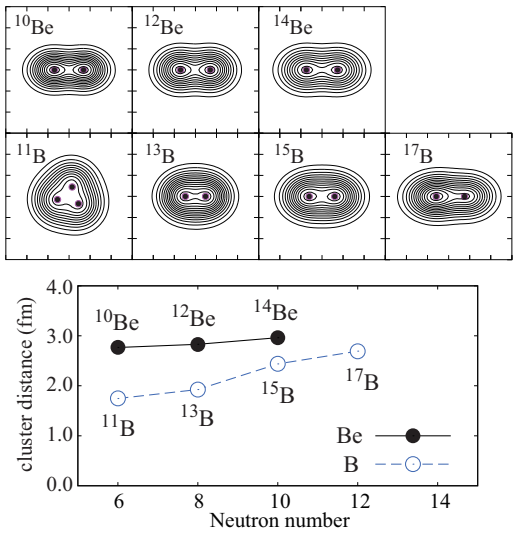

Fig. 1. Upper panels show the intrinsic proton density distribution where peaks of the density distribution are plotted by filled circles. Lower panel shows the distance between cluster centroids, *i.e.* inter-cluster distance.

To quantitatively evaluate He cluster formation and relate it to ^{4}He knockout reaction, we calculated the reduced width amplitude (RWA).

$$r\mathcal{Y}(r) = \sqrt{\binom{A}{A'}}\,\langle \delta(x-r)\,\Phi_{\rm He}\,\Phi_{A'}\,Y_{l=0}(\hat{x})]_0|\,\Phi_{\rm A}\rangle\,, \tag{1}$$

where $\Phi_{\rm He}$, $\Phi_{A'}$ and Φ_A denote the wave functions of the He cluster, daughter, and target nuclei. RWA is the probability amplitude to determine the He cluster at distance r from the daughter nucleus. Hence, its square integral (herein referred to as S-factor) defines the cluster formation probability.

The results are denoted by solid lines in Fig. 2. Unexpectedly, the S-factor decreases as neutron number increases. This contradicts the results illustrated in Fig. 1 and previous expectation;[3)] however, this trend remains consistent in Sn isotopes.[1)] To resolve this issue, we investigated the formation probabilities of ^{6}He and ^{8}He clusters (Fig. 2). The ^{6}He and ^{8}He clusters dominate over the ^{4}He cluster as neutron number increases. Considering the sum of the formation probabilities of He isotopes, we observe an increasing trend, as shown in Fig. 1.

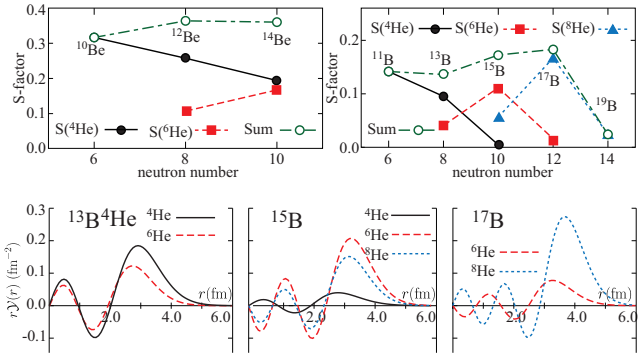

Fig. 2. Upper panels show the ^{4}He, ^{6}He and ^{8}He cluster formation probabilities. The lower panels show the RWA of the ^{4}He, ^{6}He and ^{8}He clusters in B isotopes.

The aforementioned results may be summarized as follows: In neutron-rich Be and B isotopes, ^{4}He is formed as a cluster core; however, but it is always accompanied by excess neutrons. As a result, we should sum up the ^{4}He clusters and ^{6,8}He clusters to accurately evaluate the cluster formation probability. We believe that this new insight is important for future studies to understand the relationship between clustering and excess neutrons.

† Condensed from the articles in Eur. Phys. J. A **57**, 1 (2021) and Prog. Theor. Exp. Phys. **2022**, 113D01 (2022)
*1 Department of Physics, Hokkaido University
*2 Research Center for Nuclear Physics, Osaka University
*3 School of Science, Huzhou University
*4 Institute of Modern Physics, Fudan University
*5 RIKEN Nishina Center

References

1) J. Tanaka *et al.*, Science **371**, 260 (2021).
2) Q. Zhao *et al.*, Eur. Phys. J. A **57**, 1 (2021).
3) Y. Kanada-En'yo *et al.*, Phys. Rev. C **52**, 647 (1995).
4) H. Motoki *et al.*, Prog. Theor. Exp. Phys. **2022**, 113D01 (2022).

Energy spectrum of $^{15}_{\Xi}$C and the ΞN two-body interaction†

Y. Tanimura,[*1,*2] H. Sagawa,[*3,*4] T. -T. Sun,[*5] and E. Hiyama[*1,*4]

Studying the interaction of the strangeness $S = -2$ sector is important in hypernuclear physics for a unified understanding of baryon-baryon interaction. To this end, it is crucial to study the structure of double-strangeness hypernuclei, such as double-Λ and Ξ hypernuclei.

In this work, we focused on new experimental data, IRRAWADDY event,[1)] of a $^{15}_{\Xi}$C nucleus observed at $B_\Xi = 6.27 \pm 0.27$ MeV. We estimate the strengths of the $N\Xi$ interaction and give a consistent interpretation for all the events[1–4)] of the Ξ hypernucleus including IRRAWADDY. In addition to our previous work based on the relativistic mean-field (RMF) model,[5)] we introduce an $N\Xi$ residual interaction and infer that KINKA ($B_\Xi = 8.00 \pm 0.77$ or 4.96 ± 0.77 MeV) and IRRAWADDY events[1)] are the ground-state spin doublet with the Ξ particle in the s orbit and that IBUKI ($B_\Xi = 1.27 \pm 0.21$ MeV) and KISO ($B_\Xi = 3.87 \pm 0.21$ or 1.03 ± 0.18 MeV) events[2,4)] are members of the excited-state multiplets with the Ξ particle in the p orbits.

To describe the $^{15}_{\Xi}$C nucleus and estimate its energy spectrum, we employ an RMF model and spin-isospin dependent residual interaction. Within the RMF model, we adopt the PK1 parameter set[6)] for the nucleon-meson couplings, while the coupling constants in the hyperon sector are fitted to roughly reproduce the observed spectrum. Moreover, the effect of the residual interaction is estimated by first-order perturbation theory with the RMF wave functions taken as the unperturbed states. The ^{14}N subsystem of the $^{15}_{\Xi}$C nucleus is described as the $p_{1/2}$ neutron and proton coupled to spin-parity $J^{\pi_{np}}_{np} = 1^+$ and isospin $T_{np} = 0$ on top of the inert ^{12}C core. The Ξ particle is then coupled to the nucleon pair to make the total quantum number $J^\pi T$, where J^π is the total spin-parity of the system, and $T = 1/2$ in the case of $^{15}_{\Xi}$C.

We consider a residual interaction acting on s and p waves. The s-wave interaction is given by

$$V_{N\Xi} = \sum_{i\in\text{nucleons}} (v_\sigma \boldsymbol{\Sigma}_i \cdot \boldsymbol{\Sigma}_\Xi + v_\tau \vec{\tau}_i \cdot \vec{\tau}_\Xi + v_{\sigma\tau} \boldsymbol{\Sigma}_i \cdot \boldsymbol{\Sigma}_\Xi \vec{\tau}_i \cdot \vec{\tau}_\Xi)\delta(\mathbf{r}_i - \mathbf{r}_\Xi), \quad (1)$$

where $\boldsymbol{\Sigma}$ is the spin operator acting on a Dirac spinor and $\vec{\tau}$ are the isospin operators. The strength parameters of $V_{N\Xi}$ are fixed based on the HAL QCD ΞN potential.[7)] We further introduce a p-wave spin-dependent interaction given by

$$V^p_{N\Xi} = \sum_{i\in\text{nucleons}} v^p_\sigma \boldsymbol{\Sigma}_i \cdot \boldsymbol{\Sigma}_\Xi \overleftarrow{\nabla} \cdot \delta(\mathbf{r}_i - \mathbf{r}_\Xi) \overrightarrow{\nabla}, \quad (2)$$

where v^p_σ is a parameter to be optimized by the measured energies of IRRAWADDY and KINKA events.

Fig. 1(a) shows the energy spectrum of $^{15}_{\Xi}$C as a function of v^p_σ, which is obtained by assuming that the IRRAWADDY event is the ground state of $^{15}_{\Xi}$C. It is seen that $v^p_\sigma \sim -150$ MeV.fm^5 and $\sim$100 MeV.fm^5 give spectra consistent with all the experimental data. Fig. 1(b) shows the energy spectrum obtained by assuming that the lower candidate of the KINKA event is the ground state. In this case, $v^p_\sigma \sim -150$ MeV.fm^5 and $\sim$125 MeV.fm^5 give results consistent with the data.

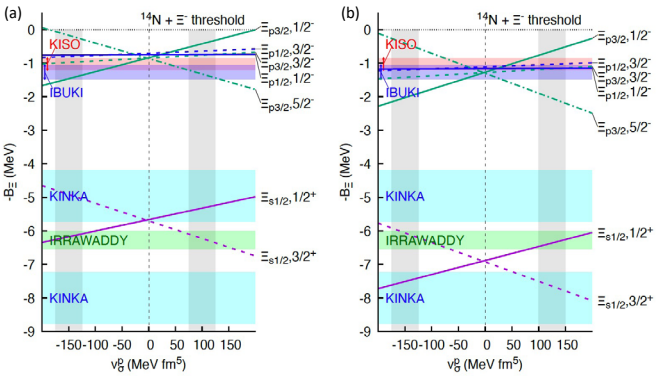

Fig. 1. Estimated energy spectrum of $^{15}_{\Xi}$C nucleus as a function of the p-wave spin-spin interaction strength v^p_σ. The energies of the levels labeled by the orbital occupied by the Ξ^- particle, Ξ_{lj}, and the total spin parity, J^π, are represented by lines. The experimental data of B_{Ξ^-} are shown by color bands.

† Condensed from the article in Phys. Rev. C **105**, 044324 (2022)

*1 Department of Physics, Tohoku University
*2 Graduate Program on Physics for the Universe, Tohoku University
*3 Center for Mathematics and Physics, the Univertysi of Aizu
*4 RIKEN Nishina Center
*5 School of Physics and Microelectronics, Zhengzhou Univeristy

References

1) M. Yoshimoto *et al.*, Prog. Theor. Expt. Phys. **2021**, 073D02 (2021).
2) K. Nakazawa *et al.*, Prog. Theor. Expt. Phys. **2015**, 033D02 (2015)
3) E. Hiyama *et al.*, Annu. Rev. Nucl. Sci. **68**, 131 (2018).
4) S. H. Hayakawa *et al.*, Phys. Rev. Lett. **126**, 062501 (2021).
5) T. T. Sun *et al.*, Phys. Rev. C **94**, 064319 (2016).
6) W. H. Long *et al.*, Phys. Rev. C **69**, 034319 (2004).
7) K. Sasaki *et al.*, Nucl. Phys. A **998**, 121737 (2020).

Microscopic collective inertial masses for nuclear reactions in the presence of the nucleonic effective mass†

K. Wen*1 and T. Nakatsukasa*1,*2

A theoretical description of low-energy nuclear reactions with a solid microscopic foundation is still a challenging subject in nuclear physics. It may provide us with a deep insight into the reaction mechanisms and quantum dynamics of many-nucleon systems. Our strategy is as follows. First, we find a collective subspace spanned by a few selected collective canonical variables, which is decoupled from the intrinsic excitations. The collective subspace and collective variables can be extracted using the adiabatic self-consistent collective coordinate (ASCC) method.[1] The collective subspace in the adiabatic regime is given by a series of time-even Slater determinants and generators of the collective coordinates and momenta locally defined for each state. We apply the method to low-energy nuclear reactions, to identify the optimal reaction path and canonical variables. The self-consistently determined collective reaction path is requantized. The procedure results in the reaction model

$$\left\{-\frac{d}{dR}\frac{1}{2M(R)}\frac{d}{dR}+\frac{\ell(\ell+1)}{2\mathcal{J}(R)}+V(R)\right\}u_\ell(R) = Eu_\ell(R), \quad (1)$$

where R is the relative distance between the projectile and the target nuclei. The wave function for the relative motion is given by $\psi(\mathbf{R}) = u_l(R)Y_{lm}(\hat{R})/R$.

The key ingredients of the requantization procedure are the potential $V(R)$, the inertial mass parameters with respect to the collective coordinates $M(R)$, and the rotational moment of inertia $\mathcal{J}(R)$ in Eq. (1). For the nuclear reaction, the relative distance R between two colliding nuclei should be properly chosen collective coordinates in the asymptotic region ($R \to \infty$). The corresponding inertial mass should be the reduced mass $\mu_{\rm red} = A_P A_T m/(A_P+A_T)$, where A_P (A_T) is the mass number of the projectile (target) nucleus and m is the bare nucleon mass. The moment of inertia $\mathcal{J}(R)$ in Eq. (1) also has an asymptotic value, $\mathcal{J}(R) \to \mu_{\rm red}R^2$ at $R \to \infty$. Therefore, the theory can be tested by examining its asymptotic limit. However, the inertial masses in the interior region where two nuclei touch each other are highly nontrivial. Thus, a microscopic theory for calculating the mass over the entire reaction path is necessary.

In our previous studies,[2] we calculated the ASCC inertial masses for the relative motion between two nuclei for the velocity-independent mean-field potential. We also examined those of the cranking formula, which turned out to be almost identical to the ASCC mass at $R \to \infty$. However, this is not true in general. In particular, the nonlocal mean-field potential produces the effective mass $m^*/m < 1$. In this case, in order to guarantee the Galilean invariance of the energy density functional, we need densities that are time-odd with respect to the time-reversal transformation. The time-odd mean fields play important roles in the time-dependent dynamics because the time-odd densities are nonzero in general for the time-dependent states. Since the ASCC equations are derived from the time-dependent mean-field theory, they are able to take into account the effects of the time-odd mean fields in calculations of the inertial masses. We have found that the ASCC inertial masses reproduce the correct asymptotic values, whereas the cranking formula fails to do so.

Figure 1 shows the results for the moments of inertia $\mathcal{J}(R)$. The velocity dependence in the mean-field potential violates the local Galilean invariance. The calculated cranking moments of inertia (dashed line) are significantly smaller than the rigid-body value $\mathcal{J}_{\rm rig}$ (dotted line). They are also smaller than the point-particle value $\mu_{\rm red}R^2$ (dash-dot line) at large R. In contrast, the ASCC calculation (solid) includes the residual effects of the time-odd mean fields, which restore the local Galilean invariance, nicely reproducing $\mu_{\rm red}R^2$ at $R > 7.5$ fm. Near the equilibrium state ($R \sim 5.5$ fm), it also reproduces the rigid-body value.

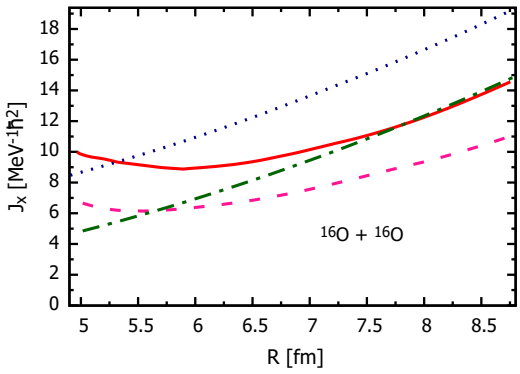

Fig. 1. Rotational moments of inertia as a function of the relative distance R for ^{16}O+^{16}O. See text for details.

References
1) T. Nakatsukasa *et al.*, Rev. Mod. Phys. **88**, 045004 (2016).
2) K. Wen *et al.*, Phys. Rev. C **94**, 054618 (2016); *ibid.* **96**, 014610 (2017).

† Condensed from the article in Phys. Rev. C **105**, 034603 (2022)

*1 Center for Computational Sciences, University of Tsukuba
*2 RIKEN Nishina Center

Gamow-Teller transitions in magic nuclei calculated based on the charge-exchange subtracted second random phase approximation†

M. J. Yang,*1 C. L. Bai,*1 H. Sagawa,*2,*3 and H. Q. Zhang*4

We studied the Gamow-Teller (GT) transitions in four magic nuclei, *i.e.*, ^{48}Ca, ^{90}Zr, ^{132}Sn, and ^{208}Pb based on a self-consistent Hartree-Fock (HF) + subtracted second random phase approximation (SSRPA) model with different Skyrme energy density functionals (EDFs). The SSRPA model describes systematically and quantitatively the GT strength distribution in the four nuclei better than the RPA model.

The results of SAMi-T[1] with and without tensor terms are shown in Fig. 1. Specifically, SGII[2] and SAMi-T EDFs well reproduce the strength distributions of the main GT peaks in terms of the excitation energy and peak height in comparison with the experimental data, except for ^{90}Zr, in which the calculated peak height is approximately two times larger than the experimental result. We examined the effect of tensor terms of the SAMi-T EDF and found that the terms shift the main peaks downward by approximately 1 MeV in ^{48}Ca, ^{132}Sn, and ^{208}Pb; however, they hardly affect ^{90}Zr. The quenching factor has increased slightly; however these values with the tensor interactions are still about a half of the experimental quenching factors. We explored the possibility whether the tensor force with different strengths further enhances the quenching factor of the GT strength. To this end, we adopt the T21, T44, and T55 EDFs from the TIJ family[3] with different values of of the tensor terms. We realized that none of these three parameter sets well described the strength distributions. However, the T55 EDF produces large quenching factors: 30% for ^{48}Ca, 25% for ^{90}Zr, 27% for ^{132}Sn, and 19% for ^{208}Pb. In ^{208}Pb, the quenching factors are smaller, which is related to the insufficient cutoff energy of $2p$-$2h$ configurations.

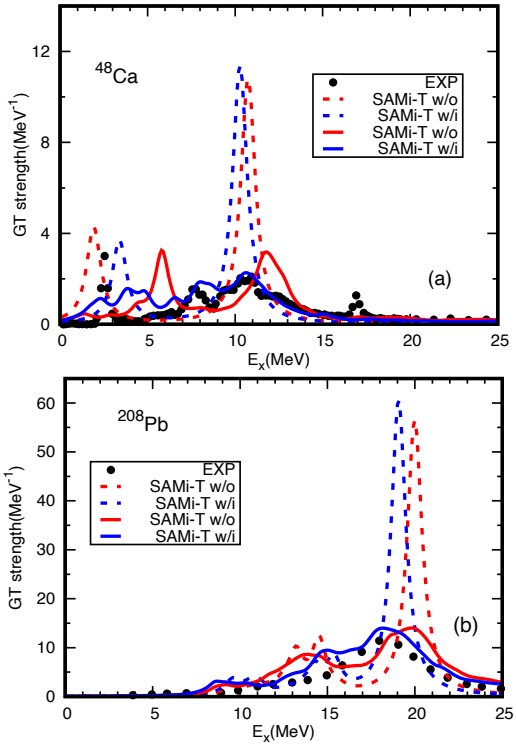

Fig. 1. GT$_-$ strength distributions of ^{48}Ca [panel (a)], and ^{208}Pb [panel (b)] calculated with SAMi-T by RPA (dash lines) and SSRPA (solid lines) with or without tensor terms. The red lines represent SAMi-T without tensor terms labeled w/o, and the blue lines represent SAMi-T with tensor terms labeled w/i. Experimental data are taken from Ref. 4) for ^{48}Ca and Ref. 5) for ^{208}Pb.

Further we studied the role of tensor interactions in quenching with the parameter sets, *i.e.*, SGII + Te1, SGII + Te2, and SGII + Te3 keeping the central part unchanged. With these parameter sets, we found that the tensor interactions significantly affect the strength distributions of GT peaks, *i.e.*, strong effect on the spreading of the strength distribution and shift of the excitation energy. Among the parameters, SGII + Te1 best reproduces the GT strength distributions in the four nuclei. While the SGII + Te1 and SGII + Te3 EDFs, in which the strengths of the triplet-odd tensor term are significantly different even in the sign, produce large quenching factors similar to those of T55. In addition, as SGII is optimized excluding J^2 terms, we performed the calculations in which the J^2 terms are excluded in HF and SSRPA for the SGII EDF. The calculations indicate that the exclusion of J^2 terms originated from the momentum dependent interactions generates larger quenching factors, close to experiments. However, the systematical description of the strength distributions in the four nuclei has not improved much compared to those with the J^2 terms. It is still a challenge to describe realistic strength distributions and large quenching factors with Skyrme EDFs.

† Condensed from the article in Phys. Rev. C **106**, 014219 (2022)
*1 College of Physics, Sichuan University
*2 RIKEN Nishina Center
*3 Center for Mathematics and Physics, University of Aizu
*4 China Institute of Atomic Energy

References
1) S. H. Shen *et al.*, Phys. Rev. C **99**, 034322 (2019).
2) C. L. Bai *et al.*, Phys. Rev. C **83**, 054316 (2011).
3) T. Lesinsky *et al.*, Phys. Rev. C **76**, 014312 (2008).
4) K. Yako *et al.*, Phys. Rev. Lett. **103**, 012503 (2009).
5) T. Wakasa *et al.*, Phys. Rev. C **85**, 064606 (2012).

Indication of α clustering in the density profiles of ^{44,52}Ti†

W. Horiuchi[*1,*2,*3,*4] and N. Itagaki[*1,*2]

The standard nuclear structure is shell structure; however, α-cluster structure often appears in the ground and excited states of light nuclei. Here, we discuss the α-cluster structure in medium mass nuclei, ^{44}Ti and ^{52}Ti, and show that the development of core+α structure can be quantified in the density profiles near the nuclear surface using proton-nucleus elastic scattering.

In the present study, we examine two different density profiles. Shell- and α-cluster configurations are generated by utilizing the basis states of the antisymmetrized quasi-cluster model (AQCM),[1] which can describe both the j-j coupling shell and α-cluster configurations in a single scheme. The AQCM basis for the core (^{40}Ca or ^{48}Ca) plus α cluster is expressed by the antisymmetrized product of the core and α-cluster wave functions, with R being their distance. The wave function of the core nucleus is constructed based on the multi-α cluster model at the zero-distance limit, corresponding to the $N = 20$ closure for ^{40}Ca and eight neutrons are additionally put for the $N = 28$ closure of ^{48}Ca. The size parameters of the core and α-cluster wave functions are taken as the same for simplicity.

The shell-model wave functions for ^{44,52}Ti are obtained by taking $R \to 0$. The size parameter is fixed to reproduce the measured charge radius of ^{44}Ti or ^{52}Ti. We call this shell-model wave function as S-type.

For the α-cluster wave function, we determine the size parameter to reproduce the measured charge radius of the core nucleus and set the R value to reproduce the charge radius of ^{44}Ti or ^{52}Ti. We call this α-cluster wave function as C-type. The determined R value is large (2.85 fm) for ^{44}Ti, indicating a well-developed α-cluster structure. The charge radius of ^{52}Ti is not known. However, to understand the role of excess neutrons, we assume $R = 3$ fm for ^{52}Ti, which is comparable to that of ^{44}Ti.

Although both S- and C-types reproduce the charge radius data, we discover that α clustering significantly changes the density profiles near the surface. To quantify these changes, we evaluate the nuclear "diffuseness,"[2] which is practically obtained by a two-parameter Fermi function, $\rho_0/\{1+\exp[(r-\bar{R})/a]\}$, where the radius ($\bar{R}$) and diffuseness ($a$) parameters are determined by the least-square fitting with the obtained one-body density. The a values for S- and C-types are 0.56 fm and 0.63 fm for ^{44}Ti and 0.58 fm and 0.61 fm for ^{52}Ti, respectively. The α clustering significantly changes the nuclear surface diffuseness, especially for ^{44}Ti, owing to the occupation of the diffused low-angular momentum orbit, *i.e.*, $1p$ orbit. For ^{52}Ti, the difference between S- and C-types is less significant that of ^{44}Ti because the shell-model configuration $(1p_{3/2})^4$ already has a diffused nuclear surface.

We show that this difference can be detected by measuring proton-nucleus elastic scattering at intermediate energies. The proton-nucleus differential elastic scattering cross sections are calculated by the optical-limit approximation in the Glauber model. Inputs to the reaction model are one-body density distributions and profile function. By using the standard profile function, we confirm that the theory reproduces the experimental cross sections for ^{40}Ca and ^{48}Ca using the wave functions obtained by the AQCM approach without introducing any adjustable parameter.

Figure 1 plots the proton-nucleus differential elastic scattering cross sections at 320 MeV/nucleon at around the first peak position, where the difference of the nuclear diffuseness is well reflected.[2] For ^{44}Ti, we see that the difference between the S- and C-type cross sections is large, considering that the uncertainties of the experimental proton-^{40}Ca cross sections at around the first peak position is only ≈4%.[3] The difference is smaller for ^{52}Ti, but it is significant.

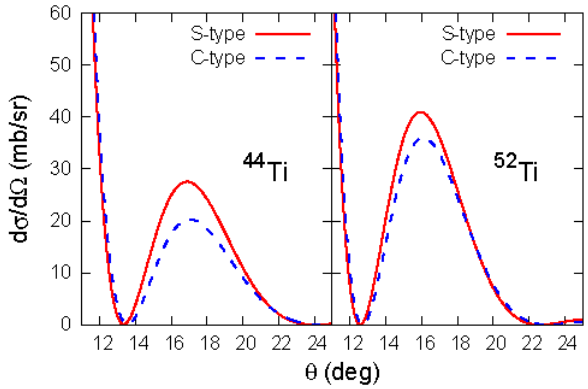

Fig. 1. Proton-^{44,52}Ti differential elastic scattering cross sections at 320 MeV/nucleon for scattering angles near the first peak position.

In summary, we have investigated the density profiles of ^{44}Ti and ^{52}Ti with the shell and α-cluster configurations and found that these two aspects can be distinguished by measuring the proton-nucleus differential elastic scattering cross sections up to the first peak position.

† Condensed from the article in Phys. Rev. C **106**, 044330 (2022)

*1 Department of Physics, Osaka Metropolitan University
*2 Nambu Yoichiro Institute of Theoretial and Experimental Physics, Osaka Metropolitan University
*3 RIKEN Nishina Center
*4 Department of Physics, Hokkaido University

References

1) N. Itagaki *et al.*, Phys. Rev. C **71**, 064307 (2005).
2) S. Hatakeyama *et al.*, Phys. Rev. C **97**, 054607 (2018).
3) J. J. Kelly *et al.*, Phys. Rev. C **44**, 2602 (1991).

Enhanced moments of inertia for rotation in neutron-rich nuclei†

K. Yoshida*1

Nuclear rotational motion emerges due to the spontaneous breaking of rotational symmetry. As stepping away from the magic numbers, the first $I^\pi = 2^+$ state becomes lower in energy: The collective mode of excitation changes its character from vibration to rotation as the deformation develops.

Recently, various spectroscopic studies have been conducted to explore unique structures in neutron-rich nuclei. The excitation energy of the 2_1^+ state, $E(2_1^+)$, is often among the first quantities accessible in experiments and systematic measurements have revealed the evolution of the shell structure. Besides the change of the shell structure associated with the onset of deformation, the $E(2_1^+)$ value may provide rich information on exotic nuclei. A significant lowering of $E(2_1^+)$, observed in a near-drip-line nucleus ^{40}Mg, could be a signal of new physics in drip-line nuclei,[1] as the theoretical calculations have predicted that the magnitude of deformation is not enhanced in ^{40}Mg compared to the Mg isotopes with fewer neutrons.[2]

There are 657 even-even nuclei with known $E(2_1^+)$. In the present study, I limit the scope by excluding the very light nuclei ($Z < 10$), for which mean-field theory is least justified. This eliminates 22 nuclei. The experimental data evaluated as $3/E(2_1^+)$ for 635 nuclei are displayed in Fig. 1 as 'Exp.' There is no collective rotation in spherical nuclei where the MoI is zero. I defined the spherical nuclei if the calculated MoI was less than 0.1 MeV^{-1}. An additional 273 nuclei have been eliminated for that reason, leaving 362 nuclei in the present analysis.

To quantitatively measure the theoretical accuracy, I compared theory and experiment, and examined the statistical properties of the quantity $R = \mathcal{J}_{\rm th}/\mathcal{J}_{\rm exp}$. Here, $\mathcal{J}_{\rm th}$ and $\mathcal{J}_{\rm exp}$ are the theoretical and experimental MoI. For the SkM* functional, the average is $\bar{R} = 1.02$. Here, the Yamagami-Shimizu-Nakatsukasa pairing functional[3] was adopted. When excluding the weakly deformed nuclei with the deformation parameter $\beta < 0.1$, $\bar{R} = 1.07$ for 332 data. Therefore, the present model overestimates the MoI by about 10%. This analysis indicates that the 2_1^+ state is mostly governed by the rotational MoI of the ground state, and the self-consistent cranking model describes the MoI surprisingly well for nuclei with a finite β value.

I investigate the MoI of neutron-rich nuclei, and discussed the unique features near the drip line. A striking feature observed in the result shown in Fig. 1 is that the deformation is strong in the neutron-rich lanthanide nuclei around $N = 100$ and the MoI is large accordingly. Furthermore, the MoI in nuclei near the drip line is comparable to that of heavy actinide nuclei, despite a mass number difference of about 40. The MoI in the lanthanides with $N \sim 150$ is about twice as large as that in the $N \sim 100$ region, although the deformation of protons is almost the same. Because the neutrons are spatially extended, β of neutrons and matter are both smaller than those in the $N \sim 100$ region, which is against a simple perspective for a large MoI. The density dependence of a pairing functional employed in the calculation is the origin of this unique feature near the drip line, and that weak binding plays a minor role.

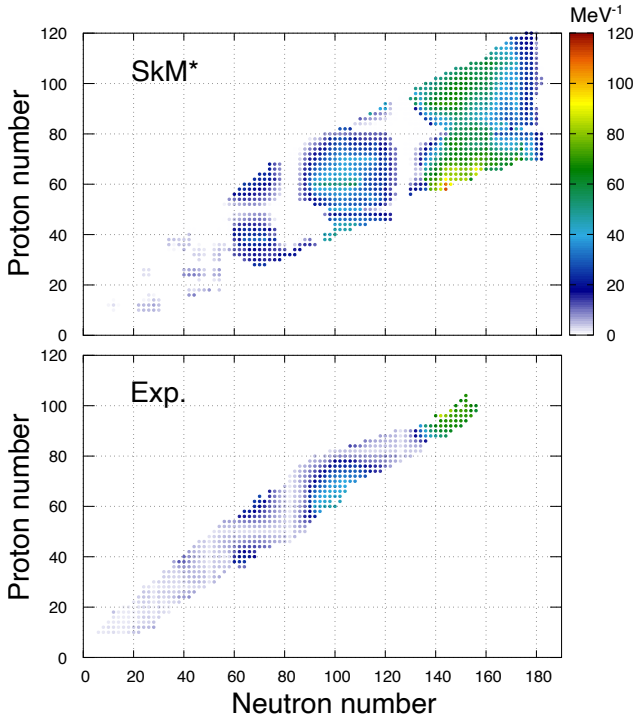

Fig. 1. Calculated moments of inertia $\mathcal{J}$ for the SkM* functional. The experimental data are taken from NNDC, which is evaluated as $3/E(2_1^+)$.

References

1) H. L. Crawford *et al.*, Phy. Rev. Lett. **122**, 052501 (2019).
2) J. Terasaki *et al.*, Nucl. Phys. A **621**, 706 (1997).
3) M. Yamagami *et al.*, Phys. Rev. C **80**, 064301 (2009).

† Condensed from the article in Phys. Lett. B **834**, 137458 (2022)

*1 Research Center for Nuclear Physics, Osaka University

Does the second-order operator in the adiabatic expansion contribute to the collective mass?

K. Sato*1,*2

The adiabatic self-consistent collective coordinate (ASCC) method[1] is a practical method for describing large-amplitude collective motion in atomic nuclei with superfluidity and an advanced version of the adiabatic time-dependent Hartree-Fock-Bogoliubov (HFB) theory. According to the generalized Thouless theorem, the state vector in the ASCC theory can be written in the form

$$|\phi(q,p)\rangle = e^{i\hat{G}(q,p)}|\phi(q)\rangle,$$

where $\hat{G}(q,p)$ is a linear combination of the $a^\dagger a^\dagger$ and aa terms. We shall call the $a^\dagger a^\dagger$ and aa terms as A-terms, and the $a^\dagger a$ and $aa^\dagger$ terms as B-terms. Recently, the ASCC theory including a second-order collective operator has been proposed.[2] There, $\hat{G}(q,p)$ is expanded as

$$\hat{G}(q,p) = p\hat{Q}^{(1)}(q) + \frac{1}{2}p^2\hat{Q}^{(2)}(q). \tag{1}$$

In the conventional ASCC theory, only the first-order collective operator $\hat{Q}^{(1)}$ is included. However, as shown in Refs. 2) and 3), the second-order collective operator $\hat{Q}^{(2)}$ is involved in the moving-frame equations of motion. Moreover, $\hat{Q}^{(2)}$ contributes to the collective mass as

$$\begin{aligned} B(q) =& -\langle\phi(q)|[[\hat{H},\hat{Q}^{(1)}],\hat{Q}^{(1)}]|\phi(q)\rangle \\ &+\langle\phi(q)|[\hat{H},i\hat{Q}^{(2)}]|\phi(q)\rangle. \end{aligned} \tag{2}$$

It is worth mentioning that the second term on the right-hand side gives a contribution of the same order as the first term.

The fundamental equations in the ASCC theory consist of the moving-frame HFB and quasiparticle random phase approximation (QRPA) equations and the canonical-variable conditions, which are derived from the invariance principle of the Schrödinger equation and the canonicity conditions, respectively. The former is the equation of motion, and the latter the conditions for the collective variables to be canonical. In the conventional ASCC theory, only the canonical-variable conditions of $O(1)$ and $O(p)$ have been taken into account, while the equations of motion up to $O(p^2)$ are solved to determine the state vector and collective operators, from which the collective Hamiltonian is calculated. In Ref. 3), the ASCC theory including the second-order collective operator $\hat{Q}^{(2)}$ was successfully applied to the Lipkin model, and it was shown that the inclusion of $\hat{Q}^{(2)}$ improves the agreement with the exact solution.

*1 Faculty of Education, Kochi University
*2 RIKEN Nishina Center

We consider the case where the pairing correlation is not taken into account, and the Hamiltonian does not include the three-body interaction. Then, we shall show that the second-order collective operator $\hat{Q}^{(2)}$ does not directly contribute to the collective mass if the second-order canonical-variable condition

$$\langle\phi(q)|[\hat{Q}^{(1)},\hat{Q}^{(2)}]|\phi(q)\rangle = 0 \tag{3}$$

is imposed.[2,3] Noting that $\hat{Q}^{(2)}$ is written in terms of A-terms only and that the Hamiltonian can be written in terms of A-terms, B-terms, and normally ordered quartic terms, one can easily see that

$$\langle\phi(q)|[\hat{H},i\hat{Q}^{(2)}]|\phi(q)\rangle = \langle\phi(q)|[\hat{H}_A,i\hat{Q}^{(2)}]|\phi(q)\rangle. \tag{4}$$

Here, $\hat{H}_A$ denotes the A-part of $\hat{H}$.

From the moving-frame Hartree-Fock equation, we obtain

$$\hat{H}_A = \partial_q V\hat{Q}^{(1)}. \tag{5}$$

By substituting Eq. (5) into Eq. (4), we obtain

$$\begin{aligned} &\langle\phi(q)|[\hat{H},i\hat{Q}^{(2)}]|\phi(q)\rangle \\ &\quad = i\partial_q V\langle\phi(q)|[\hat{Q}^{(1)},\hat{Q}^{(2)}]|\phi(q)\rangle = 0 \end{aligned} \tag{6}$$

if the second-order canonical-variable condition in Eq. (3) is met. Then, the inertial mass $B(q)$ is

$$B(q) = -\langle\phi(q)|[[\hat{H},\hat{Q}^{(1)}],\hat{Q}^{(1)}]|\phi(q)\rangle. \tag{7}$$

The second-order collective operator $\hat{Q}^{(2)}$ does not contribute to the inertial mass directly, but it can contribute only through the equations of motion. $\hat{Q}^{(2)}$ contributes to the first- and second-order moving-frame equations of motion, which may affect the state vector $|\phi(q)\rangle$.

Here, we have concentrated on the case without the pairing correlation. When the pairing correlation is taken into account, the $\hat{Q}^{(2)}$ term in the inertial mass in Eq. (2) does not vanish even if the condition in Eq. (3) is imposed. Before ending this report, we add one remark. It is not trivial whether one should/can include the second-order canonical-variable condition in Eq. (3) in the set of fundamental equations of the ASCC theory. If it is imposed in addition to the first-order canonical-variable conditions, there may be too many conditions to determine the unknown quantities, and the problem may be overdetermined. This point will be investigated and reported in a future publication.

References

1) M. Matsuo *et al.*, Prog. Theor. Phys. **103**, 959 (2000).
2) K. Sato, Prog. Theor. Exp. Phys. **2018**, 103D01 (2018).
3) K. Sato, Prog. Theor. Exp. Phys. **2017**, 033D01 (2017).

3. Nuclear Data

EXFOR compilation of RIBF data in 2022

S. Shin,[*1] S. Watanabe,[*1] M. Kimura,[*2,*3] M. Aikawa,[*2,*3] and N. Otuka[*4,*3]

Nuclear databases are crucial for providing the best estimates of nuclear reactions to a wide range of data users in various scientific and related fields. Among them, nuclear reaction data support the most important aspects of nuclear technology (nuclear power generation, nuclear fuel cycle, environmental monitoring, dosimetry, radiation safety, radioisotope production, radiation therapy, medical diagnosis, *etc.*) and science (nuclear physics, nuclear chemistry, geophysics, space physics, *etc.*).

The EXFOR library (EXchange FORmat for experimental nuclear reaction data) is the largest and most globally used publicly available database.[1] It is maintained by the International Network of Nuclear Reaction Data Centers (NRDC) under the auspices of the International Atomic Energy Agency (IAEA).[2] The scope of the EXFOR library covers a wide range of nuclear reactions such as neutron-induced, charged-particle, and photon-induced reactions.

The Hokkaido University Nuclear Reaction Data Center (JCPRG)[3] was established in 1973 and joined NRDC in 1975 as the first member from Asian countries. The JCPRG is responsible for compiling nuclear reaction data with charged particles and photons measured at Japanese facilities,[4] and its contribution to the EXFOR database amounts to approximately 10% of the total database. The database compilation process begins with scanning of peer-reviewed journal papers published within the scope of EXFOR. Subsequently selected papers are assigned to unique entry numbers and entered into the EXFOR library, where the editorial progress can be monitored. Bibliographic information, experimental equipment, physical quantities measured, numerical data measured, and error information are extracted and entered into a single EXFOR entry. During this process, we communicate with the authors, asking questions regarding the content of their paper, and requesting numerical data.

Aiming to increase the availability of RIBF data, JCPRG has been compiling data obtained from RIBF since 2010 in cooperation with the RIKEN Nishina Center. The new EXFOR data related to RIBF experiment are as follows. We have compiled 40 new papers and revised 3 old entries, of which 17 were from RIKEN; 17 new papers. We can access these data based on the entry numbers presented in Table 1.

Collaboration with RIKEN has aided in the establishment of an efficient procedure for compilation. Much of the RIKEN data was compiled soon after the publication of the papers, allowing for smooth access by end users. We are also grateful to the authors of the RIKEN papers who have provided us with numerical data. This has greatly helped to improve the accuracy and quality of the database.

Table 1. Entry numbers with references compiled from RIBF data in 2022.

		Entries	
New	E2620[5]	E2659[6]	E2682[7]
	E2685[8]	E2687[9]	E2689[10]
	E2693[11]	E2697[12]	E2698[13]
	E2703[14]	E2704[15]	E2705[16]
	E2712[17]	E2713[18]	E2715[19]
	E2722[20]	E2723[21]	
Total		17	

We would like to take this opportunity to express our thanks to the authors of these papers for their kind cooperation with the EXFOR compilation process.

*1 Graduate School of Science, Hokkaido University
*2 Faculty of Science, Hokkaido University
*3 RIKEN Nishina Center
*4 Nuclear Data Section, International Atomic Energy Agency

References

1) N. Otuka *et al.*, Nucl. Data Sheets **120**, 272 (2014).
2) IAEA Nuclear Data Services, `https://www-nds.iaea.org/`.
3) Hokkaido University Nuclear Reaction Data Centre, `https://www.jcprg.org/`.
4) M. Kimura, AAPPS Bulletin **28**, 24 (2018).
5) S. Wimmer *et al.*, Phys. Lett. B **785**, 441 (2018).
6) A. Frotscher *et al.*, Phys. Rev. Lett. **125**, 012501 (2020).
7) Z. Tsoodolés *et al.*, Appl. Radiat. Isot **168**, 109448 (2021).
8) H. Suzuki *et al.*, Phys. Rev. C **102**, 064615 (2020).
9) L. Yang *et al.*, Phys. Lett. B **813**, 136045 (2021).
10) Z. H. Yang *et al.*, Phys. Rev. Lett. **126**, 082501 (2021).
11) M. Aikawa *et al.*, Nucl. Instrum. Methods Phys. Res. B **498**, 23 (2021).
12) D. Ichinkhorloo *et al.*, Nucl. Instrum. Methods Phys. Res. B **499**, 46 (2021).
13) M. M. Juhasz *et al.*, Phys. Lett. B **814**, 136108 (2021).
14) M. Sakaguchi *et al.*, Appl. Radiat. Isot **176**, 109826 (2021).
15) M. M. Juhasz *et al.*, Phys. Rev. C **103**, 064308 (2021).
16) D. Bazin *et al.*, Phys. Rev. C **103**, 064318 (2021).
17) H. Suzuki *et al.*, Nucl. Instrum. Methods Phys. Res. B **317**, 756 (2013).
18) F. Browne *et al.*, Phys. Rev. Lett. **126**, 252501 (2021).
19) M. Aikawa *et al.*, Nucl. Instrum. Methods Phys. Res. B **508**, 29 (2021).
20) M. Aikawa *et al.*, Nucl. Instrum. Methods Phys. Res. B **515**, 1 (2022).
21) K. Sugihara *et al.*, Nucl. Instrum. Methods Phys. Res. B **512**, 102 (2022).

Measurement of isotopic production cross section on ^{99}Tc *via* proton- and deuteron-induced reactions

R. Matsumura,[*1,*2] H. Otsu,[*1] H. Wang,[*3] H. Sakurai,[*1] D. Nishimura,[*4] H. Takahashi,[*4] S. Takeshige,[*5] M. Tanaka,[*1] and Y. Togano[*1,*5] for the RIBF-TM2021 Collaboration

In order to evaluate the reactions of the long-lived fission products (LLFPs) with neutron, we have measured systematically the proton- and deuteron-induced cross sections for ^{90}Sr,[1] ^{137}Cs,[1] ^{93}Zr,[2] ^{107}Pd,[3] *etc.* As a next step, we started a study on ^{99}Tc, which is known to be one of the LLFPs.

A secondary beam including ^{99m}Tc was produced by the in-flight fission of ^{238}U at 345 MeV/nucleon on a 3-mm-thick ^{9}Be target, selected and identified event-by-event using the TOF-$B\rho$-ΔE method[4] in BigRIPS. It also included ^{99m}Tc ($T_{1/2}$ = 6 h), which is indistinguishable by the same method, was irradiated to a 3-mm-thick Al plate and studied for the production ratio by in-flight fission using the Ge detector. Cocktail beams of ^{99}Tc and ^{99m}Tc at 114 MeV/nucleon were bombarded with CH_2, CD_2, and C reaction targets placed at the entrance of ZD spectrometer (ZDS). The residual nuclei produced in the reactions were identified in ZDS. Since the momentum acceptance of ZDS is limited to ±3%, the measurement was conducted using 5 different momentum settings ($\Delta(B\rho)/B\rho = -9$, -6, -3, 0, and $+3$%) for each target to accept a wide range of the mass-to-charge ratio A/Q.

Figure 1 shows particle identification of residual nuclei was realized by combining A/Q and atomic number Z, derived from the measured information in ZDS. The A/Q (relative RMS) resolution was 0.20%, which corresponds to 5.4σ separation. On the other hand, the Z resolution was 0.80%, not achieving even 3σ separation. This is probably because the integration time of the F11IC[5] Shaping Amp. was unintentionally adjusted to be too short. Although the identification resolution is insufficient compared to the previous experiments, the yield can be counted up with the superposition of 2-D Gaussian functions.

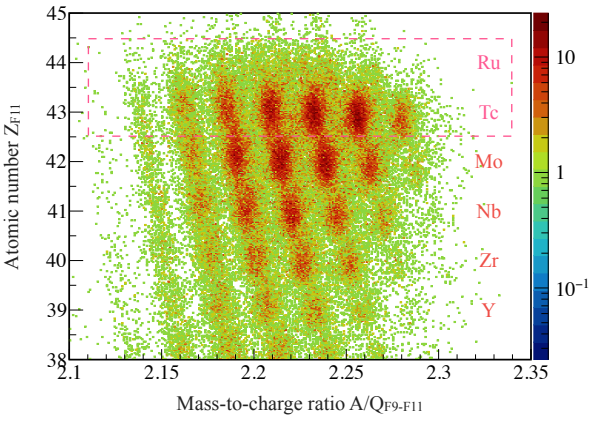

Fig. 1. Particle identifications of residual nuclei were produced in reactions with the CH_2 target at the $\Delta(B\rho)/B\rho = -6$% setting on ZDS.

Moreover, the Ru isotopes from the ^{99}Tc beam are scarcely observed in the region indicated by the dashed line in Fig. 1. It was confirmed that the Ru and Tc isotopes with large pulse heights were overflowing in some or all of the ADCs with 6 channel readout. The number of overflowed channels causes a difference in the peak position of each isotope in the A/Q spectrum. In Fig. 2, the A/Q spectrum is plotted for that overflow bit information. The peaks indicated in the blue curve are almost consistent with the unique A/Q of the Tc isotopes. Whereas the red curve is considered to be the sum of both responses because it has a peak in the middle of each A/Q of Tc and Ru. We plan to decompose the red curve into each response from the strictly defined A/Q peak positions.

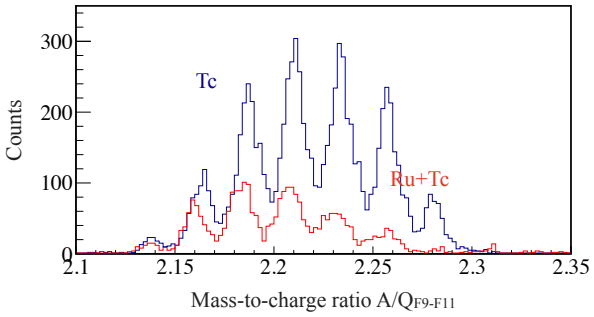

Fig. 2. A/Q spectra showing the dashed line region in Fig. 1, these are imposed overflow bit = 5, 6 for red curve and 1 for blue curve.

We have started a new study of proton- and deuteron-induced cross sections on ^{99}Tc. After the analysis method is finalized, the other remaining targets will be analyzed.

*1 RIKEN Nishina Center
*2 Department of Physics, Saitama University
*3 RIKEN Cluster for Pioneering Research
*4 Department of Natural Sciences, Tokyo City University
*5 Department of Physics, Rikkyo University

References

1) H. Wang *et al.*, Phys. Lett. B **754**, 104 (2016).
2) S. Kawase *et al.*, Prog. Theor. Exp. Phys. **2017**, 093D03 (2017).
3) H. Wang *et al.*, Prog. Theor. Exp. Phys. **2017**, 021D01 (2017).
4) N. Fukuda *et al.*, Nucl. Instrum. Methods Phys. Res. B **317**, 323 (2013).
5) K. Kimura *et al.*, Nucl. Instrum. Methods Phys. Res. A **538**, 608 (2005).

Generating scattering data using Gaussian process regression†

S. Watanabe,[*1] F. Minato,[*2,*3] M. Kimura,[*4] N. Iwamoto,[*2] and S. Yoshida[*5]

Recently, several studies[1,2] have employed machine learning algorithms to improve the accuracy of nuclear data evaluation and reduce the production cost. Herein, we introduce a framework which combines Gaussian process regression (GPR) with a nuclear reaction model code, *i.e.*, 'CCONE'.[3,4] The framework determines model parameters required by CCONE to reproduce and predict nuclear reaction data.

Figures 1 and 2 demonstrate how the proposed framework works. In this example, we used the experimental data of neutron elastic scattering on ^{54}Fe at incident energies of E = 6, 10, 15, and 17 MeV as input.[5] In the first step, by combining CCONE and Bayesian optimization with the Gaussian process (BO-GP), we optimize the depth of the real part of the optical potential, which is denoted by $v_R^0(E)$, to reproduce these data. The obtained optimal values of $v_R^0(E)$ at each energy is plotted by open circles in Fig. 1.

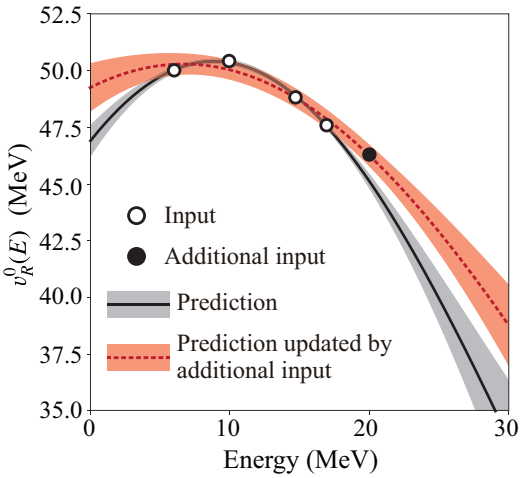

Fig. 1. Open circles show the optimal values of $v_R^0(E)$ at E = 6, 10, 15 and 17 MeV obtained by BO-GP. With these input, GPR predicts $v_R^0(E)$ as shown by solid line with shadowed area. With additional input at E = 20 MeV denoted by filled circle, GPR updates the prediction as shown by dotted line with shadowed area.

In the second step, using optimal values as inputs, $v_R^0(E)$ as a function of E is predicted by GPR, as denoted by the solid line with a shadowed area in Fig. 1.

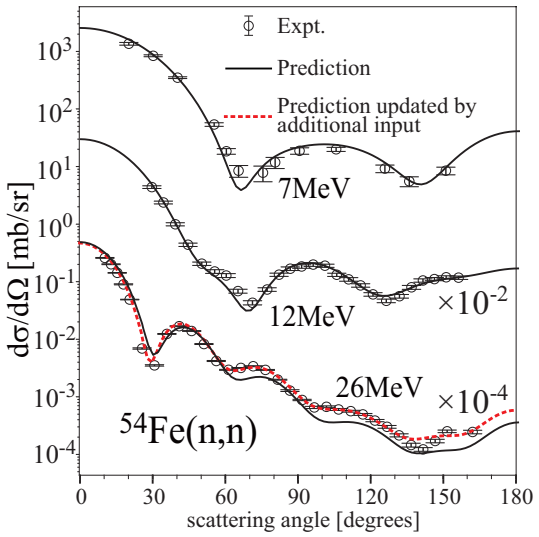

Fig. 2. Predicted and observed angular distributions of ^{54}Fe(n,n) at the incident energies of E = 7, 12, and 26 MeV.

Then, using CCONE and the predicted value of $v_R^0(E)$, our framework predicts unknown cross sections. Figure 2 shows the comparison of the prediction results for E = 7, 12, and 26 MeV with the actual experimental data. The framework works quite effectively to predict data at E = 7 and 12 MeV, which correspond to the interpolation of the known data. Even in the case of the extrapolation of the known data, *i.e.*, E = 26 MeV, it can perform a plausible prediction.

This framework can investigate how new experimental data improve prediction. Herein, we add a new data set at E = 20 MeV, and calculate the optimal $v_R^0(E)$ at this energy, as denoted by the filled circle in Fig. 1. With this additional input, GPR can enhance the prediction of $v_R^0(E)$, as denoted by the dashed line with a shadowed area. With this enhanced $v_R^0(E)$, the cross section at E = 26 MeV is calculated as plotted as a dotted line in Fig. 2, where we see considerable improvement in backward angles.

The development of this framework is in progress, and we expect that it will generate accurate nuclear reaction databases enhanced with a large amount of experimental data produced at RIBF.

† Condensed from the articles in J. Nucl. Sci. Technol. **59**, 1399 (2022)
*1 Department of Physics, Hokkaido University
*2 Nuclear Data Center, Japan Atomic Energy Agency
*3 Department of Physics, Kyushu University
*4 RIKEN Nishina Center
*5 Institute for Promotion of Higher Academic Education, Utsunomiya University

References

1) A. E. Lovell *et al.*, J. Phys. G **47**, 114001 (2020).
2) H. Iwamoto *et al.*, J. Nucl. Sci. Technol. **57**, 932 (2020).
3) S. Watanabe *et al.*, J. Nucl. Sci. Technol. **59**, 1399 (2022).
4) S. Watanabe *et al.*, Eur. Phys. J. Conf. Ser. (in press).
5) All experimental data are collected from EXFOR database.

4. Hadron Physics

Transverse single spin asymmetry for forward neutron production in polarized $p + p$ collisions at $\sqrt{s} = 510$ GeV

M. H. Kim*1 for the RHICf Collaboration

Transverse single spin asymmetry ($A_{\rm N}$) is defined by a left-right cross-section asymmetry with respect to the beam polarization. In high-energy polarized $p + p$ collisions, $A_{\rm N}$ of the forward (pseudorapidity $\eta > 6$) particle is a unique observable for studying the spin-involved diffractive particle production mechanism.

$A_{\rm N}$ for forward neutron production has been explained by the interference between the spin flip (π exchange) and nonflip (a_1 exchange) amplitudes with a nonzero phase shift. This π and a_1 exchange model predicted that the neutron $A_{\rm N}$ would increase in magnitude with the transverse momentum ($p_{\rm T}$) and explained the PHENIX data, which had been measured with three different collision energies, 62.4, 200, and 500 GeV.[1] Recent PHENIX results,[2] which unfolded $A_{\rm N}$ on $p_{\rm T}$ at $\sqrt{s} = 200$ GeV, were also in good agreement with the prediction of the π and a_1 exchange model. However, the π and a_1 exchange model predicted the neutron $A_{\rm N}$ only in the range of $p_{\rm T} < 0.4$ GeV/c.

In June 2017, the RHICf experiment[3] measured $A_{\rm N}$ for forward neutron production in polarized $p+p$ collisions at $\sqrt{s} = 510$ GeV by installing an electromagnetic calorimeter,[4] the RHICf detector, at the zero-degree area of the STAR experiment at the Relativistic Heavy Ion Collider. We measured the neutron $A_{\rm N}$ over a wider range of $0 < p_{\rm T} < 1$ GeV/c to compare the results with those of PHENIX and to test the π and a_1 exchange model in the higher p_T region. In this article, we report the preliminary results of the neutron $A_{\rm N}$ measured by the RHICf experiment.

Neutrons were separated from the photon background using the difference between their shower developments in the detector. Once the neutron candidates were selected, Bayesian unfolding,[5] which is available in the RooUnfold library,[6] was applied to estimate the true longitudinal momentum fraction ($x_{\rm F}$) and $p_{\rm T}$ distributions. $A_{\rm N}$ could be calculated because unfolding was applied for events from both spin-up and spin-down polarizations. Because finite photon and charged hadron backgrounds were included in the neutron candidates, the $A_{\rm N}$ backgrounds were subtracted by estimating their fractions. Refer to Ref. 7) for a more detailed analysis procedure.

Figure 1 shows the preliminary results for the forward neutron $A_{\rm N}$ as a function of $p_{\rm T}$. The systematic uncertainties due to unfolding, the beam center calculation, polarization estimation, and background subtraction are included. In the range $p_{\rm T} < 0.2$ GeV/c, the values of the forward $A_{\rm N}$ measured by RHICf are consistent with those of PHENIX, even though the collision energies are different. In the range $x_{\rm F} > 0.46$, $A_{\rm N}$ increases in magnitude with $p_{\rm T}$, even in the $p_{\rm T}$ range beyond where $A_{\rm N}$ was calculated theoretically. Comparing the data points in $x_{\rm F} < 0.46$ and $x_{\rm F} > 0.46$, there is a gap, which indicates that the neutron $A_{\rm N}$ is possibly dependent on $x_{\rm F}$, which has not been predicted.

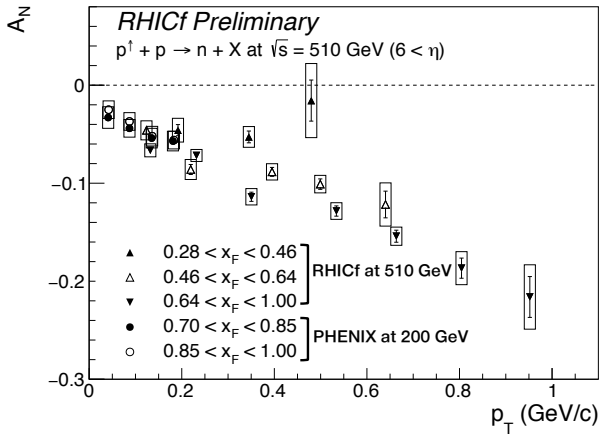

Fig. 1. Forward neutron $A_{\rm N}$ as a function of $p_{\rm T}$ for different $x_{\rm F}$ regions. The triangular and circular data points are the RHICf and PHENIX results, respectively. The error bars indicated by lines and boxes correspond to the statistical and systematic uncertainties, respectively.

In the preliminary results, large systematic uncertainties are assigned to background subtraction because an analysis of the front counter, which had been installed in front of the RHICf detector to suppress the charged hadron background, was not complete. However, the final results will be released soon because the background study has been recently completed.

*1 RIKEN Nishina Center

References

1) B. Z. Kopeliovich *et al.*, Phys. Rev. D **84**, 114012 (2011).
2) U. A. Acharya *et al.* (PHENIX Collaboration), Phys. Rev. D **105**, 032004 (2022).
3) RHICf Collaboration, arXiv:1409.4860v1.
4) K. Kawade *et al.*, J. Instrum. **9**, P03016 (2014).
5) G. D'Agostini, Nucl. Instrum. Methods Phys. Res. A **362**, 487 (1995).
6) T. Adye, arXiv:1105.1160.
7) M. H. Kim for the RHICf Collaboration, https://doi.org/10.5281/zenodo.7271694 .

EIC activities in Japan

Y. Goto*1 for the EIC-Japan Group

The Electron-Ion Collider (EIC) is the highest priority future project in nuclear physics field in the United States and is the world's first polarized electron + polarized proton and nuclei collider to be constructed at Brookhaven National Laboratory (BNL).[1] The EIC User Group was established in 2016, with participants from the U.S., Europe, Asia, and other regions numbering more than 1,300 members. In Japan, the EIC-Japan Group was established at approximately the same time and has been very active. The EIC project has now been authorized by the U.S. Department of Energy to begin the project execution phase, and this year we will prepare a Technical Design Report for the next phase. The EIC-Japan group is also participating in the design of the detector for the ePIC international collaboration experiment to be conducted at the first collision point of the EIC.

In 2022, the EIC-Japan Group submitted a proposal to the Science Council of Japan's "Future Science Promotion Initiative" as part of the "International High Energy Quantum Science Frontier: QCD Research at Overseas Facilities." The proposal aims to promote QCD research to be developed at overseas facilities, including high-density QCD at GSI-FAIR, high-temperature QCD at CERN-LHC, nucleon and nuclear structure studies at BNL-EIC, and theoretical research and computational research of QCD. The proposal was discussed and granted by the Japanese Nuclear Physics Committee.

As part of our participation in the ePIC detector, we aim to contribute to three subsystems. (1) For the Zero-Degree Calorimeter (ZDC), we are leading the design (Fig. 1), simulation calculation, and performance evaluation, and further evaluation is underway as the basic design.[2] The electromagnetic calorimeter technology in this design uses the tungsten/silicon detector of ALICE-FoCal-E calorimeter,[3] which is promoted mainly by the University of Tsukuba group. Test beam evaluations of the prototype detectors are conducted at CERN and Tohoku University's ELPH facility, and radiation tolerance tests of the silicon detectors are conducted at the RIKEN RANS neutron facility. (2) The construction of a barrel detector using AC-LGAD (Low-Gain Avalanche Detector), which has excellent timing and position resolution, is intended to be conducted with the contribution of the EIC-Japan Group. We plan to evaluate a test board shown in Fig. 2 that combines a sensor manufactured at BNL and a readout ASIC manufactured in France. In addition, we will develop a sensor with Hamamatsu Photonics K. K. in Japan. Simulation calculations for design evaluation in combination with the ePIC detector are in progress. (3) Discussion of contributions to the Free Streaming DAQ system will proceed.

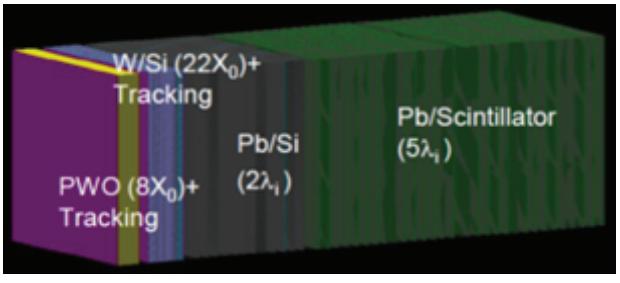

Fig. 1. A design of the ZDC.

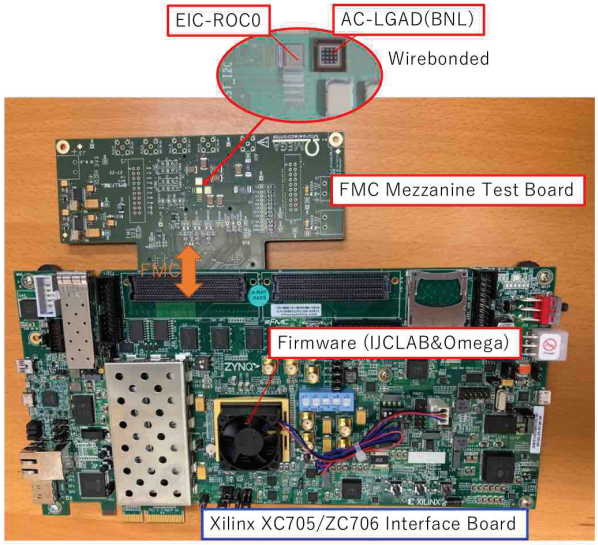

Fig. 2. A test board of the AC-LGAD.

Discussions are underway for cooperation with the Asian region, particularly the South Korean and Taiwanese groups, which began in late 2022. In addition to the three subsystems mentioned above, we will also deepen regional cooperation on projects led by other Asian groups. Cooperation between the nuclear physics and high-energy physics fields will also be expanded and developed in the future.

References

1) R. A. Khalek *et al.*, Nucl. Phys. A **1026**, 122447 (2022).
2) S. Shimizu *et al.*, in this report.
3) ALICE Collaboration, ALICE-PUBLIC-2019-005.

*1 RIKEN Nishina Center

Impact studies for transverse spin measurements at the EIC†

R. Seidl*1

The ECCE proposal was one of three proposals for the project detector of the Electron Ion Collider to be built at Brookhaven national laboratory. It has since been chosen and forms the baseline of the ePIC collaboration that has been formed recently. One of the goals of the EIC is the extraction of the three-dimensional transverse spin and momentum structure of the nucleon. These can generally be accessed via semi-inclusive deeply inelastic scattering (SIDIS) events where in addition to the scattered lepton also a final-state hadron is detected and its transverse momentum and azimuthal asymmetries are extracted. Within the ECCE proposal several full detector simulations were performed using GEANT4 and PYTHIA6 as generators. While transverse momentum dependence is reasonably described in the generator, transverse spin effects are not included. Those were artificially included based on global fits of existing data by reweighting each event according to these parameterizations. In doing so azimuthal single spin asymmetries such as the so-called Sivers and Collins asymmetries could be generated and reconstructed after the full simulations.

An example is shown in Fig. 1 for the Collins asymmetry of charged pions in two kinematic example bins as a function of the hadron fractional momentum z. In the higher x bin, where x describes the momentum fraction the struck parton carries, a sizeable asymmetry is visible for both charges. The reconstructed asymmetries are able to reproduce these results rather well, suggesting little smearing of all kinematic variables involved. Extrapolating these simulations to the expected accumulated luminosities of 10 fb^{-1} and assigning discrepancies between generated and reconstructed asymmetries as maximal systematic uncertainties, the expected precision of the EIC measurements can be evaluated, as shown in Fig. 2. These expected uncertainties can then be fed into the aforementioned global fits to extract the impact of the EIC measurements on the transverse polarization of quarks in the nucleon, its integrals the tensor charges, and the Sivers function, as previously performed in Ref. 1). It was found that the ECCE detector proposal fullfills the requirements of the Yellow Report[2] well and the impact on the transverse spin and momentum structure of the nucleon is immense. As example the impact on the uncertainties of the tensor charged for up and down quarks is shown in Fig. 3 in comparison to the current precision and the Lattice QCD predictions. Eventually, discrepancies between Lattice and measurements could hint at physics beyond the standard model once the phenomenological description is sufficiently improved.

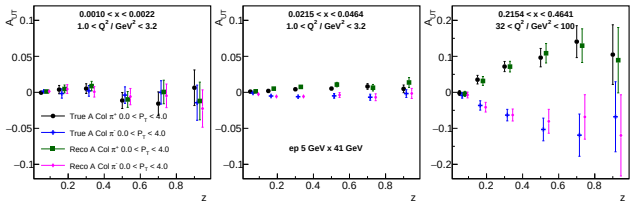

Fig. 1. Example of the positive (generated: black, reconstructed: green) and negative (generated: blue, reconstructed: purple) pion Collins asymmetries as a function of momentum fraction z, in three example bins of DIS variables x and Q^2 in 5 GeV × 41 GeV e-p collisions. For simplicity, transverse momentum was integrated over.

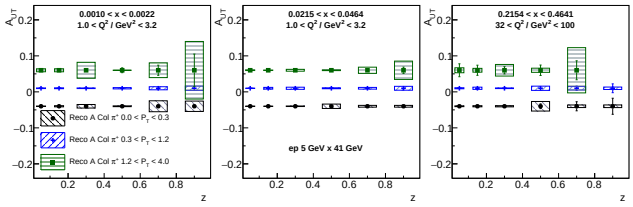

Fig. 2. Expected uncertainties for positive pion Collins asymmetries in three transverse momentum bins as a function of momentum fraction z, in three example bins of DIS variables x and Q^2 in 5 GeV × 41 GeV e-p collisions.

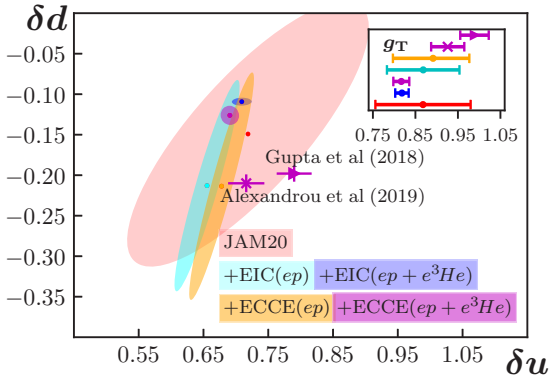

Fig. 3. Expected impact on the tensor charges under inclusion of the expected ECCE uncertainties. The small differences between Yellow Report and ECCE impact values arise from the different pseudo-data sets resulting is slightly different central values.

† Condensed from the article in Nucl. Instrum. Methods Phys. Res. A **1049**, 168017 (2023)

*1 RIKEN Nishina Center

References

1) L. Gamberg *et al.*, Phys. Lett. B **816**, 136255 (2021).
2) R. Abdul Khalek *et al.*, arXiv:2103.05419.

Zero degree calorimeter for the ePIC experiment

S. Shimizu[*1,*2] for the EIC Japan group

The Electron Ion Collider (EIC) is the next collider scheduled to be built at the Brookhaven National Laboratory in US. It collides electrons and protons or nuclei and will provide a powerful measure to examine the structure of protons and nuclei. In 2022, a new collaboration was formed, named ePIC, as an experiment at the interaction point IP6. The ePIC detector will be a multi-purpose detector, with suites of detectors in the far-forward and far-backward regions of the ion-beam direction.

The Zero Degree Calorimeter (ZDC) is one of the far-forward detector systems. It is used to detect photons and neutrons coming from the interaction point. The ZDC enables measurements for several key EIC physics programs[1)] such as exclusive vector meson production in $e+A$ collisions or spectator-neutron-tagged $e+d$ deep inelastic scattering. Its first design was considered for EIC in the previous report.[2)] It comprises a crystal calorimeter and three types of sampling calorimeters.

The same ZDC design was adopted to the ePIC detector as a baseline ePIC ZDC design. In the ePIC collaboration, a new software framework was developed and the ZDC design was migrated there. Figure 1 shows a schematic of the ePIC detector including the ZDC.

A few details of the ZDC design are examined and discussed: material of the crystal calorimeter, radiation resistance of photon detectors, and placement of the ZDC.

The material of the crystal calorimeter was studied by simulation. Two materials were compared: LYSO and $PbWO_4$, where the former has a >100 times higher light yield but is more expensive with respect to the latter. Considering the photon counting effect, the comparison showed no large difference in the cluster finding efficiency. Worse energy resolution was observed for $PbWO_4$, but it is still acceptable for the physics requirement of 20%. As far as the performance of the calorimeter system is sustained as designed, $PbWO_4$ can be used for the ZDC crystal calorimeter.

The crystal calorimeter requires photon detectors to detect light in the crystal, and avalanche photodiodes (APDs) are the first candidate for the ZDC. Hamamatsu APDs S8664-55 were irradiated at RANS, RIKEN Accelerator-driven compact Neutron Sources, to test their radiation resistance. Following two days of irradiation, the estimated dose on the APDs is 10^{12}–10^{13} neutrons/cm^2.[a)] All the irradiated APDs seem to lose their function. With the EIC operation for a third of a year, the EIC ZDC is expected to be exposed to 8×10^{12} $n_{\rm eq}$/cm^2 per year.[3)] The APDs do not have sufficient radiation resistance for the EIC ZDC and another technology is needed.

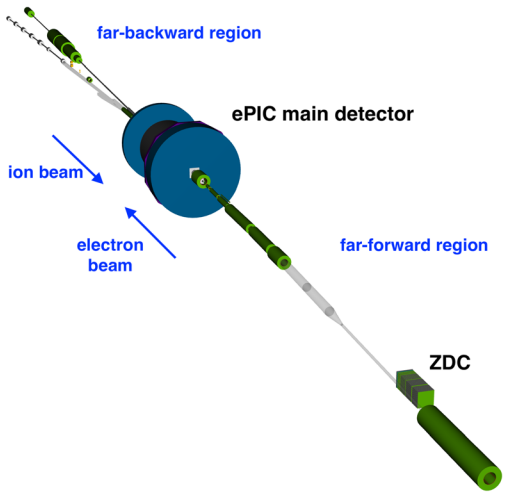

Fig. 1. A schematic of the ePIC detector, observed from the downstream of the ion beam line, as implemented in the ePIC software framework. The ion beam goes from the left side top to the right side bottom as indicated by the arrow. The large disks are calorimeter endcaps of the ePIC main detector. The ZDC is the set of rectangular solids at the bottom right. In the far-forward region, only the ion beam line is shown.

The ePIC ZDC will be situated between the electron and ion beam lines. Its placement was revised following consultations with experts in US. The ZDC has a limited space to place the front-end system close to the ZDC. Discussion on the readout system has started and is ongoing.

In summary, the previously reported ZDC design is adopted to the ePIC detector and discussions on several aspects is ongoing for realization of the design. The ZDC effort is also in close contact with the ALICE FoCal development,[4)] which had several test-beam experiments conducted in 2022, as the same technique will be used in ZDC sampling calorimeters.

*1 RIKEN Nishina Center
*2 Wako Nuclear Science Center (WNSC), IPNS, KEK

a) The dose estimation is based on the measurement using radioactivation of indium foils.

References

1) R. A. Khalek *et al.*, EIC Yellow Report, arXiv:2103.05419.
2) S. Shimizu *et al.*, RIKEN Accel. Prog. Rep. **55**, 47 (2022).
3) V. Baturin, internal document.
4) ALICE collaboration, ALICE-PUBLIC-2019-005, `https://cds.cern.ch/record/2696471` .

Centrality dependence of charm and bottom quark suppression in Au + Au collisions at RHIC†

T. Hachiya*1,*2 for the PHENIX Collaboration

Charm and bottom quarks, collectively referred as heavy flavor, are a clean probe to study the properties of quark-gluon plasma (QGP) produced in high-energy heavy-ion collisions. Because of their large mass, heavy quarks are predominantly produced at the initial stage of the collisions. Once produced, heavy flavors lose their energy as they propagate through the QGP. The energy loss of heavy quarks is expected to be suppressed by "dead cone" effect, where gluon radiation caused by bremsstrahlung is suppressed at an angle smaller than the mass-to-energy ratio of the quark.[1] Thus, energy loss is expected to follow the mass ordering of quarks and gluons, $\Delta E_g > \Delta E_{u,d} > \Delta E_c > \Delta E_b$. The PHENIX experiment previously observed the different suppression of electrons from charm and bottom hadron decays in minimum bias Au + Au collisions at $\sqrt{s_{NN}} = 200$ GeV.[2]

This article reports the centrality dependence of charm and bottom quark suppression measured at PHENIX. Using the high-statistics dataset recorded in 2014 and the updated $p + p$ reference from 2015,[3] the nuclear modification factor, R_{AA} (a ratio of yields in Au + Au to $p + p$ after normalized by number of binary collisions) of the charm and bottom electrons in four centrality classes (0–10, 10–20, 20–40 and 40–60%) of Au + Au collisions can be measured with improved precision compared with our previous results.[2]

Heavy flavor electrons are measured using the central arm PHENIX detector. An inner silicon tracker, VTX, measures the distance of closest approach of the electron track, DCA_T, to the collision vertex in the transverse plane. Using the different decay lengths of charm and bottom hadrons ($c\tau = 123$ μm for D^0 and 455 μm for B^0), electrons from these decays are statistically separated by the DCA_T. The measured electron samples contain not only heavy flavors but background electrons. The main background is photonic electrons which are photon conversions and Dalitz decays of light neutral mesons. The background is mostly rejected by the analysis cut with the hit-pair on VTX as the electron pairs from the photon conversions produce hits that are close to each other. The remaining backgrounds are estimated through the full GEANT detector simulation and subtracted from the measured electron samples. The electron samples are separated by the unfolding, which simultaneously fits the transverse momentum p_T spectrum and DCA_T distributions.

Figure 1 shows R_{AA} in 0–10% central Au + Au collisions. The blue and green lines represent the bottom- and charm electrons with 1-sigma uncertainty bands,

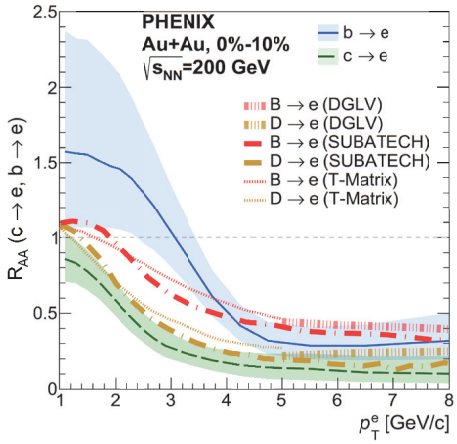

Fig. 1. R_{AA} for charm and bottom electrons compared with the theoretical models.

respectively. Significant suppression is seen for both charms and bottoms at high p_T. Charm suppression is stronger than bottom suppression for $p_T = 2$–5 GeV/c. The result was compared with the models that expect a mass ordering of energy loss in QGP. All models reproduce the data reasonably within large uncertainty.

The centrality dependence of the suppression is studied using the number of nucleon participants in the collision (N_{part}). Figure 2 shows R_{AA} vs N_{part} for three different p_T intervals. There is no suppression for both charms and bottoms in low p_T. The mid-p_T region shows a clear suppression of charm hadrons but no bottom suppression. The high-p_T region shows an increasing suppression of both charms and bottoms.

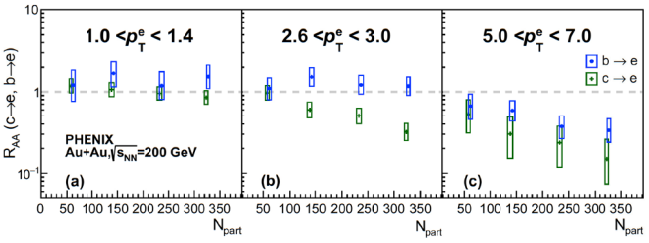

Fig. 2. R_{AA} charm and bottom electrons as a function of N_{part} for three p_T intervals.

In summary, PHENIX studied the centrality dependence of charm and bottom suppression. A clear different suppression was observed at $p_T = 2.5$ GeV/c. The suppression pattern is consistent with the models that expect mass ordering of energy loss.

† Condensed from the article in arXiv:.2023.17058

*1 Department of Mathematical and Physical Sciences, Nara Women's University
*2 RIKEN Nishina Center

References

1) Y. L. Dokshitzer *et al.*, Phys. Lett. B **519**, 199 (2001).
2) A. Adare *et al.*, Phys. Rev. C **93**, 034904 (2016).
3) C. Aidala *et al.*, Phys. Rev. D **99**, 10.1103 (2019).

Study of v_2 depending on multiplicity with ZDC energy event categorization

R. Takahama[*1,*2] for the PHENIX Collaboration

The PHENIX experiment was operated at BNL-RHIC, which collides heavy ions at relativistic energy to create a hot state in a second. In this state, quarks and gluons are deconfined, and this state is called quark-gluon plasma (QGP) the collective motion of QGP is known. In hydrodynamic models, the detailed azimuthal correlation structure of emitted particles resulting from the collective motion is typically characterized by its Fourier components, known as the elliptic flow (v_2).[1)]

In the past decade, some results have suggested the possibility of QGP-like matter creation during extremely high multiplicity events in a lighter collision system than that of heavy ions.[3–7)] However, the mechanism of that possibility has not been revealed. One helpful fact is that the ridge structure and collective motion are measured only in extremely high multiplicity events, where multiparton interactions become more relevant.[8)]

The effect of multiparton interactions in heavy ion collision is of interest to us. Selecting events with the same number of participating nucleons in the collision is crucial to study the multiparton interaction effect because much more nucleons interact in heavy ion collisions than in proton-proton collisions. We can not directory measure the number of participating nucleons because they change to new particles after interactions. However, the number of spectator (not participated in collision) neutrons can be directory detected by the zero degree calorimeter (ZDC). In high-energy heavy-ion collisions, most of the spectator nucleons outside of the overlap region are causally disconnected from the matter produced by the participating nucleons, so we measure the energy of spectator neutrons captured by ZDC. We classify the events with the number of participating nucleons in the collision as in $p+p$ collision by selecting the events with the same energy measured by ZDC, thus creating a simple situation to study multiparton collision. Furthermore, the multiplicity has a width at some ZDC energy sum events. We assumed that the effect of the multiparton interaction makes this width. If the multiparton interaction effect is more relevant, a larger multiplicity should be obtained from events with the same number of participating nucleons. Because v_2 increases as a function of the number of tracks in $p+p$ collision,[7)] v_2 will be larger in events where the multiparton interaction effect is more relevant. Analyzing v_2 as a function of multiplicity at the same energy in the ZDC detector can tell us if the multiparton interaction effect is worth consideration in heavy ion collision.

Our goal is to analyze v_2 as a function of multiplicity using the ZDC energy sum event categorization in Au + Au collision data taken at $\sqrt{s_{NN}} = 200$ GeV in the PHENIX experiment. Such an event categorization has never been used to analyze v_2, so we worked on the reaction plane angle calibration to make its distribution flat. Figure 1 shows the reaction plane angle distribution after calibration of the one of the event classes. A fitting to these distributions with a straight line gave a $\chi 2$/ndf of approximately 1.0. We checked the flatness for all event classes for all runs and finally confirmed that the calibration had been done successfully. We are now at the stage of analyzing v_2 as a function of multiplicity using calibrated events. The results will be published in the near future.

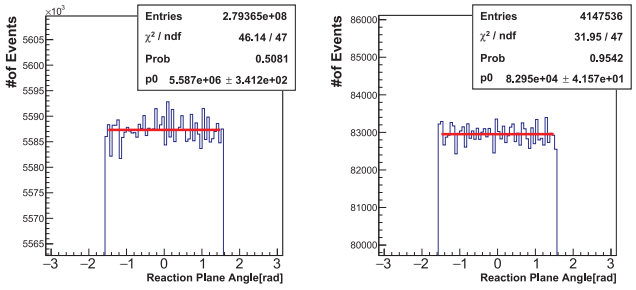

Fig. 1. Reaction plane angle distribution after calibration in events whose the number of normalized FVTX tracks is larger than 0.50 and less than 0.55. Left: with no ZDCe event selection. Right: events in 900 < ZDCe < 910.

References

1) S. Voloshin and Y. Zhang, Z. Phys. C **70**, 665 (1996).
2) S. Chatrchyan *et al.* (CMS Collaboration), Phys. Lett. B **719**, 29 (2013).
3) V. Khachatryan *et al.* (CMS Collaboration), Phys. Rev. Lett. **116**, 172302 (2016).
4) A. Adare *et al.* (PHENIX Collaboration), Phys. Rev. Lett. **114**, 192301 (2015).
5) L. Adamczyk *et al.* (STAR Collaboration), Phys. Lett. B **747**, 265 (2015).
6) A. Adare *et al.* (PHENIX Collaboration), Phys. Rev. Lett. **115**, (2015).
7) V. Khachatryan *et al.* (CMS Collaboration), Phys. Lett. B **765**, (2017).
8) W. Li, Mod. Phys. Lett. A **27**, 1230018 (2012).

*1 RIKEN Nishina Center
*2 Division of Nature Physics, Nara Women's University

Completion of Bus-Extender development for sPHENIX INTT

T. Hachiya,[*1,*2] Y. Akiba,[*2] J. Bertaux,[*3] K. Fujiki,[*2,*4] M. Fujiiwara,[*1] S. Hasegawa,[*1,*5] M. Hata,[*1,*2] H. Imai,[*2,*4] M. Kano,[*1] T. Kato,[*2,*4] T. Kondo,[*6] C. M. Kuo,[*7] R. S. Lu,[*8] I. Nakagawa,[*2] Y. Namimoto,[*1,*2] R. Nouicer,[*9] G. Nukazuka,[*2] C. W. Shih,[*7] M. Shimomura,[*1] R. Shishikura,[*2,*4] M. Stojanovic,[*3] Y. Sugiyama,[*1,*2] R. Takahama,[*1,*2] W. C. Tang,[*7] H. Tsujibata,[*1] M. Watanabe,[*1] and X. Wei[*3]

sPHENIX is a second-generation experiment at Relativistic Heavy-Ion Collider. It is scheduled to start in 2023 to explore the properties of quark-gluon plasma. The INTermediate Tracker, INTT,[1)] is a silicon strip detector placed in a tight and confined space near the beam pipe. INTT measures more than 1000 particles in a collision. Large amount of raw data is sent to the later read-out electronics placed more than 1.1 m away from INTT with a curving path for signal processing at high speed. It is difficult for commercial cables such as flex flat cable and co-ax cable to satisfy all the requirements listed below. We developed a special data cable namely "Bus Extender (BEX)" for INTT based on flexible printed circuits (FPC).

The requirements for BEX are: (1) length of 1.1 m, (2) high-density signal lines (128 lines/5 cm), (3) high-speed data transfer of 200 Mbps by LVDS with 100 Ω differential impedance, (4) flexibility, (5) mechanical reliability, and (6) radiation hardness. We developed BEX for five years to satisfy all the requirements. Instead of the standard polymide, liquid crystal polymer (LCP) was used for the substrate to reduce loss of signals transmitted at high speed. The design of BEX was optimized by the printed circuit simulation. The prototype BEX was made for testing. BEX consists of four metal layers including signal, power, and ground layers laminated by glue. The uniformity of width for signal lines is measured to be 122 ± 2 μm.

Using the prototype BEX, the electrical performance is measured with S-parameters, differential impedance, and eye-diagram and compared with the simulation. Figure 1 shows S-parameter for insertion (SDD21) and return loss (SDD11). The data and simulation are labeled as "meas" and "em," respectively. From the comparison, the simulation successfully reproduced the overall behavior of the data. The eye-diagram is often used to visually inspect the margin of the signal pulse. By comparing the mask (gray hexagonal shape) which represents the minimum requirement of the margin,

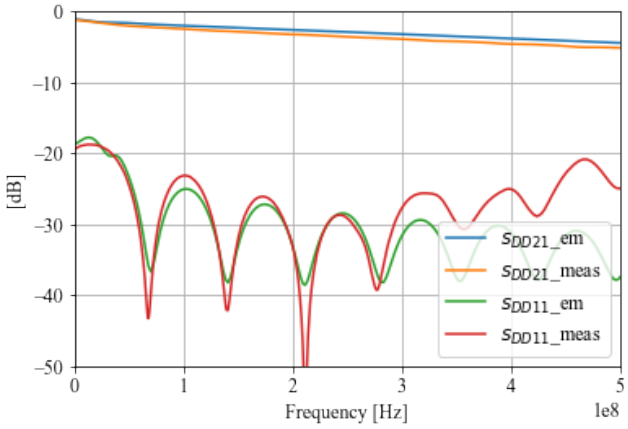

Fig. 1. Insertion and return loss.

the measured eye diagram satisfied the requirement as shown in Fig. 2. The differential impedance was estimated as 95 Ω by the time domain reflectometry. The result is slightly lower than the requirement but acceptable.

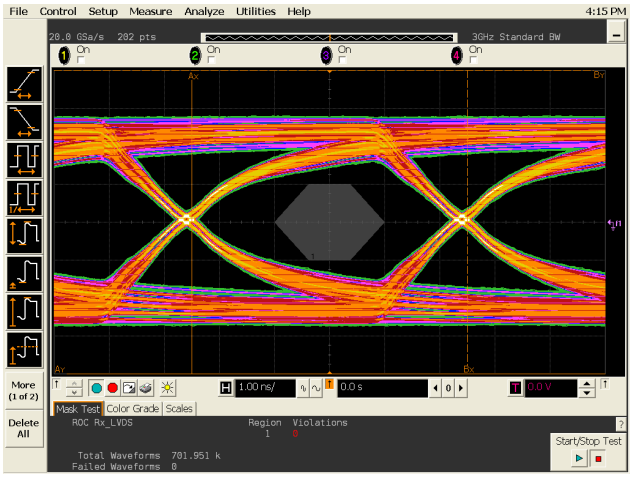

Fig. 2. Eye-diagram.

The mechanical reliability was evaluated by the peeling and the thermal shock test using the FPC samples with the same configuration. The peel strength between the laminated two layers was measured by a tensile tester. The result was more than 16 N/cm and indicates BEX has sufficient strength. We also compared the strength with radiation exposure by 5 k Gy and

*1 Department of Mathematical and Physical Sciences, Nara Women's University
*2 RIKEN Nishina Center
*3 Department of Physics and Astronomy, Purdue University
*4 Department of Physics, Rikkyo University
*5 Japan Atomic Energy Agency
*6 Tokyo Metropolitan Industrial Technology Research Institute
*7 Center for High Energy and High Field Physics and Department of Physics, National Central University
*8 Department of Physics, National Taiwan University
*9 Physics Department, Brookhaven National Laboratory

found no change. This indicates that the impedance of BEX was not changed by irradiation. The thermal shock test aimed to check the long-term stability. BEX was exposed with -15°C and 75°C for 30 min. with 5 min. interval. The rapid change in temperature puts physical stress with expansion and contraction. The electrical resistance of the signal line is increased if the signal line is damaged. After 1000 thermal cycles that are equivalent to 8 years of use, we found no resistance change. These mechanical performances are detailed in Ref. 2).

After the evaluation of the prototype, we performed the mass production of 130 BEXs. The issue with low yield rate was investigated and the tiny dust caused mis-formation of lines.[3] A visual inspection fixture was also developed to monitor the line formation during production. As a result, the mass production was completed with almost 100% yield. In summer 2022, all the BEX was assembled to the INTT barrel. INTT and BEX are ready for sPHENIX data taking in April 2023.

References

1) Conceptual design report of sPHENIX (2018).
2) T. Kondo *et al.*, Trans. J. Inst. Electron. Packag. **15**, E21 (2022).
3) T. Hachiya *et al.*, RIKEN Accel. Prog. Rep. **55**, 98 (2022).

Development of graphical user interface application for sPHENIX-INTT LV system

M. Watanabe,[*4] Y. Akiba,[*1] J. Bertaux,[*2] K. Fujiki,[*1,*3] M. Fujiiwara,[*4] T. Hachiya,[*1,*4] S. Hasegawa,[*1,*5] M. Hata,[*4] H. Imai,[*1,*3] M. Kano,[*4] T. Kato,[*1,*3] T. Kondo,[*6] C. Kuo,[*7] R.-S. Lu,[*8] I. Nakagawa,[*1] Y. Namimoto,[*1,*4] R. Nouicer,[*9] G. Nukazuka,[*1] C. Shih,[*7] M. Shimomura,[*4] R. Shishikura,[*1,*3] M. Stojanovic,[*2] Y. Sugiyama,[*4] R. Takahama,[*1,*4] W.-C. Tang,[*7] H. Tsujibata,[*4] and X. Wei[*2]

We create a Graphical User Interface (GUI) that allows you to operate the Low Voltage (LV). A control panel based on the Graphic User Interface (GUI) application is under development to operate the LV power for a Read Out Card (ROC), *i.e.*, an electronics to read out from the INTermediate Tracker (INTT) detector. The INTT is one of the three tracking detectors in the sPHENIX experiment, which is scheduled to go live in the spring of 2023. The ROC is a multi-functional circuit board and consists of as many as 3000 surface mount components. Thus ROC requires a couple of different voltages to distribute relevant voltage(s) to each component. There are 13 LV distribution modules assigned to power 8 ROCs. Each module occupies a single VME slot and supplies a preset voltage up to 10 output channels. Thus a single ROC power is provided by the multiple distribution modules with various voltage settings. The LV distribution module can be operated from a remote server (KEPServer[1]) and its output voltage and current can be readout from the KEPServer. The GUI has been developed using the commercial application called "Ignition Designer"[2,3] which runs on an Ignition Gateway PC. The KEPServer and the Ignition Gateway are linked to the OPC interoperability standard.

Shown in Fig. 1 is the main control panel of the LV control GUI. It is still under development. The panel is designed to be operated in the interactively. Clickable buttons are implemented to turn on/off all powers (11 channels) for ROC-1 at once.

Only first ROC(ROC1) has already been implemented in the image, but the plan is to introduce new buttons for ROC2, ROC3 ... ROC8. The black buttons on the left with numbers from 1 to 11 represents the slot number of the LV distribution module. The table on the right of the panel displays the history of abnormalities. It shows the channel and the time. In order to avoid the main control panel being too busy with too many buttons and voltage/current displays, a "Detail" button is implemented on the bottom left corner of the panel. A new pop-up panel, as shown in Fig. 2, appears on the screen by clicking the Detail button.

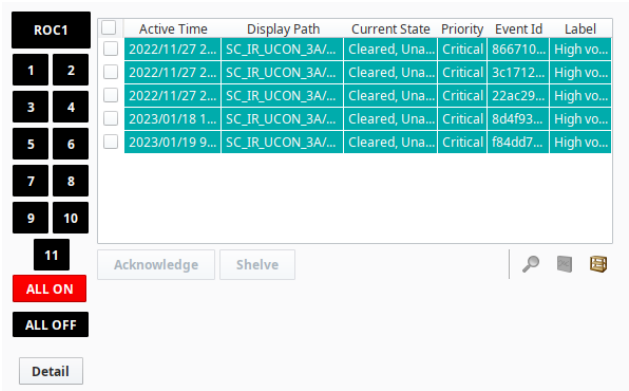

Fig. 1. The main control panel of the INTT LV distribution modules.

Fig. 2. A new pop-up panel appears by clicking "Detail" button on the main control panel.

This panel displays the latest current and voltage values of each channel of a given ROC. Further development is planned to change the color of buttons to express the power on/off status of each channel following

† Condensed from the article in Phys. Rev. Lett. **85**, 1827 (2000)

*1 RIKEN Nishina Center
*2 Department of Physics and Astronomy, Purdue University
*3 Department of Physics, Rikkyo University
*4 Department of Mathematical and Physical Sciences, Nara Women's University
*5 Japan Atomic Energy Agency
*6 Tokyo Metropolitan Industrial Technology Research Institute
*7 Department of Physics, National Central University
*8 Department of Physics, National Taiwan University
*9 Physics Department, Brookhaven National Laboratory

the same color coordinate manner of the main control panel. The green rectangles with SLOT number are also implemented to function as interactive buttons, allowing each channel to turn on/off independently. This GUI is still under development, so we would like to create buttons that can control other ROCs and ROC detail screens in the future.

References

1) https://www.kepware.com/en-us/.
2) https://docs.inductiveautomation.com/display/DOC80/Welcome.
3) https://docs.inductiveautomation.com/display/DOC80/Standard+Architecture.

Detection efficiency of sPHENIX-INTT by cosmic ray measurements and its timing dependence

Y. Namimoto,[*1,*4] Y. Akiba,[*1] J. Bertaux,[*2] K. Fujiki,[*1,*3] M. Fujiiwara,[*4] T. Hachiya,[*1,*4] S. Hasegawa,[*1,*5] M. Hata,[*4] H. Imai,[*1,*3] M. Kano,[*4] T. Kato,[*1,*3] T. Kondo,[*6] C. M. Kuo,[*7] R.-S. Lu,[*8] I. Nakagawa,[*1] R. Nouicer,[*9] G. Nukazuka,[*1] C. W. Shih,[*7] M. Shimomura,[*4] R. Shishikura,[*1,*3] M. Stojanovic,[*2] Y. Sugiyama,[*4] R. Takahama,[*1,*4] W. C. Tang,[*7] H. Tsujibata,[*4] M. Watanabe,[*4] and X. Wei[*2]

INTermediate Tracker (INTT) is one of the three tracking detectors for the sPHENIX experiment, which will be started in April 2023 at the Relativistic Heavy Ion Collider (RHIC) in Brookhaven National Laboratory. It comprises 56 ladders, each comprising two silicon strip sensor modules. One module is divided into 26 cells, and each containing 128 readout strips.

To measure the detection efficiency of INTT, we executed beam tests three times. Although the expected efficiency is approximately 100%, the observed efficiency was $96.0 \pm 0.5\%$ as the result of the second beam test at Fermilab Test Beam Facility (FTBF) in 2019.[1)] The RHIC beam bunches are synchronized with 9.4 MHz clock and so as INTT readout electronics. However, some hits can fall into possible signal processing glitch between subsequent beam clocks (BCO) because the FTBF beam is asynchronous to the RHIC-BCO. To verify the hypothesis, we executed the third beam test at the ELPH facility at Tohoku Univ. in 2021. We upgraded the DAQ system from a nominal Window-based DAQ to a CAMAC-based TDC for the timing measurement of INTT hits w.r.t. the BCO. As a result of this test, we obtained an efficiency of $99.56 \pm 0.06\%$.[2)] Unfortunately, the timing dependence measurement was unsuccessful because we discovered the beam rate exceeded the DAQ processing speed limit, and recorded data were unreliable. Therefore we should measure the detection efficiency and the BCO dependence in low beam rate conditions. The best way is to repeat the measurement with cosmic rays.

For cosmic rays measurement, we put three INTT ladders in a dark box, and two scintillation counters are set above and below the box for external triggers (Fig. 1). The internal clock of the readout electronics is used as BCO. We call the ladders from top to bottom L1, L2, and L3. CAMAC measured the ADC of scintillation counters and BCO timing.

*1 RIKEN Nishina Center
*2 Department of Physics and Astronomy, Purdue University
*3 Department of Physics, Rikkyo University
*4 Department of Mathematical and Physical Sciences, Nara Women's University
*5 Japan Atomic Energy Agency
*6 Tokyo Metropolitan Industrial Technology Research Institute
*7 Center for High Energy and High Field Physics and Department of Physics, National Central University
*8 Department of Physics, National Taiwan University
*9 Physics Department, Brookhaven National Laboratory

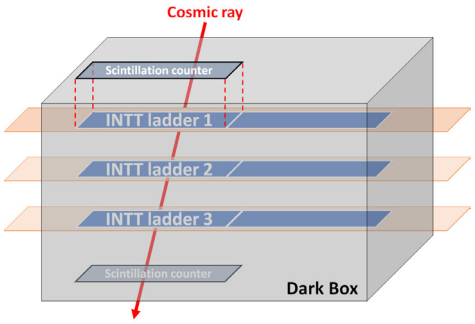

Fig. 1. Setup for cosmic rays measurements.

The efficiency of L2 layer is defined as Eq. (1). Errors were calculated by the binomial distribution.

$$\text{L2 Efficiency} = \frac{\Sigma N(\text{L1}_{\text{hit}} \cap \text{L2}_{\text{hit}} \cap \text{L3}_{\text{hit}})}{\Sigma N(\text{L1}_{\text{hit}} \cap \text{L3}_{\text{hit}})} \quad (1)$$

The observed detection efficiency is $99.54 \pm 0.06\%$, reproducing the 2021 beam test result, by requiring some zenith angle range to be nearly vertical. Then these event samples were classified into 11 relative phase categories w.r.t. BCO, and the efficiency in each phase was evaluated as shown in Fig. 2.

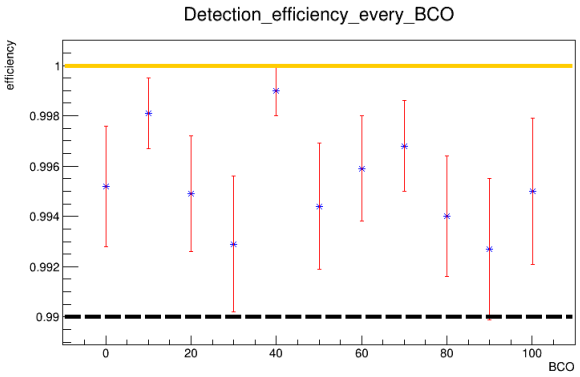

Fig. 2. Detection efficiency of every BCO.

In summary, we confirmed that the detection efficiency of INTT exceeds 99%, and it has no dependence on BCO.

References

1) A. Suzuki, Master thesis, Nara Women's University (2019).
2) M. Morita, Master thesis, Nara Women's University (2021).

MIP measurement for mass production of sPHENIX-INTT ladder with a positron beam

Y. Sugiyama,[*4] Y. Akiba,[*1] J. Bertaux,[*2] K. Fujiki,[*1,*3] M. Fujiiwara,[*4] T. Hachiya,[*1,*4] S. Hasegawa,[*1,*5] M. Hata,[*4] H. Imai,[*1,*3] M. Kano,[*4] T. Kato,[*1,*3] T. Kondo,[*6] C. M. Kuo,[*7] R. S. Lu,[*8] I. Nakagawa,[*1] Y. Namimoto,[*1,*4] R. Nouicer,[*9] G. Nukazuka,[*1] C. W. Shih,[*7] M. Shimomura,[*4] R. Shishikura,[*1,*3] M. Stojanovic,[*2] R. Takahama,[*1,*4] W. C. Tang,[*7] H. Tsujibata,[*4] M. Watanabe,[*4] and X. Wei[*2]

The sPHENIX experiment will start in 2023 at the Relativistic Heavy Ion Collider in Brookhaven National Laboratory. Intermediate Tracker (INTT) is one of the three tracking detectors used in the experiment, which consists of 56 ladders of silicon strip detectors. A half ladder is divided into 26 cells which consist of two types of silicon sensors with different strip lengths, and each cell includes 128 read-out FPHX chips.[1)]

In 2021 at ELPH, Tohoku University, we performed a test beam experiment to evaluate the performance of mass production ladders.[2)] We used the γ-ray beamline at the facility, and irradiated a positron beam with a momentum of about 1 GeV. Three halves of a ladder were used, and two scintillators were installed upstream and downstream of them, respectively.

We evaluated the performance of silicon sensor by detecting Minimum Ionizing Particles (MIP). The noise contamination to the MIP region in the energy deposit spectrum is crucial to achieve good signal-to-noise ratio. The FPHX read-out chip converts the height of the signal generated by the sensor into a 3-bit ADC. As a preparation of the signal AD conversion process, the 8-bit DAC threshold values (called DAC value) are preset with approximately 4 mV step. When the signal is processed, a corresponding DAC value is assigned and set in a data stream as a 3-bit ADC data. The ADC value relates to energy loss of a traversing charged particle. It is important to observe the entire energy deposit spectrum with a good resolution though, it is not possible by using the built-in 3-bit ADC of FPHX chip. A series of sequential measurements were executed to scan through the full DAC range by setting the DAC to cover only narrow range but fine pitch in one measurement.

In the data analysis, events which have too many hits away from the beam spot were removed. Only hits on a single strip were analyzed. A hit with the highest ADC value was excluded from the full ADC spectrum reconstruction event samples because the hit could be an overflow value. We reconstructed ADC distribution of a cell in the upstream ladder obtained from 8 runs. Then the distribution was normalized by the number of entries in two overlapping bins, shown in Fig. 1(a). Then we took the average over each overlapping bin, letting each ADC distributions of narrow region connect smoothly with the spectrum of adjacent region. It was performed in order from the smallest ADC configuration to obtain one energy deposit spectrum.

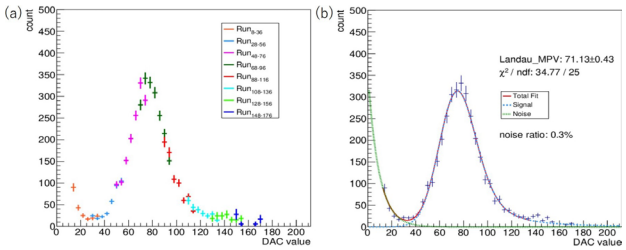

Fig. 1. (a) The ADC distribution obtained from 8 runs by normalizing entries in overlapping bins. (b) The energy deposit spectrum with the fitting results.

We applied the Landau-Gaussian convolution function[3)] to reproduce the peak shape of the MIP region, and an exponential function to express the noise contribution. The Landau most probable value indicates the peak value corresponding to the energy loss of the MIP. We fitted the energy deposit spectrum with a sum of their functions and succeeded in reproducing the experimental data, shown in Fig. 1(b).

The fitting result shows the Landau MPV was 71.13 ± 0.43 at the operation bias voltage of 50 V. The noise contamination in the MIP region from 40 to 136 is estimated to be about 0.3%. Therefore the mass production ladder is almost noiseless in the MIP region.

In summary, we obtained one exact energy deposit spectrum from measurements with 8 different ADC configurations. The experimental spectrum was well reproduced by the sum of the convolution function and the exponential function. Also, the noise contamination in the MIP region is about 0.3%. This means that the DAC threshold value can be set low, leading to high detection efficiency.

*1 RIKEN Nishina Center
*2 Department of Physics and Astronomy, Purdue University
*3 Department of Physics, Rikkyo University
*4 Department of Mathematical and Physical Sciences, Nara Women's University
*5 Japan Atomic Energy Agency
*6 Tokyo Metropolitan Industrial Technology Research Institute
*7 Center for High Energy and High Field Physics and Department of Physics, National Central University
*8 Department of Physics, National Taiwan University
*9 Physics Department, Brookhaven National Laboratory

References

1) C. Aidala *et al.*, Nucl. Instrum. Meth. Phys. Res. A **755**, 44 (2014).
2) G. Nukazuka *et al.*, ELPH Annu. Rep. (2022).
3) S. Hancock *et al.*, Phys. Rev. A **28**, 615 (1983).

The LV power system of INTT detector at RHIC

W. C. Tang,[*1] Y. Akiba,[*2] J. Bertaux,[*3] K. Fujiki,[*2,*4] M. Fujiiwara,[*5] T. Hachiya,[*2,*5] S. Hasegawa,[*2,*6] M. Hata,[*5] H. Imai,[*2,*4] M. Kano,[*5] T. Kato,[*2,*4] T. Kondo,[*7] C. M. Kuo,[*1] R. S. Lu,[*8] I. Nakagawa,[*2] Y. Namimoto,[*2,*5] R. Nouicer,[*9] G. Nukazuka,[*2] C. W. Shih,[*1] M. Shimomura,[*5] R. Shishikura,[*2,*4] M. Stojanovic,[*3] Y. Sugiyama,[*5] R. Takahama,[*2,*5] H. Tsujibata,[*5] M. Watanabe,[*5] and X. Wei[*3]

The sPHENIX experiment is an upgrade project of RHIC's former PHENIX experiment and aims to study quark-gluon plasma.[1] The INTermediate Tracker (INTT) is one of the sub-detectors of sPHENIX. INTT inherits much of the electronics, such as the readout card (ROC) and FPHX chips,[2] from the FVTX detector. The power system of INTT includes the high voltage (HV) system, which gives the bias voltage to the silicon sensors, and the low voltage (LV) system, which powers up the FPHX chips and ROC.

The INTT power system is constructed in a power crate (Fig. 1). This power crate is used for ladders testing and for detector operation. On the top of the crate is the MPOD module which can produce 100 V as the high voltage system.

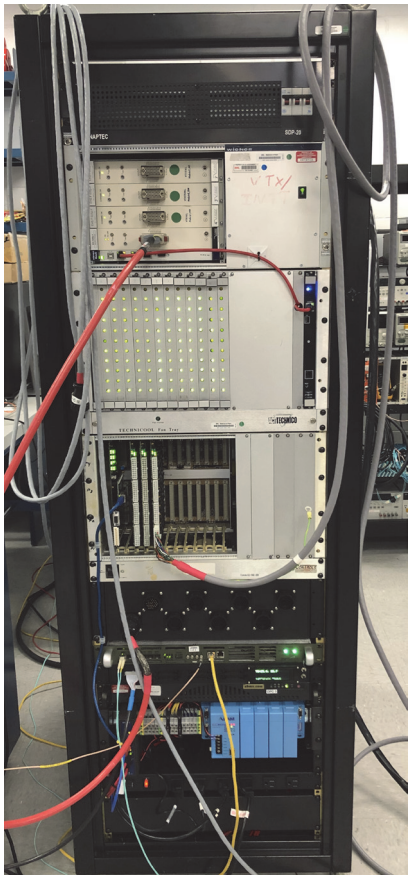

Fig. 1. INTT power crate system.

The second top of the crate is the switch distribution board. There are 13 slots for switch distribution board in total. Slots 1–11 from the left-hand side are used to power up the ROCs, and the other two slots are used to give power to the FPHX power supply system.

The third top of the crate is the FPHX power supply system which powers up the FPHX chips. The FPHX power supply system consists of a controlling board and filtering boards. A controlling board is used to give out the command to filtering boards (Fig. 2). There can be up to eight filtering boards in a system. Each filtering board can power up 8 ladders' FPHX chips, which indicates that 64 ladders' FPHX chips can be powered by one power crate.

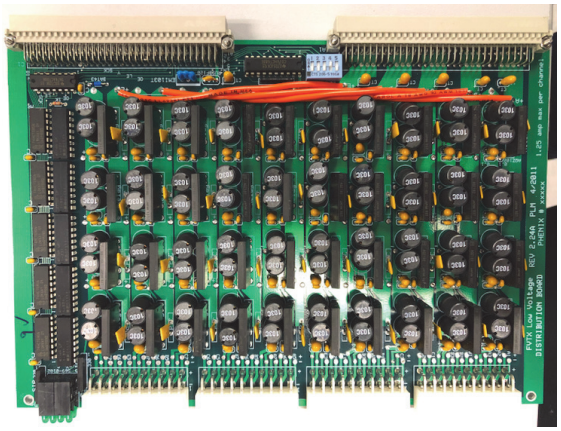

Fig. 2. FPHX power system filtering board.

The Switch distribution board and FPHX power supply system are all connected to the PC by ethernet cables. One can easily enter the rack PC by using the NoMachine, ssh through the gateway, or control it locally using the keyboard and monitor to control the whole system. The Switch distribution board can be controlled by the telnet command line, and the FPHX power supply can be controlled by a perl script respectively. There is a written script for controlling whole INTT power system including HV and LV system, which can turn on and turn off all the power systems by one command.

*1 Department of Physics, National Central University
*2 RIKEN Nishina Center
*3 Department of Physics and Astronomy, Purdue University
*4 Department of Physics, Rikkyo University
*5 Department of Mathematical and Physical Sciences, Nara Women's University
*6 Japan Atomic Energy Agency
*7 Tokyo Metropolitan Industrial Technology Research Institute
*8 Department of Physics, National Taiwan University
*9 Physics Department, Brookhaven National Laboratory

References

1) Conceptual Design Report of sPHENIX (2018).
2) "FPHX: A new silicon strip readout chip for the PHENIX experiment at RHIC," 2009 IEEE Nuclear Science Symposium Conference Record.

Signature of the gluon orbital angular momentum†

S. Bhattacharya,*1 R. Boussarie,*2 and Y. Hatta*1,*3

The Relativistic Heavy Ion Collider (RHIC) spin program at Brookhaven National Laboratory has revealed that the gluon helicity contribution ΔG to the proton spin sum rule

$$\frac{1}{2} = \frac{1}{2}\Delta\Sigma + \Delta G + L_q + L_g, \tag{1}$$

is nonvanishing and likely sizable. Together with the known quark helicity contribution $\Delta\Sigma \sim 0.3$, the result indicates that parton helicities account for a significant fraction of the proton spin. Yet, there still remain huge uncertainties about the small-x contribution to $\Delta G = \int_0^1 dx \Delta G(x)$. Resolving this issue is one of the major goals of the future Electron-Ion Collider (EIC).

Another obvious goal of the EIC is to measure the orbital angular momentum (OAM) of quarks and gluons $L_{q,g}$. However, progress in this direction is relatively slow, although there have been a few suggestions[1] for experimental observables in recent years. In this report we propose a new and promising observable for the gluon OAM in Deep Inelastic Scattering and make a quantitative prediction for the EIC.

Specifically, we calculate longitudinal double spin asymmetry (DSA) in exclusive dijet production in electron-proton collisions $ep \to \gamma^* p \to jjp'$ where both the incoming electron and proton are longitudinally polarized. The part of the cross section which depends on the proton and electron polarizations takes the form

$$d\sigma^{h_p h_l} \sim h_p h_l \cos(\phi_{l_\perp} - \phi_{\Delta_\perp}) \mathfrak{Re}(A_2 A_3^*), \tag{2}$$

where $h_l, h_p = \pm 1$ are the electron and proton helicities. $\phi_{l_\perp}$ and $\phi_{\Delta_\perp}$ are the azimuthal angles of the outgoing lepton and the proton, respectively. A_2 is the known[2] twist-2 amplitude for dijet production. A_3 is a twist-3 amplitude which contains the OAM and which is calculated for the first time in this work. The details can be found in the published letter. Here we show the final result after certain approximations

$$\mathfrak{Re}(A_2 A_3^*) \propto \mathfrak{Re}\left[\left\{\mathcal{H}_g^{(1)*} + \frac{4q_\perp^2}{q_\perp^2 + \mu^2}\mathcal{H}_g^{(2)*}\right\}\mathcal{L}_g - \mathcal{H}_g^{(1)*}\tilde{\mathcal{H}}_g\right], \tag{3}$$

where $q_\perp$ is the transverse momentum of the two jets which are assumed to be symmetric and $4\mu^2 = Q^2$ is the photon virtuality. $\mathcal{H}_g^{(1,2)}$, $\mathcal{L}_g$ and $\tilde{\mathcal{H}}_g$ are the Compton form factors of the unpolarized gluon generalized parton distribution (GPD), the gluon OAM and the gluon helciity GPD, respectively. We observe an interesting interplay between the gluon OAM and the gluon helicity. The latter contribution was missed in the previous calculation of a related observable.[1]

In Fig. 1, we show our numerical result for the cross section for the EIC kinematics at $\delta\phi = \phi_{l_\perp} - \phi_{\Delta_\perp} = 0$ for $Q^2 = 2.7$ GeV^2 plotted as a function of skewness ξ (longitudinal momentum fraction the proton loses in scattering). We see that the OAM and helicity contributions are comparable in magnitude, but with opposite signs. This is consistent with the theoretical prediction[3] that the gluon OAM and gluon helicity parton distributions cancel in the small-x region. For larger values of Q^2, our result (3) predicts that the two contributions add up. This can be tested in experiment by varying Q^2.

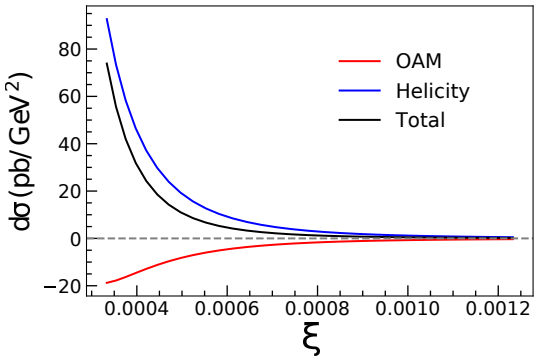

Fig. 1. Spin-dependent part of the cross section at $Q^2 = 2.7$ GeV^2 as a function of the skewness variable ξ. The 'OAM' and 'Helicity' contributions come from the $\mathcal{L}_g$ and $\tilde{\mathcal{H}}_g$ terms in (3), respectively.

In conclusion, we have made the first quantitative prediction for an observable sensitive to the parton OAM at the EIC. Our result adequately demonstrates the feasibility of accessing the gluon OAM from DSA. It also emphasizes that, due to the admixture of the gluon helicity contribution, in order to extract the OAM reliably, one needs an accurate determination of $\Delta G(x)$ down to $x \sim 10^{-3}$.

References
1) X. Ji *et al.*, Phys. Rev. Lett. **118**, 192004 (2017), arXiv:1612.02438.
2) V. M. Braun *et al.*, Phys. Rev. D **72**, 034016 (2005), arXiv:hep-ph/0505263.
3) Y. Hatta *et al.*, Phys. Lett. B **781**, 213 (2018), arXiv:1802.02716.

† Condensed from the article in Phys. Rev. Lett. **128**, 182002 (2022)

*1 Department of Physics, Brookhaven National Laboratory
*2 Ecole Polytechnique
*3 RIKEN BNL Research Center

5. Hadron Physics (Theory)

6. Particle Physics

QST algebra

Y. Akiba*1

The standard model (SM) successully describes the nature, but it has at least 25 free parameters. Simple formulas with no free parameter for 24 SM parameters have been reported:[1] 15 particle masses, 4 Cabbibo-Kobayashi-Maskawa (CKM) quark mixing parameters, 3 neutrino mixing angles, the fine structure constant, and the strong coupling constant. Moreover, the quarternion-spin-isospin (QST) model that predicts these formulas,[2] and their implications of gravity and cosmology[3] have also been reported. This article reports an update of the model.

In the QST model, the Planck time, $t_{\rm pl} = 5.3912 \times 10^{-44}$ s, is the minimum time period in nature. $t_{\rm pl}$ is a fundamental constant of nature, similar to the speed of light in vacuum c and the Planck constant $\hbar$. Consequently, the Planck length $l_{\rm pl} = ct_{\rm pl}$ is the minimum distance in nature; therefore, a spacetime point has a finite minimum size, and the number of spacetime points in a finite volume is also finite. Thus, each space-time point can be numbered.

In the QST model, the change in the state from a spacetime point $|n\rangle$ to the subsequent spacetime point $|n+1\rangle$ is described as

$$|n+1\rangle = \left(1 + d\hat{S}^{\rm EA}[n]\right) = \left(1 + \sum \delta_p[n] d\hat{S}^{\rm EA}_p\right)|n\rangle,$$

where $d\hat{S}^{\rm EA}[n] = \sum \delta_p[n] d\hat{S}^{\rm EA}_p$ is the change in the state from $|n\rangle$ to $|n+1\rangle$, and $\delta_p[n] = 0$ or 1, and $d\hat{S}^{\rm EA}_p (p = 1, \cdots, 49)$ are operators that are denoted as elementary actions (EAs). This implies that each spacetime point is associated with a 49-dimentional vector space that describes the physical action, and an EA is the basis of the vector space. We denote this vector space as the EA space. Here the coefficient of $d\hat{S}^{\rm EA}_p$ is not a real number; however it is limited to either 0 or 1. This inidicates that the coefficient field of the EA space is not real $\mathbb{R}$, but a finite field $\mathbb{F}_2 = \{0, 1\}$.

In the QST model, an EA is a 48-fold product of operators that we denote as primordial actions (PAs).

$$d\hat{S}^{\rm EA}_p = [\hat{X}_{p_1} \vee \hat{X}_{p_2} \vee \cdots \vee \hat{X}_{p_{48}}],$$

where $\vee$ is a binary product operator in the model analogous to the wedge product $\wedge$ in the exterior algebra, $\hat{X}_{p_k}$ are PAs, and [] represents a "reduction" operator that evaluates a vee product in term of normal product. A PA is one of the following 64 operators.

$$\{I^\mu \sigma^\nu \tau^a, \varepsilon\tau^a, \varepsilon i, \varepsilon I^{[c-a]}\tau^a, \varepsilon i\tau^3, -\varepsilon I^c, -\varepsilon i, \varepsilon, -\varepsilon, i, 1\},$$

where ε is the sign operator. If $\hat{X}_p\hat{X}_q = \pm\hat{X}_q\hat{X}_p$ then $\hat{X}_p(\varepsilon\hat{X}_q) = \mp\hat{X}_q(\varepsilon\hat{X}_p)$. The reduction operator evaluates a n-fold vee product of PAs as follows

- If more than one of the $\hat{X}_p$'s are identical

$$[\hat{X}_{p_1} \vee \cdots \vee \hat{X}_{p_n}] = 0.$$

- If $\hat{X}_{p_k}\hat{X}_{p_{k+1}} = \hat{X}_{p_{k+1}}\hat{X}_{p_k}$ for any k $(1 \le k < n)$,

$$[\hat{X}_{p_1} \vee \cdots \vee \hat{X}_{p_n}] = 0.$$

- If $\hat{X}_{p_k}\hat{X}_{p_{k+1}} = -\hat{X}_{p_{k+1}}\hat{X}_{p_k}$ for all k $(1 \le k < n)$,

$$[\hat{X}_{p_1} \vee \cdots \vee \hat{X}_{p_n}] = \hat{X}_{p_1} \cdots \hat{X}_{p_n}.$$

The change of physical state from $|n\rangle$ to $|n+N\rangle$ is expressed as

$$|n+N\rangle = (1 + d\hat{S}^{\rm EA}[n+N-1])(\cdots(1 + d\hat{S}^{\rm EA}[n])|n\rangle$$

In the model, it is shown that the product of any two EAs vanishes, that is, $d\hat{S}^{\rm EA}_p d\hat{S}^{\rm EA}_q = 0$. Thus

$$1 + d\hat{S}^{\rm EA}[k] = \exp(d\hat{S}^{\rm EA}[k]) = \exp\left(\sum \delta_p[k] d\hat{S}^{\rm EA}_p\right)$$

$$|n+N\rangle = \exp\left(\sum_{k=n}^{n+N-1} dS[k]\right)|n\rangle$$

This formula represents the physical action from one spacetime point $|n\rangle$ to another spacetime point $|n+N\rangle$ along with one path. Thus, the physical state $|t_f\rangle$ is the sum of all of such actions.

$$|x_f\rangle = \sum \exp\left(\sum d\hat{S}^{\rm EA}[k]\right)|x_i\rangle,$$

where the first sum runs over all possible paths from$|x_i\rangle$ to $|x_f\rangle$. This equation corresponds to the following path integral formula

$$\begin{aligned} |t_f\rangle &= \int \mathcal{D}\phi \exp\left(i dS[\phi]\right)|t_i\rangle \\ &= \int \mathcal{D}\phi \exp\left(i \int \mathcal{L}[\phi] d^4x\right)|t_i\rangle \end{aligned}$$

This indicates that an EA $d\hat{S}^{\rm EA}_p$ corresponds to a term of Lagrangian as follows

$$d\hat{S}^{\rm EA}_p \leftrightarrow \mathcal{L}_p d^4x$$

In the QST model, all terms of the standard model Lagrangian are derived as one of the 49 EAs.

A paper describing the QST model is still in progress.

*1 RIKEN Nishina Center

References
1) Y. Akiba, RIKEN Accel. Prog. Rep. **54**, 69 (2021).
2) Y. Akiba, RIKEN Accel. Prog. Rep. **54**, 70 (2021).
3) Y. Akiba, RIKEN Accel. Prog. Rep. **54**, 71 (2021).

Twelfth-order QED contributions to the muon $g-2$

R. Yamazaki[*1,*2] and M. Nio[*2,*1]

The anomalous magnetic moment of the muon, $a_\mu \equiv (g_\mu - 2)/2$, has occupied a central role in testing the validity of the standard model of elementary particles (SM). The new measurement of a_μ at Fermilab[1] is consistent with that at Brookhaven,[2] and the long-standing tension between experiment and theory remains unresolved. The average of the two experiments and the SM prediction[3] are given as

$$a_\mu(\text{Exp}) = 116\ 592\ 061\ (41) \times 10^{-11}, \quad (1)$$

$$a_\mu(\text{SM}) = 116\ 591\ 810\ (43) \times 10^{-11}, \quad (2)$$

respectively, and the difference is $(251 \pm 59) \times 10^{-11}$ corresponding to 4.2 σ.

The theoretical prediction of a_μ has been calculated by considering all three forces of SM. The contribution from the quantum electrodynamics (QED) is dominant and has been determined up to the tenth order of the perturbation theory. It has been considered sufficiently well known as its uncertainty is 1.0×10^{-12}. The assigned uncertainty was derived from the rough estimate of the leading-order contribution of the twelfth-order term. Recently, we have calculated, not guessed, the two types of Feynman diagrams shown in Fig. 1 that are supposed to give the leading contributions in the twelfth order.

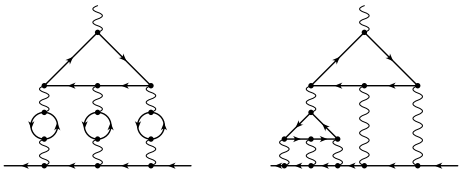

Fig. 1. Some Feynman vertex diagrams of the twelfth-order QED containing light-by-light scattering subdiagrams.

Because the muon is about two hundred times heavier than the electron, enhancement factors arise in some QED contributions to a_μ. One famous origin of the enhancement is a light-by-light scattering vertex diagram (LL6), in which an external magnetic photon is attached to an electron loop. Another is a vacuum-polarization subdiagram (VP) consisting of an electron loop. The left diagram of Fig. 1 is a combination of two enhancement mechanisms of the twelfth order of the QED perturbation theory. We have calculated its numerical contribution taking into account all possible insertions of three second-order VPs (P2s) to LL6. In addition, diagrams with insertions of one fourth-order VP (P4) and two P2s to LL6 were calculated. The coefficients of $(\alpha/\pi)^6$, where α is the fine-structure constant, are obtained as follows:

$$a_\mu^{(12)}[\text{LL6}^{(e)}\_\text{P2}^{(e)}\text{P2}^{(e)}\text{P2}^{(e)}] = 2415.256\ (53), \quad (3)$$

$$a_\mu^{(12)}[\text{LL6}^{(e)}\_\text{P2}^{(\mu)}\text{P2}^{(e)}\text{P2}^{(e)}] = 367.974\ (15), \quad (4)$$

$$a_\mu^{(12)}[\text{LL6}^{(e)}\_\text{P4}^{(e)}\text{P2}^{(e)}] = 1451.106\ (91), \quad (5)$$

where a superscript (e) or (μ) of LL6, P2, or P4 indicates a species of its fermion loop. The sum of the three gives the leading contribution of the twelfth-order QED:

$$\left(\frac{\alpha}{\pi}\right)^6 \times 4230 = 0.665 \times 10^{-12}\,. \quad (6)$$

It is within the uncertainty assigned to the QED contribution to a_μ.

A new enhancement mechanism appears at the twelfth order. The right diagram of Fig. 1 (LL6_LL6) contains a "child" LL6 as a subdiagram. When the mass of an external fermion is much heavier than that of a loop fermion, the slope of F_1 form factor of LL6 has a large enhancement factor[4]

$$m_\mu^2 \frac{dF_1(q^2)}{dq^2}\bigg|_{q^2=0} \propto \left(\frac{m_\mu}{m_e}\right)^2 \sim 40000\,. \quad (7)$$

It is uncertain that such a critical enhancement factor exists in the LL6_LL6 contribution to a_μ. Therefore, we calculated LL6_LL6 without any approximation except for numerical integration. The 360 Feynman vertex diagrams of the gauge-invariant set LL6_LL6 can be reduced to sixteen independent integrals. Each of the integrands consists of about 50 MByte text files. In principle, no renormalization is required for LL6_LL6. However, to conduct numerical integration, an integrand needs ultra-violet (UV) counter terms that cancel the UV divergences of a child LL6 vertex subdiagram and a light-by-light scattering subdiagram (LL). The UV counter terms we constructed are the form factor $F_1(0)$ for a child LL6 and the light-by-light scattering tensor $\Pi^{\mu\nu\rho\sigma}(0,0,0,0)$ for a LL. The sum of the UV counter terms exactly vanishes when all gauge-invariant diagrams are summed up. The numerical calculation has been performed, and the result will be reported elsewhere.

Numerical calculations were conducted on RIKEN's supercomputer HOKUSAI BigWaterfall. This work was partly supported by KAKENHI 16K05338, 20H05646, and 22K03646.

*1 Department of Physics, Saitama University
*2 RIKEN Nishina Center

References

1) B. Abi *et al.* (Muon g–2 Collaboration), Phys. Rev. Lett. **126**, 141801 (2021).
2) G. W. Bennett *et al.* (Muon $g-2$ Collaboration), Phys. Rev. D **73**, 072003 (2006).
3) T. Aoyama *et al.*, Phys. Rep. **887**, 1 (2020).
4) E. H. Wichmann *et al.*, Phys. Rev. **101**, 843 (1956).

7. Astrophysics and Astro-Glaciology

Demonstration of multiplexing lobster-eye optics

Y. Zhou,[*1,*3] T. Mihara,[*1,*2] T. Tamagawa,[*1,*2,*3] and K. Uchiyama[*1,*3]

Wide-field X-ray monitor is essential in astronomy to catch short-time events, such as gamma-ray bursts,[1] and neutron-star mergers.[2] The all-sky X-ray monitor, MAXI,[3] which we have operated on the ISS since 2009, has proven its usefulness. As an extension of MAXI to the soft X-ray band and precise-imaging, we introduced the multiplexing lobster-eye (MuLE) optics.[4] we have recently performed verification experiments of MuLE for the first time. In this report, we present the angular resolution of MuLE obtained with Ti Kα (4.5 keV) X-rays.

The test setup is shown in Fig. 1. We used micro porous optics (MPOs) made by NNVT company with $R = 750$ mm and the size of 43 mm square. The CMOS image sensor was Gpixel 400BSI-TVISB, whose size was 22.5 mm square. X-rays through the three MPOs focus on a single CMOS placed on the focal plane at a radius of $R/2$, where R was the curvature of MPO. The field-of-view of a mirror is 3 deg $\times$ $\pm$1.5 deg. Each mirror was centered at 0 deg, 9 deg and 18 deg like stepping stones. We added the other side at -9 deg and -18 deg to make one unit. Using 3 units, the whole $\pm$20 deg $\times$ $\pm$1.5 deg sky can be covered. This CMOS has a good energy resolution. We measured the energy resolution of the CMOS for Ti Kα to be $\Delta E/E = 3.7\%$ (FWHM) with single-pixel events at room temperature.

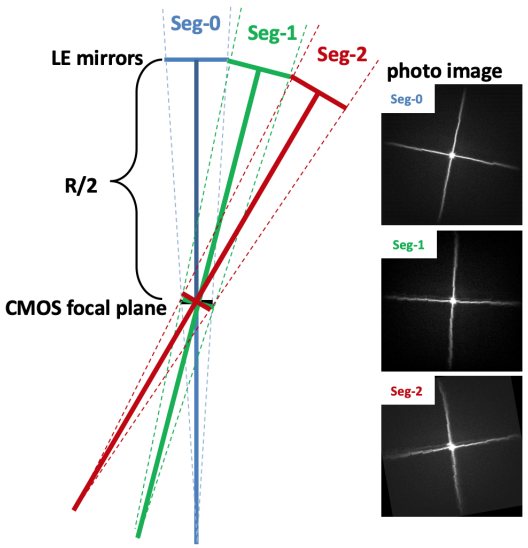

Fig. 1. MuLE experiment and X-ray images of three LE. The brightness corresponds to X-ray intensity.

We showed the focus images in Fig. 1 right. The distance of the Ti X-ray generator to the MPO was 3.85 m. The focal length was measured as 345 mm for this diverging light. In our experiment, the CMOS was set in this distance. Focal length for the parallel light was calculated to be 379 mm. It is close to the designed value (375 mm).

2 MPOs were placed on a mount, and measured Seg-0 and Seg-1 first. The Seg-0 mirror was rotated clockwise around the optical axis by 10 deg, while Seg-1 was 0 deg upright. The direction of the cross arm identifies the MPO which the X-ray comes from. After we measured Seg-0 and Seg-1 we moved the whole mount so that the Seg-1 MPO can locate Seg-2. Then we measured Seg-2. Although Seg-1 and Seg-2 are the same MPO, the image of the Seg-2 was rotated anticlockwise by 10 deg in Fig. 1 for understanding.

A demerit of the MuLE is that the CMOS is placed in a slanted way for the Seg-1 and Seg-2, which makes the image worse in the X direction in our setting.

By fitting the peak of the core in the image, the width of the focus can be measured. The angular resolution (σ) was shown in Fig. 2. It distributed between 4 arcmin to 8 arcmin, which is acceptable. Some jumping data points are due to irregularities on the LE surface.

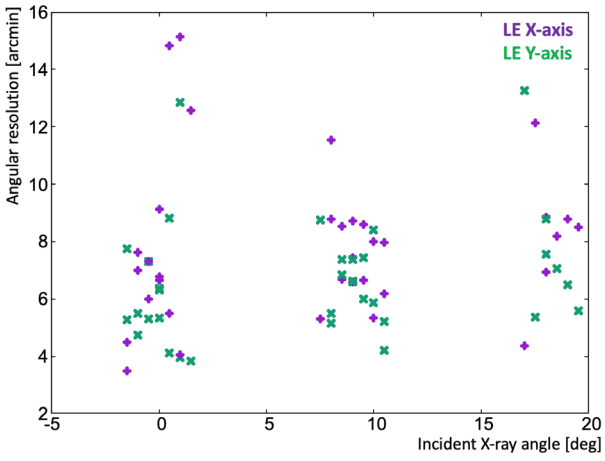

Fig. 2. Incident X-ray angle and position resolution (σ).

This report demonstrated the MuLE system worked as expected. MuLE system can be used in small satellites or ISS payloads to compensate for the soft X-ray performance of MAXI.

*1 RIKEN Nishina Center
*2 High Energy Astrophysics Laboratory, RIKEN Cluster for Pioneering Research
*3 Department of Physics, Tokyo University of Science

References

1) R. Vanderspek *et al.*, Astrophy. J. **617**, 1251 (2004).
2) B. P. Abbott *et al.*, Phys. Rev. Lett. **119**, 161101 (2017).
3) M. Matsuoka *et al.*, Publ. Astron. Soc. J. **61**, 999 (2009).
4) T. Tamagawa *et al.*, J. Astron. Telesc. Instrum. Syst. **6**, 025003 (2020).

Direct determination of the activation energy for diffusion of OH radicals on water ice†

A. Miyazaki,[*1] M. Tsuge,[*1] H. Hidaka,[*1] Y. Nakai,[*2] and N. Watanabe[*1]

Physicochemical processes such as surface reactions of radicals, photolysis by ultraviolet (UV) irradiation, and ion bombardment on interstellar icy grains are indispensable for chemical evolution during star formation. The chemical evolution begins in molecular clouds where the temperature is as low as 10 K. In molecular clouds, the hydrogenation of primordial atomic and molecular species is crucial because hydrogen atoms can migrate and encounter reaction partners on the grain surface even at ∼10 K.[1–7] During temperature elevation in star-forming regions, heavier species can diffuse on the ice and many types of complex organic molecules (COMs) are considered to be produced through reactions among heavier species, particularly radicals. Thus, the behavior of radicals on the ice surface should be investigated to understand the formation pathways of COMs. OH radical would be one of the most abundant radicals on ice surface as they can be produced through photolysis of H_2O and hydrogenation of O atoms on the ice surface. Therefore, OH radicals are expected to participate in various physicochemical processes on ice surface. However, conventional methods for detecting OH radicals, such as Raman, infrared, and electron spin resonance spectroscopies, are not applicable because of their low detection efficiencies and non-surface selectivity. In this study, we applied a combination of photostimulated desorption (PSD) and resonance-enhanced multiphoton ionization (REMPI) to facilitate direct detection of OH radicals on the ice surface.[8] Using this PSD-REMPI method, we determined the activation energy for diffusion (E_{diff}) of OH radicals on compact amorphous solid water (c-ASW), because the surface diffusion of radicals often becomes a rate-limiting process in reactions involving radicals.

The c-ASW samples were deposited on a sapphire disk at 100 K by introducing the water vapor into an ultrahigh vacuum chamber (∼10^{-8} Pa). After the preparation of ASW sample, OH radicals were produced via photolysis of water molecules using a deuterium lamp in the temperature range of 54–80 K. In this photolysis, H_2O is dissociated mainly into H + OH with minor channels, H_2 + O and 2H + O, and as secondary products, H_2 and O_2 are also produced on the surface. To avoid the undesired effect of these species other than OH, the experiments were performed at temperatures above 54 K where hydrogen and oxygen cannot stay on the surface. The OH radicals on the sample surface were detected with the PSD-REMPI method.[8] The OH radicals were photodesorbed by weak-pulsed laser radiation at 532 nm from an Nd:YAG laser. The photon energy at 532 nm is below the dissociation energy of H_2O. Photodesorbed OH radicals were selectively ionized by the (2 + 1) REMPI process above the c-ASW surface and detected with a time-of-flight mass spectrometer. We performed two types of measurements. In the first measurement, the OH intensities were monitored during UV exposure. We monitored the OH intensities in the steady state during UV irradiation. In the other measurement, the OH intensities were measured following a particular period of UV exposure. Note that we can selectively monitor OH radicals based on one-photon chemical process.[8]

When monitoring OH during UV exposure, we found that the OH intensities in steady state gradually decreased with the temperature of c-ASW in the range of approximately 60–80 K. We experimentally confirmed that OH radicals were lost through OH–OH recombination rather than thermal desorption of OH. The recombination rate should be limited by the diffusion of OH radicals on the c-ASW surface because the radical-radical reaction itself is barrierless. By analyzing the recombination rate with the Arrhenius type formula, the activation barrier of surface diffusion, E_{diff}, was evaluated to be 0.14 ± 0.01 eV (1650 ± 60 K). Furthermore, in the other measurement of OH monitoring after UV exposure, the OH intensities decreased with time after UV termination. Again, considering that this decrease is dominated by OH–OH recombination, we derived E_{diff} to be 0.13 ± 0.01 eV (1540 ± 80 K). This value is consistent with the previously obtained value.

Under a simple assumption that the activation energy of diffusion has the single value of 1650 K, the OH radicals can migrate over 100 nm on the icy dust within 105 years at temperatures above 36 ± 1 K. The present results suggest that OH reactions start at approximately 36 K and become important in the warming-up of star-forming regions. Note that we do not exclude the possibility that the OH radicals drift to a certain extent through shallower sites even at temperatures below 36 K.

References
1) N. Watanabe *et al.*, Prog. Surf. Sci. **83**, 439 (2008).
2) T. Hama *et al.*, Chem. Rev. **113**, 8783 (2013).
3) N. Watanabe *et al.*, Astrophys. J. Lett. **571**, L173 (2002).
4) S. Ioppolo *et al.*, Astrophys. J. **686**, 1474 (2008).
5) N. Miyauchi *et al.*, Chem. Phys. Lett. **456**, 27 (2008).
6) F. Dulieu *et al.*, Astron. Astrophys. **512**, A30 (2010).
7) H. Hidaka *et al.*, Chem. Phys. **13**, 15798 (2011).
8) A. Miyazaki *et al.*, Phys. Rev. A **102**, 052822 (2020).

† Condensed from the article in Astrophys. J. Lett. **940**, L2 (2022)

*1 Institute of Low Temperature Science, Hokkaido University
*2 RIKEN Nishina Center

Polarized X-rays emitted from a magnetar†

K. Uchiyama,[*1,*2] R. Taverna,[*3] R. Turolla,[*3,*6] F. Muleri,[*4] J. Heyl,[*5] S. Zane,[*6] L. Baldini,[*7,*8] D. González-Caniulef,[*5] M. Bachetti,[*9] J. Rankin,[*4] I. Caiazzo,[*10] N. D. Lalla,[*11] V. Doroshenko,[*12] M. Errando,[*13] E. Gau,[*13] D. Kırmızıbayrak,[*5] H. Krawczynski,[*13] M. Negro,[*14,*15] M. Ng,[*16] N. Omodei,[*11] A. Possenti,[*9] T. Tamagawa,[*1,*2,*17] and M. C. Weisskopf[*18] on behalf of the IXPE magnetar WG

Magnetars are neutron stars with ultra-strong magnetic fields. Magnetars exhibit steady X-ray pulsed emissions with a luminosity of approximately 10^{33}–10^{35} erg s^{-1}, spin period P of approximately 0.1–12 s, and large spin-down rates $\dot{P}$ of approximately 10^{-14}–10^{-10} s s^{-1}. This translates into magnetic fields of up to B approximately 10^{15} G, assuming a conventional spin-down model. The external magnetic field of magnetars is expected to have a toroidal component that twists the field lines. Because charged particles must flow along the closed magnetic field lines to sustain the field, the star magnetosphere becomes optically-thick during resonant Compton scattering (RCS).[1] Because of its strong magnetic field, magnetar X-ray emission is linearly polarized in two normal modes, namely, the ordinary (O) and extraordinary (X) modes, and upon reprocessing via RCS, X-mode photons become dominant.

4U 0142 + 61 is the brightest persistent magnetar with an unabsorbed flux of 6×10^{-11} erg s^{-1} cm^{-2} in the 2–10 keV range. Here, we report on the polarimetric observation of 4U 0142 + 61 conducted by the Imaging X-ray Polarimetry Explorer (IXPE) from January 31, 2022 to February 27, 2022 for a total on-source time of 840 ks.

Results are shown in Fig. 1 in the form of a polar plot where the polarization degree (PD) is the radial coordinate and polarization angle (PA) the azimuth. The measured PD is 15 ± 1% at low energies (2–4 keV). At 4–5 keV PD becomes consistent with zero and then increases to 35 ± 7% at 5.5–8 keV. The PA is approximately 50° East of North at energies below 4 keV and swings by 90°, settling at 40° West of North, above 5 keV.

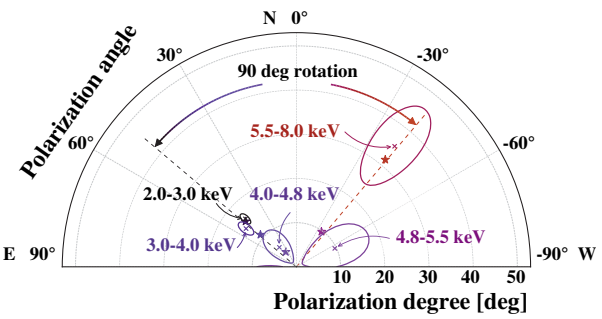

Fig. 1. Polar plot showing the energy dependence of the measured PD and PA. Contours enclose the 68.3% confidence level regions. Stars indicate the corresponding PD and PA calculated using the RCS model.

The polarization pattern as a function of energy, with a minimum of PD and swing of PA by 90° at approximately 4–5 keV, suggests that the X-ray emission from 4U 0142 + 61 is characterized by two distinct components polarized in two different normal modes. The low-energy component is thought to be produced by thermal surface emission while the high-energy component by photons up-scattered in the magnetosphere. The measured polarization fraction at high energies (35% at 5.5–8 keV) is indeed compatible with the theoretical expectations of the RCS model and suggests that X-mode photons dominate. Although the measured polarization fraction at low energies (2–4 keV) differs from the predictions of published theoretical models,[2] we found that the radiation emitted from a condensed[3] equatorial belt results in a predominance of O-mode photons with PD of approximately 15%.

In conclusion, the positive detection of polarized emission from 4U 0142 + 61 by IXPE further supports the magnetar model. In particular, the distinctive energy-dependent pattern can be explained by assuming emission from the bare condensed surface reprocessed by RCS in the twisted magnetosphere.

† Condensed from the article in Science **378**, 646 (2022)
*1 RIKEN Nishina Center
*2 Department of Physics, Tokyo University of Science
*3 Department of Physics and Astronomy, University of Padova
*4 Istituto di Astrofisica e Planetologia Spaziali
*5 Department of Physics and Astronomy, University of British Columbia
*6 Mullard Space Science Lab., University College London
*7 Dipartimento di Fisica Enrico Fermi, Università di Pisa
*8 Istituto Nazionale di Fisica Nucleare, Sezione di Pisa
*9 Osservatorio Astronomico di Cagliari, INAF
*10 TAPIR at Caltech
*11 Department of Physics, Stanford University
*12 Institut für Astronomie und Astrophysik, Universität Tübingen
*13 Physics Department and McDonnell Center for the Space Sciences, Washington University
*14 University of Maryland, Baltimore Country
*15 NASA Goddard Space Flight Center
*16 Kavli Institute for Astrophysics and Space Research, Massachusetts Institute of Technology
*17 RIKEN Cluster for Pioneering Research
*18 NASA Marshall Space Flight Center

References

1) C. Thompson *et al.*, Astrophys. J. **574**, 332 (2002).
2) R. Taverna *et al.*, Mon. Not. R. Astron. Soc. **492**, 5057 (2020).
3) A. Y. Potekhin *et al.*, Astron. Astrophys. **546**, A121 (2012).

8. Accelerator

Production of high intense Ca-ion beam for RILAC II acceleration

T. Nagatomo,[*1] Y. Higurashi,[*1] J. Ohnishi,[*1] and T. Nakagawa[*1]

Calcium(Ca)-48-ion beam is indispensable for studying light nuclei with excess neutrons. The ^{48}Ca beam was obtained from RILAC as an injector for RIBF accelerators before the upgrade of RILAC with superconducting (SC) acceleration cavities.[1] The injection line for the RIBF cyclotrons was removed owing to the construction required for the upgrade, and has not been restored at present. Currently, the only way is to use RILAC II, which is mainly used to inject heavy ion beams (krypton, xenon, uranium), as the injector for RIBF. Despite the global shortage of ^{48}Ca (natural abundance = 0.187%) samples, it is estimated that low-level enriched samples (∼20%) will be available within 2 years. However, the low enrichment of 20% implies that only 20% of the produced Ca beam can be used. Therefore, in accordance with the Ca beam acceleration scheme using RILAC II, we conducted a test to extract ultra-intense Ca^{11+}-beam above 100 μA from a SC-ECR ion source (SC-ECRIS).

The experiment was conducted using an SC-ECRIS for RILAC (R28G-K),[2,3] which exhibits the same performance as that of RILAC II. An ion-extraction voltage of 13.00 kV was applied to fit to the acceleration scheme. We selected a high-temperature oven (HTO),[4] which was used in the previous Ca^{16+} beam production last year with good results.[5] Compared to the previous test, because the Ca^{11+} has a lower charge state, the stable plasma conditions, such as the electron temperature and ion confinement time, differ. The magnetic mirror was set to lower field strength than the Ca^{16+} case, similar to the Ref. 6), resulting in the decreased electron temperature. Natural CaO samples were prepared using the same procedure as in a previous study.[5] Two evaporation methods to obtain the neutral Ca gas were attempted: direct heating of the sample at temperatures up to 2000°C (DH), and use of the redox reaction of $3CaO + 2Al \rightarrow 3Ca + Al_2O_3$ to lower the Ca evaporation temperature (RR). The DH method is the same method as in the Ca^{16+} beam production, and RR is a common method as presented in Ref. 6). The temperature was controlled by the applied power on the HTO (P_{HTO}). Oxygen (O_2) and helium (He) gases were tested as support gases (SGs) to maintain a stable plasma. The total microwave power with frequencies of 18 and 28 GHz, $P_{\mathrm{tot.}}$, as well as the SG flow rate were adjusted to optimize the beam intensity and stability.

Table 1 summarizes the obtained intensities of ^{40}Ca-ion beam extracted from R28G-K along with the experimental conditions. The data for the ionic charge state $Q = 16$ are obtained from a previous study.[5] Here, I_{start} and I_{stop} represent the beam intensities at the beginning and end of the operation (duration time Δt), respectively. As shown in Table 1, in all cases of Ca^{16+}, the beam intensity gradually increased, and eventually reached to constant values. However, the Ca^{11+} beam intensity tended to decrease with the elapsed time. This trend is more pronounced in the O_2 case than in the He case. Note that, in the previous study,[5] the Ca^{16+} beam intensity was also tested with He support gas; however, it was found to be only half that of the O_2 support gas. The DH method seems to cause a chemical reaction between the tungsten crucible and the CaO sample at elevated temperature of ∼2000°C. From the M/Q analyses using the analyzing magnet, when the P_{HTO} is 700 W, the heavy-ion beams, which appear to be tungsten ions, are not noticeable; however, as the P_{HTO} is increased to 800 W and 900 W, they become more pronounced. Owing to the chemical reaction, the RR method, which can be used at lower temperature, is preferable to produce low-charge Ca ion beams. Although the measurement time was not sufficiently long, the consumption rate of Ca was estimated to be ∼0.7 mg/h using the RR method using the He gas to produce a Ca^{11+} beam of approximately 100 μA.

Table 1. ^{40}Ca ion beam intensities with the charge state Q together with the some experimental conditions such as the support gas (SG) and the Ca evaporation method (Meth.). Measurements were performed over a period of Δt. See text for other abbreviations.

Q	SG	Meth.	$P_{\mathrm{tot.}}$ kW	P_{HTO} W	Δt hours	I_{start} μA	I_{stop} μA
11	O_2	DH	3.4	900.	9.3	242.	204.
11	O_2	DH	2.7	800.	14.3	101.	59.
11	O_2	RR	2.8	190.	17.9	74.	33.
11	He	RR	2.1	190.	7.7	105.	90.
16	O_2	DH	3.0	720.	16.3	84.	85.
16	O_2	DH	3.0	660.	39.7	35.	70.
16	O_2	DH	3.0	600.	37.1	25.	30.

This study has only just begun, and the search for conditions that reduce the Ca consumption is ongoing.

References
1) N. Sakamoto *et al.*, Proc. SRF2019, Dresden, Germany (2019), p. WETEB1.
2) T. Nagatomo *et al.*, Rev. Sci. Instrum. **91**, 023318 (2020).
3) G. D. Alton *et al.*, Rev. Sci. Instrum. **65**, 775 (1994).
4) J. Ohnishi *et al.*, Proc. ECRIS2018, Catania, Italy (2018), p. 180.
5) T. Nagatomo *et al.*, RIKEN Accel. Prog. Rep. **55**, S18 (2022).
6) J. Y. Benitez *et al.*, Rev. Sci. Instrum. **85**, 02A961 (2014).

*1 RIKEN Nishina Center

Upgrade of rf control system for RILAC injector

K. Yamada,[*1] K. Suda,[*1] T. Ohki,[*2] H. Yamauchi,[*2] K. Oyamada,[*2] M. Tamura,[*2] A. Yusa,[*2] K. Kaneko,[*2] and N. Sakamoto[*1]

The RIKEN linear accelerator (RILAC)[1,2] and its downstream superconducting linac (SRILAC)[3] actively supply beams for research studies involving super heavy element. The injection section of the RILAC was constructed in the 1990s and consists of three main instruments: a buncher, a folded-coaxial-type radio-frequency (rf) quadrupole linac (FCRFQ),[4] and a re-buncher.

The old rf control systems at RIKEN were very poor in terms of reproducibility and operability, and their old analog low-level circuits caused a lack of rf voltage and phase stability. One of the major reasons is that they are aging, having been manufactured nearly 30 years ago; another reason is that the resolution is insufficient because the set values are specified using analog voltages. In addition, the feedback parameter settings must be adjusted in the circuit itself and cannot be changed easily during operation. Therefore, we decided to improve the controllability and the resulting rf stability by upgrading the control system with a programmable logic controller (PLC) and a new digital low-level (LL) circuit.

The old control system and wiring were removed and the new system was installed from July to August 2022, and the wiring to each control target such as the resonators, amplifiers, and DC power supply was connected in September. Figure 1 depicts the front view of the new control system. The left half depicts the cabinet with the PLC and motor drivers, and the right side depicts the cabinet with digital LL circuits and oscilloscopes. All the 12 motors, three for the RFQ resonator, four for the RFQ amplifier, and five for the re-buncher resonator, were updated to new stepping motors. All devices are controlled by a single PLC, similar to other rf control systems in RIBF. The new control system allows for better reproducible positioning of each drive mechanism, and the frequency tuner, which was previously operated manually, is now controlled automatically. The rf system is interfaced by EPICS for remote operation and monitoring, which is connected to the PLC through a TCP/IP connection.

Fig. 1. New rf control system for the RILAC injector. The PLC and motor drivers are visible inside the door.

The digital LL circuit is an original one based on the circuit for SRILAC,[5] and it supports a frequency range of 17–40 MHz. The circuit integrates automatic gain control, phase-lock loop, and phase difference detection for automatic tuning. These signals acquired by on-board 16-bit ADCs are I/Q demodulated using a field programmable gate array, and a direct digital synthesizer output is I/Q modulated and output as an rf signal. Similar to the SRILAC, various parameters such as the voltage set value, phase set value, and internal status are read and written by the PLC in parallel communication with the digital LL circuit. As all communication with the circuit is done digitally, all setting parameters such as the feedback parameters and thresholds can be set reliably, and the settings can be changed remotely.

Figure 2 presents a one-day trend graph depicting the rf voltage and phase stability of the RFQ. It is clear that the new system has significantly improved the rf stability. We plan to replace the analog LL system of the RILAC and RRC with an equivalent digital LL system next fiscal year.

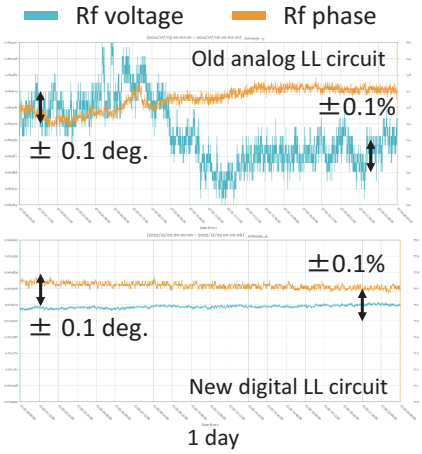

Fig. 2. Trend graph for rf voltage and phase of the RFQ before (upper panel) and after (lower panel) the upgrade.

*1 RIKEN Nishina Center
*2 SHI Accelerator Service Ltd.

References
1) M. Odera *et al.*, Nucl. Instrum. Methods Phys. Res. A **227**, 187 (1984).
2) O. Kamigaito *et al.*, Rev. Sci. Instrum. **76**, 013306 (2005).
3) K. Yamada *et al.*, Proc. SRF2021, (2021), p. 167.
4) O. Kamigaito *et al.*, Rev. Sci. Instrum. **70**, 4523 (1999).
5) K. Suda *et al.*, Proc. SRF2021, (2021), p. 666.

Beam profile measurement using helium gas light emission for superheavy element search experiment†

T. Watanabe,[*1] A. Kamoshida,[*2,*1] T. Nishi,[*1] A. Uchiyama,[*1] and K. Kaneko[*3]

The newly constructed superconducting linear accelerator (SRILAC)[1] continues to operate with the aim of discovering new superheavy elements following the discovery of 113 Nihonium,[2] and production medical radiation isotopes At.[3] In this experimental search for superheavy elements, owing to the demand to extend the durability of the expensive Cm target to the best extent possible the accelerated V beam must be adequately widened. Therefore, a He gas light emission monitor (HeLM) has been introduced to measure the beam width non-destructively and constantly.

Figure 1 shows the schematic of the differential pumping system, target chamber for the GARIS-Ⅲ, and HeLM. The beam originates from the left side and hits the Cm targets. As helium gas is flowing in the target chamber, the electrons of helium gas is excited by the collision with the beam. By monitoring the emitted light with a CCD camera when the excited electrons are de-excited, the beam profile can be obtained continuously. The image data obtained is sent to an image analysis PC with a video server for digital processing. These measurements and data analysis are controlled and programed with LabVIEW and the analyzed data are shared with a large-scale EPICS control system.

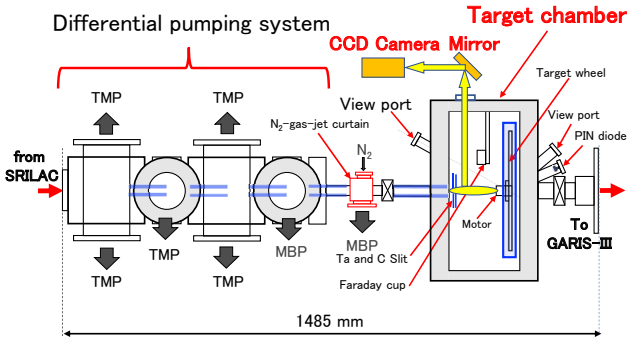

Fig. 1. Schematic of the differential pumping system, target chamber for GARIS Ⅲ and HeLM.

Figure 2 shows the front panels programmed with LabVIEW and measurement results. Recently, the beam width measurement with the HeLM and the beam optics calculation[4] facilitated the precise beam size control at the Cm target. Furthermore, the correlation between the beam size measured with the HeLM and elastic scattering counts measured with a semiconductor detector are confirmed to be quite consistent.

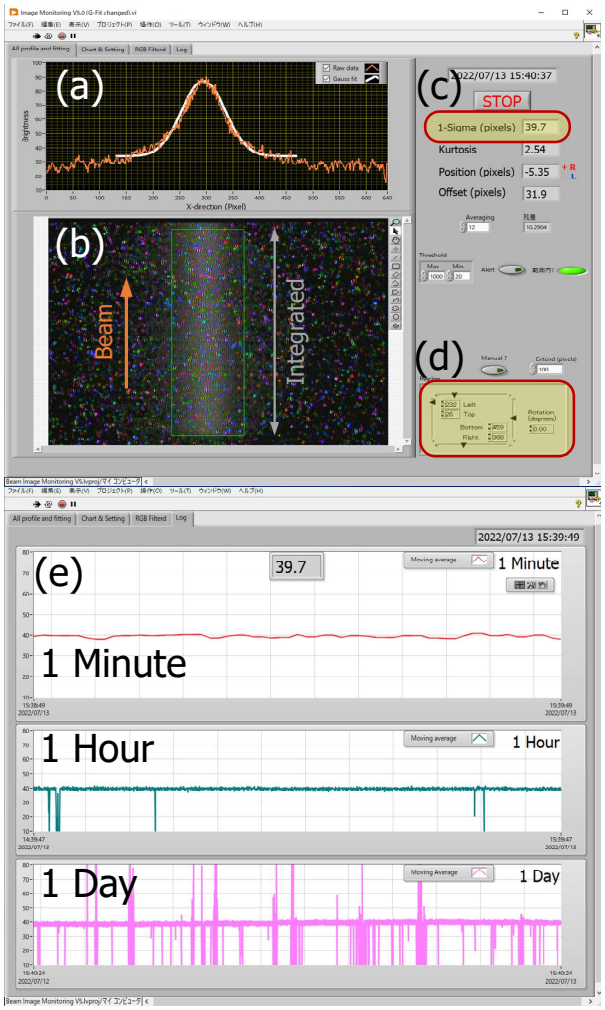

Fig. 2. The front panels programmed with LabVIEW and measurement results. (a) The integrating the brightness in the direction of travel of the beam and the result of Gauss fit, (b) image of He gas emission, (c) value of Gauss fit 1σ and the deviation from the center, (d) selection of the fitting region (manual, direct numerical input) and (e) Record of the Gauss fit 1σ.

† Condensed from the article in Proc. 19th Annu. Meeting Part. Accel. Soc. Jpn., to be published (2022)

*1 RIKEN Nishina Center
*2 National Instruments Japan Corporation
*3 SHI Accelerator Service Ltd.

References
1) N. Sakamoto, J. Part. Accel. Soc. Jpn. **17**, 70 (2020).
2) K. Morita *et al.*, J. Phys. Soc. Jpn. **81**, 103201 (2012).
3) H. Haba, Drug Deliv. Syst. **35**, 114 (2020).
4) T. Nishi *et al.*, Proc. 64th ICFA Advanced Beam Dynamics Workshop on High-Intensity and High-Brightness Hadron Beams (HB202), Illinois, USA, 2021-10, THBC1.

Improvement of the high temperature superconducting properties for the HTc SQUID current meter

T. Watanabe,[*1] I. Watanabe,[*1] and U. Widyaiswari[*1]

To measure the DC current of heavy-ion beams non-destructively at high resolution, we have developed a high critical temperature (HTc) superconducting quantum interference device (SQUID) beam current meter for use in the radioactive isotope beam factory (RIBF). Aiming at its practical use, the HTc SQUID monitor was installed at RIBF and a 1 μA heavy ion beam was successfully measuried with 100 nA resolution with this current meter.[1,2)]

Although we could measure the intensity of a sub-μA beam, a minimum current resolution of more than two orders of magnitude lower is required at the RIBF. With the aim of higher sensitivity and miniaturization of the SQUID current meter, we have started the investigation on a new method. Figure 1 shows a new scheme based on a direct coupling between an induced magnetic flux and the HTc SQUID.[3)] To fabricate an induction ring and a shielding ring, we have been investigating to coat and molten a thin layer (20–50 μm) of Bi_2-Sr_2-Ca_1-Cu_2-O_x (Bi2212) on a Ag substrate. The critical temperature of Bi2212 must be over 77 K, because it is cooled at a temperature of liquid N_2. To confirm the high critical temperature and to realize the high critical current which is related to the shielding effect of the environmental magnetic noise, we have been improving the superconducting properties. We found the properties of Bi2212 are improved by annealing it in the high purity Ar atmosphere. To obtain the better Bi2212 properties, we searched the critical temperature and critical current with a magnetic property measurement system by changing the annealing temperatures and annealing time. The measured results are shown in Fig. 2 and summarized in Table 1. The

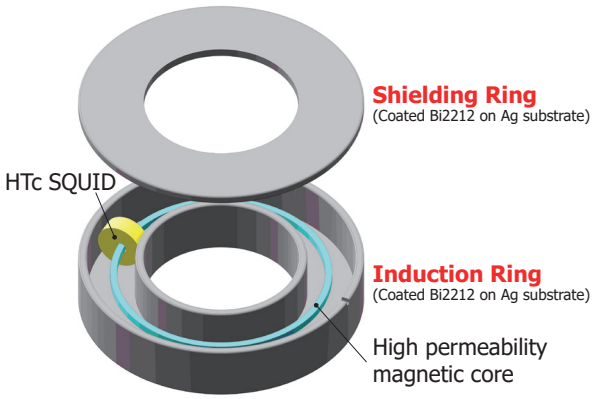

Fig. 1. A new scheme based on a direct coupling between an induced magnetic flux and the HTc SQUID.[3)]

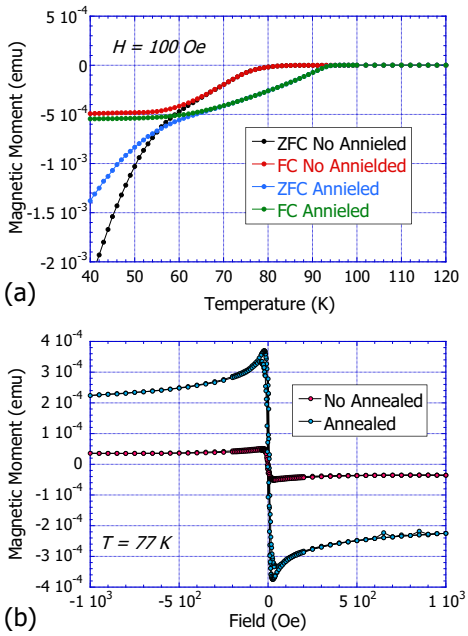

Fig. 2. Measured properties of the Bi2212 with a magnetic property measurement system.

Table 1. The obtained critical temperatures and critical currents.

	Anneiled	No anneiled
Critical temperature (K)	96	82
Critical current (A/cm^2)	422	83

critical temperatures and critical current were greatly improved by annealing at the temperature of 723 K for 24 hours in the the high purity Ar atmosphere. Currently, the Ag substrates of the induction ring and shielding ring are being coated and molten. Furthermore, a large quartz glass container used for the annealing is also being fabricated.

This work is supported by Japan Society for the Promotion of Science KAKENHI Grant Number 19H04403.

References

1) T. Watanabe *et al.*, Proc. 2010 Beam Instrumentation Workshop (BIW10), Santa Fe, US, 2010-9, p. 523.
2) T. Watanabe *et al.*, Proc. 4th International Beam Instrumentation Conference (IBIC2015), Melbourne, Australia, 2015-9, p. 590.
3) T. Watanabe *et al.*, Proc. 13th Annual Meeting of Particle Accelerator Society of Japan, 2016-8, p. 1127.

*1 RIKEN Nishina Center

Development of auto-tuning system using Bayesian optimization for ion optics in primary beam line with 26 electric nA Kr beam

T. Nishi,[*1] N. Fukuda,[*1] E. Iwai,[*2,*3] H. Maesaka,[*2] Y. Shimizu,[*1] T. Sugimoto,[*2,*3] T. Sumikama,[*1] and A. Uchiyama[*1]

We started the project to introduce the auto-tuning system of the accelerator facility to RIBF as reported last year.[1] As a first step in this project, we adopt an auto-tuning program using sequential learning based on Bayesian optimization[2] to the beam line optics from the SRC to BigRIPS first production target F0, so-called T-Course.

A test experiment for the project was conducted in May 2022 with Kr^{36+} beam to develop a new method to measure beam intensity and beam spot simultaneously for high-intensity beams. In the method, the phase ellipse and intensity of the primary beam are measured using BigRIPS nominal detectors. Because the direct measurement with these detectors limits the intensity of the primary beam, the charge-converted particles created by the 1 mm-thick Be target at F0 are measured by downstream detectors. This method enables to measure, for example, approximately 10 kcps Kr^{34+} beam at F3 as an indicator of a primary 30 electric nA Kr^{36+} beam.

In the experiment, Kr^{34+} was selected by the F1 slit and measured by PPACs and a scintillator at F3. The beam intensity was set to approximately 0.001 electric nA for the 5 different optical conditions to compare with the nominal method, and spot images were acquired with the viewer target at F0. As a result, they showed good agreement and we confirmed the measured values by F3 detectors were good indicators for the primary beam. Next step, we adjusted the optics of the T-course using the developed indicators. In the optical system tuning, it was necessary to finish the measurement and evaluation in a few tens of seconds for each parameter sets. We converted PPAC data into trajectories and beam widths within a few seconds using the newly developed BYACO[3] system and passed the data to the optimization program via EPICS. Finally, we optimized the currents of doublet quadrupole magnets QDT11a-b and QDT12a-b with 26 electric nA Kr^{36+} primary beam to maximize the scintillator count rate and minimize the beam widths at F3. Left panel of Fig. 1 shows beam spot measured by F3 PPACs before (left top) and after (left bottom) optimization. As shown in the figures, the horizontal beam widths are reduced from 1.5 to 1.1 mm (rms) at F3. The transmission efficiency was also measured for each optics with the Faraday cup at G01 and beam dump inside the D1 magnet, and it confirmed that both values agree within the errors. Graphs in the right panel of Fig. 1 show measured and calculated beam widths at the location of profile monitors in

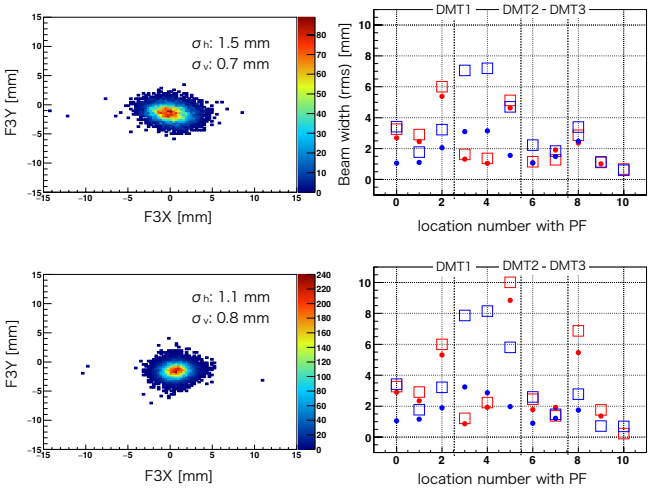

Fig. 1. (Top) Before optimization. (Bottom) After optimization. (Left) beam spot of Kr^{34+} measured by F3 PPACs. (Right) Beam widths at the location of profile monitors. Red (blue) marks correspond to horizontal (vertical) beam widths, and circle (square) marks correspond to the data measured by profile monitors (calculated by the simulation).

T-Course. The location 10 indicates F0. The calculation is based on the measured beam phase ellipse at F3. As shown in the figures, the measured and calculated values are in good agreement, except the vertical beam widths between DMT1 and DMT2. These calculations also show the optimized ion optics realized the smaller beam spot at F0.

In conclusion, we developed a new method to measure beam spot and intensity simultaneously with high-intensity primary beam. With the method we optimized ion optics in T-Course and reduce beam spot size at F0, keeping beam transmission efficiency. This new method using BYACO opens the possibility of optimizing the parameters of the beam lines using not only the beam spot, but also the signal of any downstream detector (*e.g.*, the signal-to-noise ratio of secondary particles) as an indicator. We are developing a new algorithm with safe regions to apply this method for the higher intense primary beam.

References

1) T. Nishi *et al.*, RIKEN Accel. Prog. Rep. **55**, 66 (2021).
2) E. Iwai *et al.*, Proc. PASJ2021, WEOB02 (2021).
3) T. Sumikama *et al.*, RIKEN Accel. Prog. Rep. **54**, 82 (2020).

*1 RIKEN Nishina Center
*2 RIKEN SPring-8 Center
*3 Japan Synchrotron Radiation Research Institute

Development and test operation of the prototype of the new beam interlock system for machine protection of RIBF

M. Komiyama,[*1] M. Fujimaki,[*1] A. Kamoshida,[*1,*2] M. Hamanaka,[*3] M. Nishimura,[*3] R. Koyama,[*3] K. Kaneko,[*3] A. Uchiyama,[*1] and N. Fukunishi[*1]

Continuing from 2021, we are developing a new beam interlock system (BIS) for machine protection based on CompactRIO[1] (hereafter, cRIO-BIS), a product by National Instruments, as a successor system to the BIS,[2] which has been in operation since 2006. We set up a prototype using one CompactRIO and one expansion chassis with I/O modules and developed the logic for digital input signals. The prototype signals for both a beam chopper and a beam stopper (Faraday cup) immediately after receiving an alert signal. Details are shown in Fig. 1.

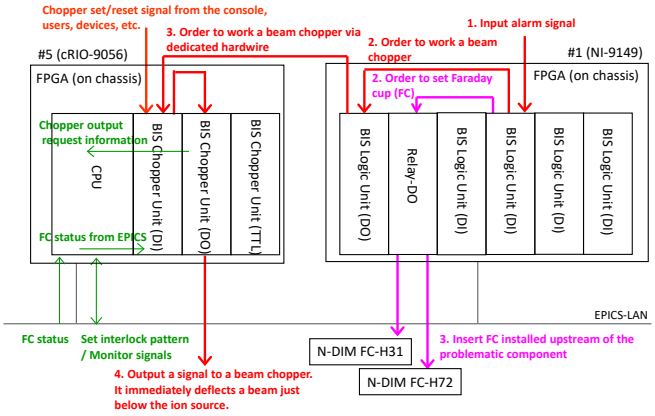

Fig. 1. Hardware configuration and process flow in the cRIO-BIS prototype.

The CompactRIO system has three layers for implementing logic for signal control: a field-programmable gate array (FPGA) layer, which is the most reliable and capable of the fastest signal processing, a real-time OS (RT-OS) layer that is positioned in the upper layer of FPGA and communicates with FPGA, and a Windows-OS layer that is positioned in the upper layer of them and communicates with them. FPGA is implemented on both CompactRIO and its expansion chassis, and RT-OS is implemented on CompactRIO. The goal of cRIO-BIS is to stop the beam within 1 ms by outputting a signal to the beam chopper from an alert signal input. Thus, interlock logic for signal input/output is implemented on the FPGA. However, signal condition setting and monitoring do not require the same speed as interlock logic. Thus, they are implemented on the RT-OS and controlled by using experimental physics and industrial control system (EPICS)[3] by setting up an EPICS server on the RT-OS.

Based on the operational experience of the BIS, cRIO-BIS implements two types of logic units; BIS Logic Unit (BLU) and BIS Chopper Unit (BCU). The BLU judges conditions such as mask and holding time for alert signal input and sends a signal to the BCU to request a signal to the beam chopper via dedicated hard wire. The BCU compares the input signal from the BLU and the insertion status of the Faraday cup and outputs a signal to the beam chopper. Since the BCU is designed to perform not only the function of BIS but also the role of the existing chopper signal control panel (it will be decommissioned in the future), it also receives signals from the console's manual switches and user's devices and outputs signal to the beam chopper.

After developing the prototype in the control room, its two stations were installed next to RIBF-BIS station 5 in the computer room of the Nishina Building and next to RIBF-BIS station 1 in the power supply room 2 of the RIBF building. The signal wiring was performed during the summer maintenance period. Since the prototype was planned to be tested in a part of the RIBF-BIS consisting of 5 stations, we connected the input signals into the prototype in parallel with the RIBF-BIS and evaluated its performance. The GUI for signal settings and prototype monitoring has been developed using the Control System Studio (CSS)[4] of EPICS, and the log system has been developed using the system in RILAC-operation.[5]

After installing the prototype, we measured the response time of the system with alert signals generated experimentally from an actual component and obtained a result of approximately 250 μs (between 229.0 μs to 260.0 μs). This is consistent with the system's response time measurements using test input signals in the control room. Furthermore, it was confirmed by the test that the response time could be reduced to less than 200 μs by adding a pull-up circuit to the signal input/output part. Since the response time of RIBF-BIS measured using the same signal was approximately 15 ms, we were able to develop a system that is approximately 100 times faster than the BIS.

We have started the test operation of the prototype during the beam service times scheduled in the latter half of the fiscal year 2022. Some minor corrections were necessary; however, no major defects were observed.

*1 RIKEN Nishina Center
*2 National Instruments Japan Corporation
*3 SHI Accelerator Service Ltd.

References

1) CompactRIO, https://www.ni.com/ja-jp/shop/compactrio.html .
2) M. Komiyama *et al.*, RIKEN Accel. Prog. Rep. **39**, 239 (2006).
3) EPICS, https://epics.anl.gov/ .
4) CSS, http://controlsystemstudio.org/ .
5) A. Uchiyama *et al.*, Proc. 18th Annual Meeting of Particle Accelerator Society of Japan (2021), p. 532.

Activation of temperature control in the RILAC cooling water

K. Yamada,[*1] M. Tamura,[*2] A. Yusa,[*2] and N. Sakamoto[*1]

Fluctuations in cooling water temperature have a significant impact on the accelerator. For example, a change in water temperature deforms the cavity resonator of the accelerator and changes its resonant frequency, resulting in a slight drift in rf voltage and phase despite feedback control. This affects the beam, causing beam loss and making it difficult to maintain a high-intensity beam. Therefore, we decided to activate the temperature control of the cooling water system of RILAC to realize a high-intensity beam and improve availability.

The cooling water of the RILAC is roughly divided into the ion source system, RFQ[1] system, RILAC[2] main system, RILAC booster[3]/SRILAC[4] system, and vacuum pump system. Except for the vacuum system, the secondary cooling water was cooled in the cooling tower, and the primary cooling water, which recovers heat from the load, was cooled through a heat exchanger. Some systems had flow control valves for temperature control, but the majority of them were disabled. In addition, all the fans in the cooling tower were constantly rotating, and the temperature of the secondary water fluctuated greatly depending on the condition of the outside air. As a result, the temperature of the primary water changed several degrees in one day.

The ion source system was originally temperature-controlled, but the cooling tower fan was rotated constantly. This secondary water was also used for the RILAC drift tube cooling system, and the temperature drop in winter caused a vacuum leak from the drift tube, resulting in a severe discharge. Therefore, a temperature controller was added on the control panel to automatically turn fans ON/OFF at 24 ± 1.5°C.

The RFQ system had a heat-exchanger bypass valve on the secondary side, which was sticking and unusable. The control panel was modified to add a primary and secondary temperature controller, and the bypass valve was replaced with a new one. The cooling tower fan is now automatically controlled ON/OFF at 23 ± 1°C, and the primary temperature automatically controls the bypass valve to keep at about ±0.1°C.

The secondary cooling water in the RILAC main system cools the resonator system, amplifier system, and irradiation vault system as the primary side. The number of cooling tower fans can be controlled by adding a temperature controller and rewriting the logic controller program by automatically turning them on and off individually. In addition, the fans are activated in sequence to reduce damage due to startups. Automatic control of the heat exchanger bypass valves in the resonator and irradiation vault systems was enabled, and both systems were maintained within ±0.2°C.

The SRILAC system was originally a cooling system for the RILAC booster, but the automatic control of the flow control valve had been disabled since the water leak in 2009. The control panel was modified to enable automatic ON/OFF control of two fans alternately, and automatic control of the primary temperature control valve was enabled. As a result, the temperature could be controlled to ±0.1°C.

The vacuum pump system used a closed cooling tower. Previously, the system froze during the cold winter, requiring repair. Thus, the control panel was modified, and a temperature controller was added. Currently, the temperature is controlled at 23 ± 2°C, and there is no longer any concern about over-cooling.

Figure 1 shows an example of one day trend for rf voltage and phase in the RILAC resonators. The rf stability is dramatically improved after activating the temperature control, contributing to a further intense-beam supply and increased availability.

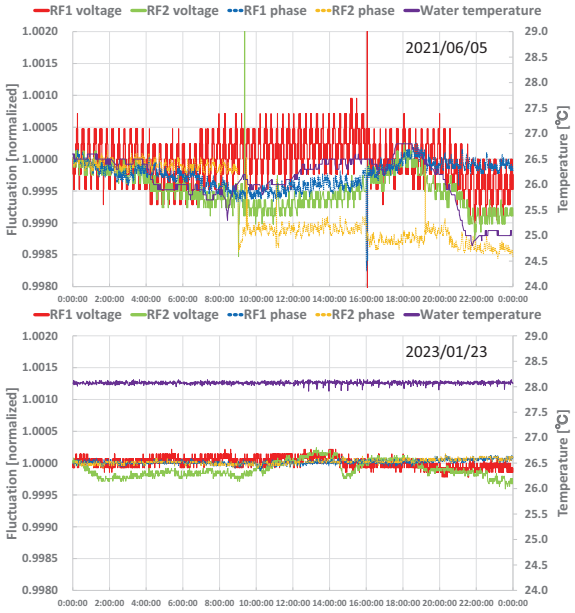

Fig. 1. One day trend of rf voltage and phase in the RILAC resonator no.1 and no.2 before (upper panel) and after (lower panel) stabilizing the water temperature.

*1 RIKEN Nishina Center
*2 SHI Accelerator Service Ltd.

References

1) O. Kamigaito *et al.*, Rev. Sci. Instrum. **70**, 4523 (1999).
2) M. Odera *et al.*, Nucl. Instrum. Methods Phys. Res. A **227**, 187 (1984).
3) O. Kamigaito *et al.*, Rev. Sci. Instrum. **76**, 013306 (2005).
4) K. Yamada *et al.*, Proc. SRF2021, (2021), p. 167.

2022 operational report of the Nishina RIBF water-cooling system

T. Maie,[*1] K. Kusaka,[*1] Y. Watanabe,[*1] M. Kidera,[*1] K. Kobayashi,[*2] J. Shibata,[*2] K. Yadomi,[*2] M. Oshima,[*3] and H. Shiraki[*3]

In 2022, the Nishina and RIBF cooling systems were operated for a slightly longer duration than the accelerator. The RIBF cooling system was operated for approximately 70 days, excluding the time of installation which was carried out continuously. Other cooling systems by Nishina (AVF standalone, AVF + RRC, AVF + RRC + IRC, and RILACII + RRC) were operated for approximately less than six months. Except for some minor problems, the cooling systems operated stably, and there were no long-term shutdowns of the accelerator. Complications regarding the SRC vacuum were experienced during the second half of the RIBF operating time, resulting in a cooling system operating time that was less than a year.

The minor problems that occurred are listed below.

(1) Cooling tower fan failure
(2) Water leakage from the joint of the cooling pipe
(3) Decline in purity of cooling water due to water leakage
(4) Cooling water pump motor bearing failure
(5) Equipment shutdown caused by momentary voltage drop due to lightning (3–4 times a year)

The afore-mentioned problems occur at approximately the same frequency every year. We experienced only minor complications because of proper periodic maintenance. Figure 1 shows a photograph of the periodic maintenance of the RIBF cooling pump. Figure 2 shows a photograph of the disassembly process of the cooling pump bearing. Periodic maintenance is planned as usual for the long-term suspension of accelerator operation in summer and winter. See the previous for details on the maintenance.

The annual cooling-equipment maintenance budget is extremely low. Maintenance is performed annually within the budget; however, the deterioration of the facilities is inevitable. The commodities and spare parts of the water-cooling pumps that have been used for the past 15 years are not produced anymore and are difficult to obtain. Aging cooling equipment is not only a causes of failure, but also one of the causes of beam instability in accelerators. Managing the costs of maintenance is an important concern for the future.

Fig. 1. RIBF water-cooling pump maintenance (Periodic maintenance).

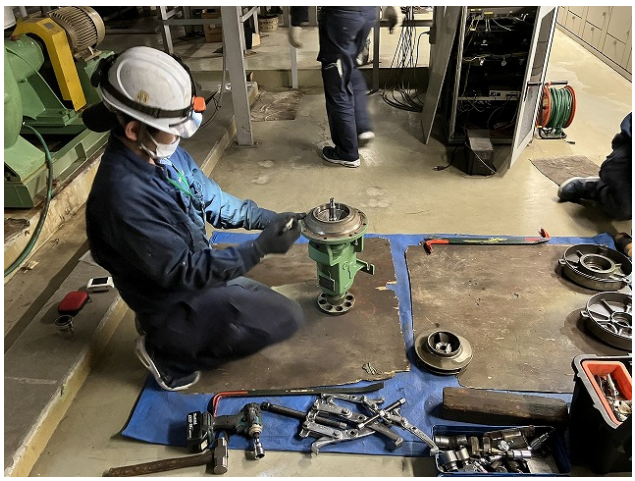

Fig. 2. Pump bearing section disassembly (Periodic maintenance).

Reference

1) T. Maie *et al.*, RIKEN Accel. Prog. Rep. **55**, 65 (2022).

[*1] RIKEN Nishina Center
[*2] SHI Accelerator Service Ltd.
[*3] Nippon Air Conditioning Service Co., Ltd.

Relationship between instantaneous voltage drops at RIKEN and influence on transmission power lines

M. Kidera,[*1] T. Maie,[*1] S. Watanabe,[*1] E. Ikezawa,[*1] Y. Watanabe,[*1] and O. Kamigaito[*1]

A stable supply of electric power is very important for accelerator facilities. Power outages and momentary voltage drops are unwelcome not only because they can shut down equipment but also because they can damage it. In addition, power problems occurring during the delivery of high-intensity, high-energy ion beams to the user are serious because they can cause a shift in the beam trajectory and lead to serious accelerator failures. The Nishina Center has a gas-turbine-type cogeneration system (CGS)[1)] in addition to the power supply an external power company. If there is a risk of a lightning strike, the CGS is activated to power the chillers that use liquid He. Information on lightning strike hazard is provided by the power company, which can be found on the internet. In this study, we report the correlation between the instantaneous voltage drops at RIKEN and influence on transmission power lines. Data on the influence on the power lines were provided by TEPCO Power Grid and data on the instantaneous voltage drop at RIKEN were provided by RIKEN's Facilities Division.

Electricity is generated by nuclear, thermal, and hydroelectric power plants and transmitted via high-voltage transmission lines. These power plants are located far from RIKEN. The transmission lines from these power plants are networked to achieve a stable power supply. Transmission from the power plants is transformed in the sequence 500 kV, 275 kV, 154 kV, 66 kV, and 22 kV along the transmission path, and wired to various residential and factory areas. The voltage of transmission line drawn into a factory or a commercial facility is determined by the electric power used by the facility. Electricity delivered to RIKEN at 66 kV from the power company, converted to 6600 V at a substation on site, and then transformed to 400 V and 200 V at a voltage transformer in the center. Table 1 shows the number of instantaneous voltage drops at RIKEN from 2017 to 2022, categorized according to the influence on power lines to each transmission line. Instantaneous voltage drops at RIKEN due to lightning strikes on the 500 kV power lines account for approximately 60% of the total, and approximately 79% if statistics are taken from lightning strikes alone. Much of the 500 kV power line network is located close to the power plant and far from RIKEN. Preparation for instantaneous voltage drops due to lightning strikes requires attention to not only the nearby lightning advisories, but also to the lightning strikes occurring in the neighboring prefectures.

Reference

1) T. Fujinawa *et al.*, J. Part. Accel. Soc. Jpn. **8**, 18 (2011).

Table 1. The number of instantaneous voltage drops at RIKEN from 2017 to 2022, categorized the influence on power lines to each transmission line.

Transmission line voltage	Lightning strike	Accident	Other
500 kV	15	1	
275 kV	1	1	
66 kV	1		
unknown	2	2	2

*1 RIKEN Nishina Center

Status of vacuum pumping systems in accelerator facilities

Y. Watanabe,[*1] M. Fujimaki,[*1] Y. Higurashi,[*1] E. Ikezawa,[*1] O. Kamigaito,[*1] M. Kidera,[*1] T. Nishi,[*1] S. Watanabe,[*1] K. Yamada,[*1] M. Nishida,[*2] K. Oyamada,[*2] J. Shibata,[*2] K. Yadomi,[*2] and A. Yusa[*2]

A vacuum pumping system in the RIBF accelerator facility comprises cryopump (CRP) systems, turbo-molecular pump (TMP) systems, rough pumping systems (mechanical booster pump + rotary pump [RP]), additional chamber pumping systems, and subpumping systems.[1] In addition, module-type vacuum gauges (total pressure gauge [TPG] controller combined with two gauges) are used in almost all vacuum pumping systems. In this study, we report the malfunction status of a vacuum pumping system encountered in 2022. Table 1 lists the number of malfunctions in the vacuum pumping systems from 2018 to 2022. The vacuum pumping systems were stable to maintain and manage in 2021 and 2022, and most malfunctions of each unit were less frequent than in other years.[2]

There was only one CRP (pump) malfunction, such as abnormal noise, vibration, and helium leakage, and the reason for this decrease is unclear. Furthermore, only one CRP compressor in the SRC malfunctioned due to a high environmental radiation dose. The reason for this decrease is due to the use of the existing old CRP compressor (model: C30V), which has a higher radiation resistance than the new CRP compressor (model: C30VRT), as long as possible. However, because the existing C30V is fewer and has been discontinued by the manufacturer, we plan to relocate eight of 13 compressors to a location far from the region of high environmental radiation (from the SRC-northeast area to the SRC-south area) in 2023.[2] Two new CRP compressors (model; C30VRT and F-50L) were purchased as spare units due to the existing discontinued CRP compressors (model; C30V, CRC-874, and P-875CA) of the AVF, SRC, RRC, fRC, and IRC. In the CRP system of AVF, RRC, and SRC, some helium leakages have occurred in some flexible hoses and couplings which were repaired by installing new parts.

Only one TMP (pump) and one power supply have malfunctioned due to age-related deterioration, such as abnormal noise, vibration, and circuit board failure, and the reason for this decrease is also unclear. In the update of large TMP systems (5000 L/s), we plan to replace the large TMP of the RILAC No.4 tank with a set of medium TMPs (800 L/s, 1100 L/s, and 2400 L/s) in 2023.

Five malfunctioned RPs were also caused by age-related deteriorations. Some oil leaks in the small RPs were repaired as usual by installing new O-rings and seals.

Age-related deteriorations also caused four malfunctioned TPG controllers. There were no malfunctioning TPG controllers when power was restored following an electrical power outage in August and October 2022.[2] Three malfunctioned gauges were replaced by spare units due to a contamination of the sensor head.

Almost all vacuum leaks at the RIBF were caused by age-related deterioration and were repaired by installing new parts, applying a repair material, or re-welding. For example, multiple water leaks from the water-cooling parts in the RRC or SRC cavities were repaired by re-welding. A vacuum leak of stainless bellows between the resonator No.2 cavity and a main chamber of the S-sector magnet in the RRC occurred for the first time in 2014 and was repaired for the third time with a sealing agent. Vacuum leaks of multiple flange welds in the AA6 chamber, installed in the fRC-IRC beam transport line, and in the RILAC cavities No.2 and No.6 were also repaired with a sealing agent. Faraday cup of the C21 chamber, a slit of A01 chamber and an O-ring of the AVF-RF No.2 were replaced with spare units or new O-ring. Finally, a vacuum leak due to beam loss damage occurred at a beam duct of the magnetic deflection channel No.3 in the SRC in December and is still under consideration.

References

1) Y. Watanabe *et al.*, RIKEN Accel. Prog. Rep. **50**, 154 (2016).
2) Y. Watanabe *et al.*, RIKEN Accel. Prog. Rep. **55**, 67 (2021).

Table 1. Number of malfunctions from 2018 to 2022.

		Number of units	2018	2019	2020	2021	2022
CRP [a]	Pump	> 80	4	6	7	6	1
	Compressor					8	5
TMP [b]	Pump	> 138	3	8	4	1	1
	Power supply					4	1
RP [c]	Pump	> 146	5	3	7	1	5
TPG [d]	Controller	> 160	4	6	9	5	4
	Gauge					7	3

[a] Includes a compressor. [b] Includes an attached power supply. [c] Excludes an oil leak. [d] Includes a controller, Pirani, and cold cathode gauge.

*1 RIKEN Nishina Center
*2 SHI Accelerator Service Ltd.

9. Instrumentation

Development of an automatic particle identification system for the BigRIPS separator

Y. Shimizu,[*1] N. Fukuda,[*1] H. Takeda,[*1] H. Suzuki,[*1] M. Yoshimoto,[*1] Y. Togano,[*1] T. Sumikama,[*1] H. Baba,[*1] and K. Yoshida[*1]

We are developing a fully automatic system for radioactive-isotope (RI) beam production based on our technological developments and experiences to reduce the operation time. In the present study, we aimed to automate particle identification (PID) for RI beams.

PID was performed event-by-event using the ΔE-TOF-$B\rho$ method to determine the mass-to-charge ratio A/Q and atomic number Z of RI beams.[1)] PID was confirmed by measuring the delayed γ-rays emitted from isomers. A PID analysis has been performed with the following procedure:

1. Find the isomers among RI beams,
2. Detect the peak energies from the delayed γ-ray spectra of the isomers,
3. Identify the isomers by comparing the detected γ energies with the known isomeric γ energies, and
4. Determine the calibration parameters for A/Q and Z.

This analysis procedure was automated using the BYACO ecosystem.[2)] The information on the isomeric nuclei observed at RIBF was stored in a relational database (RDB) based on Microsoft Access 2010.[3)] To use this information in the BYACO ecosystem, the RDB was transferred to a PostgreSQL database on a Linux server.

The automatic PID system was tested online during the ^{132}Sn-beam production required for MS-EXP22-04.[4)] Figures 1(a) and 1(b) show the PID plots without and with the delayed γ coincidence, respectively. The observation of isomers enhanced the fraction of blobs in Fig. 1(b) compared with that in Fig. 1(a). PID gates for the enhanced blobs were created and the delayed γ-ray spectra were obtained, as shown in Fig. 2. The isomers were identified by scanning the RDB for the measured peak energies, *e.g.*, blob No. 13 was identified as ^{132}Sn. The calibration parameters for PID were determined using A/Q and Z of the identified isomers. This automatic PID system was successfully demonstrated. As a result, the operation time became shorter than that of conventional manual tuning by 15 min.

The current system requires the RI-beam physicist to confirm that sufficient data have been acquired to obtain some γ-ray spectra. In future work, we will fully automate PID for RI beams.

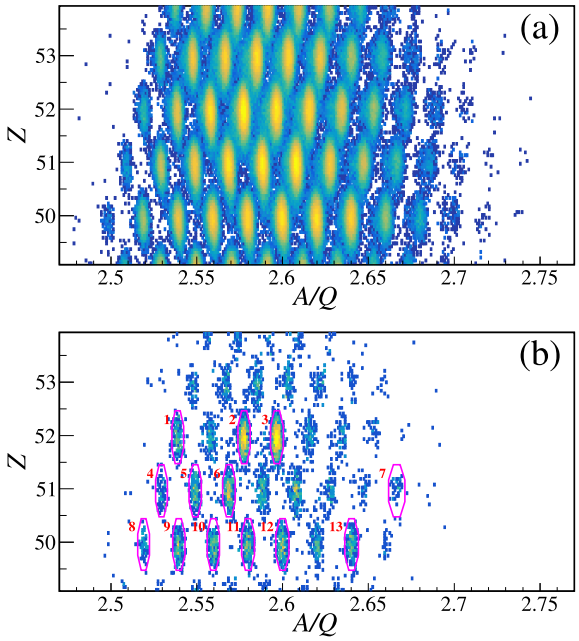

Fig. 1. Z versus A/Q PID plots (a) without and (b) with the delayed γ coincidence. The automatically generated gates for the isomers are labeled as 1: ^{132}Te, 2: ^{134}Te, 3: ^{135}Te, 4: ^{129}Sb, 5: ^{130}Sb, 6: ^{131}Sb, 7: ^{136}Sb, 8: ^{126}Sn, 9: ^{127}Sn, 10: ^{128}Sn, 11: ^{129}Sn, 12: ^{130}Sn, and 13: ^{132}Sn.

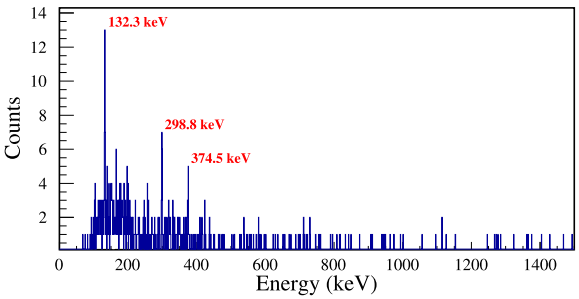

Fig. 2. Delayed γ-ray energy spectrum in coincidence with blob No. 13, which was found to be ^{132}Sn using the automatic PID system.

References

1) N. Fukuda *et al.*, Nucl. Instrum. Methods Phys. Res. B **317**, 323 (2013).
2) T. Sumikama *et al.*, RIKEN Accel. Prog. Rep. **54**, 82 (2021).
3) Y. Shimizu *et al.*, RIKEN Accel. Prog. Rep. **47**, 166 (2013).
4) Y. Shimizu *et al.*, in this report.

*1 RIKEN Nishina Center

Introduction and performance evaluation of a new data acquisition system for germanium detectors

H. Takeda,[*1] H. Baba,[*1] N. Fukuda,[*1] H. Suzuki,[*1] Y. Shimizu,[*1] M. Yoshimoto,[*1] Y. Togano,[*1] and K. Yoshida[*1]

Isomer tagging is an essential technique for unambiguous particle identification (PID) in BigRIPS[1)] and is achieved by detecting characteristic γ rays emitted from known short-lived nuclear isomers. Currently, two clover-type high-purity germanium (Ge) detectors are used for this purpose. Data acquisition (DAQ) for Ge detectors has traditionally been performed with a CAMAC-based system. However, many CAMAC modules are aging and becoming difficult to maintain due to discontinued production. Further failure of the critical modules could interfere with the isomer tagging. Therefore, considering an alternative DAQ system has been an urgent issue recently.

Mesytec MDPP-16[2)] is a promising candidate for the new DAQ system. It is a VME-based, 16-channel digital pulse processor with a fast high-resolution time and amplitude digitizer. Input signals are first amplified, filtered, and then digitally reconstructed in a hardware component, followed by detailed analysis in a digital signal processing unit implemented in a field-programmable gate array (FPGA). Among several FPGA software modules available for the MDPP-16, the standard "SCP" module suits our purpose. It delivers timing and amplitude information for standard charge-integrating preamplifier signals with 16-bit (64k) resolution. It can replace all the conventional shaping amplifiers, peak-sensitive ADCs, timing filter amplifiers, constant fraction discriminators, and TDCs.

First, we examined the ADC and TDC performance of the MDPP-16 SCP. The integral non-linearity (INL) of ADC was less than 0.1%, while the differential non-linearity (DNL) of ADC was less than 4% over the 20%–90% range of full scale. The INL and DNL of TDC were less than 0.001% and 0.03%, respectively. Time slewing with respect to the pulse height was less than 0.4 ns. These performance values were comparable to or better than the current system.

Figure 1 shows a γ-ray spectrum of a ^{60}Co source measured with the MDPP-16 SCP by the Ge detector used in the actual isomer tagging.

FWHM resolution of the 1332-keV peak was typically 4.7 keV. This value was mainly due to the accumulation of radiation damage to the Ge crystals over the years and was the same as that measured with the current system.

The isomeric γ-ray measurement using the MDPP-16 SCP was performed during the BigRIPS tuning this autumn. Figure 2 shows an atomic number (Z) versus mass-to-charge ratio (A/Q) PID plot for a ^{52}Ca-centered radioactive isotope (RI) beam.

*1 RIKEN Nishina Center

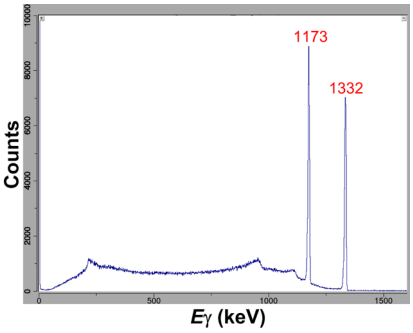

Fig. 1. γ-ray spectrum of a ^{60}Co source measured with the MDPP-16 SCP.

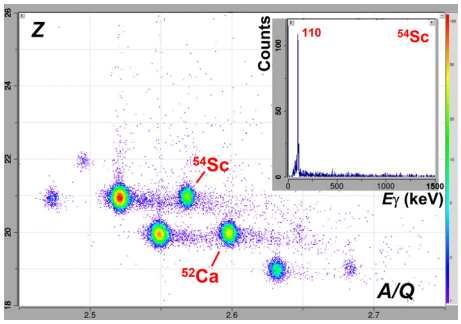

Fig. 2. Z versus A/Q PID plot of the ^{52}Ca-centered RI beam. Delayed γ-ray energy spectrum of the ^{54}Sc isomer is overlaid in the upper right corner.

The delayed γ-ray energy spectrum of the isomeric nucleus ^{54}Sc is overlaid in the upper right corner. The presence of a distinct 110-keV peak indicates that the MDPP-16 SCP can be used for isomer tagging.

Finally, we examined long-term stability, which is also important for practical operations. The energy calibration was stable within 0.5 keV over several days if no setting was changed. However, when we changed the settings, such as thresholds, the calibration was occasionally shifted from a few keV to a maximum of 10 keV. Based on oscilloscope observations, it is suspected that the baseline may shift when the settings are changed. A detailed investigation is in progress. While this issue must be resolved, the MDPP-16 SCP has the sufficient performance required for the new DAQ system of the Ge detectors. We plan to replace the current CAMAC-based system with the new system as soon as possible.

References

1) N. Fukuda *et al.*, Nucl. Instrum. Methods Phys. Res. B **317**, 323 (2013).
2) `https://www.mesytec.com/products/nuclear-physics/MDPP-16.html`.

Conceptual design of new high-power beam dump for BigRIPS

Y. Togano,[*1] N. Fukuda,[*1] H. Suzuki,[*1] Y. Shimizu,[*1] H. Takeda,[*1] M. Yoshimoto,[*1] and K. Yoshida[*1]

A new high-power beam dump situated at the exit of the first dipole magnet (D1) in the BigRIPS separator has been designed to absorb a 2 particle μA ^{238}U beam at 345 MeV/nucleon. The BigRIPS separator is equipped with beam dumps located both inside and at the exit of the D1 magnet to intercept unreacted beams resulting from primary beam + production target reactions at the focal plane F0. In the near future, the RIBF intends to utilize a 2 particle μA ^{238}U primary beam, which is 30 times more intense than the current ^{238}U beam, in order to produce a greater variety of exotic nuclei. However, the existing beam dump at the exit of the D1 magnet (hereafter referred to as the exit-beam dump) is incapable of safely absorbing such an intense beam due to insufficient cooling power. For performing experiments with 2 particle μA ^{238}U beam, a new high-power exit-beam dump, that utilizes a rotating water-cooled copper drum, has been designed.

The schematic depiction of the newly proposed exit-beam dump is illustrated in Fig. 1. The drum-shaped beam dump, measuring 300 mm in diameter and 350 mm in depth, rotates about its central axis to distribute heat and improve radiation damage resulting from the intense beam. The dump is made of a copper alloy, specifically Cu-Cr-Zr, and is equipped with 72 screw tubes (M8 tapped) to serve as water-cooling channels.[1] The water flowed in the cooling channels is pressurized at 1 MPa and runs at a velocity of 10 m/s, ensuring a high rate of heat transfer between the cooling water and the copper alloy. This M8 tapped cooling channels have already been equipped for the present exit beam dump.[2] The distance from the surface of the dump to the center of each cooling channel is 14 mm, and the pitch of the cooling channels is 12.2 mm. The rotational frequency of the dump is assumed to be sufficient to achieve a uniform temperature distribution along the circumference of the dump.

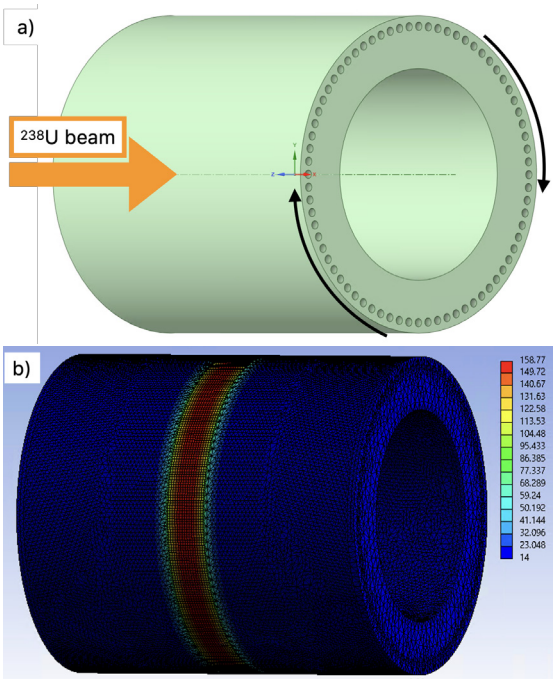

Fig. 1. a) Schematic view of the new exit beam dump. b) Caluculated temperature distribution on the surface of dump impinged by a 2 particle μA ^{238}U primary beam.

The cooling capacity of the dump is evaluated through finite element method simulation utilizing the ANSYS code. The results of the simulation are appraised against the following criteria:[2] the maximum temperature of the dump should be less than 350°C to maintain the radiation hardness of the dump, and the heat flux at the surface of the cooling channels must be less than the critical heat flux (55 MW/m^2) for stable cooling of the dump. It is known that copper alloy keeps good radiation hardness at temperatures below 400°C. Above the critical heat flux, the heat transfer rate at the cooling channel abruptly decreases as the surface of the cooling channel becomes covered with vapor generated by vigorously boiling cooling water. In the simulation, it is assumed that a 2 particle μA ^{238}U beam ($Q = 86^+$) at 345 MeV/nucleon is directly impinged on the dump as illustrated in Fig. 1a). The beam spot on the dump is of an elliptical shape due to overfocus by the D1 magnet. The ratio of magnetic rigidities between the ^{238}U beam and a beam following the central trajectory of the D1 magnet is assumed to be 0.85. The range of the 345 MeV/nucleon ^{238}U beam in copper alloy is 3.2 mm.

Figure 1b) illustrates the calculated temperature distribution on the surface of the dump upon the impingement of the 2 particle μA ^{238}U beam. The maximum temperature of the dump is 159°C and the maximum heat flux at the surface of the cooling channel is 5.4 MW/m^2. These values are below the allowable temperature and the critical heat flux, indicating that the new dump can safely absorb the 2 particle μA ^{238}U beam. The detailed design of the new exit beam dump is currently underway.

*1 RIKEN Nishina Center

References

1) J. Boscary *et al.*, Fusion Eng. Des. **43**, 147 (1998).
2) K. Yoshida *et al.*, Nucl. Instrum. Methods Phys. Res. B **317**, 373 (2013).

Energy-degraded beam on BigRIPS F0

H. Otsu,[*1] N. Fukuda,[*1] T. Nishi,[*1] and T. Sumikama[*1]

Uranium (and Xe, Kr) beams, which are accelerated up to the SRC, have a fixed beam energy of 345 MeV/nucleon because fixed-frequency accelerators are operated upstream. If a lower energy beam is required, the beam energy would be lowered with material as an energy degrader at the first stage of BigRIPS. Subsequently, the lower energy beam would be delivered into the downstream beamline. The energy-degraded beam would be transported to F2 or F3, where reaction targets would be placed. The disadvantages of the method are: 1) Transport of a relatively intense primary beam to F2 or F3 is required for the measurement of the reaction cross section, which might be subject to radiation shielding limitations. 2) Reaction products should be separated using downstream of F3 in BigRIPS, which requires a completely different approach compared to the measurement of production cross sections at 345 MeV/nucleon. This in turn might lead to large systematic errors.

Based on these reasons, the possibility of providing energy degraded beam to BigRIPS F0 was investigated and tested. A primary beam transport beamline is located from the G01 port to BigRIPS F0 downstream of the SRC exit. At an intermediate beam profile monitor port T11 beam can focus in both X and Y directions. Therefore, if this type of transport optics are used and an energy degrader material are located at T11, it is expected that the primary beam can be transported to the F0 focal plane without increasing phase space of the primary beam largely. Figure 1 shows the calculated transport from T11 to the F0 focal plane. In fact, this transport method has been previously used in dispersion matching experiments[1)] for verification of dispersion matching. Conversely, an energy degrade material has never been placed here before. This test was the first attempt to investigate the transport of energy-degraded primary beam to BigRIPS F0.

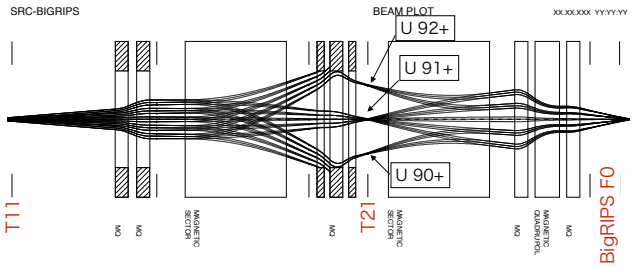

Fig. 1. Beam envelop from the T11 focus to BigRIPS F0. U beams with three different charge states are transported in the calculation.

The energy degrader plate was inserted from one of the ports at T11. It made of aluminum with 8 steps, each with a thickness ranging from 1.7 mm to 9.3 mm. After passing through each steps, uranium primary beam with 345 MeV/nucleon was degraded into 300, 250, 200, 150, 100, 75, 50 and 25 MeV/nucleon. When the energy degrader plate is withdrawn, the 345 MeV/nucleon U beam passes unchanged with the 86^+ charge 345 MeV/nucleon U beam passes unchanged with the 86^+ charge state. The beam is then transported to F0 by adjusting the magnetic field of the dipole magnets DMT2,3 to match the magnetic rigidity required for the 86^+ beam.

The U beam that has passed through the energy degrade plate has a dispersed charge state, and it is deflected by the DMT2 and DMT3 magnets from T11 and transported to F0 as shown in Fig. 1. It can be observed that a beam with a charge state whose rigidity is tuned to the central trajectory can pass through the triplet quadrupole magnets between DMT 2 and 3, while beams with neighboring charge states are considered to be partially blocked by walls in the middle of the Q magnet.

Tests of the transport were performed as a program DA03 on 2021/11 and 2022/03. Figure 2(a) shows one of the results on a profile monitor at T21 with the 250 MeV/nucleon transport. The neighboring charge state was actually observed as a separate peak on the momentum dispersion axis (X) in the profile monitor located at T21. The magnetic rigidity was set at 92^+ in the central trajectory. The results verified that the beam passing through the central orbit is 92^+ of the charge state, because 91^+ beam was observed at neighboring higher momentum while 93^+ was not observed. In this condition, the beam spread was confirmed by an alumina fluorescent plate at F0 shown in Fig. 2(b1), which is comparable with those observed at 345 MeV/nucleon (Fig. 2(b2)). At 150 MeV/nucleon, the condition was not as good as that at 250 MeV/nucleon and the T21 separation was

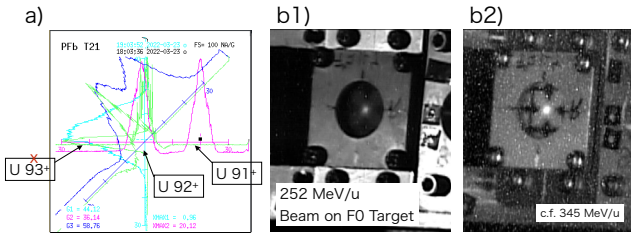

Fig. 2. a) Beam profile at T21 with U 250 MeV/nucleon. b1) Beam spot at F0 and b2) that of 345 MeV/nucleon for comparison.

*1 RIKEN Nishina Center

not sufficient. The beam spread, as monitored by the alumina fluorescent plate, was significantly larger than those at 345 or 250 MeV/nucleon.

In conclusion, the energy degraded beam from 345 MeV/nucleon at BigRIPS F0 was successfully delivered. This method proved that the energy-degraded beam can be delivered without using the first stage of BigRIPS, by utilizing the primary beam transport beamline from T11. On the other hand, it should be noted that the use of beams with different charge states are blocked by the beam duct along the beam line, especially at DMT2 or Q magnets between DMT2 and 3. Therefore, the effects of heat and radiation should be considered, not only for normal high-intensity beams but also for sufficiently reduced intensity beams.

Reference

1) T. Nishi *et al.*, Nucl. Instrum. Methods Phys. Res. B **317**, 290 (2013).

FPC board design for TOGAXSI silicon trackers

K. Higuchi,[*1,*2] J. Tanaka,[*1] T. Uesaka,[*1] H. Baba,[*1] and K. Miki[*3] for the ONOKORO collaboration

We are developing the detector array TOGAXSI[1] for realizing the ONOKORO project[2] at RIKEN. In order to accurately measure the angles of particles emitted from cluster-knockout reactions, it is necessary to track the particles with silicon strip detectors with good position resolutions. So far, we have performed test experiments using a prototype detector[3] and have established a detection and readout method for light ions. As the next step, we designed an electronics board for the silicon detector array for TOGAXSI. In experiments with scarce radioactive isotope (RI) beams, it is necessary to maximize the azimuthal-angle coverage of the detector array covering the cylindrical liquid hydrogen target STRASSE[4] to ensure adequate yields with limited beam intensity. Here, we report the design of flexible printed circuit (FPC) boards for detecting recoiled protons in cluster-knockout reactions. In order to maximize the azimuthal-angle coverage, six silicon detectors (HAMAMATSU S10938-5847, size: 51.0 mm × 78.4 mm) are arranged in a hexagonal shape as shown in Fig. 1. The distances between the six detectors should be as short as possible. In addition, these detectors have 100-μm strips in the polar-angle direction with respect to the beam axis. In terms of noise, it is essential to connect the APV25s1[5] chip, including a preamplifier circuit, to the same circuit with short wiring (a capacitance of 5 pF or less). The input-pad spacing of the APV25s1 chip was 44 μm and was routed from a 100-μm-pitch silicon detector with a line-strip spacing of 22 μm. The direction of signal readout is the direction in which the hexagonal silicon detectors are adjacent, which interferes with conventional planar printed circuit boards (PCBs). Therefore, we adopted FPC boards that can be bent 60° over a short distance between the silicon detector and the APV25s1 chip and designed a circuit that satisfies these requirements.

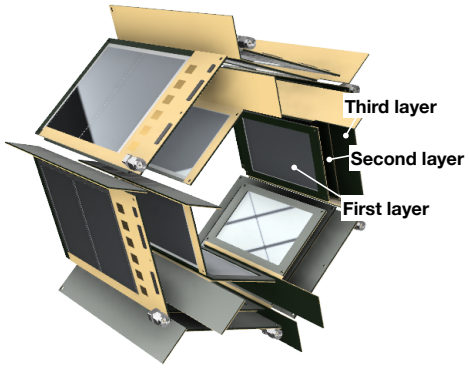

Fig. 1. CAD design of the silicon tracker of TOGAXSI.

The readout circuit is accommodated radially in six directions between the silicon wafers with respect to the beam axis. The power supply and output signals of the APV25s1 chip, and the connectors for supplying voltages to the silicon wafer are arranged on the upstream side of the beamline in the circuit, taking into account cable insertion/extraction and routing.

In addition, holes are created in the bottom of the APV25s1 chip to ensure heat conduction and to efficiently radiate the heat generated by the 300 mW consumed by one APV25s1 chip. The heat-connection part of the FPC board is designed to be thermally connected to the mounting frame. The frame is cooled by a water-cooling pipe introduced into the vacuum.

It was simultaneously confirmed that the azimuthal-angle coverage was maximized and that the requirements for the TOGAXSI silicon detectors, polar-angle coverages of 36°–67° and 8°–30° and angular resolutions of less than 3 mrad, were fulfilled as listed in Table 1.

Table 1. Calculated estimates of the polar-angle acceptances, polar angle resolutions, and azimuthal-angle acceptances of silicon detectors for recoil protons and light ions.

	Recoil protons	Light ions
Polar-angle accept.	35.3°–67.5°	8°–30°
Polar-angle resolu.	≤2.3 mrad	≤2.0 mrad
Azim.-angle accept.	∼65.8%	∼74.7%

At the time of reporting, the FPC board mentioned above is being manufactured, followed by wire bonding of the silicon wafer and mounting of the APV25s1 chip. We are also designing trapezoidal silicon wafers and FPC boards for measuring light ions by cluster knockout reactions.

*1 RIKEN Nishina Center
*2 Department of Physics, Saitama University
*3 Department of Physics, Tohoku University

References

1) T. Uesaka *et al.*, RIBF Construction Proposal, *TOGAXSI: A new detector array for inverse-kinematics cluster and nucleon knock-out reaction experiments* (2021).
2) T. Uesaka *et al.*, Grant-in-Aid for Specially Promoted Research, *Comprehensive research of cluster formation in nuclear matter* (2021).
3) K. Higuchi *et al.*, RIKEN Accel. Prog. Rep. **55**, 75 (2021).
4) H. N. Liu *et al.*, arXiv:2301.09276.
5) L. Jones, *APV25-S1 User Guide V2.2* (2001).

Study of the position dependence of the large GAGG(Ce) calorimeter

R. Tsuji,[*1,*2] J. Tanaka,[*2] T. Uesaka,[*2] J. Zenihiro,[*1] Y. Kubota,[*2] K. Higuchi,[*2,*3] T. Sugiyama,[*3] S. Kurosawa,[*4] H. Baba,[*2] S. Takeshige,[*5] Y. Hijikata,[*1,*2] S. Ogio,[*1] K. Yahiro,[*1] and T. Yano[*1]

A telescope named TOGAXSI array has been developed for proton induced cluster knockout measurements of reactions with inverse kinematics in ONOKORO project.[1,2] It consists of silicon strip detectors and total energy calorimeters which detect knock-outed cluster and the recoil proton. The requirements of the calorimeter are high energy resolution ($\sigma \sim 1$ MeV), durability for high count rate ($\leq$100 kcps) and large stopping power because the knockout clusters which has high energy up to 250 MeV/nucleon are scattered in forward angle with high count rate. We employed the large GAGG(Ce) scintillator ($35 \times 35 \times 120$ mm^3) which has high energy resolution, high stopping power, fast response and no hygroscopic nature.

In the pervious work, avalanche photo diodes which size are 10×10 mm^2 are attached to GAGG(Ce) directly and the position dependence of the light output is drastic ($\sim$30%).[3] The behavior is similar to photon collection efficiency which is mainly caused by solid angle of photo sensor.[4] The suppression of the position dependence is necessary because it cause worse energy resolution and linearity. We tested the light guide and the photo diode (Hamamatsu, S3584-08) which has relatively large effective area (28×28 mm^2) to suppress the position dependence as shown in Fig. 1.

The beam test was performed at QST HIMAC to research the response such as energy resolution and position dependence in new setup with proton and α beams at 100–230 MeV/nucleon. The energy resolution for focused proton beam at 100 MeV is about 1 MeV (σ). To measure the position dependence, the proton beam at 100 MeV was defocused and tracked by silicon strip detector. The definition of the coordinate is shown in Fig. 1. The position dependence in y and z direction is suppressed to less than 1% with the new setup.

Figure 2(a) shows the position dependence in x direction. The position dependence of left and right light output is relatively small at the region far from the each photo diodes. On the other hands, the light output of them decrease and increase near the each photo diodes. The photon collection efficiency explains this phenomenon. Figure 2(b) shows the result of the simulation of the photo collection efficiency with Monte Carlo simulation. In this simulation, the photons which are emitted isotropically from the designated point in the crystal are totally reflected at the surface of the crystal and light guide and refracted at the boundary of materials. The behavior of position

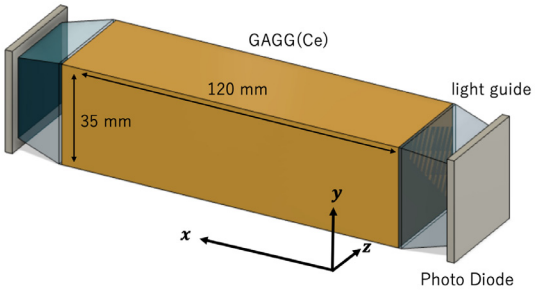

Fig. 1. The setup of GAGG(Ce) calorimeter.

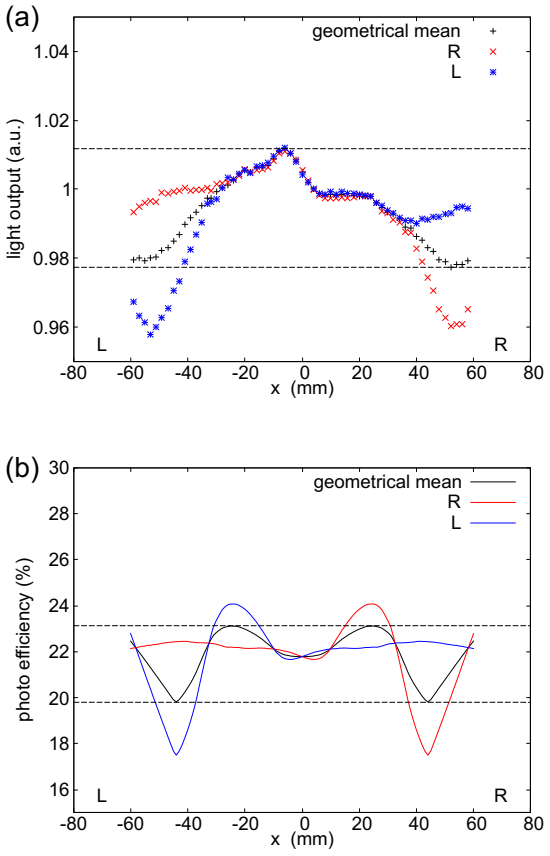

Fig. 2. The position dependence of the GAGG(Ce) calorimeter. (a) The light output measured with 100 MeV proton beam. (b) The photon collection efficiency simulated with Monte Carlo method.

*1 Department of Physics, Kyoto University
*2 RIKEN Nishina Center
*3 Department of Physics, Saitama University
*4 NICHe, Tohoku University
*5 Department of Physics, Rikkyo University

dependence near the photo diodes is similar to the experimental results but the absolute value is not duplicated. The light outputs of left and right photo diodes matches at $|x| < 30$ mm in Fig. 2(a) and it supports that effect of photon collection efficiency is small at the region far from photo diodes. Another cause of position dependence is the nonuniform composition of the crystal such as concentration of the doped cerium. The increase of the light output of both left and right photo diodes around $x = -10$ mm can be caused by this effect. In the new setup, the position dependence in y and z direction is suppressed and the total position dependence decreases under 4%. With the correction with silicon strip detectors, the energy resolution can be improved to under 1% for 100 MeV proton in this data.

References

1) T. Uesaka *et al.*, RIBF Construction Proposal, NP2112-SAMURAI72 (2021).
2) T. Uesaka *et al.* Grant-in-Aid for Specially Promoted Research, "Comprehensive research of cluster formation in nuclear matter" (2021).
3) R. Tsuji *et al.*, RIKEN Accel. Prog. Rep. **55**, 76 (2021).
4) R. Tsuji *et al.*, Master thesis, Kyoto University (2022).

Integration of VX2740B digitizer into babirl DAQ

S. Ogio,[*1] H. Baba,[*2] J. Zenihiro,[*1] R. Tsuji,[*1] and T. Yano[*1] for the ONOKORO Collaboration

We investigate cluster formation mechanism dependent on isotope and the kind of clusters by (p, pX) cluster knock-out experiments and inverse kinematics reconstruction with TOGAXSI array,[1] which named ONOKORO project.[2] It is difficult that approximately 100 ch signals from TOGAXSI array are processed in a conventional analog circuit and combined into output triggers based (p, pX) kinematics. CAEN digitizer VX2740B is a promising candidate to obtain data from GAGG scintillators of TOGAXSI array, process complex logic signals, and generate triggers.

VX2740B digitizer is an 125 MS/s ADC having 64 analog inputs, compliant with VME64X standard which has a 62.5 MHz internal clock. Pulse height is sampled by the 16-bit ADC in full-scale range of 2 Vpp. The VME crate is used only as a power supplier. Data is obtained via USB-3.0, 1/10 Gigabit Ethernet, or optical link cables attached to the front panel. Digitized signal, which is temporarily stored in 2.5 GB memory, is processed in FPGA Xilinx Zynq UltraScale+ implemented on VX2740B board. If the data rate is too high, the memory becomes full, VX2740B outputs intrinsic busy signals and the efficiency is significantly suppressed. CAEN provides firmware and C libraries named "FELib" for the basic waveform processing. Here we have developed a new program to integrate VX2740B into babirl DAQ.[3] It is called as babies for VX2740B and it utilizes FELib.

The H424 experiment[4] was carried out in PH2 course at QST, HIMAC and we confirmed that VX2740B can work properly under the experiment condition as a first development. Beam nuclide is ^{4}He, ^{16}O, ^{40}Ar and all of their energy were set to 230 MeV/nucleon. ESPRI chamber, drift chambers and ONOKORO chamber were aligned from the beam upstream to the downstream. The detector data except those of VX2740B were obtained by MPV[5] which is a VME-based DAQ system. 24 signals from GAGG in the ONOKORO chamber and 2 signals from GAGG read out with photodiodes in the ESPRI chamber were divided and entered into VX2740B and conventional CAEN ADC V785 installed in MPV. In this experiment, "scope" firmware was used to acquire waveforms by VX2740B. VX2740B was driven by a common external trigger from the babirl DAQ while data from VX2740B and the babirl DAQ were saved in separate ridf files. To synchronize the timestamp information, which eanbles merging separately stored data, a 62.5 MHz internal clock of VX2740B was distributed to MPV.

As a result, we have found that VX2740B did not output busy and then VX2740B event counts are almost the same as babirl DAQ when input channels were 26 and trigger rate was approximately 1 kHz. As shown in Fig. 1, waveforms are correctly obtained. We analyzed the ridf files unified with timestamps in order to compare the ADC values of V785 obtained by existing DAQ with the PHA values calculated from waveforms acquired by VX2740B, resulting the linear correlation event by event (Fig. 2).

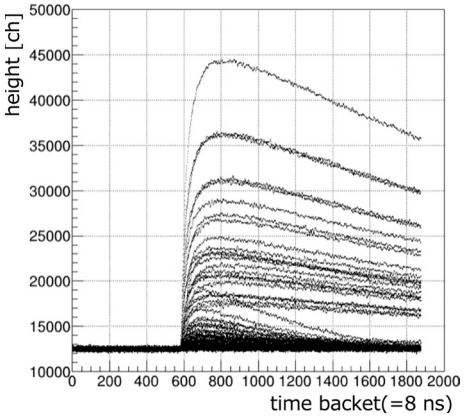

Fig. 1. Waveforms obtained by VX2470B.

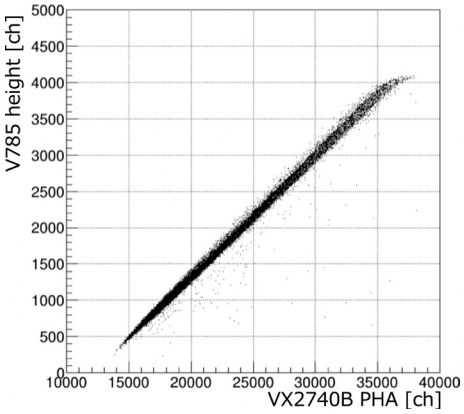

Fig. 2. Pulse height correlation.

In summary, we have developed the babies for VX2740B and succeeded in integrating it into babirl DAQ. In the HIMAC experiment, we operated it simultaneously with conventional ADC V785 and confirmed that the data was obtained correctly. In future studies, we plan to test the triggering function of VX2740B with "DPP-PHA" firmware provided by CAEN.

References

1) T. Uesaka *et al.*, RIBF Construction Proposal, NP2112-SAMURAI72 (2021).
2) T. Uesaka *et al.*, Grant-in-Aid for Specially Promoted Research (2021).
3) H. Baba *et al.*, Nucl. Instrum. Methods Phys. Res. A **616**, 65 (2010).
4) R. Tsuji *et al.*, in this report.
5) H. Baba *et al.*, IEEE Trans. Nucl. Sci. **68**, 1841 (2021).

*1 Department of Physics, Kyoto University
*2 RIKEN Nishina Center

Integration of DABC and babirl DAQ

S. Takeshige,[*1,*2] H. Baba,[*2] J. Tanaka,[*2] K. Higuchi,[*2,*3] and K. Yahiro[*2,*4]

In knockout measurements and elastic scattering measurements, such as the ONOKORO project[1] and the ESPRI project, the angle of the scattered particles must be measured with high accuracy. These projects use microstrip silicon detectors[2] as position detectors. We use DABC[3] for data acquisition in this silicon detector. DABC is a data acquisition (DAQ) system developed by GSI and established for the DAQ system of readout of these silicon detectors. In the two projects, babirl DAQ,[4] developed at RIKEN, is used for data acquisition, where babirl DAQ is DAQ software that can event-build from multiple sub-DAQ systems. We have developed additional software to link RUN operations of DAQ between DABC and babirl DAQ and merge data event-by-event to realize online analysis.

Figure 1 shows a schematic of the developed system. In this development, we have aimed to integrate and separate DABC and babirl DAQ easily in a simple design. The signals of silicon detectors are read out with analog pipeline ASIC, referred to as APV25,[5] and digitized by the ADC module, referred to as ADCMs,[6] composed of an SFP transceiver module and FPGA. These data were sent to the DABC in response to triggers from backend electronics referred to as TRB3[7] developed by GSI and Technische Universität München. DABC event-builds data from ADCM and saves it to the HLD file format. Here, the ridf-plugin was added as a DABC extension to enable communication with babirl DAQ. The ridf-plugin is a program that streams data over the network. The data event-built by DABC are sent to the *relay* program with two server sockets via the ridf-plugin. The *relay* passes the data to babies, which process this data. The processed data are sent to babirl DAQ, and event data is constructed with data from other modules. In this development, we have designed DABC and babies as clients, and the *relay* connects both. This ensures that both interprocess communications are de-coupled, and their configuration does not affect each other. For RUN synchronization, the start-stop manager referred to as babissm is used. When operating the babirl DAQ, the start/stop command is sent to babies and babissm from babicon, which is the controller of the babirl DAQ. In this case, we have added the start/stop command for DABC to the babissm. This allows both babies and DABC to operate from babicon.

Figure 2 shows a schematic of the conversion from HLD format to RIBF Data Format (RIDF). RIDF is the data format used for babirl DAQ. In RIDF, the data are identified by the segment header. The DABC event-built the data and sends as a single buffer gathering multiple event data. Therefore, developed babies decomposes the data in HLD format, attach a dedicated segment header to each event, and composes it as RIDF. Consequently, the silicon detector data sent to babirl DAQ are written to a file in RIDF along with data from other modules.

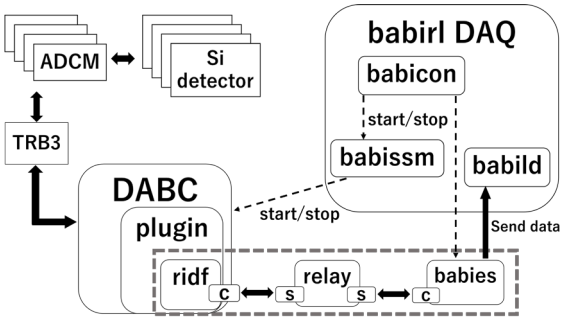

Fig. 1. Schematic of the DAQ integration system, where C and S represent client and server socket, respectively. The dotted box shows the developed part.

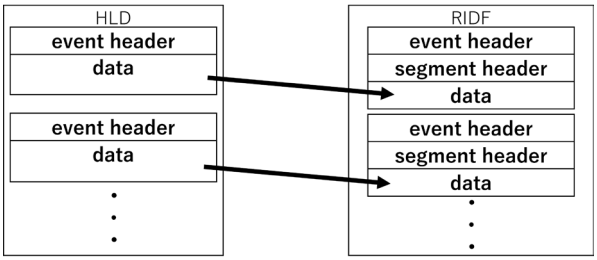

Fig. 2. Schematic of the conversion from HLD format to RIDF.

We used the system in the H424 experiment, conducted in July 2022 and January 2023 at the HIMAC of the QST. We successfully integrated DABC and babirl DAQ in this experiment. In addition, HLD format data could be converted to RIDF and merged on an event-by-event.

*1 Department of Physics, Rikkyo University
*2 RIKEN Nishina Center
*3 Department of Physics, Saitama University
*4 Department of Physics, Kyoto University

References
1) T. Uesaka *et al.*, RIKEN Accel. Prog. Rep. **55**, 28 (2021).
2) K. Higuchi *et al.*, RIKEN Accel. Prog. Rep. **55**, 75 (2021).
3) J. Adamczewski *et al.*, J. Phys. Conf. Ser. **119**, 022002 (2008).
4) H. Baba *et al.*, Nucl. Instrum. Methods Phys. Res. A **616**, 65 (2010).
5) L. Jones, APV25-S1 User Guide V2.2 (2001).
6) J. Michel, Development and Implementation of a New Trigger and Data Acquisition System for the HADES Detector (2012).
7) Michael Bohmer *et al.*, A Users Guide to the TRB3 and FPGA-TDC Based Platforms (2015).

Fokker-planck analysis for particle motion in RUNBA

M. Wakasugi,[*1,*2] R. Ogawara,[*1,*2] Y. Maehara,[*1,*2] and S. Yoshida[*1,*2]

Recycled-Unstable-Nuclear Beam Accumulator (RUNBA) is under construction at E21 room to develop beam recycling technology for research on precise nuclear reactions of rare nuclei. RUNBA requires special equipment such as Energy Dispersion Corrector (EDC) and Angular Diffusion Corrector (ADC) to compensate for the dilution of particles in 6D phase space owing to the energy and flight angle straggling generated by the internal target. The principle of operation of the RUNBA and the EDC and ADC performance required for steady beam circulation in RUNBA have been presented in previous reports.[1,2] We analyzed particle motion using the Fokker-Planck equation, thereby confirming the reliability of the RUNBA's operation. In this report, the results of the Fokker-Planck analysis are presented along the longitudinal direction because of space limitations.

Invariant of the particle motion, Q, along the longitudinal direction is expressed as

$$Q = \frac{1}{2}X^2\delta\epsilon^2 + Y\{\cos(\phi_s+\delta\phi)-\cos(\phi_s)+\delta\phi\sin(\phi_s)\}, \quad (1)$$

where $\delta\epsilon = \delta E/(M + E_k)$, $X = \eta\omega/\beta^2$, $Y = qV\eta\omega/AT\beta^2E$, η a slipping factor, ω and V are the rf angular frequency and amplitude, respectively, β a velocity, A a mass number, q a charge, T a revolution period and ϕ_s and $\delta\phi$ are synchronous phase and its difference, respectively. Beam dynamics can be understood based on an analysis of the time evolution of the provability density distribution $f(Q,t)$ as a function of the invariant Q. The time derivative of $f(Q,t)$ is expressed as the Fokker-Planck equation

$$\frac{\partial f}{\partial t} = -F\frac{\partial f}{\partial Q} + D\frac{\partial^2 f}{\partial Q^2}, \quad (2)$$

where F is a friction coefficient and D is a diffusion coefficient. The details of the derivation of F and D are not provided here, but they are expressed as follows:

$$F = \frac{X^2}{2T}\sigma_e^2 + \frac{X^2K(\lambda_e)}{T}\sigma_e^2 + \frac{K(\lambda_e)}{T}Q, \quad (3)$$

$$D = \frac{3X^4}{8T}\sigma_e^4 + \frac{X^2}{2T}\sigma_e^2Q + \frac{X^4}{4T}(2K(\lambda_e)-1)\sigma_e^4 + \frac{5X^2K(\lambda_e)}{2T}\sigma_e^2Q + \frac{3K(\lambda_e)^2}{4T}Q^2, \quad (4)$$

where σ_e is the rms energy straggling generated at target divided by the total energy $M + E_k$, $K(\lambda_e) = q\eta_{te}T_{te}\lambda_e/A\beta^2E$, η_{te} and T_{te} are the partial slipping factor and time of flight between the target and EDC, respectively, and λ_e is an energy correction parameter at EDC. The first terms in Eq. (3) and the first and second terms in Eq. (4) are the energy-straggling effects while the remaining terms are the contributions from correction at EDC.

The time evolution of $f(Q,t)$ for a 10-MeV/nucleon ^{12}C beam in a RUNBA with a 10^{18}-cm^{-2} thick internal target has been calculated using the RUNBA lattice structure and presented in a previous report.[1] Figure 1 shows the time evolution of the single-particle probability density distribution $f(Q,t)$ with and without EDC correction, assuming a Gaussian-type distribution as the initial distribution. The black and red lines in Fig. 1 show the results of the particle tracking simulation and numerical solutions of the Fokker-Planck equation, respectively. The Fokker-Planck analysis reproduces the results of the particle simulation well, and this situation is similar for the transverse analysis. Thus the Fokker-Planck analysis is a useful tool for studying beam dynamics in RUNBA.

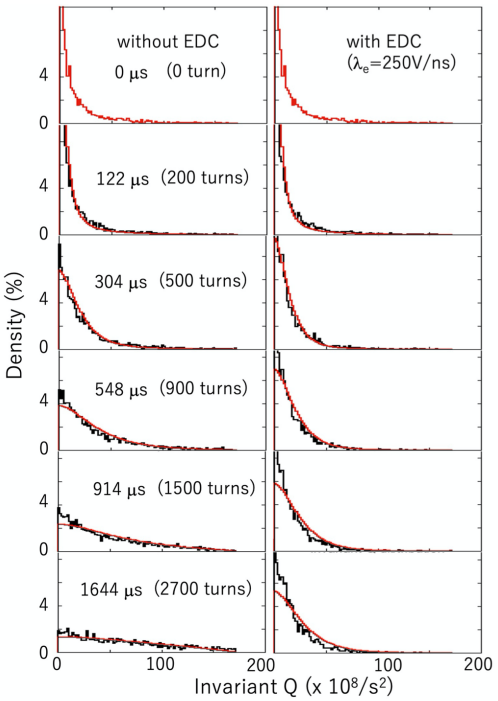

Fig. 1. Time evolution of $f(Q,t)$ without (left) and with (right) EDC correction at $\lambda_e = 250$ V/ns.

*1 Institute for Chemical Research, Kyoto University
*2 RIKEN Nishina Center

References

1) M. Wakasugi *et al.*, J. Part. Accel. Soc. Jpn. **19**, 25 (2022).
2) M. Wakasugi *et al.*, RIKEN Accel. Prog. Rep. **55**, 79, 80, 81 (2021).

Present operation status of ERIS at the SCRIT electron scattering facility

T. Ohnishi,[*1] Y. Abe,[*1] D. Abe,[*2] R. Danjyo,[*2] A. Enokizono,[*1,*3] T. Goke,[*2] M. Hara,[*1] Y. Honda,[*1,*2] T. Hori,[*1] S. Ichikawa,[*1] S. Iimura,[*1,*3] Y. Ishikura,[*2] Y. Ito,[*4] K. Kurita,[*3] C. Legris,[*2] Y. Maehara,[*4] Y. Nagano,[*5] R. Ogawara,[*1,*4] R. Ohara,[*2] T. Suda,[*1,*2] K. Tsukada,[*1,*4] M. Wakasugi,[*1,*4] M. Watanabe,[*1] H. Wauke,[*1,*2] and S. Yoshida[*4]

The electron-beam-driven radioactive isotope separator for SCRIT (ERIS)[1] at the SCRIT electron scattering facility[2] is an online isotope-separator system used to produce low-energy radioactive isotope (RI) beams using the photofission of uranium. The RI beam production at ERIS began in 2013 and has been vigorously developed. This year, two full-scale ion beam operations were conducted for physics experiments. The first was the ^{137}Cs ion-beam production for electron scattering experiment with RI. The second was the ion beam supply of Xe isotopes for the systematic study of nuclear structure using electron scattering. In this paper, we report details of both these operations.

The ^{137}Cs ion-beam production was performed in the spring of 2022. ^{137}Cs nuclei were produced via photofission of uranium, and they were ionized and extracted with the surface ionization technique. Details of the ^{137}Cs beam production are reported in Ref. 3). In this operation, self-made 48 uranium carbide disks, with thickness and diameter of 0.8 and 18 mm, respectively, were used as production targets and the total amount of uranium was approximately 28 g. A 150-MeV electron beam with beam power of approximately 15 W irradiated to the production target heated to around 2000°C using the resistive heating method. Ionized RIs were stacked in the ionization chamber for 25 ms, extracted as a pulsed beam by the exit grid of the ionization chamber, and then accelerated to 6 keV. Following mass selection, the pulsed ^{137}Cs ion beam was injected into a RFQ cooler and buncher, FRAC.[4] Approximately 10^7 ions/pulse for ^{137}Cs, accumulated for 4 s inside FRAC, were transported to the SCRIT system for the electron scattering experiment. During the measurement, which was approximately one month operation, the ERIS operation was very stable. Although there were concerns regarding the lifetime of the production target, the amount of produced RI remained almost constant because of the good quality of the target. It is important to establish a target-production method that guarantees the quality.

The ion beams of Xe isotopes have been supplied since this summver. The FEBIAD type ion source was used for the ionization of Xe, and natural Xe gas was injected directly into the ionization chamber. Details of the FEBIAD type ion source at ERIS are reported in Ref. 5). The overall efficiency, estimated as 5%, was lower than the previous result of 14%.[5] This is because no magnetic field of the FEBIAD type ion source was used to reduce the ion-beam emittance. With the optimized magnetic field, the overall efficiency became the same as the previous value. Finally, stable xenon ion beams over a wide mass range, from ^{124}Xe to ^{136}Xe, were supplied. For the supply of ^{124}Xe and ^{126}Xe, the gas supply volume was increased because the existing supply volume was insufficient owing to their low natural abundance ratio. An ion beam current, almost 1 nA, was achieved in case of ^{124}Xe, while maintaining the pressure inside the ion source in the order of 10^{-4} Pa with careful control of the gas supply. Figure 1 shows the mass spectrum. ^{124}Xe and ^{126}Xe were clearly separated and measured. After cooling and stacking inside FRAC, 10^8 ions/pulse of each Xe isotopes, including ^{124,126}Xe, were transported to the SCRIT system.

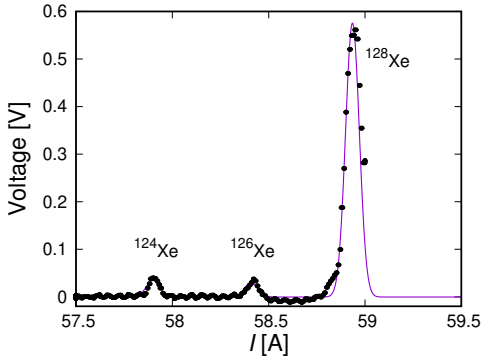

Fig. 1. Mass spectrum around ^{124}Xe and ^{126}Xe plotted with the current value of the analyzing magnet.

Currently, the experiments with Xe isotopes are still ongoing. As the next research objective, further development of ERIS is planned to accommodate the upgrade of the electron beam power to a few kW. For example, the radiation shield and the remote handling system are being considered for updates.

*1 RIKEN Nishina Center
*2 Research Center for Electron-Photon Science, Tohoku University
*3 Department of Physics, Rikkyo University
*4 Institute of Chemical Research, Kyoto University
*5 Department of Physics, Yamagata University

References

1) T. Ohnishi *et al.*, Nucl. Instrum. Methods Phys. Res. B **317**, 357 (2013).
2) M. Wakasugi *et al.*, Nucl. Instrum. Methods Phys. Res. B **317**, 668 (2013).
3) Y. Abe *et al.*, RIKEN Accel. Prog. Rep. **55**, S19 (2022).
4) M. Wakasugi *et al.*, Rev. Sci. Instrum. **89**, 095107 (2018).
5) T. Ohnishi *et al.*, Nucl. Instrum. Methods Phys. Res. B **463**, 290 (2020).

Improvement of gas inlet system for FRAC at SCRIT facility

S. Iimura,[*1,*2] T. Ohnishi,[*2] T. Yamano,[*1] Y. Abe,[*2] K. Kurita,[*1] R. Ogawara,[*3,*2] M. Wakasugi,[*3,*2] M. Watanabe,[*2] and H. Wauke[*4,*2]

At the SCRIT facility,[1] we have been studying the charge density distribution of unstable nuclei using the electron scattering method. To perform electron scattering with radioactive isotopes at a low production rate, it is necessary to convert the ions generated continuously by the ISOL-type ion separator, the electron-beam-driven RI separator for SCRIT (ERIS),[2] to a pulsed beam with an efficiency as high as possible. A fringing-RF-field-activated dc-to-pulse converter (FRAC)[3] is a gas-filled beam cooler buncher developed for this purpose and achieves an accumulation of 10^7 ions with an efficiency of approximately 90%.[4,5] However, a decrease was observed in the accumulation efficiency with a longer stacking time (see the blue squares in Fig. 2), and there were concerns that contaminants with small ionization potential in the noble gas could neutralize and molecularize the target ions. Therefore, a buffer gas purification system was introduced in the FRAC.

Figure 1 presents a schematic of the newly modified gas inlet system. Neon gas was purified to the ppb level or less of impurities using a filter (IG-105-200630, ARM Purification) and flowed into the FRAC, where the gas pressure was controlled to $\sim 10^{-3}$ Pa through differential pumping. A further improvement was the installation of a variable leak valve (951-7170, Canon ANELVA) instead of the needle valves. This valve enabled microflow control and significantly contributed to optimizing the gas pressure in the FRAC. Following assembly, all the gas lines were evacuated and baked at 110°C for nearly a day to eliminate as much residual impurity as possible.

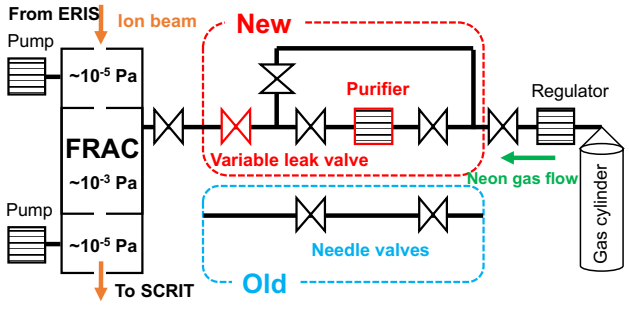

Fig. 1. Schematic of the gas inlet system before (blue frame) and after (red frame) modification. Neon gas was regulated at 0.11 MPa before the variable leak valve, and the microflow rate was controlled and introduced downstream of the valve to the FRAC.

*1 Department of Physics, Rikkyo University
*2 RIKEN Nishina Center
*3 Institute for Chemical Research, Kyoto University
*4 Research Center for Electron-Photon Science, Tohoku University

Offline experiments were performed to evaluate the improved efficiency. The $^{132}Xe^+$ ion beam delivered from ERIS was injected into the FRAC for 0.4 ms at 1 Hz ($\sim 10^7$ ions/cycle), trapped and cooled (for 1–1000 ms), and subsequently ejected into a Faraday cup located downstream of the FRAC to measure the ion current. The FRAC was operated with a 1.8 MHz, 1 kV_{pp} RF field and a DC potential of depth 30 V along the beam axis at a neon gas pressure of 2.0×10^{-4} Pa.

Figure 2 presents the offline test results of the stacking time dependence of the accumulation efficiency with and without the purifier. The efficiencies were defined as the ratio of the ion current to that without stacking in the FRAC. Before the improvement, the efficiency started decreasing after 10 ms of stacking and dropped to approximately 66% at 500 ms, whereas the introduction of gas purification enabled the efficiency to be maintained at over 90% for more than 1 s.

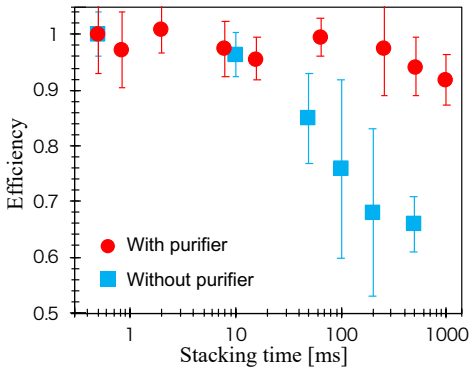

Fig. 2. Dependence of stacking time on FRAC efficiency with (red solid circles) and without (blue solid squares) purifier.

This study has established the significance of buffer gas purity, and the possibility of longer accumulation times and more efficient cooling at higher pressures has indicated the possibility of the electron scattering of exotic nuclei with small production yields in the future.

References

1) M. Wakasugi *et al.*, Nucl. Instrum. Methods Phys. Res. B **317**, 668 (2013).
2) T. Ohnishi *et al.*, Nucl. Instrum. Methods Phys. Res. B **317**, 357 (2013).
3) M. Wakasugi *et al.*, Rev. Sci. Instrum. **89**, 095107 (2018).
4) S. Sato *et al.*, RIKEN Accel. Prog. Rep. **52**, 144 (2019).
5) S. Sato *et al.*, RIKEN Accel. Prog. Rep. **53**, 111 (2020).

Charge state distributions of ^{138}Ba ions trapped in the SCRIT

R. Ogawara,[*1,*2] Y. Abe,[*1] T. Ohnishi,[*1] A. Enokizono,[*1] K. Kurita,[*3] Y. Maehara,[*1] K. Tsukada,[*1,*2] M. Wakasugi,[*1,*2] M. Watanabe,[*1] and H. Wauke[*1,*4]

The self-confining radioactive isotope ion target (SCRIT) method is an internal-target-forming technique for realizing electron scattering with unstable nuclei.[1] Target ions are injected into the SCRIT device and are trapped transversely by periodic focusing forces from electron beam bunches and longitudinally by the electrostatic well potential.[2] While the target ions are trapped in the SCRIT device, SCRIT performance (number of trapped ions, charge distributions, *etc.*) continues to change. Previous studies have shown that the instability of the electron beam is one of the major sources of trapped ions escaping from the SCRIT.[3] The trapping lifetime of the ions with a small mass-to-charge ratio (A/q) is shorter than that of the ions with a large A/q. Therefore, to optimize SCRIT performance, it is necessary to evaluate the charge state distribution of the trapped ions.

After trapping ions in the SCRIT device, the target ions are extracted and transported to an ion analyzer consisting of a total charge monitor, an $E \times B$ velocity filter (Model 600-B, Colutron Research Corp.), and a 43-channeltron array (Photonis Scientific, Inc.).[3] In previous work,[2] the charge state distributions of ^{133}Cs ions were measured by an ion analyzer with fixed electric and magnetic fields in the $E \times B$ velocity filter. The $^{133}Cs^{1+} \sim {}^{133}Cs^{3+}$ ions were identified clearly, but it was difficult to evaluate the abundance ratio of the$^{133}Cs^{1+} \sim {}^{133}Cs^{3+}$ ions because of the difficulty associated with correcting the detection efficiencies of the channeltrons, which depended on the position and angle of incidence and the individual differences in the channeltrons.

We developed a measurement method for the ion analyzer using a fixed magnetic field and an electric field scanning in the $E \times B$ velocity filter. In this method, the same number of trapped ions are injected into all channeltrons by electric field scanning so the detection efficiencies of all channeltrons can be measured simultaneously with measurements of the charge state distributions. The charge state distributions measured by each channeltron are corrected for the detection efficiencies and added to improve the statistical accuracy. The performance of the developed method was evaluated by simulating ^{138}Ba ion trajectories using the Runge-Kutta method, and it was confirmed that $^{138}Ba^{1+} \sim {}^{138}Ba^{10+}$ ions can be identified.

We measured charge state distributions of ^{138}Ba ions using the developed method while varing the trapping times. The incident energy of $^{138}Ba^{1+}$ ions to the SCRIT device was 6 keV. The energy and current of the electron beam were 150 MeV and 210–270 mA, respectatively. The fixed magnetic field was 1850 G, and the range of supply voltages for electric field scanning were 0–2400 V in 10 V steps.

Figures 1 (a), (b), and (c) show the charge state distributions of ^{138}Ba ions at trapping times of 30, 100, and 200 ms, respectatively. The $^{138}Ba^{1+} \sim {}^{138}Ba^{7+}$ ions were clearly identified, comfirming that the ions in higher charge states can be identified compared to measurements for ^{133}Cs ions.[2] The $^{138}Ba^{1+}$ ions were dominant at a short trapping time of 30 ms, but the charge state distributions of the ^{138}Ba ions were bred and spread with increasing the trapping time. The average charge states at trapping times of 30, 100, and 200 ms were 1.3, 2.5, and 3.6, respectatively. These results show that the developed method is useful for evaluating the charge state distributions of trapped ions in the SCRIT.

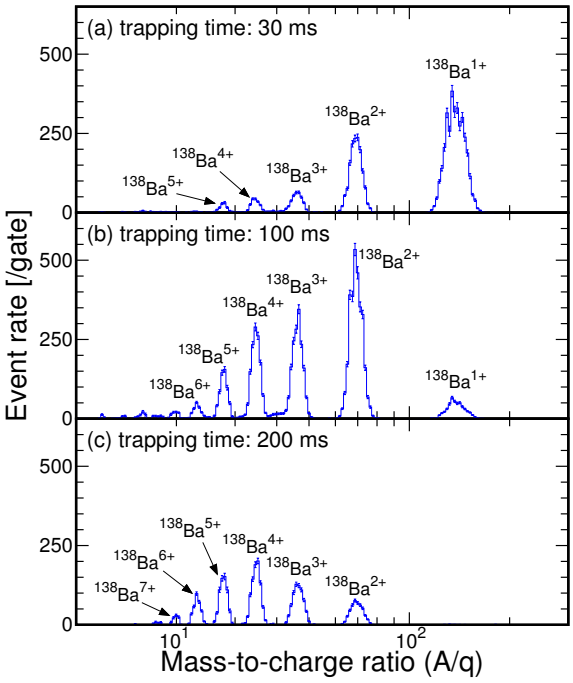

Fig. 1. Charge state distributions of ^{138}Ba ions with trapping times of (a) 30, (b) 100, and (c) 200 ms.

*1 RIKEN Nishina Center
*2 Institute for Chemical Research, Kyoto University
*3 Department of Physics, Rikkyo University
*4 Research Center for Electron Photon Science, Tohoku University

References

1) K. Tsukada *et al.*, Phys. Rev. Lett. **118**, 262501 (2017).
2) M. Wakasugi *et al.*, Nucl. Instrum. Methods Phys. Res. B **317**, 368 (2013).
3) R. Ogawara *et al.*, Nucl. Instrum. Methods Phys. Res. B **317**, 674 (2013).

Installation of the NEBULA-Plus neutron array

N. A. Orr,[*1] J. Gibelin,[*1] Y. Kondo,[*2] and H. Otsu[*3]
on behalf of the NEBULA-Plus Collaboration[*1,*2,*3,*4]

The direct investigation, through high-energy reactions and invariant mass spectroscopy, of neutron unbound states and systems requires the detection of one or more neutrons. In the case of the RIBF, the principal permanently available fast neutron detector is the two-wall 120-element NEBULA array,[1] which has been in operation since the commissioning of the SAMURAI setup in 2012. In order to augment the detection efficiency, in particular for multineutron channels, an upgrade comprising two supplementary walls to be located just forward of NEBULA (Fig. 1) has been built within the context of the French ANR funded project EXPAND.[2]

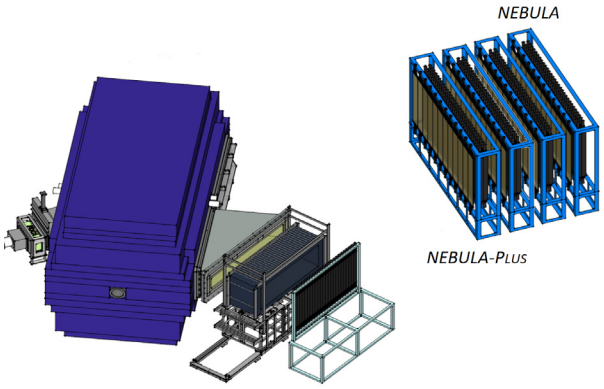

Fig. 1. Schematic view of the SAMURAI setup including the NEBULA-Plus and NEBULA arrays.

The NEBULA-Plus walls are composed of a total of 90 plastic scintillator bars (Eljen EJ200), with dimensions identical to those of NEBULA,[1] read out by Hamamatsu H11284 PMT assemblies. Each wall is composed of two layers - with each layer in the first wall comprising 22 bars and in the second wall 23 bars. As for NEBULA, each of the walls is preceded by a layer of thin (1 cm thick) large area charged-particle veto detectors. The read out of the PMT signals is performed using the FASTER digital electronics and acquisition system[3] developed at LPC-Caen. Whilst FASTER has been conceived as a triggerless system, it has been modified for use with NEBULA-Plus to generate a trigger (derived from the coincidence between the signals from the two PMTs of each bar) so as to allow for its integration into the SAMURAI data acquisition system (DAQ).

*1 LPC-Caen, France
*2 Department of Physics, Tokyo Institute of Technology
*3 RIKEN Nishina Center
*4 Department of Physics, Tokyo City University

After detailed acceptance testing of all the bars and PMTs at LPC-Caen and optimization of the operation of the FASTER electronics (in particular the timing and charge measurements) NEBULA-Plus was shipped to the RIBF in summer 2022, following the easing of covid travel restrictions. The mechanical installation and cabling were completed in early October (Fig. 2) and were followed by the installation of the high voltage system and electronics. Extensive testing was then performed during October and early November using cosmic rays and γ-ray sources with NEBULA-Plus running in a stand alone mode with FASTER. Subsequently the effort has been focused on the coupling of the FASTER electronics and DAQ with that of SAMURAI. At the time of writing (January 2023) this work and that required to merge the NEBULA-Plus data with that from the SAMURAI detectors has been completed and tested with cosmic ray data acquired with NEBULA and NEBULA-Plus operated in tandem. Initial in-beam commissioning is planned to be undertaken using the well-known ^{7}Li(p, n) reaction which will also enable the single-neutron detection efficiency of NEBULA-Plus to be determined.[4]

Fig. 2. View of the NEBULA-Plus array, including the veto detectors, prior to the installation of the electronics.

References

1) T. Nakamura *et al.*, Nucl. Instrum. Methods Phys. Res. B **376**, 156 (2016).
2) EXPAND: "Explorations Beyond the Neutron Dripline," ANR-14-CE33-0022-02.
3) `http://faster.in2p3.fr/`.
4) Y. Kondo *et al.*, Nucl. Instrum. Methods Phys. Res. B **463**, 178 (2020).

Silicon tracker array for RIB experiments at SAMURAI†

A. I. Stefanescu,[*1,*2,*3] V. Panin,[*4] L. Trache,[*1] D. Tudor,[*1,*2] I. C. Stefanescu,[*1,*2] J. Tanaka,[*3] H. Otsu,[*3] T. Motobayashi,[*3] A. Spiridon,[*1] and T. Uesaka[*3] for HI-p Collaboration

A silicon tracker for use in front of the SAMURAI spectrometer at the RIBF facility of the Nishina Center of RIKEN, Wako, Japan was designed, built and tested.[1)] The tracker consists of two pairs of single-sided microstrip detectors that determine the (x, y) position at two locations along the beamline after the target. The system provides particle identification from protons up to $Z \sim 50$ heavy fragments with energies 100–350 MeV/nucleon. GLAST-type 325 μm thick detectors were used. The inherent problems stemming from the large granularity, the required very large dynamic range and counting rate were handled using two matched ASICs: a dual-gain preamplifier DGCSP and the HINP16 pulse processing system.

Combining the HINP16 ASICs with the newly developed dual-gain preamplifiers, produces $2 \times 4 \times 128 = 1024$ channels. (Lo/Hi gain $\times$ 4 Si each with 128 channels.) This system yields a very large dynamic range of $\sim 10^4$. It can work in a self-triggering mode or in slave mode where it requires an external trigger and can tolerate very large input capacitance. The large dynamic range, provided by the dual-channel preamplifier, makes it possible to measure a wide range of nuclear charges. Parts of the system were tested with beams from the HIMAC facility in Chiba, Japan, to show that it can measure energy losses from 100 keV (protons) to 600–900 MeV (for heavy fragments up to $Z = 50$), which makes it appropriate for the studies with radioactive ion beams at intermediate energies.

The whole system was used and characterized in two RIBF experiments (NP1412-SAMURAI29 and NP1406-SAMURAI24), using the SAMURAI magnetic spectrometer. The silicon detection system was successfully used to track protons and heavy fragments simultaneously in the breakup of the proton-rich nuclei, (like ^{9}C and ^{66}Se) to reconstruct the reaction vertex, the emerging angles of the particles, the momentum distributions of the protons and the relative energy spectra. We run the system with 1.2×10^3 Hz ^{132}Xe beam rate during the HIMAC test and with 4×10^4 Hz of ^{9}C beam, and we assume that the maximum rate can be higher. However, the damage of the detector may become important. The problem becomes more complex because the center of the detector system takes a larger rate of hits and will lead to local damages. And it is more important for heavier (secondary) beams. This will be addressed by replacing the detectors when necessary.

To achieve the science objectives of the experiments with proton-rich radioactive beams in which we have to measure the proton and the heavy ion remnant, the essential tracking performances are: the atomic number identification, the vertex reconstruction resolution, the angular resolution and the momentum reconstruction resolution. All these are required to determine with a good energy resolution the missing mass spectra. We illustrate these with the case of the proton breakup of ^{9}C at 160 MeV/nucleon. The physics objectives are to disentangle the E1 and E2 contributions to the Coulomb dissociation process on a lead target and to evaluate the astrophysical factor, $S_{18}(0)$ by separating the contribution of the resonance at 918 keV. The resolutions obtained with the silicon system are resulting from the incoming beam phase space characteristics, the strip pitch size (0.684 mm), the distance between target and the first pair of detectors and the distance between the two pairs of detectors. With the 4 silicon detectors used in the configuration presented in the article, the resolution of the longitudinal distance (σ = 35 mm) is sufficient to separate the spurious events induced by the beam in the other materials around the target, as illustrated in Fig. 10(b) of Ref. 1). The angular resolution obtained for the laboratory opening angle is 3.5 mrad and the largest contribution is coming from the proton straggling in the first two silicon layers (straggling in 0.650 mm Si $\approx$ 2.8 mrad). By using these silicon detectors for proton tracking together with the proton drift chambers mounted at the exit of the SAMURAI superconducting magnet, we got for proton momentum resolution: $\Delta P/P \approx 0.065\%$. Considering these resolutions, we expect that at 1 MeV relative energy of p-^{8}B we get the energy resolution of $\approx$100 keV, about 2.5 times better than without the silicon tracker, which is sufficient to determine the cross section at energies below the resonance and to evaluate $S_{18}(0)$ by extrapolation.

This silicon tracker dramatically extends the research opportunities with the SAMURAI spectrometer especially for systems with two or more charged particles, which had been too difficult with the standard detectors equipped in SAMURAI.

Reference

1) A. I. Stefanescu *et al.*, Eur. Phys. J. A **58**, 223 (2022).

† Condensed from the article in Eur. Phys. J. A **58**, 223 (2022)

*1 Horia Hulubei National Institute for R&D in Physics and Nuclear Engineering
*2 Doctoral School of Physics, University of Bucharest
*3 RIKEN Nishina Center
*4 GSI Helmholtzzentrum für Schwerionenforschung GmbH

Development of a new configuration for the liquid hydrogen target

X. Wang,[*1] M. Kurata-Nishimura,[*2] H. Wang,[*3] T. Gao,[*2,*4] K. Horikawa,[*5] H. Otsu,[*2] and K. Takahashi[*5]

This study reports the development of a new configuration for the liquid hydrogen target, using a cryogenic proton and alpha target system (CRYPTA).[1] We study the complete kinematics of p(^{10}Be, pd) reactions at 230 MeV/nucleon. Recoil protons and deuterons exhibits a large scattering angular range (0°–70°). To cover these particles, we develop a new configuration for the liquid hydrogen target system located inside the CAesium iodide array for γ-ray Transitions in Atomic Nuclei at high isospin Asymmetry (CATANA)[2] frame.

Figure 1(a) shows the conceptional image of the new configuration and (b) shows the internal structure of the vacuum chamber. A 70-cc copper (Cu) buffer tank is connected to the first stage of a Gifford-McMohon cycle refrigerator (ULVAC R20) using a 45-cm long Cu pipe. A SUS O-ring is used to avoid leakage, and a small Cu ring is inserted to improve heat conductivity. The target cell is made of oxygen-free Cu and connected to the buffer tank by two Cu tubes, which are used for inlet (green) and outlet (magenta), respectively. Havar foil with a thickness of 6.5 μm was glued to the Cu window of the target cell and sandwiched by a Kapton ring. Figure 1(c) shows the size of the target cell. The thickness of the target cell is 15 mm. The deformation of the Havar foil was measured to be 2 mm with a difference of 1.2 atm. In the new configuration, the target cell is located at the downstream side of the vacuum chamber near the exit window (Fig. 1(b)). The chamber will be inserted into the CATANA frame. As a result, the center of the target is 25 cm more downstream than the center of the cryogenic head along the beam direction, thus covering a solid angle of approximately 2π.

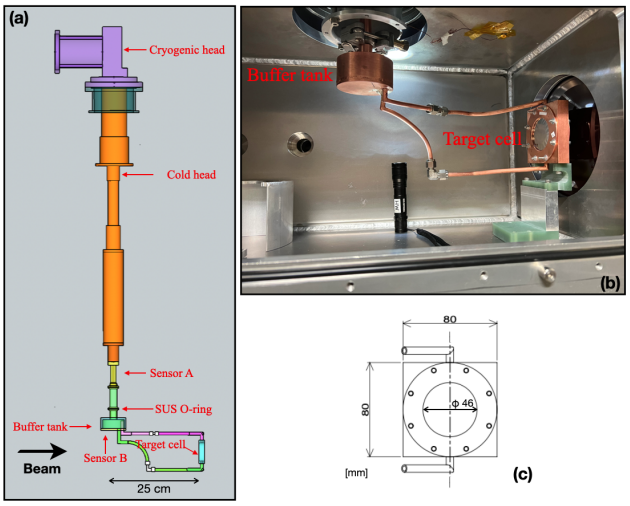

Fig. 1. New configuration: (a) conceptional image; (b) inside of the vacuum chamber; (c) the size of the target cell.

Temperature is monitored using two silicon diode thermometers (Scientific Instruments Si410AA). The thermometers are labeled as "Sensor A" (SA) (placed below the heater) and "Sensor B" (SB) (placed at the bottom of the buffer tank) (Fig. 1(a)). Figure 2 shows the variation in temperature and pressure with cooling time in a cooling test. The target cell and buffer tank was firstly pumped out at room temperature. It took less than 3 hours to cool SA from room temperature to 20 K, whereas SB was at 25 K. Then the heater started to operate and SA was maintained at 20 K. SB was cooled down to approximately 24 K with vacuum, and the system achieved dynamic equilibrium. Hydrogen gas was filled into the cell at 1650 hPa and liquefied near the cold head. Liquid hydrogen flew down gradually and cooled the system down to 21 K (Fig. 2(b)). Finally, the pressure was stabled at 1111 hPa, which is 33% lower than the pressure at which hydrogen gas was filled, indicating that the buffer tank and target cell was fully filled by liquid hydrogen. It took approximately 1.5 hours to completely filled the buffer tank and target cell. In the new configuration, it takes 4.5 hours to cool down and fully fill the system with liquid hydrogen.

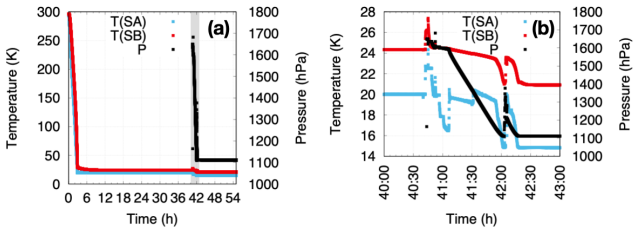

Fig. 2. Variation in temperature and pressure with time in a cooling test: (a) overall variation; (b) zoom-in view of the hatch area illustrated in (a).

In summary, we have developed a new configuration for the liquid hydrogen target system based on CRYPTA. By implanting the buffer tank, the target cell is placed near the center of CATANA. The system will be used first in the SAMURAI-53 experiment. Moreover, such a new configuration can be applied to the DALI2 array to study in-beam γ-ray spectroscopy.

*1 Research Center for Nuclear Physics, Osaka University
*2 RIKEN Nishina Center
*3 High Energy Nuclear Physics Laboratory, RIKEN
*4 Department of Physics, University of Hong Kong
*5 Department of Physics, Tokyo Institute of Technology

References

1) H. Ryuto *et al.*, Nucl. Instrum. Methods Phys. Res. A **555**, 1 (2005).
2) Y. Togano *et al.*, Nucl. Instrum. Methods Phys. Res. B **463**, 195 (2020).
3) S. Koyama and D. Suzuki, RIKEN Acce. Prog. Rep. **52**, 148 (2019).

Improvements in cooling operations of the SAMURAI magnet

H. Sato,[*1] H. Otsu,[*1] M. Kurata-Nishimura,[*1] M. Ohtake,[*1] and K. Kusaka[*1]

The operational policy for the SAMURAI superconducting dipole magnet is that the magnet is cooled for each SAMURAI campaign experiment and warmed after the experiments in order to save operating time and thus extend the cryocooler maintenance cycle. In line with this policy, the magnet has been at room temperature since 2020. Cooling operation of the magnet was performed from 2022/5/9 to 2022/6/2 for the upcoming experiments. Previously, we reported on the first magnet cooling conducted in 2014.[1)] This report describes the improvements made to the work environment and operating procedures since then.

The procedure for cooling is as follows:

(1) evacuation of the vacuum layers of the coil vessels,
(2) pre-cooling of the coils with liquid nitrogen,
(3) removal of liquid nitrogen,
(4) replacement of the inside of the coil vessels with gaseous helium,
(5) transfer of liquid helium into the coil vessels.

This series of operations are performed in parallel, shifting by one week for the upper and lower coils.

For (2), we have extended the liquid nitrogen inlet to be closer to the magnet (Fig. 1). As a result, the handling of liquid nitrogen filling was improved, the filling operation was reduced from three days to two days for a coil, and total liquid nitrogen was reduced from 7125 L (2014) to 5700 L (2022).

For (5), a new gaseous helium recovery port was installed near the magnet to facilitate recovery line preparation and effective collection of gaseous helium (Fig. 1(b)). We also introduced a 1000 L liquid helium container and a long transfer tube. Previously, more than five 250 L containers were needed to cool a coil. In practice, two containers were used one after the other, making it laborious to refill liquid helium and transport the containers from the RIBF building to the helium liquefaction building in the south area of the Wako campus. After introducing the 1000 L container, it was only necessary to transport one 1000 L and one 250 L container at a time. Furthermore, because of the long transfer tube, liquid helium could be poured from the containers placed on the floor (Fig. 2). In addition, as the container only needs to be exchanged once, the loss of liquid helium was reduced, resulting in a reduction in total liquid helium from 3145 L (2014) to 2237 L (2022). The filling process was also reduced for a coil from two days to one day.

One of the remaining issues to be improved would be to place the exhaust port near the magnet for gaseous nitrogen generated during pre-cooling. Currently, we use the port located in the ceiling of the elevator hall.

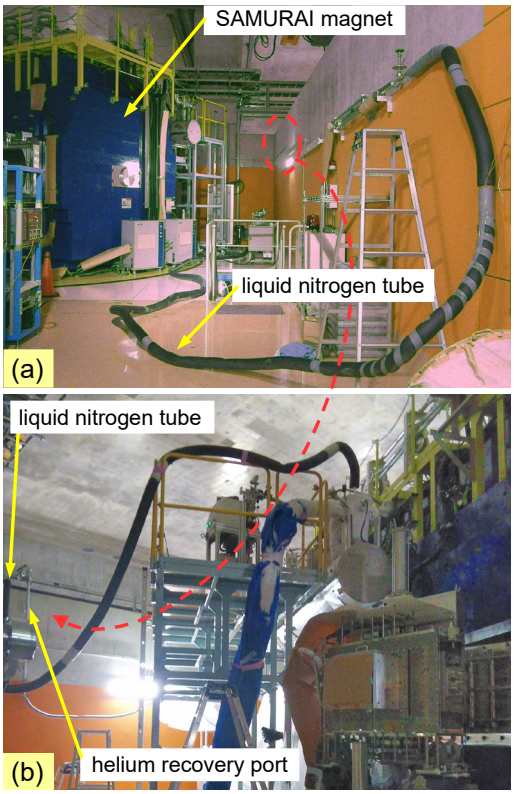

Fig. 1. The tube for liquid nitrogen and the recovery port for gaseous helium. (a) photo in 2014. There was no recovery port near the magnet. (b) photo in 2022.

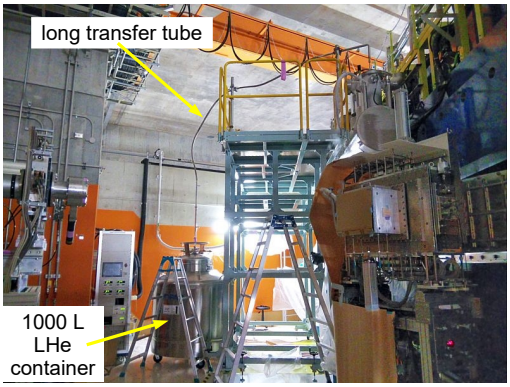

Fig. 2. Liquid helium transfer to the lower coil using the 1000 L container with the long transfer tube.

Reference
1) H. Sato *et al.*, RIKEN Accel. Prog. Rep. **48**, 201 (2015).

*1 RIKEN Nishina Center

The extraction test aiming for the laser spectroscopy of actinoid elements by PALIS

T. Sonoda,[*1] V. Sonnenschein,[*2] H. Iimura,[*3] H. Miura,[*2] Y. Hirayama,[*4] D. Hou,[*4] S. Iimura,[*1] H. Ishiyama,[*1] I. Katayama,[*1] T. M. Kojima,[*1] S. Nishimura,[*1] M. Rosenbusch,[*3] A. Takamine,[*1] H. Tomita,[*2] M. Wada,[*4] Y. X. Watanabe,[*4] W. Xian,[*4] J. M. Yap,[*4,*5] and BigRIPS Collaborators[*1]

The laser spectroscopy of actinide RIs offers an opportunity to study atomic/nuclear structure in terms of relativistic effects, nuclear shell effects, deformations *etc.* The BigRIPS provides a wide variety of actinide RI-beams by using in-flight projectile fragmentation of uranium. In this year, we were granted 24 hours beam time for the extraction test of actinide isotopes and simultaneously performing a commissioning test for the low-energy RI-beam production system by laser ionization(PALIS),[1)] in a director's beam times.

During the beam time, the BigRIPS optics were taken over from the previous beam user's setup. The main beam optics was ^{225}Ac ($T_{1/2}$ = 10 d), which was expedient for the extraction test of actinides. However as the half-life of ^{225}Ac was too long to measure for our experimental setup, we fully opened the F1 slits at BigRIPS to obtain more yield of the relatively short-lived ^{223}Ac ($T_{1/2}$ = 2.1 min). Figure 1 shows the expected RI-beams and its intensity which were implanted to the PALIS gas cell, simulated by LISE.

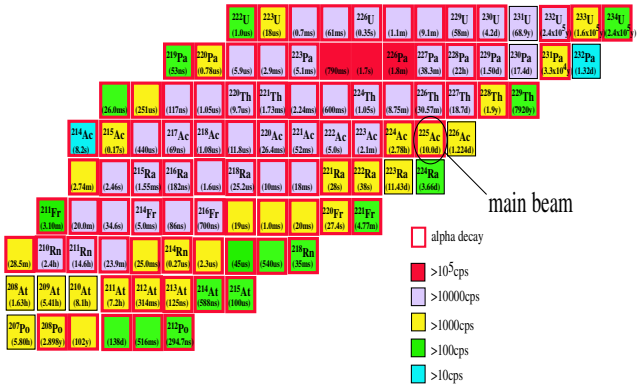

Fig. 1. Expected RI-beams and its beam intensity (primary beam 1 particle nA, fully opened F1 slits) by LISE.

To confirm the low-energy RI-beam extraction, the α-rays produced via α decays were detected at the silicon detector, which was placed in the differential pumping area at the PALIS, as shown in Fig. 2. The stopped and extracted RIs from the gas cell were transported through the sextupole and quadrupole ion beam guides, respectively, and then deposited to the surface of the silicon detector. To reduce the background, the beam was stopped during α-ray measurement.

*1 RIKEN Nishina Center
*2 Faculty of Engineering, Nagoya University, Nagoya
*3 Japan Atomic Energy Agency
*4 Wako Nuclear Science Center (WNSC), IPNS, KEK
*5 Department of Physics, University of Hong Kong

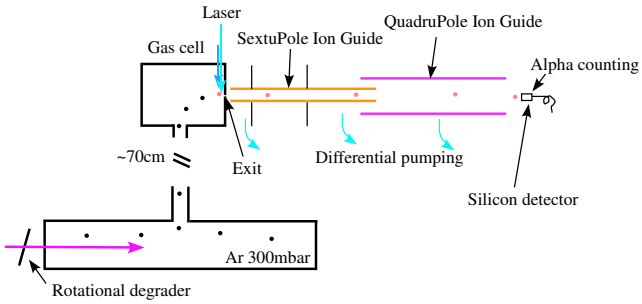

Fig. 2. PALIS experimental setup.

Figure 3 shows the energy spectra of detected alpha particles, taken with a primary beam intensity of 10 particle nA and implantation/measurement period of 300 s each. The rate enhancement of the alpha counting by laser effect was not clearly confirmed, implying that the extracted alpha emitters were ions that survived against neutralization inside the gas cell. The insensitivity of the laser effect is attributed to the impossibility of identifying only ^{223}Ac from the superimposed α-ray's spectra by many types of α emitters, which hindered the optimization of the proper degrader thickness for ^{223}Ac. In addition, the evaluation of laser effect was distorted by other alpha-rays. Next we will utilize a precise mass identification device for extracted RIs.

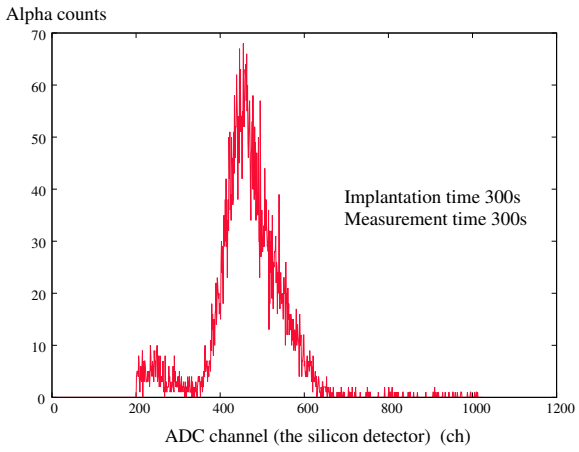

Fig. 3. Observed alpha spectra at silicon detector.

We successfully observed the extracted RIs as a low-energy RI-beam. The efficiency improvement and the installation of the mass identification are in progress.

Reference

1) T. Sonoda *et al.*, Prog. Theor. Exp. Phys. **113**, D02 (2019).

Charge population investigation for the ^{248}Cm fission products extracted from a helium gas catcher

A. Takamine,[*1] M. Rosenbusch,[*2] J. M. Yap,[*1,*3] H. Ishiyama,[*1] M. Wada,[*2] S. Chen,[*3,*4] T. Gao,[*1,*3] D. Hou,[*5,*6] S. Iimura,[*1,*7] S. Kimura,[*1] T. M. Kojima,[*1] S. Nishimura,[*1] T. Niwase,[*3] P. Schury,[*2] T. Sonoda,[*1] H. Ueno,[*1] P. Vi,[*1] Y. X. Watanabe,[*2] and W. Xian[*3]

We are developing a helium gas catcher using the RF ion guide technique and a multi-reflection time-of-flight mass spectrograph downstream of the ZeroDegree spectrometer, referred to as ZD MRTOF-MS.[1] We aim to convert BigRIPS beams to ultra low energy beams and precisely measure the atomic masses of unstable nuclei.

After highly charged radioactive ion beams enter the gas cell, their energy deposition results in the ionization of helium atoms and even impurities, and they undergo charge exchange with the helium and impurities. The charge state that will be dominant depends on the ionization potentials of the elements, as discussed in Ref. 2). Although it is naively expected that charge exchange with helium would stop when the ionization potential falls below the first ionization potential of helium, the mechanism for determining the charge population is complex because it also depends on the level of impurities in the helium gas. For efficient online experiments, *a priori* knowledge of the element dependent charge population is essential. Recently, a ^{248}Cm fission source with a 2-μm-thick Ti degrader was installed outside the cryogenic gas cell (Fig. 1). The ^{248}Cm source has an activity of 10 kBq with branching ratios of 91.6% and 8.4% for alpha and spontaneous fission decays, respectively. The emitted alpha particles and the spontaneous fission products enter the gas cell through a 6-μm-thick Mylar window. This setup facilitates tests with a consistent and knowable intensity of ions under a fair approximation of online conditions.

We performed the charge population measurements for ^{100}Y, ^{100,103}Zr, ^{100,103,104}Nb, ^{103,104}Mo, and ^{104}Tc ions produced by spontaneous fission decay from the ^{248}Cm source offline. The cryogenic gas cell temperature was approximately 80 K, and the gas density was equivalent to 200 mbar at room temperature (293.15 K). Their count rates for the singly, doubly, and triply charged states were measured with the MRTOF mass spectrograph detector. Their fractional charge population is shown in Fig. 2 with their second and third ionization potentials. It is reasonable that the doubly charged states were predominantly extracted from the helium gas. The fraction of triply charged ions decreases consistently with the increase in the third ionization potential. In contrast, Zr and Y exhibited smaller triple charge fractions than that of Nb despite the third ionization potentials of Y and Zr being less than Nb. This result could imply a significant molecularization probability leading to the loss of atomic Zr and Y ions. The charge populations are expected to depend significantly on the gas cell conditions such as temperature, cleanliness, *etc.* Further investigations with various conditions and elements and the searching for the molecularized fission products are in progress.

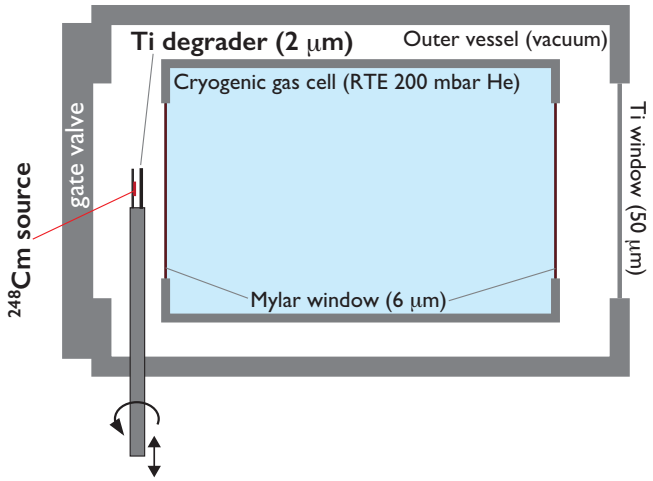

Fig. 1. Schematic of the gas catcher cell of the ZD-MRTOF (top view). The ions are transported upwards, out of the page. The fission source holder attached with the Ti degrader is movable and rotatable.

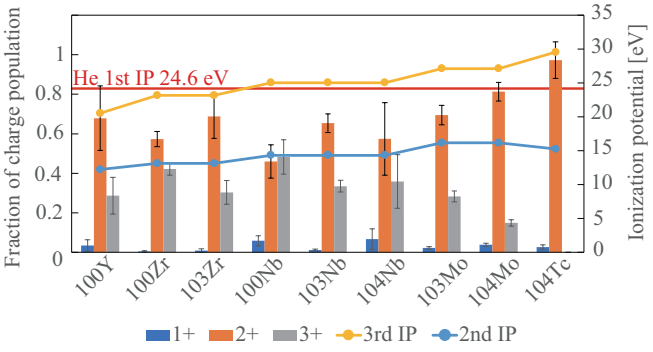

Fig. 2. Charge population of ^{100}Y, ^{100,103}Zr, ^{100,103,104}Nb, ^{103,104}Mo, and ^{104}Tc extracted from a helium gas cell. The 2nd and 3rd ionization potentials for Y, Zr, Nb, and Mo are plotted. The red line shows the first ionizaton potential of helium.

*1 RIKEN Nishina Center
*2 Wako Nuclear Science Center (WNSC), IPNS, KEK
*3 Department of Physics, University of Hong Kong
*4 Faculty of Science, University of York
*5 Institute of Modern Physics, Chinese Academy of Sciences
*6 School of Nuclear Science and Technology, Lanzhou University
*7 Department of Physics, College of Science, Rikkyo University

References
1) M. Rosenbusch *et al.*, Nucl. Instrum. Methods Phys. Res. A **1047**, 167824 (2023).
2) P. Schury *et al.*, Nucl. Instrum. Methods Phys. Res. B **407**, 160 (2017).

Offline measurement of ^{248}Cm fission products at ZD-MRTOF

J. M. Yap,[*1,*2] A. Takamine,[*2] M. Rosenbusch,[*3] S. Chen,[*1,*4] T. Gao,[*1,*2] D. Hou,[*5,*6] S. Iimura,[*2,*7] H. Ishiyama,[*2] S. Kimura,[*2] T. M. Kojima,[*2] J. Lee,[*1] S. Nishimura,[*2] T. Niwase,[*3] P. Schury,[*3] T. Sonoda,[*2] P. Vi,[*2] M. Wada,[*3] Y. X. Watanabe,[*3] and W. Xian[*1]

A 10-kBq ^{248}Cm (SF: 8.39%) fission source was installed in the gas catcher[1] downstream from the ZeroDegree spectrometer to study the ion transport from the gas cell to the ZeroDegree Multi-reflection Time-of-flight Mass Spectrograph (ZD-MRTOF)[2] in offline tests, providing pseudo conditions similar to online beam experiments. The fission source is placed between the inner gas cell and outer vessel chambers such that it can be removed for beam-time experiments. A 2-μm Ti degrader is attached to the source to reduce the kinetic energy of fission products and match the stopping power of the gas cell. The degrader can also be rotated to increase effective thickness. The transport test of the fission products, $^{104–106}$Nb, Mo, Tc, and Ru, was performed shortly after installation. The stopped fission products were extracted mostly as doubly charged ions, and high-precision mass measurements were made after transportation to ZD-MRTOF. This measurement also serves as an ion counter for transport efficiency measurements from the gas cell to ZD-MRTOF.

A degrader thickness scan was performed by measuring the doubly charged ion count rate at various degrader angles to search for the condition of maximum stopping efficiency. Figure 1 depicts the ion count rate of nine fission products. A similar peak count rate was determined at the approximate angles of 45° and −60°. This difference in the positive and negative peak angular positions is likely caused by the asymmetric structure of the gas cell, such as the DC gradient field applied to collect ions at the RF carpet located on one side of the gas cell.

The maximum count rate of fission products was found at a degrader rotation of approximately 45°, with an effective thickness of 2.83 µm. The stopping efficiency of the gas cell in this condition was 4.9%, roughly estimated by simulation, considering the solid angle, energy, energy spread,[3] energy losses, and range in the material of the fission products. Table 1 lists the observed count rates and transport efficiencies of doubly charged ions. The transport efficiency is obtained after correcting for the stopping efficiency from the total efficiency based on the fission yields of ^{248}Cm provided by JAEA[4] and the observed count rate. In the mass region of $A = 104 - 106$, the Mo and Tc isotopes have a transport efficiency of approximately 12%, whereas the Nb isotopes have a relatively low efficiency of approximately 5%. The low transport efficiency of the Nb isotopes could be attributed to the different charge distribution from the slightly lower second ionization potential.[5] Another possible factor is molecular formation of Nb isotopes with contaminant molecules. Further investigations on Nb isotopes will be carried out. The offline transport efficiency measurement forms a baseline for future improvements. Two such upgrade plans, the addition of an RF-wire curtain and modification of the RF carpet scheme from the RF + 4-phase AF to 4-phase RF, will be tested with the fission source.

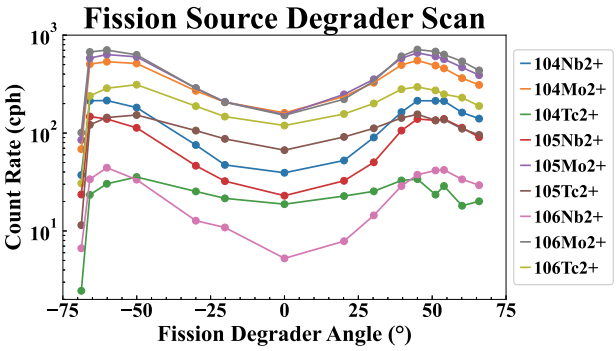

Fig. 1. Count rate (cph) of $^{104–106}$Nb, Mo, and Tc within the degrader angles of −70° to 70°. The positive angles denote counter-clockwise rotation, towards the RF carpet.

Table 1. Observed count rate (cph) and transport efficiency of doubly charged $^{104–106}$Nb, Mo, and Tc ions at a degrader angle of 45°. The uncertainty is specified in parentheses.

Isotope	Count rate (cph)	Transport eff. (%)
^{104}Nb	214 (3)	4.7 (24)
^{105}Nb	139 (3)	5.3 (17)
^{106}Nb	38 (1)	4.0 (25)
^{104}Mo	550 (5)	14.0 (45)
^{105}Mo	658 (6)	11.7 (37)
^{106}Mo	712 (6)	13.5 (43)
^{104}Tc	34 (1)	11.1 (71)
^{105}Tc	155 (3)	13.5 (87)
^{106}Tc	296 (4)	10.6 (34)

*1 Department of Physics, University of Hong Kong
*2 RIKEN Nishina Center
*3 Wako Nuclear Science Center (WNSC), IPNS, KEK
*4 School of Physics, Engineering and Technology, University of York
*5 Institute of Modern Physics, Chinese Academy of Sciences
*6 School of Nuclear Science and Technology, Lanzhou University
*7 Department of Physics, College of Science, Rikkyo University

References
1) A. Takamine *et al.*, RIKEN Accel. Prog. Rep. **53**, 108 (2019).
2) M. Rosenbusch *et al.*, Nucl. Instrum. Methods Phys. Res. A **1047**, 167824 (2023).
3) A. Benoufella *et al.*, Nucl. Phys. A **565**, 563 (1993).
4) J. Katakura *et al.*, EPJ Web Conf. **111**, 08004 (2016).
5) A. Takamine *et al.*, in this progress report.

Development of a high-speed digital data acquisition system for the ZD-MRTOF and β-decay experiments at F11

V. H. Phong,[*1,*2] S. Nishimura,[*1] M. Rosenbusch,[*3] A. Takamine,[*3] M. Wada,[*3] H. Ishiyama,[*1] P. Schury,[*3] and J. M. Yap[*4] for the ZD-MRTOF Collaboration

A new project ZD-MRTOF has been launched to survey the masses of exotic nuclei using high-intensity radioactive isotope beams at RIBF.[1] Optimizing the degrader thickness online is essential to maximize the stopping efficiency of rare isotopes in the He gas cell during the experiment.[2] Here, we report the performance of the newly introduced data acquisition system designed for the ZD-MRTOF experiments using high-speed digitizers during the Spring campaign of the ZD-MRTOF in 2022, where identification of rare isotopes under the beam rate of about 10^4 cps has been confirmed with minimum event loss. The system is based on the CAEN VME digitizers equipped with Field Programmable Gate Arrays (FPGAs), where signals that exceed programmable thresholds are digitized and processed to extract amplitude and timing information.[3] The recorded signals are time-stamped and synchronized with the existing DAQ systems at RIBF thanks to the use of LUPO modules,[4] which distribute common 50 MHz clock signals to all digitizers.

Data acquisition is carried out using RCDAQ software.[5] To combine online data from different DDAQ subsystems for Zerodegree, ZD-MRTOF and β-decay setups, the ZeroMQ protocol[6] was implemented. The acquired data are distributed to data analysis computers on the network, where event reconstruction and time correlations are performed online or offline.

The performance of the DDAQ system under high rate conditions was tested using a cocktail beam of neutron-rich Fe-Ge isotopes during the ZD-MRTOF experiment NP2012-RIBF202. Signals from ZeroDegree spectrometer beamline detectors were readout using the CAEN V1730 digitizers running the DPP-PSD and DPP-PHA firmwares. Figure 1 demonstrates the improvement in deadtime using our DDAQ compared to the existing CAMAC DAQ system, where deadtime and event rate are evaluated based on a fit of the distribution of time intervals between subsequent events to a non-extended deadtime model.[7] A particle identification (PID) plot obtained using our DDAQ system is also shown. With the extracted event rate of 13.5 kHz, a dead time of $\approx$4 μs was obtained for our DDAQ system, compared to $\approx$377 μs for the CAMAC DAQ.

Our DDAQ system has also been successfully employed to readout the TOF signals of the ZD-MRTOF system, providing possibility to combine with the ZeroDegree spectrometer PID information to monitor online the absolute efficiency of the ZD-MRTOF setup. Figure 2 shows a TOF spectrum obtained with a ^{248}Cm fission source,[8] where the start signals of the mirror ejection and the stop signals of the fast ion impact detector (ETP 14DM572)[1] were recorded using a CAEN V1730 digitizer running the DPP-PSD firmware.

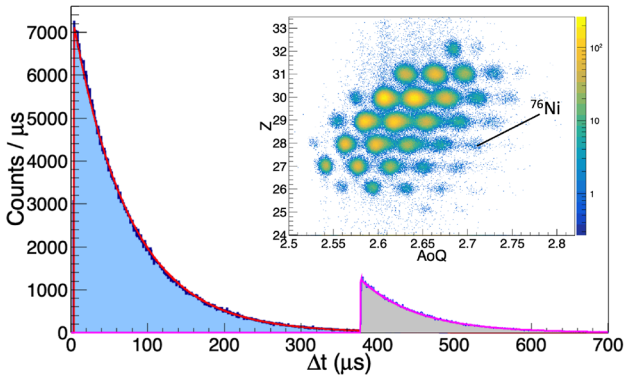

Fig. 1. Fitted distribution of the time interval between subsequent events (blue-filled) and a PID plot (inset) obtained with our DDAQ system compared to the distribution obtained with the BigRIPS CAMAC DAQ (gray-filled).

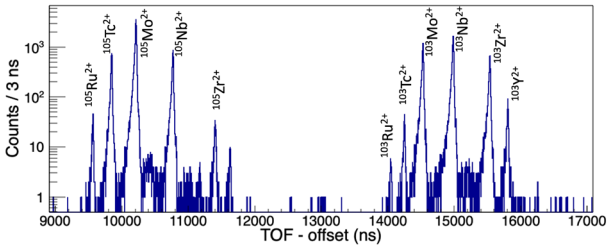

Fig. 2. TOF spectrum obtained with our DDAQ system.

*1 RIKEN Nishina Center
*2 University of Science, Vietnam National University, Hanoi
*3 Wako Nuclear Science Center (WNSC), IPNS, KEK
*4 Department of Physics, University of Hong Kong

References

1) M. Rosenbusch *et al.*, Nucl. Instrum. Methods Phys. Res. A **1047**, 167824 (2023).
2) S. Chen, RIKEN Accel. Prog. Rep. **54**, 97 (2021).
3) `https://www.caen.it/subfamilies/dpp/`.
4) H. Baba *et al.*, Nucl. Instrum. Methods Phys. Res. A **777**, 75 (2015).
5) M. L. Purschke, 2012 18th IEEE-NPSS Real Time Conference (IEEE, 2012).
6) ZeroMQ, `https://zeromq.org/`.
7) J. W. Müller, Nucl. Instrum. Methods Phys. Res. A **301**, 543 (1991).
8) J. M. Yap *et al.*, in this report.

The new MRTOF mass spectrograph following the ZeroDegree spectrometer at RIKEN's RIBF facility†

M. Rosenbusch,[*1] M. Wada,[*1] S. Chen,[*2,*3] A. Takamine,[*4] S. Iimura,[*1,*4,*5,*6] D. S. Hou,[*7,*8] W. Xian,[*2] S. Yan,[*9] P. Schury,[*1] Y. Hirayama,[*1] Y. Ito,[*10] H. Ishiyama,[*4] S. Kimura,[*4] T. M. Kojima,[*4] J. Lee,[*2] J. Liu,[*2,*7] S. Michimasa,[*11] H. Miyatake,[*1] J. Y. Moon,[*12] M. Mukai,[*4] S. Naimi,[*4] S. Nishimura,[*4] T. Niwase,[*1] T. Sonoda,[*4] Y. X. Watanabe,[*1] and H. Wollnik[*14]

The newly assembled multi-reflection time-of-flight mass spectrograph (MRTOF-MS) at RIKEN's RIBF facility has been finalized and became fully operational after its first online operation in the spring of 2020. Further modifications and performance tests using stable ions were completed in early 2021. This system was coupled with a cryogenic helium-filled gas cell[1)] located behind the ZeroDegree (ZD) spectrometer to slow down the high-energy reaction products from initially relativistic energies to thermal equilibrium with the helium gas, and perform high-precision mass measurements of radioactive ions at low kinetic energies.

The setup underwent a successful commissioning[2)] leading to first important mass results recently published.[3)] Follow-up mass measurements were performed in dedicated beam times using the SRC accelerator[4)] (NP2012-RIBF 199/202).

A new optimization procedure for electrostatic mirror voltages has been implemented, which uses the pulsed-drift-tube technique to modify the ions' energy in a wide range and optimize the isochronicity of the system. The TOF could be made insensitive to the kinetic energy of the ions in a wide range. This procedure provided valuable initial settings of the mirror voltages, which have been used for further fine tuning. Figure 1 shows drift corrected TOF spectra obtained after the full optimization, which show a mass resolving power of $R_m \approx 1\,000\,000$. This result was reached for a total time-of-flight of only 12.5 ms for $A \sim 40$, which denotes a world record for such mass spectrometers. The new capabilities may allow for the study of short-lived nuclei possessing low-lying isomers.

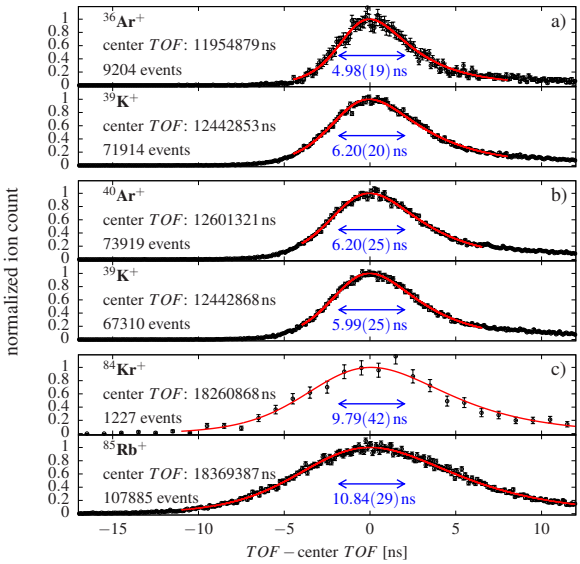

Fig. 1. Pairs of TOF spectra for one hour measurement time (Ar/Kr from gas cell K/Rb and from a thermal ion source). Numbers below double arrows: FWHM of the TOF signals.

Furthermore, a first accuracy benchmark of the setup was performed using isobaric species including stable molecules and well-known radioactive ions from BigRIPS. The mass deviations are shown with uncer-

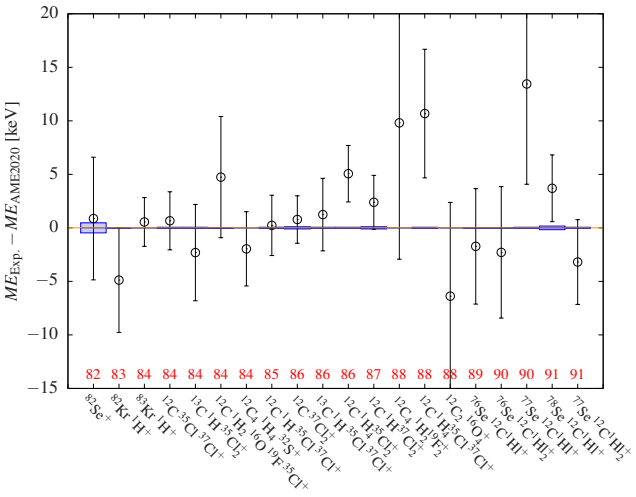

Fig. 2. Benchmark of the mass accuracy using well-known species between $A = 82$ and $A = 91$.

† Condensed from the article in Nucl. Instrum. Methods Phys. Res. A **1047**, 167824 (2023)

*1 Wako Nuclear Science Center (WNSC), IPNS, KEK
*2 Department of Physics, University of Hong Kong
*3 School of Physics, University of York
*4 RIKEN Nishina Center
*5 Department of Physics, Rikkyo University
*6 Department of Physics, Osaka University
*7 Institute of Modern Physics, Chinese Academy of Sciences
*8 School of Nuclear Science and Technology, Lanzhou University
*9 Institute of Mass Spectrometry and Atmospheric Environment, Jinan University
*10 Advanced Science Research Center, Japan Atomic Energy Agency
*11 Center for Nuclear Study, University of Tokyo
*12 Institute for Basic Science
*13 GSI Helmholtzzentrum für Schwerionenforschung GmbH
*14 New Mexico State University

tainties in Fig. 2. The precisely known masses of the analyte ions could be reproduced with an overall mean deviation of $\delta m/m = 2.8(99) \times 10^{-8}$, which is a value competitive with Penning-trap systems.

References
1) A. Takamine *et al.*, RIKEN Accel. Prog. Rep. **52**, 139 (2019).
2) M. Rosenbusch *et al.*, RIKEN Accel. Prog. Rep. **54**, S28 (2021).
3) S. Iimura *et al.*, Phys. Rev. Lett. **130**, 012501 (2023).
4) M. Rosenbusch *et al.*, RIKEN Accel. Prog. Rep. **55**, 86 (2022).

Improvements in the performance of the KISS MRTOF

P. Schury,[*1] T. Niwase,[*1,*2,*3] M. Wada,[*1] Y. Hirayama,[*1] H. Miyatake,[*1] M. Mukai,[*2] M. Rosenbusch,[*1] and Y. X. Watanabe[*1]

The KISS facility uses mutinucleon transfer reactions to produce nuclides which are difficult to produce by fusion or by in-flight fission and fragmentation reactions. Many of these nuclides are close to stability, and typically the more stable isobars are produced with orders of magnitude greater rates. This has made it difficult to access some desirable nuclides, such as ^{188}W, $^{198,\,199}$Ir, and $^{238,\,239}$Pa, as resolving such nuclides from the next stabler isobar requires a high mass resolving power not only in terms of full-width at half-maximum but in terms of full-width at 1%—*i.e.* minimal tails.

Until recently, the MRTOF at KISS has achieved a maximum mass resolving power of $\Delta m/m \sim 200{,}000$ and the peak shape had a strong asymmetry, with the relative amplitude at $\Delta m \approx +20$ ppm being ≈1% of maximum. This was not sufficient to the task of resolving interesting nuclides nearer stability. However, in the past year the performance of the MRTOF installed at the KISS facility has improved. The mass resolving power has increased to $\Delta m/m \sim 400{,}000$ while the peak shape has been made significantly more Gaussian. The improvement is shown in the top panel of Fig. 1. The lower panel of Fig. 1 demonstrates how the new peak shape will allow for discernment of ^{199}Ir which was previously not possible.

By carefully adjusting the biasing of the MRTOF optical elements, it was possible to both improve the peak shape and the resolving power. This effort was made reasonable by the use of purpose-built high-voltage power supplies[1)] which achieve a high-stability without requiring long time-constant capacitive filtering. As these power supplies settle in under one minute, it was possible to efficiently perform multi-parameter optimizations. With further tuning we anticipate that $\Delta m/m > 500{,}000$ with a Gaussian profile can be achieved, which will greatly improve our ability to resolve isobars near stability

In future experiments, we plan to use the MRTOF as a very high-resolution isobar purifier to deliver isobarically (and possibly isomerically) pure beam of radioactive ions for *e.g.* decay studies. This will require a high stability in the peak position. We have found that the power supplies contribute a temperature dependent drift of $\Delta m/\Delta T = 2.36(4)$ ppm/K while thermal expansion of the MRTOF itself results in $\Delta m/\Delta T = 20.4(6)$ ppm/K. In the past we observed very large shifts in the MRTOF peak position as the room warmed due to the presence of numerous experimenters during online measurements. To try to reduce this effect, we gently heated the MRTOF chamber using a PID regulated baking system. The result is shown in Fig. 2. In the future we will try improving the thermal regulation.

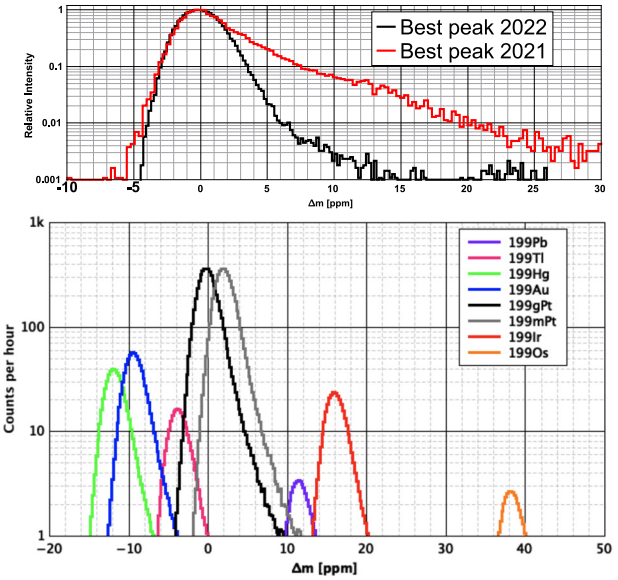

Fig. 1. (top) Comparison of MRTOF peak shape from 2021 with the improved peak shape achieved in 2022. (bottom) Simulated spectrum for $A = 199$ isobars based on measured MRTOF peak shape and calculated production yields. Prior to improving the peak shape it was very difficult to observe ^{199}Ir ions as they produced only a small fluctuation in the tail of the ^{199}Pt ion peak.

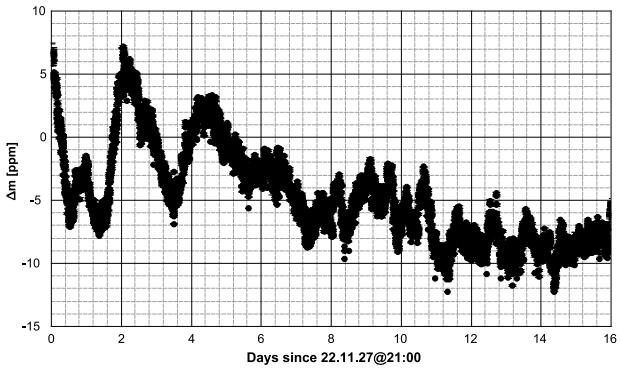

Fig. 2. Drift of the peak position over 16 days of measurement while roughly regulating the MRTOF chamber at 38°C. The maximum fluctuation is consistent with a thermal fluctuation of $\Delta T_{pk-pk} \approx 0.75$ K.

*1 Wako Nuclear Science Center (WNSC), IPNS, KEK
*2 RIKEN Nishina Center
*3 Department of Physics, Kyushu University

Reference
1) P. Schury, *et al.*, Rev. Sci. Instrum. **91**, 014702 (2020).

Development of cryogenic helium gas cell at KISS

Y. Hirayama,[*1] M. Mukai,[*2] P. Schury,[*1] Y. X. Watanabe,[*1] S. Iimura,[*2] H. Ishiyama,[*2] S. C. Jeong,[*1] H. Miyatake,[*1] T. Niwase,[*1] M. Rosenbusch,[*1] A. Takamine,[*2] A. Taniguchi,[*3] and M. Wada[*1]

We have developed a cryogenic helium gas cell to efficiently extract unstable nuclei produced by multi-nucleon transfer (MNT) reactions of ^{136}Xe beam impinging a ^{198}Pt target at the KEK Isotope Separation System (KISS).[1] Unstable nuclei implanted in such a helium (ionization potential (IP): 24.6 eV) gas cell can survive as singly or doubly charged ions depending on their ionization potential. In contrast to the laser ionization used with the present argon (IP: 15.8 eV)-filled KISS gas cell, a helium gas cell offers faster, more efficient, and element-independent extraction of ions. Delivering such wide isobaric cocktail beams to the existing multi-reflection time-of-flight mass spectrograph (MRTOF-MS) will allow for high-efficacy mass measurements as the device can simultaneously analyze numerous ion species. For example, in decay studies, the MRTOF-MS could be used to provide an isobarically (or even isomerically) pure sample. Therefore, the use of a helium gas cell could provide at least one order of magnitude improvement in experimental efficacy over the existing argon gas cell.

Interactions of target-like and projectile-like MNT products and scattered primary beams, with the helium gas result in a strong plasma of He^{2+} and e^-. To efficiently transport the desired radioactive ions in such a plasma, we manufactured a radio-frequency (RF) wire-carpet unit for use with a 4-phase RF traveling wave (RFTW) technique.[2] The RF wire carpet unit consists of 224 beryllium-copper wires (100 μm in diameter) with 600 μm pitch arranged in a plane. A negative DC bias applied to the wire carpet accumulates ions near the wires, while a superposed 4-phase RFTW moves the ions across the structure. Figure 1 shows a cross-sectional view of the helium gas cell installed at KISS. In the helium gas cell, a system of two RF wire carpet units accumulates and transports ions to a RF carpet on a Kapton substrate from which the ions are extracted from the gas cell. The gas cell was cooled to $T \approx 70$ K to freeze out unwanted impurities by combining a cryo-cooler and liquid nitrogen.

We performed initial offline tests to optimize the DC and RF conditions using stable $^{85}Rb^+$ emitted from an alkali ion source installed in the gas cell. The performance was then confirmed in online tests by extracting the MNT products implanted in the gas cell under the dense plasma condition. We measured the extraction yield as a function of the primary beam intensity, as shown in Fig. 2, using the MRTOF-MS to identify and count $^{198}Pt^{2+}$ ions extracted from the gas cell. The extraction efficiency from the gas cell was determined to be approximately 1%, indicating more than one order of magnitude improvement over the argon gas cell. Futhermore, the extraction yield increased linearly in proportion to the primary beam intensity up to at least 100 particle nA, in contrast with the performance of the argon gas cell wherein yields typically saturate above 50 particle nA. In total, we expect more than a 20-fold gain in extraction yield by using the helium gas cell. We plan to measure the masses of unstable nuclei in the vicinity of $N = 126$ with this system in the near future.

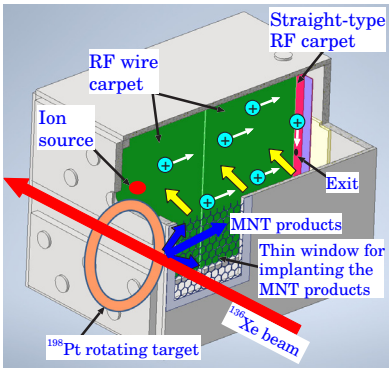

Fig. 1. Cross-sectional view of the helium gas cell. MNT products (blue lines) are implanted into the gas cell through a thin window. The flow of ions toward the gas cell exit by DC field and RFTW is shown by yellow and white arrows, respectively.

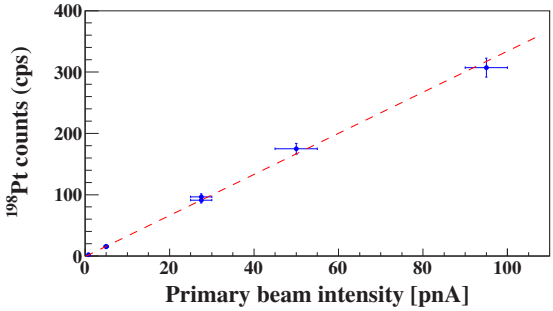

Fig. 2. Measured extraction yield of $^{198}Pt^+$ as a function of the primary beam intensity.

*1 Wako Nuclear Science Center (WNSC), IPNS, KEK
*2 RIKEN Nishina center
*3 Institute for Integrated Radiation and Nuclear Science, Kyoto University (KURNS)

References

1) Y. Hirayama *et al.*, Nucl. Instrum. Methods Phys. Res. B **463**, 425 (2020).
2) K. R. Lund *et al.*, Nucl. Instrum. Methods Phys. Res. B **463**, 378 (2020).

Development of light collection system for collinear laser spectroscopy

M. Tajima,[*1] A. Takamine,[*1] H. Iimura,[*1] M. Wada,[*2] and H. Ueno[*1]

The laser spectroscopy of atomic transitions can aid in clarifying the nuclear structures in ground and isomeric states. We are preparing for the collinear laser spectroscopy (CLS) of rare isotopes (RIs) at the upcoming thermalized RI beam facility using an He gas catcher, referred to as SLOWRI.[1] Barium isotopes were measured as a first offline demonstration of our CLS setup.[2] Thereafter, offline measurements of stable Zr isotopes were performed.[3] An unstable refractory element isotope such as a radioactive Zr isotope is a candidate for an online experiment in the intermediate mass region. As the intensity of exotic Zr isotopes is limited in the online experiment, the detection efficiency should be improved for precise measurement. This report describes a next step to improve the light collection efficiency.

We have performed CLS by changing the velocity, that is, Doppler tuning, of the ion beam using post-acceleration electrodes in the region where a photomultiplier tube (PMT) is placed as a fluorescence monitor. Figures 1(a) and (b) depict the top and side views of the primary design of the electrodes, respectively. Ion beams and the spectroscopy laser pass collinearly through them (from left to right). A post-acceleration voltage up to ±3 kV is applied on a long electrode at the center, divided by each resistor connected to each thin electrode, and grounded at both ends. A sheet of metal mesh is attached on both sides at the center. It avoids optical pumping outside of the region and enables the spectroscopy laser to be locked. Figure 1(e) presents a schematic around the center electrode. The PMT is placed in front of the mesh and a cylindrical mirror is placed on the opposite side, so that light from these two open sides can be detected.

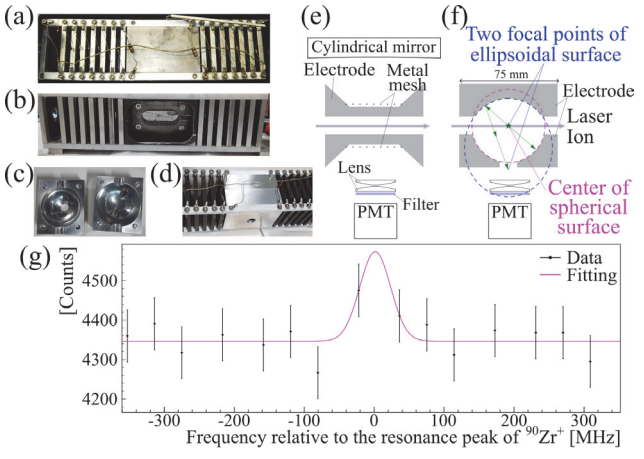

Fig. 1. Post-acceleration electrodes: (a) top and (b) side view of the old ones, (c) inner surfaces, and (d) assembled view of the new ones. Schematics of the (e) previous and (f) new design of the center electrode. (g) Observed spectrum of $^{90}Zr^{+}$ with 10^3 ions per bunch and Voigt fitting.

We constructed a new pair of mirror-shaped electrodes to improve the light collection efficiency. Figure 1(c) depicts the inner surfaces of the new electrodes: one is spherical with a hole at the center (left) and the other is ellipsoidal (right); these were originally designed by M. Baba[4] for molecular spectroscopy. They are made of aluminum, and the inner surfaces are polished. Figure 1(d) presents an integrated view with the new pair of electrodes at the center. Figure 1(f) presents a schematic where blue and magenta dashed lines correspond to the ellipsoidal and spherical surfaces, respectively. The center of the spherical surface is one of two simultaneous focal points of the ellipsoidal surface. If a point-like light source is placed at the center, reflected light on the spherical surface returns and re-passes the spherical center, and then re-reflected light on the ellipsoidal surface focuses onto the other focal point, which is observed using the PMT through the hole. It allows 90% of solid angle coverage for the pointlike source. In CLS, however, 40% of coverage is estimated when the interaction region is 4 cm in length.

We performed the CLS of $^{90}Zr^{+}$ this new apparatus. The overall efficiency is improved by a factor of 2.3 over the original detection setup. The absolute value is estimated at more than 4×10^{-6}, though it is necessary to determine the exact number of ions that contribute to the optical detection. So far, a resonance peak was observed for the intensity of down to 10^3 ions per bunch of repetition of 2 Hz, as depicted in Fig. 1(g). Further improvement such as one-to-one coincidence with ion detection is necessary to reduce the background rate for the exotic RIs with intensity lower than 100 pps. Further, the reflectivity of the surface of the electrode in this wavelength region, which is currently estimated at less than 50%, can be improved up to 60% by polishing.[5]

*1 RIKEN Nishina Center
*2 Wako Nuclear Science Center (WNSC), IPNS, KEK

References

1) M. Wada *et al.*, Nucl. Instrum. Methods Phys. Res. B **204**, 570 (2003).
2) M. Tajima *et al.*, RIKEN Accel. Prog. Rep. **53**, 15 (2020).
3) M. Tajima *et al.*, RIKEN Accel. Prog. Rep. **55**, 90 (2022).
4) M. Baba *et al.*, J. Chem. Phys. **131**, 224318 (2009).
5) K. Minamisono *et al.*, Nucl. Instrum. Methods Phys. Res. A **709**, 85 (2013).

Measuring the stopping position of the energetic radioactive Rb beams in superfluid helium

M. Ito,[*1,*2] K. Imamura,[*1] S. Akimoto,[*1,*2] A. Takamine,[*1] K. Kikuchi,[*1,*2] R. Mitsuyasu,[*1,*2] T. Miwa,[*1,*2] A. Gladkov,[*1] M. Tajima,[*1] S. Go,[*1] M. Mukai,[*1] H. Endo,[*1,*2] S. Sasamori,[*1,*2] S. Takahashi,[*1,*2] Y. Fukuzawa,[*1,*2] M. Hase,[*3] K. Kawata,[*1,*4] A. Kitagawa,[*5] T. Wakui,[*5] H. Ueno,[*1] and Y. Matsuo[*1,*2]

We are developing a laser spectroscopy technique called OROCHI (Optical RI-atom Observation in Condensed Helium as Ion-catcher) to study the nuclear structure of short-lived and low-yield radioisotopes produced at accelerator facilities.[1)] In OROCHI, ion beams are injected into superfluid helium (He II), where the ions are slowed down, stopped in a small volume, and neutralized with nearly 100% efficiency. Nuclear spins/moments are derived from the measurements of the Zeeman/hyperfine splitting energy using the laser-radio frequency (RF)/laser-microwave (MW) double resonance. The feasibility of this method for measuring the hyperfine splitting energy with an accuracy of six orders of magnitude was demonstrated in off-line experiments conducted with Cs atoms.[2)] Therefore, this method is expected to be promising for short-lived unstable nuclei applications.

In previous online experiments,[1)] our group observed laser-RF double resonance spectra for $^{84-87}$Rb ion beams provided by the RIKEN RIPS at ∼60 MeV/nucleon. In the future, we plan to conduct measurements on low-yield unstable nuclear atoms, such as Ag, which are provided at energies as high as ∼300 MeV/nucleon at the RIKEN BigRIPS facility. To demonstrate the applicability of our method to high energy beams, we conducted experiments at the QST-HIMAC SB2 beamline, which can deliver a beam in excess of 350 MeV/nucleon. Among the single-valence-electron alkali atoms, Rb is one of the atoms whose behavior in superfluid helium is well studied. Furthermore, ^{84}Rb is estimated to be produced with the highest yield with a primary beam of ^{84}Kr according to the LISE++ simulation. This is why we employed ^{84}Rb as the target atom in our experiments. Because the number of atoms stopped in the observation region in He II is small, a LIF (laser-induced fluorescence) detection mechanism with high efficiency is needed. Therefore, the accurate measurement of the beam stopping position at HIMAC SB2 beamline is one of the important developments for the future double resonance measurement of atoms with unstable nuclei.

So far, in FY2019, we measured the beam yields of a high-energy ^{84}Rb beam at the HIMAC SB2 beamline using liquid nitrogen as a stopping material to estimate the number of stopped atoms in the possible LIF observation region.[3)] Then, in FY2021, we successfully observed the LIF of ^{84}Rb atoms in superfluid helium (He II) at the HIMAC SB2 beamline.[4)]

In FY2022, the number of measurement points was increased compared to the beam experiment conducted in FY2021 to more precisely determine the beam stopping position. Two measurement methods were performed as shown in Fig. 1. (1) measurement of the number of injected ions that penetrated the plastic scintillator placed in the center of the cryostat in normal fluid liquid helium and (2) measurement of LIF from atoms stopped in superfluid helium in the cryostat. A taper-amplified laser light[5)] was used for the irradiation of the cryostat center with a cross section size of 3 mm × 6 mm. These two types of measurements were performed while varying the thickness of the Al degrader every 100 μm to optimize the degrader thickness for efficient LIF collection from ^{84}Rb atoms. We are currently in the process of data analysis.

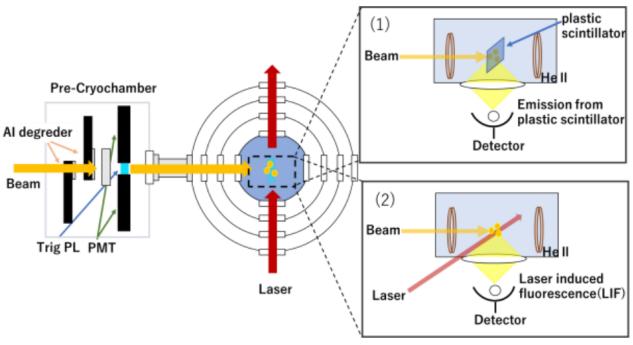

Fig. 1. Schematics of RI beam introduction to helium at HIMAC SB2 beamline.

*1 RIKEN Nishina Center
*2 Department of Advanced Sciences, Hosei University
*3 National Institute for Materials Science (NIMS)
*4 Center for Nuclear Study, University of Tokyo
*5 Institute for Quantum Medical Science, National Institutes for Quantum and Radiological Science and Technology (QST-iQMS)

References
1) X. F. Yang *et al.*, Phys. Rev. A **90**, 052516 (2014).
2) K. Imamura *et al.*, Hyperfine Interact. **73**, 230 (2015).
3) K. Tsubura *et al.*, RIKEN Accel. Prog. Rep. **53**, 132 (2020).
4) K. Tsubura *et al.*, RIKEN Accel. Prog. Rep. **55**, 91 (2022).
5) R. Mitsuyasu *et al.*, in the abstract of 25th Congress of the International Commission for Optics (2022).

Highly-efficient γ-ray linear polarization measurement by multi-layer CdTe Compton Camera

S. Go,[*1] Y. Tsuzuki,[*2,*3,*1] Y. Ichikawa,[4,*1] T. Ikeda,[*1] N. Imai,[*5] K. Imamura,[*1] M. Niikura,[*1] D. Nishimura,[*6,*1] R. Mizuno,[*2,*1] S. Takeda,[*3,*1] H. Ueno,[*1] S. Watanabe,[*7,*3,*1] T. Y. Saito,[*5] S. Shimoura,[*5,*1] S. Sugawara,[*6,*1] A. Takamine,[*1] H. Yoneda,[*1] and T. Takahashi[*2,*3,*1]

Linear-polarization measurements of photons are typically applied to determine the electromagnetic character of gamma-ray transitions. However, the measurement has not been applied in the wide range of nuclei because it needs to measured the azimuth and polar scattering angle of Compton Scattering events. As for the performance for the polarimeter, a figure of merit was proposed as:[1)]

$$F = \epsilon Q^2, \tag{1}$$

where ϵ is the efficiency of the detector to measure Compton-scattering events and Q is the polarization sensitivity of the polarimeter. The development of the γ-ray polarimeters which has a sufficient figure of merit is important for the linear polarization measurements on rare isotopes.

Therefore, we implement a multi-layer semiconductor Compton Camera,[2,3)] which has been developed originally for the X- and gamma-ray observatory in space, for the linear polarization measurement. The detector consists of 20-layer pixelated cadmium telluride. The thickness of each layer is 0.75 mm and the effective area of 51.2×51.2 mm^2 is pixelated into 16×16. The detector measured the intensity distribution of Compton-scattering events of γ ray as a function of azimuth angle.

To demonstrate the capability of measuring the linear polarization for sub-MeV γ-ray, the experiment was conducted at the RIKEN Pelletron facility in May 2022. The performance as a polarimeter was investigated with polarized γ-ray.[4)] The iron target foil of 10 μm was irradiated with the proton beam energy around 3.1 MeV. The first excited 2^+ state of ^{56}Fe was populated by the proton inelastic reactions. The azimuth angle distribution of 847-keV γ ray were measured by the detector placed at 90° degrees to the beam direction. The segmented Ge detector (CNS-GRAPE[5)]) with a lead collimator was also placed at 90° to the beam direction to measure the axial asymmetry of scattered radiation as described in Ref. 6).

The intensity distribution of Compton scattering events as a function of azimuth angle obtained by the Compton Camera is shown in Fig. 1. The curve was obtained by calculating the ratio of the experimental and simulated azimuth angle intensity for polarized and unpolarized photons, respectively. The known electric character of the γ-ray was successfully confirmed. Further analysis to quantify the polarization sensitivity and figure of merit of the polarimeter is in progress.

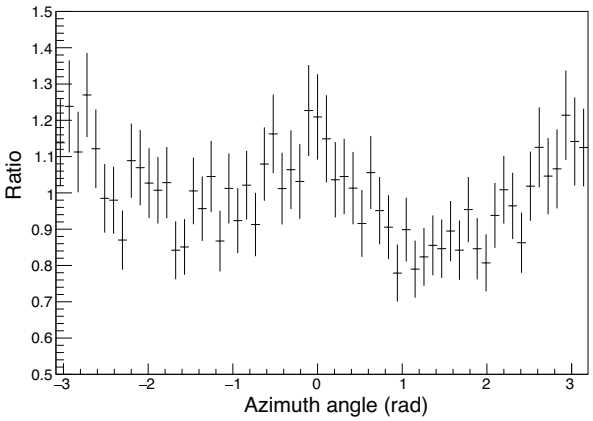

Fig. 1. Intensity distribution of Compton scattering events of the 847-keV γ-ray as a function of azimuth angle.

References

1) B. A. Logan *et al.*, Nucl. Instrum. Methods Phys. Res. **108**, 603 (1973).
2) T. Takahashi, Nucl. Phys. B (Proc. Suppl.) **134**, 191 (2004).
3) S. Watanabe *et al.*, Nucl. Instrum. Methods Phys. Res. A **505**, 118 (2003).
4) J. Simpson *et al.*, Nucl. Instrum. Methods Phys. Res. **204**, 463 (1983).
5) S. Shimoura *et al.*, Nucl. Instrum. Methods Phys. Res. A **525**, 188 (2004).
6) P. A. Butler *et al.*, Nucl. Instrum. Methods Phys. Res. **108**, 497 (1973).

*1 RIKEN Nishina Center
*2 Department of Physics, University of Tokyo
*3 Kavli Institute for the Physics and Mathematics of the Universe, Institutes for Advanced Study
*4 Department of Physics, Kyushu University
*5 Center for Nuclear Study, University of Tokyo
*6 Department of Physics, Tokyo City University
*7 Institute of Space and Astronautical Science, Japan Aerospace Exploration Agency

Charge-exchange reaction of francium ions using an yttrium neutralizer

H. Nagahama,[*1] K. Nakamura,[*1] N. Ozawa,[*2] M. Sato,[*3,*4] T. Nakashita,[*3,*4] S. Nagase,[*2] M. Fukase,[*2] D. Uehara,[*2] Y. Kotaka,[*1] K. Kamakura,[*1] T. Aoki,[*4] H. Haba,[*3] A. Takamine,[*3] H. Ueno,[*3] and Y. Sakemi[*1]

The large imbalance in the amounts of matter and antimatter currently observed in the universe demands physics beyond the standard model, which violates fundamental symmetries.[1] Recently, the search for a nonzero permanent electric dipole moment (EDM) of an elementary particle has taken place actively world-wide, because the existence of EDM violates charge conjugation parity symmetry.

It is predicted that the EDM of an electron (eEDM) is enhanced in paramagnetic atoms.[2] Francium (Fr), being the heaviest alkali element, is known to possess the largest eEDM enhancement factor amongst any ground-state atom.[3] Therefore, we aim to search for the eEDM with unprecedented precision using Fr atoms trapped in an optical lattice. To achieve this goal, it is necessary to prepare a large number of Fr atoms trapped in a magneto-optical trap (MOT) before transporting them to an optical lattice. The number of trapped atoms in a MOT strongly depends on the desorption efficiency of Fr atoms from a neutralizer, where the charge-exchange reaction of Fr ions takes place. Here, we report the characterization of the efficiency of Fr atoms desorbed from an yttrium (Y) neutralizer during beam time in 2022.

An $^{18}O^{6+}$ beam (7 MeV/nucleon) provided by the AVF cyclotron in RIKEN RIBF is irradiated on the gold target to induce the following fusion reactions: $^{197}\mathrm{Au}(^{18}\mathrm{O}, xn)^{215-x}\mathrm{Fr}$. Heating up the target using an infrared radiation heater results in thermal diffusion of the produced Fr, and some fractions will reach the surface. Subsequently, most of the Fr on the surface will be thermally ionized and extracted as a secondary beam (100 eV, typically 5×10^6 s^{-1} for ^{210}Fr). The Fr ions are transported through the electrostatic beam line and irradiated on a Y foil for 3 minutes. The Y foil is then moved mechanically to the so-called silicon semiconductor detector (SSD) chamber to characterize the number of Fr atoms deposited on the surface of the foil. After the characterization, the foil is transported to the so-called neutralization chamber to heat the foil up to a maximum of 750°C and release the Fr as neutral atoms into a vacuum. Finally, the foil is transported back to the SSD chamber to characterize the number of Fr atoms remaining on the surface. Before conducting this experiment, the Y foil is bombarded by an argon (Ar) ion beam (10^{-2} A m^{-2}, 500 eV, 300 K) for 1.5–2 hours to clean its surface.

Figure 1 shows an example of count rate of alpha particles emitted via the alpha decay of $^{208-211}$Fr detected by an SSD, as a function of time. By evaluating all the data collected during the beam time, we derived a desorption efficiency of $\epsilon_{\mathrm{des}} = 29 \pm 15\%$, when the foil was heated to 750°C for approximately 3 seconds. Considering an experiment to measure the desorption energy of rubidium (Rb) on a Y surface,[4] almost all the Fr on the surface should be released into the vacuum by heating the foil up to 350°C for several seconds. Note that Rb is an alkali element akin to Fr and has chemical properties similar to those of Fr. This discrepancy implies that the cleaning procedure of the Y surface before the measurement was insufficient to realize an ideal surface, which does not have any impurities nor passive layers.

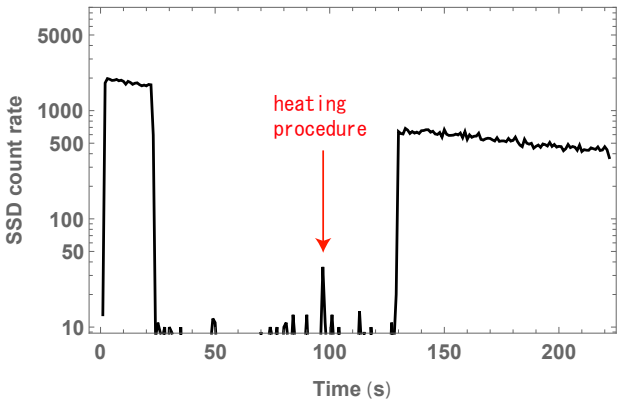

Fig. 1. Count rate of alpha particles emitted via alpha decay of $^{208-211}$Fr detected by a silicon semiconductor detector (SSD), as a function of time.

In 2023, we are planning to realize an ideal Y surface by optimizing the sputtering procedure using the Ar ion beam and by annealing the Y foil to reconstruct the surface structure. Consequently, this will allow the more efficient release of Fr on the surface at a minimum heating temperature, which will enable us to maximize the MOT efficiency of the Fr atoms.

*1 Center for Nuclear Study, University of Tokyo
*2 Department of Physics, University of Tokyo
*3 RIKEN Nishina Center
*4 Graduate School of Arts and Sciences, University of Tokyo

References
1) A. D. Sakharov, Sov. Phys. Usp. **34**, 392 (1991).
2) M. Popeslov *et al.*, Annu. Phys. **318**, 119 (2005).
3) N. Shitara *et al.*, J. High Energy Phys. **JHEP02**, 124 (2021).
4) M. P. Cox *et al.*, Surf. Sci. **129**, 375 (1983).

Absorption spectroscopy measurements of molecular iodine for magneto-optical trapping of francium atoms

K. Nakamura,[*1] S. Nagase,[*2] T. Nakashita,[*3,*4] T. Hayamizu,[*4] T. Aoki,[*3] H. Nagahama,[*1] N. Ozawa,[*2] M. Sato,[*3,*4] M. Fukase,[*2] D. Uehara,[*2] A. Takamine,[*4] and Y. Sakemi[*1]

We have demonstrated absorption spectroscopy measure-ments of molecular iodine (I_2) to develop a permanent electric dipole moment (EDM) measurement system with ^{210}Fr atoms in E7 and ^{221}Fr atoms in the hot lab. Laser cooling of the atoms makes it possible to elongate the interaction time in the EDM measurement. During a few years, the number of Fr atoms produced has been gradually improved toward the realization of the MOT. The laser frequency used to trap the atoms has to be red-detuned by several tens of MHz from the resonance frequency of the trapping transition ($7S_{1/2}$ $F = 13/2 \rightarrow 7P_{3/2}$ $F = 15/2$ for ^{210}Fr, $7S_{1/2}$ $F = 3 \rightarrow 7P_{3/2}$ $F = 4$ for ^{221}Fr). The frequency range where the atoms can be trapped is ∼10 MHz.[1)] We have used the high performance wavelength meter (HighFinesse, WS8-2) with an absolute frequency accuracy of 10 MHz to search for the appropriate frequency for MOT by varying the laser frequency in the vicinity of the Fr trapping transition frequencies reported by previous studies,[1–4)] but have not yet achieved MOT. The frequency references that they rely upon and the wavelength meter that we rely upon are different and not traceable. The Fr trapping transition frequencies with references to the I_2 absorption lines have been reported.[1,2)] In this study we perform I_2 absorption spectroscopy and discuss the Fr trapping transition frequencies based on the results obtained.

The experimental setup for I_2 absorption spectroscopy is shown in Fig. 1(a). In this spectral region, the I_2 cell must be heated above 570 K to observe the absorption well.[1)] It has been reported that the ^{210}Fr trapping laser frequency (−31 MHz detuning[3)]) is +3.38(8) GHz away from the I_2 Doppler broadened P(78)1-9 transition (commonly known as atlas[5)] line number 381) frequency[1)] whereas the ^{221}Fr trapping transition frequency is −0.5(1) GHz away from the I_2 Doppler broadened R(113)3-10 transition (atlas[5)] line number 380) frequency[2)] (Fig. 1(b)). However, these studies do not describe the cell temperature. The I_2 absorption spectrum is a composite of several Doppler broadened hyperfine structure spectra.[6)] Therefore, the peak frequency of the I_2 absorption spectrum may shift at different cell temperatures. We performed absorption spectroscopy of line numbers 380 and 381 at cell temperatures $T = 570$, 590, 610, and 630 K, respectively. The absolute frequency of line 381 ($T = 590$ K) was 417 409 191(10) MHz, that is, −57 MHz away from the I_2 atlas [417 409 248(57) MHz].[5)] Whereas, that of line 380 ($T = 570$ K) was 417 400 090(11) MHz, that is, +40 MHz away from the I_2 atlas [417 400 050(51) MHz].[5)] The trapping transition frequencies for ^{210}Fr and ^{221}Fr reported by previous studies are shown in Figs. 1(c)–(d). They used I_2 atlas,[1)] wavelength meter,[2,3)] and optical resonator[4)] as frequency reference, respectively. Ref. 2) states that the absolute frequency of the I_2 380 line was +30 MHz away from the atlas[5)] with reference to their wavelength meter. Consequently, the present I_2 absorption spectroscopy found that the Fr trapping transition frequencies shown in Refs. 1) and 2) were shifted by −57 MHz ($T = 590$ K) and +10 MHz ($T = 570$ K), respectively, when using our wavelength meter as the frequency reference (red dots in Figs. 1(c)–(d)). Depending on the cell temperature, the center frequency of the absorption spectrum was shifted by up to 28 MHz (No. 381) and 31 MHz (No. 380), respectively. Till date, we have used the frequency range in the blue dashed rectangular (Figs. 1(c)–(d)) as the expected frequencies in MOT searches; however, they must be extended further.

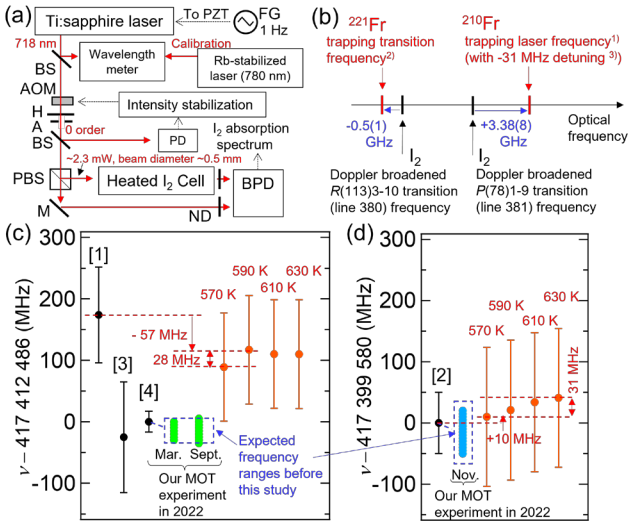

Fig. 1. (a) Experimental setup for I_2 absorption spectroscopy. (b) I_2 lines and Fr trapping transition frequencies. Trapping transition frequencies of (c) ^{210}Fr and (d) ^{221}Fr, respectively.

*1 Center for Nuclear Study, University of Tokyo
*2 Department of Physics, University of Tokyo
*3 Graduate School of Arts and Sciences, University of Tokyo
*4 RIKEN Nishina Center

References
1) J. E. Simsarian *et al.*, Phys. Rev. Lett. **76**, 3522 (1996).
2) Z. -T. Lu *et al.*, Phys. Rev. Lett. **79**, 994 (1997).
3) E Gomez *et al.*, Rep. Prog. Phys. **69**, 79 (2006).
4) S. Sanguinetti *et al.*, Opt. Lett. **34**, 893 (2009).
5) S. Gerstenkorn *et al.*, *Atlas Du Spectre D'Absorption De la Molecule D'Iode* (Laboratoire Aime Cotton, Orsay, France, 1982).
6) P. Dubé *et al.*, J. Opt. Soc. Am. B **21**, 1113 (2004).

Improved ^{6}He beam production at CRIB with MWDC and degraders

H. Yamaguchi,[*1] M. Sferrazza,[*2] S. Hayakawa,[*1] K. Okawa,[*1] Q. Zhang,[*1,*3] S. Cherubini,[*4] M. La Cognata,[*4] R. G. Pizzone,[*4] T. Chillery,[*1] S. Hanai,[*1] N. Imai,[*1] S. Masuoka,[*1] and K. Yako[*1]

The first production test of ^{6}He beam at CRIB was performed in 2021,[1] in which ^{6}He beams at two different energies (8.0 and 5.7 MeV/nucleon) were successfully produced with an intensity of the order of 10^{5}–10^{6} pps. However, the practical beam intensity was limited to $\sim 2 \times 10^{5}$ pps due to the low detection efficiency of the PPAC for such a light-ion beam. The ^{6}He beam purity was 73% for the 8 MeV/nucleon beam, where the main contaminant was $^{3}H^{1+}$, having an almost identical charge-to-mass ratio as $^{6}He^{2+}$.

The second test was carried out in Oct. 2022 as a two-day machine study (MS-EXP22-05), to improve the effective intensity and purity of the ^{6}He beam by introducing wire chambers (MWDC[2]) and degraders. The primary beam was $^{7}Li^{3+}$ accelerated with the AVF cyclotron to an energy of 8.3 MeV/nucleon, and the RI beam was produced with the ^{7}Li$(d,^{3}$He$)^{6}$He reaction in inverse kinematics. The major differences from the first test were the maximum ^{7}Li beam current of 1.5 particle μA (= 4.4 electric μA) at the entrance of CRIB and the pressure of the production target (around 410 Torr), which were both lower than the previous values (3 particle μA and 730 Torr, respectively).

To purify the ^{6}He beam, we installed degraders with two different thicknesses (10-μm-thick aluminized and 20-μm-thick normal Mylar films) at the F1 (momentum dispersive) focal plane. We confirmed a position offset between ^{6}He and ^{3}H was produced at F2 with each degrader, as shown in Fig. 1. Using the 20-μm-thick degrader, the beam purity at F3 measured with a plastic scintillator was 91%, much improved from the previous value, 73%.

The MWDC had already been developed and used at CNS for SHARAQ/OEDO experiments,[2] and introduced for the first time at CRIB. In the present test, we employed two MWDCs operated at 10 kPa (76 Torr), having an XX-YY anode configuration and cell sizes of 3 mm and 5 mm for the upstream and downstream ones, respectively. Even with a high-rate secondary beam at 6.0×10^{5} pps, the MWDCs maintained an efficiency $\epsilon > 90\%$ with high voltages of up to 900 V, and no significant reduction of the efficiency was observed. This is in contrast to the previous test, where we had to limit the primary beam current to 0.3 particle μA in order to keep the stable PPAC operation with an acceptable efficiency ($\epsilon = 70\%$). The

*1 Center for Nuclear Study, University of Tokyo
*2 Department of Physics, Université Libre de Bruxelles
*3 Department of Physics, Lanzhou University
*4 Laboratori Nazionali del Sud, Istituto Nazionale di Fisica Nucleare (INFN)

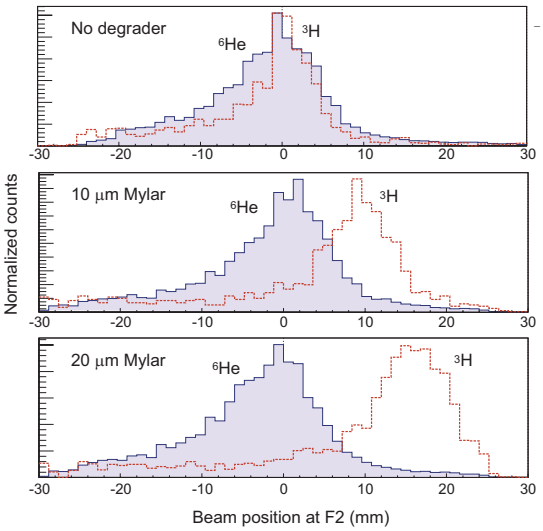

Fig. 1. The beam profiles of ^{6}He (solid line) and ^{3}H (dashed line), with different degrader settings. The counts are scaled to show the profiles as similar heights.

basic beam parameters are summarized in Table 1 and compared with those of the optimum case in the previous test. The new ^{6}He rate is roughly consistent with the previous value, considering the higher ^{7}Li beam current (×5) and nearly half F0 pressure. However, the previous rate (200 kcps) was severely limited with the PPAC, while in the present work we successfully obtained a higher ^{6}He rate (520 kcps) with a better beam purity (91%), even though the F0 pressure was not at its best value. The new condition well satisfies the requirements by the approved experiments,[3] to be performed in the near future.

Table 1. Summary of the basic beam parameters. ϵ is the efficiency of the beam-monitoring detector.

Test year	^{7}Li (particle μA)	F0 Pres. (Torr)	ϵ	^{6}He purity	^{6}He rate (kcps)
2021	0.3	730	70%	73%	200
2022	1.5	410	94%	91%	520

References

1) H. Yamaguchi *et al.*, RIKEN Accel. Prog. Rep. **55**, 94 (2022).
2) H. Miya *et al.*, Nucl. Instrum. Meth. Phys. Res. B **317**, 701 (2013).
3) M. Sferrazza *et al.*, proposal for RIBF NP-PAC-21, NP2021-AVF70 (2020, unpublished) and others.

Progress on double photon coincidence imaging with ^{67}Cu and ^{169}Yb

K. Shimazoe,[*1] M. Uenomachi,[*2] H. Takahashi,[*1] Y. Shigekawa,[*3] A. Nambu,[*3] X. Yin,[*3] and H. Haba[*3]

In nuclear medical imaging, positron emission tomography (PET) and single photon emission computed tomography (SPECT) are two important imaging modalities; however, the imaging principles of these modalities have remained the same for more than 50 years. We have proposed and investigated a novel imaging method referred to as double photon emission coincidence imaging (DPECI) utilizing two successive gamma-rays emitted from cascade nuclides.[1,2] The coincidence detection of two gamma-rays enables the localization of radioisotope with a single event. Previous studies have shown the increase in signal to noise ratio (SNR) and reduction of cross-talks between nuclides through the application of selection with timing information using ^{111}In and ^{177}Lu, which are clinically used radioisotopes for diagnosis and therapy.[3,4] Furthermore, in addition to the conventional accumulation imaging of radioisotope, the hyperfine interaction of intermediate state in cascade nuclides with the external field can be used to detect the chemical information using the successive gamma-ray photons as reported in previous studies.[5,6]

Here we investigate the possible use of ^{67}Cu and ^{169}Yb for DPECI with collimator-based imaging system. ^{67}Cu and ^{169}Yb were produced in the ^{70}Zn$(d,\alpha n)^{67}$Cu and ^{169}Tm$(d,2n)^{169}$Yb reactions at the RIKEN AVF cyclotron. ^{67}Cu emits two gamma-rays with energies of 91.3 and 93.3 keV with the time constant of 9.1 μs in a cascade decay. ^{169}Yb also emits two gamma-rays with the combination of 63.1–177 keV, 63.1–198 keV, and 63.1–307.7 keV in cascade decays and the time constant is approximately 659.9 ns. The relatively long intermediate time constant could be useful to detect the hyperfine interaction through the gamma-ray distribution. In this study, we demonstrate DPECI method using the combination of slit and parallel-hole collimators achieving higher sensitivity than parallel-hole only collimators using ^{67}Cu.[7]

Figure 1 shows the experimental setup of DPECI to visualize ^{67}Cu radioisotope using the coincidence detection of two gamma-rays. ^{67}Cu with the activity of 2.12 MBq was enclosed in the U-shape phantom and measured for 16 hours. The time window was set to 10 μs. The shape of U is successfully visualized by considering the intersection of a plane determined by slit collimators and a line by parallel-hole collimators. The slit width of collimator was 1.6 mm with thickness of 15 mm. The gamma-rays were detected by 2.5 mm × 2.5 mm × 4 mm (D) HR-GAGG scintillation crystals arrays coupled to SiPM arrays.

For evaluating the feasibility of coincidence detection of two successive gamma-rays from ^{169}Yb, ring-shape GAGG-SiPM detector arrays including 512 channels were used. The left panel in Fig. 2 shows the time difference between two gamma-rays and the decay time constant of 659.9 ns is successfully observed. The right panel shows the energy spectrum obtained from the time-over-threshold (ToT) measurement, which indicates that the gamma ray energy is correctly identified.

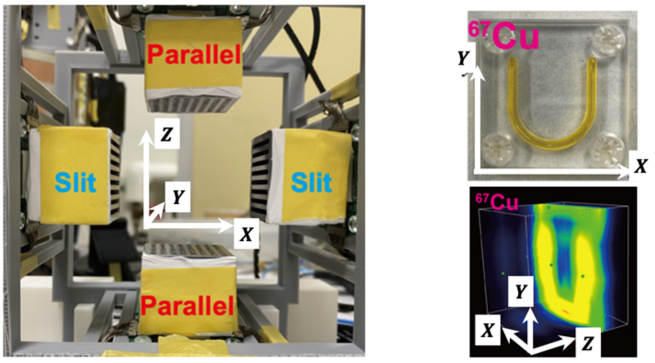

Fig. 1. Geometry of DPECI for visualizing ^{67}Cu radioisotope enclosed in U shape phantom and its image.

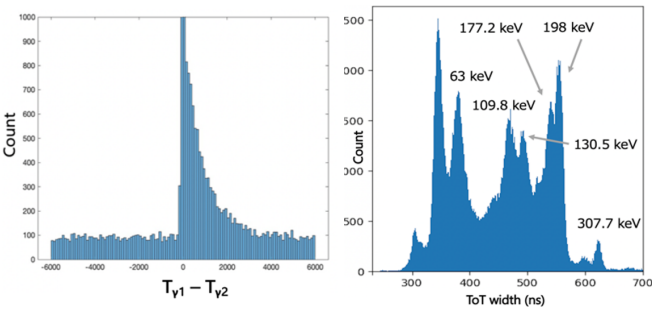

Fig. 2. Coincidence time histogram of two gamma-rays from ^{169}Yb and the measured energy spectra with GAGG-SiPM arrays.

In summary, we have proposed a new method (DPECI) using double photon emitting nuclides and the imaging capability and coincidence detection was demonstrated with ^{67}Cu and ^{169}Yb fabricated at RIKEN AVF cyclotron.

*1 School of Engineering, University of Tokyo
*2 Unit of Synergetic Studies for Space, Kyoto University
*3 RIKEN Nishina Center

References

1) K. Shimazoe *et al.*, J. Instrum. **12**, C12055 (2017).
2) M. Uenomachi *et al.*, Bull. Am. Meteorol. Soc. **18**, 120 (2022).
3) M. Uenomachi *et al.*, Sci. Rep. **11**, 13330 (2021).
4) M. Uenomachi *et al.*, J. Instrum. **17**, P04001 (2022).
5) K. Shimazoe *et al.*, Commun. Phys. **5**, 1 (2022).
6) K. Shimazoe *et al.*, Bull. Am. Meteorol. Soc. **18**, 127 (2022).
7) L. Yan *et al.*, Nucl. Instrum. Methods Phys. Res. A **1053**, 168305 (2023).

Status of the J-PARC E16 experiment in 2022

S. Yokkaichi*1 for the J-PARC E16 Collaboration

We proposed the experiment E16[1] to measure the vector meson decays in nuclei in order to investigate the chiral symmetry restoration in dense nuclear matter. The experiment started at the J-PARC Hadron Experimental Facility.

This experiment aims to systematically study the spectral modification of vector mesons in nuclei, particularly the ϕ meson, using the e^+e^- decay channel with statistics that are two orders larger in magnitude than those of the prior E325[2] experiment performed at KEK-PS. In other words, it aims to accumulate 1×10^5 to 2×10^5 events for each nuclear target (H, C, Cu, and Pb) and deduce the dependence of the spectral modification on the size of nucleus and meson momentum. The number of modified mesons could be larger for larger nucleus and lower momentum mesons because the decay probability inside the nucleus is enhanced for such cases.

The proposed spectrometer comprises 26 modules. As shown in Fig. 1, a module consists of Lead-glass calorimeter (LG) and Hadron-blind detector (HBD) for electron identification, as well as three-layers of GEM Trackers (GTR) and a single layer of silicon strip detector (SSD) as the tracking devices.

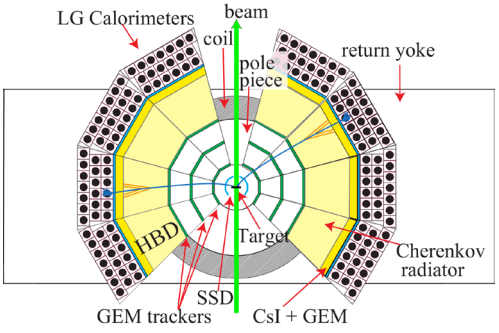

Fig. 1. Cross-sectional plan view of the E16 spectrometer in the eight-module configuration for Run-1.

Commissioning runs, in total 403 hours as summarized in Table 1, were performed in 2020-21 at the newly constructed 'High-momentum beam line'.[3] Owing to budget limitations, a limited number of modules were installed in the commissioning runs. In these runs, electron identification performance was confirmed.[4] The read out circuit for the data collection is described in Ref.[5]

In the next beam time planned in 2023, full eight modules shown in Fig. 1 will be operated. In the previous runs, six modules of SSD was borrowed from J-PARC E07 group. However, they will be replaced by the newly developed eight modules with the cooperation of the CBM group at GSI.

Table 1. Run-time summary. Run-0d demonstrates prospect.

	Run-0a 2020	Run-0b 2021	Run-0c 2021	Total	Run-0d 2023
Period	6/4-20	2/11-28	5/28-6/9		(5-6)
Days	17	18	12	47	
Beam time (h)	159	110	134	403	100
Raw data (TB)	33	28	46	97	-

The major issue detected in the commissioning runs is the micro beam structures, which deteriorate the DAQ performance[3] due to the time-localized high beam intensity. It was typically ten times as high as the nominal value of the beam intensity. In other words, the typical beam rate is 5 GHz because the intensity is 1×10^{10} protons per 2 sec duration; however, the actual beam rate increased to 50 GHz locally due to the micro structures.

Some countermeasures have been discussed and will be applied in the next beam time. Before Run-1 (physics run), we plan to perform a beam study to check whether the countermeasures can improve the DAQ performance, and construct the acceptable trigger rate by tuning threshold, coincidence pattern and time window, and beam intensity, with the upgraded DAQ system.

In Aug. 2022, our proposal for Run-1 based on the updated technical design report was reviewed. The approval for Run-1 was deferred, and only 200 hours of beam time was approved for the beam study (101 hours) and trigger study (100 hours) as mentioned above.

In J-PARC, an upgrade work of MR[a] was performed from 2021 summer (just after the Run-0c) to 2022 autumn, and a test operation of MR had started. Owing to the malfunction of the septum magnet and so on, we expect the next beam time, namely, a slow extraction beam for users, in May 2023 at the earliest case.

References

1) S. Yokkaichi *et al.*, J-PARC proposal No. 16 (`http://j-parc.jp/researcher/Hadron/en/pac_0606/pdf/p16-Yokkaichi_2.pdf`); M. Ichikawa *et al.*, Acta Phys. Pol. B Proc. Suppl. **16**, 1-A143 (2023).
2) R. Muto *et al.*, Phys. Rev. Lett. **98**, 042501 (2007).
3) S. Yokkaichi, RIKEN Accel. Prog. Rep. **55**, 54 (2022).
4) S. Nakasuga *et al.*, Nucl. Instrum. Methods Phys. Res. A **1041**, 167335 (2022).
5) T. N. Takahashi *et al.*, IEEE Trans. Nucl. Sci. **68**, 1907 (2021).

*1 RIKEN Nishina Center

a) J-PARC Main Ring Accelerator

Preparation status for sPHENIX experiment and INTT detector for Run23 at RHIC

I. Nakagawa,[*1] Y. Akiba,[*1] J. Bertaux,[*2] K. Fujiki,[*1,*3] M. Fujiiwara,[*4] T. Hachiya,[*1,*4] S. Hasegawa,[*1,*5] M. Hata,[*4] H. Imai,[*1,*3] M. Kano,[*4] T. Kato,[*1,*3] T. Kondo,[*6] C. M. Kuo,[*7] R. S. Lu,[*8] Y. Namimoto,[*1,*4] R. Nouicer,[*9] G. Nukazuka,[*1] C. W. Shih,[*7] M. Shimomura,[*4] R. Shishikura,[*1,*3] M. Stojanovic,[*2] Y. Sugiyama,[*4] R. Takahama,[*1,*4] W. C. Tang,[*7] H. Tsujibata,[*4] M. Watanabe,[*4] and X. Wei[*2]

The sPHENIX experiment is the next generation jet detector which is under construction at RHIC as the upgrade of former PHENIX experiment.[1] The installation of a time projection chamber (TPC) detector has been completed by the middle of January, 2023 as shown in Fig. 1. The silicon strip intermediate (INTT) detector, developed by mainly Japanese group,[2] is to be implemented next inside of the TPC. The assembly of the INTT silicon ladders has been completed by Spring of 2022.

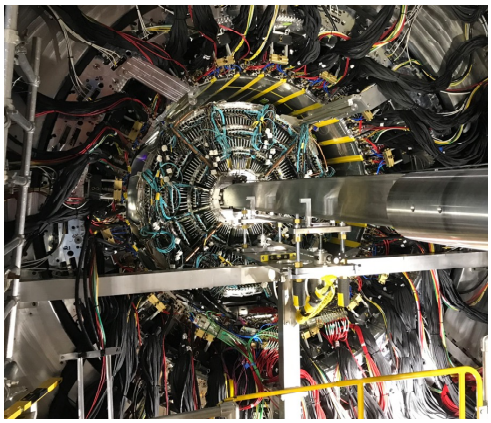

Fig. 1. Installed TPC in the sPHENIX detector.

The barrel type INTT detector consists of the inner and outer layers of INTT ladders. Shown in Fig. 2 is the pair of an INTT half barrel. 24 and 32 ladders were installed as the inner and outer barrels, respectively. The signal readout response of every single ladder was tested before and after the barrel construction using a built-in calibration system which injects an artificial pulse to an analogue to digital conversion chip implemented right next to the silicon sensors. The INTT detector is scheduled to be installed to sPHENIX in March 2023.

*1 RIKEN Nishina Center
*2 Department of Physics and Astronomy, Purdue University
*3 Department of Physics, Rikkyo University
*4 Department of Mathematical and Physical Sciences, Nara Women's University
*5 Japan Atomic Energy Agency
*6 Tokyo Metropolitan Industrial Technology Research Institute
*7 Center for High Energy and High Field Physics and Department of Physics, National Central University
*8 Department of Physics, National Taiwan University
*9 Physics Department, Brookhaven National Laboratory

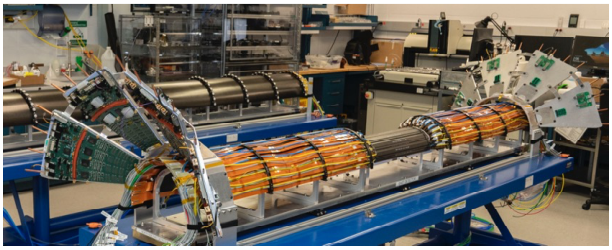

Fig. 2. INTT half barrels.

A μ-coax technology (Fig. 3) was employed as the last piece of the readout cable series[3] for the INTT ladder. This technology has certain advantage in the flexibility for a high signal density cable compared to the flexible print cable (FPC) one. On the other hand, a material "fluorinated resin" used as an insulator for the μ-coax harness is known to be weak against radiation compared to popular insulator materials like polyimide or liquid crystal polymer which are typically used for the FPC[4] Therefore the radiation hardness of the μ-coax harness was examined at RANS facility at RIKEN. The harness was exposed to the RANS neutron beam upto 4×10^{12} equivalent neutrons which is an order of more dose than expected during the INTT operation within 3 years of sPHENIX running. The signal transmission performance was compared before and after the irradiation. No degradation was observed due to the radiation as a result.

Fig. 3. Readout cables for the INTT ladder based on the μ-coax technology.

References

1) Technical Design Report of sPHENIX (2019), https://indico.bnl.gov/event/7081/.
2) Nikkei Science, June (2023).
3) Trans. Jpn. Inst. Electron. Packag. **15**, E21-007 (2022).
4) L. Whinnery *et al.*, SAND2017-9103C (2017), https://www.osti.gov/servlets/purl/1467983.

Preliminary results of INTT beam test 2021 at ELPH†

C. W. Shih,[*1] Y. Akiba,[*2] J. Bertaux,[*3] K. Fujiki,[*2,*4] M. Fujiiwara,[*5] T. Hachiya,[*2,*5] S. Hasegawa,[*2,*6] M. Hata,[*5] H. Imai,[*2,*4] M. Kano,[*5] T. Kato,[*2,*4] T. Kondo,[*7] C. M. Kuo,[*1] R. -S. Lu,[*8] I. Nakagawa,[*2] Y. Namimoto,[*2,*5] R. Nouicer,[*9] G. Nukazuka,[*2] M. Shimomura,[*5] R. Shishikura,[*2,*4] M. Stojanovic,[*3] Y. Sugiyama,[*5] R. Takahama,[*2,*5] W. -C. Tang,[*1] H. Tsujibata,[*5] M. Watanabe,[*5] and X. Wei[*3]

The Intermediate silicon Tracker, INTT, is one among the sub-detectors of sPHENIX tracking system.[1] A beam test experiment was performed with INTT ladders at the end of 2021 at ELPH, Japan. In the experiment, a telescope of 4 INTT ladders was installed, and 3 ladders were operated. The positron beam with the energy of 1 GeV was delivered. One of the goals of this experiment was to demonstrate the detection efficiency of INTT ladder. As the radiation length of INTT ladder was 1.08% X_0, the track was assumed to be a straight line.

This study focused on the column with the highest events.[2] The clustering was performed on 3 ladders, the adjacent fired channels in a column were grouped to form a hit cluster. The cluster position y in vertical direction was determined by $y = \Sigma_i E_i \cdot y_i / \Sigma_i E_i$, where E is the energy deposit. The track reconstruction was performed by the upstream ladder, L0, and downstream ladder, L2, and the detection efficiency of the middle ladder, L1, was measured. In the reconstruction process, no cluster in the adjacent columns of all ladders was required, and the number of clusters was required to be one on the same column for L0 and L2. The tracks passing the criteria were considered as track candidates. The residual r is defined as $r \equiv (y + C_y) - y_{pred}$, where y_{pred} is the y position at L1 predicted by the track candidate, and C_y is an offset term indicating the misalignment. An alignment correction of $-C_y$ was applied in the study.

Several cuts were applied to maximize the authenticity of the results. For L0 and L2, the single-hit cluster was rejected to minimize the false track candidates based on accidental noise hits. The track candidates within five channels from the edges were rejected to suppress the misalignment effect (edge effect). In addition, the track candidates with large deviation in the angle (±0.01 radian) from the beam axis were excluded (Slope cut). The track candidates that passed all criteria were considered as good tracks. Subsequently, the clusters in L1 were checked. Three categories were considered:

(1) The closest cluster is close to y_{pred} (N_{good}),
(2) The closest cluster is far from y_{pred} (N_{far}),
(3) No cluster was found (N_{no_hit}).

The residual distribution of the first two categories is shown in Fig. 1. The first category requires $|r| < 0.234$ mm (Residual cut).

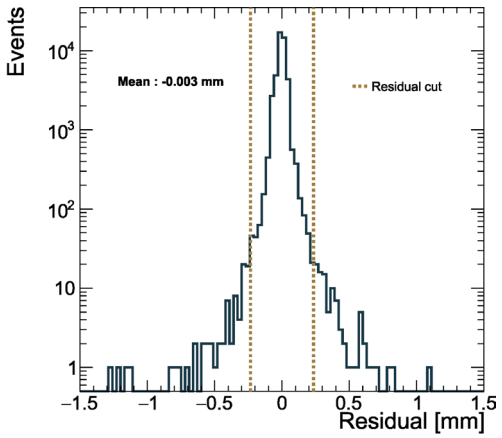

Fig. 1. Residual distribution in L1.

The equation of detection efficiency of L1 is defined as $\frac{N_{\rm good}}{N_{\rm no\_hit}+N_{\rm good}+N_{\rm far}} \times 100\%$. The systematic uncertainties associated with the detection efficiency originate from the determinations of the three cut values, the **slope cut**, **edge effect**, and **residual cut**. Scanning cut values provides the variation of each source, and the variation average estimates the uncertainties. The numerical values are summarized in Table 1.

Table 1. Sources of the systematic uncertainties affecting the detection efficiency calculation.

Sources	Scan range	Uncertainty (%)
Residual cut	0.164–0.304 mm	0.063
Slope cut	0.0088–0.0112 radian	3e-3
Edge effect	0–10 channels	4e-4
Total		0.063

Considering the systematic uncertainty, the detection efficiency of ladder L1 was 99.33 ± 0.04 (stat) ±0.06 (syst)%. The performance of INTT ladder is excellent enough for the sPHENIX experiment.

References

1) Conceptual Design Report of sPHENIX (2018).
2) G. Nukazuka *et al.*, ELPH Annu. Rep. (2022).

† Condensed from the article in ELPH Annu. Rep. (2022)

*1 Center for High Energy and High Field Physics and Department of Physics, National Central University
*2 RIKEN Nishina Center
*3 Department of Physics and Astronomy, Purdue University
*4 Department of Physics, Rikkyo University
*5 Department of Mathematical and Physical Sciences, Nara Women's University
*6 Japan Atomic Energy Agency
*7 Tokyo Metropolitan Industrial Technology Research Institute
*8 Department of Physics, National Taiwan University
*9 Physics Department, Brookhaven National Laboratory

Accelerator report INTT onlmon progress summary 2023

J. Bertaux,[*2] Y. Akiba,[*1] K. Fujiki,[*1,*3] M. Fujiiwara,[*4] T. Hachiya,[*1,*4] S. Hasegawa,[*1,*5] M. Hata,[*4] H. Imai,[*1,*3] M. Kano,[*4] T. Kato,[*1,*3] T. Kondo,[*6] C. M. Kuo,[*7] R. S. Lu,[*8] I. Nakagawa,[*1] Y. Namimoto,[*1,*4] R. Nouicer,[*9] G. Nukazuka,[*1] C. W. Shih,[*7] M. Shimomura,[*4] R. Shishikura,[*1,*3] M. Stojanovic,[*2] Y. Sugiyama,[*4] R. Takahama,[*1,*4] W. C. Tang,[*7] H. Tsujibata,[*4] M. Watanabe,[*4] and X. Wei[*2]

The sPHENIX OnlMon framework is designed to facilitate the monitoring of detector subsystems during data collection. Raw data is continuously unpacked and used to maintain ROOT[1)] histograms stored on a server. A client can request these histograms and use them to convey information to a user via a graphical interface, also generated using ROOT.[1)] Each subsystem of the sPHENIX experiment is responsible for implementing the unique methods needed for its framework.

The Intermediate Silicon Tracker (INTT) subsystem's implementation must be sufficiently comprehensive to show the readout status of the smallest partitions of its active area, yet compact enough so that a user can diagnose any issue at a glance. The hardware of the INTT is organized into four concentric layers of 12, 12, 16, 16 ladders (innermost layer to outermost layer). Each ladder is divided into north and south halves, and each half-ladder has 26 chips arranged in 2 rows of 13. Each chip has 128 channels which can further specify an analogue to digital conversion (ADC) value ranging 0 to 7. This is too much to show concurrently, and the compromise is to have multiple types of displays.

The GUI has two types of displays: a main display that shows the INTT at the level of individual chips, and a secondary display that will show an individual chip at the level of channels or ADC values. The main display exhibits four histograms, representing each layer, with a bin for each chip. The bin will be colored depending on a user specified option, such as the raw number of counts registered to the chip, a weighted-average ADC value, or the number of channels exhibiting statistically significant behavior when compared to others at similar pseudorapidity (Fig. 1).

From the main display, a user can click a bin to launch a second GUI that shows a single histogram representing the chip, with bins for each channel and possibly ADC value, again colored by the same user specified option, the raw number of counts in each channel,

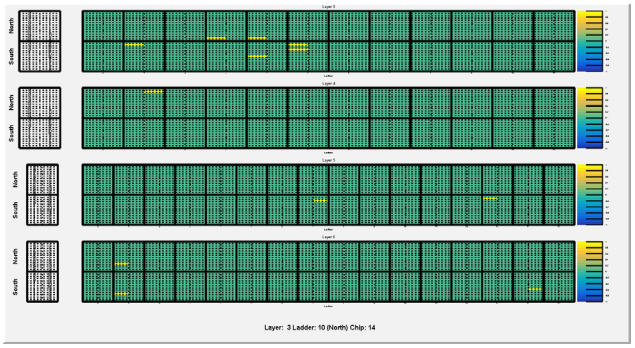

Fig. 1. A primary GUI where bin values are the number of statistically significant channels (see Fig. 2) in the chip the bin represents. In this case, there are only 12 chips with at least one significant channel (the yellow bins). Thick, black lines denote ladders and their north/south halves, thin dotted lines denote chips, a key shows the chip layout in one ladder, and text shows which chip the user's mouse is over.

the exact ADC distribution across all channels, or the likelihood of an issue with the channel based on its comparative performance (Fig. 2).

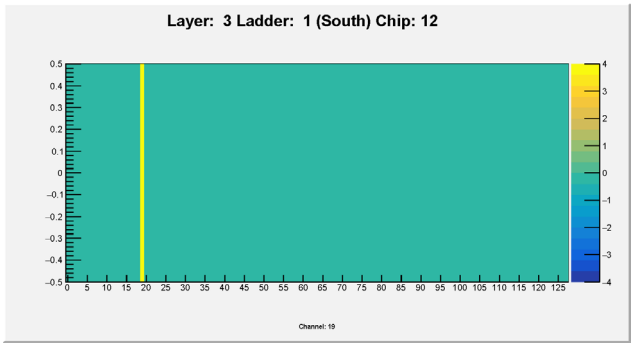

Fig. 2. A secondary GUI where bin values are the statistical significance (z-score) of the channel it represents when compared to all channels at similar pseudorapidity. Here, any $z < -2$ or $z > +2$ is considered significant and will be colored differently; in this case, there is only one (the yellow bin). Text at the bottom shows which channel the user's mouse is over.

*1 RIKEN Nishina Center
*2 Department of Physics and Astronomy, Purdue University
*3 Department of Physics, Rikkyo University
*4 Department of Mathematical and Physical Sciences, Nara Women's University
*5 Japan Atomic Energy Agency
*6 Tokyo Metropolitan Industrial Technology Research Institute
*7 Center for High Energy and High Field Physics and Department of Physics, National Central University
*8 Department of Physics, National Taiwan University
*9 Physics Department, Brookhaven National Laboratory

Reference
1) R. Brun and F. Rademakers, Nucl. Instrum. Methods Phys. Res. A **389**, 81 (1997).

Performance of a new operating system by FELIX board for INTT in sPHENIX

G. Nukazuka,[*1] Y. Akiba,[*1] J. Bertaux,[*2] K. Fujiki,[*1,*3] M. Fujiiwara,[*4] T. Hachiya,[*1,*4] S. Hasegawa,[*1,*5] M. Hata,[*4] H. Imai,[*1,*3] M. Kano,[*4] T. Kato,[*1,*3] T. Kondo,[*6] C. M. Kuo,[*7] R. S. Lu,[*8] I. Nakagawa,[*1] Y. Namimoto,[*1,*4] R. Nouicer,[*9] C. W. Shih,[*7] M. Shimomura,[*4] R. Shishikura,[*1,*3] M. Stojanovic,[*2] Y. Sugiyama,[*4] R. Takahama,[*1,*4] W. C. Tang,[*7] H. Tsujibata,[*4] M. Watanabe,[*4] and X. Wei[*2]

sPHENIX is scheduled to start operationsn at the Relativistic Heavy Ion Collider at Brookhaven National Laboratory in 2023 to study quark-gluon plasma and cold-QCD.[1)] The Intermediate Tracker (INTT) is a silicon barrel tracker located between the other two tracking detectors of the sPHENIX detector complex. INTT is responsible for tracking and jet flavor tagging with high precision and low background. It inherits much of the electronics, such as the readout card (ROC), from the FVTX detector[2)] in the PHENIX experiment to significantly reduce development time and cost. FVTX is controlled by slow control commands from the VME modules, Front-End Module (FEM), and FEM Interface Board (FEM-IB), and data from the detector was initially processed by FEM and recorded by Data Collecting Module-II (DCM-II) and other equipment (Fig. 1).

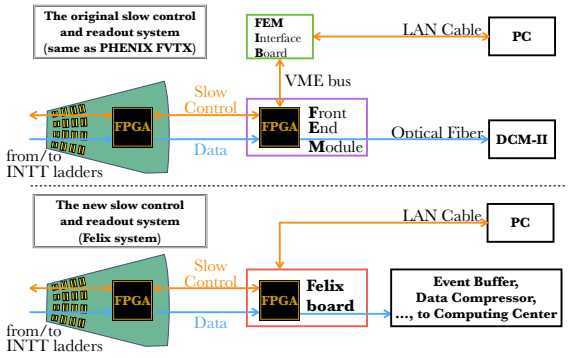

Fig. 1. Schema of the INTT operating system using the FEM/FEM-IB (top) or the Felix board (bottom).

As part of the transition from PHENIX to sPHENIX, all tracking detectors including INTT adopted a streaming readout (data readout without triggering). The streaming readout can collect two to three orders of magnitude more data than calorimeter triggers and eliminate trigger bias.[1)] To enable streaming readout, the Felix board[3)] used in ATLAS experiment at CERN was hired and optimized for each detector. INTT has almost completed the migration to the new system with Felix (Fig. 1), although the initial plan was to assume control of the FEM/FEN-IB system from FVTX.

To evaluate the performance of the Felix system, measurements of pulses generated by the ROC, referred to as *calibration*, were performed. The chips received pulses with various amplitude and performed analog-to-digital conversion. Further, *caliblation* provides the correlation between analog amplitude and digitized value. Another crucial performance evaluated from *calibration* is the number of the chip responses, which can be predicted, as the readout system must receive signals from the chip under many restrictions such as timing. Figure 2 shows the channel distribution of a readout chip, comprising 128 channels, from the calibration performed with the FEM/FEM-IB or Felix systems. Both measurements yielded consistent results. The slight differences are owing to fluctuations around the thresholds. Calibration with the Felix system was continuously performed to confirm good stability. The difference in the number of data from the expectation was no more than 0.1% provided as the data in the low amplitude noisy region were excluded. The INTT operation with Felix was confirmed stable and consistent with the FEM/FEM-IB system.

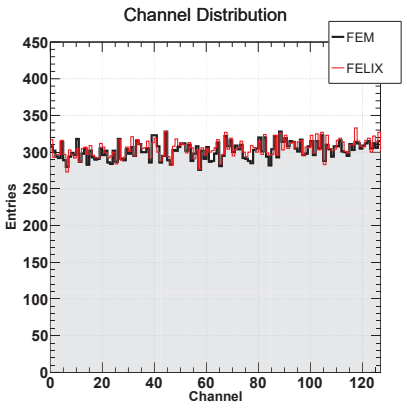

Fig. 2. Comparison of the channel distribution of a readout chip using the FEM (black) or the Felix (red) system.

*1 RIKEN Nishina Center
*2 Department of Physics and Astronomy, Purdue University
*3 Department of Physics, Rikkyo University
*4 Department of Mathematical and Physical Sciences, Nara Women's University
*5 Japan Atomic Energy Agency
*6 Tokyo Metropolitan Industrial Technology Research Institute
*7 Department of Physics, National Central University
*8 Department of Physics, National Taiwan University
*9 Physics Department, Brookhaven National Laboratory

References

1) sPHENIX collaboration, sPHENX Beam Use Proposal (2020).
2) C. Aidala *et al.*, Nucl. Instrum. Methods Phys. Res. A **755**, 44 (2014).
3) J. Anderson, *et al.* (ATLAS Collaboration), J. Phys. Conf. Ser. **664**, 082050 (2015).

Development of a control application for sPHENIX-INTT detector operation

H. Imai,[*1,*3] Y. Akiba,[*1] J. Bertaux,[*2] K. Fujiki,[*1,*3] M. Fujiiwara,[*4] T. Hachiya,[*1,*4] S. Hasegawa,[*1,*5] M. Hata,[*4] M. Kano,[*4] T. Kato,[*1,*3] T. Kondo,[*6] C. Kuo,[*7] R.-S. Lu,[*8] I. Nakagawa,[*1] Y. Namimoto,[*1,*4] R. Nouicer,[*9] G. Nukazuka,[*1] C. Shih,[*7] M. Shimomura,[*4] R. Shishikura,[*1,*3] M. Stojanovic,[*2] Y. Sugiyama,[*4] R. Takahama,[*1,*4] W.-C. Tang,[*7] H. Tsujibata,[*4] M. Watanabe,[*4] and X. Wei[*2]

The sPHENIX experiment will begin at Brookhaven National Laboratory (BNL) in 2023 to study quark-gluon plasma (QGP) using Relativistic Heavy Ion Collider (RHIC). We have developed a tracking detector which is named INTT for several years and the barrel assembly was completed by the end of 2022.[1)]

The INTT barrel consists of 56 silicon ladders. The analog signal from the silicon sensor is amplified, digitized, and transmitted downstream in an integrated circuit chip (FPHX) mounted right next to the silicon sensors. There are as many as 2912 FPHX implemented in the entire INTT barrel, and each can be customized operation parameter such as gain, threshold, *etc.* Developing a software application to centralize the control of FPHX chips all at once is mandatory. The application is called "expert GUI."

The development of the expert GUI can be divided into the following three categories.

1) Graphic User Interface (GUI) is designed to be intuitive for a user and interactively allows operation; 2) setting up a database to store the latest operation parameters for the FPHX chips; 3) establishing the communication between the server (Felix)[2)] which collects data from the FPHX chips and the client PC using Remote Procedure Call (RPC) protocol.

The front-end code is written in Python3, especially using Tkinter as a toolkit for developing GUI. Figure 1 shows the main control panels of the expert GUI. The left panel displays the cross-section layout of the INTT barrel, and the right represents the layout of Read Out Cards (ROC). The ROC relays data from FPHX to the downstream server (Felix). The trapezoid objects are clickable and will launch a new pop-up window with fields where the user can type in a desired value of a parameter for a given FPHX chips. The color of objects shows the LV power status of ROC and ladders.

As the database engine, PostgreSQL[3)] is used. It is operated on a dedicated server. We introduced four categorized tables to be stored in the database. They are 1) operation parameters for FPHX chips, 2) status of channel masks, 3) ladders and ROCs, and 4) ROCs and Felix servers.

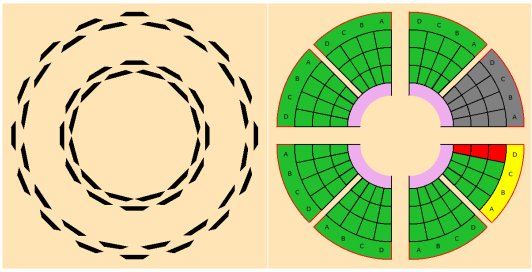

Fig. 1. The main control panel of the expert GUI.

Our choice of the RPC framework is gRPC[4)] as the communication protocol between the Felix server and the client PC where the GUI runs. The infrastructure of the communication can be established by setting up a gRPC-server on the server end and registering all functions to be executed on the server. Once it is established, the user can send a request for a function to be executed on the server from the client's PC.

The initial communication test was carried out by sending a function from the GUI to the Felix server using established RPC and checking the resulting response from the server. The function executed was "establish the optical communication between the ROC and the Felix." Then the GUI received the response from the server, which tells "the requested communication was established successfully," as shown in Fig. 2. Development of the expert GUI is ongoing.

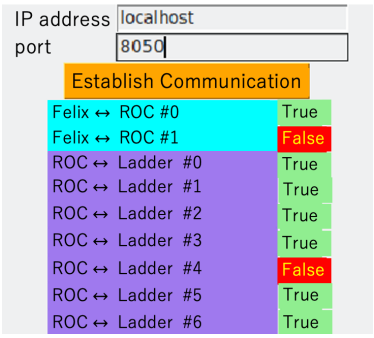

Fig. 2. Result of the attempt to establish communication using gRPC. Neither ROC#1 nor ladder#4 are physically not connected.

*1 RIKEN Nishina Center
*2 Department of Physics and Astronomy, Purdue University
*3 Department of Physics, Rikkyo University
*4 Department of Mathematical and Physical Sciences, Nara Women's University
*5 Japan Atomic Energy Agency
*6 Tokyo Metropolitan Industrial Technology Research Institute
*7 Department of Physics, National Central University
*8 Department of Physics, National Taiwan University
*9 Physics Department, Brookhaven National Laboratory

References

1) I. Nakagawa *et al.*, in this report.
2) G.Nukazuka *et al.*, in this report.
3) `https://www.postgresql.org/`.
4) `https://grpc.io/`.

Forward calorimeter upgrade project in ALICE†

T. Chujo,[*1] Y. Goto,[*2] M. Inaba,[*3] and M. H. Kim[*2] for the ALICE-FoCal Collaboration

A new forward high-resolution calorimeter, called FoCal (Forward Calorimeter) is being planned as one of the upgrade projects for the ALICE experiment at CERN. FoCal will be installed during LS3 (2026–2028) for physics data taking in LHC Run-4 (2029–2032). The letter of Intent for FoCal[1] has been submitted to the LHCC, and the FoCal project has been endorsed for the final R&D process for the Technical Design Report (TDR).

FoCal is a highly granular silicon-tungsten electromagnetic calorimeter combined with a conventional sampling hadronic calorimeter covering pseudorapidities of $3.2 < \eta < 5.8$. It provides to the LHC the unique capabilities to probe small-x gluon distributions via prompt photon production. FoCal significantly enhances the scope of existing ALICE physics programs by providing measurements of inclusive production cross-sections and correlations of neutral mesons, prompt photons, and jets at high rapidities, to explore the unknown dynamics of quarks and gluons inside a nucleus at small momentum fraction, $x = 10^{-6}$ for the first time. It is also expected to elucidate the existence of the color glass condensate (CGC),[2,3] which describes the dynamics of very densely populated gluon states at very small momentum fractions x in the nucleus and is expected to be important for the early stage formation of quark-gluon plasma in heavy-ion collisions.

FoCal will be located outside the ALICE solenoid magnet, at a distance of 7 m from the ALICE interaction point. The FoCal electromagnetic calorimeter (FoCal-E) is a compact silicon-tungsten sampling electromagnetic calorimeter with longitudinal segmentation. The current design comprises 18 layers of tungsten and silicon pads (FoCal-E PAD) with a granularity of 1 cm^2 and two layers of tungsten and silicon pixels (FoCal-E PIXEL) with a high granularity (30×30 μm^2). The pad layers provide measurements of the shower energy and profile, while the pixel layers enable two-photon separation down to a few mm, to discriminate between isolated photons and merged showers of decay photon pairs from neutral pions. The total silicon sensor area for FoCal-E is approximately 12 m^2 with approximately 150 thousand individual pad channels and approximately 8 thouasnd pixel sensors.

The FoCal hadron calorimeter (FoCal-H) is a Cu-scintillating fiber spaghetti calorimeter with a high granularity of approximately 2×2 cm^2, which provides good hadronic energy resolution and compensation. FoCal-H contributes to the measurement of photon isolation energy, to improve the selection of prompt photons, and to jet measurements.

In 2022, prototypes of three FoCal subsystems, namely FoCal-E PAD, PIXEL, and FoCal-H, were built and tested at the PS and SPS beam lines (Fig. 1). We (Tsukuba/RIKEN/Grenoble LPSC groups) constructed 18 layers of FoCal-E PAD prototype based on p-type silicon sensors with 320 μm thickness, 8×9 pad segmentation with 1 cm^2 pad size, and tungsten plates. HGCROC[4] readout ASICs were used for the PAD detector and successfully read out thorough data aggregation, a common readout unit (CRU), and a first level processor (FLP) together with other subsystems for the first time. The test beam data analysis is ongoing.[5] We also performed an irradiation test with neutrons by using the RIKEN accelerator-driven compact neutron source (RANS). We irradiated monitor silicon sensors (p-substrate and n-substrate) and measured IV characteristics. The total neutron dose at RANS at this time reached up to 10^{14} NEQ (1 MeV neutron equivalent fluence). The performance evaluation of irradiated sensors is also ongoing. Based on test results, TDR will be prepared for the final review of the detector construction and integration into ALICE in 2023.

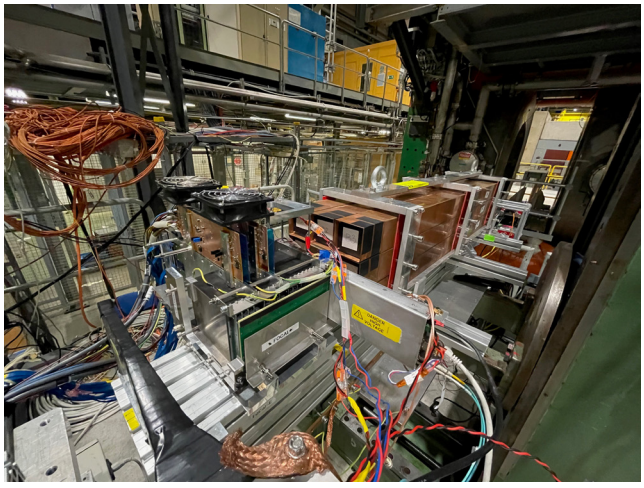

Fig. 1. FoCal prototype at CERN SPS test beam line in the experimental hall H2 (Nov., 2022).

References
1) Letter of Intent, A Forward Calorimeter (FoCal) in the ALICE experiment (ALICE Collaboration), CERN-LHCC-2020-009.
2) L. D. McLerran *et al.*, Phys. Rev. D **49**, 3352 (1994).
3) F. Gelis, Int. J. Mod. Phys. A **28**, 133000 (2013).
4) The Phase-2 Upgrade of the CMS Endcap Calorimeter (CMS Collaboration), CERN-LHCC-2017-023; CMS-TDR-019.
5) M. H. Kim, in this report.

† Condensed from the article in EP Newsletter, CERN, March 14, 2022

*1 Faculty of Pure and Applied Sciences, University of Tsukuba
*2 RIKEN Nishina Center
*3 Faculty of Industrial Technology, Tsukuba University of Technology

Beam test data analysis of the ALICE FoCal-E pad prototype

M. H. Kim*1 for the ALICE FoCal-E detector Collaboration

The ALICE FoCal-E detector[1] is an electromagnetic sampling calorimeter with a total depth of 20 radiation length (X_0), which aims to measure the direct photons produced by quark-gluon Compton scattering to explore the small-x parton structure of nucleons and nuclei. It is composed of 18 low-granularity silicon pad layers, with a cell size of 1×1 cm^2 for energy measurement, and 2 high-granularity silicon pixel layers, with a cell size of 30×30 μm^2 for position measurement and photon shower separation because the direct photons should be distinguished from those decayed from π^0. All layers have the tungsten sheets with a thickness of 1 X_0 followed by silicon layers.

FoCal-E has been developed since 2016 to be used for physics data collection in 2029. Now, we are studying the detector performance to write a technical design report and optimize the final design. A FoCal-E prototype with a transverse dimension of 9×8 cm^2 was prepared and tested using high-energy electron beams from 20 to 350 GeV at CERN-SPS in September and November 2022. In this article, we report the status and plan of the pad data analysis.

FoCal-E pad will use the HGCROC chip, which is being developed by the CMS experiment for a high-granularity calorimeter.[2] It provides ADC for signals up to 100 Minimum Ionizing Particles (MIP), which is used for energy calibration of each pad and time-over-threshold (TOT), which is fired from 100 MIP for large signals to measure photon energy up to 2 TeV. TOT is a technique that obtains the energy by measuring the pulse width of the digital output. Although it allows us to measure large signals, nonlinearity between the TOT and energy and the reliability of energy measurement in the intermediate dynamic range where it is converted from ADC to TOT need to be carefully studied.

A pad layer of the prototype consists of 72 cells. When the TOT values of all cells in the eighth layer, which is one of the shower maximum layers, were summed up for a 150-GeV beam energy, two peaks were observed. One was the case when all TOT values were zero. The other was a Gaussian peak around a non-zero value.

In the electron beam, a finite fraction of the hadron background exists. We assumed the former comes from the hadron background and the latter comes from the electron. This assumption is reasonable because the maximum energy deposit of a cell in the eighth layer by the electron was predicted by simulation to be larger than a level of 200 MIP, which is sufficient to fire the TOT even though the electron hits the edge of a cell. Therefore, events where at least one cell has non-zero TOT value in the eighth layer were selected to enhance the electron event. Mean of TOT sum, $\langle$TOT sum$\rangle$, was calculated for all pad layers to estimate the detector performance from the longitudinal shower profile.

Figure 1 shows the longitudinal shower profiles of the FoCal-E pad prototype with four different beam energies. As the beam energy increases, not only does the $\langle$TOT sum$\rangle$ increase but also the shower max layers move backward.

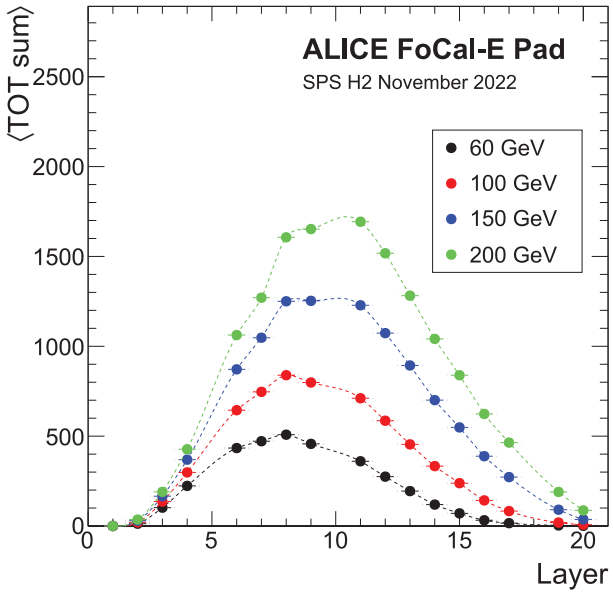

Fig. 1. Longitudinal shower profiles of the FoCal-E pad prototype, which shows the $\langle$TOT sum$\rangle$ with four different beam energies over the layers. Layer 5 and 10 are the pixel layers. Layer 18 is not shown due to a gain problem.

The FoCal-E pad prototype showed a reasonable performance even though the analysis cut condition was simple. However, the estimated energy resolution was 1.5 times worse than that expected by simulation. We are now processing the quality assurance (QA) for each run. After QA, more strict conditions will be applied to separate the electron from the hadron background. Calibration parameters will also be provided to combine the TOT and ADC and also to reduce the TOT nonlinearity. Taking these factors into account, precise detector performances will be studied.

References

1) ALICE Collaboration, CERN-LHCC-2020-009 (2020).
2) CMS Collaboration, CERN-LHCC-2017-023 (2017).

*1 RIKEN Nishina Center

Activation measurement of copper by ^{238}U irradiation

A. Akashio,[*1] K. Tanaka,[*1] N. Shigyo,[*1,*2] and K. Sugihara[*1,*2,*3]

γ-ray residual radiation dose around the copper beam dump of BigRIPS, where the highest radiation dose rate is expected at RIBF, is occasionally estimated by Monte-Carlo radiation transport code such as PHITS.[1)] However, there are no measured data for the activation caused by uranium beam and the accuracy of the calculation remains unknown. Therefore, 345 MeV/nucleon uranium beams were irradiated on a stack of copper sheets, which is the material of the beam dump, to measure the produced radioisotopes and compare them with the PHITS calculation.[1)]

Ten 1 mm thick copper sheets were stacked. A 10 mm thick copper plate was applied as the radiation sample. After the irradiation of the uranium beam, γ rays were measured with a germanium detector to identify the nuclide and quantity of the produced radioisotopes. To consider long-lived radiation from the beam dump, the γ rays were measured nine months after the irradiation. Figure 1 shows the depth dependence of the observed radioactive nuclei. The depth was reduced from the copper sheet number. The amount of the radioisotopes was evaluated from the individual measurements of the copper sheets. The range of 345 MeV/nucleon uranium-238 beam in copper was approximately 3.3 mm. Manganese-54, cobalt-56, -57, -58, and cobalt-60 were observed at all the copper sheets. Therefore, the isotopes of manganese and cobalt in the range 1–3 mm were produced through a reaction between the uranium and copper nuclei. The isotopes deeper than 4 mm were produced by a nuclear reaction of secondary neutrons with copper nuclei. Further, the secondary neutron was produced from the reaction with uranium beam and copper. Consequently, osmium-185, hafnium-175, zirconium-97, and ruthenium-103 were observed in the depth range of 4–6 mm. As nuclei of mass number of approximately 180 are heavier than typical fission fragments of uranium which mass are approximately 140, osmium and hafnium are supposed to be produced by projectile fragmentation of uranium beam. Zirconium and ruthenium, with approximate mass number of 100, are typical nuclides from in-flight fission of uranium beam. The range of produced nuclei in copper was longer than the 3.3 mm range of uranium beam because their atomic number are smaller than that of uranium. Moreover, the nuclei produced by fission were not observed at 7 mm depth and beyond.

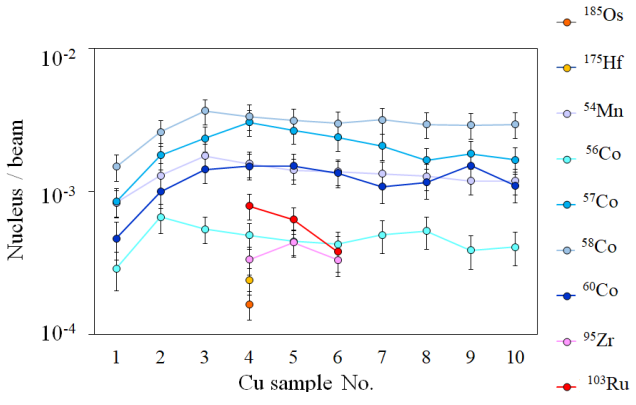

Fig. 1. Depth dependence of the observed radioactive nuclei in the copper sheets. The depth was converted from the number of the sheets.

The measured activity of nuclei was compared with the calculation by PHITS. Figure 2 shows the activity ratio of the calculated to measured value.

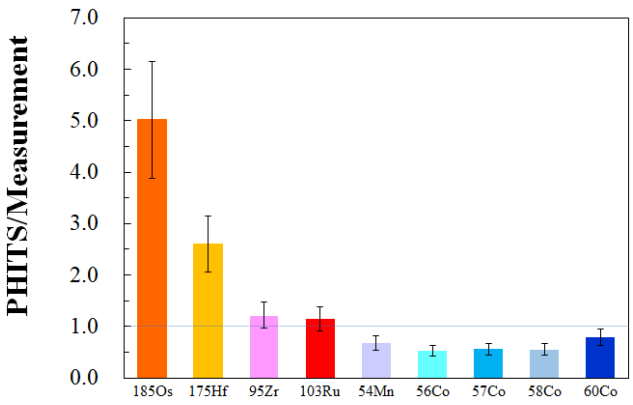

Fig. 2. Ratio of nuclei calculated evaluation by PHITS to measured values.

The calculated activation rate of copper by the secondary neutron was approximately 50% of measured value. The calculated production rate of projectile-fragmentation nuclides of osmium-185 and hafnium-175 were several times higher than measured values. However, the ratios of the fission nuclei zirconium-97, and rutheniu-103 were approximately identical to the measured values.

Consequently, the benchmark of activation for 345 MeV/nucleon uranium-beam irradiation on copper material was obtained. The PHITS evaluation was consistent the measured values within a factor of several.

*1 RIKEN Nishina Center
*2 Department of Applied Quantum Physics and Nuclear Engineering, Kyushu University
*3 High Energy Accelerator Research Organization (KEK)

Reference
1) T. Sato *et al.*, J. Nucl. Sci. Tech. **55**, 684 (2018).

RIKEN Wi-Fi service in the RIBF experimental area

H. Baba,[*1] H. Honda,[*2] and M. Kurokawa[*2]

Internet service is one of the essential infrastructures for research activities. For information security, networks are required to be separated depending on users and purposes. In the RIBF, an easy-to-use and secure network environment is necessary because many external researchers participate in experiments one after another. For example, a dedicated network has been constructed in the RIBF experimental area for data acquisition during experiments using the BigRIPS beam line. However, access to the Internet is accessed through RIKEN's intranetwork, and there are concerns about network separation for external researchers.

To achieve secure network separation, Eduroam and guest Wi-Fi services provided by RIKEN Information System Divisions for external researchers were introduced in the B1F and B3F measurement rooms of the RIBF experimental area. The B1F and B3F measurement rooms (each floor has an area of approximately 2000 m^2) are located apart from each other, and some rooms are separated by walls. This required the installation of a large number of wireless access points to provide wireless signals to the entire area. By adopting leaky coaxial (LCX) cables[1,2] as wireless antennas, we have successfully established a cost-efficient and easy-to-maintain Wi-Fi environment.

An LCX cable is a type of antenna in which slots are placed in the outer conductor of a coaxial cable to enable wireless communication. Figure 1 shows the structure of an LCX cable. We adopted LCX cables (Proterial Ltd. F-8D-LCX) that can be extended to a maximum cable length of 100 m and are compatible with the 2.4 and 5 GHz Wi-Fi bands. A diagram of the wiring in the B1F and B3F measurement rooms of the RIBF building is shown in Fig. 2. Boxes labeled with **AP**, circles, and bold lines are the access point, experimental room, and LCX cables, respectively. An HPE Aruba AP-504 access point, which is compliant with the 2.4 and 5 GHz Wi-Fi bands, was adopted. Two LCX cables are connected to each access point, and

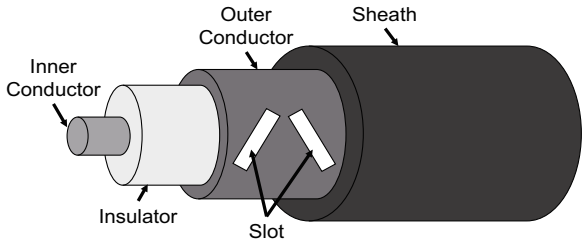

Fig. 1. Structure of an LCX cable.

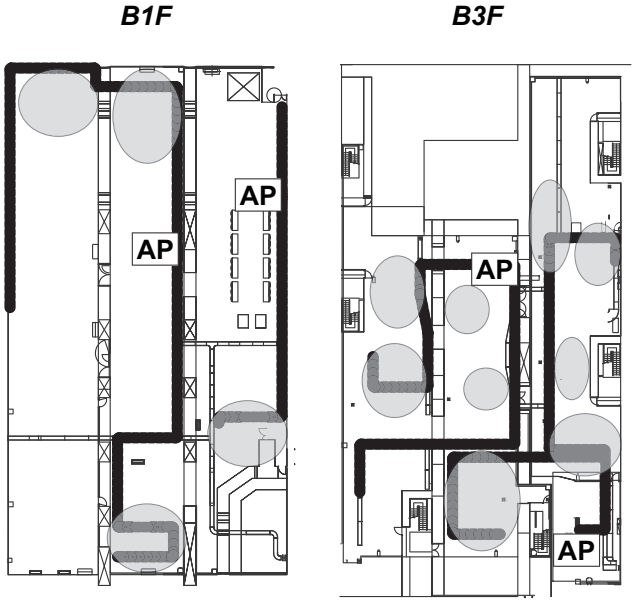

Fig. 2. Wiring diagram for the B1F and B3F measurement rooms in the RIBF building.

two access points were installed on each floor. Eight LCX cables (15, 38, 40, 50, 50, 60, 67, and 80 m) were used, and the total length was 400 m. Cables were routed along walls or cable racks on the ceiling. As shown in Fig. 2, four access points and eight LCX cables were sufficient to cover all the B1F and B3F measurement rooms.

The Wi-Fi signal strength is generally considered good if it is above −50 dBm. Near the access point, the Wi-Fi signal strength was approximately −40 dBm for both the 2.4 and 5 GHz bands. At a distance of 80 m from the access point, the signal strength was about −70 dBm for the 2.4 GHz band and less than −90 dBm for the 5 GHz band. However network communication was possible with the 2.4 GHz Wi-Fi band.

These results show that the Wi-Fi environment using LCX cables is effective in an experimental area such as the RIBF, where several measurement rooms are separately located. In the future, we plan to construct a Wi-Fi environment with LCX cables in the measurement rooms of the Nishina Building.

References

1) `https://ww.hcnet.co.jp/products/wireless/lcx/lcx.html`.
2) T. Igarashi *et al.*, in *Computers in Railways IX*, edited by J. Allan *et al.*, (WIT Press, 2004), p. 455.

*1 RIKEN Nishina Center
*2 RIKEN Information Systems Division

Computing and network environment at the RIKEN Nishina Center

T. Ichihara,[*1] Y. Watanabe,[*1] and H. Baba[*1]

We operate the Linux cluster systems[1] at the RIKEN Nishina Center (RNC).

Figure 1 shows the current configuration of the Linux servers at the RNC. Scientific Linux (SL) 7 and CentOS Stream 8 have been installed in these systems.

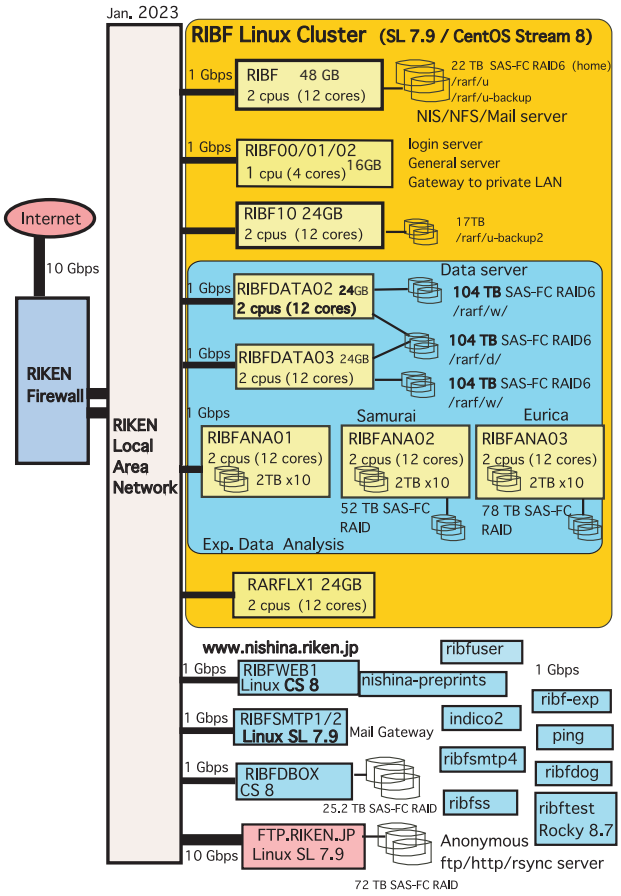

Fig. 1. Configuration of the RIBF Linux cluster.

Among these servers, the hardware of *RIBFSMTP1, RIBFSMTP2, INDICO2, RIBFSS*, and *RIBFUSER* are HP ProLiant DL320e. Because the hardware support of the HP DL320e was ending in December 2022, we replaced the hardware of the *RIBFSMTP1* with the newly installed HP DL160 in November.

HP ProLiant servers were repaired for 8 times. They were faults of two batteries and one capacitor for cache memories, and five hard disk drive units.

The hosts *RIBFSMTP1/2* are the mail gateways used for tagging spam emails and isolating virus-infected emails. The latest version of Sophos Email Protection-Advanced (PMX 6.4.9) was installed. However, as the support for Sophos PMX is scheduled to end in July 2023, we are preparing for a new mail system without using Sophos PMX. Figure 2 shows the email trends in 2022. Approximately 59% of the incoming emails were blocked by the PMX ip-blocker, and the number of the blocked emails (mostly spams) was increasing monthly.

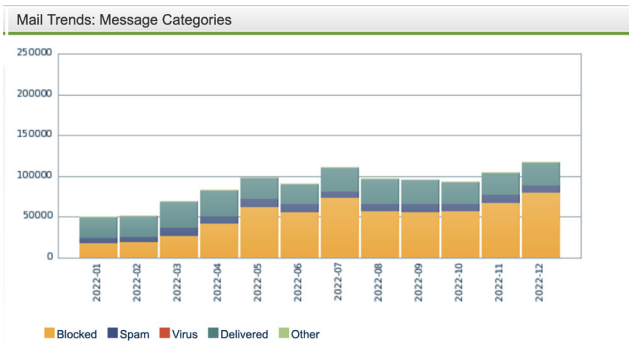

Fig. 2. Mail trends: message categories in 2022.

We tested Clam AV,[2] a free anti-virus software, on the test server *RIBFSMTP4* and found it working well. This could be one possibility for virus protection of emails when we drop Sophos PMX in 2023. We have also tested Rocky Linux 8 on *RIBFTEST* as a new operating system and the installation possibility of indico,[3] which is not supported in RHEL8.

An anonymous ftp server, *FTP.RIKEN.JP*, is managed and operated at the RNC. Major Linux distributions are mirrored daily for the convenience of the users. A memory leak was observed, and a workaround is in progress. It was announced in December 2022 that the CERN and Fermilab jointly plan to provide AlmaLinux as the standard distribution for experiments at our facilities, reflecting recent experience and discussions with experiments.[4] Therefore, our new servers may soon adopt AlmaLinux as an operating system.

We have been operating approximately 70 units of wireless LAN access points in RNC for the convenience of experiments and daily work. Two old and degraded access points, WAPS-APG600H, were replaced by new access points, WAPM-1266R.

*1 RIKEN Nishina Center

References

1) T. Ichihara *et al.*, RIKEN Accel. Prog. Rep. **55**, 102 (2022).
2) `https://www.clamav.net/`.
3) `https://getindico.io/`.
4) `https://linux.web.cern.ch/`.

CCJ operations in 2022

S. Yokkaichi,[*1] Y. Akiba,[*1] T. Ichihara,[*1] and Y. Watanabe[*1]

Overview

The RIKEN Computing Center in Japan (CCJ)[1] commenced operations in June 2000 as the largest offsite computing center for the PHENIX[2] experiment being conducted at RHIC. Since then, CCJ has been providing numerous services as a regional computing center in Asia. We have transferred several hundred terabytes of raw data files and nDST[a] files from the USA.

Many analysis and simulation projects are being conducted at CCJ, which are listed on the web page `http://ccjsun.riken.jp/ccj/proposals/`. As of December 2022, CCJ has contributed to 47 published papers and 45 doctoral theses.

Computing hardware and software

The network configuration and computing hardware (nodes) and software (OS, batch queuing systems, database engine, *etc.*) are nearly the same as described in the previous APR,[3] and the number of servers are summarized in Table 1. The main server (users' home directory, NIS, DNS, and NTP), SAS RAID for the server (15.5 TB), and one login server were replaced, and a new interactive server was deployed in Oct. 2022. Interactive servers are used for the compilation and test runs for the jobs before the submission to the computing nodes. Two spare machines for interactive and login servers were prepared.

Table 1. Number of servers and disk sizes, as of 2022 Dec. Dagger(†) shows replacement and newly deploying in this year (detail is in the text).

	number	disk size (TB/node)	type
main server	1	6(built-in) + 15.5(RAID)	DL360G10†
login server	2	-	DL20G9/DL20G10†
interactive server	4	-	-/DL320G6/ DL160G9/DL20G10†
calculation node 1	16	10	DL180G6
calculation node 2	8	20	DL180G6
work disk server	2	26 / 39	DL180G9/DL385G10
DB server	1	1	DL145G3
library(AFS) server	1	9	DL180G6
transfer server	2	12 / 39	DL180G9/DL380G10
docker test server	1	-	DL20G9

In addition, we operate one dedicated server for the RHICf group[4] and two servers for the J-PARC E16 group[5] in order to maintain their dedicated compilation and library environments along with some data.

We operate 26 computing nodes, and 352 (= 8 × 17 nodes + 24 × 9 nodes) jobs can be processed simultaneously via these computing nodes using a batch queuing system, LSF 9.1.3.[6] Table 2 lists the number of malfunctioning SATA or SAS disks in the HP servers, namely, computing nodes and NFS/AFS servers. The OS of nine calculation nodes and of two interactive servers operated in SL7.9[7] and the rest are still old. Two old interactive servers will be shutdown following the upgrade of the computing nodes.

Table 2. Number of malfunctioning HDDs in HP servers during 2011–2022.

Type (TB)	total	11	12	13	14	15	16	17	18	19	20	21	22
SATA (1.0)	192	9	20	16	11	14	8	18	16	8	9	10	5
SATA (2.0)	120	4	5	2	0	10	2	10	2	10	5	9	7
SATA (4.0)	26	-	-	-	-	-	-	-	0	0	0	2	0
SATA (6.0)	20	-	-	-	-	-	-	-	0	0	0	0	0
SAS (0.15)	38	1	1	0	2	3	5	1	3	6	3	5	2
SAS (0.3)	26	1	0	0	1	1	0	1	0	2	1	2	1

Three 10-KVA UPSs are operated as power supplies for these CCJ nodes. The next replacement is planned in Mar. 2026 considering the 5-year battery life. Rearrangement of AC power lines for the nodes from these UPSs was performed for the re-balancing of load, immediately after the deployment of new servers, during the planned power outage in Wako Campus.

The replacement of the main switch is planned in 2023, to support the 10 GBASE-T network for servers, while 10 GBASE-LR and SR are used now only for the uplink to RIKEN-LAN and for the downlink to edge switches for the calculation nodes, respectively.

Joint operation with ACCC/HOKUSAI

CCJ and the RIKEN IT division have been jointly operated since July 2009. In April 2015, "HOKUSAI Greatwave"[8] system was launched and the joint operation with CCJ continued, with the inclusion of a new hierarchical archive system wherein approximately 1070 TB of CCJ data were stored as of December 2022. A breakdown of the data is presented in Table 3.

Table 3. Tape usage in Hokusai as of December 2022.

user	total	PHENIX official	KEK/ J-PARC	RHICf	user-level archive
size (TB)	1068	749	173	8	137

[*1] RIKEN Nishina Center

[a] term for a type of summary data files in PHENIX

References

1) `http://ccjsun.riken.jp/ccj/`.
2) `http://www.phenix.bnl.gov/`.
3) S. Yokkaichi *et al.*, RIKEN Accel. Prog. Rep. **55**, 103 (2022).
4) Y. Itow *et al.*, arXiv:1409.4860.
5) S. Yokkaichi, in this report.
6) `https://www.ibm.com/docs/en/spectrum-lsf/`.
7) `http://www.scientificlinux.org/`.
8) `https://i.riken.jp/supercom/`.

III. RESEARCH ACTIVITIES II
(Material Science and Biology)

1. Atomic and Solid State Physics (Ion)

Control of electrical conductivity in diamond by boron-implantation using an ECR ion source

H. Yamazaki,[*1] T. Minamidate,[*2] M. Kidera,[*1] A. Yamamoto,[*3] R. Kato,[*4] and H. Ueno[*1]

Diamond is an excellent electrical insulator with a large band gap of 5.5 eV. It becomes a semiconductor when doped with a small amount of boron (for p-type) or phosphorus (for n-type). When doped beyond the metal-to-insulator transition at a boron density of $n_B \sim 3 \times 10^{20}$ B/cm^3, boron-doped diamond exhibits superconductivity in the samples grown by the high-pressure and high-temperature synthesis.[1)] Theoretically, the superconducting critical temperature T_c can be significantly increased by reducing the effects of disorder in boron-doping processes.[2)] For a higher T_c, more subtle control of doping using CVD and/or MBE methods is highly required. However, a different method based on ion implantation is also worth investigating as it enables selective ion doping in a controlled manner. This has great potential for future device applications. Successful inclusion of boron ions by the implantation technique has been confirmed using SEM/EDS measurements. The surface image of our sample and its EDS spectrum are shown in Fig. 1. At 0.19 keV, we can see an energy peak from the boron ions embedded in the diamond.

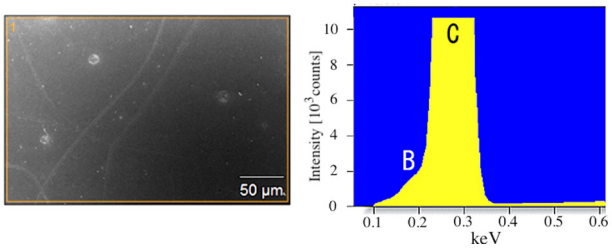

Fig. 1. Left: SEM image of our sample with a boron concentration of $n_B \sim 6.8 \times 10^{22}$ B/cm^3; right: EDS spectrum obtained with an acceleration voltage of 7.0 kV. The strongest peak comes from the carbon atoms in the diamond.

For the past few years, we have been trying to control the electrical conductivity in Ib-type diamonds using boron-ion implantation. To reduce the lattice damage produced during the implantation, we performed annealing treatments after implantation. As the phase diagram of carbon shows, the diamond is not stable at low pressures; therefore, we annealed the samples at 800°C and 4 GPa for 1 hour. Contrary to our expectations, the annealed samples exhibited no sign of superconductivity. The laser Raman spectra (632.8 nm excitation) indicated that the annealing promoted the formation of NV$^-$ centers, which behave as carrier traps in the diamond.

In this fiscal year, to decrease the NV$^-$ defect density, we used single-crystals of IIa-type diamond with a nitrogen concentration of less than 8 ppm (Fig. 2, right). We also investigated the dependence of boron-implantation yield on the crystallographic orientation of diamond surface: (100) and (111). Using an ECR ion source,[3)] boron ions were implanted into the diamond crystals at 5 keV corresponding to an implantation depth of ∼10 nm. Five samples of different concentrations from $n_B \sim 5 \times 10^{20}$ to 2×10^{22} B/cm^3 were prepared. These samples were annealed under the same conditions as noted above.

Fig. 2. Pristine single-crystals of IIa-type diamond (right) and Ib-type diamond (left, for comparison). The size of each crystal is approximately $1 \times 1 \times 0.3$ mm^3.

Figure 3 shows a sample and some parts of high-pressure media after removing the sample. For comparison, the implanted samples without annealing were also prepared. We are now ready to measure the samples with different combinations of the conditions: (a) five different n_B's, (b) two types of surface orientations: (100) and (111), and (c) with/without annealing treatment after implantation.

Fig. 3. The boron-implanted diamond (arrowhead) after the process of high-temperature and high-pressure annealing. Parts of high-pressure media are also shown.

*1 RIKEN Nishina Center
*2 Faculty of Science, Tokyo University of Science
*3 Graduate School of Engineering and Science, Shibaura Institute of Technology
*4 Condensed Molecular Materials Laboratory, RIKEN

References

1) E. A. Ekimov *et al.*, Nature **428**, 542 (2004).
2) T. Shirakawa *et al.*, J. Phys. Soc. Jpn. **76**, 014711 (2007).
3) M. Kidera *et al.*, Eur. J. Mass Spectrom. **13**, 239 (2007).

Lattice sites of ^{23}Ne implanted in single-crystal ZnO studied by β-NMR/NQR spectroscopy

H. Yamazaki,[*1] H. Nishibata,[*2] A. Gladkov,[*1] T. Kawaguchi,[*3] H. Ueno,[*1] Y. Ichikawa,[*2] A. Takamine,[*1] T. Sato,[*1] K. Kawata,[*1,*4] W. Kobayashi,[*3] M. Sanjo,[*3] L. C. Tao,[*5] Y. Nakamura,[*3] T. Asakawa,[*3] Y. Sasaki,[*3] K. Totsuka,[*3] K. Doi,[*3] T. Yada,[*3] K. Asahi,[*1] Y. Ishibashi,[*6] K. Imamura,[*1] T. Fujita,[*7] G. Georgiev,[*8] and J. M. Daugas[*9]

Zinc oxide is a II-VI binary compound that crystalizes in a hexagonal wurtzite structure. The compound has received significant attention because of its potential for application in optoelectronic devices and transparent conducting films as well as in space environments owing to its radiation hardness. In particular, owing to wide and direct band gap of 3.4 eV at room temperature, ZnO can be utilized in next-generation devices for short-wavelength optoelectronics such as light-emitting diodes operating in the spectral range from blue to ultraviolet. For utilizing ZnO as semiconductors, both n-type and p-type doped ZnO are necessary. We can fabricate n-type ZnO through the partial substitution of Zn with Al, Ga, or In, whereas fabricating a reliable high-quality p-type ZnO still remains a challenge. Despite considerable research conducted so far, high-quality p-type ZnO has not been fabricated.

Recently, first-principles calculations performed by Malyi *et al.* indicated that a noble gas (He, Ne, or Ar) implanted in ZnO can serve as a new type of dopant.[1)] In spite of its fully occupied atomic orbitals, the noble gas strongly changes the surrounding electronic states by pushing away the electrons around it. This suggests that a noble gas can be a functional dopant in ZnO, and the investigation of ZnO using noble-gas nuclei as local probes is much anticipated. In this study, we investigate, in particular, Ne implantation into single-crystal ZnO.

For details of the experimental setup, see our earlier report.[2)] First, using the β-NMR method, we determined the nuclear g-factor for the radioactive ^{23}Ne isotope (nuclear spin $I = 5/2$) that decays through β-emission into the nucleus ^{23}Na with a half-life of $T_{1/2} = 37$ s. Thereafter, we implanted the ^{23}Ne isotopes as probe nuclei in ZnO and measured the electric field gradient (EFG) at the ^{23}Ne stopping sites using β-NQR method. EFGs are highly sensitive to the electronic density in the vicinity of the relevant nucleus. This sensitivity can be used to identify the crystallographic sites for the implanted ^{23}Ne and to study the effect of ^{23}Ne implantation on the charge distribution around the nucleus. The β-NQR spectrum obtained at 47 K is depicted in Fig. 1.

We determined the electric field gradient Vzz at the position of ^{23}Ne in ZnO. The value of $(3.1 \pm 0.3) \times 10^{20}$ [V/m^2] for ^{23}Ne compare well with that for ^{20}Na on the interstitial site (see Table 1). Although Ne occupies an octahedral interstitial site (the lowest energy site for Ne),[1)] Na in the form of ion (Na^+) is shifted by 0.23 Å from the ideal octahedral site parallel to the c-axis.[6)] Considering that both Ne and Na^+ have the same electron configuration $1s^2 2s^2 2p^6$, we must study the position dependence of V_{zz} further in detail theoretically.

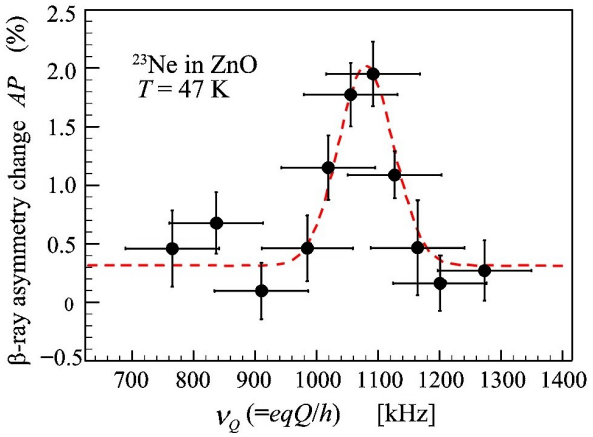

Fig. 1. β-NQR spectrum of ^{23}Ne implanted in ZnO single crystal. The dashed line represents the least χ-square fitting result to a Gaussian function.

Table 1. Experimental results of the electric field gradient V_{zz} in ZnO for the β-NQR probes of ^{8}Li, ^{12}N, and ^{20}Na.

Implanted probe	^{8}Li [3)]	^{12}N [4)]	^{20}Na [5)]
V_{zz} [10^{20} V/m^2] Lattice site	1.342±0.001 interstitial site close to octahedral site 0.6029±0.0004 Zn substitutional site	0.86 ±0.11 site unclear	2.7 interstitial site close to octahedral site[6)] 1.8 Zn substitutional site[6)]

*1 RIKEN Nishina Center
*2 Department of Physics, Kyushu University
*3 Department of Physics, Hosei University
*4 Center for Nuclear Study, University of Tokyo
*5 School of Physics, Peking University
*6 Cyclotron and Radioisotope Center, Tohoku University
*7 Department of Physics, Osaka University
*8 CSNSM, CNRS/IN2P3, Université Paris-Sud
*9 CEA/DAM-Ile de France

References
1) O. I. Malyi *et al.*, npj Comput. Mater. **5**, 38 (2019).
2) H. Nishibata *et al.*, RIKEN Accel. Prog. Rep. **52**, 56 (2018).
3) J. R. Adelman *et al.*, Phys. Rev. B **106**, 035205 (2022).
4) R. Matsumiya *et al.*, Hyperfine Interact. **178**, 63 (2007).
5) K. Minamisono *et al.*, Nucl. Instrum. Methods Phys. Res. A **616**, 45 (2010).
6) U. Wahl *et al.*, Semicond. Sci. Technol. **31**, 095005 (2016).

Evaluation of horizontal irradiation for SiC vertical diodes

M. Iwata,[*1] M. Takahashi,[*1] N. Ohtani,[*1] N. Nemoto,[*1] and H. Shindou[*1]

Silicon carbide (SiC) devices are the candidates for next generation power device for space applications because of their excellent electric property. To clarify the destruction mechanism of SiC devices caused by heavy ions, which is a critical issue for usage in harsh radiation environments, we have conducted experiments under various irradiation conditions.

The test was conducted on the 650 V commercial SiC vertical diodes with a junction barrier Schottky (JBS) structure, which is the same as in the previous report.[1] Test devices were decapped and irradiated with ^{84}Kr ions at room temperature in air using RIKEN AVF coupled with the RIKEN Ring Cyclotron (RRC). The energy of ion at incident edge of the device was 3040 MeV. Irradiations were performed from different sides: one was from the upper side, the other was from the left side, horizontal to the device surface, as shown in Fig. 1. A reverse voltage (V_R) was applied to the device and the leakage current (I_R) was continuously monitored during irradiation. Further, V_R was initialized at 240 V and increased in 40 V steps after the total fluence at each V_R reached 1.0×10^6 ions/cm^2. The maximum V_R in this test was 640 V, which was close to the rated voltage of the test device.

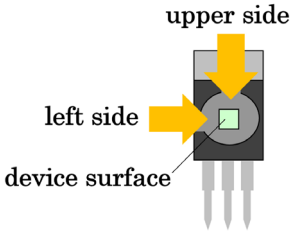

Fig. 1. Irradiation direction to the device.

Figure 2(a) shows the transition of I_R at the end of irradiation at each V_R. The device irradiated from the left side was broken at V_R = 600 V, whereas that irradiated from the upper side was not broken until the maximum V_R. Figure 2(b) shows the transition of I_R with increasing fluence at V_R = 600 V irradiated from the left side; I_R abruptly increased and reached approximately 6 mA.

The same test was conducted for different samples to confirm the effects of crystal direction relative to ion tracks. The samples were 650 V SiC diodes created by the same company; however its structure was planar type, which does not have p+ regions at the Schottky contact. No increase in I_R was observed when irradiated from both sides, which implies that interaction between the p+ regions and charges generated by a heavy ion affected the device breakdown more than crystal direction.

*1 Research and Development Directorate, Japan Aerospace Exploration Agency

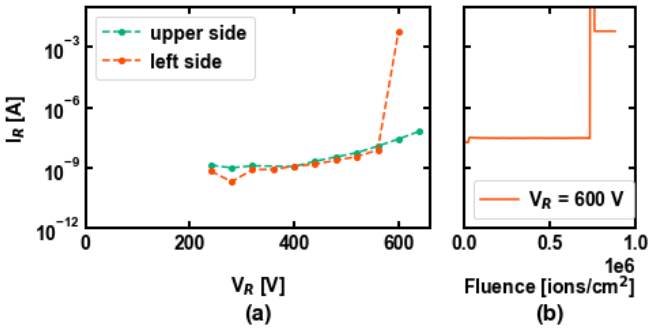

Fig. 2. (a) Transition of I_R during irradiation and (b) Transition of I_R at V_R = 600 V irradiated from left side.

Follwing the test, a surface damage considered evidence of single-event burnout (SEB) was observed on the device irradiated from the left side. It was located approximately 320–450 μm from the left edge of the device. Focusing on linear energy transfer (LET) transition in the device, the highest LET with a Bragg peak was 43.8 MeV/(mg/cm^2) at 383 μm, which is approximately the center of the damage site. Note that incidence position in device thickness direction remained unclear in this test; however, for triggering SEB, an ion was introduced into the depletion layer because deposited charges must be accelerated by the electric field.

The electric field lines within depletion layer are perpendicular to the surface under certain V_R; thus, charges generated by an ion move vertically in vertical diodes. These charges are amplified in the collection process, which can cause device degradation or destruction. Although less amplification can be expected for horizontal irradiation because reduction in charge multiplication with increasing tilt angle has been reported,[2] a rapid increase in I_R and surface damage were observed in the device irradiated from the left side. The same behavior could not be observed at normal incidence (*i.e.*, perpendicular to the device surface) with the same ion and device; gradual increase of I_R at lower V_R was observed instead. Focusing on a small vertical region in the device, charges generated by horizontal irradiation are considered to exist as a point, and all charges including amplified charges might be collected in an extremely short period of time. However, the time for all charges to be collected at normal incidence might be longer than horizontal irradiation because charges are generated in a vertical line along an ion track. This difference in collecting time period might affect the difference in destruction mode.

References

1) M. Iwata *et al.*, RIKEN Accel. Prog. Rep. **5**, 106 (2022).
2) A. Javanainen *et al.*, IEEE Trans. Nucl. Sci. **64**, 2031 (2017).

Improvement of the signal-to-noise ratio of Rb D1 fluorescence in superfluid helium using picosecond time-resolved detection

H. Endo,[*1,*2] K. Ishii,[*3] K. Imamura,[*2] A. Takamine,[*2] Y. Matsuo,[*1,*2] T. Tahara,[*3] and H. Ueno[*2]

Our research group is developing a laser spectroscopy technique (OROCHI) for atoms in superfluid helium (He II). When atoms are injected into He II, the surrounding helium atoms are pushed out by the Pauli repulsion force.[1] The resulting vacuum region is referred to as an atomic-bubble. As the shape of the electron orbit of the impurity atom is deformed according to its energy state, the atomic bubble is also deformed following the shape change of the atomic orbit. The wavelengths of the atomic transitions for both the absorption and emission in He II are shifted from those in vacuum due to this deformation cycle.[2] It is estimated that the bubble deformation requires an order of a few picoseconds;[1] however, till date, the relaxation time has not been measured in the time domain in bulk He II. Because the emission wavelength is expected to change with the degree of the bubble deformation, we aim to determine the relaxation time of Rb atomic bubbles in He II through time-resolved emission measurements at different wavelengths.[3]

We have successfully observed laser-induced fluorescence (LIF) from Rb atoms of the D1 line (absorption center wavelength in He II: 778.0 nm) picosecond laser excitation and detection with time-correlated single photon counting (TCSPC).[3] To measure the fluorescence that is weaker at shorter wavelengths than the center wavelength, the signal-to-noise ratio must be increased. Here, we report the introduction of a metal cell with anti-reflection (AR) coated windows instead of a conventional quartz-cell to reduce the effect of scattered light from the excitation laser.

Figure 1 shows the experimental setup. We used a picosecond mode-locked Ti:sapphire laser (laser power: 100 mW, repetition rate: 80 MHz, pulse width: 1.6 ps, center wavelength: 778.2 nm) as the excitation laser. LIF was detected using an avalanche photodiode (APD) through a monochromator. The transmission of AR-coated windows is greater than 99.4% in the wavelength range of 780 nm to 830 nm. Because a large proportion of the background photons are considered to originate from the scattered light on the surface of the quartz cell, the introduction of the AR-coated windows is expected to reduce the scattered light, in the LIF detection efficiency.

Figure 2 shows the observed photon intensities as a function of delay time. The peaks in Fig. 2 are at the time of the excitation laser incidence, from which the Rb atoms decay along their spontaneous emission life-

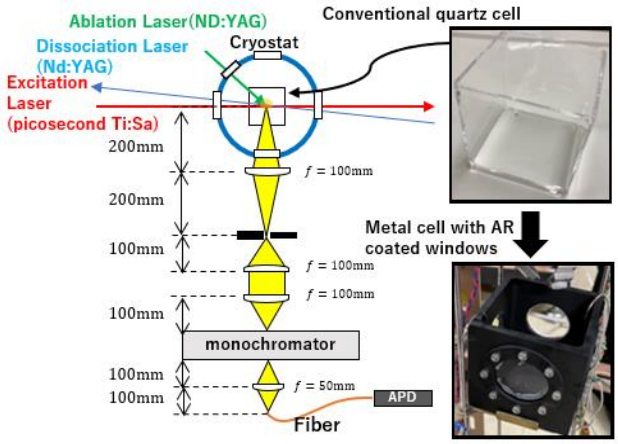

Fig. 1. Experimental setup of LIF detection.

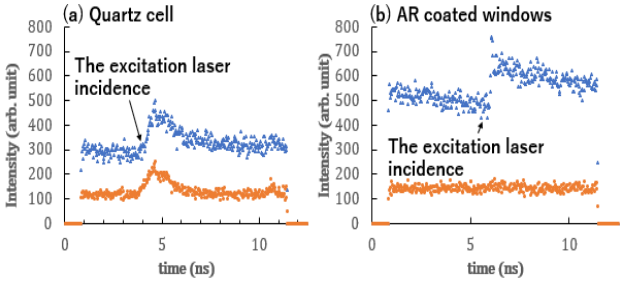

Fig. 2. Intensity detected by TCSPC using (a) a quartz cell, (b) AR coated windows.

time of 27 ns. Figure 2(a) shows the result of the LIF observation using the conventional quartz cell without AR coating. Both the LIF signal (blue) and a relatively large amount of laser-scattered light (orange) were observed. Note that the background also contains ambient light other than the laser in the environment and areas with a value of 0 correspond to the timing when the detection device can not count photons. Figure 2(b) shows that LIF increased when AR-coated windows were used, whereas laser scattered light was almost negligible. We plan to observe weaker emission on the short wavelength side through further improvement of the signal-to-noise ratio by increasing the data acquisition time.

References

1) B. Tabbert *et al.*, J. Low Temp. Phys. **109**, 653 (1997).
2) Y. Takahashi *et al.*, Phys. Rev. Lett. **71**, 1035 (1993).
3) Y. Takeuchi *et al.*, RIKEN Accel. Prog. Rep. **54**, 105 (2020).

*1 Department of Advanced Sciences, Hosei University
*2 RIKEN Nishina Center
*3 RIKEN Center for Advanced Photonics

Development of a spin polarized RI atomic beam apparatus the using atomic resonance method

K. Imamura,[*1] Y. Fukuzawa,[*1,*2] A. Takamine,[*1] S. Go,[*1] A. Gladkov,[*1] M. Tajima,[*1] and H. Ueno[*1]

We are currently developing a spin-polarized radioactive isotope (RI) atomic beam apparatus using the atomic beam magnetic resonance (ABR) method to apply RIs to nuclear structure study and material sciences. The apparatus mainly consists of the following two parts: i) An RI ion neutralizer based on a radio frequency (RF) trap and laser cooling technique for generating a low-energy RI atomic beam. ii) An ABR apparatus consisting of a sextupole magnet, dipole magnet, quadrupole magnet, and RF cavity for producing a highly polarized RI atomic beam.[1)] In our method, RI and laser-cooled ions are simultaneously trapped in a linear Paul trap at first. Then, the energy of trapped RI ions is sympathetically decreased by the Coulomb interaction between laser-cooled and trapped RI ions (sympathetic cooling).[2)] After cooling the RI ions, an ion neutralization gas is blown against the trapped ions. An RI atomic beam produced by the above neutralization process is delivered to the ABR apparatus. In the ABR apparatus, spin polarization is achieved by a combination of double spin selection using a magnetic field gradient generated by a sextupole and quadrupole magnet and single spin flip by magnetic resonance with an RF cavity assembled in a uniform magnetic field generated by a dipole magnet. In the development process, establishing highly efficient RI ion neutralization and RI atomic beam transport method is crucial because the ABR method itself is a well-established technique in the field of measuring nuclear electromagnetic moment of stable isotopes. In this study, we report on an offline laser cooling experiment conducted using singly charged ^{88}Sr ions toward sympathetic cooling for developing the neutralizer.

Figure 1 shows (a) the schematic of the setup and (b) corresponding energy levels of the $^{88}Sr^{+}$ ion in the experiment. Laser pulses from a Nd: YAG laser (wavelength: 1064 nm, repetition rate: 1 Hz, pulse duration: 5 ns, intensity: ∼2.5 mJ) were focused on a $SrTiO_3$ plate (width × hight × thickness = 10 × 10 × 0.5 mm^3) using a convex lens with a mm focal length of 350 mm. The $^{88}Sr^{+}$ ions produced by laser ablation were trapped at the center electrode (denoted as "C" in Fig. 1) in our linear Paul trap. For ion trapping, we introduced He as the buffer gas whose pressure was approximately 2.0×10^{-2} Pa for buffer gas cooling. After 200 s of buffer gas cooling, the buffer gas was quickly pumped out and pressure was maintained in the range of 10^{-6}–10^{-7} Pa. To produce laser-cooled $^{88}Sr^{+}$ ions, we prepared two lasers. One was the cooling laser with

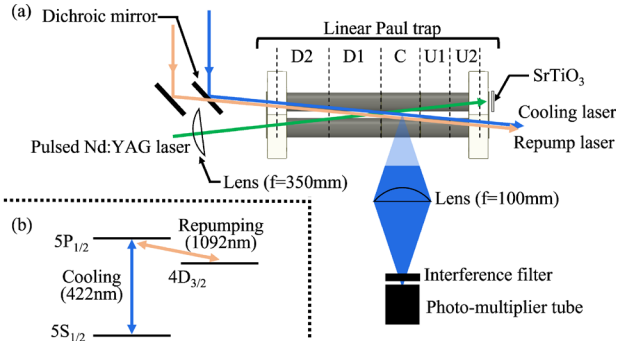

Fig. 1. (a)The schematic of the experimental setup. (b) The related energy levels of Sr ion in the experiment.

awavelength of 422 nm corresponding to the D1 ($5S_{1/2}$–$5P_{1/2}$) transition of the $^{88}Sr^{+}$ ion. The other was the repump laser (wavelength: 1092 nm) used to pump $^{88}Sr^{+}$ ions de-excited in the $4D_{3/2}$ metastable state to the $5P_{1/2}$ excited state. We irradiated the trapped ions with both lasers in a co-propagation configuration. The optical paths of the lasers were spatially combined using a dichroic mirror (Thorlabs, DMLP650). The laser powers of the cooling laser and the repump laser were 1.5 mW and 5 mW, respectively. The laser induced-fluorescence (LIF) emitted from $^{88}Sr^{+}$ ions was collected using a convex lens with a focal length of 100 mm and detected using a photo-multiplier tube (Hamamatsu photonics, H16721-50). In order to reduce the background stray light, an interference filter with a bandwidth of 435 ± 20 nm (Edmund optics, Fluorescence band-pass filter) was mounted in front of the PMT. We obtained the LIF spectra by scanning the laser frequency of the cooling laser. So far, we have confirmed the onset of laser cooling effect by observing the narrowing of the line width and change of line shape under different RF voltages applied to the trap electrodes. Further optimization of the experimental parameters, such as the applied laser power, number of trapped ions, and so on, is under investigation.

Along with the development of the neutralizer, an RF cavity is being developed. We have designed the RF cavity, whose resonance frequency is approximately 3 GHz, as a prototype. Currently, preparations to evaluate the performace of the cavity using an Rb vapor enclosed glass cell is in progress now.

*1 RIKEN Nishina Center
*2 Department of Advanced Science, Hosei University

References

1) H. T. Duong *et al.*, Nucl. Instrum. Methods Phys. Res. A **325**, 465 (1993).
2) D. J. Larson *et al.*, Phys. Rev. Lett. **57**, 70 (1986).

Application of ^{21}O β-NMR spectroscopy to study the microscopic properties of CuO single crystal

A. Gladkov,[*1] H. Yamazaki,[*1] Y. Ichikawa,[*1] A. Takamine,[*1] H. Nishibata,[*2] K. Asahi,[*1] K. Kawata,[*1,*3] K. Imamura,[*1] M. Tajima,[*1] K. Tsubura,[*1] S. Go,[*1] H. Endo,[*1] R. Mitsuyasu,[*1] K. Kikuchi,[*1] S. Takahashi,[*1] S. Akimoto,[*1] Y. Fukuzawa,[*1] M. Ito,[*1] M. Mukai,[*1] and H. Ueno[*1]

Since the discovery of high-T_c superconductivity in cuprates, copper ions coordinated by oxygen have been extensively studied. The multiferroic phase of CuO exists between 213 K and 230 K, a much higher temperature range than the multiferroic phase of other known compounds. When the temperature of the CuO sample is decreased from $T > 230$ K (the paramagnetic phase) to 230 K $> T >$ 213 K (the multiferroic phase), it is expected that the electric field gradient (EFG) at oxygen sites will be changed due to the multiferroic transition. By substituting the O sites in CuO with polarized ^{21}O ions, this hypothesized change in EFG can be detected by the β-detected nuclear quadrupole resonance (β-NQR) method, providing the microscopic information on the "improper" ferroelectric phase. The advantages of using ^{21}O relative to other oxygen isotopes have been discussed in a previous report.[1)]

Previously, we have successfully measured the ground-state magnetic dipole and electric quadrupole moments of ^{21}O[2,3)] by means of β-detected nuclear magnetic resonance (β-NMR) spectroscopy. Thus, in the present study, the microscopic properties of CuO are investigated by using the ^{21}O isotope as a spectroscopic probe.

The experiment was carried out using the RIPS separator at the RIBF facility. The experimental settings for the production of spin-polarized ^{21}O secondary fragments were the same as the optimized settings for the previously conducted measurement of the quadrupole moment in TiO_2 single crystal.[2)] A ^{21}O beam was produced in the projectile fragmentation reaction of a ^{22}Ne beam at 70 MeV/nucleon on a 185 mg/cm^2 Be target. The momentum window and emission angle of the secondary fragments were selected to be $p_F = p_0 \times (0.97 \pm 0.03)$ and $\theta_F > 1.5°$, respectively.

The secondary beam of ^{21}O was then purified by the RIPS separator and implanted into the single-crystal CuO sample located in the cryostat in the center of the β-NMR apparatus. The well-established method of β-NMR/NQR spectroscopy[4)] in combination with the adiabatic fast passage technique[5)] was used to measure the anticipated change in the EFG around the 210–230 K temperature region.

In order to record a successful β-NQR measurement, it is important to know the EFG orientation throughout the sample. For this purpose, the present sample of the single-crystal CuO has been studied using scanning electron microscope imaging, before being placed in the experimental setup so that the main component of the EFG is parallel to the static magnetic field. The β-NQR measurements of the EFG have been obtained at different temperatures in the multiferroic phase region, as well as at 100 K and at room temperature.

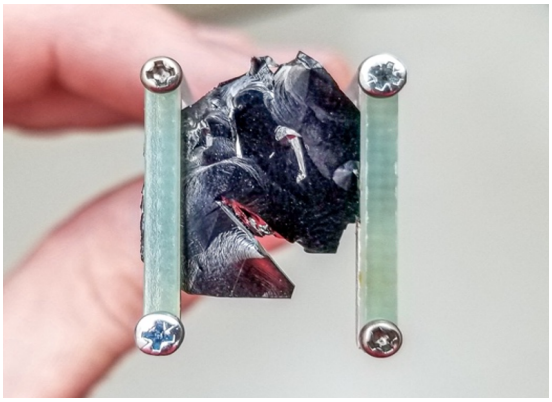

Fig. 1. An image of the sample of single-crystal CuO used in the present experiment.

Unlike the ^{21}O β-NMR measurements for the TiO_2 crystal, where a prominent resonant spectrum was directly observed, no resonance could be distinguished from the measurements of the single-crystal CuO. The obtained β-NMR spectra require further comprehensive analysis to be able to determine the microscopic properties of CuO. This work is in progress and the results will be reported in due course.

*1 RIKEN Nishina Center
*2 Department of Physics, Kyushu University
*3 Center for Nuclear Study, University of Tokyo

References
1) T. Kimura *et al.*, Nat. Mater. **7**, 291 (2008).
2) A. Gladkov *et al.*, RIKEN Accel. Prog. Rep. **54**, 28 (2021).
3) Y. Ishibashi *et al.*, Phys. Rev. C **107**, 024306 (2023).
4) D. Nagae *et al.*, Nucl. Instrum. Methods Phys. Res. B **266**, 4612 (2008).
5) A. Abragam, *The Principles of Nuclear Magnetism* (Clarendon, Oxford, 1961).

Precise measurement of diffraction structures in capillary laser sight for ion microbeam irradiation to mammalian cells

M. Kurino,[*1,*2] T. Ikeda,[*2,*1] K. Inayoshi,[*1,*2] R. Otani,[*1,*2] and W. -G. Jin[*1]

Glass capillary optics has been utilized in emitting ion microbeam (μm-order diameter) irradiation to single mammalian cells and *Escherichia coli* cells at the RIKEN Pelletron accelerator facility in the Nishina R&D Building.[1)] The typical ion energy is a few MeV whose range in water is from 10 to 100 μm for a H ion and approximately 10 μm for a He ion. The ranges are close to cell sizes, and are controlled with 1 μm resolution by selecting an appropriate initial energy. To avoid mis-hitting the target area in ion irradiation, a laser sighting operation will be performed[2)] prior to the ion shooting, which is realized by a dual-microbeam capillary optics method. However, the micrometer-sized spot of the laser-sight encompasses not only the center spot but also surrounding ring structures, which causes a larger laser spot and increases the mis-hitting probability. Here, we report a new precise laser spot mapping method and analyze the decomposition of the diffraction pattern. Figure 1 shows the experimental setup implemented at Toho University. A laser beam from an Ar^+ laser source enters the glass capillary optics. A digital camera equipped with a transmissive screen or power meter probe was located at a distance of 65–70 mm downstream of the capillary outlet. Figure 2(a) depicts a typical ring pattern taken by the camera, showing the center spot, thin rings, and bright ring groups. We aim to investigate (1) the origin of the thin rings, (2) dependence of the diameters of the 1st and 2nd bright ring groups on capillary outlet size a, and (3) power ratio of each group. Accordingly, a power meter probe with a 70 $\mu m\phi$-aperture was newly installed to measure the absolute value of power density driven by a 2-dimentional high position-resolution (0.5 μm) stage. The green curve with dots connected by lines depicted in Fig. 2(b) denotes the measured power density along a horizontal line including the

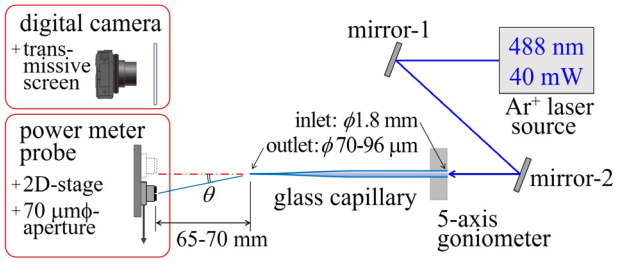

Fig. 1. Setup of the laser microbeam profile measurement.

*1 Department of Physics, Toho University
*2 RIKEN Nishina Center

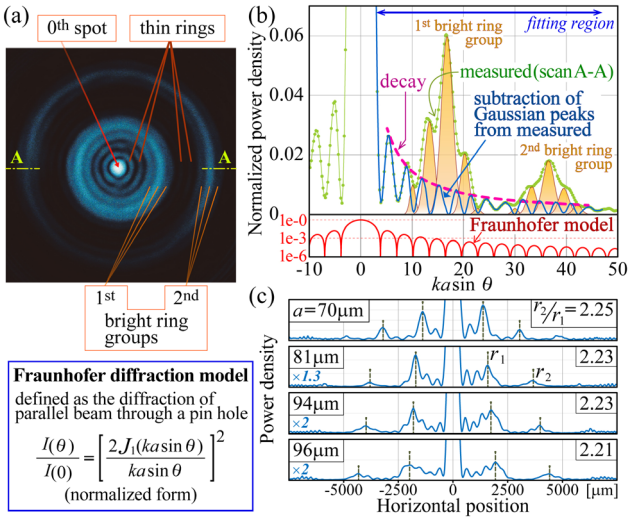

Fig. 2. (a) Photo of typical ring pattern. (b) Power density as a function of $ka\sin\theta$, showing measured (green) and fitted Gaussian peaks (orange), as well as Fraunhofer diffraction model in a logarithmic scale (red). (c) Comparison of the ring diameters according to the outlet size a.

spot center defined in Fig. 2(a) for a capillary with $a = 94$ μm. Horizontal axis is in the unit of $ka\sin\theta$, where k is wave number and θ is the probe angle in Fig. 1. Each Gaussian peak comprises more than 10 measurement points, which are large enough to use fitting methods. The thin rings in Fig. 2(a) are assumed to extend beyond the 2nd bright ring group. However, the spread is hidden behind the bright rings. To remove the bright rings from the green curve, they were expressed as 5 and 3 Gaussian peaks, and the shapes were determined by fitting. The solid blue curve represents the result of subtracting of the Gaussian peaks (orange) from the green curve. The fitting did not impose a Fraunhofer condition; however, the oscillation period of the blue curve is the same as that of the Fraunhofer model (red). Although the decay of the (dashed) curve seems to be slower than that of the red curve, the behavior of blue curve including the center spot is similar to a Fraunhofer model. The slow decay might be due to the focused light beam inside the capillary body. Using the precise peak positions of the bright ring groups, it was found that the diameters of the groups increase with a (Fig. 2(c)), while the ratios of the diameters of 2nd to 1st groups remains constant with respect to a. The power ratios of 0th, 1st, and 2nd groups were also obtained. The

ratio of the 0th spot was 37% of the entire spot for $a = 96$ μm. However, a ratio of 62% was achieved for smaller $a = 70$ μm. This means a smaller microbeam has less power of bright ring groups. In conclusion, the thin rings originate in the Fraunhofer diffraction at the outlet. To obtain a high-contrast laser microspot with smaller bright ring groups, it is necessary to use the capillaries with smaller outlets.

References

1) T. Ikeda, Quantum Beam Sci. **4**, 1 (2020).
2) K. Inayoshi *et al.*, RIKEN Accel. Prog. Rep. **55**, 107 (2022).

2. Atomic and Solid State Physics (Muon)

DFT investigations on magnetic properties with Muon in La_2CuO_4 using LSDA + U functional

S. Charoenphon,[*1,*2] P. Reunchan,[*1] and I. Watanabe[*2]

Lanthanum cuprate (La_2CuO_4, LCO) is a typical Mott insulator exhibiting a strong covalent state of Cu-3d with O-2p within the two-dimensional (2D) CuO_2 plane. In a previous study, LCO has been well investigated experimentally and theoretically; however, questions regarding electromagnetic states remain unanswered. The primary concern is the on-site Coulomb potential, U, and the covalent state of the electronic orbitals of Cu. The muon spin resonance technique (μSR) can provide information on local magnetic fields at the muon site. However, obtaining the muon effect in the structure.[5)] In this study, we apply the density functional theory (DFT) + U to comprehensively investigate the electronic structure surrounding the muon. Our attempt to solve the problem within the DFT framework has yielded mixed results. Notably, most studies have attempted to correct the antiferromagnetic (AFM) ground state model of LCO and have failed to provide a handle on the key experimentally observed properties of LCO. More specifically, the local-spin-density approximation (LSDA) incorrectly predicts LCO to be nonmagnetic (NM) metals in complete disagreement with the experimental value. The generalized gradient approximation (GGA) produces a weak AFM. Thus, the development of methods that have stronger electron correlations to stabilize the AFM ground state is necessary. DFT + U is a method that was proposed to improve the strong correlation system.[6)] Among the most implemented methods in the DFT + U realm is the LSDA + U method.

The DFT calculation was performed using the RIKEN-integrated HOKUSAI Supercomputing Facility. Ab initio calculations were performed in the Vienna ab initio simulation package (VASP) with an energy cutoff of 400 eV for the plane-wave basis set. We employed the Hubbard parameter U = 4.87 eV.[4)] We use a 28-atoms primitive cell with a $6\times6\times3$ Γ-centered k-point mesh for the Brillouin zone integrations to calculate the fundamental properties of LCO shown in Fig. 1(a). In addition, a supercell structure containing 252 atoms ($3\times3\times1$ unit cell) was adopted for a calculation to consider the effect of the relaxation of muon position.

The lattice parameters calculated based on LSDA + U, band gap, and magnetic moment are listed in Table 1. The experimental values. The calculated bandgap was obtained as 1.15 eV, slightly higher than the experimental value of 1 eV.[3)] Next step, the LSDA + U was conducted, including the muon, to reproduce the μSR results. We estimate the initial position of muon injection in LCO obtained from the electrostatic potential. There are three possible local minimum potential positions that the muons can stop in a structure: M1, M2, and M3 as shown in Fig. 1(c), compared with muon spin resonance technique μSR results.[4,5)] Our method is fundamentally similar to the GGA functional method[4)] except for the difference in the functional. This is important for investigating the effect of the difference in the functional in the previous result.

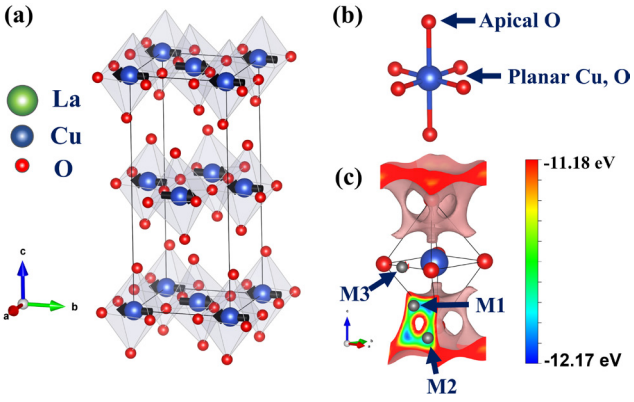

Fig. 1. (a) Crystal structure of LCO in the LTO phase with copper, oxygen, and lanthanum atom indicated as blue, red, and green spheres, respectively. (b) Schematic of a CuO_6 octahedral showing the O apical site and Cu, O in the planar site. (c) Electrostatic potential calculation result. The grey sphere indicates three local-minimum potential positions as candidates for initial muon-stopped positions.

Table 1. Calculation of structural parameter, band gap, and magnetic moment of a unit cell of LCO.

Function	Lattice parameter			The band gap (eV)	Magnetic moment (μ_B)
	a	b	c		
Exp.	5.357[1]	5.406[1]	13.143[1]	1[3]	0.48 ± 0.15[2]
LSDA+U	5.196	5.246	12.903	1.15	0.469

The final muon position and local deformations of the crystal structure estimated from our LSDA + U + μ calculations are shown in Fig. 2. We calculated the magnetic moment of Cu without muon to be 0.450 μ_B. Following relaxation, the magnetic moment calculation of Cu changed to 0.414, 0.453, and 0.449 μ_B for M1, M2, and M3, respectively.

*1 RIKEN Nishina Center
*2 Department of Physics, Kasetsart University

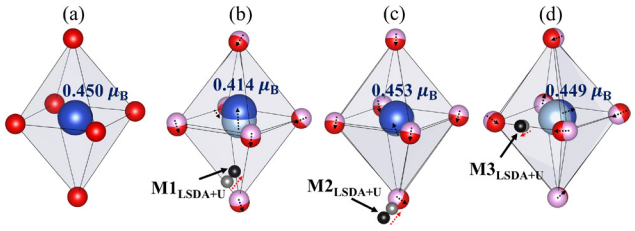

Fig. 2. (a) Structure of LCO without muon. The final muon position after relaxation for (b) M1, (c) M2, and (d) M3, respectively. The Grey spheres indicate the initial position. The black spheres indicate the final position of the muon after relaxation.

In conclusion, the role of muon perturbation was found to deform the local crystal structure in the immediate vicinity of the muon. This effect resulted in a slight reduction in the magnetic moment surrounding the muon. Moreover, a new result is that LSDA + U is clearly proven to be not suitable for describing the electronic state of a strongly correlated system, particularly LCO.

References

1) M. Reehuis *et al.*, Phys. Rev. B **73**, 144513 (2006).
2) D. Vaknin *et al.*, Phys. Rev. Lett. **58**, 2802 (1987).
3) S. Uchida *et al.*, Phys. Rev. B **43**, 7942 (1991).
4) R. Ramadhan *et al.*, Phys. Rev. R **4**, 033044 (2022).
5) J. S. Möller *et al.*, Phys. Scr. **88**, 068510 (2013).
6) M. Yu *et al.*, npj Comput. Mater. **6**, 180 (2020).

The effect of particle size on magnetic properties regarding La_2CuO_4 nanoparticles

A. E. Putri,[*1,*2] B. Kurniawan,[*2] and I. Watanabe[*1]

The nano size effect is an interesting physical phenomenon because it shows unique properties compared to those observed in a bulk condition. One example is the gold (Au). When the particle size of Au was reduced to be in the nano-scale size, ferromagnetic behavior was observed, whose origin is still unknown.[1] Changes in magnetic properties due to particle size reductions were also observed in the La-based high-T_c superconducting oxide, $La_{2-x}Sr_xCuO_4$ (LSCO).[2] Synthesizing LSCO nanoparticles experiences numerous difficulties regarding the control of defects and impurities.[3] Thus, an investigation to optimize sample preparation is a prerequisite.

The La_2CuO_4 (LCO), a parental compound of LSCO exhibiting antiferromagnetic Mott insulator behavior at $T_N \approx 300$ K,[4] will be investigated considering a nano-size particle. LCO nanoparticle were synthesized using sol-gel method with lanthanum oxide, La_2O_3 (99.99%), and cooper oxide, CuO (99.99%), as a raw material similar to a previous research.[5] Particles size of LCO can be controlled by varying the sintering temperature at 650°C, 700°C, 750°C, 800°C, and 1100°C over 6 hours which produce 43 nm, 54 nm, 70 nm, 90 nm, and 161 nm particle size, respectively. Rietveld refinement method is used to analyze the X-ray diffractometer (XRD) pattern, which exhibit an orthorhombic crystal structure with Bmab-space group. Small impurities were detected at the lowest sintering temperature of 650°C, which correspond to approximately 1.3% of La_2O_3 coming from the raw material. Because La_2O_3 has no magnetic component, the magnetic properties of this sample should not be affected. The LCO particle size (D) estimated using the Debye Scherrer method is express using the following equation:

$$D = \kappa\lambda/\beta\cos\theta \quad (1)$$

where κ is the Scherrer constant (0.9), λ is the wavelength of Cu-K_α (1.5406 Å) obtained from XRD measurements, β denotes the full width of half maximum intensity observed from XRD pattern and θ is the Braggs angle.

The La_2CuO_4 is composed of a basic unit of CuO_6 octahedron crystal structure, which has been thoroughly investigated in the past. Changing the particle size of LCO affects the antiferromagnetic transition temperature (T_N), as shown in Fig 1. Reducing the particle size of LCO up to 43 nm can decrease the T_N down to 65 K. This nano-size effect was also investigated on magnetic materials, such as CuO. Accordingly, it was reported that the Néel temperature, T_N, of CuO could be reduced from 290 K down to 40 K when CuO particle size was reduced to approximately 5 nm.[6] Those studies indicated that the magnetic exchange interaction would be affected by the reduction of particle size.

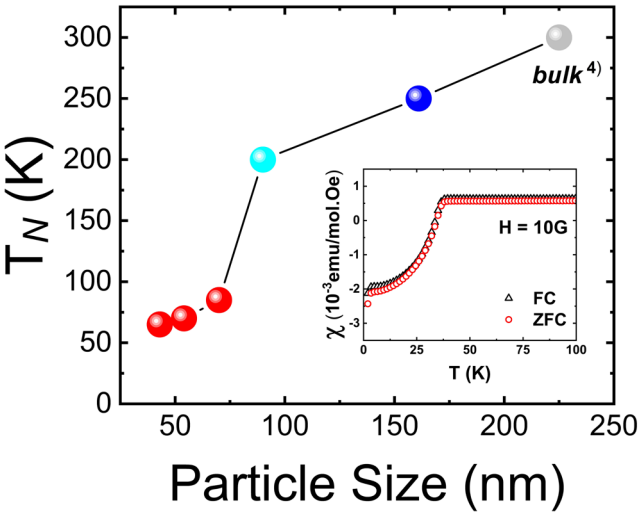

Fig. 1. Particle size dependance of the antiferromagnetic transition temperature, determined from the χ measurement at 0.0001 T with zero field cooled method using Superconducting Quantum Interference Device (SQUID) magnetometer MPMS. The insert figure demonstrates the temperature dependance of magnetic susceptibility for sample A.

The largest particle size exhibits a superconducting state below 40 K, which corresponds to the transition temperature of LSCO doped with 15% strontium.[2] The antiferromagnetic long-range order was suppressed and superconductivity occurred owing to the excess oxygen inside the LCO sample,[7] which led to the phase separation of partial superconductivity. Interestingly, reducing the particle size of LCO down to nano-size suppressed the superconductivity behavior below 40 K, which occurred owing to the excess oxygen. Otherwise, magnetic susceptibility of LCO nanoparticle below 50 K can be fit using Curie-Weiss equation, showing that the magnetic free spins increase by decreasing the particle size.

*1 RIKEN Nishina Center
*2 Department of Physics, Universitas Indonesia

References

1) Y. Yamamoto *et al.*, Phys. Rev. Lett. **93**, 116801 (2004).
2) Y. Yin *et al.*, Phys. Chem. C **117**, 3028 (2013).
3) S. Winarsih *et al.*, Mater. Sci. Forum **966**, 357 (2019).
4) P. A. Lee, *et al.*, Rev. Mod. Phys. **78** (2006).
5) A. E. Putri *et al.*, Mater. Sci. Forum **1028**, 44 (2021).
6) X. G. Zheng *et al.*, Phys. Rev. B **72**, 014464 (2005).
7) Y. Okajima *et al.*, Physica C **282–287**, 1319 (1997).

Sample synthesis of $Nd_2Ru_2O_7$ for researches by using quantum beams

M. A. Syakuur,[*1] U. Widyaiswari,[*1] and I. Watanabe[*1]

The pyrochlore system, $A_2B_2O_7$, is a frustrated magnet with corner-sharing crystal structure.[1] Frustrated is defined as a condition where a system cannot minimize its total energy.[1] Frustration caused by the lattice geometry in the crystal structure is classified as geometrical frustration.

There are a series of $A_2B_2O_7$ shows a variety of unique electronic states. Among them, an interesting example but not yet well studied is $Nd_2Ru_2O_7$, which shows a magnetic fragmentation state with a monopole or multipole state at the A site.[2] This system has the Kramer's ion Nd at the A site and the 4*d* element Ru with a magnetic moment at the B site. The Ru magnetic moment shows a magnetic ordering below 145 K and the Nd magnetic moment indicates an ordered state as well below 2 K.[2] An anomaly in the temperature dependence of the magnetic susceptibility was reported to be approximately 25 K. The origin of this anomaly was not clear and show the sample dependence.[3]

Mother materials of Nd_2O_3 and RuO_2 were used to synthesize $Nd_2Ru_2O_7$. Hence the chemical reaction efficiency between Nd and Ru is not so good and the vaporization temperature of those elements is different, it is not so easy to obtain a single-phase sample even for a powder one.

Furthermore, a single crystal is necessary to investigate the magnetic fragmentation and the monopole/multipole states. This has not yet been achieved yet until now due to those difficulties of the sample synthesis. We are now trying to develop the sample synthesis method to get a single-phase powder sample which is necessary for the single crystal growth.

We mixed the mother powder samples as much as possible by using a ball mill and adjusted the sintering temperature and atmospheric gases, and we confirmed that the anomaly observed around 25 K was due to Nd_3RuO_7 which showed a ferromagnetic ordering.[3]

Figure 1(a), the results of the X-ray diffraction measurement show that there is no other phase besides $Nd_2Ru_2O_7$ for a mixing time of 12 hours. While the mixing time using a ball mill for 6, 24, or 96 hours gives rise to other phases besides $Nd_2Ru_2O_7$.

Figure 1(b), the temperature dependence of susceptibility graph, χ, shows a transition at 145 K which corresponds to the magnetic transition of Ru^{4+} moments of $Nd_2Ru_2O_7$ as reported in previous studies.[2–5] This magnetic transition temperature decreases, with increasing ball mill time which is not good to maintain a single phase sample. In this 12 hours ball mill sample, we confirmed that there is no anomaly peak around 25 K which corresponds to other phases, namely Nd_3RuO_7.[3]

By using this single phase sample, a single crystal synthesis process will then be carried out using the floating zone method, Bridgman technique, and the complete sealed sample cell with high temperature synthesis for researches by using quantum beams such as neutron and muon spin relaxation (μSR).

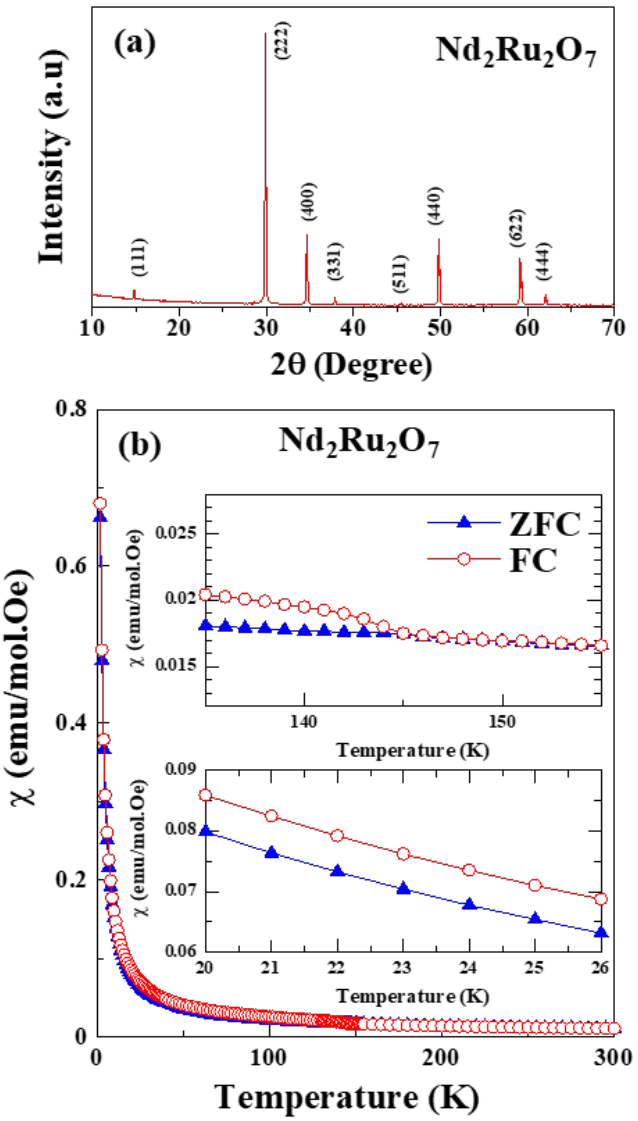

Fig. 1. (a) X-ray diffraction patterns of $Nd_2Ru_2O_7$. (b) Temperature dependence of the magnetic susceptibility, χ, measured from 2 to 300 K at $H = 0.1$ kOe.

References

1) J. S. Gardner *et al.*, Rev. Mod. Phys. **82**, 53 (2010).
2) S. T. Ku *et al.*, J. Phys. Condens. Matt. **30**, 155601 (2018).
3) Utami *et al.*, Mater. Sci. Forum **1028**, 3 (2021).
4) M. Gaultois *et al.*, J. Phys. Condens. Matt. **25**, 186004 (2013).
5) N. Taira *et al.*, J. Solid State Chem. **152**, 441 (2000).

*1 RIKEN Nishina Center

Probing internal fields induced by Ru and Nd spin ordering on $Nd_2Ru_2O_7$ using continuous muon beam

U. Widyaiswari,[*1,*2] H. Sakai,[*3] N. Hanasaki,[*3] and I. Watanabe[*1,*2]

Pyrochlore oxides have the general formula $A_2B_2O_7$ (A = trivalent rare-earth ion; B = tetravalent transition metal ion), with corner-sharing tetrahedral lattice networks of A and B sites.[1] The magnetic frustration, competition between the exchange and dipolar interactions, and crystal electric field effect control the nature of the ground state of the pyrochlore oxide.[2]

Nd pyrochlores have been intensively investigated owing to their exotic properties exhibiting the coexistence of static ordering and the dynamic behavior of Nd spin.[3–5] $Nd_2Ru_2O_7$ is a stable Nd pyrochlore, in which both Nd and Ru are magnetic ions. The magnetic ground state of $Nd_2Ru_2O_7$ is interesting from the perspective of research, as we may investigate the coupling between Nd and Ru spins and how it affects the coexistence of static and dynamic Nd spins. $Nd_2Ru_2O_7$ exhibits a magnetic transition around 1.8 and 146 K, corresponding to the ordering of Nd and Ru spins, respectively.[6–8] In addition to macroscopic measurements using, for example, the Magnetic Properties Measurement System (MPMS), the magnetic properties of $Nd_2Ru_2O_7$ were investigated using a local magnetic probe such as muon spin relaxation (μSR) measurement. We explore the ordering of both Ru and Nd spins using μSR and determine the internal field induced by the ordered spins.

Polycrystalline $Nd_2Ru_2O_7$ was prepared using a solid-state reaction method. From previous μSR measurements using a pulsed muon beam, we confirmed the ordering of Ru and Nd spins based on the decrease in the initial asymmetry.[9] The decrease in the initial asymmetry indicates fast muon spin precession in the early time spectra. The expected internal field surrounding the muon-stopping site is higher than 500 G, beyond the time window of the pulsed muon beam. Therefore, a continuous muon beam is necessary to determine the internal field induced by the ordering of Ru and Nd spins. In this report, we present the μSR data obtained using a continuous muon beam on the DOLLY and GPS spectrometers at Paul Scherrer Institute (PSI), Switzerland. We measured the μSR time spectra in the zero-field (ZF) condition in the temperature range of 2–250 K on GPS, whereas the time spectra below 3 K down to 0.3 K were obtained on DOLLY.

Figure 1(a) and (b) display the ZF-μSR time spectra. The appearance of the Ru order state was confirmed by the appearance of muon spin precession below 145 K. Below 120 K, a beating pattern appears in the oscillating time spectra, indicating two frequencies of muon spin precession associated with the two internal fields. The origin of these two internal fields might be attributed to two muon-stopping sites or two sources of the field. Because at a high-temperature range, only the Ru spins were ordered, the internal fields were attributed to the two muon-stopping sites. A linearity exists between the two internal fields down to 2 K. Below 2 K, one frequency becomes more prominent than the other one, and the linearity of these two fields is broken. The enhancement of the internal field below 2 K might be related to the ordering of Nd spins.

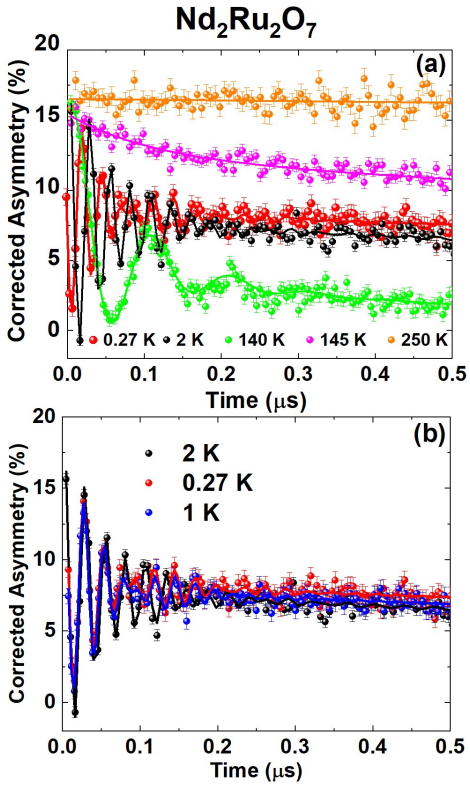

Fig. 1. (a) ZF-μSR time spectra of $Nd_2Ru_2O_7$ from 250 K down to 0.27 K. (b) ZF-μSR time spectra of $Nd_2Ru_2O_7$ below 2 K indicates a change in the frequency of the muon spin precession.

*1 RIKEN Nishina Center
*2 Department of Condensed Matter Physics, Hokkaido University
*3 Department of Physics, Graduate School of Science, Osaka University

References
1) J. S. Gardner *et al.*, Rev. Mod. Phys. **82**, 53 (2010).
2) B. C. Dem Hertog *et al.*, Phys. Rev. Lett. **84**, 3430 (2000).
3) J. Xu *et al.*, Phys. Rev. B **94**, 064425 (2016).
4) S. Petit *et al.*, Nat. Phys. **12**, 746 (2016).
5) V. K. Anand *et al.*, Phys. Rev. B **95**, 224420 (2017).
6) S. T. Ku *et al.*, J. Phys. Condens. Matt. **30**, 155601 (2018).
7) M. W. Gaultois *et al.*, J. Phys. Condens. Matt. **25**, 186004 (2013).
8) U. Widyaiswari *et al.*, Mater. Sci. Forum **1028**, 3 (2021).
9) U. Widyaiswari *et al.*, RIKEN Accel. Prog. Rep. **55**, 110 (2022).

Magnetic short-range order in a hyperkagome lattice alloy Mn_3CoSi

D. P. Sari,[*1] H. Yamauchi,[*2] A. E. Hall,[*3] K. M. Kojima,[*4] D. Arseneau,[*4] G. Morris,[*4] B. Hitti,[*4] A. Berlie,[*5] I. Watanabe,[*6] P. -T. Hsu,[*7] Y. -S. Chen,[*8] M. K. Lee,[*7] B. Geetha,[*3] L. -J. Chang,[*7,*9] and S. Shamoto[*7,*10,*11]

We found a magnetic short-range order (SRO) in a hyperkagome lattice alloy of Mn_3RhSi up to 720 K.[1] The onset temperature is the highest among any magnets, to our knowledge. Because of the historical record, the magnetic cluster may be topologically protected in a paramagnetic state. To reveal the possible mechanism, we have studied Mn_3TX (T: Co, Rh, and Ir, X: Si and Ge) family alloys by μSR, where the cubic lattice parameter varies together with the electronic bandwidth. The lattice parameter of Mn_3CoSi is close to that of β-Mn, which is known as a non-Fermi liquid and spin-liquid candidate compound.[2,3] The β-Mn is also the heavy electron metal (γ = 70 mJ/Mn K^2).[3] Mn_3CoSi with the smallest cubic lattice parameter (a = 6.26 Å) locates near the quantum critical point, then with increasing the cubic lattice parameter, the magnetic transition temperature increases, and the electronic specific heat γ decreases in the Mn_3TX system. In the case of Mn_3RhSi with a lattice parameter of $a = 6.45$ Å, the Néel temperature T_N becomes 190 K and γ decreases to 12.1 mJ/Mn K^2. Our magnetic pair distribution function analysis revealed that the magnetic SRO originated from the other magnetic structure different from the long-range order (LRO) magnetic structure.[4] In addition, a similar magnetic SRO is recently discovered in a skyrmion alloy $Co_7Zn_7Mn_6$ with the same β-Mn structure.[5]

Here, we report the μSR result of the single crystal Mn_3CoSi measured at M20 of TRIUMF (M2201) and ARGUS of ISIS (2070006). The transverse field (TF) time spectra of Mn_3CoSi were analyzed using a Gaussian damped oscillation function. The temperature dependence in Fig. 1 clearly shows the drop in the initial asymmetry. The onset temperature is about 240 K. Figure 2 shows the phase diagram of the Mn_3TSi system. The result suggests that SRO and LRO temperatures decrease to a quantum critical point. In addition, the initial asymmetry drop also decreases to the quantum critical point. The ratios were about 20% and 1% for Mn_3RhSi and Mn_3CoSi, respectively.

In summary, we have studied Mn_3CoSi crystal by μSR. The SRO and LRO temperatures depend on the lattice parameter, suggesting the bandwidth effect. To further explore the magnetic SRO, it is necessary for us to study Mn_3IrSi with a lattice parameter of $a = 6.50$ Å by μSR. These alloys have spiral structures of Mn triangular units, resulting in the noncentrosymmetric space group. Neutron scattering measurements may be required to study further the magnetic SRO related to a topological magnetic cluster by using single crystals. We acknowledge the present μSR measurements at M20 of TRIUMF (M2201) in 2022 and ARGUS of ISIS (2070006) in 2020.

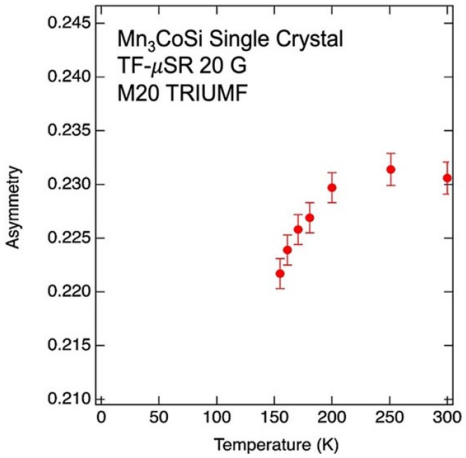

Fig. 1. Initial asymmetry obtained from the Mn_3RhSi single crystal under a transverse magnetic field of 20 G.

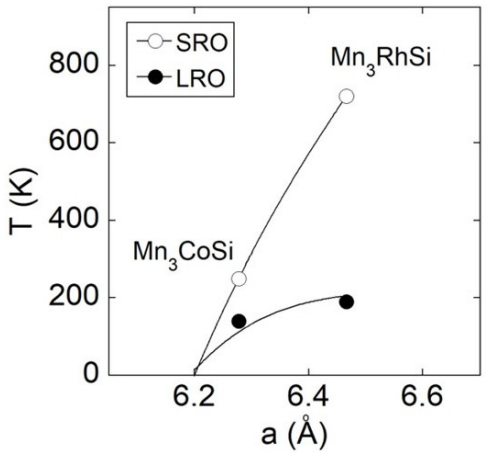

Fig. 2. Tentative phase diagram of Mn_3TSi system.

*1 Department of Physics, Shibaura Institute of Technology
*2 Material Science Research Center, Japan Atomic Energy Agency
*3 Department of Physics, University of Warwick
*4 Physical Sciences Division, TRIUMF
*5 RAL, ISIS
*6 RIKEN Nishina Center
*7 Department of Physics, National Cheng Kung University
*8 National Synchrotron Radiation Research Center (NSRRC)
*9 Institute of Physics, Academia Sinica Academia Sinica
*10 Comprehensive Research Organization for Science and Society (CROSS)
*11 Advanced Science Research Center, Japan Atomic Energy Agency

References

1) H. Yamauchi *et al.*, Commun. Math. Phys. **1**, 43 (2020).
2) J. R. Stewart *et al.*, Phys. Rev. Lett. **89**, 186403 (2002).
3) H. Nakamura *et al.*, J. Phys. Condens. Matt. **9**, 4701 (1997).
4) K. Kodama *et al.*, J. Phys. Soc. Jpn. **90**, 074710 (2021).
5) V. Ukleev *et al.*, npj Quantum Mater. **6**, 40 (2021).

TF-μSR study of $YbCu_4Ni$

T. Taniguchi,[*1] K. Osato,[*1,*2] H. Okabe,[*1] J. Nakamura,[*3] A. Koda,[*3] and M. Fujita[*1]

Several examples of quantum critical phenomena have been reported in f electron systems.[1] The reason is that the energy scale is so small that it can be controlled by the pressure and magnetic field generated in a laboratory system. Thus, it is an ideal situation for investigating quantum critical phenomena as a whole. However, there are few examples of materials near the quantum critical point at ambient pressure and zero magnetic field. Therefore, the search for such materials is a significant challenge..

We focused on $YbCu_4Ni$, which has a large electronic specific heat coefficient.[2] Recently, we have succeeded in synthesizing pure materials. We have also succeeded in using $YbCu_4Ni$ as a magnetic refrigeration material by exploring its large electronic specific heat coefficient.[3] However, there are two possible origins of the large value: (i) Kondo disorder, (ii) quantum criticality. To determine the actual origin, we performed TF-μSR experiments.

The purpose of this study is to determine the origin of the large electronic specific heat coefficient of $YbCu_4Ni$. The linewidth of the μSR spectrum increases with a decrease in the temperature when the Kondo disorder is dominant, as noted in previous studies on UCu_4Pd,[4,5] $CeRhRuSi_2$,[6] and $YbRh_2Si_2$.[7] To obtain the information on $YbCu_4Ni$, we compared the μSR spectra at 10 K and 35 mK under TF-300 G. The μSR measurements were performed with a dilution refrigerator using the D1 μSR spectrometer at Materrials and Life Science Experimental Facility (MLF) in J-PARC, Japan. The powder sample was placed on a silver plate and covered with silver foil.

Figure 1 shows the 10 K and 35 mK μSR spectra; the spectrum at 35 mK is narrower than that at 10 K. This rejects the main magnetic contribution of the Kondo disorder. Therefore, we determined that $YbCu_4Ni$ is a quantum critical material. Previous studies on $YbCu_{5-x}Au_x$ reported that the smaller the lattice constant, the closer to the quantum critical point.[8–12] However, it is difficult to syntheize the samples with small value of x because of the change in crystal structure at ambient pressure. Because $YbCu_4Ni$ has a smaller lattice constant than these samples, the quantum criticality may be observed at ambient pressure and zero magnetic field.

In this study, we performed TF-μSR experiments to investigate the origin of the large electronic specific heat coefficient of $YbCu_4Ni$. The spectrum at 35 mK was observed to be narrower than that at 200 K, suggesting that $YbCu_4Ni$ has a quantum criticality. In future studies, we will determine the origin of quantum criticality by synthesizing pure single crystals and determining the band structure. Further, μSR measurements will be carried out in collaboration with KEK and RIKEN groups.

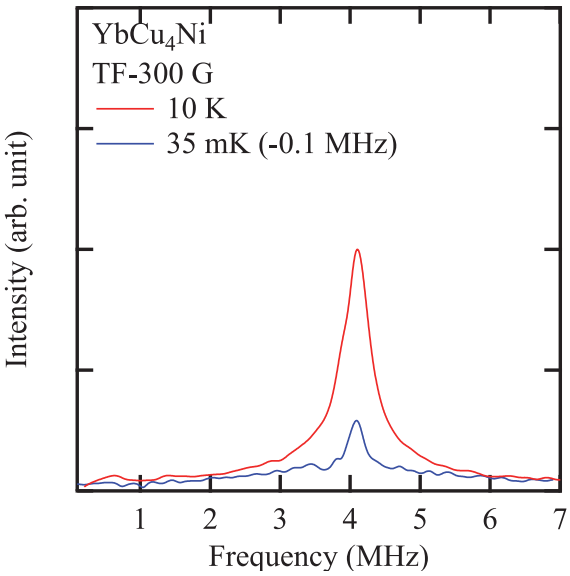

Fig. 1. μSR spectra of $YbCu_4Ni$ at 10 K and 35 mK.

We thank I. Watanabe from RIKEN and D. P. Sari from College of Engineering Shibaura Institute of Technology for stimulating discussions. The μSR measurement at the Materials and Life Science Experimental Facility of J-PARC (Proposal No. 2022A0064) was performed under user program.

References

1) G. R. Stewart, Rev. Mod. Phys. **56**, 755 (1984).
2) J. G. Sereni *et al.*, Phys. Rev. B **98**, 094420 (2018).
3) Y. Shimura *et al.*, J. Appl. Phys. **131**, 013903 (2022).
4) D. E. MscLauglin *et al.*, Phys. Rev. B **58**, R11849(R) (1998).
5) D. E. MscLauglin *et al.*, Physica B **289-290**, 15 (2000).
6) C. -Y. Liu *et al.*, Phys. Rev. B **61**, 432 (2000).
7) K. Ishida *et al.*, Phys. Rev. B **68**, 184401 (2003).
8) K. Yoshimura *et al.*, J. Alloys Compd. **317-318**, 465 (2001).
9) M. Giovannini *et al.*, Intermetallics **16**, 399 (2008).
10) P. Carretta *et al.*, Phys. Rev. B **79**, 020401(R) (2009).
11) I. Čurlik *et al.*, Phys. Rev. B **90**, 224409 (2014).
12) M. Giovannini *et al.*, J. Alloys Compd. **627**, 20 (2015).

*1 Institute for Materials Research, Tohoku University
*2 Department of Physics, Tohoku University
*3 Institute of Materials Structure Science, KEK

μSR study of slightly pressurized organic superconductor κ-$(ET)_4Hg_{2.89}Br_8$, II

D. P. Sari,[*1,*2] Y. Cai,[*3,*4] K. Kojima,[*3,*4] I. Watanabe,[*2] Y. Ishii,[*1] and H. Taniguchi[*5]

The hole-doped organic superconductor κ-$(ET)_4Hg_{2.89}Br_8$, (κ-HgBr), where bis (ethylenedithio) tetrathiafulvalene is abbreviated as ET, is a key to bridge the knowledge gap between half-filled organics and doped cuprate systems. Both κ-HgBr and cuprate superconductors exhibit a peculiar metallic state at high temperature and pressure where their resistivity exhibits a linear temperature dependence, $\rho \propto T$; this is non-Fermi-liquid (FL) behavior. In κ-HgBr, this non-FL region gradually changes to the FL state by owing to pressure,[1,2] similar to the change in metallic state from optimally doped to overdoped cuprates. A heat capacity study suggested that the enhanced antiferromagnetic fluctuations toward low-temperature cause the non-FL behavior of κ-HgBr.[3] This evidence may locate the superconducting κ-HgBr state near the quantum critical point in between the FL and localized states; incoherent conductivity was observed in its non-FL state.[1,2] In this region, low superfluid density was proposed by the macroscopic measurement.[4]

Our zero-field μ^+SR experiment indicated that the relaxation rate from a temperature of approximately 10 K down to 0.3 K is temperature-independent.[5] This is consistent with a superconducting state that preserves time-reversal symmetry. Furthermore, we measured the transverse-field (TF) μ^+SR on ARGUS at the RIKEN-RAL/ISIS muon facility. There was almost no change in the 10 mT of transverse-field-μ^+SR time spectra at 0.3 K and above superconducting (SC) temperature $T_c = 4.6(3)$ K, indicating that the London penetration depth λ_{bc}, is longer than the order of micrometer, that is, low superfluid density. To confirm this result, measurements using ano-ther geometric setup are necessary to minimize the sample misalignment and determine the absolute value of λ_{bc}.

Further, we performed the μ^+SR experiment at the M15 beamline at TRIUMF. The μ^+ spin rotator was used so that the sample setup illustrated in Fig. 1 could be arranged. In all, 100 mg of the sample was used. The plate-like crystals we aligned so that the magnetic field is perpendicular to the conducting bc-plane. Using this setup on the M15 beamline, the crystal misalignment can be minimized, and larger TF 10 times higher than $H_{c1} = 25(5)$ Oe, which lies in the vortex solid regime[6] can be applied.

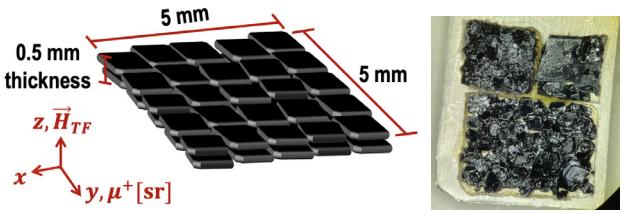

Fig. 1. Sample setup in the perpendicular mode μ^+[sr] stand for the muon beam with a spin rotator. In the perpendicular mode, the TF is applied perpendicular to the plate-like conducting plane. The right panel displays a photograph of the sample setup on top of Ag plate of the cryostat sample holder.

Furthermore, the bulk SC state must be confirmed. Therefore, we first measure the TF-μ^+SR upon zero-field cooling and compare the spectra above and below $T_c = 4.6(3)$ K. Figure 2 depicts the TF-μ^+SR time spectra measured at 0.3 and 10 K under 50 mT, respectively. The spectrum measured at 0.3 K was clearly damped compared to that at 10 K owing to the bulk SC state. The spectra were analyzed by applying the Gaussian-type-damped cosine equation (represented by lines in Fig. 2) as,

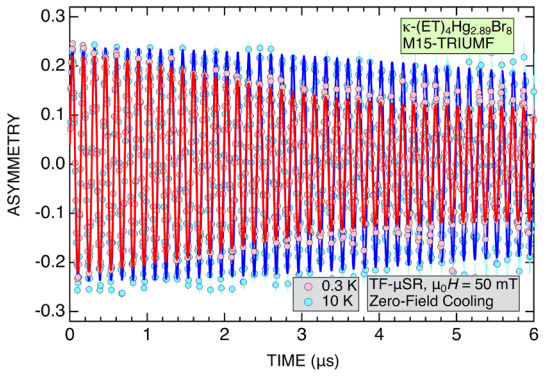

Fig. 2. TF-μ^+SR time spectra upon zero-field cooling in κ-HgBr. The pink and cyan circles represent TF-μ^+SR time spectra measured at 0.3 and 10 K, respectively. The red and blue solid lines represent the fitting lines for the 0.3 and 10 K data, respectively.

$$A(t) = A_1 \exp[-\sigma^2 t^2] \cos(\gamma_\mu B_1 t + \phi) + A_2 \cos(\gamma_\mu B_2 t + \phi), \quad (1)$$

where the first and second terms on the right-hand side

*1 College of Engineering, Shibaura Institute of Technology
*2 Meson Science Laboratory, RIKEN
*3 SBQM Institute, University British Columbia
*4 CMMS, TRIUMF
*5 Department of Physics, Saitama University

describe muon components from the sample and background, respectively. The damping rate σ at 0.3 K was determined as 0.53 μs^{-1}. The next step is to measure the temperature dependence of the London penetration depth in the vortex state under the field cooling condition.

References

1) H. Taniguchi *et al.*, J. Phys. Soc. Jpn. **76**, 113709 (2007).
2) H. Oike *et al.*, Nat. Commun. **8**, 756 (2017).
3) A. Naito *et al.*, Phys. Rev. B **71**, 054514 (2005).
4) K. Wakamatsu *et al.*, arXiv.2201.10714.
5) D. P. Sari *et al.*, J. Phys. Conf. Ser. **2462**, 012061 (2023).
6) D. P. Sari *et al.*, in *Materials Science Forum*, Vol. 966 (Trans Tech Publications Ltd., Sanur, Bali, Indonesia, 2019), p. 296.

3. Radiochemistry and Nuclear Chemistry

Extraction behavior of Nb and Ta in HF solution with F-form TOMA resin

S. Goto*1 and M. Higuchi*1

Elements with atomic numbers ≥104 are called superheavy elements. The purpose of Db chemistry research is to investigate the relativistic effects of orbital electrons, which are more pronounced in heavier elements. Furthermore, in the search for new elements, if the anchor nucleus (last nucleus in the observed decay chain) is a neutron-rich Db isotope, the chemical identity of the Db can determine the formation of the new element, because such isotopes have a relatively long half-life.

Group 5 elements, including Db in hydrofluoric acid, form fluorine-containing complexes very quickly, making this reaction system suitable for on-line chemical experiments with short-lived Db isotopes. However, group 5 elements may also form oxyfluoride complexes, thus a method to identify the chemical species is desired.[1] We have studied solid-phase extraction of Nb and Ta anion complexes from hydrofluoric acid using Aliquat 336-supported resin.[2] This extraction system differs from anion exchange in that the distribution coefficients of Nb is very different from Ta; however, the extracted chemical species are not yet clearly known. The resin used in this study was trioctyl methyl ammonium chloride (TOMA-Cl), one of the main components of Aliquat 336. The counter ions in Aliquat 336 and TOMA are generally chloride ions. In order to clarify the effect of chloride ions in solid-phase extraction with hydrofluoric acid, we prepared resins in which the chloride ion was replaced with an anion originating from the hydrofluoric acid, and investigated the extraction behavior of Nb and Ta.

Radiotracers, ^{95g}Nb ($T_{1/2}$ = 34.991 d) and ^{179}Ta ($T_{1/2}$ = 1.82 y), were produced with deuteron irradiation on Zr and Hf metallic foil targets with natural isotopic abundance, respectively, using the RIKEN K70 AVF cyclotron. The radiotracers in the targets were chemically isolated by anion exchange. The 40-wt% TOMA-Cl resin was prepared by mixing TOMA-Cl dissolved in methanol with MCI GEL CHP20/P30 for approximately 1 day.[3] To obtain Cl^- free F-type resin the TOMA-Cl resin was shaken well with 10 M HF, and then dried. A 400 μL of 1–27 M HF solution containing ^{95g}Nb and ^{179}Ta tracers was shaken with approximately 11 mg of TOMA resin for 1 h using a syringeless filter. After filtering the resin, the 250 μL solution was aliquoted and the radioactivity was measured with an HPGe detector. Aqueous solution control samples without resin were also measured to determine the radioactivity of the resin. The distribution coefficients K_d for ^{95g}Nb and ^{179}Ta were obtained from the following equation:

$$K_d = \frac{(A_{ini} - A_a)/m_r}{A_a/V_a}, \quad (1)$$

where the subscripts a and r represent the aqueous phase and the resin, respectively, for the radioactivity A, mass m, and volume V. A_{ini} is the radioactivity relative to the control sample.

According to the reported dissociation constant for hydrofluoric acid,[4] the anions originating from HF are mostly HF_2^- at the concentrationns of HF in this study. The dependence of K_d on the HF_2^- concentration is shown in Fig. 1. For both Nb and Ta, K_d was smaller in pure hydrofluoric acid than in the aqueous phase containing Cl^-. This may indicate a difference in the adsorption of Cl^- and HF_2^- on the resin. However, further investigation is needed because the formation of complexes containing Cl is also possible when Cl-form resins were used.

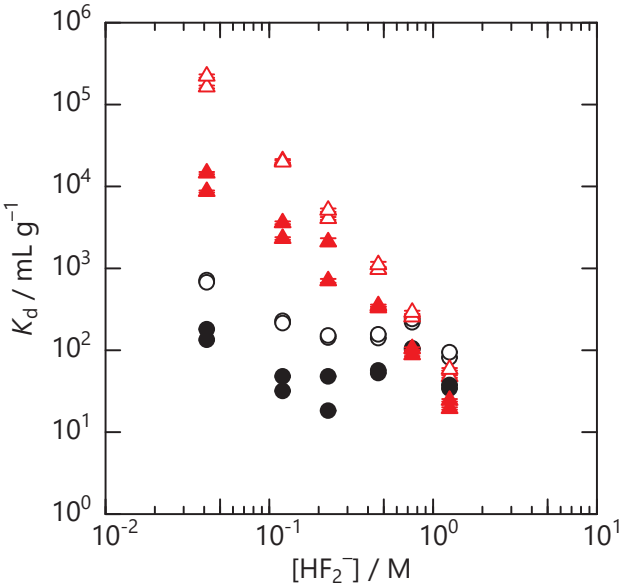

Fig. 1. Dependence of the distribution coefficients K_d for Nb (black) and Ta (red) on [HF_2^-] with F-type (solid symbols) and Cl-type (hollow symbols) TOMA resins.

*1 Graduate School of Science and Technology, Niigata University

References
1) O. L. Keller, Jr., Inorg. Chem. **2**, 783 (1963).
2) D. Sato *et al.*, RIKEN Accel. Prog. Rep. **50**, 246 (2017).
3) H. Haba *et al.*, Radiochim. Acta **95**, 1 (2007).
4) H. H. Broene *et al.*, J. Am. Chem. Soc. **69**, 1644 (1947).

Online solid-liquid extraction of ^{255}No with the polymer-supported crown ether

E. Watanabe,[*1,*2] R. Nakanishi,[*1,*2] S. Otaka,[*1,*2] R. Wang,[*1,*2] Y. Itakura,[*2,*3] R. Masuda,[*1,*2] Y. Shigekawa,[*2] A. Nambu,[*2] X. Yin,[*2] T. Yokokita,[*4] H. Haba,[*2] A. Shinohara,[*1,*5] and Y. Kasamatsu[*1,*2]

Nobelium (No) is an actinide element with an atomic number of 102. In aqueous solutions, No is considered to form a +2 valence state stably, while other f-block elements are stable at +3 or higher valence states. Previous ion-exchange experiments have reported that No exhibits similar chemical behavior to that of Ca^{2+} and Sr^{2+}.[1] Our group has recently demonstrated that No^{2+} shows different coprecipitation behavior from alkaline earth metal ions, using the samarium hydroxide coprecipitation method.[2] Further systematic studies are needed on No^{2+} compared with the group II elements from the viewpoint of molecular structure in the solution and its electronic structure.

We focus on solid-liquid extraction using the polymer-supported crown ether. The Sr resin (Eichrom Inc.) contains 4,4′ (5′)-di-tert-butylcyclohexano-18-crown-6 ether (DtBuCH18C6) and has strong extraction selectivity for Sr^{2+}. The selectivity of alkaline earth ion is affected by a changes in the acidity of a liquid phase and its concentration.[3,4] In the extraction in HNO_3 system, the extracted species of Sr is deduced to be $Sr(NO_3)_2$DtBuCH18C6.[5] Previously, we found that the extraction reaction of alkaline earth elements with the Sr resin rapidly (∼1 min) reached the equilibrium state and the solid-liquid extraction is suitable for ^{255}No experiment. We have obtained the distribution coefficients (K_d) of Ca, Sr, Ba, and Ra with the Sr resin in HNO_3, HCl, and $HClO_4$ as comparison data for No.

In this work, we performed online solid-liquid extraction experiments with ^{255}No to obtain its K_d values and to investigate the complexation between No^{2+} and DtBuCH18C6. To obtain the K_d values of No under equilibrium state, we used a batch-type solid-liquid extraction apparatus called AMBER.[6]

We produced ^{255}No ($T_{1/2}$ = 211 s) and ^{162}Yb ($T_{1/2}$ = 18.9 min) by the ^{248}Cm(^{12}C, $5n$)^{255}No and ^{nat}Gd(^{12}C, xn)^{162}Yb reactions with the AVF cyclotron at RIKEN. The reaction products were transported by the He/KCl gas-jet system to the chemistry room and dissolved in 3.5 MHNO_3 or 7.6 M HCl solutions. The solution sample was injected into a chemical reaction container containing the Sr resin. After shaking the container for 60 or 180 s, only the solution phase was discharged from the container through a PTFE filter. Subsequently, the discharged sample was evaporated to dryness and subjected to alpha particle measurement by the automated rapid α/SF detection system.

After α-particle measurement, we measured γ-ray activities of ^{162}Yb in the samples with Ge detectors to calculate the chemical yield of each extraction.

We carried out 48 extraction and 24 control cycles and observed a total of 173 α events from the decay of ^{255}No, as shown in Fig. 1. The production cross-section of ^{255}No was estimated to be approximately 500 nb, and the value is consistent with that determined in the previous report.[7] The half-life of ^{255}No was estimated to be 212±24 s, which is in good agreement with the previously reported value (211 ± 11 s).[8] The K_d value of ^{154,155}Er and ^{254,255}Fm (byproduct α-emitters) is ∼1 mL g^{-1}, which is within the value of other f-block elements previously reported.[4] Thus, it was demonstrated that the α events in the region of interest for ^{255}No in the α-particle spectrum properly originate from only ^{255}No and that reliable K_d values were obtained in the present solid-liquid extraction experiments using AMBER. The K_d values of No are under estimation.

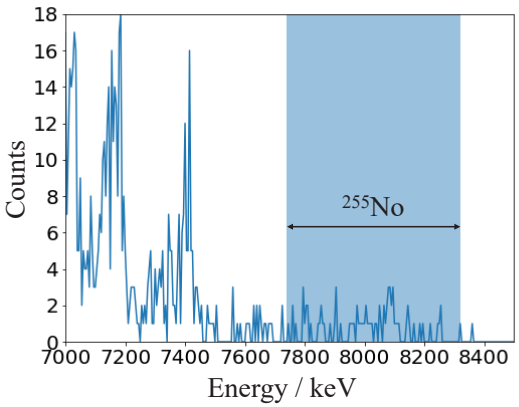

Fig. 1. α-spectrum for ^{255}No obtained in control experiment without the resin with 60-s shaking.

In the future, we will discuss the extraction behavior of No based on the comparison of the K_d values of ^{255}No with those of alkaline earth metal ions. Additionally, we will perform relativistic quantum chemical calculations and analyze the electronic states of extracted species of No.

*1 Graduate School of Science, Osaka University
*2 RIKEN Nishina Center
*3 School of Science, Osaka University
*4 Salesian Polytechnic
*5 Osaka Aoyama University

References

1) R. J. Silva *et al.*, J. Inorg. Nucl. Chem. **38**, 1207 (1976).
2) H. Ninomiya *et al.*, RIKEN Accel. Prog. Rep. **52**, 184 (2019).
3) E. P. Horwitz *et al.*, Solv. Extr. Ion Exch. **10**, 313 (1992).
4) D. V. Filosofov *et al.*, Solv. Extr. Ion Exch. **33**, 496 (2015).
5) M. L. Dietz *et al.*, Talanta **62**, 109 (2004).
6) Y. Kasamatsu *et al.*, Radiochim. Acta **103**, 513 (2015).
7) T. Sikkeland *et al.*, Phys. Rev. **172**, 1232 (1968).
8) M. Asai *et al.*, Phys. Rev. C **83**, 1 (2011).

Coprecipitation behavior of element 102, nobelium, with barium sulfate

S. Otaka,[*1,*2] E. Watanabe,[*1,*2] R. Nakanishi,[*1,*2] R. Masuda,[*1,*2] R. Wang,[*1,*2] Y. Itakura,[*2,*3] T. Yokokita,[*2,*4] Y. Shigekawa,[*2] A. Nambu,[*2] X. Yin,[*2] H. Haba,[*2] A. Shinohara,[*5] and Y. Kasamatsu[*1,*2]

The orbital electrons of heavy elements with $Z \geq 101$, synthesized by heavy-ion-induced nuclear reactions, are affected by significant relativistic effects. Therefore, the chemical properties of the heavy elements might be different from those expected from the periodicity of the homologues in the periodic table, and it is very interesting to investigate their chemical behavior.

We focus on element 102, nobelium (No). No is reported to exist as M^{2+} ion in aqueous solutions, whereas the other heavy actinides all form M^{3+}.[1,2] In the previous chemical experiments on No, the behavior of No was compared with those of divalent transition metal elements and the alkaline earth metal, barium (Ba). As a result, it has been reported that No behaves similarly to Ba. Thereafter, No was reported to have similar chemical behavior to those of calcium (Ca) and strontium (Sr), which have similar ionic radii to No, instead of other alkaline earth metal elements.[4] Recently, our research group focused on sulfate precipitates of alkaline earth metal elements and established the barium-sulfate-coprecipitation method which is applicable to No.[3] According to the results obtained in the preliminary experiments with Ca, Sr, Ba, and Ra, we found that the precipitation behavior in the present reaction system is sensitive to the ionic radii of the alkaline earth metal elements. In addition, it is expected that a difference in chemical bonding properties of No from those of alkaline earth metal elements will be observed. In this study, we applied the above method to No.

We produced ^{255}No ($T_{1/2}$ = 211 s) and ^{162}Yb ($T_{1/2}$ = 18.9 min) by the ^{248}Cm(^{12}C, $5n$)^{255}No and ^{nat}Gd(^{12}C, xn)^{162}Yb reactions, respectively, using the AVF cyclotron at RIKEN RIBF. The reaction products were transported by the He/KCl gas-jet system to the chemistry room and dissolved in a dilute HCl solution. When a precipitated sample is prepared, 20 μg of Ba and 2 mL of 0.1 M or 2.0 M ammonium sulfate were added into the dissolved solution in a 5-mL microtube, and the solution was stirred for 5 min at room temperature using a Vortex mixer. Then, the solution containing the precipitate was filtrated using the suction filtration apparatus controlled by PC. The precipitated sample was dried with He gas at 100°C. When determining the total amount of dissolved species (a standard sample is prepared), the reaction products were dissolved in dilute HCl solution, and the solution was put on a Ta plate. The sample was evaporated to dryness by He gas at 600°C and a halogen heat lamp. Finally, these dried precipitated and standard samples were subjected to alpha-particle measurement by the automated rapid alpha/SF detection system. After the alpha-particle measurement, gamma-ray activities of ^{162}Yb in the samples were measured with a Ge detector to monitor the chemical yields and coprecipitation behavior of Yb.

We successfully prepared 17 coprecipitated samples and 41 standard samples. Alpha-particle spectrum for the standard samples is shown in Fig. 1. Based on the alpha counts, we estimated the coprecipitation yields of ^{255}No and ^{162}Yb, considering various corrections such as the differences in the cooling times before the measurements and detection efficiency. As a result, a high coprecipitation yield of around 80% was obtained for ^{255}No in the case of adding 2.0 M ammonium sulfate. A detailed analysis is underway. We plan to discuss the sulfate complexation properties of ^{255}No based on the comparison with those of alkaline earth metal elements. In addition, we will compare the results with those obtained by quantum chemical calculations which were previously performed[4] to discuss the chemical bonding properties of No.

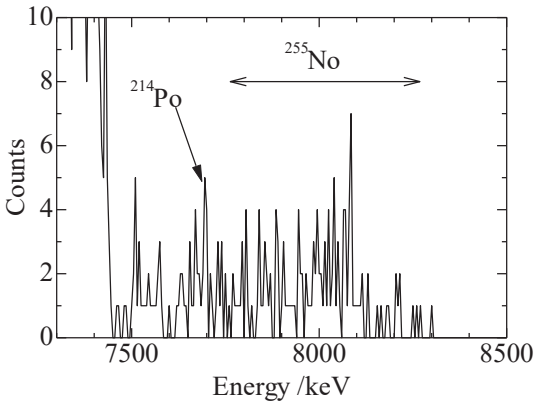

Fig. 1. Alpha-particle spectrum for the ^{255}No standard sample.

References
1) J. Maly *et al.*, Science **160**, 1114 (1963).
2) G. T. Seaborg, in *The Transuranium Elements* (McGraw-Hill, New York, 1949), p.1492.
3) R. J. Silva *et al.*, Inorg. Chem. **13**, 2233 (1974).
4) S. Hayami, MS thesis, Osaka University (2021).

*1 Graduate School of Science, Osaka University
*2 RIKEN Nishina Center
*3 Department of Chemistry, Osaka University
*4 Salesian Polytechnic
*5 Osaka Aoyama University

Coprecipitation of ^{133}Ba, ^{226}Ra, and ^{152}Eu with calcium oxalate for the chemical study of nobelium

R. Nakanishi,[*1,*2] E. Watanabe,[*1,*2] S. Otaka,[*1,*2] R. Masuda,[*1,*2] R. Wang,[*1,*2] Y. Itakura,[*2,*3] T. Yokokita,[*2,*4] Y. Shigekawa,[*2] A. Nambu,[*2] X. Yin,[*2] H. Haba,[*2] A. Shinohara,[*5] and Y. Kasamatsu[*1,*2]

Superheavy elements (SHEs) with $Z \geq 101$ are synthesized by heavy-ion-induced nuclear reactions. The production rates of these elements are very low, and their half-lives are usually short.[1] Therefore, it is difficult to investigate their chemical properties. Element 102, nobelium (No), is one of the actinide elements. No has unique property that the element exists stably as No^{2+} ion in aqueous solutions,[2] whereas all lanthanide and actinide elements have the most stable valency of +3 or higher. Previous chemical studies on No have reported that No exhibits similar chemical behavior to those of the group 2 elements in the periodic table.[3] In this study, we focused on oxalic acid, which precipitates the group 2 elements by bonding with metal ions, and malonic acid, which has a slightly longer carbon chain length than oxalic acid. We expect that the complexation behavior of these dicarboxylic acids with No can be investigated by the coprecipitation method. Studies for complexation with organic ligands are scarce in SHE chemistry, and through the present study, the dependence of the No behavior on the ligand size and shape is expected to be discussed. In this report, we present the results of the precipitation and coprecipitation experiments of Ca, Sr, Ba, Ra, and Eu with oxalic acid. We determined the suitable experimental conditions for investigating the properties of No-oxalic complexes.

Oxalic acid precipitation experiments for Ca, Sr, and Ba were performed to determine the carrier metal elements that rapidly and fully precipitate by bonding with oxalic acid. The precipitation experiments were performed at pH = 2, 3, 4, and 5 with reaction times of 3 min. 5 mL of 2 mM Ca^{2+}, Sr^{2+}, or Ba^{2+} hydrochloric acid (pH = 2, 3, 4, or 5) was mixed with 5 mL of 4, 20, and 200 mM oxalic acid (pH = 2, 3, 4, or 5). The amounts of Ca and Sr in the precipitate and filtrate samples were analyzed by EDTA titration and that of Ba was determined by γ-ray measurement for ^{133}Ba tracer with a Ge semiconductor detector. The precipitation yields were estimated from the amounts.

Based on the precipitation results, coprecipitation experiments of ^{133}Ba, ^{226}Ra, and ^{152}Eu with calcium oxalate were performed using Ca as the carrier at pH = 3. 20 μL of hydrochloric acid (pH = 3) containing ^{133}Ba, ^{226}Ra, and ^{152}Eu was added to 230 μL of 2.17 mM Ca^{2+} hydrochloric acid (pH = 3), which was followed by addition of 250 μL of 20 and 200 mM oxalic acid (pH = 3). The mixture was shaken for 5 min. The coprecipitation yield of each element was determined by γ-ray measurement for ^{133}Ba and ^{152}Eu with the Ge semiconductor detector, and by α-particle measurement with a Si detector for ^{226}Ra.

The results of the oxalic acid precipitation experiments of Ca, Sr, and Ba showed that the precipitation yield of Ca rapidly reached about 100%, and a clear difference in the precipitation yields of Ca (92.6 ± 4.9%), Sr (5.8%), and Ba (0.6 ± 0.3%) was observed under the condition of 10 mM oxalic acid at pH = 3. Consequently, we determined suitable experimental conditions, as Ca carrier will be used in coprecipitation at pH = 3, to observe the similarity of No behavior to which group 2 element.

Figure 1 shows the coprecipitation yields of ^{133}Ba, ^{226}Ra, and ^{152}Eu with calcium oxalate. The yields for ^{133}Ba and ^{226}Ra were low and increased with increasing oxalic acid concentration, in the range 10–40% for ^{133}Ba and 5–20% for ^{226}Ra. The coprecipitation yields for ^{152}Eu were over ∼90% at all oxalic acid concentrations studied. The coprecipitation yields were in the order of Ca ≈ ^{152}Eu > ^{133}Ba > ^{226}Ra, which is inverse order of the ionic radius[4]: Ca^{2+} (1.12 Å) ≈ Eu^{3+} (1.066 Å) < Ba^{2+} (1.42 Å) < Ra^{2+} (1.48 Å). This suggests that smaller metal ions tend to match the size of oxalic acid and stably form complexes. We plan to investigate the coprecipitation behavior of No with oxalic acid to discuss the ionic radius of No.

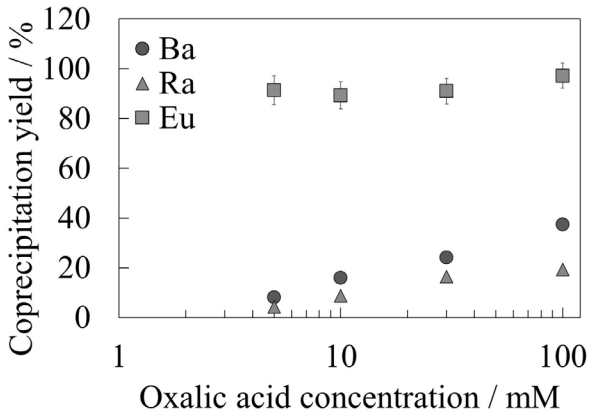

Fig. 1. Coprecipitation yield of ^{133}Ba, ^{226}Ra, and ^{152}Eu.

*1 Graduate School of Science, Osaka University
*2 RIKEN Nishina Center
*3 Department of Chemistry, Osaka University
*4 Salesian Polytechnic
*5 Osaka Aoyama University

References
1) J. Maly *et al.*, Science **160**, 1114 (1963).
2) A. Toyoshima *et al.*, J. Am. Chem. Soc. **131**, 9180 (2009).
3) R. J. Silva *et al.*, Inorg. Chem. **13**, 2233 (1974).
4) R. D. Shannon, Acta Cryst. A **32**, 751 (1976).

Improved chemical separation scheme of Pa isotopes from a ^{232}Th target toward observing the radiative decay of ^{229m}Th using ^{229}Pa

Y. Shigekawa,[*1] X. Yin,[*1] A. Nambu,[*1] Y. Wang,[*1] and H. Haba[*1]

The first excited state of the ^{229}Th nucleus (^{229m}Th) has an excitation energy of ∼8.3 eV (150 nm),[1] potentially leading to an ultraprecise nuclear clock. We aim to observe the radiative decay (γ rays) of ^{229m}Th and determine its radiative half-life; this is an important parameter to develop the nuclear clock by doping a CaF_2 crystal with ^{229}Pa, which decays to ^{229m}Th with negligibly small recoil energy.[2–4] In a previous study,[4] we ionized ^{233}Pa and implanted it into a CaF_2 crystal with a total efficiency of 0.53(1)% using the surface ionization technique. However, when we tried the ionization and implantation of ^{229}Pa that was produced in the ^{232}Th$(p, 4n)^{229}$Pa reaction and chemically purified,[3] the efficiency was limited to ∼0.1%. A probable reason for the low efficiency is that some amount of ^{232}Th and impurities remain in the purified ^{229}Pa solution and inhibit the ionization of Pa. Therefore, we improved the chemical separation scheme in this study by adding a separation step using the CL resin (Triskem).[5] Moreover, for faster separation, we increased the flow rate of eluents during column chromatography by a factor of ∼10, compared with our previous separation experiments.[2,3]

The chemical separation scheme was developed using ^{230}Pa ($T_{1/2}$ = 17.4 d) and ^{233}Pa ($T_{1/2}$ = 27.0 d) produced in the ^{232}Th$(d, 4n)^{230}$Pa and ^{232}Th$(d, n)^{233}$Pa reactions at the RIKEN AVF cyclotron. Two ^{232}Th foils (70 mg/cm^2 × 2, ∼140 mg) were irradiated with 9.1 μA of a 24-MeV deuteron beam for 70 min. The foils were dissolved with concentrated HCl and 0.05 M $(NH_4)_2SiF_6$[6] 62 days after the irradiation. The chemical separation of the Pa isotopes was performed following the scheme shown in Fig. 1, which consists of three column separations using anion-exchange resin (Column A and C) and the CL resin (Column B). The flow rate of every eluent was set to 1–2 mL/min by pushing the air in the column using a peristaltic pump. The radioactivity of Pa isotopes and fission products (FPs) for each fraction was measured via γ-ray spectroscopy using a Ge detector to check chemical yields and radioactive impurities. The final Pa fraction was subjected to inductively coupled plasma mass spectrometry (ICP-MS) to check the chemical purity.

The separation by Column A removed the majority of ^{232}Th and FPs, and the Pa fraction that eluted from Column A included radioactive impurities of ^{95}Zr ($T_{1/2}$ = 64.0 d), ^{95}Nb ($T_{1/2}$ = 35.0 d), and ^{103}Ru ($T_{1/2}$ = 39.2 d). The separation with Column B reduced

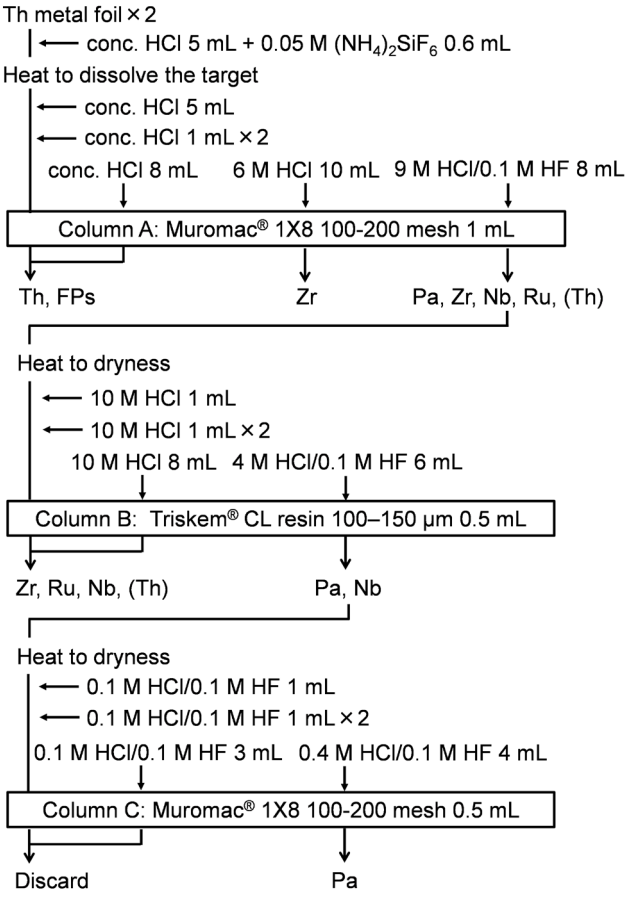

Fig. 1. Chemical separation scheme of Pa.

^{95}Zr and ^{103}Ru to levels less than the detection limits of the γ-ray measurement. ^{95}Nb, which behaves similarly to Pa, was separated with Column C by a decontamination factor of 220, which is high enough for the experiment of ^{229}Pa. It was reported that Nb can be separated with the Eichrom DGA resin;[5] thus, we checked the performance of this method. However, the decontamination factor was measured to be only 12, and thus, we selected the method in Fig. 1. The chemical yields of Pa isotopes for Columns A, B, and C were 95(4)%, 96(3)%, and 95(3)%, respectively (total yield 86(5)%), meaning that the separation at the high flow rate does not lead to the loss of Pa. We expect that the whole separation will be finished in ∼4 h, which is ∼3 times shorter than that of the previous scheme, minimizing the decay loss of ^{229}Pa. For the ICP-MS measurement of the purified Pa solution, the impurities of >100 ng were Mg (627 ng), Al (284 ng), Zn (141 ng), and Th (167 ng). Therefore, the amount

*1 RIKEN Nishina Center

of ^{232}Th was reduced to the same level as other impurities.

We are now developing a new Pa implantation apparatus that enables in varying the implantation energy of ^{229}Pa in the range of 0.5–30 keV, not limited to 15 keV.[4] In a preliminary experiment using the purified ^{230,233}Pa solution and the new apparatus, the total ion implantation efficiency was measured to be ∼0.2%, which is higher than the previous value using ^{229}Pa (∼0.1%), probably due to the improved chemical purification scheme. Higher efficiency may be further obtained by improving and optimizing the new apparatus.

References

1) B. Seiferle *et al.*, Nature **573**, 243 (2019).
2) Y. Shigekawa *et al.*, RIKEN Accel. Prog. Rep. **54**, 143 (2021).
3) Y. Shigekawa *et al.*, RIKEN Accel. Prog. Rep. **55**, 124 (2022).
4) Y. Shigekawa *et al.*, RIKEN Accel. Prog. Rep. **55**, 126 (2022).
5) T. Mastren *et al.*, Anal. Chem. **90**, 7012 (2018).
6) V. Radchenko *et al.*, Radiochim. Acta **104**, 291 (2016).

Preparation of a small high-density ^{229}Th target for the X-ray pumping of the ^{229}Th nuclear clock isomer

Y. Shigekawa,[*1] K. Okai,[*2] Y. Fukunaga,[*2] K. Yoshimura,[*2] and H. Haba[*1]

The first excited state of the ^{229}Th nucleus (^{229m}Th) has an excitation energy of ∼8.3 eV,[1] which allows laser excitation and spectroscopy of the nucleus. One application is ultraprecise nuclear clocks with unprecedented uncertainty.[2] Our group aims to observe the γ-rays emitted from ^{229m}Th, which is an important step for realizing nuclear clocks. In 2019, we succeeded in actively producing ^{229m}Th by populating the 29.2-keV second excited state of ^{229}Th using X-rays at SPring-8.[3] With this technique, we are now trying to detect γ-rays of ^{229m}Th produced in a ^{229}Th-doped CaF_2 crystal, in which the internal conversion process of ^{229m}Th would be inhibited. For every beamtime at Spring-8, we have to precisely adjust the energy of X-rays for the resonant excitation of ^{229}Th to the 29.2-keV state. For the energy adjustment, we have used a source containing 0.24 μg of ^{229}Th placed in a hole with a diameter of 0.4 mm on a graphite plate. Owing to the small amount of ^{229}Th, searching for the resonant X-ray energy has required more than 14 h. The above ^{229}Th source was prepared by performing the ∼7000 sets of dropping a small amount of ^{229}Th solution (5 nL per drop) into the hole and evaporating it by heating. The amount of ^{229}Th that can be poured into the small hole was limited because the nanoscale drop was not stable and the density of the ^{229}Th sample was lower than expected, probably owing to the repeated rapid evaporation processes. In this study, we developed a new simple method and successfully prepared a small high-density ^{229}Th source, which is used to search for the resonant X-ray energy for the 29.2-keV state.

The new source-preparation method is drying one drop (∼1 μL) of nitric acid containing ^{229}Th on a Teflon plate. Owing to the high water repellency of Teflon, the shape of the drop remains spherical during the evaporation process, and the drop size becomes much less than 1 mm just before it is completely dried. We prepared two types of Teflon plates shown in Fig. 1. The type A plate has a small taper hole made by drilling, where the ^{229}Th solution is dropped. The hole in the type B plate was manually prepared by heating the Teflon plate and deforming it with a conical die. We found that a drop on the type B plate was evaporated and retained a spherical shape. In contrast, a drop on the type A plate slightly expanded, and the size of the residues became larger than 1 mm. The images obtained by scanning electron microscopy (SEM) for the type A plate (Fig. 2) showed scratches made by drilling, which would be the reason for the lower water repellency. The type B plate showed a smooth surface (Fig. 2); thus, we adopted the type B plate to prepare the ^{229}Th source.

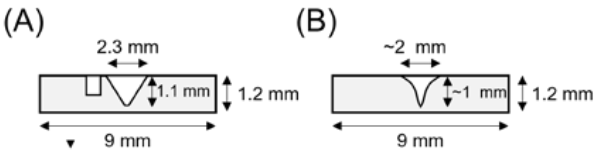

Fig. 1. Schematics of the Teflon plates of types A (left) and B (right).

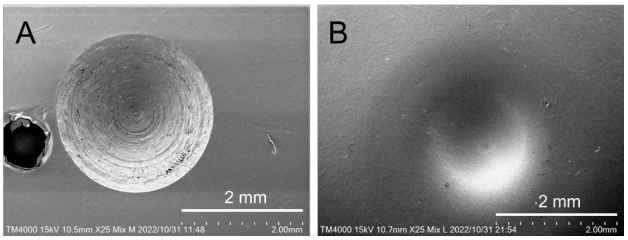

Fig. 2. SEM images of the Teflon plates of types A (left) and B (right).

^{229}Th was first purified via anion exchange chromatography using high-purity acids (metal impurities <100 ppt). The purified ^{229}Th was dissolved with 10 μL of 1-M HNO_3. The solution was dropped on a Teflon sheet and evaporated. Then, the residue was dissolved with 1 μL of 1-M HNO_3 and dropped on the type B plate placed on a hot plate. We washed the Teflon sheet with 1 μL of 1-M HNO_3, which was then added to the drop on the type B plate. The temperature of the hot plate was first maintained at ∼45°C for 20 min to slowly evaporate the majority of the solution. It was then increased to ∼120°C over 11 min and maintained at that temperature for 9 min. The temperature was then raised to 200°C over 13 min and maintained at that temperature for 19 min for complete dryness.

The ^{229}Th source shown in Fig. 3 had a residue with a diameter of ∼0.7 mm. The amount of ^{229}Th in the source was measured to be 1.61(2) μg by γ-ray spectroscopy, which is 6.7 times larger than the amount of the previous ^{229}Th source that we have used.[3] X-ray fluorescent measurements performed at SPring-8 showed that a large amount of ^{229}Th was condensed within a diameter of 0.65 mm. By using this new ^{229}Th source, we were able to finish the X-ray en-

*1 RIKEN Nishina Center
*2 Research Institute for Interdisciplinary Science, Okayama University

ergy search for the excitation to the 29.2-keV state four times faster than that for the previous source.

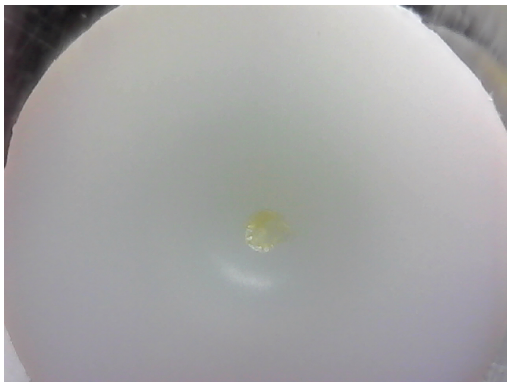

Fig. 3. Photograph of the prepared ^{229}Th target.

References
1) B. Seiferle *et al.*, Nature **573**, 243 (2019).
2) E. Peik *et al.*, Europhys. Lett. **61**, 181 (2003).
3) T. Masuda *et al.*, Nature **573**, 238 (2019).

Development of ^{211}Rn/^{211}At generator through liquid phase recovery of radon and ionic liquid extraction of astatine

Y. Nagai,[*1] Y. Ganaha,[*1] A. Yokoyama,[*2,*3] K. Washiyama,[*4] I. Nishinaka,[*5] X. Yin,[*3] A. Nambu,[*3] Y. Shigekawa,[*3] and H. Haba[*3]

The short path length and high linear energy transfer of α particles are expected to facilitate targeted alpha therapy for the treatment of tumor. A promising nuclide among various α emitters is ^{211}At with a half-life of 7.21 h, which has gained popularity owing to its appropriate life and potential to synthesize labeled compounds as a halogen element. This has led to several preclinical studies on At chemistry.[1] To improve the availability of ^{211}At, a ^{211}Rn/^{211}At generator was developed via the extraction using organic solvent of DIPE or MIBK for expanding nuclide production away from accelerator facilities because ^{211}Rn, which has a half-life of 14.6 h, is the parent nuclide of ^{211}At.[2] In this study, we proved the wet chemistry processes through liquid phase recovery of radon and ionic liquid extraction of astatine for the generator.

In recent years, ionic liquids have attracted attention as an alternative to organic solvents from the perspective of green chemistry. Ionic liquids exist in the liquid phase at room temperature, have low volatility, and are flame-retardant; therefore, the environmental load or risk of accidents is minimal. Further, the amount of radioactive waste can be reduced compared to that using organic solvents owing to their repeated usability. In addition, ionic liquids are considered promising solvents for extracting ^{211}At as per the reports on radiation resistance.[3]

The nuclide of ^{211}At was produced via the ^{209}Bi(α, $2n$) reaction at the RIKEN AVF cyclotron or the decay of ^{211}Rn from the ^{209}Bi(^{7}Li, $5n$) reaction at the JAEA tandem Van de Graaff accelerator. The irradiated Bi target was dissolved in 6 M HNO_3 and finally the ^{211}At nuclide was collected in dodecane solvent although the At species may differ depending on the procedures of preparation. The ^{211}At was further extracted to 3 M HCl solution. Subsequently, ^{211}At was extracted into an ionic liquid (IL) of $[C_8mim]^+$ $[Tf_2N]^-$, where $[C_8mim]^+$ and $[Tf_2N]^-$ are alkylimidazolium ion and bis (trifluoromethanesulfonyl) imide ions, respectively. Finally, it was back-extracted into 0.1 M NaOH solutions. The α radioactivity of ^{211}At was measured using a liquid scintillation counter to determine extraction rates of the nuclide for the relevant extraction procedures.

Figure 1 shows the extraction rates of ^{211}At from dodecane into HCl solution, from HCl solution into IL, and from IL into NaOH solution. Species in dodecane were found to be dependent on the preparation of At as observed upon the comparison of the results. Following the extraction in HCl solution, At species appeared to behave in a similar manner.

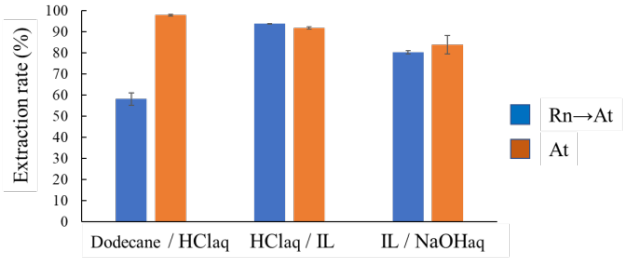

Fig. 1. Extraction rates for At from the decay of Rn (Rn → At) and directly produced At (At).

Figure 2 shows the same extraction rates of ^{211}At from the decay of ^{211}Rn, as in Fig. 1, but for with and without H_2O_2 as a reductant. Reduction of At species enhanced extraction into HCl and worked the other way in back-extraction with NaOH. This suggests that solvent extraction in practical applications necessitates the adjustment of chemical species to have a good recovery of At.

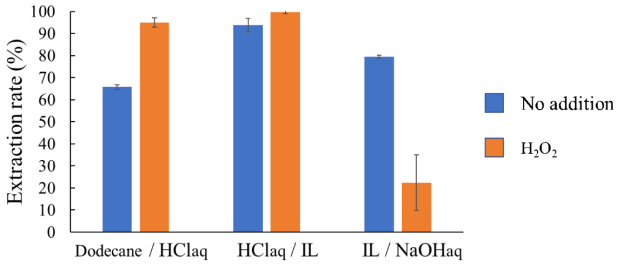

Fig. 2. Extraction rates for At from the decay of Rn with and withou without H_2O_2.

*1 Graduate School of Natural Science and Technology, Kanazawa University
*2 Institute of Science and Engineering, Kanazawa University
*3 RIKEN Nishina Center
*4 Fukushima Global Medical Science Center, Fukushima Medical University
*5 Quantum Beam Science Research Directorate, National Institutes for Quantum Science and Technology

References

1) F. Guérard *et al.*, Cancer Biother. Radiopharm. **28**, 1 (2013).
2) E. Maeda *et al.*, J. Radioanal. Nucl. Chem. **303**, 1465 (2015).
3) L. Yuan *et al.*, J. Phys. Chem. B **113**, 8948 (2009).

The feasibility study for the medical radioisotope: astatine-211 production by the gas cell-based laser ionization technique

T. Sonoda,[*1] T. Nakashita,[*1] H. Haba,[*1] H. Tomita,[*2] and H. Ishiyama[*1]

Astatine-211 is one of remarkable advantage isotopes for targeted α-particle therapy. RIKEN Nishina Center has been providing many types of medical radioisotopes, particularly a large amount of ^{211}At.[1] Astatine-211 can be produced from natural bismuth target via the ^{209}Bi$(\alpha, 2n)^{211}$At nuclear reaction. The adjustment of α-particle energy is constrained from maximizing ^{211}At production to avoid production of ^{210}At, which yields the undesirable α-particle emitting daughter, ^{210}Po. The chemical separation of ^{211}At and ^{210}At is, in principle, incompatible in the recovery process of ^{211}At from the target.

Here, we propose a new idea to use the physical separation of ^{211}At and ^{210}At by the gas cell-based laser ionization technique. This technique utilizes an isotope separation by the element and mass selective low-energy beam transportation. Figure 1 shows the conceptual diagram for this technique. The bismuth target irradiated by the cyclotron beam is installed into the gas cell. Atomic/ionic At or any other isotopes are evaporated from the target by resistive heat transfer and then they are transported to the exit area by an inert gas flow. Three-color pulsed laser beams are sent to the gas cell exit area for laser ionization of At.[2] The laser wavelength enables element selective ionization by using a resonant excitation scheme in the atomic structure. The excitation energy for the removal of single electron is acquired stepwise by laser photons. Photo-ionized astatine isotopes are sent to the quadrupole mass separator for the separation of ^{211}At and ^{210}At via multipole ion beam guide in the differential pumping stage. Consequently, a highly pure ^{211}At ion beam is collected. The radioactive contamination can be minimized by using the closed gas circulation[3] and by installing the entire system in a draft chamber.

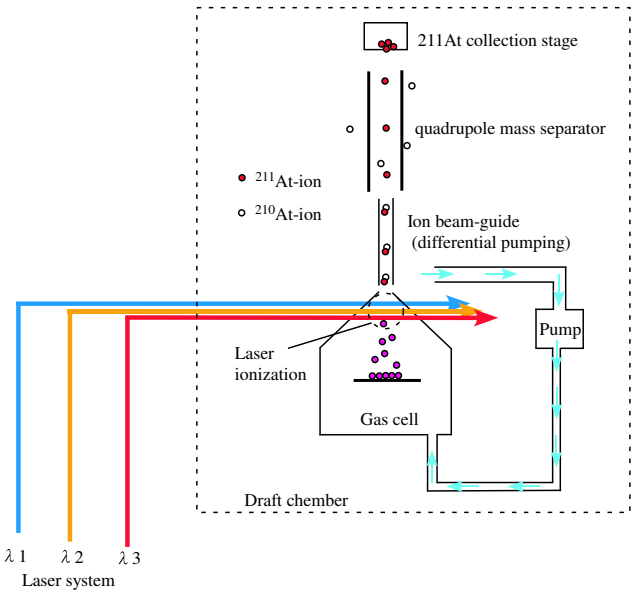

Fig. 1. Conceptual diagram for ^{211}At production. The whole system is as small as to be placed in the general draft chamber.

In 2023, we will start the feasibility study for this technique as the following steps:

- Laser ionization test for astatine isotope in vacuum to investigate efficient ionization scheme.
- Extraction and collection test for ^{211}At.
- Evaluation of the radioactive purity and collection efficiency.

The potential advantage of this technique is expected in the following parts: (1) Facilitate use of the best α-particle energy for the cyclotron for the maximum production of ^{211}At, without worrying about any other isotope production, such as ^{210}At. This will result in 3-5 gain in the production efficiency. (2) Minimization in human exposure/contamination against alpha emitting radioactivity and radiation. For the first test, we will install the highly activated target into the gas cell manually. In future, the bismuth target including gas cell will be set on the beam axis of the cyclotron beam line, then the gas cell unit can be treated instead of dealing the target by human hands. This is crucial if the cyclotron beam intensity is very high.

The feasibility study for new production technique of ^{211}At has been started. The fabrication and development of the whole system is in progress. If the feasibility is confirmed, this technique will be extended to other medical radioisotope productions such as ^{213}Bi, ^{111}In, and ^{225}Ac.

*1 RIKEN Nishina Center
*2 Faculty of Engineering, Nagoya University

References

1) Y. Wang *et al.*, RIKEN Accel. Prog. Rep. **53**, 192 (2019).
2) S. Rothe *et al.*, Nat. Commun. **4**, 1835 (2013).
3) T. Sonoda *et al.*, Rev. Sci. Instrum. **87**, 065104 (2016).

Progress of ^{211}At production at the RIKEN AVF cyclotron

X. Yin,[*1] N. Sato,[*1] A. Nambu,[*1] Y. Shigekawa,[*1] and H. Haba[*1]

^{211}At is one of the most promising radionuclides for targeted α-particle therapy. The most common method for ^{211}At production is to irradiate natural Bi with α particles via the ^{209}Bi$(\alpha, 2n)^{211}$At reaction. We have been developing production technologies of ^{211}At at the RIKEN AVF cyclotron.[1–3] In our current method,[3] a metallic ^{209}Bi target with a typical thickness of 20 mg/cm^2 on a 1-mm Al backing is irradiated with a 28.0-MeV α beam at an angle of 15° to the beam axis. During the irradiation, the target is cooled with circulating water (1.5 L/min, 10°C) and He gas (30 L/min). The maximum beam intensity of 10 particle μA (pμA) can produce ^{211}At with a thick target yield of 48 MBq/pμA h. After the irradiation, the target was placed in a quartz tube, was heated up to 850°C, and kept for 10 min with O_2-gas flowing at 10 mL/min. ^{211}At sublimated from the target was trapped by a PFA tube cooled at −96°C. 200–400 μL $CHCl_3$ was used to wash the PFA tube to collect ^{211}At in a glass v-vial. Finally, the $CHCl_3$ solution was dried to obtain a dry ^{211}At in the v-vial with N_2-gas flowing at 100 mL/min.

The demand for RIKEN ^{211}At is increasing every year. It is desirable to increase the production yield of ^{211}At by irradiating the ^{209}Bi target with a more intense beam. Due to the poor thermal conductivity (9.79 W/(m·K)) and a low melting point (272°C) of Bi, an effective cooling system is essential. In this work, we modified the channel of the cooling water to increase its flow rate from 1.5 to 4.0 L/min. We also lowered the temperature of the water from 10 to 5°C. However, we could prepare only one dry ^{211}At in a single drying and it took approximately 15 min to dry 200 μL of $CHCl_3$. To increase the productivity of the dry ^{211}At, we developed a rapid drying apparatus that makes it possible to simultaneously produce 4 v-vials of dry ^{211}At within less time.

The ^{209}Bi targets with thicknesses of 17.7 mg/cm^2 and 18.6 mg/cm^2 were irradiated for 40 mins with a 28-MeV α beam using the previous and new irradiation systems, respectively. The beam intensity was 25 particle μA. After the irradiations, the targets were subjected to γ-ray spectrometry to determine the activity of ^{211}At.

In a separate experiment, 642 MBq of ^{211}At in 300 μL of $CHCl_3$ was divided into 3 v-vials of 100 μL each and dried simultaneously in the rapid drying apparatus with N_2-gas flowing at 3 L/min at room temperature and 100 kPa. The N_2 gas was aspirated by a chemical pump and exhausted through 1 M $Na_2S_2O_5$ solution and a charcoal trap (Fig. 1(b)). The v-vials were subjected to γ-ray spectrometry before and after drying.

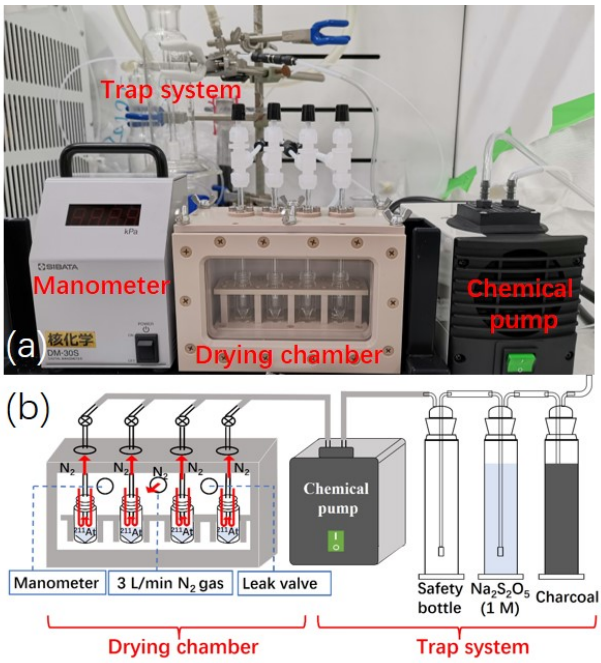

Fig. 1. (a) Photo and (b) schematic of rapid drying apparatus for ^{211}At.

Figures 2(a) and 1(b) show photos of the irradiated ^{209}Bi targets with the previous and new irradiation systems, respectively. The target cooled with 1.5-L/min water at 10°C was damaged severely. The produced ^{211}At activity of 503 ± 16 MBq is only 61% compared with the theoretical yield.[4] The damage of the target cooled with the 4.0-L/min water at 5°C with the new system seems smaller, and the produced ^{211}At activity of 667 ± 23 MBq is 82% of the theoretical yield.[4] As expected, a higher flow rate and lower temperature of cooling water help to produce ^{211}At more quantitatively. Our current production yield of ^{211}At (1.0 GBq/h at 28.0 MeV with a 25-particle μA α beam) was increased by a factor of 2.1 compared to our previous one by a 10-particle μA α beam irradiation.[1]

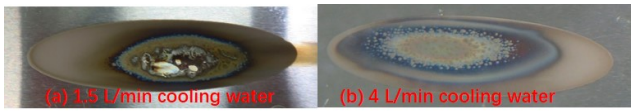

Fig. 2. Photos of the ^{209}Bi targets irradiated with the previous (a) and new (b) irradiation system at the 1.5 and 4.0 L/min flow rate of cooling water, respectively.

[*1] RIKEN Nishina Center

Each 100 μL of the ^{211}At $CHCl_3$ solution in the 3 v-vials was dried within 5 min. The activities of ^{211}At before and after drying were consistent with each other after the decay corrections. With the rapid drying apparatus, the time required to dry ^{211}At was significantly reduced.

References

1) N. Sato *et al.*, RIKEN Accel. Prog. Rep. **50**, 262 (2017).
2) S. Yano *et al.*, RIKEN Accel. Prog. Rep. **50**, 263 (2017).
3) Y. Wang *et al.*, RIKEN Accel. Prog. Rep. **53**, 192 (2019).
4) S. M. Qaim *et al.*, IAEA Technical Report Series No.473, IAEA, Vienna, Austria (2011).

Improvement of chemical separation method for theranostic radionuclide ^{141}Ce

K. Ooe,[*1] T. Watabe,[*2,*3] Y. Shirakami,[*3] A. Nambu,[*4] H. Haba,[*4] and J. Hatazawa[*5]

Radionuclides are widely used in the treatment of tumors. In Japan, all therapeutic radionuclides used in clinical practice are imported from other countries. Domestic production using accelerators is desirable for a stable supply of therapeutic radionuclides.

One of the candidate radionuclides for theranostics (therapeutics + diagnosis) that can be produced by using accelerators is cerium-141 (^{141}Ce, $T_{1/2}$ = 32.5 d). This nuclide emits β-particles (maximum β energy: 580.7 keV), which can be used for tumor therapy. It also emits a γ-ray with an energy of 145.4 keV (branching ratio: 48.2%), which can be used for imaging by single photon emission computed tomography (SPECT). One of the production reactions for ^{141}Ce using accelerators is the ^{138}Ba$(\alpha, n)^{141}$Ce reaction. However, ^{141}Ce has rarely been used in the field of nuclear medicine, and investigation of accelerator production and chemical separation conditions will be necessary.

We have previously reported the accelerator production and chemical separation of ^{141}Ce.[1)] BaO was selected as a suitable target material for the production of ^{141}Ce by the α beam using an accelerator. Chemical separation of ^{141}Ce from the irradiated BaO target was also achieved through column chromatography using a Ln resin (extraction chromatographic resin with di (2-ethylhexyl) phosphoric acid). However, it took approximately 4 h for the chemical separation of ^{141}Ce because there was no eluent pumping.

In this study, the rapid chemical separation of ^{141}Ce from the Ba target using the Ln resin cartridge was investigated with increasing eluent flow rate.

^{141}Ce was produced in the ^{nat}Ba$(\alpha, xn)^{141}$Ce reaction with a 29-MeV alpha beam using the RIKEN K70 AVF cyclotron. ^{nat}BaO pellet was used as the target material. The irradiated ^{nat}Ba target (approximately 100 mg) was dissolved in 3 mL of 1 M HCl. After evaporation to dryness, the residue was dissolved in 10 mL of 0.03 M HCl solution The solution was filled into a 10 mL syringe and then injected into the Ln resin cartridge column (resin volume: 2 mL) at a flow rate of 1 drop per 1–2 seconds. Each 1 mL of the eluents was corrected with sample tubes. The ^{nat}Ba was washed out from the cartridge with 0.03 M HCl, and then ^{141}Ce was eluted with 1 M HCl solution. Each eluted sample was subjected to γ-ray spectrometry with a Ge detector for the determination of ^{141}Ce radioactivity. After measurement with the Ge detector, the concentration of ^{nat}Ba in each eluted sample was measured by ICP-MS.

The elution curves for ^{nat}Ba and ^{141}Ce, from the Ln resin cartridge, were shown in Fig. 1. The time required for the separation of ^{141}Ce with the Ln resin cartridge was less than 1 h, significantly reduced compared to the previous study (approximately 4 h) by increasing the eluent flow rate. The most of ^{nat}Ba was eluted at elution volume of around 15 mL with 0.03 M HCl. After elution of ^{nat}Ba, ^{141}Ce was recovered by elution with 1 M HCl. Although a small amount of ^{141}Ce leakage was observed around 10 mL of 0.03 M HCl, probably due to the increased eluent flow rate, the recovery yield for ^{141}Ce with 1 M HCl was as high as 96%. The contamination of ^{nat}Ba in the ^{141}Ce fractions was calculated to be approximately 0.6 μg in the ICP-MS measurement, which is also improved compared to the previous separation (contamination of ^{nat}Ba was approximately 3 μg).[1)] The separation factor of ^{141}Ce for Ba is estimated to be approximately 10^5.

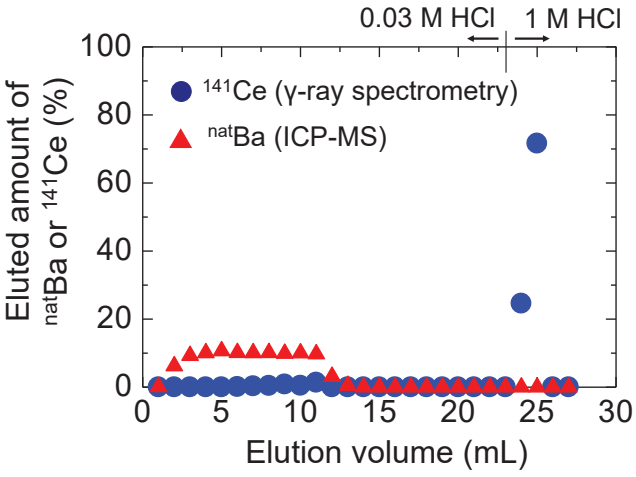

Fig. 1. Elution curves of ^{nat}Ba and ^{141}Ce in chromatographic separation with Ln resin cartridge.

In the next study, the radiopharmaceutical labeling of ^{141}Ce using DOTA (1, 4, 7, 10-Tetraazacyclododecane-1, 4, 7, 10-tetraacetic Acid), which is widely used for chelate labeling of therapeutic radionuclides, will be investigated.

Reference

1) K. Ooe *et al.*, RIKEN Accel. Prog. Rep. **55**, 130 (2022).

*1 Radioisotope Research Center, Institute for Radiation Sciences, Osaka University
*2 Department of Nuclear Medicine and Tracer Kinetics, Osaka University Graduate School of Medicine
*3 Institute for Radiation Sciences, Osaka University
*4 RIKEN Nishina Center
*5 Research Center for Nuclear Physics, Osaka University

Chemical separation of ^{139}Ce from a ^{nat}La target using LN resin

K. Akiyama,[*1,*2] A. Tamura,[*1] and H. Haba[*2]

Endohedral metallofullerenes are clathrate compounds in which metal atoms and metal carbon clusters are included in a fullerene, which is a cage-like molecule composed of sp^2 carbons.[1] In particular, radioactive metallofullerenes encapsulating radioisotopes (RIs) are expected to be applied to radiopharmaceuticals such as a drug delivery system for transporting an RI to affected organs by chemical modification of the fullerene surface. We have studied the production of endohedral metallofullerenes containing lanthanide and actinide elements and their chemical properties. In these studies, it is necessary to use well-characterized radioactive Ce-encapsulated metallofullerenes as the comparators for the metallofullerenes encapsulating RIs which are carrier-free or without any stable isotopes such as promethium and actinide elements. So far, we have used chemically separated ^{139}Ce produced by the ^{139}La$(d, 2n)^{139}$Ce reaction in the RIKEN AVF cyclotron with the target material of ^{nat}La for our metallofullerene research.[2] However, it is necessary to use the highly toxic $K_2Cr_2O_7$ as an oxidizing agent for Ce in the solvent extraction method by di-(2-ethylhexyl) phosphoric acid (HDEHP), which we employed so far, and is not preferable for the application of radioactive metallofullerenes for nuclear medicine in future work. Therefore, we use LN resin (Eichrom Technologies, Inc.) (see Fig. 1), which is an extraction chromatography resin specialized for the separation of rare-earth elements using HDEHP, for the separation of ^{139}Ce from a target material containing La in large quantities. The purpose of this work was to separate and purify a trace amount of ^{139}Ce from La as a target by extraction chromatography using LN resin.

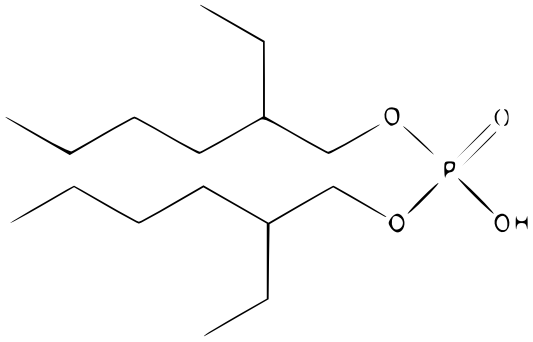

Fig. 1. Structure of the LN resin extractant.

About 1 g of a La plate as a target was irradiated with 24 MeV deuterons at a beam intensity of 5 μA in the RIKEN AVF cyclotron, and ^{139}Ce was produced by the ^{139}La$(d, 2n)^{139}$Ce reaction. The irradiated La target was dissolved in concentrated nitric acid to obtain a ^{139}Ce solution. A polyethylene column with a hight of 50 mm and a diameter of 7 mm was filled with LN resin and loaded with 100 μL of ^{139}Ce solution. A total of 25 mL of 0.15 M nitric acid was added to this column, and the eluate was collected every 5 mL. Then, a total of 10 mL of 6 M nitric acid was added to wash the column. Gamma rays with an energy of 165 keV of ^{139}Ce emitted from each fraction were measured with a Ge semiconductor detector. After gamma-ray measurement, 4-(2-pyridylazo) resorcinol (PAR) was added to each fraction to confirm the elution position of La by the ultraviolet/visible (UV/vis) absorption.

Figure 2 shows the elution behavior of ^{139}Ce during extraction chromatography, monitored by the relative radioactivity of 165 keV emitted from each fraction. The shaded fractions indicate the fractions containing La confirmed by UV/vis absorption. From these results, it is found that ^{139}Ce was sufficiently separated from La and that the proposed separation method is excellent for the separation of ^{139}Ce from a large amount of La used as a target material. Using this purified ^{139}Ce, we are currently researching metallofullerenes encapsulating ^{143}Pm and carrier-free endohedral metallofullerenes encapsulating ^{177}Lu.

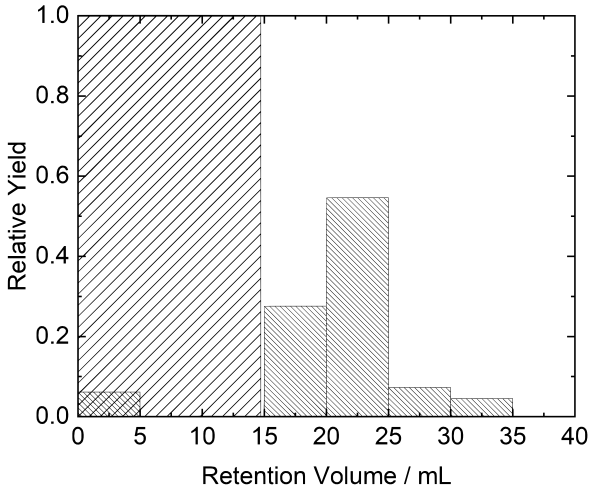

Fig. 2. Elution behavior of ^{139}Ce on LN resin. The shaded fractions indicate the fractions containing La, as confirmed by UV/vis absorption. The radioactivity in each fraction was normalized to that of loaded ^{139}Ce.

*1 Department of Chemistry, Tokyo Metropolitan University
*2 RIKEN Nishina Center

References

1) H. Shinohara, Rep. Prog. Phys. **63**, 843 (2000).
2) K. Akiyama *et al.*, RIKEN Accel. Prog. Rep. **53**, 194 (2019).

Astatine-211-labeled gold nanoparticles for targeted alpha-particle therapy via intravenous injection†

X. Huang,[*1] K. Kaneda-Nakashima,[*2,*3] Y. Kadonaga,[*4] K. Kabayama,[*1,*2,*3] A. Shimoyama,[*1,*2,*3] K. Ooe,[*2,*3] H. Kato,[*4] A. Toyoshima,[*2,*3] A. Shinohara,[*2,*5] H. Haba,[*6] Y. Wang,[*6] and K. Fukase[*1,*2,*3]

Recently, much attention has been directed towards the powerful cancer therapeutic potential of targeted alpha-particle therapy (TAT). Globally, particularly in Japan, the α-particle emitting radionuclide astatine-211 (^{211}At) has garnered significant attention for its use in TAT.

One of the crucial challenges in TAT is the delivery of ^{211}At to the tumor tissues. In a previous study, we discovered that ^{211}At could be efficiently incorporated into gold nanoparticles (AuNPs) through a simple mixing process for 5 min, leading to a high radiochemical yield (RCY) without the need for purification. Furthermore, our research revealed that the intratumoral administration of ^{211}At-AuNPs effectively suppresse tumor growth and demonstrate the stability of ^{211}At-AuNPs in the body.[1)] For systemic metastatic tumors, intravenous injection is a promising method of delivery. In this study, we investigated the substantial potential of AuNPs as carriers for the targeted delivery of ^{211}At via intravenous administration.

^{211}At was produced at RIKEN using a short-lived RI supply platform. The separation and purification of ^{211}At was achieved through dry distillation. Four types of functional AuNPs were synthesized through surface modification using methoxy polyethylene glycol (mPEG) or tumor-targeting peptides (H16 or RGD). The astatine labeling reaction was evaluated using centrifugation, as described previously.[1)]

Tumor xenograft models were established thorough the subcutaneous transplantation of human pancreatic cancer cells (PANC-1) in BALB/c-nu/nu mouse. Four types of ^{211}At-AuNPs were administered to PANC-1 xenograft mice to evaluate their biodistribution at 3 and 24 h. The treatment effect of 5 nm ^{211}At-AuNPs@mPEG was evaluated using the PANC-1 xenograft model. All the animal experiments were conducted according to the guidelines of the Animal Research: Reporting In Vivo Experiments and the Osaka University Animal Experiment Regulations, and approved by the Osaka University Animal Experiment Committee.

Four types of ^{211}At-labeled functional AuNPs (5 nm ^{211}At-AuNPs@mPEG, 30 nm ^{211}At-AuNPs@mPEG, 5 nm ^{211}At-AuNPs@H16, and 5 nm ^{211}At-AuNPs@H16/RGD), as shown in Fig. 1, can be labeled with ^{211}At in a high RCY.

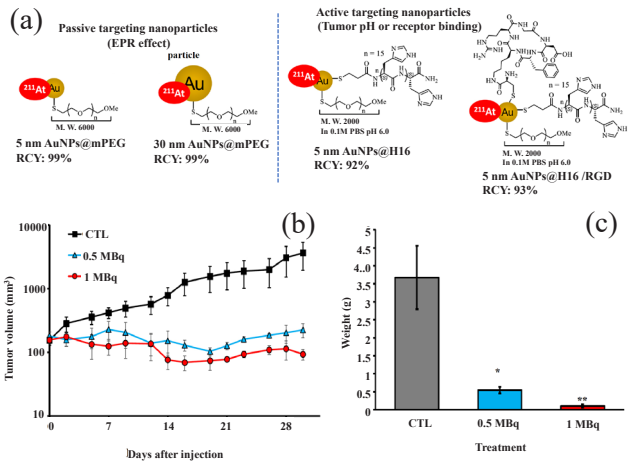

Fig. 1. (a) Four types of ^{211}At-labeled functional AuNPs designed for the study. (b) Change in the tumor size following the administration of 5 nm ^{211}At-AuNPs@mPEG or control (CTL) (saline). (c) Weight of enucleated tumors 30 d after injection.

The in *vivo* biodistribution results indicated a higher accumulation of 5 nm ^{211}At-AuNPs@mPEG in tumors (2.25%ID/g) in 3 h when compared with 30 nm ^{211}At-AuNPs@mPEG based on the enhanced permeability and retention (EPR) effect with a long retention time in tumors for 24 h. The intravenous administration of 5 nm ^{211}At-AuNPs@mPEG was found to significantly inhibit tumor growth in a pancreatic cancer model.

Gold nanoparticles (AuNPs) are an ideal carrier for ^{211}At delivery, owing to their facile and efficient synthesis processes and high stability. The results of this study indicate that the intravenous administration of 5 nm ^{211}At-AuNPs@mPEG exhibits a potent antitumor effect. These results provide a novel framework for the design of nanoparticles suitable for targeted alpha-particle therapy via intravenous injection.[2)]

References

1) H. Kato *et al.*, J. Nanobiotechnology **19**, 1 (2021).
2) X. Huang *et al.*, Pharmaceutics **14**, 2705 (2022).

† Condensed from the article in Pharmaceutics **14**, 2705 (2022)

*1 Graduate School of Science, Osaka University
*2 Institute for Radiation Sciences, Osaka University
*3 Forefront Research Center, Osaka University
*4 Graduate School of Medicine, Osaka University
*5 Osaka Aoyama University
*6 RIKEN Nishina Center

Efficacy of nuclear medicine therapy with $^{67}CuCl_2$ in mice bearing LS180 colon cancer

Y. Fujisawa,[*1] Y. Sugiura,[*1] H. Haba,[*2] A. Nambu,[*2] Y. Shigekawa,[*2] X. Yin,[*2] Y. Magata,[*3] and Y. Iida[*1]

Nuclear medicine is one of the effective methods for early diagnosis and therapy of cancer, and various radioisotopes (RI) have been used. Among them, radioactive Cu is expected to be a promising RI with diagnostic and therapeutic properties. Radioactive Cu includes ^{60}Cu, ^{61}Cu, ^{62}Cu, and ^{64}Cu, which are effective for PET diagnosis, and ^{67}Cu, which can be applied for treatment. ^{67}Cu is a therapeutic radionuclide that emits β-particles of energy 0.392 to 0.577 MeV with a half-life of 61.8 h. Although the β-particle energy of ^{67}Cu is low, it is expected to be effective in treating small cancers.[1] RIs that have high-energy β-particles, such as ^{90}Y, show a good therapeutic effect, but they also have a large effect on surrounding tissues, and the injected dose is limited by exposure to other organs.[2] ^{67}Cu has a low-energy β-particles and can be administered in large doses, leading to effective and efficient treatment.[3] Another advantage of ^{67}Cu is the ability to calculate exposure doses accurately. Injected doses of radiopharmaceuticals used in nuclear medicine therapy are calculated from the exposure doses. ^{67}Cu-labeled drugs can accurately calculate the exposure doses with ^{64}Cu-labeled ones, contributing to safe and effective personalized medicine.

Various studies have been conducted on cancer diagnosis and therapy using radioactive Cu-labeled drugs, and in recent years, the possibility of PET diagnosis using $^{64}CuCl_2$ has been demonstrated. Copper transporter protein 1 (CTR1) is overexpressed in various cancers, suggesting that ^{64}Cu accumulates in cancer via CTR1.[4] Based on these studies, the tumor accumulation of $^{67}CuCl_2$ was also evaluated, and it was found to have the same pharmacokinetics as $^{64}CuCl_2$.[5] In this study, we investigated the therapeutic effect of $^{67}CuCl_2$ on tumor-bearing mice to clarify the potential of cancer therapy using $^{67}CuCl_2$.

Tumor-bearing mice were prepared by implantation of LS180 tumor cells (5×10^6 cells) in 0.1 mL PBS into the flanks of nude mice (BALB/c-nu/nu, male). Biodistribution experiments were performed by intravenously administering $^{67}CuCl_2$. The mice were killed at 1, 24 and 48 h after administration, and tissues of interest were excised and weighed before their radioactivity was measured. LS180 tumors were grown in BALB/c mice in the same way for therapeutic studies. Mice were administered with 17.0–23.2 MBq of $^{67}CuCl_2$ intravenously. Saline-treated mice were used as a control. Mice were weighed and tumor diameters were recorded regularly. The diameters of tumorswere measured with a caliper, and tumor volumes were determined using the formula: (longer diameter) $\times$ (shorter diameter)^2/2. This study was performed in accordance with the recommendations by the Guide for the Care and Use of Laboratory Animals of the Suzuka University of Medical Science.

$^{67}CuCl_2$ showed high accumulation in the tumor, 6.50 ± 2.34, 6.85 ± 1.83, and 5375 ± 1.26% ID/g at 1, 24, and 48 h after administration, as shown in a previous study. Tumor size reduction was observed in all mice treated with $^{67}CuCl_2$ (Fig. 1). However, but relatively significant weight loss was also observed in them (Fig. 2). Therefore, ^{67}Cu is a promising RI for

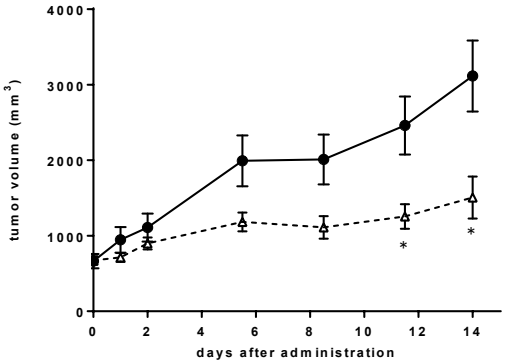

Fig. 1. Therapeutic studies of $^{67}CuCl_2$ in LS180 tumor-bearing mice. (•; saline ($n = 7$), △; $^{67}CuCl_2$ ($n = 4$). *, $p < 0.05$ (2-way ANOVA followed by sidack-test).

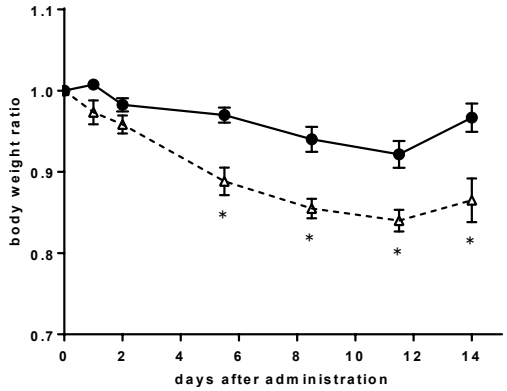

Fig. 2. Changes in body weight of mice after saline or $^{67}CuCl_2$ administration. (•; saline ($n = 7$), △; $^{67}CuCl_2$ ($n = 4$). *, $p < 0.05$ (2-way ANOVA followed by sidack-test).

*1 Faculty of Pharmaceutical Sciences, Suzuka University of Medical Science
*2 RIKEN Nishina Center
*3 Department of Molecular Imaging, Hamamatsu University School of Medicine

the treatment of cancer, but the use of ^{67}Cu-labeled drugs that selectively accumulate in cancer cells are thought to be more suitable for cancer therapy.

References

1) Y. Fujisawa *et al.*, RIKEN Accel. Prog. Rep. **53**, 175 (2019).
2) G. A. Wiseman *et al.*, Eur. J. Nucl. Med. **27**, 766 (2000).
3) Y. Fujisawa *et al.*, RIKEN Accel. Prog. Rep. **55**, 141 (2021).
4) C. Qin *et al.*, J. Nucl. Med. **55**, 812 (2014).
5) Y. Sugo *et al.*, J. Phys. Soc. Jpn. **86**, 023201 (2017).

Accelerator-based synthesis of rhenium-186 that enables high spatial resolution imaging

S. Takeda,[*1] I. O. Umeda,[*1] M. Katsuragawa,[*1] A. Yagishita,[*1] A. Nambu,[*2] X. Yin,[*2] H. Haba,[*2] and T. Takahashi[*1]

Radiotheranostics is the integration of targeted radionuclide therapy with molecular imaging techniques such as Positron Emission Tomography (PET) and Single Photon Emission Computed Tomography (SPECT). The exponential growth of radiotheranostics in the field of oncology is due to its unique mechanism of action, which allows for the targeted elimination of tumor cells with minimal adverse effects. The radionuclides, used for diagnosis, emit β^+ particles in PET and γ rays in SPECT. In contrast, for cancer therapy, radionuclides that emit energetic α, β^-, and auger electron particles are utilized.

Rhenium radioactive isotopes are an attractive option for radiotheranostics, as they emit both particles suitable for targeted therapy and photons useful for diagnosis, and can aid in developing radiopharmaceuticals. Rhenium belongs to the same chemical family as technetium. Technetium-99m (^{99m}Tc) is the most widely used radionuclide in nuclear medicine imaging, due to its short half-life and favorable physical properties such as low radiation exposure to patients. Many ^{99m}Tc-labeled probes have been developed and are used clinically to diagnose of various diseases. Most of the ligands and chelation chemistry developed for technetium can be also applied to rhenium. ^{186}Re is typically produced through neutron irradiation in reactors in other countries, but production in Japan is challenging due to the difficulty of reactor production. Additionally, ^{186}Re produced in reactors includes a large amount of carrier Re as raw material. At the RIKEN RI Beam Factory, carrier-free ^{186}Re can be produced through proton and heavy ion-induced reactions of ^{186}W using the RIKEN AVF cyclotron. Our goal is to develop new radiotheranostics using ^{186}Re.[1,2)]

^{186}Re emits gamma-rays at 137 keV, allowing visualization of biobehavior of ^{186}Re-labeled radiopharmaceuticals. However, the emission yield of 137 keV photons is as small as 9.4%. Therefore, high-sensitivity and high-resolution imaging have been challenging since the signals (137 keV photons) are prone to be contaminated by the continuum background constituted by scattering of high-energy gamma-rays caused by contamination of rhenium isotopes other than ^{186}Re. In our previous experiment, ^{186}Re was produced in the ^{186}W$(d, 2n)^{186}$Re reaction using the 24-MeV d beam. We found that the byproduct of ^{184}Re significantly contributed to the contamination and caused significant degradation in imaging quality.

To improve imaging quality, it is essential to increase the radionuclidic purity of ^{186}Re. In this study, we produced ^{186}Re in the ^{186}W$(p, n)^{186}$Re reaction using the 14.8-MeV proton beam on target and successfully improved the radionuclidic purity of ^{186}Re from 94.43% to 99.56%.

A 19-MeV proton beam delivered from the RIKEN AVF cyclotron was degraded to 14.8 MeV through a Ta plate (192.6 μm) and irradiated onto a $^{186}WO_3$ powder (isotope enrichment of ^{186}W: 99.79%; thickness: $\sim$200 mg/cm^2). After irradiation, ^{186}Re was purified by chemical separation.[3)] 3 MBq of ^{186}Re in 200 μL of 0.01 M HCl was shipped to National Cancer Center Research Center for the imaging experiment.

We demonstrated the effectiveness of the purification for imaging using CdTe-DSD SPECT[4)] (Fig. 1) developed by the IPMU team. CdTe-DSD SPECT is a novel small animal imaging system consisting of 8 modules of CdTe Double-sided Strip Detectors[5)] and a multi-pinhole collimator made of tungsten. The detector has an energy resolution of 1–2 keV (FWHM) in 10–100 keV and 1.6% (FWHM) at 140 keV, which is around three times better than those of currently available high-grade semiconductor SPECT systems. An ultra-high spatial resolution of better than 350 μm is possible. Figure 2 compares phantom imaging results for ^{186}Re with a purity of 94.43% (left) and 99.56% (right). The image was noisy for lower purity because of the continuum background produced by ^{184}Re. On the other hand, the preferred image was obtained for high-purity ^{186}Re. This is a promising result, and we will proceed to in-vivo imaging with mice.

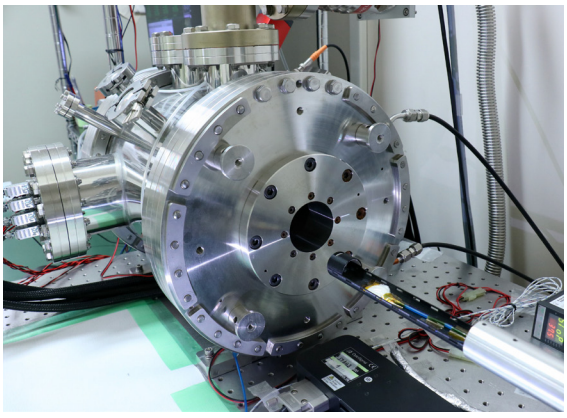

Fig. 1. CdTe-DSD SPECT viewed from the entrance window for small animals.

*1 Kavli Institute for the Physics and Mathematics of the Universe, University of Tokyo
*2 RIKEN Nishina Center

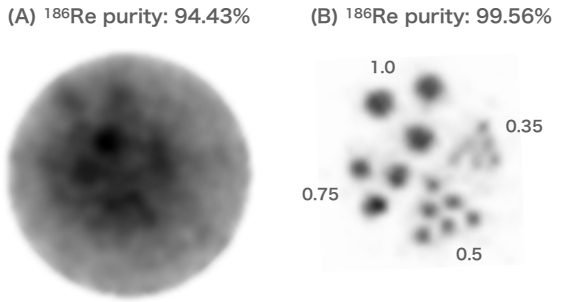

Fig. 2. The comparison of phantom imaging results for ^{186}Re with a radionuclidic purity of 94.43% (left) and 99.56% (right) taken with CdTe-DSD SPECT.

References

1) I. O. Umeda *et al.*, RIKEN Accel. Prog. Rep. **54**, 157 (2021).
2) I. O. Umeda *et al.*, RIKEN Accel. Prog. Rep. **55**, 139 (2022).
3) N. Shigeta *et al.*, J. Radioanal. Nucl. Chem. **205**, 85 (1996).
4) S. Takeda *et al.*, IEEE Trans. Radiat. Plasma Med. Sci. (to be submitted).
5) S. Takeda *et al.*, Nucl. Instrum. Methods Phys. Res. A **912**, 57 (2018).

^{44m}Sc-DOTA-TATE imaging with a cancer disease mouse model for multiple-isotope PET imaging

T. Fukuchi,[*1] Y. Kanayama,[*1] Y. Nakatani,[*1] A. Nambu,[*2] S. Usuda,[*2] Y. Shigekawa,[*2] X. Yin,[*2] H. Haba,[*2] and Y. Watanabe[*1]

Positron emission tomography (PET) is a powerful tool for the visualization of radiotracer distribution used for imaging diagnosis in medical and fundamental life sciences. However, standard PET is only useful for single-tracer imaging because of the energy constancy of annihilation photons, which are utilized for PET imaging. To enhance the usefulness of PET, we developed a new PET system that can be used for simultaneous multi-tracer PET imaging, named multiple-isotope PET (MI-PET).[1,2)]

A positron emitter ^{44m}Sc is one of the MI-PET nuclides. MI-PET utilizes a prompt γ-ray to identify the tracer nuclide in addition to coincidence measurement of positron-electron annihilation photons, which is used for conventional PET systems. ^{44m}Sc is a beta-plus decay nuclide with a half-life of 58.6 h and emits 1157 keV prompt γ-ray successively after positron emission. As a preliminary study for future multi-tracer imaging, we conducted single-tracer PET imaging experiment using a cancer mouse model with ^{44m}Sc labelled drug.

For future multi-tracer imaging, we synthesized a tracer labelled by an MI-PET nuclide ^{44m}Sc (positron prompt γ-ray emitter) and tested for accumulation on cancer cells. For the experiment, we synthesized a ^{44m}Sc labelled DOTA-TATE (DOTA-[Tyr^3]-octreotide), which is a compound containing tyrosine^3-octreotate and somatostatin receptor for numerous malignancies. The labelling protocol was based on a method developed by Huclier-Markai *et al.*[3,4)] DOTA-TATE was purchased from BACHEM (Switzerland). ^{44m}Sc was produced *via* the reaction of ^{44}Ca$(d, 2n)^{44m}$Sc with a 24-MeV deuteron beam at the RIKEN AVF cyclotron and purified by ion-exchanges. The produced ^{44m}Sc was transported to the RIKEN Kobe campus for the drug synthesis. A total of 0.2 nmol of DOTA-TATE and 5 MBq of ^{44m}Sc were added into NaOH 95°C for 30 min with shaking. After incubation, 1.1 MBq of 95°C for 30 min with shaking. After incubation, 1.1 MBq of ^{44m}Sc labelled DOTA-TATE was purified using a C18 solidphase extraction column. The labelling ratio for ^{44m}Sc-DOTA-TATE was approximately 30%.

We prepared an 8-week-old immunodeficient male mouse transplanting pancreatic tumoral cell (AR42J)[5)] as a cancer disease animal model. For the imaging experiment, 1.1 MBq of ^{44m}Sc-DOTA-TATE was administered *via* the tail vein. After 1 min from administration, a 90-min scan of the mouse abdomen was performed under anaesthesia using the MI-PET system.[1)] The experimental setting for the mouse imaging is shown in Fig. 1. All animal experiments in this study received ethical approval by the institutional review board of RIKEN and were performed in accordance with the guidelines for care and use of laboratory animals.

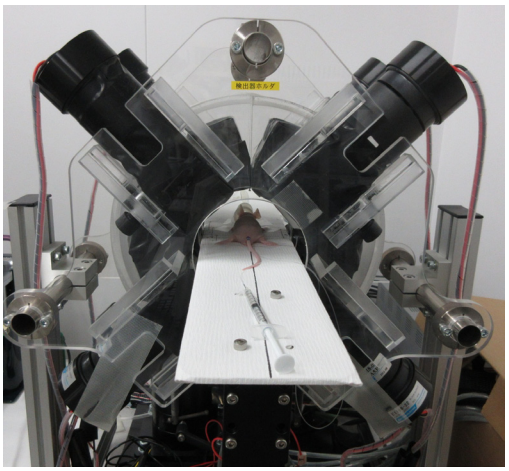

Fig. 1. Experimental setting for the mouse imaging using MI-PET system.

Figure 2 shows a photograph and reconstructed image of a mouse. In this reconstructed image, we

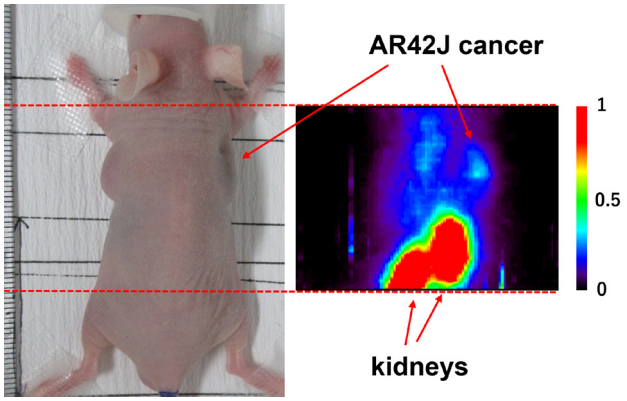

Fig. 2. A photograph (left) and reconstructed image (right) of a mouse administrated with ^{44m}Sc-DOTA-TATE. Image is reconstructed by conventional PET events, namely coincidence measurement of the annihilation photons without prompt γ-ray detection.

*1 RIKEN Center for Biosystems Dynamics Research
*2 RIKEN Nishina Center

can clearly observe the accumulation of ^{44m}Sc-DOTA-TATE in AR42J cancer. In the future, we will perform imaging experiments for multi-drug comparison on animal disease models using ^{44m}Sc-DOTA-TATE and other PET tracers, such as ^{18}F-FDG.

References

1) T. Fukuchi *et al.*, Med. Phys. **40**, 2257 (2017).
2) T. Fukuchi *et al.*, J. Instrum. **16**, P01035 (2021).
3) S. Huclier-Markai *et al.*, Nucl. Med. Biol. **41**, e36 (2014).
4) T. Fukuchi *et al.*, RIKEN Accel. Prog. Rep. **55**, 142 (2022).
5) J. Christophe, Am. J. Physiol. **266**, G963 (1994).

Source preparation technique for Ag^{211}At for alpha spectroscopy

S. Fujino,[*1] T. Kojima,[*2] K. Mori,[*1] T. Yamada,[*1,*3] Y. Wang,[*4] X. Yin,[*4] and H. Haba[*4]

^{211}At has attracted a considerable amount of interest because of its potential advantages in targeted alpha therapy. High-resolution alpha spectrometry is one of the most important techniques in radiochemical analyses and precise radioactivity measurements. Electroplating is widely used as a conventional technique to prepare α sources. However, there are several difficulties in applying this method to the measurement of ^{211}At such as its short half-life and high volatility. To overcome such difficulties, we studied another practical approach using a Ag plate without electroplating.

In this study, carrier-free ^{211}At was produced by the ^{209}Bi$(\alpha, 2n)^{211}$At reaction using the RIKEN AVF cyclotron.[1] Three different chemical forms of 100 kBq/mL of ^{211}At solutions were prepared as listed in Table 1. To reduce the radioactivity loss due to the volatility of At, ascorbic acid (AA) was added to solution (II) considering the result of a previous study on At retention using AA by Toyoshima *et al.*[2] At is also expected to have stable alkalinity; thus, NaOH was added to solution (III). Ag plates with a thickness of 0.1 mm were used to fix ^{211}At. Approximately 30 μL of each ^{211}At solution in Table 1 was directly dropped onto a Ag plate. Sources were dried in a desiccator with silica gel. After drying process, sources were measured using a ZnS (Ag) scintillation detector with a 2π geometry to evaluate the deposition yield of ^{211}At on silver. A Si detector was also used to obtain an α spectrum from each source with the defined sources-detector geometry in vacuum. In addition, imaging plate (IP) was used to confirm the distribution of radioactivity in an active area on the Ag plate with ^{211}At solution (I).

Table 1. ^{211}At solutions used in the present study.

^{211}At solutions		Chemical form
(I)	^{211}At	^{211}At in H_2O
(II)	^{211}At+AA	^{211}At in 1 μg/mL AA aqueous solution
(III)	^{211}At+NaOH	^{211}At in 50 μg/mL NaOH aqueous solution

Figure 1 shows the measured α spectra obtained by three different types of sources. Two major peaks of ^{211}At (E_α = 5.87 MeV) and ^{211}Po (E_α = 7.45 MeV)

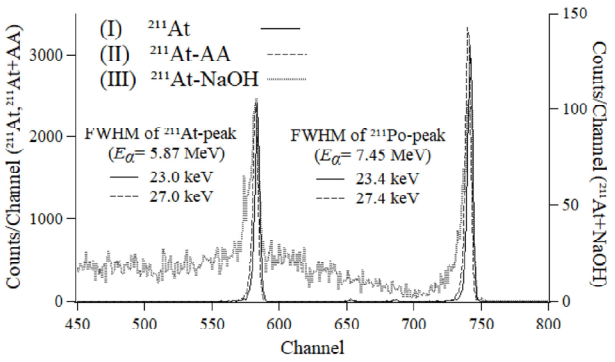

Fig. 1. Measured α spectra obtained by ^{211}At sources.

were observed in each spectrum. As shown in Fig. 1, the ^{211}Po peaks obtained by source (II) shifted to the lower energy side by approximately 20 keV compared to those for source (I). This could be due to self-absorption caused by AA. However, the full width at half maximum (FWHM) of the ^{211}At peak of source (II) increased by only 4 keV compared with that for source (I); thus, it could not cause a large uncertainty in the activity measurement. In contrast, a significant degradation in the spectrum was observed for source (III) compared with the two other sources. The deposition yield of each ^{211}At source was determined as a ratio of the $2\pi\alpha$ count rate to the activity of ^{211}At. The resulting deposition yields were 88.3% ± 1.2%, 98.4% ± 1.3%, and 40.3% ± 6.8% for sources (I), (II), and (III), respectively, indicating that AA contributes to the retention of ^{211}At during drying. However, the results obtained for source (III) may be affected by self-absorption, resulting in underestimation of the deposition yield.

Figure 2 shows the distribution of ^{211}At on a Ag plate for ^{211}At solution (I) with an IP. Although the

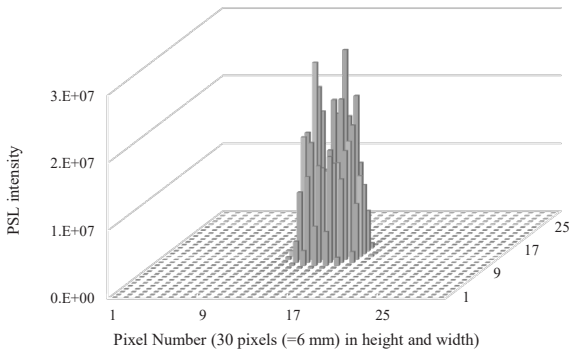

Fig. 2. Distribution of ^{211}At on a Ag plate.

*1 Graduate School of Science and Engineering, Kindai University
*2 School of Science and Engineering, Kindai University
*3 Atomic Energy Research Institute, Kindai University
*4 RIKEN Nishina Center

diameter of the ^{211}At solution drop before drying was around 6 mm, 99% of the radioactivity of the source was concentrated within a diameter of 2 mm. In the measurements with a defined solid angle, an extension of the active area might increase the uncertainty in the evaluation of the geometric efficiency. Therefore, a source with a small active area, such as that prepared in the present study, could have the advantage that the activity could be determined with a smaller uncertainty.

References

1) Y. Wang *et al.*, RIKEN Accel. Prog. Rep. **53**, 192 (2019).
2) A. Toyoshima *et al.*, Radiat. Saf. Manage. **18**, 13 (2019).

Radioactivity calibrations of ^{225}Ac and ^{211}At

K. Arai,[*1] M. Imamura,[*1] D. Mori,[*1] H. Ishizu,[*1] Y. Sato,[*2] H. Haba,[*3] X. Yin,[*3] Y. Wang,[*3] and Y. Wakitani[*1]

^{225}Ac and ^{211}At are short half-life α-emitters that have attracted attention as radiopharmaceuticals. The minimum requirements for radiopharmaceuticals, the radioactivity of most preparations is specified as 90–110%. To confirm of fulfill the specification, the calibration of measuring instruments, and thus standard sources with small uncertainties to the best extent possible is essential. However, certain issues plague the radioactivity calibration. First, ^{213}Po, which is one of the progenies of ^{225}Ac, interferes with the measurement. The short half-life of 3.70 μs[1)] of ^{213}Po causes counting loss owing to the β-rays emitted from its parent ^{213}Bi when measured using a commercial liquid scintillation counter (LSC) with dead time of a few μs. Thus, a correction for counting efficiency is necessary. Second, ^{211}At is highly volatile; however, there is minimal knowledge on suitable samples for the LSC measurement. In addition, ^{207}Bi, which is one of the progenies of ^{211}At, is not in radiative equilibrium; thus, the contribution of ^{207}Bi and its uncertainty on the calibration must be evaluated. In this study, our radioactivity calibration methods for ^{225}Ac and ^{211}At were examined to solve the above problems through comparisons with the results obtained from the National Institute of Advanced Industrial Science and Technology (AIST).

The commercial LSC, Tricarb 4810TR (Perkinelmer Inc.) and the custom-build LSC with variable dead time, LSC0001 were used in the radioactivity measurements of ^{225}Ac and ^{211}At. To correct for the counting loss of ^{213}Po in an ^{225}Ac solution, the dead time of LSC0001 was set to 100 μs, and a correction factor was calculated from the ratio of the count rate measured by LSC0001 to that measured by 4810TR. The radioactivity was calculated by the CIEMAT-NIST method[2)] for both Japan Radioisotope Association (JRIA) and AIST.

^{211}At was produced in the ^{209}Bi$(\alpha, 2n)^{211}$At reaction at the RIKEN AVF cyclotoron.[3)] ^{211}At was dissolved with 1.2% ascorbic acid in 5/15 M phosphate buffer or 1 M sodium hydroxide aqueous solution;[4,5)] the sodium hydroxide solution was selected to suppress loss of volatile ^{211}At. The contribution of ^{207}Bi to the measurement at 24 h after distillation was estimated to be approximately 0.1%. Therefore, measurements were performed using Tricarb 4810TR within 2 half-lives after dry distillation to minimize the contribution of ^{207}Bi as low as possible. After ^{211}At had decayed sufficiently (above 10 days), the contribution of ^{207}Bi was evaluated through re-measurements. The radioactivity of ^{211}At was also calculated by the CIEMAT-NIST method.[2)]

The radioactivities of ^{225}Ac and ^{211}At were measured to be 318.9 ± 4.6 kBq/g ($k = 2$) and 3.155 ± 0.064 kBq/g ($k = 2$), respectively, and they are shown in Fig. 1. Most of the uncertainty components were uncertainties in the calculations by the CIEMAT-NIST method. In addition, the radioactivities of ^{225}Ac and ^{211}At by AIST were 317.1 ± 4.8 kBq/g ($k = 2$) and 3.143 ± 0.025 kBq/g ($k = 2$), respectively, and both were consistent with our data within the uncertainty range.

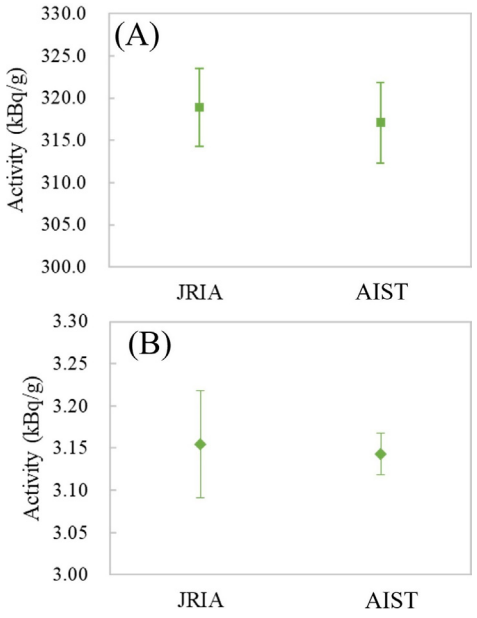

Fig. 1. Intercomparison result of (A) ^{225}Ac and (B) ^{211}At radioactivity.

In summary, the radioactivities of ^{225}Ac and ^{211}At were measured and compared with those by AIST. Consistent results were obtained for both nuclides. JRIA is an accredited calibration laboratory related radiation and radioactivity in Japan Calibration Service System (JCSS). Accredited calibration laboratories, which satisfy the requirements of the measurement act can issue calibration certificate with the "JCSS" logo. Furthermore, we are ready to calibrate ^{225}Ac radioactivity for JCSS calibration. In the future, where ^{211}At is scheduled to applied for JCSS calibration nuclide and is already available for a general calibration.

*1 R&D Section, Japan Radioisotope Association
*2 National Metrology Institute of Japan (NMIJ), National Institute of Advanced Industrial Science and Technology
*3 RIKEN Nishina Center

References
1) M. -M. Bé *et al.*, Table of Radionuclides (Bureau International des Poids et Mesures, Sèvres, 2010), Vol. 5, p. 59.
2) A. G. Malonda, Free Parameter Models in *Liquid Scintillation Counting* (Centro de Investigaciones Energéticas, Medioambientales y Tecnológicas, Madrid, 1999).
3) Y. Wang *et al.*, RIKEN Accel. Prog. Rep. **53**, 192 (2019).
4) A. Toyoshima and A. Shinohara., Radioisotopes **67**, 461 (2018).
5) T. Watabe *et al.*, J. Nucl. Med. **60**, 1301 (2019).

Activation cross sections of ^{28}Mg via α-particle-induced reaction on ^{27}Al

M. Aikawa,[*1,*2] H. Huang,[*3,*2] G. Damdinsuren,[*3,*2] S. Ebata,[*4,*2] H. Haba,[*2] S. Takács,[*5,*2] F. Ditrói,[*5,*2] and Z. Szücs[*5,*2]

Magnesium-28 ($T_{1/2}$ = 20.9 h) decays with emission of a β^- particle and γ rays. This radionuclide can be used as a radiotracer in several applications.[1] The promising production reaction of ^{28}Mg is the α-particle-induced reaction on ^{27}Al targets. Ten experimental studies on the cross sections of the ^{27}Al$(\alpha, 3p)^{28}$Mg reaction were found in the EXFOR library.[2] However, the cross sections of the previous studies are broadly scattered. Therefore, we performed an experiment to obtain reliable cross sections of the ^{27}Al$(\alpha, 3p)^{28}$Mg reaction.

An experiment using a 50.7-MeV α-particle beam was conducted at the RIKEN AVF cyclotron employing the stacked-foil activation technique and high-resolution γ-ray spectrometry.

Pure metallic foils of ^{27}Al (>99% purity, 50 and 5 μm thick) and ^{nat}Ti (99.6% purity, 5 μm thick) were purchased from Nilaco Corp., Japan. The 50- and 5-μm Al foils were used as target and catcher foils, respectively. The Ti foil was used for the ^{nat}Ti$(\alpha, x)^{51}$Cr monitor reaction. The size and weight of all foils were measured for the average thicknesses. The thicknesses of the Al target, Al catcher, and Ti monitor foils were determined as 13.2, 1.22, and 2.37 mg/cm^2, respectively. The foils were cut into a 10 × 10 mm size and stacked in a target holder that served as a Faraday cup.

The stacked target was irradiated for 30 min with a 50.7-MeV α-particle beam. The initial beam energy was determined using the time-of-flight method.[3] The average beam intensity measured using the Faraday cup was obtained as 205 nA. The beam energy degradation in the stacked target was calculated using stopping powers obtained from the SRIM code.[4] γ rays emitted from the irradiated foils were measured using a high-purity germanium detector (ORTEC GEM30P4-70) and dedicated analysis software (SEIKO EG&G Gamma Studio) without chemical separation.

The cross sections of the ^{nat}Ti$(\alpha, x)^{51}$Cr monitor reaction were derived using the γ line at 320 keV (I_γ = 9.91%) from the decay of ^{51}Cr ($T_{1/2}$ = 27.7 d). The derived cross sections were compared with the International Atomic Energy Agency recommended values.[5] For best agreement between the measured and recommended values, the incident beam energy and thickness of Al target foils were corrected within their uncertainties by +0.2 MeV and −1%, respectively. The other measured parameters were adopted without correction. The corrected cross sections were consistent with the recommended values, indicating proper beam parameters and energy loss determination within the stack, as shown in Fig. 1.

The cross sections of the ^{27}Al$(\alpha, 3p)^{28}$Mg reaction were determined using the γ line at 1342 keV (I_γ = 54%), which was emitted with the decay of ^{28}Mg ($T_{1/2}$ = 20.9 h). Figure 2 shows our preliminary result with the earlier experimental data obtained from the EXFOR library[2] and the TENDL-2021 theoretical values.[6] The theoretical values are considerably lower than the experimental data.

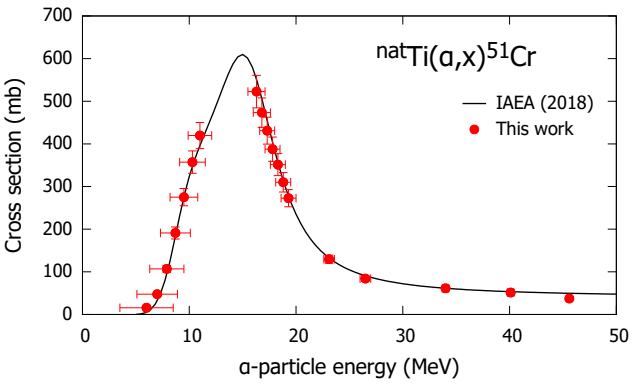

Fig. 1. Cross sections of the ^{nat}Ti$(\alpha, x)^{51}$Cr monitor reaction with the IAEA recommended values.[5]

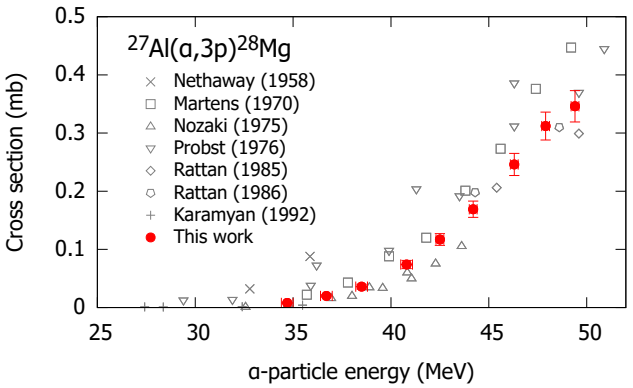

Fig. 2. Measured cross sections of the ^{27}Al$(\alpha, 3p)^{28}$Mg reaction with the literature data and the TENDL-2021 values.[6]

*1 Faculty of Science, Hokkaido University
*2 RIKEN Nishina Center
*3 Graduate School of Biomedical Science and Engineering, Hokkaido University
*4 Graduate School of Science and Engineering, Saitama University
*5 Institute for Nuclear Research (ATOMKI)

References
1) N. P. van der Meulen *et al.*, Appl. Radiat. Isot. **115**, 125 (2016).
2) N. Otuka *et al.*, Nucl. Data Sheets **120**, 272 (2014).
3) T. Watanabe *et al.*, Proc. 5th Int. Part. Accel. Conf. (IPAC2014), (2014), p. 3566.
4) J. F. Ziegler *et al.*, Nucl. Instrum. Methods Phys. Res. B **268**, 1818 (2010).
5) A. Hermanne *et al.*, Nucl. Data Sheets **148**, 338 (2018).
6) A. J. Koning *et al.*, Nucl. Data Sheets **155**, 1 (2019).

Production cross sections of ^{47}Sc via α-particle induced reactions on ^{nat}Ca†

M. Aikawa,[*1,*2] Y. Hanada,[*3,*2] D. Ichinkhorloo,[*4,*2] H. Haba,[*2] S. Takács,[*5,*2] F. Ditrói,[*5,*2] and Z. Szücs[*5,*2]

Scandium-47 ($T_{1/2}$ = 3.3492 d) is a potential radionuclide for therapy.[1] Owing to the relatively small abundance of ^{46}Ca (0.004%) and ^{48}Ca (0.187%) in natural calcium, its most possible production route for practical use is expected to be the α-particle-induced reaction on ^{44}Ca (2.086%).

In a literature survey, we found only one experimental study of the ^{44}Ca$(\alpha,p)^{47}$Sc reaction.[2] Therefore, we performed an experiment to provide more credible cross sections of the ^{nat}Ca$(\alpha,x)^{47}$Sc reaction. In addition to the production cross sections of ^{47}Sc, the activation cross sections for ^{46,44m,44g,43}Sc and ^{47}Ca were also determined simultaneously.

In the experiment, a 29-MeV α-particle beam was used to activate the targets at the AVF cyclotron in RIKEN. The stacked-foil activation technique and high resolution γ-ray spectrometry were adopted to perform the measurement.

Calcium-fluoride (CaF_2) was deposited on a high-purity ^{27}Al backing foil (Al_H, 99.999% purity, Goodfellow Co. Ltd., UK) and used as the ^{nat}Ca target. Metallic foils of ^{nat}Ti (99.5% purity) for the ^{nat}Ti$(\alpha,x)^{51}$Cr monitor reaction and low-purity ^{27}Al (Al_L, >99% purity) to catch recoiled products were purchased from Nilaco Corp., Japan and inserted into the stack. The average thicknesses of the Al_H, Al_L, and ^{nat}Ti foils were 2.57, 1.50, and 2.30 mg/cm^2, respectively, determined from the measured lateral sizes and weights of the foils. The thickness of the deposited CaF_2 layer was 0.135 mg/cm^2, which was derived from the measured deposited area and net weight. All foils were cut into a size of 10×10 mm to fit a target holder that also served as a Faraday cup. Each ^{nat}Ca target comprised two CaF_2 layers sandwiched between the Al_H backing foils. Twelve ^{nat}Ca targets were stacked with seven sets of ^{nat}Ti-Al_L foils in the target holder.

The stacked target was irradiated with an α-particle beam for 30 min. The measured average beam intensity and energy were 175 nA and 29.0 ± 0.2 MeV, respectively. The energy degradation in the stacked target was calculated using stopping powers obtained from the SRIM code.[3]

The high-resolution γ-ray spectrometry using a high-purity germanium detector was performed without chemical separation. The spectra of the ^{nat}Ca targets were measured with cooling times ranging from 3.2 h to 77 d.

The derived cross sections of the ^{nat}Ti$(\alpha,x)^{51}$Cr monitor reaction were compared with the IAEA recommended values[4] to assess beam parameters and target thicknesses. The beam intensity and thicknesses of both Al_H and Al_L foils were corrected within their uncertainties by +5.6% and −1%, respectively. The measured thicknesses of the ^{nat}Ti monitor foil and the CaF_2 layer were adopted without any correction.

^{47}Sc could be produced directly in the ^{44}Ca$(\alpha,p)^{47}$Sc reaction and indirectly by decay of the co-produced ^{47}Ca ($T_{1/2}$ = 4.536 d) and ^{47}K ($T_{1/2}$ = 17.50 s). The indirect contribution was at a negligible level because ^{47}Ca and ^{47}K can be formed only on the lower-abundant ^{46}Ca and ^{48}Ca isotopes. The activity of ^{47}Sc was determined by measuring the γ line at 159.381 keV ($I_\gamma = 68.3\%$) from the decay of ^{47}Sc. The derived cross sections of the ^{nat}Ca$(\alpha,x)^{47}$Sc reaction are shown in Fig. 1 compared with the literature data[2] and the theoretical values provided in the TENDL-2019 library.[5] The literature data on ^{44}Ca targets were normalized to those on ^{nat}Ca targets. The newly obtained data correspond to a smooth excitation function, in contrast to the literature data. The TENDL-2019 calculation overestimates both the experimental datasets. Thus, the data are expected to contribute to practical use in nuclear medicine and aid in improving the theoretical models.

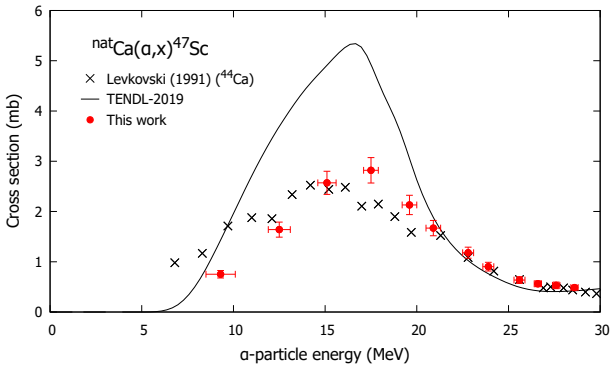

Fig. 1. Measured cross sections of the ^{nat}Ca$(\alpha,x)^{47}$Sc reaction with normalized literature data[1] and TENDL-2019 values.[5]

This work was supported by the Japan-Hungary Research Cooperative Program between JSPS and HUS, Grant number JPJSBP120193808 and NKM-43/2019.

† Condensed from the article in Nucl. Instrum. Methods Phys. Res. B **515**, 1 (2022)

*1 Faculty of Science, Hokkaido University
*2 RIKEN Nishina Center
*3 Graduate School of Biomedical Science and Engineering, Hokkaido University
*4 Nuclear Research Center, National University of Mongolia
*5 Institute for Nuclear Research (ATOMKI)

References
1) I. F. Chaple *et al.*, J. Nucl. Med. **59**, 1655 (2018).
2) V. N. Levkovski, Cross Sections of Medium Mass Nuclide Activation (A = 40–100) by medium energy protons and alpha particles (E = 10–50 MeV) (Inter-Vesi, Moscow, USSR, 1991).
3) J. F. Ziegler *et al.*, Nucl. Instrum. Methods Phys. Res. B **268**, 1818 (2010).
4) A. Hermanne *et al.*, Nucl. Data Sheets **148**, 338 (2018).
5) A. J. Koning *et al.*, Nucl. Data Sheets **155**, 1 (2019).

Production cross sections of ^{52g}Mn in α-particle-induced reactions on ^{nat}V†

G. Damdinsuren,[*1,*2] M. Aikawa,[*1,*2,*3] Kh. Tegshjargal,[*4] N. Erdene,[*4] S. Ebata,[*5,*2] and H. Haba[*2]

Manganese-52 has the longer-lived ground state ^{52g}Mn ($T_{1/2}$ = 5.6 d, $\varepsilon + \beta^+$: 100%) and the shorter-lived excited state ^{52m}Mn ($T_{1/2}$ = 21.1 min, IT: 1.78%, $\varepsilon + \beta^+$: 98.22%). The decay processes of ^{52g}Mn are electron capture (70.6%) and positron emission (29.4%, $\langle E_{\beta^+} \rangle$ = 242 keV).[1] The positrons emitted from the decay of ^{52g}Mn can be used for Positron Emission Tomography (PET).[2] The direct routes to produce ^{52g}Mn involve charged-particle-induced reactions on chromium and vanadium. Whereas, the indirect route involves the internal transition of ^{52m}Mn co-produced simultaneously in the reactions. This study, we focused on the α-particle-induced reaction on ^{nat}V. Eleven experimental cross section data of the ^{nat}V$(\alpha, x)^{52g}$Mn reactions were found in the EXFOR library.[3] However, their data are largely scattered. Therefore, we measured the excitation function of the ^{nat}V$(\alpha, x)^{52g}$Mn reaction up to 50 MeV. The obtained cross sections were compared with the literature data and theoretical calculation in the TENDL-2019 library.[4]

The stacked-foil activation technique and high-resolution γ-ray spectrometry were used to measure the cross sections. Pure metallic foils of ^{nat}V (25-μm thick, 99% purity), ^{nat}Ti (5-μm thick, 99.6% purity), and ^{27}Al (5-μm thick, >99% purity) were purchased from Nilaco Corp., Japan, and used for the stacked target. The ^{nat}Ti foils were interleaved for the ^{nat}Ti$(\alpha, x)^{51}$Cr monitor reaction. The ^{27}Al foils were used to catch recoiled products from the ^{nat}V and ^{nat}Ti foils. The average target thicknesses were derived from the measured size and weight of the original foils. Derived average thicknesses of ^{nat}V, ^{nat}Ti, and ^{27}Al foils were 20.4, 2.24, and 1.22 mg/cm^2, respectively. The original foils were cut into a size of 8 × 8 mm. Eleven sets of V-Al-Ti-Ti-Al foils were stacked into a target holder, which served as a Faraday cup.

The stacked target was irradiated with an α-particle beam for 30 min. The primary beam energy was measured by the time-of-flight method.[5] The measured beam energy was 50.6 ± 0.2 MeV. Consequently, the energy degradation in the stacked target was calculated using stopping powers obtained from the SRIM code.[6] The average beam intensity measured using the Faraday cup was 194 nA.

γ rays emitted from each irradiated foil were measured by a high-resolution HPGe detector (ORTEC GEM-25185-P), which was calibrated with a multiple gamma-ray emitting point source. The spectra were analyzed using dedicated software (SEIKO EG&G Gamma Studio). Each ^{nat}V foil with the following ^{27}Al catcher foil was measured several times. The distance between the detector and foils was arranged to ensure a dead time of less than 3%.

The cross sections of the ^{nat}Ti$(\alpha, x)^{51}$Cr monitor reaction were derived and used to assess the beam parameters and target thicknesses. The measurement of the γ line at 320.08 keV (I_γ = 9.91%) from the decay of ^{51}Cr ($T_{1/2}$ = 27.7025 d) was performed following a cooling time of 3 days. Only the Ti foils at the beam downstream of each Ti-Ti foil pair in the stack were used for cross section deduction because the compensation of recoiled ^{51}Cr was expected. The dead time during the measurements was maintained at less than 1%. Subsequently, the derived cross sections were compared with the IAEA-recommended values[7] and found to be consistent with each other. We adopted the measured beam parameters and target thicknesses without any corrections for data analyses.

The cross sections of the ^{nat}V$(\alpha, x)^{52g}$Mn reaction were derived. The γ line at 935.544 keV (I_γ = 94.5%) from the decay of ^{52g}Mn was measured following a cooling time of 17 d. During the cooling time, the excited state ^{52m}Mn completely decayed to the ground state ^{52g}Mn or the stable nuclide ^{52}Cr. The cumulative cross

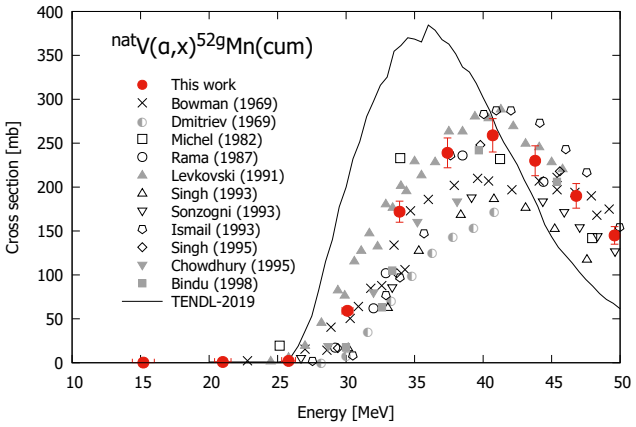

Fig. 1. Excitation functions of the ^{nat}V$(\alpha, x)^{52g}$Mn reaction.

† Condensed from the article in Appl. Radiat. Isot. **184**, 110204 (2022)

*1 Graduate School of Biomedical Science and Engineering, Hokkaido University
*2 RIKEN Nishina Center
*3 Faculty of Science, Hokkaido University
*4 School of Engineering and Applied Sciences, National University of Mongolia
*5 Graduate School of Science and Engineering, Saitama University

sections could be derived from the measured net counts of the γ line. The excitation functions are shown in Fig. 1 along with the literature data and TENDL-2019 values.[4] The measured cross sections exhibited a smooth curve and agreement with part of the previous experimental data. However, the shape of the TENDL-2019 values was largely different from the experimental data.

G. Damdinsuren was granted a scholarship by the M-JEED project (Mongolian-Japan Engineering Education Development Program, J11B16).

References

1) Y. Dong *et al.*, Nucl. Data Sheets **128**, 185 (2015).
2) F. Bianchi *et al.*, Appl. Radiat. Isot. **166**, 109329 (2020).
3) N. Otuka *et al.*, Nucl. Data Sheets **120**, 272 (2014).
4) A. J. Koning *et al.*, Nucl. Data Sheets **155**, 1 (2019).
5) T. Watanabe *et al.*, Proc. 5th Int. Part. Accel. Conf. (IPAC 2014), (2014), p. 3566.
6) J. F. Ziegler *et al.*, Nucl. Instrum. Methods Phys. Res. B **268**, 1818 (2010).
7) F. Tárkányi *et al.*, IAEA-TECDOC-1211 (2007).

Activation cross sections of deuteron-induced reactions on ^{nat}Cr up to 24 MeV†

H. Huang,[*1,*2] M. Aikawa,[*1,*2,*3] Y. Hanada,[*1,*2] and H. Haba[*2]

Many radioisotopes are used for medical applications. ^{51}Cr ($T_{1/2}$ = 27.8 d) decays through the electron capture process with the emission of 320-keV γ rays. The radionuclide is used to label red blood cells.[1] Another medical radionuclide ^{52g}Mn ($T_{1/2}$ = 5.591 d), decays via the electron capture and positron emission processes. The emitted positrons can be used for imaging of positron emission tomography (PET).[2] Further, ^{48}V ($T_{1/2}$ = 15.97 d) can be used for tumor imaging.[3] Among the possible reactions to produce the medical radionuclides, we focused on the deuteron-induced reaction on ^{nat}Cr. The reactions are also related to the effects on the anti-corrosion coating of chromium and the iron-chromium alloy in fusion reactors.[4] Reliable experimental and evaluated excitation functions of the reactions are required. Therefore, we aim to obtain a new set of experimental data for the reactions up to 24 MeV.

We adopted the well-established stacked-foil activation technique and high-resolution γ-ray spectrometry. The stacked target comprised foils of nickel-chromium (NiCr) alloy (99.9% purity, Goodfellow Co., Ltd., UK), ^{nat}Ti (99.6% purity, Nilaco Corp., Japan), and ^{27}Al (>99% purity, Nilaco Corp., Japan). The ^{nat}Ti foil was used for the ^{nat}Ti$(d,x)^{48}$V monitor reaction. ^{27}Al foil was interleaved to collect recoiled products. The average foil thicknesses were derived from their measured weight and size. We analyzed the elemental ratio of the NiCr alloy foil (Cr 21.5%, Ni 76.7%, Mn 1.7%) by a scanning electron microscope with an energy dispersive X-ray spectrometer (Hitachi TM4000 Plus II). The original foils were cut into squares of 8 × 8 mm to fit a target holder. Thirteen sets of NiCr-NiCr-Al-Ti-Ti-Al foils were stacked as the target. In addition, the loss recoiled from the second foils was assumed to be compensated by that from the first foils. Only γ spectra from each second foil were measured.

The stacked target was irradiated for 30 min using a 24-MeV deuteron beam at the AVF cyclotron at RIKEN. The average intensity and primary energy of the beam were measured as 105 nA and 24.0 ± 0.1 MeV, respectively. Energy degradation in the stacked target was calculated using stopping powers obtained by the SRIM code.[5]

The γ rays emitted from the foils were detected seven times using a high-purity germanium detector (ORTEC GEM30P4-70). To assess the radionuclides with different half-lives, the measurements were performed with cooling times of 1 h–32 d, and the associated dead time was less than 5.2%.

The cross sections of the ^{nat}Ti$(d,x)^{48}$V monitor reaction were derived and compared with the recommended values of International Atomic Energy Agency.[6] According to the comparison, the beam intensity was decreased by 1.1% within the uncertainty (5%). The other parameters, such as primary beam energy and target thicknesses, were adopted without correction.

The production cross sections of ^{52g}Mn were determined using the 935.544-keV γ line (I_γ = 94.5%), following a cooling time of 1.8 d. The short-lived isomer ^{52m}Mn ($T_{1/2}$ = 21.1 min) decayed to ^{52g}Mn via isomeric transition, with a branching ratio of 1.78%. Consequently, the derived cross sections were cumulative. Our result was consistent with the recent studies while slightly smaller than the others (Fig. 1). The predicted values in the TENDL-2019 library[8] are larger than the experimental data at the peak between 15–20 MeV.

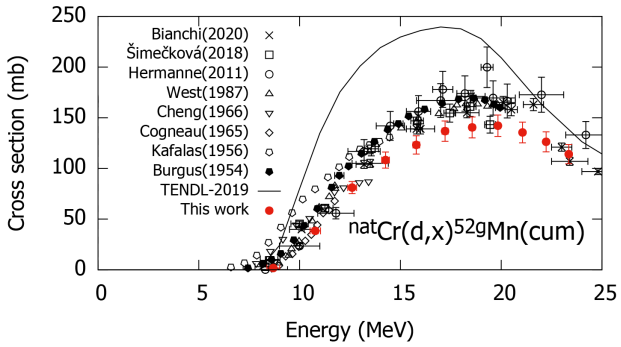

Fig. 1. Cumulative cross sections of the ^{nat}Cr$(d,x)^{52g}$Mn reaction compared with those in previous studies found in the EXFOR library[7] and the TENDL-2019 values.[8]

References
1) S. J. Gray *et al.*, J. Clin. Invest. **29**, 1604 (1950).
2) M. Pagani *et al.*, Eur. J. Nucl. Med. **24**, 1301 (1997).
3) K. Iwai *et al.*, Int. J. Rad. Appl. Instrum. B **16**, 783 (1989).
4) P. P. Liu *et al.*, J. Nucl. Mater. **459**, 81 (2015).
5) J. F. Ziegler *et al.*, SRIM: the Stopping and Range of Ions in Matter (2008), `http://www.srim.org`.
6) A. Hermanne *et al.*, Nucl. Data Sheets **148**, 338 (2018).
7) N. Otuka *et al.*, Nucl. Data Sheets **120**, 272 (2014).
8) A. J. Koning *et al.*, Nucl. Data Sheets **113**, 2841 (2012).

† Condensed from the article in Nucl. Instrum. Methods Phys. Res. B **530**, 23 (2022)

*1 Graduate School of Biomedical Science and Engineering, Hokkaido University
*2 RIKEN Nishina Center
*3 Faculty of Science, Hokkaido University

Activation cross sections of alpha-particle-induced reactions on natural lanthanum up to 50 MeV†

S. Ebata,[*1,*2] M. Aikawa,[*3,*2] G. Damdinsuren,[*4,*2] and H. Haba[*2]

In the medical field, radionuclides have been applied to therapy and diagnosis for decades. Ensuring the accuracy of nuclear data is essential for the safe and effective production of radionuclides. Recently, there have been investigations into radionuclides that can be used for both therapy and diagnosis. The radionuclide ^{142}Pr ($T_{1/2}$ = 19.12 h) is among the applicable candidates.[1] The alpha-particle-induced reaction on lanthanum is a practical method to generate ^{142}Pr. We found only two experimental studies of the ^{nat}La$(\alpha, x)^{142g}$Pr reaction,[2,3] for which the data are scattered and not fully consistent (Fig. 1). Therefore, we measured the production cross-sections of the ^{nat}La$(\alpha, x)^{142}$Pr reaction using the activation method.

Two independent experiments were performed using 50 (#1) and 29 MeV (#2) α beams at the RIKEN AVF cyclotron. To determine the excitation function, we applied the stacked-foil technique, and used a high-resolution germanium detector to measure the γ rays from generated radionuclides. The stacked targets comprised ^{nat}La (99% purity), ^{27}Al (>99% purity) and ^{nat}Ti (99.6% purity) metal foils purchased from Nilaco Corp., Japan. The actual thicknesses were derived as 15.4, 2.25, and 1.22 mg/cm^2 for the ^{nat}La, ^{nat}Ti, and ^{27}Al foils, respectively. The ^{nat}Ti foils were inserted into the stack for the ^{nat}Ti$(\alpha, x)^{51}$Cr monitor reaction to assess the beam parameters, energy loss of the particles, and target thicknesses through comparisons of the measured data with the recommended values.[4] The initial beam parameters were accepted; however, the thicknesses of ^{nat}La foils were corrected by +2% within the uncertainties (2%).

The ^{27}Al foils were used as catchers of recoiled products and for energy degradation. In experiment #1, eighteen sets of La-Al-Ti-Ti, and in experiment #2, eight La-Al-Ti foils were stacked into the target holders and served as Faraday cups. The energy degradation of the beam in the target was calculated using stopping powers obtained from the SRIM code.[5] Both targets were irradiated for 30 min. The average beam intensities were 196 (#1) and 210 nA (#2), and the measured primary beam energies were 50.6 (#1) and 29.0 MeV (#2).

The ^{nat}La foils with the following ^{27}Al catcher foil were measured together using a high-purity germanium detector after cooling times of 7–28 h. The γ line at 1575.85 keV (I_γ = 3.7%) with no interferences from decay of ^{142g}Pr was analyzed to derive the cross-sections of the ^{nat}La$(\alpha, x)^{142}$Pr reaction. The ^{142m}Pr isomer ($T_{1/2}$ = 14.6 min) produced simultaneously in the reaction decayed by IT decay mode to the ground state during the cooling time. The cross-sections derived from the γ ray spectra were cumulative owing to the contribution from the decay of its isomer.

The results of the experiments #1 and #2 are shown in Fig. 1 and compared with the previous studies[2,3] and the TENDL-2021 values.[6] Data from our experiments were consistent with each other. However, our cross-sections were slightly larger than the previous data above 17 MeV. The TENDL curve underestimated all data above 17 MeV, its peak was located at slightly lower energy and its width was narrower than those of all data.

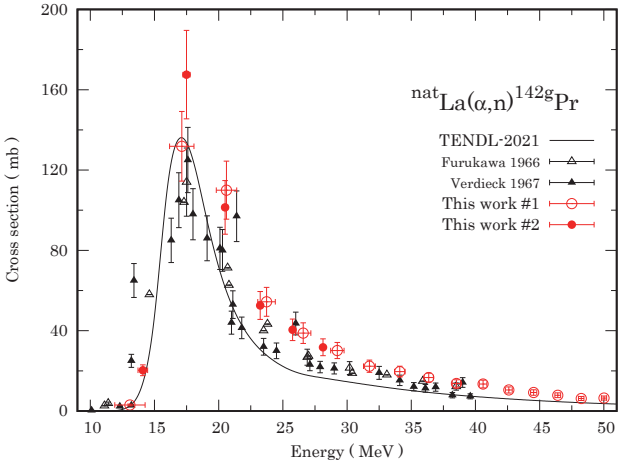

Fig. 1. Cumulative cross-sections of the ^{nat}La$(\alpha, n)^{142g}$Pr reaction in comparison with the previous data[2,3] and the TENDL-2021 curve (solid line).[6]

In addition to ^{142}Pr, production cross-sections for $^{139,\,138m}$Pr and $^{141,\,139g}$Ce were also obtained in this study. Furthermore, data of ^{139g}Ce and ^{138m}Pr were determined for the first time.

References

1) M. Sadeghi *et al.*, J. Radioanal. Nucl. Chem. **288**, 937 (2011).
2) M. Furukawa, Nucl. Phys. **77**, 565 (1966).
3) E. V. Verdiegk *et al.*, Phys. Rev. **153**, 1253 (1967).
4) F. Tárkányi *et al.*, IAEA-TECDOC-1211 (2007).
5) J. F. Ziegler *et al.*, Nucl. Instrum. Methods Phys. Res. B **268**, 1818 (2010).
6) A. J. Koning *et al.*, Nucl. Data. Sheets **155**, 1 (2019).

† Condensed from the article in Nucl. Instrum. Methods Phys. Res. B **530**, 18 (2022)

*1 Department of Physics, Saitama University
*2 RIKEN Nishina Center
*3 Faculty of Science, Hokkaido University
*4 Graduate School of Biomedical Science and Engineering, Hokkaido University

Reexamination of production cross sections of ^{153}Sm via α-particle induced reactions on ^{nat}Nd†

M. Aikawa,[*1,*2] M. Sakaguchi,[*3,*2] N. Ukon,[*4,*2] Y. Komori,[*2] H. Haba,[*2] N. Otuka,[*5,*2] and S. Takács[*6,*2]

Samarium radionuclides, ^{153}Sm ($T_{1/2}$ = 46.3 h) and ^{145}Sm ($T_{1/2}$ = 340 d), can be used in nuclear medicine.[1,2] Among the possible production routes of these medical radionuclides, we studied the α-particle-induced reactions on ^{nat}Nd.[3] However, the measured cross sections of the ^{nat}Nd$(\alpha,x)^{153}$Sm reaction were found to largely deviate from the data studied in a previous study.[4] The peak amplitude of the cross sections was very different in the two experiments. Therefore, we performed two additional experiments to determine the activation cross sections of the reactions with primary focus on the peak amplitude of the ^{nat}Nd$(\alpha,x)^{153}$Sm reaction.

Two experiments (#1 and #2) were conducted at the RIKEN AVF cyclotron. Well-established methods for activation cross section measurements were adopted, including the stacked-foil activation technique and high-resolution γ-ray spectrometry.

The two stacked targets comprised pure metallic foils of ^{nat}Nd (99% purity, Goodfellow Co., Ltd., UK) and ^{nat}Ti (99.6% purity, Nilaco Corp., Japan). The ^{nat}Ti foils were interleaved for the ^{nat}Ti$(\alpha,x)^{51}$Cr monitor reaction to assess the incident beam parameters and target thicknesses. The average thicknesses of the foils were derived from the measured size and weight of the original ^{nat}Nd and ^{nat}Ti foils. The derived thicknesses were 16.7 and 2.25 mg/cm^2, respectively. The foils were cut into a size of 10 × 10 mm to fit the target holders served as Faraday cups.

Both targets were independently irradiated for 33 min with α-particle beams. The measured incident beam energy of both beams was 28.9 MeV. The energy degradation of the beams in the stacked targets was calculated using the stopping powers obtained from the SRIM code.[5] The average beam intensities measured by the Faraday cups were 103 nA (#1) and 104 nA (#2). The γ rays emitted from the irradiated foils were measured without chemical separation using high-purity germanium detectors.

Cross sections of the ^{nat}Ti$(\alpha,x)^{51}$Cr monitor reaction were used for final assessment of the beam parameters and target thicknesses. Based on the comparison with the recommended values,[6] the measured values were corrected within their uncertainties. The thickness of the ^{nat}Nd foil was decreased by 2% and the initial beam energy was increased by 0.2 MeV. In addition, the beam intensity of the second experiment (#2) was corrected by +2%.

The activation cross sections of ^{153}Sm were determined using the spectra measured after cooling times of 6.0–19.5 h (#1) and 10.9–24.9 h (#2) when the parent ^{153}Pm ($T_{1/2}$ = 5.25 min) had completely decayed to ^{153}Sm. The net counts of the γ line at 103.18 keV (I_γ = 29.25%) emitted from the decay of ^{153}Sm were measured. The low energy γ rays were expected to be absorbed in the ^{nat}Nd foil. The absorption probability of 2.1% was calculated using the target thickness and mass attenuation coefficients.[8] The cumulative cross sections were then determined using the counts corrected for absorption. The results are shown in Fig. 1 along with the experimental data published earlier[3,4] and the TENDL-2021 values.[7] The results obtained in this work are consistent with each other and also with our previous study.[3] In contrast, the other literature data[4] are inconsistent. The TENDL-2021 values are slightly deviated from our data, however, they support the smaller amplitude. The experimental cross sections derived in this work can increase the reliability of the excitation function of this reaction.

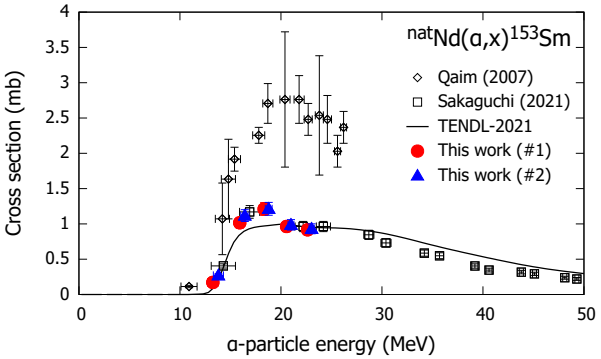

Fig. 1. Cross sect ions of the ^{nat}Nd$(\alpha,x)^{153}$Sm reactioreaction with previous experimental data data[3,4] and the TENDL TENDL-20 21 values.[7]

References
1) I. G. Finlay *et al.*, Lancet Oncol. **6**, 392 (2005).
2) R. G. Fairchild *et al.*, Phys. Med. Biol. **32**, 847 (1987).
3) M. Sakaguchi *et al.*, Appl. Radiat. Isot. **176**, 109826 (2021).
4) S. M. Qaim *et al.*, Radiochim. Acta **95**, 313 (2007).
5) J. F. Ziegler *et al.*, SRIM: the Stopping and Range of Ions in Matter (2008), `http://www.srim.org/`.
6) A. Hermanne *et al.*, Nucl. Data Sheets **148**, 338 (2018).
7) A. J. Koning *et al.*, Nucl. Data Sheets **155**, 1 (2019).
8) J. H. Hubble *et al.*, X-Ray Mass Attenuation Coefficients, NIST Standard Reference Database **126**, `https://dx.doi.org/10.18434/T4D01F`.

† Condensed from the article in Appl. Radiat. Isot. **187**, 110345 (2022)

*1 Faculty of Science, Hokkaido University
*2 RIKEN Nishina Center
*3 Graduate School of Biomedical Science and Engineering, Hokkaido University
*4 Advanced Clinical Research Center, Fukushima Medical University
*5 Nuclear Data Section, International Atomic Energy Agency
*6 Institute for Nuclear Research (ATOMKI)

Activation cross sections of ^{7}Li-induced reactions on ^{nat}Sm

M. Aikawa,[*1,*2] G. Damdinsuren,[*3,*2] S. Ebata,[*4,*2] N. Ukon,[*5,*2] and H. Haba[*2]

Terbium radionuclides can be used for nuclear medicine.[1] High specific activities of the Tb radionuclides can be obtained using charged-particle-induced reactions on neighbor elements, such as Gd, Er and Sm. We focused on ^{7}Li-induced reactions on Sm. We found two experimental studies for fusion reactions on ^{144,152}Sm enriched targets in a literature survey.[2,3] The data shortage of the experimental cross sections motivated us to experiment with ^{7}Li-induced reactions on ^{nat}Sm. Due to the isotopic ratio of ^{nat}Sm (^{144}Sm 3.08%, ^{147}Sm 15.00%, ^{148}Sm 11.25%, ^{149}Sm 13.82%, ^{150}Sm 7.37%, ^{152}Sm 26.74% and ^{154}Sm 22.74%), the reactions can produce Tb radionuclides simultaneously.

The experiment using a ^{7}Li beam was conducted at the RIKEN AVF cyclotron. We adopted well-established methods, such as stacked-foil activation technique and γ-ray spectrometry, to determine activation cross sections.

Two ^{nat}Sm (5-μm thick, 99% purity, Nilaco Corp., Japan) and one ^{27}Al (5-μm thick, >99% purity, Nilaco Corp., Japan) foils were purchased for the stacked target. The size and weight of the foils were measured to derive the average thicknesses. The measured thicknesses of the two ^{nat}Sm and ^{27}Al foils were 4.07, 4.20, and 1.21 mg/cm^2, respectively. The foils were cut into a size of 10 × 10 mm. Nineteen sets of Sm-Sm-Al-Al foils were stacked in a target holder that served as a Faraday cup.

Irradiation with a 72-MeV ^{7}Li beam on the stacked target lasted for 48 min. The incident beam energy was measured using the time-of-flight method. The beam energy degraded at each foil was calculated using the measured foil thicknesses and stopping powers retrieved from the SRIM code.[4] The average beam intensity measured using the Faraday cup was 48.9 nA.

The γ rays emitted from the irradiated foils were measured using a high-resolution HPGe detector (ORTEC GMX30P4-70) and dedicated software (SEIKO EG&G Gamma Studio). The γ-ray measurements of the ^{nat}Sm foils were repeated five times with a cooling time of 1.1 h–2.7 d. The associated dead time was less than 2.2%. The nuclear data required for the deduction of the cross sections were retrieved from NuDat 3.0.[5]

The cross sections of the ^{nat}Sm(^{7}Li, x)^{152}Tb reaction were determined from net counts of the γ line at 344.2785 keV (I_γ = 63.5%) emitted from the decay of ^{152}Tb ($T_{1/2}$ = 17.5 h). The spectra measured with the cooling time of 9.6–27.4 h were adopted. Possible interferences in the γ line were assessed. The ground state ($T_{1/2}$ = 13.517 y) and excited state of ^{152}Eu ($T_{1/2}$ = 9.3116 h) emit the same energy γ rays in the decay. The long-lived ^{152g}Eu decayed less during the measurements. The contribution from ^{152m}Eu (I_γ = 2.4%) could be neglected because no peak of the more intense γ line (I_γ = 14.2%) was found. Another possible interference of the 344.90-keV γ line (I_γ = 2.12%) from ^{151}Pm ($T_{1/2}$ = 28.40 h) was negligibly small because the more intense γ line at 340.08 keV (I_γ = 22.5%) was missing in the spectra. The count rate of the 344.3-keV γ peak decreased with the half-life of ^{152}Tb, indicating less contribution from other radionuclides.

The result is shown in Fig. 1. No previous study of the reaction was found. According to the threshold energies (Table 1), the first peak at 40 MeV comprises reactions on several Sm isotopes. Above 60 MeV, the reaction on ^{154}Sm can be dominant. We will finish analyses to determine the cross sections of ^{152}Tb and other Tb radionuclides.

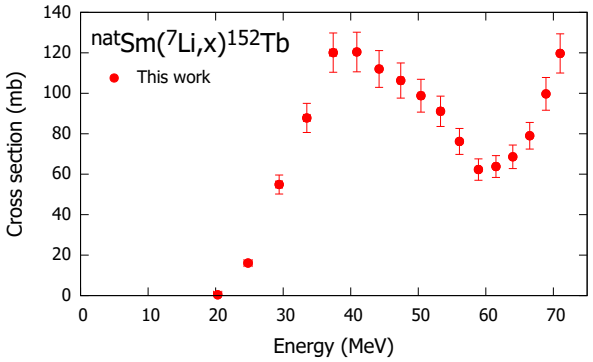

Fig. 1. Measured cross sections of the ^{nat}Sm(^{7}Li, x)^{152}Tb reaction.

Table 1. Q value and threshold energy (E_{th}) of the reaction on each Sm isotope target for ^{152}Tb production.

Reaction	Q value (MeV)	E_{th} (MeV)
^{147}Sm(^{7}Li,2n)^{152}Tb	−5.7	6.0
^{148}Sm(^{7}Li,3n)^{152}Tb	−13.9	14.5
^{149}Sm(^{7}Li,4n)^{152}Tb	−19.8	20.7
^{150}Sm(^{7}Li,5n)^{152}Tb	−27.7	29.1
^{152}Sm(^{7}Li,7n)^{152}Tb	−41.6	43.6
^{154}Sm(^{7}Li,9n)^{152}Tb	−55.4	58.1

*1 Faculty of Science, Hokkaido University
*2 RIKEN Nishina Center
*3 Graduate School of Biomedical Science and Engineering, Hokkaido University
*4 Graduate School of Science and Engineering, Saitama University
*5 Advanced Clinical Research Center, Fukushima Medical University

References
1) C. Müller *et al.*, J. Nucl. Med. **53**, 1952 (2012).
2) P. K. Rath *et al.*, Phys. Rev. C **88**, 044617 (2013).
3) M. S. Gautam *et al.*, Int. J. Mod. Phys. E **29**, 2050029 (2020).
4) J. F. Ziegler *et al.*, Nucl. Instrum. Methods Phys. Res. B **268**, 1818 (2010).
5) National Nuclear Data Center, The NuDat 3.0 database, `http://www.nndc.bnl.gov/nudat3/`.

Activation cross sections of deuteron-induced reactions on natural gadolinium up to 24 MeV†

D. Ichinkhorloo,[*1,*2] M. Aikawa,[*1,*3,*4] Ts. Zolbadral,[*2,*3,*4] Y. Komori,[*3] and H. Haba[*3]

Terbium (Tb) and gadolinium (Gd) radionuclides can be used for medical applications. For example, ^{161}Tb ($T_{1/2}$ = 6.89 d) can be used for targeted β^- radionuclide therapy.[1] The production cross sections of the radionuclide are important nuclear data in terms of practical use. The radionuclide can be produced via charged-particle-induced reactions on ^{nat}Gd, of which can yield the compositions as follows: ^{152}Gd (0.2%), ^{154}Gd (2.2%), ^{155}Gd (14.8%), ^{156}Gd (20.5%), ^{157}Gd (15.7%), ^{158}Gd (24.8%), and ^{160}Gd (21.8%). In this study, we focused on the deuteron-induced reactions on ^{nat}Gd. In the literature survey, only two experimental studies of the cross sections were found.[2,3] However, the experimental data show a discrepancy between them. Therefore, we performed to measure cross sections of the deuteron-induced reaction on ^{nat}Gd. The result was compared with the literature data[2,3] and the TENDL-2021 values.[4]

The experiment to determine the activation cross sections was conducted at the RIKEN AVF cyclotron. The stacked-foil activation technique and the high-resolution γ-ray spectrometry were adopted. The stacked target comprised foils cut from ^{nat}Gd (0.025 × 50 × 100 mm, 99.9% purity, Nilaco Corp., Japan) and ^{nat}Ti foils (0.005×50×100 mm, 99.6% purity, Nilaco Corp., Japan). The thicknesses of the ^{nat}Gd and ^{nat}Ti foils were derived from the measured size and weight and found to be 25.3 and 2.34 mg/cm^2, respectively. ^{nat}Ti foils were used for the ^{nat}Ti$(d,x)^{48}$V monitor reaction to assess the beam parameters and target thicknesses. The foils were cut into a size of 8 × 8 mm and stacked into a target holder that served as a Faraday cup.

The stacked target was irradiated with a deuteron beam for 60 min. The average beam intensity measured by the Faraday cup was 98.1 nA. The beam energy measured by the time-of-flight method[5] was 24.1 MeV. Further, the energy degradation in the stacked target was calculated using the target thicknesses and stopping powers derived from the SRIM code.[6]

The γ rays emitted from each irradiated foil were measured using a high-resolution HPGe detector (ORTEC GMX30P4-70) and the dedicated software (SEIKO EG&G Gamma Studio). The spectra of each foil were measured four times with different cooling time and distance. The associated dead time was less than 6.3%. Comparisons indicated that the beam intensity was corrected by +6.5% within its uncertainty (7%).

The cross sections of the ^{nat}Ti$(d,x)^{48}$V monitor reaction, beam energy and measured foil thicknesses were adopted without any correction. The cross sections using the corrected parameters were consistent with the recommended values.

The cross sections of the ^{nat}Gd$(d,x)^{161}$Tb reaction were derived using the γ line at 74.57 keV (I_γ = 10.2%). The self-absorption of the low-energy γ line in each ^{nat}Gd foil was estimated as 9.5%. The measurements were performed following a cooling time of 39–42 d. The co-produced parent ^{161}Gd ($T_{1/2}$ = 3.66 min) decayed during the cooling time.

The cumulative cross sections are shown in Fig. 1 with the literature data[2,3] and the TENDL-2021 values.[5] Both experimental data were consistent our data below 12 MeV with deviations observed above 12 MeV. The TENDL-2021 values were smaller than the experimental data.

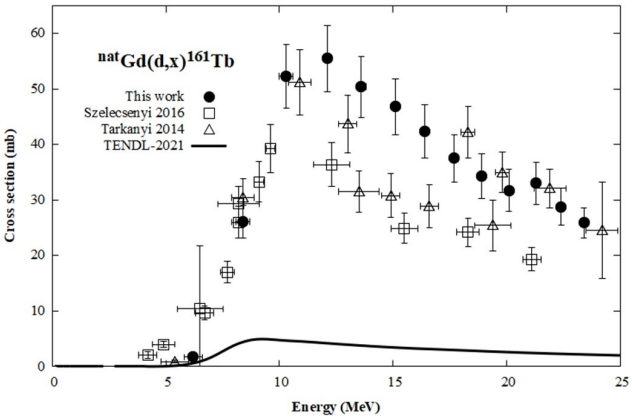

Fig. 1. Excitation function of the ^{nat}Gd$(d,x)^{161}$Tb reaction with the previous data[2,3] and the TENDL-2021 data.[4]

In addition to ^{161}Tb, we also determined the production cross sections of ^{153,154m1,154m2,155,156,160}Tb and ^{153,159}Gd. The cross sections are almost consistent with the experimental data studied earlier. The results are expected to contribute to development of theoretical model calculation and nuclear medicine.

References
1) C. Müller *et al.*, J. Nucl. Med. **53**, 1951 (2012).
2) F. Szelecsényi *et al.*, J. Radioanal. Nucl. Chem. **307**, 1877 (2016).
3) F. Tárkányi *et al.*, Appl. Radiat. Isot. **83**, 25 (2014).
4) A. J. Koning *et al.*, Nucl. Data Sheets **155**, 1 (2019).
5) T. Watanabe *et al.*, Proc. 5th Int. Part. Accel. Conf. (IPAC 2014) (2014), p. 3566.
6) J. F. Ziegler *et al.*, SRIM: the Stopping and Range of Ions in Matter, `http://www.srim.org`.
7) A. Hermanne *et al.*, Nucl. Data Sheets. **148**, 338 (2018).

† Condensed from the article in Nucl. Instrum. Methods Phys. Res. B **536**, 30 (2023)

*1 Faculty of Science, Hokkaido University
*2 Nuclear Research Center, National University of Mongolia
*3 RIKEN Nishina Center
*4 Graduate School of Biomedical Science and Engineering, Hokkaido University

Production yields of ^{165}Er and ^{169}Yb via 24-MeV deuteron induced reactions

Y. Shigekawa,[*1] A. Nambu,[*1] Y. Kumakura,[*2] and H. Haba[*1]

The use of Auger electrons for cancer therapy has been widely investigated owing to their higher linear energy transfer than β^- particles. ^{165}Er ($T_{1/2}$ = 10.4 h) and ^{169}Yb ($T_{1/2}$ = 32.0 d), which decay purely via electron capture (EC), are promising candidates for targeted radionuclide therapy using Auger electrons.[1,2] Moreover, the decay of ^{169}Yb accompanies the emission of cascade γ-rays potentially applicable to nuclear-medicine imaging that can prove the local chemical environment.[3] In order to perform nuclear-medicine studies with ^{165}Er and ^{169}Yb, we need to produce >1 GBq of ^{165}Er and >100 MBq of ^{169}Yb and chemically purify them without adding carriers. The production cross sections for these isotopes were reported for the ^{165}Ho$(d,2n)^{165}$Er[4,5] and ^{169}Tm$(d,2n)^{169}$Yb reactions.[6–8] In this study, we confirmed the production yields of ^{165}Er and ^{169}Yb via 24-MeV deuteron induced reactions using thick target foils to determine the irradiation conditions to obtain sufficient radioactivity for nuclear-medicine studies.

We irradiated ^{165}Ho and ^{169}Tm targets with a 23.9-MeV deuteron beam at the RIKEN AVF cyclotron. The ^{165}Ho target consisted of four ^{165}Ho foils (10 × 10 mm, 219.9 mg/cm^2, purity 99.9%) and was irradiated with an average beam intensity of 102 nA for 30 min. The ^{169}Tm target consisted of nine ^{169}Tm foils (8 × 8 mm, 94.5 mg/cm^2, purity 99%) and was irradiated with an average beam intensity of 105 nA for 3 h. After irradiation, γ-ray spectroscopy was performed using high-purity Ge detectors.

The radioactivity of ^{169}Yb was determined with the γ peaks of 177.2 and 307.7 keV. For ^{165}Er, no-γ rays are emitted; thus, the-X rays of Ho emitted after the EC decay were used to quantify ^{165}Er. The X-rays of Ho (46.7, 47.5, 53.7, 53.9, and 55.3 keV) were observed as three peaks in the γ-ray spectra. The peak corresponding to the 53.7- and 53.9-keV X-rays was useful to quantify ^{165}Er because the other X-rays overlap with the Er X-rays emitted from ^{166}Ho ($T_{1/2}$ = 26.8 h) produced in the ^{165}Ho$(d,p)^{166}$Ho reaction. The count rate for the peak of the 53.7- and 53.9-keV X-rays was obtained by fitting a Gaussian function to each dataset. The X-ray count rate as a function of the elapsed time decreased with the half-life of ^{165}Er (10.4 h), meaning that interference from radioactive impurities was negligibly small. To determine the radioactivity of ^{165}Er, the self-absorption of X-rays by the thick Ho foils was corrected using the γ-ray measurements for the two sides of each foil and a database of the X-ray absorption coefficients.[9]

The cross sections of ^{165}Er and ^{169}Yb (Figs. 1 and 2) are almost consistent with those of previous studies.[4–8] The total radioactivity of ^{165}Er at the end of bombardment (EOB) was 19.7(12) MBq, and the impurity was 3.2(3) MBq of ^{166}Ho. The total radioactivity of ^{169}Yb at the EOB was 2.06(3) MBq, and the impurities were 0.071(1) MBq of ^{168}Tm and 0.16(3) MBq of ^{167}Tm. Hence, the thick target yields for ^{165}Er and ^{169}Yb were determined to be 390(24) and 6.58(14) MBq/μAh, respectively. Via irradiation

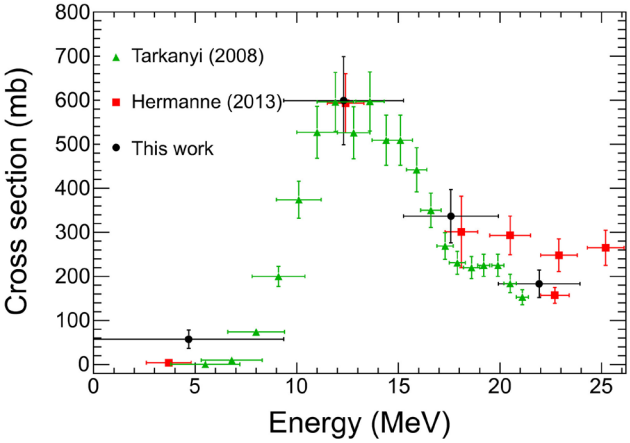

Fig. 1. Excitation function of the ^{165}Ho$(d,2n)^{165}$Er reaction measured in this work. The values measured in previous studies[4,5] are also shown for comparison.

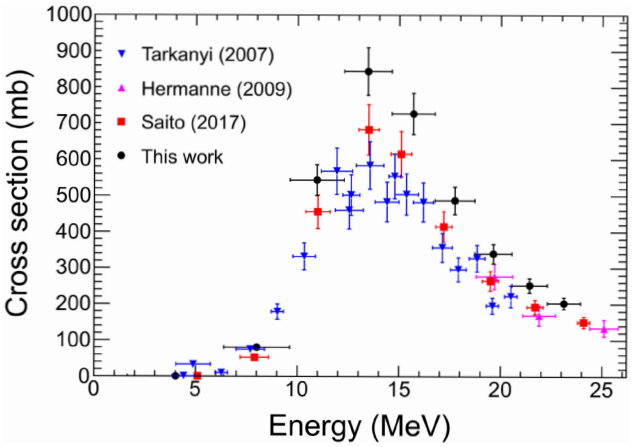

Fig. 2. Excitation function of the ^{169}Tm$(d,2n)^{169}$Yb reaction measured in this work. The values measured in previous studies[6–8] are also shown for comparison.

*1 RIKEN Nishina Center
*2 Faculty of Medicine, Saitama Medical University

with a 5-μA deuteron beam, we will be able to produce 1 GBq of ^{165}Ho in 0.5 h and 100 MBq of ^{169}Yb in 3 h, which are sufficient for nuclear-medicine studies.

References

1) I. D. Silva *et al.*, Molecules **26**, 7513 (2021).
2) S. M. Qaim *et al.*, Radiochim. Acta **95**, 313 (2007).
3) K. Shimazoe *et al.*, Commun. Phys. **5**, 24 (2022).
4) F. Tarkanyi *et al.*, Nucl. Instrum. Methods Phys. Res. B **266**, 3529 (2008).
5) A. Hermanne *et al.*, Nucl. Instrum. Methods Phys. Res. B **311**, 102 (2013).
6) F. Tarkanyi *et al.*, Appl. Radiat. Isot. **65**, 663 (2007).
7) A. Hermanne *et al.*, Nucl. Instrum. Methods Phys. Res. B **267**, 727 (2009).
8) M. Saito *et al.*, Appl. Radiat. Isot. **125**, 23 (2017).
9) M. J. Berger *et al.*, XCOM: Photon Cross Section Database (version 1.5), National Institute of Standards and Technology, Gaithersburg, MD (2010).

Activation cross sections of α-particle-induced reactions on ^{nat}Ta

S. Takács,[*1,*2] F. Ditrói,[*1,*2] Z. Szücs,[*1,*2] M. Aikawa,[*2,*3,*4] G. Damdinsuren,[*2,*4] H. Haba,[*2] and S. Ebata[*2,*5]

Tantalum is a frequently used material in accelerator technology exploiting its proper physical characteristics. However, by irradiating it with energetic alpha particles several longlived radionuclides are produced. To estimate the possible activity produced during an irradiation, knowledge of the excitation functions of the possible reactions is required. In a literature survey, several experimental studies were found reporting data on different reactions. As significant difference exists in the peak position and amplitude among the different datasets, we decided to perform an experiment to investigate the ^{nat}Ta(α, x) reactions and to deduce more reliable cross-sections data of these reactions. Furthermore, the obtained results were compared with theoretical model prediction available in TENDL-2021 data library.[1)]

The experiment was performed at the AVF cyclotron of RIKEN RI Beam Factory employing the stacked-foil target, activation method and high-resolution γ-ray spectrometry. The target comprised pure metallic foils of ^{nat}Ta (nominal thickness 9 μm, 99.99% purity, from Goodfellow, UK) and ^{nat}Ti (nominal thickness 5 μm, 99.6% from Nilaco Co., Japan). The ^{nat}Ti foils served as catcher foils to stop and collect the recoiled reaction products and also as monitor foils for the ^{nat}Ti$(\alpha, x)^{51}$Cr monitor reaction. The average foil thickness was determined from the measured lateral size and weight of the original foils. The derived thicknesses of ^{nat}Ta and ^{nat}Ti foils were 14.37 and 2.24 mg/cm^2, respectively. Subsequently, the original foils were cut into a size of 10×10 mm and stacked into a target holder served as a Faraday cup to measure the incident beam intensity. Every Ta foil was set together with a Ti catcher foil. The other Ti foils were inserted into the stack at certain positions for monitoring, to obtain maximum information on the beam parameters and the energy loss of the beam in the target stack. The stacked target was irradiated with a 50.5 $\pm$ 0.2 MeV α-particle beam for 1 hour. The primary beam energy was measured employing the time-of-flight method.[2)] Energy degradation in the target was calculated using stopping power data derived from the SRIM code.[3)] The average beam intensity measured on the Faraday cup was 203 nA.

The γ-ray spectra of the Ta and its Ti catcher foil pairs, as well as of the Ti monitor foils were measured by a high-resolution HPGe detector (ORTEC GEM-25185-P) and analyzed using dedicated software (SEIKO EG&G Gamma Studio and Genie2000). The spectra of each foil were measured several times to follow the decay of the reaction products. To maintain a low dead time the detector to foil distance was adjusted.

The cross-sections of the ^{nat}Ti$(\alpha, x)^{51}$Cr monitor reaction were derived using the γ-line at 320.08 keV (I_γ = 9.910%) from the decay of ^{51}Cr ($T_{1/2}$ = 27.7025 d) and were compared with the recommended values of IAEA.[4)] Based on the comparison, the incident beam energy was increased by 0.13% to 50.6 MeV, and thickness of the ^{nat}Ta foil was reduced by 0.12% to 14.36 mg/cm^2. Moreover, owing the escaping secondary electrons, the beam intensity was reduced by 3% to 197.2 nA. With these adopted changes, good agreement was reached with the recommended values.

Activation cross-sections can be deduced for several Re, W, Ta, Hf, and Lu reaction products. A preliminary result cross-section for the ^{nat}Ta$(\alpha, x)^{182g}$Re reaction is presented in Fig. 1 together with the previous experimental data and the TENDL-2021 values.[1)] Data were assessed using the γ-line at 1427.3 keV (I_γ = 9.8%) emitted following the decay of ^{182g}Re. Measurements were performed after a cooling time of 48 h. This gamma line can be considered as interference free, because only decay of possible co-produced ^{176}Ta may contribute above 38 MeV with a negligible, two orders of magnitude lower intensity. The earlier experimental data were consistent in terms of position of the maximum; however, certain differences exist in the am-

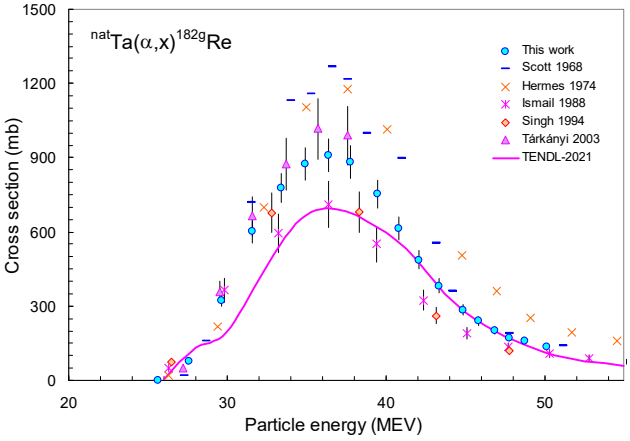

Fig. 1. Experimental cross-sections of the ^{nat}Ta$(\alpha, x)^{182g}$Re reaction in comparison with TENDL-2021 values.

*1 Institute for Nuclear Research (ATOMKI)
*2 RIKEN Nishina Center
*3 Faculty of Science, Hokkaido University
*4 Graduate School of Biomedical Science and Engineering, Hokkaido University
*5 Graduate School of Science and Engineering, Saitama University

plitude. The TENDL-2021 values disagreed with the experimental data both in peak position and in amplitude. Preliminary results for the activation cross-sections have already been deduced for several reactions; however, owing to the long half lives of several reaction products, the γ-ray spectrometry measurements are still required and thus continued. Final results are expected in the second half of the year 2023.

References

1) A. J. Koning *et al.*, Nucl. Data Sheets **155**, 1 (2019).
2) T. Watanabe *et al.*, Proc. 5th Int. Part. Accel. Conf. (IPAC 2014), (2014), p. 3566.
3) J. F. Ziegler *et al.*, Nucl. Instrum. Methods Phys. Res. B **268**, 1818 (2010).
4) A. Hermanne *et al.*, Nucl. Data Sheets **148**, 338 (2018).

Activation cross sections of deuteron-induced reactions on ^{nat}Re

M. Aikawa,[*1,*2] Y. Toyoeda,[*3,*2] G. Damdinsuren,[*4,*2] S. Ebata,[*5,*2] H. Haba,[*2] S. Takács,[*6,*2] F. Ditrói,[*6,*2] and Z. Szücs[*6,*2]

The ground states of ^{186}Re ($T_{1/2}$ = 3.7186 d) and ^{188}Re ($T_{1/2}$ = 17.003 h) decay with the emission of β^- particles and γ rays. Both rhenium radionuclides can be used for theranostics, which combines therapy and diagnosis.[1,2] The radionuclides can be produced through neutron-capture reactions on rhenium and charged-particle-induced reactions on tungsten and rhenium targets. The possible production reactions should be investigated for practical use. In this work, we focused on the deuteron-induced reactions on rhenium. In a literature survey, we found only two experimental studies of cross sections[3,4] and their data were largely scattered. Therefore, we performed an experiment to measure the cross sections of the reactions.

In the experiment a 24-MeV deuteron beam delivered from the RIKEN AVF cyclotron was used to irradiate the stacked target. We adopted well-established methods, such as stacked-foil activation technique and off-line high-resolution γ-ray spectrometry.

The stacked target consisted of thin and pure metallic foils of ^{nat}Re (0.0125 × 50 × 50 mm, 99.98% purity, Goodfellow Co., Ltd., UK) and ^{nat}Ti (0.005 × 50 × 100 mm, 99.6% purity, Nilaco Corp., Japan). The ^{nat}Ti foils were interleaved for the ^{nat}Ti$(d,x)^{48}$V monitor reaction. The lateral size and weight of each foil were measured. The average thicknesses of the ^{nat}Re and ^{nat}Ti foils were found to be 24.9 and 2.24 mg/cm^2, respectively. The original foils were then cut into a size of 8 × 8 mm. Sixteen sets of Re-Re-Ti-Ti foils were stacked in a target holder.

The target was irradiated with a 24-MeV deuteron beam for 1 h. The initial beam energy was determined by the time-of-flight method. The average beam intensity determined using the charge collected by the Faraday cup was 105 nA. The beam energy at each foil was calculated using stopping powers derived from the SRIM code.[5]

γ-ray spectra of irradiated foils were measured using a high-purity germanium detector and dedicated software. The associated dead time was less than 4.4%.

Cross sections of the ^{nat}Ti$(d,x)^{48}$V monitor reaction were derived. The cross sections using the measured beam parameters and target thicknesses agreed well with the IAEA recommended values,[6] as shown in Fig. 1. The measured parameters were adopted without any correction to determine cross sections of the reaction on the Re targets.

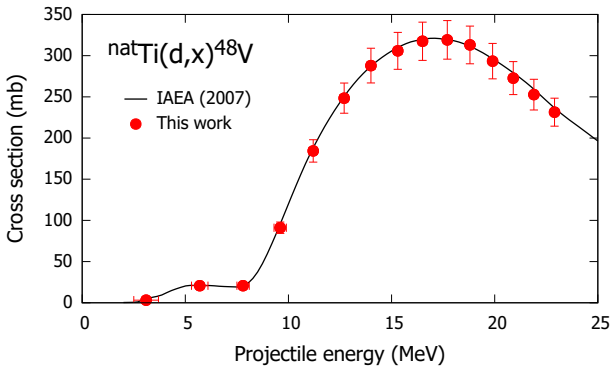

Fig. 1. Cross sections of the ^{nat}Ti$(d,x)^{48}$V monitor reaction with the IAEA recommended values.[7]

The cross sections of the ^{nat}Re$(d,x)^{188g}$Re reaction were determined using the γ line at 155.044 keV (I_γ = 15.49%). The preliminary result is shown in Fig. 2 with the literature data[3,4] and the TENDL-2019 values.[7] The data of Natowitz *et al.*[4] using ^{187}Re enriched targets were normalized to those using ^{nat}Re targets. The normalized data are consistent with our result, while the data by Ditroi *et al.*[3] are higher. The TENDL-2019 values are lower than all experimental data.

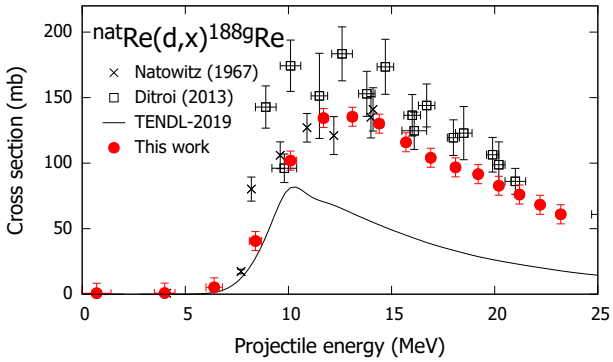

Fig. 2. Measured cross sections of the ^{nat}Re$(d,x)^{188g}$Re reaction with the literature data[3,4] and the TENDL-2021 values.[7] The literature data on enriched ^{187}Re[4] were normalized to those on ^{nat}Re.

*1 Faculty of Science, Hokkaido University
*2 RIKEN Nishina Center
*3 School of Science, Hokkaido University
*4 Graduate School of Biomedical Science and Engineering, Hokkaido University
*5 Graduate School of Science and Engineering, Saitama University
*6 Institute for Nuclear Research (ATOMKI)

References
1) A. M. Denis-Bacelar *et al.*, Eur. J. Nucl. Med. Mol. Imaging **44**, 620 (2017).
2) I. G. Finlay *et al.*, Lancet Oncol. **6**, 392 (2005).
3) F. Ditroi *et al.*, Nucl. Instrum. Methods Phys. Res. B **296**, 92 (2013).
4) J. B. Natowitz *et al.*, Phys. Rev. **155**, 1352 (1967).
5) J. F. Ziegler *et al.*, Nucl. Instrum. Methods Phys. Res. B **268**, 1818 (2010).
6) F. Tárkányi *et al.*, IAEA-TECDOC-1211 (2007).
7) A. J. Koning *et al.*, Nucl. Data Sheets **155**, 1 (2019).

Production cross sections of ^{189g}Ir in α-particle-induced reactions on ^{nat}Re

G. Damdinsuren,[*1,*2] M. Aikawa,[*1,*2,*3] S. Ebata,[*4,*2] H. Haba,[*2] S. Takács,[*5,*2] F. Ditrói,[*5,*2] and Z. Szücs[*5,*2]

Iridium-189 has the ground state ^{189g}Ir ($T_{1/2}$ = 13.2 d, ε: 100%) and two short-lived excited states ^{189m1}Ir and ^{189m2}Ir ($T_{1/2}$ = 13.3 and 3.7 ms, IT: 100%). The radionuclide ^{189g}Ir is an Auger electron emitter and can be used for therapy in nuclear medicine.[1] Charged-particle-induced reactions on osmium and rhenium are possible production routes of ^{189g}Ir. In this work, we focused on the α-particle-induced reactions on ^{nat}Re targets. In a literature survey, three experimental studies of the cross sections of the ^{nat}Re$(\alpha,x)^{189}$Ir reactions were found.[2–4] The previous experimental data are significantly different in peak position and amplitude. Therefore, we performed an experiment to measure reliable cross sections of the ^{nat}Re$(\alpha,x)^{189}$Ir reaction. The result was compared with the experimental data published earlier and the TENDL-2021 values.[5]

The experiment was conducted at the AVF cyclotron of the RIKEN RI Beam Factory. The stacked-foil technique, activation method, and high-resolution γ-ray spectrometry were used. The stacked target consisted of pure metallic foils of ^{nat}Re (12.5-μm thick, 99.99% purity), ^{nat}Ti (5-μm thick, 99.6% purity), and ^{27}Al (5-μm thick, 99.9% purity). All foils were purchased from Nilaco Corp., Japan. The ^{nat}Ti foils were used for the ^{nat}Ti$(\alpha,x)^{51}$Cr monitor reaction. The ^{27}Al foils were inserted to catch reaction products recoiled from the ^{nat}Re and ^{nat}Ti foils. The target thicknesses were derived from the measured size and weight of the foils. The derived thicknesses of ^{nat}Re, ^{nat}Ti, and ^{27}Al foils were 25.3, 2.24, and 1.22 mg/cm^2, respectively. The original foils were then cut into a size of 10 × 10 mm to fit in a target holder that served as a Faraday cup. Fifteen sets of Re-Al-Ti-Al foils were stacked in the target holder.

The stacked target was irradiated with a 50.6 ± 0.2 MeV α-particle beam for 30 min. The primary beam energy was measured by the time-of-flight method.[6] Energy degradation in the stacked target was calculated using stopping powers derived from the SRIM code.[7] The average beam intensity measured by the Faraday cup was 203 nA.

The γ-ray spectra were measured using a high-resolution HPGe detector (ORTEC GEM-25185-P) and analyzed using dedicated software (SEIKO EG&G Gamma Studio). The spectra of each ^{nat}Re foil and the following ^{27}Al catcher foil were measured several times. The distance between the detector and the foils was set to keep dead time below 1%.

To assess the beam parameters and target thicknesses, the ^{nat}Ti$(\alpha,x)^{51}$Cr monitor reaction cross sections were derived. The γ line at 320.08 keV (I_γ = 9.910%) from the decay of ^{51}Cr ($T_{1/2}$ = 27.7025 d) was measured after a cooling time of 2 d.

The derived cross sections were compared with the IAEA-recommended values.[8] Based on the comparison, the incident beam energy and thickness of the ^{nat}Re foil were corrected within the uncertainties by +0.2 MeV and −1%, respectively.

The measurement of the γ line at 245.1 keV (I_γ = 6.0%) emitted with the decay of ^{189g}Ir was performed after a cooling time of 36 d. The two short-lived excited states with shorter half-lives ($T_{1/2}$ = 13.3 and 3.7 ms, IT: 100%) decayed to ^{189g}Ir during the irradiation. The cumulative cross sections of the ^{nat}Re$(\alpha,x)^{189g}$Ir reaction were derived from measured net counts. The preliminary result of the cross sections of $^{189(g+m1+m2)}$Ir is shown in Fig. 1, together with the previous experimental data[2–4] and the TENDL-2021 values.[5] The experimental data of Singh and Gadkari[4] are higher than our data, while the peak position is located at nearly the same energy. The data of Goncharov *et al.*[2] and Ismail[3] are largely different from ours in both peak amplitude and position. The TENDL-2021 values agree well with ours.

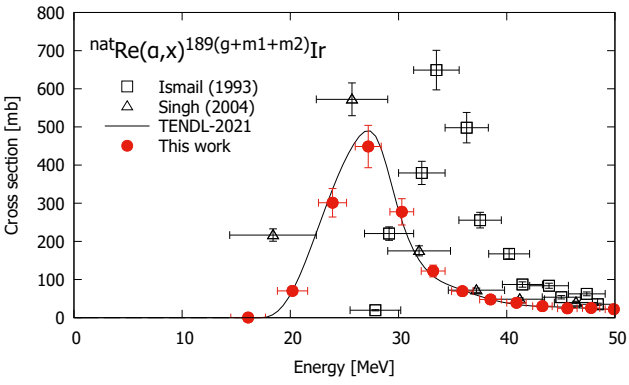

Fig. 1. Cumulative cross sections of the ^{nat}Re$(\alpha,x)^{189g}$Ir reaction.

The analyses to determine the final cross sections of ^{189g}Ir and other co-products are continued. The thick

*1 Graduate School of Biomedical Science and Engineering, Hokkaido University
*2 RIKEN Nishina Center
*3 Faculty of Science, Hokkaido University
*4 Graduate School of Science and Engineering, Saitama University
*5 Institute for Nuclear Research (ATOMKI)

target yields of the products can be calculated using the measured cross sections. The finalized results are expected to contribute to the practical use of radionuclides in nuclear medicine.

G. Damdinsuren was granted a scholarship by the M-JEED project (Mongolian-Japan Engineering Education Development Program, J11B16).

References

1) D. Filosofov *et al.*, Nucl. Med. Biol. **94**, 1 (2021).
2) K. S. Goncharov *et al.*, Sov. J. Nucl. Phys. **32**, 319 (1980).
3) M. Ismail, Pramana - J. Phys. **40**, 227 (1993).
4) N. L. Singh *et al.*, Can. J. Phys. **82**, 227 (2004).
5) A. J. Koning *et al.*, Nucl. Data Sheets **155**, 1 (2019).
6) T. Watanabe *et al.*, Proc. 5th Int. Part. Accel. Conf. (IPAC 2014), (2014), p. 3566.
7) J. F. Ziegler *et al.*, Nucl. Instrum. Methods Phys. Res. B **268**, 1818 (2010).
8) F. Tárkányi *et al.*, IAEA-TECDOC-1211 (2007).

Production cross sections of ^{198g}Au in proton-induced reactions on ^{nat}Pt†

G. Damdinsuren,[*1,*2] M. Aikawa,[*1,*2,*3] Kh. Tegshjargal,[*4] N. Erdene,[*4] N. Ukon,[*5,*2] and H. Haba[*2]

Gold-198 has two long-lived states, the ground state ^{198g}Au ($T_{1/2}$ = 2.6941 d, β^-: 100%) and the excited state ^{198m}Au ($T_{1/2}$ = 2.272 d, IT: 100%). The ground state ^{198g}Au can be used in nuclear medicine, such as brachytherapy[1] and nanoparticles.[2] The neutron capture reaction on the monoisotopic element ^{197}Au in a reactor can produce a considerable amount of ^{198g}Au. However, this method yields only the low specific activity of ^{198g}Au owing to the difficulty encountered in separating ^{198g}Au from the Au target. The high specific activity ^{198g}Au can be produced using charged-particle-induced reactions on platinum. In this study, the proton-induced reactions on ^{nat}Pt targets were investigated. Moreover, the literature survey, only two experimental studies of cross sections of the ^{nat}Pt$(p,x)^{198g}$Au reaction were found.[3,4] The literature data have large uncertainties and show discrepancy. Therefore, we conducted an experiment to provide reliable cross sections of the ^{nat}Pt$(p,x)^{198g}$Au reaction. Thus, the results of this study were compared with the previous data and theoretical model calculation in the TENDL-2019 library.[5]

The stacked-foil activation technique and high-resolution γ-ray spectrometry were used for cross section. Pure metallic foils of ^{nat}Pt (20-μm thick, 99.95% purity) and ^{nat}Ti (5-μm thick, 99.6% purity) were purchased from Nilaco Corp., Japan. The stacked target was composed of ^{nat}Pt and ^{nat}Ti foils. The ^{nat}Ti foils were used for the ^{nat}Ti$(p,x)^{48}$V monitor reaction for assessment of the beam parameters and the target thicknesses. Size and weight of the original foils were measured and the average foil thicknesses were derived. The derived average thicknesses of the ^{nat}Pt and ^{nat}Ti foils were 39.2, and 2.24 mg/cm^2, respectively. Both original foils were cut into a size of 10 × 10 mm. Twenty-five sets of Pt-Pt-Ti-Ti foils were stacked in a target holder served as a Faraday cup.

The stacked target was irradiated with a proton beam. The irradiation lasted for 30 min. The primary beam energy measured by the time-of-flight method[6] was 30.1 ± 0.1 MeV. Consequently, the beam energy at each foil was calculated using stopping powers derived from the SRIM code.[7] The average beam intensity was 101 nA, which was derived from irradiation period and charge collected by the Faraday cup.

γ rays emitted from irradiated foils were measured by a high-resolution HPGe detector (ORTEC GEM-25185-P) and analyzed using dedicated software (SEIKO EG&G Gamma Studio). Only the second foil of the same element pairs was measured because products recoiled from the second foil were assumed to be compensated from the first foil. The dead time throughout the measurement was less than 4.7%.

Cross sections of the ^{nat}Ti$(p,x)^{48}$V monitor reaction were derived using the γ line at 983.5 keV (I_γ = 99.98%) from the decay of ^{48}V ($T_{1/2}$ = 15.9735 d). The derived cross sections were consistent with the IAEA-recommended values.[8] Thus, the measured beam parameters and target thicknesses were adopted without corrections for deduction of cross sections.

The cross sections of the ^{nat}Pt$(p,x)^{198g}$Au reaction were determined using the measurement of the γ line at 411.80205 keV (I_γ = 95.62%) from the decay of ^{198g}Au. The measurement was performed following a cooling time of 13 d. The possible contribution through decay of ^{198m}Au ($T_{1/2}$ = 2.272 d, IT: 100%) was negligibly small because intense γ lines of ^{198m}Au could not be found in any spectra. Figure 1 shows the derived cross sections in comparison with the previous experimental data[3,4] and TENDL-2019 values.[3] The excitation function exhibited a smooth curve and was consistent with previous experimental data within the uncertainty; although certain data points of Tárkányi *et al.*[3] were deviated. The peak amplitude and position of the TENDL-2019 values were slightly different from the experimental cross sections although the trend was similar.

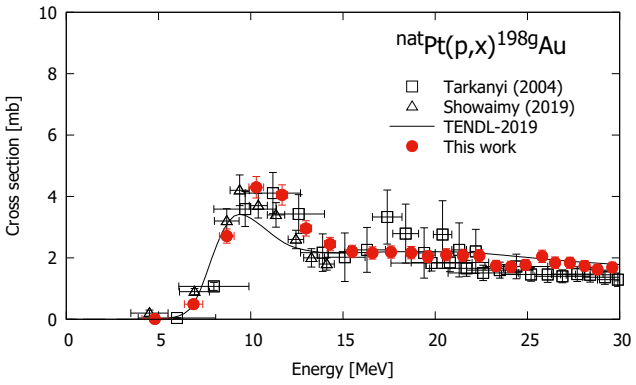

Fig. 1. Excitation function of the ^{nat}Pt$(p,x)^{198g}$Au reaction.

† Condensed from the article in Appl. Radiat. Isot. **192**, 110621 (2023)

*1 Graduate School of Biomedical Science and Engineering, Hokkaido University
*2 RIKEN Nishina Center
*3 Faculty of Science, Hokkaido University
*4 School of Engineering and Applied Sciences, National University of Mongolia
*5 Advanced Clinical Research Center, Fukushima Medical University

G. Damdinsuren was granted a scholarship by the M-JEED project (Mongolian-Japan Engineering Education Development Program, J11B16). This work was partially supported by JSPS KAKENHI Grant No. 22H04961.

References

1) M. Konishi *et al.*, J. Radiat. Res. **62**, 871 (2021).
2) R. Chakravarty *et al.*, Nucl. Med. Biol. **72**, 1 (2019).
3) F. Tárkányi *et al.*, Radiochim. Acta **92**, 223 (2004).
4) H. Showaimy *et al.*, Radiat. Phys. Chem. **157**, 97 (2019).
5) A. J. Koning *et al.*, Nucl. Data Sheets **155**, 1 (2019).
6) T. Watanabe *et al.*, Proc. 5th Int. Part. Accel. Conf. (IPAC 2014), (2014), p.3566.
7) J. F. Ziegler *et al.*, Nucl. Instrum. Methods Phys. Res. B **268**, 1818 (2010).
8) F. Tárkányi *et al.*, IAEA-TECDOC-1211 (2007).

Production cross sections of ^{211}Rn *via* ^{7}Li-induced reaction on ^{209}Bi

N. Ukon,[*1,*2] K. Washiyama,[*1] M. Aikawa,[*3,*2] G. Damdinsuren,[*4,*2] S. Ebata,[*5,*2] and H. Haba[*2]

Astatine-211 possesses a half-life of 7.214 h and is a promising radionuclide for targeted α-particle therapy.[1] ^{211}Rn ($T_{1/2}$ = 14.6 h) is the longer-lived parent nuclide of ^{211}At and is expected for a ^{211}Rn/^{211}At generator.[2] One possible reaction to produce ^{211}Rn is Li-induced reactions on the mononuclidic element ^{209}Bi. Thus, we focused on the ^{7}Li-induced reaction on ^{209}Bi. Based on our survey, three experimental studies were found, and their data were scattered.[2–4] Therefore, we conducted experiments on the ^{209}Bi(^{7}Li, $5n$)^{211}Rn reaction to measure cross sections and thick target yield.

We conducted three experiments, *i.e.*, two for excitation functions and one for the thick target yield, using 72-MeV ^{7}Li beams at the RIKEN AVF cyclotron. γ-ray spectrometry was used to identify radioactive products. The stacked-foil activation technique was employed to measure the excitation functions.

To measure the excitation functions (#1 and #2), independent stacked targets were prepared. For the targets, small pieces of Bi (purity: 99.999%) and three Al foils (purity: >99%, thickness: 10, 18, and 5 μm, size: 100 × 100 mm) were purchased from Nilaco Corp., Japan. The 10-μm and 18-μm Al foils were used as backing foils for targets #1 and #2, respectively, and the 5-μm Al foil was used to cover the deposited Bi layer. The lateral size and weight of the Al foils were measured, and their average thicknesses of the 10-, 18- and 5-μm Al foils were 2.17, 4.79, and 1.21 mg/cm^2, respectively. The Al backing foils were cut into a size of 25 × 25 mm for the vacuum evaporation method. The Bi pieces were evaporated and deposited on a circular area with a diameter of 20 mm of the Al backing foils. The weight of the Al backing foils before and after the deposit process were measured, and the thicknesses of the Bi layers ranged from 5.46 to 10.9 mg/cm^2. The Bi layers on the Al backing and cover foils were cut into a size of 8 × 8 mm to fit target holders served as Faraday cups. Two stacked targets comprised 20 sets of Al(5 μm)/Bi/Al(10 μm) for target #1 and 16 sets of Al(5 μm)/Bi/Al(18 μm) for target #2.

To measure the thick target yield (#3), a Bi sheet (purity: 99.999%, thick: 1 mm, size: 25 × 25 mm, Goodfellow Co., Ltd., UK) was used. The Bi sheet and 5-μm Al cover foil were cut into a size of 10 × 10 mm to fit another target holder.

Targets #1, #2, and #3 were irradiated with the ^{7}Li beams for 60, 57, and 20 min, respectively. The average beam intensities measured using the Faraday cups were 147 (#1), 147 (#2), and 142 nA (#3). The beam energy common in the three experiments was 71.9 MeV. The energy degradation in the targets was calculated using stopping powers obtained from the SRIM code.[5] Target #3 was sufficiently thick to stop the beam.

γ rays emitted from the irradiated foils and sheet were measured using a high-purity germanium detector with different cooling times ranging from 1.0 h to 33 d.

The production cross sections of ^{211}Rn ($T_{1/2}$ = 14.6 h) were determined using the γ line at 674.1 keV (I_γ = 45.4%). The γ line overlapped with others at 672.82 keV (I_γ = 3.27%) from ^{209}At ($T_{1/2}$ = 28.5 min) and 675.15 keV (I_γ = 6.8%) from ^{207}At ($T_{1/2}$ = 1.80 h). The measurements with cooling times of 1.4–2.3 d were adopted to neglect the contributions of the γ lines from the shorter-lived co-products.

The preliminary results with the previously studied experimental data[2–4] are shown in Fig. 1. The results obtained from targets #1 and #2 are slightly scattered but consistent. The peak amplitudes of the previously studied experimental data are lower than those of the data of this study.

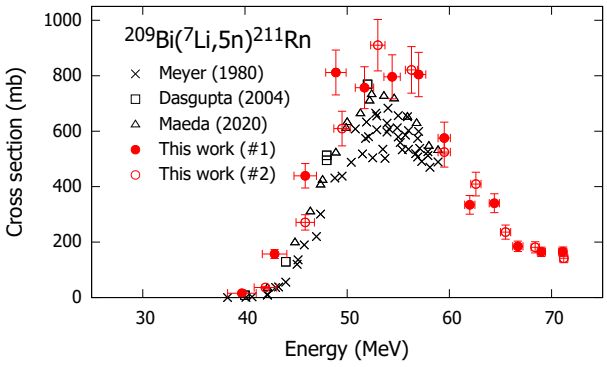

Fig. 1. Measured cross sections of the ^{209}Bi(^{7}Li, $5n$)^{211}Rn reaction with the literature data.[2–4]

Hereafter, we will determine the production cross sections of ^{211}Rn. The thick target yield will be calculated using the measured cross sections and compared with the experimental result.

*1 Advanced Clinical Research Center, Fukushima Medical University
*2 RIKEN Nishina Center
*3 Faculty of Science, Hokkaido University
*4 Graduate School of Biomedical Science and Engineering, Hokkaido University
*5 Graduate School of Science and Engineering, Saitama University

References

1) F. Guérard *et al.*, Cancer Biother. Radiopharm. **28**, 1 (2013).
2) E. Maeda *et al.*, J. Radioanal. Nucl. Chem. **323**, 921 (2020).
3) G. J. Meyer *et al.*, Appl. Radiat. Isot. **31**, 351 (1980).
4) M. Dasgupta *et al.*, Phys. Rev. C **70**, 024606 (2004).
5) J. F. Ziegler *et al.*, Nucl. Instrum. Methods Phys. Res. B **268**, 1818 (2010).

4. Radiation Chemistry and Biology

Sample preparation for ion-beam irradiation for biological experiments

Y. Hayashi*1 and T. Abe*1

RIKEN has developed a unique technology for mutation induction by using heavy-ion beams from particle accelerators at the RI Beam Factory (RIBF). At relatively low doses, ion beams induced mutations at a high rate without severely inhibiting growth. The irradiation treatment given to the various plant materials is quick, lasting between a few seconds and a few minutes, but is sufficient to induce mutation. By using this method, RIKEN has already put 39 new varieties on the market in Japan, the United States, and the European Union since 2001.[1,2] Furthermore, high-yielding rice, good growth wakame (*Undaria pinnatifida*), lettuce with low browning, microalgae with high oil content, and larger rotifer were identified as beneficial mutants.

We have developed an automatic irradiation system consisting of a range shifter and an automatic sample changer to cope with numerous requests with various biological samples such as dry seeds, wet seeds, callus, cultured tissue materials, pollens, seedings, cuttings *etc.*[3] Biological samples are stored in sample containers. Typical sample containers include plant boxes for regenerated plants and seedlings, 35-, 60-, and 90 mm-diameter plastic petri dishes for cultured tissues and seeds, and square plastic boxes for cuttings. The sample containers containing biological samples are attached to unique frames that support each sample containers.[4] Irregularly shaped samples placed in zipper bags or hybri-bags are fixed directly to the frame in line with the irradiation position. For example, Arabidopsis seeds were placed in a hybri-bag and arranged in a single layer by deaeration, then we found the most effective LET for mutation induction.[5] A uniform dose distribution is important for reproducible treatment on biological materials using ions with stable LET. The thickness of the sample is limited by the irradiation conditions. Therefore, it is necessary to place the sample in the most suitable container and attach the container to the frame.

We built a new beam line, 'WACAME,' to increase available nuclides with higher LETs and longer ranges. The Ar-ion beams are accelerated by RRC and IRC to 160 MeV/nucleon and sent to the E5 beam lines. Ar-ion irradiation is now available in tubes, increasing the number of microbes and microalgae users. We have created two types of cassettes for liquid cultures of microbes and microalgae (Fig. 1). One is for 15 mL centrifuge tube, and the other is for 1.5 mL micro and 200 μL PCR tubes. The first one is also available for cuttings that do not fit into square plastic boxes. The second one is rubber lined to prevent slipping down of tubes. Samples are fixed by springs to adapt various size of samples in both cassettes. Holes were drilled in the frame to check the sample's center. Each cassette also has a hole, and by aligning it with the hole in the frame, accurate placement in the irradiation position was made possible. In addition, yellow stickers were placed on the plates so that the irradiation field could be seen. We will continue to develop new frames and cassettes that promote efficiency in irradiation experiments as a tailor-made mutagen treatment technology to meet user requirements.

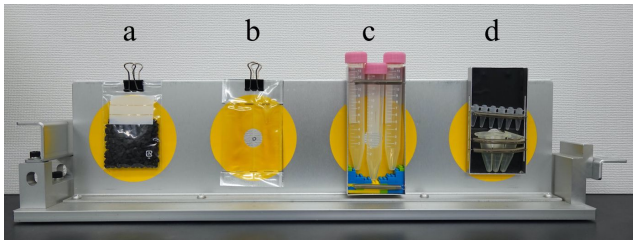

Fig. 1. Various samples set in the frame of automatic sample changer.
a: seed in the zipper bag, b: liquid sample in the hybri-bag, c: centrifuge tube fixed in the cassette, d: micro tube and PCR tube fixed in the cassette.

Table 1. Sample containers available in the frames of automatic sample changer.

Samples	Containers
Cultured tissues	Petri dish, Plant box
Seeds	Petri dish, Zipper bag, Square plastic box, Hybri-bag
Cuttings	Zipper bag, Square plastic box
Liquid	Centrifuge tube (15 ml), Micro tube (1.5-2 ml), 8 strips PCR tube*1, Hybri-bag*2

*1: Use 6 strips in the middle and cut off the both ends.
*2: The thickness of sample for Fe-ion irradiation must be less than 2 mm.

*1 RIKEN Nishina Center

References
1) T. Abe *et al.*, in *Ion beam radiation mutagenesis in Plant Mutation Breeding and Biotechnology*, (Oxfordshire UK, 2012), p. 99.
2) T. Abe *et al.*, Nucl. Phys. News **25**, 30 (2015).
3) H. Ryuto *et al.*, J. Biomed. Nanotechnol. **2**, 88 (2006).
4) H. Ryuto *et al.*, Plant Biotechnol. **25**, 119 (2008).
5) Y. Kazama *et al.*, Plant Biotechnol. **25**, 113 (2008).

Identification of causal site for an *Arabidopsis* C30-144-as3 mutant

A. D. Nagalla,[*1] S. Ohbu,[*1] K. Ishii,[*1,*2] Y. Kazama,[*1,*3] T. Hirano,[*1,*4] and T. Abe[*1]

Mutations are one of the crucial factors for natural selection and species evolution. They occur frequently in nature. With the development of science and technology, we can create artificial mutagenesis and manually search for desirable characters. Among those artificial mutagenesis techniques, heavy-ion beam irradiation has been established as a reliable approach in plant breeding.[1)] An important parameter for ion-beam mutagenesis can be identified as linear energy transfer (LET). The LET implies the amount of energy deposited per unit length of a particle's path (keV/μm). The C-ion irradiation (30 keV/μm) on Arabidopsis seeds has a high mutation frequency[2)] and results mainly in single nucleotide variants (SNVs), small indels (<100 bp), in the responsible genes for mutant phenotypes. The number of homozygous mutated genes per genome is approximately five, making it easy to identify the causative gene.[3)]

In this study, we irradiated Arabidopsis (Col-0) seeds with 400 Gy C-ions (30 keV/μm). The resulting mutant plants were isolated, allowing further generations to be selfed, and screened for interesting phenotypes. The C30-144-as3 mutant was identified as later flowering and round rosette leaves containing plant (Fig. 1). After the whole genome sequencing, mutation calling was conducted using the AMAP: A pipeline for whole-genome mutation detection.[4)] This analysis resulted in homozygous SNVs, a large deletion, and intrachromosomal translocations (ITX) occurred in genic regions (Table 1). In order to identify the candidate gene, we planned to perform a linkage analysis using a backcrossed (BC) population. The BC_1F_2 population consists of 84 plants. Phenotype scoring referred to the perfect C30-144-as3 plant (M_3) with later flowering and round rosette leaves.

Fig. 1. Ion beam mutant C30-144-as3 shows later flowering and round rosette leaves containing plant (b) compared to Col-0 plant (a) on 31 days after germination.

Table 1. Homozygous mutated genes found in C30-144-as3.

Chr.	Position	Type	Size	Affected genes
1	13088360-13167752	ITX	79.39Kb	AT1G06917
2	19600910	SNV	1bp	AT2G47860
3	11316869-12608684	DEL	1.29Mb	111 genes
3	23056674	SNV	1bp	AT3G62300
4	998176	SNV	1bp	AT4G02280
4	9318677	SNV	1bp	AT4G16550

A total of 17 plants showed mutant phenotype. The segregation of the F2 population fitted the 3 : 1 segregation ratio (wild-type: mutant = 67 : 17, χ^2 = 1.02). Therefore, we hypothesize that this mutation was caused by a recessive single gene. Linkage analysis was performed for all the homozygous mutated genes using 17 F_2 plants, which showed the mutated phenotype. The AMAP pipeline revealed large deletion of approximately 1.29 Mb in M_3 plants. This deletion has lost a total of 111 genes, according to the Arabidopsis genome browser. We used two primer pairs and Sanger sequencing of PCR products for genotyping experiments. Linkage analysis resulted in 16 homozygous plants linked with the above large deletion (one of the plants among 17 plants resulted in non-reproducible linkage analysis result, which could be due to contaminated DNA), indicating responsible gene might be included in the deleted fragment. Because among the homozygous mutated genes, only the 1.29 Mb deletion showed the linkage. Next, we checked the gene description of all 111 genes and found a single gene responsible for regulating flowering time and leaf shape. It's the gene AT3G30260 and already identified as *AGAMOUS-LIKE 79* (*AGL79*).[5)] The non-functional mutants were reported to show later flowering and round rosette leaves. Then we presumed *AGL79* gene was the causative gene for the C30-40 mutant.

*1 RIKEN Nishina Center
*2 Department of Radiation Measurement and Dose Assessment, National Institute of Radiological Sciences
*3 Faculty of Bioresources, Fukui Prefectural University
*4 Faculty of Agriculture, University of Miyazaki

References

1) T. Abe *et al.*, *Plant mutation breeding and biotechnology* (Oxfordshire UK: CABI, 2012), p. 99.
2) Y. Kazama *et al.*, Plant Biotechnol. **25**, 113 (2008).
3) Y. Kazama *et al.*, BMC Plant Biol. **11**, 161 (2011).
4) K. Ishii *et al.*, Genes Genet. Syst. **91**, 229 (2016).
5) R. Gao *et al.*, Front. Plant Sci. **8**, 2226 (2018).

Analysis of splicing patterns in *Arabidopsis egy1-4* carrying argon-induced mutations in the intron 3-exon 4 region

A. Sanjaya,[*1,*2] Y. Fujii,[*1] M. Asano,[*1] T. Abe,[*3] Y. Kazama,[*2,*3] and M. Fujiwara[*1,*3]

Eukaryotic gene expression involves the splicing of precursor messenger RNAs before the translation. The U2 spliceosome, a nuclear ribonucleoprotein complex, is important in the process of splicing, and recognizes certain conserved "canonical" sequences in introns, including a GU at the 5' end, an adenine known as the "branchpoint" located 20–50 bases upstream of the 3' end, and an AG at the 3' end. Based on the mechanism of intron excision discovered, the intron 5' splice and intron 3' splice sites are referred to as the splice donor site and the splice acceptor site, respectively. Splicing begins at the 5' splice site and involves the formation of an intron lariat at the branchpoint as the cleaved 5' end of the intron becomes attached to it. The excision of the intron lariat from the 3' splice site then allows for the ligation of the exons.

Mutations at such canonical intron sites typically cause inefficient and/or cryptic splicings.[1)] In *Arabidopsis thaliana*, mutations of the intron 3' splice site, either "AG to AA" or "AG to GG," are known to activate only cryptic 3' splice sites but not 5' splice sites.[1,2)] A 3' splice site mutation resulting in cryptic 5' splice site activation has never been reported.

In *A. thaliana*, the *Ethylene-dependent Gravitro-pism-deficient and Yellow-green 1* (*EGY1*) gene (AGI code: At5g35220) encodes a chloroplast-targeted metalloprotease and is composed of 10 exons and 9 introns. During its functional analysis, an argon-ion-induced allele, *egy1-4* (Ar-28-pg1[3)]), has been noted as it contains an AG to AC transition at the 3'-end of intron 3, in addition to 4-bp substitutions and a 5-bp deletion in the downstream exon 4.[4)] To determine whether these mutations in the intron 3-exon 4 junction region of *egy1-4* affect the splice site selection in *EGY1*, the total RNAs were extracted from 2-week-old seedlings of wild-type and *egy1-4*, and analyzed using RT-PCR with primers binding to the *EGY1* 5'-untranslated region and exon 5. The amplified PCR products were ligated to a vector and transformed into an *E. coli* DH5α strain. The resulting colonies were subsequently cultured for the propagation of plasmids, which were then Sanger-sequenced. The sequence of *EGY1* cDNAs around intron 3 was then compared between the wild-type and *egy1-4*.

Only one splicing pattern of intron 3 was observed in the wild-type by sequencing 30 clones (Fig. 1; Table 1). However, among 58 cDNA clones of *egy1-4* examined, 42 exhibited no splicing of intron 3 (unspliced pattern). The rest exhibited distinct splicing patterns from the wild-type ones: 5 and 8 clones exhibited activation of upstream and downstream cryptic 3' splice sites, respectively. Moreover, a new splicing pattern, exhibiting activation of cryptic 5' splice site alongside activation of 3' splice site, was found in 3 clones (Fig. 1; Table 1).

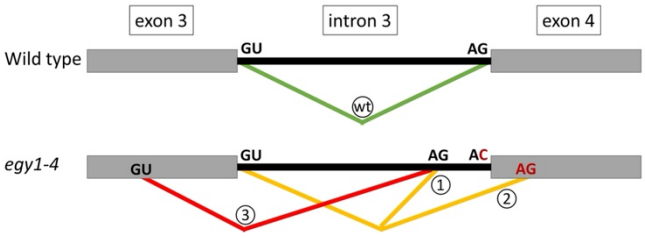

Fig. 1. Schematic comparison of *EGY1* transcript splicing patterns between the wild-type and *egy1-4*. Sole splicing pattern (wt) was observed in the wild-type. Cryptic 3' splice sites were activated without (patterns 1 and 2) or with (pattern 3) the activation of cryptic 5' splice site in *egy1-4*. The nucleotide letters in red denote that they are uniquely produced in *egy1-4* by argon-ion-irradiation.[3)]

Table 1. RT-PCR and cloning analysis of intron 3 splicing patterns in wild-type and *egy1-4*.

Plant line	Intron 3 splicing pattern	Number of cDNA clones sequenced	Relative frequency
Wild type	wt	30	100 %
	Total:	30	100 %
egy1-4	(unspliced)	42	72.4 %
	1	5	8.6 %
	2	8	13.8 %
	3	3	5.2 %
	Total:	58	100 %

As sole splicing patterns were observed in all the other introns for both wild-type and *egy1-4* (unpublished results), the pale green phenotype of *egy1-4* plants[4)] was attributed to the expression of truncated forms of EGY1. This is due to premature stop codons in the mutant exon 3 or exon 4 in any spliced/unspliced variants. Our finding demonstrates that mutations induced by heavy-ion irradiation significantly impact on the terminal phenotype of plant bodies via interference of splicing.

*1 Graduate School of Science and Technology, Sophia University
*2 Graduate School of Bioscience and Biotechnology, Fukui Prefectural University
*3 RIKEN Nishina Center

References
1) J. W. S. Brown, Plant J. **10**, 771 (1996).
2) M. A. Schuler, in *Splice Site Requirements and Switches in Plants*, edited by A. S. N. Reddy and M. Golovkin (Springer, Berlin, 2008), p. 39.
3) T. Hirano *et al.*, Mutat. Res. **735**, 19 (2012).
4) A. Sanjaya *et al.*, Plants **10**, 1254 (2021).

Irradiation of seeds with C-ion and Ar-ion beams for *Streptocarpus* mutagenesis to understand leaf meristem genetics

K. Nishii,[*1,*2] M. Möller,[*1] N. Kelso,[*1] H. France,[*1] S. Barber,[*1] Y. Hayashi,[*3] K. Ishii,[*3] and T. Abe[*3]

Streptocarpus Lindl. (Gesneriaceae) attract developmental biologists owing to their variable shoot/leaf forms, which include caulescents with ordinary shoot apical meristem (SAM) and acaulescent (unifoliates and rosulates) lacking SAMs (*e.g.*, Figs. 1a–c). Anisocotyly (Fig. 1b), the unequal cotyledon development producing a macrocotyledon also marks this genus/family.[1)] *Streptocarpus rexii* Lindl. is rosulate and has been studied as a model to understand their unique cotyledon and leaf development. Previous results have shown relocated expression of SAM genes in their leaf meristems.[1)] Thus, the genetic and functional shift of meristems from the shoot apex laterally to the leaf might result in their unique acaulescent forms. This work is important to understand plant meristems and their effects on plant form. To date, a genetic map, transcriptome, and genome have been generated for *S. rexii*,[2)] which are important resources to isolate the underlying genetic loci. Here, we use forward genetics utilizing heavy-ion mutagenesis to facilitate this aim.[3)]

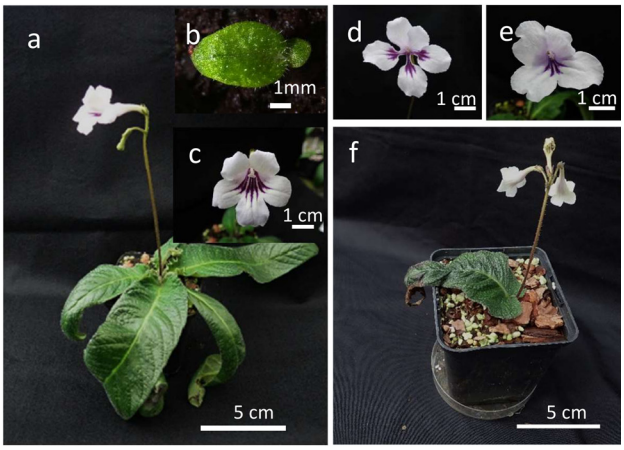

Fig. 1. Images of *Streptocarpus rexii* wild type and heavy-ion irradiated mutants. a-b) *S. rexii* wild type. b) Anisocotyly. c) Wild type flower. d-e) C200 flower mutations. f) C200 qualifier "JW" M_1 plant showing delayed leaf initiation phenotype.

Seeds of *S. rexii* (RBGE 20170766*A) cultivated in the glasshouses at Royal Botanic Garden Edinburgh (RBGE) were harvested in October 2018, certified at Science & Advice for Scottish Agriculture (SASA; Phytosanitary Certificate No. SG/SASA/2018/033), and transported to RIKEN (Wako, Japan). C-ion ($^{12}C^{6+}$) and Ar-ion ($^{40}Ar^{17+}$) irradiations were conducted at RIBF. The high linear energy transfer (LET) value of C-ion was set to 30 keV μm^{-1}, and that of Ar-ion to 184 keV μm^{-1}. For C-ion, doses of 50, 100, 150, 200, 300 and 400 Gy, and for Ar-ion, 10, 20 and 50 Gy were used, labelled C50, C100, C150, C200, C300, C400, Ar10, Ar20, and Ar50, respectively. The lethal effects of the treatments were assessed as the germination rate and seedling growth. The seeds were sown in Petri dishes on filter paper soaked with tap water and examined 2 and 3 weeks later. The growth of seedlings (the cotyledon size) was measured 7 weeks after sowing. The flower phenotype was also observed for mutations in the M_1 generation from 20–26 plants per treatment. To obtain larger M_2 populations for screening, M_1 seeds of selected treatments were sown and cultivated. The vegetative phenotype was observed while focusing on mutations in leaf initiation. Germination was observed in all treatments; however, it was delayed in C400 and Ar50. The final germination rate was low only for Ar50 (Table 1). A strong suppression of seedling growth was observed in C300, C400, and Ar50, and all seedlings eventually died. Over 20% of M_1 plants of C150, C200, Ar10 and Ar20 showed flower mutations, such as split corollas and shift in symmetry (Figs. 1c–e).

Table 1. Effects of heavy-ion irradiation on Streptocarpus rexii.

	Germination% 2 weeks	Germination% 3 weeks	Macrocotyledon size (μm^2)	Num. of flower mutants per total plants observed
	average ± SE, *N*=10, biological triplicates or duplicate*			
Wild type	78 ± 7	78 ± 7	2724 ± 88	0/20
C50	62 ± 2	72 ± 2	6380 ± 1564	2/23
C100	81 ± 3	83 ± 2	4453 ± 925	1/23
C150	67 ± 1	75 ± 5	3689 ± 861	6/26
C200	70 ± 11	76 ± 6	1984 ± 38	6/26
C300	66 ± 10	71*	965 ± 63	lethal
C400	45 ± 6	73 ± 8	703 ± 36	lethal
Ar10	71 ± 13	76 ± 11	4148 ± 1064	5/24
Ar20	76 ± 4	85 ± 4	5332 ± 877	7/26
Ar50	46 ± 18	53 ± 17	964 ± 36	lethal

Considering all results together, C150, C200, and Ar20 were just below the lethal dosage, and showed clear flower mutations. Thus, they were selected for large scale mutant screening. More than 1000 M_1 plants of C150, C200, and Ar20 were cultivated to obtain M_2 seeds. The estimated fertility rates (in May

*1 Royal Botanic Garden Edinburgh
*2 The Research Institute for Integrated Science, Kanagawa University
*3 RIKEN Nishina Center

2021) were 62, 47, and 40% for C150, C200, and Ar20, respectively. Five of C200 M_1 plants, and 25 of Ar20 showed a delayed leaf initiation phenotype (Table 1; Fig. 1f). M_2 seeds of these were harvested from four C200 and 12 Ar20 plants. Now, these mutant phenotypes were observed for mutant stability in following generations.

References

1) K. Nishii *et al.*, Dev. Genes Evol. **220**, 25 (2010).
2) K. Nishii *et al.*, Plant Direct **6**, e388 (2022).
3) T. Abe *et al.*, Nucl. Phys. News **25**, 30 (2015).

Comprehensive effects of heavy-ion beam irradiation on sweet potato (*Ipomoea batatas* [L.] Lam.)†

H. Park,[*1] Y. Narasako,[*2] T. Abe,[*3] H. Kunitake,[*4] and T. Hirano[*3,*4]

Sweet potato is one of the most important food crops and plays a critical role in food supply and safety worldwide. Although the main feature of sweet potato is the formation of tuberous roots, the detailed mechanisms of how tuberous root formation is controlled by the factors are still unknown. Therefore, an advanced strategy is required for the investigation of molecular functions. Heavy-ion beam has been applied for mutation breeding in various plants and genetic studies.[1,2] In this study, Ar- and C-ion beam irradiation was applied to *in vitro* cultured shoots of sweet potato, and mutant lines were established to screen the mutants on tuberous root formation.

In vitro cultured shoots with an axillary bud of sweet potato (*Ipomoea batatas* 'Beniharuka') were irradiated with $^{12}C^{6+}$ ions (LET; 30 keV μm^{-1}) at absorbed doses of 5.0, 10.0, and 20.0 Gy, or $^{40}Ar^{17+}$ ions (LET; 184 keV μm^{-1}) at absorbed doses of 1.0, 2.5, and 5.0 Gy. The regenerated shoot was cut into nodes, each with an axillary bud, after three months of culture. Three lines were separated from each irradiated shoot. The irradiated lines were acclimatized in the greenhouse and then cultivated in the field.

The shoot formation was decreased at high-dose irradiation of both ion beams. Shoulder doses on the shoot formation curve were considered 10 Gy for the C-ion beam and 2.5 Gy for the Ar-ion beam. We have obtained 335 lines, which consist of 104 and 231 lines derived from Ar- and C-ion irradiation, respectively. After the acclimatization, 116 and 211 irradiated lines survived and were used for the mutant screening in the fields in 2020 and 2021, respectively. The irradiated lines demonstrated a wide range of phenotype variations in the tuberous roots (Fig. 1). Generally, the total weight of the tuberous roots tends to decrease in the C- and Ar-ion irradiated lines. The high-yield lines, with an increase of more than 180%, were derived from Ar-ion irradiation. Considerable inhibition of tuberous root formation was observed in the lines derived from C- and Ar-ion irradiation. It was indicated that heavy-ion beam mutagenesis is effective in broadening the range of the phenotypes corresponding to tuberous root formation. These mutant candidates are expected to enhance our understanding of the mechanisms related to tuberous root formation.

References

1) T. Abe *et al.*, Nucl. Phys. News **25**, 30 (2015).
2) T. Hirano *et al.*, Cytologia **87**, 3 (2022).

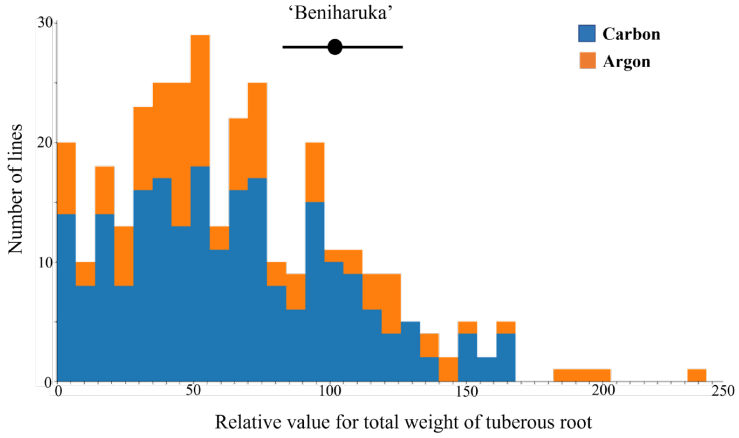

Fig. 1. Frequency distribution of the relative total weight of tuberous roots in C- and Ar-ion irradiated lines. The data represents the combined results for 2020 and 2021. The circle and bar represent the mean (100) and range of 'Beniharuka,' respectively.

† Condensed from the article in Plant Biotechnol. **39**, 311 (2022)

*1 Interdisciplinary Graduate School of Agriculture and Engineering, University of Miyazaki
*2 Kushima AoiFarm Co.
*3 RIKEN Nishina Center
*4 Faculty of Agriculture, University of Miyazaki

Growth inhibition of marine red alga *Agardhiella subulata* through C-ion beam irradiation

K. Tsuneizumi,[*1] M. Yamada,[*1] M. Mogamiya,[*2] Y. Sato,[*2] and T. Abe[*1]

In the Japanese way of life, seaweeds such as laver, kelp, wakame, and hijiki have a long history of use and are consumed in large quantities. Recently, seaweeds have gained attention as materials for the production of carrageenan, alginic acid, and agar,[1] and their production has been increasing in Asia as an aquaculture marine resource rather than for food. Furthermore, seaweeds contain fucoidan, which has proven to be effective in hair growth promotion,[2] immunostimulatory activities,[3] and anti-aging.[4] This information has led to increasing attention to seaweeds as raw materials for functional materials.

Agardhiella subulata, commonly known as edible red algae, has been discovered as a new material that produces fucoidan,[5] and there is much interest in increasing the production of its active ingredients. Breeding new cultivars with properties such as high yield, high environmental adaptability, and high concentrations of constituents with human health benefits is desirable for enhanced value. In this report, to determine the effective conditions of the C-ion beam for red algae mutagenesis, we calculated the growth in the area of irradiated regenerating buds.

Small fragments of *A. subulata* were cultured with NORI SEED (Daiichi Seimo Co., Ltd.), a highly enriched culture solution. A culture medium was prepared using 160 μL of NORI SEED diluted with 300 mL of autoclaved sea water. Small fragments developed into regenerating buds for three weeks in a stirred 300-mL marine flask containing the culture medium. The flask was placed at 25°C for a 12 hours photoperiod with a light intensity of 50 μmol photons $\cdot$ m^{-2}s^{-1}, and the culture medium in the flask was replaced every week. The regenerating buds were replaced into 5-mL tubes at each irradiation condition.

Heavy-ion-beam irradiation was performed using C (LET = 30 keV/μm) at 8 irradiation doses of 5, 10, 20, 40, 70, 100, 200, and 400 Gy generated at the RIKEN RIBF.[6] Four hours after irradiation, eight regenerating buds were inoculated into each 36-mm dish containing 3 mL of fresh culture medium for each irradiation condition. The dishes were placed at 25°C for a 12 hours photoperiod with a light intensity of 50 μmol photons $\cdot$ m^{-2}s^{-1}, and 150 μL of the 20-fold concentrated culture medium was added every 2–3 d. The regenerating buds were photographed every few days and the sizes of 8 reproducing individuals ($n = 8$) were calculated using Image J software version 1.5.1[7] (Fig. 1).

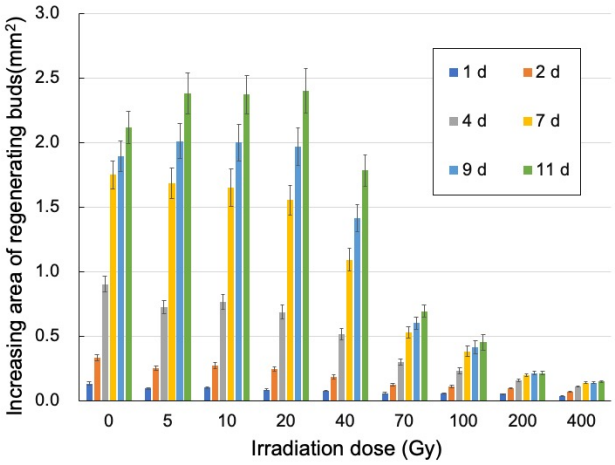

Fig. 1. Correlation between increasing area of regenerating buds and C-irradiation dose. A correlation chart using the average values of increasing area was constructed for the unirradiated control and irradiated regenerating buds. The vertical vars represent the standard errors.

An increase in the area representing the regenerating buds irradiated up to 20 Gy in the correlation chart indicates that they proliferate in the same way as unirradiated controls (Fig. 1). In contrast, the growth inhibition of the regenerating buds is observed in a dose-dependent manner effected by 40–400 Gy C-ion beams (Fig. 1). In future studies, we will carry out large-scale screening under each irradiation condition, and the optimum irradiation conditions will be determined based on the frequency of the appearances of the mutant lines.

*1 RIKEN Nishina Center
*2 Riken Food Co., Ltd.

References

1) Y. C. Liao *et al.*, Bioengineered **12**, 3787 (2021).
2) I. S. Moon *et al.*, Hear. Res. **282**, 236 (2011).
3) R. Li *et al.*, Mar. Drugs **21**, 18 (2023).
4) R. Zhang *et al.*, Carbohydr. Polym. **15**, 228 (2020).
5) C. Faggio *et al.*, Nat. Prod. Res. **30**, 2016 (2015).
6) T. Abe *et al.*, in *Plant Mutation Breeding and Biotechnology*, edited by Q. Y. Shu *et al.* (CABI, Oxfordshire, 2012), p. 99.
7) C. Schneider *et al.*, Nat. Methods **9**, 671 (2021).

Semi-automated high-throughput microbial DNA extraction protocol for population-scale mutation analysis

Y. Nishimiya,[*1] N. Lei,[*1] and H. Ichida[*1]

At RIKEN Nishina Center for Accelerator-Based Science, one active area of research is the application of heavy-ion beams to mutation breeding, where we utilise next-generation sequencing and the massively parallel supercomputer "HOKUSAI" to characterise irradiation-induced DNA damage and subsequent genetic mutations statistically. In recent years, we have demonstrated the efficacy thereof using various model organisms, efficient identification of mutations through whole-genome and exome sequencing in *Nicotiana tabacum* L., and the applicability of the redundant sequence elimination algorithm in analysing data obtained from a complex genome such as wheat. We accordingly developed a versatile and high-accuracy mutation-detection pipeline.

Historically, only indirect measurements such as the survival rate and albino emergence rate were available to estimate the mutation-induction efficiency approximately. Whole-genome sequencing (WGS), on the other hand, enables one to count the exact number of mutations in each sample, which presents two crucial advantages: (i) The smaller error margin enables a more sensitive differentiation of the mutation-induction efficiency. (ii) Significantly fewer samples are required to estimate the optimal experimental condition compared to conventional indirect methods.

Therefore, we began testing the WGS-based mutation-induction optimisation methodology against the survival-rate-based estimates using budding yeast with a small genome size. However, investigating the multitude of irradiation conditions (ion type, linear energy transfer, and irradiation dose) and genetic backgrounds (wild type and DNA-repair deficient mutants), where all combinations thereof require several (at least 10) samples, necessitates the simultaneous cultivation of cultures on a considerable scale whilst maintaining the overall pace of execution to control for their time-sensitive nature properly.

To overcome this challenge, we devised a series of techniques to achieve efficiency based on the knowledge that 500 μL of culture per sample is sufficient for DNA extraction and sequencing. This small volume requirement permits us to use 96 deep-well plates with significantly high density (a desktop incubator can cultivate up to 384 samples) and higher ease of manipulation than conventional test tubes. Moreover, after centrifugation and a brief lysis procedure, we can directly transfer them onto the automated liquid-handling robot (OT-2, Opentrons) in a smooth production-line-like manner. Eliminating the necessity to pipette the liquid culture from one tube to another ensures that the entire volume of the obtained culture proceeds for DNA extraction, reducing human labour and risks of cross-contamination. The 96 deep-well plates we tested can also be used for cryogenic storage of the liquid culture.

Hence, we tested the yeast DNA extraction through the automated procedure. Following trial and error, we verified the robot's reliability to automatically execute a protocol consisting of (i) cell-wall digestion with Zymolyase, (ii) extraction of DNA using magnetic beads, and (iii) elution of the extracted DNA. Although the reagents must be carefully prepared in advance, we estimate that the combined use of 96 deep-well plate cultivation and robot DNA extraction would require as little human labour as approximately half an hour in all to prepare up to 192 DNA samples per day, in comparison with the 4.5 hours including active and standby time required for the manual alternative. Figure 1 presents an example of concentrations in ng/μL of the DNA thereby extracted across the well plate. From past trials, we know that 700 ng is adequate for sequencing. Thus, when the final elution volume is specified as 100 μL, the minimum concentration of 7 ng/μL suffices.

	1	2	3	4	5	6	7	8	9	10	11	12
A	15.5	20.3	22.9	12.3	24.1	17.0	19.4	20.5	15.8	15.5	15.5	21.9
B	15.6	17.7	21.9	16.1	21.2	21.4	21.8	23.0	20.6	15.5	18.3	22.9
C	16.8	19.5	21.1	13.6	21.5	19.7	16.5	15.0	16.4	14.4	18.5	21.2
D	9.9	19.6	23.3	14.2	19.5	21.2	19.0	20.1	19.5	14.6	18.5	24.1
E	16.5	19.4	25.3	7.4	24.3	17.5	14.1	17.1	15.0	13.5	18.1	22.8
F	17.0	19.9	24.9	20.6	28.4	7.3	19.6	18.2	14.4	14.5	15.5	24.0
G	15.2	16.5	22.8	13.3	16.1	19.8	18.2	20.6	16.2	16.1	13.0	21.0
H	17.5	16.1	25.5	14.7	19.2	22.8	20.9	22.4	22.1	17.8	17.6	20.7

Fig. 1. Example distribution of extracted DNA concentration in ng/μL on a grid corresponding to the 96 deep-well plate. The blue-red bi-colour scale represents the increasing yield.

At the time of writing this manuscript, we had acquired approximately 700 distinct yeast DNA samples following irradiation with carbon, argon, and iron beams, the WGS data of which are presently being analysed. Our current objectives are to establish the population-scale WGS-based mutation analysis protocol as a more efficient and accurate method to advance our understanding of heavy-ion beam-induced mutations, DNA repair mechanisms, and their applications to mutation breeding technology, and to develop statistical models to efficiently learn about and infer from the newly acquired rich source of genomic data.

*1 RIKEN Nishina Center

Heavy-ion irradiation enhanced the post-transcriptional modification of CtIP

M. Izumi,[*1] T. Tsukada,[*1] and T. Abe[*1]

Among DNA damages caused by ionizing radiation, DNA double strand breaks (DSBs) are the most lethal as misrepaired or unrepaired DSBs can cause a loss of genetic information, canceration, and cell death. Mammalian cells have four pathways to repair DSBs: canonical non-homologous end joining (NHEJ), homologous recombination (HR), alternative NHEJ (alt-NHEJ), and single strand annealing (SSA). Accelerated heavy-ion particles with high linear energy transfer (LET) induce complex clustered DNA damage including DSBs, single strand breaks, and base damages within one or two helical turns of DNA. The clustered DNA damage is considered as an obstacle to efficient repair and affects the pathway choice for DSB repair.

After exposure to low-LET radiation, NHEJ is the dominant repair pathway throughout the cell cycle, whereas HR works only in the late S/G2 phase. Alt-NHEJ and SSA are considered to be functional only when both the NHEJ and HR are impaired.[1)] However, the repair mechanism after heavy-ion irradiation has not been fully understood. Our previous study using mammalian cells and specific inhibitors against NHEJ or HR suggests that NHEJ is the major repair pathway after 2 Gy of heavy-ion irradiation.[2)] In addition, we have shown that HR is favored after heavy-ion irradiation in G2-phase, although HR repairs DSBs less efficiently after heavy-ion irradiation than after X-ray irradiation.[3)] Moreover, recruitment of Rad51 (HR factor) to DSB is suppressed by high dose (>15 Gy) heavy-ion irradiation,[4)] suggesting that the pathway choice is dependent on the cell cycle, LET, and dose.

In this study, we examined the modification of CTBP-interacting protein (CtIP) after heavy-ion irradiation. CtIP is involved in end-resection of DSBs for generating 3′-single strand DNA, which promotes HR, SSA, and alt-NHEJ.[5)] CtIP is phosphorylated by active ATM as well as cyclin-dependent kinase in S/G2 phase. Phosphorylation of CtIP facilitates its interaction with BRCA1 and Mre11/Rad50/Nbs1 nuclease complex. Recent studies suggest that the balance between 53BP1-Rif1 and CtIP-BRCA1 controls the pathway choice. Thus, the choice between NHEJ and HR/alt-NHEJ/SSA is determined by which among end-joining or end resection occurs first.[6)]

Exponentially growing HeLa cells were irradiated with argon ions (LET = 300 keV/μm) of different doses (2–30 Gy), and chromatin fractions were obtained and subjected to an immunoblot analysis (Fig. 1). In unirradiated cell extracts (at 0 hour), both phosphorylated and non-phosphorylated forms of CtIP were detected. The level of phosphorylated forms increased after both 15 and 30 Gy of X-ray irradiation. Argon-ion irradiation induced phosphorylation at the lower dose (2–5 Gy), suggesting that the end-resection is enhanced after heavy-ion irradiation. In addition, we found a more retarded form of CtIP after high dose (>15 Gy) of argon-ion irradiation. The retarded form may be hyperphosphorylated or modified by small proteins such as ubiquitin or SUMO. Moreover, we observed the same form after the carbon-ion (LET = 80 keV/μm) irradiation (data not shown).

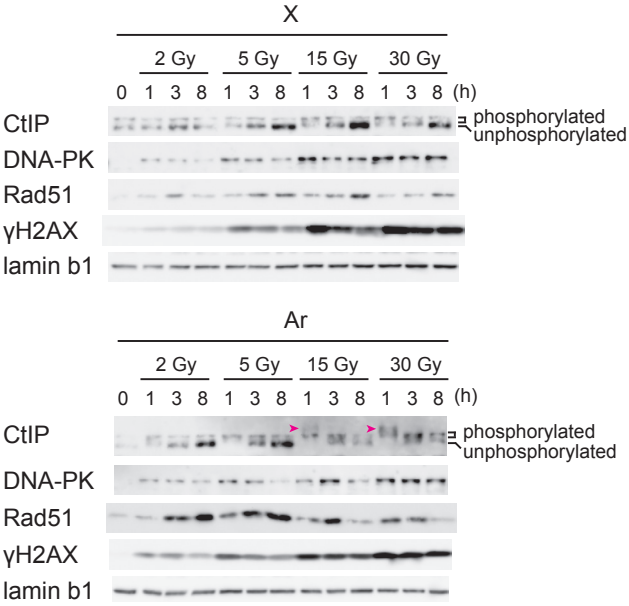

Fig. 1. Immunoblot analysis of chromatin-bound repair proteins after irradiation. HeLa cells were irradiated with indicated doses of X ray or Ar ions. Triton-insoluble fractions (chromatin fractions) were prepared at indicated time points following irradiation and subjected to immunoblot. CtIP, phosphorylated DNA-PK, Rad51, and phosphorylated histone H2AX (γH2AX) were detected. Arrowheads indicate the retarded modified forms, which were absent in X-ray irradiated extracts. Lamin B1 was detected as a loading control.

We also detected phosphorylated DNA-PK (NHEJ factor) and Rad51 (Fig. 1). The amount of phosphorylated DNA-PK was dependent on the dose, whereas that of Rad51 increased up to 5 Gy after argon-irradiation and decreased at 15 Gy irradiation as previously reported.[4)] These results suggest that CtIP can promote alt-NHEJ and/or SSA at high doses (>15 Gy).

*1 RIKEN Nishina Center

References
1) R. Ceccaldi *et al.*, Trends Cell Biol. **26**, 52 (2016).
2) M. Izumi *et al.*, RIKEN Accel. Prog. Rep. **53**, 24 (2020).
3) M. Izumi *et al.*, RIKEN Accel. Prog. Rep. **54**, 33 (2021).
4) M. Izumi *et al.*, RIKEN Accel. Prog. Rep. **55**, 174 (2022).
5) P. Cejka *et al.*, Annu. Rev. Genet. **55**, 285 (2021).
6) C. Escribano-Diaz *et al.*, Mol. Cell **49**, 872 (2013).

Examination of the direct visualization toward adverse events caused by space radiation

A. Sakaue-Sawano,[*1] M. Izumi,[*2] T. Abe,[*2] and A. Miyawaki[*1]

The cellular response to DNA damage varies according to the cell types and the cell cycle phases as well as the extent of DNA damage. In the early 1960s, Terasima *et al.*[1] employed a method of selectively harvesting cells in M-phase (mitotic shake-off) to examine cell cycle-dependent responses to DNA damage caused by X-ray irradiation in HeLa cells. They concluded that cell survival was minimal when irradiation was executed during the mitotic (M) and late G1 or early DNA synthesis (early S) phases whereas it was maximal during the early postmitotic (early G1) and premitotic (S to G2) phases. This view has been widely accepted to date. However, conventional methods that use pharmacological reagents and the above-mentioned mitotic shake-off method should have artifactual effects on cells or may be incapable of complete cell-cycle synchronization, especially of highly proliferative tumor cells.

Recently, various cell-cycle visualization methods using fluorescent proteins (FP) have been developed, making it possible to directly analyze the cell cycle stages without synchronization and thus without affecting normal cell functions. Our original Fucci (fluorescent ubiquitination-based cell cycle indicator) technique skillfully utilizes the degradation properties of Cdt1 and Geminin (which undergo cell cycle-dependent proteolysis), two important proteins that contribute to normal cell cycle progression. When the degradation domains of Cdt1 and Geminin are conjugated to Red or Green FP, respectively, the cell cycle transition from G1 to S phase is highlighted with high color contrast, like a traffic light: red to green which mean "stop" and "go," respectively (Fig. 1).[2] We will not go into details here, *i.e.* Fucci (SA) highlights nuclei of cells in G1 phase in red and those of cells in S-G2-M phases in green. Furthermore, the improved Fucci (CA) is able to identify clear interphase boundaries between G1, S, and G2 phases (it highlights G1 phase in red, S phase in green, and G2-M phases in yellow). Then we have successfully demonstrated S phase maximal sensitivity of HeLa cells to UV radiation.[3]

In the coming era when humans are once again traveling to the Moon and Mars as represented by "Artemis mission," it should be necessary to reevaluate the impact of space risks such as radiation and microgravity.[4] Various FP-based approaches have been initiated to directly study the effects of space radiation on living cells.[5,6] Live imaging technology using FPs is expected to make significant contributions to the direct visualization and detailed understanding of radiation-related adverse events.

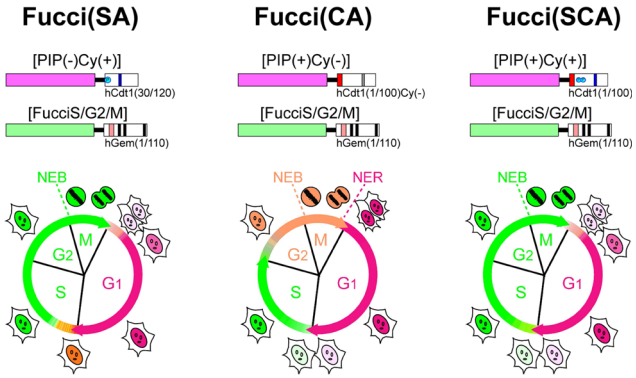

Fig. 1. Cell cycle-phasing capabilities of the Fucci technology. Domain structures of each Fucci repertoire (upper) and cell-cycle phasing capabilities (lower) are shown. For reasons of space, we will not go into details, but please review the original paper to understand Fucci's technology in general. Data were adapted from Sakaue-Sawano *et al.*[3]

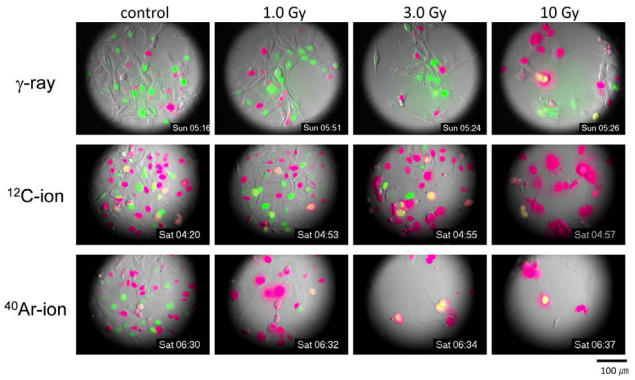

Fig. 2. Example of an experiment to evaluate the effects of heavy-ion irradiation using Fucci Live Imaging. The human Fibrosarcoma cell line; HT1080/Fucci (CA) 5 cells were irradiated with indicated doses for γ-ray, carbon-ion (LET = 50.9 keV/μm) or argon-ion (LET = 185 keV/μm), respectively. Live cell imaging was immediately performed using an LCV100 computer-assisted fluorescence microscope capable of visualizing eight samples simultaneously.[2,3] The data are superimposed snapshots of DIC, Green FP and Red FP 36 hours after irradiation.

We planned to use Fucci (CA) to visualize responses

*1 RIKEN Center for Brain Science
*2 RIKEN Nishina Center

to different types and doses of heavy-ion irradiation to understand the heterogeneity or plasticity of cultured tumor cells or non-tumor cells. However, the establishment of a seamless experimental system for time-lapse imaging of living cells before and after a series of irradiations is too challenging due to various physical limitations. Accordingly, we have compromised to use the E5 beamline at the RIKEN RRC for visualizing live cell behavior immediately after heavy-ion irradiation. We proceeded to evaluate the response patterns of cell-cycle populations, their heterogeneity and reproducibility (Fig. 2). Due to the insufficient number of experiments to verify biological differences, we would like to carry our conclusions to the next report. We will conduct further replicated experiments for a comprehensive understanding based on quantitative analysis.

References

1) T. Terasima *et al.*, Nature **190**, 1210 (1961).
2) A. Sakaue-Sawano *et al.*, Cell **132**, 487 (2008).
3) A. Sakaue-Sawano *et al.*, Mol. Cell **68**, 626 (2017).
4) E. Afshinnekoo *et al.*, Cell **183**, 1162 (2020).
5) S. Furukawa *et al.*, Biomed. Res. Int. **2020**, 4703286 (2020).
6) K. Takahashi *et al.*, NPJ Microgravity **7**, 2 (2021).

Effects of heavy-ion beam irradiation on non-model fruit fly, *Drosophila miranda*

M. Ogawa,[*1] K. Tsuneizumi,[*2] T. Abe,[*2] and M. Nozawa[*1,*3]

Irradiation has been a useful tool for making deletion mutants and establishing strains with balancer chromosomes in *Drosophila melanogaster*.[1] These flies have been fundamental resources in the fields of genetics, development, evolutionary biology, and so on. However, irradiation has so far been applied primarily only to this model species of *Drosophila*. If the same resources become available for other *Drosophila* species, researchers working on other fly species can utilize these resources for a variety of studies. For example, *D. miranda* acquired the so-called neo-sex chromosomes by fusing an autosome with the ordinary Y chromosome approximately a million years ago, and it has a high potential for elucidating the early evolutionary phase of sex chromosomes.[2,3] The purpose of this study is, therefore, to examine the effects of heavy-ion beam irradiation on the fertility and the genome of *D. miranda*.

We irradiated the iron (Fe)-ion beam (806 keV/μm; 0.5, 1, or 2 Gy) to the flies with 3–4 days after eclosion. For irradiation, 15-mL tubes were used, in which 3 mL of the medium consisting of 1% agar and 50% grape juice was poured at an angle of 30°. Five males with the irradiation of the Fe-ion beam were then crossed with five virgin females on the same (zeroth) day of the irradiation in a vial containing a normal corn medium (Fig. 1). On the 1st, 4th, and 7th days after irradiation, only the males were transferred to a new vial and crossed with another five virgin females. After 3 days of crossing, all the females were discarded from each vial. All the males were also discarded with females on the 10th day. The number of F_1 flies eclosed in each vial was counted. To consider variations, we prepared four vials (that is, 5 males × 4 vials) for each irradiation condition as replicates. Among the F_1 individuals (Fig. 2), we extracted genomic DNA from each of the five males from the 1–3 days vials derived from the males with irradiation of 2 Gy indicating a lower fertility, and resequenced the genomes using Illumina HiSeq X. Following sequencing, the regions with mapping depth of zero in the F_1 individual but of at least 1 in the wildtype individuals were regarded as the candidate regions of deletions. The same experiments were also conducted for the argon-ion beam (Ar, 189 keV/μm; 1 Gy) and the carbon-ion beam (C, 30 keV/μm; 5 Gy) and the genomes of two F_1 males were sequenced for each ion beam.

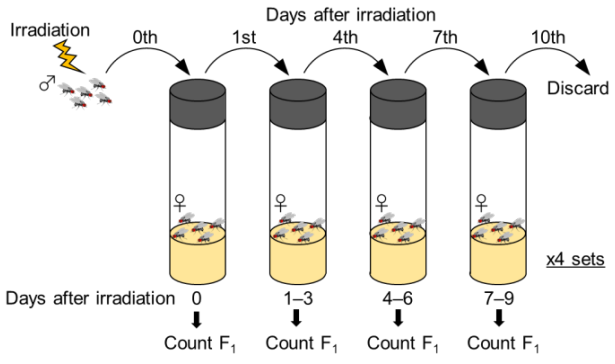

Fig. 1. Crossing experiments following irradiation.

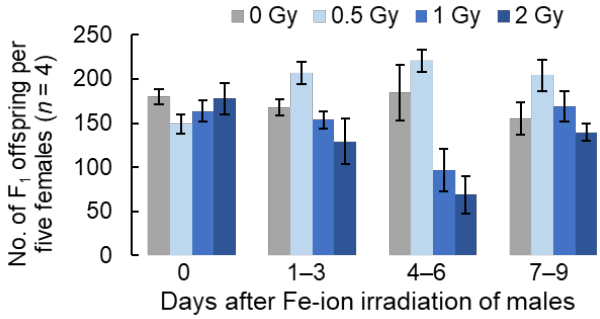

Fig. 2. Transition of male fertility after Fe-ion irradiation.

Using the strategy described, we successfully detected a number of genes containing the candidate regions of deletions on the Y/neo-Y chromosomes (Table 1). However, deletions were also detected on the X/neo-X chromosomes, which was not expected because the X/neo-X chromosomes were inherited only

Table 1. Number of genes in which deletions were detected.

Chr.	Assembly size (Mb)	Average no. of genes* in which deletions were detected		
		Fe, 2 Gy	Ar, 1 Gy	C, 5 Gy
Y/Neo-Y	101.5	6.5	6.5	36.0
X/Neo-X	103.0	7.7	4.0	25.5

* The average number of genes with deletions per individual is shown. Only the genes in which deletions were detected within the exons were counted.

*1 Department of Biological Sciences, Tokyo Metropolitan University
*2 RIKEN Nishina Center
*3 Research Center for Genomics and Bioinformatics, Tokyo Metropolitan University

from the non-irradiated females. We speculate that sequence polymorphism between each F_1 male and reference genomes caused such erroneous identifications. We would like to optimize the conditions for making mutants with large deletions in future studies by repeating the irradiations under various conditions.

This research was supported by the KAKENHI (21H02539), granted to MN.

References

1) R. F. Grell *et al.*, DIS **30**, 71 (1956).
2) D. Bachtrog *et al.*, Nature **416**, 323 (2002).
3) M. Nozawa *et al.*, Nat. Commun. **7**, 13659 (2016).

IV. OPERATION RECORDS

Program Advisory Committee meetings for nuclear physics and for materials and life sciences

H. Ueno *1

There are two Program Advisory Committees (PACs) that are responsible for reviewing submitted proposals in the fields of nuclear physics (NP-PAC) and materials and life science (ML-PAC). The NP-PAC is co-organized by the RIKEN Nishina Center (RNC), the Center for Nuclear Study (CNS), the University of Tokyo, and the Wako Nuclear Science Center (WNSC), Institute of Particle and Nuclear Studies (IPNS), KEK. The NP-PAC reviews experimental programs at RI Beam Factory (RIBF), whereas the ML-PAC reviews those at the Rutherford Appleton Laboratory (RAL) and RIBF.

NP-PAC

The 23rd NP-PAC meeting was held in a hybrid format on December 5–7, 2022 at 9:00–18:30 JST,[1] where 40 proposals were submitted and reviewed. One letter-of-intent was also submitted. For the first time in three years, the committee members and the experiment representatives participated in a face-to-face meeting, although the audience participated online. Proposals were evaluated on the basis of five grades: S, A, B, C, and D. Those with a grade of B or higher were approved, of which those with a rating of S or A will be given priority for beamtime allocation. Table 1 summarizes the outcome of the 23rd NP-PAC meeting.

The members of the 23rd NP-PAC meeting were M. J. G. Borge (Chair, Consejo Superior de Investigaciones Científicas), S. Grevy (Centre dÉtudes Nucléaires de Bordeaux Gradignan), M. Dasgupta (The Australian National Univ.), J. Dilling (Ork Ridge National Laboratory), M. Gorska (GSI Darmstadt), T. Kawabata (Osaka Univ.), M. Matsuo (Niigata Univ.), R. Zegers (Michigan State Univ.), N. Aoi (Osaka Univ.), R. Charity (Washington Univ. in St. Louis), G. Martínez-Pinedo (Technische Univ. Darmstadt / GSI), I. Moore (Univ. Jyväskylä), T. Saito (RIKEN), P. J. Woods (Univ. Edinburgh), A. Vitturi (Univ. Padova), and X. Zhou (Chinese Academy of Sciences).

Table 1. Summary of the outcome of the 23rd NP-PAC meeting. The sum of the proposals ranked with S and A is listed in the "approval" columns.

	23rd NP-PAC (December 5–7, 2022)			
	proposal number		beam time (days)	
	request	approval	request	approval
RILAC (GARIS, ...)	0	0	0	0
AVF (CRIB, ...)	3	1	32.5	11
RRC (KISS, ...)	4	3	41	18
BigRIPS/ZD	25	10	151.85	45
SHARAQ/OEDO	1	1	6	2.5
Rare-RI Ring	1	1	17.5	9
SAMURAI	6	4	63.5	25.5
(BigRIPS-related	33	16	238.85	82)
Total	40	20	312.35	111

ML-PAC

The 23rd ML-PAC meeting was held in January 2023.[2] At this meeting, only proposals for the use of the RIBF were solicited, and not proposals for the use of muon beams at RAL. The one submitted RIBF proposals was reviewed, where the review was conducted through email, in consideration of the number of applications. For experimental proposals using RIBF, the same evaluation grade as for NP-PAC was adopted. The outcome of the meeting is summarized in Table 2.

The members of the 23rd ML-PAC meeting were A. D. Hillier (Chair, RAL-ISIS), T. Adachi (Sophia Univ.), J. Kishine (The Open Univ. Japan), Y. Kobayashi (The Univ. Electro-Communications), Y. Miyazawa (Yamagata Univ.), K. Shimomura (KEK), T. Takayanagi (Saitama Univ.), Z. Qin (CAS-IMP), and I. Yamauchi (Saga Univ.).

Table 2. Summary of the outcome of the 23rd ML-PAC meeting. For the RIBF proposals, the sum of the proposals ranked with S and A is listed in the "approval" columns.

	23rd ML-PAC (January 2023)			
	proposal number		beam time (days)	
	request	approval	request	approval
RAL	*—no call for proposals—*			
RIBF				
AVF	1	1	6	4
Total	1	1	6	4

References

1) http://www.nishina.riken.jp/RIBF/NP-PAC/.
2) http://www.nishina.riken.jp/RIBF/ML-PAC/.

*1 RIKEN Nishina Center

Electric power consumption of RIKEN Nishina Center in 2022

M. Kidera,[*1] T. Maie,[*1] S. Watanabe,[*1] E. Ikezawa,[*1] and O. Kamigaito[*1]

A comparison of the electricity consumption of RIKEN Nishina Center (RNC) for each month in 2022 with those in 2020 and 2021 is presented in Fig. 1. The large increase in power consumption in March 2022 as compared with that in March 2021 may be attributed to the RI Beam Factory (RIBF) experiment started on March 18, 2022, whereas, in 2021, it started in April. The lower power consumption in November 2022 compared to that in November 2021 was caused by a delay in the commencement of the RIBF experiment owing to the failure of the BigRIPS chiller.

In 2022, the total annual power consumption of the RNC was 67,338 MWh, an increase of 6% when compared 2021. This increase could be attributed primarily to the RIBF experiment conducted in the previous period, as mentioned earlier. The total power of the RNC reached a maximum of 16.6 MW in April 16th when the uranium (^{238}U) beam was being tuned for the RIBF experiment.

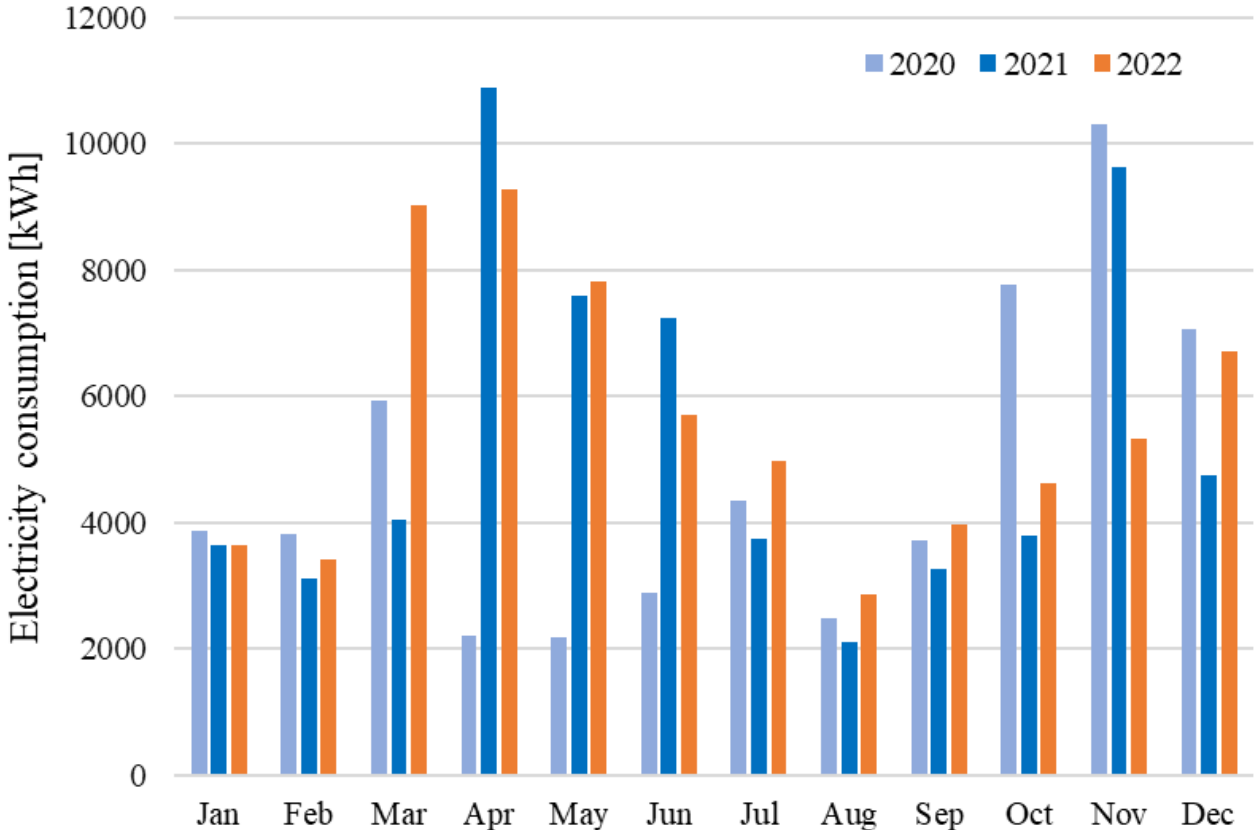

Fig. 1. Electricity consumption at RNC for each month in 2022 when compared with that in 2020 and 2021.

*1 RIKEN Nishina Center

RILAC operation

H. Yamauchi,[*1] M. Fujimaki,[*2] N. Fukunishi,[*2] H. Hasebe,[*2] Y. Higurashi,[*2] E. Ikezawa,[*2] H. Imao,[*2] O. Kamigaito,[*2] K. Kaneko,[*1] M. Kidera,[*2] M. Komiyama,[*2] R. Koyama,[*1] K. Kumagai,[*2] T. Maie,[*2] T. Nagatomo,[*2] T. Nakagawa,[*2] T. Nishi,[*2] T. Ohki,[*1] J. Ohnishi,[*2] H. Okuno,[*2] K. Oyamada,[*1] K. Ozeki,[*2] N. Sakamoto,[*2] K. Suda,[*2] J. Suzuki,[*1] M. Tamura,[*1] A. Uchiyama,[*2] S. Watanabe,[*2] T. Watanabe,[*2] Y. Watanabe,[*2] K. Yamada,[*2] and A. Yusa[*1]

We report on RILAC operations in 2022. Beam service started in January 2021, and is frequently interrupted due to high X-rays from the first and last cryomodules (CM1, CM3) of SRILAC.[1] These X-rays were caused by field emission from the cavities and have been handled by changing the balance of the acceleration voltage. To improve the condition of cavities, we applied pulsed high-power radio-frequency (RF) processing in November and successfully reduced the field emissions. The beam service was restarted in December and continued up to the present. Some statistical data regarding the RILAC operation from January 1st to December 31st, 2022, are provided in Table 1.

Table 1. Statistical data of RILAC operation from January 1st to December 31st, 2022.

Operation time of RILAC	3856.9	h
Mechanical problems	27.0	h
Standalone RILAC	3352.5	h
Injection into RRC	0.0	h
Total beam service time of RILAC	3352.5	h

During the summer maintenance period, we updated the RF control panel for the RILAC injector system, and all the RF systems at RILAC can now be operated remotely. Other maintenance works performed during the reporting period are listed below.

(1) Replacement of TMPs for tank #5, coupler of middle cryomodule of SRILAC (CM2) and RFQ.
(2) Replacement of power supplies for transistor amp. of tank #1, auto gain controller of A1 and A2, and filament of tank #5.
(3) Parallelization of cooling water lines for vacuum pump of tank #5, #6 .
(4) Renewal of chillers for INCAP in tank #1, #2, #5, #6.
(5) Installation of Direct-Current Current Transformer (DCCT) for power supplies of steerer magnets in High Energy Beam Transport line.
(6) Replacement of valves and joints of cooling system for A1, A2 cavities from brass to stainless steel.
(7) Repairment of vacuum leakage in tank #2 and A1 cavity.

We encountered several machine troubles during the reporting beam service period, which are listed as follows.

(1) Repairment of water leakage from the middle stage amp. of tank #6 and end drift tube of A1 cavity.
(2) Malfunction and repairment of the power supply for D2 magnet.
(3) Malfunction and replacement of Auto Phase Control (APC) system of tank #3, power supplies for middle and end stage filament, PLC unit of A2 cavity and wide band amp. of tank #1.
(4) Malfunction and repairment of DC24V control unit and remote switch for APC of tank #4.
(5) Falling the profile monitor at e12 into beam line by the trouble of the cylinder.
(6) Thermo-senser trouble of RFQ.
(7) Vacuum deterioration at G3DP by lack of rotary pump oil.
(8) Trouble and re-calibration of OUTCAP position monitor of tank #6.

All the problems were successfully fixed, and the beam service was recovered instantly. The RF system became more stable owing to the temperature control operation of the second-stage cooling system introduced last year.[2]

*1 SHI Accelerator Service Ltd.
*2 RIKEN Nishina Center

References

1) N. Sakamoto *et al.*, Proc. SRF2019, (paper WETEB1, Dresden, 2019), p. 750.
2) K. Yamada *et al.*, in this report.

Operation report on the RIKEN AVF cyclotron for 2022

K. Yadomi,[*1] K. Ozeki,[*2] J. Ohnishi,[*2] S. Fukuzawa,[*1] M. Hamanaka,[*1] S. Ishikawa,[*1] K. Kobayashi,[*1] R. Koyama,[*1] R. Moteki,[*1] T. Nakamura,[*1] M. Nishida,[*1] M. Nishimura,[*1] J. Shibata,[*1] N. Tsukiori,[*1] T. Adachi,[*2] M. Fujimaki,[*2] N. Fukunishi,[*2] H. Hasebe,[*2] Y. Higurashi,[*2] H. Imao,[*2] O. Kamigaito,[*2] M. Kidera,[*2] M. Komiyama,[*2] K. Kumagai,[*2] T. Maie,[*2] Y. Miyake,[*2] T. Nagatomo,[*2] T. Nakagawa,[*2] T. Nishi,[*2] H. Okuno,[*2] N. Sakamoto,[*2] K. Suda,[*2] A. Uchiyama,[*2] S. Watanabe,[*2] T. Watanabe,[*2] Y. Watanabe,[*2] K. Yamada,[*2] K. Kamakura,[*3] and Y. Kotaka[*3]

The annual report on the operation of the RIKEN AVF cyclotron (hereafter denoted as AVF) for the period January-December 2022 is presented.

AVF delivers beams to the following experimental courses as a stand-alone operation: C01 (machine study; MS), C03 (RI production), E7V (CNS experiments and RI production), E7A (CRIB experiments), and E7B (student experiments and RI production). In addition, AVF is operated as an injector of RIKEN ring cyclotron (RRC).

The yearly changes in operation statistics since 2019, and the beams accelerated using AVF in the period are summarized in Tables 1 and 2. The operation times for stand-alone operation and injection to RRC in the period were 2287 hours and 1574 hours, respectively. The beam service interrupt time caused by trouble of AVF was 0.7 hours. Because the RIBF experiments using light-ion beams were not scheduled, AVF-RRC-SRC experiments were not performed.

Table 1. Comparison of AVF operation statistics with that in the previous years.

AVF stand-alone operation	Year	2019	2020	2021	2022
Tuning of AVF	[h]	1314	744	1149	1212
Trouble of AVF	[h]	0	1	5	0
C01 MS	[h]	0	12	35	32
C03 Exp.	[h]	873	631	672	491
E7V Exp.	[h]	36	18	95	94
E7A Exp.	[h]	790	12	48	302
E7B Exp.	[h]	153	101	96	155
Sub total	[h]	3166	1519	2100	2287
AVF operation as injector of RRC	Year	2019	2020	2021	2022
Tuning of AVF	[h]	118	178	214	273
Trouble of AVF	[h]	0	5	1	1
RRC Exp. & RRC-IRC Exp.	[h]	320	999	834	1300
RRC-SRC Exp.	[h]	0	0	767	0
Sub total	[h]	438	1182	1816	1574
Total	[h]	3604	2702	3916	3860

Development of Xe beam with an energy of approximately 36 MeV/nucleon is now in progress. Although the Xe beam accelerated using RILAC2-RRC mode so far (∼10 MeV/nucleon at the exit of RRC) has already been supplied to the industrial application experiments, we aim to supply Xe beam with higher energy using AVF-RRC mode, which is frequency-variable. Required beam current is small, 20 nA or more. As part of the beam development, the tests of the acceleration harmonics $H = 3$ using $^{84}Kr^{14+}$ at 2 MeV/nucleon and $^{84}Kr^{17+}$ at 2.4 MeV/nucleon, and the extraction of Xe beams from the 18-GHz ECR ion source were performed. Furthermore, the change of operation permission for radiation safety was required to accelerate Xe beam. After those preparations, we successfully extracted 900 nA of $^{136}Xe^{27+}$ at 2.4 MeV/nucleon. However, the beam current of $^{136}Xe^{37+}$ after charge-stripping, which is required to accelerate at the RRC, was too low to extract from the RRC. Therefore, in the next machine study, we plan to use $^{129}Xe^{35+}$ instead of $^{136}Xe^{37+}$ with the same energy because an ion yield after charge-stripping is expected to be nearly an order of magnitude higher.

Table 2. AVF beam list in 2022.

AVF stand-alone operation			
Particle	Energy [MeV/nucleon]		Experimental Course
$^{1}H^{+}$		19	E7V
		30	C03
$^{2}H^{+}$		12	C03, E7B
$^{4}He^{2+}$		6.5	E7B
		7.25	C03, E7B
		12.5	C03
$^{7}Li^{2+}$		6	C03
$^{7}Li^{3+}$		8.3	E7A
	1st beam	10	C03
$^{12}C^{4+}$		7.3	C03
$^{18}O^{6+}$		7	E7V
$^{24}Mg^{8+}$		7.25	E7A
$^{84}Kr^{14+}$	1st beam	2	C01
$^{84}Kr^{17+}$	1st beam	2.4	C01

AVF operation as injector of RRC			
Particle	Energy [MeV/nucleon]		Experimental Course
$^{12}C^{4+}$		7	RRC-RARF
$^{14}N^{4+}$		4	RRC-RARF
$^{20}Ne^{7+}$		7	RRC-RARF
$^{22}Ne^{6+}$		4	RRC-RARF
$^{40}Ar^{11+}$		3.8	RRC-IRC-E5B
		5.2	RRC-RARF
$^{56}Fe^{15+}$		5.01	RRC-RARF
$^{84}Kr^{20+}$		3.97	RRC-RARF
$^{136}Xe^{27+}$	1st beam	2.4	RRC-RARF

To improve equipment, an upgrade of phase probe (AVF-PP) used for isochronous tuning was performed. A channel switch of the AVF-PP malfunctioned possibly due to age deterioration. The channel switch was upgraded to a newer model because we have a policy to replace CIM/DIM system[1)] to N-DIM[2)] as an aging management.

*1 SHI Accelerator Service Ltd.
*2 RIKEN Nishina Center
*3 Center for Nuclear Study, University of Tokyo

References

1) K. Shimizu, Nucl. Instrum. Methods Phys. Res. A **236**, 109 (1985).
2) M. Fujimaki *et al.*, RIKEN Accel. Prog. Rep. **37**, 279 (2004).

Operation report on ring cyclotrons in the RIBF accelerator complex

K. Kobayashi,[*1] K. Suda,[*2] T. Adachi,[*2] T. Dantsuka,[*2] M. Fujimaki,[*2] T. Fujinawa,[*2] N. Fukunishi,[*2] S. Fukuzawa,[*1] M. Hamanaka,[*1] H. Hasebe,[*2] Y. Higurashi,[*2] E. Ikezawa,[*2] H. Imao,[*2] S. Ishikawa,[*1] O. Kamigaito,[*2] Y. Kanai,[*2] M. Kidera,[*2] M. Komiyama,[*2] R. Koyama,[*1] K. Kumagai,[*2] T. Maie,[*2] Y. Miyake,[*2] R. Moteki,[*1] T. Nagatomo,[*2] T. Nakagawa,[*2] M. Nakamura,[*2] T. Nakamura,[*1] M. Nishida,[*1] M. Nishimura,[*1] J. Ohnishi,[*2] H. Okuno,[*2] K. Ozeki,[*2] N. Sakamoto,[*2] J. Shibata,[*1] N. Tsukiori,[*1] A. Uchiyama,[*2] S. Watanabe,[*2] T. Watanabe,[*2] Y. Watanabe,[*2] K. Yadomi,[*1] and K. Yamada[*2]

This paper presents an operation report on ring cyclotrons in the RIBF accelerator complex from January to December 2022. Table 1 summarizes the beams accelerated by these cyclotrons. Availability can be defined as the ratio of the actual beam service time to the scheduled beam service time, which is an index of stable operation of accelerators. When calculating each availability for beam service times completed earlier than scheduled, we regarded scheduled times as actual times. The total actual beam service time was 2403.2 hours. The ratio of the beam service time between the experiments conducted in the old (RARF) and new (RIBF) facilities was 49 : 51. In the RARF, the actual beam service time was 1178.8 hours with an availability of 99.1%.

In the RIBF, three beam services were conducted. The actual beam service time was 1224.4 hours with an availability of 96.3%. The beam services of ^{238}U 345 MeV/nucleon were conducted primarily to compensate the beam supply suspended owing to the issue of BigRIPS in December 2021. No major problem occurred during the experiment. The maximum beam intensity was 82.6 particle nA, and the availability was 97.8%.

In the ^{78}Kr beam supply, we recorded the highest ever beam intensity of 690 particle nA. The power supply of the IRC main coil failed twice because the flow meter malfunctioned. It took three hours for recovery. As the beam tuning time was shorter than the expected time and the beam service for 20 days started earlier than scheduled, the availability was 103.0%.

In the ^{70}Zn beam service conducted in December 2022, severe failures occurred. The fRC-W plate power supply failed to generate 12 kV DC owing to the ground fault of the high-voltage transformer. It took 15 hours to replace the transformer. A beam supply was unstable overnight because a fluctuation in the receiving voltage in the Nishina memorial building affected the RF systems of RRC and fRC. To protect equipments, the beam intensity was reduced to 2/3 of the maximum value using a slit placed after the ion source. However, the beam service was suspended owing to a vacuum leakage in SRC-MDC3 caused by beam loss. The beam service time was only 148.5 hours, and the availability was 77.4%.

The total availability in the RARF and RIBF was 97.6%.

Table 1. Summary of accelerated beams in 2022.

	Beam particle	Energy (MeV/nucleon)	Acceleration mode	Beam course	Beam intensity (particle nA)		Beam service time (h)		Availability (%)
					Requested	Actual	Scheduled	Actual	
RARF	^{12}C	135	AVF-RRC	E5B (Biology)	2	550.0	24.5	12.9	100.0
	^{14}N	70		E3B (RI Production)	100	111.0	6.0	5.9	100.0
	^{20}Ne	135		E5B (Biology)	2	120.0	3.0	1.2	100.0
	^{22}Ne	70		E6 (RIPS)	500	530.0	120.0	119.3	99.4
	^{40}Ar	95		E5A (Industry)	1	85.3	192.0	143.8	100.0
	^{56}Fe	90		E5B (Biology)	2	6.3	12.0	3.7	100.0
	^{84}Kr	70		E3A (Industry)	1	7.4	30.0	30.0	100.0
				E5A (Industry)	1	9.8	336.0	269.9	100.0
	^{136}Xe	35.7		E5A (MS)	1	0.1	0.0	0.0	0.0
	^{4}He	7.25	RILAC2-RRC	E3B (RI Production)	10000	10000.0	24.0	19.0	100.0
	^{51}V	6		E6 (KEK/MRTOF)	5000	3306.0	288.0	284.1	100.0
	^{136}Xe	10.75		E2B (KEK/KISS)	200	240.0	108.0	107.9	99.9
				E3A (JAXA)	100	125.0	36.0	35.0	100.0
				E5A (Industry)	1	100.0	48.0	46.1	100.0
	^{238}U	10.75		E2B (KEK/KISS)	2	314.3	96.0	89.5	93.2
	^{40}Ar	160	AVF-RRC-IRC	E5B (Biology)	2	29.4	28.5	10.7	100.0
						Subtotal	1352.0	1178.8	99.1
RIBF	^{70}Zn	345	RILAC2-RRC-fRC-IRC-SRC	BigRIPS/ZDS/SHARAQ	1000	818.0	192.0	148.5	77.4
	^{78}Kr			BigRIPS/ZDS/SHARAQ	700	690.0	384.0	395.4	103.0
	^{238}U			BigRIPS/ZDS/F12/SLOWRI/SHARAQ	120	82.6	696.0	680.4	97.8
						Subtotal	1272.0	1224.4	96.3
						Total	2624.0	2403.2	97.6

*1 SHI Accelerator Service Ltd.
*2 RIKEN Nishina Center

Present status of liquid-helium supply and recovery system

T. Dantsuka,[*1] H. Okuno,[*1] M. Nakamura,[*1] S. Tsuruma,[*1] M. Takahashi,[*1] M. Ohshima,[*2] H. Shiraki,[*2] H. Hirai,[*2] K. Kimura,[*2] S. Okada,[*2] A. Mikami,[*2] M. Nagano,[*2] H. Shiba,[*2] and H. Hazama[*2]

A liquid-helium supply and recovery system,[1)] which can produce liquid helium at a liquefaction rate of 200 L/h from pure helium gas, has been under stable operation since the beginning of April 2001. However, due to increased operational failures caused by deterioration over time, the liquefier was duplicated in 2017. The new liquefier can produce liquid helium at a liquefaction rate of 220 L/h from pure helium gas. Although the older helium liquefier has been failing since the summer of 2018, the new helium liquefier provides a constant supply of liquid helium. The older helium liquefier was repaired in February 2020.

The volumes of liquid helium supplied each year from 2001 to 2021 are illustrated in Fig. 1. From 2001 to 2013, there was a gradual increase in the supplied volume, with two decrements in 2009 and 2011. In 2014, the supplied volume decreased owing to a system malfunction. However, in 2015, it returned to its original value. In 2016, the supplied volume decreased, whereas it increased slightly in 2017 and significantly in 2018. In 2019, approximately 140,000 L of liquid helium was supplied despite the high price of helium gas. In 2020, a supply volume decrease of approximately 15,000 L was caused by the influence of the new coronavirus.

Moreover, the purity of helium gas recovered from the laboratories has gradually deteriorated. Currently, the impurity concentration in the recovered gas is approximately 1700 ppm, which affects the liquefaction process and makes continuous operation difficult. Therefore, improving the purity of the recovered helium gas is necessary. As one of the causes, the purity of the recovered gas from gas holder E was found to be down to about 95%.

Furthermore, the volume of helium gas recovered from each building in the Wako campus as well as the volume transported to the liquid-helium supply and recovery system were measured. The recovery efficiency was calculated as the ratio of the amount of recovered helium gas to the amount of supplied liquid helium. The recovery efficiency for the buildings on the south side of the Wako campus, *i.e.*, the Cooperation Center building of the Advanced Device Laboratory, Chemistry and Material Physics building, and Nanoscience Joint Laboratory building, increased to approximately 98%.

Reference

1) K. Ikegami *et al.*, RIKEN Accel. Prog. Rep. **34**, 349 (2001).

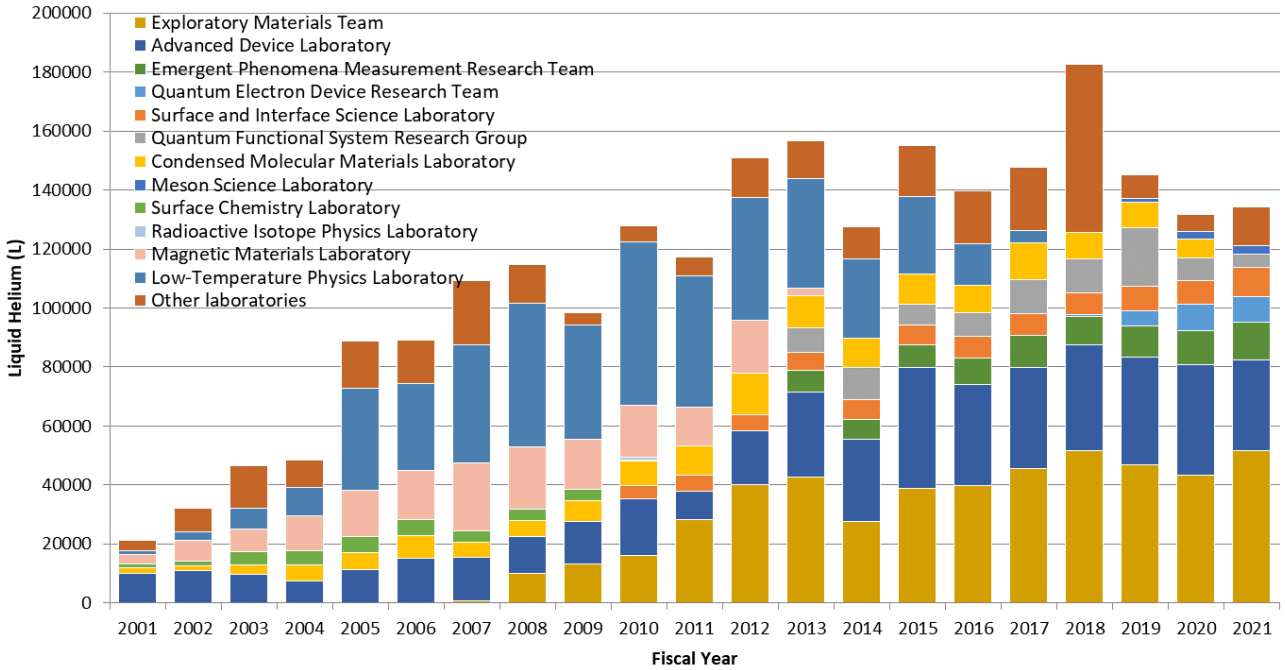

Fig. 1. Volumes of liquid helium supplied to various laboratories for each fiscal year from 2001 to 2021.

*1 RIKEN Nishina Center
*2 Nippon Air Conditioning Service K.K.

Operation of BigRIPS cryogenic plant

K. Kusaka,[*1] M. Ohtake,[*1] K. Yoshida,[*1] M. Ohshima,[*2] A. Mikami,[*2] H. Hazama,[*2] H. Shiraki,[*2] H. Hirai,[*2] K. Kimura,[*2] M. Nagano,[*2] H. Shiba,[*2] and S. Okada[*2]

Following the accident that occurred on December 3, 2021,[1] the main motor of the BigRIPS compressor unit was shipped to the manufacturer's factory and disassembled. Damages were found in the bearing units on both the coupling and anticoupling sides. In particular the bearing unit on the coupling side was heavily damaged such that the ribbon retainer was destroyed and the surfaces of the bearing balls and rings were ruined (Fig. 1). We also found that the size of the housing for the damaged bearing unit was 20 μm larger than its standard dimension (+0 to 25 μm). After cleaning the rotor and stator, the motor unit was reassembled using new bearing units and the re-manufactured bracket housing. In addition to mechanical maintenance, the insulation was also examined, and little deterioration of the stator insulation was noticed. We decided to replace the motor unit in the summer maintenance period.

Fig. 1. Damaged bearing unit, disassembled from the coupling side of the motor unit.

Fig. 2. Compressor unit with the new motor.

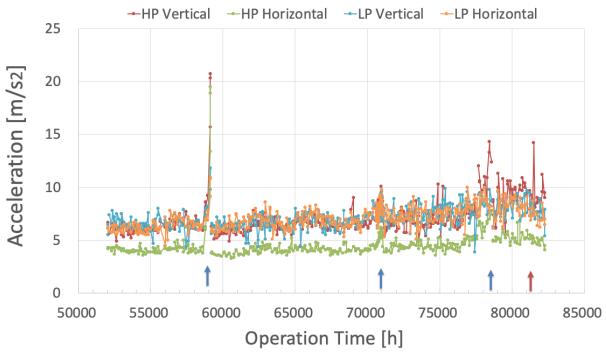

Fig. 3. Vibration acceleration of the compressor unit.

We performed two continuous operations of the BigRIPS cryogenic plant in 2022. The first operation period was from February 22 to June 13 and the second was from November 16 to December 28. Between these dates, we replaced the motor unit with a new one (Fig. 2). Figure 3 depicts the vibration accelerations in the vertical and horizontal directions as functions of the total operation time. Three rapid increases in the vibration acceleration at the operation times of 59,000, 71,000, and 78,541 indicate that the damage in the bearing unit occurred in December 2016, June 2019, and December 2022.[1] The red arrow at the operation time of 81,235 hours indicates the replacement of the motor unit. Although the vibration acceleration does not change significantly, the typical operation current of the motor unit decreased from 30.0 to 26.6 A.

In 2022, another incident occurred: the damage of the first expansion turbine T1 in the refrigerator. We visually inspected T1 and T2 turbines during every summer maintenance. It was found that the blades of the expansion wheel of the T1 turbine were broken (Fig. 4). The T1 cartridge was then sent to its manufacturer, Linde, and disassembled. Linde reports that the fractured surface indicates the typical characteristics of a low-cycle fatigue (LCF). The expan-

*1 RIKEN Nishina Center
*2 Nippon Air Conditioning Services Co., Ltd.

sion and compressor turbine wheels are replaced with new ones and re-assembled with new axial bearings. Before remounting the T1 cartridge on the refrigerator, we investigated the inside of the refrigerator using a fiberscope. No fragments but tiny metal dust was found in the downstream piping of the T1 expansion turbine. After the dust was removed using a vacuum cleaner, the T1 turbine was mounted on the refrigerator. We switched the refrigerator on for pre-cooling on November 16, and the STQ1-5 cryostats were filled with liquid helium on December 3. Although the average liquefaction rate of 26 m^3/h is the same as before, the rotation speed of 4450 rps of the T1 turbine during the steady-state operation was lower than its design value of 4600 rps. The origin of the LFC and the lower rotation speed of the T1 turbine are currently under investigation.

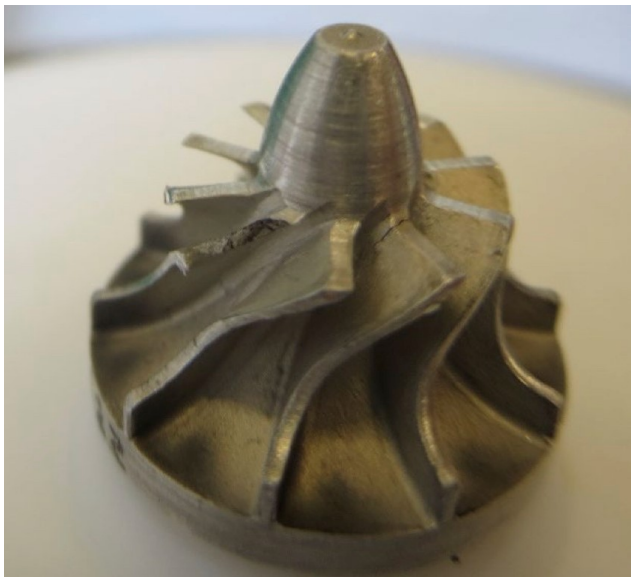

Fig. 4. T1 expansion turbine wheel with broken blades.

Reference

1) K. Kusaka *et al.*, RIKEN Accel. Prog. Rep. **55**, 182 (2022).

Operation of Pelletron tandem accelerator

T. Ikeda,[*1] K. Inayoshi,[*2,*1] and H. Sato[*1]

The Pelletron tandem accelerator (5SDH-2) provides ion beams accelerated by up to 1.7 MV for sample irradiation, material analysis, and developments of detectors used in RIBF. This accelerator is registered as a joint-use equipment (ID: WE0429)[1] at the Wako campus and is managed by the Detector Team of RNC. Fig. 1 shows the configuration of the accelerator, four beam lines, and two ion sources. One ion source is the RF charge-exchange type, referred to as Alphatross and is used to generate He^- ions. The other is the Source of Negative Ions by Cesium Sputtering (SNICS), which can generate almost all other negative ions. Till date, ion species of H, He, B, C, O, and Au have been mainly accelerated in the range of 0.5–1.7 MV. For example, the energies of He^{2+} and $^{12}C^{6+}$ are 5.1 and 11.9 MeV, respectively, upon the application of 1.7 MV.

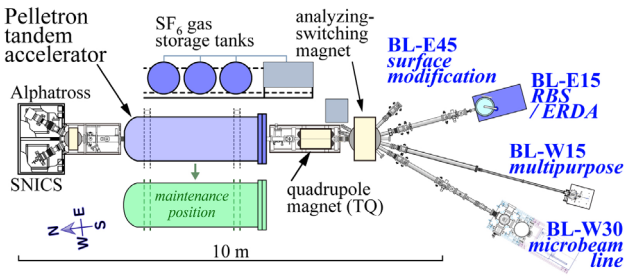

Fig. 1. Pelletron tandem accelerator and beam lines at Nishina R&D Building.

BL-E45 is dedicated to a sub-mm sized beam irradiation for samples in liquid.[2] BL-E15 is used by users in the field of material science to perform Rutherford backscattering (RBS) spectrometry analysis[3,4] and elastic recoil detection analysis (ERDA). The RBS/ERDA apparatus (Charles Evans and Associates Model RBS-400) comprises a goniometer to rotate a sample and particle detectors. Further, the detectors are located at backward and forward positions to measure the energies of backscattered (He^{2+}) ions and recoiled particles from the sample, respectively. The samples and the detectors are inside a vacuum chamber with a vacuum level of the order of 10^{-4} Pa. The intensity of the input He^{2+} beam of 2.28 MeV is greater than 10 nA according to the collimated beam size of 5–10 mm in diameter. On the west side, BL-W15 is employed as a multipurpose line for various equipment. Test systems have been constructed for profile measurements of ion microbeam produced by glass capillary[5] and microbeam irradiation to induce damage in DNA of mammalian cells.[6] The production of γ rays based on proton-induced resonance reactions is available for a cross-section measurement in an international summer school, Nishina School, and for calibration of Ge detectors using high energy γ rays up to 10.8 MeV. Although the 992-keV proton resonance in the reaction of $^{27}Al(p,\gamma)^{28}Si$.[7] BL-W30 was previously used for detector calibration;[8] however, since 2020, it has been dedicated to a new cell irradiation port equipped with a glass capillary microbeam generator[9–11] and an Olympus research microscope. This line has a unique feature to irradiate living cells in liquid medium with a short ion range (<100 μm) and a stopping power (>200 keV/μm), which is sufficiently high to induce double strand breaks of DNA in cell nucleus.

The total machine time (MT) from January 1 to December 31, 2022, was 27 days as presented in Table 1. The MT included a machine study (MS) on acceleration, whereas excluded the conditioning of the ion sources.

Table 1. Beam conditions.

Ion	Energy [MeV]	Beam current [particle nA]	Experiment	Operation time [days]
$^{1}H^{+}$	1.0–3.2	0.05–980	Irradiation	23
$^{4}He^{2+}$	2.28	5–58	RBS	3
$B^{1,2,3+}$	1.0–2.0	7	MS	1

The experiments performed in this facility are listed below, along with the beam lines and number of days of MT. The Nishina School in 2022 was postponed.

(1) Microbeam performance study with H ions using glass capillaries at BL-W15 and -W30 (9 days)
(2) RBS/ERDA experiments at BL-E15 (4 days)
(3) Educational experiment of proton capture by carbon/boron-nucleus for the Nishina School (0 days)
(4) Development of a charged-particle/γ-ray detector to be used for RIBF experiments including MS (14 days)

The fluctuation of the acceleration voltage of the Pelletron improved from 2 to 0.1% following the overhaul from February to March. The achieved stability was the best in the last decade and realized the beam position fluctuation of less than 1 mm (beam size is 10–20 mm) at the samples.

*1 RIKEN Nishina Center
*2 Department of Physics, Toho University

References

1) Research support system, R-COMS (RIKEN ID is necessary), `https://riken.simprent.jp/`
2) T. Kobayashi *et al.*, Surf. Coat. Technol. **331**, 206 (2017).
3) L. Jianjun *et al.*, Chem. Sci. **12**, 10354 (2021).
4) S. R. Lee *et al.*, Phys. Status Solidi A **219**, 23, 2200318 (2022).
5) T. Ikeda *et al.*, Nucl. Instrum. Methods Phys. Res. B **470**, 42 (2020).
6) T. Ikeda *et al.*, RIKEN Accel. Prog. Rep. **53**, 215 (2020).
7) R. Mizuno *et al.*, RIKEN Accel. Prog. Rep. **55**, S20 (2022).
8) F. P. Gustafsson *et al.*, RIKEN Accel. Prog. Rep. **50**, 209 (2017).
9) T. Ikeda, Jpn. Soc. Appl. Phys. Rev. **2022**, 220205 (2022).
10) K. Inayoshi *et al.*, RIKEN Accel. Prog. Rep. **55**, 107 (2022).
11) M. Kurino *et al.*, in this report.

Radiation safety management at RIBF

K. Tanaka,[*1] H. Sakamoto,[*1] R. Hirunuma-Higurashi,[*1] H. Mukai,[*1] A. Akashio,[*1] T. Okayasu,[*1] R. Suzuki,[*2] M. Takekoshi,[*2] T. Sato,[*2] K. Igarashi,[*1] S. Iizuka,[*1] N. Usudate,[*1] Y. Shioda,[*1] and M. Murata[*1]

The results of radiation monitoring at RIBF, conducted at the border of the facility and the radiation-controlled area are reported. The residual doses along the accelerator setups are also presented. In 2022, ^{238}U beam of approximately 345 MeV/nucleon was provided at an intensity of 70 particle nA in April. Then ^{75}Kr beam of about 345 MeV/nucleon of 600 particle nA were used in May and June. Further, ^{70}Zn beam of approximately 345 MeV/nucleon of 400 particle nA were used in December.

The dose rates at the boundary of the radiation-controlled area were monitored. Neutron and γ-ray monitors were used at three locations: roofs of the RRC, IRC, and BigRIPS. Figure 1 shows the annual neutron dose at these positions. As the thickness of the radiation shield at IRC roof was relatively small, the dose rate was high. In 2017, additional local-concrete shield of 1 meter thick was set on a beamline in IRC room. The dose was successfully reduced. In 2022, even the highest annual dose of 4.1 μSv/y at the IRC roof was lower than the legal limit of 5.2 mSv/y. The dose at IRC roof at 2022 is sensitive to IRC and SRC operation time. In 2022, these were operated for only four months. Therefore, the annual dose of IRC roof was small.

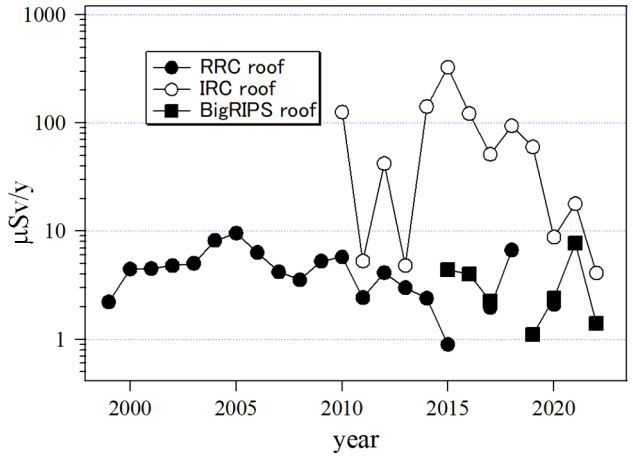

Fig. 1. Radiation dose at the boundary of the radiation-controlled area.

The dose rates at the site boundary with Wako city, where the legal limit is 1 mSv/y, were monitored by neutron and γ-ray monitors. The annual dose in 2022 was 9.0 μSv neutrons after the background correction. The annual dose of the γ-ray was under the background level. Therefore, the radiation dose rate was considerably lower than the legal limit.

The residual radioactivity at the deflectors of the cyclotrons was measured immediately before the maintenance work. The residual dose is dependent on factors such as the beam intensity, accelerator operation time, and cooling time. The data have been obtained at the cyclotrons maintenance works, when the deflectors were able to accessible. Therefore, the cooling times were not constant. The dose rates from 1986 are shown in Fig. 2. The dose rates for FRC, IRC, and SRC are shown for the years after 2006, when the RIBF operation started. For AVF, the dose rate increased in 2006 because the radioisotope production was started, and the beam intensity increased.

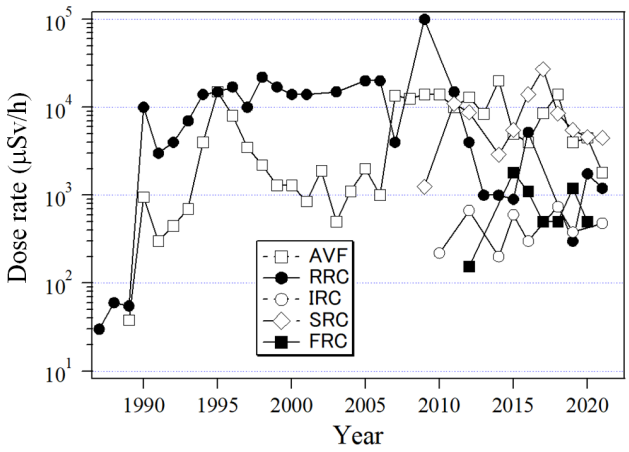

Fig. 2. Dose rates of residual radioactivity at the deflectors of 5 cyclotrons.

The residual radioactivity along the beam lines was measured after almost every experiment. Figure 3 shows the locations of the measurement points where high residual-doses rates greater than 100 μSv/h were observed. Table 1 lists the dose rates, beam conditions, and cooling time at the measurement points. The maximum dose was 28 mSv/h at point 15, which is near the beam dump of BigRIPS.

The radioactivity in the closed cooling system at BigRIPS was measured. The water for the F0 target, exit beam dump, and side-wall dump were sampled in March 2022. The water in the closed cooling systems were partly replaced on October 2021. The results are shown in Table 2. A liquid scintillation counter (LSC-7400, Hitachi Co. Ltd.) was used for the low energy β ray of 18 keV from H-3 nuclide. A Ge detector (GC2019, Canbbera Co. Ltd.) was used for γ rays emitted from other radionuclides. The radionuclides,

*1 RIKEN Nishina Center
*2 Daiwa Atomic Engineering Corporation

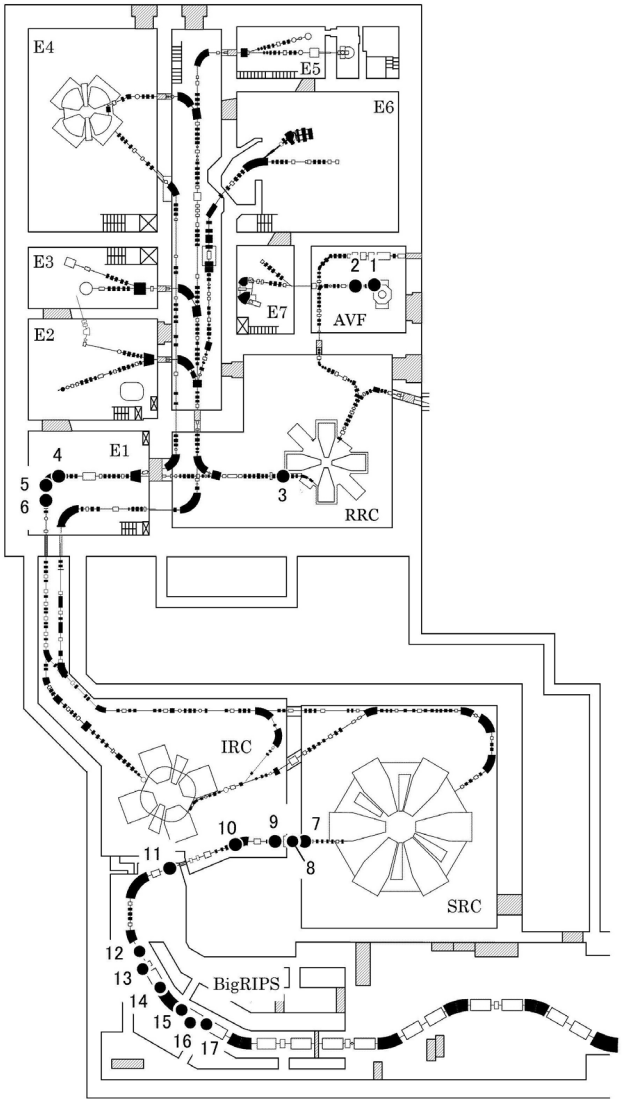

Fig. 3. Layout of the beam lines at RIBF. The measurement locations listed in Table 1 are indicated.

except for H-3, were already filtered by an ion exchange resin set in the closed cooling systems. Although the overall value of contamination was less than the legal limit for drain water, as shown in Table 2, the water from the closed cooling system will be dumped into the drain tank prior to the subsequent operation to prevent contamination in the room in case of a water leakage.

The E-learning module, which can be accessed anytime and from anywhere (even from the outside RIKEN), has been used for the re-training to the radiation workers at RIBF. Approximately 612 radiation workers have completed the training in 2022.

As described above, radiation management to comply with lows and to maintain a radiation level as low as usual has been conducted successfully.

Table 1. Dose rates measured at beam lines in 2021. Points 1–17 indicate the locations where measurements were taken as shown in Fig. 3.

Point	Dose rate (μSv/h	Date (M/D)	Particle	Energy (MeV/u)	Intensity (pnA)	Decay period (h)
1	130	7/27	α	7.3	2500	362
2	260	7/27	α	7.3	2500	362
3	300	7/27	U-238	10.8	300	343
4	2200	6/14	Kr-78	50	940	269
5	1700	6/14	Kr-78	50	940	269
6	130	6/14	Kr-78	50	940	269
7	4400	6/14	Kr-78	345	631	269
8	6900	6/14	Kr-78	345	631	269
9	140	6/14	Kr-78	345	631	269
10	200	6/14	Kr-78	345	631	269
11	100	6/14	Kr-78	345	631	269
12	730	6/14	Kr-78	345	631	269
13	2380	6/14	Kr-78	345	631	269
14	3650	6/14	Kr-78	345	631	269
15	27500	6/14	Kr-78	345	631	269
16	910	6/14	Kr-78	345	631	269
17	470	6/14	Kr-78	345	631	269

Table 2. Concentrations of radionuclide in the cooling water at BigRIPS, allowable legal limits for drain water, and ratios of concentration to the allowable limit.

Cooling water	Nuclide	Concentration[a] (Bq/cm^3)	Limit[b] (Bq/cm^3)	Ratio to limit [a/b]
BigRIPS F0 target	H-3	2.0	60	3.3e-2
			summation	3.3e-2
BigRIPS exit beam dump	H-3	9.3	60	1.6e-1
	Be-7	4.3e-3[1)]	30	1.4e-4
	Mn-54	5.0e-3	1	5.0e-3
	Co-56	8.2e-4	0.3	2.8e-3
	Co-57	7.4e-3	4	1.8e-3
	Co-58	3.9e-3	1	3.9e-2
	Co-60	6.7e-3	0.2	3.4e-2
			summation	0.20
BigRIPS side-wall beam dump	H-3	15.8	60	4.3e-1
	Be-7	3.7e-3	30	1.2e-4
	Co-57	4.4e-4	4	1.1e-4
	Co-60	6.0e-4	0.2	3.0e-3
			summation	0.43

1) read as 4.3×10^{-3}

Variation of impurity gas in recovered helium gas for liquid-helium supply and recovery system

M. Nakamura,[*1] T. Dantsuka,[*1] H. Okuno,[*1] S. Turuma,[*1] M. Ohshima,[*2] H. Hirai,[*2] H. Shiraki,[*2] H. Shiba,[*2] K. Kimura,[*2] S. Okada,[*2] A. Mikami,[*2] H. Hazama,[*2] M. Nagano,[*2] and M. Nakayama[*2]

We use recovered helium gas for the liquid-helium supply system. To measure the purity of the recovered helium gas, we introduce a gas chromatography equipment and monitor the recovered gas. We observed the impurities concentration and the recovered helium gas condition for effective operation.[1)] In this study, we report the changes in the concentration of the impurity gases observed in 2022.

The recovered helium was analyzed by SHIMADZU 2014, except on Saturdays and holidays. The data from January 4 to December 28, 2022, is shown in Fig. 1. The left-side axis shows the concentration of N_2 and O_2, and the right-side axis shows that of H_2, CO_2, and CO. The black, gray, red, blue, and green lines correspond to the N_2, O_2, H_2, CO_2, and CO concentrations, respectively.

The fluctuation N_2 concentration was mostly between 1600 to 1800 and O_2 concentration was between 1200 to 1400, almost co-varying with each other. The N_2 concentration is at the same level as that of O_2 from October to December in 2021. The O_2 concentration seems to be slightly higher than that of N_2 2021. We hypothesize that the presence of N_2 and O_2 is due to air entrainment during the recovery process.[1)] However, the ratio of N_2 and O_2 in our analysis is about 0.7 and not the same as 0.25 of the air. The reason for this discrepancy cannot be explicated.

The fluctuation of H_2 concentration was significant. Typically, H_2 concentration stabilized at between 0.1 to 0.2 ppm. The H_2 concentration suddenly increased to 0.5–1.5 ppm on several occasions. However, such a sudden increase in concentration was limited to a single day, and the liquid-helium supply and recovery system was not damaged. The correlation of H_2 concentration fluctuation with that of N_2 and O_2 is unclear. We presume that H_2 impurity intermixed into the recovered helium gas by a different mechanism for N_2 and O_2.

CO_2 was detected almost daily from July to September. CO_2 concentration suddenly increased to 1.2–10 ppm on several occasions. It seems that CO_2 was detected before and after the sudden increase in H_2 concentration. The reason for this phenomenon cannot be explicated. However, CO_2 can be eliminated immediately from the system because the melting point of CO_2 is much higher than that of N_2 and O_2. Therefore, no problem occurred during the operation because of CO_2.

We cannot estimate the concentration of CO impurity because these gases were observed only a few times in this year.

In 2022, we had no serious troubles in the liquid-helium supply and recovery system operations. Especially, our system was not damaged by impurity gases. However, the concentration of impurity gases continued to exhibit chronic elevation. The concentrations of N_2 and O_2 annually become slightly higher. Dealing with such issues will be a critical topic in the near future. Coping with such problems is an important subject in near future.

Reference

1) M. Nakamura *et al.*, RIKEN Accel. Prog. Rep. **55**, 181 (2022).

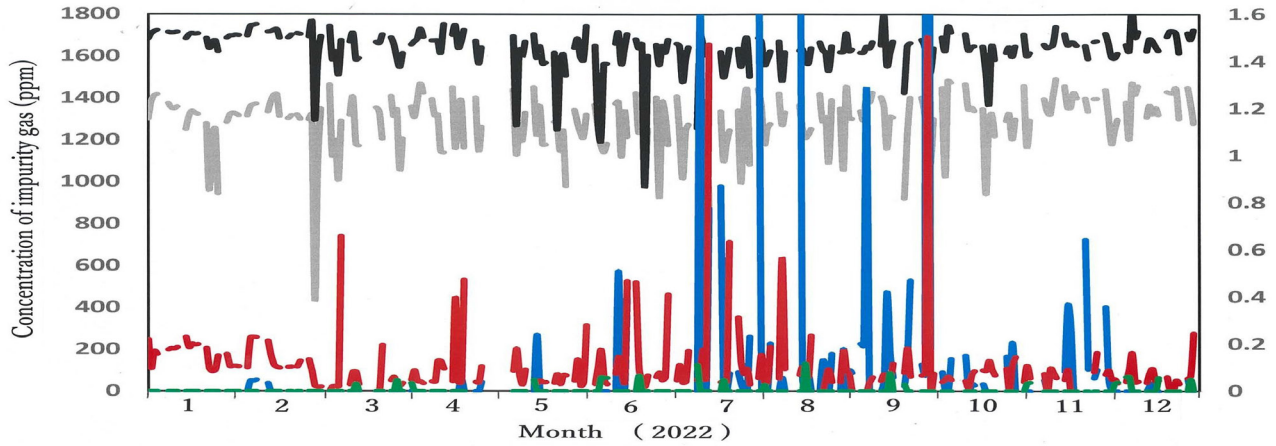

Fig. 1. Impurity concentration in recovered helium gas in 2022.

*1 RIKEN Nishina Center
*2 Nippon Air Conditioning Service KK

Fee-based activities performed by the RI application research group

A. Nambu,[*1] H. Haba,[*1] A. Yoshida,[*1] K. Watanabe,[*1] and T. Kambara[*1]

This article summarizes the fee-based activities performed by the RI Application Research Group in 2022, which include the distribution of radioisotopes (RIs) and utilization of heavy-ion beams in the industry.

Since 2007, RIKEN has distributed RIs to users in Japan for a fee in collaboration with the Japan Radioisotope Association[1] (JRIA). The nuclides include ^{65}Zn ($T_{1/2}$ = 244 d), ^{109}Cd ($T_{1/2}$ = 463 d), ^{88}Y ($T_{1/2}$ = 107 d), ^{85}Sr ($T_{1/2}$ = 65 d), and ^{67}Cu ($T_{1/2}$ = 61.8 h) produced in the RIKEN AVF cyclotron by the Nuclear Chemistry Research Team of the RI Application Research Group.

According to a material transfer agreement (MTA) drawn between JRIA and RIKEN, JRIA mediates the transaction of RIs and distributes them to users. ^{65}Zn and ^{109}Cd are delivered approximately two weeks after the acceptance of an order. ^{85}Sr, ^{88}Y, and ^{67}Cu, which have short half-lives, are not stocked like ^{65}Zn and ^{109}Cd; instead, they are produced in a scheduled beamtime after an order is accepted. Therefore, they are delivered after two or more months. Details regarding RIKEN RIs can be found on the online ordering system, J-RAM,[2] of JRIA. In 2022, we delivered 5, 1, 5, and 1 shipments of ^{65}Zn, ^{109}Cd, ^{85}Sr, and ^{67}Cu with a total activity of 17.7, 5, 11.7, and 10 MBq, respectively; there was no shipment of ^{88}Y. The ^{67}Cu delivery was the second since the beginning of its distribution in 2018. The final recipients of RIs included six universities, one research institute, and two private companies. Figure 1 shows the yearly trends in the number of orders and amount of distributed RIs. Compared with 2021, the amounts of distributed ^{109}Cd and ^{67}Cu increased, and those of ^{65}Zn, ^{88}Y, and ^{85}Sr decreased. The amount of ^{85}Sr distributed in 2022 was still the second highest since the beginning of its distribution. The number of orders for ^{65}Zn in 2022 increased again and reached its highest in the last eight years.

In addition, we also provide ^{211}At ($T_{1/2}$ = 7.2 h) through an MTA drawn between Osaka University and RIKEN, and among University of Tokyo, Saitama Medical University, and RIKEN. ^{211}At is delivered to the universities directly from RIKEN due to its short half-life. In 2022, we delivered a total of 5.4 GBq of ^{211}At to Osaka University in 11 shipments, and 250 MBq to University of Tokyo in 5 shipments.

The Industrial Application Research Team of the RI Application Research Group promotes the utilization of heavy-ion beams in the industry. The RIKEN Nishina Center allows the use of the AVF cyclotron, RILAC2, and RIKEN Ring Cyclotron (RRC) by private companies in Japan for a fee.[3] Currently, the main users include semiconductor companies that irradiate space-use semiconductor devices with ^{40}Ar, ^{84}Kr, or ^{136}Xe ions from the RRC to simulate single-event effects due to the heavy-ion components of cosmic radiation.

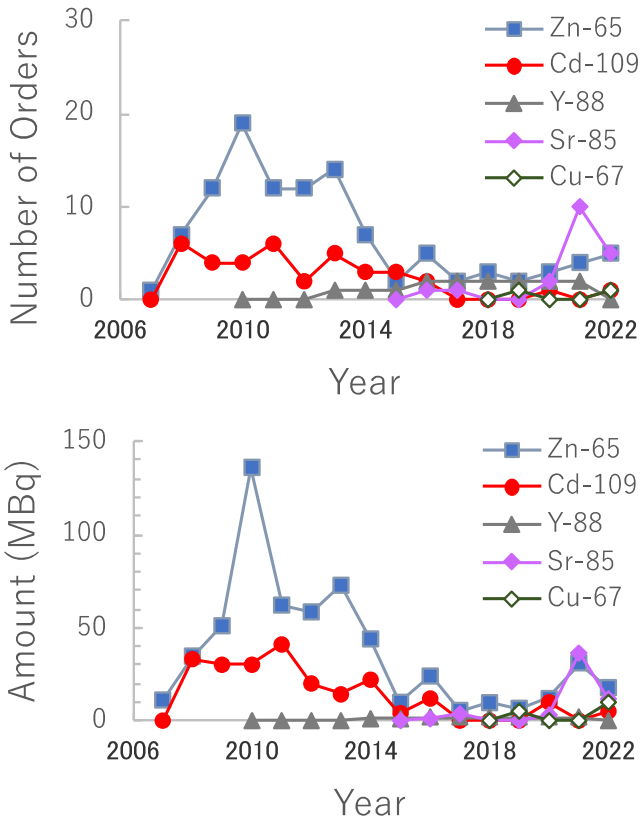

Fig. 1. Number of orders (upper) and amount (lower) of RIs distributed annually from 2007 to 2022. The distribution of ^{88}Y, ^{85}Sr, and ^{67}Cu started in 2010, 2015, and 2018, respectively.

The proposals for beam utilization are reviewed by a program advisory committee dedicated to industrial use (In-PAC).

In January 2022, In-PAC reviewed and approved two proposals via e-mail. In July, In-PAC held its 19th meeting, where it reviewed and approved seven proposals, including four new proposals.

In 2022, seven companies executed 25 fee-based beamtimes, 14 of which used a ^{84}Kr beam with a total beamtime of 234 hours, 9 utilized an ^{40}Ar beam with a total beamtime of 129 hours, and 2 utilized a ^{136}Xe beam with a total beam time of 20 hours.

References

1) http://www.jrias.or.jp/ (Japanese), http://www.jrias.or.jp/e/ (English).
2) https://j-ram.org/ (Japanese).
3) http://ribf.riken.jp/sisetu-kyoyo/HIbeam/ (Japanese).

*1 RIKEN Nishina Center

V. EVENTS

Research strategy with open-closed data utilization in nuclear physics experiments

H. Baba*1

A workshop on Research strategy with open-closed data utilization in nuclear physics experiments[1] was held on March 7th, 2022 at Integrated Innovation Building of RIKEN Kobe campus in a hybrid format with both on-site and remote participation. This workshop was supported by RIKEN's internal fund dedicated to data utilization promotion support.

Open science and open data schemes are currently being attempted worldwide. RIKEN has also been promoting open science especially in the fields of life and medical science.[2] For example, in accelerator based sciences, some particle physics experimental data are opened at CERN.[3] Even in open science approaches, it is recommended that open-closed data be strategically selected, rather than all data being open. For example, regarding satellite data for astronomy, for which open access is common, the spokesperson is often given a period of several years of occupied use. This workshop was held to discuss "What kind of demands and effects can be expected by open data of nuclear physics experiments at RIBF?."

There were 19 participants from RIKEN Nishina Center, RIKEN Information R&D and Strategy Headquarters, Japan Atomic Energy Agency, Hokkaido University, Konan University, Kyoto University, Kyushu University, Research Center for Nuclear Physics, Osaka University, University of Miyazaki, University of Tsukuba, Tohoku University, Tokyo City University, and Yokohama National University. 9 regular talks and 8 short talks were presented:

- Background and purpose of this workshop
- RIKEN's open science initiatives for maximizing research results
- Activities on nuclear data
- Past nuclear data research activities and latest initiatives
- Suggestions from the nuclear engineering community regarding RIBF data
- Suggestions from theoretical studies regarding RIBF data
- Research and education at the University of Miyazaki
- Research and education at Tokyo City University
- Current status and future of research and education at Konan University
- Comments from Nishina Center Promotion Office (short talk)
- Comments from Tohoku University (short talk)
- Comments from Kyoto University (short talk)
- Comments from Research Center for Nuclear Physics, Osaka University (short talk)
- Comments from RIKEN Slow RI Data Team (short talk)
- Comments from RIKEN Radioactive Isotope Physics Laboratory (short talk)
- Comments from experimentalist of RIBF User Executive Committee (short talk)
- Comments from theorist of RIBF User Executive Committee (short talk).

As a result of active discussion, several initiatives were proposed.

1) A detailed database of experiments conducted at RIBF: make a table of nuclei, energies, targets, measured quantities of approved experiments at RIBF to understand what kind of experiments are planned.

2) RIBF experiments assuming data sharing : try to share not only data but also analysis methods to accumulate knowledge and experience as a software library.

3) Registration to nuclear data: not all RIBF experimental results will be registered, especially those of master's thesis. We will continue to discuss methods of registration.

We are continuing our discussions on how to realize open-closed data in the nuclear field, starting from this workshop.

References

1) https://indico2.riken.jp/event/4016/.
2) https://metadb.riken.jp/osp/.
3) https://opendata.cern.ch/.

*1 RIKEN Nishina Center

RIKEN open day 2022

T. Ikeda,[*1] Y. Watanabe,[*1] N. Miyauchi,[*1] Y. Hayashi,[*1] and T. Abe[*1]

RIKEN open day, on which its research activities are showcased to the public, was held in the RIKEN Wako campus on Saturday, April 23, 2022 in a hybrid style. Employing an advance reservation system, it was the first attempt to invite visitors to the campus under the spread of COVID-19. The number of the visitors was limited to 300 for each morning and afternoon slot. The number of applications was 766 and 795, respectively, for the two slots and those of the visitors on site was 208 and 198, respectively. All visitors were supposed to spend their time in the Administrative Headquarters (AH) bldg. in the campus, except when taking group tours to a few selected research centers.

The contents of the activities from Nishina Center were (1) group tours for Cyclopedia and RIBF (Fig. 1), (2) exhibition of a large photo panel of the Superconducting Ring Cyclotron (SRC) at the AH bldg. as well as a poster presentation (Fig. 2), and (3) an online laboratory tour with a navigator to the Nishina accelerators using RIBF-VR360 (Fig. 3(a)).[1)] Online movies made before 2022 were also available. These contents included collaborations with the Center for Nuclear Study (CNS) at University of Tokyo and the Wako Nuclear Science Center (WNSC), IPNS, KEK. A tin-badge event was held at the AH bldg., in which visitors could make badges by themselves. The badges related to the Nishina Center, as shown in Fig. 3(b), were well-received by the participants. The details of the various activities are in Figs. 1 and 2.

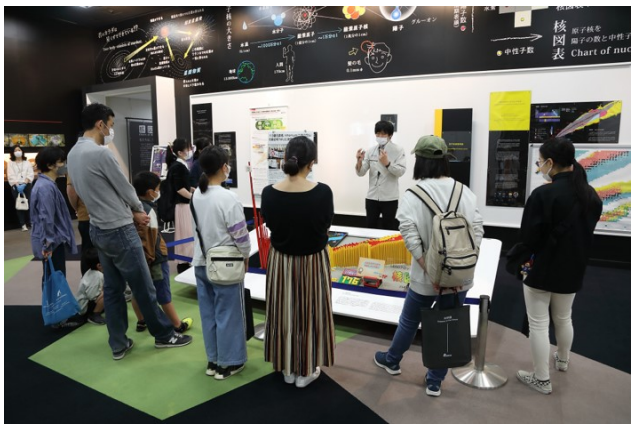

Fig. 1. Group tour to the Nishina Center RIBF bldg., including an explanation session at Cyclopedia followed by visits to SRC and BigRIPS.

For COVID-19 infection control, the group tours to the Nishina RIBF bldg. were designed carefully. The tours titled "*Everything you want to know about state-of-the-art accelerator is right here!*" were held twice in the morning and also twice in the afternoon. The tour attendance was limited to 12 visitors, who were escorted by RIKEN staff members between the AH bldg. and the RIBF bldg., so that each group tour finished within an hour. The participants were welcomed at Cyclopedia for an explanation by the Nishina staff instructors, and then enjoyed the views of SRC and BigRIPS from the MB2 floor with guidance by the other instructors. At the end of the tour, they got RIBF souvenirs and left with the RIKEN staff members.

In the AH bldg., a booth with the title "*A huge ac-*

*1 RIKEN Nishina Center

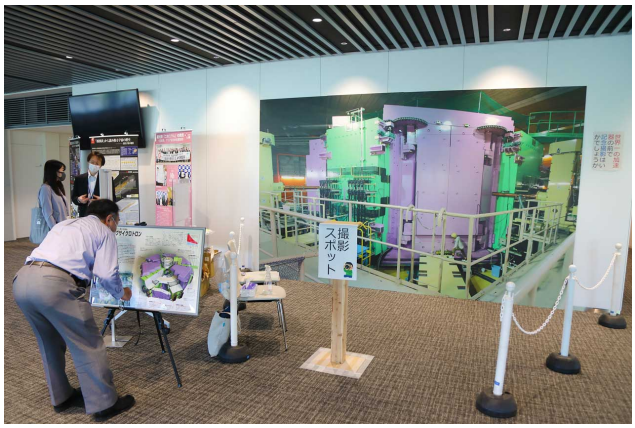

Fig. 2. A large photo panel of SRC displayed as a photogenic place at the Administrative Headquarters bldg.

Fig. 3. (a-1) Online tour using RIBF-VR360 with a navigator for interactive communication. (a-2) the title page (b) three badges marked with yellow circles were designed by Nishina Center. The flowering plant in (i) is the "Nishina Otome" cherry blossom produced in this center. The symbol "Nh" in (ii) and (iii) stands for the element Nihonium, that was synthesized in the center for the first time in the world.

celerator facility where elements are freely created like magic" was opened, where a 2.5-m high photo panel of SRC (Fig. 2), large enough for visitors to take photos as if they were at the SRC site, was on display. Nearby, several posters introducing the entire Nishina Center were displayed, where two Nishina staff members were assigned to provide explanation.

The online laboratory tour titled "*RI Beam Factory: A reclining dragon-like huge underground accelerator complex*" using the RIBF-VR360 was carried out through a zoom meeting system, where ion sources, RILAC, RRC, fRC, IRC, and SRC were introduced by a navigator (Fig. 3(a-1)). The virtual tour achieved 111 net views, which was the highest number among the four virtual tours, including the other centers.

The RIKEN open day 2023 is scheduled on October 14, 2023, which is the first trial of the autumn season.

Reference

1) RIBF-VR360 (in Japanese): `https://vr.riken.jp/ribf/` .

Physics of RI: Recent progress and perspectives

M. Kimura[*1] and T. Uesaka[*1] for the Physics of RI Organizing Committee

Introduction: The "Physics of RI: Recent Progress and Perspectives" conference[1)] was held from May 30 to June 1, 2022 at RIKEN RIBF, co-organized by RIKEN Nishina Center and Yukawa Institute for Theoretical Physics (YITP).

The conference adopted a hybrid format, combining in-person and Zoom participation, with approximately 40 in-person attendees, including 3 international participants, and approximately 50 online participants. The conference was held in coordination with the YITP's long-term workshop "Mean-field and Cluster Dynamics in Nuclear Systems (MCD2022)," which focuses on the theoretical aspects of mean-field and cluster dynamics. The purpose of "Physics of RI" conference was to complement this with experimental aspects, presenting the latest experimental results obtained at the experimental facilities regarding unstable nuclei such as RIBF, along with related theoretical research, and discussing future research directions.

The conference focused on several main topics, including:

(1) Comprehensive reports from experimental facilities including RIKEN RIBF
(2) Fundamental properties of unstable nuclei, such as mass, lifetime, radius, and moment
(3) Disappearance of magic numbers, shell evolution, and related gamma-ray spectroscopy experiments
(4) Phenomena in the vicinity of drip lines and beyond, such as tetra-neutrons
(5) Experimental and theoretical studies on cluster formation in nuclei
(6) Experimental and theoretical studies on nuclear matter properties and EOS
(7) Applications of nuclear technology, such as nuclear conversion
(8) Advances in Ab-initio nuclear structure calculations

The conference resulted in several significant outcomes:

- The conference provided an opportunity for active in-person discussions, which had been limited due to the COVID-19 pandemic, fostering exchange between experimental and theoretical researchers.
- The conference provided a clear outlook on recent progress and future research directions, which holds great importance for future experimental and theoretical research at RIKEN.
- Young researchers were given opportunities for oral presentations, promoting their participation and contribution to the field.

In conclusion, the "Physics of RI: Recent Progress and Perspectives" conference was a successful event that brought together researchers in the field of nuclear physics. The conference provided a platform for comprehensive discussions on various topics related to unstable nuclei, including experimental results, theoretical research, and future research directions. The exchange of ideas and discussions among researchers from different backgrounds facilitated the advancements in the field and promoted collaborations between experimental and theoretical researchers.

The organizers express their gratitude to RIKEN Nishina Center and its staff for their support in hosting the conference.

Reference

1) https://indico2.riken.jp/event/4120/.

*1 RIKEN Nishina Center

Predictions for sPHENIX

M. E. Connors,[*1] Y. M.-Tani,[*2,*3] G. Nukazuka,[*2] D. V. Perepelitsa,[*4] and A. Sickles[*5]

To complete the RHIC mission, sPHENIX was specifically designed to measure jet and heavy-flavor observables with an exceptional level of precision not previously achievable at RHIC. This will enhance our understanding of the quark-gluon plasma (QGP) properties and their temperature dependence beyond what is possible with existing and planned data obtained from the LHC and other RHIC experiments.

A major goal of the sPHENIX program is to address questions regarding the approach to thermalization of the quark-gluon plasma and its transport properties using hard probes, such as jets and heavy-flavor particles. The current three-year run plan includes Au + Au, p + Au, and $p + p$ collisions at 200 GeV.[1)] The Au + Au dataset provides a large QGP system to study the QGP properties. The p + Au dataset will allow for additional studies regarding the intriguing behavior other RHIC experiments observed in flow measurements, as well as transport properties of cold QCD matter and proton/nuclear structure. The $p + p$ collisions provide a necessary reference for Au + Au and p + Au collisions and allow for additional studies of proton structure. The upgraded sPHENIX data acquisition system will enable data collection at a high rate to achieve the statistical precision needed for measurements with rare probes. Anticipated measurements include, but are not limited to, jet substructure observables, photon and heavy-flavor tagged jets and comparisons of the production mechanisms of the different upsilon states in all three collision systems.

To maximize the rich physics sPHENIX is capable of accessing, a workshop was hosted July 20–22, 2022 at Brookhaven National Lab (BNL). The goal of the workshop was to enhance the discussions between the experimentalists extracting the measurements and the theorists whose models will be tested and constrained by the new data. Because sPHENIX will start collecting data in Spring of 2023, this workshop was timely for theorists wishing to make final predictions regarding the anticipated observables before data collection commences. In addition, it provided an opportunity for theorists and experimentalists to propose and discuss new observables.

The workshop was very successful and attracted 106 registered participants. The format of the workshop was hybrid with slightly less than half of the participants attending in person at BNL and the others joining remotely via Zoom. The full agenda is available on Indico at `https://indico.bnl.gov/event/15482/` . The 30 talks included both experimentalists and theorists, resulting in productive discussions. The experimental talks covered current results obtained from experiments at RHIC and LHC, as well as the capabilities and planned measurements for sPHENIX. The theory talks represented various theoretical approaches and topics. An important outcome of this workshop was the decision to write a paper collecting the latest theoretical predictions from the presenters. The goal is to submit the paper for publication before sPHENIX starts collecting its first physics data. This collection of theoretical predictions for sPHENIX will be an extremely useful resource and particularly helpful for citing the theories in future sPHENIX publications.

*1 Department of Physics and Astronomy, Georgia State University
*2 RIKEN BNL Research Center
*3 Brookhaven National Laboratory
*4 Department of Physics, University of Colorado Boulder
*5 Department of Physics, University of Illinois Urbana Champaign

Reference

1) sPHENIX Beam Use Proposal 2022, sPH-TRG-2022-001, `https://indico.bnl.gov/event/15148/attachments/40846/68568/sPHENIX_Beam_Use_Proposal_2022.pdf` .

International workshop on "Hadron physics with Kaon beam and related topics"

F. Sakuma*1 for the Workshop Organizer

The international workshop on "Hadron Physics with Kaon Beam and Related Topics" was held online on October 3–4, 2022. It was organized by RIKEN Nishina Center and Grant-In-Aid for Specially Promoted Research "Toward revolutionary Nuclear Study via revealing Internal Structure of Kaonic Nuclei" (MEXT Kakenhi 22H04917), and supported by Hadron Hall User Association (HUA), KEK Theory Center, RCNP, ELPH, and JAEA ASRC.

The workshop focused on the recent experimental and theoretical developments in kaon interactions with nucleons and nuclei, particularly those activities using the unique kaon beams available at J-PARC and DAΦNE. The topics covered by the workshop were:

- kaonic nuclei
- Γ(1405)
- kaonic atoms
- kaon-nucleon scattering

The workshop was held fully online using Zoom, which included 82 participants from 10 countries, with 27 participants from abroad. The scientific program comprises plenary sessions held by invited speakers. The structure of the sessions was set to be accessible to Asian and European participants. Sessions on both days ran from 16:00 to approximately 23:00 Japan time, with lunch (dinner) breaks as reported in Table 1. A screenshot of participants is shown in Fig. 1.

Table 1. Timetable of the workshop.

Oct. 3	JST		
	16:00	17:30	opening & theoretical overview
	17:30	17:45	*break*
	17:45	19:15	konic-nuclei
	19:15	20:15	*dinner/lunch break*
	20:15	21:45	konic-nuclei
	21:45	22:00	*break*
	22:00	23:00	Λ(1405)
Oct. 4	**JST**		
	16:00	17:30	lattice QCD & Λ(1405)
	17:30	17:45	*break*
	17:45	19:15	Λ1405 & kaonic-atoms
	19:15	20:15	*dinner/lunch break*
	20:15	21:45	kaonic-atoms
	21:45	22:00	*break*
	22:00	23:40	$K^{bar}N$ scatt & closing

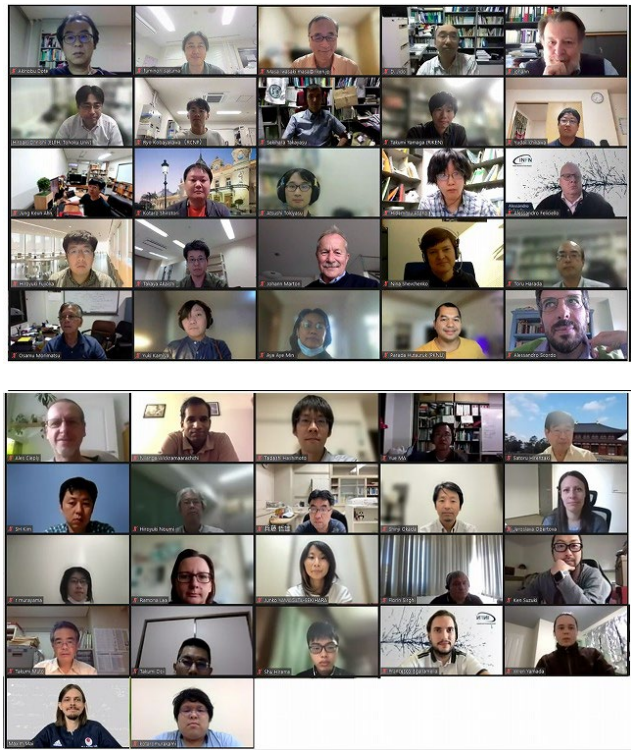

Fig. 1. Screenshot of online participants.

There were 24 talks, including opening and closing remarks. The session began with the theoretical overviews of low-energy kaon physics, which is an important probe to understand low-energy QCD. Following that, the latest results and future experimental prospects at J-PARC, DAΦNE, SPring-8, and LHC, as well as the latest theoretical developments, were presented. There, discussions were given on the recent major topics of kaonic nuclei and atoms, Γ(1405), and $K^{bar}N$ scattering, including the latest topics on lattice QCD calculations. The full program and presentation files are available online at the workshop website.[1)]

Following the success of the workshops, we are planning to conduct a second workshop around FY2024-25 to continuously discuss physics at the J-PARC and related facilities.

Reference

1) `https://kds.kek.jp/event/43204/` (Access key required) .

*1 RIKEN Nishina Center

The 10th users' meeting on mutation breeding in RIBF "Sustainable society and creation of specialty products realized by ion-beam breeding"

T. Abe,[*1] Y. Hayashi,[*1] Y. Watanabe,[*1] N. Fukunishi,[*1] K. Ishii,[*1,*2] K. Tsuneizumi,[*1] Y. Shirakawa,[*1] S. Ohbu,[*1] and N. Asakawa[*1]

The users' meeting on mutation breeding in RIBF has been held the RIKEN Symposium every two years since 2003. Moreover, we have published the RIKEN Symposium abstracts and user reports. The 10th symposium was initially scheduled to be held in January 2022; however due to the Covid-19 pandemic, it was postponed until January 19–20, 2023. The RIKEN Symposium was held in a hybrid manner with 32 on-site and 50 online participants. Online participation from remote locations was effective. The participants' research fields were categorized by biology (development of fundamental technologies and gene isolation) and breeding as targets (microorganisms, trees, food crops and flowering plants). In the 10th meeting, there were no tree-breeding researchers, and the number of microalgae researchers increased. The proportion of other specialities remained relatively the same from recent trends (Fig. 1).[1)]

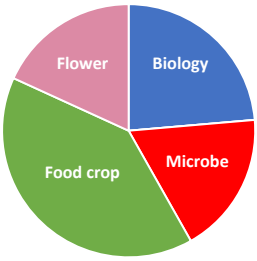

Fig. 1. The specializations of symposium participants in 2022.

The meeting featured ten presentations and two invited lectures on three research topics: developing breeding techniques, identification of novel genes using mutants and analysis of gene function, and breeding new varieties. The invited talks were on biorefinery using microalgae and upgrade concept of the RIBF accelerators. In addition, a tour of the accelerator facility was conducted before the meeting.

(1) Development of breeding technology

It is clear that mutations at 30 keV/μm, which have a high mutation rate in *Arabidopsis thaliana*, are often base substitutions or small deletions of a few bp. Whereas those at 290 keV/μm, which have a high lethal effect, are often large deletions of 100 bp or more and chromosome rearrange- ments. Similar results were observed with rice.[2)] Furthermore,we investigated genomic mutations of carbon and argon ions at 100–300 keV/μm to identify the LETs that increase the rate of large deletions and chromosomal rearrangements in *Arabidopsis*.

Fig. 2. Photograph of on-site participants.

(2) Identification of novel genes using mutants and analysis of gene function

A sex-determining gene located on the Y chromosome in a dioecious plant, *Silene latifolia*, was determined.[3)] Other discovered genes can be used for seed size increase in *Arabidopsis*,[4)] heat-stress marker in rice[5)] and breeding in wheat.

(3) Breeding new varieties

New varieties applied for variety registration in 2018–2022 were three cherry blossoms and one hibiscus by the farmers, two *Chrysanthemum* that blooms in all three colors during the Bon Festival by the Nagasaki Prefecture, and a Satsuma mandarin that can be harvested one month late and suitable for long-term storage by the Shizuoka Prefecture.

Users could deepen their understanding of accelerator facilities and accelerator science through invited lectures and a tour of the accelerator. In the other special lecture, useful mutants, such as those yielding high oil production, have been obtained even in microalgae. It was confirmed that to realize a sustainable world, we will continuously contribute to solving problems of energy, environment and food, and create local speciality products by ion-beam breeding. The next meeting is scheduled to be held in January 2025.

*1 RIKEN Nishina Center
*2 National Institute of Radiological Sciences, National Institutes for Quantum Science and Technology

References
1) T. Abe *et al.*, RIEKN Accel. Prog. Rep. **53**, 231 (2020).
2) R. Morita *et al.*, Cytologia **86**, 303 (2021).
3) Y. Kazama *et al.*, Mol. Biol. Evol. **39**, msac195 (2022).
4) V. Q. Nhat *et al.*, Plants **10**, 1252 (2021).
5) R. Tabassum *et al.*, Plant Prod. Sci. **24**, 230 (2021).

VI. ORGANIZATION AND ACTIVITIES OF RIKEN NISHINA CENTER

(Activities, Members, Publications & Presentations)

1. Organization

1.1 Organization Chart as of March 31, 2023 (End of FY2022)

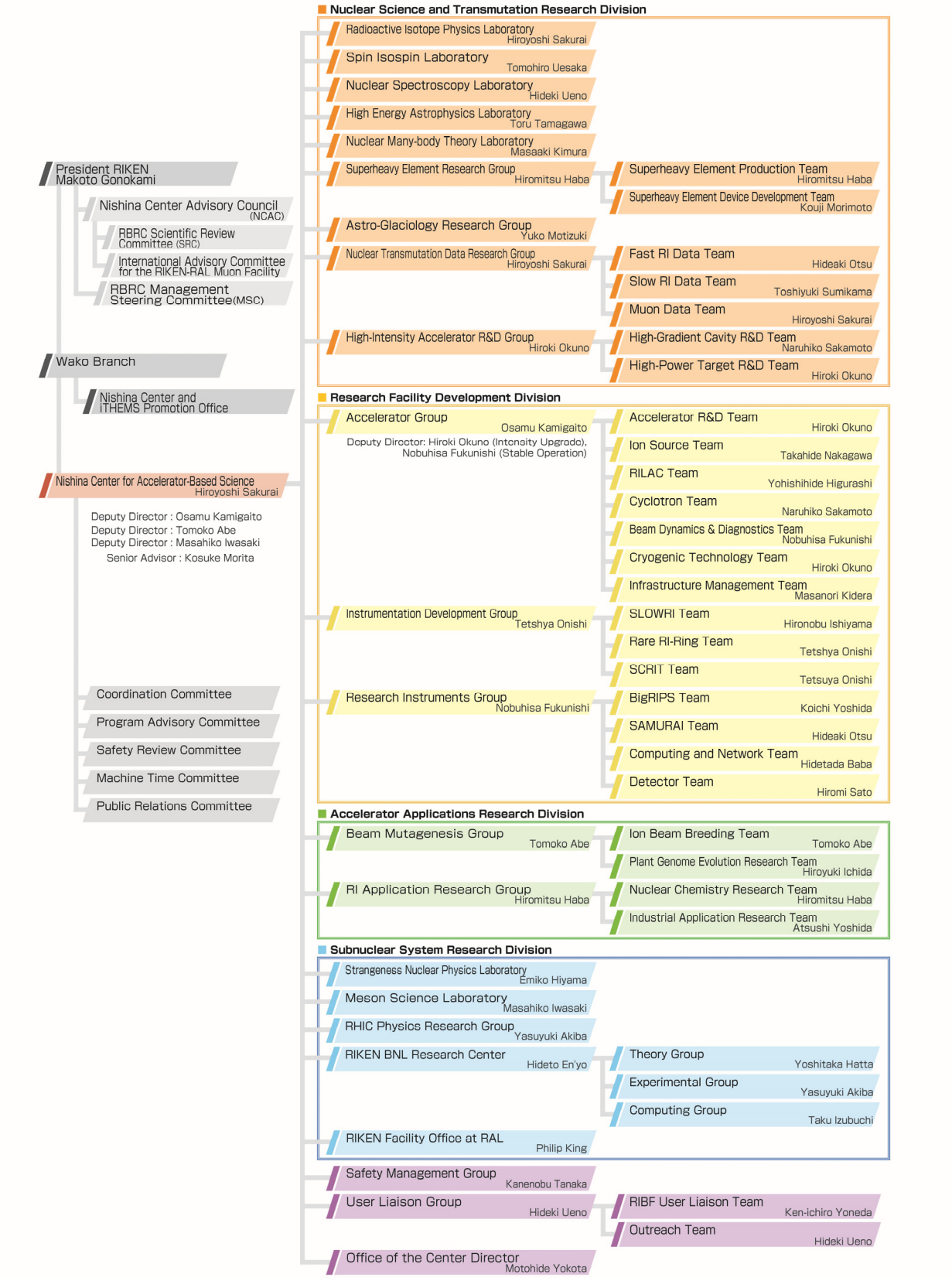

1.2 Topics in FY2022

Year	Date	Topics in Management
2022	Apr. 1	Newly appointed: Director of RHIC Physics Research Group: Yasuyuki AKIBA
2022	Oct. 1	Newly appointed: Team Leader of RILAC Team: Yoshihide HIGURASHI
2022	Oct. 1	Newly appointed: Director of Instrumentation Development Group, Team Leader of Rare RI-Ring Team and SCRIT Team: Tetsuya OHNISHI

2. Finances

A transition of the RNC budget for the past four years is shown in following graph.

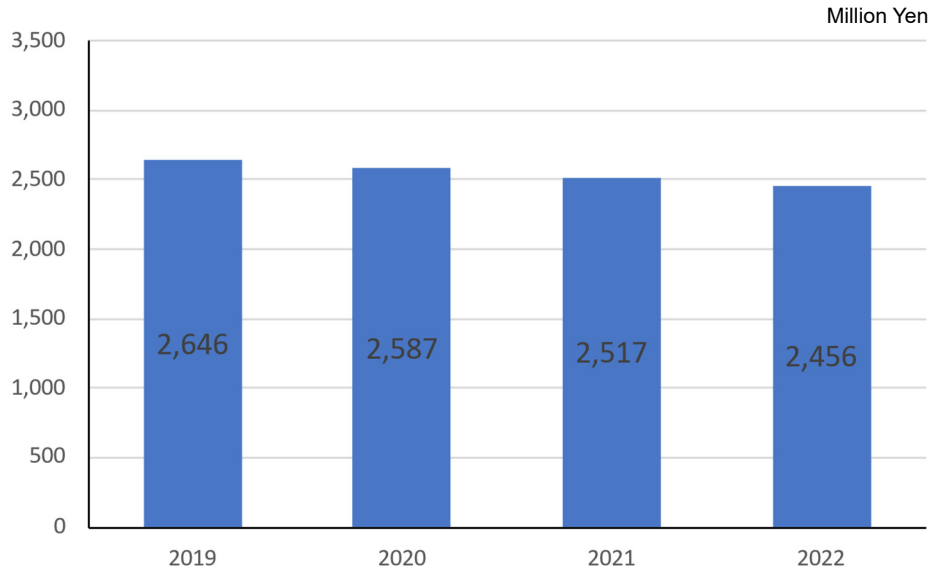

3. Staffing

At the start of FY2022, there were 127 personnel affiliated with RNC and 386 researchers visiting RNC for research purpose. The following graphs show a breakdown of personnel into six categories as of April 1, 2022, and a transition of the number of each category.

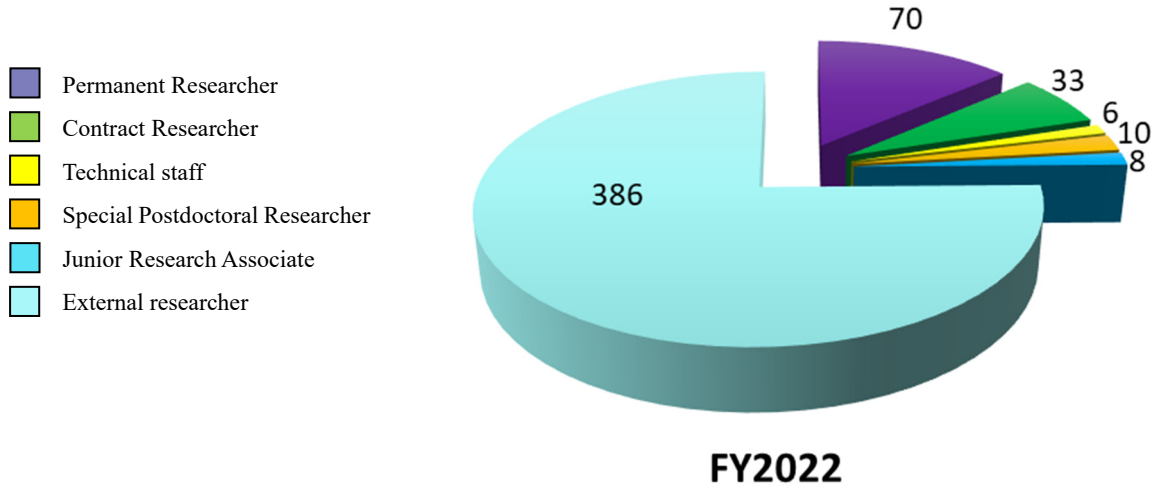

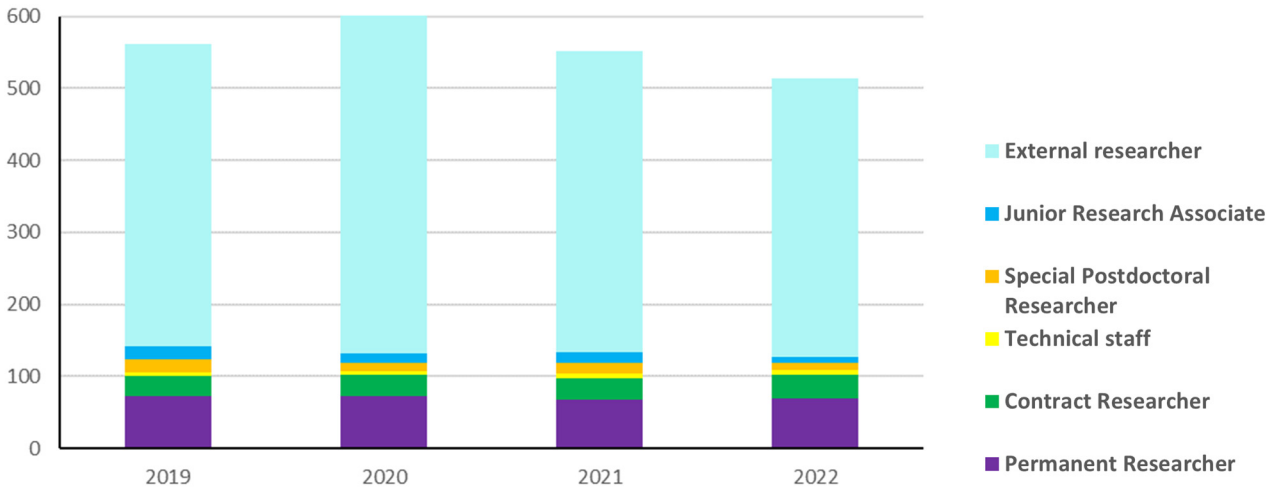

4. Research publication

The number of papers published annually from RNC is shown graphically using the data obtained from Clarivate Analytics' Web of Science Documents.

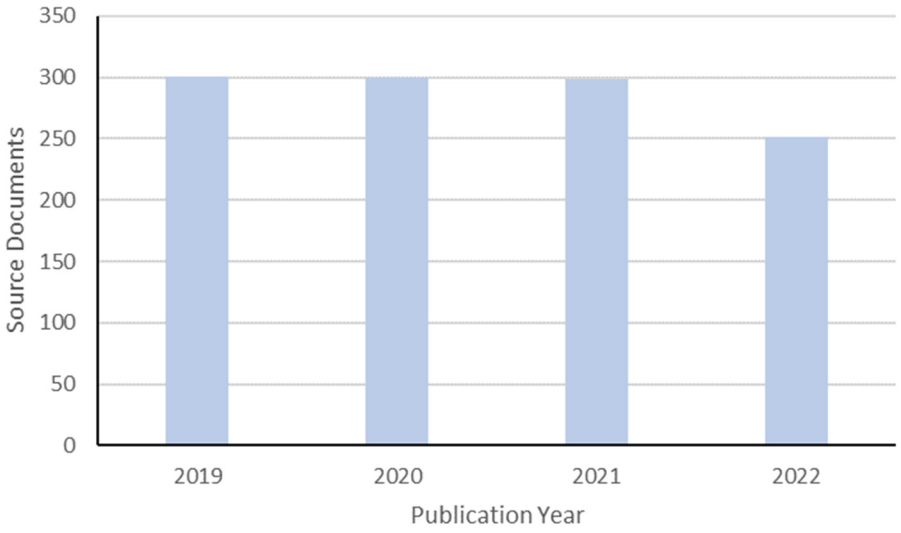

Citation analysis for the past four years

As of April 2023

Indicators \ Year	2019	2020	2021	2022
Total number of papers	301	300	298	251
Percentage of papers in top 1%	1.00	1.33	3.4	0.8
Percentage of papers in top 10%	9.63	12.67	14.1	9.6

5. Management

Headed by the RNC Director Hiroyoshi SAKURAI, the RIKEN Nishina Center for Accelerator-Based Science (RNC) consists of:

- 7 Laboratories
- 12 Groups with 27 Teams
- 2 overseas research centers with 3 Groups

as of the end of FY2022. There are also two 'Partner Institutes' which conduct research in the laboratories set up in RNC. RNC is managed by its Director who takes into consideration the majority decision of the RNC Coordination Committee. The management of RNC is supported by the following committees:

- Coordination Committee
- Program Advisory Committee
- Safety Review Committee
- RIBF Machine Time Committee
- Public Relations Committee

There are also committees to support the President of RIKEN and/or the Director of RNC such as:

- Nishina Center Advisory Council with three subcommittees:
  - ・RBRC Scientific Review Committee (SRC)
  - ・International Advisory Committee for the RIKEN-RAL Muon Facility
  - ・RBRC Management Steering Committee (MSC)

Nishina Center for Accelerator-based Science

Executive Members (as of March 31, 2023)

Hiroyoshi SAKURAI	Director
Osamu KAMIGAITO	Deputy Director (Research Facility Development Division)
Tomoko ABE	Deputy Director (Accelerator Applications Research Division)
Masahiro IWASAKI	Deputy Director (Subnuclear System Research Division)
Kosue MORITA	Senior Advisor

RNC Coordination Committee

The following subjects relevant to the RNC management are deliberated under the chairmanship of the RNC Director:

- Establishment of the new organization or reorganization in RNC
- Personnel management of RNC researchers
- Research themes and research budget
- Approval of the Partner Institutes
- Evaluation of the management of RNC and the response to the recommendations by external evaluation

The RNC Coordination Committee is held monthly.

Members (as of March 31, 2023)

Hiroyoshi SAKURAI	Director, RNC; Director, Radioactive Isotope Physics Laboratory and Nuclear Transmutation Data Research Group; Team Leader, Muon Date Team
Osamu KAMIGAITO	Deputy Director, RNC; Director, Accelerator Group
Tomoko ABE	Deputy Director, RNC; Director, Beam Mutagenesis Group; Team Leader, Ion Beam Breeding Team
Masahiko IWASAKI	Deputy Director, RNC; Director, Meson Science Laboratory
Tomohiro UESAKA	Director, Spin Isospin Laboratory
Hideki UENO	Director, Nuclear Spectroscopy Laboratory and User Liaison Group; Team Leader, Outreach Team
Toru TAMAGAWA	Director, High Energy Astrophysics Laboratory
Emiko HIYAMA	Director, Strangeness Nuclear Physics Laboratory
Masaaki KIMURA	Director, Nuclear Many-body Theory Laboratory
Yuko MOTIZUKI	Director, Astro-Glaciology Research Group
Kosuke MORITA	Senior Advisor, RNC
Hiroki OKUNO	Deputy Group Director, Accelerator Group; Director, High-Intensity Accelerator R&D Group; Team Leader, Accelerator R&D Team, Cryogenic Technology Team, and High-Power Target R&D Team
Nobuhisa FUKUNISHI	Deputy Group Director, Accelerator Group; Director, Research Instruments Group; Team Leader, Beam Dynamics & Diagnostics Team
Tetsuya ONISHI	Director, Instrumentation Development Group; Team Leader, Rare RI-Ring Team and SCRIT Team
Hiromitsu HABA	Director, Superheavy Element Research Group, RI Application Research Group; Team Leader, Nuclear Chemistry Research Team and Superheavy Element Production Team

Kanenobu TANAKA	Director, Safety Management Group
Hideaki OTSU	Team Leader, SAMURAI Team and Fast RI Data Team
Naruhiko SAKAMOTO	Team Leader, Cyclotron Team and High-Gradient Cavity R&D Team
Hiromi SATO	Team Leader, Detector Team
Toshiyuki SUMIKAMA	Team Leader, Slow RI Data Team
Takahide NAKAGAWA	Team Leader, Ion Source Team
Koji MORIMOTO	Team Leader, Superheavy Element Device Development Team
Atsushi YOSHIDA	Team Leader, Industrial Application Research Team
Koichi YOSHIDA	Team Leader, BigRIPS Team
Ken-ichiro YONEDA	Team Leader, RIBF User Liaison Team
Hironobu ISHIYAMA	Team Leader, SLOWRI Team
Hidetada BABA	Team Leader, Computing and Network Team
Hiroyuki Ichida	Team Leader, Plant Genome Evolution Research Team
Masanori Kidera	Team Leader, Infrastructure Management Team
Yoshihide HIGURASHI	Team Leader, RILAC Team
Hideto EN'YO	Director, RIKEN BNL Research Center
Yoshitaka HATTA	Group Leader, Theory Group, RIKEN BNL Research Center
Yasuyuki AKIBA	Director, RHIC Physics Research Group; Group Leader, Experimental Group, RIKEN BNL Research Center
Taku IZUBUCHI	Group Leader, Computing Group, RIKEN BNL Research Center
Motohide YOKOTA	Office of the Center Director
Toshinari ANZO	Director, Nishina Center and iTHEMS Promotion Office

Program Advisory Committee

The Program Advisory Committee reviews experimental proposals submitted by researchers and reports the approval/disapproval of the proposals to the RNC Director. The Committee also reports to the RNC Director the available days of operation at RIBF or the Muon Facility at RAL allocated to researchers. The Committee is divided into three categories according to the research field.

- Nuclear Physics Experiments at RIBF (NP-PAC): academic research in nuclear physics
- Materials and Life Science Researches at RNC (ML-PAC): academic research in materials science and life science
- Industrial Program Advisory Committee (In-PAC): non-academic research

Program Advisory Committee for Nuclear Physics Experiments at RI Beam Factory (NP-PAC)

The 23rd NP-PAC was held on December 5−7, 2022 at RIBF

Members (as of March 31, 2023)

Maria J.G. BORGE (Chair)	Consejo Superior de Investigaciones Científicas
Stéphane Grevy	Centre d'Etudes Nucléaires de Bordeaux Gradignan
Mahananda Dasgupta	The Australian National University
Jens Dilling	Ork Ridge National Laboratory
Magdalena Gorska	GSI Darmstadt
Takahiro Kawabata	Osaka University
Masayuki Matsuo	Niigata University
Remco Zegers	Michigan State University
Nori AOI	RCNP, Osaka University
Robert CHARITY	Washington University in St. Louis
Gabriel MARTINEZ-PINEDO	Technische Universität Darmstadt, GSI Helmholtzzentrum für Schwerionenforschung
Iain MOORE	University of Jyväskylä
Takehiko SAITO	RIKEN
Philip J. WOODS	University of Edinburgh
Andrea VITTURI	Universita' di Padova
Xiaohong ZHOU	Chinese Academy of Sciences

Program Advisory Committee for Materials and Life Science Researches at RIKEN Nishina Center (ML-PAC)

The 22nd ML-PAC was held on August 22−25, 2022 via e-mail and Web meeting.
The 23rd ML-PAC was held between December 23, 2022 and January 10, 2023 via e-mail.

Members (as of March 31, 2023)

Adrian HILLIER (Chair)	ISIS, RAL (UK)
Zhi QIN	Chinese Academy of Sciences
Toshiyuki TAKAYANAGI	Saitama University
Yoshio KOBAYASHI	The University of Electro-Communications
Yutaka MIYAZAWA	Yamagata University
Tadashi ADACHI	Sophia University
Ichihiro YAMAUCHI	Saga University
Koichiro SHIMOMURA	KEK
Jun-ichiro KISHINE	The Open University of Japan

Industrial Program Advisory Committee (In-PAC)

The 19th In-PAC was held on July 22, 2022 via Web meeting.
The 20th In-PAC was held between December 12, 2022 and January 6, 2023 via e-mail.

Safety Review Committee

The Safety Review Committee is composed of two sub committees, the Safety Review Committee for Accelerator Experiments and the Hot-Lab Safety Review Committee. These Committees review the safety regarding the usage of radiation generating equipment based on the proposal submitted to the RNC Director from the spokesperson of the approved experiment.

Safety Review Committee for Accelerator Experiments

Members (as of March 31, 2023)

Hiromi SATO (Chair)	Team Leader, Detector Team
Kouji MORIMOTO	Team Leader, Superheavy Element Device Development Team
Takashi NAGATOMO	Senior Technical Scientist, Ion Source Team
Hiromitsu HABA	Team Leader, Nuclear Chemistry Research Team
Atsushi YOSHIDA	Team Leader, Industrial Application Research Team
Koichi YOSHIDA	Team Leader, BigRIPS Team
Naoki FUKUDA	Technical Scientist, BigRIPS Team
Naruhiko SAKAMOTO	Team Leader, Cyclotron Team
Daisuke SUZUKI	Research Scientist, Radioactive Isotope Physics Laboratory
Masaki SASANO	Senior Research Scientist, Spin Isospin Laboratory
Shunji NISHIMURA	Senior Research Scientist, Radioactive Isotope Physics Laboratory

External members

Shinichiro MICHIMASA	Assistant Professor, Center for Nuclear Study, University of Tokyo
Hidetoshi YAMAGUCHI	Lecturer, Center for Nuclear Study, University of Tokyo
Yutaka WATANABE	Associate Professor, High Energy Accelerator Research Organization, KEK

Ex officio members

Kanenobu TANAKA	Director, Safety Management Group
Hisao SAKAMOTO	Technical Scientist, Safety Management Group

Hot-Lab Safety Review Committee

Members (as of March 31, 2023)

Tetsuya OHNISHI (Chair)	Director, Instrumentation Development Group
Kanenobu TANAKA	Director, Safety Management Group
Hisao SAKAMOTO	Technical Scientist, Safety Management Group
Hiroki MUKAI	Technical Staff I, Safety Management Group
Rieko HIGURASHI	Technical Scientist, Safety Management Group
Hiromitsu HABA	Team Leader, Nuclear Chemistry Research Team

RIBF Machine Time Committee

Upon request of the RNC Director, the RIBF Machine Time Committee deliberates on the machine time schedule of RIBF and reports the results to the Director.

Members (as of March 31, 2023)

Hideki UENO (Chair)	Director, User Liaison Group and Nuclear Spectroscopy Laboratory
Osamu KAMIGAITO	Director, Accelerator Group
Tetsuya ONISHI	Director, Instrumentation Development Group
Tomohiro UESAKA	Director, Spin Isospin Laboratory
Nobuhisa FUKUNISHI	Director, Research Instruments Group and Deputy Group Director, Accelerator Group
Hiroki OKUNO	Deputy Group Director, Accelerator Group
Shunji NISHIMURA	Senior Research Scientist, Radioactive Isotope Physics Laboratory
Tomoko ABE	Director, Beam Mutagenesis Group
Hiromitsu HABA	Director, RI Application Research Group
Kanenobu TANAKA	Director, Safety Management Group
Ken-ichiro YONEDA	Team Leader, RIBF User Liaison Team
Kouji MORIMOTO	Team Leader, Superheavy Element Device Development Team
Koichi YOSHIDA	Team Leader, BigRIPS Team

External members

Kentaro YAKO	Associate Professor, Center for Nuclear Study, University of Tokyo
Hidetoshi YAMAGUCHI	Lecturer, Center for Nuclear Study, University of Tokyo
Yutaka WATANABE	Associate Professor, High Energy Accelerator Research Organization, KEK

Observers

Hiroyoshi SAKURAI	Director, RNC; Director, Radioactive Isotope Physics Laboratory and Nuclear Transmutation Data Research Group; Team Leader, Muon Date Team
Yasuhiro SAKEMI	Director, Center for Nuclear Study, University of Tokyo
Michiharu WADA	Director, KEK Wako Nuclear Science Center
Hiroari MIYATAKE	Professor, High Energy Accelerator Research Organization, KEK
Daisuke SUZUKI	Chair, The RIBF Users Executive Committee (RIBF-UEC); Research Scientist, Radioactive Isotope Physics Laboratory
Tohru MOTOBAYASHI	Senior Advisor, RNC
Hideyuki SAKAI	Senior Advisor, RNC
Hideaki OTSU	Team Leader, Fast RI Date Team and SAMURAI Team
Atsushi YOSHIDA	Team Leader, Industrial Application Research Team
Hironobu ISHIYAMA	Team Leader, SLOWRI Team
Toshinari ANZO	Director, Nishina Center and iTHEMS Promotion Office
Soh OSUKA	Manager, Nishina Center and iTHEMS Promotion Office

Public Relations Committee

Upon request of the RNC Director, the Public Relations Committee deliberates and coordinates the following matters:

- Creating public relations system for RNC
- Prioritization of the public relations activities for RNC
- Other general and important matters concerning the public relations of RNC

Members (as of March 31, 2023)

Toshinari ANZO (Chair)	Director, Nishina Center and iTHEMS Promotion Office
Osamu KAMIGAITO	Deputy Director, RNC; Director, Accelerator Group
Tomoko ABE	Deputy Director, RNC; Director, Beam Mutagenesis Group
Masahiko IWASAKI	Deputy Director, RNC; Director, Meson Science Laboratory
Tomohiro UESAKA	Director, Spin Isospin Laboratory
Hideki UENO	Director, Nuclear Spectroscopy Laboratory and User Liaison Group
Yuko MOTIZUKI	Director, Astro-Glaciology Research Group
Narumasa MIYAUCHI	Technical Staff I, Outreach Team
Yasushi WATANABE	Special Temporary Research Scientist, Outreach Team
Motohide YOKOTA	Director, Office of the Center Director

RBRC Management Steering Committee (MSC)

RBRC MSC is set up according to the Memorandum of Understanding between RIKEN and BNL concerning the collaboration on the Spin Physics Program at the Relativistic Heavy Ion Collider (RHIC). The 28th MSC was held on May 26, 2021.

Members (as of March 31, 2023)

Shigeo KOYASU	Executive Director, RIKEN
Hiroyoshi SAKURAI	Director, RNC
Shoji NAGAMIYA	Senior Visiting Scientist, RNC
Robert TRIBBLE	Deputy Director for Science and Technology, BNL
Dmitori DENISOV	Deputy Associate Laboratory Director for High Energy Physics, BNL
Haiyan GAO	Associate Laboratory Director for Nuclear and Particle Physics, BNL

6. International Collaboration (as of March 31, 2023)

Country	Partner Institute	Objects	RNC contact person
China	China Nuclear Physics Society	Creation of the council for China -Japan research collaboration on nuclear physics	Hiroyoshi SAKURAI, Director, Radioactive Isotope Physics Laboratory
	Peking University	Nuclear Science	Hiroyoshi SAKURAI, Director, Radioactive Isotope Physics Laboratory
	Institute of Modern Physics, Chinese Academy of Science	Physics of heavy ions	Hiroyoshi SAKURAI, Director, Radioactive Isotope Physics Laboratory
	Department of Physics, Faculty of Science, The University of Hong Kong	Experimental and educational research collaboration in experimental nuclear physics	Hiroyoshi SAKURAI, Director, Radioactive Isotope Physics Laboratory
	School of physics, Nankai University	Framework	Emiko HIYAMA, Director, Strangeness Nuclear Physics Laboratory
	School of Physical Sciences, USTC	Framework	Masahiko IWASAKI, Director, Meson Science Laboratory
Finland	University of Jyvaskyla	Basic nuclear physics and related instrumentation	Hironobu ISHIYAMA, Team Leader, SLOWRI Team
France	National Institute of Nuclear Physics and Particle Physics (IN2P3)	Physics of heavy ions	Tomohiro UESAKA, Director, Spin Isospin Laboratory
	Normandy University	Framework	Tomohiro UESAKA, Director, Spin Isospin Laboratory
	Commissariat à l'énergie atomique et aux énergies alternatives (CEA, French Alternative Energies and Atomic Energy Commission)・Direction des Sciences de la Matière” (DSM)		Tomohiro UESAKA, Director, Spin Isospin Laboratory
	The Institut National de Physique Nucléaire et de Physique des Particules CNRS (CNRS/IN2P3)	Experiments with NEBULA-Plus array	Tomohiro UESAKA, Director, Spin Isospin Laboratory
Germany	GSI	Physics of heavy ions and accelerator	Hiroyoshi SAKURAI, Director, Radioactive Isotope Physics Laboratory
	Department of Physics, Technische Universität Darmstadt	Framework	Emiko HIYAMA, Director, Strangeness Nuclear Physics Laboratory
Hungary	The Institute of Nuclear Research of the Hungarian Academy of Sciences (ATOMKI)	Nuclear physics, Atomic Physics	Tomohiro UESAKA, Director, Spin Isospin Laboratory
Indonesia	ITB, UNPAD, ITS, UGM, UI	Material science using muons at the RIKEN-RAL muon facility	Masahiko IWASAKI, Director, Meson Science Laboratory
	Hasanuddin University	Agricultural science and related fields involving heavy-ion beam mutagenesis using Indonesian crops	Tomoko ABE, Director, Beam Mutagenesis Group
	Institut Teknologi Bandung	Framework	Hideki UENO, Director, Nuclear Spectroscopy Laboratory
	Universitas Padjadjaran	Framework	Hideki UENO, Director, Nuclear Spectroscopy Laboratory
Italy	National Agency for New Technologies, Energy and the Environment (ENEA)	Framework	Hiroyoshi SAKURAI, Director, Radioactive Isotope Physics Laboratory
	European Center for Theoretical Studies in Nuclear Physics and Related Areas (ECT*)	Theoretical physics	Masaaki KIMURA Director, Nuclear Many-body Theory Laboratory

Country	Partner Institute	Objects	RNC contact person
Italy	Istituto Nazionale di Fisica Nucleare (INFN)	Physics of heavy ions	Hiroyoshi SAKURAI, Director, Radioactive Isotope Physics Laboratory
Korea	College of Natural Science, Seoul National University	Nishina School	Hiroyoshi SAKURAI, Director, Radioactive Isotope Physics Laboratory
	College of Natural Science, Ewha Women's University	Framework	Tomohiro UESAKA, Director, Spin Isospin Laboratory
	College of Natural Sciences, INHA University	Framework	Emiko HIYAMA, Director, Strangeness Nuclear Physics Laboratory
Malaysia	Universiti Sains Malaysia	Muon Science	Masahiko IWASAKI, Director, Meson Science Laboratory
Norway	Faculty of Mathematics and Natural Science, University of Oslo（UiO MN）	Framework	Hiroyoshi SAKURAI, Director, Radioactive Isotope Physics Laboratory
Poland	The Henryk Niewodniczanski Institute of Nuclear Physics, Polish Academy of Sciences (IFPAN)	Framework	Hiroyoshi SAKURAI, Director, Radioactive Isotope Physics Laboratory
Romania	"Horia Hulubei" National Institute of Physics and Nuclear Engineering Bucharest-Magurele, Romania	Framework	Tomohiro UESAKA, Director, Spin Isospin Laboratory
Russia	Joint Institute for Nuclear Research (JINR)	Framework	Tomohiro UESAKA, Director, Spin Isospin Laboratory
	Russian Research Center "Kurchatov Institute"	Framework	Hiroyoshi SAKURAI, Director, Radioactive Isotope Physics Laboratory
Switzerland	Paul Scherrer Institute	Improve the performance and reliability of accelerator systems	Osamu KAMIGAITO, Director, Accelerator Group
Taiwan	Taiwan Instrumentation Detector Consortium（TIDC）	Framework	Itaru Nakagawa, Senior Research Scientist, RHIC Physics Research Group
	Center for High Energy and High Field Physics, Taiwan（CHiP）	High energy and nuclear physics	Yasuyuki AKIBA, Director, RHIC Physics Research Group
USA	Brookhaven National Laboratory	Framework	Yasuyuki AKIBA, Director, RHIC Physics Research Group
	Columbia University	The development of QCDCQ	Yasuyuki AKIBA, Director, RHIC Physics Research Group
	Michigan State University	Comprehensive The use of TPC (Time Projection Chamber)	Tomohiro UESAKA, Director, Spin Isospin Laboratory
UK	The ISIS Neutron and Muon Source at the Science and Technology Facilities Council, part of United Kingdom Research and Innovation, Rutherford Appleton Laboratory	Framework	
Vietnam	Vietnam Atomic Energy Commission	Framework	
Europe	The European Organization for Nuclear Research (CERN)	R&D and application of micro-pattern gas detectors (MPGD) technology (RD51 Collaboration)	Yasuyuki AKIBA, Director, RHIC Physics Research Group
	The European Organization for Nuclear Research (CERN)	Collaboration in the ALICE Experiment	Yasuyuki AKIBA, Director, RHIC Physics Research Group
	EURO-LABS	Framework	Tomohiro UESAKA, Director, Spin Isospin Laboratory

7. Awards

Awardee, Laboratory / Team	Award	Organization	Date
Tomoko ABE, Director of the Beam Mutagenesis Group	The 10th Wada Memorial Award	The Japan Mendel Society	Apr. 17
Pieter Christiaan DOORNENBAL, Senior Research Scientist at the Radioactive Isotope Physics Laboratory	Friedrich Wilhelm Bessel Research Award	Alexander von Humboldt Foundation	Apr. 25
Kimiko SEKIGUCHI, Visiting Scientist at the Spin Isospin Laboratory	The 42nd Saruhashi Prize	一般財団法人 女性科学者に明るい未来をの会	May 29
Kai KIKUCHI, Student Trainee at the Nuclear Spectroscopy Laboratory	29th International Conference on Low Temperature Physics (LT29) Poster Award	29th International Conference on Low Temperature Physics (LT29) organizing committee	Aug. 24
Kenta SUGIHARA, Visiting Scientist at the Safety Management Group	The Atomic Energy Society of Japan (AESJ) Data Division Encouragement Award	Atomic Energy Society of Japan	Sep. 9
Rurie Mizuno, Student Trainee at the Radioactive Isotope Laboratory	The Outstanding Presentation Award	Japanese Society of Radiation Chemistry	Sep. 12
Tomoko ABE, Director of the Beam Mutagenesis Group	Japanese Society of Breeding Award	Japanese Society of Breeding	Sep. 20
Yusuke KAZAMA, Visiting Scientist of the Ion Beam Breeding Team	Japanese Society of Breeding Award	Japanese Society of Breeding	Sep. 20
Tomoya HIRANO, Visiting Scientist of the Ion Beam Breeding Team	Japanese Society of Breeding Award	Japanese Society of Breeding	Sep. 20
Tomoko ABE, Director of the Beam Mutagenesis Group	Japanese Society of Crop Science (CSSJ) Best Paper Award.	Crop Science Society of Japan	Oct. 18
Hiroyuki ICHIDA, Team Leader of the Plant Genome Evolution Research Team	Japanese Society of Crop Science (CSSJ) Best Paper Award.	Crop Science Society of Japan	Oct. 18
Ryohei MORITA, Technical Scientist at the Ion Beam Breeding Team	Japanese Society of Crop Science (CSSJ) Best Paper Award.	Crop Science Society of Japan	Oct. 18
Yasuyuki MORITA, Special Post Doctoral Researcher at the Ion Source Team	The Young Presentation Award by the Beam Physics Study Group	The Beam Physics Study Group	Mar. 10

8. RIKEN Awards

Awardee	Award	Laboratory	Date
Shigekawa YUDAI	Ohbu Award (桜舞賞) The 14th RIKEN Research Incentive Awards (研究奨励賞)	Nuclear Chemistry Research Team	Mar. 23
Yasushi ABE	Ohbu Award (桜舞賞) The 14th RIKEN Technology Incentive Awards (技術奨励賞)	SCRIT Team	Mar. 23
Hiromitsu HABA	Eiho Award (栄峰賞)	Nuclear Chemistry Research Team	Mar. 23

Takashi ABE, Takaharu OTSUKA	Baiho Award (梅峰賞)	Nuclear Spectroscopy Laboratory	Mar. 23
Yoshitaka YAMAGUCHI	Baiho Award (梅峰賞)	Rare RI-Ring Team	Mar. 23

The Center Director

Meeting Attendance as Ex Officio

International Meetings

[NuPECC associate member]

∗ May 6–7, 2022, hybrid.
∗ December 1–2, 2022, hybrid.

[IUPAP WG9]

∗ June 14–15, 2022, hybrid.

Domestic Meetings

[核物理委員会]

仁科センター報告, オンライン, 2022 年 7 月 18 日.
仁科センター報告, オンライン, 2022 年 9 月 7 日.
仁科センター報告, オンライン, 2022 年 10 月 13 日.
仁科センター報告, オンライン, 2022 年 12 月 11 日.
仁科センター報告, オンライン, 2022 年 12 月 12 日.
仁科センター報告, オンライン, 2022 年 12 月 22 日.
仁科センター報告, オンライン, 2023 年 3 月 23 日.

List of Presentations

Presentations

[Domestic Conferences/Workshops]

H. Sakurai (invited), “A brief overview of RIBF,” RIBF User Meeting, Online, September 20, 2022.

H. Sakurai (invited), “A brief overview of RIBF,” SAMURAI Workshop, Online, September 2, 2022.

櫻井博儀（招待講演）,「安心安全な新たな核エネルギー創出のための元素変換研究の推進」, 日本学術会議物理学委員会素粒子物理学・原子核物理学分科会, 東京大学, 2022 年 9 月.

Nuclear Science and Transmutation Research Division
Radioactive Isotope Physics Laboratory

1. Abstract

This Laboratory works as one of core research groups conducting programs at the world-premiere heavy-ion accelerator facility of RIKEN "RI Beam Factory (RIBF)." The Laboratory explores exotic nuclear structures and dynamics in exotic nuclei that have never been investigated before, such as those with largely imbalanced proton and neutron numbers. Our aim is to develop new experimental techniques utilizing fast radioactive isotope (RI) beams at RIBF, to discover new phenomena and properties in exotic nuclei. The Laboratory is focusing three major subjects; shell evolution of very neutron-rich nuclei, the *r*-process path and equation-of-state in asymmetric nuclear matter. The Laboratory has initiated international collaborations for in-beam gamma spectroscopy, decay spectroscopy and heavy-ion induced reactions, and has formed a discussion forum for next generation gamma-ray detectors.

2. Major Research Subjects

(1) Study of structure and dynamics of exotic nuclei through developments of new tools in terms of reaction- and technique-based methodology
(2) Research on EOS in asymmetric nuclear matter via heavy-ion induced reactions
(3) Detector developments for spectroscopy and reaction studies

3. Summary of Research Activity

(1) In-beam gamma spectroscopy

In the medium and heavy mass region explored at RIBF, collective natures of nuclei are one of important subjects, which are obtained through production and observation of high excited and high spin states. To populate such states, heavy-ion induced reactions such as fragmentation, fission are useful. So far, we have developed two-step fragmentation method as an efficient method to identify and populate excited states, and lifetime measurements to deduce transition strength.

Devices utilized for the in-beam gamma spectroscopy are ZeroDegree spectrometer (ZDS) and a NaI array DALI2. Since the end of 2008, the first spectroscopy on nuclei island-of-inversion region was performed, we have explored step-by-step new and unknown regions in the nuclear chart. The second campaign in 2009 was organized to study background components originating from atomic processes in a heavy target. Neutron-rich nuclei at $N = 20$ to 28 were studied in 2010. In 2011–2013, we conducted experiment programs for Ca-54, Ni-78, neutron-rich nuclei at $N = 82$ and neutron-deficient nuclei at $Z = 50$.

A multitude of data obtained with inelastic, nucleon knock-out, fragmentation channels have been analyzed and published. In 2011–2013, collective natures of Mg-36, 38 and Si-42 were both published in PRL. Excited states firstly observed in Ca-54 were reported in Nature to demonstrate a new nuclear magic number of 34. Fragmentation reaction has been found efficient for nuclei with $A > 100$ and low-lying excited state in Pd-126 has been successfully observed and reported in PRC. In 2019, results of the first spectrosocpy of ^{40}Mg was published in PRL, to demonstrate the exotic structure which is very different from in other neutron-rich Mg isotopes.

To further strengthen the in-beam gamma spectroscopy at RIBF, we have proposed a new setup of MINOS + DALI2 to search for the 1st excited states in even-even neutron-rich nuclei with $Z \sim 20$ to 40. The program was submitted to the PAC 2013 as a new category of proposal, "proposal for scientific program" and was S-ranked. A dedicated collaboration "SEASTAR" has been established as a subset of in-beam gamma collaboration "SUNFLOWER." The three campaigns were organized in 2014, 2015 and 2017 to study very neutron-rich isotopes, and were very productive to access very neutron-rich nuclei such as Ar-52, Ca-56, Ni-78, Kr-100, Zr-110. In 2019, the result of the first spectroscopy of Ni-78 was published in Nature.

A new project of high resolution gamma spectroscopy with fast beams "HiCARI" was proposed at PAC 2018. MINIBALL and several Ge tracking detectors from Japan, Europe, the USA and Korea were combined to form an array of germanium detectors. The new setup aims to accelerate researches of the nuclear structure by observing gamma-lines in even-odd nuclei and measuring lifetimes of excited states. The two workshops were organized in 2019, and the machine time of 43.5 days in total was approved at PAC 2019. The experiments with the MINOS setup were canceled due to the travel difficulties of COVID-19 for French engineers. The 31.5days experiments were successfully conducted in 2020 and 2021.

Concerning a next generation detector, a discussion forum has been established to write up a white paper on tracking germanium detectors and high-efficient crystal detectors such $LaBr_3$ and GAGG.

(2) Decay spectroscopy

Beta- and isomer-spectroscopy is an efficient method for studying nuclear structure, especially for non-yrast levels. We had accumulated experimental techniques at the RIPS facility to investigate nuclear structure in light mass region via beta-gamma and beta-p coincidence. Concerning the medium and heavy mass region available at RIBF, we have developed two position-sensitive active-stoppers, strip-silicon detectors and a cylindrical active stopper called CAITEN, to achieve a low-background measurement by taking correlation between heavy ion stop position and beta-ray emission position. A site of decay-spectroscopy at the new facility of RIBF is the final focal plane of ZDS, where high precision of TOF in particle identification is obtained due to a long flight path from BigRIPS to ZDS.

At the end of 2009, the first decay spectroscopy was organized with a minimum setup of four clover gamma detectors and silicon strip detectors, to study neutron-rich nuclei with $A \sim 110$. The first campaign was found successful and efficient to publish four

letter articles in 2011, two PRL's and two PLB's. One of the PRL papers is associated to the *r*-process path where half-lives for 18 neutron-rich nuclei were determined for the first time. The other PRL paper reported a finding of deformed magic number 64 in the Zr isotopes.

The success of the first decay-spectroscopy campaign stimulated to form a new large-scale collaboration "EURICA," where a twelve Euroball cluster array is coupled with the silicon-strip detectors to enhance gamma efficiency by a factor of 10. A construction proposal of "EURICA" was approved in the PAC 2011, and the commissioning was successfully organized in spring 2012. Since then, physics runs had been conducted for programs approved to survey nuclei of interest as many as possible, such as Ni-78, Pd-128, Sn-100. The EURICA collaboration finished its physics programs in summer 2016. So far, 54 papers including 14 PRL's and 13 PLB's were published. One of the highlights is discovery of a seniority isomer in Pd-128, of which cascade gamma decay gives the energy of first excited state and robustness of $N = 82$ magic number, and the other is a half-life measurement for 110 neutron-rich nuclei across the $N = 82$ shell gap, which shows implications for the mechanism and universality of the *r*-process path.

Beta-delayed neutron emission probability of medium and heavy neutron-rich nuclei is important to understand nuclear structure and the *r*-process path. In 2013, a new collaboration "BRIKEN" has been established to form a He-3 detector array. A present design of the array has neutron efficiency as high as 70% up to 3 MeV. The array was coupled with the AIDA silicon strip system. A construction proposal was approved at the PAC 2013. The commissioning run was conducted in autumn 2016. The major physics runs were conducted in 2017–2021. One of the recent highlights is "Beta-Delayed One and Two Neutron Probabilities Southeast of Sn-132 and the Odd-Even Systematics in *r*-Process Nuclide Abundances," published in PRL, 2022.

A new project "IDATEN" has been launched in 2021 to measure lifetime of excited states with a large size $LaBr_3$ array, which is formed by combination of FATIMA and Khala arrays. The construction proposal was submitted to PAC, 2021, and proposals with IDATEN were evaluated at PAC, 2022. The project has been conducted under UK, Korea, China, and Japan.

The CAITEN detector was successfully tested with fragments produced with a Ca-48 beam in 2010.

(3) Equation-of-state via heavy-ion central collisions

Equation-of-state in asymmetric nuclear matter is one of major subjects in physics of exotic nuclei. Pi-plus and pi-minus yields in central heavy ion collisions at the RIBF energy are considered as one of EOS sensitive observables at the RIBF energy. To observe charged pions, a TPC for the SAMURAI spectrometer is being constructed under an international collaboration "SπRIT," Construction proposal was submitted at the PAC 2012, and physics proposals were approved at the PAC 2012 and 2013. The physics runs were successfully conducted in spring 2016. The first three papers were published in 2020 and 2021. One of them, which was published in PRL, has been ranked as the TOP 1% paper by WoS.

An international symposium "NuSYM" on nuclear symmetry energy was organized at RIKEN July 2010 to invite researchers in three sub-fields, nuclear structure, nuclear reaction and nuclear astrophysics, and to discuss nuclear symmetry energy together. Since then, the symposium series have been held every year and been useful to encourage theoretical works and to strengthen the collaboration.

(4) Nucleon correlation and cluster in nuclei

Nucleon correlation and cluster in nuclei are matters of central focus in a "beyond mean-field" picture. The relevant programs with in-beam gamma and missing-mass techniques are to depict nucleon condensations and correlations in nuclear media as a function of density as well as temperature. Neutron-halo and -skin nuclei are objects to study dilute neutron matter at the surface. By changing excitation energies in neutron-rich nuclei, clustering phenomena and role of neutrons are to be investigated.

In 2013, two programs were conducted at the SAMURAI spectrometer. One is related to proton-neutron correlation in the C-12 nucleus via *p*-*n* knockout reaction with a carbon target. The other is to search for a cluster state in C-16, which was populated via inelastic alpha scattering. The data is being analyzed.

In 2018, a new project based on missing mass spectroscopy was launched to investigate an exotic cluster state in a very proton-rich nucleus. The experiment was organized at GANIL with combination of RIKEN liquid hydrogen target CRYPTA and the MUST2 detector array.

Members

Director

Hiroyoshi SAKURAI

Senior Research Scientists

Pieter C. DOORNENBAL
Tadaaki ISOBE
Akihisa KOHAMA
Yoichi NAKAI
Shunji NISHIMURA

Research Scientist

Daisuke SUZUKI

Contract Researcher

Nobuya NISHIMURA

Special Postdoctoral Researchers

Martha Liliana CORTES SUA
Masaomi TANAKA

Postdoctoral Researchers

Shoya TANAKA
Zuxing YANG
Phong VI

International Program Associates

Ting GAO (University of Hong Kong)
Jinn Ming YAP (University of Hong Kong)

Special Temporary Research Scientist

Takashi ICHIHARA

Research Consultants

Masayasu ISHIHARA
Kenichi MATSUYANAGI

Senior Visiting Scientists

Shigeru KUBONO (Univ. of Tokyo)
Tetsuya MURAKAMI

Visiting Scientists

Nori AOI (Osaka Univ.)
Frank BROWNE (CERN)
Hue M. BUI (Vietnam Academy of Sci. and Tech.)
Giordano CERIZZA (Michigan State Univ.)
Sidong CHEN (Univ. of York)
Silvio CHERUBINI (Univ. of Catania)
Xiaohua FAN (Southwest Univ.)
Chaoyi FU (Univ. of Hong Kong)
Mitsunori FUKUDA (Osaka Univ.)
Byungsik HONG (Korea Univ.)
Kei IIDA (Kochi Univ.)
Natsumi IKENO (Tottori Univ.)
Takuji IZUMIKAWA (Niigata Univ.)
Takashi KISHIDA (Aoyama Gakuin Univ.)
Gabor KISS (Inst. for Nuclear Res. (ATOMKI))
Asahi KOHDA (Osaka Univ.)
Khiem LE (Vietnam Academy of Sci. and Tech.)
Xiaoyu LIU (Univ. of Hong Kong)
Byul MOON (The Inst. for Basic Sci. (IBS))
Yoshiharu MORI (Kyoto Univ.)
Evgueni NIKOLSKI (Kurchatov Inst.)
Daiki NISHIMURA (Tokyo City Univ.)
Takashi OHTSUBO (Niigata Univ.)
Hooi Jin ONG (IMP, CAS)
Akira ONO (Tohoku Univ.)
Naohiko OTSUKA (IAEA)
Kazuhiro OYAMATSU (Aichi Shukutoku Univ.)
Paer-Anders SOEDERSTROEM (IFIN-HH, Romania)
Ryo TANIUCHI (Univ. of York)
Rensheng WANG (Soochow Univ.)
Yijie WANG (Tsinghua Univ.)
Hiroshi WATANABE (Beihang Univ.)
Kathrin WIMMER (GSI)
Jin WU (Brookhaven Nat'l Lab.)
Yasutaka YAMAMOTO (Osaka Univ.)

Visiting Researcher

Umesh GARG (JSPS)

Student Trainees

Mei AMITANI (Tokyo City Univ.)
Takamichi AOKI (Univ. of Tokyo)
Takumi AOKI (Univ. of Tokyo)
Linh BUI (Vietnam Atomic Energy Inst.)
Hiroaki FUKUSHIMA (Rikkyo Univ.)
Miki FUKUTOME (Osaka Univ.)
Jiseok KIM (Korea Univ.)
Yukiya KOBAYASHI (Niigata Univ.)
Kei KOKUBUN (Univ. of Tokyo)
Rurie MIZUNO (Univ. of Tokyo)
Nurhafiza MOHAMAD NOR (Osaka Univ.)
Yuki NAKAMURA (Tokyo City Univ.)
Thomas G. PARRY (Univ. of Surrey)
Yuhao QIN (Tsinghua Univ.)
Sora SUGAWARA (Tokyo City Univ.)
Ryo TAGUCHI (Osaka Univ.)
Hiroyuki TAKAHASHI (Tokyo City Univ.)
Kazuya TAKATSU (Niigata Univ.)
Gen TAKAYAMA (Osaka Univ.)
Takumi TOMIYAMA (Tokyo City Univ.)
Tik Tsun YEUNG (Univ. of Tokyo)
Boyuan ZHANG (Tsinghua Univ.)

Research Part-time Workers

Kiyomi ARAI
Mie DOI
Miki KANOU
Eiko MIZUMOTO
Noriko OKAYASU
Mayumi SAITO
Tsuneyo SUZUKI
Miyuki TAMABAYASHI

List of Publications & Presentations

Publications

[Original Papers]

M. Enciu, H. N. Liu, A. Obertelli, P. Doornenbal, F. Nowacki, K. Ogata, A. Poves, K. Yoshida, N. L. Achouri, H. Baba, F. Browne, D. Calvet, F. Chateau, S. Chen, N. Chiga, A. Corsi, M. L. Cortes, A. Delbart, J. -M. Gheller, A. Giganon, A. G illibert, C. Hilaire, T. Isobe, T. Kobayashi, Y. Kubota, V. Lapoux, T. Motobayashi, I. Murray, H. Otsu, V. Panin, N. Paul, W. Rodriguez, H. Sakurai, M. Sasano, D. Steppenbeck, L. Stuhl, Y. L. Sun, Y. Togano, T. Uesaka, K. Wimmer, K. Yoneda, O. Aktas, T. Aumann, L. X. Chung, F. Flavigny, S. Franchoo, I. Gasparic, R. -B. Gerst, J. Gibelin, K. I. Hahn, D. Kim, Y. Kondo, P. Koseoglou, J. Lee, C. Lehr, P. J. Li, B. D. Linh, T. Lokotko, M. MacCormick, K. Moschner, T. Nakamura, S. Y. Park, D. Rossi, E. Sahin, P. -A. Soderstrom, D. Sohler, S. Takeuchi, H. Toernqvist, V. Vaquero, V. Wagner, S. Wang, V. Werner, X. Xu, H. Yamada, D. Yan, Z. Yang, M. Yasuda, and L. Zanetti, "Extended $p_{3/2}$ neutron orbital and the $N = 32$ shell closure in ^{52}Ca," Phys. Rev. Lett. **129**, 262501 (2022).

B. Moon, C. -B. Moon, A. Odahara, R. Lozeva, S. Nishimura, C. Yuan, F. Browne, P. Doornenbal, G. Lorusso, Z. Patel, S. Rice, L. Sinclair, P. -A. Söderström, T. Sumikama, H. Watanabe, J. Wu, Z. Y. Xu, A. Yagi, D. S. Ahn, H. Baba, F. L. Bello Garrote, R. Daido, J. M. Daugas, F. Didierjean, Y. Fang, N. Fukuda, B. Hong, E. Ideguchi, N. Inabe, T. Ishigaki, T. Isobe, H. S. Jung, D. Kameda, I. Kojouharov, T. Komatsubara, T. Kubo, Y. K. Kwon, C. S. Lee, P. Lee, S. Morimoto, D. Murai, M. Niikura, H. Nishibata, I. Nishizuka, H. Sakurai, Y. Shimizu, H. Suzuki, H. Takeda, K. Tshoo, and R. Yokoyama, "Gamow-teller decay of ^{142}Te to ^{142}I," Phys. Rev. C **107**, 014311 (2023).

S. Iimura, M. Rosenbusch, A. Takamine, Y. Tsunoda, M. Wada, S. Chen, D. S. Hou, W. Xian, H. Ishiyama, S. Yan, P. Schury, H. Crawford, P. Doornenbal, Y. Hirayama, Y. Ito, S. Kimura, T. Koiwai, T. M. Kojima, H. Koura, J. Lee, J. Liu, S. Michimasa, H. Miyatake, J. Y. Moon, S. Naimi, S. Nishimura, T. Niwase, A. Odahara, T. Otsuka, S. Paschalis, M. Petri, N. Shimizu, T. Sonoda, D. Suzuki, Y. X. Watanabe, K. Wimmer, and H. Wollnik, "Study of the $N = 32$ and $N = 34$ shell gap for Ti and V by the first high-precision multireflection time-of-flight mass measurements at BigRIPS-SLOWRI," Phys. Rev. Lett. **130**, 012501 (2023).

M. Rosenbusch, M. Wada, S. Chen, A. Takamine, S. Iimura, D. Hou, W. Xian, S. Yan, P. Schury, Y. Hirayama, Y. Ito, H. Ishiyama, S. Kimura, T. Kojima, J. Lee, J. Liu, S. Michimasa, H. Miyatake, J. Y. Moon, M. Mukai, S. Naimi, S. Nishimura, T. Niwase, T. Sonoda, Y. X. Watanabe, and H. Wollnik, "The new MRTOF mass spectrograph following the ZeroDegree spectrometer at RIKEN's RIBF facility," Nucl. Instrum. Methods Phys. Res. A **1047**, 167824 (2023).

J. Wu, S. Nishimura, P. -A. Söderström, A. Algora, J. J. Liu, V. H. Phong, Y. Q. Wu, F. R. Xu, J. Agramunt, D. S. Ahn, T. A. Berry, C. G. Bruno, J. J. Bundgaard, R. Caballero-Folch, A. C. Dai, T. Davinson, I. Dillmann, A. Estrade, A. Fijalkowska, N. Fukuda, S. Go, R. K. Grzywacz, T. Isobe, S. Kubono, G. Lorusso, K. Matsui, A. I. Morales, N. Nepal, S. E. A. Orrigo, B. C. Rasco, K. P. Rykaczewski, H. Sakurai, Y. Shimizu, D. W. Stracener, T. Sumikama, H. Suzuki, J. L. Tain, H. Takeda, A. Tarifeño-Salvidia, A. Tolosa-Delgado, M. Wolińska-Cicocka, and R. Yokoyama, "First observation of isomeric states in ^{111}Zr, ^{113}Nb, and ^{115}Mo," Phys. Rev. C **106**, 064328 (2022).

V. H. Phong, S. Nishimura, G. Lorusso, T. Davinson, A. Estrade, O. Hall, T. Kawano, J. Liu, F. Montes, N. Nishimura, R. Grzywacz, K. P. Rykaczewski, J. Agramunt, D. S. Ahn, A. Algora, J. M. Allmond, H. Baba, S. Bae, N. T. Brewer, C. G. Bruno, R. Caballero-Folch, F. Calviño, P. J. Coleman-Smith, G. Cortes, I. Dillmann, C. Domingo-Pardo, A. Fijalkowska, N. Fukuda, S. Go,1 C. J. Griffin, J. Ha, L. J. Harkness-Brennan, T. Isobe, D. Kahl, L. H. Khiem, G. G. Kiss, A. Korgul, S. Kubono, M. Labiche, I. Lazarus, J. Liang, Z. Liu, K. Matsui, K. Miernik, B. Moon, A. I. Morales, P. Morrall, N. Nepal, R. D. Page, M. Piersa-Silkowska, V. F. E. Pucknell, B. C. Rasco, B. Rubio, H. Sakurai, Y. Shimizu, D. W. Stracener, T. Sumikama, H. Suzuki, J. L. Tain, H. Takeda, A. Tarifeño-Salvidia, A. Tolosa-Delgado, M. Wolińska-Cicocka, P. J. Woods, and R. Yokoyama, "β-delayed one and two neutron emission probabilities southeast of ^{132}Sn and the odd-even systematics in r-process nuclide abundances," Phys. Rev. Lett. **129**, 172701 (2022).

G. G. Kiss, A. Vitéz-Sveiczer, Y. Saito, A. Tarifeño-Salvidia, M. Pallas, J. L. Tain, I. Dillmann, J. Agramunt, A. Algora, C. Domingo-Pardo, A. Estrade, C. Appleton, J. M. Allmond, P. Aguilera, H. Baba, N. T. Brewer, C. Bruno, R. Caballero-Folch, F. Calviño, P. J. Coleman-Smith, G. Cortes, T. Davinson, N. Fukuda, Z. Ge, S. Go, C. J. Griffin, R. K. Grzywacz, O. Hall, A. Horváth, J. Ha, L. J. Harkness-Brennan, T. Isobe, D. Kahl, T. T. King, A. Korgul, S. Kovács, R. Krücken, S. Kubono, M. Labiche, J. Liu, J. Liang, M. Madurga, K. Miernik, F. Molina, A. I. Morales, M. R. Mumpower, E. Nacher, A. Navarro, N. Nepal, S. Nishimura, M. Piersa-Silkowska, V. Phong, B. C. Rasco, B. Rubio, K. P. Rykaczewski, J. Romero-Barrientos, H. Sakurai, L. Sexton, Y. Shimizu, M. Singh, T. Sprouse, T. Sumikama, R. Surman, H. Suzuki, T. N. Szegedi, H. Takeda, A. Tolosa, K. Wang, M. Wolińska-Cicocka, P. Woods, R. Yokoyama, and Z. Xu, "Measuring the β-decay properties of neutron-rich exotic Pm, Sm, Eu, and Gd isotopes to constrain the nucleosynthesis yields in the rare-earth region," Astrophys. J. **936**, 107 (2022).

A. Vitéz-Sveiczera, A. Algoraa, A. I. Morales, B. Rubioa, G. G. Kiss, P. Sarrigurene, P. Van Isacker, G. de Angelis, F. Recchia, S. Nishimura, J. Agramunt, V. Guadilla, A. Montaner-Pizá, S. E. A. Orrigo, A. Horváth, D. Napoli, S. Lenzi, A. Boso, V. H. Phong, J. Wu, P. -A. Söderström l, T. Sumikama, H. Suzuki, H. Takeda, D. S. Ahn, H. Baba, P. Doornebal, N. Fukuda, N. Inabe, T. Isobe, T. Kubo, S. Kubono, H. Sakurai, Y. Shimizu, C. Sidong, B. Blank, P. Ascher, M. Gerbaux, T. Goigoux, J. Giovinazzo, S. Grévy, T. Kurtukián Nieto, C. Magron, W. Gelletly, Zs. Dombrádi, Y. Fujita, M. Tanaka, P. Aguilera, F. Molina, J. Eberth, F. Diel, D. Lubos, C. Borcea, E. Ganioglu, D. Nishimura, H. Oikawa, Y. Takei, S. Yagi, W. Korten, G. de France, P. Davies, J. Liu, J. Lee, T. Lokotko, I. Kojouharov, N. Kurz, H. Shaffner, and A. Petrovici, "The β-decay of ^{70}Kr into ^{70}Br: Restoration of the pseudo-SU(4) symmetry," Phys. Lett. B **830**, 137123 (2022).

V. Girard Alcindor, A. Mercenne, I. Stefan, F. de Oliveira Santos, N. Michel, M. Ploszajczak, M. Assie, A. Lemasson, E. Clement, F. Flavigny, A. Matta, D. Ramos, M. Rejmund, J. Dudouet, D. Ackermann, P. Adsley, M .Assuncao, B. Bastin, D. Beaumel, G. Benzoni, R. Borcea, A. J. Boston, D. Brugnara, L. Caceres, B. Cederwall, I. Celikovic, V. Chudoba, M. Ciemala, J. Collado, F. C. L. Crespi, G. D'Agata, G. De France, F. Delaunay, C. Diget, C. Domingo-Pardo, J. Eberth, C. Fougeres, S. Franchoo, F. Galtarossa, A. Georgiadou, J. Gibelin, S. Giraud, V. Gonzalez, N. Goyal, A. Gottardo, J. Goupil, S. Grevy, V. Guimaraes, F. Hammache, L. J. Harkness-Brennan, H. Hess, N. Jovancevic, D. S. Judson Oliver, O. Kamalou, A. Kamenyero, J. Kiener, W. Korten, S. Koyama, M. Labiche, L. Lalanne,

V. Lapoux, S. Leblond, A. Lefevre, C. Lenain, S. Leoni, H. Li, A. Lopez-Martens, A. Maj, I. Matea, R. Menegazzo, D. Mengoni, A. Meyer, B. Million, B. Monteagudo, P. Morfouace, J. Mrazek, M. Niikura, J. Piot, Zs. Podolyak, C. Portail, A. Pullia, B. Quintana, F. Recchia, P. Reiter, K. Rezynkina, T. Roger, J. S. Rojo, F. Rotaru, M. D. Salsac, A. M. Sanchez-Benitez, E. Sanchis, M. Senyigit, N. de Sereville, M. Siciliano, J. Simpson, D. Sohler, O. Sorlin, M. Stanoiu, C. Stodel, D. Suzuki, C. Theisen, D. Thisse, J. C. Thomas, P. Ujic, J. J. Valiente-Dobon, and M. Zielinska, "New narrow resonances observed in the unbound nucleus ^{15}F," Phys. Rev. C **105**, L051301 (2022).

L. Lalanne, O. Sorlin, A. Poves, M. Assié, F. Hammache, S. Koyama, D. Suzuki, F. Flavigny, V. Girard-Alcindor, A. Lemasson, A. Matta, T. Roger, D. Beaumel, Y. Blumenfeld, B. A. Brown, F. De Oliveira Santos, F. Delaunay, N. de Séréville, S. Franchoo, J. Gibelin, J. Guillot, O. Kamalou, N. Kitamura, V. Lapoux, B. Mauss, P. Morfouace, M. Niikura, J. Pancin, T. Y. Saito, C. Stodel, and J. -C. Thomas, "Structure of ^{36}Ca under the coulomb magnifying glass," Phys. Rev. Lett. **129**, 122501 (2022).

B. Le Crom, M. Assié, Y. Blumenfeld, J. Guillot, H. Sagawa, T. Suzuki, M. Honma, N. L. Achouri, B. Bastin, R. Borcea, W. N. Catford, E. Clément, L. Caceres, M. Caamano, A. Corsi, G. De France, F. Delaunay, N. De Séréville, B. Fernandez-Dominguez, M. Fisichella, S. Franchoo, A. Georgiadou, J. Gibelin, A. Gillibert, F. Hammache, O. Kamalou, A. Knapton, V. Lapoux, S. Leblond, A. O. Macchiavelli, F. M. Marques, A. Matta, L. Ménager, P. Morfouace, N. A. Orr, J. Pancin, X. Pereira-Lopez, L. Perrot, J. Piot, E. Pollacco, D. Ramos, T. Roger, F. Rotaru, A. M. Sánchez-Benítez, M. Sénoville, O. Sorlin, M. Stanoiu, I. Stefan, C. Stodel, D. Suzuki, J. -C. Thomas, M. Vandebrouck, "Neutron-proton pairing in the $N = Z$ radioactive *fp*-shell nuclei ^{56}Ni and ^{52}Fe probed by pair transfer," Phys. Lett. B **829**, 137057 (2022).

L. Zago, A. Gottardo, J. J. Valiente-Dobon, G. Benzoni, A. Gadea, M. Gorska, S. Lunardi, Zs. Podolyak, P. H. Regan, D. Rudolph, A. Algora, G. de Angelis, D. Bazzacco, J. Benlliure, P. Boutachkov, A. Bracco, A. M. Bruce, F. Camera, E. Casarejos, M. L. Cortes, F. C. L. Crespi, A. Corsi, C. Domingo-Pardo, M. Doncel, T. Engert, H. Geissel, J. Gerl, A. Goasduff, N. Goel, J. Grebosz, E. Gregor, T. Habermann, S. Klupp, I. Kojouharov, N. Kurz, S. M. Lenzi, S. Leoni, S. Mandal, R. Menegazzo, D. Mengoni, B. Million, A. I. Morales, D. R. Napoli, F. Naqvi, C. Nociforo, M. Pfutzner, S. Pietri, A. Prochazka, F. Recchia, E. Sahin, H. Schaffner, A. Sharma, B. Sitar, D. Siwal, P. Strmen, I. Szarka, C. A. Ur, P. M. Walker, H. Weick, O. Wieland, H. -J. Wollersheim, "High-spin states in ^{212}Po above the α-decaying (18^+) isomer," Phys. Lett B **834**, 137457 (2022).

S. M. Cha, K. Y. Chae, K. Abe, S. Bae, D. N. Binh, S. H. Choi, N. N. Duy, Z. Ge, K. I. Hahn, S. Hayakawa, B. Hong, N. Iwasa, D. Kahl, L. H. Khiem, A. Kim, D. Kim, E. J. Kim, G. W. Kim, M. J. Kim, K. Kwak, M. S. Kwag, E. J. Lee, S. I. Lim, B. Moon, J. Y. Moon, S. Y. Park, V. H. Phong, H. Shimizu, H. Yamaguchi, and L. Yang, "Investigation of ^{22}Mg levels via resonant scattering of ^{22}Ne+α," Front. Phys. **11**, 375 (2023).

X. -H. Fan, Z. -X. Yang, P. Yin, P. -H. Chen, J. -M. Dong, Z. -P. Li, and H. Liang, "A local-density-approximation description of high-momentum tails in isospin asymmetric nuclei," Phys. Lett. B **834**, 10 (2022).

P. -H. Chen, H. Wu, Z. -X. Yang, X. -H. Zeng, Z. -Q. Feng, "Prediction of synthesis cross sections of new moscovium isotopes in fusion-evaporation reactions," Nucl. Sci. Tech. **34**, 7 (2023).

Z. -X. Yang, X. -H. Fan, Z. -P. Li, and H. Liang, "A Kohn-Sham scheme based neural network for nuclear systems," Phys. Lett. B **840**, 10 (2023).

W. P. Liu, Z. H. Li, J. J. He, X. D. Tang, G. Lian, J. Su, Y. P. Shen, Z. An, F. Q. Chao, J. J. Chang, L. H. Chen, H. Chen, X. J. Chen, Y. H. Chen, Z. J. Chen, B. Q. Cui, X. C. Du, X. Fang, C. B. Fu, L. Gan, B. Guo, Z. Y. Han, X. Y. Guo, G. Z. He, J. R. He, A. Heger, S. Q. Hou, H. X. Huang, N. Huang, B. L. Jia, L. Y. Jiang, S. Kubono, J. M. Li, M. C. Li, K. A. Li, E. T. Li, T. Li, Y. J. Li, M. Lugaro, X. B. Luo, H. Y. Ma, S. B. Ma, D. M. Mei, W. Nan, W. K. Nan, N. C. Qi, Y. Z. Qian, J. C. Qin, J. Ren, C. S. Shang, L. T. Sun, W. L. Sun, W. P. Tan, I. Tanihata, S. Wang, P. Wang, Y. B. Wang, Q. Wu, S. W. Xu, S. Q. Yan, L. T. Yang, Y. Yang, X. Q. Yu, Q. Yue, S. Zeng, L. Zhang, H. Zhang, H. Y. Zhang, L. Y. Zhang, N. T. Zhang, P. Zhang, Q. W. Zhang, T. Zhang, X. P. Zhang, X. Z. Zhang, W. Zhao, J. F. Zhou, and Y. Zhou, "Progress of underground nuclear astrophysics experiment JUNA in China," Few-Body Syst. **63**, 43 (2022).

Y. H. Lam, N. Lu, A. Heger, A. M. Jacobs Nadezda, A. Smirnova, T. K. Nieto, Z. Johnston, and S. Kubono, "The regulated NiCu cycles with the new ^{57}Cu$(p,\gamma)^{58}$Zn reaction rate and its influence on type I X-ray bursts: the GS 1826–24 clocked burster," Astrophys. J. **929**, 73 (2022).

B. Gao, T. Y. Jiao, Y. T. Li, H. Chen, W. P. Lin, Z. An, L. H. Ru, Z. C. Zhang, X. D. Tang, X. Y. Wang, N. T. Zhang, X. Fang, D. H. Xie, Y. H. Fan, L. Ma, X. Zhang, F. Bai, P. Wang, Y. X. Fan, G. Liu, H. X. Huang, Q. Wu, Y. B. Zhu, J. L. Chai, J. Q. Li, L. T. Sun, S. Wang, J. W. Cai, Y. Z. Li, J. Su, H. Zhang, Z. H. Li, Y. J. Li, E. T. Li, C. Chen, Y. P. Shen, G. Lian, B. Guo, X. Y. Li, L. Y. Zhang, J. J. He, Y. D. Sheng, Y. J. Chen, L. H. Wang, L. Zhang, F. Q. Cao, W. Nan, W. K. Nan, G. X. Li, N. Song, B. Q. Cui, L. H. Chen, R. G. Ma, Z. C. Zhang, S. Q. Yan, J. H. Liao, Y. B. Wang, S. Zeng, D. Nan, Q. W. Fan, N. C. Qi, W. L. Sun, X. Y. Guo, P. Zhang, Y. H. Chen, Y. Zhou, J. F. Zhou, J. R. He, C. S. Shang, M. C. Li, S. Kubono, and W. P. Liu, "Deep underground laboratory measurement of ^{13}C$(\alpha,n)^{16}$O in the gamow windows of the *s* and *i* processes," Phys. Rev. Lett. **129**, 132701 (2022).

A. Miyazaki, M. Tsuge, H. Hidaka, Y. Nakai, and N. Watanabe, "Direct determination of the activation energy for diffusion of OH radicals on water ice," Astrophys. J. Lett. **940**, L2 (2022).

[Proceedings]

M. Pallas, A. Tarifeno-Saldivia, G. G. Kiss, J. L. Tain, A. Tolosa-Delgado, A. Vitez-Sveiczer, F. Calvino, J. Agramunt, P. Aguilera, A. Algora, J. M. Allmond, H. Baba, N. T. Brewer, R. Caballero-Folch, P. J. Coleman-Smith, G. Cortes, T. Davinson, I. Dillmann, C. Domingo-Pardo, A. Estrade, N. Fukuda, S. Go, C. J. Griffin, R. K. Grzywacz, O. Hall, L. J. Harkness-Brennan, T. Isobe, D. Kahl, T. T. King, A. Korgul, S. Kovacs, S. Kubono, M. Labiche, J. Liu, M. Madurga, K. Miernik, F. Molina, N. Mont-Geli, A. I. Morales, E. Nácher, A. Navarro, N. Nepal, S. Nishimura, M. Piersa-Silkowska, V. Phong, B. C. Rasco, J. Romero-Barrientos, B. Rubio, K. P. Rykaczewski, Y. Saito, H. Sakurai, Y. Shimizu, M. Singh, T. Sumikama, H. Suzuki, T. N. Szegedi, H. Takeda, K. Wang, M. Wolińska-Cichocka, P. J. Woods, R. Yokoyama and for the BRIKEN Collaboration, "Study of decay properties of Ba to Nd nuclei ($A \approx 160$) relevant to the formation of the *r*-process rare-earth peak," EPJ Web Conf. **284**, 02005 (2023).

H. Yamaguchi, S. Hayakawa, N. Ma, H. Shimizu, K. Okawa, Q. Zhang, L. Yang, D. Kahl, M. La Cognata, L. Lamia, K. Abe, O. Be-

liuskina, S. Cha, K. Chae, S. Cherubini, P. Figuera, Z. Ge, M. Gulino, J. Hu, A. Inoue, N. Iwasa, A. Kim, D. Kim, G. Kiss, S. Kubono, M. La Commara, M. Lattuada, E. Lee, J. Moon, S. Palmerini, C. Parascandolo, S. Park, V. Phong, D. Pierroutsakou, R. Pizzone, G. Rapisarda, S. Romano, C. Spitaleri, X. Tang, O. Trippella, A. Tumino, N. Zhang, Y. Lam, A. Heger, A. Jacobs, S. Xu, S. Ma, L. Ru, E. Liu, T. Liu, C. Hamill, A. S. J. Murphy, J. Su, X. Fang, M. Kwag, N. Duy, N. Uyen, D. Kim, J. Liang, A. Psaltis, M. Sferrazza, Z. Johnston, and Y. Li, "RIB induced reactions: Studying astrophysical reactions with low-energy RI beam at CRIB," EPJ Web Conf. **275**, 01015 (2023).

S. Tanaka, N. Nishimura, I. Nishimura, and Y. Aritomo, "The evaluation of the fission mode and fragment yields of neutron-rich nucleiby the ynamical model," EPJ Web Conf. **279**, 11021 (2023).

Presentations

[International Conferences/Workshops]

H. Sakurai (invited), "Neutron-rich nuclei, a treasure-chest of discovery and application," The 28th International Nuclear Physics Conference (INPC 2022), Cape Town, South Africa, September 11–16, 2022.

H. Sakurai (invited) "Recent progress and plans at RIBF," Pioneer symposium in Korean Physical Society, Hybrid, April 21, 2022.

H. Sakurai (invited) "Recent progress and plans at RIBF," CPS-APS-IOP-JPS-DPG Joint Session on Large-Scale Facilities for Science in Chinese Physical Society, Hybrid, November 18–22, 2022.

S. Nishimura (invited), "Dense matter from nuclear reactions in astro- and heavy-ion physics," Intersection of Nuclear Structure and High-Energy Nuclear Collisions, Washington University (INT), Seattle, USA, January 23–27, 2023.

S. Nishimura (invited), "Exotic nuclei: Toward the dripline," Nuclear Physics in Astrophysics -X, CERN, Geneva, Switzerland, September 4–9, 2022.

S. Nishimura (invited), "Experiments Relevant to *r*-Process Nucleosynthesis," The 15th Asian Pacific Physics Conference (APPC15), August 21–26, 2022.

S. Nishimura (invited), "Experiments related to *r*-process nucleosynthesis," Mean-field and Cluster Dynamics in Nuclear Systems 2022 (MCD2022), May 9–June 17, 2022.

P. Doornenbal (invited), "First Spectroscopy of ^{56,58}Ca," Reimei Workshop, Darmstadt, Germany, October 10–12, 2022.

D. Suzuki (invited), "Spectroscopy of ^{8}C: mirror symmetry beyond the proton drip line," Halo Week 2022, Bergen, Norway, July 20–15, 2022.

M. L. Cortés (invited), "In-beam gamma-ray spectroscopy towards ^{100}Sn: Recent results and future perspectives" Reimei workshop on "Unveiling nuclear shells and correlations in exotic nuclei through knockout reactions," TU Darmstadt, Germany, October 9–11, 2022.

Y. Nakai (poster), W. M. C. Sameera, K. Furuya, H. Hidaka, A. Ishibashi, and N. Watanabe, "Methanol production through irradiation of low-energy CH_3^+ ions on a water ice surface," Symposium on Next Generation Astrochemistry, Tokyo, Japan, November 29–December 2, 2022.

V. H. Phong (invited), "Experimental studies of the β-decay properties among other important nuclear data inputs for the *r*-process nucleosynthesis at the RIKEN RIBF," International Symposium on Origin of Matter and Evolution of Galaxies OMEG16 2022, Hanoi, Vietnam, October 24–28, 2022.

V. H. Phong (oral), "Beta-delayed one and two neutron emission probabilities south-east of ^{132}Sn : Impact on the odd-even abundance pattern of the second *r*-process peak," UKAKUREN-RCNP Conference on AstroNuclear Physics ANP2022, Osaka, Japan, July 20–21, 2022.

V. H. Phong (oral), "Beta-Delayed Neutron-Emission Probabilities of 20 neutron-rich Ag, Cd, In and Sn isotopes: Impacts on the second *r*-process peak formation," Astrophysics with Radioactive Isotopes 2022, Budapest, Hungary, June 12–17, 2022.

V. H. Phong (oral), "20 β-delayed neutron emission probabilities across the $Z = 50$ and $N = 82$ shell closure: Implication on the formation of the second *r*-process peak," International Nuclear Physics Conference (INPC) 2022, Cape Town, South Africa, September 11–16, 2022.

Y. Aritomo (poster), S. Tanaka, N. Nishimura, and I. Nishimura, "The evaluation of the fission mode and fragment yields of neutron-rich nuclei by the dynamical model," Nuclear Physics in Astrophysics-X, Geneva, Switzerland, September 5–9, 2022.

F. Minato (poster), S. Tanaka, and N. Nishimura, "Fission fragment yields of neutron-rich nuclei evaluated by the Langevin model calculation," 2022 Symposium on Nuclear Data, Osaka, Japan, November 17–18, 2022.

[Domestic Conferences/Workshops]

西村俊二（招待講演), 「中性子捕獲反応と元素合成: 鍵を握る原子核データの収集と研究戦略」, 中性子捕獲反応で迫る宇宙の元素合成, 東京大学本郷キャンパス, 2023 年 2 月 9–10 日.

鈴木大介（一般講演), 「非束縛核 ^{8}C におけるミラー対称性の研究」, 2022 年日本物理学会秋季大会, 岡山県岡山市 (岡山理科大学), 2022 年 9 月 6–8 日.

鈴木大介（招待講演), 「RI ビームファクトリーにおける超新星爆発下の核反応研究」, 中性子捕獲反応で迫る宇宙の元素合成, 東京都文京区 (東京大学), 2023 年 2 月 9–10 日.

鈴木大介（招待講演), 「RI ビームを用いた高速陽子捕獲反応の研究」, 星の進化と爆発天体における核反応の物理, 埼玉県和光市 (理化学研究所), 2023 年 2 月 20–21 日.

中井陽一 (口頭発表), 「低エネルギーイオンと低温氷表面との反応」, 文科省科研費 学術変革領域（A）次世代アストロケミストリー 気相実験ワークショップ, 宮崎県宮崎市 (KITEN ビルコンベンションホール), 2022 年 9 月 7 日.

中井陽一 (口頭発表), 日高宏, 渡部直樹, 「低エネルギーイオンと氷表面との反応実験」, 日本物理学会 2022 年秋季大会, 東京都目黒区 (東京工業大学), 2022 年 9 月 12–15 日.

中井陽一 (口頭発表), 「低エネルギーイオンと極低温氷表面との分子生成反応」, 学術変革領域次世代アストロケミストリー 第 3 回 領域全体集会, 東京都文京区 (東京大学), 2022 年 3 月 7–9 日.

中井陽一 (口頭発表), 渡部直樹, 柘植雅士, 副島浩一, 「極低温氷表面に存在する OH ラジカルの可視域光による光脱離」, 日本物理学会 2023 年春季大会, オンライン, 2023 年 3 月 22–25 日.

P. Doornenbal (invited), "Past achievements and future perspectives for in-beam gamma-ray spectroscopy at the isospin frontier at the RIBF," Physics of RI: Recent progress and perspectives workshop, Wako, Japan, May 30–June 1, 2022.

M. L. Cortés (invited), "In-beam gamma-ray spectroscopy towards ^{100}Sn: Recent results and future perspectives" RIBF Users Meeting 2022, RIBF, RIKEN, Japan, September 20–22, 2022.

有友嘉浩 (口頭発表), 田中翔也, 西村信哉, 西村紘志, 「r プロセス計算へ向けた動力学模型による核分裂研究」, 日本物理学会 2022 年秋季大会, 岡山県岡山市 (岡山理科大学), 2022 年 9 月 6–8 日.

湊太志 (ポスター), 田中翔也, 西村信哉, 「r プロセス計算へ向けた中性子過剰核領域における核分裂収率の理論評価」, 2022 (令和 4) 年度 国立天文台 CfCA ユーザーズミーティング, 東京都三鷹市 (国立天文台), 2023 年 1 月 26–27 日.

有友嘉浩 (口頭発表), 田中翔也, 西村信哉, 湊太志, 西村紘志, 「r プロセス計算へ向けた核分裂の評価」, [RIBF-ULIC-miniWS038] 理論と実験で拓く中性子過剰核の核分裂, 東京都和光市 (理化学研究所), 2023 年 2 月 16–17 日.

有友嘉浩 (口頭発表), 田中翔也, 西村信哉, 西村紘志, 湊太志, 「動力学模型による中性子過剰核の核分裂収率計算」, 日本原子力学会 2023 年春の年会, 東京都目黒区 (東京大学), 2023 年 3 月 13–15 日.

湊太志 (口頭発表), 田中翔也, 西村信哉, 「ランジュバン計算と統計模型を用いた核分裂収率および即発中性子の評価」, 日本物理学会 2023 年春季大会, オンライン, 2023 年 3 月 22–25 日.

[Seminars]

D. Suzuki (invited), "Radioactive isotope physics," INTPART School 2023, Okinawa, Japan, February 20–March 3, 2023.

P. Doornenbal, "Latest Results and Future Potential for In-Beam γ-Ray Spectroscopy at the RIBF," SFB Seminar, Darmstadt, Germany, May 19, 2022.

田中翔也, 「動力学模型による核分裂の理論計算」, 第 57 回「基礎科学セミナー」, 千葉県習志野市 (千葉工業大学), 2023 年 2 月 25 日.

Press Releases

極低温氷表面での OH ラジカルの動きやすさを初めて測定—宇宙の氷微粒子上で分子進化が活性化する温度が明らかに—, 北海道大学, 理化学研究所, 2022 年 11 月 24 日, https://www.riken.jp/press/2022/20221124_1/index.html .

加速器実験による r 過程の同位体比の再現に成功—宇宙初期と太陽系のバリウムは中性子星合体が起源か？ — 2022 年 10 月 19 日, https://www.riken.jp/press/2022/20221019_1/index.html .

Awards

P. Doornenbal, Friedrich Wilhelm Bessel Research Award, 2022.

水野るり惠, 放射線化学討論会, 優秀発表賞 (学生), 2022 年 9 月.

Outreach Activities

櫻井博儀,「理研で進展する元素変換科学—宇宙での元素進化—」, 埼玉県立春日部高等学校, 2023 年 2 月.

櫻井博儀, 2022 年度「はかる! 」, 埼玉県立不動岡高等学校.

Nuclear Science and Transmutation Research Division
Spin isospin Laboratory

1. Abstract

The Spin Isospin Laboratory pursues research activities putting primary focus on interplay of spin and isospin in exotic nuclei. Understanding nucleosyntheses in the universe, especially those in *r*- and *rp*-processes is another big goal of our laboratory.

Investigations on isospin dependences of nuclear equation of state, spin-isospin responses of exotic nuclei, occurrence of various correlations at low-densities, evolution of spin-orbit coupling are main subjects along the line. We are leading a mass measurement project with the Rare RI Ring project, too. Through the experimental studies, we will be able to elucidate a variety of nuclear phenomena in terms of interplay of spin and isospin, which will in turn, lead us to better understanding of our universe.

2. Major Research Subjects

(1) Direct reaction studies of neutron-matter equation of state
(2) Study of spin-isospin responses with RI-beams
(3) *r*-process nucleosynthesis study with heavy-ion storage ring
(4) Application of spin-polarization technique to RI-beam experiments and other fields
(5) Development of special targets for RI-beam experiments

3. Summary of Research Activity

(1) Direct reaction studies of neutron matter equation of state

Direct reactions induced by light-ions serve as powerful tools to investigate various aspects of nuclei. We are advancing experimental programs to explore equation of state of neutron matter, via light-ion induced reactions with RI-beams.

(1-1) Determination of a neutron skin thickness by proton elastic scattering

A neutron skin thickness is known to have strong relevance to asymmetry terms of nuclear equation of state, especially to a term proportional to density. The ESPRI project aims at determining density distributions in exotic nuclei precisely by proton elastic scattering at 200–300 MeV/nucleon. An experiment for ^{132}Sn that is a flagship in this project has been successfully performed.

(1-2) Asymmetry terms in nuclear incompressibility

Nuclear incompressibility represents stiffness of nuclear matter. Incompressibility of symmetric nuclear matter is determined to be 230 ± 20 MeV, but its isospin dependence still has a large uncertainty at present. A direct approach to the incompressibility of asymmetric nuclear matter is an experimental determination of energies of isoscalar giant monopole resonances (GMR) in heavy nuclei. We have developed, in close collaboration with Center for Nuclear Study (CNS) of University of Tokyo, an active gas target for deuteron inelastic scattering experiments to determine GMR energies. The active gas target has been already tested with oxygen and xenon beams at HIMAC and finally has been applied to a ^{132}Sn experiment at RIBF.

(1-3) Multi-neutron and α-cluster correlations at low densities

Occurrences of multi-neutron and α-cluster correlations are other interesting aspects of nuclear matter and define its low-density behavior. The multi-neutron and α-cluster correlations can be investigated with the large-acceptance SAMURAI spectrometer. The SAMURAI has been already applied to experiments to explore light neutron-rich nuclei close to the dripline. We plan to reinforce experimental capabilities of the SAMURAI by introducing advanced devices such as MINOS (Saclay) and NeuLAND (GSI).

(1-4) Fission barrier heights in neutron-rich heavy nuclei

The symmetry energy has a strong influence on fission barrier heights in neutron-rich nuclei. Knowledge on the fission barrier heights, which is quite poor at present, is quite important for our proper understanding on termination of the *r*-process. We are planning to perform, in collaboration with the TU Munich group, $(p, 2p)$-delayed fission experiments at the SAMURAI to determine the fission barrier heights in neutron-rich nuclei in Pb region.

(2) Study of spin-isospin responses with RI-beams

The study of spin-isospin responses in nuclei forms one of the important cores of nuclear physics. A variety of collective states, for example isovector giant dipole resonances, isobaric analogue states, Gamow-Teller resonances, have been extensively studied by use of electromagnetic and hadronic reactions from stable targets.

The research opportunities can be largely enhanced with light of availabilities of radioactive isotope (RI) beams and of physics of unstable nuclei. There are three possible directions to proceed. The first direction is studies of spin-isospin responses of unstable nuclei via inverse-kinematics charge exchange reactions. A neutron-detector array WINDS has been constructed, under a collaboration of CNS, Tokyo and RIKEN, for inverse kinematics (p, n) experiments at the RI Beam Factory. We have already applied WINDS to the (p, n) experiments for ^{12}Be, ^{132}Sn and plan to extend this kind of study to other exotic nuclei.

The second direction is studies with RI-beam induced charge exchange reaction. RI-beam induced reactions have unique properties which are missing in stable-beam induced reactions and can be used to reach the yet-to-be-discovered states. We have constructed the SHARAQ spectrometer and the high-resolution beam-line at the RI Beam Factory to pursue the capabilities of RI-beam induced reactions as new probes to nuclei. One of the highlights is an observation of β^+ type isovector spin monopole resonances (IVSMR) in ^{208}Pb and ^{90}Zr via the $(t, ^3\mathrm{He})$ reaction at 300 MeV/nucleon.

The third direction is studies of neutron- and proton-rich nuclei via stable-beam induced charge exchange reactions, which is conducted under collaboration with Research Center for Nuclear Physics (RCNP), Osaka University. We have performed the double

charge exchange ^{12}C(^{18}O, ^{18}Ne)^{12}Be reaction at 80 MeV/nucleon to investigate structure of a neutron-rich ^{12}Be nucleus. Peaks corre- sponding to ground and excited levels in ^{12}Be have been clearly observed. Another double charge exchange reaction, (^{12}C, ^{12}Be(0^+)) are being used to search for double Gamow-Teller resonances.

(3) *r*-process nucleosynthesis study with heavy-ion storage ring

Most of the *r*-process nuclei become within reach of experimental studies for the first time at RI Beam Factory at RIKEN. The Rare RI Ring at RIBF is the unique facility with which we can perform mass measurements of *r*-process nuclei. Construction of the Rare RI Ring started in FY2012 in collaboration with Tsukuba and Saitama Universities. A major part of the ring has been completed and the commissioning run is planned in FY2014.

We are planning to start precise mass measurements of *r*-process nuclei soon. A series of experiments will start with nuclei in the $A = 80$ region and will be extended to heavier region.

(4) Application of spin-polarization technique to RI-beam experiments and other fields

A technique to produce nuclear polarization by means of electron polarization in photo-excited triplet states of aromatic molecules can open new applications. The technique is called "Tripletd-DNP." A distinguished feature of Triplet-DNP is that it works under a low magnetic field of 0.1–0.7 T and temperature higher than 100 K, which exhibits a striking contrast to standard dynamic nuclear polarization (DNP) techniques working in extreme conditions of several Tesla and sub-Kelvin.

We have constructed a polarized proton target system for use in RI-beam experiments. Recent experimental and theoretical studies have revealed that spin degrees of freedom play a vital role in exotic nuclei. Tensor force effects on the evolution of shell and possible occurrence of *p*-*n* pairing in the proton-rich region are good examples of manifestations of spin degrees of freedom. Experiments with the target system allow us to explore the spin effects in exotic nuclei. It should be noted that we have recently achieved a proton polarization of 40% at room temperature in a pentacene-d_{14} doped *p*-terphenyl crystal.

Another interesting application of Triplet-DNP is sensitivity enhancement in NMR spectroscopy of biomolecules. We started a new project to apply the Triplet-DNP technique to study protein-protein interaction via two-dimensional NMR spectroscopy, in close collaboration with biologists and chemists.

(5) Development of special targets for RI-beam experiments

For the research activities shown above, we are developing and hosting special targets for RI-beam experiments listed below:

(a) Polarized proton target (described in (4))
(b) Thin solid hydrogen target
(c) MINOS (developed at Saclay and hosted by the Spin Isospin Laboratory)

Members

Director

Tomohiro UESAKA

Senior Research Scientists

Masaki SASANO
Juzo ZENIHIRO
Ken-ichiro YONEDA

Research Scientists

Sarah NAIMI
Kenichiro TATEISHI

Research & Development Scientist

Yohei SHIMIZU

Postdoctoral Researcher

Junki TANAKA

Junior Research Associates

Shutaro HANAI
Tomoya HARADA

International Program Associates

Siwei HUANG
Yutian LI

Research Consultants

Harutaka SAKAGUCHI (Osaka Univ.)
Kazuko TANABE
Yasuyuki SUZUKI

Senior Visiting Scientist

Hiroyuki SAGAWA (Univ. of Aizu)

Visiting Scientists

Satoshi ADACHI (Osaka Univ.)
Hidetoshi AKIMUNE (Konan Univ.)
Didier BEAUMEL (Inst. de Phys.Nucl.)
Konstanze BORETZKY (GSI)
Anna CORSI (CEA Saclay)
Masanori DOZONO (Kyoto Univ.)
Zoltan ELEKES (ATOMKI)
Zsolt FULOP (ATOMKI)
Tatsuya FURUNO (Osaka Univ.)
Igor GASPARIC (Rudjer Boskovic Inst.)
Valdir GUIMARAES (Inst.o de Fisica da Univ. de Sao Paulo)
Zoltan HALASZ (ATOMKI)
Kaori KAKI (Shizuoka Univ.)
Takahiro KAWABATA (Osaka Univ.)
Yuma KIKUCHI (NIT, Tokuyama College)
Yosuke KONDO (Tokyo Tech)
Zeren KORKULU (Inst. for Basic Sci. (IBS))
Attila KRASZNAHORKAY (ATOMKI)
Dorottya KUNNE SOHLER (ATOMKI)
Istvan KUTI (ATOMKI)
Valerie LAPOUX (Inst.ion CEA-Saclay)
Yury LITVINOV (GSI)
Hongna LIU (TU Darmstadt)
Yohei MATSUDA (Konan Univ.)
Kenjiro MIKI (Tohoku Univ.)
Tetsuaki MORIGUCHI (Tsukuba Univ.)
Sarah NAIMI (IJCLab (Laboratoire de physique des 2 infinis - Irene Joliot-Curie))
Takashi NAKAMURA (Tokyo Tech)
Noritsugu NAKATSUKA (Tokyo Tech)
Alexandre OBERTELLI (TU Darmstadt)
Kazuyuki OGATA (Osaka Univ.)
Valerii PANIN (GSI)
Aldric REVEL (CEA Saclay)
Kimiko SEKIGUCHI (Tokyo Tech)
Laszlo STUHL (Inst. for Basic Sci. (IBS))
Baohua SUN (Beihang Univ.)
Yelei SUN (TU Darmstadt)
Shinji SUZUKI (Chinese Academy of Sci.)
Satoru TERASHIMA (Beihang Univ.)
Yasuhiro TOGANO (Rikkyo Univ.)
Takashi WAKUI (QST)
Atomu WATANABE (JSPS)
Takayuki YAMAGUCHI (Saitama Univ.)
Zaihong YANG (Osaka Univ.)
Juzo ZENIHIRO (Kyoto Univ.)
Yuhu ZHANG (IMP, CAS)

Visiting Technicians

Denis CALVET (CEA)
Alain DELBART (CEA/CE Saclay)
Clement HILAIRE (CEA Saclay)
Shoji SUZUKI (KEK)
Olivier TELLIER (CEA Saclay)

Student Trainees

Tomoki ADACHI (Kyushu Univ.)
Sota ANDO (Kyushu Univ.)
Paul ANDRE (CEA Saclay)
Naoki EBINA (Tokyo Tech)
Shiyo EN'YO (Kyoto Univ.)
Yuki FUJIKAWA (Kyoto Univ.)
Saiya FUJIWARA (Kyushu Univ.)
Jian GAO (Peking Univ.)
Shutaro HANAI (Univ. of Tokyo)
Sakumi HARAYAMA (Saitama Univ.)
Koshi HIGUCHI (Saitama Univ.)
Kouta HORIKAWA (Tokyo Tech)
Kento INABA (Kyoto Univ.)
Kakeru ISOBE (Tokyo Tech)
Koki KAMEYA (Tohoku Univ.)
Naoto KANAME (Tsukuba Univ.)
Masanori KANDA (Saitama Univ.)
Fumiya KAWAGUCHI (Tokyo Tech)
Yusuke KAWASHIMA (Kyushu Univ.)
Kanki KISHIMOTO (Kyushu Univ.)
Sho KITAYAMA (Tohoku Univ.)
Yukari KOIZUMI (Saitama Univ.)
Hyeji LEE (Tokyo Tech.)
Hongfu LI (IMP, CAS)
Yoshiki MARUTA (Tohoku Univ.)
Takaya MATSUI (Tohoku Univ.)
Tomoki MATSUI (Tokyo Tech)
Riku MATSUMURA (Saitama Univ.)
Atsuyuki MORIYAMA (Tsukuba Univ.)
Shintaro OKAMOTO (Kyoto Univ.)
Kengo OKUBO (Saitama Univ.)
Misaki OTSU (Saitama Univ.)
Yuko SAITO (Tohoku Univ.)
Kosuke SAKANASHI (Osaka Univ.)
Kenta SASAKI (Saitama Univ.)
Hibiki SEKI (Saitama Univ.)
Yusuke SHINOHARA (Kyushu Univ.)
Naru SHINOZAKI (Saitama Univ.)
Kohei TAKAHASHI (Tokyo Tech)
Ryotaro TSUJI (Kyoto Univ.)
Ren URAYAMA (Tohoku Univ.)
Kanta YAHIRO (Kyoto Univ.)
Kohei YAMAMOTO (Tohoku Univ.)
Wataru YAMASHITA (Kyushu Univ.)
Asahi YANO (Tsukuba Univ.)
Nozomi YOKOTA (Kyushu Univ.)
Chieko YONEMURA (Kyushu Univ.)
Ryohsuke YOSHIDA (Kyoto Univ.)

Assistants

Emiko ISOGAI Yuri TSUBURAI

List of Publications & Presentations

Publications

[Original Papers]

V. P. Ladygin, A. V. Averyanov, E. V. Chernykh, D. Enache, Yu. V. Gurchin, A. Yu. Isupov, M. Janek, J. -T. Karachuk, A. N. hrenov, D. O. Krivenkov, P. K. Kurilkin, N. B. Ladygina, A. N. Livanov, O. Mezhenska, S. M. Piyadin, S. G. Reznikov, Y. T. Skhomenko, A. A. Terekhin, A. V. Tishevsky, T. Uesaka, and I. S. Volkov, "Deuteron analyzing powers A_y, A_{yy}, and A_{xx} in dp-elastic scattering at large transverse momenta," JPS Conf. Proc. **37**, 020902 (2022).

T. Aumann, W. Bartmann, O. Boine-Frankenheim, A. Bouvard, A. Broche, F. Butin, D. Calvet, J. Carbonell, P. Chiggiato, H. De Gersem, R. De Oliveira, T. Dobers, F. Ehm, J. Ferreira Somoza, J. Fischer, M. Fraser, E. Friedrich, A. Frotscher, M. Gomez-Ramos, J. -L. Grenard, A. Hobl, G. Hupin, A. Husson, P. Indelicato, K. Johnston, C. Klink, Y. Kubota, R. Lazauskas, S. Malbrunot-Ettenauer, N. Marsic, W. F. O Müller, S. Naimi, N. Nakatsuka, R. Necca, D. Neidherr, G. Neyens, A. Obertelli, Y. Ono, S. Pasinelli, N. Paul, E. C. Pollacco, D. Rossi, H. Scheit, M. Schlaich, A. Schmidt, L. Schweikhard, R. Seki, S. Sels, E. Siesling, T. Uesaka, M. Vilén, M. Wada, F. Wienholtz, S. Wycech, and S. Zacarias, "PUMA, antiProton unstable matter annihilation," Eur. Phys. J. A **58**, 88 (2022).

V. P. Ladygin, A. V. Averyanov, E. V. Chernykh, D. Enache, Y. V. Gurchi, A. Y. Isupov, M. Janek, J. T. Karachuk, A. N. Khrenov, D. O. Krivenkov, P. K. Kurilkin, N. B. Ladygina, A. N. Livanov, S. M. Piyadin, S. G. Reznikov, A. A. Terekhin, A. V. Tishevsky, T. Uesaka, and I. S. Volkov, "Angular dependences of the deuteron analyzing powers in elastic dp scattering at large transverse momenta," Phys. Part. Nucl. **53**, 251 (2022).

M. Duer, T. Aumann, R. Gernhäuser, V. Panin, S. Paschalis, D. M. Rossi, N. L. Achouri, D. Ahn, H. Baba, C. A. Bertulani, M. Böhmer, K. Boretzky, C. Caesar, N. Chiga, A. Corsi, D. Cortina-Gil, C. A. Douma, F. Dufter, Z. Elekes, J. Feng, B. Fernández-Domínguez, U. Forsberg, N. Fukuda, I. Gasparic, Z. Ge, J. M. Gheller, J. Gibelin, A. Gillibert, K. I. Hahn, Z. Halász, M. N. Harakeh, A. Hirayama, M. Holl, N. Inabe,T. Isobe, J. Kahlbow, N. Kalantar-Nayestanaki, D. Kim, S. Kim, T. Kobayashi, Y. Kondo, D. Körper, P. Koseoglou, Y. Kubota, I. Kuti, P. J. Li, C. Lehr, S. Lindberg, Y. Liu,F. M. Marqués, S. Masuoka, M. Matsumoto, J. Mayer, K. Miki, B. Monteagudo, T. Nakamura, T. Nilsson, A. Obertelli, N. A. Orr, H. Otsu, S. Y. Park, M. Parlog, P. M. Potlog, S. Reichert, A. Revel, A. T. Saito, M. Sasano, H. Scheit, F. Schindler, S. Shimoura, H. Simon, L. Stuhl, H. Suzuki, D. Symochko, H. Takeda, J. Tanaka, Y. Togano, T. Tomai, H. T. Törnqvist, J. Tscheuschner, T. Uesaka, V. Wagner, H. Yamada, B. Yang, L. Yang, Z. H. Yang, M. Yasuda, K. Yoneda, L. Zanetti, J. Zenihiro and M. V. Zhukov, "Observation of a correlated free four-neutron system," Nature **606**, 678 (2022).

A. I. Stefanescu, V. Panin, L. Trache, T. Motobayashi, H. Otsu, A. Saastamoinen, T. Uesaka, L. Stuhl, J. Tanaka, D. Tudor, I. C. Stefanescu, A. E. Spiridon, K. Yoneda, H. Baba, M. Kurokawa, Y. Togano, Z. Halasz, M. Sasano, S. Ota, Y. Kubota, D. S. Ahn, T. Kobayashi, Z. Elekes, N. Fukuda, H. Takeda, D. Kim, E. Takada, H. Suzuki, K. Yoshida, Y. Shimizu, H. N. Liu, Y. L. Sun, T. Isobe, J. Gibelin, P. J. Li, J. Zenihiro, F. M. Marqués, M. N. Harakeh, G. G. Kiss, A. Kurihara, M. Yasuda, T. Nakamura, S. Park, Z. Yang, T. Harada, M. Nishimura, H. Sato, I. S. Hahn, K. Y. Chae, J. M. Elson, L. G. Sobotka, and C. A. Bertulani, "Silicon tracker array for RIB experiments at SAMURAI," Eur. Phys. J. A **58**, 223 (2022).

M. Enciu, H. N. Liu, A. Obertelli, P. Doornenbal, F. Nowacki, K. Ogata, A. Poves, K. Yoshida, N. L. Achouri, H. Baba, F. Browne, D. Calvet, F. Château, S. Chen, N. Chiga, A. Corsi, M. L. Cortés, A. Delbart, J. -M. Gheller, A. Giganon, A. Gillibert, C. Hilaire, T. Isobe, T. Kobayashi, Y. Kubota, V. Lapoux, T. Motobayashi, I. Murray, H. Otsu, V. Panin, N. Paul, W. Rodriguez, H. Sakurai, M. Sasano, D. Steppenbeck, L. Stuhl, Y. L. Sun, Y. Togano, T. Uesaka, K. Wimmer, K. Yoneda, O. Aktas, T. Aumann, L. X. Chung, F. Flavigny, S. Franchoo, I. Gasparic, R. -B. Gerst, J. Gibelin, K. I. Hahn, D. Kim, Y. Kondo, P. Koseoglou, J. Lee, C. Lehr, P. J. Li, B. D. Linh, T. Lokotko, M. Maccormick, K. Moschner, T. Nakamura, S. Y. Park, D. Rossi, E. Sahin, P. -A. Söderström, D. Sohler, S. Takeuchi, H. Toernqvist, V. Vaquero, V. Wagner, S. Wang, V. Werner, X. Xu, H. Yamada, D. Yan, Z. Yang, M. Yasuda, and L. Zanetti, "Extended $p_{3/2}$ Neutron Orbital and the $N = 32$ Shell Closure in ^{52}Ca ," Phys. Rev. Lett. **129**, 262501 (2022).

T. Nishi, K. Itahashi, D. Ahn, G. P. A. Berg, M. Dozono, D. Etoh, H. Fujioka, Naoki Fukuda, N. Fukunishi, H. Geissel, E. Haettner, T. Hashimoto, R. S. Hayano, S. Hirenzaki, H. Horii, N. Ikeno, N. Inabe, M. Iwasaki, D. Kameda, K. Kisamori, Y. Kiyokawa, T. Kubo, K. Kusaka, M. Matsushita, S. Michimasa, G Mishima, H. Miya, D. Murai, H. Nagahiro, M. Niikura, N. N. -Togawa, S. Ota, N. Sakamoto, K. Sekiguchi, Y. Shiokawa, H. Suzuki, K. Suzuki, M. Takaki, H. Takeda, Y. K. Tanaka, T. Uesaka, Y. Wada, A. Watanabe, Y. N. Watanabe, H. Weick, H. Yamakami, Y. Yanagisawa, K. Yoshida, and piAF Collaboration, "Chiral symmetry restoration at high matter density observed in pionic atoms," Nat. Phys. **19**, 788–793 (2023). DOI:10.1038/s41567-023-02001-x .

Y. Kawashima, T. Hamachi, A. Yamauchi, K. Nishimura, Y. Nakashima, S. Fujiwara, N. Kimizuka, T. Ryu, T. Tamura, M. Saigo, K. Onda, S. Sato, Y. Kobori, K. Tateishi, T. Uesaka, G. Watanabe, K. Miyata and N. Yanai, "Singlet fission as a polarized spin generator for dynamic nuclear polarization," Nat. Commun. **14**, 1056 (2023).

K. Nishimura, R. Yabuki, T. Hamachi, N. Kimizuka, K. Tateishi, T. Uesaka, and N. Yanai, "Dynamic electron polarization lasting more than 10 μs by hybridizing porphyrin and TEMPO with flexible linkers," J. Phys. Chem. B **127**, 1219 (2023).

H. F. Li, S. Naim, T. M. Sprouse, M. R. Mumpower, Y. Abe, Y. Yamaguchi, D. Nagae, F. Suzaki, M. Wakasugi, H. Arakawa, W. B. Dou, D. Hamakawa, S. Hosoi, Y. Inada, D. Kajiki, T. Kobayashi, M. Sakaue, Y. Yokoda, T. Yamaguchi, R. Kagesawa, D. Kamioka, T. Moriguchi, M. Mukai, A. Ozawa, S. Ota, N. Kitamura, S. Masuoka, S. Michimasa, H. Baba, N. Fukuda, Y. Shimizu, H. Suzuki, H. Takeda, D. S. Ahn, M. Wang, C. Y. Fu, Q. Wang, S. Suzuki, Z. Ge, Yu. A. Litvinov, G. Lorusso, P. M. Walker, Zs. Podolyak, and T. Uesaka, "First application of mass measurements with the Rare-RI Ring reveals the solar r-process abundance trend at $A = 122$ and $A = 123$," Phys. Rev. Lett. **128**, 152701 (2022).

S. Kaur, R. Kanungo, W. Horiuchi, G. Hagen, J. D. Holt, B. S. Hu, T. Miyagi, T. Suzuki, F. Ameil, J. Atkinson, Y. Ayyad, S. Bagchi, D. Cortina-Gil, I. Dillmann, A. Estradé, A. Evdokimov, F. Farinon, H. Geissel, G. Guastalla, R. Janik, R. Knöbel, J. Kurcewicz,

Y. A. Litvinov, M. Marta, M. Mostazo, I. Mukha, C. Nociforo, H. J. Ong, T. Otsuka, S. Pietri, A. Prochazka, C. Scheidenberger, B. Sitar, P. Strmen, M. Takechi, J. Tanaka, I. Tanihata, S. Terashima, J. Vargas, H. Weick, and J. S. Winfield, "Proton distribution radii of $^{16\text{–}24}$O: signatures of new shell closures and neutron skin," Phys. Rev. Lett. **129**, 142502 (2022).

K. Yoshida and J. Tanaka, "α knockout reaction as a new probe for α formation in α-decay," Phys. Rev. C **106**, 014621 (2022).

H. Sagawa, S. Yoshida, T. Naito, T. Uesaka, J. Zenihiro, J. Tanaka, and T. Suzuki, "Isovector density and isospin impurity in ^{40}Ca," Phys. Lett. B **829**, 137072 (2022).

M. Heil, A. Kelić-Heil, L. Bott, T. Almusidi, H. Alvarez-Pol, L. Atar, L. Atkins, T. Aumann, J. Benlliure, K. Boretzky, B. Brückner, P. Cabanelas, C. Caesar, E. Casarejos, J. Cederkall, L. Chulkov, A. Corsi, J. Dueñas, P. Erbacher, S. E. Rodriguez, A. Falduto, M. Feijoo, A. Frotscher, J. Frühauf, I. Gašparić, M. J. G. Borge, J. Gerbig, R. Gernhäuser, M. Gilbert, J. Glorius, B. Gnoffo, K. Göbel, D. G. Caamaño, A. Grein, A. -L. Hartig, H. Heggen, M. Heine, A. Heinz, M Holl, I. Homm, A. Horvat, H. T. Johansson, B. Jonson, N. Kalantar-Nayestanaki, A. Kamenyero, A. Khodaparast, O. Kiselev, P. Klenze, M. Knösel, K. Koch, D. Körper, T Kröll, D Kurtulgil, N Kurz, B Löher, C Langer, C Lehr, Y Litvinov, H Liu, S Murillo Morales, E Nácher, T Nilsson, J Park, S. Paschalis, L. Pellegri, A. Perea, M. Petri, T. Pohl, L. Ponnath, R. Popočovski, R. Reifarth, H. -B. Rhee, J. L. Sanchez, D. Rossi, C. Sürder, A. M. Sánchez-Benítez, D. Savran, H. Scheit, H. Simon, Z. Slavkovská, S. Storck-Dutine, Y. Sun, H. T. Törnqvist, J. Tanaka, O. Tengblad, B. Thomas, L. Varga, M. Volknandt, V. Wagner, F. Wamers, L. Zanetti, "A new Time-of-flight detector for the R3B setup," Eur. Phys. J. A **58**, 248 (2022).

T. Koiwai, K. Wimmer, P. Doornenbal, A. Obertelli, C. Barbieri, T. Duguet, J. Holt, T. Miyagi, P. Navrátil, K. Ogata, N. Shimizu, V. Somà, Y. Utsuno, K. Yoshida, N. Achouri, H. Baba, F. Browne, D. Calvet, F. Château, S. Chen, N. Chiga, A. Corsi, M. Cortés, A. Delbart, J. -M. Gheller, A. Giganon, A. Gillibert, C. Hilaire, T. Isobe, T. Kobayashi, Y. Kubota, V. Lapoux, H. Liu, T. Motobayashi, I. Murray, H. Otsu, V. Panin, N. Paul, W. Rodriguez, H. Sakurai, M. Sasano, D. Steppenbeck, L. Stuhl, Y. Sun, Y. Togano, T. Uesaka, K. Yoneda, O. Aktas, T. Aumann, L. Chung, F. Flavigny, S. Franchoo, I. Gasparic, R. -B. Gerst, J. Gibelin, K. Hahn, D. Kim, Y. Kondo, P. Koseoglou, J. Lee, C. Lehr, B. Linh, T. Lokotko, M. MacCormick, K. Moschner, T. Nakamura, S. Park, D. Rossi, E. Sahin, P. -A. Söderström, D. Sohler, S. Takeuchi, H. Toernqvist, V. Vaquero, V. Wagner, S. Wang, V. Werner, X. Xu, H. Yamada, D. Yan, Z. Yang, M. Yasuda, and L. Zanetti, "A first glimpse at the shell structure beyond ^{54}Ca: Spectroscopy of ^{55}K, ^{55}Ca, and ^{57}Ca," Phys. Lett. B **827**, 136953 (2022).

B. Le Croma, M. Assi'ea, Y. Blumenfelda, J. Guillota, H. Sagawab, T. Suzukic, M. Honmab, N. L. Achourid, B. Bastine, R. Borceaf, W. N. Catfordg, E. Cl'emente, L. C'acerese, M. Caama'noh, A. Corsii, G. De Francee, F. Delaunayd, N. De S'er'evillea, B. Fernandez-Dominguezh, M. Fisichellaj, S. Franchooa, A. Georgiadoua, J. Gibelind, A. Gilliberti, F. Hammachea, O. Kamaloue, A. Knaptong, V. Lapouxi, S. Leblondd, A. O. Macchiavellik, F. M. Marqu'esd, A. Mattag, L. M'enagere, P. Morfouacea, N. A. Orrd, J. Pancine, X. Pereira-Lopezd,h, L. Perrota, J. Piote, E. Pollaccoi, D. Ramos, T. Rogere, F. Rotaruf, A. M. S'anchez-Ben'ıtezl, M. S'enovillei, O. Sorline, M. Stanoiuf, I. Stefana, C. Stodele, D. Suzukia, J. -C. Thomase, and M. Vandebrouck, "Neutron-proton pairing in the $N = Z$ radioactive fp-shell nuclei ^{56}Ni and ^{52}Fe probed by pair transfer," Phys. Lett. B **829**, 137057 (2022).

Y. Tanimura, H. Sagawa, T. Sun, and E. Hiyama, "Xi hypernuclei ^{15}XiC, ^{12}XiBe and Xi-N two-body interaction," Phys. Rev. C **105**, 044324 (2022).

M. J. Yang, C. L. Bai, H. Sagawa, and H. Q. Zhang, "The Gamow-Teller transitions in magic nuclei calculated by the charge-exchange subtracted second random phase approximation," Phys. Rev. C **106**, 014319 (2022).

J. -Y. Xu, Z. -Z. Li, B. -H. Sun, Y. -F. Niu, X. Roca-Maza, H. Sagawa, and I. Tanihata, "Constraining equation of state of nuclear matter by charge-changing cross section measurements of mirror nuclei," Phys. Lett. B **833**, 137333 (2022).

K. Hagino and H. Sagawa, "Spatial correlation of a particle-hole pair with a repulsive isovector interaction," Phys. Phys. C **106**, 034313 (2022).

T. Naito, X. Roca-Maza, G. Colo, H. Liang, and H. Sagawa, "Isospin symmetry breaking in the charge radius difference of mirror nuclei," Phys. Rev. C **106**, L061306 (2022).

M. J. Yang, H. Sagawa, C. L. Bai, and H. Q. Zhang, "Effects of two particle-two hole configurations and tensor force on beta decay of magic nuclei," Phys. Rev. C **107**, 014325 (2023).

N. Matsumoto, K. Nishimura, N. Kimizuka, Y. Nishiyama, K. Tateishi, T. Uesaka, and N. Yanai, "Proton hyperpolarization relay from nanocrystals to liquid water," J. Am. Chem. Soc. **144**, 18023 (2022).

T. Furuno, T. Doi, K. Himi, T. Kawabata, S. Adachi, H. Akimune, S. Enyo, Y. Fujikawa, Y. Hijikata, K. Inaba, M. Itoh, S. Kubono, Y. Matsuda, I. Murat, M. Murata, S. Okamoto, K. Sakanash, and S. Tamaki, "Measurement of ^{12}C(n, n') reaction cross section to determine triple-alpha reaction rate in high-density environments," EPJ Web Conf. **260**, 11010 (2022).

M. Abdullah, S. Bagchi, M. N. Harakeh, and the E497 collaboration, "Effect of ground-state shape deformation on the isoscalar giant monopole resonance in Nd isotopes," Proc. DAE Symp. Nucl. Phys. **66**, 94 (2022).

Presentations

[International Conferences/Workshops]

H. Sagawa (invited), "What can we learn from the nuclear ground state densities?," 6th Topical Workshop on Modern Aspects in Nuclear Stracutre, Bormio, Italy, February 6–11, 2022.

H. Sagawa (invited), "Beyond mean field model for nuclear collective states," The 16th International Symposium on Origin of Matter and Evolution of Galaxies (OMEG2022), Hanoi, Vietnam, October 25–28, 2022.

H. Sagawa (invited), "What can we learn from the nuclear ground state densities?," Physics of RI: Recent progress andperspectives, RIKEN, Saitama, Japan, May 30–June 1, 2022.

H. Sagawa (oral), "Some topics of isoscalar spin-triplet pairing," YIPQS long-term workshop, "Mean-field and cluster dynamics in nuclear systems 2022 (MCD2022), Kyoto University, Kyoto, May 9–June 17, 2023.

H. Sagawa (invited), "What can we learn from the nuclear ground state densities?," Focus Program: A quest for exotica in rare-earth elements, Pohang, Korea, August 22–26, 2022.

J. Tanaka (invited), "Clustering phenomena in dilute neutron-rich matter," The 15th Asia Pacific Physics Conference (APPC15) August 21–26, 2022.

Y. Kubota (invited), "Surface localization of the dineutron in nuclei," in Halo Week 2022, Bergen, Norway, 2022.

Y. Kubota (oral), "Recent updates on SAMURAI18 experiment," in SAMURAI International Collaboration Workshop 2022, Ookayama, Japan, 2022.

Y. Kubota (oral), "SAMURAI: Recent advances in analysis and prospects for future experiments," in RIBF Users Meeting 2022.

Y. Hijikata (oral), "Developmetn of gaseous Xe scintillator for particle identification of high-intensity RI beams," The 2022 Annual Meeting of the JSPS/NSFC/NRF A3 Foresight Program, Osaka, Japan, February 14, 2023.

T. Tsuji (oral), "Development of TOGAXSI array," SAMURAI International Collaboration Workshop 2022, Meguro-ku, Tokyo (Tokyo titech University), September 2–3, 2022.

T. Tsuji (oral), "Development of large GAGG:Ce calorimeter for measurements of the cluster knockout reactions," A3 Foresight Annual Meeting 2022, Osaka, Japan (OsakaInternational Convention Center), February 13–15, 2023.

T. Uesaka (invited), "Clustering in heavy nuclei probed with knockout reactions," 6th Topical Workshop on Modern Aspects in Nuclear Stracutre, Bormio, Italy, February 6–11, 2022.

T. Uesaka (invited), "Recent progress in nuclear cluster physics," 28th International Nuclear Physics Conference (INPC 2022), Cape town, South Africa, September 11–16, 2022.

T. Uesaka (invited), "ONOKORO project—knockout reaction studies of clusters in heavy nuclei—," Direct Reactions with Exotic Beams (DREB2022), Santiago de Compostela, Spain, June 26–July 1, 2022.

J. Tanaka (poster), "Detector array TOGAXSI for inverse-kinematics cluster and nucleon knockout reaction experiment," EMIS 2022, Daejeon, Korea, October 3–7, 2022.

Y. Hijikata (poster), "Development of gaseous Xe scintillator for particle identification of high-intensity and heavy-ion beams," EMIS 2022, Daejeon, Korea, October 3–7, 2022.

R. Tsuji (poster) , "Development of large GAGG:Ce calorimeter for measurements of the cluster knockout reactions," EMIS2022, Dejean, Korea, October 3–7, 2022.

K. Higuchi (poster), "Development of silicon-strip for cluster knockout reactions," EMIS2022, Daejon, Korea, October 3–7, 2022.

[Domestic Conferences/Workshops]

田中純貴（招待講演), 「原子核基底状態のアルファクラスターと ONOKORO プロジェクト」, 日本物理学会 2023 年春季大会, シンポジウム講演, 2023 年 3 月 22–25 日.

久保田悠樹（招待講演), 「ノックアウト反応で調べるボロミアン核のダイニュートロン相関」, RCNP 研究会「微視的系と巨視的系における核子対凝縮相」, 茨木市 (大阪大学核物理研究センター), 2022 年 9 月 26–28 日.

立石健一郎（口頭論文), 「トリプレット DNP による室温核偏極: 原理・装置・現状の課題」, DNP 研究会, 豊中市 (大阪大学南部陽一郎ホール), 2022 年 7 月 12 日.

立石健一郎（口頭論文), 「核スピン偏極技術とその応用」, 第 4 回若手放談会: エキゾチック核物理の将来, 神戸市 (理研神戸), 2023 年 3 月 15–17 日.

立石健一郎（口頭論文), 「Development of High-temperature Nuclear Polarization Method for Hypersensitive NMR Spectroscopy」, Frontier of Dynamic Structural Biology, 吹田市 (大阪大学), 2022 年 10 月 17–18 日.

土方佑斗（口頭論文), 「錫 112 の弾性散乱と錫同位体でのアイソスカラー・アイソベクトル密度分布変化」, おのころ戸隠夏合宿, 長野市 (JA 長野県ビル), 2022 年 7 月 29–31 日.

樋口浩志（口頭論文), 「クラスターノックアウト反応に向けた荷電粒子用シリコン・ストリップ検出器の開発」, 日本物理学会 2022 年春季大会, 2022 年 3 月 15–18 日.

樋口浩志（口頭論文), 「Strip-Si detector performance report from HIMAC exp」, おのころプロジェクトローカルコラボレーションミーティング, 京都市, 2022 年 5 月 19–20 日.

樋口浩志（口頭論文), 「TOGAXSI で調べる核内クラスターのシェル構造」, おのころプロジェクト戸隠夏合宿, 長野市 (JA 長野県ビル), 2022 年 7 月 29–30 日.

辻崚太郎（口頭論文), 「GAGG(Ce) performance; report from HIMAC exp」, おのころプロジェクトローカルコラボレーションミーティング, 京都市, 2022 年 5 月 19–20 日.

辻崚太郎（口頭論文), 「$^{40-52}$Ca(p, pX) とクラスター種の同位体依存性」, おのころプロジェクト戸隠夏合宿, 長野市 (JA 長野県ビル), 2022 年 07 月 29–30 日.

土方佑斗（ポスター), 「原子核実験の先端データ収集システム—標準化と将来—」, 茨木市 (大阪大学 RCNP), 2023 年 3 月 16 日.

Awards

久保田悠樹, 第 29 回 原子核談話会新人賞.

久保田悠樹, 第 17 回 日本物理学会若手奨励賞.

Other

土方佑斗（パネルディスカッション), 「原子核実験の先端データ収集システム—標準化と将来—」, 茨木市（大阪大学 RCNP), 2023 年 3 月 16 日.

Nuclear Science and Transmutation Research Division
Nuclear Spectroscopy Laborarory

1. Abstract

The research group has conducted nuclear-physics studies utilizing stopped/slowed-down radioactive-isotope (RI) beams mainly at the RIBF facility. These studies are based on the technique of nuclear spectroscopy such as β-ray-detected NMR (β-NMR), γ-PAD (Perturbed Angular Distribution), laser, and Mössbauer among other methods that takes advantage of intrinsic nuclear properties such as nuclear spins, electromagnetic moments, and decay modes. In particular, techniques and devices for the production of spin-controlled RI beams have been developed and combined to the spectroscopic studies, which enable high-sensitivity measurements of spin precessions/resonances through a change in the angular distribution of radiations. Anomalous nuclear structures and properties of far unstable nuclei are investigated from thus determined spin-related observables. The group also aims to apply such techniques to interdisciplinary fields such as fundamental physics and materials science by exploiting nuclear probes.

2. Major Research Subjects

(1) Nuclear spectroscopy utilizing spin-oriented fast RI beams
(2) Nuclear/Atomic laser spectroscopy & SLOWRI R&D
(3) Application of RI probes to materials science
(4) Fundamental physics: Study of symmetry

3. Summary of Research Activity

(1) Nuclear spectroscopy utilizing spin-oriented fast RI beams

Measurements of static electromagnetic nuclear moments over a substantial region of the nuclear chart have been conducted for structure studies on the nuclei far from the β-decay stability. Utilizing nuclear spin orientation phenomena of RIs created in the projectile-fragmentation reaction, ground- and excited-state electromagnetic nuclear moments been determined by means of the β-ray-detected nuclear magnetic resonance (β-NMR) and the γ-ray time differential perturbed angular distribution (γ-TDPAD) methods. In particular, a new method developed for controlling spin in a system of rare RIs, taking advantage of the mechanism of the two-step projectile fragmentation reaction combined with the momentum-dispersion matching technique, has been developed and employed making fully use of world's highest intensity rare RIBs delivered from BigRIPS for rare isotopes.

(2) Nuclear/Atomic laser spectroscopy & SLOWRI R&D

The group has been conducting system development for nuclear laser spectroscopy from the following two approaches in order to realize experiments for rare isotopes at RIBF. One is collinear laser spectroscopy for a large variety of elements using slowed-down RI beams produced via a projectile-fragmentation reaction, which can be achieved only by the universal low-energy RI-beam delivery system, SLOWRI, under installation in collaboration with the SLOWRI Team. This slowed-down RI-beam scheme enables to perform high-precision laser spectroscopy even with fast-fragmentation-based RIBs without the elemental limitation problematic in the ISOL-based RIBs.

The other approach is a new method utilizing superfluid helium (He II) as a stopping medium of energetic RI beams, in which the characteristic atomic properties of ions surrounded by superfluid helium enables us to perform unique nuclear laser spectroscopy. RI ions trapped in He II are known to exhibit a characteristic excitation spectrum significantly blue-shifted compared with the emission one. Consequently, the background derived from the excitation-laser stray light, which often causes serious problems in measurements, can be drastically reduced.

(3) Application of RI probes to materials science

The application of RI and heavy ion beams as a probe for condensed matter studies is also conducted by the group. The microscopic material dynamics and properties have been investigated through the deduced internal local fields and the spin relaxation of RI probes based on various spectroscopies utilizing RI probes such as β-NMR/NQR spectroscopy, Mössbauer spectroscopy, the γ-ray time differential perturbed angular correlation (γ-TDPAC) spectroscopy. Furthermore, studies on the control of electrical conductivity of diamond by boron and nitrogen implantation are ongoing.

Provided that highly spin-polarized RI probes are produced independently of their element properties and doped into a substance as an impurity, the constituent particle of the substance can be substituted by the same element RI probe without changing the material structure. This scheme provides a new opportunity for materials-science researches, but a key technology, production of element-independent highly spin-polarized RI beams, has not yet been achieved. In this subject, the group has conducted R&D studies to realize an ultra-slow & highly-spin-polarized RI beams, based on the technique of the atomic beam resonance.

(4) Fundamental physics: Study of symmetry

The nuclear spins of stable and unstable isotopes sometimes play important roles in fundamental physics research. New experimental methods and devices have been developed for studies of the violation of time reversal symmetry (T-violation) using spin-polarized nuclei. These experiments aim to detect the small frequency shift in the spin precession arising from new mechanisms beyond the Standard Model.

Members

Director

Hideki UENO

Research/Technical Scientists

Hiroki YAMAZAKI (Senior Research Scientist)
Isao WATANABE (Senior Research Scientist)
Aiko TAKAMINE (Research Scientist)
Shintaro GO (Research Scientist)

Research & Development Scientist

Tetsu SONODA

Contract Researcher

Takashi ABE

Special Postdoctoral Researcher

Momo MUKAI

Postdoctoral Researchers

Minori TAJIMA
Kei IMAMURA (CPR)

Research Associate

Aleksey A. GLADKOV

International Program Associate

Muhammad A. SYAKUUR (Univ. Padjadjaran)

Senior Visiting Scientists

Yukari MATSUO (Hosei Univ.)
Takaharu OTSUKA (Univ. of Tokyo)

Visiting Scientists

Dimiter Loukanov BALABANSKI (IFIN-HH)
Jean-Michel DAUGAS (CNRS)
Georgi GEORGIEV (CNRS-IN2P3)
Yuichi ICHIKAWA (Kyushu Univ.)
Anders KASTBERG (Univ. of Tokyo)
Yoshio KOBAYASHI (Univ. of Electro-Commun.)
Kenya M. KUBO (Int'l Christian Univ.)
Jun MIYAZAKI (Tokyo Denki Univ.)
Takamasa MOMOSE (The Univ. of British Columbia)
Jin NAKAMURA (Univ. of Electro-Commun.)
Hiroki NISHIBATA (Kyushu Univ.)
Tomoya SATO (Tokyo Tech)
Wataru SATO (Kanazawa Univ.)
Tadayuki TAKAHASHI (Univ. of Tokyo)
Shinichiro TAKEDA (Univ. of Tokyo)
Satoshi TSUTSUI (Japan Synchrotron Radiation Res. Inst.)
Shin WATANABE (JAXA)
Deyan T. YORDANOV (CNRS)
Akihiro YOSHIMI (Okayama Univ.)

Student Trainees

Sai AKIMOTO (Hosei Univ.)
Manami ITO (Hosei Univ.)
Satoshi TANAKA (Hosei Univ.)
Hiroki ENDO (Hosei Univ.)
Yusuke FUKUZAWA (Hosei Univ.)
Kai KIKUCHI (Hosei Univ.)
Rikuta MITSUYASU (Hosei Univ.)
Takaya MIWA (Hosei Univ.)
Shoki TAKAHASHI (Hosei Univ.)
Shinya SASAMORI (Hosei Univ.)
Yutaka TSUZUKI (Univ. of Tokyo)
Mio YOSHIDA (Univ. of Electro-Commun.)
Yoko KIMURA (Osaka Univ.)
Takato SUGISAKI (Osaka Univ.)
Roman L. WIXINGER (Univ. of Tokyo)
Konstantin STOYCHEV (Univ. of Paris-Saclay)

Assistant

Izumi YOSHIDA

List of Publications & Presentations

Publications

[Original Papers]

M. Mukai, Y. Hirayama, Y. X. Watanabe, H. Watanabe, H. Koura, S. C. Jeong, H. Miyatake, M. Brunet, S. Ishizawa, F. G. Kondev, G. J. Lane, Yu. A. Litvinov, T. Niwase, M. Oyaizu, Zs. Podolyák, M. Rosenbusch, P. Schury, M. Wada, and P. M. Walker, "Ground-state β-decay spectroscopy of ^{187}Ta," Phys. Rev. C **105**, 034331-1–6 (2022). DOI: 10.1103/PhysRevC.105.034331 .

Y. Ishibashi, A. Gladkov, Y. Ichikawa, A. Takamine, H. Nishibata, T. Sato, H. Yamazaki, T. Abe, J. M. Daugas, T. Egami, T. Fujita, G. Georgiev, K. Imamura, T. Kawaguchi, W. Kobayashi, Y. Nakamura, A. Ozawa, M. Sanjo, N. Shimizu, D. Tominaga, L. C. Tao, K. Asahi, and H. Ueno, "Nuclear magnetic moment of the neutron-rich nucleus ^{21}O," Phys. Rev. C **107**, 024306-1–7 (2023). DOI: 10.1103/PhysRevC.107.024306 .

S. Iimura, M. Rosenbusch, A. Takamine, Y. Tsunoda, M. Wada, S. Chen, D. Hou, W. Xian, H. Ishiyama, S. Yan, P. Schury, H. Crawford, P. Doornenbal, Y. Hirayama, Y. Ito, S. Kimura, T. Koiwai, T. Kojima, H. Koura, J. Lee, J. Liu, S. Michimasa, H. Miyatake, J. Moon, S. Naimi, S. Nishimura, T. Niwase, A. Odahara, T. Otsuka, S. Paschalis, M. Petri, N. Shimizu, T. Sonoda, D. Suzuki, Y. Watanabe, K. Wimmer, and H. Wollnik, "Study of the $N = 32$ and $N = 34$ shell gap for Ti and V by the first high-precision multireflection time-of-flight mass measurements at BigRIPS-SLOWRI," Phys. Rev. Lett. **130**, 012501-1–6 (2023). DOI: 10.1103/PhysRevLett.130.012501 .

T. Otsuka, T. Abe, T. Yoshida, Y. Tsunoda, N. Shimizu, N. Itagaki, Y. Utsuno, J. Vary, P. Maris, and H. Ueno, "α-clustering in atomic nuclei from first principles with statistical learning and the Hoyle state character," Nat. Commum. **13**, 2234-1–10 (2022). DOI: 10.1038/s41467-022-29582-0 .

K. Nakamura, S. Nagase, T. Nakashita, T. Hayamizu, T. Aoki, H. Nagahama, N. Ozawa, M. Sato, K. Yamane, M. Fukase, D. Uehara, A. Takamine, and Y. Sakemi, "Development of a laser frequency stabilization and an optical transmission system for the francium electric dipole moment search," J. Phys. Conf. Ser. **2249**, 012010-1–7 (2022). DOI: 10.1088/1742-6596/2249/1/012010 .

T. Hashimoto, S. Aikawa, T. Akaishi, H. Asano, M. Bazzi, D. A. Bennett, M. Berger, D. Bosnar, A. D. Butt, C. Curceanu, W. B. Doriese, M. S. Durkin, Y. Ezoe, J. W. Fowler, H. Fujioka, J. D. Gard, C. Guaraldo, F. P. Gustafsson, C. Han, R. Hayakawa, R. S. Hayano, T. Hayashi, J. P. Hays-Wehle, G. C. Hilton, T. Hiraiwa, M. Hiromoto, Y. Ichinohe1, M. Iio, Y. Iizawa, M. Iliescu, S. Ishimoto, Y. Ishisaki, K. Itahashi, M. Iwasaki, Y. Ma, T. Murakami, R. Nagatomi, T. Nishi, H. Noda, H. Noumi, K. Nunomura, G. C. O'Neil, T. Ohashi, H. Ohnishi, S. Okada, H. Outa, K. Piscicchia, C. D. Reintsema, Y. Sada, F. Sakuma, M. Sato, D. R. Schmidt, A. Scordo, M. Sekimoto, H. Shi, K. Shirotori, D. Sirghi, F. Sirghi, K. Suzuki, D. S. Swetz, A. Takamine, K. Tanida, H. Tatsuno, C. Tripp, J. Uhlig, J. N. Ullom, S. Yamada, T. Yamaga, T. Yamazaki, and J. Zmeskal (J-PARC E62 Collaboration), "Measurements of strong-interaction effects in kaonic-helium isotopes at sub-eV precision with X-ray microcalorimeters," Phys. Rev. Lett. **128**, 112503-1–6 (2022). DOI: 10.1103/PhysRevLett.128.112503 .

M. Rosenbusch, M. Wada, S. Chen, A. Takamine, S. Iimura, D. Hou, W. Xian, S. Yan, P. Schury, Y. Hirayama, Y. Ito, H. Ishiyama, S. Kimura, T. Kojima, J. Lee, J. Liu, S. Michimasa, H. Miyatake, M. Mukai, J. Y. Moon, S. Nishimura, S. Naimi, T. Niwase, T. Sonoda, Y. X. Watanabe, and H. Wollnik, "The new MRTOF mass spectrograph following the ZeroDegree spectrometer at RIKEN's RIBF facility," Nucl. Instrum. Methods Phys. Res. A **1047**, 167824-1–12 (2022). DOI: 10.1016/j.nima.2022.167824 .

D. S. Ahn, J. Amano, H. Baba, N. Fukuda, H. Geissel, N. Inabe, S. Ishikawa, N. Iwasa, T. Komatsubara, T. Kubo, K. Kusaka, D. J. Morrissey, T. Nakamura, M. Ohtake, H. Otsu, T. Sakakibara, H. Sato, B. M. Sherrill, Y. Shimizu, T. Sumikama, H. Suzuki, H. Takeda, O. B. Tarasov, H. Ueno, Y. Yanagisawa, and K. Yoshida, "Discovery of ^{39}Na," Phys. Rev. Lett. **129**, 212502-1–7 (2022). DOI: 10.1103/PhysRevLett.129.212502 .

G. G. Kiss, A. Vitéz-Sveiczer, Y. Saito, A. Tarifeño-Saldivia, M. Pallas, J. L. Tain, I. Dillmann, J. Agramunt, A. Algora, C. Domingo-Pardo, A. Estrade, C. Appleton, J. M. Allmond, P. Aguilera, H. Baba, N. T. Brewer, C. Bruno, R. Caballero-Folch, F. Calvino, P. J. Coleman-Smith, G. Cortes, T. Davinson, N. Fukuda, Z. Ge, S. Go, C. J. Griffin, R. K. Grzywacz, O. Hall, A. Horváth, J. Ha, L. J. Harkness-Brennan, T. Isobe, D. Kahl, T. T. King, A. Korgul, S. Kovács, R. Krücken, S. Kubono, M. Labiche, J. Liu, J. Liang, M. Madurga, K. Miernik, F. Molina, A. I. Morales, M. R. Mumpower, E. Nacher, A. Navarro, N. Nepal, S. Nishimura, M. Piersa-Siłkowska, V. Phong, B. C. Rasco, B. Rubio, K. P. Rykaczewski, J. Romero-Barrientos, H. Sakurai, L. Sexton, Y. Shimizu, M. Singh, T. Sprouse, T. Sumikama, R. Surman, H. Suzuki, T. N. Szegedi, H. Takeda, A. Tolosa, K. Wang, M. Wolinska-Cichocka, P. Woods, R. Yokoyama, and Z. Xu, "Measuring the β-decay properties of neutron-rich exotic Pm, Sm, Eu, and Gd isotopes to constrain the nucleosynthesis yields in the rare-earth region," Astrophys. J. **936**, 107-1–18 (2022). DOI: 10.3847/1538-4357/ac80fc .

V. H. Phong, S. Nishimura, G. Lorusso, T. Davinson, A. Estrade, O. Hall, T. Kawano, J. Liu, F. Montes, N. Nishimura, R. Grzywacz, K. P. Rykaczewski, J. Agramunt, D. S. Ahn, A. Algora, J. M. Allmond, H. Baba, S. Bae, N. T. Brewer, C. G. Bruno, R. Caballero-Folch, F. Calviño, P. J. Coleman-Smith, G. Cortes, I. Dillmann, C. Domingo-Pardo, A. Fijalkowska, N. Fukuda, S. Go, C. J. Griffin, J. Ha, L. J. Harkness-Brennan, T. Isobe, D. Kahl, L. H. Khiem, G. G. Kiss, A. Korgul, S. Kubono, M. Labiche, I. Lazarus, J. Liang, Z. Liu, K. Matsui, K. Miernik, B. Moon, A. I. Morales, P. Morrall, N. Nepal, R. D. Page, M. Piersa-Siłkowska, V. F. E. Pucknell, B. C. Rasco, B. Rubio, H. Sakurai, Y. Shimizu, D. W. Stracener, T. Sumikama, H. Suzuki, J. L. Tain, H. Takeda, A. Tarifeño-Saldivia, A. Tolosa-Delgado, M. Wolińska-Cichocka, P. J. Woods, and R. Yokoyama, "β-delayed one and two neutron emission probabilities southeast of ^{132}Sn and the odd-even systematics in r-process nuclide abundances," Phys. Rev. Lett. **129**, 172701-1–7 (2022). DOI: 10.1103/PhysRevLett.129.172701 .

M. Tanaka, P. Brionnet, M. Du, J. Ezold, K. Felker, B. J. P. Gall, S. Go, R. Grzywacz, H. Haba, K. Hagino, S. Hogle, S. Ishizawa, D. Kaji, S. Kimura, T. T. King, Y. Komori, R. K. Lemon, M. G. Leonard, K. Morimoto, K. Morita, D. Nagae, N. Naito, T. Niwase, B. C. Rasco, J. B. Roberto, K. P. Rykaczewski, S. Sakaguchi, H. Sakai, Y. Shigekawa, D. W. Stracener, S. VanCleve, Y. Wang, K. Washiyama, and T. Yokokita, "Probing optimal reaction energy for synthesis of element 119 from ^{51}V + ^{248}Cm reaction with quasielastic barrier distribution measurement," J. Phys. Soc. Jpn. **91**, 084201-1–17 (2022). DOI: 10.7566/JPSJ.91.084201 .

Y. Hirayama, M. Mukai, Y. X. Watanabe, P. Schury, H. Nakada, J. Y. Moon, T. Hashimoto, S. Iimura, S. C. Jeong, M. Rosenbusch,

M. Oyaizu, T. Niwase, M. Tajima, A. Taniguchi, M. Wada, and H. Miyatake, "In-gas-cell laser resonance ionization spectroscopy of ^{200,201}Pt," Phys. Rev. C **106**, 034326-1–11 (2022). DOI: 10.1103/PhysRevC.106.034326 .

C. Amsler, H. Breuker, S. Chesnevskaya, G. Costantini, R. Ferragut, M. Giammarchi, A. Gligorova, G. Gosta, H. Higaki, E. D. Hunter, C. Killian, V. Kletzl, V. Kraxberger, N. Kuroda, A. Lanz, M. Leali, V. Mäckel, G. Maero, C. Malbrunot, V. MascagnaY. Matsuda, S. Migliorati, D. J. Murtagh, Y. Nagata, A. Nanda, L. Nowak, E. Pasino, M. Romé, M. C. Simon, M. Tajima, V. Toso, S. Ulmer, L. Venturelli, A. Weiser, E. Widmann, T. Wolz, Y. Yamazaki, and J. Zmeskal, "Reducing the background temperature for cyclotron cooling in a cryogenic Penning-Malmberg trap," Phys. Plasmas **29**, 083303-1–12 (2022). DOI: 10.1063/5.0093360 .

H. F. Li, S. Naimi, T. M. Sprouse, M. R. Mumpower, Y. Abe, Y. Yamaguchi, D. Nagae, F. Suzaki, M. Wakasugi, H. Arakawa, W. B. Dou, D. Hamakawa, S. Hosoi, Y. Inada, D. Kajiki, T. Kobayashi, M. Sakaue, Y. Yokoda, T. Yamaguchi, R. Kagesawa, D. Kamioka, T. Moriguchi, M. Mukai, A. Ozawa, S. Ota, N. Kitamura, S. Masuoka, S. Michimasa, H. Baba, N. Fukuda, Y. Shimizu, H. Suzuki, H. Takeda, D. S. Ahn, M. Wang, C. Y. Fu, Q. Wang, S. Suzuki, Z. Ge, Yu. A. Litvinov, G. Lorusso, P. M. Walker, Zs. Podolyak, and T. Uesaka, "First application of mass measurements with the Rare-RI Ring reveals the solar *r*-process abundance trend at $A = 122$ and $A = 123$," Phys. Rev. Lett. **128**, 152701-1–6 (2022). DOI: 10.1103/PhysRevLett.128.152701 .

B. Moon, A. Gargano, H. Naidja, C. -B. Moon, A. Odahara, R. Lozeva, S. Nishimura, C. Yuan, F. Browne, P. Doornenbal, G. Lorusso, Z. Patel, S. Rice, M. Si, L. Sinclair, P. -A. Soderstrom, T. Sumikama, H. Watanabe, J. Wu, Z. Y. Xu, A. Yagi, D. S. Ahn, H. Baba, F. L. Bello Garrote, R. Daido, J. M. Daugas, F. Didierjean, Y. Fang, N. Fukuda, B. Hong, E. Ideguchi, N. Inabe, T. Ishigaki, T. Isobe, H. S. Jung, D. Kameda, I. Kojouharov, T. Komatsubara, T. Kubo, Y. K. Kwon, C. S. Lee, P. Lee, S. Morimoto, D. Murai, M. Niikura, H. Nishibata, I. Nishizuka, H. Sakurai, Y. Shimizu, H. Suzuki, H. Takeda, K. Tshoo, and R. Yokoyama, "First observation of the $\pi 0h_{11/2} \otimes \nu 0h_{9/2}$ partner orbital configuration in the odd-odd ^{138}I nucleus," Phys. Rev. C **105**, 034334-1–7 (2022). DOI: 10.1103/PhysRevC.105.034334 .

A. Yagi, A. Odahara, H. Nishibata, R. Lozeva, C. B. Moon, S. Nishimura, K. Yoshida, N. Yoshinaga, C. Watanabe, K. Higashiyama, T. Shimoda, R. Daido, Y. Fang, P. S. Lee, B. Moon, P. Doornenbal, G. Lorusso, P. A. Söderström, T. Sumikama, H. Watanabe, T. Isobe, H. Baba, H. Sakurai, F. Browne, Z. Patel, S. Rice, L. Sinclair, J. Wu, Z. Y. Xu, R. Yokoyama, T. Kubo, N. Inabe, H. Suzuki, N. Fukuda, D. Kameda, H. Takeda, D. S. Ahn, Y. Shimizu, D. Murai, F. L. Bello Garrote, J. M. Daugas, F. Didierjean, E. Ideguchi, S. Iimura, T. Ishigaki, H. S. Jung, T. Komatsubara, Y. K. Kwon, C. S. Lee, S. Morimoto, M. Niikura, I. Nishizuka, and K. Tshoo, "Various nuclear structures in ^{140}Xe studied by β decay of ground and isomeric states in ^{140}I," Phys. Rev. C **105**, 044325-1–14 (2022). DOI: 10.1103/PhysRevC.105.044325 .

D. Little, A. D. Ayangeakaa, R. V. F. Janssens, S. Zhu, Y. Tsunoda, T. Otsuka, B. A. Brown, M. P. Carpenter, A. Gade, D. Rhodes, C. R. Hoffman, F. G. Kondev, T. Lauritsen, D. Seweryniak, J. Wu, J. Henderson, C. Y. Wu, P. Chowdhury, P. C. Bender, A. M. Forney, and W. B. Walters, "Multistep Coulomb excitation of ^{64}Ni: Shape coexistence and nature of low-spin excitations," Phys. Rev. C **106**, 044313-1–13 (2022). DOI: 10.1103/PhysRevC.106.044313 .

T. Niwase, W. Xian, M. Wada, M. Rosenbusch, S. Chen, A. Takamine, J. Liu, S. Iimura, D. Hou, S. Yan, H. Ishiyama, H. Miyatake, S. Nishimura, D. Kaji, K. Morimoto, Y. Hirayama, Y. X. Watanabe, S. Kimura, P. Schury, and H. Wollnik, "Development of a β-TOF detector: An enhancement of the α-TOF detector for use with β-decaying nuclides," Prog. Theor. Exp. Phys. **2023**, 50934006-1–9 (2023). DOI: 10.1093/ptep/ptad039 .

[Book]

Y. Tsunoda and T. Otsuka, "Configuration interaction approach to atomic nuclei: The shell model," in *Handbook of Nuclear Physics*, edited by I. Tanihata, H. Toki, and T. Kajino (Springer, Singapore, 2022). DOI: 10.1007/978-981-15-8818-1_17-1 .

Presentations

[International Conferences/Workshops]

T. Abe (oral), "Alpha-cluster structure from first principles," YIPQS long-term workshop "Mean-field and Cluster Dynamics in Nuclear Systems 2022" (MCD2022), Kyoto, Japan & Online (Hybrid), May 9–June 17, 2022.

T. Abe (oral), "Alpha-cluster structure from first principles," RIKEN-YITP Workshop "Physics of RI: Recent Progress and Perspectives," Wako (RIKEN), Japan & Online (Hybrid), May 30–June 1, 2022.

K. Nakamura (oral), S. Nagase, T. Nakashita, T. Hayamizu, T. Aoki, H. Nagahama, N. Ozawa, K. Yamane, M. Fukase, D. Uehara, A. Takamine, and Y. Sakemi, "400-m-Long polarization-maintaining fibers for magneto-optical trapping of francium atoms," The 15th Pacific Rim Conference on Lasers and Electro-Optics (CLEO Pacific Rim, CLEO-PR 2022); International Symposium on Imaging, Sensing, and Optical Memory 2022 (ISOM'22); and the 13th International Conference on Optics-photonics Design and Fabrication (ODF'22), Sapporo, Japan, July 31–August 5, 2022.

K. Kikuchi (poster) *et al.*, "Optimization of the stopping position of a highly energetic ^{84}Rb atoms injected into superfluid helium," 29th International Conference on Low Temperature Physics (LT29), Sapporo, Japan & Online (Hybrid), August 18–24, 2022.

H. Endo (poster) *et al.*, "LIF spectrum analysis for measurement of Rb atomic bubble relaxation time in superfluid helium," 29th International Conference on Low Temperature Physics (LT29), Sapporo, Japan & Online (Hybrid), August 18–24, 2022.

M. A. Syakuur (oral), A. R. Noviyanti, U. Widyaiswari, T Saragi, Risdiana, and I. Watanabe, "Comparison of effective magnetic moment on impurity substitution dependence of $Eu_{2-x}Ce_xCu_{1-y}(Zn, Ni)_yO_{4+a-d}$," 29th International Conference on Low Temperature Physics (LT29), Sapporo, Japan & Online (Hybrid), August 18–24, 2022.

K. Imamura (poster) *et al.*, "Laser spectroscopic method for the investigation of nuclear structure utilizing superfluid helium as a host matrix of radioisotope atoms," 29th International Conference on Low Temperature Physics (LT29), Sapporo, Japan & Online (Hybrid), August 18–24, 2022.

S. Go (invited), "Overview of RIBF" and "Spectroscopy of exotic nuclei," The 21st CNS International Summer School (A3F-CNSSS22), Kumagaya, Saitama, August 20–24, 2022.

R. Mitsuyasu (poster) *et al*., "Spectral optimization of laser for excitation of Rb atoms in superfluid helium in accelerator experiments," The 25th Congress of the International Commission for Optics (ICO), Dresden, Germany & Online (Hybrid), September 5–9, 2022.

S. Akimoto (poster) *et al*., "Development of an efficient fluorescence detection system for radioisotope atoms generated at accelerators," The 25th Congress of the International Commission for Optics (ICO), Dresden, Germany & Online (Hybrid), September 5–9, 2022.

A. Takamine (invited), M. Rosenbusch, M. Wada, S. Iimura, D. Hou, W. Xian, S. Chen, S. Yan, H. Ishiyama, T. Niwase, S. Kimura, Y. Hirayama, Y. Ito, T. Kojima, J. Lee, S. Michimasa, H. Miyatake, J. Y. Moon, M. Mukai, S. Naimi, T. Sonoda, P. Vi, J. M. Yap, T. T. Yeung, and H. Wollnik, "Nuclear mass measurements with the new MRTOF-MS system at the ZeroDegree spectrometer of BigRIPS," 28th International Nuclear Physics Conference (INPC 2022), Cape Town, South Africa, September 11–16, 2022.

S. Go (oral), "High-spin states in ^{35}S: the promotion of isoscalar pair at high spin," 28th International Nuclear Physics Conference (INPC 2022), Cape Town, South Africa, September 11–16, 2022.

A. Takamine (oral), "Development of the new helium gas catcher and nuclear mass measurements with the new MRTOF-MS behind the ZeroDegree spectrometer at RIKEN BigRIPS," The 19th International Conference on Electromagnetic Isotope Separators and Related Topics (EMIS 2022), Daejeon, Korea, October 3–7, 2022.

M. Tajima (poster), A. Takamine, H. Iimura, M. Wada, S. Kimura, T. Niwase, P. Schury, A. Schuessler, J. Lassen, and H. Ueno, "Offline development for collinear laser spectroscopy at the SLOWRI facility," The 19th International Conference on Electromagnetic Isotope Separators and Related Topics (EMIS 2022), Daejeon, Korea, October 3–7, 2022.

A. Gladkov (poster), Y. Ishibashi, H. Yamazaki, Y. Ichikawa, A. Takamine, H. Nishibata, K. Asahi, T. Sato, T. Abe, M. Tajima, S. Go, A. Ozawa, N. Shimizu, T. Fujita, L. C. Tao, T. Egami, D. Tominaga, T. Kawaguchi, M. Sanjo, W. Kobayashi, K. Imamura, Y. Nakamura, G. Georgiev, J. M. Daugas, and H. Ueno, "β-NMR measurements of neutron-rich isotopes for nuclear structure and materials science," The 19th International Conference on Electromagnetic Isotope Separators and Related Topics (EMIS 2022), Daejeon, Korea, October 3–7, 2022.

P. Schury (oral), D. Kaji, M. Wada, T. Niwase, S. Kimura, H. Koura, H. Miyatake, H. Ishiyama, K. Morimoto, M. Rosenbusch, A. Takamine, Y. Hirayama, Y. Ito, Y. X. Watanabe, P. Brionnet, and H. Wollnik, "Multi-reflection time-of-flight mass spectroscopy of superheavy nuclides," The 19th International Conference on Electromagnetic Isotope Separators and Related Topics (EMIS 2022), Daejeon, Korea, October 3–7, 2022.

J. Y. Moon (poster), M. Wada, P. Schury, T. Hashimoto, Y. X. Watanabe, Y. Hirayama, M. Rosenbusch, Y. Ito, S. Iimura, J. Lee, S. Kimura, Z. Korkulu, H. Miyatake, T. Niwase, A. Takamine, and H. Wollnik, "Construction of the Multi-reflection time-of-flight mass spectrograph (MRTOF-MS) at RAON," The 19th International Conference on Electromagnetic Isotope Separators and Related Topics (EMIS 2022), Daejeon, Korea, October 3–7, 2022.

M. Mukai (oral), "Laser ionization spectroscopy of neutron-rich Ir isotopes and recent works at KISS," Workshop on Laser Spectroscopy/Analysis of Radioactive Isotope and Related Topics, Nagoya, Japan, October 20, 2022.

M. A. Syakuur (poster), A. R. Noviyanti, U. Widyaiswari, T. Saragi, Risdiana, and I. Watanabe, "Sample synthesis of a single phase $Nd_2Ru_2O_7$," Asia-Pacific Conference on Condensed Matter Physics 2022 (AC2MP2022), Sendai, Japan & Online (Hybrid), November 21–23, 2022.

M. A. Syakuur (poster), A. R. Noviyanti, A. R. Noviyanti, U. Widyaiswari, T. Saragi, Risdiana, D. P. Sari, H. Sakai, N. Hanasaki, and I. Watanabe, "Sample synthesis of a single phase $Nd_2Ru_2O_7$," The 6th International Conference on Functional Materials Science 2022 (ICFMS 2022), Bali, Indonesia & Online (Hybrid), November 29–30, 2022.

T. Otsuka (invited), "Emerging of alpha clustering due to nuclear forces," Mean-field and Cluster Dynamics in Nuclear Systems 2022 (MCD2022) First Week, Kyoto, Japan & Online (Hybrid), May 9–13, 2022.

T. Otsuka (invited), "Alpha clustering from first principles for Be and C isotopes including the Hoyle state," 8th Workshop on Level Density and Gamma Strength, Oslo, Norway, May 9–13, 2022.

T. Otsuka (oral), "New facets of alpha-clustering and deformation towards driplines depicted by nuclear forces," Mean-field and Cluster Dynamics in Nuclear Systems 2022 (MCD2022) Third Week, Kyoto, Japan & Online (Hybrid), May 23–27, 2022.

T. Otsuka (invited), "Emerging concepts in nuclear structure based on the shell model," Symposium "Frontiers in Nuclear Structure Theory" on the Occasion of the 90th Birthday of Prof. Jan Blomquist, Online, May 23–25, 2022.

T. Otsuka (invited), "Prevailing triaxiality of heavy deformed nuclei," Shapes and Symmetries in Nuclei: from Experiment to Theory (SSNET'22), Paris, France, May 30–June 3, 2022.

T. Otsuka (invited), "Structure evolutions towards neutron driplines," Mean-field and Cluster Dynamics in Nuclear Systems 2022 (MCD2022) Fifth Week, Kyoto, Japan, June 6–10, 2022.

T. Otsuka (invited), "Monopole-quadrupole interplay in nuclear structure and resulting self-organization phenomena," Mean-field and Cluster Dynamics in Nuclear Systems 2022 (MCD2022) Sixth Week, Kyoto, Japan & Online (Hybrid), June 13–17, 2022.

T. Otsuka (oral), "What locates neutron driplines?" Direct Reactions with Exotic Beams 2022 (DREB2022), Santiago de Compostela, Spain, June 27–July 1, 2022.

T. Otsuka (invited), "Prevailing triaxiality in nuclear shapes," 55th Zakopane Conference on Nuclear Physics, Zakopane, Poland, August 29–September 2, 2022.

T. Otsuka (invited), "Shell evolution and emerging paradigm changes," 28th International Nuclear Physics Conference (INPC 2022), Cape Town, South Africa, September 11–16, 2022.

T. Otsuka (invited), "Prevailing triaxiality in heavy deformed nuclei and possible experimental observation by M1 excitation," SFB 1245 Annual Workshop, Darmstadt, Germany, October 4–7, 2022.

T. Otsuka (invited), "Knocking out nucleons and alphas to see novel nuclear structures," REIMEI Workshop "Unveiling Nuclear Shells and Correlations in Exotic Nuclei through Knockout Reactions," Darmstadt, Germany, October 10–12, 2022.

T. Otsuka (invited), "(A) Triaxial ellipsoids probed by the RHC and a possible paradigm change in nuclear structure (B) Progress report on ^{96}Zr and ^{96}Ru," EMMI Rapid Reaction Task Force (RRTF) "Nuclear physics Confronts Relativistic Collisions of Isobars," Heidelberg, Germany, October 12–14, 2022.

T. Otsuka (invited), "Prevailing triaxiality driven by the tensor force," The 6th Topical Workshop on Modern Aspects in Nuclear Structure (BORMIO-2023), Bormio, Italy, February 6–11, 2022.

T. Otsuka (invited), "New aspects of nuclear structure (Impacts from modern Shell Model)," INTPART School 2023, Okinawa, Japan, February 20–March 3, 2023.

[Domestic Conferences/Workshops]

今村慧 (依頼講演), 「RI 原子線共鳴装置の開発:イオントラップ部」, 新学術領域研究「宇宙観測検出器と量子ビームの出会い. 新たな応用の架け橋. 」領域研究会 (第 4 回領域全体会議), オンライン, 2022 年 5 月 20–21 日.

上野秀樹 (依頼講演), 「計画研究 B03 班 高偏極 RI ビームの生成と核・物質科学研究への応用」, 新学術領域研究「宇宙観測検出器と量子ビームの出会い. 新たな応用の架け橋. 」領域研究会 (第 4 回領域全体会議), オンライン, 2022 年 5 月 20–21 日.

光安陸大, 高峰愛子, 今村慧, 秋元彩, 伊藤愛美, 螺良健太, 菊地快, 上野秀樹, 松尾由賀利, 「加速器実験における超流動ヘリウム中 Rb 原子励起用レーザーのスペクトル最適化」, 第 18 回原子・分子・光科学 (AMO) 討論会, 東京 (東京大学本郷キャンパス) & オンライン ハイブリッド開催, 2022 年 6 月 10–11 日.

菊地快, 今村慧, 高峰愛子, 螺良健太, 秋元彩, 伊藤愛美, 光安陸大, A. Gladkov, 田島美典, 郷慎太郎, 向井もも, 遠藤宏紀, 長谷正司, 川田敬太, 西畑洸希, 市川雄一, 北川敦志, 涌井崇志, 上野秀樹, 松尾由賀利, 「超流動ヘリウム中レーザー分光のための不安定核原子 ^{84}Rb の停止位置最適化」, 第 18 回原子・分子・光科学 (AMO) 討論会, 東京 (東京大学本郷キャンパス) & オンライン ハイブリッド開催, 2022 年 6 月 10–11 日.

遠藤宏紀, 石井邦彦, 今村慧, 高峰愛子, 竹内由衣花, 田原太平, 上野秀樹, 松尾由賀利, 「超流動ヘリウム中 Rb 原子バブル緩和時間測定に向けたスペクトル解析」, 第 18 回原子・分子・光科学 (AMO) 討論会, 東京 (東京大学本郷キャンパス) & オンライン ハイブリッド開催, 2022 年 6 月 10–11 日.

大塚孝治, 「炭素 12 の第一原理計算とホイル状態」, RCNP 研究会「原子核反応研究の最近の話題と展望」 河合光路先生を偲ぶ会, 大阪府茨木 (大阪大学吹田キャンパス), 2022 年 7 月 8–9 日.

水野るり恵, 池田時浩, 郷慎太郎, 櫻井博儀, 齋藤岳志, 新倉潤, 松崎禎市郎, 道正新一郎, 「1 MeV 陽子ビームを用いた広ダイナミックレンジ光子検出器の性能評価実験」, 第 34 回タンデム加速器及びその周辺技術の研究会, オンライン, 2022 年 7 月 21–22 日.

安藤蒼太, 市川雄一, 佐藤智哉, 篠原雄介, 西畑洸希, 岸本侃己, 山下渉, 横田望海, 立川柊平, 竹中京平, 梶原孝文, 荒殿和希, 郷慎太郎, 高峰愛子, 上野秀樹, 旭耕一郎, 「EDM 測定に向けたガラスセル中 Xe 原子のスピン緩和機構の評価 II」, 日本物理学会 2022 年秋季大会, 岡山市 (岡山理科大学岡山キャンパス), 2022 年 9 月 6–8 日.

篠原悠介, 市川雄一, 郷慎太郎, 西畑洸希, 安藤蒼太, 荒殿和希, 旭耕一郎, 馬場秀忠, 福田直樹, G. Georgiev, A. Gladkov, 今村慧, 梶原孝文, 岸本侃己, R. Lozeva, 向井もも, 新倉潤, M. N. Nurhafiza, 小田原厚子, 清水陽平, M. Si, K. Stoychev, 鈴木宏, 立川柊平, 田島美典, 高峰愛子, 竹田浩之, 竹中京平, 武重祥子, 上野秀樹, 若狭智嗣, 山下渉, 山崎展樹, 横田望海, 吉本雅浩, J. -M. Daugas, 「分散整合二回散乱法による ^{99}Zr アイソマー状態のスピン整列」, 日本物理学会 2022 年秋季大会, 岡山市 (岡山理科大学岡山キャンパス), 2022 年 9 月 6–8 日.

向井もも, 平山賀一, 渡邉裕, P. Schury, S. C. Jeong, 宮武宇也, 庭瀬暁隆, 小柳津充宏, M. Rosenbusch, 上野秀樹, 和田道治, 「MRTOF と組み合わせた崩壊核分光のための飛行時間検出器の開発」, 日本物理学会 2022 年秋季大会, 岡山市 (岡山理科大学岡山キャンパス), 2022 年 9 月 6–8 日.

飯村俊, M. Rosenbusch, 高峰愛子, 和田道治, S. Chen, D. Hou, J. Liu, W. Xian, S. Yan, P. Schury, 木村創大, 庭瀬暁隆, 伊藤由太, 園田哲, 小島隆夫, 渡辺裕, 平山賀一, 宮武宇也, S. Naimi, 道正新一郎, 西村俊二, 小田原厚子, 石山博恒, 角田佑介, 清水則孝, 大塚孝治, 「理研 BigRIPS SLOWRI における ZD-MRTOF 装置を用いた中性子過剰 Sc, Ti, V 核の系統的核構造研究」, 日本物理学会 2022 年秋季大会, 岡山市 (岡山理科大学岡山キャンパス), 2022 年 9 月 6–8 日.

鈴木大介, 小山俊平, Assié, M., L. Lalanne, O. Sorlin, 阿部喬, D. Beaumel, Y. Blumenfeld, L. Caceres, de Oliveira F. Santos, F. Delaunay, F. Flavigny, S. Franchoo, J. Gibelin, Girard-V. Alcindor, J. Guillot, F. Hammache, O. Kamalou, A. Kamenyero, 北村徳隆, V. Lapoux, A. Lemasson, A. Matta, B. Mauss, P. Morfouace, 新倉潤, 大津秀暁, J. Pancin, T. Roger, 齋藤岳志, 櫻井博儀, C. Stodel, and J. -C. Thomas, 「非束縛核 ^{8}C におけるミラー対称性の研究」, 日本物理学会 2022 年秋季大会, 岡山市 (岡山理科大学岡山キャンパス), 2022 年 9 月 6–8 日.

平山賀一, 向井もも, 渡辺裕, P. Schury, S. C. Jeong, 庭瀬暁隆, 小柳津充広, M. Rosenbusch, 谷口秋洋, 宮武宇也, 和田道治, 「KISS での低温ヘリウムガスセル開発」, 日本物理学会 2022 年秋季大会, 岡山市 (岡山理科大学岡山キャンパス), 2022 年 9 月 6–8 日.

庭瀬暁隆, 渡辺裕, 平山賀一, 向井もも, P. Schury, N. Andreyev, 飯村俊, 石山博恒, S. C. Jeong, 宮武宇也, M. Rosenbusch, 谷口秋洋, 和田道治, 「精密質量測定による新同位体 ^{241}U の発見」, 日本物理学会 2022 年秋季大会, 岡山市 (岡山理科大学岡山キャンパス), 2022 年 9 月 6–8 日.

洲嵜ふみ, 西尾勝久, A. N. Andreyev, 廣瀬健太郎, R. Orlandi, 牧井宏之, J. Smallcombe, 伊藤由太, 浅井雅人, 塚田和明, 佐藤哲也, 小川達彦, 宮武宇也, 渡邉裕, 平山賀一, S. C. Jeong, 向井もも, 庭瀬暁隆, 久保野茂, 岩佐直仁, 「JAEA 反跳生成核分離装置を用いた多核子移行反応の研究」, 日本物理学会 2022 年秋季大会, 岡山市 (岡山理科大学岡山キャンパス), 2022 年 9 月 6–8 日.

角田佑介, 清水則孝, 大塚孝治, 「モンテカルロ殻模型による $N = 50$ 近傍の核構造の研究」, 日本物理学会 2022 年秋季大会, 岡山市 (岡山理科大学岡山キャンパス), 2022 年 9 月 6–8 日.

阿部喬 (基調講演), 「富岳で探る炭素 12 のホイル状態」, 富岳で加速する素粒子・原子核・宇宙・惑星シンポジウム, 神戸大学先端融合研究環統合研究拠点 & オンライン ハイブリッド開催, 2022 年 12 月 12–13 日.

阿部喬, 「モンテカルロ殻模型による第一原理計算の最近の進展」, 富岳で加速する素粒子・原子核・宇宙・惑星シンポジウム, オンライン, 2022 年 1 月 17–18 日

小澤直也, 長濱弘季, 中村圭佑, 佐藤幹, 中下輝士, 永瀬慎太郎, 上原大祐, 深瀬実来, 青木貴稔, 山口敦史, 高峰愛子, 上野秀樹,

酒見泰寛, 「永久電気双極子能率探索を目指した冷却フランシウム原子源の開発」, 日本物理学会 2023 年春季大会, オンライン, 2023 年 3 月 22–25 日.

深瀬実来, 長濱弘季, 中村圭佑, 小澤直也, 佐藤幹, 中下輝士, 永瀬慎太郎, 上原大祐, 高峰愛子, 上野秀樹, 酒見泰寛, 「フランシウム原子の永久電気双極子能率探索に向けた高周波二重極質量フィルターの開発」, 日本物理学会 2023 年春季大会, オンライン, 2023 年 3 月 22–25 日.

上原大祐, 長濱弘季, 中村圭佑, 佐藤幹, 中下輝士, 小澤直也, 永瀬慎太郎, 深瀬実来, 青木貴稔, 山口敦史, 高峰愛子, 上野秀樹, 酒見泰寛, 「レーザー冷却フランシウム源実現に向けた金属表面における中性脱離反応の研究」, 日本物理学会 2023 年春季大会, オンライン, 2023 年 3 月 22–25 日.

立川柊平, 市川雄一, 佐藤智哉, 安藤蒼太, 篠原悠介, 谷本昂平, 山本陽介, 西畑洸希, 若狭智嗣, 岸本侃己, 山下渉, 横田望海, 竹中京平, 梶原孝文, 荒殿和希, 郷慎太郎, 高峰愛子, 上野秀樹, 旭耕一郎, 「EDM 測定に向けた能動帰還型核スピンメーザーの開発」, 日本物理学会 2023 年春季大会, オンライン, 2023 年 3 月 22–25 日.

今村慧, 高峰愛子, 福澤悠亮, A. Gladkov, 郷慎太郎, 田島美典, 上野秀樹, 「原子ビーム共鳴法を利用したスピン偏極 RI 原子ビーム生成に向けた中性化装置開発」, 日本物理学会 2023 年春季大会, オンライン, 2023 年 3 月 22–25 日.

菊地快, 今村慧, 高峰愛子, 螺良健太, 秋元彩, 伊藤愛美, 光安陸大, A. Gladkov, 田島美典, 郷慎太郎, 向井もも, 遠藤宏紀, 長谷正司, 川田敬太, 西畑洸希, 市川雄一, 北川敦志, 涌井崇志, 上野秀樹, 松尾由賀利, 「レーザー誘起蛍光観測による超流動ヘリウム中不安定核原子 ^{84}Rb の停止位置最適化」, 日本物理学会 2023 年春季大会, オンライン, 2023 年 3 月 22–25 日.

光安陸大, 高峰愛子, 今村慧, 秋元彩, 伊藤愛美, 螺良健太, 菊地快, 上野秀樹, 松尾由賀利, 「HIMAC における超流動ヘリウム中不安定核原子 ^{84}Rb の蛍光検出高感度化の試み」, 日本物理学会 2023 年春季大会, オンライン, 2023 年 3 月 22–25 日.

向井もも, 平山賀一, 渡邉裕, P. Schury, S. C. Jeong, 宮武宇也, 庭瀬暁隆, M. Rosenbusch, 上野秀樹, 和田道治, 「安定イリジウム同位体周辺核の直接質量測定」, 日本物理学会 2023 年春季大会, オンライン, 2023 年 3 月 22–25 日.

田島美典, 黒田直史, 桧垣浩之, 松田恭幸 (ASACUSA-CUSP Collaboration), 「反陽子蓄積リング施設 ELENA における反陽子トラップ」, 日本物理学会 2023 年春季大会, オンライン, 2023 年 3 月 22–25 日.

阿部喬, 「第一原理計算によるホイル状態のクラスター構造」, 日本物理学会 2023 年春季大会, オンライン, 2023 年 3 月 22–25 日.

角田佑介, 清水則孝, 大塚孝治, 「モンテカルロ殻模型による $N = 50$ 近傍の核構造の研究」, 日本物理学会 2023 年春季大会, オンライン, 2023 年 3 月 22–25 日.

高峰愛子, 「原子物理分光技術で覗く原子核の世界」, 第 30 回原子衝突セミナー, オンライン, 2022 年 3 月 30–31 日.

Award

K. Kikuchi (Hosei Univ.), "Optimization of the stopping position of a highly energetic ^{84}Rb atoms injected into superfluid helium," Poster Award of the 29th International Conference on Low Temperature Physics (LT29), August 23, 2022.

Press Releases

プレスリリース: 「スーパーコンピュータ『富岳』で探る炭素の起源―第一原理計算で導かれたアルファクラスターの構造」, 理研, 東京大学, 日本原子力研究開発機構共同プレスリリース, 2022 年 4 月 27 日.

新聞掲載: 「理研, C12 原子核の量子構造解明 炭素起源理解に期待」, 日刊工業新聞, 2022 年 4 月 28 日.

Outreach Activities

アウトリーチ: 高峰愛子 (理研), インタビュー記事 Web 掲載 (高校・大学生向けイベント) 「見たい! 知りたい! 原子核サイエンス最前線仁科加速器科学研究センター応援団」, 2022 年 7 月 1 日.

理研広報誌掲載: 「炭素はどのようにしてつくられたのか」, 理研クローズアップ科学道 2022 (理研, 2022 年 9 月 12 日).

理研広報誌掲載: "Calculations reveal three helium nuclei lurking inside carbon nuclei," RIKEN Research (RIKEN, Winter 2022 issue), p. 14.

Nuclear Science and Transmutation Research Division
High Energy Astrophysics Laborarory

1. Abstract

In the immediate aftermath of the Big Bang, the beginning of our universe, only hydrogen and helium existed. However, nuclear fusion in the interior of stars and the explosion of supernovae in the universe over 13.8 billion years led to the evolution of a world brimming with the many different elements we have today. By using scientific satellites or balloons to observe X-rays and gamma-rays emitted from celestial objects, we are observing the synthesis of the elements at their actual source. Our goal is to comprehensively elucidate the scenarios for the formation of the elements in the universe, together with our research on sub-atomic physics through the use of an accelerator.

2. Major Research Subjects

(1) History of nucleosynthesis in the universe
(2) Physics in extreme conditions in the universe
(3) Research and development of innovative radiation detectors
(4) Apply radiation technology for human to live in space

3. Summary of Research Activity

High Energy Astrophysics Laboratory started in April 2010. The goal of our research is to reveal the mechanism of nucleosynthesis and the evolution of elements in the universe, and to observe/discover exotic physical phenomena in extremely strong magnetic and/or gravitational fields. We have observed supernova remnants, strongly magnetized neutron stars, pulsars, black holes and galaxies with X-ray astronomical satellites, balloons and ground-based telescopes.

(1) Nucleosynthesis in the universe

(1-1) XRISM

X-Ray Imaging and Spectroscopy Mission (XRISM) is a new X-ray astrophysics observatory developed by a joint effort between Japan and US with the participation of Europe. XRISM aims to recover the high-resolution X-ray spectroscopy of hot plasma in the Universe initiated by the short-lived Hitomi satellite, which was lost in 2016 by accident one month after the launch. In FY2022, the development and tests of the satellite have been completed successfully. XRISM is ready for launch in the summer of 2023. A major milestone was also achieved in the science observation program. The observation targets for the Performance Verification (PV) phase have been selected and released to public and a new program called the XRISM Guest Scientist has started to offer researchers in the astrophysics community an opportunity to participate in scientific activities with the observations in the PV phase.

(1-2) MAXI and OHMAN

Since April 2018, High Energy Astrophysics Laboratory has hosted MAXI (Monitor of All-sky X-ray Image) onboard International Space Station (ISS), which was attached to ISS in 2009. MAXI is a RIKEN-led project collaborating with JAXA and other universities. Since MAXI scans X-ray all-sky every 90 minutes, many new transient objects, including outbursts of neutron stars or blackhole binaries, can be found. All the data go public soon after they are taken, and almost all groups in high-energy phenomena rely on the MAXI data. In FY2022, MAXI has directly linked to NICER (Neutron Star Interior Composition Explorer; highly sensitive X-ray detector but narrow field of view) operated by the US on the ISS (the OHMAN project; On-orbit Hookup of MAXI And NICER). The connection was completed in August 2022 after a few years of preparation and has successfully transferred MAXI transient discovery alerts to NICER in as little as 100 s. Detections associated with the neutron star merger event have yet to be made but are ready to respond anytime.

(2) Extremely strong magnetism and gravity

(2-1) IXPE

We have contributed to NASA's world-first X-ray polarimeter mission IXPE (Imaging X-ray Polarimeter Explorer). High Energy Astrophysics Laboratory is responsible for providing the gas electron multipliers (GEMs) to the IXPE mission: the GEM is a key device of the X-ray polarimeter and is produced based on our patent for space use. The IXPE satellite was successfully launched from Florida on December 9, 2021. After one month of commissioning in orbit, IXPE started scientific observations of X-ray stellar objects on January 11, 2022. The international science team has written over 30 discovery papers (including 3 Nature and 2 Science papers) during 1.5 years of operation.

Using the IXPE mission, we aim to prove the strong magnetism of Magnetars, one of the species of neutron stars with ultra-strong magnetic field $B > 10^{11}$ T. In such ultra-strong magnetic field, higher-order diagrams, $\mathrm{O}(eB/m^2)$, $\mathrm{O}(eB/m^2)^2$ *etc.*, never ignored in the QED perturbation theory. As a result, we observe newly-emerging phenomena such as vacuum polarization, vacuum birefringence, *etc.* The RIKEN team is the core member of the science working group on Magnetars, leading observations and data analysis. In 4U 0142+61 Magnetar observation, we have confirmed that the results are consistent with the model with an ultra-strong magnetic field above 10^{10} T. We have also discovered that contrary to theoretical expectations, there is no atmosphere on the magnetar surface, and the condensed surface is exposed to space (press released at RIKEN). This may be because the atmosphere condenses due to the strong magnetic field. The further study of a strong magnetic field, one of the key parameters of neutron stars, hints at the study of neutron star nuclear matter.

(2-2) Astrophysical data analysis

In parallel with the mission development/operations, we are studying gamma-ray binary systems, which are one of the most important astrophysical targets in the MeV gamma-ray band. We analyzed the broad-band emission of gamma-ray binary LS 5039, a bright gamma-ray object in the MeV band, using NuSTAR and Fermi. The obtained spectrum with the highest available statistics shows that the emission from MeV to sub-GeV bands is difficult to explain with current theoretical models, suggesting particle acceleration there is much more efficient than well-known standard diffusive shock acceleration.

(3) Innovative breakthrough in astrophysics with a small satellite

We are developing technology and acquiring the know-how to make space observation, which requires a lot of money, possible with small satellites at a low cost. NASA and other space agencies around the world have realized the importance of these opportunities and have started space observation activities using small satellites. NinjaSat is a micro-satellite mission (6U CubeSat; $30\times20\times10$ cm^3) led by RIKEN in collaboration with universities. NinjaSat will be launched on October 2023. Although several science missions have recently been conducted using micro-satellites, NinjaSat is the world's first general-purpose CubeSat mission to observe X-ray sources. NinjaSat carries two Xe-filled gas detectors with 2-degree-wide collimators and performs spectroscopy between 2–50 keV and timing observation with a timing resolution of about 61 μs. Since the effective area is not large ($\sim$32 cm^2 at 6 keV), the target of the NinjaSat is long-term monitoring of bright X-ray sources which are discovered by MAXI *etc.* In general, bright objects are difficult to observe, and continuous observations for a long period are impossible with large satellite missions. NinjaSat aims to perform observations that are difficult to perform on larger missions. For example, NinjaSat observes the time variability of binary neutron stars and binary black holes in conjunction with the ground-based optical, radio, and gravitational telescopes. We installed the X-ray detectors into the satellite bus in FY2022.

(4) Future X-ray and gamma-ray detectors

As an successor of the MAXI mission, we are also verifying the principle of a new concept, multiplexing lobster-eye (MuLE) optics, to monitor the entire sky with a wide field-of-view for detecting and immediate reporting transient objects such as a neutron star merger. We published a paper on the conceptual design of MuL, and proved the concept by a simple experiment.

To explore the MeV gamma-ray sky in the Universe, we are working on the technical development of the GRAMS (Gamma-Ray and AntiMatter Survey) project, which aims at future MeV gamma-ray observations with a Compton telescope using a liquid argon time projection chamber. We developed two types of event reconstruction algorithms for multiple Compton scattering events using probabilistic and neural network methods. Based on them, we confirmed that the advantage of the GRAMS project, which is an observation with an effective area larger than previous by 1-2 orders magnitudes, can be achievable with a current mission concept.

Members

Director

Toru TAMAGAWA

Research/Technical Scientist

Tatehiro MIHARA (Senior Research Scientist)

Special Postdoctoral Researcher

Hiroki YONEDA

Visiting Scientists

Aya BAMBA (Univ. of Tokyo)
Naohisa INADA (NIT, Nara College)
Satoru KATSUDA (Saitama Univ.)
Tomoko KAWATE (Nat'l Inst. of Natural Sci.)
Tomoki KIMURA (Tokyo Univ. Sci.)
Kazuki KOMIYA (Tokyo Metroporitan Industrial Tech. Res. Inst.)
Toru MISAWA (Shinshu Univ.)
Ikuyuki MITSUISHI (Nagoya Univ.)
Yujin NAKAGAWA (JAMSTEC)
Nobuyuki NAKAMURA (Univ. of Electro-Commun.)
Hirofumi NODA (Osaka Univ.)
Hirokazu ODAKA (Univ. of Tokyo)
Yuki OKURA (NAOJ/Nat'l Inst. of Natural Sci.)
Hiroyuki SAKAUE (Nat'l Inst. of Natural Sci.)
Rohta TAKAHASHI (NIT, Tomakomai College)
Yoko TAKEUCHI (Tokyo Metroporitan Industrial Tech. Res. Inst.)
Takaaki TANAKA (Konan Univ.)
Yukikatsu TERADA (Saitama Univ.)
Masahiro TSUJIMOTO (JAXA)
Hiroyuki UCHIDA (Kyoto Univ.)
Masaki WAKABAYASHI (Jakulin Commercial Company LC)
Shinya YAMADA (Rikkyo Univ.)
Hiroya YAMAGUCHI (JAXA)

Student Trainees

Yuki AMANO (Kyoto Univ.)
Syoki HAYASHI (Tokyo Univ. Sci)
Arata JUJO (Tokyo Univ. Sci)
Miki KURIHARA (Univ. of Tokyo)
Yuken OHSHIRO (Univ. of Tokyo)
Naoyuki OTA (Tokyo Univ. Sci)
Satoshi TAKASHIMA (Univ. of Tokyo)
Moto TOGAWA (Univ. of Heidelberg)
Keisuke UCHIYAMA (Tokyo Univ. Sci)
Sota WATANABE (Tokyo Univ. Sci)
Yuanhui ZHOU (Tokyo Univ. Sci)

Research Part-time Worker

Naoyuki OTA (Tokyo Univ. Sci)

List of Publications & Presentations

Publications

[Original Papers]

M. C. Weisskopf, P. Soffitta, L. Baldini, B. D. Ramsey, S. L. O'Dell, R. W. Romani, G. Matt, W. D. Deininger, W. H. Baumgartner, R. Bellazzini, E. Costa, J. J. Kolodziejczak, L. Latronico, H. L. Marshall, F. Muleri, S. D. Bongiorno, A. Tennant, N. Bucciantini, M. Dovciak, F. Marin, A. Marscher, J. Poutanen, P. Slane, R. Turolla, W. Kalinowski, A. D. Marco, S. Fabiani, M. Minuti, F. L. Monaca, M. Pinchera, J. Rankin, C. Sgrò, A. Trois, F. Xie, C. Alexander, D. Z. Allen, F. Amici, J. Andersen, A. Antonelli, S. Antoniak, P. Attiná, M. Barbanera, M. Bachetti, R. M. Baggett, J. Bladt, A. Brez, R. Bonino, C. Boree, F. Borotto, S. Breeding, D. Brienza, H. K. Bygott, C. Caporale, C. Cardelli, R. Carpentiero, S. Castellano, M. Castronuovo, L. Cavalli, E. Cavazzuti, M. Ceccanti, M. Centrone, S. Citraro, F. D'Amico, E. D'Alba, L. D. Gesu, E. D. Monte, K. L. Dietz, N. D. Lalla, G. D. Persio, D. Dolan, I. Donnarumma, Y. Evangelista, K. Ferrant, R. Ferrazzoli, M. Ferrie, J. Footdale, B. Forsyth, M. Foster, B. Garelick, S. Gunji, E. Gurnee, M. Head, G. Hibbard, S. Johnson, E. Kelly, K. Kilaru, C. Lefevre, S. L. Roy, P. Loffredo, P. Lorenzi, L. Lucchesi, T. Maddox, G. Magazzu, S. Maldera, A. Manfreda, E. Mangraviti, M. Marengo, A. Marrocchesi, F. Massaro, D. Mauger, J. McCracken, M. McEachen, R. Mize, P. Mereu, S. Mitchell, I. Mitsuishi, A. Morbidini, F. Mosti, H. Nasimi, B. Negri, M. Negro, T. Nguyen, I. Nitschke, A. Nuti, M. Onizuka, C. Oppedisano, L. Orsini, D. Osborne, R. Pacheco, A. Paggi, W. Painter, S. D. Pavelitz, C. Pentz, R. Piazzolla, M. Perri, M. Pesce-Rollins, C. Peterson, M. Pilia, A. Profeti, S. Puccetti, J. Ranganathan, A. Ratheesh, L. Reedy, N. Root, A. Rubini, S. Ruswick, J. Sanchez, P. Sarra, F. Santoli, E. Scalise, A. Sciortino, C. Schroeder, T. Seek, K. Sosdian, G. Spandre, C. O. Speegle, T. Tamagawa, M. Tardiola, A. Tobia, N. E. Thomas, R. Valerie, M. Vimercati, A. L. Walden, B. Weddendorf, J. Wedmore, D. Welch, D. Zanetti, and F. Zanetti, "Imaging X-ray polarimetry explorer: prelaunch," J. Astron. Telesc. Instrum. Syst. **8**, 026002 (2022).

R. Taverna, R. Turolla, F. Muleri, J. Heyl, S. Zane, L. Baldini, D. Gonzalez-Caniulef, M. Bachetti, J. Rankin, I. Caiazzo, N. D. Lalla, V. Doroshenko, M. Errando, E. Gau, D. Kırmızıbayrak, H. Krawczynski, M. Negro, M. Ng, N. Omodei, A. Possenti, T. Tamagawa, K. Uchiyama, M. C. Weisskopf, I. Agudo, L. A. Antonelli, W. H. Baumgartner, R. Bellazzini, S. Bianchi, S. D. Bongiorno, R. Bonino, A. Brez, N. Bucciantini, F. Capitanio, S. Castellano, E. Cavazzuti, S. Ciprini, E. Costa, A. D. Rosa, E. D. Monte, L. D. Gesu, A. D. Marco, I. Donnarumma, M. Dovˇciak, S. R. Ehlert, T. Enoto, Y. Evangelista, S. Fabiani, R. Ferrazzoli, J. A. Garcia, S. Gunji, K. Hayashida, W. Iwakiri, S. G. Jorstad, V. Karas, T. Kitaguchi, J. J. Kolodziejczak, F. L. Monaca, L. Latronico, I. Liodakis, S. Maldera, A. Manfreda, F. Marin, A. Marinucci, A. P. Marscher, H. L. Marshall, G. Matt, I. Mitsuishi, T. Mizuno, S. C. -Y. Ng, S. L. O'Dell, C. Oppedisano, A. Papitto, G. G. Pavlov, A. L. Peirson, M. Perri, M. Pesce-Rollins, M. Pilia, J. Poutanen, S. Puccetti, B. D. Ramsey, A. Ratheesh, R. W. Romani, C. Sgr'o, P. Slane, P. Soffitta, G. Spandre, F. Tavecchio, Y. Tawara, A. F. Tennant, N. E. Thomas, F. Tombesi, A. Trois, S. S. Tsygankov, J. Vink, K. Wu, and F. Xie, "Polarized X-rays from a magnetar," Science **378**, 646 (2022).

I. Liodakis, A. P. Marscher, I. Agudo, A. V. Berdyugin, M. I. Bernardos, G. Bonnoli, G. A. Borman, C. Casadio, V. Casanova, E. Cavazzuti, N. R. Cavero, L. D. Gesu, N. D. Lalla, I. Donnarumma, S. R. Ehlert, M. Errando, J. Escudero, M. Garcıa-Comas, B. Agıs-González, C. Husillos, J. Jormanainen, S. G. Jorstad, M. Kagitani, E. N. Kopatskaya, V. Kravtsov, H. Krawczynski, E. Lindfors, E. G. Larionova, G. M. Madejski, F. Marin, A. Marchini, H. L. Marshall, D. A. Morozova, F. Massaro, J. R. Masiero, D. Mawet, R. Middei, M. A. Millar-Blanchaer, I. Myserlis, M. Negro, K. Nilsson, S. L. O'Dell, N. Omodei, L. Pacciani, A. Paggi, G. V. Panopoulou, A. L. Peirson, M. Perri, P. -O. Petrucci, J. Poutanen, S. Puccetti, R. W. Romani, T. Sakanoi, S. S. Savchenko, A. Sota, F. Tavecchio, S. Tinyanont, A. A. Vasilyev, Z. R. Weaver, A. V. Zhovtan, L. A. Antonelli, M. Bachetti, L. Baldini, W. H. Baumgartner, R. Bellazzini, S. Bianchi, S. D. Bongiorno, R. Bonino, A. Brez, N. Bucciantini, F. Capitanio, S. Castellano, S. Ciprini, E. Costa, A. D. Rosa, E. D. Monte, A. D. Marco, V. Doroshenko, M. Dovˇciak, T. Enoto, Y. Evangelista, S. Fabiani, R. Ferrazzoli, J. A. Garcia, S. Gunji, K. Hayashida, J. Heyl, W. Iwakiri, V. Karas, T. Kitaguchi, J. J. Kolodziejczak, F. L. Monaca, L. Latronico, S. Maldera, A. Manfreda, A. Marinucci, G. Matt, I. Mitsuishi, T. Mizuno, F. Muleri, S. C. -Y. Ng, C. Oppedisano, A. Papitto,G. G. Pavlov, M. Pesce-Rollins, M. Pilia, A. Possenti, B. D. Ramsey, J. Rankin, A. Ratheesh, C. Sgró, P. Slane, P. Soffitta, G. Spandre, T. Tamagawa, R. Taverna, Y. Tawara, A. F. Tennant, N. E. Thomas, F. Tombesi, A. Trois, S. Tsygankov, R. Turolla, J. Vink, M. C. Weisskopf, K. Wu, F. Xie, and S. Zane, "Polarized blazar X-rays imply particle acceleration in shocks," Nature **611**, 677 (2022).

S. R. Ehlert, R. Ferrazzoli, A. Marinucci, H. L. Marshall, R. Middei, L. Pacciani, M. Perri, P. -O. Petrucci, S. Puccetti, T. Barnouin, S. Bianchi, I. Liodakis, G. Madejski, F. Marin, A. P. Marscher, G. Matt, J. Poutanen, K. Wu, I. Agudo, L. A. Antonelli, M. Bachetti, L. Baldini, W. H. Baumgartner, R. Bellazzini, S. D. Bongiorno, R. Bonino, A. Brez, N. Bucciantini, F. Capitanio, S. Castellano, E. Cavazzuti, S. Ciprini, E. Costa, A. D. Rosa, E. D. Monte, L. D. Gesu, N. D. Lalla, A. D. Marco, I. Donnarumma, V. Doroshenko, M. Dovˇciak, T. Enoto, Y. Evangelista, S. Fabiani, J. A. Garcia, S. Gunji, K. Hayashida, J. Heyl, W. Iwakiri, S. G. Jorstad, V. Karas, T. Kitaguchi, J. J. Kolodziejczak, H. Krawczynski, F. L. Monaca, L. Latronico, S. Maldera, A. Manfreda, F. Massaro, I. Mitsuishi, T. Mizuno, F. Muleri, M. Negro, C. -Y. Ng, S. L. O'Dell, N. Omodei, C. Oppedisano, A. Papitto, G. G. Pavlov, A. L. Peirson, M. Pesce-Rollins, M. Pilia, A. Possenti, B. D. Ramsey, J. Rankin, A. Ratheesh, R. W. Romani, C. Sgr'o, P. Slane, P. Soffitta, G. Spandre, T. Tamagawa, F. Tavecchio, R. Taverna, Y. Tawara, A. F. Tennant, N. E. Thomas, F. Tombesi, A. Trois, S. Tsygankov, R. Turolla, J. Vink, M. C. Weisskopf, F. Xie, S. Zane, J. Rodi, E. Jourdain, and J. -P. Roques, "Limits on X-ray polarization at the core of centaurus A as observed with the imaging X-ray polarimetry explorer," Astrophys. J. **935**, 116 (2022).

V. Doroshenko, J. Poutanen, S. S. Tsygankov, V. F. Suleimanov, M. Bachetti, I. Caiazzo, E. Costa, A. D. Marco, J. Heyl, F. L. Monaca, F. Muleri, A. A. Mushtukov, G. G. Pavlov, B. D. Ramsey, J. Rankin, A. Santangelo, P. Soffitta, R. Staubert, M. C. Weisskopf, S. Zane, I. Agudo, L. A. Antonelli, L. Baldini, W. H. Baumgartner, R. Bellazzini, S. Bianchi, S. D. Bongiorno, R. Bonino, A. Brez, N. Bucciantini, F. Capitanio, S. Castellano, E. Cavazzuti, S. Ciprini, A. D. Rosa, E. D. Monte, L. D. Gesu, N. D. Lalla, I. Donnarumma, M. Dovčiak, S. R. Ehlert, T. Enoto, Y. Evangelista, S. Fabiani, R. Ferrazzoli, J. A. Garcia, S. Gunji, K. Hayashida, W. Iwakiri,

S. G. Jorstad, V. Karas, T. Kitaguchi, J. J. Kolodziejczak, H. Krawczynski, L. Latronico, I. Liodakis, S. Maldera, A. Manfreda, F. Marin, A. Marinucci, A. P. Marscher, H. L. Marshall, G. Matt, I. Mitsuishi, T. Mizuno, C. -Y. Ng, S. L. O'Dell, N. Omodei, C. Oppedisano, A. Papitto, A. L. Peirson, M. Perri, M. Pesce Rollins, M. Pilia, A. Possenti, S. Puccetti, A. Ratheesh, R. W. Romani, C. Sgr'o, P. Slane, G. Spandre, R. A. Sunyaev, T. Tamagawa, F. Tavecchio, R. Taverna, Y. Tawara, A. F. Tennant, N. E. Thomas, F. Tombesi, A. Trois, R. Turolla, J. Vink, K. Wu, and F. Xie, "Determination of X-ray pulsar geometry with IXPE polarimetry," Nat. Astron. **6**, 1433 (2022).

H. Krawczynski, F. Muleri, M. Dovčiak, A. Veledina, N. R. Cavero, J. Svoboda, A. Ingram, G. Matt, J. A. Garcia, V. Loktev, M. Negro, J. Poutanen, T. Kitaguchi, J. Podgorný, J. Rankin, W. Zhang, A. Berdyugin, S. V. Berdyugina, S. Bianchi, D. Blinov, F. Capitanio, N. D. Lalla, P. Draghis, S. Fabiani, M. Kagitani, V. Kravtsov, S. Kiehlmann, L. Latronico, A. A. Lutovinov, N. Mandarakas, F. Marin, A. Marinucci, J. M. Miller, T. Mizuno, S. V. Molkov, N. Omodei, P. -O. Petrucci, A. Ratheesh, T. Sakanoi, A. N. Semena, R. Skalidis, P. Soffitta, A. F. Tennant, P. Thalhammer, F. Tombesi, M. C. Weisskopf, J. Wilms, S. Zhang, I. Agudo, L. A. Antonelli, M. Bachetti, L. Baldini, W. H. Baumgartner, R. Bellazzini, S. D. Bongiorno, R. Bonino, A. Brez, N. Bucciantini, S. Castellano, E. Cavazzuti, S. Ciprini, E. Costa, A. D. Rosa, E. D. Monte, L. D. Gesu, A. D. Marco, I. Donnarumma, V. Doroshenko, S. R. Ehlert, T. Enoto, Y. Evangelista, R. Ferrazzoli, S. Gunji, K. Hayashida, J. Heyl, W. Iwakiri, S. G. Jorstad, V. Karas, J. J. Kolodziejczak, F. L. Monaca, I. Liodakis, S. Maldera, A. Manfreda, A. P. Marscher, H. L. Marshall, I. Mitsuishi, C. -Y. Ng, S. L. O'Dell, C. Oppedisano, A. Papitto, G. G. Pavlov, A. L. Peirson, M. Perri, M. Pesce-Rollins, M. Pilia, A. Possenti, S. Puccetti, B. D. Ramsey, R. W. Romani, C. Sgr'o, P. Slane, G. Spandre, T. Tamagawa, F. Tavecchio, R. Taverna, Y. Tawara, N. E. Thomas, A. Trois, S. Tsygankov, R. Turolla, J. Vink, K. Wu, F. Xie, and S. Zane, "Polarized X-rays constrain the disk-jet geometry in the black hole X-ray binary Cygnus X-1," Science **378**, 650 (2022).

J. Vink, D. Prokhorov, R. Ferrazzoli, P. Slane, P. Zhou, K. Asakura, L. Baldini, N. Bucciantini, E. Costa, A. D. Marco, J. Heyl, F. Marin, T. Mizuno, C. -Y. Ng, M. Pesce-Rollins, B. D. Ramsey, J. Rankin, A. Ratheesh, C. Sgró, P. Soffitta, D. A. Swartz, T. Tamagawa, M. C. Weisskopf, Y. -J. Yang, R. Bellazzini, R. Bonino, E. Cavazzuti, L. Costamante, N. D. Lalla, L. Latronico, S. Maldera, A. Manfreda, F. Massaro, I. Mitsuishi, N. Omodei, C. Oppedisano, S. Zane, I. Agudo, L. A. Antonelli, M. Bachetti, W. H. Baumgartner, S. Bianchi, S. D. Bongiorno, A. Brez, F. Capitanio, S. Castellano, S. Ciprini, A. D. Rosa, E. D. Monte, L. D. Gesu, I. Donnarumma, V. Doroshenko, M. Dovčiak, S. R. Ehlert, T. Enoto, Y. Evangelista, S. Fabiani, J. A. Garcia, S. Gunji, K. Hayashida, W. Iwakiri, S. G. Jorstad, V. Karas, T. Kitaguchi, J. J. Kolodziejczak, H. Krawczynski, F. L. Monaca, I. Liodakis, A. Marinucci, A. P. Marscher, H. L. Marshall, G. Matt, F. Muleri, S. L. O'Dell, A. Papitto, G. G. Pavlov, A. L. Peirson, M. Perri, M. Pilia, A. Possenti, J. Poutanen, S. Puccetti, R. W. Romani, G. Spandre, F. Tavecchio, R. Taverna, Y. Tawara, A. F. Tennant, N. E. Thomas, F. Tombesi, A. Trois, S. Tsygankov, R. Turolla, K. Wu, and F. Xie, "X-ray polarization detection of cassiopeia A with IXPE," Astrophys. J. **938**, 40 (2022).

F. Xie, A. D. Marco, F. L. Monaca, K. Liu, F. Muleri, N. Bucciantini, R. W. Romani, E. Costa, J. Rankin, P. Soffitta, M. Bachetti, N. D. Lalla, S. Fabiani, R. Ferrazzoli, S. Gunji, L. Latronico, M. Negro, N. Omodei, M. Pilia, A. Trois, E. Watanabe, I. Agudo, L. A. Antonelli, L. Baldini, W. H. Baumgartner, R. Bellazzini, S. Bianchi, S. D. Bongiorno, R. Bonino, A. Brez, F. Capitanio, S. Castellano, E. Cavazzuti, S. Ciprini, A. D. Rosa, E. D. Monte, L. D. Gesu, I. Donnarumma, V. Doroshenko, M. Dovčiak, S. R. Ehlert, T. Enoto, Y. Evangelista, J. A. Garcia, K. Hayashida, J. Heyl, W. Iwakiri, S. G. Jorstad, V. Karas, T. Kitaguchi, J. J. Kolodziejczak, H. Krawczynski, I. Liodakis, S. Maldera, A. Manfreda, F. Marin, A. Marinucci, A. P. Marscher, H. L. Marshall, F. Massaro, G. Matt, I. Mitsuishi, T. Mizuno, C. -Y. Ng, S. L. O'Dell, C. Oppedisano, A. Papitto, G. G. Pavlov, A. L. Peirson, M. Perri, M. Pesce-Rollins, P. -O. Petrucci, A. Possenti, J. Poutanen, S. Puccetti, B. D. Ramsey, A. Ratheesh, C. Sgró, P. Slane, G. Spandre, T. Tamagawa, F. Tavecchio, R. Taverna, Y. Tawara, A. F. Tennant, N. E. Thomas, F. Tombesi, S. S. Tsygankov, R. Turolla, J. Vink, M. C. Weisskopf, K. Wu, and S. Zane, "Vela pulsar wind nebula X-rays are polarized to near the synchrotron limit," Nature **612**, 658 (2022).

H. L. Marshall, M. Ng, D. Rogantini, J. Heyl, S. S. Tsygankov, J. Poutanen, E. Costa, S. Zane, C. Malacaria, I. Agudo, L. A. Antonelli, M. Bachetti, L. Baldini, W. H. Baumgartner, R. Bellazzini, S. Bianchi, S. D. Bongiorno, R. Bonino, A. Brez, N. Bucciantini, F. Capitanio, S. Castellano, E. Cavazzuti, S. Ciprini, A. D. Rosa, E. D. Monte, L. D. Gesu, N. D. Lalla, A. D. Marco, I. Donnarumma, V. Doroshenko, M. Dovčiak, S. R. Ehlert, T. Enoto, Y. Evangelista, S. Fabiani, R. Ferrazzoli, J. A. Garcia, S. Gunji, K. Hayashida, W. Iwakiri, S. G. Jorstad, V. Karas, T. Kitaguchi, J. J. Kolodziejczak, H. Krawczynski, F. L. Monaca, L. Latronico, I. Liodakis, S. Maldera, A. Manfreda, F. Marin, A. Marinucci, A. P. Marscher, G. Matt, I. Mitsuishi, T. Mizuno, F. Muleri, C. -Y. Ng, S. L. O'Dell, N. Omodei, C. Oppedisano, A. Papitto, G. G. Pavlov, A. L. Peirson, M. Perri, M. Pesce Rollins, P. -O. Petrucci, M. Pilia, A. Possenti, S. Puccetti, B. D. Ramsey, J. Rankin, A. Ratheesh, R. W. Romani, C. Sgr'o, P. Slane, P. Soffitta, G. Spandre, T. Tamagawa, F. Tavecchio, R. Taverna, Y. Tawara, A. F. Tennant, N. E. Thomas, F. Tombesi, A. Trois, R. Turolla, J. Vink, M. C. Weisskopf, K. Wu, F. Xie, N. S. Schulz, and D. Chakrabarty, "Observations of 4U 1626-67 with the imaging X-ray polarimetry explorer," Astrophys. J. **940**, 70 (2022).

A. Marinucci, F. Muleri, M. Dovciak, S. Bianchi, F. Marin, G. Matt, F. Ursini, R. Middei, H. L. Marshall, L. Baldini, T. Barnouin, N. C. Rodriguez, A. De Rosa, L. Di Gesu, D. Harper, A. Ingram, V. Karas, H. Krawczynski, G. Madejski, C. Panagiotou, P. O. Petrucci, J. Podgorny, S. Puccetti, F. Tombesi, A. Veledina, W. Zhang, I. Agudo, L. A. Antonelli, M. Bachetti, W. H. Baumgartner, R. Bellazzini, S. D. Bongiorno, R. Bonino, A. Brez, N. Bucciantini, F. Capitanio, S. Castellano, E. Cavazzuti, S. Ciprini, E. Costa, E. Del Monte, N. Di Lalla, A. Di Marco, I. Donnarumma, V. Doroshenko, S. R. Ehlert, T. Enoto, Y. Evangelista, S. Fabiani, R. Ferrazzoli, J. A. Garcia, S. Gunji, K. Hayashida, J. Heyl, W. Iwakiri, S. G. Jorstad, T. Kitaguchi, J. J. Kolodziejczak, F. La Monaca, L. Latronico, I. Liodakis, S. Maldera, A. Manfreda, A. P. Marscher, I. Mitsuishi, T. Mizuno, C. -Y. Ng, S. L. O'Dell, N. Omodei, C. Oppedisano, A. Papitto, G. G. Pavlov, A. L. Peirson, M. Perri, M. Pesce-Rollins, M. Pilia, A. Possenti, J. Poutanen, B. D. Ramsey, J. Rankin, A. Ratheesh, R. W. Romani, C. Sgrš, P. Slane, P. Soffitta, G. Spandre, T. Tamagawa, F. Tavecchio, R. Taverna, Y. Tawara, A. F. Tennant, N. E. Thomas, A. Trois, S. S. Tsygankov, R. Turolla, J. Vink, M. C. Weisskopf, K. Wu, F. Xie, and S. Zane, "Polarization constraints on the X-ray corona in Seyfert Galaxies: MCG-05-23-16," Mon. Not. R. Astron. Soc. **516**, 5907 (2022).

L. D. Gesu, I. Donnarumma, F. Tavecchio, I. Agudo, T. Barnounin, N. Cibrario, N. D. Lalla, A. D. Marco, J. Escudero, M. Errando, S. G. Jorstad, D. E. Kim, P. M. Kouch, I. Liodakis, E. Lindfors, G. Madejski, H. L. Marshall, A. P. Marscher, R. Middei, F. Muleri, I. Myserlis, M. Negro, N. Omodei, L. Pacciani, A. Paggi, M. Perri, S. Puccetti, L. A. Antonelli, M. Bachetti, L. Baldini, W. H. Baumgartner, R. Bellazzini, S. Bianchi, S. D. Bongiorno, R. Bonino, A. Brez, N. Bucciantini, F. Capitanio, S. Castellano, E. Cavazzuti, S. Ciprini, E. Costa, A. D. Rosa, E. D. Monte, V. Doroshenko, M. Dovčiak, S. R. Ehlert, T. Enoto, Y. Evangelista, S. Fabiani, R. Fer-

razzoli, J. A. Garcia, S. Gunji, K. Hayashida, J. Heyl, W. Iwakiri, V. Karas, T. Kitaguchi, J. J. Kolodziejczak, H. Krawczynski, F. L. Monaca, L. Latronico, S. Maldera, A. Manfreda, F. Marin, A. Marinucci, F. Massaro, G. Matt, I. Mitsuishi, T. Mizuno, C. -Y. Ng, S. L. O'Dell, C. Oppedisano, A. Papitto, G. G. Pavlov, A. L. Peirson, M. Pesce-Rollins, P. -O. Petrucci, M. Pilia, A. Possenti, J. Poutanen, B. D. Ramsey, J. Rankin, A. Ratheesh, R. W. Romani, C. Sgr'o, P. Slane, P. Soffitta, G. Spandre, T. Tamagawa, R. Taverna, Y. Tawara, A. F. Tennant, N. E. Thomas, F. Tombesi, A. Trois, S. Tsygankov, R. Turolla, J. Vink, M. C. Weisskopf, K. Wu, F. Xie, and S. Zane, "The X-ray polarization view of mrk 421 in an average flux state as observed by the imaging X-ray polarimetry explorer," Astrophys. J. Lett. **938**, L7 (2022).

S. S. Tsygankov, V. Doroshenko, J. Poutanen, J. Heyl, A. A. Mushtukov, I. Caiazzo, A. D. Marco, S. V. Forsblom, D. González-Caniulef, M. Klawin, F. L. Monaca, C. Malacaria, H. L. Marshall, F. Muleri, M. Ng, V. F. Suleimanov, R. A. Sunyaev, R. Turolla, I. Agudo, L. A. Antonelli, M. Bachetti, L. Baldini, W. H. Baumgartner, R. Bellazzini, S. Bianchi, S. D. Bongiorno, R. Bonino, A. Brez, N. Bucciantini, F. Capitanio, S. Castellano, E. Cavazzuti, S. Ciprini, E. Costa, A. D. Rosa, E. D. Monte, L. D. Gesu, N. D. Lalla, I. Donnarumma, M. Dovčiak, S. R. Ehlert, T. Enoto, Y. Evangelista, S. Fabiani, R. Ferrazzoli, J. A. Garcia, S. Gunji, K. Hayashida, W. Iwakiri, S. G. Jorstad, V. Karas, T. Kitaguchi, J. J. Kolodziejczak, H. Krawczynski, L. Latronico, I. Liodakis, S. Maldera, A. Manfreda, F. Marin, A. Marinucci, A. P. Marscher, G. Matt, I. Mitsuishi, T. Mizuno, C. -Y. Ng, S. L. O'Dell, N. Omodei, C. Oppedisano, A. Papitto, G. G. Pavlov, A. L. Peirson, M. Perri, M. Pesce-Rollins, P. -O. Petrucci, M. Pilia, A. Possenti, S. Puccetti, B. D. Ramsey, J. Rankin, A. Ratheesh, R. W. Romani, C. Sgr'o, P. Slane, P. Soffitta, G. Spandre, T. Tamagawa, F. Tavecchio, R. Taverna, Y. Tawara, A. F. Tennant, N. E. Thomas, F. Tombesi, A. Trois, J. Vink, M. C. Weisskopf, K. Wu, F. Xie, S. Zane, "The X-ray polarimetry view of the accreting pulsar cen X-3," Astrophys. J. Lett. **941**, L14 (2022).

Q. Abarr, B. Beheshtipour, M. Beilicke, R. Bose, D. Braun, G. d. Geron- imo, P. Dowkontt, M. Errando, T. Gadson, V. Guarino, S. Heatwole, M. Hossen, N. Iyer, F. Kislat, M. Kiss, T. Kitaguchi, H. Krawczynski, J. Lanzi, S. Li, L. Lisalda, T. Okajima, M. Pearce, Z. Peterson, L. Press, B. Rauch, G. Simburger, D. Stuchlik, H. Takahashi, J. Tang, N. Uchida, and A. West, "Performance of the X-Calibur hard X-ray polarimetry mission during its 201819 long-duration balloon flight," Astron. J. **143**, 102749 (2022).

K. Asai, T. Mihara, and M. Matsuoka, "Decades-long variations in NS-LMXBs observed with MAXI/GS, RXTE/ASM, and Ginga/ASM," Publ. Astron. Soc. Jpn. **74**, 974 (2022).

M. Sugizaki, T. Mihara, K. Kobayashi, H. Negoro, M. Shidatsu, S. N. Pike, W. Iwakiri, S. Urabe, M. Serino, N. Kawai, M. Nakajima, J. A. Kennea, and Z. Liu, "Discovery of a new supergiant fast X-ray transient MAXI J0709159 associated with the Be star LY Canis Majoris," Publ. Astron. Soc. Jpn. **74**, 1131 (2022).

S. N. Pike, H. Negoro, J. A. Tomsick, M. Bachetti, M. Brumback, R. M. T. Connors, J. A. García, B. Grefenstette, J. Hare, F. A. Harrison, A. Jaodand, R. M. Ludlam, G. Mastroserio, T. Mihara, M. Shidatsu, M. Sugizaki, and R. Takagi, "MAXI and NuSTAR observations of the faint X-ray transient MAXI J1848-015 in the GLIMPSE-C01 cluster," Astrophys. J. **927**, 190 (2022).

[Proceeding]

W. Kamogawa, H. Matsumoto, Q. Abarr, H. Awaki, R. Bose, D. Braun, G. d. Geronimo, P. Dowkontt, T. Enoto, M. Errando, Y. Fukazawa, A. Furuzawa, T. Gadson, E. Gau, V. Guarino, S. Gunji, K. Harmon, K. Hayashida, S. Heatwole, F. Imazato, K. Ishibashi, M. Ishida, N. K. Iyer, F. Kislat, M. Kiss, T. Kitaguchi, H. Krawczynski, J. Lanzi, L. Lisalda, Y. Maeda, H. Matake, T. Mineta, T. Miyazawa, T. Mizuno, T. Okajima, M. Pearce, Z. Peterson, B. Rauch, N. R. Cavero, F. Ryde, T. -A. Stana, D. Stuchlik, G. Simburgeb, S. Spooner, H. Takahashi, T. Takeda, M. Takeo, T. Tamagawa, H. Tsunemi, N. Uchida, Y. Uchida, K. Uchiyama, A. West, E. A. Wulf, and Y. Yoshida, "Optical performance of the X-ray telescope for the XL-Calibur experiment," Proc. SPIE **12181**, 1218171 (2022).

Presentations

[International Conferences/Workshops]

T. Tamagawa (invited), "A review of MPGD applications in space missions," The 7th International Conference on Micro Pattern Gaseous Detectors (MPGD2022), Rehovot, Israel, December 11–16, 2022.

T. Takeda, T. Tamagawa, T. Enoto, T. Kitaguchi, Y. Kato, T. Mihara, W. Iwakiri, M. Numazawa, Y. Zhou, K. Uchiyama, Y. Yoshida, N. Ota, S. Hayashi, S. Watanabe, A. Jujo, H. Sato, C. P. Hu, H. Takahashi, H. Odaka, T. Tamba, and K. Taniguchi, "Gas selection for Xe-based LCP-GEM detectors onboard the CubeSat X-ray observatory NinjaSat," The 7th International Conference on Micro Pattern Gaseous Detectors (MPGD2022), Rehovot, Israel, December 11–16, 2022.

N. Ota, T. Tamagawa, T. Enoto, T. Kitaguchi, Y. Kato, T. Mihara, W. Iwakiri, M. Numazawa, Y. Zhou, K. Uchiyama, T. Takeda, Y. Yoshida, S. Hayashi, S. Watanabe, A. Jujo, H. Sato, C. P. Hu, H. Takahashi, H. Odaka, T. Tamba, and K. Taniguchi, "Development of miniaturized circuit boards for GEM detectors onboard the CubeSat X-ray observatory NinjaSat," The 7th International Conference on Micro Pattern Gaseous Detectors (MPGD2022), Rehovot, Israel, December 11–16, 2022.

[Domestic Conferences/Workshops]

玉川徹 (招待講演), 「X 線偏光観測—宇宙を見る新しい手段の開拓—」, 日本光学会年次学術講演会, 宇都宮市 (栃木県総合文化センター), 2022 年 11 月 15 日.

玉川徹 (招待講演), 「超小型衛星 NinjaSat プロジェクトと科学教育利用の試み」, 第 14 回小型衛星の科学教育利用を考える会, 調布市 (成城大学), 2023 年 3 月 17–18 日.

郡司修一, 渡邉瑛里, 寺島政伸, 管佑真, 上小林柾, 玉川徹, 北口貴雄, 榎戸輝揚, 内山慶祐, 武田朋志, 三石郁之, 柏倉一斗, 田原譲, 深沢泰司, 水野恒史, 高橋弘充, Zhang Sixuan, 岩切渉, 林田清, 朝倉一統, Martin Weisskopf, Brian Ramsey, Stephen O'Dell, Paolo Soffitt, Luca Baldini, ほか IXPE 衛星チーム, 「IXPE 衛星による初期科学観測」, 日本物理学会 2022 年秋季大会, 岡山市 (岡山理科大), 2022 年 9 月 6–8 日.

水野恒史, 深沢泰司, 高橋弘充, Zhang Sixuan, 郡司修一, 渡邉瑛里, 寺島政伸, 管佑真, 上小林柾, 玉川徹, 北口貴雄, 榎戸輝揚, 内山慶祐, 武田朋志, 三石郁之, 柏倉一斗, 田原譲, 岩切渉, 林田清, 朝倉一統, Martin Weisskopf, Brian Ramsey, Stephen O'Dell, Paolo

Soffitta, Luca Baldini, ほか IXPE 衛星チーム, 「IXPE 衛星による「かに星雲・パルサー」の X 線偏光観測」, 日本物理学会 2022 年秋季大会, 岡山市 (岡山理科大), 2022 年 9 月 6–8 日.

渡邉瑛里, 郡司修一, 柴田晋平, 大野寛, 寺島政伸, 管佑真, 上小林柾, 玉川徹, 北口貴雄, 榎戸輝揚, 内山慶祐, 武田朋志, 三石郁之, 柏倉一斗, 田原譲, 深沢泰司, 水野恒史, 高橋弘充, Zhang Sixuan, 岩切渉, 林田清, 朝倉一統, Martin Weisskopf, Brian Ramsey, Stephen O'Dell, Paolo Soffitta, Luca Baldini, ほか IXPE 衛星チーム, 「カニ星雲を用いた Chandra と IXPE のジョイント解析による偏光解析手法の開発」, 日本物理学会 2022 年秋季大会, 岡山市 (岡山理科大), 2022 年 9 月 6–8 日.

管佑真, 郡司修一, 渡邉瑛里, 寺島政伸, 上小林柾, 玉川徹, 北口貴雄, 榎戸輝揚, 内山慶祐, 武田朋志, 三石郁之, 柏倉一斗, 田原譲, 深沢泰司, 水野恒史, 高橋弘充, Zhang Sixuan, 岩切渉, 林田清, 朝倉一統, Martin Weisskopf, Brian Ramsey, Stephen O'Dell, Paolo Soffitta, Luca Baldini, ほか IXPE 衛星チーム, 「IXPE 衛星を用いたブラックホールスピンの決定方法」, 日本物理学会 2022 年秋季大会, 岡山市 (岡山理科大), 2022 年 9 月 6–8 日.

寺島政伸, 郡司修一, 渡邉瑛里, 管佑真, 上小林柾, 玉川徹, 北口貴雄, 榎戸輝揚, 内山慶祐, 武田朋志, 三石郁之, 柏倉一斗, 田原譲, 深沢泰司, 水野恒史, 高橋弘充, Zhang Sixuan, 岩切渉, 林田清, 朝倉一統, Martin Weisskopf, Brian Ramsey, Stephen O'Dell, Paolo Soffitta, Luca Baldini, ほか IXPE 衛星チーム, 「IXPE における増光天体の観測検討とアラートシステムの構築」, 日本物理学会 2022 年秋季大会, 岡山市 (岡山理科大), 2022 年 9 月 6–8 日.

内田悠介, Quin Abarr, 青柳美緒, 朝倉一統, 粟木久光, Matthew G. Baring, Richard Bose, Dana Braun, Gianluigi de Geronimo, Paul Dowkontt, John Elliot, 榎戸輝揚, Manel Errando, 深沢泰司, 古澤彰浩, Thomas Gadson, Epharaim Gau, Victor Guarino, 郡司修一, 袴田知宏, 萩原涼太, Kenny Hall, 花岡真帆, Keon Harmon, 服部憲吾, 林田清, Scott Heatwole, Arman Hossen, 井出峻太郎, 今村竜太, 今里郁弥, 今澤遼, 石橋和紀, 石田学, 石倉彩美, 石渡幸太, Nirmal Kumar Iyer, Fabian Kislat, Mozsi Kiss, 亀谷紀香, 鴨川航, 北口貴雄, David Kotsifakis, Henric Krawczynski, James Lanzi, Lindsey Lisalda, 前田良知, 松下友亮, 眞武寛人, 松本浩典, 峯田大晴, 宮本明日香, 宮澤拓也 R, 水野恒史, 中庭望, 野田博文, 大出優一, 岡島崇, 岡崎貴樹, Izabella Pastrani, Mark Pearce, Zachary Peterson, Helen Poon, Chris Purdy, Brian Rauch, Felix Ryde, 斎藤芳隆, 佐久間翔太郎, 佐藤淳矢, 澤上拳明, Chris Shreeves, Garry Simburger, Carl Snow, Sean Spooner, Theodor-Adrian Stana, David Stuchlik, 鈴木瞳, 高橋弘充, 武田朋志, 武尾舞, 玉川徹, 田村啓輔, 常深博, 内田和海, 内山慶祐, Brett Vincent, Andrew West, Eric Wulf, 山本龍哉, 楊冲, 米山友景, 吉田勇登, 善本真梨那, 「硬 X 線偏光観測気球実験 XL-Calibur の 2022 年スウェーデンフライトの状況報告」, 日本物理学会 2022 年秋季大会, 岡山市 (岡山理科大), 2022 年 9 月 6–8 日.

北口貴雄, 玉川徹, 榎戸輝揚, 加藤陽, 三原建弘, 岩切渉, 沼澤正樹, 周圓輝, 内山慶祐, 武田朋志, 吉田勇登, 大田尚享, 林昇輝, 重城新大, 渡部蒼汰, 佐藤宏樹, Chin-Ping Hu, 高橋弘充, 小高裕和, 丹波翼, 谷口絢太郎 H 「超小型 X 線衛星 NinjaSat の開発進捗」, 日本物理学会 2022 年秋季大会, 岡山市 (岡山理科大), 2022 年 9 月 6–8 日.

玉川徹, 北口貴雄, 榎戸輝揚, 内山慶祐, 武田朋志, 三石郁之, 柏倉一斗, 田原譲, 郡司修一, 渡邉瑛里, 寺島政伸, 管佑真, 上小林柾, 深沢泰司, 水野恒史, 高橋弘充, Zhang Sixuan, 岩切渉, 林田清, 朝倉一統, Martin Weisskopf, Brian Ramsey, Stephen O'Dell, Paolo Soffitta, Luca Baldini, ほか IXPE 衛星チーム, 「X 線偏光観測衛星 IXPE の現状 (2)」, 日本天文学会 2022 年秋季年会, 新潟市 (新潟大), 2022 年 9 月 13–15 日.

高橋弘充, 阪本菜月, 今里郁弥, 山本龍哉, 今澤遼, 眞武寛人, Poon Helen, 楊冲, 水野恒史, 深沢泰司, 内田悠介, 峯田大靖, 鴨川航, 松本浩典, 服部兼吾, 井出峻太郎, 米山友景, 岡崎貴樹, 朝倉一統, 石倉彩美, 佐久間翔太郎, 花岡真帆, 澤上拳明, 松下友亮, 善本真梨那, 大出優一, 佐藤淳矢, 袴田知宏, 佐藤淳矢, 青柳美緒, 石渡幸太, 萩原涼太, 野田博文, 林田清, 常深博, 前田良知, 石田学, 内田和海, 宮澤拓也, 石橋和紀, 中庭望, 武尾舞, 鈴木瞳, 宮本明日香, 今村竜太, 亀谷紀香, 粟木久光, 古澤彰浩, 北口貴雄, 玉川徹, 榎戸輝揚, 内山慶祐, 武田朋志, 吉田勇登, 郡司修一, 岡島崇, 田村啓輔, Henric Krawczynski, Fabian Kislat, 他 XL-Calibur チーム, 「硬 X 線偏光観測実験 XL-Calibur 気球の 2022 年フライトにおける現地準備状況」, 日本天文学会 2022 年秋季年会, 新潟市 (新潟大), 2022 年 9 月 13–15 日.

大田尚享, 玉川徹, 榎戸輝揚, 北口貴雄, 加藤陽, 三原建弘, 岩切渉, 沼澤正樹, 周圓輝, 内山慶祐, 武田朋志, 吉田勇登, 林昇輝, 重城新大, 渡部蒼汰, 佐藤宏樹, Chin-Ping Hu, 高橋弘充, 小高裕和, 丹波翼, 谷口絢太郎, 小平聡, 「超小型 X 線衛星 NinjaSat の開発進捗」, 日本天文学会 2022 年秋季年会, 新潟市 (新潟大), 2022 年 9 月 13–15 日.

北口貴雄, 玉川徹, 榎戸輝揚, 加藤陽, 三原建弘, 岩切渉, 沼澤正樹, 周圓輝, 内山慶祐, 武田朋志, 吉田勇登, 大田尚享, 林昇輝, 重城新大, 渡部蒼汰, 佐藤宏樹, Chin-Ping Hu, 高橋弘充, 小高裕和, 丹波翼, 谷口絢太郎, 「超小型 X 線衛星 NinjaSat に搭載するガス X 線検出器のオンボード信号処理」, 日本天文学会 2022 年秋季年会, 新潟市 (新潟大), 2022 年 9 月 13–15 日.

林昇輝, 玉川徹, 榎戸輝揚, 北口貴雄, 加藤陽, 三原建弘, 岩切渉, 沼澤正樹, 周圓輝, 内山慶祐, 武田朋志, 吉田勇登, 大田尚享, 重城新大, 渡部蒼汰, 佐藤宏樹, Chin-Ping Hu, 高橋弘充, 小高裕和, 丹波翼, 谷口絢太郎, 「超小型 X 線衛星 NinjaSat 搭載のガス X 線検出器のエネルギー較正」, 日本天文学会 2022 年秋季年会, 新潟市 (新潟大), 2022 年 9 月 13–15 日.

玉川徹, 北口貴雄, 榎戸輝揚, 内山慶祐, 武田朋志, 三石郁之, 柏倉一斗, 田原譲, 郡司修一, 渡邉瑛里, 寺島政伸, 管佑真, 上小林征, 深沢泰司, 水野恒史, 高橋弘充, Sixuan Zhang, 岩切渉, 林田清, 朝倉一統, Martin Weisskopf, Brian Ramsey, Stephen O'Dell, Paolo Soffitta, Luca Baldini, ほか IXPE 衛星チーム, 「X 線偏光観測衛星 IXPE ー現状と最新成果」, 宇宙科学シンポジウム 2023, 相模原市 (JAXA 宇宙科学研究所), 2023 年 1 月 5–6 日.

水野恒史, 玉川徹, 北口貴雄, 榎戸輝揚, 内山慶祐, 武田朋志, 三石郁之, 柏倉一斗, 田原譲, 郡司修一, 渡邉瑛里, 寺島政伸, 管佑真, 上小林征, 深沢泰司, 高橋弘充, Sixuan Zhang, 岩切渉, 林田清, 朝倉一統, Martin Weisskopf, Brian Ramsey, Stephen O'Dell, Paolo Soffitta, Luca Baldini, ほか IXPE 衛星チーム, 「IXPE 衛星による「かに星雲・パルサー」の X 線偏光観測」, 水野恒史宇宙科学シンポジウム 2023, 相模原市 (JAXA 宇宙科学研究所), 2023 年 1 月 5–6 日.

寺島政伸, 郡司修一, 渡邉瑛里, 管佑真, 上小林柾, 玉川徹, 北口貴雄, 内山慶祐, 武田朋志, 岩切渉, 三石郁之, 田原譲, 柏倉一斗, 林田清, 朝倉一統, 榎戸輝揚, 水野恒史, 深沢泰司, 高橋弘充, Zhang Sixuan, Michela Negro, Niccoló Di Lalla, Nicola Omodei, Stefano Silvestri, Alberto Manfreda, Peter Veres, Eric Burns, Martin Weisskopf, Brian Ramsey, Stephen L. O'Dell, Luca Baldini, ほか IXPE 衛星チーム, 「IXPE 衛星による GRB221009A の観測」, 宇宙科学シンポジウム 2023, 相模原市 (JAXA 宇宙科学研究所), 2023 年 1 月 5–6 日.

内山慶祐, 玉川徹, 北口貴雄, 榎戸輝揚, 郡司修一, 渡邉瑛里, 寺島政伸, 管佑真, 上小林柾, 水野恒史, 深沢泰司, 高橋弘充, ZhangSixuan, 林田清, 朝倉一統, 三石郁之, 田原譲, 柏倉一斗, 岩切渉, 武田朋志, 「X 線偏光観測衛星 IXPE によるマグネターの偏光観測」, 宇

宙科学シンポジウム 2023, 相模原市 (JAXA 宇宙科学研究所), 2023 年 1 月 5–6 日.

玉川徹, 北口貴雄, 加藤陽, 三原建弘, 榎戸輝揚, 岩切渉, 武田朋志, 吉田勇登, 大田尚享, 林昇輝, 内山慶祐, 渡部蒼太, 重城新大, 周圓輝, 佐藤宏樹, 沼澤正樹, Chin-Ping Hu, 高橋弘充, 小高裕和, 丹波翼, 谷口絢太郎, 「6U X 線天文衛星 NinjaSat」, 超小型衛星利用シンポジウム 2023, 中央区 (X-NIHONBASHI), 2023 年 2 月 21 日.

玉川徹, 北口貴雄 (理研), 榎戸輝揚 (京都大), 内山慶祐, 武田朋志, 三石郁之, 柏倉一斗, 田原譲, 郡司修一, 渡邉瑛里, 寺島政伸, 管佑真, 上小林柾, 深沢泰司, 水野恒史, 高橋弘充, Zhang Sixuan, 岩切渉, 林田清, 朝倉一統, Martin Weisskopf, Brian Ramsey, Stephen O'Dell, Paolo Soffitta, Luca Baldini, ほか IXPE 衛星チーム, 「X 線偏光観測衛星 IXPE の現状 (3)」, 日本天文学会 2023 年春季年会, 豊島区 (立教大), 2023 年 3 月 13–16 日.

高橋弘充, 阪本菜月, 今里郁弥, 今澤遼, 眞武寛人, 水野恒史, 深沢泰司, 内田悠介, 峯田大靖, 鴨川航, 倉本春希, 松本浩典, 服部兼吾, 井出峻太郎, 岡崎貴樹, 朝倉一統, 石倉彩美, 佐久間翔太郎, 花岡真帆, 澤上拳明, 松下友亮, 善本真梨那, 大出優一, 佐藤淳矢, 袴田知宏, 佐藤淳矢, 青柳美緒, 石渡幸太, 萩原涼太, 野田博文, 林田清, 常深博, 前田良知, 石田学, 宮澤拓也, 石橋和紀, 中庭望, 武尾舞, 鈴木瞳, 宮本明日香, 今村竜太, 亀谷紀香, 粟木久光, 古澤彰浩, 北口貴雄, 玉川徹, 榎戸輝揚, 郡司修一, 岡島崇, 田村啓輔, Henric Krawczynski, Fabian Kislat, 他 XL-Calibur チーム, 「硬 X 線集光偏光計 XL-Calibur 気球実験の 2022 年フライトと今後」, 日本天文学会 2023 年春季年会, 豊島区 (立教大), 2023 年 3 月 13–16 日.

武田朋志, 玉川徹, 榎戸輝揚, 北口貴雄, 加藤陽, 三原建弘, 岩切渉, 沼澤正樹, 内山慶祐, 吉田勇登, 大田尚享, 林昇輝, 重城新大, 渡部蒼汰, 佐藤宏樹, Chin-Ping Hu, 高橋弘充, 小高裕和, 丹波翼, 谷口絢太郎, 岸本俊二, 「超小型 X 線衛星 NinjaSat の開発進捗 (2)」, 日本天文学会 2023 年春季年会, 豊島区 (立教大), 2023 年 3 月 13–16 日.

榎戸輝揚, 辻直希, 長岡央, 加藤陽, 谷口絢太郎, 大竹淑恵, 若林泰生, 高梨宇宙, 岩本ちひろ, 玉川徹, 晴山慎, 小林泰三, 池永太一, 中野雄貴, 塚本雄士, 草野広樹, 星野健, 唐牛譲, 上野宗孝, 森本健志, 吉浦伸太郎, 本間希樹, 高橋弘充, 木坂将大, 中澤知洋, 山岡和貴, 仏坂健太, 「MoMoTarO 計画—月面の水資源探査と基礎科学への活用」, 日本物理学会 2023 年春季大会, オンライン, 2023 年 3 月 22–25 日.

谷口絢太郎, 榎戸輝揚, 辻直希, 長岡央, 加藤陽, 鶴見美和, 大竹淑恵, 若林泰生, 高梨宇宙, 岩本ちひろ, 玉川徹, 晴山慎, 小林泰三, 池永太一, 中野雄貴, 塚本雄士, 草野広樹, 星野健, 唐牛譲, 上野宗孝, 小松龍世, 「MoMoTarO 計画—月周回軌道を使った中性子寿命の測定」, 日本物理学会 2023 年春季大会, オンライン, 2023 年 3 月 22–25 日.

辻直希 , 榎戸輝揚, 長岡央, 加藤陽, 谷口絢太郎, 大竹淑恵, 若林泰生, 高梨宇宙, 岩本ちひろ, 玉川徹, 晴山慎, 小林泰三, 池永太一, 中野雄貴, 塚本雄士, 草野広樹, 星野健, 唐牛譲, 上野宗孝, 「MoMoTarO 計画—中性子とガンマ線の測定を目指す検出器開発」, 日本物理学会 2023 年春季大会, オンライン, 2023 年 3 月 22–25 日.

高橋弘充, Quin Abarr, 青柳美緒, 朝倉一統, 粟木久光, Matthew G. Baring, Richard Bose, Dana Braun, Gianluigi de Geronimo, Paul Dowkontt, John Elliot, 榎戸輝揚, Manel Errando, 深沢泰司, 古澤彰浩, Thomas Gadson, Epharaim Gau, Victor Guarino, 郡司修一, 袴田知宏, 萩原涼太, Kenny Hall, 花岡真帆, Keon Harmon, 服部憲吾, 林田清, Scott Heatwole, Arman Hossen, 井出峻太郎, 今村竜太, 今里郁弥, 今澤遼, 石橋和紀, 石田学, 石倉彩美, 石渡幸太, Nirmal Kumar Iyer, 亀谷紀香, 鴨川航, Fabian Kislat, Mozsi Kiss, 北口貴雄, David Kotsifakis, Henric Krawczynski, 倉本春希, James Lanzi, Lindsey Lisalda, 前田良知, 松下友亮, 眞武寛人, 松本浩典, 峯田大晴, 宮本明日香, 宮澤拓也, 水野恒史, 中庭望, 野田博文, 大出優一, 岡島崇, 岡崎貴樹, Izabella Pastrani, Mark Pearce, Zachary Peterson, Chris Purdy, Brian Rauch, Felix Ryde, 斎藤芳隆, 阪本菜月, 佐久間翔太郎, 佐藤淳矢, 澤上拳明, Chris Shreeves, Garry Simburger, Carl Snow, Sean Spooner, Theodor-Adrian Stana, David Stuchlik, 鈴木瞳, 武尾舞, 玉川徹, 田村啓輔, 常深博, 内田和海, 内田悠介, Brett Vincent, Andrew West, Eric Wulf, 米山友景, 善本真梨那, XL-Calibur チーム, 「硬 X 線集光偏光計 XL-Calibur 気球実験の 2022 年フライトと今後」, 日本物理学会 2023 年春季大会, オンライン, 2023 年 3 月 22–25 日.

上小林柾, 郡司修一, 渡邉瑛里, 寺島政伸, 管佑真, 玉川徹, 北口貴雄, 榎戸輝揚, 内山慶祐, 武田朋志, 三石郁之, 柏倉一斗, 田原譲, 深沢泰司, 水野恒史, 高橋弘充, Zhang Sixuan, 岩切渉, 林田清, 朝倉一統, Martin Weisskopf, Brian Ramsey, Stephen O'Dell, Paolo Soffitta, Luca Baldini, ほか IXPE 衛星チーム「Crab Pulsar を用いた IXPE 衛星の Encircled Energy Fraction の評価」, 日本物理学会 2023 年春季大会, オンライン, 2023 年 3 月 22–25 日.

澤野達哉, 米徳大輔, 三原建弘, 有元誠, 鈴木大晴, 吉田翼, 池田博一「X 線突発天体監視速報衛星こようフライトモデル開発報告」, 日本物理学会 2023 年春季大会, オンライン, 2023 年 3 月 22–25 日.

小高裕和, 市橋正裕, 高嶋聡, 丹波翼, 南木宙斗, 馬場彩, 青山一天, 櫻井真由, 田中雅士, 中曽根太地, 寄田浩平, 一戸悠人, Dmitry Khangulyan, 井上芳幸, 内田悠介, 須田祐介, 高橋弘充, 深沢泰司, 辻直美, 広島渚, 八幡和志, 米田浩基, 渡辺伸, Tsuguo Aramaki, Georgia Karagiorgi, Reshmi Mukherjee, GRAMS コラボレーション, 「GRAMS 実験 9: ステータス報告」, 日本物理学会 2023 年春季大会, オンライン, 2023 年 3 月 22–25 日.

青山一天, 岩澤広大, 櫻井真由, 清水虎冴, 田中雅士, 谷口日奈子, 中島理幾, 中曽根太地, 寄田浩平, 小高裕和, 高嶋聡, 米田浩基, GRAMS コラボレーション, 「GRAMS-AM 実験 4 大気球搭載液体アルゴン TPC を用いた宇宙反物質探索実験」, 日本物理学会 2023 年春季大会, オンライン, 2023 年 3 月 22–25 日.

櫻井真由, 青山一天, 岩澤広大, 清水虎冴, 田中雅士, 谷口日奈子, 中島理幾, 中曽根太地, 寄田浩平, 小高裕和, 高嶋聡, 米田浩基, GRAMS コラボレーション, 「GRAMS-AM 実験 5 $30 \times 30 \times 30$ cm^3 液体アルゴン TPC の製作と性能評価」, 日本物理学会 2023 年春季大会, オンライン, 2023 年 3 月 22–25 日.

谷口日奈子, 青山一天, 岩澤広大, 櫻井真由, 清水虎冴, 田中雅士, 中島理幾, 中曽根太地, 寄田浩平, 小高裕和, 高嶋聡, 米田浩基, GRAMS コラボレーション, 「GRAMS-AM 実験 6 反粒子同定手法検証のための宇宙線ミューオンを用いた地上実験の現状」, 日本物理学会 2023 年春季大会, オンライン, 2023 年 3 月 22–25 日.

中曽根太地, 青山一天, 岩澤広大, 櫻井真由, 清水虎冴, 田中雅士, 谷口日奈子, 中島理幾, 寄田浩平, 小高裕和, 高嶋聡, 米田浩基, GRAMS コラボレーション, 「GRAMS-AM 実験 7 反粒子同定手法検証のための加速器ビームテスト計画と開発課題」, 日本物理学会 2023 年春季大会, オンライン, 2023 年 3 月 22–25 日.

米田浩基, 新井翔大, 市橋正裕, 小高裕和, 高嶋聡, 丹波翼, 南木宙斗, 馬場彩, 青山一天, 岩澤広大, 櫻井真由, 清水虎冴, 田中雅士, 谷口日奈子, 中島理幾, 中曽根太地, 寄田浩平, 一戸悠人, Dmitry Khangulyan, 井上芳幸, 内田悠介, 須田祐介, 高橋弘充, 深沢泰司, 辻直美, 廣島渚, 八幡和志, 渡辺伸, Tsuguo Aramaki, Georgia Karagiorgi, Reshmi Mukherjee, GRAMS コラボレーション, 「GRAMS 実験 10: ステータス報告」, 日本物理学会 2023 年春季大会, オンライン, 2023 年 3 月 22–25 日.

高嶋聡 , 新井翔大, 市橋正裕, 小高裕和, 馬場彩, 青山一天, 櫻井真由, 田中雅士, 中曽根太地, 寄田浩平, 米田浩基, 渡辺伸, GRAMS コラボレーション, 「GRAMS 実験 11: 液体アルゴンコンプトンカメラ実証機の開発状況」, 日本物理学会 2023 年春季大会, オンライン, 2023 年 3 月 22–25 日.

市橋正裕, 高嶋聡, 新井翔大, 小高裕和, 南木宙斗, 馬場彩, 青山一天, 櫻井真由, 田中雅士, 中曽根太地, 寄田浩平, 米田浩基, 八幡和志, GRAMS コラボレーション, 「GRAMS 実験 12: シンチレーション光検出器系の開発」, 日本物理学会 2023 年春季大会, オンライン, 2023 年 3 月 22–25 日.

田中雅士, 青山一天, 石川皓貴, 岩澤広大, 内海和伸, 櫻井真由, 清水虎冴, 谷口日奈子, 中島理幾, 中曽根太地, 寄田浩平, 新井翔大, 市橋正裕, 高嶋聡, 馬場彩, 小高裕和, 米田浩基, Tsuguo Aramaki, Georgia Karagiorgi, GRAMS コラボレーション, 「GRAMS-AM 実験 8 大気球搭載液体アルゴン TPC を用いた宇宙反物質探索実験」, 日本物理学会 2023 年春季大会, オンライン, 2023 年 3 月 22–25 日.

櫻井真由, 青山一天, 石川皓貴, 岩澤広大, 内海和伸, 清水虎冴, 田中雅士, 谷口日奈子, 中島理幾, 中曽根太地, 寄田浩平, 新井翔大, 市橋正裕, 高嶋聡, 馬場彩, 小高裕和, 米田浩基, Tsuguo Aramaki, Georgia Karagiorgi, GRAMS コラボレーション, 「GRAMS-AM 実験 9 宇宙線 μ^+/μ^- を用いた粒子反粒子識別試験における LArTPC の性能評価」, 日本物理学会 2023 年春季大会, オンライン, 2023 年 3 月 22–25 日.

中曽根太地, 青山一天, 石川皓貴, 岩澤広大, 内海和伸, 櫻井真由, 清水虎冴, 田中雅士, 谷口日奈子, 中島理幾, 寄田浩平, 新井翔大, 市橋正裕, 高嶋聡, 馬場彩, 小高裕和, 米田浩基, Tsuguo Aramaki, Georgia Karagiorgi, GRAMS コラボレーション, 「GRAMS-AM 実験 10 J-PARC ハドロンホール K1.8BR における LArTPC を用いた反粒子同定手法検証のための開発状況」, 日本物理学会 2023 年春季大会, オンライン, 2023 年 3 月 22–25 日.

Nuclear Science and Transmutation Research Division
Nuclear Many-Body Theory Laborarory

1. Abstract

The nuclear many-body theory laboratory aims to understand various aspects of nuclear structure and reactions due to the assembly and disassembly of protons and neutrons in the nuclear many-body systems. For this purpose, we construct theoretical models and conduct numerical calculations to describe them. Our research topics include nuclear structure issues such as nuclear deformation, shell structure, and clustering of unstable nuclei, and nuclear reactions in the Universe where elements originate. In addition to fundamental research, we are also developing nuclear reaction database by combining the nuclear models and machine learning. The database will be used for various scientific and technological applications such as nuclear reactors, medicine and industry.

2. Major Research Subjects

(1) Structure and reactions of unstable nuclei
(2) Nuclear clustering and related nuclear reactions
(3) Nuclear reactions in the universe
(4) Research and development of the nuclear reaction database for applications

3. Summary of Research Activity

(1) Structure and reactions of unstable nuclei

The study of the structure and reactions of unstable nuclei is an important subject of the Nishina Center, as well as one of the core issues in modern nuclear physics. Our group approaches this problem by performing numerical calculations using theoretical models such as antisymmetrized molecular dynamics and density functional theory.

The research highlights in this fiscal year are as follows: (1) Description of neutron-halo and resonances near and beyond dripline within the framework of molecular dynamics. We have developed the numerical technique to describe the neutron halos with heavier masses by the molecular dynamics models. Combining this technique with the method of analytical continuation of the coupling constant (ACCC), our model can also describe the resonances beyond the neutron dripline. As a benchmark calculation, the method has been successfully applied to a neutron halo nucleus ^{31}Ne and an unbound nucleus ^{25}O. This success opened the way to study nuclei beyond the drip line in a fully microscopic model. (2) Study of the total reaction cross sections of unstable nuclei. Combining the microscopic nuclear structure models and a reaction model (Glauber model), we have investigated how the ground-state structure of unstable nuclei affects the reaction cross section. In the study of the oxygen isotopes, the signature of the new shell closure and the growth of the neutron skin were found.

(2) Nuclear clustering and related nuclear reactions

The nuclear clustering, in which nucleons are confined into into several subunits (clusters), is an eligible research subject for understanding the correlation of nucleons interacting with strong force. Since the clusters are linked to the nuclear reaction channels, they also appear as the intermediate states of various nuclear reaction dynamics.

The research highlights in this fiscal year are as follows: (1) Study of the formation probabilities of α cluster at the surface of unstable nuclei. Using the antisymmetrized molecular dynamics model, we have investigated how the α cluster formation probability in unstable Be and C isotopes changes as function of neutron skin thickness. We have demonstrated that the α cluster formation is hindered by the growth of the neutron skin, which is consistent with the experimental data reported for the Sn isotopes. (2) α cluster formation and total reaction cross section. The formation of α clusters should affect the density profile at the nuclear surface. Consequently, the signature of the clustering can be observed in the total reaction cross section. We have discussed such effect in the case of light stable nuclei.

(3) Nuclear reactions in the universe

Fusion reactions that occur in stellar and explosive astronomical events are key to understanding the origin of the elements. However, many reactions have extremely small cross sections, making direct experimental measurement difficult, and estimating reaction rates by theoretical calculation is critically important.

In this fiscal year, using the antisymmetrized molecular dynamics, we have provided an estimate of the reaction rate of ^{12}C +^{12} C fusion, which is a key reaction for understanding the steller evolution and superburst. We have shown that there are many resonances within the Gamow window, and hence, the reaction rate at steller temperatures are not hindered but are enhanced in contradiction to the estimation by a phenomenological model. Using several different nuclear density functionals, we have shown how the uncertainity of the nuclear models propages to the raction rate.

(4) Research and development of the nuclear reaction database for applications

Evaluated nuclear data are indispensable in the field of nuclear science and technology, and the demand of nuclear data is altering year by year with technical developments of nuclear science and technology. To meet such demands, an effective and accurate method that can regularly generate evaluated nuclear data has been highly desired.

The machine learning technologies can be an answer to this demand, and we are training nuclear reaction models by adopting the Bayesian optimization (BO) to effectively produce the nuclear data. In this fiscal year, we have improved a prototype system which combines the assembly of the nuclear reaction codes CCONE and BO with Gaussian regression. We have demonstrated that

the optical potentials at different incident energies can be predicted by using Gaussian Process (GP). Using this method, future RIBF experimental data can be used to determine optical potentials at arbitrary energies.

Members

Director
Masaaki KIMURA

Contract Researcher
Dang NGUYEN DINH

Visiting Scientists
Wataru HORIUCHI (Osaka Metropolitan Univ.)
Phuc LE (Duy Tan Univ.)
Futoshi MINATO (JAEA)
Takashi NAKATSUKASA (Tsukuba Univ.)
Hung NGUYEN (Duy Tan Univ.)
RHINE KUMAR ARAYAKKANDI KEECH (Cochin Univ. of Sci. and Tech.)
Koichi SATO (Kochi Univ.)
Kazuyuki SEKIZAWA (Tokyo Tech)
Yasutaka TANIGUCHI (NIT, Kagawa College)
Kenichi YOSHIDA (Kyoto Univ.)

Student Trainees
Tatsuhiro HATTORI (Tokyo Tech)
Riku ICHIHASHI (Tokyo Tech)
Shoto WATANABE (Hokkaido Univ.)
Kenta YOSHIMURA (Tokyo Tech)

Visiting Scientists
Kenichi YOSHIDA (Kyoto Univ.)
Kazuyuki SEKIZAWA (TITECH)
Futoshi MINATO (JAEA)
Koichi SATO (Kochi Univ.)

Assistant
Izumi YOSHIDA

List of Publications & Presentations

Publications

[Original Papers]

Q. Zhao, M. Kimura, B. Zhou, and S. Shin, "α formation probability in ^{10}Be and ^{12}Be within a microscopic cluster model," Phys. Rev. C **106**, 054313 (2022).

H. Motoki, Y. Suzuki, T. Kawai, and M. Kimura, "Cluster formation in neutron-rich Be and B isotopes," Prog. Theor. Exp. Phys. **2022**, 113D01 (2022).

T. Baba, Y. Taniguchi, and M. Kimura, "4α linear-chain state produced by ^{9}Be +^{9} Be collisions," Phys. Rev. C **105**, L061301 (2022).

H. Masui, W. Horiuchi, and M. Kimura, "Two-Neutron Halo Structure and Anti-halo Effect in ^{31}F," Few-Body Syst. **63**, 20 (2022).

S. Watanabe, F. Minato, M. Kimura, and N. Iwamoto, "Nuclear data generation by machine learning (I) application to angular distributions for nucleon-nucleus scattering," J. Nucl. Sci. and Technol. **59**, 1399 (2022).

Y. Suzuki, W. Horiuchi, and M. Kimura, "Erosion of $N = 28$ shell closure: Shape coexistence and monopole transition," Prog. Theor. Exp. Phys. **2022**, 063D02 (2022).

J. X. Han *et al*., "Observation of the $\pi^2\sigma^2$-bond linear-chain molecular structure in ^{16}C," Phys. Rev. C **105**, 044302 (2022).

Q. Zhao, B. Zhou, M. Kimura, H. Motoki, and S. Shin, "Microscopic calculations of ^{6}He and ^{6}Li with real-time evolution method," Eur. Phys. J. A **58**, 25 (2022).

M. Kimura, Y. Suzuki, T. Baba, and Y. Taniguchi, "Description of isospin mixing by a generator coordinate method," Phys. Rev. C **105**, 014311 (2022).

R. Takatsu, Y. Suzuki, W. Horiuchi, and M. Kimura, "Microscopic study of the deformed neutron halo of ^{31}Ne," Phys. Rev. C **107**, 024314 (2023).

T. Nakatsukasa, "Fermi operator expansion method for nuclei and inhomogeneous matter with a nuclear energy density functional," Phys. Rev. C **107**, 015802 (2023).

S. Kaur *et al*., "Proton distribuition radii of $^{16-24}$O: Signatures of new shell closures and neutron skin," Phys. Rev. Lett. **129**, 142502 (2022).

H. Tajima, H. Moriya, W. Horiuchi, K. Iida, and E. Nakano, "Resonance-to-bound transition of ^{5}He in neutron matter and its analogy with heteronuclear Feshback molecule," Phys. Rev. C **106**, 045807 (2022).

W. Horiuchi and N. Itagaki, "Density profiles near nuclear surface of ^{44,52}Ti: An indication of α clustering," Phys. Rev. C **106**, 044330 (2022).

W. Horiuchi and N. Itagaki, "Imprints of α clustering in the density profiles of ^{12}C and ^{16}O," Phys. Rev. C **107**, L021304 (2023).

H. Moriya, W. Horiuchi, J. Casal, and L. Fortunato, "Three-α configurations of the second $J^\pi = 2^+$ state in ^{12}C," Eur. Phys. J. A **59**, 37 (2023).

Presentations

[International Conferences/Workshops]

M. Kimura (invited) and Y. Taniguchi, "Astrophysical S-factor for ^{12}C + ^{12}C fusion reaction from a full-microscopic nuclear model," Annual Topical Meeting of IReNA - FA1 Nuclear reaction measurements in Underground Laboratories, Online, April 5–8, 2022.

M. Kimura (invited) and Y. Taniguchi, "Low energy monopole strength: A novel approach to the astrophysical fusion reactions," ECT* Workshop, Advances On Giant Nuclear Monopole Excitations And Applications To Multi-Messenger Astrophysics, Online, July 10–14, 2022.

M. Kimura (invited), "Monopole transitions as a probe for nuclear shape and clusters," Developments of Physics of Unstable Nuclei (YKIS2022b), Kyoto, Japan, May 23–27, 2022.

M. Kimura (invited), "Alpha cluster formation at the surface of stable and unstable nuclei," Korean Physical Society Spring meeting 2022, Online, April 4–8, 2022.

M. Kimura (invited), "Shape coexistence and electromagnetic moments/transitions," VI Topical Workshop on Modern Aspects in Nuclear Structure, Bormio, Italy, February 6–11, 2023.

Y. Taniguchi (invited) and M. Kimura, "Microscopic estimation of ^{12}C + ^{12}C fusion reaction rate at astrophysical energies," YIPQS long-term workshop Mean-field and Cluster Dynamics in Nuclear Systems 2022 (MCD2022), Kyoto, Japan, May 9–June 17, 2022.

F. Minato (invited), "Theoretical studies of beta-decay half-lives," JSPS/NSFC/NRF A3 Foresight Program Nuclear Physics in the 21st Century, Osaka, February 13–15, 2023.

F. Minato (invited), "Predictions of beta-decay half-lives and neutron capture cross sections of neutron-rich nuclei," RIKEN Workshop Physics of RI; Recent progress and perspectives, Wako, May, 2022.

K. Yoshida (invited), "Mean-field based approach for collective excitations in neutron-rich nuclei," YKIS2022b: Developments of Physics of Unstable Nuclei, Kyoto, Japan, May 23–27, 2022.

K. Yoshida (invited), "Pairing in neutron-rich nuclei investigated by responses," Physics of RI: Recent progress and perspectives, Wako, Japan, May 30–June 1, 2022.

K. Yoshida (invited),"Skyrme-QRPA for monopole modes of excitation," Advances on Giant Monopole Excitations and Applications to Multi-messenger Astrophysics, ECT*, Trento, Italy & Online, July 11–15, 2022.

K. Sato (invited), "Nuclear density functional calculation with proton-neutron mixing," YITP Workshop Fundamentals in Density Functional Theory (DFT2022), Kyoto University, December, 2022.

Y. Taniguchi (oral), "^{12}C + ^{12}C fusion reaction rate from a microscopic nuclear model," PANDORA Wrokshop, Onna, Japan, March 5–7, 2023.

Y. Taniguchi (oral), "^{12}C + ^{12}C fusion reaction rate from a full-microscopic nuclear model," The 16th International Symposium on Origin of Matter and Evolution of Galaxies, Hanoi, Vietnam, October 24–28, 2022.

Y. Taniguchi (oral), "^{12}C + ^{12}C fusion astrophysical S-factor from a full-microscopic nuclear model," Developments of Physics of Unstable Nuclei (YKIS2022b), Kyoto, Japan, May 23–27, 2022.

F. Minato (oral), "Evaluation of fission fragment yields and parameter optimization in CCONE code system," 2nd RCM on Updating Fission Yield Data for Applications, December, 2022.

F. Minato (oral), "Effects of continuum states on particle emissions from muon captures," YIPQS long-term workshop on Mean-field and Cluster Dynamics in Nuclear Systems 2022 (MCD 2022), Kyoto, May, 2022.

F. Minato (oral), "Study of particle emissions following beta-decays and muon captures," Shapes and Symmetries in Nuclei: from Experiment to Theory (SSNET'22 Conference), Orsay, May, 2022.

K. Sato (oral), "Large-amplitude collective dynamics with the adiabatic SCC theory including the second-order collective operator," YIPQS long-term workshop Mean-field and Cluster Dynamics in Nuclear Systems 2022 (MCD2022), Yukawa Institute for Theoretical Physics, Kyoto University, Japan, May 7–June 17, 2022.

S. Watanabe (oral), M. Kimura, F. Minato, S. Yoshida, and N. Iwamoto, "Nuclear data generation by machine learning," YIPQS long-term workshop "Mean-field and Cluster Dynamics in Nuclear Systems 2022 (MCD2022), Kyoto, Japan, May 9–June 17, 2022.

S. Watanabe, M. Kimura, F. Minato, S. Yoshida, and N. Iwamoto, "Generating nucleon-nucleus scattering data by Gaussian process regression," 15th International Conference on Nuclear Data for Science and Technology (ND2022), Online, July 24–29, 2022.

[Domestic Conferences/Workshops]

谷口億宇 (招待講演), 「基底および共鳴状態におけるクラスター相関と天体核反応」, おのころ戸隠夏合宿, JA 長野県ビル, 長野, 2022 年 7 月 29, 30 日.

谷口億宇 (招待講演), 木村真明, 「低エネルギー ^{12}C + ^{12}C 核融合反応率の微視的模型による評価」, 低エネルギー核物理と高エネルギー天文学で読み解く中性子星, 大阪大学核物理研究センター, 2022 年 8 月 3–5 日.

谷口億宇 (招待講演), 木村真明, 「X 線バーストを引き起こす ^{12}C + ^{12}C 分子共鳴状態」, 核反応シミュレーションと機械学習による核反応模型の発展, 北海道大学, 2022 年 12 月 13–15 日.

谷口億宇 (招待講演), 木村真明, 「^{12}C + ^{12}C molecular resonances that enhance the fusion reaction rate」, 星の進化と爆発天体における核反応の物理, 理化学研究所, 2023 年 2 月 20–21 日.

谷口億宇 (招待講演), 木村真明, 「天体核融合とノックアウト反応の微視的模型による研究」, 日本物理学会春季大会, オンライン, 2023 年 3 月 22–25 日.

湊太志 (招待講演), 「実験データからの拘束条件下での中性子捕獲断面積の理論予測」, 第 2 回 研究用原子炉を用いた原子核素粒子物理学（FPUR-II), 2023 年 3 月 16 日.

湊太志 (招待講演), 「中性子過剰核のベータ崩壊と遅発中性子」, 理化学研究所 RIBF ミニワークショップ「理論と実験で拓く中性子過剰核の核分裂」, 和光市, 2023 年 2 月 16–17 日.

湊太志 (招待講演), 「様々な拘束条件下での中性子過剰核の捕獲断面積の不定性」, 研究会「中性子捕獲反応で迫る宇宙の元素合成」, 東京, 2023 年 2 月 9–10 日.

湊太志 (招待講演), 「ミュオン捕獲後の粒子放出と半導体ソフトエラー」, 北大情報基盤セ萌芽型共同研究研究会「核反応シミュレーションと機械学習による核反応模型の発展」, 札幌, 2022 年 12 月.

湊太志 (招待講演), 「原子核構造モデルによるミュオン捕獲後の粒子放出計算」, ミューオンソフトエラー研究会, 九州大学筑紫キャンパス, 2022 年 11 月.

湊太志 (招待講演), 「Skyrme EDF+QRPA による beta 崩壊半減期の研究」, UKAKUREN-RCNP Conference on AstroNuclear Physics (ANP2022), 豊中, オンライン, 2022 年 7 月.

湊太志 (招待講演), 「中性子過剰核の keV 領域の中性子捕獲反応の理論予測」, RCNP 研究会「研究用原子炉を用いた原子核素粒子物理学」, 茨木, 2022 年 5 月.

谷口億宇 (口頭発表), 木村真明, 「クラスター共鳴による天体における ^{12}C + ^{12}C 核融合反応率の増大」, 原子核におけるクラスター物理の新展開, 大阪公立大学, 2022 年 10 月 19–20 日.

谷口億宇 (口頭発表), 木村真明, 「天体における ^{12}C + ^{12}C 核融合反応率の微視的評価」, 日本物理学会 2022 年秋季大会, 岡山理科大学, 2022 年 9 月 6–8 日.

谷口億宇 (口頭発表), 木村真明, 「^{12}C + ^{12}C fusion reaction rate at low temperature from a microscopic nuclear model」, UKAKUREN-RCNP Conference on AstroNuclear Physics (ANP2022), 大阪大学, 2022 年 7 月 20–21 日.

谷口億宇 (口頭発表), 木村真明, 「天体エネルギーにおける ^{12}C + ^{12}C 核融合反応率の微視的評価」, RCNP 研究会「原子核反応研究の最近の話題と展望」, 大阪大学核物理研究センター, 2022 年 7 月 8–9 日.

湊太志 (口頭発表), 「ミュオン捕獲後の粒子放出」, 日本物理学会 2022 年秋季大会, 岡山市, 2022 年 9 月.

堀内渉 (口頭発表), 板垣直之, 「原子核密度分布にみる α クラスター状態」, 大阪公立大研究会「原子核におけるクラスター物理の新展開」, 大阪公立大学杉本キャンパス, 2022 年 10 月 19–20 日.

堀内渉 (口頭発表), 鈴木宜之, M. Shalchi, L. Tomio, 「カルシウム 62, 72 のエキゾチックハロー構造発現の可能性について」, 日本物理学会 2022 年秋季大会, 岡山理科大学, 2022 年 9 月 6–8 日.

堀内渉 (口頭発表), 稲倉恒法, 「中性子過剰鉛同位体における芯核増大現象」, 日本物理学会 2022 年秋季大会, 岡山理科大学, 2022 年 9 月 6–8 日.

森谷元 (口頭発表), 堀内渉, Jeśus Casal, Lorenzo Fortunato, 「直交条件模型を用いた炭素 12 第二 2^+ 状態の研究」, 日本物理学会 2022 年秋季大会, 岡山理科大学, 2022 年 9 月 6–8 日.

槇口雄二 (口頭発表), 堀内渉, 「高エネルギー原子核衝突における不完全吸収反応」, 日本物理学会 2022 年秋季大会, 岡山理科大学, 2022 年 9 月 6–8 日.

堀内渉 (口頭発表), 板垣直之, 「陽子弾性散乱でみる原子核のクラスター構造」, 日本物理学会 2023 年春季大会, オンライン, 2023 年 3 月 22–25 日.

山口雄紀 (口頭発表), 堀内渉, 板垣直之, 「ネオン 20 のクラスター構造と陽子弾性散乱断面積」, 日本物理学会 2023 年春季大会, オンライン, 2023 年 3 月 22–25 日.

森谷元 (口頭発表), 堀内渉, Bo Zhou, 「パウリ原理を考慮した新しい多クラスター系の基底関数 II」, 日本物理学会 2023 年春季大会, オンライン, 2023 年 3 月 22–25 日.

吉田賢市 (口頭発表), "Neutron stars tell us the shapes of nuclei," RCNP 研究会「低エネルギー核物理と高エネルギー天文学で読み解く中性子星」, 大阪大学核物理研究センター, 2022 年 8 月 3–5 日.

吉田賢市 (口頭発表), "Enhanced moments of inertia in neutron-rich nuclei: A role of pair correlations," 日本物理学会 2022 年秋季大会, 岡山理科大学, 2022 年 9 月 6–8 日.

吉田賢市 (口頭発表), "Collectivity of proton-neutron pairing," RCNP 研究会「微視的系と巨視的系における核子対凝縮相」, 大阪大学核物理研究センター, 2022 年 9 月 26–28 日.

吉田賢市 (口頭発表), "Linear-response TDDFT for rotating nuclei—Nuclear DFT for rovibrational motions—" Domestic Molecule Type Workshop Fundamentals in density functional theory, 京都大学基礎物理学研究所, 2022 年 12 月 7–20 日.

佐藤弘一 (口頭発表), 「高次の集団座標演算子を入れた大振幅集団運動への断熱的アプローチ II」, 日本物理学会 2022 年秋季大会, 岡山理科大学, 2022 年 9 月.

佐藤弘一 (口頭発表), 「ATDHF/ASCC 方程式における解の一意性の破れ」, 日本物理学会 2023 年春季大会, オンライン, 2023 年 3 月.

渡辺証斗 (口頭発表), 木村真明, 湊太志, 吉田聡太, 岩本信之, 「機械学習を用いた核データ生成」, 日本原子力学会 2022 年秋の年会大会, 茨城大学, 2022 年 8 月 6–9 日.

[Seminars]

W. Horiuchi, "What can we learn from nuclear density profiles ?," The 311th RIKEN RIBF nuclear physics seminar, RIKEN Nishina Center (Hybrid), Wako, Japan, November 17, 2022.

吉田賢市, "Shell effects in non-axial-shape excitations," 第 977 回九大原子核セミナー, 九州大学, 2023 年 1 月 24 日.

Nuclear Science and Transmutation Research Division
Superheavy Element Research Group

1. Abstract

The heavy elements with atomic numbers exceeding 103 are called superheavy elements (SHEs). In Superheavy Element Research Group, Superheavy Element Production Team and Superheavy Element Devise Development Team work together to investigate synthesis of SHEs, nuclear properties of SHE nuclei, and chemical properties of SHEs. We also develop and maintain SHE production and separation devices, detectors, and chemistry apparatuses.

2. Major Research Subjects

(1) Search for new superheavy elements
(2) Decay spectroscopy of the heaviest nuclei
(3) Study of reaction mechanisms for production of the heaviest nuclei
(4) Study of chemical properties of the heaviest elements
(5) Development, maintenance, and operation of GARIS, GARIS-II, and GARIS-III
(6) Development and maintenance of detector and DAQ system of GARIS, GARIS-II, and GARIS-III
(7) Development and maintenance of target system of GARIS, GARIS-II, and GARIS-III

3. Summary of Research Activity

See the subsections of Superheavy Element Production Team and Superheavy Element Device Development Team.

Member

Director

Hiromitsu HABA

List of Publication

Publication

See the subsections of Superheavy Element Production Team and Superheavy Element Device Development Team.

Nuclear Science and Transmutation Research Division
Superheavy Element Research Group
Superheavy Element Production Team

1. Abstract

The elements with atomic number $Z \geq 104$ are called as trans-actinide or superheavy elements (SHEs). Superheavy Element Production Team synthesizes SHE nuclei including new elements and investigates synthesis mechanisms of SHE nuclei, nuclear properties of SHE nuclei, and chemical properties of SHEs in collaboration with Superheavy Element Devise Development Team and Nuclear Chemistry Research Team of RIKEN Nishina Center.

2. Major Research Subjects

(1) Search for new superheavy elements
(2) Decay spectroscopy of the heaviest nuclei
(3) Study of reaction mechanisms for production of the heaviest nuclei
(4) Study of chemical properties of the heaviest elements

3. Summary of Research Activity

(1) Search for new superheavy elements

In November 2016, the 7th period of the periodic table was completed with the official approval of four new elements, nihonium (Nh, $Z = 113$), moscovium (Mc, $Z = 115$), tennessine (Ts, $Z = 117$), and oganesson (Og, $Z = 118$) by International Union of Pure and Applied Chemistry. We have started to search for new elements to expand the chart of the nuclides toward to the island of stability and the periodic table of the elements toward the 8th period. In January 2020, RIKEN heavy-ion Linear ACcelerator (RILAC) was upgraded as Superconducting RIKEN heavy-ion Linear ACcelerator (SRILAC). We installed the new gas-filled recoil ion separator GARIS-III on the beam line of SRILAC. In June–July 2020, we conducted the commissioning of SRILAC and GARIS-III using the ^{169}Tm + ^{40}Ar, ^{208}Pb + ^{40}Ar, and ^{208}Pb + ^{51}V reactions. Since October 2020, we have been conducting a synthesis experiment of isotopes of new element 119 in the ^{248}Cm + ^{51}V reaction under the nSHE collaboration.

(2) Study of reaction mechanisms for production of the heaviest nuclei

SHE nuclei have been produced by complete fusion reactions of two heavy nuclei. However, the reaction mechanism of the fusion process is still not well understood both theoretically and experimentally. In 2022, the quasielastic barrier distribution of the ^{51}V + ^{248}Cm reaction was extracted by measuring the excitation function of quasielastic backscattering using GARIS-III at SRILAC. The result was utilized to estimate the optimal incident beam energy for production of isotopes of new element 119 in the ^{248}Cm(^{51}V, xn)$^{299-x}$119 reactions. We also measured the excitation functions for the evaporation residues and the quasielastic scattering of the ^{51}V + ^{159}Tb reaction to deepen our understanding of the ^{51}V-induced reaction on the deformed target.

(3) Study of chemical properties of the heaviest elements

Chemical characterization of newly-discovered SHEs is an extremely interesting and challenging research subject in modern nuclear and radiochemistry. In collaboration with Nuclear Chemistry Research Team of RIKEN Nishina Center, we are developing SHE production systems as well as rapid single-atom chemistry apparatuses for chemistry studies of SHEs. We installed a gas-jet transport system to the focal plane of GARIS at RILAC. This system is a promising approach for exploring new frontiers in SHE chemistry: the background radiations from unwanted products are strongly suppressed, the intense primary heavy-ion beam is absent in the gas-jet chamber, and hence the high gas-jet extraction yield is attained. Furthermore, the beam-free conditions make it possible to investigate new chemical systems. In 2022, we continued to develop an ultra-rapid gas-chromatograph apparatus, which consists of an RF carpet gas cell and a cryo-gas-chromatograph column with a Si detector array, at the focal plane of GARIS for the gas chemistry of SHEs. To realize aqueous chemistry studies of Sg ($Z = 106$) and Bh ($Z = 107$), we have been developing a continuous and rapid solvent extraction apparatus which consists of a continuous dissolution apparatus Membrane DeGasser (MDG), a Flow Solvent Extractor (FSE), and a liquid scintillation detector for α/SF-spectrometry. In collaboration with Osaka University, co-precipitation behavior of No ($Z = 102$) with $BaSO_4$ and CaC_2O_4 was also investigated with ^{255}No produced in the ^{248}Cm(^{12}C, $5n$)^{255}No reaction at the AVF cyclotron.

Members

Team Leader

Hiromitsu HABA

Research & Development Scientist

Daiya KAJI

Visiting Scientists

Marc ASFARI (IPHC/Univ. of Strasbourg)
Mahananda DASGUPTA (Australian Nat'l Univ.)
Olivier DORVAUX (Univ. of Strasbourg)
Benoit Jean-Paul GALL (Univ. of Strasbourg)
Zaiguo GAN (Inst. of Modern Phys./Chinese Academy of Sci.)
David HINDE (Australian Nat'l Univ.)
Minghui HUANG (Inst. of Modern Phys./Chinese Academy of Sci.)
Kieran KESSACI (Univ. of Strasbourg)
Hiroyuki KOURA (JAEA)
Daisuke NAGAE (Tokyo Tech)
Satoshi SAKAGUCHI (Kyushu Univ.)
Mirei TAKEYAMA (Yamagata Univ.)
Taiki TANAKA (Australian Nat'l Univ.)
Huabin YANG (Inst. of Modern Phys./Chinese Academy of Sci.)
Zhiyuan ZHANG (Inst. of Modern Phys./Chinese Academy of Sci.)

Student Trainees

Margaux S.A. FORGE (Univ. of Strasbourg)
Takumi FUKATSU (Kyushu Univ.)
Yuichi ISHIBASHI (Kyushu Univ.)
Sotaro MATSUNAGA (Kyushu Univ.)
Haruki MATSUURA (Kyushu Univ.)
Yuya MICHIMOTO (Kyushu Univ.)
Mikito NOMI (Kyushu Univ.)
Koichi SUGIYAMA (Kyushu Univ.)
Yuki YAMANOUCHI (Kyushu Univ.)

Intern

Margaux S.A. FORGE (Univ. of Strasbourg)

List of Publications & Presentations

Publications

[Original Papers]

A. Yakushev, L. Lens, Ch.E. Düllmann, J. Khuyagbaatar, E. Jäger, J. Krier, J. Runke, H. M. Albers, M. Asai, M. Block, J. Despotopulos, A. Di Nitto, K. Eberhardt, U. Forsberg, P. Golubev, M. Götz, S. Götz, H. Haba, L. Harkness-Brennan, R.-D. Herzberg, F. P. Heßberger, D. Hinde, A. Hübner, D. Judson, B. Kindler, Y. Komori, J. Konki, J. V. Kratz, N. Kurz, M. Laatiaoui, S. Lahiri, B. Lommel, M. Maiti, A. Mistry, Ch. Mokry, K. J. Moody, Y. Nagame, J. P. Omtvedt, P. Papadakis, V. Pershina, D. Rudolph, L. G. Samiento, T. K. Sato, M. Schädel, P. Scharrer, B. Schausten, D. A. Shaughnessy, J. Steiner, P. Thörle-Pospiech, A. Toyoshima, N. Trautmann, K. Tsukada, J. Uusitalo, K.-O. Voss, A. Ward, M. Wegrzecki, N. Wiehl, E. Williams, and V. Yakusheva, "On the adsorption and reactivity of element 114, flerovium," Front. Chem. **10**, published online (August 25, 2022). DOI: 10.3389/fchem.2022.976635 .

M. Tanaka, P. Brionnet, M. Du, J. Ezold, K. Felker, B. J. P. Gall, S. Go, R. K. Grzywacz, H. Haba, K. Hagino, S. Hogle, S. Ishizawa, D. Kaji, S. Kimura, T. T. King, Y. Komori, R. K. Lemon, M. G. Leonard, K. Morimoto, K. Morita, D. Nagae, N. Naito, T. Niwase, B. C. Rasco, J. B. Roberto, K. P. Rykaczewski, S. Sakaguchi, H. Sakai, Y. Shigekawa, D. W. Stracener, S. VanCleve, Y. Wang, K. Washiyama, and T. Yokokita, "Probing optimal reaction energy for synthesis of element 119 from ^{51}V + ^{248}Cm reaction with quasielastic barrier distribution measurement," J. Phys. Soc. Jpn. **91**, 084201-1–11 (2022).

A. C. Berriman, D. J. Hinde, D. Y. Jeung, M. Dasgupta, H. Haba, T. Tanaka, K. Banerjee, T. Banerjee, L. T. Bezzina, J. Buete, K. J. Cook, S. Parker-Steele, C. Sengupta, C. Simenel, E. C. Simpson, M. A. Stoyer, B. M. A. Swinton-Bland, and E. Williams, "Energy dependence of p + ^{232}Th fission mass distributions: Mass-asymmetric standard I and standard II modes, and multichance fission," Phys. Rev. C **105**, 064614-1–18 (2022).

H. Sakai, H. Haba, K. Morimoto, and N. Sakamoto, "Facility upgrade for superheavy-element research at RIKEN," Eur. Phys. J. A **58**, 238-1–15 (2022).

[Review Article]

羽場宏光, 「人工元素合成」, 科学 **92**, 846–851 (2022).

[Books]

羽場宏光, 「元素探索と RI 製造」 in 「量子ビーム科学の基礎と応用」, NSA/Commentaries **27**, 一般社団法人日本原子力産業協会 原子力システム研究懇話会, 195 ページ, 2023 年 3 月 24 日, p. 26–39.

桜井弘（編), 荒野泰, 小谷明, 高妻孝光, 佐治英郎, 鈴木晋一郎, 中山祐正, 根矢三郎, 羽場宏光, 廣田俊, 藤井敏司, 「ブルーバックス 元素 118 の新知識 第 2 版」, 講談社, 2023 年 3 月 20 日, p. 560.

[Proceeding]

H. Sakai, H. Haba, K. Morimoto, and N. Sakamoto, "Facility upgrade for SHE research at RIKEN Nishina Center," Acta Phys. Pol. B Proc. Suppl. **16**, 4-A10-1–12 (2023).

Presentations

[International Conferences/Workshops]

H. Haba (invited), "Production and applications of radioisotopes at RIKEN RI Beam Factory—Search for new elements through diagnosis and therapy of cancer—," Laser Solutions for Space and the Earth 2022 in OPTICS & PHOTONICS International Congress 2022 (OPIC 2022), Yokohama, Japan & Online, April 18–22, 2022.

M. Tanaka (invited) for nSHE Collaboration, "Quasielastic backscattering measurement for ^{51}V + ^{248}Cm reaction toward element-119 synthesis at RIKEN," 19th Workshop on Recoil Separator for Superheavy Element Chemistry & Physics (TASCA 22), Darmstadt, Germany & Online, May 10–12, 2022.

H. Haba (invited), "Production and applications of radioisotopes at RIKEN RI Beam Factory—Search for new elements through diagnosis and therapy of cancer—," IAEA/RCA RTC on Good Manufacturing Practice (GMP) and Radiation Safety Aspects of Radiopharmaceutical Production Using Medical Cyclotron, Online, May16–20, 2022.

H. Sakai (invited), H. Haba, K. Morimoto, and N. Sakamoto, "Facility upgrade for SHE research at RIKEN," Zakopane Conference on Nuclear Physics, "Extremes of the Nuclear Landscape," Zakopane, Poland, August 28–September 4, 2022.

M. Tanaka (oral) for nSHE Collaboration, "Optimal energy for element 119 synthesis via ^{51}V + ^{248}Cm reaction probed by quasielastic barrier distribution measurement," Zakopane Conference on Nuclear Physics, "Extremes of the nuclear landscape," Zakopane, Poland, August 28–September 4, 2022.

S. Sakaguchi (poster) and M. Tanaka for nSHE Collaboration, "Probing optimal energy for synthesis of element 119 from ^{51}V+^{248}Cm reaction," The 28th International Nuclear Physics Conference (INPC 2022), Cape Town, South Africa, September 11–16, 2022.

A. Takamine (invited), D. Kaji, H. Haba, M. Wada, P. Schury, H. Koura, H. Wollnik, H. Miyatake, H. Ishiyama, K. Morimoto, M. Rosenbusch, S. Kimura, T. Niwase, Y. Hirayama, Y. Ito, Y. Watanabe, and P. Brionnet, "Multi-reflection time-of-flight mass spectroscopy of superheavy nuclides," 19th International Conference on Electromagnetic Isotope Separators and Related Topics (EMIS 2022), Daejeon, Korea, October 3–7, 2022.

M. Tanaka (oral), "Optimal reaction energy for synthesis of element 119 via ^{51}V + ^{248}Cm reaction probed by quasielastic barrier distribution measurement," 19th International Conference on Electromagnetic Isotope Separators and Related Topics (EMIS 2022), Daejeon, Korea, October 3–7, 2022.

P. Brionnet (poster), R. Grzywacz, D. Kaji, T. King, T. Niwase, K. Morimoto, and K. Rykaczewski, "Development and optimization of the digital electronic for the search of new super heavy element at RIKEN on GARIS-III," 19th International Conference on Electromagnetic Isotope Separators and Related Topics (EMIS 2022), Daejeon, Korea, October 3–7, 2022.

H. Haba (invited), "Production and distribution of radioisotopes at RIKEN RI Beam Factory," PRISMAP Workshop on Emerging Infrastructures and Technical Developments, Padova, Italy & Online, November 21–22, 2022.

H. Haba (invited), "Production of radioisotopes for application studies at RIKEN RI Beam Factory—Search for new elements through diagnosis and therapy of cancer," The Fifth International Conference on Application of RadiotraCers and Energetic Beams in Sciences (ARCEBS 2023), Purulia, India, January 31–February 5, 2023.

[Domestic Conferences/Workshops]

永井歩夢 (口頭発表), 細川浩由, 中島朗久, 坂口綾, 南部明弘, 重河優大, 羽場宏光, 横山明彦, 「^{232}Th + ^{7}Li 核反応によって生成する U 同位体の ICP-MS による定量」, 日本放射化学会第 66 回討論会 (2022), 文京区, 2022 年 9 月 15–17 日.

渡邉瑛介 (口頭発表), 笠松良崇, 横北卓也, 中西諒平, 大髙咲希, 板倉悠大, 益田遼太郎, 王瑞麟, 重河優大, 南部明弘, 殷小杰, 羽場宏光, 高宮幸一, 篠原厚, 「クラウンエーテルを用いた 102 番元素ノーベリウムの硝酸系固液抽出実験」, 日本放射化学会第 66 回討論会 (2022), 文京区, 2022 年 9 月 15–17 日.

中西諒平 (口頭発表), 渡邉瑛介, 大髙咲希, 王瑞麟, 板倉悠大, 速水翔, 羽場宏光, 南部明弘, 篠原厚, 笠松良崇, 「Rf の共沈実験に向けた Zr, Hf, Th のシュウ酸, マロン酸系でのフロー式共沈実験」, 日本放射化学会第 66 回討論会 (2022), 文京区, 2022 年 9 月 15–17 日.

羽場宏光 (依頼講演), 「新元素でがん治療〜理研 RI ビームファクトリーがつくるラジオアイソトープ〜」, 放射線安全フォーラム第 75 回放射線防護研究会, 「短寿命核種の利用の拡大に向けて」, 文京区 & オンライン, 2022 年 10 月 29 日.

山ノ内邑希 (ポスター発表), 坂口聡志, Pierre Brionnet for nSHE Collaboration, 「新元素合成のための最適反応エネルギー推定に向けた ^{51}V + ^{159}Tb 融合反応の励起関数測定」, 日本物理学会 2023 年春季大会, オンライン, 2023 年 3 月 22–25 日.

深津巧光 (ポスター発表), 坂口聡志, Pierre Brionnet for nSHE Collaboration, 「新元素合成のための最適反応エネルギー推定に向けた ^{51}V + ^{159}Tb 融合反応の障壁分布測定 I」, 日本物理学会 2023 年春季大会, オンライン, 2023 年 3 月 22–25 日.

道本優也 (ポスター発表), 坂口聡志, Pierre Brionnet for nSHE Collaboration, 「新元素合成のための最適反応エネルギー推定に向けた ^{51}V + ^{159}Tb 融合反応の障壁分布測定 II」, 日本物理学会 2023 年春季大会, オンライン, 2023 年 3 月 22–25 日.

Outreach Activities

羽場宏光 (依頼講演), 「新元素でがん治療—RIBF がつくるラジオアイソトープ—」, 理研と未来を創る会第 28 回講演会, 和光市, 2022 年 9 月 6 日.

羽場宏光 (依頼講演), 「ニホニウム発見への道のり」, 山梨県立吉田高等学校理研見学会, 和光市, 2022 年 11 月 16 日.

Nuclear Science and Transmutation Research Division
Superheavy Element Research Group
Superheavy Element Device Development Team

1. Abstract

A gas-filled recoil ion separator has been used as a main experimental device for the study of superheavy elements. This team is in charge of maintaining, improving, developing, and operating the separators and related devices. In the RIBF facility, three gas-filled recoil ion separators are installed at RILAC and RRC facility. One is GARIS that is designed for a symmetric reaction such as coldfusion reaction, and the other two are developed for an asymmetric reaction such as hot-fusion reaction, GARIS-II and GARIS-III. New elements ^{278}113 were produced by ^{70}Zn + ^{209}Bi reaction using GARIS. Further the new element search is currently in progress by using GARIS-II and GARIS-III.

2. Major Research Subjects

(1) Maintenance of GARIS, GARIS-II and development of new separator GARIS-III
(2) Maintenance and development of detector and DAQ system for superheavy element research
(3) Maintenance and development of target system for GARIS, GARIS-II and GARIS-III

3. Summary of Research Activity

The GARIS-II and III are newly developed which has an acceptance twice as large as existing GARIS, in order to realize higher transmission. A new element search program aiming to element 119 was started using GARIS-II. And new separator GARIS-III was developed and installed into the RILAC experimental hall. After the some commissioning works of GARIS-III, new 119th element search has been started. We will also offer user-support if a researcher wishes to use the devices for his/her own research program.

Members

Team Leader
Kouji MORIMOTO

Senior Technical Scientists
Masaki FUJIMAKI
Daiya KAJI

Postdoctoral Researchers
Pierre BRIONNET
Sota KIMURA

Visiting Scientists
Shin-ichi GOTO (Niigata Univ.)
Katsuhisa NISHIO (JAEA)
Eiji IDEGUCHI (Osaka Univ.)
Toshitaka NIWASE (KEK)
Yuta ITO (JAEA)
Fuyuki TOKANAI (Yamagata Univ.)

Student Trainee
Kosaku KURAMOTO (Yamagata Univ.)

List of Publications & Presentations

Publications

[Original Papers]

P. Brionnet, R. K. Grzywacz, D. Kaji, T. T. King, T. Niwase, K. Morimoto, K. P. Rykaczewski, and H. Sakai, "Development of digital electronics for the search of SHE nuclei using GARIS-II/III at RIKEN," Nucl. Instrum. Methods Phys. Res. A **1049**, 168068 (2023).

H. Sakai, H. Haba, K. Morimoto, and N. Sakamoto, "Facility upgrade for superheavy-element research at RIKEN," Eur. Phys. J. A **58**, 238 (2022).

M. Tanaka, P. Brionnet, M. Du, J. Ezold, K. Felker, B. J. P. Gall, S. Go, R. K. Grzywacz, H. Haba, K. Hagino, S. Hogle, S. Ishizawa, D. Kaji, S. Kimura, T. T. King, Y. Komori, R. K. Lemon, M. G. Leonard, K. Morimoto, K. Morita, D. Nagae, N. Naito, T. Niwase, B. C. Rasco, J. B. Roberto, K. P. Rykaczewski, S. Sakaguchi, H. Sakai, Y. Shigekawa, D. W. Stracener, S. VanCleve, Y. Wang, K. Washiyama, and T. Yokokita, "Probing optimal reaction energy for synthesis of element 119 from ^{51}V + ^{248}Cm reaction with quasielastic barrier distribution measurement," J. Phys. Soc. Jpn. **91**, 084201 (2022).

T. Niwase, Y. X. Watanabe, Y. Hirayama, M. Mukai, P. Schury, A. N. Andreyev, T. Hashimoto, S. Iimura, H. Ishiyama, Y. Ito, S. C. Jeong, D. Kaji, S. Kimura, H. Miyatake, K. Morimoto, J. -Y. Moon, M. Oyaizu, M. Rosenbusch, A. Taniguchi, and M. Wada, "Discovery of new isotope ^{241}U and systematic high-precision atomic mass measurements of neutron-rich Pa-Pu nuclei produced via multinucleon transfer reactions," Phys. Rev. Lett. **130**, 132502 (2023).

T. Niwase, W. Xian, M. Wada, M. Rosenbusch, S. Chen, A. Takamine, J. Liu, S. Iimura, D. Hou, S. Yan, H. Ishiyama, H. Miyatake, S. Nishimura, D. Kaji, K. Morimoto, Y. Hirayama, Y. X Watanabe, S. Kimura, P. Schury, and H. Wollnik, "Development of a β-TOF detector: An enhancement of the α-TOF detector for use with β-decaying nuclides," Prog. Theor. Exp. Phys. **2023**, 031H01 (2023).

M. Rosenbusch, M. Wada, S. Chen, A. Takamine, S. Iimura, D. Hou, W. Xian, S. Yan, P. Schury, Y. Hirayama, Y. Ito, H. Ishiyama, S. Kimura, T. Kojima, J. Lee, J. Liu, S. Michimasa, H. Miyatake, M. Mukai, J. Y. Moon, S. Nishimura, S. Naimi, T. Niwase, T. Sonoda, Y. X. Watanabe, and H. Wollnik, "The new MRTOF mass spectrograph following the ZeroDegree spectrometer at RIKEN's RIBF facility," Nucl. Instrum. Methods Phys. Res. A **1047**, 167824 (2023).

S. Iimura, M. Rosenbusch, A. Takamine, Y. Tsunoda, M. Wada, S. Chen, D. S. Hou, W. Xian, H. Ishiyama, S. Yan, P. Schury, H. Crawford, P. Doornenbal, Y. Hirayama, Y. Ito, S. Kimura, T. Koiwai, T. M. Kojima, H. Koura, J. Lee, J. Liu, S. Michimasa, H. Miyatake, J. Y. Moon, S. Naimi, S. Nishimura, T. Niwase, A. Odahara, T. Otsuka, S. Paschalis, M. Petri, N. Shimizu, T. Sonoda, D. Suzuki, Y. X. Watanabe, K. Wimmer, and H. Wollnik, "Study of the $N = 32$ and $N = 34$ shell gap for Ti and V by the first high-precision multireflection time-of-flight mass measurements at BigRIPS-SLOWRI," Phys. Rev. Lett. **130**, 012501 (2023).

[Proceeding]

H. Sakai, H. Haba, K. Morimoto, and N. Sakamoto, "Facility upgrade for SHE research at RIKEN Nishina Center," Acta Phys. Pol. B Proc. Suppl. **16**, 4-A10-1–12 (2023).

Presentations

[International Conferences/Workshops]

H. Sakai (invited), "Facility upgrade for SHE research at RIKEN Nishina Center," 57th Zakopane Conference on Nuclear Physics, Zakopane, Poland, August 28–September 4, 2022.

K. Morimoto (oral), "Present status and plans of GARIS-II and GARIS-III," SSRI-PNS Collaboration Meeting 2022, Wako, Saitama & Online, September 1, 2022.

S. Kimura (oral), "Study of the neutron-rich ^{252}Cf-fission-fragments with MRTOF-MS," The 16th International Symposium on Origin of Matter and Evolution of Galaxies (OMEG16), Hanoi, Vietnam, October 24–28, 2022.

M. Tanaka (poster) and S. Sakaguchi for nSHE Collaboration, "Probing optimal energy for synthesis of element 119 from ^{51}V + ^{248}Cm reaction," The 28th International Nuclear Physics Conference (INPC 2022), South Africa, September 11–16, 2022.

P. Brionnet (invited), "Upgrade of the detection setup of the gas-filled recoil separator GARIS-III," 19th TASCA22 Workshop, GSI Darmstadt, Germany & Online, May 10–12, 2022.

P. Brionnet (poster), "Development and optimization of the digital electronic for the search of new super heavy element at RIKEN on GARIS-III," 19th International Conference on Electromagnetic Isotope Separators and Related Topics, EMIS 2022, Daejeon, South Korea, October 3–7, 2022.

[Seminar]

H. Sakai, "Facility upgrade for SHE research at RIKEN Nishina Center," C2R2 Seminer, IBS CENS, September 29, 2022.

[Domestic Conferences/Workshops]

倉本幸作 (ポスター発表), 森本幸司, 加治大哉, 武山美麗, 門叶冬樹, 「超重核実験用ピクセル型大面積半導体検出器の性能評価」, 第 37 回 研究会「放射線検出器とその応用」, 茨城県つくば市 (高エネルギー加速器研究機構放射線科学センター), 2023 年 1 月 25–27 日.

倉本幸作 (ポスター発表), 森本幸司, 加治大哉, 武山美麗, 門叶冬樹, 「超重核実験用ピクセル型大面積半導体検出器の性能評価」, 第 83 回応用物理学会秋季学術講演会, 東北大学川内北キャンパス & オンライン, 2022 年 9 月 20–23 日.

倉本幸作 (口頭発表), 森本幸司, 加治大哉, 武山美麗, 門叶冬樹, 「超重核実験用ピクセル型半導体検出器の不感層評価」, 第 59 回 アイソトープ・放射線研究発表会, オンライン, 2022 年 7 月 6–8 日.

Nuclear Science and Transmutation Research Division
Astro-Glaciology Research Group

1. Abstract

Our Astro-Glaciology Laboratory promotes both experimental and theoretical studies to open up the new interdisciplinary research field of astro-glaciology, which combines astrophysics, astrochemistry, glaciology, and climate science.

On the experimental side, we measure isotopic and ionic concentrations in ice cores drilled at Dome Fuji station, Antarctica, in collaboration with the National Institute of Polar Research (NIPR, Tokyo). Here, the ice cores are time capsules which preserve atmospheric information of the past. In particular, the ice cores obtained around the Dome Fuji site are very unique, because they contain much more information on the stratosphere than any other ice cores obtained from elsewhere on Earth. This means that we have significant advantages in using Dome Fuji ice cores if we wish to study the Universe, since UV photons, gamma-rays, and high energy protons emitted by astronomical phenomena affect the stratosphere.

Our principal aim is thus to acquire and interpret information preserved in ice cores regarding:

- Signatures of past volcanic eruptions and solar cycles;
- Relationship between climate change and solar activity;
- Traces of past supernovae in our galaxy, in order to understand better the rate of galactic supernova explosions.

Moreover, we are promoting experimental projects on:

- Development of an automated laser melting sampler for analyzing ice cores with high depth resolution;
- Development of precise analytical techniques of high sensitivity for analyzing ice cores;
- The application of analytical methods for measuring isotopes in ice cores to archaeological artifacts;
- The evolution of molecules in space;

On the theoretical side, we are simulating numerically:

- Chemical effects of giant solar flares and supernovae on the Earth's atmosphere;
- The explosive and the *r*-process nucleosynthesis in core-collapse supernovae;

Combining our experimental evidence and theoretical simulations, we are promoting the researches mentioned above. These all will contribute to understanding relationships between the Universe and Earth. In particular, climate change is the most critical issue facing the world in the 21st century. It is also emphasized that the frequency of supernova explosions in our galaxy has not yet been fully understood, and it is the key to understand the *r*-process nucleosynthesis.

Members

Director

Yuko MOTIZUKI

Senior Research Scientist

Yoichi NAKAI

Special Temporary Research Scientist

Kazuya TAKAHASHI

Technical Staff

Yu Vin SAHOO

Senior Visiting Scientists

Yasushige YANO (Nishina Memorial Foundation)
Kunihiko KODERA (Meteorological Res. Inst.)
Hideharu AKIYOSHI (National Institute for Environmental Studies)

Visiting Scientists

Hisashi HAYAKAWA (Nagoya Univ.)
Kazuho HORIUCHI (Hirosaki Univ.)
Hideki MADOKORO (Mitsubushi Heavy Industries, Ltd.)
Akira HORI (Kitami Inst. of Tech.)

Visiting Technicians

Junya HIROSE (Fusion Tech. Co., Ltd.)
Yuma HASEBE (Denryoku Comp. Ctr., Ltd.)

Research Part-time Worker

Kazuhito ITO

Administrative Part-time Worker
Kanako FUJITA

Assistant
Asako SAKIHAMA

List of Publications & Presentations

Publications

[Original Papers]

S. Katsuda, T. Enoto, A. N. Lommen, K. Mori, Y. Motizuki, M. Nakajima, N. C. Ruhl, K. Sato, G. Stober, M. S. Tashiro, Y. Terada, and K. S. Wood, "Long-term density trend in the mesosphere and lower thermosphere from occultations of the crab nebula with X-ray astronomy satellites," J. Geophys. Res. Space Phys. **128**, e2022JA030797 (2023).

A. Miyazaki, M. Tsuge, H. Hidaka, Y. Nakai, and N. Watanabe, "Direct determination of the activation energy for diffusion of OH radicals on water ice," Astrophys. J. Lett. **940**, L2 (2022).

Y. Miyake, N. Ikoma, K. Takahashi, Y. V. Sahoo, and H. Okuno, "Test of ^{107}Pd transmutation with macroscopic quantities," J. Nucl. Sci. Technol. **59**, 1536 (2022).

K. Takahashi, Y. V. Sahoo, Y. Nakai, H. Motoyama, and Y. Motizuki, "Annually resolved profiles of δ^{34}S and sulfate in shallow ice core DF01 (Dome Fuji, Antarctica) spanning the nineteenth century and their geochemical implications," J. Geophys. Res. Atmos. **127**, e2021JD036137 (2022).

Presentations

[International Conferences/Workshops]

Y. Motizuki (invited), "Verifying footprints of solar cycles and supernovae in polar ice cores," International Conference on Astrophysics with Radioactive Isotopes (AwRI), Budapest & Online, June 12–17, 2022.

S. Katsuda (poster), T. Enoto, A. N. Lommen, K. Mori, Y. Motizuki, M. Nakajima, N. C. Ruhl, K. Sato, G. Stober, M. S. Tashiro, Y. Terada, and K. S. Wood, "Measuring vertical density profiles of Earth's upper atmosphere using X-ray astronomy satellites," AGU Fall Meeting 2022, Chicago & Online, December 12–16, 2022.

Y. Motizuki (poster), Y. Nakai, K. Takahashi, T. Imamura, and H. Motoyama, "Eleven-year, 22-year and ~90-year solar cycles discovered in nitrate concentrations in a Dome Fuji (Antarctica) ice core," The 5th ISEE International Symposium: Toward the Future of Space-Earth Environmental Research, Nagoya & Online, November 15–17, 2022.

[Domestic Conferences/Workshops]

望月優子 (招待講演), 「地質学的試料に残った超新星の痕跡について」, 新学術領域「地下から解き明かす宇宙の歴史と物質の進化」主催第 9 回超新星ニュートリノ研究会, 九州大学・伊都キャンパス & オンライン, 2023 年 3 月 2–3 日.

望月優子 (招待講演), 「南極アイスコアから探る太陽活動と気候変動〜太陽の鼓動—星と私たちの繋がりを通して」, お茶の水女子大学理学部主催第 10 回宇宙講演会, 東京, 2022 年 12 月 10 日.

望月優子 (招待講演), 「南極の氷からひもとく地球と宇宙の歴史」, 朝日カルチャーセンター新宿教室, オンライン, 2022 年 8 月 27 日.

望月優子 (招待講演), 「Solar activity signatures embedded in ice cores」, 宇核連—RCNP 研究会「宇宙核物理の展開」, 豊中 & オンライン, 2022 年 7 月 20–21 日.

中井陽一, 渡部直樹, 柘植雅士, 副島浩一, 「極低温氷表面に存在する OH ラジカルの可視域光による光脱離」, 日本物理学会 2023 年春季大会, オンライン, 2023 年 3 月 22–25 日.

中井陽一, 「低エネルギーイオンと極低温氷表面との分子生成反応」, 学術変革領域次世代アストロケミストリー第 3 回領域全体集会, 東京, 2023 年 3 月 7–9 日.

勝田哲, 榎戸輝揚, L. Andrea, 森浩二, 望月優子, 中島基樹, R. Nathaniel, 佐藤浩介, S. Gunter, 田代信, 寺田幸功, W. Kent, 「X線天文衛星を用いた地球超高層大気の密度鉛直構造の測定〜長期トレンドの調査〜」, 地球電磁気・地球惑星圏学会 第 152 回総会及び講演会 (2022 年秋学会), 相模原, 2022 年 11 月 3–7 日.

Press Releases

勝田哲, 榎戸輝揚, L. Andrea, 森浩二, 望月優子, 中島基樹, R. Nathaniel, 佐藤浩介, S. Gunter, 田代信, 寺田幸功, W. Kent, 「地球温暖化に伴う超高層大気の収縮を X 線天文衛星で解明」, 2023 年 2 月 2 日, https://www.riken.jp/press/2023/20230222_2/ .

宮崎彩音, 柘植雅士, 日髙宏, 中井陽一, 渡部直樹, 「極低温氷表面での OH ラジカルの動きやすさを初めて測定—宇宙の氷微粒子上で分子進化が活性化する温度が明らかに—」, 2022 年 11 月 24 日, https://www.riken.jp/press/2022/20221124_1/ .

Nuclear Science and Transmutation Research Division
Nuclear Transmutation Data Research Group

1. Abstract

The nuclear waste problem is an inevitable subject in nuclear physics and nuclear engineering communities. Since the Chicago Pile was established in 1942, nuclear energy has become one of major sources of energy. However, nowadays the nuclear waste produced at nuclear power plants has caused social problems. Minor actinide components of the waste have been studied well as a fuel in fast breeder reactors or ADS. Long-lived fission products (LLFP) in waste, on the other hand, have not been studied extensively. A deep geological disposal has been a policy of several governments, but it is difficult to find out location of the disposal station in terms of security, sociology and politics. To solve the social problem, a scientific effort is necessary for nuclear physics community to find out efficient methods for reduction of nuclear waste radioactivity. In the world-wide situation above, our Group aims to obtain reaction data of LLFP at RIBF and other muon facilities for muon capture data. These data are necessary to design an accelerator-based system for transmutation, and also may lead to a new discovery and invention for peaceful use of nuclear power and the welfare of humanity.

2. Major Research Subjects

The Group is formed by three research teams. The first two Teams, “Fast RI Data Team” and “Slow RI Data Team,” are in charge of proton- and deuteron-induced reaction data of LLFP in inverse kinematics at RIBF. The third Team “Muon Data Team” is to obtain muon capture data of LLFP at muon facilities. All of the teams are focusing to obtain high-quality data which are essentially necessary to establish reliable reaction models. Each team has its own subjects and promotes LLFP reaction programs based on their large experiences, techniques and skills.

3. Summary of Research Activity

In 2014, all the teams polished up experimental strategies, formed collaboration and prepared experiments. Physics runs for spallation reaction were successfully organized at RIBF in 2015–2017. The muon program started at RCNP, Osaka University in spring 2016 and the data for Pd isotopes were successfully obtained in 2017–2019 via in-beam method with DC beams at RCNP, and via activation method with pulsed beams at J-PARC and ISIS-RAL/RIKEN facilities.

The reaction data obtained with both fast and energy-degraded beams at RIBF encouraged the nuclear data group of JAEA, and a new database called “JENDLE/ImPACT-2018” has been released. The new database has been generated by a newly developed reaction model “DEURACS” which treats deuteron-induced reactions. DEURACS reproduces very well cross section data, and much better than other reaction models. A simulation code “PHITS” has been re-coordianted to use the database information.

In December 2018, the Team leader, Hideaki Otsu, was invited to join Technical Meeting of IAEA, entitled “Novel Multidisciplinary Applications with Unstable Ion Beams and Complementary Techniques.” Our activity has been demonstrated and recognized internationally. In November 2020, Hideaki Otsu organized a domestic conference entitled “RIKEN Sympoium on Nuclear Data 2020.”

At the end of fiscal year 2021, the spallation reaction data with ^{99}Tc beam was obtained and a secondary beam test for ^{237}Np production was conducted. The data analysis is in progress.

Member

Director

Hiroyoshi SAKURAI

List of Presentation

Presentation

[Domestic Conference/Workshop]

櫻井博儀（招待講演）, 「核変換とミュオン」, 日本中間子科学会「中間子科学の将来討論会」, 和光市 (理化学研究所), 2022 年 11 月.

Nuclear Science and Transmutation Research Division
Nuclear Transmutation Data Research Group
Fast RI Data Team

1. Abstract

Fast RI data team aims at obtaining and accumulating the cross section data for long lived fission products (LLFPs) in order to explore the possibility of using accelerator for nuclear transmutation.

LLFPs as nuclear waste have been generated continuously in nuclear power plants for wealth for human lives, while people noticed the way of disposal has not necessarily been established, especially after the Fukushima Daiichi power plant disaster. One of the ways to reduce the amount of LLFP or to recover them as recycled resources is nuclear transmutation technique.

RIBF facility has a property to generate such LLFP as a secondary beam and the beam species are identified by event by event. Utilizing the property, absolute values of the cross section of various reactions on LLFPs are measured and accumulated as a database.

In addition, a project to obtain nuclear reaction data on stable nuclei by means of inverse kinematic technique to provide the distribution of reaction residue nuclides. It will be utilized on Pb/Bi for ADS neutron generator materials or on Li/Be for blanket on nuclear fusion reactors.

Furthermore, we started to obtain production cross section to minor actinide (MA) nuclide from primary uranium beam. This methods will provide an opportunity to study MA nuclides by distributing them as a secondary beam in near future.

2. Major Research Subjects

(1) Measurement of reaction products by the interaction of LLFPs with proton, deuteron, and photon to explore candidate reactions for the transmutation of LLFPs
(2) Evaluation of the cross section data for the neutron induced reactions from the obtained data

3. Summary of Research Activity

(1) Acting as a collaboration hub on many groups which plan to take data using fast RI beams in RIBF facility
(2) Concentrating on taking data for proton and deuteron induced spallation reactions with inverse kinematics
(3) Accumulating the cross section data and evaluating them as evaluated nuclear data
(4) Evaluating cross section of neutron induced reaction on LLFP by collaborating with the nuclear model calculation and evaluation group

Members

Team Leader

Hideaki OTSU (Concurrent: Team Leader, SAMURAI Team)

Junior Research Associate

Riku MATSUMURA

Visiting Scientists

Takashi TERANISHI (Kyushu Univ.)
Ayano MAKINAGA (Teikyo Univ.)
Shin'ichiro MEIGO (JAEA)
Keita NAKANO (JAEA)

List of Publications & Presentations

Presentations

[Domestic Conferences/Workshops]

R. Matsumura, "New analytical model for momentum distribution on the spallation reaction in inverse kinematics," 2022 Symposium on Nuclear Data, Kinki University, Osaka, Japan, November 17–18, 2022.

R. Matsumura, "New analytical model for momentum distribution on the spallation reaction in inverse kinematics," JSPS/NRF/NSFC A3 Foresight Program, "Nuclear Physics in the 21st Century," Osaka International Convention Center, Osaka, Japan, February 13–15, 2023.

Other

[Bachlar Thesis]

福嶋千隼, 卒業論文, 「理研 RI ビームファクトリーでのネプツニウム 237 同位体の生成」, 東京都市大学, 2023 年 3 月.

Nuclear Science and Transmutation Research Division
Nuclear Transmutation Data Research Group
Slow RI Data Team

1. Abstract

This team is in charge of the development of low-energy RI beams of long-lived fission fragments (LLFP) or minor actinides (MA) from the ^{238}U by means of degrading the energy of beams produced by the BigRIPS fragment separator.

2. Major Research Subjects

Studies of the slowing down and purification of RI beams are the main subjects of the team. Developments of devices used for the slowing down of RI beams are also an important subject.

(1) Study and development of the slowed-down methods for LLFP
(2) Operation of the BigRIPS separator and supply the low energy LLFP beam to the experiment in which the cross sections of LLFP are measured at the low energy.
(3) Development of MA (such as Np) beams for the nuclear data
(4) Development of the framework to seamlessly handle device, detector, DAQ, and analysis for the easy control of the complicate slowed-down RI beam production and its development.

3. Summary of Research Activity

A new OEDO beam line, designed for the slowed-down RI beams, was constructed under the collaboration with CNS, the University of Tokyo. Our group was responsible for the construction of the infrastructure such as the cooling water and the electrical equipment, and the movement and alignment of existing vacuum chambers, quadrupole magnets. The power supply for the Superconducting Triplet Quadrupoles (STQ) was made, which had a stability also under the low current condition.

Slowed-down ^{93}Zr beams with 20 or 50 MeV/nucleon were successfully developed in June 2016 for the first time. The methods to obtain the narrow energy, position, and angle distribution were developed. The methods of the energy adjustment and the particle identification at 50 MeV/nucleon were developed. The ^{93}Zr and ^{107}Pd beams with 50 MeV/nucleon were produced for the nuclear-transmutation experiments using proton or deuteron targets in October 2016. The commissioning experiment of the OEDO beam line was successfully performed in June 2017. The first transmutation experiments using OEDO beam line were performed with ^{93}Zr, ^{107}Pd, and ^{79}Se around 20 MeV/nucleon.

With our developments, the slowed-down RI beams became ready for the transmutation experiments. On the other hand, the procedure to make the slowed-down RI beams became highly specialized. To easily produce the slowed-down RI beam, the framework, called BYACO, is being developed to seamlessly handle the device, detector, DAQ, and analysis. The procedure of the RI-beam energy control was implemented in the web application. The BYACO system was used also for an RI-beam automatic tuning project by the BigRIPS team. The automatic tuning of the RI beam becomes one of the categories in the RNC's use case of the TRIP project. BYACO needs to be upgraded when the automatic tuning is used under the operation. Future developments were considered in 2022.

The extension of the RI-beam separation using the $B\rho$-ΔE-$B\rho$ method by the charge state of RI beam was found to be essential to produce the heavy RI beams. The simulation tool of this extended separation, called Q^+ separation, was developed and implemented into BYACO in 2021. With this tool, we succeeded to produce a ^{237}Np beam as a secondary beam by collaborating mainly with the fast RI data team and the BigRIPS team.

Members

Team Leader
Toshiyuki SUMIKAMA

Visiting Scientist
SungHan BAE (Inst. for Basic Sci.)

Student Trainee
Masaya OISHI (Kyushu Univ.)

List of Presentation

Presentation

[Domestic Conference/Workshop]

炭竈聡之（招待講演）, 「理研・低速 RI データチームから」, 原子核物理学実験におけるデータ利活用による研究戦略, オンライン, 2022 年 3 月 7 日.

Nuclear Science and Transmutation Research Division
Nuclear Transmutation Data Research Group
Muon Data Team

1. Abstract

Dr. Yoshio Nishina observed muons in cosmic rays in 1937. The muon is an elementary particle similar to electron and classified to lepton group. The muon has positive or negative electric charge, and the lifetime is 2.2 μsec. The negative muon (μ^-) is 207 times heavier than the electron and behaves as a "heavy electron" in materials. The negative muon is captured by atomic orbits of nuclei to form a muonic atom and cascades down to the $1s$ orbit to make muon nuclear capture. The muon is combined with a proton in the nucleus to convert to a neutron and a neutrino. The muon nuclear capture reaction on a nucleus ($^A_Z N$) with the atomic number Z and mass number A generates the isotopes of $^{A-x}_{Z-1}N$ ($x = 0, 1, 2, 3, 4$) by emitting some neutrons in the reaction. The phenomenon is called "muon nuclear transmutation." The reaction branching ratio of $^A_Z N(\mu^-, x n\nu)^{A-x}_{Z-1}N$ reactions ($x = 0, 1, 2, 3, 4$) is one of important factors toward various applications with nuclear transmutation technique. From a viewpoint of the nuclear physic, the muon nuclear capture reaction is very unique and interesting. A high-energy compound nuclear state is suddenly generated in the nuclei associated with a weak conversion process of proton to neutron and neutrino. Many experimental results have been so far reported, however, the reaction mechanism itself is not well clarified. The research team aims at obtaining the experimental data to investigate the reaction mechanism of muon nuclear capture, and also at theoretical understanding on the nuclear capture reaction.

2. Major Research Subjects

(1) Experimental clarification on the mechanism of nuclear muon capture reaction
(2) Theoretical understanding on the nuclear muon capture reaction
(3) Interdisciplinary applications with the nuclear transmutation technique

3. Summary of Research Activity

There are two experimental methods to study the muon nuclear capture reaction. The first one is "muon in-beam spectroscopy method." The neutron and γ-ray emissions from the excited states of $^{A-x}_{Z-1}N$ nuclei are prompt events and are observed by the "muon in-beam spectroscopy method" with a DC muon beam. The reaction branching ratio is directly determined by measuring the neutron multiplicity in the reaction. The DC muon beam is available at the MuSIC (Muon Science Innovative Channel) muon facility in the Research Center for Nuclear Physics (RCNP) at Osaka University. The second one is "muon activation method" with the pulsed muon beam. The produced unstable nuclei $^{A-x}_{Z-1}N$ make $\beta^{+/-}$ decays. The γ-rays associated with $\beta^{+/-}$ decays to the daughter nuclei are observed in the experiment. The build-up curve of γ-ray yield at muon beam-on and the decay curve at beam-off are measured. Since the half-lives and decay branching ratios of $\beta^{+/-}$-γ decays are known, the reaction branching ratios to the $^{A-x}_{Z-1}N$ nuclei are determined by the γ-ray yield curves. The pulsed muon beam is available at the RIKEN-RAL Muon Facility in the UK and J-PARC muon facility.

Muon nuclear capture reactions are studied on five isotope-enriched palladium targets (^{104,105,106,108,110}Pd) and five isotope-enriched zirconium targets (^{90,91,92,94,96}Zr) employing two experimental methods. By obtaining the experimental data on the Pd and Zr targets, the reaction mechanism is investigated experimentally, and the results are compared with appropriate theoretical calculations. The ^{107}Pd is classified to a long-lived fission product (LLFP) and is contained in a spent nuclear fuel. The study of muon nuclear capture on the Pd and Zr targets is aiming at exploring a possible reaction path to make the nuclear transmutation of the Pd and Zr metal extracted from the spent nuclear fuel without an isotope separation process. This research was funded by the ImPACT Program of Council for Science, Technology and Innovation (Cabinet Office, Government of Japan).

(1) Experiments with "muon in-beam spectroscopy method"

Muon nuclear capture reactions were investigated on five palladium targets (^{104,105,106,108,110}Pd) by employing the DC muon beam at MuSIC. The γ-ray and neutron in the muon nuclear capture reaction were measured with the time information relative to muon beam arrival. The measured neutron multiplicity gives the reaction branching ratio of $^A_{46}\mathrm{Pd}(\mu^-, x n\nu)^{A-x}_{45}\mathrm{Rh}$ reactions, where $A = 104, 105, 106, 108, 110$ and $x = 0, 1, 2, 3, 4$.

Employing a newly built neutron spectrometer, the neutron was measured to obtain the reaction branching ratios of muon capture reactions on the Pd targets. We have constructed a neutron spectrometer named "Seamine": **S**cintillator **E**nclosure **A**rray for **M**uon **I**nduced **N**eutron **E**mission. The spectrometer consists of 21 liquid scintillation counters, 2 Ge γ-ray detectors, 7 BaF_2 counters. The Pd target, muon beam counters and muon degraders are placed at the center of spectrometer. The neutron counter is a BC-501A liquid scintillation counter with 20 cm diameter and 5 cm depth and is connected to a 5" photo multiplication tube (H4144-01). The total neuron detection efficiency is estimated 5%, where the distance is 4 cm from the target to neutron counters. The Ge γ-ray detectors are placed at 10 cm form the target, and the typical detection efficiency is 0.5% for 200 keV γ-ray. The BaF_2 counters are located beneath the target to detect fast γ-rays emitted from the compound nucleus formed in the reactions. Signals from the liquid scintillation counters are processed in a CAEN V1730B waveform digitizer (16 channel, 14 bit, 500 M samplings/sec.). The neuron-γ discrimination is performed on-line during the experiment, and the detailed data analysis is conducted off-line after the experiment. The neutron energy spectrum is constructed in the digitizer. Signals from Ge detectors are also processed in the digitizer to obtain the energy and time spectrum of γ-rays associated with the reaction. Signals from the BaF_2 counters and muon beam counters are sent to the digitizer to make the fast timing signals.

We have established the muon in-beam spectroscopy method employing the "Seamine" spectrometer. The neutron data analysis

is in progress to obtain the multiplicity, the energy and the TOF spectrum using start signals given by γ-rays detected in the BaF_2 counters. The γ-ray data gives the energy spectrum of prompt γ-rays and muonic X-rays originated from the ^{104,105,106,108,110}Pd targets.

(2) Experiments with "muon activation method" at the RIKEN-RAL Muon Facility

We conducted the experiments on the muon nuclear capture employing the muon activation method at the RIKEN-RAL Muon Facility in the UK. The pulsed muon beam was irradiated on the ^{104,105,106,108,110}Pd targets. The γ-rays were detected by a Ge detector located at the downstream of the Pd targets to maximize the detection efficiency. The build-up and decay curves of γ-ray intensities were measured associated with $\beta^{+/-}$ decays of produced unstable nuclei to daughter nuclei. The γ-ray-yield curves give the absolute radiation activity produced by the reaction, and the reaction branching ratios are determined for ${}^{A}_{46}\mathrm{Pd}(\mu^-, xn\nu){}^{A-x}_{45}\mathrm{Rh}$ reactions. The decay curves of γ-rays from the produced nuclei with long half-lives were measured under low γ-ray background at an experimental apparatus built in a separated room. The detailed off-line data analysis is in progress.

(3) Experiments with "muon activation method" at J-PARC muon facility

The experiments employing the muon activation method were performed at J-PARC muon facility. The five isotope-enriched Pd targets (^{104,105,106,108,110}Pd) were irradiated by the pulsed muon beam, and the build-up and decay curves of γ-ray intensities were measured.

In addition to the Pd targets, the experiments on five isotope-enriched Zr target (^{90,91,92,94,96}Zr) were conducted to obtain the reaction branching ratios of ${}^{A}_{40}\mathrm{Zr}(\mu^-, xn\nu){}^{A-x}_{39}\mathrm{Y}$ reactions, where $A = 90, 91, 92, 94, 96$. The obtained reaction branching ratios on the Pd and Zr targets are important to understand the reaction mechanism of muon nuclear capture. The ^{93}Zr is one of the LLFP and is contained in a spent nuclear fuel. The experiment on the Zr targets is to explore a possibility to realize the nuclear transmutation of the Zr metal extracted from the spent nuclear fuel.

In order to obtain the reaction branching ratio of ${}^{107}_{46}\mathrm{Pd}(\mu^-, xn\nu){}^{107-x}_{45}\mathrm{Rh}$ reactions, the muon activation experiment was performed employing a Pd target containing ^{107}Pd of 15.3%. The γ-ray intensities associated with $\beta^{+/-}$ decays of produced unstable nuclei were measured to obtain the build-up and decay curves. Once the branching ratios of the reactions on the ^{104,105,106,108,110}Pd targets are obtained, these contributions are extracted from the branching-ratio data obtained for the Pd target with ^{107}Pd. The reaction branching ratio of ${}^{107}_{46}\mathrm{Pd}(\mu^-, xn\nu){}^{107-x}_{45}\mathrm{Rh}$ reactions is finally determined. The detailed off-line data analysis is in progress.

(4) Comparison with theory

The muon activation method gives the reaction branching ratios. The muon in-beam spectroscopy method gives the neutron multiplicity and the neutron energy spectrum. These experimental results are important to understand the compound nuclear state and neutron emission mechanism. The reaction branching ratios obtained by the muon activation method are compared with the results of neutron multiplicity measurements. The neutron energy spectrum is considered to be reflected by the energy distribution of compound nuclear state and neutron emission mechanism. The experimental results are compared with the appropriate calculations employing the neutron emission mechanisms due to an evaporation, a cascade and a direct emission processes with assuming the energy distribution at compound nuclear state.

Members

Team Leader

Hiroyoshi SAKURAI

Contract Researcher

Megumi NIIKURA

Senior Visiting Scientist

Teiichiro MATSUZAKI

List of Publications & Presentations

Publications

[Original Papers]

T. Nishi *et al.*, "Chiral symmetry restoration at high matter density observed in pionic atoms," Nat. Phys. **19**, 788 (2023).

A. Yagi *et al.*, "Various nuclear structures in ^{140}Xe studied by beta decay of ground and isomeric states in ^{140}I," Phys. Rev. C **105**, 044325 (2022).

B. Moon *et al.*, "First observation of the $\pi 0h_{(11/2)} \times \nu 0h_{(9/2)}$ partner orbital configuration in the odd-odd ^{138}I nucleus," Phys. Rev. C **105**, 034334 (2022).

B. Moon *et al.*, "Gamow-Teller decay of ^{142}Te to ^{142}I," Phys. Rev. C **107**, 014311 (2023).

[Proceeding]

S. Manabe *et al.*, "Emissions of hydrogen isotopes from the nuclear muon capture reaction in ^{nat}Si," EPJ Web Conf. **284**, 01029 (2023).

Presentations

[International Conferences/Workshops]

M. Niikura (oral), "Nuclear physics with muon," Physics of RI: Recent progress an dperspective, RIKEN, Wako, May, 2022.

M. Niikura (oral), "Study of muon-induced fission for spectroscopy of the muonic atom with unstable nuclei," Open CHRISP Users Meeting, PSI, Villigen, Switzerland, January, 2023.

R. Mizuno *et al*. (poster), "Measurement of muon-induced nuclear transmutation for Si isotopes," Transscale Quantum Science, Univ. of Tokyo, November, 2022.

R. Mizuno *et al*. (oral), "Measurement of nuclear transmutation via muon capture reaction for Si isotopes," VIth Topical Workshop on Modern Aspects in Nuclear Structure, Bormio, Italy, February, 2023.

[Domestic Conferences/Workshops]

新倉潤 (口頭発表), "Study of muon-induced fission for spectroscopy of the muonic atom with unstable nuclei," Fission Workshop, 和光市 (理科学研究所), 2023 年 1 月.

新倉潤 (招待講演), 「ミューオン原子核物理」, 中間子科学の将来検討会, 和光市 (理化学研究所), 2022 年 11 月.

水野るり恵, 他 7 名 (口頭発表), 「1 MeV 陽子ビームを用いた広ダイナミックレンジ光子検出器の性能評価実験」, タンデム加速器及びその周辺技術の研究会, オンライン, 2022 年 7 月.

水野るり恵, 他 7 名 (口頭発表), 「Ge 検出器を用いた光子検出器システムの広ダイナミックレンジにおける性能評価実験」, 放射線化学討論会, オンライン, 2022 年 9 月.

[Seminar]

M. Niikura, "Development of muonic X-ray spectrometer for element analysis," LMU seminar at Paul Scherrer Institut (PSI), Online, April, 2022.

Nuclear Science and Transmutation Research Division
High-Intensity Accelerator R&D Group

1. Abstract

The High-Intensity Accelerator R&D group, consisting of two teams, develops elemental technology of high-power accelerators and high-power targets, aiming at future applications to nuclear transmutations of long-lived fission product into short-lived nuclides. The research subjects are superconducting rf cavities for low-velocity ions, design of high-power accelerators, high-power target systems and related technologies.

Nuclear transmutation with high-intensity accelerators is expected to reduce the high-level radioactive wastes and to recycle the precious resources such as rare-earth materials in future. This method is one of the important applications of the ion-accelerator technologies that have been developed at RIKEN for a long time. Under the framework of ImPACT Fujita Program, we have conducted R&D of elemental technology related to the high-power accelerators and high-power targets, from FY2014 to FY2018. We gained a lot of experiences in these R&Ds. Among them, the development of a superconducting rf cavity has become the basis of the upgrade program of the RILAC facility which started in 2016.

2. Major Research Subject

R&D of elemental technology of high-power accelerators and high-power targets.

3. Summary of Research Activity

(1) A high-gradient rf cavity has been constructed and tested based on the superconducting rf technology.
(2) Several candidates for the high-power target have been proposed and their prototypes have been tested.
(3) A high-current deuteron RFQ has been designed.

Members

Director

Hiroki OKUNO
(concurrent: Deptuy Group Director, Accelerator Group)

Visiting Scientist

Hideyuki Watanabe (AIST)

Nuclear Science and Transmutation Research Division
High-Intensity Accelerator R&D Group
High-Gradient Cavity R&D Team

1. Abstract

Superconducting linacs are suitable for high-power beam facilities, such as spallation neutron sources. The mission of this team is to develop a highly efficient superconducting linac with a high acceleration voltage, capable of handling high beam intensity and ensuring high availability, drawing from the operational experiences of SRILAC.

2. Major Research Subjects

(1) Development of high-gradient cavites for low beta ions
(2) Development of power saving cryomodules
(3) Operation wigh high availability

3. Summary of Research Activity

Development of highly efficient superconducting accelerator modules

Members

Team Leader

Naruhiko SAKAMOTO

Research/Technical Scientists

Yutaka WATANABE
Kazutaka OZEKI

Research & Development Scientist

Kenji SUDA

Nuclear Science and Transmutation Research Division
High-Intensity Accelerator R&D Group
High-Power Target R&D Team

1. Abstract

The subjects of this team cover R&D studies with respect to target technology for the transmutation of the LLFPs.

2. Major Research Subjects

(1) Liquid lithium target for production of neutron or muon
(2) Beam window without solid structure

3. Summary of Research Activity

(1) Liquid lithium target for production of neutron or muon (H. Okuno)
(2) Beam window with solid structure (H. Okuno)

Members

Team Leader

Hiroki OKUNO

Visiting Scientist

Katsuyoshi TSUMORI (Nat'l Inst. Fusion Science)

List of Publication

Publication

[Original Paper]

Y. Miyake *et al.*, "Test of ^{107}Pd transmutation with macroscopic quantities," J. Nucl. Sci. Technol. **59**, 1536 (2022).

Research Facility Development Division
Accelerator Group

1. Abstract

The Accelerator Group, consisting of seven teams, pursues various upgrade programs on the world-leading heavy-ion accelerator facility, RI Beam Factory (RIBF), to enhance the accelerator performance and operation efficiency. The programs include the R&D of superconducting ECR ion source, charge stripping systems, beam diagnostic devices, radio-frequency systems, control systems, and beam simulation studies. We are also maintaining the large infrastructure to realize effective operation of the RIBF. Moreover, we are actively promoting the applications of the facility to various research fields.

Our primary mission is to supply intense, stable heavy-ion beams for the users through effective operation, maintenance, and upgrade of the RIBF accelerators and related infrastructure. The director members oversee the development programs that are not dealt with by a single team, such as intensity upgrade and effective operation. We also discuss the future plans of RIBF along with other laboratories belonging to the RIBF research division.

2. Major Research Subjects

(1) Intensity upgrade of RIBF accelerators (Okuno)
(2) Effective and stable operation of RIBF accelerators (Fukunishi)
(3) Stable operation of the upgraded RILAC facility
(4) Promotion of applied research through collaborations
(5) Promotion of the RIBF upgrade plan

3. Summary of Research Activity

(1) Various improvements and developments have been carried out for the RIBF accelerators in order to upgrade the beam intensities and stability. Owing to the efforts, we succeeded in accelerating the zinc beam of 830 particle nA through SRC in December 2022, which corresponds to the beam power of 20 kW.
(2) In December 2022, the high intensity zinc beam damaged the beam pipe in the last magnetic deflection channel (MDC3) in SRC, causing a vacuum leak and stopping beam service. We plan to repair the damaged part, investigate the cause, and implement remedial measures.
(3) In the upgraded RILAC, replacement of the low-level rf control units has been carried out with newly developed ones based on digital circuit technology. The temperature control device for the cooling water in the normal-conducting cavity has been improved, and the accuracy of the temperature has been dramatically improved. Pulsed-rf conditioning of the superconducting cavities, where field emission had become severe, was also successfully performed. So far, a high-intensity vanadium beam has been stably supplied to the experiments for the synthesis of a new superheavy element.
(4) We have supplied a wide variety of beams for applied research aimed at solving social problems, such as ion beam breeding, irradiation of semiconductors for space applications, and radioactive isotope production. Since 2017, we have cooperated in producing and supplying At-211 to various research activities. In particular, we contributed to the initiation of a physician-led clinical trial at Osaka University in 2021. A high-power target for mass production of At-211 is under development with RI Application Research Group of RNC, using the high-intensity alpha beam from RRC. It will be installed and tested in the SRILAC facility in near future.
(5) An intensity-upgrade plan of the RIBF has been further investigated. The main focus of this plan is to increase the effective transmission efficiency of the accelerator chain from the current 5% to 50% by installing two Charge Stripper Rings (CSRs). The final goal of this plan is to increase the uranium beam intensity by 20 times of the present value, namely up to 2000 particle nA, at the exit of SRC. Detailed orbit calculations for the first of these CSRs have progressed, and design, prototyping, and testing of focusing and extraction magnets have been carried out with the involvement of companies. Good results have been obtained so far. In 2022, a detailed study of the entire plan, including the elements other than CSR, was initiated by young group members.

Members

Director
Osamu KAMIGAITO

Deputy Directors
Hiroki OKUNO (for intensity upgrade)
Nobuhisa FUKUNISHI (for stable and efficient operation)

Research Consultants
Tadashi FUJINAWA
Masayuki KASE

Visiting Scientists

Eiji KAKO (KEK)
Hirotaka NAKAI (KEK)
Kensei UMEMORI (KEK)
Hiroshi SAKAI (KEK)
Masahiro OKAMURA (BNL)
Noboru SASAO (Okayama Univ.)
Yasutaka IMAI (Okayama Univ.)

Assistant

Karen SAKUMA

Administrative Part-time Worker

Ryoko UMEZAKI

List of Presentation

Presentation

[International Conference/Workshop]

O. Kamigaito (invited), "High beam power operations at RIKEN RIBF: Technical developments, challenges and resolutions," 15th International Conference on Heavy Ion Accelerator Technology (HIAT2022), Darmstadt, Germany, June 27–July 1, 2022.

Research Facility Development Division
Accelerator Group
Accelerator R&D Team

1. Abstract

We are developing the key hardware in upgrading the RIBF accelerator complex. Our primary focus and research is charge stripper which plays an essential role in the RIBF accelerator complex. Charge strippers remove many electrons in ions and realize efficient acceleration of heavy ions by greatly enhancing charge state. The intensity of uranium beams is limited by the lifetime of the carbon foil stripper conventionally installed in the acceleration chain. The improvement of stripper lifetimes is essential to increase beam power towards the final goal of RIBF in the future. We are developing charge strippers for high power beams, such as low-Z gas stripper, highly oriented graphene films and liquid lithium films. Another our focus is the upgrade of the world's first superconducting ring cyclotron.

2. Major Research Subjects

(1) Development of charge strippers for high power beams (highly oriented graphene film, low-Z gas, liquid lithium films)
(2) Upgrade of the superconducting ring cyclotron
(3) Maintenance and R&D of the electrostatic deflection/inflection channels for the beam extraction/injection

3. Summary of Research Activity

(1) Development of charge strippers for high power beams (foil, low-Z gas, liquid lithium film)

(H. Hasebe, H. Imao, Y. Miyake, and H. Okuno)

We are developing the charge strippers for high intensity heavy ion beams. We are focusing on the developments on highly oriented carbon graphite films, gas strippers including He gas stripper and liquid lithium films.

(2) Upgrade of the superconducting ring cyclotron

(J. Ohnishi, Y. Miyake, and H. Okuno)

We are focusing on the upgrade of the superconducting ring cyclotron.

(3) Maintenance and R&D of the electrostatic deflection/inflection channels for the beam extraction/injection

(J. Ohnishi, Y. Miyake, and H. Okuno)

We are developing high-performance electrostatic channels for high power beam injection and extraction.

Members

Team Leader
Hiroki OKUNO

Senior Research Scientist
Hiroshi IMAO

Technical Scientists
Hiroo HASEBE
Yasuto MIYAKE

Special Temporary Technical Scientist
Jun-ichi OHNISHI

Visiting Scientist
Noriyosu HAYASHIZAKI (Tokyo Tech)

List of Publication

Publications

[Original Papers]

Y. Miyake *et al*., "Test of ^{107}Pd transmutation with macroscopic quantities," J. Nucl. Sci. Technol. **59**, 1536 (2022).

Research Facility Development Division
Accelerator Group
Ion Source Team

1. Abstract

Our aim is to operate and develop the ECR ion sources for the accelerator-complex system of the RI Beam Factory. We focus on further upgrading the performance of the RI Beam Factory through the design and fabrication of a superconducting ECR ion source for production of high-intensity heavy ions.

2. Major Research Subjects

(1) Operation and development of the ECR ion sources
(2) Development of a superconducting ECR heavy-ion source for production of high-intensity heavy ion beams

3. Summary of Research Activity

(1) Operation and development of ECR ion sources

(T. Nakagawa, M. Kidera, Y. Higurashi, T. Nagatomo, Y. Kanai, G. M Q. Saquilayan, and H. Haba)

We routinely produce and supply various kinds of heavy ions such as zinc and calcium ions for the super-heavy element search experiment as well as uranium ions for RIBF experiments. We also perform R&D's to meet the requirements for stable supply of high-intensity heavy ion beams.

(2) Development of a superconducting ECR ion source for use in production of a high-intensity heavy ion beam

(T. Nakagawa, J. Ohnishi, M. Kidera, Y. Higurashi, G. M Q. Saquilayan, and T. Nagatomo)

The RIBF is required to supply heavy ion beams with very high intensity so as to produce RI's and for super-heavy element search experiment. We have designed and are fabricating an ECR ion source with high magnetic field and high microwave- frequency, since the existing ECR ion sources have their limits in beam intensity. The coils of this ion source are designed to be superconducting for the production of high magnetic field. We are also designing the low-energy beam transport line of the superconducting ECR ion source.

Members

Team Leader

Takahide NAKAGAWA

Senior Technical Scientists

Yoshihide HIGURASHI
Takashi NAGATOMO

Postdoctoral Researcher

Glynnis Mae Q. SAQUILAYAN

Research Consultant

Yasuyuki KANAI

List of Presentation

Presentation

[International Conference/Workshop]

T. Nakagawa (invited), "High performance ECR ion sources development at RIKEN and their impact to heavy ion accelerators," 23rd International Conference on Cyclotrons and their Applications (CYC2022), Beijing, China, December 5–9, 2022.

Research Facility Development Division
Accelerator Group
RILAC Team

1. Abstract

Our team is responsible for the operation, maintenance, and upgrade of the RIKEN heavy-ion linear accelerator (RILAC), a unique variable-frequency linac that has been in operation since 1980. RILAC was upgraded in the 1990s as part of the RI Beam Factory (RIBF) project, and made a significant contribution to the synthesis and discovery of the element 113, Nihonium. In 2019, a superconducting linac booster, SRILAC, was installed, and it will play a major role in the synthesis of heavier new elements, development of the technologies for production of medical radioisotopes, and as a powerful injector to RIBF. We successfully avoided major troubles by effectively planning and implementing maintenance and upgrades of outdated equipment within a limited budget.

2. Major Research Subjects

(1) Efficient operation, maintenance and management of the vacuum equipment in the RIBF accelerators
(2) Development of technology to operate RILAC with high intensity and high stability
(3) Construction and maintenance of the RILAC beamlines

3. Summary of Research Activity

In 2022 we have made various improvements of the whole RILAC with the cooperation of other teams of the Accelerator Group, in order to provide high-intensity beams more stably to the new element synthesis experiments being conducted at GARIS III. For example, activate the temperature control of the cooling water system of RILAC. With these efforts, the beam availability has been improved significantly.

A beamline is being prepared at the RILAC facility for mass production of ^{211}At, which has potential medical applications. Under the leadership of the RI Application Research Group and with the help of other teams of the Accelerator Group, the optical calculations, electromagnet design, radiation shielding design, and overall beamline installation were undertaken and the beamline is almost complete.

As in the past, we maintained the vacuum system of the whole accelerators at RIBF. While taking into consideration the aging of the vacuum pumps, an efficient maintenance plan was established and cost-conscious maintenance was executed.

Members

Team Leaders
Yoshihide HIGURASHI　　Osamu KAMIGAITO

Deputy Team Leader
Naruhiko SAKAMOTO

Research/Technical Scientists
Yutaka WATANABE (Senior Technical Scientist)　　Takahiro NISHI (Research Scientist)

Research Consultant
Eiji IKEZAWA

List of Publication & Presentations

Publication

[Proceeding]

H. Yamauchi, T. Ohki, K. Oyamada, M. Tamura, Y. Akira, K. Kaneko, T. Nishi, N. Sakamoto, M. Fujimaki, H. Imao, M. Kidera, T. Nagatomo, K. Ozeki, K. Suda, A. Uchiyama, T. Watanabe, Y. Watanabe, K. Yamada, O. Kamigaito, "Present status of RILAC," Proceedings of the 19th Annual Meeting of Particle Accelerator Society of Japan, Kyushu University, Online, Japan, October 18–21, 2022, TFP009, 1144–1147 (2022). https://www.pasj.jp/web_publish/pasj2022/proceedings/PDF/TFP0/TFP009.pdf .

Presentations

[Domestic Conferences/Workshops]

山内啓資, 西隆博, 大木智則, 小山田和幸, 田村匡史, 遊佐陽, 金子健太, 坂本成彦, 今尾浩士, 内山暁仁, 大関和貴, 須田健嗣, 長友傑, 藤巻正樹, 山田一成, 渡邉環, 渡邉裕, 上垣外修一, 「理研重イオンリニアックの現状報告」, 日本加速器学会, オンライン, 2022 年 10 月 10 日.

T. Nishi (invited), "Development of automatic optical tuning system for primary line using Gaussian process at RIKEN," ML@HEP, Tokyo, Japan, July, 2022.

T. Nishi, "Development of auto tuning system using Bayesian optimization for heavy ion optics," Workshop on Machine Learning for Accelerator and Beam Physics, RCNP, Osaka, March, 2023.

Outreach Activity

[Lecture]

T. Nishi, “AI based accelerator operation,” KEK IINAS 5th International School on Beam Dynamics and Accelerator Technology, Hiroshima, Japan, October, 2022.

Research Facility Development Division
Accelerator Group
Cyclotron Team

1. Abstract

The mission of the RIKEN Radioactive Isotope Beam Facility (RIBF)[1] is to improve our understanding of the mechanism of element synthesis in the universe through experiments using intense heavy-ion beams. According to the medium-term targets of the RNC, our team's mission is to maintain and improve the highly reliable operation of the RIBF accelerator complex, in collaboration with other teams of the RNC. The stable operation of the RF system is crucial for handling very high-power beams. Our goal is to develop a highly reliable/stable radio-frequency (RF) system for RIBF cyclotrons and linacs, enabling high-power beam operations. Recently, we successfully achieved energy and intensity upgrades for the injector RILAC, which are required for super-heavy element synthesis experiments, by introducing the superconducting linac SRILAC. After three years of hardware improvements on the linac, we achieved a beam intensity of 4.2 particle μA with a duty factor of 86%.[1] Since FY2021, this team has been assigned to take over the duties under an outsourcing contract for the operation staff.

Reference
1) K. Yamada *et al.*, Proc. SRF2023.

2. Major Research Subjects

(1) Room-temerature and superconducting RF technology for heavy-ion accelerators
(2) Development of superconducting linac
(3) Operation of RIBF accelerator complex

3. Summary of Research Activity

- Room-temperature and superconducting RF technology for heavy-ion accelerators. We have successfully constructed a superconducting linac for the SHE experiment. Thanks to the newly developed digital feedback circuit, the amplitude and phase of the accelerating electric field are highly stabilized. The existing analog feedback circuits for the room-temperature RF system will be replaced by the newly developed digital feedback circuit.
- After commissioning the hardware of the superconducting linac, the next target is to achieve long-term operation with high reliability. One of the most significant issues with superconducting cavities is the increase in field emission due to prolonged operation. We are currently working on finding a solution to restore the original performance of the superconducting cavity by utilizing high-power pulsed conditioning.
- User beam services are performed by the operation staff. To ensure effective operation and software and hardware maintenance, a weekly operation meeting is held. During these meetings, problems and difficulties are discussed among members of the hardware groups and the safety management group.

Members

Team Leader

Naruhiko SAKAMOTO

Research/Technical Scientists

Kazutaka OZEKI (Senior Technical Scientist)
Kenji SUDA (Technical Scientist)

List of Publications & Presentations

Publications

[Original Paper]

H. Sakai, H. Haba, K. Morimoto, and N. Sakamoto, "Facility upgrade for superheavy-element research at RIKEN," Eur. Phys. J. A **58**, 238 (2022).

[Review Article]

N. Sakamoto and T. Nagatomo, "Superconducting linac booster for super-heavy element experiments at RIKEN radioactive isotope beam factory," Nucl. Phys. News **32**, 21 (2022).

[Proceedings]

K. Yadomi, K. Ozeki, S. Fukuzawa, M. Hamanaka, S. Ishikawa, K. Kobayashi, R. Koyama, R. Moteki, T. Nakamura, M. Nishida, M. Nishimura, J. Shibata, N. Tsukiori, T. Adachi, M. Fujimaki, N. Fukunishi, H. Hasebe, Y. Higurashi, H. Imao, O. Kamigaito, M. Kidera, M. Komiyama, K. Kumagai, T. Maie, Y. Miyake, T. Nagatomo, T. Nakagawa, T. Nishi, J. Ohnishi, H. Okuno, N. Sakamoto, K. Suda, A. Uchiyama, S. Watanabe, T. Watanabe, Y. Watanabe, K. Yamada, K. Kamakura, and Y. Kotaka, "Status report on the operation of RIKEN AVF cyclotron," Proceedings of the 19th Annual Meeting of Particle Accelerator Society of Japan, Kyushu

University, Online, Japan, October 18–21, 2022, TWP001, 1075–1078 (2022), https://www.pasj.jp/web_publish/pasj2022/proceedings/PDF/TWP0/TWP001.pdf.

K. Kobayashi, K. Suda, S. Fukuzawa, M. Hamanaka, S. Ishikawa, R. Koyama, R. Moteki, T. Nakamura, M. Nishida, M. Nishimura, J. Shibata, N. Tsukiori, K. Yadomi, T. Adachi, T. Dantsuka, M. Fujimaki, T. Fujinawa, N. Fukunishi, H. Hasebe, Y. Higurashi, E. Ikezawa, H. Imao, O. Kamigaito, Y. Kanai, M. Kidera, M. Komiyama, K. Kumagai, T. Maie, Y. Miyake, T. Nagatomo, T. Nakagawa, M. Nakamura, J. Ohonishi, H. Okuno, K. Ozeki, N. Sakamoto, A. Uchiyama, S. Watanabe, T. Watanabe, Y. Watanabe, and K. Yamada, "Status report on the operation of RIKEN AVF cyclotron," Proceedings of the 19th Annual Meeting of Particle Accelerator Society of Japan, Kyushu University, Online, Japan, October 18–21, 2022, TWP003, 1084–1088 (2022), https://www.pasj.jp/web_publish/pasj2022/proceedings/PDF/TWP0/TWP003.pdf.

H. Yamauchi, T. Ohki, K. Oyamada, M. Tamura, Y. Akira, K. Kaneko, T. Nishi, N. Sakamoto, M. Fujimaki, H. Imao, M. Kidera, T. Nagatomo, K. Ozeki, K. Suda, A. Uchiyama, T. Watanabe, Y. Watanabe, K. Yamada, and O. Kamigaito, "Present status of RILAC," Proceedings of the 19th Annual Meeting of Particle Accelerator Society of Japan, Kyushu University, Online, Japan, October 18–21, 2022, TFP009, 1144–1147 (2022), https://www.pasj.jp/web_publish/pasj2022/proceedings/PDF/TFP0/TFP009.pdf.

Presentations

[International Conferences/Workshops]

K. Yamada, "Operational status of SRILAC at RIKEN," Tesla Technology Collaboration Meeting, Rokkasho, Japan, October 11–14, 2022.

K. Ozeki, "Present stautus of RIKEN power coupler," Tesla Technology Collaboration Meeting, Rokkasho, Japan, October 11–14, 2022.

[Domestic Conferences/Workshops]

K. Yadomi, K. Ozeki, S. Fukuzawa, M. Hamanaka, S. Ishikawa, K. Kobayashi, R. Koyama, R. Moteki, T. Nakamura, M. Nishida, M. Nishimura, J. Shibata, N. Tsukiori, T. Adachi, M. Fujimaki, N. Fukunishi, H. Hasebe, Y. Higurashi, H. Imao, O. Kamigaito, M. Kidera, M. Komiyama, K. Kumagai, T. Maie, Y. Miyake, T. Nagatomo, T. Nakagawa, T. Nishi, J. Ohnishi, H. Okuno, N. Sakamoto, K. Suda, A. Uchiyama, S. Watanabe, T. Watanabe, Y. Watanabe, K. Yamada, K. Kamakura, and Y. Kotaka, "Status report on the operation of RIKEN AVF cyclotron," The 19th Annual Meeting of Particle Accelerator Society of Japan, Kyushu University, Online, Japan, October 18–21, 2022.

K. Kobayashi, K. Suda, S. Fukuzawa, M. Hamanaka, S. Ishikawa, R. Koyama, R. Moteki, T. Nakamura, M. Nishida, M. Nishimura, J. Shibata, N. Tsukiori, K. Yadomi, T. Adachi, T. Dantsuka, M. Fujimaki, T. Fujinawa, N. Fukunishi, H. Hasebe, Y. Higurashi, E. Ikezawa, H. Imao, O. Kamigaito, Y. Kanai, M. Kidera, M. Komiyama, K. Kumagai, T. Maie, Y. Miyake, T. Nagatomo, T. Nakagawa, M. Nakamura, J. Ohonishi, H. Okuno, K. Ozeki, N. Sakamoto, A. Uchiyama, S. Watanabe, T. Watanabe, Y. Watanabe, and K. Yamada, "Status report on the operation of RIKEN AVF cyclotron," The 19th Annual Meeting of Particle Accelerator Society of Japan, Kyushu University, Online, Japan, October 18–21, 2022.

H. Yamauchi, T. Ohki, K. Oyamada, M. Tamura, Y. Akira, K. Kaneko, T. Nishi, N. Sakamoto, M. Fujimaki, H. Imao, M. Kidera, T. Nagatomo, K. Ozeki, K. Suda, A. Uchiyama, T. Watanabe, Y. Watanabe, K. Yamada, and O. Kamigaito, "Present status of RILAC," The 19th Annual Meeting of Particle Accelerator Society of Japan, Kyushu University, Online, Japan, October 18–21, 2022.

Research Facility Development Division
Accelerator Group
Beam Dynamics & Diagnostics Team

1. Abstract

Aiming at stable and efficient operation of the RIBF cascaded cyclotron system, Beam Dynamics and Diagnostics Team develops power supplies, beam instrumentation, computer control, and beam dynamic studies. We have successfully increased the beam availability for user experiments to over 98%. We have also established small-beam-loss operations, which strongly contribute to recent high-power operations at RIBF.

2. Major Research Subjects

(1) Efficient and stable operations of the RIBF cascaded cyclotron system
(2) Maintenance and development of the beam instrumentation
(3) Developments of the computer control system for more intelligent and efficient operations
(4) Maintenance and improvements of the magnet power supplies for more stable operations
(5) Upgrade of the existing beam interlock system for high-power beams with a few tens of kW

3. Summary of Research Activity

(1) High-intensity heavy-ion beams such as 117-particle-nA (particle nA) uranium, 173-particle nA xenon, 690-particle nA krypton, 830-particle nA Zinc and, 740-particle nA calcium beams, have been obtained.
(2) The world-first high-Tc SQUID beam current monitor has been developed. The Beam Energy and Position Monitor has been successfully developed and introduced into the beamline of the superconducting rilac (SRILAC). Construction of a new Faraday cup capable of withstanding 50-kW beams is nearly completed by the end of FY2022.
(3) The replacement and upgrade of the old power supplies used in Riken Ring Cyclotron (RRC) are in progress. Two-thirds of the outdated power supplies that energize the trim coils of RRC have been replaced with new ones. The power supplies applying currents to beam injection and extraction systems have been upgraded in their current feedback systems, improving long-term stability.
(4) The new beam interlock system with a response time of less than 1 ms has been successfully developed utilizing National Instruments' CompactRIO technology.
(5) The RIBF control system has been operated stably by replacing legacy hardware controllers inherited from our old facility with new ones. Several useful operation tools are also developed.

Members

Team Leader
Nobuhisa FUKUNISHI

Senior Technical Scientists
Masaki FUJIMAKI
Kazunari YAMADA
Taihei Adachi
Tamaki WATANABE
Akito UCHIYAMA

Expert Technician
Misaki KOMIYAMA

Research Associate
Hiroki FUJII

Special Temporary Technical Scientist
Keiko KUMAGAI

Visiting Scientists
Shin-ichiro HAYASHI (Hiroshima Int'l Univ.)
Atsushi KAMOSHIDA (Nat'l Instruments Japan Corporation)
Takuya MAEYAMA (Kitasato Univ.)

List of Publications & Presentations

Publications

[Original Paper]

T. Maeyama, A. Mochizuki, K. Yoshida, N. Fukunishi, K. L. Ishikawa, and S. Fukuda, "Radio-fluorogenic nanoclay gel dosimeters with reduced linear energy transfer dependence for carbon beam radiotherapy," Med. Phys. **50**, 1073 (2023). https://doi.org/10.1002/mp.16092 .

[Proceedings]

T. Watanabe, A. Kamoshida, T. Nishi, A. Uchiyama, and K. Kaneko, "Beam profile measurement using helium gas light emission for superheavy element search experiment," Proceedings of the 19th Annual Meeting of Particle Accelerator Society of Japan, October 18–21, 2022, Online (Kyushu University), Japan, p. 764.

A. Uchiyama A. M. Kidera, M. Komiyama, and K. Kaneko, "Deployment of archiver appliance to RIBF control system," Proceedings of the 19th Annual Meeting of Particle Accelerator Society of Japan, October 18–21, 2022, Online (Kyushu University), Japan, p. 9.

K. Yamada, "Upgrade and current status of high-frequency systems for RIKEN Ring Cyclotron," Proc. 23rd International Conference on Cyclotrons and their Applications (CYC2022), Beijing, China, December 5–9, 2022, MOAI02.

A. Uchiyama, K. Kumagai, M. Komiyama, and N. Fukunishi, "Evaluation of PLC-based EtherNet/IP communication for upgrade of electromagnet power supply control at RIBF," Proc. 23rd International Conference on Cyclotrons and their Applications (CYC2022), Beijing, China, December 5–9, 2022, TUBO04.

Presentations

[International Conferences/Workshops]

K. Yamada (invited), "Upgrade and current status of high-frequency systems for RIKEN Ring Cyclotron," 23rd International Conference on Cyclotrons and their Applications (CYC2022), Beijing, China, December 5–9, 2022.

A. Uchiyama (oral), K. Kumagai, M. Komiyama, and N. Fukunishi, "Evaluation of PLC-based EtherNet/IP communication for upgrade of electromagnet power supply control at RIBF," 23rd International Conference on Cyclotrons and their Applications (CYC2022), Beijing, China, December 5–9, 2022.

[Domestic Conferences/Workshops]

T. Watanabe (poster), A. Kamoshida, T. Nishi, A. Uchiyama, and K. Kaneko, "Beam profile measurement using helium gas light emission for superheavy element search experiment," 19th Annual Meeting of Particle Accelerator Society of Japan, October 18–21, 2022, Kyushu University, Online, Japan.

A. Uchiyama (oral), M. Kidera, M. Komiyama, and K. Kaneko, "Deployment of archiver appliance to RIBF control system," 19th Annual Meeting of Particle Accelerator Society of Japan, October 18–21, 2022, Kyushu University, Online, Japan.

Research Facility Development Division
Accelerator Group
Cryogenic Technology Team

1. Abstract

We are operating the cryogenic system for the superconducting ring cyclotron in RIBF. We are operating the helium cryogenic system in the south area of RIKEN Wako campus and delivering the liquid helium to users in RIKEN. We are trying to collect efficiently gas helium after usage of liquid helium.

2. Major Research Subjects

(1) Operation of the cryogenic system for the superconducting ring cyclotron in RIBF
(2) Operation of the helium cryogenic plant in the south area of Wako campus and delivering the liquid helium to users in Wako campus

3. Summary of Research Activity

(1) Operation of the cryogenic system for the superconducting ring cyclotron in RIBF (H. Okuno, T. Dantsuka, M. Nakamura)
(2) Operation of the helium cryogenic plant in the south area of Wako campus and delivering the liquid helium to users in Wako campus (T. Dantsuka, S. Tsuruma, M. Kuroiwa, M. Takahashi, H. Okuno).

Members

Team Leader
Hiroki OKUNO

Senior Technical Scientist
Masato NAKAMURA

Technical Scientist
Tomoyuki DANTSUKA

Research Part-time Worker
Mamoru TAKAHASHI

Administrative Part-time Workers
Shizuho TSURUMA Mayumi KUROIWA

List of Publication & Presentation

Outreach Activity

段塚知志,「実験を止めない! 理研のヘリウムリサイクル」, クローズアップ科学道 2022, 2022 年 10 月 17 日, https://www.riken.jp/pr/closeup/2022/20221017_1/index.html .

Research Facility Development Division
Accelerator Group
Infrastructure Management Team

1. Abstract

Our team oversees the design, operation, and maintenance of the large-scale infrastructure for the entire RI Beam Factory (RIBF), including cooling water, air conditioning, and electrical equipment, as well as the research and development of their advanced management. In order to operate the RIBF efficiently, it is very important to ensure the sound operation of these infrastructures that lead to the stable functioning of various devices. Another important mission is to coordinate the scheduling of major construction and repair work related to the RIBF so that beamtime runs smoothly.

The recent issue is the aging of infrastructure equipment. In line with these measures, we are making modifications that contribute to the stability of accelerator equipment and energy saving. In addition, infrastructure equipment has many sensors for management, and a huge amount of measurement data from these sensors is archived. We are planning to use this data to build a more advanced management system.

2. Major Research Subjects

(1) Operation, maintenance, and monitoring of infrastructure of RI Beam Factory
(2) Development of advanced management of infrastructure that contributes to accelerator and beam stability
(3) Coordination of large construction work and modification related to RI Beam Factory

Members

Team Leader
Masanori KIDERA

Technical Scientist
Takeshi MAIE

Special Temporary Technical Scientist
Shu WATANABE

List of Publications & Presentations

Publications

[Proceedings]

内山暁仁, 金子健太, 木寺正憲, 込山美咲,「アーカイバーアプライアンスの RIBF 制御系への展開」, “Deployment of archiver appliance to RIBF control system,” Proceedings of the 19th Annual Meeting of Particle Accelerator Society of Japan, Kyushu University, Online, Japan, October 18–21, 2022, pp. 9–13.

矢冨一慎, 大関和貴, 福澤聖児, 濱仲誠, 石川盛, 小林清志, 小山亮, 茂木龍一, 仲村武志, 西田稔, 西村誠, 柴田順翔, 月居憲俊, 足立泰平, 藤巻正樹, 福西暢尚, 長谷部裕雄, 日暮祥英, 今尾浩士, 上垣外修一, 木寺正憲, 込山美咲, 熊谷桂子, 真家武士, 三宅泰斗, 長友傑, 中川孝秀, 西隆博, 大西純一, 奥野広樹, 坂本成彦, 須田健嗣, 内山暁仁, 渡部秀, 渡邉環, 渡邉裕, 山田一成, 鎌倉恵太, 小高康照, 「理研 AVF サイクロトロン運転の現状報告」, “Status report on the operation of RIKEN AVF cyclotron,” Proceedings of the 19th Annual Meeting of Particle Accelerator Society of Japan, Kyushu University, Online, Japan, October 18–21, 2022, pp. 1075–1078.

小林清志, 須田健嗣, 福澤聖児, 濱仲誠, 石川盛, 小山亮, 茂木龍一, 仲村武志, 西田稔, 西村誠, 柴田順翔, 月居憲俊, 矢冨一慎, 足立泰平, 段塚知志, 藤巻正樹, 藤縄雅, 福西暢尚, 長谷部裕雄, 日暮祥英, 池沢英二, 今尾浩士, 上垣外修一, 金井保之, 木寺正憲, 込山美咲, 熊谷桂子, 真家武士, 三宅泰斗, 長友傑, 中川孝秀, 中村仁音, 大西純一, 奥野広樹, 大関和貴, 坂本成彦, 内山暁仁, 渡部秀, 渡邉環, 渡邉裕, 山田一成,「理研 RIBF におけるリングサイクロトロンの運転報告」, “Status report of the operation of RIBF ring cyclotrons,” Proceedings of the 19th Annual Meeting of Particle Accelerator Society of Japan, Kyushu University, Online, Japan, October 18–21, 2022, pp. 1084–1088.

山内啓資, 西隆博, 大木智則, 小山田和幸, 田村匡史, 遊佐陽, 金子健太, 坂本成彦, 今尾浩士, 内山暁仁, 大関和貴, 木寺正憲, 須田健嗣, 長友傑, 藤巻正樹, 山田一成, 渡邉環, 渡邉裕, 上垣外修一, 「理研重イオンリニアックの現状報告」, “Present status of RILAC,” Proceedings of the 19th Annual Meeting of Particle Accelerator Society of Japan, Kyushu University, Online, Japan, October 18–21, 2022, pp. 1144–1147.

Research Facility Development Division
Instrumentation Development Group

1. Abstract

This group develops the core-experimental instruments at the RI Beam Factory. Three projects are currently going on. SCRIT is the world's first experimental facility for electron scattering of unstable nuclei and was constructed off the main beamline of RIBF. The first physic result was demonstrated in 2017. After years of developments and improvements, the world's first electron scattering experiment with online-produced radioactive isotopes has been successfully conducted in 2022. An upgrade of the electron beam power that drives RI beam production is currently underway. The Rare-RI Ring is an event-by-event-operated heavy ion storage ring for precise mass measurement of extremely rare exotic nuclei. It is currently accepting applications for experimental proposals and has already conducted PAC-approved experiments and published its first physics results. In 2022, we confirmed that the new capacitors of the kicker-magnet system worked well during long-time test. Thus, the problem in the operation has been solved so far. More improvements are currently underway to achieve more precise mass measurements and stable operation. The compact heavy-ion storage ring RUNBA is an R&D machine for the development of beam recycling techniques for nuclear reaction research on rare elements. This is currently under construction and some of the critical components of the ring are currently undergoing technical development.

All instrumentations are designed to maximize the research potential of the world's most intense RI beams, and dedicated RI Beam Factory equipment makes the experimental challenge possible. The experimental technique and experience accumulated in this group provide opportunities for new experimental challenges and form the basis for the future development of the RIBF.

2. Major Research Subjects

(1) SCRIT Project (electron scattering off unstable nuclei)
(2) Rear RI Ring Project (precise mass measurement)
(3) RUNBA project (Beam recycling techniques)

3. Summary of Research Activity

We are developing beam manipulation techniques to carry out the above projects. These are high-quality slow RI beam generation technology (SCRIT), beam cooling and stopping technology (SCRIT) and beam accumulation technology in a storage ring (Rare RI Ring, RUNBA). The technical know-how accumulated in the project will play a major role in the next generation of RIBF. The current status and future plans for SCRIT and Rare-RI Ring are described in the respective sections.

In 2022, we successfully conducted the world's first electron scattering experiment with online-produced unstable nuclei, which is ^{137}Cs isotopes, through years of the developments and improvements. We are in the process of power upgrading of the electron beam from the RTM, which is the driving for RI production, and expanding the nuclei that can be accessed. The Rare RI Ring is an event-by-event based mass measurement system, designed specifically for extremely low-producing isotopes. We carried out PAC-approved experiments and successfully measured the masses of ^{74,76}Ni, ^{122}Rh, ^{123,124}Pd and ^{125}Ag for the first time. To improve mass resolution and efficiency, the first-response kicker system and optical tuning system are being improved. To ensure stable operation, the new capacitors were tested with a kicker manet system with good results. According to the future plans of Nishina center, a beam re-cycling technique is under development. Beam recycling technology allows the circulation of RI beams to be maintained in a storage ring with a thin internal target until a nuclear reaction occurs. In order to establish beam recirculation, the increase in energy width and emittance needs to be compensated for using a fast feedback system. We have demonstrated the possibility of compensation in an analytical way and found the properties of EDC and ADC devices necessary for compensation. To develop these new technologies, a compact heavy ion storage ring (RUNBA) connected to ISOL (ERIS) is under construction at the SCRIT facility. Under a research cooperation agreement with ICR in Kyoto University, technical development of the main components required for RUNBA *i.e.* the charge breeder, energy dispersion corrector, angular diffusion corrector and internal target system are underway. We developed the prototype devices for EDC and ADC devices, and further improvements are ongoing. Furthermore, we also developed the simulation code based on the analytical model, and evaluated the performance of RUNBA.

Members

Directors

Tetsuya OHNISHI
Masanori WAKASUGI

Contract Researcher

Ryo OGAWARA

Visiting Scientists

Shun IIMURA (Rikkyo Univ.)
Daisuke NAGAE (Tokyo Tech)
Ryo OGAWARA (Kyoto Univ.)
Akira OZAWA (Tsukuba Univ.)
Fumi SUZAKI (JAEA)
Kyo TSUKADA (Kyoto Univ.)
Masanori WAKASUGI (Kyoto Univ.)

Student Trainees

Yuki ITO (Kyoto Univ.)
Yusei MAEDA (Kyoto Univ.)
Yoshiki MAEHARA (Kyoto Univ.)
Mariko TACHIBANA (Kyoto Univ.)
Fuuma TOUJOU (Rikkyo Univ.)
Tsubasa YAMANO (Rikkyo Univ.)
Satoru YOSHIDA (Kyoto Univ.)

Administrative Part-time Worker

Midori TAKEMON

List of Publication & Presentations

Publication

[Review Article]

M. Wakasugi, Y. Abe, Y. Ito, T. Ohnishi, R. Ogawara, K. Kuze, S. Takagi, K. Tsukada, H. Tongu, Y. Maehara, and Y. Yamaguchi, "Recycled-Unstable-Nuclear Beam Accumulator (RUNBA) for developing beam recycling technique toward the study of nuclear reaction for rare RIs," J. Part. Accl. Soc. Jpn. **19**, 25 (2022).

Presentations

[Domestic Conferences/Workshops]

小川原亮 (口頭発表), 「RI-RI 反応実験を目的としたビームリサイクル技術開発用蓄積リング（RUNBA）の動作原理」, 日本物理学会 第 77 回年次大会, オンライン, 2022 年 3 月 15–19 日.

小川原亮 (口頭発表), 「ビームリサイクル技術開発を目的とした重イオン蓄積リング RUNBA の動作原理」, 第 19 回日本加速器学会年会, オンライン, 2022 年 10 月 18–21 日.

Research Facility Development Division
Instrumentation Development Group
SLOWRI Team

1. Abstract

The SLOWRI team develops, operates and improves SLOW RI beam production devices and related systems, and uses these devices and systems to conduct experimental programs at RIBF. As the heart of SLOWRI, we have developed RF carpet type cryogenic He gas catchers (RFGC). Two RFGCs are currently in operation to deliver slow RI beams converted from fast RIs produced with fragmentation or inflight fission on RIPS and BigRIPS. These RFGCs are directly combined with muti-reflection time-of-flight mass spectrographs (MRTOF-MS) for precise mass measurements tailored to user's experimental programs. Especially, the RFGC combined with a MRTOF-MS installed behind ZeroDegree spectrometer of BigRIPS is being operated symbiotically reusing RIs from other experiment conducted upstream without extra costs. To date, masses on more than 80 RIs provided with BigRIPS have been successfully measured. A lot of user's experimental programs for precise mass measurements will be conducted in SLOWRI project soon. An Ar gas catcher at F2 of BigRIPS was also installed to rescue RI that would otherwise be discarded without being used for experiments. The RI is caught with the Ar gas catcher, laser resonant ionized and delivered as a slow RI beam in parasitic operating mode (PALIS). The off- and online-commissioning of PALIS is underway.

2. Major Research Subjects

(1) Development, operation and upgrade of SLOW RI beam production devices and related systems
(2) Development and operation of multi-reflection time-of-flight mass spectrographs and to conduct precision mass measurements of short-lived nuclei
(3) Development of a parasitic slow RI beam production method using resonance laser ionization

3. Summary of Research Activity

(1) Development of RF carpet type cryogenic He gas catchers (RFGCs)

The fast (>100 MeV/nucleon) RI beams can be stopped in helium gas and extracted as slow (<100 eV) RI beams from a RF carpet type cryogenic He gas cell (RFGC). At RIBF, two RFGCs are in operation at the SLOWRI project: one is a 30-cm-long RFGC consisting of DC ring electrodes and a RF carpet. It is located behind GARIS-II at E6 of RIBF and is used in combination with a MRTOF-MS for precise mass measurements of superheavy nuclides. Also, a 9 MBq ^{252}Cf fission source has recently been installed just in front of the He gas catcher. Even off-line, mass measurements on fission fragments have continued and several first mass measurements were performed.

Second one is a 50-cm-long RFGC installed behind ZeroDgree spectrometer of BigRIPS. This RFGC contains a three stage RF-carpet structure: a gutter RF carpet (1st carpet) for the collection thermal ions in the cell into a small slit, a narrow (about 10 mm) traveling-wave RF-carpet (2nd carpet) for collection of ions from the gutter carpet and for transporting the ions towards the exit, and a small RF carpet for extraction from the gas cell. The off-line test has been completed in FY2019. The on-line commissioning has been successfully performed symbiotically using RIs provided with BigRIPS during HiCARI campaign in FY2020. During the on-line commissioning, precise mass measurements were also performed. In FY2021, the first experiment approved in NP-PAC of RNC has been performed, which has aimed the mass measurement in the vicinity of the double magic nucleus of ^{78}Ni. As the result, masses of ^{74}Ni and ^{75}Ni have been measured with high precision less than 20 keV. In FY 2022, a ^{248}Cm source has been installed just behind the mylar window of the gas cell. The measured extraction efficiencies on the fission products emitted from the source after stopping in the He gas have been currently reached several to about 30% of the sum of singly-, doubly- and triply-charged ions, depending on elements. Several improvements in order to improve the efficiencies are underway using the fission fragments from the source. Mass measurements on experimental programs already approved in NP-PAC of RIBF will be performed soon. A final version of the RFGC, 1 m long and with increased helium gas pressure, is also in preparation and will be installed in SD4 at BigRIPS.

(2) Conduct of precise mass measurements using MRTOF-MSs combined with RFGCs

The MRTOF, called as SHE-MASS, is combined with the RFGC behind GARIS-II of E6. Mass measurements of superheavy elements of Db isotopes have been conducted. As a result, the mass on ^{257}Db superheavy nucleus was determined for the first time. The mass measurements on superheavy nuclide, proton rich nuclide and fission products emitted from intense Cf source have been performed.

The MRTOF-MS, called as ZD-MRTOF, is located behind ZDS of BigRIPS in combination with the 50 cm-long RFGC. Currently, the mass resolving power has been reached at 1 million. Since the location of the ZD-MRTOF is just in front of the beam dump of ZDS, mass measurements have been conducted symbiotically re-using RIs from other experiment conducted upstream without extra costs. To date, the masses on more than 80 RIs provided from BigRIPS have been measured. Among them, three isotope masses have been measured for the first time and mass uncertainties of eleven isotope have been significantly improved from the previous ones. For example, the mass uncertainties have been reduced down to the order of 10 keV for ^{56,58}Ti and $^{56\text{-}59}$V and nonexistence of the N = 34 empirical two neutron shell-gaps on Ti and V isotopes are revealed experimentally with the new precision achieved.

We have a plan to increase this versatile and portable instrumentation at RIBF: an MRTOF-MS is being installed behind GARIS-III, and a plan is underway to install an MRTOF-MS with the RFGC behind SD4 at BigRIPS, which will lead to more opportunities to study unexplored nuclear species.

(3) Development of a parasitic slow RI beam production method using resonance laser ionization (PALIS)

More than 99% of RIs produced in projectile fission or fragmentation at BigRIPS of RIBF are simply dumped into the first dipole magnet and the slits. The SLOWRI project proposed a new method called PALIS, which uses a compact Ar gas catcher and resonant laser ionization to rescue such precious RI. The thermalized RIs in a cell filled with Ar gas can be quickly neutralized and transported to the exit of the cell by gas flow. Irradiation of resonance lasers at the exit ionizes neutral RI atoms selectively. PALIS is located at F2 of BigRIPS and is undergoing off- and on-line commissioning.

At F2, due to high radiation from a beam dump, it was found to be not easy to handle ions using electric ion guides. Therefore, a 70-cm-long gas pipe from the Ar gas cell was newly installed to transport RIs to relatively low radiation area thanks for the Ar gas flow. In FY2021, we have confirmed the transport of ions of interest downstream of the ion guide behind the gas pipe using α-emitting Ac isotopes provided with BigRIPS. Also, we have found a lot of contaminant ions from the gas cell, which are originated from impurities in the gas. To reduce the influence of such contaminant, a quadrupole mass filter has been installed downstream of the ion guide. In FY2023, an on-line test for resonant laser ionization is planned.

Members

Team Leader
Hironobu ISHIYAMA

Senior Research Scientist
Takao KOJIMA

Research Scientist
Aiko TAKAMINE

Technical Scientist
Tetsu SONODA

Research Consultant
Hideki IIMURA

Visiting Scientists
Minoru TANIGAKI (Kyoto Univ.)
Hideki TOMITA (Nagoya Univ.)

List of Publications & Presentations

Publications

[Original Papers]

S. Iimura, M. Rosenbusch, A. Takamine, Y. Tsunoda, M. Wada, S. Chen, D. S. Hou, W. Xian, H. Ishiyama, S. Yan, P. Schury, H. Crawford, P. Doornenbal, Y. Hirayama, Y. Ito, S. Kimura, T. Koiwai, T. M. Kojima, H. Koura, J. Lee, J. Liu, S. Michimasa, H. Miyatake, J. Y. Moon, S. Nishimura, S. Naimi, T. Niwase, A. Odahara, T. Otsuka, S. Paschalis, M. Petri, N. Shimizu, T. Sonoda, D. Suzuki, Y. X. Watanabe, K. Wimmer, and H. Wollnik, "A new study of the $N = 32$ and $N = 34$ shell gap for Ti and V by the first high-precision MRTOF mass measurements at BigRIPS-SLOWRI," Phys. Rev. Lett. **130**, 012501 (2023).

M. Rosenbusch, M. Wada, S. Chen, A. Takamine, S. Iimura, D. Hou, W. Xian, S. Yan, P. Schury, Y. Hirayama, Y. Ito, H. Ishiyama, S. Kimura, T. Kojima, J. Lee, J. Liu, S. Michimasa, H. Miyatake, M. Mukai, J. Y. Moon, S. Nishimura, S. Naiumi, T. Niwase, T. Sonoda, Y. X. Watanabe, and H. Wolnik, "The new MRTOF mass spectrograph following the ZeroDegree spectrometer at RIKEN's RIBF facility," Nucl. Instrum. Methods Phys. Res. B **1047**, 167824 (2023).

Y. Hirayama, M. Mukai, Y. X. Watanabe, P. Schury, H. Nakada, J. Y. Moon, T. Hashimoto, S. Iimura, S. C. Jeong, M. Rosenbusch, M. Oyaizu, T. Niwase, M. Tajima, A. Taniguchi, M. Wada, and H. Miyatake, "In-gas-cell laser resonance ionization spectroscopy of ^{200,201}Pt," Phys. Rev. C **106**, 034326 (2022).

Presentations

[International Conferences/Workshops]

S. Iimura (invited), "A new study of $N = 34$ subshell structure probed by high-precision mass measurements," JSPS/NSFC/NRF A3 Foresight Program, "Nuclear Physics in the 21st Century," Osaka, Japan, February 13–15, 2023.

A. Takamine, M. Rosenbusch, M. Wada, S. Iimura, D. Hou, W. Xian, S. Chen, J. M. Yap, H. Ishiyama, P. Schury, S. Nishimura, T. Niwase, S. Kimura, Y. Hirayama, Y. Ito, T. M. Kojima, J. Lee, J. Liu, S. Michimasa, H. Miyatake, J. Y. Moon, M. Mukai, S. Naimi, T. Sonoda, H. Ueno, P. Vi, Y. X. Watanabe, S. Yan, T. T. Yeung, and H. Wollnik, "Development of the new helium gas catcher and nuclear mass measurements with the new MRTOF-MS system behind the ZeroDegree spectrometer at RIKEN BigRIPS," The 19th International Conference on Electromagnetic Isotope Separators and Related Topics (EMIS 2022), Daejong, Korea, October 3–7, 2022.

M. Rosenbusch, M. Wada, S. Chen, A. Takamine, S. Iimura, D. Hou, W. Xian, S. Yan, P. Schury, Y. Hirayama, Y. Ito, H. Ishiyama, S. Kimura, J. Lee, J. Liu, S. Michimasa, H. Miyatake, J. Y. Moon, S. Nishimura, S. Naimi, T. Niwase, Y. X. Watanabe, P. Vi, H. Wollnik, and J. M. Yap, "High-precision MRTOF mass measurements of radioactive isotopes at RIKEN's RIBF facility: Recent projects for mirror potentials, wideband mass accuracy, and ion selection," The 19th International Conference on Electromagnetic Isotope Separators and Related Topics (EMIS 2022), Daejong, Korea, October 3–7, 2022.

M. Rosenbusch, "Exploring exotic nuclei by high-precision MRTOF mass measurements: The new ion catcher and mass spectrograph at RIKEN's RIBF facility," The 8th International Conference on Trapped Charged Particles and Fundamental Physics (TCP 2022), Glashütten, Germany, September 25–30, 2022.

H. Ishiyama, "Toward mass measurement of neutron-rich nuclei in the vicinity of $N = 126$," Workshop for Uniqueness of the ^{208}Pb beam at RIBF, Online, September 27, 2022.

M. Rosenbusch (invited), "New nuclear masses, recent and present developments, and future opportunities of the MRTOF-MS at the ZeroDegree spectrometer," RIBF Users Meeting 2022, Online, September 20–22, 2022.

S. Iimura (invited), "A new study of the $N = 32$ and $N = 34$ shell gap for Ti and V by the first high-precision MRTOF mass measurements at BigRIPS-SLOWRI," RIBF Users Meeting 2022, Online, September 20–22, 2022.

A. Takamine (invited), "Nuclear mass measurements with the new MRTOF-MS system at the ZeroDegree spectrometer of BigRIPS," 28th International Nuclear Physics Conference (INPC 2022), Cape Town, South Africa, September 11–16, 2022.

H. Ishiyama (invited), "Present status of SLOWRI," SSRI-PNS collaboration meeting 2022, Online, September 1–2, 2022.

[Domestic Conferences/Workshops]

M. Rosenbusch, S. Iimura, A. Takamine, Y. Tsunoda, M. Wada, S. Chen, D. S. Hou, W. Xian, H. Ishiyama, S. Yan, P. Schury, H. Crawford, P. Doornenbal, Y. Hirayama, Y. Ito1, S. Kimura, T. Koiwai, T. M. Kojima, H. Koura, J. Lee, J. Liu, S. Michimasa, H. Miyatake, J. Y. Moon, S. Naimi, S. Nishimura, T. Niwase, A. Odahara, T. Otsuka, S. Paschalis, M. Petri, N. Shimizu, T. Sonoda, D. Suzuki, Y. X. Watanabe, K. Wimmer, and H. Wollnik, "The SLOWRI/MRTOF-MS project at BigRIPS/ZeroDegree," 日本物理学会 2022 年度春季年会, オンライン, 2023 年 3 月 23–25 日.

飯村俊, M. Rosenbusch, 高峰愛子, 和田道治, S. Chen, D. Hou, J. Liu, W. Xian, S. Yan, P. Schury, 木村創大, 庭瀬暁隆, 伊藤由太, 園田哲, 小島隆夫, 渡辺裕, 平山賀一, 宮武宇也, S. Naimi, 道正新一郎, 西村俊二, 小田原厚子, 石山博恒, 角田佑介, 清水則孝, 大塚孝治, 「BigRIPS SLOWRI における ZD-MRTOF 装置を用いた中性子過剰 Sc, Ti, V 核の系統的核構造研究」, 日本物理学会 2022 年度秋季大会, 岡山市 (岡山理科大学), 2022 年 9 月 6–8 日.

庭瀬暁隆, 渡辺裕, 平山賀一, 向井もも, P. Schury, A. N. Andreyev, 飯村俊, 石山博恒, 鄭淳讃, 宮武宇也, M. Rosenbusch, 谷口秋洋, 和田道治, 「精密質量測定による新同位体 ^{241}U の発見」, 日本物理学会 2022 年度秋季大会, 岡山市 (岡山理科大学), 2022 年 9 月 6–8 日.

[Seminar]

M. Rosenbusch (invited), "A first review of the SLOWRI-MRTOF mass spectrograph following the ZeroDegree spectrometer at BigRIPS," RIBF seminar, Wako, Japan, February 14, 2023.

Press Release

マルコローゼンブッシュ, 飯村俊, 他, 「チタン・バナジウム中性子過剰同位体で新魔法数の消失を観測—精密質量測定による原子核構造のより深い理解に期待—」, KEK, RIKEN, 大阪大学, 2023 年 1 月 6 日.

Research Facility Development Division
Instrumentation Development Group
Rare RI-ring Team

1. Abstract

The aim of Rare-RI Ring (R3) is to measure the masses of short-lived unstable nuclei far from the beta-stability line. In particular, a high-precision mass measurement for nuclei located around the *r*-process path (rare-RI) is required in nucleosynthesis point of view. Through the commissioning experiments by 2017, we confirmed the high ability of R3 as a storage ring capable of handling one event, and demonstrated that it is possible to perform the time-of-flight Isochronous Mass Spectrometry (IMS) in shorter than 1 millisecond. In 2018, we performed mass measurement experiments for the first time. In 2020, the kicker system was modified to flatten the magnetic field distribution, and the performance study using unstable nuclei was successfully conducted. In 2021, we performed mass measurement experiments using the upgraded kicker system. The results of the experiment dispelled concerns about the results of the previous experiment that the injection angle might greatly affected the accuracy of the mass determination. On the other hand, a failure occurred in the kicker power supply that interfered with the progress of experiments. The cause of the failure was investigated and resolved in this fiscal year. We have plan to conduct a beam test to confirm the stable operation of the kicker system before resuming the mass measurement experiments.

2. Major Research Subjects

(1) Further improvement of mass measurement efficiency and precision
(2) Precision mass measurement for rarely produced isotopes related to *r*-process

3. Summary of Research Activity

In the commissioning experiments up to 2017, we confirmed the unique performances of R3 and demonstrated the time-of-flight isochronous mass measurement method. We have realized in forming the precise isochronous field of less than 5 ppm with wide momentum range of $\Delta p/p = \pm 0.5\%$. Another performance required for R3 is to efficiently seize hold of an opportunity of the mass measurement for rare-RIs produced unpredictably. It was realized by constructing the Isotope-Selectable Self-trigger Injection (ISSI) scheme which pre-identified rare-RI itself triggers the injection kicker magnets. Key device was a fast response kicker system that has been successfully developed. Full activation of the kicker magnetic field can be completed within the flight time of the rare-RI from an originating point (F3 focal point in BigRIPS) of the trigger signal to the kicker position in R3.

Since R3 circulates, in principle, only one event, we fabricated high-sensitive beam diagnostic devices in the ring. One of them is a cavity type of Schottky pick-up installed in a straight section of R3. The Schottky pick-up successfully monitored a single $^{78}Kr^{36+}$ ion circulation with the measurement time of less than 10 milliseconds in the first commissioning experiment. We also confirmed that it is useful for fine tuning of the isochronous field.

We performed mass measurement in the third commissioning experiment by using unstable nuclei which masses are well-known. The masses of ^{79}As, ^{77}Ga, ^{76}Zn, and ^{75}Cu relative to ^{78}Ge were deduced with the accuracy of several ppm. In addition, we have improved the extraction efficiency to 2% by considering the matching condition between the emittance of injection events and the acceptance of R3 in the fourth commissioning experiment. This extraction efficiency was sufficient to conduct the accepted two proposals: mass measurements of Ni isotopes and south-west region of ^{132}Sn.

In November 2018, we conducted the first experiment using R3 to measure the masses for ^{74,76}Ni in 4 days. After that, we also measured the masses for ^{122}Rh, ^{123,124}Pd, and ^{125}Ag in 4.5 days. These nuclei were successfully extracted from R3 with the efficiency of 1–2%. However, unexpected deviation from the evaluated values of literature remained in the masses obtained by detailed analysis. This was thought to be due to the following two reasons. One is that due to the kicker field distribution is not flattened, the injection angle is different between the reference and target nucleus, and therefore the relative value of TOF is incorrect. The other is that the absolute value of beta or magnetic rigidity determined for each extracted event is incorrect.

In 2020, we modified the kicker system to flatten the magnetic field distribution as well as to dispel the concerns of the results of first experiment. As a result of performance study using unstable nuclei, we succeeded in forming the kicker field with 100 ns flat-top for injection and long flat-top of 350 ns or more for extraction. The experimental efficiency had been improved by a factor of two or more than previous condition because all nuclides can be extracted at once thanks to the long flat-top.

Using this upgraded kicker system, we measured the mass for ^{74}Ni again in April 2021. Although the kicker field distribution was flattened, the results of masses were the same as those of the first experiment. In other words, concerns about the effects of differences in injection angles have been dispelled. As a subsequent analysis, it was clarified that the reason is the second concern described above. Recently, the mass of ^{123}Pd was determined precisely and its effect on heavy element synthesis was investigated with collaborators. We concluded that the composition around ^{123}Pd observed in the solar system can only be reproduced using the new mass values, and published a paper in early 2022. The final mass values of other measured nuclei, such as Ni-isotopes, will be determined soon.

The insulation breakdown of a ceramic capacitor used as the charging circuit of the kicker system, which occurred frequently during the experiment conducted in November 2021, significantly affected the progress of the experiment. We investigated the cause of the problem, but found no external factors, and considered the problem to be the capacitor itself. It was difficult to determine the exact cause due to so severe damage, but it was found that the central part of the three-layer structure was particularly damaged inside the molded resin. Therefore, we decided to use a single-layer capacitor to avoid overheating of the central part. A five-days continuous test was conducted in November 2022 to compare the old and new capacitors. As a result, the old capacitor failed again while the new

capacitor was fine. We will replace all the capacitors and conduct a performance test of the kicker system in 2023.

Members

Team Leaders

Tetsuya OHNISHI Masanori WAKASUGI

Technical Scientist

Yoshitaka YAMAGUCHI

List of Publications & Presentations

Publications

[Original Papers]

H. F. Li, S. Naimi, T. M. Sprouse, M. R. Mumpower, Y. Abe, Y. Yamaguchi, D. Nagae, F. Suzaki, M .Wakasugi, H. Arakawa, W. B. Dou, D. Hamakawa, S. Hosoi, Y. Inada, D. Kajiki, T. Kobayashi, M .Sakaue, Y. Yokoda, T. Yamaguchi, R. Kagesawa, D. Kamioka, T. Moriguchi, M. Mukai, A. Ozawa, S. Ota, N. Kitamura, S. Masuoka, S. Michimasa, H. Baba, N. Fukuda, Y. Shimizu, H. Suzuki, H. Takeda, D. S. Ahn, M. Wang, C. Y. Fu, Q. Wang, S. Suzuki, Z. Ge, Yu. A. Litvinov, G. Lorusso, P. M. Walker, Zs. Podolyak, and T. Uesaka, "First application of mass measurements with the Rare-RI Ring Reveals the solar *r*-process abundance at $A = 122$ and $A = 123$," Phys. Rev. Lett. **128**, 152701 (2022).

ナイミ・サラ, リ・ホンフー, 山口由高, 上坂友洋, 「元素起源の謎解明に向けた超高速質量測定法の実現」, Isotope News **785**, 32 (2023).

Presentations

[Domestic Conferences/Workshops]

山口貴之 (招待講演), 「多価イオンビームによる２光子稀崩壊の観測」, 新学術領域研究「宇宙観測検出器と量子ビームの出会い. 新たな応用への架け橋」, 領域研究会, オンライン, 2022 年 5 月 20–21 日.

篠崎稔 (口頭発表), 「稀少 RI リングのための GAGG:Ce シンチレータを用いた重イオンビーム飛行時間兼全エネルギー検出器の開発」, 日本物理学会 2022 年秋季大会, 岡山市 (岡山理科大学), 2022 年 9 月 6–8 日.

神田真矩 (口頭発表), 「稀少 RI リングのためのプラスチックシンチレータと WLS ファイバーを用いた位置検出器の開発」, 日本物理学会 2022 年秋季大会, 岡山市 (岡山理科大学), 2022 年 9 月 6–8 日.

大久保研吾 (口頭発表), 「デルタ線を利用した重イオンビーム飛行時間検出器の開発」, 日本物理学会 2023 年秋季大会, オンライン, 2023 年 3 月 15–19 日.

佐々木健太 (口頭発表), 「稀少 RI リングのためのシンチレーションファイバーを用いた位置検出器の開発」, 日本物理学会 2023 年秋季大会, オンライン, 2023 年 3 月 15–19 日.

Press Release

「元素起源の謎の解明に向けた世界最速質量測定が始動—稀少 RI リングを用いた短寿命放射性同位体の質量測定に成功—」 , 理化学研究所, 筑波大学, 埼玉大学, 東京大学, 2022 年 4 月 28 日.

Research Facility Development Division
Instrumentation Development Group
SCRIT Team

1. Abstract

The SCRIT Electron Scattering Facility has been constructed at RIKEN RIBF. This aims at investigation of internal nuclear structure for short-lived unstable nuclei by means of electron scattering. SCRIT (Self-Confining RI Ion Target) is a novel method to form internal targets in an electron storage ring. This is a unique method for making electron scattering experiments for unstable nuclei possible. Construction of the facility has been started in 2009. This facility consists of an electron accelerator (RTM), a SCRITequipped electron storage ring (SR2), an electron-beam-driven RI separator (ERIS), and a window-frame spectrometer for electron scattering (WiSES) which consists of a large window-frame dipole magnet, drift chambers and trigger scintillators. Installation of all components in the facility was completed in 2015. After the comprehensive test and tuning, the luminosity was reached to $3 \times 10^{27}/(\mathrm{cm}^2\mathrm{s})$ with the number of injected ions of 3×10^8. In 2016, we successfully completed a measurement of diffraction of scattered electrons from ^{132}Xe nuclei and determined the charge density distribution for the first time. Through years of developments and improvements, in 2022, we successfully conducted the world's first electron scattering experiment with online-produced unstable nuclei. Using ^{137}Cs ions of 10^7 ions/pulse at 0.25 Hz, the luminosity was achieved to $0.9 \times 10^{26}/(\mathrm{cm}^2\mathrm{s})$ with about 250 mA-electron beam. In addition, we started the study of the isotope dependence of charge density distribution using Xe stable isotopes.

2. Major Research Subjects

Development of SCRIT electron scattering technique and measurement of the nuclear charge density distributions of unstable nuclei.

3. Summary of Research Activity

SCRIT is a novel technique to form internal target in an electron storage ring. Positive ions are three dimensionally confined in the electron beam axis by transverse focusing force given by the circulating electron beam and applied electrostatic longitudinal mirror potential. The created ion cloud composed of RI ions injected from outside works as a target for electron scattering. Construction of the SCRIT electron scattering facility has been started in 2009. The electron accelerators RTM and the storage ring SR2 were successfully commissioned in 2010. Typical accumulation current in SR2 is 250–300 mA at the energy range of 120–300 MeV that is required energy range in electron scattering experiment. The SCRIT device was inserted in the straight section of SR2 and connected to an ISOL named ERIS (Electron-beam-driven RI separator for SCRIT) by 20-m long low energy ion transport line. A buncher system based on RFQ linear trap named FRAC (Fringing-RF-field-Activated dc-to-pulse converter) was inserted in the transport line to convert the continuous beam from ERIS to pulsed beam, which is acceptable for SCRIT. The detector system WiSES consisting of a high-resolution magnetic spectrometer, drift chambers and trigger scintillators, was constructed, and it has a solid angle of 100 msr, energy resolution of 10^{-3}, and the scattering angle coverage of 25–55 degrees. A wide range of momentum transfer, 80–300 MeV/c, is covered by changing the electron beam energy from 150 to 300 MeV.

We successfully measured a diffraction pattern in the angular distribution of scattered electron from ^{132}Xe isotope at the electron beam energy of 150 MeV, 200 MeV, and 300 MeV, and derived the nuclear charge distribution by assuming two-parameters Fermi model for the first time. At this time, luminosity was reached to $3 \times 10^{27}/(\mathrm{cm}^2\mathrm{s})$ at maximum and the averaged value was $1.2 \times 10^{27}/(\mathrm{cm}^2\mathrm{s})$ with the number of injected target ions of 3×10^8.

We are now under preparation for going to the experiments for unstable nuclei. There are some key issues for that. They are increasing the intensity of the RI beams from ERIS, efficient DC-to-pulse conversion at FRAC, improving the transmission efficiency from FRAC to SCRIT, and effective suppression of the background in measurement of scattered electrons. RI beam intensity will be improved by upgrading the electron beam power from 10 W to 60 W, increasing the contained amount of U in the target ion source, and some modifications in mechanical structure in the ion source. For upgrading the electron beam power, the RF system of RTM has been maintained intensively, and we will continue the development of RTM. For efficient DC-to-pulse conversion, we established the two-step bunching method, which is time compression at FRAC in combination with pre-bunching at the ion source using grid action. Furthermore, we will improve the conversion efficiency and the transmission efficiency from FRAC to the SCRIT device by cooling the trapped ions using minuscule amounts of a buffer gas. These improvements on FRAC were already confirmed in off-line test. Since one of significant contribution to the background for scattered electron is scattering from massive structural objects around the trapping region originated from halo components of the electron beam, we remodeled the SCRIT electrodes. The vacuum pump system at the SCRIT device has been upgraded to reduce the contribution of residual gases. Luminosity for radioactive Xe isotopes is expected to be more than $10^{26}/(\mathrm{cm}^2\mathrm{s})$ after these improvements. Then, we will be able to start experiments for unstable nuclei. When further upgrading in the RTM power planned to be 3 kW will be achieved, we can extend the measurements to more exotic nuclei.

In 2018, we developed several instruments. One is the introduction of the surface-ionization type ion source at ERIS in order to increase kinds of radioactive beam and to produce high intensity beam. Another development is the upgrading of the drift chamber located in front of the magnetic spectrometer of WiSES to improve the momentum resolution and angular acceptance. These developments help us to realize experiments for unstable nuclei.

In 2019, we installed a newly designed SCRIT electrodes. The main purpose of the replacement was to lower the background during the measurement due to the electron scattering from the SCRIT electrodes itself but not from the ion targets for the experiment. For that purpose, we employed thin metal wires to construct the electrodes rather than metal plates nor blocks. In addition, we

modified the inside structure of the SCRIT chamber to symmetrize the electric ground potential affecting the potential curve inside the electrodes.

In 2020, we tested accelerators RTM and SR2 if they bear for long term experiment for 24 hours. In 2021, we commissioned the new SCRIT electrodes using ^{138}Ba ion beams produced by the surface-ionization type ion source at ERIS. After the RI production test, ERIS became ready to provide enough ions for the experiment of unstable nuclei.

In 2022, we successfully conducted the world's first electron scattering experiment with online-produced unstable nuclei. The ^{137}Cs ion beams, almost 10^7 ions/pulse at 0.25 Hz, produced by ERIS and FRAC was injected to the SCRIT device, and the luminosity was reached as $0.9 \times 10^{26}/(\mathrm{cm}^2\mathrm{s})$ with about 250-mA electron beam. Scattering electrons by ^{137}Cs targets were clearly analyzed and measured by WiSES, and the obtained angular distribution of ^{137}Cs is consistent to the calculated results. The paper will be published soon. In addition, we started the study of the isotope dependence of charge density distribution using Xe stable isotopes. This study will be expected to help to understand the nuclear structure precisely. First, we measured the angular distribution of $^{130, 132, 134, 136}$Xe isotopes. Those of remained Xe isotopes, $^{124, 126, 128}$Xe, will be measured soon.

Members

Team Leaders

Tetsuya OHNISHI
Masanori WAKASUGI

Senior Research Scientist

Masamitsu WATANABE

Senior Technical Scientist

Tetsuya OHNISHI

Contract Researcher

Yasushi ABE

Junior Research Associate

Hikari WAUKE

Research Consultants

Takashi EMOTO
Toshitada HORI
Masahiro HARA

Visiting Scientists

Akitomo ENOKIZONO (Rikkyo Univ.)
Toshimi SUDA (Tohoku Univ.)
Yuki HONDA (Tohoku Univ.)
Shuo WANG (Shandong Univ.)
Takahiro IWATA (Yamagata Univ.)

Student Trainees

Daiki ABE (Tohoku Univ.)
Evelyn MORRIS (Tohoku Univ.)
Rika DANJO (Tohoku Univ.)
Yuka NAGANO (Yamagata Univ.)
Taiga GOKE (Tohoku Univ.)
Ryo OBARA (Tohoku Univ.)
Yuma ISHIKURA (Tohoku Univ.)
Hikari WAUKE (Tohoku Univ.)
Clement LEGRIS (Tohoku Univ.)

List of Publications & Presentations

Publications

[Original Paper]

T. Suda, "Study of radii of proton and nuclei by electron scattering," JAEA-Conf **2022-001**, 51 (2022).

[Review Article]

T. Suda, "Electron Scattering Off Stable and Unstable Nuclei," in *Handbook of Nuclear Physics*, I. Tanihata, H. Toki, and T. Kajino (eds), (Springer, Singapore, 2023), https://doi.org/10.1007/978-981-15-8818-1_8-1 .

[Proceedings]

J. Bernauer, R. Corliss, S. Gardner, M. Hasinoff, R. Kanungo, J. Martin, R. Milner, K. Pachal, T. Suda, and S. Yen, "Scientific opportunities at the ARIEL electron linac," Proceedings of "Workshop on New Scientific Opportunities with the TRIUMF ARIEL e-linac," J. Phys. Conf. Ser. **2391**, 012001 (2022).

T. Suda, "Low-energy electron scattering facilities in Japan," Proceedings of "Workshop on New Scientific Opportunities with the TRIUMF ARIEL e-linac," J. Phys. Conf. Ser. **2391**, 012004 (2022).

Presentations

[International Conferences/Workshops]

T. Suda (invited), "Low-energy electron scattering facilities in Japan," New Scientific Opportunities with the TRIUMF ARIEL e-linac, Vancouver, Canada, May 25–27, 2022.

T. Suda (invited), "Low-energy electron scattering—proton radius and beyond," International STRONG workshop on the Proton Charge Radius and related topics, Paris, France, June 20–23, 2022.

K. Tsukada (oral), "Electron scattering from unstable nuclei at SCRIT facility," 28th International Nuclear Physics Conference (INPC2022), Cape Town, South Africa, September 11–16, 2022.

R. Ogawara (poster), "Ion-trapping properties of SCRIT: time evolution of charge state distributions of ^{138}Ba ions," The 19th International Conference on Electromagnetic Isotope Separators and Related Topics (EMIS 2022), Daejeon, South Korea, October 3–7, 2022.

T. Ohnishi (invited), "The SCRIT electron scattering facility at RIKEN RI Beam Factory," The 19th International Conference on Electromagnetic Isotope Separators and Related Topics (EMIS 2022), Daejeon, South Korea, October 3–7, 2022.

[Domestic Conferences/Workshops]

塚田暁 (口頭発表), 「電子・不安定核散乱実現に向けた SCRIT 電子散乱施設の現状と展望」, 日本物理学会 2022 年秋季大会, 岡山市 (岡山理科大), 2022 年 9 月 6–8 日.

小川原亮 (口頭発表), 「SCRIT における ^{138}Ba 標的の価数分布とその時間発展」, 日本物理学会 2022 年秋季大会, 岡山市 (岡山理科大), 2022 年 9 月 6–8 日.

和宇慶ひかり (口頭発表), 「SCRIT 電子散乱施設における電荷分布の同位体・同調体依存性測定」, 日本物理学会 2022 年秋季大会, 岡山市 (岡山理科大), 2022 年 9 月 6–8 日.

大西哲哉 (口頭発表), 「理研 SCRIT 施設における電子ビーム RI セパレーター ERIS の現状と展望」, 日本物理学会 2022 年秋季大会, 岡山市 (岡山理科大), 2022 年 9 月 6–8 日.

和宇慶ひかり (口頭発表), 「SCRIT 電子散乱施設における電荷分布の同位体・同調体依存性測定」, 日本物理学会 2023 年春季大会, オンライン, 2023 年 3 月 23 日.

[Seminars]

T. Suda, "Electron scattering and nuclear matrix elements of the double-beta decay process," 二重ベータ崩壊核行列要に関する実験理論合同研究会, Research Center for Nuclear Physics, Osaka, Japan, October 3–4, 2022.

T. Suda (invited), "Proton Radius," Australian National University Director's Colloquium, Canberra, Australia, October 22, 2022.

T. Suda (invited), "Proton Radius," Physics Colloquium of Univ. Melbourne, Melbourne, Australia, October 26, 2022.

T. Suda, "Proton Radius," 京都大学物理学科セミナー, 京都大学, 2022 年 12 月 2 日.

K. Tsukada, "Electron scattering from unstable nuclei at SCRIT facility," GSI NUstar seminar, GSI, Germany, February 13, 2023.

K. Tsukada, "Present status and future prospects of the SCRIT project," CEA ESNT seminar, CEA-Saclay, France, February 15, 2023.

塚田暁, 「エキゾチックな原子核を造る・観る」, 京都大学丸の内セミナー, 京都大学 東京オフィス (新丸ビル 10 階), 2023 年 3 月 10 日.

Outreach Activity

須田利美, 特別講義「陽子などの物の大きさはどう測る？」, 埼玉県立熊谷高等学校, 2023 年 1 月 21 日.

Research Facility Development Division
Research Instruments Group

1. Abstract

The Research Instruments Group is the driving force at RI Beam Factory (RIBF) for continuous enhancement of activities and competitiveness of experimental research. Consisting of four teams, we are in charge of the operation, maintenance, and improvement of the core research instruments at RIBF, such as the BigRIPS in-flight RI separator, ZeroDegree spectrometer and SAMURAI spectrometer, and the related infrastructure and equipment. We are also in charge of the production and delivery of RI beams using the BigRIPS separator. The group also conducts related experimental research as well as R&D studies on the research instruments.

2. Major Research Subjects

Design, construction, operation, maintenance, and improvement of the core research instruments at RIBF and related R&D studies. Experimental studies on exotic nuclei.

3. Summary of Research Activity

The current research subjects are summarized as follows:

(1) Production and delivery of RI beams and related research;
(2) Design, construction, operation, maintenance, and improvement of the core research instruments at RIBF and their related infrastructure and equipment;
(3) R&D studies on the core research instruments and their related equipment at RIBF;
(4) Experimental research on exotic nuclei using the core research instruments at RIBF.

Members

Director

Nobuhisa Fukunishi

Research Consultant

Toshiyuki KUBO

Senior Visiting Scientist

Toshio KOBAYASHI (Tohoku Univ.)

Student Trainees

Fumitaka ENDO (Tohoku Univ.)
Kosuke ICHIMURA (Tohoku Univ.)
Shojiro ISHIO (Tohoku Univ.)

List of Publication

Publication

[Original Paper]

D. S. Ahn, J. Amano, H. Baba, N. Fukuda, H. Geissel, N. Inabe, S. Ishikawa, N. Iwasa, T. Komatsubara, T. Kubo, K. Kusa,a, D. J. Morrossey, T. Nakamura, M. Ohtake, H. Otsu, T. Sakakibara, H. Sato, B. M. Sherrill, Y. Shimizu, T. Sumikawa, H. Suzuki, H. Takeda, O. B. Tarasov, H. Ueno, Y. Yanagisawa, and K. Yoshida, "Discovery of ^{39}Na," Phys. Rev. Lett. **129**, 215020 (2022). DOI: 10.1103/PhysRevLett.129.212502 .

Research Facility Development Division
Research Instruments Group
BigRIPS Team

1. Abstract

This team is in charge of design, construction, development and operation of BigRIPS in-flight separator and its related research instruments at RI beam factory (RIBF). They are employed not only for the production of RI beams but also the experimental studies using RI beams.

2. Major Research Subjects

Design, construction, development and operation of BigRIPS in-flight separator, RI-beam transport lines, and their related research instruments.

3. Summary of Research Activity

This team is in charge of design, construction, development and operation of BigRIPS in-flight separator, RI-beam transport lines, and their related research instruments such as ZeroDegree spectrometer at RI beam factory (RIBF). They are employed not only for the production of RI beams but also various kinds of experimental studies using RI beams. The research subjects may be summarized as follows:

(1) General studies on RI-beam production using in-flight scheme;
(2) Studies on ion-optics of in-flight separators, including particle identification of RI beams;
(3) Simulation and optimization of RI-beam production;
(4) Development of beam-line detectors and their data acquisition system;
(5) Experimental studies on production reactions and unstable nuclei;
(6) Experimental studies of the limits of nuclear binding;
(7) Development of superconducting magnets and their helium cryogenic systems;
(8) Development of a high-power production target system;
(9) Development of a high-power beam dump system;
(10) Development of a remote maintenance and remote handling systems;
(11) Operation, maintenance and improvement of BigRIPS separator system, RI-beam transport lines, and their related research instruments such as ZeroDegree spectrometer and so on;
(12) Experimental research using RI beams.

Members

Team Leader

Koichi YOSHIDA

Senior Research Scientists

Yoshiyuki YANAGISAWA
Naohito INABE
Kensuke KUSAKA
Masao OHTAKE

Technical Scientists

Naoki FUKUDA
Yohei SHIMIZU
Hiroshi SUZUKI
Hiroyuki TAKEDA

Contract Researcher

Yasuhiro TOGANO

Postdoctoral Researcher

Masahiro YOSHIMOTO

Visiting Scientists

Deuk Soon AHN (Inst. for Basic Sci.)
Daniel P. BAZIN (Michigan State Univ.)
Hans GEISSEL (GSI)
Naohito IWASA (Tohoku Univ.)
Yutaka MIZOI (Univ. of Electro-Commun.)
Sadao MOMOTA (Kochi Univ. Tech.)
David MORRISSEY (Michigan State Univ.)
Oleg TARASOV (Michigan State Univ.)

Student Trainees

Mika EGETA (Tohoku Univ.)
Taiga HAGINOUCHI (Tohoku Univ.)

List of Publications & Presentations

Publications

[Original Papers]

M. Duer, T. Aumann, R. Gernhäuser, V. Panin, S. Paschalis, D. M. Rossi, N. L. Achouri, D. Ahn, H. Baba, C. A. Bertulani, M. Böhmer, K. Boretzky, C. Caesar, N. Chiga, A. Corsi, D. Cortina-Gil, C. A. Douma, F. Dufter, Z. Elekes, J. Feng, B. Fernández-Domínguez, U. Forsberg, N. Fukuda, I. Gasparic, Z. Ge, J. M. Gheller, J. Gibelin, A. Gillibert, K. I. Hahn, Z. Halász, M. N. Harakeh, A. Hirayama, M. Holl, N. Inabe, T. Isobe, J. Kahlbow, N. Kalantar-Nayestanaki, D. Kim, S. Kim, T. Kobayashi, Y. Kondo, D. Körper, P. Koseoglou, Y. Kubota, I. Kuti, P. J. Li, C. Lehr, S. Lindberg, Y. Liu, F. M. Marqués, S. Masuoka, M. Matsumoto, J. Mayer, K. Miki, B. Monteagudo, T. Nakamura, T. Nilsson, A. Obertelli, N. A. Orr, H. Otsu, S. Y. Park, M. Parlog, P. M. Potlog, S. Reichert, A. Revel, A. T. Saito, M. Sasano, H. Scheit, F. Schindler, S. Shimoura, H. Simon, L. Stuhl, H. Suzuki, D. Symochko, H. Takeda, J. Tanaka, Y. Togano, T. Tomai, H. T. Törnqvist, J. Tscheuschner, T. Uesaka, V. Wagner, H. Yamada, B. Yang, L. Yang, Z. H. Yang, M. Yasuda, K. Yoneda, L. Zanetti, J. Zenihiro, and M. V. Zhukov, "Observation of a correlated free four-neutron system," Nature **606**, 678 (2022).

H. F. Li, S. Naimi, T. M. Sprouse, M. R. Mumpower, Y. Abe, Y. Yamaguchi, D. Nagae, F. Suzaki, M. Wakasugi, H. Arakawa, W. B. Dou, D. Hamakawa, S. Hosoi, Y. Inada, D. Kajiki, T. Kobayashi, M. Sakaue, Y. Yokoda, T. Yamaguchi, R. Kagesawa, D. Kamioka, T. Moriguchi, M. Mukai, A. Ozawa, S. Ota, N. Kitamura, S. Masuoka, S. Michimasa, H. Baba, N. Fukuda, Y. Shimizu, H. Suzuki, H. Takeda, D. S. Ahn, M. Wang, C. Y. Fu, Q. Wang, S. Suzuki, Z. Ge, Yu. A. Litvinov, G. Lorusso, P. M. Walker, Zs. Podolyak, and T. Uesaka, "First application of mass measurements with the Rare-RI Ring reveals the solar *r*-process abundance trend at $A = 122$ and $A = 123$," Phys. Rev. Lett. **128**, 152701 (2022).

V. H. Phong, S. Nishimura, G. Lorusso, T. Davinson, A. Estrade, O. Hall, T. Kawano, J. Liu, F. Montes, N. Nishimura, R. Grzywacz, K. P. Rykaczewski, J. Agramunt, D. S. Ahn, A. Algora, J. M. Allmond, H. Baba, S. Bae, N. T. Brewer, C. G. Bruno, R. Caballero-Folch, F. Calviño, P. J. Coleman-Smith, G. Cortes, I. Dillmann, C. Domingo-Pardo, A. Fijalkowska, N. Fukuda, S. Go, C. J. Griffin, J. Ha, L. J. Harkness-Brennan, T. Isobe, D. Kahl, L. H. Khiem, G. G. Kiss, A. Korgul, S. Kubono, M. Labiche, I. Lazarus, J. Liang, Z. Liu, K. Matsui, K. Miernik, B. Moon, A. I. Morales, P. Morrall, N. Nepa, R. D. Page, M. Piersa-Siłkowska, V. F. E. Pucknell, B. C. Rasco, B. Rubio, H. Sakurai, Y. Shimizu, D. W. Stracener, T. Sumikama, H. Suzuki, J. L. Tain, H. Takeda, A. Tarifeño-Saldivia, A. Tolosa-Delgado, M. Wolińska-Cichocka, P. J. Woods, and R. Yokoyama, "β-delayed one and two neutron emission probabilities southeast of ^{132}Sn and the odd-even systematics in *r*-process nuclide abundances," Phys. Rev. Lett. **129**, 172701 (2022).

D. S. Ahn, J. Amano, H. Baba, N. Fukuda, H. Geissel, N. Inabe, S. Ishikawa, N. Iwasa, T. Komatsubara, T. Kubo, K. Kusaka, D. J. Morrissey, T. Nakamura, M. Ohtake, H. Otsu, T. Sakakibara, H. Sato, B. M. Sherrill, Y. Shimizu, T. Sumikama, H. Suzuki, H. Takeda, O. B. Tarasov, H. Ueno, Y. Yanagisawa, and K. Yoshida, "Discovery of ^{39}Na," Phys. Rev. Lett. **129**, 212502 (2022).

A. Vitéz-Sveiczer, A. Algora, A. I. Morales, B. Rubio, G. G. Kiss, P. Sarriguren, P. Van Isacker, G. de Angelis, F. Recchia, S. Nishimura, J. Agramunt, V. Guadilla, A. Montaner-Pizá, S. E. A. Orrigo, A. Horváth, D. Napoli, S. Lenzi, A. Boso, V. H. Phong, J. Wu, P. -A. Söderström, T. Sumikama, H. Suzuki, H. Takeda, D. S. Ahn, H. Baba, P. Doornebal, N. Fukuda, N. Inabe, T. Isobe, T. Kubo, S. Kubono, H. Sakurai, Y. Shimizu, C. Sidong, B. Blank, P. Ascher, M. Gerbaux, T. Goigoux, J. Giovinazzo, S. Grévy, T. Kurtukián Nieto, C. Magron, W. Gelletly, Zs. Dombrádi, Y. Fujita, M. Tanaka, P. Aguilera, F. Molina, J. Eberth, F. Diel, D. Lubos, C. Borcea, E. Ganioglu, D. Nishimura, H. Oikawa, Y. Takei, S. Yagi, W. Korten, G. de France, P. Davies, J. Liu, J. Lee, T. Lokotko, I. Kojouharov, N. Kurz, H. Shaffner, and A. Petrovici, "The β-decay of ^{70}Kr into ^{70}Br: Restoration of the pseudo-SU(4) symmetry," Phys. Lett. B **830**, 137123 (2022).

S. Kim, J. W. Hwang, Y. Satou, N. A. Orr, T. Nakamura, Y. Kondo, J. Gibelin, N. L. Achouri, T. Aumann, H. Baba, F. Delaunay, P. Doornenbal, N. Fukuda, N. Inabe, T. Isobe, D. Kameda, D. Kanno, N. Kobayashi, T. Kobayashi, T. Kubo, S. Leblond, J. Lee, F. M. Marqués, R. Minakata, T. Motobayashi, D. Murai, T. Murakami, K. Muto, T. Nakashima, N. Nakatsuka, A. Navin, S. Nishi, S. Ogoshi, H. Otsu, H. Sato, Y. Shimizu, H. Suzuki, K. Takahashi, H. Takeda, S. Takeuchi, R. Tanaka, Y. Togano, A. G. Tuff, M. Vandebrouck, and K. Yoneda, "Unbound states in ^{17}C and *p-sd* shell-model interactions," Phys. Lett. B **836**, 137629 (2022).

B. Moon, A. Gargano, H. Naïdja, C. -B. Moon, A. Odahara, R. Lozeva, S. Nishimura, C. Yuan, F. Browne, P. Doornenbal, G. Lorusso, Z. Patel, S. Rice, M. Si, L. Sinclair, P. -A. Söderström, T. Sumikama, H. Watanabe, J. Wu, Z. Y. Xu, A. Yagi, D. S. Ahn, H. Baba, F. L. Bello Garrote, R. Daido, J. M. Daugas, F. Didierjean, Y. Fang, N. Fukuda, B. Hong, E. Ideguchi, N. Inabe, T. Ishigaki, T. Isobe, H. S. Jung, D. Kameda, I. Kojouharov, T. Komatsubara, T. Kubo, Y. K. Kwon, C. S. Lee, P. Lee, S. Morimoto, D. Murai, M. Niikura, H. Nishibata, I. Nishizuka, H. Sakurai, Y. Shimizu, H. Suzuki, H. Takeda, K. Tshoo, and R. Yokoyama, "First observation of the $\pi 0h_{11/2} \otimes \nu 0h_{9/2}$ partner orbital configuration in the odd-odd ^{138}I nucleus," Phys. Rev. C **105**, 034334 (2022).

A. Yagi, A. Odahara, H. Nishibata, R. Lozeva, C. -B. Moon, S. Nishimura, K. Yoshida, N. Yoshinaga, C. Watanabe, K. Higashiyama, T. Shimoda, R. Daido, Y. Fang, P. S. Lee, B. Moon, P. Doornenbal, G. Lorusso, P. -A. Söderström, T. Sumikama, H. Watanabe, T. Isobe, H. Baba, H. Sakurai, F. Browne, Z. Patel, S. Rice, L. Sinclair, J. Wu, Z. Y. Xu, R. Yokoyama, T. Kubo, N. Inabe, H. Suzuki, N. Fukuda, D. Kameda, H. Takeda, D. S. Ahn, Y. Shimizu, D. Murai, F. L. Bello Garrote, J. -M. Daugas, F. Didierjean, E. Ideguchi, S. Iimura, T. Ishigaki, H. S. Jung, T. Komatsubara, Y. K. Kwon, C. S. Lee, S. Morimoto, M. Niikura, I. Nishizuka, and K. Tshoo, "Various nuclear structures in ^{140}Xe studied by β decay of ground and isomeric states in ^{140}I," Phys. Rev. C **105**, 044325 (2022).

M. Tanaka, M. Takechi, A. Homma, A. Prochazka, M. Fukuda, D. Nishimura, T. Suzuki, T. Moriguchi, D. S. Ahn, A. Aimaganbetov, M. Amano, H. Arakawa, S. Bagchi, K. -H. Behr, N. Burtebayev, K. Chikaato, H. Du, T. Fujii, N. Fukuda, H. Geissel, T. Hori, S. Hoshino, R. Igosawa, A. Ikeda, N. Inabe, K. Inomata, K. Itahashi, T. Izumikawa, D. Kamioka, N. Kanda, I. Kato, I. Kenzhina, Z. Korkulu, Y. Kuk, K. Kusaka, K. Matsuta, M. Mihara, E. Miyata, D. Nagae, S. Nakamura, M. Nassurlla, K. Nishimuro, K. Nishizuka, K. Ohnishi, M. Ohtake, T. Ohtsubo, S. Omika, H. J. Ong, A. Ozawa, H. Sakurai, C. Scheidenberger, Y. Shimizu, T. Sugihara, T. Sumikama, H. Suzuki, S. Suzuki, H. Takeda, Y. Tanaka, Y. K. Tanaka, I. Tanihata, T. Wada, K. Wakayama, S. Yagi, T. Yamaguchi, R. Yanagihara, Y. Yanagisawa, K. Yoshida, and T. K. Zholdybayev, "Charge-changing cross sections for $^{42-51}$Ca and effect of charged-particle evaporation induced by neutron-removal reactions," Phys. Rev. C **106**, 014617 (2022).

J. Wu, S. Nishimura, P. -A. Söderström, A. Algora, J. J. Liu, V. H. Phong, Y. Q. Wu, F. R. Xu, J. Agramunt, D. S. Ahn, T. A. Berry, C. G. Bruno, J. J. Bundgaard, R. Caballero-Folch, A. C. Dai, T. Davinson, I. Dillmann, A. Estrade, A. Fijałkowska, N. Fukuda, S. Go, R. K. Grzywacz, T. Isobe, S. Kubono, G. Lorusso, K. Matsui, A. I. Morales, N. Nepal, S. E. A. Orrigo, B. C. Rasco, K. P. Rykaczewski, H. Sakurai, Y. Shimizu, D. W. Stracener, T. Sumikama, H. Suzuki, J. L. Tain, H. Takeda, A. Tarifeño-Saldivia, A. Tolosa-Delgado, M. Wolinska-Cichocka, and R. Yokoyama, "First observation of isomeric states in ^{111}Zr, ^{113}Nb, and ^{115}Mo," Phys. Rev. C **106**, 064328 (2022).

J. W. Lee, M. B. Tsang, C. Y. Tsang, R. Wang, J. Barney, J. Estee, T. Isobe, M. Kaneko, M. Kurata-Nishimura, W. G. Lynch, T. Murakami, A. Ono, S. R. Souza, D. S. Ahn, L. Atar, T. Aumann, H. Baba, K. Boretzky, J. Brzychczyk, G. Cerizza, N. Chiga, N. Fukuda, I. Gasparic, B. Hong, A. Horvat, K. Ieki, N. Ikeno, N. Inabe, G. Jhang, Y. J. Kim, T. Kobayashi, Y. Kondo, P. Lasko, H. S. Lee, Y. Leifels, J. Łukasik, J. Manfredi, A. B. McIntosh, P. Morfouace, T. Nakamura, N. Nakatsuka, S. Nishimura, H. Otsu, P. Pawłowski, K. Pelczar, D. Rossi, H. Sakurai, C. Santamaria, H. Sato, H. Scheit, R. Shane, Y. Shimizu, H. Simon, A. Snoch, A. Sochocka, T. Sumikama, H. Suzuki, D. Suzuki, H. Takeda, S. Tangwancharoen, Y. Togano, Z. G. Xiao, S. J. Yennello, and Y. Zhang (the SπRIT Collaboration), "Isoscaling in central Sn+Sn collisions at 270 MeV/nucleon," Eur. Phys. J. A **58**, 201 (2022).

A. I. Stefanescu, V. Panin, L. Trache, T. Motobayashi, H. Otsu, A. Saastamoinen, T. Uesaka, L. Stuhl, J. Tanaka, D. Tudor, I. C. Stefanescu, A. E. Spiridon, K. Yoneda, H. Baba, M. Kurokawa, Y. Togano, Z. Halasz, M. Sasano, S. Ota, Y. Kubota, D. S. Ahn, T. Kobayashi, Z. Elekes, N. Fukuda, H. Takeda, D. Kim, E. Takada, H. Suzuki, K. Yoshida, Y. Shimizu, H. N. Liu, Y. L. Sun, T. Isobe, J. Gibelin, P. J. Li, J. Zenihiro, F. M. Marqués, M. N. Harakeh, G. G. Kiss, A. Kurihara, M. Yasuda, T. Nakamura, S. Park, Z. Yang, T. Harada, M. Nishimura, H. Sato, I. S. Hahn, K. Y. Chae, J. M. Elson, L. G. Sobotka and C. A. Bertulani, "Silicon tracker array for RIB experiments at SAMURAI," Eur. Phys. J. A **58**, 223 (2022).

G. G. Kiss, A. Vitéz-Sveiczer, Y. Saito, A. Tarifeño-Saldivia, M. Pallas, J. L. Tain, I. Dillmann, J. Agramunt, A. Algora, C. Domingo-Pardo, A. Estrade, C. Appleton, J. M. Allmond, P. Aguilera, H. Baba, N. T. Brewer, C. Bruno, R. Caballero-Folch, F. Calvino, P. J. Coleman-Smith, G. Cortes, T. Davinson, N. Fukuda, Z. Ge, S. Go, C. J. Griffin, R. K. Grzywacz, O. Hall, A. Horváth, J. Ha, L. J. Harkness-Brennan, T. Isobe, D. Kahl, T. T. King, A. Korgul, S. Kovács, R. Krücken, S. Kubono, M. Labiche, J. Liu, J. Liang, M. Madurga, K. Miernik, F. Molina, A. I. Morales, M. R. Mumpower, E. Nacher, A. Navarro, N. Nepal, S. Nishimura, M. Piersa-Siłkowska, V. Phong, B. C. Rasco, B. Rubio, K. P. Rykaczewski, J. Romero-Barrientos, H. Sakurai, L. Sexton, Y. Shimizu, M. Singh, T. Sprouse, T. Sumikama, R. Surman, H. Suzuki, T. N. Szegedi, H. Takeda, A. Tolosa, K. Wang, M. Wolinska-Cichocka, P. Woods, R. Yokoyama, and Z. Xu, "Measuring the β-decay properties of neutron-rich exotic Pm, Sm, Eu, and Gd isotopes to constrain the nucleosynthesis yields in the rare-earth region," Astrophys. J. **936**, 107 (2022).

[Proceeding]

S. Kim, J. Hwang, Y. Satou, N. A. Orr, T. Nakamura, Y. Kondo, J. Gibelin, N. L. Achouri, T. Aumann, H. Baba, F. Delaunay, P. Doornenbal, N. Fukuda, N. Inabe, T. Isobe, D. Kameda, D. Kanno, N. Kobayashi, T. Kobayashi, T. Kubo, S. Leblond, J. Lee, F. M. Marqués, R. Minakata, T. Motobayashi, D. Murai, T. Murakami, K. Muto, T. Nakashima, N. Nakatsuka, A. Navin, S. Nishi, S. Ogoshi, H. Otsu, H. Sato, Y. Shimizu, H. Suzuki, K. Takahashi, H. Takeda, S. Takeuchi, R. Tanaka, Y. Togano, A. G. Tuff, M. Vandebrouck, and K. Yoneda, "Spectroscopy of ^{17}C above the neutron separation energy," Few-Body Syst. **63**, 21 (2022).

Presentations

[International Conferences/Workshops]

H. Suzuki (invited), "Studies of the two-step scheme with a ^{132}Sn beam for next-generation RI-beam production in the medium-heavy very-neutron-rich region," The 19th International Conference on Electromagnetic Isotope Separators and Related Topics (EMIS), Daejeon, Korea, October 3–7, 2022.

M. Yoshimoto (oral), N. Fukuda, H. Otsu, Y. Shimizu, T. Sumikama, H. Suzuki, H. Takeda, J. Tanaka, K. Yoshida, R. Matsumura, D. Nishimura, and H. Takahashi, "Development of new ionization chamber specialized in high-Z beam," The 19th International Conference on Electromagnetic Isotope Separators and Related Topics (EMIS), Daejeon, Korea, October 3–7, 2022.

K. Yoshida (oral), Y. Yanagisawa, M. Ohtake, and T. Kubo, "Operational experiences of high-power production target and high-power beam dump at BigRIPS separator at RIKEN RI beam factory," The 19th International Conference on Electromagnetic Isotope Separators and Related Topics (EMIS), Daejeon, Korea, October 3–7, 2022.

[Domestic Conferences/Workshops]

金子雅紀 (口頭発表), 村上哲也, 磯部忠昭, 倉田 (西村) 美月, 小野章, 池野なつ美, J. Barney, G. Cerizza, J. Estee, G. Jhang, J. W. Lee, W. G. Lynch, C. Santamaria, C. Y. Tsang, M. B. Tsang, R. Wang, D. S. Ahn, G, L. Atar, H, T. Aumann, 馬場秀忠, K. Boretzky, J. Brzychczyk, 千賀信幸, 福田直樹, I. Gašparić, B. Hong, A. Horvat, 市原卓, 家城和夫, 稲辺尚人, Y. J. Kim, 小林俊雄, 近藤洋介, P. Lasko, H. S. Lee, Y. Leifels, J. Łukasik, J. Manfredi, A. B. McIntosh, P. Morfouace, 中村隆司, 中塚徳継, 西村俊二, R. Olsen, 大津秀暁, P. Pawłowski, K. Pelczar, D. Rossi, 櫻井博儀, 佐藤広海, H. Scheit, R. Shane, 清水陽平, H. Simon, 炭竈聡之, 鈴木大介, 鈴木宏, 竹田浩之, S. Tangwancharoen, 栂野康宏, H. Törnqvist, H, Z. Xiao, S. J. Yennello, J. Yurkon, Y. Zhang, 「RI ビームを用いた重イオン衝突における水素同位体生成と高密度核物質の対称エネルギー」, 日本物理学会第 77 回年次大会 (2022 年), オンライン, 2022 年 3 月 15–19 日.

篠原悠介 (口頭発表), 市川雄一, 郷慎太郎, 西畑洸希, 安藤蒼太, 荒殿和希, 旭耕一郎, 馬場秀忠, 福田直樹, G. Georgiev, A. Gladkov, 今村慧, 梶原孝文, 岸本侃己, R. Lozeva, 向井もも, 新倉潤, M. N. Nurhafiza, 小田原厚子, 清水陽平, M. Si, C, K. Stoychev, 鈴木宏, 立川柊平, 田島美典, 高峰愛子, 竹田浩之, 竹中京平, 武重祥子, 上野秀樹, 若狭智嗣, 山下渉, 山崎展樹, 横田望海, 吉本雅浩, J. M. Daugas, 「分散整合二回散乱法による ^{99}Zr アイソマー状態のスピン整列」, 日本物理学会 2022 年秋季大会, 岡山市 (岡山理科大学), 2022 年 9 月 6–8 日.

H. Lee(oral), T. Nakamura, N. Nakatsuka, A, Y. Kondo, K. J. Cook, S. Ogoshi, A. T. Saito, N. L. Achouri, T. Aumann, E, H. Baba, F. Delaunay, Q. Deshayes, P. Doornenbal, N. Fukuda, J. Gibelin, J. W. Hwang, N. Inabe, T. Isobe, D. Kameda, D. Kanno, S. Kim,

N. Kobayashi, T. Kobayashi, T. Kubo, S. Leblond, J. Lee, F. M. Marques, R. Minakata, T. Motobayashi, K. Muto, T. Murakami, D. Murai, T. Nakashima, A. Navin, S. Nishi, N. A. Orr, H. Otsu, H. Sato, Y. Satou, Y. Shimizu, H. Suzuki, K. Takahashi, H. Takeda, S. Takeuchi, R. Tanaka, Y. Togano, J. Tsubota, A. G. Tuff, M. Vandebrouck, and K. Yoneda, "Coulomb dissociation of ^{17}B," 日本物理学会 2022 年秋季大会, 岡山市 (岡山理科大学), 2022 年 9 月 6–8 日.

Research Facility Development Division
Research Instruments Group
SAMURAI Team

1. Abstract

In collaboration with research groups in and outside RIKEN, the team designs, develops and constructs the SAMURAI spectrometer and relevant equipment that are and will be used for reaction experiments using RI beams at RI Beam Factory. The SAMURAI spectrometer consists of a large superconducting dipole magnet and a variety of detectors to measure charged particles and neutrons. After the commissioning experiment in March 2012, the team prepared and conducted, in collaboration with researchers in individual experimental groups, the first series of experiments with SAMURAI in May 2012. Then, amount numbers of experiments were well performed until now utilizing the property of SAMURAI. The team also provides a basis for research activities by, for example, organizing collaboration workshops by researchers who are interested in studies or plan to perform experiments with the SAMURAI spectrometer.

2. Major Research Subjects

Design, operation, maintenance and improvement of the SAMURAI spectrometer and its related research instruments. Support and management for SAMURAI-based research programs. Generate future plans for next generation instruments for nuclear reaction studies.

3. Summary of Research Activity

The current research subjects are summarized as follows:

(1) Operation, maintenance and improvement of a large superconducting dipole magnet, the main component of the SAMURAI spectrometer
(2) Design, development and construction of various detectors that are used for nuclear reaction experiments using the SAMURAI spectrometer
(3) Preparation for planning experiments using SAMURAI spectrometer
(4) Maintenance and improvement of the SAMURAI beam line
(5) Formation of a collaboration platform called "SAMURAI collaboration"
(6) Preparation for next generation spectrometer for nuclear reaction studies

Members

Team Leader
Hideaki OTSU

Research & Development Scientist
Mizuki NISHIMURA

List of Publications & Presentations

Publications

[Original Papers]

T. Phol *et al*., "Multiple mechanisms in proton-induced nucleon removal at 100 MeV/nucleon," Phys. Rev. Lett. **130**,172501 (2023).

A. Corsi *et al*., "Searching for universality of dineutron correlation at the surface of Borromean nuclei," Phys. Lett. B **840**, 137875 (2023).

S. Kim *et al*., "Unbound states in ^{17}C and *p-sd* shell-model interactions," Phys. Lett. B **836**, 137629 (2023).

A. I. Stefanescu *et al*., "Silicon tracker array for RIB experiments at SAMURAI," Eur. Phys. J. A **58**, 223 (2022).

M. Kaneko *et al*., "Multiplicity trigger detector for the SπRIT experiment," Nucl. Instrum. Methods Phys. Res. A **1039**, 167010 (2022).

M. Enciu *et al*., "Extended $p_{3/2}$ neutron orbital and the N = 32 shell closure in ^{52}Ca," Phys. Rev. Lett. **129**, 262501 (2022).

Z. Elekes *et al*., "Southwestern boundary of the N = 40 island of inversion: First study of low-lying bound excited states in ^{59}V and ^{61}V," Phys. Rev. C **106**, 064321 (2022).

J. W. Lee *et al*., "Isoscaling in central Sn+Sn collisions at 270 MeV/nucleon," Eur. Phys. J. A **58**, 201 (2022).

M. Duer *et al*., "Observation of a correlated four-neutron system," Nature **606**, 678–682 (2022).

M. Holl *et al*., "Border of the island of inversion: Unbound states in ^{29}Ne," Phys. Rev. C **105**, 034301 (2022).

T. Koiwai *et al*., "A first glimpse at the shell structure beyond ^{54}Ca: Spectroscopy of ^{55}K, ^{55}Ca, and ^{57}Ca," Phys. Lett. B **827**, 136953 (2022).

Presentations

[International Conferences/Workshops]

SAMURAI International Collaboration Workshop 2022, Tokyo Institute of Technology, Tokyo & Online, September 2–3, 2022. https://indico2.riken.jp/event/4219/ .

T. Nakamura (invited), "Spectroscopy of nuclei near and beyond the neutron dripline," ECT* Workshop on "Nuclear Physics at the Edge of Stability," Online & Trento, Italy (Hybrid), July 4–8, 2022.

T. Nakamura (plenary/invited), "Summary Talk," The 11th International Conference on Direct Reactions with Exotic Beams (DREB2022), Santiago de Compostela, Spain, June 26–July 1, 2022.

Y. Kondo (invited), "Experimental studies near and beyond the dripline at SAMURAI," Halo Week 2022, Bergen, Norway (Grand Hotel Terminus), July 10–15, 2022.

Y. Kondo (invited), "Experimental studies of nuclei in the vicinity of the neutron-drip line at SAMURAI," Physics of RI: Recent progress and perspectives, RIKEN, Saitama, Japan, May 30–June 1, 2022.

[Domestic Conferences/Workshops]

久保田悠樹 (招待講演), 若手奨励賞講演, 「^{11}Li 原子核中でのダイニュートロンの表面局在」, 日本物理学会春季大会, オンライン, 2023 年 3 月.

松井智輝, 「中性子過剰 He 同位体における多中性子系クラスターの探索」, 日本物理学会 2023 年春季大会, オンライン, 2023 年 3 月.

H. Lee, "Coulomb Dissociation of ^{17}B," 日本物理学会 2022 年秋季大会, 岡山市 (岡山理科大学), 2022 年 9 月.

磯部駆, 「中性子過剰核における短距離相関対探索のための後方散乱粒子検出器の開発」, 日本物理学会秋季大会, 岡山市 (岡山理科大学), 2022 年 9 月.

松井智輝, 「多中性子クラスター探索実験に向けた反跳陽子検出器のテスト実験」, 日本物理学会秋季大会, 岡山市 (岡山理科大学), 2022 年 9 月.

Press Release

"Observation of a correlated free four-neutron system," June 23, 2022, https://www.riken.jp/press/2022/20220623_1/index.html .

Master Theses

堀川晃太, 「中性子過剰核における短距離相関探索実験」, 東京工業大学, 2023 年 2 月.

松井智輝, 「中性子過剰 He 同位体における多中性子クラスターの探索」, 東京工業大学, 2023 年 2 月.

Research Facility Development Division
Research Instruments Group
Computing and Network Team

1. Abstract

This team is in charge of development, management and operation of the computing and network environment, mail and information services and data acquisition system and management of the information security of the RIKEN Nishina Center.

2. Major Research Subjects

(1) Development, management and operation of the general computing servers
(2) Development, management and operation of the mail and information servers
(3) Development, management and operation of the data acquisition system
(4) Development, management and operation of the network environment
(5) Management of the information security

3. Summary of Research Activity

This team is in charge of development, management and operation of the computing and network environment, mail and information services and data acquisition system and management of the information security of the RIKEN Nishina Center.The details are described elsewhere in this progress report.

(1) Development, management and operation of the general computing servers

We are operating Linux cluster system for the data analysis of the experiments and general computing. This cluster system consists of eight computing servers with 74 CPU cores and totally 500 TB RAID of highly-reliable Fibre-channel interconnection. There are approximately 100 active user accounts on this cluster system. We are adopting the latest version of the Linux operating system. In addition to the cluster system, we have constructed analysis environment on the private could system of HOKUSAI Sailing Ship operated by Information Systems Division in RIKEN. As computational resources for data analysis of RIBF experiments, 80 core and 150 TB diskspace are reserved. These resources are dynamically allocated to several experimental projects.

(2) Development, management and operation of the mail and information servers

We are operating RIBF.RIKEN.JP server as a mail/NFS/NIS server. This server is a core server of RIBF Linux cluster system. Postfix has been used for mail transport software and dovecot has been used for imap and pop services. These software packages enable secure and reliable mail delivery. We are operating several information servers such as Web servers, Integrated Digital Conference (INDICO) server, Wiki servers, Groupware servers, Wowza streaming servers.

(3) Development, management and operation of the data acquisition system

We have developed the standard data-acquisition system named as RIBFDAQ. This system can process up to 40 MB/s data. By using crate-parallel readout from front-end systems such as CAMAC and VME, the dead time could be minimized. To synchronize the independent DAQ systems, the time stamping system has been developed. The resolution and depth of the time stamp are 10 ns and 48 bits, respectively. This time stamping system is very useful for beta decay experiments such as EURICA, BRIKEN and VANDLE projects. One of the important tasks is the DAQ coupling, because detector systems with dedicated DAQ systems are transported to RIBF from other facilities. In case of SAMURAI Silicon (NSCL/TUM/WUSTL), the readout system is integrated into RIBFDAQ. The projects of MUST2 (GANIL), MINOS (CEA Saclay), NeuLAND (GSI) and TRB3 (TUM) cases, data from their DAQ systems are transferred to RIBFDAQ and merged online. For SPIRIT (RIKEN/GANIL/CEA Saclay/NSCL), RIBFDAQ is controlled from the NARVAL-GET system that is a large-scale signal processing system for the time projection chamber. EURICA (GSI), BRIKEN (GSI/Univ. Liverpool/IFIC), VANDLE (UTK) and OTPC (U. Warsaw) projects, we adopt the time stamping system to apply individual trigger for each detector system. In this case, data are merged in offline. In addition, we are developing intelligent circuits based on FPGA. General Trigger Operator (GTO) is an intelligent triggering NIM module. To improve the data readout speed of VME system, we have successfully developed the MPV system which is a parallel readout extension of the VME system. Thanks to the MPV system, now the DAQ system in RIBF is 10 times faster than in 2007. Toward to the next generation DAQ system, we have started to develop a real-time data processing unit based on Xilinx RFSoC that includes FPGA and 4 GHz FADC for TOF measurements of plastic scintillators. For gaseous detectors like PPAC and drift chamber, the development of FPGA-based dead-time free TDC is now in progress. For Silicon semiconductor detectors, waveform digitizer based front-end electronics is commissioned. From 2022, Signal processing and data acquisition infrastructure (SPADI) alliance is launched to advance collaborative DAQ development in Japanese nuclear physics community. This team participates as one of the core members of the SPADI alliance.

(4) Development, management and operation of the network environment

We have been managing the network environment collaborating with Information Systems Division in RIKEN. All the Ethernet ports of the information wall sockets are capable of the Gigabit Ethernet connection (10/100/1000 bps). In addition, some 10 Gbps networks port has been introduced to RIBF experimental area. We have been operating approximately 70 units of wireless LAN access points in RNC. Almost the entire radiation-controlled area of the East Area of RIKEN Wako campus is covered by wireless LAN for the convenience of experiments and daily work. In 2022, wireless LAN system (including Guest and Eduroam network) operated by

RIKEN Information Systems Division is additionally introduced in the measurement rooms in RIBF B1F and B3F.

(5) Management of the information security

It is essential to take proper information security measures for information assets. We are managing the information security of Nishina Center collaborating with Information Systems Division in RIKEN.

Members

Team Leader

Hidetada BABA

Junior Research Associate

Shoko TAKESHIGE (Rikkyo Univ.)

Special Temporary Research Scientists

Takashi ICHIHARA

Yasushi WATANABE

Visiting Scientists

Kazuo IEKI (Rikkyo Univ.)

Shoichiro KAWASE (Kyushu Univ.)

Student Trainee

Shoko TAKESHIGE (Rikkyo Univ.)

List of Presentations

Presentations

[International Conference/Workshop]

S. Takeshige, H. Baba *et al*. (poster), "Time determination method using digital waveform processing with RFSoC for RI beam experiments," 23rd Virtual IEEE Real Time Conference, Online, August 1–5, 2022.

[Domestic Conference/Workshop]

馬場秀忠 (口頭発表),「WG2（時刻同期・通信）報告と展望」, 原子核実験の先端データ収集システム—標準化と将来—, 茨木市 (大阪大学 RCNP), 2022 年 5 月 17 日.

Research Facility Development Division
Research Instruments Group
Detector Team

1. Abstract

This team is in charge of maintenance and improvement of detectors which are used at BigRIPS separator and its succeeding beam lines for beam diagnosis and particle identification of RI beams. We are also engaged in R&D of new detectors that can be used for higher-intensity RI beams. In addition, we are doing the R&D which uses the pelletron accelerator together with other groups.

2. Major Research Subjects

Development, fabrication, and operation of beam-line detectors which are used for the production and delivery of RI beams (beam diagnosis and particle identification). R&D which uses the pelletron accelerator.

3. Summary of Research Activity

The current research subjects are summarized as follows:

(1) Maintenance and improvement of the beam-line detectors which are used at BigRIPS separator and its succeeding beam lines
(2) Development of new beam-line detectors with radiation hardness and tolerance for higher counting rates
(3) Management of the pelletron accelerator and R&D which uses the pelletron

Members

Team Leader

Hiromi SATO

Research/Technical Scientist

Tokihiro IKEDA (Senior Research Scientist)

Student Trainees

Kotoko INAYOSHI (Toho University)
Ryusei OTANI (Toho University)
Mai KURINO (Toho University)

List of Publications & Presentations

Publications

[Original Papers]

S. R. Lee, A. Kim, S. Choi, T. Ikeda, T. Isoshima, S. Cho, and Y. Kim, "Amorphous to polycrystalline phase transition in La_2O_3 films grown on a silicon substrate forming Si-doped La_2O_3 films," Phys. Status Solidi **219**, 2200318 (2022).

D. S. Ahn, J. Amano, H. Baba, N. Fukuda, H. Geissel, N. Inabe, S. Ishikawa, N. Iwasa, T. Komatsubara, T. Kubo, K. Kusaka, D. J. Morrissey, T. Nakamura, M. Ohtake, H. Otsu, T. Sakakibara, H. Sato, B. M. Sherrill, Y. Shimizu, T. Sumikama, H. Suzuki, H. Takeda, O. B. Tarasov, H. Ueno, Y. Yanagisawa, and K. Yoshida, "Discovery of ^{39}Na," Phys. Rev. Lett. **129**, 212502 (2022).

A. I. Stefanescu, V. Panin, L. Trache, T. Motobayashi, H. Otsu, A. Saastamoinen, T. Uesaka, L. Stuh, J. Tanaka, D. Tudor, I. C. Stefanescu, A. E. Spiridon, K. Yoneda, H. Baba, M. Kurokawa, Y. Togano, Z. Halasz, M. Sasano, S. Ota, Y. Kubota, D. S. Ahn, T. Kobayashi, Z. Elekes, N. Fukuda, H. Takeda, D. Kim, E. Takada, H. Suzuki, K. Yoshida, Y. Shimizu, H. N. Liu, Y. L. Sun, T. Isobe, J. Gibelin, P. J. Li, J. Zenihiro, F. M. Marqués, M. N. Harakeh, G. G. Kiss, A. Kurihara, M. Yasuda, T. Nakamura, S. Park, Z. Yang, T. Harada, M. Nishimura, H. Sato, I. S. Hahn, K. Y. Chae, J. M. Elson, L. G. Sobotka, and C. A. Bertulani, "Silicon tracker array for RIB experiments at SAMURAI," Eur. Phys. J. A **58**, 223 (2022).

S. Kim, J. W. Hwang, Y. Satou, N. A. Orr, T. Nakamura, Y. Kondo, J. Gibelin, N. L. Achouri, T. Aumann, H. Baba, F. Delaunay, P. Doornenbal, N. Fukuda, N. Inabe, T. Isobe, D. Kameda, D.Kanno, N. Kobayashi, T. Kobayashi, T. Kubo, S. Leblond, J. Lee, F. M. Marqués, R. Minakata, T. Motobayashi, D. Murai, T. Murakami, K. Muto, T. Nakashima, N. Nakatsuka, A. Navin, S. Nishi, S. Ogoshi, H. Otsu, H. Sato, Y. Shimizu, H. Suzuki, K. Takahashi, H. Takeda, S. Takeuchi, R. Tanaka, Y. Togano, A. G. Tuff, M. Vandebrouck, and K. Yoneda, "Unbound states in ^{17}C and *p-sd* shell-model interactions," Phys. Lett. B **836**, 137629 (2023).

[Review Articles]

池田時浩, 「MeV イオンビームのガラスキャピラリーによるマイクロビーム化とその応用」, 応用物理 **91**, 542–647 (2022).

T. Ikeda, "Production of MeV ion microbeams using glass capillary optics and its applications," JSAP Review **2022**, 220205 (2022).

Presentations

[International Conferences/Workshops]

K. Inayoshi (poster), T. Ikeda, K. Ono, and W. -G. Jin, "Density enhancement of ion microbeams with miniature quadrupole magnets for tapered glass capillary opticss," ICACS & SHIM 2022, Helsinki, Finland & Online, June 19–24, 2022.

T. Ikeda (oral), “Glass capillary optics as an ion microbeam generator and its applications,” 2nd Annual Meeting of MRS-Japan 2022, Yokohama, Japan, December 5–7, 2022.

[Domestic Conferences/Workshops]

稲吉琴子 (口頭発表), 池田時浩, 金衛国, 「小型四重極永久磁石を用いたガラスキャピリー内のイオンビームの通過特性の研究」, 第 34 回タンデム加速器及びその周辺技術の研究会, オンライン, 2022 年 7 月 21–22 日.

水野るり惠 (口頭発表), 池田時浩, 郷慎太郎, 櫻井博儀, 齋藤岳志, 新倉潤, 松崎禎市郎, 道正新一郎, 「1 MeV 陽子ビームを用いた広ダイナミックレンジ光子検出器の性能評価実験」, 第 34 回タンデム加速器及びその周辺技術の研究会, オンライン, 2022 年 7 月 21–22 日.

池田時浩 (口頭発表), 稲吉琴子, 佐藤広海, 「理化学研究所におけるタンデム加速器の現状（2020–2021 年度）」, 第 34 回タンデム加速器及びその周辺技術の研究会, オンライン, 2022 年 7 月 21–22 日.

稲吉琴子 (ポスター発表), 池田時浩, 金衛国, 「小型四重極永久磁石によるビーム拡がり抑制のキャピラリーマイクロビームへの応用」, 原子衝突学会 第 47 回年会, 宮崎市 (宮崎大学), 2022 年 9 月 8–9 日.

池田時浩 (ポスター発表), 「絶縁体キャピラリーによるイオンビームガイディング: 20 年の歩み」, 原子衝突学会 第 47 回年会, 宮崎市 (宮崎大学), 2022 年 9 月 8–9 日.

水野るり惠 (口頭発表), 池田時浩, 郷慎太郎, 齋藤岳志, 櫻井博儀, 新倉潤, 松崎禎市郎, 道正新一郎, 「Ge 検出器を用いた光子検出器システムの広ダイナミックレンジにおける性能評価実験」, 第 65 回放射線化学討論会, オンライン, 2022 年 9 月 10–12 日.

稲吉琴子 (口頭発表), 池田時浩, 金衛国, 「ガラスキャピラリー内部のイオンビーム軌道制御のための小型四重極永久磁石の作製」, 日本物理学会 2022 年秋季大会, 目黒区 (東京工業大学), 2022 年 9 月 12–15 日.

稲吉琴子 (ポスター発表), 池田時浩, 金衛国, 「キャピラリー内イオン衝突抑制のための小型四重極永久磁石の作製」, 第 42 回 原子衝突若手の会 秋の学校, 高崎市 (榛名湖温泉ゆうすげ), 2022 年 10 月 8–10 日.

Accelerator Applications Research Division
Beam Mutagenesis Group

1. Abstract

This group promotes biological applications of ion beams from RI Beam Factory (RIBF). Ion Beam Breeding Team studies various biological effects of fast heavy ions and develops new technology to breed plants and microbes by heavy-ion irradiations. Plant Genome Evolution Research Team choose baker's yeast and the legume *Lotus japonicus* as model systems to characterize genomic mutations using the population genomics approach with robust molecular biology and bioinformatics techniques.

2. Major Research Subjects

(1) Biological effects of fast heavy ions
(2) Molecular nature of DNA alterations induced by heavy-ion irradiation
(3) Research and development of heavy-ion breeding
(4) Genomics-based approach to revolutionize the mutagenesis in plants and microbes

3. Summary of Research Activity

Summary of research activities of the two teams are given in the sections of each team.

Members

Director

Tomoko ABE

Senior Visiting Scientist

Yutaka ARIMOTO

Accelerator Applications Research Division
Beam Mutagenesis Group
Ion Beam Breeding Team

1. Abstract

Ion beam breeding team studies various biological effects of fast heavy ions. It also develops new technique to breed plants and microbes by heavy-ion irradiations. Fast heavy ions can produce dense and localized ionizations in matters along their tracks, in contrast to photons (X rays and gamma rays) which produce randomly distributed isolated ionizations. These localized and dense ionization can cause double-strand breaks of DNA which are not easily repaired and result in mutation more effectively than single-strand breaks. A unique feature of our experimental facility at the RIKEN Ring Cyclotron (RRC) is that we can irradiate living tissues in atmosphere since the delivered heavy-ion beams have energies high enough to penetrate deep in matter. This team utilizes a dedicated beam line (E5B) of the RRC to irradiate microbes, plants and animals with beams ranging from carbon to iron. Its research subjects cover study of ion-beam radiation mutagenesis, genome-wide analyses of mutation, and development of new plants and microbial varieties by heavy-ion irradiation. Thirty-nine new varieties have already been brought to the market.

2. Major Research Subjects

(1) Study on the biological effects by heavy-ion irradiation
(2) Study on the molecular nature of DNA alterations induced by heavy-ion irradiation
(3) Innovative applications of heavy-ion irradiation

3. Summary of Research Activity

We study biological effects of fast heavy ions from the RRC using 135 MeV/nucleon C, N, Ne ions, 95 MeV/nucleon Ar ions, 90 MeV/nucleon Fe ions and from the IRC using 160 MeV/nucleon Ar ions. We also develop breeding technology of microbes and plants. Main subjects are:

(1) Study on the biological effects by heavy-ion irradiation

Heavy-ion beam deposits a concentrated amount of dose at just before stop with severely changing the linear energy transfer (LET). The peak of LET is achieved at the stopping point and known at the Bragg peak (BP). Adjusting the BP to target malignant cells is well known to be effective for cancer therapy. On the other hand, a uniform dose distribution is a key to the systematic study for heavy-ion mutagenesis, thus to the improvement of the mutation efficiency. Plants and microbes therefore, are irradiated using ions with stable LET. We investigated the effect of LET ranging from 23 to 640 keV/μm, on mutation induction using dry seeds of the model plants Arabidopsis thaliana and rice (*Oryza sativa* L.). The most effective LET (LETmax) was 30 keV/μm in *Arabidopsis*. LETmax irradiations showed the same mutation rate as that by chemical mutagens, which typically cause high mutation rate. The LETmax was 23–39 keV/μm in buckwheat, 23–50 keV/μm in rice and 50–70 keV/μm in wheat. By contrast, when LET was 290 keV/μm, the mutation rate was low and the survival rate was greatly reduced in plants. In the case of microbe, filamentous fungus (*Neurospora crassa*), the Ar ions at 290 keV/μm demonstrated higher mutagenic activity than the Fe-ions at 640 keV/μm. Thus, the LET is an important factor to be considered in heavy-ion mutagenesis.

(2) Study on the molecular nature of DNA alterations induced by heavy-ion irradiation

A whole-genome analysis with high-throughput sequencing is a powerful tool used to characterize the nature of induced mutations. We have been using whole genome sequencing to analyze DNA mutations in *Arabidopsis* and rice genomes. C ions with LETmax mainly induced single nucleotide variants (SNVs) and small insertions and deletions (InDels), while the number of large deletions and chromosomal rearrangements was low in *Arabidopsis*. However, 290 keV/μm Ar ions showed a different mutation spectrum: SNVs and number of small InDels was low, while the number of large deletions ($\geq$100 bp) and chromosomal rearrangements was high. Number of mutated gene induced by C-ion and Ar-ion irradiation is less than 10, relatively small, and often only 1 mutation is found near the mapped location. Thus, irradiation with these ions can efficiently generate knockout mutants of a target gene and can be applied to reverse genetics. Rice mutants of the causative gene induced by ion-beam irradiation were compared at 23–50 keV/μm and 290 keV/μm with typical LETs. The most mutations irradiated with C ion at 23–50 keV/μm were small deletions (<100 bp). Irradiation with 290 keV/μm Ar-ion resulted in the highest number of large deletions and decreased small deletions. In rice, as in *Arabidopsis*, the LETmax with high mutagenic effects was dominated by SNVs and small deletion mutations, while large deletions and chromosomal rearrangement mutations dominated LETs with high lethal effects.

(3) Innovative application of heavy-ion irradiation

In 1999, we formed a consortium for ion-beam breeding consisting of 24 groups. In 2022, the consortium grew to 184 groups from Japan and 22 from overseas. Previously, the ion-beam breeding procedures were carried out using mainly flowers and ornamental plants. We have recently put a new non-pungent and tearless onion, 'Smile Ball,' on the market along with 'Kiku Meigetsu,' an edible late flowering chrysanthemum. In addition, a new project was launched to expand the cultivation area of this variety of chrysanthemum in Yamagata prefecture. Beneficial variants have been grown for various plant species, such as high yield sea weeds, lipids hyperaccumulating unicellular alga, medicinal plant with high productivity of medicinal ingredient, peanuts without major allergens, oranges with delayed coloring and one-month late harvest, and lettuce with a low browning property as a cut vegetable. As

a result of a collaborative study with Shizuoka prefecture, we have created a new variety of 'Haru Shizuka,' which is late coloring. The harvest time of the Satsuma mandarin has tended to come earlier due to global warming, 'Haru Shizuka' is harvested about a month later than the original variety, but the fruits are sour when harvested. 'Haru Shizuka' is suitable for long-term storage and the fruits turn into good quality sweet oranges during storage till April. By broadening the target of heavy-ion breeding extending from flowers to crops, the technology will contribute to solving the global problems of food shortage and environmental destruction.

Members

Team Leader

Tomoko ABE

Research/Technical Scientists

Tokihiro IKEDA (Senior Research Scientist)
Masako IZUMI (Senior Research Scientist)
Ryouhei MORITA (Technical Scientist)
Teruyo TSUKADA (Senior Research Scientist)
Kazuhide TSUNEIZUMI (Senior Research Scientist)

Postdoctoral Researcher

Asanga D. N. IMIHAMI MUDIYANSELAGE

Technical Staffs

Yoriko HAYASHI
Yuki SHIRAKAWA
Sumie OHBU
Mieko YAMADA

Special Temporary Technical Scientists

Hiroshi ABE
Katsunori ICHINOSE

Research Consultant

Masahiro MII (Chiba Univ.)

Visiting Scientists

Tory CHHUN (Prek Leap Nat'l Inst. of Agriculture)
Ayumi DEGUCHI (Chiba Univ.)
Makoto FUJIWARA (Sophia Univ.)
Eitaro FUKATSU (Forestry and Forest Products Res. Inst.)
Tomonari HIRANO (Univ. of Miyazaki)
Akiko HOKURA (Tokyo Denki Univ.)
Kotaro ISHII (QST)
Yusuke KAZAMA (Fukui Prefectural Univ.)
Yutaka MIYAZAWA (Yamagata Univ.)
Kazumitsu MIYOSHI (Chiba Univ.)
Koji MURAI (Fukui Prefectural Univ.)
Kyosuke NIWA (Tokyo Univ. of Marine Sci. and Tech.)
Tadashi SATO (Tohoku Univ.)
Yoichi SATO (Riken Food Co., Ltd.)
Kenichi SUZUKI (Suntory Flowers Co., Ltd.)
Hinako TAKEHISA (Nat'l Agriculture and Food Res. Org.)
Masao WATANABE (Tohoku Univ.)
Alexis Kooichi VIDAL TAKASAKI (Pontificia Universidad Católica de Valparaíso)

Visiting Technicians

Yukiko KANAZAWA (Nippon Beet Sugar Manufacturing Co., Ltd.)
Norihide KISHINO (Sanwa Norin Co. Ltd.)
Miho MOGAMIYA (Riken Food Co., Ltd.)
Daisuke SAITO (Riken Food Co., Ltd.)

Research Fellow

Hirokazu SAIDO (Saitama Agricultural Tech. Res. Center)

Student Trainee

Yuzo MARUYAMA (Tokyo Denki Univ.)

Part-timer Worker

Haruka WATANABE

List of Publications & Presentations

Publications

[Original Papers]

A. Deguchi, F. Tatsuzawa, K. Ishii, T. Abe, and K. Miyoshi, "Localized repression of two bHLH genes is involved in the formation of white margins and white abaxial surfaces in carnation petals by inducing the absence of anthocyanin synthesis," Hortic. Sci. **91**, 68 (2022).

橋口太亮, 飯山光太郎, 長井純一, 藤川和博, 石井公太郎, 阿部知子, 「サツマイモ『シロユタカ』と外観識別可能な『こなみずき』欠刻葉系統の作出」, 日本作物学会九州支部会報 **88**, 22 (2022).

H. Park, Y. Narasako, T. Abe, H. Kunitake, and T. Hirano, "Comprehensive effects of heavy-ion beam irradiation on sweet potato (*Ipomoea batatas [L.] Lam.*)," Plant Biotechnol (Tokyo) **39**, 311 (2022).

Y. Kazama, M. Kitoh, T. Kobayashi, K. Ishii, M. Krasovec, Y. Yasui, T. Abe, S. Kawano, and D. A. Filatov, "A CLAVATA3-like gene acts as a gynoecium suppression function in white campion," Mol. Biol. Evol. **39**, 10 (2022).

阿部知子, 林依子, 大野豊, 畑下昌範, 高城啓一, 「イオンビーム育種技術の開発に取り組む加速器施設」, アグリバイオ **6**, 8 (2022).

平野智也, 「イオンビームを用いた花き植物の品種改良」, アグリバイオ **6**, 14 (2022).

中村茂和, 阿部知子, 「長期貯蔵に適した温州みかん新品種『春しずか』の育成」, アグリバイオ **6**, 24 (2022).

風間裕介, 畑下昌範, 木元久, 櫻井明彦, 「イオンビームを用いた微生物の品種改良」, アグリバイオ **6**, 29 (2022).

H. J. Kim, K. Nakammura, Y. Sakakura, K. Suga, K. Tsuneizumi, T. Abe, M. Yamada, M. Kawada, T. Katayama, N. Tezuka, T. Kobayashi, M. Koiso, and A. Hagiwara, "Effects of dietary microalgal species and hormone treatment on the lorica size and reproductivity of heavy-ion beam irradiated rotifers," Fish. Sci. **89**, 61 (2023).

[Review Articles]

T. Hirano, Y. Kazama, H. Kunitake, and T. Abe, "Mutagenic effects of heavy-ion beam irradiation to plant genome," Cytologia **87**, 3 (2022).

阿部知子, 「イオンビーム育種技術の開発—農学と加速器物理学のシナジー効果」, アグリバイオ **6**, 6 (2022).

Presentations

[International Conferences/Workshops]

T. Abe (invited), Y. Hayashi, R. Morita, Y. Shirakawa, and H. Ichida, "Ion-beam mutagenesis for creation of new varieties and discovery of genes," Bangabandhu International Conference on Sustainable Agriculture through Nuclear and Frontier Research (Webinar), Online, January 19–21, 2022.

Y. Kazama (oral) and T. Abe, "Effect of linier energy transfer in the heavy-ion mutagenesis and breeding," The 32nd Annual Meeting of MRS-J, Yokohama, Japan, December 5–7, 2022.

T. Mayuzumi (poster), A. Matsuta, M. Hatashita, K. Takagi, T. Abe, K. Murai, and Y. Kazama, "Heavy-ion beams with high linear energy transfer frequently produces morphological mutants in the M1 generation of an ornamental plant *Torenia fournieri*," The 32nd Annual Meeting of MRS-J, Yokohama, Japan, December 5–7, 2022.

[Domestic Conferences/Workshops]

石井公太郎 (口頭発表), 風間裕介, 浅野円花, 竹下毅, 阿部知子, 河野重行, 「クロレラの内部倍数性と Ar・Fe イオンビーム照射による染色体の分断化と再構成」, 日本藻類学会 第 45 回大会, オンライン, 2022 年 3 月 16–17 日.

石井公太郎 (口頭発表), 風間裕介, 平野智也, J. A. Fawcett, 酒井富士子, 白川侑希, 大部澄江, 阿部知子, 「重イオンビームで誘発される欠失変異と必須遺伝子のシロイヌナズナゲノム上での分布に関する俯瞰的解析」, 日本育種学会 第 141 回講演会, オンライン, 2022 年 3 月 20–21 日.

杉田和陽 (口頭発表), サンジャヤ アルビン, 西嶋遼, 村井耕二, 阿部知子, 風間裕介, 「シロイヌナズナの新規染色体再編成変異体で見られたダイナミックな形態変化」, 同上.

黛隆宏 (口頭発表), 松田彩花, 畑下昌範, 高城啓一, 阿部知子, 村井耕二, 風間裕介, 「トレニアの新規フリル変異体で見られた花弁の細胞サイズの変化」, 同上.

H. Park (口頭発表), 奈良迫洋介, 阿部知子, 國武久登, 平野智也,「重イオンビーム照射がサツマイモの塊根形成に及ぼす影響」, 同上.

小林壮生 (ポスター発表), 高橋真佐子, 杉山立志, 石井公太郎, 河野重行, 風間裕介, 「根端分裂組織の細胞周期の同調に着目したヒロハノマンテマの染色体標本作製方法」, 同上.

椎槙子 (ポスター発表), 加治屋優希, 阿部知子, 星野洋一郎, 國武久登, 平野智也, 「アルゴンイオンビーム照射雄性配偶子の受精機構解析」, 園芸学会令和 4 年度秋季大会, 山形市 (山形大学), 2022 年 9 月 7–13 日.

武田信哉 (口頭発表), 市田裕之, 阿部知子, 有村慎一, 風間智彦, 陳孫禄, 金岡義高, 貴島祐治, 鳥山欽哉, 「台中 65 号の細胞質およびアフリカイネの核を持つ TG-CMS の原因遺伝子解析とその稔性回復様式の調査」, 第 39 回日本植物バイオテクノロジー学会, 堺市 (大阪公立大学), 2022 年 9 月 11–13 日.

生駒拓也 (ポスター発表), サンジャヤ アルビン, 池田美穂, 西嶋遼, 村井耕二, 阿部知子, 風間裕介, 「シロイヌナズナ染色体における遺伝子量補正の調査」, 日本遺伝学会第 94 回大会, 札幌市 (北海道大学), 2022 年 9 月 14–17 日.

杉田和陽 (ポスター発表), サンジャヤアルビン, 西嶋遼, 田中裕之, 伊藤武彦, 村井耕二, 阿部知子, 風間裕介, 「シロイヌナズナの新規染色体部分的重複変異体における遺伝子発現変動とクロマチン動態」, 同上.

小川雅文 (ポスター発表), 常泉和秀, 阿部知子, 野澤昌文, 「重粒子線照射によるショウジョウバエ Y 染色体の部分破壊: 遺伝子量補償の即時性の検証に向けて」, 同上.

池田公季 (ポスター発表), 旭置桐哉, 風間裕介, 石井公太郎, 阿部知子, 國武久登, 平野智也, 「シロイヌナズナ petal compensation exhibiting 変異体における花器官細胞サイズ制御機構の解析」, 日本植物学会第 86 回大会, 京都市 (京都府立大), 2022 年 9 月 15–19 日.

石井公太郎 (口頭発表), 浅野円花, 阿部知子, 河野重行, 「クロレラゲノム配列の更新と重イオンビーム誘導変異体の染色体再編成の解析」, 同上.

田中朋之 (口頭発表), 小林麻子, 阿部知子, 「高温感受性イネ突然変異体 flo11-2 を用いた白未熟粒発生機構の解析」, 第 254 回日本作物学会講演会, 福島市 (福島大学), 2022 年 9 月 20–21 日.

市田裕之 (口頭発表), Ni Lei, 森田竜平, 阿部知子, 「機械学習による変異バリデーション法の開発と検証」, 日本育種学会 第 142 回講演会, 帯広市 (帯広畜産大学), 2022 年 9 月 23–25 日.

上田純平 (口頭発表), 風間裕介, 阿部知子, 村井耕二, 「時計遺伝子 WPCL1 の欠失による一粒系コムギ早生変異体の早生性を抑制するイオンビーム変異体 late-heading1 の解析」, 同上.

杉田和陽 (口頭発表), サンジャヤアルビン, 西嶋遼, 田中裕之, 伊藤武彦, 村井耕二, 阿部知子, 風間裕介, 「染色体再編成が植物ゲノムに及ぼす影響」, 北陸植物学会第 12 回大会, 富山市 (富山大学), 2022 年 11 月 13 日.

生駒拓也 (口頭発表), サンジャヤアルビン, 池田美穂, 西嶋遼, 村井耕二, 阿部知子, 風間裕介, 「シロイヌナズナで遺伝子量補正は起きるのか」, 同上.

黛隆宏 (口頭発表), 松田彩花, 畑下昌範, 高城啓一, 阿部知子, 村井耕二, 風間裕介, 「重イオンビームを用いた園芸植物トレニアの花形変異体の作出」, 同上.

鬼頭萌 (口頭発表), 小林壮生, 石井公太郎, M. Krasovic, 安井康夫, 阿部知子, 河野重行, D. A. Filaotv, 風間裕介, 「雌雄異株植物ヒロハノマンテマの決定候補遺伝子 GSFY の同定」, 同上.

小林壮生 (口頭発表), 鬼頭萌, D. A. Filaotv, 風間裕介, 「ヒロハノマンテマ性決定遺伝子の X 染色体連鎖パラログ GSFX の機能解析」, 同上.

風間裕介 (口頭発表), 鬼頭萌, 小林壮生, 石井公太郎, M. Krasovic, 安井康夫, 阿部知子, 河野重行, D. A. Filaotv, 「CLV3 様ペプチドはヒロハノマンテマの性を決定する」, 植物化学調節学会第 57 回大会, 吉田郡 (福井県立大), 2022 年 11 月 25–27 日.

Award

阿部知子, 第 10 回和田賞, 公益財団法人日本メンデル協会, 4 月, 2022.

Press Releases

「春先に出荷可能な温州みかんの作出に成功」, 2021 年 12 月 8 日.

“Accelerators accelerate many fields,” T. Abe, RIKEN People, December 20, 2021.

研究最前線「重イオンビームで温州みかんの品種改良」, RIKEN News 481, 18 (2022).

「巨大 Y 染色体発見から 99 年目の快挙—ヒロハノマンテマの性決定遺伝子の同定に成功—」, 2022 年 9 月 28 日.

Patent

蝶野真喜子, 神山紀子, 阿部知子, 「種子の白色性を向上させたコムギ」, 特許出願番号 2021-166243, 出願日 2021 年 10 月 8 日.

Outreach Activities

阿部知子, 「重イオンビームを用いて新しい品種を創る」, 第 9 回 理研イノベーションセミナー, オンライン, 2022 年 1 月 21 日.

阿部知子, 「重イオンビームを用いて新しい品種を創る」, 理研と未来を創る会第 28 回講演会・見学会, 和光市, 2022 年 9 月 6 日.

阿部知子,「加速器を用いた重イオンビーム育種の発展」, シンポジウム「理化学研究所仁科研究室のキセキ」, 和光市, 2022 年 10 月 28 日.

We established the “Asagao (morning glory) club” to deepen the understanding of our technology of mutation breeding. The club distributes the morning glory seeds irradiated with C-ion on request, and collects and compiles the observation reports of their growth.

Accelerator Applications Research Division
Beam Mutagenesis Group
Plant Genome Evolution Research Team

1. Abstract

Established in May 2018 and succeed in October 2020, the plant genome evolution research team studies the effect of heavy-ion induced mutations on plant and microbial phenotypes. Chromosome rearrangements including translocations, inversions, and deletions are thought to play an important role in evolution and have a greater potential to achieve large phenotypic changes. However, this potential has not been fully investigated due to the lack of an effective method to induce and analyze complexed mutations. We employ the population genomics approach with robust molecular biology and bioinformatics techniques to characterize genomic mutations in model and non-model plant and microbial species, and create the future of mutation breeding.

2. Major Research Subjects

(1) Genomics-based approach to revolutionize the mutagenesis in model and non-model plants and microbes
(2) De novo genome sequencing and assembly of cultivars and isolates, and its application to evolution and breeding studies

3. Summary of Research Activity

(1) Genomics-based approach to revolutionize the mutagenesis in model and non-model plants and microbes

Recent advances in genome sequencing and bioinformatics technology enabled us to obtain a genome-wide view of the induced mutations in unselected populations. We chose baker's yeast and a legume *Lotus japonicus* as model systems, irradiated different doses of carbon-ion beams to these organisms, and determined the dose-survival correlation. We isolated a semi-dwarf *L. japonicus* mutant, identified the responsible mutation by whole-genome sequencing, and started to characterize the phenotypic traits of this mutant. Phenotyping analysis indicated that the isolated semi-dwarf mutant shows significantly shortened internode length while still maintaining good seed production equivalent to the wild-type plants. The semi-dwarf *L. japonicus* mutant is suitable for high-density cultivation in the laboratory environment and may serve as an efficient model platform for legume- *Rhizobium* symbiosis.

(2) *De novo* genome sequencing and assembly of new cultivars and isolates, and its application to evolution and breeding studies

We apply the latest *de novo* genome sequencing technology to elucidate genome sequences in different cultivars and isolates and successfully created some high-quality draft genome sequences. The determined and assembled draft genome sequences are subjected to gene predictions and functional annotations, then shared in a searchable data visualization and analysis system accessible through the internet. With these fundamental genome information resources, we and our collaborators work together to achieve new findings that will achieve major advances in both science and practical applications. These resources as well as the overall experimental techniques and the analysis pipeline are essential to further expand our genome-wide mutation and evolution approach to previously uncharacterized non-model species.

Members

Team Leader

Hiroyuki ICHIDA

Postdoctoral Researcher

Ni LEI

Administrative Part-time Workers

Yusaku NISHIMIYA
Chiharu HINO
Keiko UEDA

List of Publications & Presentations

Publications

[Original Papers]

H. Ichida, T. Kazama, S. Arimura, and K. Toriyama, "The mitochondrial and plastid genomes of *Oryza sativa* L. cv. Taichung 65," Plant Biotechnol. **40**, 109 (2023).

H. Murata, N. Nakamura, A. Ohta, and H. Ichida, "A semisolid plate method to isolate mycelia maintaining chlamydospore formation in *Tricholoma bakamatsutake*," Bulletin of FFPRI **22**, 13 (2023).

[Review Article]

H. Murata, A. Yamada, H. Ichida, N. Nakamura, and H. Neda, "Biodiversity of *Tricholoma matsutake* (syn. *T. nauseosum*) and its related species based on repetitive DNA and genomics," Botany (April 5, 2023), https://doi.org/10.1139/cjb-2022-0122 .

Presentations

[International Conference/Workshop]

T. Abe (invited), Y. Hayashi, R. Morita, Y. Shirakawa, and H. Ichida, “Ion-beam mutagenesis for creation of new varieties and discovery of genes,” Bangabandhu International Conference on Sustainable Agriculture through Nuclear and Frontier Research, Online, January, 2022.

[Domestic Conferences/Workshops]

高塚歩, 風間智彦, 市田裕之, 阿部知子, 鳥山欽哉, 「Tadukan 型細胞質雄性不稔性イネのミトコンドリア RNA プロセッシングに関わる PPR 遺伝子の推定」, 第 10 回 植物 RNA 研究ネットワーク シンポジウム, 文京区, 2022 年 12 月.

市田裕之, Ni Lei, 森田竜平, 阿部知子, 「機械学習による変異バリデーション法の開発と検証」, 日本育種学会 第 142 回講演会, 帯広市, 2022 年 9 月.

稲田裕介, 高塚歩, 市田裕之, 鳥山欽哉, 「CW 型細胞質雄性不稔性イネに対するインディカ品種 Samba Mahsuri 由来の新規稔性回復遺伝子のマッピング」, 日本育種学会 第 142 回講演会, 帯広市, 2022 年 9 月.

高塚歩, 風間智彦, 市田裕之, 阿部知子, 鳥山欽哉, 「Tadukan 型細胞質雄性不稔性イネを稔性回復させる遺伝子の探索」, 日本育種学会 第 142 回講演会, 帯広市, 2022 年 9 月.

高塚歩, 風間智彦, 市田裕之, 阿部知子, 鳥山欽哉, 「Tadukan に由来する細胞質雄性不稔性イネの稔性回復候補遺伝子」, 第 39 回日本植物バイオテクノロジー学会（堺）大会, 堺市, 2022 年 9 月.

武田信哉, 市田裕之, 阿部知子, 有村慎一, 風間智彦, 陳孫禄, 金岡義高, 貴島祐治, 鳥山欽哉, 「台中 65 号の細胞質とアフリカイネの核を持つ TG-CMS の原因遺伝子とその稔性回復様式の調査」, 第 39 回日本植物バイオテクノロジー学会（堺）大会, 堺市, 2022 年 9 月.

Accelerator Applications Research Division
RI Application Research Group

1. Abstract

RI Application Research Group promotes industrial applications of radioisotopes (RIs) and ion beams at RIKEN RI Beam Factory (RIBF). Nuclear Chemistry Research Team develops production technologies of useful RIs for application studies in nuclear and radiochemistry. The team also develops technologies of mass spectrometry for trace-element and isotope analyses and apply them to the research fields such as cosmochemistry, environmental science, archaeology, and so on. Industrial Application Research Team promotes industrial applications of the accelerator facility and its related technologies.

2. Major Research Subjects

(1) Research and development of RI production technologies at RIBF
(2) RI application research
(3) Distribution of RIs produced at RIBF
(4) Development of radioactive targets and sources
(5) Development of trace element analyses using accelerator techniques and their applications to geoscience and archaeological research fields
(6) Development of chemical materials for ECR ion sources of the RIBF accelerators
(7) Development of technologies on industrial utilization and novel industrial applications of RIBF
(8) Support of industrial utilization of the heavy-ion beams at RIBF
(9) Support of materials science experiments

3. Summary of Research Activity

See the subsections of Nuclear Chemistry Research Team and Industrial Application Research Team.

Member

Director

Hiromitsu HABA

List of Publications & Presentations

See the subsections of Nuclear Chemistry Research Team and Industrial Application Research Team.

Accelerator Applications Research Division
RI Application Research Group
Nuclear Chemistry Research Team

1. Abstract

The Nuclear Chemistry Research Team develops production technologies of unique radioisotopes (RIs) at RIKEN RI Beam Factory (RIBF) and applies them in the research fields of physics, chemistry, biology, engineering, medicine, pharmaceutical and environmental sciences. The purified RIs such as ^{65}Zn, ^{67}Cu, ^{85}Sr, ^{88}Y, and ^{109}Cd are delivered to universities and institutes through Japan Radioisotope Association. We also develop new technologies of mass spectrometry for the trace-element analyses using accelerator techniques and apply them to the research fields such as cosmochemistry, environmental science, archaeology, and so on. We perform various isotopic analyses on the elements such as S, Pd, and Pb using ICP-MS, TIMS, and IRMS. We also develop radioactive targets and sources, and chemical materials such as metallic ^{238}U, $^{238}UO_2$, and ^{48}CaO for ECR ion sources of the heavy-ion accelerators at RIBF.

2. Major Research Subjects

(1) Research and development of RI production technologies at RIBF
(2) RI application research
(3) Development of trace element analyses using accelerator techniques and their applications to geoscience and archaeological research fields
(4) Development of radioactive targets and sources, and chemical materials for ECR ion sources of the heavy-ion accelerators at RIBF

3. Summary of Research Activity

(1) Research and development of RI production technologies at RIBF and RI application research

Due to its high sensitivity, the radioactive tracer technique has been successfully applied for investigations of the behavior of elements in the fields of chemistry, biology, engineering, medicine, pharmaceutical and environmental sciences. We have been developing production technologies of useful radioisotopes (RIs) at RIBF and conducting their application studies in collaboration with many researchers in various fields. With 30-MeV proton, 24-MeV deuteron, 50-MeV alpha, and 70-MeV ^{7}Li beams from the AVF cyclotron, we presently produce about 100 RIs from ^{7}Be to ^{236}Np. Among them, ^{65}Zn, ^{67}Cu, ^{85}Sr, ^{88}Y, and ^{109}Cd are delivered to Japan Radioisotope Association for fee-based distribution to the general public in Japan. Our RIs are also distributed to researchers under the Supply Platform of Short-lived Radioisotopes for Fundamental Research, supported by MEXT KAKENHI in FY2016-2027. On the other hand, RIs of a large number of elements are simultaneously produced from metallic targets such as ^{nat}Ti, ^{nat}Ag, ^{nat}Hf, ^{197}Au, and ^{232}Th irradiated with a 135 MeV/nucleon ^{14}N beam from the RIKEN Ring Cyclotron. These multitracers are also supplied to universities and institutes as collaborative research.

In 2022, we developed production technologies of RIs such as ^{28}Mg, ^{44m}Sc, ^{44}Ti, ^{67}Cu, ^{86}Y, ^{111}Ag, ^{139}Ce, ^{141}Ce, ^{155}Tb, ^{165}Er, ^{169}Yb, ^{186}Re, ^{195}Au, ^{211}At, ^{212}Pb, ^{224}Ra, ^{225}Ac, ^{229}Pa, and ^{236}Np which were strongly demanded but lack supply sources in Japan. We also investigated the excitation functions for the ^{27}Al(α, x), ^{nat}Zn(p, x), ^{nat}Sm(^{7}Li, x), ^{nat}Gd(p, x), ^{nat}Re(d, x), ^{nat}Re(α, x), ^{nat}Ta(α, x), ^{nat}W(p, x), ^{nat}Pt(p, x), ^{nat}Pt(α, x), and ^{209}Bi(^{7}Li, x) reactions to effectively and quantitatively produce useful RIs. We used radiotracers of ^{139}Ce, ^{211}At, and ^{229}Pa for application studies in chemistry, ^{44m}Sc, ^{67}Cu, ^{111}Ag, ^{141}Ce, ^{186}Re, ^{211}At, and ^{225}Ac in nuclear medicine, and ^{28}Mg, ^{44m}Sc, ^{67}Cu, ^{86}Y, ^{169}Yb, ^{186}Re, and ^{211}At in engineering. We also produced ^{65}Zn, ^{67}Cu, ^{85}Sr, ^{88}Y, and ^{109}Cd for our scientific research on a regular schedule and supplied the surpluses through Japan Radioisotope Association to the general public. In 2022, we accepted 4 orders of ^{65}Zn with a total activity of 12.7 MBq, 4 orders of ^{85}Sr with 6.7 MBq, and 1 order of ^{88}Y with 0.1 MBq. We also distributed ^{28}Mg (1 MBq × 2), ^{67}Cu (10 MBq × 1 and 100 MBq × 1), ^{86}Y (5 MBq × 1), ^{88}Zr (1 MBq × 2), ^{95}Nb (2 MBq × 2), ^{111}Ag (1 MBq × 1), ^{141}Ce (0.24 MBq × 1), ^{175}Hf (1 MBq × 2), ^{179}Ta (1 MBq × 1), and ^{211}At (5 MBq × 4, 10 MBq × 1, 30 MBq × 2, 50 MBq × 1, 80 MBq × 2, 90 MBq × 1, and 100 MBq × 2) under the Supply Platform of Short-lived Radioisotopes for Fundamental Research.

(2) Superheavy element chemistry

Chemical characterization of newly-discovered superheavy elements (SHEs, atomic number $Z \geq 104$) is an extremely interesting and challenging research subject in modern nuclear and radiochemistry. We are developing SHE production systems as well as rapid single-atom chemistry apparatuses at RIBF. Using heavy-ion beams from SRILAC and AVF, ^{261}Rf (Z = 104), ^{262}Db (Z = 105), ^{265}Sg (Z = 106), and ^{266}Bh (Z = 107) are produced in the ^{248}Cm(^{18}O, 5n)^{261}Rf, ^{248}Cm(^{19}F, 5n)^{262}Db, ^{248}Cm(^{22}Ne, 5n)^{265}Sg, and ^{248}Cm(^{23}Na, 5n)^{266}Bh reactions, respectively, and their chemical properties are investigated.

We installed a gas-jet transport system to the focal plane of the gas-filled recoil ion separator GARIS at SRILAC. This system is a promising approach for exploring new frontiers in SHE chemistry: the background radiations from unwanted products are strongly suppressed, the intense primary heavy-ion beam is absent in the gas-jet chamber, and hence the high gas-jet extraction yield is attained. Furthermore, the beam-free condition makes it possible to investigate new chemical systems. In 2022, we continued to develop an ultra-rapid gas-chromatograph apparatus, which consists of an RF carpet gas cell and a cryo-gas-chromatograph column with a Si detector array, at the focal plane of GARIS for the future gas-phase chemistry of the short-lived SHEs (half-life $T_{1/2}$ < 1 s). To realize aqueous chemistry studies of Sg and Bh, we have been developing a continuous and rapid solvent extraction apparatus which

consists of a continuous dissolution apparatus Membrane DeGasser (MDG), a Flow Solvent Extractor (FSE), and a liquid scintillation detector for α/SF-spectrometry. On the other hand, in collaboration with Osaka University, co-precipitation behavior of No (Z = 102) with $BaSO_4$ and CaC_2O_4 was investigated with ^{255}No produced in the ^{248}Cm(^{12}C, 5n)^{255}No reaction at the AVF cyclotron. We also produced radiotracers of ^{88}Zr, ^{95}Nb, ^{175}Hf, and ^{179}Ta at the AVF cyclotron and conducted model experiments for aqueous chemistry studies on Rf and Db.

(3) Development of trace element analyses using accelerator techniques and their applications to geoscience and archaeological research fields

We have been developing the ECR Ion Source Mass Spectrometer (ECRIS-MS) for trace element analyses. We renovated the detection system of ECRIS-MS and evaluated its sensitivity and mass resolution power. We equipped a laser-ablation system with an ion source and a pre-concentration system to achieve high-resolution analyses for noble gases such as Kr and Xe.

Using the ICP-MS, TIMS, IRMS, and so on, we studied Pb and S isotope ratios on cinnabar and asphalt samples from ancient ruins in Japan to elucidate the distribution of goods in the archaic society. We have established a sampling technique for pigment without any damages on the artifacts or wall paintings, using a sulfur-free adhesive tape since 2019. This technique was applied to analyze vermilion samples collected from archaeological sites. In FY2022, three types of vermilion were analyzed. The first was vermilion excavated from tombs dating from the Yayoi Period to the Kofun Period in Japan, the second was excavated from tombs dating from the Pre-Qin Period (the Shang, Spring and Autumn, Warring States Period, *etc*.) in China, and the third was used for murals on the Roman sites in the Iberian Peninsula. Furthermore, since 2021, we have been developing a method for the analyses of 3 isotopic abundance ratios (^{32}S, ^{33}S, and ^{34}S) of sulfur as a new parameter for identification of source mine. We analyzed the possibility of exploring the MIF (mass-independent-fractionation) effect. This is also expected to provide a new parameter for the analysis of environmental dynamics.

In FY2022, we operated ICP-MS, making it a shared-use instrument, and analyzed 294 samples from seven laboratories.

(4) Development of chemical materials for ECR ion sources of the heavy-ion accelerators at RIBF

In 2022, we prepared $^{238}UO_2$ on a regular schedule for ^{238}U-ion accelerations with the 28-GHz ECR of RILAC2.

Members

Team Leader
Hiromitsu HABA

Technical Scientist
Hiroo HASEBE

Contract Researcher
Xiaojie YIN

Postdoctoral Researcher
Yudai SHIGEKAWA

Technical Staff
Akihiro NAMBU

Special Temporary Research Scientist
Kazuya TAKAHASHI

Junior Research Associates
Teruhito NAKASHITA
Motoki SATO

Research Part-time Workers
Michiko KITAGAWA
Nozomi SATO
Sachiko USUDA
Minako OSANAI

Research Consultant
Hisaaki KUDO (Niigata Univ.)

Visiting Scientists
Msayuki AIKAWA (Hokkaido Univ.)
Kazuhiko AKIYAMA (Tokyo Metropolitan Univ.)
Takatoshi AOKI (Univ. of Tokyo)
Masato ASAI (JAEA)
Ferenc DITROI (ATOMKI)
Shuichiro EBATA (Saitama Univ.)
Osuke FUJIMOTO (PDRadiopharma Inc.)
Yuichi FUNASE (PDRadiopharma Inc.)
Takahiro HIRAKI (Okayama Univ.)
Hayato IKEDA (Tohoku Univ.)
Masamichi KAJITA (PDRadiopharma Inc.)
Yoshitaka KASAMATSU (Osaka Univ.)
Hiroshi KATO (PDRadiopharma Inc.)
Mayeen U. KHANDAKER (Sunway Univ.)

Hidetoshi KIKUNAGA (Tohoku Univ.)
Yoshikatsu KOGA (Nat'l Cancer Center)
Shoko KUBOTA (PDRadiopharma Inc.)
Takumi KUBOTA (Kyoto Univ.)
Takahiko MASUDA (Okayama Univ.)
Toshimitsu MOMOSE (Int'l Univ. of Health and Welfare)
Eri NAKAMURA (PDRadiopharma Inc.)
Kenichiro OGANE (Int'l Univ. of Health and Welfare)
Miki OHTSUKA (Waseda Univ.)
Kazuhiro OOE (Osaka Univ.)
Kai ORIHARA (PDRadiopharma Inc.)
Shinobu OSHIKIRI (PDRadiopharma Inc.)
Yasutaka SAITO (PDRadiopharma Inc.)
Aya SAKAGUCHI (Univ. of Tsukuba)
Miho SATAKE (PDRadiopharma Inc.)
Tetsuya SATO (JAEA)
Yuki SATO (PDRadiopharma Inc.)
Kenji SHIMAZOE (Univ. of Tokyo)
Keisuke SUEKI (Univ. of Tsukuba)
Kentaro SUZUKI (PDRadiopharma Inc.)
Zoltan SZUCS (ATOMKI)
Sandor TAKACS (ATOMKI)
Hiroyuki TAKAHASHI (Univ. of Tokyo)
Miho TAKAHASHI (Tokyo Univ. of Marine Sci. and Tech.)
Hiroki TAKASHIMA (Nat'l Cancer Center)
Sayuri TAKATORI (Okayama Univ.)
Atsushi TOYOSHIMA (Osaka Univ.)
Kazuaki TSUKADA (JAEA)
Mizuki UENOMACHI (Kyoto Univ.)
Naoyuki UKON (Fukushima Medical Univ.)
Takahiro YAMADA (Kindai Univ.)
Takuya YOKOKITA (Salesian Polytechnic)
Akihiko YOKOYAMA (Kanazawa Univ.)
Zenko YOSHIDA (ATOX Co., Ltd.)
Koji YOSHIMURA (Okayama Univ.)

Visiting Technicians

Hideyuki ARAI (Metal Tech. Co., Ltd.)
Hiroshi ARATA (Metal Tech. Co., Ltd.)
Mai FUKUMORI (ATOX Co., Ltd.)
Masataka IMAMURA (Japan Radioisotope Association)
Shota KIMURA (Japan Radioisotope Association)
Yukiyoshi KON (Osaka Univ.)
Takashi KURIHARA (Metal Tech. Co., Ltd.)
Daiki MORI (Japan Radioisotope Association)
Shingo NAKAMURA (Metal Tech. Co., Ltd.)
Yuki TAKEMURA (ATOX Co., Ltd.)
Shusaku TAZAWA (ATOX Co., Ltd.)
Sho TOMITA (ATOX Co., Ltd.)
Yuichirou WAKITANI (Japan Radioisotope Association)
Kaede YAMADA (ATOX Co., Ltd.)
Mami YUKI (ATOX Co., Ltd.)

Visiting Researcher

Mizuki UENOMACHI (Kyoto Univ.)

Student Trainees

Kjeld A.A.G. BEEKS (Vienna Univ. of Tech.)
Desheng CHEN (Univ. of Chinese Academy of Sci.)
Gantumur DAMDINSUREN (Hokkaido Univ.)
Shunsuke FUJINO (Kindai Univ.)
Yuta FUKUNAGA (Okayama Univ.)
Ming GUAN (Okayama Univ.)
Hiroyuki HOSOKAWA (Kanazawa Univ.)
Xuan HOU (Univ. of Tokyo)
He HUANG (Hokkaido Univ.)
Yuki ISHII (Kanazawa Univ.)
Yudai ITAKURA (Osaka Univ.)
Donghwan KIM (Univ. of Tokyo)
Hongchang LIN (Univ. of Tokyo)
Ryoutarou MASUDA (Osaka Univ.)
Kenichi MORI (Kindai Univ.)
Ayumu NAGAI (Kanazawa Univ.)
Ryohei NAKANISHI (Osaka Univ.)
Teruhito NAKASHITA (Univ. of Tokyo)
Koichi OKAI (Okayama Univ.)
Saki OTAKA (Osaka Univ.)
Yuma SAKAKIEDA (Univ. of Tsukuba)
Motoki SATO (Univ. of Tokyo)
Hodaka TAKAHASHI (Univ. of Tsukuba)
Katsuyuki TOKOI (Osaka Univ.)
Yutaka TOYOEDA (Hokkaido Univ.)
Taisei UEKI (Univ. of Tokyo)
Ruilin WANG (Osaka Univ.)
Eisuke WATANABE (Osaka Univ.)

List of Publications & Presentations

Publications

[Original Papers]

K. Ohnuki, M. Yoshimoto, H. Haba, S. Manabe, H. Takashima, M. Yasunaga, Y. Takenaka, and H. Fujii, "Protection from contamination by ^{211}At, an enigmatic but promising alpha-particle-emitting radionuclide," EJNMMI Phy. **9**, 39 (2022).

M. Aikawa, M. Sakaguchi, N. Ukon, Y. Komori, H. Haba, N. Otuka, and S. Takács, "Production cross sections of samarium-153 and -145 via alpha-particle-induced reactions on natural neodymium," Appl. Radiat. Isot. **187**, 110345 (2022).

A. Yakushev, L. Lens, Ch. E. Düllmann, J. Khuyagbaatar, E. Jäger, J. Krier, J. Runke, H. M. Albers, M. Asai, M. Block, J. Despotopulos, A. Di Nitto, K. Eberhardt, U. Forsberg, P. Golubev, M. Götz, S. Götz, H. Haba, L. Harkness-Brennan, R. -D. Herzberg, F. P. Heßberger, D. Hinde, A. Hübner, D. Judson, B. Kindler, Y. Komori, J. Konki, J. V. Kratz, N. Kurz, M. Laatiaoui, S. Lahiri, B. Lommel, M. Maiti, A. Mistry, Ch. Mokry, K. J. Moody, Y. Nagame, J. P. Omtvedt, P. Papadakis, V. Pershina, D. Rudolph, L. G. Samiento, T. K. Sato, M. Schädel, P. Scharrer, B. Schausten, D. A. Shaughnessy, J. Steiner, P. Thörle-Pospiech, A. Toyoshima, N. Trautmann, K. Tsukada, J. Uusitalo, K. -O. Voss, A. Ward, M. Wegrzecki, N. Wiehl, E. Williams, and V. Yakusheva, "On the adsorption and reactivity of element 114, flerovium," Front. Chem. **10**, published online (August 25, 2022). DOI: 10.3389/fchem.2022.976635 .

T. Watabe, Y. Liu, K. Kaneda-Nakashima, T. Sato, Y. Shirakami, K. Ooe, A. Toyoshima, E. Shimosegawa, Y. Wang, H. Haba, T. Nakano, A. Shinohara, and J. Hatazawa, "Comparison of the therapeutic effects of [^{211}At]NaAt and [^{131}I]NaI in an NIS-expressing thyroid cancer mouse model," Int. J. Mol. Sci. **23**, 9434 (2022).

M. Tanaka, P. Brionnet, M. Du, J. Ezold, K. Felker, B. J. P. Gall, S. Go, R. K. Grzywacz, H. Haba, K. Hagino, S. Hogle, S. Ishizawa, D. Kaji, S. Kimura, T. T. King, Y. Komori, R. K. Lemon, M. G. Leonard, K. Morimoto, K. Morita, D. Nagae, N. Naito, T. Niwase, B. C. Rasco, J. B. Roberto, K. P. Rykaczewski, S. Sakaguchi, H. Sakai, Y. Shigekawa, D. W. Stracener, S. VanCleve, Y. Wang, K. Washiyama, and T. Yokokita, "Probing optimal reaction energy for synthesis of element 119 from ^{51}V + ^{248}Cm reaction with quasielastic barrier distribution measurement," J. Phys. Soc. Jpn. **91**, 084201 (2022).

A. C. Berriman, D. J. Hinde, D. Y. Jeung, M. Dasgupta, H. Haba, T. Tanaka, K. Banerjee, T. Banerjee, L. T. Bezzina, J. Buete, K. J. Cook, S. Parker-Steele, C. Sengupta, C. Simenel, E. C. Simpson, M. A. Stoyer, B. M. A. Swinton-Bland, and E. Williams, "Energy dependence of p+^{232}Th fission mass distributions: Mass-asymmetric standard I and standard II modes, and multichance fission," Phys. Rev. C **105**, 064614 (2022).

S. Ebata, M. Aikawa, D. Gantumur, and H. Haba, "Activation cross sections of alpha-particle-induced reactions on natural lanthanum up to 50 MeV," Nucl. Instrum. Methods Phys. Res. B **530**, 18 (2022).

H. Huang, M. Aikawa, Y. Hanada, and H. Haba, "Activation cross sections of deuteron-induced reactions on natural chromium up to 24 MeV," Nucl. Instrum. Methods Phys. Res. B **530**, 23 (2022).

A. Aso, K. Kaneda-Nakashima, H. Nabetani, Y. Kadonaga, Y. Shirakami, T. Watabe, T. Yoshiya, M. Mochizuki, Y. Koshino, K. Ooe, A. Kawakami, N. Jinno, A. Toyoshima, H. Haba, Y. Wang, J. Cardinale, F. L. Giesel, A. Shimoyama, and K. Fukase, "Substrate study for dihydroxyboryl astatine substitution reaction with Fibroblast Activation Protein Inhibitor (FAPI)," Chem. Lett. **51**, 1091 (2022).

T. Watabe, K. Kaneda-Nakashima, Y. Shirakami, Y. Kadonaga, K. Ooe, Y. Wang, H. Haba, A. Toyoshima, J. Cardinale, F. L. Giesel, N. Tomiyama, and K. Fukase, "Targeted α-therapy using astatine (^{211}At)-labeled PSMA1, 5, and 6: a preclinical evaluation as a novel compound," Eur. J. Nucl. Med. Mol. Imaging **50**, 849 (2023).

H. Sakai, H. Haba, K. Morimoto, and N. Sakamoto, "Facility upgrade for superheavy-element research at RIKEN," Eur. Phys. J. A **58**, 238 (2022).

X. Huang, K. Kaneda-Nakashima, Y. Kadonaga, K. Kabayama, A. Shimoyama, K. Ooe, H. Kato, A. Toyoshima, A. Shinohara, H. Haba, Y. Wang, and K. Fukase, "Astatine-211-labeled gold nanoparticles for targeted alpha-particle therapy via intravenous injection pharmaceutics," Pharmaceutics **14**, 2705 (2022).

H. Takashima, K. Ohnuki, S. Manabe, Y. Koga, R. Tsumura, T. Anzai, Y. Wang, X. Yin, N. Sato, Y. Shigekawa, A. Nambu, S. Usuda, H. Haba, H. Fujii, and M. Yasunaga, "Tumor targeting of ^{211}At-labeled antibody under sodium ascorbate protection against radiolysis," Mol. Pharm. **20**, 1156 (2023).

K. Kaneda-Nakashima, Y. Shirakami, T. Watabe, K. Ooe, T. Yoshimura, A. Toyoshima, Y. Wang, H. Haba, and K. Fukase, "Effect to therapy of sodium-iodine symporter expression by alpha-ray therapeutic agent via sodium/iodine symporter," Int. J. Mol. Sci. **23**, 15509 (2022).

M. Uenomachi, K. Shimazoe, and H. Takahashi, "Double photon coincidence crosstalk reduction method for multi-nuclide Compton imaging," J. Instrm. **17**, P04001 (2022).

Y. Kasamatsu, M. Nagase, H. Ninomiya, E. Watanabe, Y. Shigekawa, N. Kondo, K. Takamiya, T. Ohtsuki, N. Shiohara, and A. Shinohara, "Coprecipitation with samarium hydroxide using multitracer produced through neutron-induced fission of ^{235}U toward chemical study of heavy elements," Appl. Radiat. Isot. **179**, 110006 (2022).

Y. Miyake, N. Ikoma, K. Takahashi, Y. V. Sahoo, and H. Okuno, "Test of ^{107}Pd transmutation with macroscopic quantities," J. Nucl. Sci. Technol. **59**, 1536 (2022).

青木貴稔, 佐藤拓海, 池田英彦, 岡本直大, 鳥井寿夫, 中村圭佑, 永瀬慎太郎, 長濱弘季, 小澤直也, 佐藤幹, 中下輝士, 山根風樹, 松田恭幸, 酒見泰寛, 早水友洋, 大塚未来, 高峰愛子, 上野秀樹, 羽場宏光, 田中香津生, 原田健一, 川村広和, 井上壮志, 内山愛子, 畠山温, 市川雄一, 田中聡, 松尾由賀利, R. Sreekantham, B. K. Sahoo, B. Arora, and A. Kastberg, 「量子エンタングル Fr 原子を用いた電子 EDM の量子センシング」, 電気学会研究会資料 **40-44**, 17 (2022).

D. Gantumur, M. Aikawa, T. Khishigjargal, E. Norov, N. Ukon, and H. Haba, "Activation cross sections of proton-induced reactions on natural platinum up to 30 MeV," Appl. Radiat. Isot. **192**, 110621 (2023).

D. Ichinkhorloo, M. Aikawa, Z. Tsoodol, Y. Komori, and H. Haba, "Production cross sections of terbium and gadolinium radioisotopes from the deuteron-induced reactions on natural gadolinium up to 24 MeV," Nucl. Instrum. Methods Phys. Res. B **536**, 30 (2023).

Y. Osuka, K. Ii, K. Tsuchiya, M. Nemoto, Y. V. Sahoo, K. Takahashi, and M. Tanaka, "Molecular speciation of isopolyoxomolybdates and isopolyoxotungstates with silicic acid in aqueous solution using ESI-MS," J. Solution Chem., published online (February 27, 2023). DOI: 10.1007/s10953-023-01255-6 .

[Review Articles]

羽場宏光, 「人工元素合成」, 科学 **92**, 846 (2022).

羽場宏光, 「加藤セチ」, 和光純薬時報 **91**, 32 (2023).

[Books]

羽場宏光, 「元素探索と RI 製造」 in 「量子ビーム科学の基礎と応用」, NSA/Commentaries No. 27, 一般社団法人日本原子力産業協会原子力システム研究懇話会, 195 ページ, 2023 年 3 月 24 日, pp. 26–39.

桜井弘（編), 荒野泰, 小谷明, 高妻孝光, 佐治英郎, 鈴木晋一郎, 中山祐正, 根矢三郎, 羽場宏光, 廣田俊, 藤井敏司, 「ブルーバックス 元素 118 の新知識 第 2 版」, 講談社, 560 ページ, 2023 年 3 月 20 日.

上条信彦, 高橋和也, 「アスファルト分析」 in 「杉沢 C 遺跡第 1・2 次発掘調査報告書」（山形県埋蔵文化財センター調査報告書,

第 246 集), 公益財団法人山形県埋蔵文化財センター, 256 ページ, 2023 年 3 月, pp. 208–210.

[Proceedings]

H. Sakai, H. Haba, K. Morimoto, and N. Sakamoto, "Facility upgrade for SHE research at RIKEN Nishina Center," Acta Phys. Pol. B Proc. Suppl. **16**, 4-A10 (2023).

K. Nakamura, S. Nagase, T. Nakashita, T. Hayamizu, T. Aoki, H. Nagahama, N. Ozawa, M. Sato, K. Yamane, M. Fukase, D. Uehara, A. Takamine, and Y. Sakemi, "400-m-long polarization-maintaining fibers for magneto-optical trapping of francium atoms," Proc. 2022 Conf. on Lasers and Electro-Optics Pacific Rim, Technical Digest Series (Optica Publishing Group, 2022), CTuP7C_03, pp. 1–2.

A. Mukai, S. Hara, K. Yamagishi, R. Terabayashi, K. Shimazoe, Y. Tamura, H. Woo, T. Kishimoto, H. Kogami, Z. Zhihong, M. Uenomachi, A. Nurrachman, H. Takahashi, H. Asama, F. Ishida, H. Ebi, E. Takada, J. Kawarabayashi, K. Tanabe, K. Kamada, and H. Tomita, "Optimization of detector movement algorithm using decision trees analysis for radiation source identification based on 4π gamma imaging," 2022 IEEE/SICE International Symposium on System Integration (SII), Narvik, Norway, 2022, pp. 1026–1029.

Presentations

[International Conferences/Workshops]

H. Haba (invited), "Production and applications of radioisotopes at RIKEN RI Beam Factory—Search for new elements through diagnosis and therapy of cancer—," Laser Solutions for Space and the Earth 2022 in OPTICS & PHOTONICS International Congress 2022 (OPIC 2022), Yokohama, Japan & Online, April 18–22, 2022.

M. Tanaka (invited) for nSHE Collaboration, "Quasielastic backscattering measurement for ^{51}V + ^{248}Cm reaction toward element-119 synthesis at RIKEN," 19th Workshop on Recoil Separator for Superheavy Element Chemistry and Physics (TASCA 22), Darmstadt, Germany & Online, May 10–12, 2022.

K. Ooe (oral), S. Naka, Y. Shirakami, E. Shimosegawa, H. Kato, M. Tatsumi, H. Haba, A. Toyoshima, and T. Watabe, "Manufacturing of [^{211}At]NaAt for the first-in-human clinical trial of targeted alpha therapy for differentiated thyroid cancer at Osaka University Hospital," SNMMI 2022 Annual Meeting, Vancouver, Canada, June 11–14, 2022.

Y. Shirakami (oral), T. Watabe, K. Kaneda, Y. Kadonaga, K. Ooe, Y. Wang, H. Haba, A. Toyoshima, and K. Fukase, "Synthesis and preclinical evaluation of PSMA ligands labeled with astatine-211," SNMMI 2022 Annual Meeting, Vancouver, Canada, June 11–14, 2022.

T. Watabe (oral), K. Kaneda-Nakashima, Y. Shirakami, Y. Kadonaga, K. Ooe, Y. Wang, H. Haba, A. Toyoshima, and K. Fukase, "Targeted alpha therapy using astatine (^{211}At)-labeled PSMA5: a preclinical evaluation as a new novel compound," SNMMI 2022 Annual Meeting, Vancouver, Canada, June 11–14, 2022.

H. Haba (invited), "Production and applications of radioisotopes at RIKEN RI Beam Factory—Search for new elements through diagnosis and therapy of cancer—," IAEA/RCA RTC on Good Manufacturing Practice (GMP) and Radiation Safety Aspects of Radiopharmaceutical Production Using Medical Cyclotron, Online, May16–20, 2022.

M. Uenomachi (oral), T. Ueki, K. Shimazoe, H. Takahashi, Y. Shigekawa, A. Nambu, X. Yin, Y. Wang, and H. Haba, "Simultaneous multi-nuclide double photon coincidence imaging with parallel and slit collimators," 9th Conference on New Developments in Photodetection, Troyes, France, July 4–8, 2022.

K. Nakamura (oral), S. Nagase, T. Nakashita, T. Hayamizu, T. Aoki, H. Nagahama, N. Ozawa, M. Sato, K. Yamane, M. Fukase, D. Uehara, A. Takamine, and Y. Sakemi, "400-m-long polarization-maintaining fibers for magneto-optical trapping of francium atoms," The 15th Pacific Rim Conference on Lasers and Electro-Optics (CLEO Pacific Rim, CLEO-PR 2022), Sapporo & Online, July 31–August 5, 2022.

H. Sakai (invited), H. Haba, K. Morimoto, and N. Sakamoto, "Facility upgrade for SHE research at RIKEN," Zakopane Conference on Nuclear Physics "Extremes of the Nuclear Landscape," Zakopane, Poland, August 28–September 4, 2022.

M. Tanaka (oral) for nSHE Collaboration, "Optimal energy for element 119 synthesis via ^{51}V + ^{248}Cm reaction probed by quasielastic barrier distribution measurement," Zakopane Conference on Nuclear Physics "Extremes of the Nuclear Landscape," Zakopane, Poland, August 28–September 4, 2022.

A. Yamaguchi (invited), Y. Shigekawa, H. Haba, M. Wada, and H. Katori, "Laser spectroscopy of triply charged thorium ions towards a nuclear clock," 2022 URSI-Japan Radio Science Meeting (URSI-JRSM 2022), Bunkyo-ku, Tokyo, September 1–2, 2022.

W. Xian (oral), S. Chen, M. Rosenbusch, S. Yan, D. Hou, S. Iimura, A. Takamine, M. Wada, J. Lee, J. Liu, P. Schury, F. Browne, F. Flavigny, H. Haba, S. Kimura, H. Koura, T. Niwase, Y. Ito, T. Sonoda, T. M. Kojima, Y. X. Watanabe, S. Naimi, S. Michimasa, H. Miyatake, J. Y. Moon, S. Nishimura, H. Ishiyama, and H. Wollnik, "New mass measurements of neutron-rich nuclei of Ge, As, and Se, and an accuracy study of the new ZD-MRTOF system," The 28th International Nuclear Physics Conference (INPC 2022), Cape Town, South Africa, September 11–16, 2022.

S. Sakaguchi (poster) and M. Tanaka for nSHE Collaboration, "Probing optimal energy for synthesis of element 119 from ^{51}V + ^{248}Cm reaction," The 28th International Nuclear Physics Conference (INPC 2022), Cape Town, South Africa, September 11–16, 2022.

A. Takamine (invited), D. Kaji, H. Haba, M. Wada, P. Schury, H. Koura, H. Wollnik, H. Miyatake, H. Ishiyama, K. Morimoto, M. Rosenbusch, S. Kimura, T. Niwase, Y. Hirayama, Y. Ito, Y. Watanabe, and P. Brionnet, "Multi-reflection time-of-flight mass spectroscopy of superheavy nuclides," 19th International Conference on Electromagnetic Isotope Separators and Related Topics (EMIS 2022), Daejeon, Korea, October 3–7, 2022.

G. Damdinsuren (poster), M. Aikawa, K. Tegshjargal, N. Erdene, N. Ukon, and H. Haba, "Production cross sections of ^{198g}Au in proton-induced reactions on natural platinum," 2022 Symposium on Nuclear Data, Higashiosaka, Japan, November 17–18, 2022.

H. Haba (invited), "Production and distribution of radioisotopes at RIKEN RI Beam Factory," PRISMAP workshop on emerging infrastructures and technical developments, Padova, Italy & Online, November 21–22, 2022.

H. Haba (invited), "Production of radioisotopes for application studies at RIKEN RI Beam Factory—Search for new elements through diagnosis and therapy of cancer," The Fifth International Conference on Application of RadiotraCers and Energetic Beams in Sciences (ARCEBS 2023), Purulia, India, January 31–February 5, 2023.

Y. Shigekawa (oral), W. Yang, Y. Xiaojie, A. Nambu, and H. Haba, "Progress toward observing γ-rays emitted from ^{229m}Th by doping fluoride crystals with ^{229}Pa," The Fifth International Conference on Application of RadiotraCers and Energetic Beams in Sciences (ARCEBS 2023), Purulia, India, January 31–February 5, 2023.

H. Haba (invited), "Synthesis of radioactive isotope for gamma-ray imaging," Workshop on Double Photon Emission Computed Tomography and beyond, Bunkyo-ku, Japan, March 24, 2023.

[Domestic Conferences/Workshops]

髙島大輝 (口頭発表), 大貫和信, 眞鍋史乃, 古賀宣勝, 津村遼, 安西高廣, Wang Yang, Yin Xiaojie, 佐藤望, 重河優大, 南部明弘, 臼田祥子, 羽場宏光, 藤井博史, 安永正浩, 「アスコルビン酸 Na は放射線分解による能動的標的化の障害からアスタチン-211 結合抗体を保護する」, 第 38 回日本 DDS 学会学術集会, オンライン, 2022 年 6 月 29–30 日.

髙島大輝 (口頭発表), 眞鍋史乃, 大貫和信, 古賀宣勝, 津村遼, 安西高廣, Wang Yang, Yin Xiaojie, 佐藤望, 重河優大, 南部明弘, 臼田祥子, 羽場宏光, 藤井博史, 松村保広, 安永正浩, 「アルファ線放出核種アスタチン-211 結合抗体の前臨床試験」, 第 26 回日本がん分子標的治療学会学術集会, 金沢市, 2022 年 6 月 29 日–7 月 1 日.

渡部直史 (口頭発表), 仲定宏, 大江一弘, 豊嶋厚史, 王洋, 羽場宏光, 白神宜史, 「難治性甲状腺がんに対するアスタチンを用いた医師主導治験」, 第 59 回アイソトープ・放射線研究発表会, オンライン, 2022 年 7 月 6 日–8 日.

藤野隼輔 (口頭発表), 森健一, 山田崇裕, 羽場宏光, Wang Yang, Yin Xiaojie, 南部明弘, 「液体シンチレーション検出器を用いた効率トレーサ法による ^{211}At 放射能測定法の検討」, 第 59 回アイソトープ・放射線研究発表会, オンライン, 2022 年 7 月 6 日–8 日.

新井香純 (口頭発表), 今村正隆, 森大輝, 石津秀剛, 佐藤泰, 羽場宏光, Xiaojie Yin, Yang Wang, 脇谷雄一郎, 「Ac-225, At-211 放射能校正の検討」, 第 59 回アイソトープ・放射線研究発表会, オンライン, 2022 年 7 月 6 日–8 日.

岡井晃一 (口頭発表), Kjeld Beeks, 藤本弘之, 福永優太, 管明, 羽場宏光, 原秀明, 平木貴宏, 稲垣新, 小早川大貴, 笠松良崇, 北尾真司, 小無健司, 増田孝彦, 宮本祐樹, 笹尾登, Thorsten Schumm, 瀬戸誠, 重河優大, 高取沙悠理, 玉作賢治, 植竹智, 渡部司, 渡部信, 山口敦史, 安田勇輝, 依田芳卓, 吉見彰洋, 吉村浩司, 吉村太彦, 「トリウム 229 アイソマー状態からの脱励起に伴う真空紫外光の探索」, 日本物理学会 2022 秋季大会, 岡山市, 2022 年 9 月 6–8 日.

Guan Ming (口頭発表), 岡井晃一, Kjeld Beeks, 藤本弘之, 福永優太, 羽場宏光, 原秀明, 平木貴宏, 稲垣新, 小早川大貴, 笠松良崇, 北尾真司, 小無健司, 増田孝彦, 宮本祐樹, 笹尾登, Thorsten Schumm, 瀬戸誠, 重河優大, 高取沙悠理, 玉作賢治, 植竹智, 渡部司, 渡部信, 山口敦史, 安田勇輝, 依田芳卓, 吉見彰洋, 吉村浩司, 吉村太彦, "New methods in searching for vacuum ultraviolet signal from the isomeric state of 229-thorium," 日本物理学会 2022 秋季大会, 岡山市, 2022 年 9 月 6–8 日.

渡部直史 (口頭発表), 兼田加珠子, 白神宜史, 角永悠一郎, 大江一弘, 王洋, 羽場宏光, 豊嶋厚史, 深瀬浩一, 「^{211}At 標識 PSMA-5 を用いた標的アルファ線治療: 非臨床での評価」, 第 62 回日本核医学会学術総会, 京都市, 2022 年 9 月 7–11 日.

白神宜史 (口頭発表), 渡部直史, 兼田加珠子, 角永悠一郎, 大江一弘, 羽場宏光, 豊嶋厚史, 深瀬浩一, 「前立腺癌の α 線核医学治療に用いるアスタチン-211 標識 PSMA の調製」, 第 62 回日本核医学会学術総会, 京都市, 2022 年 9 月 7–11 日.

大江一弘 (口頭発表), 仲定宏, 白神宜史, 下瀬川恵久, 加藤弘樹, 巽光朗, 羽場宏光, 豊嶋厚史, 渡部直史, 「分化型甲状腺がんのアルファ線核医学治療第 I 相試験のためのアスタチン化ナトリウムの製造」, 第 62 回日本核医学会学術総会, 京都市, 2022 年 9 月 7–11 日.

青木貴稔 (口頭発表), 鳥井寿夫, 早水友洋, 中村圭佑, 長濱弘季, 田中香津生, 原田健一, 内山愛子, 畠山温, 高峰愛子, 上野秀樹, 市川雄一, 松田恭幸, 羽場宏光, 酒見泰寛, 「量子エンタングル Fr 原子を用いた電子 EDM の量子センシング」, 電子回路研究会「次世代周波数精密計測に向けた研究開発」, 小金井市, 2022 年 9 月 8 日.

山口敦史 (口頭発表), 重河優大, 羽場宏光, 和田道治, 香取秀俊, 「原子核時計実現にむけたトリウムイオントラップ装置の開発」, 日本物理学会 2022 秋季大会（物性）, 目黒区, 2022 年 9 月 12–15 日.

南部明弘 (ポスター発表), 殷小杰, 重河優大, 羽場宏光, 富田翔, 福森麻衣, 田沢周作, 「α 線核医学治療用核種 Pb-212 の製造に向けた Th-228 線源の取扱方法の検討」, 日本放射化学会第 66 回討論会 (2022), 文京区, 2022 年 9 月 15–17 日.

大江一弘 (ポスター発表), 渡部直史, 白神宜史, 南部明弘, 羽場宏光, 畑澤順, 「核医学利用に向けた Ce-141 の加速器製造と分離精製の検討」, 日本放射化学会第 66 回討論会 (2022), 文京区, 2022 年 9 月 15–17 日.

殷小杰 (ポスター発表), 南部明弘, 押切忍, 鈴木健太郎, 日野明弘, 羽場宏光, 「Production cross sections of ^{225}Ac and ^{225}Ra in the ^{232}Th(^{14}N, $xnyp$) reactions (2)」, 日本放射化学会第 66 回討論会 (2022), 文京区, 2022 年 9 月 15–17 日.

殷小杰 (ポスター発表), 福地知則, 渡辺恭良, 羽場宏光, 「Production of ^{44}Ti via the ^{45}Sc(p, $2n$)^{44}Ti reaction for ^{44}Ti/^{44g}Sc generator development」, 日本放射化学会第 66 回討論会 (2022), 文京区, 2022 年 9 月 15–17 日.

床井健運 (ポスター発表), 青戸宏樹, 渡邉瑛介, 篠原厚, 王洋, 羽場宏光, 笠松良崇, 豊嶋厚史,「ガスクロマトグラフィーを用いた At のハロゲン結合エネルギーの導出法の開発」, 日本放射化学会第 66 回討論会 (2022), 文京区, 2022 年 9 月 15–17 日.

細川浩由 (ポスター発表), 瀬戸彩乃, 永井歩夢, 中島朗久, 坂口綾, 羽場宏光, 横山明彦, 「Th ターゲット中に生成する Np の単離を目的とした高除染係数溶媒抽出法の検討」, 日本放射化学会第 66 回討論会 (2022), 文京区, 2022 年 9 月 15–17 日.

寺本高啓 (ポスター発表), 加納英明, WANG Yang, 羽場宏光, 豊嶋厚史, 「アスタチン化合物の表面増強ラマン分光」, 日本放射化学会第 66 回討論会 (2022), 文京区, 2022 年 9 月 15–17 日.

秋山和彦 (ポスター発表), 諏訪智也, 羽場宏光, 菊永英寿, 久冨木志郎, 「Pm を内包した二金属内包フラーレンの安定性に関する研究」, 日本放射化学会第 66 回討論会 (2022), 文京区, 2022 年 9 月 15–17 日.

益田遼太郎 (ポスター発表), 安田勇輝, 澤村慶, 重河優大, 宮本祐樹, 吉村浩司, 篠原厚, 笠松良崇, 「^{229m}Th の γ 線測定に向けた希ガスマトリックス単離装置の開発」, 日本放射化学会第 66 回討論会 (2022), 文京区, 2022 年 9 月 15–17 日.

永井雄太 (口頭発表), 我那覇功也, 西中一朗, 鷲山幸信, 殷小杰, 南部明弘, 羽場宏光, 横山明彦, 「Rn の液相回収と At のイオン液体

抽出による ^{211}Rn/^{211}At ジェネレータシステムの開発」, 日本放射化学会第 66 回討論会 (2022), 文京区, 2022 年 9 月 15–17 日.

我那覇功也 (口頭発表), 永井雄太, 西中一朗, 鷲山幸信, 股小杰, 南部明弘, 羽場宏光, 横山明彦, 「DIPE/HCl 系と HCl/イオン液体系の ^{211}At 溶媒抽出における線量効果について」, 日本放射化学会第 66 回討論会 (2022), 文京区, 2022 年 9 月 15–17 日.

久下恒明 (口頭発表), 増田寛喜, 杜婉瑩, 保田智彦, 杉山暁, 羽場宏光, 巽俊文, 秋光信佳, 熊倉嘉貴, 吉田寛, 瀬戸康之, 和田洋一郎, 野村幸世, 「胃癌腹膜播種モデルマウスを用いた ^{211}At 標識抗 FGFR4 抗体による放射線免疫療法の検討」, 日本放射化学会第 66 回討論会 (2022), 文京区, 2022 年 9 月 15–17 日.

中川創太 (口頭発表), 角永悠一郎, 大江一弘, 寺本高啓, 床井健運, 永田光知郎, 吉村崇, 羽場宏光, 王洋, 笠松良崇, 豊嶋厚史, 深瀬浩一, 篠原厚, 「電解酸化反応を用いたチロシン上ヨウ素-アスタチン置換反応」, 日本放射化学会第 66 回討論会 (2022), 文京区, 2022 年 9 月 15–17 日.

永井歩夢 (口頭発表), 細川浩由, 中島朗久, 坂口綾, 南部明弘, 重河優大, 羽場宏光, 横山明彦, 「^{232}Th + ^{7}Li 核反応によって生成する U 同位体の ICP-MS による定量」, 日本放射化学会第 66 回討論会 (2022), 文京区, 2022 年 9 月 15–17 日.

重河優大 (口頭発表), Wang Yang, Yin Xiaojie, 南部明弘, 羽場宏光, 「Th-229*m* の γ 線観測に向けた Pa-229 のフッ化物結晶への導入法及び光子測定装置の開発」, 日本放射化学会第 66 回討論会 (2022), 文京区, 2022 年 9 月 15–17 日.

渡邉瑛介 (口頭発表), 笠松良崇, 横北卓也, 中西諒平, 大髙咲希, 板倉悠大, 益田遼太郎, 王瑞麟, 重河優大, 南部明弘, 殷小杰, 羽場宏光, 高宮幸一, 篠原厚, 「クラウンエーテルを用いた 102 番元素ノーベリウムの硝酸系固液抽出実験」, 日本放射化学会第 66 回討論会 (2022), 文京区, 2022 年 9 月 15–17 日.

中西諒平 (口頭発表), 渡邉瑛介, 大髙咲希, 王瑞麟, 板倉悠大, 速水翔, 羽場宏光, 南部明弘, 篠原厚, 笠松良崇, 「Rf の共沈実験に向けた Zr, Hf, Th のシュウ酸, マロン酸系でのフロー式共沈実験」, 日本放射化学会第 66 回討論会 (2022), 文京区, 2022 年 9 月 15–17 日.

黒田拓真 (口頭発表), 西村峻, 秋山和彦, 羽場宏光, 高宮幸一, 久冨木志郎, 「ランタノイド内包フラーレン（$Ln^{3+}@C_{82}{}^{3-}$）における HPLC 溶出挙動の熱力学的解析」, 日本放射化学会第 66 回討論会 (2022), 文京区, 2022 年 9 月 15–17 日.

白神宜史 (口頭発表), 角永悠一郎, 渡部直史, 兼田加珠子, 神野直哉, 大江一弘, 羽場宏光, 豊嶋厚史, 深瀬浩一, 「^{211}At 標識 PSMA 誘導体による前立腺がん α 線核医学治療」, 第 5 回日本核医学会分科会放射性薬品科学研究会/第 21 回放射性医薬品・画像診断薬研究会, 福井市, 2022 年 9 月 17 日.

高橋浩之 (口頭発表), 島添健次, 関野正樹, 鎌田圭, 羽場宏光, 百瀬敏光, 「2 光子ガンマ線の多次元空間の相関を用いた高次イメージング法の研究」, 2022 年第 83 回応用物理学会秋季学術講演会, 仙台市 & オンライン, 2022 年 9 月 20–23 日.

久下恒明 (口頭発表), 増田寛喜, 杜婉瑩, 保田智彦, 杉山暁, 羽場宏光, 巽俊文, 秋光信佳, 熊倉嘉貴, 吉田寛, 瀬戸泰之, 和田洋一郎, 野村幸世, 「胃癌腹膜播種モデルマウスを用いた腹膜播種に対する ^{211}At 標識抗 FGFR4 抗体による放射線免疫療法の検討」, 第 81 回日本癌学会学術総会, 横浜市, 2022 年 9 月 29 日–10 月 1 日.

高島大輝 (口頭発表), 大貫和信, 眞鍋史乃, 古賀宣勝, 津村遼, 安西高廣, 王洋, 殷小杰, 佐藤望, 重河優大, 南部明弘, 臼田祥子, 羽場宏光, 藤井博史, 安永正浩, 「アスコルビン酸 Na は放射線分解による能動的標的化の障害からアスタチン-211 結合抗体を保護する」, 第 81 回日本癌学会学術総会, 横浜市, 2022 年 9 月 29 日–10 月 1 日.

重河優大 (招待講演), 「超低エネルギー励起核 U-235*m* と Th-229*m* の核壊変特性に関する研究」, 電気学会 2022 年度第 1 回調査専門委員会, 文京区, 2022 年 10 月 28 日.

羽場宏光 (依頼講演), 「新元素でがん治療〜理研 RI ビームファクトリーがつくるラジオアイソトープ〜」, 放射線安全フォーラム第 75 回放射線防護研究会「短寿命核種の利用の拡大に向けて」, 文京区 & オンライン, 2022 年 10 月 29 日.

藤野隼輔 (口頭発表), 森健一, 山田崇裕, 羽場宏光, Wang Yang, Yin Xiaojie, 南部明弘, 「^{211}At 固体線源作成手法の検討」, 第 4 回日本保健物理学会・日本放射線安全管理学会合同大会, 福岡市, 2022 年 11 月 24–26 日.

横田望海 (口頭発表), 若狭智嗣, 西畑洸希, 岸本侃己, 米村千恵子, 笹野匡紀, 三木謙二郎, 今井伸明, 上坂友洋, 浦山廉, 大田晋輔, 亀谷晃毅, 竹田浩之, 波多野雄治, 羽場宏光, 早水友洋, 原正憲, 道正新一郎, 他 RIBF-SHARAQ11 Collaboration, 「^{3}H(t,^{3}He)^{3}n 反応による 3 中性子系探索に向けた中性子測定系の開発」, 第 128 回日本物理学会九州支部例会, 熊本市, 2022 年 12 月 3 日.

山口敦史 (招待講演), 重河優大, 羽場宏光, 和田道治, 香取秀俊, 「原子核時計実現にむけたトリウムイオンのトラップとレーザー分光」, レーザー学会学術講演会第 43 回年次大会, 名古屋市, 2023 年 1 月 18–20 日.

重河優大 (口頭発表), 「Th-229*m* イオンの引き出しとイオントラップ実験の現状」, 2022 重元素化学研究会, あわら市, 2023 年 3 月 20 日–21 日.

田中聡 (口頭発表), 石川知輝, 河西壱輝, 岡本直大, 早水友洋, A. Kastberg, B. K. Sahoo, B. P. Das, 西野仁, 小野崇人, 羽場宏光, 東條賢, 酒見泰寛, 松尾由賀利, 鳥井寿夫, 青木貴稔, 「ダークマター探索のための Cs 原子の磁気光学トラップ」, 日本物理学会 2023 年春季大会, オンライン, 2023 年 3 月 22–25 日.

福永優太 (口頭発表), Kjeld Beeks, 藤本弘之, 平木貴宏, 管明, 羽場宏光, 笠松良崇, 北尾真司, 小無健司, 増田孝彦, 永澤延元, 岡井晃一, 笹尾登, Fabian Schaden, Thorsten Schumm, 瀬戸誠, 重河優大, 高取沙悠理, 玉作賢治, 植竹智, 渡部司, 渡部信, 山口敦史, 安田勇輝, 依田芳卓, 吉見彰洋, 吉村浩司, 吉村太彦, 「トリウム 229 アイソマー準位探索のための核共鳴散乱標的の開発」, 日本物理学会 2023 年春季大会, オンライン, 2023 年 3 月 22–25 日.

平木貴宏 (口頭発表), Kjeld Beeks, 藤本弘之, 福永優太, 管明, 羽場宏光, 笠松良崇, 北尾真司, 小無健司, 増田孝彦, 永澤延元, 岡井晃一, 笹尾登, Fabian Schaden, Thorsten Schumm, 瀬戸誠, 重河優大, 高取沙悠理, 玉作賢治, 植竹智, 渡部司, 渡部信, 山口敦史, 安田勇輝, 依田芳卓, 吉見彰洋, 吉村浩司, 吉村太彦, 「トリウム 229 アイソマー状態からの脱励起真空紫外光の探索」, 日本物理学会 2023 年春季大会, オンライン, 2023 年 3 月 22–25 日.

高取沙悠理 (口頭発表), Kjeld Beeks, 藤本弘之, 福永優太, 管明, 羽場宏光, 平木貴宏, 笠松良崇, 北尾真司, 小無健司, 増田孝彦, 永澤延元, 岡井晃一, 笹尾登, Fabian Schaden, Thorsten Schumm, 瀬戸誠, 重河優大, 玉作賢治, 植竹智, 渡部司, 渡部信, 山口敦史, 安田勇輝, 依田芳卓, 吉見彰洋, 吉村浩司, 吉村太彦, 「固体原子核時計の実現へ向けた放射光 X 線を用いたトリウム 229 結晶の特性評価」, 日本物理学会 2023 年春季大会, オンライン, 2023 年 3 月 22–25 日.

眞鍋史乃 (口頭発表), 高島大輝, 羽場宏光, 安永正浩, 藤井博史, 「有機化学・医学・核化学融合による α 線治療への試み」, 日本薬

学会第 143 年会, 札幌市, 2023 年 3 月 25–28 日.

山ノ内邑希 (ポスター発表), 坂口聡志, Pierre Brionnet for nSHE Collaboration, 「新元素合成のための最適反応エネルギー推定に向けた ^{51}V + ^{159}Tb 融合反応の励起関数測定」, 日本物理学会 2023 年春季大会, オンライン, 2023 年 3 月 22–25 日.

深津巧光 (ポスター発表), 坂口聡志, Pierre Brionnet for nSHE Collaboration, 「新元素合成のための最適反応エネルギー推定に向けた ^{51}V + ^{159}Tb 融合反応の障壁分布測定 I」, 日本物理学会 2023 年春季大会, オンライン, 2023 年 3 月 22–25 日.

道本優也 (ポスター発表), 坂口聡志, Pierre Brionnet for nSHE Collaboration, 「新元素合成のための最適反応エネルギー推定に向けた ^{51}V + ^{159}Tb 融合反応の障壁分布測定 II」, 日本物理学会 2023 年春季大会, オンライン, 2023 年 3 月 22–25 日.

上原大祐 (口頭発表), 長濱弘季, 中村圭佑, 佐藤幹, 中下輝士, 小澤直也, 永瀬慎太郎, 深瀬実来, 青木貴稔, 山口敦史, 高峰愛子, 上野秀樹, 酒見泰寛, 「レーザー冷却フランシウム源実現に向けた金属表面における中性脱離反応の研究」, 日本物理学会 2023 年春季大会, オンライン, 2023 年 3 月 22–25 日.

深瀬実来 (口頭発表), 長濱弘季, 中村圭佑, 小澤直也, 佐藤幹, 中下輝士, 永瀬慎太郎, 上原大祐, 高峰愛子, 上野秀樹, 酒見泰寛, 「フランシウム原子の永久双極子能率探索に向けた高周波二重極質量フィルターの開発」, 日本物理学会 2023 年春季大会, オンライン, 2023 年 3 月 22–25 日.

小澤直也 (口頭発表), 長濱弘季, 中村圭佑, 佐藤幹, 中下輝士, 永瀬慎太郎, 上原大祐, 深瀬実来, 青木貴稔, 山口敦史, 高峰愛子, 上野秀樹, 酒見泰寛, 「永久電気双極子能率探索を目指した冷却フランシウム原子源の開発」, 日本物理学会 2023 年春季大会, オンライン, 2023 年 3 月 22–25 日.

Press Release

難治性前立腺がんをアルファ線で攻撃—阪大発の治療薬を用いた医師主導治験の準備を開始—, 大阪大学, 理化学研究所, アルファフュージョン社, 2022 年 11 月 17 日, https://www.riken.jp/press/2022/20221117_2 .

Awards

羽場宏光, 「アルファ線核医学治療に向けたアスタチン-211 の大量製造技術の開発」, 2022 年度理研栄峰賞, 2023 年 3 月 22 日.

重河優大, 「Estimation of radiative half-life of ^{229m}Th by half-life measurement of other nuclear excited states in ^{229}Th (^{229}Th 原子核の励起準位の半減期測定による ^{229m}Th の γ 線放出半減期の推定)」, 第 14 回理研研究奨励賞 (桜舞賞), 2023 年 3 月 22 日.

Outreach Activities

羽場宏光 (依頼講演), 「新元素でがん治療—RIBF がつくるラジオアイソトープ—」, 理研と未来を創る会第 28 回講演会, 和光市, 2022 年 9 月 6 日.

羽場宏光 (依頼講演), 「ラジオアイソトープの製造を通じた産業振興」, シンポジウム「理化学研究所仁科研究室のキセキ」, 和光市 & オンライン, 2022 年 10 月 28 日.

羽場宏光 (依頼講演), 「ニホニウム発見への道のり」, 山梨県立吉田高等学校理研見学会, 和光市, 2022 年 11 月 16 日.

Accelerator Applications Research Division
RI Application Research Group
Industrial Application Research Team

1. Abstract

Industrial application research team handles non-academic activities at RIBF corresponding mainly to industries.

2. Major Research Subjects

Support of industrial utilization of the RIBF accelerator beam.

3. Summary of Research Activity

RNC promote facility-sharing program "Promotion of applications of high-energy heavy ions and RI beams." In this program, RNC opens a part of the RIBF facility, which includes the AVF cyclotron, RIKEN Ring Cyclotron and experimental instruments, to non-academic proposals from users including private companies. The proposals are reviewed by a program advisory committee, industrial PAC (IN-PAC). The proposals which have been approved by the IN-PAC are allocated with beam times and the users pay RIKEN the beam time fee. The intellectual properties obtained by the use of RIBF belong to the users. In order to encourage the use of RIBF by those who are not familiar with utilization of ion beams, the first two beam times of each proposal can be assigned to trial uses which are free of beam time fee.

In July 2022, the IN-PAC met and approved fee-based proposals from private companies; four proposals from new companies and three proposals from continuously using companies. In January 2023, the IN-PAC held a mail review and approved five fee-based proposals from continuous users. In 2022, five companies executed 15 fee-based beamtimes, ten of which utilized a Kr beam with a total beam time of 146 hours, four utilized an Ar beam with a total beam time of 65 hours and one of which utilized a C beam with a total beam time of 11 hours.

Members

Team Leader
Atsushi YOSHIDA

Special Temporary Technical Scientist
Kowashi WATANABE

Research Consultant
Tadashi KAMBARA

List of Publications & Presentations

Publication

[Book]

吉田敦, 「2.2 応用研究 I—宇宙開発と加速器」, 量子ビーム科学の基礎と応用: 原子力システム研究懇話会 (NSA コメンタリーシリーズ), NSA/COMMENTARIES: No.27, pp. 40–45, ISBN978-4-88911-315-0.

Presentation

[Seminar]

吉田敦, 「照射施設利用の効率化について〜理研・仁科加速器センターの取り組み〜」, 経産省: 放射線試験・ソフトエラー対策に関する勉強会 (第 10 回), オンライン, 2022 年 5 月 13 日.

Other

Fee-based beamtimes for private companies: Kr beam 146 hours, Ar beam 65 hours, C beam 1 hour; 222 hours in total.

Subnuclear System Research Division
Strangeness Nuclear Physics Laboratory

1. Abstract

Unlike many-body systems, few-body systems can be described with microscopic theories that can be solved without approximations. To this end the laboratory uses numerical techniques to exactly solve the equations describing few-body quantum systems. In particular, an accurate calculation method called the 'Gaussian Expansion Method using infinitesimally shifted Gaussian lobe basis function' has been developed. This method makes calculations tractable up to five bodies even with complicated interactions. It has been applied to various three-, four- and five-body calculations in hypernuclei, light nuclear systems, as well as cold-atom systems. These calculations have provided new insights into these various fields of physics.

2. Major Research Subjects

(1) Structure of hypernuclei
(2) Neutron-rich nuclei
(3) Few-body universality in nuclear and atomic systems
(4) Structure of exotic hadron system
(5) Equation of state for neutron stars

3. Summary of Research Activity

(1) Hypernuclei

We have investigated the role of hyperons in the structure of atomic nuclei. Using the antisymmetrized quasi-cluster model (AQCM), we investigated the role of up to two Λ hyperons in isotopes of Be and C. The presence of the Λ hyperons attract the α clusters to distances where the spin-orbit interaction can break the cluster structure. We found that while the reduction of the cluster structure is significant in C, it remains limited for Be. We have also proposed a new way to study the spin-isospin dependence of the ΞN interaction by adding α particles in order to make a ΞN pair bound without altering its spin-isospin structure. The energy levels were calculated by the Gaussian Expansion Method (GEM) using ab-initio ΞN potentials obtained from lattice QCD calculations. It was found that the pair becomes bound in the presence of two α particles, leading to spin-doublet bound states in both the isospin triplet and singlet channels. The calculation predicts that the spin-doublet energies are inverted when the isospin configuration is changed, revealing the isospin dependence of the ΞN interaction. We proposed to check these predictions in experiments involving K mesons on ^{10}B targets to produce Ξ$N\alpha\alpha$ bound states.

(2) Neutron-rich nuclei

We have investigated the possible exis tence of a ^{7}H resonant state, by modelling this system as an effective ^{3}H-n-n 5-body system solved with the GEM. We found no narrow resonance but a broad structure at $E_R \approx 9$ MeV above this threshold corresponding to the ^{7}H ground state. In a separate work, we have devised a reaction model to describe the fast removal of the α-particle in ^{8}He nucleus leading to the emission of 4 neutrons. Our model explains the energy peak observed in experiment as consequence of dineutron-dineutron correlation rather than the existence of a hypothetical tetraneutron.

(3) Few-body universality

We have investigated the universal geometry of three-body halos made of loosely bound core and two particles, such as two-neutron halo nuclei. This geometry could be calculated analytically. It was found that in absence of resonance between the two particles, the size of the halo increases logarithmically with the inverse of the binding energy, but close to the resonance between the two particles, it becomes proportional to the inverse of the binding energy. These analytical universal properties were also shown to apply to Efimov states that are observable in cold-atom experiments. In a different work, we looked at the specific case of the two-neutron halo of ^{19}B, computing its properties numerically using the GEM and the Faddeev method. These calculations confirmed that its geometrical properties are model-independent.

(4) Exotic hadron systems

We have used chiral effective theories of diquarks and quark-diquark to investigate doubly heavy tetraquarks $Q_{\bar{q}\bar{q}}$ and singly heavy baryons Q_{qq}. We also used extended quark models to investigate the fully charmed tetraquark resonant states $cc\bar{c}\bar{c}$ as well as p-wave B_S states. From these calculations, we could reproduce some experimental data and make predictions for unobserved states. In addition, we investigated the hadron mass spectrum of two-color QCD at finite density using the linear sigma model, as well as lattice calculations. Other research activities include the study of SU(N) Yang-Mills theory and the Dirac Kondo effect under magnetic catalysis.

(5) Equation of state for neutron stars

To obtain the equation of state of neutron stars at the hadron-quark crossover we interpolated the relativistic mean-field (RMF) model and Nambu-Jona-Lasinio (NJL) model with an interpolation method that reduces randomness. In a different work, we also resolved the technical problem of spurious states appearing the numerical solutions of the Dirac equation solved with the finite-difference method.

Members

Director
Emiko HIYAMA

Senior Research Scientists
Takumi DOI
Pascal NAIDON

Contract Researcher
Etsuko ITOU

Special Postdoctoral Researchers
Tokuro FUKUI
Daisuke YOSHIDA
Daiki SUENAGA

Postdoctoral Researchers
Lucas M.C. HAPP
Akira MATSUMOTO

Research Consultants
Shoji SHINMURA
Wolfram WEISE (TU Munich)

Senior Visiting Scientist
Makoto OKA (JAEA)

Visiting Scientists
Masayuki ASAKAWA (Osaka Univ.)
Kadir Utku CAN (The Univ. of Adelaide)
Jaume CARBONELL (I'rene Joliot-Curie Lab.)
Akinobu DOTE (KEK)
Shimpei ENDO (Tohoku Univ.)
Tobias FREDERICO (Technological Inst. of Aeronautics)
Tomokazu FUKUDA (Univ. of Electro-Commun.)
Yasuro FUNAKI (Kanto Gakuin Univ.)
Takenori FURUMOTO (Yokohama Nat'l Univ.)
Philipp GUBLER (JAEA)
Satoru HIRENZAKI (Nara Women's Univ.)
Atsushi HOSAKA (Osaka Univ.)
Jinniu HU (Nankai Univ.)
Tetsuo HYODO (Tokyo Metropolitan Univ.)
Yoichi IKEDA (Osaka Univ.)
Masahiro ISAKA (Hosei Univ.)
Souichi ISHIKAWA (Hosei Univ.)
Daisuke JIDO (Tokyo Tech)
Hyun-Chul KIM (Inha Univ.)
Toshio MOTOBA (Univ. of Electro-Commun.)
Takayuki MYO (Osaka Inst. of Tech.)
Sho NAGAO (Univ. of Tokyo)
Satoshi NAKAMURA (Univ. of Tokyo)
Kazuma NAKAZAWA (Gifu Univ.)
Hidekatsu NEMURA (Kyoto Univ.)
Jean-Marc RICHARD (Lyon Univ.)
Thomas RIJKEN (Univ. Of Nijmegen)
Shoichi SASAKI (Tohoku Univ.)
Hans-Josef SCHULZE (INFN)
Tingting SUN (Zhengzhou Univ.)
Masanori TACHIKAWA (Yokohama City Univ.)
Hiroyuki TAJIMA (Univ. of Tokyo)
Masaaki TOKIEDA (The Nat'l Inst. for Res. in Computer Sci. and Automation (INRIA))
Hui TONG (Tianjin Normal Univ.)
Atsushi UMEYA (Nippon Inst. of Tech.)
Shin WATANABE (NIT, Gifu College)
Chengjun XIA (Yangzhou Univ.)
Masanobu YAHIRO (Kyushu Univ.)
Ulugbek YAKHSHIEV (Inha Univ.)
Taiichi YAMADA (Kanto Gakuin Univ.)
Yasuo YAMAMOTO (Tsuru Univ.)
Nodoka YAMANAKA (Nagoya Univ.)
Takuma YAMASHITA (Tohoku Univ.)
Ying ZHANG (Tianjin Univ.)
Xian-Rong ZHOU (East China Normal Univ.)

Student Trainees
Moemi MATSUMOTO (Tohoku Univ.)
Shuhei OHNO (Yokohama City Univ.)

Administrative Part-time Worker
Yoko FUJITA

List of Publications & Presentations

Publications

[Original Papers]

N. Itagaki and E. Hiyama, "Cluster-shell competition and effect of adding hyperons," Phys. Rev. C **107**, 024309 (2023).

E. Hiyama, M. Isaka, T. Doi, and T. Hatsuda, "Probing the ΞN interaction through inversion of spin-doublets in $\Xi N\alpha\alpha$ nuclei," Phys. Rev. C **106**, 064318 (2022).

E. Hiyama, R. Lazauskas, J. Carbonell, and T. Frederico, "Scaling of the ^{19}B two-neutron halo properties close to unitarity," Phys. Rev. C **106**, 064001(2022).

E. Hiyama, R. Lazauskas, and J. Carbonell, "^{7}H ground state as a ^{3}H + 4n resonance," Phys. Lett. B **833**, 137367 (2022).

S. Choi, E. Hiyama, C. -H. Hyun, and M. -K. Cheoun, "Effects of many-body interactions in hypernuclei with Korea-IBS-Daegu-SKKU functionals," Eur. Phys. J. A **58**, 8 (2022).

T. Yamashita, Y. Kino, E. Hiyama, S. Jonsell, and P. Froelich, "Near-threshold behavior of positronium-antihydrogen scattering cross sections," Phys. Rev. A **105**, 052812 (2022).

K. Murakami, Y. Akahoshi, S. Aoki, T. Doi, and K. Sasaki (HAL QCD Collaboration), "Lattice quantum chromodynamics (QCD) studies on decuplet baryons as meson-baryon bound states in the HAL QCD method," Prog. Theor. Exp. Phys. **2023**, 043B05 (2023).

Y. Lyu, T. Doi, T. Hatsuda, Y. Ikeda, J. Meng, K. Sasaki, and T. Sugiura, "Attractive N-phi interaction and two-pion tail from lattice QCD near physical point," Phys. Rev. D **106**, 074507 (2022).

Y. Lyu, H. Tong, T. Sugiura, S. Aoki, T. Doi, T. Hatsuda, J. Meng, and T. Miyamoto, "Optimized two-baryon operators in lattice QCD," Phys. Rev. D **105**, 074512 (2022).

P. Naidon, L. Pricoupenko, and C. Schmickler, "Shallow trimers of two identical fermions and one particle in resonant regimes," SciPost Phys. **12**, 185 (2022).

Z. Yang, G. J. Wang, J. J. Wu, M. Oka, and S. L. Zhu, "The investigations of the P-wave B_S states combining quark model and lattice QCD in the coupled channel framework," J. High Energy Phys. **01**, 058-1–19 (2023).

G. J. Wang, Q. Meng, and M. Oka, "The S-wave fully-charmed tetraquark resonant states," Phys. Rev. D **106**, 096005-1–9 (2022).

N. Yamanaka and M. Oka, "Weinberg operator contribution to the CP-odd nuclear force in the quark model," Phys. Rev. D **106**, 075021-1–15 (2022).

Y. Kim, M. Oka, and K. Suzuki, "Doubly heavy tetraquarks in a chiral-diquark picture," Phys. Rev. D **105**, 074021-1–17 (2022).

Y. Kim, M. Oka, D. Suenaga, and K. Suzuki, "Strong decays of singly heavy baryons from a chiral effective theory of diquarks," Phys. Rev. D **107**, 074015 (2023).

D. Suenaga and M. Kitazawa, "Effective model for pure Yang-Mills theory on $T^2 \times R^2$ with Polyakov loops," Phys. Rev. D **107**, 074502 (2023).

D. Suenaga, K. Murakami, E. Itou, and K. Iida, "Probing the hadron mass spectrum in dense two-color QCD with the linear sigma model," Phys. Rev. D **107**, 054001 (2023).

M. Furushima, M. Takagi, D. Yoshida, Y. Kita, T. Shimazaki, and M. Tachikawa, "Theoretical investigations of positron affinities and their structure-dependent properties of carbon dioxide clusters $(CO_2)_n$ (n = 1–5)," Phys. Chem. Chem. Phys. **25**, 625 (2022).

D. Yoshida, Y. Kita, T. Shimazaki, and M. Tachikawa, "A comprehensive theoretical study of positron binding and annihilation properties of hydrogen bonded binary molecular clusters," Phys. Chem. Chem. Phys. **24**, 26898 (2022).

[Proceedings]

T. Yamashita, E. Hiyama, K. Piszczatowski, S. Jonsell, and P. Froelich, "A four-body calculation of s-wave resonant scattering between positronium and antihydrogen atom," JJAP Conf. Proc. **9**, 011002 (2023).

T. Doi, Y. Lyu, H. Tong, T. Sugiura, S. Aoki, T. Hatsuda, J. Meng, and T. Miyamoto, "Finite volume analysis on systematics of the derivative expansion in HAL QCD method," PoS LATTICE **2021**, 564 (2022).

Y. Lyu, H. Tong, T. Sugiura, S. Aoki, T. Doi, T. Hatsuda, J. Meng, and T. Miyamoto, "Most charming dibaryon near unitarity," PoS LATTICE **2021**, 606 (2022).

T. Sugiura, Y. Akahoshi, T. Aoyama, T. M. Doi, and T. Doi, "Nuclear force with LapH smearing," PoS LATTICE **2021**, 565 (2022).

Y. Akahoshi, S. Aoki, and T. Doi, "Emergence of the rho resonance from the HAL QCD potential," PoS LATTICE **2021**, 625 (2022).

Y. Kamiya, K. Sasaki, T. Fukui, T. Hyodo, K. Morita, K. Ogata, A. Ohnishi, and T. Hatsuda, "Femtoscopic study on the ΛΛ-NΞ interaction," Supl. Rev. Mex. Fis. **3**, 0308124 (2022).

A. Ohnishi, Y. Kamiya, K. Sasaki, T. Fukui, T. Hyodo, K. Morita, K. Ogata, and T. Hatsuda, "Femtoscopic study of coupled-channel baryon-baryon interactions with $S = -2$," Proc. Sci. **380**, 212 (2022).

K. Murakami, D. Suenaga, E. Itou, and K. Iida, "Measurement of hadron masses in 2-color finite density QCD," PoS LATTICE **2022**, 154 (2023).

D. Suenaga, "Roper-like singly heavy baryons in a chiral model," Rev. Mex. Fis. Suppl. **3**, 0308025 (2022).

Presentations

[International Conferences/Workshops]

E. Hiyama (invited), "Structure of light Ξ hypernuclei and ΞN interaction," 66th OMEG-SSANP Workshop, Seoul, Korea, February 22, 2023.

E. Hiyama (invited), "Structure of heavy hydrogen nucleus, ^{7}H with t + 4n cluster model," Fudan Frontiers of Nuclear Physics Open Forum, Online, January 11, 2023.

E. Hiyama (invited), "Structure of Ξ hypernuclei and ΞN interaction," EMMI Workshop "Meson and Hyperon Interactions with Nuclei" Kitzbühel, Austria, September 14–16, 2022.

E. Hiyama (invited), "The resonance of ^{7}H with t + 4n model," Nuclear Physics at the Edge of Stability, Trento Italy, July 4–8, 2022.

E. Hiyama (invited), "Structure of light Ξ hypernuclei," 14th International Conference on Hypernuclear and Strange Particle Physics (HYP2022), Prague, Czech Republic & Online, June 27–July 1, 2022.

T. Doi and G. Mantzaridis (invited), "$p\Omega$ and ΛΞ: experimental and theoretical overview," workshop on Femtoscopy in high-energy collisions at ALICE (FemTUM 2022), Munich, Germany & Online, August 31–September 2, 2022.

T. Doi for HAL QCD Collaboration (invited), "Nuclear physics from lattice QCD," 15th Asia Pacific Physics Conference (APPC15), Seoul, Korea & Online, August 21–26, 2022.

T. Doi for HAL QCD Collaboration (invited), "Lattice QCD study of hadron interactions with strangeness," 14th International Conference on Hypernuclear and Strange Particle Physics (HYP2022), Prague, Czech & Online, June 27–July 1, 2022.

P. Naidon (invited), "Universal geometry of Borromean halo states," The 3rd Japan-France Workshop "Few-body problems in Physics—From atoms to quarks," Tohoku University, Sendai, Japan, February 27–March 3, 2023.

P. Naidon (invited), "Few- and many-body physics of mass-imbalanced two-component systems," Lecture at the programme "Living Near Unitarity," Kavli Institute for Theoretical Physics, UC Santa Barbara, Santa Barbara, U. S. A, May 12, 2022.

M. Oka, "Chiral effective theory of diquarks and application to heavy hadron spectrum," 14th International Conference on Hypernuclear and Strange Particle Physics (HYP2022), Prague, Czech Republic & Online, June 27–July 1, 2022.

T. Fukui (oral), "Shell model study of chiral three-nucleon force," Physics of RI: Recent Progress and Perspectives, RIKEN, Wako, Japan, May 31–June 1, 2022.

T. Fukui (oral), "Shell model study of chiral three-nucleon force," Developments of Physics of Unstable Nuclei (YKIS2022b), YITP, Kyoto University, Kyoto, Japan, May 9 –June 17, 2022.

D. Suenaga (oral), "Modifications of diquark masses at finite density," 3rd J-PARC HEF-ex WS, Tokai, Japan, March 14–16, 2023.

D. Suenaga (oral), "Phase structure of pure Yang-Mills theory in an anisotropic system: A new extreme condition of QCD" The 9th International Conference on Quarks and Nuclear Physics, Online, September 5–9, 2022.

D. Suenaga (oral), "Phase structure of pure Yang-Mills theory in an anisotropic system: A new extreme condition of QCD," The XVth Quark Confinement and the Hadron Spectrum Conference, University of Stavanger, Stavanger, Norway, August 1–6, 2022.

L. Happ (invited), "Universal effects in one dimension," The 3rd Japan-France Workshop "Few-body problems in Physics—From atoms to quarks," Sendai, Japan, February 27–March 3, 2023.

[Domestic Conferences/Workshops]

肥山詠美子 (招待講演), 「少数多体系物理からみたハイパー核の現在と将来」, 「ハイパー核研究の進展と未来〜格致日新〜」, 仙台市 (東北大学), 2022 年 12 月 17 日.

肥山詠美子 (口頭発表), 「クラスター観点からみた軽い中性子過剰原子核とハイパー核の構造」, 大阪公立大研究会「原子核におけるクラスター物理の新展」, 大阪市 (大阪公立大学), 2022 年 10 月 19–20 日.

土井琢身 for HAL QCD collaboration (口頭発表), 「物理点 QCD 配位におけるバリオン間相互作用 (Strangeness = −4, 0) 」, 日本物理学会 2023 年春季大会, オンライン, 2023 年 3 月 22–25 日.

P. Naido (invited), "Mass-imbalanced two-component system," 基研・iTHEMS 国内モレキュール型研究会 2022 「少数系の量子ダイナミクス」, 京都市 (京都大学基礎物理学研究所), 2022 年 8 月 22 日–26 日.

P. Naidon (invited), "Efimov physics and low-energy universality in few-body systems," The YONUPA Summer School, Online, August 7–9, 2022.

岡眞, "Fully-charmed tetraquark and quark confinement," ELPH 研究会 C033「ハドロン分光に迫る反応と構造の物理」, 仙台市 (ELPH), 2022 年 12 月 6–7 日.

M. Oka, D. Jido, G. J. Wang, 「マルチクォーク系のクォーク閉込めポテンシャル」, 日本物理学会 2022 年秋季大会, 岡山市 (岡山理科大学), 2022 年 9 月 6–8 日.

福井徳朗（口頭発表）, 「カイラル相互作用による軽い核のクラスター構造の理解に向けて」, 大阪公立大研究会「原子核におけるクラスター物理の新展開」, 大阪市 (大阪公立大学), 2022 年 10 月 19–20 日.

T. Fukui (oral), L. Coraggio, G. De Gregorio, A. Gargano, N. Itaco, 「カイラル 3 体力のテンソル構造と軽い核のスピン軌道分離」, 日本物理学会 2022 年秋季大会, 岡山市 (岡山理科大学), 2022 年 9 月 6–8 日.

末永大輝 (口頭発表), "Mass modifications of diquarks in medium from chiral symmetry and anomaly," J-PARC ハドロン研究会 2023, オンライン, 2023 年 3 月 27–29 日.

末永大輝 (口頭発表), 「NJL 模型に基づいた有限密度系のダイクォークの性質変化」, 日本物理学会 2023 年春季大会, オンライン, 2023 年 3 月 22–25 日.

末永大輝 (口頭発表), "Modifications of diquark masses at finite density with chiral symmetry restoration," RCNP workshop on Hadron Physics at the LEPS2 photon beamline, 佐用郡 (SPring-8), 2023 年 3 月 6–7 日.

末永大輝 (招待講演), "Pentaquark picture for singly heavy baryons from chiral symmetry and anomaly," Physics of heavy-quark and exotic hadrons 2023, 那珂郡 (J-PARC), 2023 年 1 月 30–31 日.

末永大輝 (口頭発表), 「カイラル対称性とアノマリーに着目したペンタクォーク的ヘビーバリオンの性質」, ELPH 研究会 C033「ハドロン分光に迫る反応と構造の物理」, 仙台市 (ELPH), 2022 年 12 月 6–7 日.

末永大輝 (基調講演), 「非等方空間における pure Yang-Mills 理論の相構造: QCD の新しい極限環境としての非等方系」, 熱場の量子論 2022, 京都市 (京都大学基礎物理学研究所), 2022 年 9 月 20–22 日.

末永大輝 (口頭発表), 「線形シグマ模型を用いた 2 カラー QCD 物質中のハドロン質量変化」, 日本物理学会 2022 年秋季大会, 岡山市 (岡山理科大学), 2022 年 9 月 6–8 日.

末永大輝 (口頭発表), 「QCD の新しい極限環境としての非等方ユークリッド空間」, 日本物理学会 2022 年秋季大会, 岡山市 (岡山理科大学), 2022 年 9 月 6–8 日.

伊藤駿平, 吉田大輔, 北幸海, 島崎智実, 立川仁典 (口頭発表), 「量子モンテカルロ法を用いた分子ジアニオンの陽電子束縛に関する理論研究」, 第 16 回分子科学討論会, 横浜市 (慶應義塾大学), 2022 年 9 月 19–22 日.

伊藤駿平, 吉田大輔, 北幸海, 島崎智実, 立川仁典 (口頭発表), 「アニオン 2 量体の陽電子化合物に対する量子モンテカルロ法を用

いた第一原理理論研究」, 日本物理学会 2022 年秋季大会, 目黒区 (東京工業大学), 2022 年 9 月 12–15 日.

吉田大輔, 北幸海, 島崎智実, 立川仁典 (口頭発表), 「2 成分水素結合クラスターにおける陽電子束縛及び対消滅機構に関する理論研究」, 第 24 回理論化学討論会, 金沢市 (金沢商工会議所), 2022 年 5 月 17–20 日.

L. Happ (invited), "Universality in one-dimensional quantum three-body systems," Mini-workshop on ultracold-atom theory, Wako-shi, Japan, November 22, 2022.

[Seminars]

T. Doi, "Hybrid quantum annealing via molecular dynamics," Seminar at RIKEN R-CCS, Online, Wako, Japan, June 14, 2022.

T. Doi, "Nuclear physics from lattice QCD," Seminar at KMI Colloquium, Online, Nagoya University, Nagoya, Japan, June 8, 2022.

P. Naidon (invited), "Universal few-body clusters of heavy and light particles," seminar at Institut Pluridisciplinaire Hubert Curien, CNRS/Université de Strasbourg, Strasbourg, France, December 13, 2022.

P. Naidon (invited), "Miscibility and Polaron physics in two-component BEC," Seminar at CESQ, Université de Strasbourg, Strasbourg, France, December 7, 2022.

P. Naidon, "Mass-imbalanced two-component system," "Mini-workshop on ultracold-atom theory," RIKEN, Wako, Japan, November 22, 2022.

T. Fukui, "Theoretical study of three-nucleon force," GPPU Seminar, Graduate Program on Physics for the Universe, Tohoku University, Sendai, Japan, July 15, 2022.

D. Suenaga, "Heavy-quark spin polarization induced by the Kondo effect in a magnetic field," QCD theory seminar, Online, January 16, 2023.

末永大輝, "Continuous transformation from hadrons to quarks in medium by means of a quark model," 文京区 (東京大学), 2022 年 11 月 11 日.

D. Suenaga, "Singly heavy baryons from chiral symmetry," Asia Pacific Center for Theoretical Physics, Korea, June 23, 2022.

末永大輝, "Heavy-quark spin polarization induced by the Kondo effect in a magnetic field," 京都市 (京都大学基礎物理学研究所), 2022 年 6 月 3 日.

末永大輝, "Singly heavy baryons from chiral symmetry," 目黒区 (東京工業大学), 2022 年 5 月 16 日.

Award

T. Fukui, Presentation Award of FY2022 SPDR Presentation of Research Results, RIKEN, January 18, 2023.

Others

P. Naidon: Chairman at the International Symposium on Clustering as a Window on the Hierarchical Structure of Quantum Systems (CLUSHIQ2022), Sendai International Center, Sendai, October 31–November 3, 2022.

T. Fukui: RIKEN Wako Open Campus 2022, RIKEN, Saitama, Japan, April 23, 2022.

Subnuclear System Research Division
Meson Science Laboratory

1. Abstract

Particles like muons, pions, and kaons have finite lifetimes, so they do not exist in natural nuclei or matters. By implanting these particles into nuclei/matters, exotic phenomena in various objects can be studied from new point of view.

For example, kaon is the second lightest meson, which has strange quark as a constituent quark. It is expected that if one embeds mesons into nuclei, the sizes of the nuclei become smaller, and one can form a high-density object beyond the normal nuclear density. Study of this object could lead to better understanding of the origin of the mass of the matter and may reveal the quark degree of freedom beyond the quark-confinement. The other example is the weak interaction in nuclear matter. It can only be studied by the weak decay of hypernuclei, which have Lambda particle in the nuclei.

Muon provides even wider scope of studies, covering condensed matter physics as well as nuclear and atomic physics, and we are trying to extend the application field further into chemical and biological studies. For instance, stopping positively charged muon in a material, we obtain information on the magnetic properties or the local field at the muon trapped site (μSR). Injecting negatively charged muon to hydrogen gas, muonic hydrogen atom (μp) is formed. We use muonic atoms for proton magnetic radius measurement, muon catalyzed fusion and elemental analysis with muonic X-rays. We are also interested in precision measurement of muon property itself, such as muon anomalous magnetic moment (g_2).

In our research, we introduce different kind of impurities into nuclei/matters, and study new states of matter, new phenomena, or the object properties.

2. Major Research Subjects

(1) Study of meson property and interaction in nuclei
(2) Origin of matter mass/quark degree of freedom in nuclei
(3) Condensed matter and material studies with muon
(4) Nuclear and particle physics studies via muonic hydrogen
(5) Development of ultra cold muon beam, and its application from material science to particle physics

3. Summary of Research Activity

(1) Hadron physics at J-PARC, RIKEN-RIBF, GSI and SPring-8

Kaon and pion will shed a new insight to the nuclear physics. The recent discovery of deeply bound pionic atom enables us to investigate the properties of mesons in nuclear matter. At RIKEN-RIBF, we are preparing precise experimental study of the pionic atom. Very lately, we succeeded to discover kaonic nuclear bound state, "*K-pp*," at J-PARC. The yield dependence on momentum-transfer shows that observed system is unexpectedly small. We extended our study on $\Lambda(1405)$ that could be *K-p* bound state. By these experiments, we are studying the KN^- interaction, and clarify the nature of kaon in nuclei. At Spring-8 and at GSI, we are planning to study omega and η^1 nuclei. By these experiments, we aim to be a world-leading scientific research group using these light meta-stable particles.

(1-1) Deeply bound kaonic nuclei

J-PARC E15 experiment had been performed to explore the simplest kaonic nuclear bound state, "K^-pp." Because of the strong attraction between KN^-, the K^- in nuclei may attract surrounding nucleons, resulting in forming a deeply bound and extremely dense object. Measurement of the kaon properties at such a high-density medium will provide precious information on the origin of hadron masses, if the standard scenario of the hadron-mass-generation mechanism, in which the hadron masses are depends on matter density and energy, is correct. Namely, one may study the chiral symmetry breaking of the universe and its partial restoration in nuclear medium.

The E15 experiment was completed to observe the "K^-pp" bound state by the in-flight ^{3}He(K^-, n) reaction, which allows us the formation via the invariant-mass spectroscopy by detecting decay particles from "K^-pp." For the experiment, we constructed a dedicated spectrometer system at the secondary beam-line, K1.8BR, in the hadron hall of J-PARC.

With the Λpn final states obtained in the first stage experiment, we observed a kinematic anomaly in the Λp invariant mass near the mass threshold of M(K^-pp) (total mass of kaon and two protons) at the lower momentum transfer q region. We conducted a successive experiment to examine the nature of the observed kinematical anomaly in the Λpn final state, and we confirmed the existence of the bound state below the mass threshold of M(K^-pp) at as deep as the binding energy of 40 MeV. The momentum transfer q naturally prefers lower momentum for the bound state formation, but the observed event concentration extended having the form-factor parameter ~400 MeV/c. Based on the PWIA calculation, the data indicated that the "K^-pp" system could be as small as ~0.6 fm. It is astonishingly compact in contrast to the mean nucleon distance ~1.8 fm.

This observed signal shows that ***a meson*** $(\boldsymbol{qq^-})$ ***forms a quantum state where baryons (qqq) exist as nuclear medium***, *i.e.*, a highly excited novel form of nucleus with a kaon, in which ***the mesonic degree-of-freedom still holds***. This is totally new form of nuclear system, which never been observed before.

(1-2) Precision X-ray measurement of kaonic atom

To study the KN^- interaction at zero energy from the atomic state level shift and width of kaon, we have performed an X-ray spectroscopy of atomic $3d \rightarrow 2p$ transition of negatively charged K-mesons captured by helium atoms. However, our first experiment is insufficient in energy resolution to see the K^--nucleus potential. Aiming to provide a breakthrough from atomic level observation,

we introduce a novel X-ray detector, namely superconducting transition-edge-sensor (TES) microcalorimeter offering unprecedented high energy resolution, being more than one order of magnitude better than that achieved in the past experiments using conventional semiconductor detectors. The experiment J-PARC E62 aims to determine $2p$-level strong interaction shifts of kaonic ^{3}He and ^{4}He atoms by measuring the atomic $3d \rightarrow 2p$ transition X-rays using TES detector with 240 pixels having about 23 mm^2 effective area and the average energy resolution of 7 eV (FWHM) at 6 keV. We carried out the experiment at J-PARC in June 2018 and successfully observed distinct X-ray peaks from both atoms. The energies were determined to be 6224.5 +/ 0.4 (stat) +/ 0.2 (syst) eV and 6463.7 +/ 0.3 (stat) +/ 0.1 (syst) eV, and widths to be 2.5 +/ 1.0 (stat) +/ 0.4 (syst) eV and 1.0 +/ 0.6 (stat) +/ 0.3 (syst) eV, for kaonic ^{3}He and ^{4}He, respectively. These values are nearly 10 times more precise than in previous measurements. The results exclude the large strong-interaction shifts and widths that are suggested by a coupled-channel approach and agree with calculations based on optical-potential models.

Another important X-ray measurement of kaonic atom would be $2p \rightarrow 1$ stransition of kaonic deuteron (K^--d). We have measured same transition of kaonic hydrogen (K^--p), but the width and shift from electro-magnetic (EM) value reflect only isospin average of the $K^{\rm bar}N$ interaction. We can resolve isospin dependence of the strong interaction by the measurements both for K^--p and K^--d. The experiment J-PARC E57 aims at pioneering measurement of the X-rays from K^--d atoms. Prior to full (stage-2) approval of the E57 proposal, we performed a pilot run with hydrogen target in March 2019.

(1-3) Deeply bound pionic atoms and η^1 mesonic nuclei

We have been working on precision spectroscopy of pionic atoms systematically, which leads to understanding of the non-trivial structure of the vacuum and the origin of hadron masses. The precision data set stringent constraints on the chiral condensate at nuclear medium. We are presently preparing for the precision systematic measurements at RIBF. A pilot experiment performed in 2010 showed a unprecedented results of pionic atom formation spectra with finite reaction angles. The measurement of pionic ^{121}Sn performed in 2014 provided high-precision data and set constraints on the pion-nucleus strong interaction, which led to deduction of the chiral condensate at the normal nuclear density. In 2021, systematic high precision spectroscopy of pionic Sn atoms were performed and the analysis is ongoing.

We are also working on spectroscopy of η^1 mesonic nuclei in GSI/FAIR. Theoretically, peculiarly large mass of η^1 is attributed to UA (1) symmetry and chiral symmetry breaking. As a result, large binding energy is expected for η^1 meson bound states in nuclei (η^1-mesonic nuclei). From the measurement, we can access information about gluon dynamics in the vacuum via the binding energy and decay width of η^1-nuclear bound state. In 2022, we performed a new experiment using a large solid angle detector of WASA at GSI to search for the η^1-nucleus bound state with an enhanced signal-to-noise ratio.

(1-4) $^3_\Lambda$H^{3,4}H lifetime puzzle and our approach

Three recent heavy ion experiments (HypHI, STAR, and ALICE) announced surprisingly short lifetime for $^3_\Lambda$H hyper-nucleus's *Mesonic Weak Decay* (MWD), which seems to be inconsistent with the fact that the $^3_\Lambda$H is a very loosely bound system. It is very interesting to study this with a different experimental approach. We proposed a direct measurement of $_\Lambda$H MWD lifetime with resolution at J-PARC hadron facility by using K-meson beam at 1 GeV/c. As for the feasibility test, we also measure $^{4\Lambda}$H lifetime.

A Cylindrical Detector System (CDS) used in J-PARC E15/E31 experiment is employed to capture the delayed π^- as a weak decay product from $^{3,4}_\Lambda$H a calorimeter is installed in the very forward region to tag fast π^0 meson emission at ~0 degree, which ensures that the Λ hyperon production with small recoil momentum. By this selection, we can improve the ratio between $^{3,4}_\Lambda$H and quasi-free Λ and Σ background. A test beam for feasibility study with ^{4}He target has been conditionally approved by J-PARC PAC. We will conduct the experiment and to present the data in short.

(1-5) Study of properties of vector mesons in nuclei

Preparation of the experiment E16 at J-PARC Hadron Experimental Facility is underway with several Grant-in-Aids. This experiment aims to perform a systematic study of the spectral modification of low-mass vector mesons in nuclei through the dielectron decay channel, in order to explore the physics of chiral symmetry breaking and restoration in dense nuclear matter.

In JFY 2020, a new primary beam line for E16 was completed in J-PARC. Commissioning runs of the beam line and of our spectrometer were performed. The detectors almost satisfied the design performance. Unexpected beam micro structures which deteriorates the DAQ performance were found, and countermeasures were proposed. They will be applied in the test beam time, which is planned in 2023. Based on the result, approval of physics beam time will be discussed in PAC held in Winter 2023–24.

This activity was moved to Meson Science Laboratory after the closing of Radiation Laboratory.

(2) Muon science at RIKEN-RAL branch

The research area ranges over particle physics, condensed matter studies, chemistry and life science. Our core activities are based on the RIKEN-RAL Muon Facility located at the Rutherford-Appleton Laboratory (UK), which provides intense pulsed-muon beams. We have variety of important research activities such as particle/nuclear physics studies with muon's spin and condensed matter physics by muon spin rotation/relaxation/resonance (μSR).

(2-1) Condensed matter/materials studies with μSR

We share experimental equipment with those of RAL in order to make organization of RIKEN beam time schedules easier and to enhance the efficiency to carry out RIKEN's experiments. We use shared cryostats and manpower supports available from RAL as well we other experimental areas. Both two μSR spectrometers, ARGUS (Port-2) and CHRNUS (Port-4), are working well with maintenance supports provide from RAL. Among our scientific activities on μSR studies from year 2017 to 2022, following studies are most important subjects of material sciences at the RIKEN-RAL muon facility:

(1) Multi magnetic transitions in the Ru-based pyrochlore systems, $R_2Ru_2O_7$;

(2) Magnetic properties of the nano-cluster gold in the border of macro- and micro- scale;

(3) Novel magnetic and superconducting properties of nano-size La-based high-TC superconducting curates;
(4) Novel superconducting properties in quasi two-dimensional organic molecular systems.
(5) Determination of muon positions estimated from density functional theory (DFT) and dipole-field calculations;
(6) Chemical muonic states in DNA molecules.

(2-2) Nuclear and particle physics studies via ultra-cold muon beam and muonic atoms

If we can improve muon beam emittance, timing and energy dispersion (so-called "ultra-cold muon"), then the capability of μSR studies will be drastically improved. The ultra-cold muon beam can stop in a thin foil, multi-layered materials and artificial lattices, so one can apply the μSR techniques to surface and interface science. The development of ultra-cold muon beam is also very important as the source of pencil-like small emittance muon beam for muon $g-2$ measurement. Ultra-cold muon beam has been produced by laser ionization of muoniums in vacuum (bound system of μ^+ and electron). We developed a very promising materials for muonium production, laser ablated silica aerogel. We also developed a high power Lyman-α laser in collaboration with laser group at RIKEN. In this laser development, we succeeded to synthesize novel laser crystals Nd:YGAG and Nd:YSAG, which has an ideal wavelength property for laser amplification to generate Lyman-α by four-wave mixing in Kr gas cell. We are now building the actual muon source to be used for muon g-2. The first part of the muon ionization chamber was manufactured and is being tested using the muon beam at J-PARC.

(3) QED study of the lepton g-2

We are conducting research on Quantum Electrodynamics (QED) theory related to the determination of the theoretical and experimental values of the lepton anomalous magnetic moment (g-2). The contribution of QED to g-2 can be obtained through perturbative calculations using Feynman diagrams. We are carrying out both analytical validation and numerical computation improvements to determine the value of the 10th-order perturbation term. Additionally, we are also investigating the quantum corrections by QED to the experimental determination formula of the electron g-2.

Members

Director
Masahiko IWASAKI

Senior Research Scientists
Kenta ITAHASHI
Yue MA
Haruhiko OUTA
Fuminori SAKUMA
Isao WATANABE
Satoshi YOKKAICHI

Senior Scientist
Makiko NIO

Contract Researchers
Katsuhiko ISHIDA
Tomonori TAKAHASHI

Special Postdoctoral Researcher
Koki KANNO

Postdoctoral Researchers
Koki KANNO
Rie MURAYAMA

Junior Research Associate
Tomoki MURAKAMI

International Program Associates
Supparat CHAROENPHON (Kasetsart Univ.)
Muhammad H.B. CHE LAH (Univ. Sains Malaysia)
Li DENG (The Univ. of Sci. and Tech. of China)
Anita E. PUTRI (Univ. of Indonesia)

Research Consultant
Masayasu KAMIMURA

Senior Visiting Scientists
Hiroyuki NOUMI (Osaka Univ.)
Kazuhiro TANAKA (KEK)

Visiting Scientists
Tadashi ADACHI (Sophia Univ.)
Kazuya AOKI (KEK)
Tatsumi AOYAMA (KEK)
Retno ASIH (Inst. Teknologi Sepuluh Nopember)
Fahmi ASTUTI (Inst. Teknologi Sepuluh Nopember)
Wen-Chen CHANG (Inst. of Phys., Academia Sinica)
Catalina Oana CURCEANU (INFN)
Zyun EZAWA (Tohoku Univ.)
Hiroyuki FUJIOKA (Tokyo Tech)
Masaki FUJITA (Tohoku Univ.)

Shuhei FUKUOKA (Hokkaido Univ.)
Takayuki GOTO (Sophia Univ.)
Masashi HAYAKAWA (Nagoya Univ.)
Wataru HIGEMOTO (JAEA)
Ko-ichi HIRAKI (Fukushima Medical Univ.)
Satoru HIRENZAKI (Nara Women's Univ.)
Koichi ICHIMURA (Hokkaido Univ.)
Yasuyuki ISHII (Shibaura Inst. of Tech.)
Ryosuke KADONO (KEK)
Takayuki KAWAMATA (Tokyo Denki Univ.)
Seiko KAWAMURA (JAEA)
Hikomitsu KIKUCHI (Univ. of Fukui)
Takuya KOBAYASHI (Saitama Univ.)
Yoji KOIKE (Tohoku Univ.)
Kenji MATSUDA (Univ. of Toyama)
Hiroyasu MATSUURA (Univ. of Tokyo)
Mototsugu MIHARA (Osaka Univ.)
Takaaki MINAMIDATE (Tokyo Univ. Sci)
Yasuhiro MIYAKE (KEK)
Yuhei MORINO (KEK)
Wataru NAKAI (KEK)
Takehito NAKANO (Ibaraki Univ.)
Takahiro NAMIKI (Univ. of Toyama)
Megumi NARUKI (Kyoto Univ.)
Katsuhiko NISHIMURA (Univ. of Toyama)
Agustinus NUGROHO (Inst. Teknologi Bandung)
Kazuki OHISHI (Comprehensive Res. Org. for Sci. and Soc.)
Yu OISHI (KEK)
Kyoichiro OZAWA (KEK)
Dita PUSPITA SARI (Shibaura Inst. of Tech.)
Muhammad R. RAMADHAN (Univ. Pertahanan Republik Indonesia)
Irwan RAMLI (Univ. Cokroaminoto Palopo)
RISDIANA (Padjadjaran Univ.)
Lusi SAFRIANI (Padjadjaran Univ.)
Naohito SAITO (KEK)
Shinichi SHAMOTO (Comprehensive Res. Org. for Sci. and Soc.)
Ichiro SHIRAKI (Univ. of Yamanashi)
Shukri SULAIMAN (Univ. Sains Malaysia)
Takao SUZUKI (Shibaura Inst. of Tech.)
Takanori TANIGUCHI (Tohoku Univ.)
Andrea VACCHI (Udine Univ. (Italy))
Eberhard WIDMANN (Stefan Meyer Inst.)
Yasuhiro YAMAGUCHI (Nagoya Univ.)
Ichihiro YAMAUCHI (Saga Univ.)
Yukio YASUI (Meiji Univ.)
Masaru YOSOI (Osaka Univ.)
Wan Nurfadhilah B. ZAHARIM (UNIVERSITI SAINS MALAYSIA)
Xu-Guang ZHENG (Saga Univ.)
Johann ZMESKAL (Austrian Academy of Sci.)

Visiting Technician

Che-Sheng LIN (Academia Sinica)

Research Fellow

Harison B. ROZAK (Shibaura Inst. of Tech.)

Student Trainees

Tomoya ASANO (Saitama Univ.)
Masaya ICHIKAWA (Kyoto Univ.)
Shota MATSUMOTO (Kyoto Univ.)
Shunnosuke NAGAFUSA (Kyoto Univ.)
Satomi NAKASUGA (Kyoto Univ.)
Shuta OCHIAI (Kyoto Univ.)
Po-Hung WANG (Nat'l Central Univ.)
Utami WIDYAISWARI (Univ. Indonesia)
Kanako YAMAGUCHI (Kyoto Univ.)
Ryota YAMAZAKI (Saitama Univ.)

Research Part-time Worker

Utami WIDYAISWARI

Assistants

Kumiko TAKAHASHI
Mitsue YAMAMOTO

List of Publications & Presentations

Publications

[Original Papers]

A. Jamaludin *et al*., "Density functional theory investigation of muon hyperfine interaction in guanine-cytosine double-strand DNA," J. Phys. Soc. Jpn. **91**, 024301 (2022).

M. Redo Ramadhan *et al*., "Estimation of the on-site coulomb potential and covalent state in La_2CuO_4 by muon spin rotation and density functional theory calculations," Phys. Rev. Res. **4**, 033044 (2022).

A. Ito *et al*., "Antiferromagnetic ordering of organic mott insulator λ-(BEDSe-TTF)^{2}GaCl$_4$," Phys. Rev. B **106**, 045114 (2022).

W. N. Zaharim *et al*., "Density functional theory study of muon hyperfine interactions in 12 mer single-strand adenine, cytosine, and thymine oligomers," J. Phys. Soc. Jpn. **91**, 094301 (2022).

T. Takayama *et al*., "Competing spin-orbital singlet states in the $4d^4$ honeycomb ruthenate $Ag_3LiRu_2O_6$," Phys. Rev. Res. **4**, 043079 (2022).

M. Cataldo *et al*., "A novel non-destructive technique for cultural heritage: Depth profiling and elemental analysis underneath the surface with negative muons," J. Phys. Soc. Jpn. **91**, 024301 (2022).

C. Zhang *et al*., "Modeling the diffusion of muonium in silica aerogel and its application to a novel design of multi-layer target for thermal muon generation," Nucl. Instrum. Methods Phys. Res. A **1042**, 167443 (2022).

G. A. Green *et al*., "Negative muons reveal the economic chaos of rome's AD 68/9 civil wars," Archaeol. Anthropol. Sci. **14**, 165 (2022).

J-PARC E31 Collaboration, "Pole position of Λ (1405) measured in $d(K^-, n)^\pi\Sigma$ reactions," Phys. Lett. B **837**, 137637 (2023).

T. Nishi *et al*., piAF Collaboration, "Chiral symmetry restoration at high matter density observed in pionic atoms," Nat. Phys. **19**, 788 (2023).

N. Ikeno *et al*., "Pion-nucleon sigma term $\sigma\pi N$ and deeply bound pionic atoms," Prog. Theor. Exp. Phys. **2023**, 033D03 (2023).

[Books]

A. D. Hillier *et al*., "Depth-dependent bulk elemental analysis using negative muons," in *Handbook of Cultural Heritage Analysis*, S. D'Amico and V. Venuti (eds.), Springer 2022, pp. 23–44.

K. Itahashi, "Pionic Atoms in Experiment," in *Handbook of Nuclear Physics*, I. Tanihata, H. Toki, and T. Kajino, (eds.), Springer, Singapore, https://doi.org/10.1007/978-981-15-8818-1_36-1.

[Proceedings]

Y. Ma *et al*., "Status of J-PARC E73 experiment: first direct Hypertriton lifetime measurement with ^{3}He(K^-,*pi*0)H^{3}L reaction," Suplemento de la Revista Mexicana de Fisica **30308120**, 1 (2022).

F. Sakuma *et al*., "J-PARC hadron experimental facility extension project," EPJ Web Conf. **271**, 11001 (2022).

F. Sakuma *et al*., "Summary of the K^-pp bound-state observation in E15 and future prospects," EPJ Web Conf. **262**, 01008 (2022).

S. Nakasuga *et al*., "Commissioning of the electron identification system for Dilepton measurement in pA collisions at J-PARC," Nucl. Instrum. Methods Phys. Res. A **1041**, 167335 (2022).

K. Ozawa *et al*., "Towards the measurement of the mass modifications of vector mesons in a finite density matter," Acta Phys. Pol. A **142**, 399 (2022).

M. Ichikawa *et al*., "Commissioning runs of J-PARC E16 experiment," Acta Phys. Pol. B Proc. Suppl. **16**, 1-A143 (2023).

K. Ozawa *et al*., "J-PARC heavy ion project," EPJ Web Conf. **271**, 11004 (2022).

Ce Zhang, T. Hiraki, K. Ishida, S. Kamal, S. Kamioka, T. Mibe, A. Olin, N. Saito, K. Suzuki, S. Uetake, and Y. Mao, "Modeling the diffusion of muonium in silica aerogel and its application to a novel design of multi-layer target for thermal muon generation," Nucl. Instrum. Methods Phys. Res. A **1042**, 167443G (2022).

Presentations

[International Conferences/Workshops]

T. Yamaga (invited), "Kaonic nuclei at J-PARC," Third International Workshop on the Extension Project for the J-PARC Hadron Experimental Facility (3rd J-PARC HEF-ex WS), J-PARC, March 14–16, 2023.

T. Hashimoto (invited), "Experimental study of the four-body kaonic nuclear state, KbarNNN," EXOTICO: EXOTIc Atoms Meet Nuclear Collisions for a New Frontier Precision Era in Low Energy Strangeness Nuclear Physics ECT*, Trento, Italy, October 17, 2022.

T. Yamaga (invited), "Result of KbaRNN search at J-PARC and future projects," EXOTICO: EXOTIc Atoms Meet Nuclear Collisions for a New Frontier Precision Era in Low Energy Strangeness Nuclear Physics ECT*, October 17, 2022.

T. Yamaga (invited), "Experimental investigation of KbarNN state using K^- + ^{3}He reaction at J-PARC," EMMI workshop, "Meson and hyperon interactions with nuclei," Kitzbuhel, Austria, September 14–16, 2022.

M. Iwasaki (invited), "Kbar nuclear bound state—Toward revolutionary Nuclear Study via revealing Internal Structure of Kaonic Nuclei," The 28th International Nuclear Physics Conference (INPC 2022), Cape Town, South Africa, September 11–16, 2022.

T. Yamaga (invited), "Experimental study of KbarNN and future Kbar-nuclei experiments at J-PARC," The 9th International Conference on Quarks and Nuclear Physics (QNP2022), Online, September 5–9, 2022.

T. Hashimoto (invited), "Experimental study of kaonic nuclei and kaonic atoms at J-PARC," the 15th Asia Pacific Physics Conference (APPC15), South Korea, August 21–26, 2022.

F. Sakuma (invited), "J-PARC hadron hall extension project," 14th International Conference on Hypernuclear and Strange Particle Physics - HYP2022, Prague, Czech Republic, June 27–July 1, 2022.

T. Yamaga (invited), "Experimental study of KbarNN and future experiments for kaonic nuclei," 14th International Conference on Hypernuclear and Strange Particle Physics - HYP2022, Prague, Czech Republic, June 27–July 1, 2022,

Y. Ma (invited), "Current status of hypertriton lifetime measurement with J-PARC E73 experiment," 14th International Conference on Hypernuclear and Strange Particle Physics - HYP2022, Prague, Czech Republic, June 27–July 1, 2022.

T. Hashimoto (oral), "Search for the KbarNNN bound state in the Λ dn final states of the in-flight K- reaction on ^{4}He," 14th International Conference on Hypernuclear and Strange Particle Physics - HYP2022, Prague, Czech Republic, June 27–July 1, 2022.

K. Kanno (oral), "Commissioning of a hadron blind detector for dielectron measurement in pA reactions at J-PARC," MPGD2022, Weizmann Institute, Rehovot, Israel/Hybrid, December 11–16, 2022.

S. Yokkaichi (invited), "Measurements of spectral change of vector mesons in nuclear matter at finite density," Third International Workshop on the Extension Project for the J-PARC Hadron Experimental Facility, J-PARC, Tokai, Japan & Online, March 14–16, 2023.

K. Ishida on behalf of the J-PARC muon g-2/EDM Collaboration (E34), "Muon g-2/EDM experiment at J-PARC," Fifth Plenary Workshop of the Muon g-2 Theory Initiative, Edinburgh, September 5–9, 2022.

K. Itahashi (invited), "What ca npionic atoms tell about the QCD vacuum," XVth Quark confinement and the hadron spectrum, Stavanger,

August 1–6, 2022.

K. Itahashi (invited), "Pionic atoms and chiral symmetry," 4th Jagiellonian Symposium, Krakow, July, 2022.

[Domestic Conferences/Workshops]

山我拓巳 (招待講演), "Study of mesonic decay of KNN and perspectives of kaonic nuclei experiments at J-PARC," J-PARC ハドロン研究会, 東海村 (KEK), 2023 年 3 月 27–29 日.

橋本直 (招待講演), 「J-PARC における K 中間子原子核研究の状況と展望」, ELPH 研究会 C033「ハドロン分光に迫る反応と構造の物理」, 仙台市 (東北大学電子光理学研究センター), 2022 年 12 月 6–7 日.

高橋智則 (口頭発表), 「J-PARC E16 実験の DAQ の現状と課題」, RCNP 研究会「原子核実験の次世代データ収集システム基盤開発にむけて」, 茨木市 (RCNP) & オンライン, 2022 年 5 月 16–17 日.

T. N. Takahashi (招待講演), "Development of continuous readout electronics for precise measurement of dielectron spectra at J-PARC," 第 8 回クラスター階層領域研究会, 大阪大学 & オンライン, 2023 年 2 月 9–11 日.

石田勝彦, 「ラザフォードアップルトン研究所ミュオン施設の紹介」, 第 7 回文理融合シンポジウム 量子ビームで歴史を探る—加速器が紡ぐ文理融合の地平—, つくば市 (KEK), 2022 年 11 月 3 日.

石田勝彦, 「ミュオン触媒核融合の利用」, 中間子科学の将来討論会, 和光市 (理研), 2022 年 11 月 9–11 日.

石田勝彦, 「理研 RAL 施設と原子・原子核研究」, 第 13 回 muon 科学と加速器研究研究会, 和光市 (理研), 2023 年 1 月 10–11 日.

[Seminar]

四日市悟, 「J-PARC E16 実験の現状と展望」, 第 14 回 J-PARC-HI の物理を語る夕べ (セミナーシリーズ), オンライン, 2022 年 8 月 19 日.

Press Releases

「K 中間子と陽子が織りなす風変わりなバリオンを測定」, 大阪大学核物理研究センター, 高エネルギー加速器研究機構, J-PARC センター, 理化学研究所, 日本原子力開発機構, 東北大学電子光理学研究センター, INFN-LNF, SMI 共同プレスリリース, 2023 年 1 月 26 日.

「π で探る真空の秘密」, 理化学研究所, 奈良女子大, 鳥取大学, 阪大核物理研究センター, 共同プレスリリース, 2023 年 3 月 27 日.

Subnuclear System Research Division
RHIC Physics Research Laboratory

1. Abstract

RHIC Physics Research laboratory study the strong interaction with PHENIX and sPHENIX experiment at RHIC collider in Brookhaven National Laboratory in the U.S.A. This laboratory is formed in 2022 to be the RIKEN base of RIKEN BNL Research Center after the Radiation Laboratory was closed. The two physics goals of RHIC are (1) to study quark-gluon plasma produced in heavy ion collisions and (2) to study the spin structure of the proton. The second physics program has been promoted by RIKEN's leadership.

The aim of Heavy ion physics at RHIC is to re-create Quark Gluon Plasma (QGP), the state of Universe just after the Big Bang. Two important discoveries, jet quenching effect and strong elliptic flows, have established that new state of dense matter is indeed produced in heavy ion collisions at RHIC. RIKEN group has played a leading role in the study of QGP. In particular we achieved the first observation of thermal photons from QGP and estimated its initial temperature. The temperature is approximately 350 MeV, well above the transition temperature to QGP (~160 MeV).

The original goals of RHIC spin program are to measure the gluon spin contribution to the proton and to measure ani-quark polarization with the $W \to e$ and $W \to \mu$ measurement. rsults from PHENIX π^0 measurement and STAR jet measurement has shown that gluons in the proton carry about 30% of the proton spin. This is a major milestone of the RHIC spin program. The final results of $W \to e$ measurement was published in 2016 and the final results of $W \to \mu$ was published in 2018. The focus of the RHIC spin program is moved to study of transverse spin measurement.

PHENIX completed its data taking in 2016 to be upgraded a new experiment and detector, sPHENIX. sPHENIX will measure jets, photons, and Upsilon particles and will complete the scientific mission of RHIC. We constructed a intermediate-silicon tracker INTT for sPHENIX. INTT was completed in 2022 and it was installed in sPHENIX in March 2023. The sPHENIX will start taking data in 2023.

2. Major Research Subjects

(1) Experimental Studies of the Spin Structure of the Nucleon
(2) Study of Quark-Gluon Plasma at RHIC
(3) sPHENIX INTT detector

3. Summary of Research Activity

We study the strong interactions (QCD) using the RHIC accelerator at Brookhaven National Laboratory, the world first heavy ion collider and polarized $p + p$ collider. We have three major activities: Spin Physics at RHIC, Heavy ion physics at RHIC, and detector upgrades of PHENIX experiment. Y. Akiba (Laboratory Director) is the Spokesperson of PHENIX experiment since 2016.

Research Activity of this laboratory has large overlap with that of RBRC Experimental group since this laboratory is the RIKEN Wako campus base of RBRC. In the below, recent results reported in the report of RBRC experimental group is excluded.

(1) Experimental study of spin structure of proton using RHIC polarized proton collider

How is the spin of proton formed with 3 quarks and gluons? This is a very fundamental question in Quantum Chromodynamics (QCD), the theory of the strong nuclear forces. The RHIC Spin Project has been established as an international collaboration between RIKEN and Brookhaven National Laboratory (BNL) to solve this problem by colliding two polarized protons for the first time in history. This project also has extended the physics capabilities of RHIC.

The first goal of the Spin Physics program at RHIC is to determine the gluon contribution to proton spin. It is known that the spin of quark accounts for only 25% of proton spin. The remaining 75% should be carried either by the spin of gluons or the orbital angular momentum of quarks and gluons. One of the main goals of the RHIC spin program has been to determine the gluon spin contribution. Before the start of RHIC, there was little experimental constraint on the gluon polarization, ΔG.

PHENIX measures the double helicity asymmetry (A_{LL}) of π^0 production to determine the gluon polarization. Our most recent publication of $\pi^0 A_{LL}$ measurement at 510 GeV shows non-zero value of A_{LL}, indicating that gluons in the proton is polarized. Global analysis shows that approximately 30% of proton spin is carried by gluon spin. PHENIX measured the parity-violating single spin asymmetry A_L of the W boson production in $p + p$ in wide rapidity range. The results of the W boson measurements were published in 2016 and 2018, and these results give constraints on the anti-quark polarization in the proton. The focus of the spin physics is now moved to the measurements of the single transverse spin asymmetry A_N.

In 2017, an electromagnetic calorimeter RHICf detector was installed in the most forward area of the STAR experiment to obtain polarized proton collision data for neutral particle production (neutrons, photons, neutral pions) as the RHICf experiment. In addition to the already obtained asymmetry of neutral pions, the analyses of the production cross section of photons and asymmetry of neutrons were almost completed and presented at international conferences and workshops. The photon production cross sections are compared with results from proton collisions at higher energies at the CERN-LHC, and the results support a scaling law that is independent of collision energy. These results provide new data necessary for the development of event generation codes to reproduce ultra-high energy cosmic ray collision events with the atmosphere. The data analysis of high statistics for neutron asymmetries has yielded results that cover a wide transverse momentum region with the expected high resolution, and the data are very interesting, showing large asymmetries. A theoretical study is also being conducted to investigate the origin of these asymmetries, and comparisons with

experimental data are being made. The final results of both studies are being prepared for publication.

It is aiming to obtain physics data in 2024 to further elucidate the neutral production cross sections and asymmetries discovered by the RHICf experiment. Although this experiment has not yet been approved, it will use silicon detector technology developed in the ALICE-FoCal upgrade project at the LHC to introduce a larger detector with higher position resolution. Therefore, the collaboration with ALICE has been resumed as an associated member and the detector is being jointly developed with the FoCal group. The development of this new detector technology is also part of an essential R&D program for a zero-degree calorimeter (ZDC) detector for EIC. As a result of the fabrication of a prototype detector, its testing and evaluation in the laboratory, test beams at the ELPH facility at Tohoku University and the CERN-PS and SPS accelerators, and radiation tolerance tests at the RIKEN RANS neutron irradiation facility, the selection of silicon detector technology for the actual detector was almost completed and the next stage of detector fabrication is about to begin.

(2) Experimental study of Quark-Gluon Plasma using RHIC heavy-ion collider

The goal of high energy heavy ion physics at RHIC is study of QCD in extreme conditions *i.e.* at very high temperature and at very high energy density. Experimental results from RHIC have established that dense partonic matter is formed in Au + Au collisions at RHIC.

PHENIX completed its data taking after the 2016 run. We continue data analysis of PHENIX data. Recent highlights of study of QGP by PHENIX is presented in the report by RBRC experimental group.

(3) sPHENIX INTT detector

We constructed intermediate silicon tracker INTT for sPHENIX, a new experiment at RHIC that will start taking data in 2023. The INTT detector consists of 56 ladders, which are arranged to two layers of barrels. A ladder is shown in Fig. 1. It is a basic building block of the INTT.

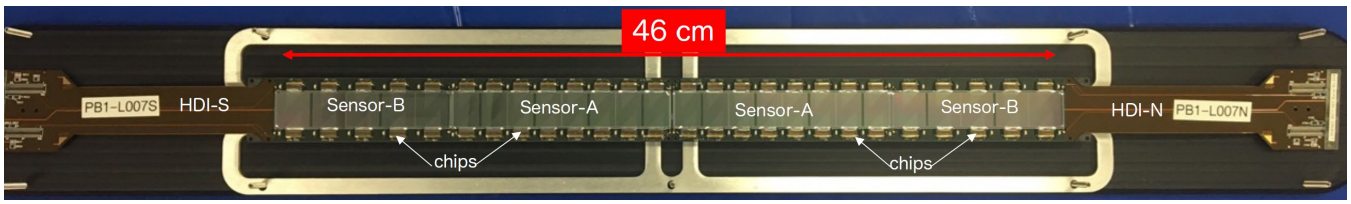

Fig. 1. Left: Completed two halves of INTT detector with members of INTT teams. Right: INTT detector and INTT team just after installation to sPHENIX.

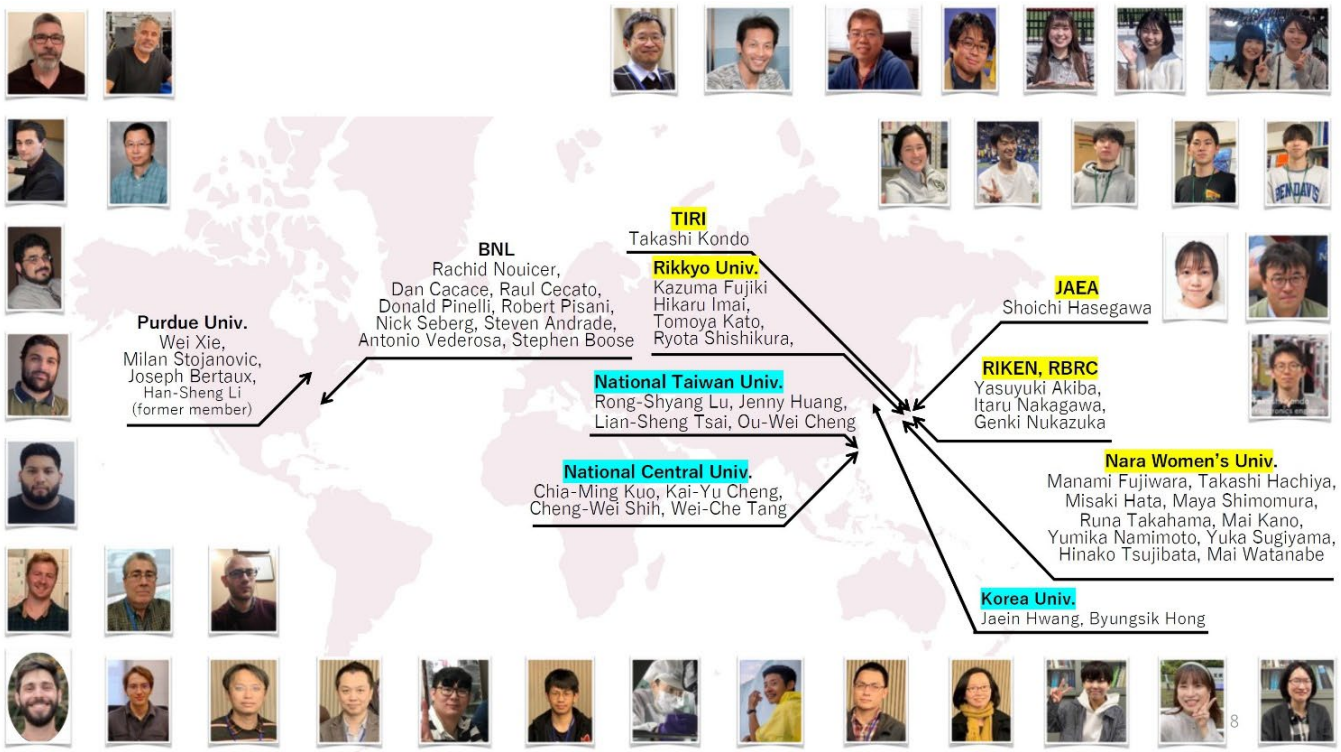

Fig. 2. INTT collaboration.

In the development of INTT, the first step was to make a prototype of one ladder of INTT. The performance of the prototype was then evaluated to confirm that it meets the required performance. If not, improvements were made. After this process was repeated and the ladder prototype meets the required performance, mass production of the ladder started. In this development process process was done by an international collaboration of INTT detector group led by Dr. Nakagawa of this laboratory and Dr. Rachid Nouicer of Brookhaven National Laboratory. The collaboration is shown in Fig. 2.

In the fall of 2022, the construction of the INTT was completed. The detector was in stalled in the sPHENIX in March 2023. The commissioning of the detector started. sPHENIX will start taking data in June 2023.

Members

Director

Yasuyuki AKIBA

Senior Research Scientists

Yuji GOTO
Itaru NAKAGAWA
Ralf SEIDL
Satoshi YOKKAICHI

Special Postdoctoral Researcher

Minho KIM

Special Temporary Research Scientist

Yasushi WATANABE

Visiting Scientists

Tatsuya CHUJO (Tsukuba Univ.)
Takashi HACHIYA (Nara Women's Univ.)
Shoichi HASEGAWA (JAEA)
Motoi INABA (Tsukuba Univ. of Tech.)
Shunzo KUMANO (Japan Women's Univ.)
Ken-ichi NAKANO (Univ. of Virginia USA)
Masahiro OKAMURA (BNL)
Toshiaki SHIBATA (Nihon Univ.)
Kenta SHIGAKI (Hiroshima Univ.)
Maya SHIMOMURA (Nara Women's Univ.)
Kiyoshi TANIDA (JAEA)

Student Trainees

Misaki HATA (Nara Women's Univ.)
Yumika NAMIMOTO (Nara Women's Univ.)
Yuka SASAKI (Nara Women's Univ.)
Yuka SUGIYAMA (Nara Women's Univ.)
Runa TAKAHAMA (Nara Women's Univ.)
Mai WATANABE (Nara Women's Univ.)

Interns

Kazuma FUJIKI (Rikkyo Univ.)
Tomoya KATO (Rikkyo Univ.)
Ryota SHISHIKURA (Rikkyo Univ.)

List of Publications & Presentations

Publications

[Original Papers]

N. J. Abdulameer *et al*., "Improving constraints oon gluon spin-momentum correlations in transversely polarized protons vias midrapidity open-heavy flavor electrons in $p + p$ collisions at $\sqrt{s}$ = 200 GeV," Phys. Rev. D **107**, 052012 (2023).

N. J. Abdulameer *et al*., "Low p_T direct-photon production in Au + Au collisions at $\sqrt{s_{NN}}$ = 39 and 62.4 GeV," Phys. Rev. C **107**, 024914 (2023).

N. J. Abdulameer *et al*., "Measurement of second-harmonic Fourier coefficients from azimuthal anisotropies in $p + p$, p + Au, d + Au, and ^{3}He + Au at $\sqrt{s_{NN}}$ = 200 GeV," Phys. Rev. C **107**, 024907 (2023).

N. J. Abdulameer *et al*., "Measurement of ϕ-meson production in Cu + Au at $\sqrt{s_{NN}}$ = 200 GeV and U + U collisions at $\sqrt{s_{NN}}$ = 193 GeV," Phys. Rev. C **107**, 014907 (2022).

U. A. Acharya *et al*., "ϕ meson production in p + Al, p + Au, d + Au, ^{3}He + Au collisions at $\sqrt{s_{NN}}$ = 200 GeV," Phys. Rev. C **106**, 014908 (2022).

U. A. Acharya *et al*., "Measurement of $\psi(2S)$ nuclear modification at backward and forward rapidity in $p+p$, $p+$Al, and $p+$Au collisions at $\sqrt{s_{NN}}$ = 200 GeV," Phys. Rev. C **105**, 064912 (2022).

U. A. Acharya *et al*., "Systematic study of nuclear effects in p + Al, p + Au, d + Au, and ^{3}He + Au collisions at $\sqrt{s_{NN}}$ = 200 GeV using π^0 production," Phys. Rev. C **105**, 064902 (2022).

Award

Y. Akiba, "Research of High temperature and high density matter through relativistic heavy ion collisions," Commendation for Science and Technology by the Minister of Education, Culture, Sports, Science, and Technology for 2023.

Subnuclear System Research Division
RIKEN BNL Research Center

1. Abstract

The RIKEN BNL Research Center was established in April 1997 at Brookhaven National Laboratory with Professor T. D. Lee of Columbia University as its initial Director. The Center is dedicated to the study of strong interactions, including spin physics, lattice QCD and RHIC physics through the nurturing of a new generation of young physicists. Professor Lee was succeeded by BNL Distinguished Scientist, the former BNL director, N. P. Samios, who served until 2013. The other former BNL director, S. H. Aronson led the Center from 2013. Hideto En'yo succeeded the director position starting from JFY 2017. Support for RBRC was initially for five years and has been renewed four times, and presently extends to March 2023. The five year extension from April 2023 is agreed between BNL and RIKEN in order to cover the era of sPHENIX experiment which is the upgraded of the PHENIX experiment. Theoretical activities in the RBRC Theory and Computing Groups are closely and intimately related to those of the Nuclear Theory, High Energy Theory and Lattice Gauge Theory Groups at BNL. The RBRC Experimental Group jointly works with RHIC Physics Research Laboratory at Wako RIKEN, the RHIC Spin Group at BNL, the RHIC Spin Physics community, and the PHENIX/sPHENIX collaboration. Radiation Laboratory at Wako was closed in March 2022, and its functions are taken over by the new laboratory "RHIC Physics Research Laboratory" headed by Y. Akiba. BNL provides office space, management, computing, and administrative support. The Deputy Director of RBRC is D. Morrison (BNL). In May 2021, Y. Hatta (BNL) becomes Theory Group leader, succeeding D. Kharzeev. Y. Akiba (RIKEN) is Experimental Group leader and T. Izubuchi (BNL) is Computing Group leader. From April 2023, Robert Tribble, the former deputy director for Science and Technology of BNL assumes the director of RBRC, after Hideto En'yo's retirement.

2. Major Research Subjects

Major research subjects of the theory group are
(1) Spin structure of proton;
(2) Gluon saturation at small-x;
(3) Physics of quark gluon plasma.

Major research subjects of the computing group are
(1) Search for new law of physics through tests for Standard Model of particle and nuclear physics;
(2) Dynamics of QCD and related theories;
(3) Theoretical and algorithmic development for lattice field theories, QCD machine design.

Major research subject of the experimental group are
(1) Experimental Studies of the Spin Structure of the Nucleon;
(2) Study of Quark-Gluon Plasma at RHIC;
(3) sPHENIX detector construction.

3. Summary of Research Activity

Summary of Research Activities of the three groups of the Center are given in the sections of each group.

Members

Director

Hideto EN'YO

Deputy Director

David P. MORRISON

Administrative Staffs

Keiko IWANO (Administration Manager)
Pamela ESPOSITO (Administrative Assistant)
Maureen MCNEIL-SHEA (Administrative Assistant)

List of Publications & Presentations

Publications

[Original Papers]

See the lists of the research groups.

Presentations

[Seminars]

H. En'yo, "My forty years of looking up to the world of Nambu (in Japanese)," Final lecture supported by the Chief Scientist Assembly and Nishina Center of RIKEN, Wako, Saitama, Japan (RIKEN) & Online, March 2, 2023.

H. En'yo, "My forty years of looking up to the world of Nambu (in English)," the special RBRC Seminar Celebrating the Retirement of Dr. Hideto En'yo, the director of RIKEN BNL Research Center, Upton NY, USA (Brookhaven National Laboratory) & Online, March 23, 2023.

Subnuclear System Research Division
RIKEN BNL Research Center
Theory Group

1. Abstract

The efforts of the RBRC theory group are concentrated on the major topics of interest in High Energy Nuclear Physics, in particular, the physics explored by the RHIC experiment at Brookhaven National Laboratory (BNL). This includes: understanding of the Quark-Gluon Plasma (QGP); the nature of dense quark matter; the initial state in high energy collisions, the Color Glass Condensate and its evolution to QGP through a Glasma; QCD spin physics; physics relevant to the future Electron-Ion Collider at BNL.

2. Major Research Subjects

(1) Heavy Ion Collisions, QCD phase diagram
(2) Perturbative Quantum Chromo-Dynamics (QCD)
(3) Nucleon structure, mass and spin

3. Summary of Research Activity

(1) Chiral and trace anomalies in Deeply Virtual Compton Scattering

Y. Hatta, S. Bhattacharya and a collaborator discovered novel 'anomaly poles' in QCD Compton scattering. These are poles $1/t$ in momentum transfer t in off-forward scattering and are manifestations of the underlying QCD chiral and trace anomalies. This has significant implications for the future tomographic study of the nucleon through the generalized parton distributions (GPDs).

(2) Gravitational form factors in holographic QCD

Y. Hatta and collaborators computed one of the gravitational form factors, the so-called D-term, in holographic QCD using the Sakai-Sugimoto model. This is the first computation of the gravitational form factors in top-down holographic QCD. They found that the D-term exhibits the phenomenon of glueball dominance, similar to the vector meson dominance of the electromagnetic form factors.

(3) Small-x behavior of the GPD $Eg(x)$

Y. Hatta and a collaborator derived, for the first time, the small-x evolution equation for the gluon GPD $Eg(x)$. It has been shown that, despite its association with nucleon helicity-flip processes, $Eg(x)$ grows rapidly with decreasing x in exactly the same way as the BFKL Pomeron.

(4) Lee-Yang edge singularity

V. Skokov and collaborators employ the functional renormalization group approach at next-to-leading order of the derivative expansion to refine their earlier findings for the universal location of the Yang-Lee edge singularity in classic O(N) universality classes. To this date, it is the most precise determination of the Yang-Lee edge singularity.

(5) CGC for ultraperipheral nuclear collisions

V. Skokov and collaborators provided the first calculation of two-gluon production at mid-rapidity in ultra-peripheral collisions in the Color Glass Condensate framework. To estimate systematic uncertainty associated with poor understanding of the wave function of the nearly real photon, they consider two diametrically different models: the dilute quark-antiquark dipole approximation and a vector meson, in which color charge density is approximated by McLerran-Venugopalan model.

(6) Simulating the tiniest fluids in 3 + 1 dimensions

Employing a dynamical initial state model coupled to (3 + 1)D viscous relativistic hydrodynamics, C. Shen and collaborators explored the rapidity dependence of anisotropic flow in the Relativistic Heavy-Ion Collider (RHIC) small system scan at 200 GeV center of mass energy [6]. They demonstrate that approximately 50% of the p_T-differential triangular flow difference between the measurements by the STAR and PHENIX Collaborations can be explained by the use of reference flow vectors from different rapidity regions. This emphasizes the importance of longitudinal flow decorrelation for anisotropic flow measurements in asymmetric nuclear collisions and the need for (3 + 1)D simulations.

(7) Multi-scale imaging of nuclei geometry at high energy

C. Shen and collaborators showed that the failure to describe the v_2 ratio in central UU and AuAu collisions at RHIC was due to inappropriate treatments of well-deformed nuclei in modeling the initial conditions of the QGP [8]. With rigorous input from Skyrme density functional calculations, they show that correcting nuclear deformations in hydrodynamic simulations restores agreement with BNL RHIC data. This brings consistency to the results of nuclear experiments across energy scales and demonstrates the impact of the hexadecapole deformation of Uranium nucleus on high-energy collisions.

(8) Renormalization of jet quenching parameter

Y. Mehtar-Tani and collaborators demonstrated that the leading quantum corrections to parton energy loss can be resummed and incorporated through a renormalization of the jet quenching parameter, while still preserving the classical tree-level framework. The renormalized jet quenching now depends on the length of the medium, owing to non-local quantum effects, resulting in a weakly non-Markovian dynamics. Based on this theory result, they developed a systematic approach with significant implications for jet quenching phenomenology.

Members

Group Leader

Yoshitaka HATTA

RBRC Researchers

Yacine MEHTAR-TANI
Chun SHEN
Vladimir SKOKOV
Bhattacharya SHOHINI

List of Publications & Presentations

Publications

[Original Papers]

Y. Hatta, B. Xiao, and F. Yuan, "Semi-inclusive diffractive deep inelastic scattering at small-x," Phys. Rev. D **106**, 094015 (2022).

M. Fujita, Y. Hatta, S. Sugimoto, and T. Ueda, "Nucleon D-term in holographic quantum chromodynamics," Prog. Theor. Exp. Phys, **2022**, 093B06 (2022).

Y. Hatta and J. Zhou, "Small-x evolution of the gluon GPD Eg," Phys. Rev. Lett. **129**, 25 (2022).

S. Bhattacharya, Y. Hatta, and W. Vogelsang, "Chiral and trace anomalies in deeply virtual Compton scattering," Phys. Rev. D **107**, 014026 (2023).

A. Kumar *et al*. [JETSCAPE], "Inclusive jet and hadron suppression in a multistage approach," Phys. Rev. C **107**, 034911 (2023).

K. J. Sun, R. Wang, C. M. Ko, Y. G. Ma, and C. Shen, "Unveiling the dynamics of nucleosynthesis in relativistic heavy-ion collisions," arXiv:2207.12532.

W. Fan *et al*. [JETSCAPE], "Multiscale evolution of charmed particles in a nuclear medium," Phys. Rev. C **107**, 054901 (2023).

H. Alalawi, J. Boyd, C. Shen, and M. Strickland, "Impact of fluctuating initial conditions on bottomonium suppression in 5.02 TeV heavy-ion collisions," Phys. Rev. C **107**, L031901 (2023).

L. Du, C. Shen, S. Jeon, and C. Gale, "Probing initial baryon stopping and equation of state with rapidity-dependent directed flow of identified particles," arXiv:2211.16408.

W. Zhao, S. Ryu, C. Shen, and B. Schenke, "3D structure of anisotropic flow in small collision systems at energies available at the BNL Relativistic Heavy Ion Collider," Phys. Rev. C **107**, 014904 (2023).

Y. Tachibana *et al*. [JETSCAPE], "Hard jet substructure in a multi-stage approach," arXiv:2301.02485.

W. Ryssens, G. Giacalone, B. Schenke, and C. Shen, "Evidence of hexadecapole deformation in uranium-238 at the relativistic heavy ion collider," accepted by Phys. Rev. Lett, arXiv:2302.13617.

H. Mäntysaari, B. Schenke, C. Shen, and W. Zhao, "Multi-scale imaging of nuclear deformation at the electron ion collider," arXiv:2303.04866.

T. Schaefer and V. Skokov, "Dynamics of non-Gaussian fluctuations in model A," Phys. Rev. D **106**, 014006 (2022).

H. Duan, A. Kovner, and V. V. Skokov, "CGC for ultra-peripheral Pb + Pb collisions at the Large Hadron Collider: a more realistic calculation," J. High Energy Phys. **12**, 077 (2022).

G. Johnson, F. Rennecke, and V. V. Skokov, "Universal location of Yang-Lee edge singularity in classic O(N) universality classes," arXiv:2211.00710.

H. Duan, A. Kovner, and V. V. Skokov, "Classical entanglement and entropy," arXiv:2301.05735.

P. Caucal and Y. Mehtar-Tani, "Universality aspects of quantum corrections to transverse momentum broadening in QCD media," J. High Energy Phys. **09**, 023 (2022).

P. Caucal and Y. Mehtar-Tani, "Transverse momentum broadening from NLL BFKL to all orders in pQCD," arXiv:2209.08900.

Y. Mehtar-Tani, S. Schlichting, and I. Soudi, "Jet thermalization in QCD kinetic theory," arXiv:2209.10569.

[Proceedings]

Y. Hatta, "Nucleon EDM from polarized DIS," JPS Conf. Proc. **37**, 020601 (2022).

S. Benic, Y. Hatta, A. Kaushik, and H. Li, "A novel contribution to single spin asymmetries in SIDIS at two loops," JPS Conf. Proc. **37**, 020203 (2022).

S. Bhattacharya, K. Cichy, M. Constantinou, J. Dodson, X. Gao, A. Metz, S. Mukherjee, A. Scapellato, F. Steffens, and Y. Zhao, "GPDs in asymmetric frames," PoS Lattice **2022**, 095 (2023).

H. Mäntysaari, B. Schenke, C. Shen, and W. Zhao, "Bayesian inference of the fluctuating proton shape in DIS and hadronic collisions," Acta Phys. Polon. Supp. **16**, 33 (2023).

V. Vovchenko, V. Koch, and C. Shen, "Proton number cumulants and correlation functions from hydrodynamics and the QCD phase diagram," Acta Phys. Polon. Supp. **16**, 83 (2023).

C. Shen, W. Zhao, and B. Schenke, "Collectivity in ultra-peripheral heavy-ion collisions," EPJ Web Conf. **276**, 01002 (2023).

Y. Tachibana, C. Shen *et al*. [JETSCAPE], "Comprehensive study of multi-scale jet-medium interaction," arXiv:2212.12188.

Presentations

[International Conferences/Workshops]

Y. Hatta (invited), "EIC science: ep reactions," Town hall meeting on hot & cold QCD, USA (MIT), September 20–22, 2022.

Y. Hatta (invited), "Nucleon D-term in the Sakai-Sugimoto model," INT Workshop on Origin of the Visible Universe: Unraveling the Proton Mass, USA (University of Washington), June 13–17, 2022.

Y. Hatta (invited), "Experimental observables to access GTMDs," Towards improved hadron femtography with hard exclusive reactions, USA (Virginia Tech University), July 18–22, 2022.

Y. Hatta (invited), "Nucleon EDM and polarized DIS," QCD evolution, University of Virginia, May 9–13, 2022.

Y. Hatta (invited), "Azimuthal angular correlation of jets from soft gluon radiation," RBRC workshop on predictions for sPHENIX, USA (BNL), July 20–22, 2022.

S. Bhattacharya (invited), "Hunting for gluon orbital angular momentum at the EIC," XXIX Cracow Epiphany Conference on Physics at the EIC and Future Facilities, Cracow, Poland, January 18, 2023.

S. Bhattacharya (invited), "Chiral and trace anomalies in DVCS," CFNS Meetings, USA (Stony Brook University), March 10, 2023.

C. Shen (selected contributed talk), "Collectivity and baryon junctions in ultra-peripheral heavy-ion collisions," the 20th International Conference on Strangeness in Quark Matter, June 14, 2022.

C. Shen (invited), "Going beyond flow: Did we hit the precision wall?," First CMS Heavy-Ion Workshop, August 8, 2022.

C. Shen (invited), "Multi-messenger heavy-ion physics with JETSCAPE," 13th International workshop on Multiple Partonic Interactions at LHC, November 15, 2022.

C. Shen (invited), "3D modeling of the RHIC isobar collisions," Intersection of Nuclear Structure and High-energy Nuclear Collisions, February 17, 2023.

C. Shen (invited), "Illuminating early-stage dynamics of heavy-ion collisions through photons at RHIC BES energies," 11th International Conference on Hard and Electromagnetic Probes of High-Energy Nuclear Collision, March 29, 2023.

Y. Mehtar-Tani (invited), "Quantum induced anomalous diffusion in QCD matter," Jet Quenching In The Quark-Gluon Plasma workshop, ECT*, Trento, June 13–17, 2022.

Y. Mehtar-Tani (invited), "Transverse momentum broadening from NLL BFKL to all orders in pQCD," Resummation Evolution Factorization, October 31–November 4, 2022.

Y. Mehtar-Tani (invited), "Jet energy loss and heavy flavor, Heavy Flavors from small to large systems," Institut Pascal Program, Orsay, France (Paris-Saclay University), October 3–21, 2022.

Y. Mehtar-Tani (invited), "Transverse momentum broadening from NLL BFKL to all orders in pQCD," 13th international workshop on Multiple Partonic Interactions at the LHC, Madrid, Spain, November 14–18, 2022.

[Domestic Conference/Workshop]

Y. Hatta (invited), "Nucleon graivitational form factors in holographic QCD," Third International Workshop on the Extension Project for the J-PARC, Hadron experimental facility, Japan (J-PARC), March 14–16, 2023.

[Seminars]

Y. Hatta, "QCD spin physics at the EIC," Heavy-ion tea seminar, USA (Lawrence Berkeley National Laboratory), October 14, 2022.

Y. Hatta, "Chiral and trace anomalies in DVCS," Stony Brook, USA, November 2, 2022.

Y. Hatta, "Azimuthal angular asymmetry of soft gluons in jet production, USA (Yale University), April 28, 2022.

Y. Hatta, "Near-threshold quarkonium production and the nucleon gravitational form factors," CFNS seminar, USA (Stony Brook University), August 25, 2022.

S. Bhattacharya, "Primary observables to access orbital angular momentum of partons," Nuclear Physics Seminar, USA (University of Illinois Urbana-Champaign), February 13, 2023.

S. Bhattacharya, "Computing PDFs and GPDs in Lattice QCD: Recent Progress," Center for Nuclear Theory seminar, USA (Stony Brook University), February 22, 2023.

C. Shen, "Longitudinal dynamics and particle production in relativistic nuclear collisions," RBRC seminar, July 7, 2022.

C. Shen, "Flowing through the nuclear phase diagram at the highest temperatures and densities," Physics colloquium at Wayne State University, October 6, 2022.

C. Shen, "3D modeling of the collective behaviors in relativistic heavy-ion collision," Nuclear Seminar at HENPIC-EVO, December 22, 2022.

C. Shen, "3D modeling of the collective behaviors in relativistic heavy-ion collisions," Nuclear Seminar at Iowa State University, February 23, 2023.

Y. Mehtar-Tani, "The hottest matter under the microscope: probing the quark gluon plasma at colliders," BNL lecture, Upton (BNL), December 14, 2022.

Y. Mehtar-Tani, "Quantum induced anomalous diffusion in QCD matter," Teilchentee seminar at ITP, Heidelberg, Germanuy (Heidelberg

University), June 2, 2022.

Y. Mehtar-Tani, "3D-structure of the proton: from partons to strong fields," UCLA Nuclear Physics Group, Los Angeles, CA (UCLA), September 15, 2022.

Press Release

S. Bhattacharya, R. Boussarie, and Y. Hatta, "Theorists propose a novel way to measure gluons' orbital motion," DOE highlights, November 10, 2022.

Awards

C. Shen, 2023 Outstanding Junior Faculty Award, Wayne State Academy of Scholars, https://academy.wayne.edu/junior-award.

V. Skokov, LeRoy and Elva Martin Award for Teaching Excellence (NCSU).

Subnuclear System Research Division
RIKEN BNL Research Center
Experimental Group

1. Abstract

RIKEN BNL Research Center (RBRC) Experimental Group studies the strong interactions (QCD) using RHIC accelerator at Brookhaven National Laboratory, the world first heavy ion collider and polarized $p + p$ collider. We have three major activities: Spin Physics at RHIC, Heavy ion physics at RHIC, and detector upgrades of PHENIX experiment at RHIC.

We study the spin structure of the proton using the polarized proton-proton collisions at RHIC. This program has been promoted by RIKEN's leadership. The first focus of the research is to measure the gluon spin contribution to the proton spin. Results from PHENIX π^0 measurement and STAR jet measurement has shown that gluons in the proton carry about 30% of the proton spin. This is a major milestone of the RHIC spin program. The second goal of the spin program is to measure the polarization of anti-quarks in the proton using $W \to e$ and $W \to \mu$ decays. The results of $W \to e$ measurement was published in 2016. The final results of $W \to \mu$ was published in 2018. The focus of the RHIC spin program is moved to study of transverse spin measurement.

The aim of Heavy ion physics at RHIC is to re-create Quark Gluon Plasma (QGP), the state of Universe just after the Big Bang. Two important discoveries, jet quenching effect and strong elliptic flows, have established that new state of dense matter is indeed produced in heavy ion collisions at RHIC. We are now studying the property of the QGP. We measured direct photons in Au + Au collisions for $1 < p_{\mathrm{T}} < 3$ GeV/c, where thermal radiation from hot QGP is expected to dominate. The comparison between the data and theory calculations indicates that the initial temperature of 300 MeV to 600 MeV is achieved. These values are well above the transition temperature to QGP, which is calculated to be approximately 160 MeV by lattice QCD calculations.

We had major roles in detector upgrades of PHENIX experiment, namely, the silicon vertex tracker (VTX) and muon trigger upgrades. The VTX is the main device to measure heavy quark (charm and bottom) production and the muon trigger is essential for $W \to \mu$ measurement. The results from the first run with VTX detector in 2011 was published. The results show that electrons from bottom quark decay is strongly suppressed at high p_{T}, but the suppression is weaker than that of charm decay electron for $3 < p_{\mathrm{T}} < 4$ GeV/c. PHENIX recorded 10 times as much Au + Au collisions data in each of the 2014 run and 2016 run. A paper on the suppression of electrons from charm and bottom decays in the 2014 run was submitted for publication. The data shows clear different of the suppression of $b \to e$ and $c \to e$.

PHENIX completed its data taking in 2016, and construction of a new detector, sPHENIX, as upgrade of PHENIX was started. sPHENIX will measure jets, photons, and Upsilon particles and will complete the scientific mission of RHIC. We constructed a intermediate-silicon tracker INTT for sPHENIX. INTT was completed in 2022 and it was installed in sPHENIX in March 2023. The sPHENIX will start taking data in 2023.

2. Major Research Subjects

(1) Experimental Studies of the Spin Structure of the Nucleon
(2) Study of Quark-Gluon Plasma at RHIC
(3) sPHENIX INTT detector

3. Summary of Research Activity

We study the strong interactions (QCD) using the RHIC accelerator at Brookhaven National Laboratory, the world first heavy ion collider and polarized $p + p$ collider. We have three major activities: Spin Physics at RHIC, Heavy ion physics at RHIC, and detector upgrades of PHENIX experiment. Y. Akiba (Experimental Group Leader) is the Spokesperson of PHENIX experiment since 2016.

(1) Experimental study of spin structure of proton using RHIC polarized proton collider

How is the spin of proton formed with 3 quarks and gluons? This is a very fundamental question in Quantum Chromodynamics (QCD), the theory of the strong nuclear forces. The RHIC Spin Project has been established as an international collaboration between RIKEN and Brookhaven National Laboratory (BNL) to solve this problem by colliding two polarized protons for the first time in history. This project also has extended the physics capabilities of RHIC.

The first goal of the Spin Physics program at RHIC is to determine the gluon contribution to proton spin. It is known that the spin of quark accounts for only 25% of proton spin. The remaining 75% should be carried either by the spin of gluons or the orbital angular momentum of quarks and gluons. One of the main goals of the RHIC spin program has been to determine the gluon spin contribution. Before the start of RHIC, there was little experimental constraint on the gluon polarization, ΔG.

PHENIX measures the double helicity asymmetry (ALL) of π^0 production to determine the gluon polarization. Our most recent publication of $\pi^0 A_{LL}$ measurement at 510 GeV shows non-zero value of A_{LL}, indicating that gluons in the proton is polarized. Global analysis shows that approximately 30% of proton spin is carried by gluon spin. PHENIX measured the parity-violating single spin asymmetry A_L of the W boson production in $p + p$ in wide rapidity range. The results of the W boson measurements were published in 2016 and 2018, and these results give constraints on the anti-quark polarization in the proton. The focus of the spin physics is now moved to the measurements of the single transverse spin asymmetry A_N.

PHENIX measured A_N of single electrons from heavy flavored hadrons at mid rapidity. Production of heavy quarks (charm and bottom) is dominated by gluon-gluon fusion, and the measurement is sensitive to the gluon correlators that are related to the orbital angular momentum of gluons via theoretical models. Figure 1 shows the A_N of single electrons from heavy flavor decays. The data

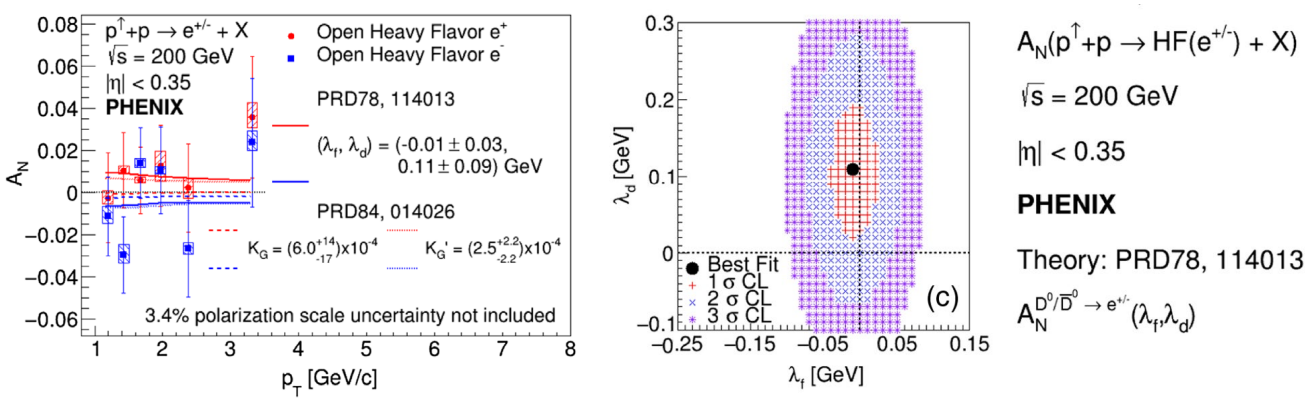

Fig. 1. The single spin asymmetry A_N of heavy flavor decay electrons (left) and the constraint on the model parameter from the data (right). Published in Phys. Rev. D **107**, 052012 (2023).

are compared with a theoretical model by Z. Kang and J. Qiu, and the two parameters λ_f and λ_d of the model are constrained from the data. The right panel of Fig. 1 shows the constraint on the model parameters. The parameters are determined as $\lambda_f = -0.01 \pm 0.03$ GeV and $\lambda_d = 0.11 \pm 0.09$ GeV. The size of these parameters are expected to be O(0.1)GeV. This is the first constraints on these model parameters. These results are published in Physical Review D.

(2) Experimental study of Quark-Gluon Plasma using RHIC heavy-ion collider

The goal of high energy heavy ion physics at RHIC is study of QCD in extreme conditions *i.e.* at very high temperature and at very high energy density. Experimental results from RHIC have established that dense partonic matter is formed in Au + Au collisions at RHIC. The matter is very dense and opaque, and it has almost no viscosity and behaves like a perfect fluid. These conclusions are primarily based on the following two discoveries:

- Strong suppression of high transverse momentum hadrons in central Au + Au collisions (jet quenching);
- Strong elliptic flow.

These results are summarized in PHENIX White paper, which has more than 3400 citations to date. The focus of the research in heavy ion physics at RHIC is now to investigate the properties of the matter. RBRC have played the leading roles in some of the most important results from PHENIX in the study of the matter properties. These include (1) measurements of heavy quark production from the single electrons from heavy flavor decay (2) measurements of J/ψ production (3) measurements of di-electron continuum and (4) measurements of direct photons.

Our most important result is the measurement of direct photons for $1 < p_{\rm T} < 5$ GeV/c in $p+p$ and Au + Au through their internal conversion to $e+e^-$ pairs. If the dense partonic matter formed at RHIC is thermalized, it should emit thermal photons. Observation of thermal photon is direct evidence of early thermalization, and we can determine the initial temperature of the matter. It is predicted that thermal photons from QGP phase is the dominant source of direct photons for $1 < p_{\rm T} < 3$ GeV/c at the RHIC energy. We measured the direct photon in this $p_{\rm T}$ region from measurements of quasi-real virtual photons that decays into low-mass $e+e^-$ pairs. Strong enhancement of direct photon yield in Au + Au over the scaled $p+p$ data has been observed. Several hydrodynamical models can reproduce the central Au + A data within a factor of two. These models assume formation of a hot system with initial temperature of $T_{\rm init} = 300$ MeV to 600 MeV. This is the first measurement of initial temperature of quark gluon plasma formed at RHIC. Y. Akiba received 2011 Nishina memorial Prize mainly based on this work.

PHENIX experiment recently measured the flow in small collision systems (p + Au, d + Au, and ^{3}He + Au), and observed strong flow in all of these systems. Theoretical models that assume formation of small QGP droplets best describe the data. These results are published in Nature Physics in 2019.

We constructed VTX detector of PHENIX. VTX is a 4-layer silicon tracker and it is the main device for measurement of charm and bottom quark production in PHENIX. VTX took data from the 2011 to 2016 when PHENIX completed data taking. PHENIX recorded high statistics Au + Au data, approximately 20 billion events with VTX in each of the 2014 run and the 2016 run. A paper reporting the results of 2014 run was submitted to Physical Review C.

PHENIX measured the nuclear modification factor of J/ψ and $\psi(2S)$ in the forward and the backward direction in p + Au and d + Au collisions at $\sqrt{s_{NN}} = 200$ GeV. The results are shown in Fig. 2.

In the forward rapidity region, the suppression of J/ψ and $\psi(2S)$ is similar. This indicates that initial state effects such as shadowing dominates in this region. In the backward rapidity region, the stronger suppression of $\psi(2S)$ than J/ψ is observed. This result suggests presence of final state effect in p + Au collisions. The paper reporting these results was published in Physical Review C and it was selected as Editor's suggestion.

PHENIX measured low $p_{\rm T}$ direct photons in Au + Au collisions at $\sqrt{s_{NN}} = 39$ and 62 GeV. The yield of these photons exceeds what is expected from $p+p$ collisions at the same energy and it is consistent with large contribution from thermal photons from a hot quark-gluon plasma. Compared with the data of other collision energies, the data suggest that the bulk of thermal photons are

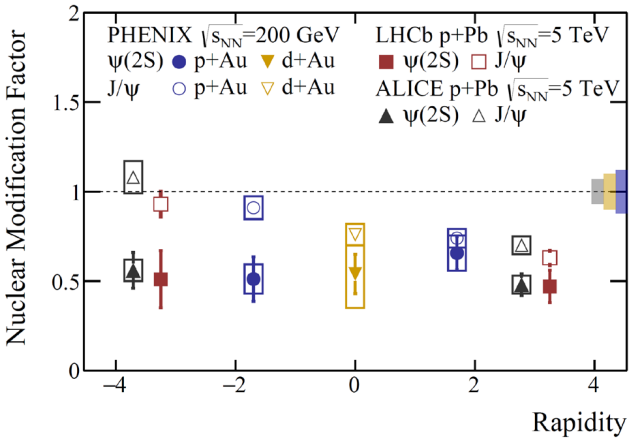

Fig. 2. The nuclear modification factor of J/ψ and $\psi(2S)$ in small collision systems as function of rapidity. Published in Phys. Rev. C **105**, 064912 (2022).

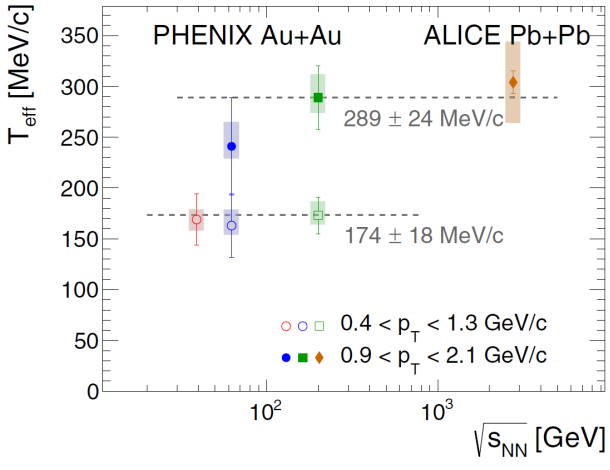

Fig. 3. Effective temperature, T_{eff}, from the low p_T direct photon spectra as function of the collision energy. Published in Phys. Rev. C **107**, 024914 (2023).

emitted near the transition of the quark-gluon plasma. The paper reporting these results was published in Physical Review C, and it was selected as Editor's suggestion.

(3) sPHENIX INTT detector

The group had major roles in several PHENIX detector upgrades, namely, the silicon vertex tracker (VTX) and muon trigger upgrades. VTX is a high precision charged particle tracker made of 4 layers of silicon detectors. It is jointly funded by RIKEN and the US DOE. The inner two layers are silicon pixel detectors and the outer two layers are silicon strip detectors. Y. Akiba is the project manager. The VTX detector was completed in November 2010 and subsequently installed in PHENIX. The detector started taking data in the 2011 run. With the new detector, we measure heavy quark (charm and bottom) production in $p + p$, A + A collisions to study the properties of quark-gluon plasma. The final result of the 2011 run was published. The result show that single electrons from bottom quark decay is suppressed, but not as strong as that from charm decay in low p_T region ($3 < p_T < 4$ GeV/c). This is the first measurement of suppression of bottom decay electrons at RHIC and the first observation that bottom suppression is smaller than charm. We have recorded 10 times as much Au + Au collisions data in each of the 2014 run and 2016 run. The results of bottom/charm ratios in $p + p$ collisions at 200 GeV from the 2015 run was published (Phys. Rev. D **99**, 092003 (2019)). A paper reporting measurements of the nuclear suppression factor R_{AA} of charm and bottom in Au + Au collisions from the 2014 data was submitted for publication to Physical Review C.

PHENIX completed its data taking in 2016. We constructed intermediate silicon tracker INTT for sPHENIX, a new experiment at RHIC that will start taking data in 2023. INTT was completed in fall 2022 and it was installed in sPHENIX in March 2023. sPHENIX will start taking data in June 2023.

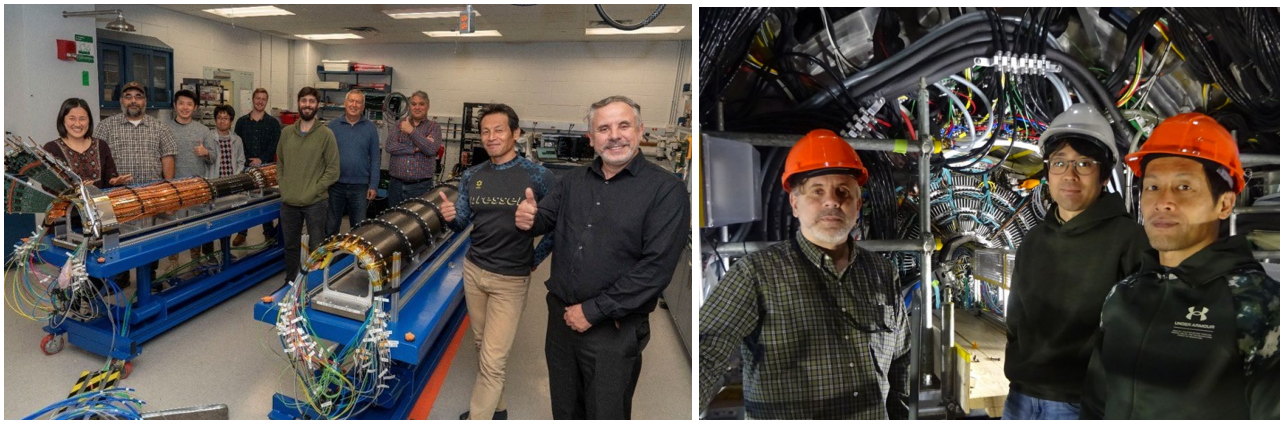

Fig. 4. Left: Completed two halves of INTT detector with members of INTT teams. Right: INTT detector and INTT team just after installation to sPHENIX.

Members

Group Leader

Yasuyuki AKIBA

RBRC Researchers

Jan C. BERNAUER
Genki NUKAZUKA
Yuji GOTO
Itaru NAKAGAWA
Ralf SEIDL
Atsushi TAKETANI

Special Postdoctoral Researcher

Minho KIM

Junior Research Associate

Takuya KUMAOKA

Special Temporary Research Scientists

Takashi ICHIHARA
Yasushi WATANABE

Senior Visiting Scientist

Rachid NOUICER (BNL)

Visiting Scientists

Stefan BATHE (City Univ. of New York)
Takashi HACHIYA (Nara Women's Univ.)
Gaku MITSUKA (KEK)
Takao SAKAGUCHI (BNL)
Takashi SAKO (Univ. of Tokyo)
Milan STOJANOVIC (Purdue Univ.)

Visiting Researcher

Shima SHIMIZU (JSPS)

Student Trainees

Joseph T. BERTAUX (Purdue Univ.)
Kai-Yu CHENG (Nat'l Central Univ.)
Jaein HWANG (Korea Univ.)
Seunghwan LEE (Sejong Univ.)
Han-Sheng LI (Purdue Univ.)
Cheng Wei SHIH (Nat'l Central Univ.)
Wei-Che TANG (Nat'l Central Univ.)
Maki WAKATA (Rikkyo Univ.)

Research Part-time Worker

Hikaru IMAI

List of Publications

Publications

[Original Papers]

N. J. Abdulameer *et al*., "Improving constraints oon gluon spin-momentum correlations in transversely polarized protons vias midrapidity open-heavy flavor electrons in $p + p$ collisions at $\sqrt{s}$ = 200 GeV," Phys. Rev. D **107**, 052012 (2023).

N. J. Abdulameer *et al*., "Low p_{T} direct-photon production in Au + Au collisions at $\sqrt{s_{NN}}$ = 39 and 62.4 GeV," Phys. Rev. C **107**, 024914 (2023).

N. J. Abdulameer *et al*., "Measurement of second-harmonic Fourier coefficients from azimuthal anisotropies in $p + p$, p + Au, d + Au, and ^{3}He + Au at $\sqrt{s_{NN}}$ = 200 GeV," Phys. Rev. C **107**, 024907 (2023).

N. J. Abdulameer *et al*., "Measurement of ψ-meson production in Cu + Au at $\sqrt{s_{NN}}$ = 200 GeV and U + U collisions at $\sqrt{s_{NN}}$ = 193 GeV," Phys. Rev. C **107**, 014907 (2022).

U. A. Acharya *et al*., "ψ meson production in p + Al, p + Au, d + Au, ^{3}He + Au collisions at $\sqrt{s_{NN}}$ = 200 GeV," Phys. Rev. C **106**, 014908 (2022).

U. A. Acharya *et al*., "Measurement of $\psi(2S)$ nuclear modification at backward and forward rapidity in $p+p$, $p+$Al, and $p+$Au collisions at $\sqrt{s_{NN}}$ = 200 GeV," Phys. Rev. C **105**, 064912 (2022).

U. A. Acharya *et al*., "Systematic study of nuclear effects in p + Al, p + Au, d + Au, and ^{3}He + Au collisions at $\sqrt{s_{NN}}$ = 200 GeV using π^0 production," Phys. Rev. C **105**, 064902 (2022).

Award

Y. Akiba, "Research of High temperature and high density matter through relativistic heavy ion collisions," Commendation for Science and Technology by the Minister of Education, Culture, Sports, Science, and Technology for 2023.

Subnuclear System Research Division
RIKEN BNL Research Center
Computing Group

1. Abstract

The computing group founded in 2011 as a part of the RIKEN BNL Research Center established at Brookhaven National Laboratory in New York, USA, and dedicated to conduct researches and developments for large-scale physics computations important for high energy particle and nuclearphysics. The group was forked from the RBRC Theory Group.

The main mission of the group is to provide important numerical information that is indispensable for theoretical interpretation of experimental data from the first principle theories of particle and nuclear physics. Their primary area of research is lattice quantum chromodynamics (QCD), which describes the sub-atomic structures of hadrons, which allow the ab-initio investigation for strongly interacting quantum field theories beyond perturbative analysis.

The RBRC group and its collaborators have emphasized the necessity and importance of precision calculations, which will precisely check the current understandings of nature, and will have a potential to find a physics beyond the current standard model of fundamental physics. The first-principle studies also elucid intrecate nature of various phenomena in quantitive and unambiguous manners. We have therefore adopted techniques that aim to control and reduce any systematic errors. This approach has yielded many reliable results.

The areas of the major activities are R&D for high performance computing codes, developments for computing algorithms, and researches of particle, nuclear, and lattice theories. Since the inception of RBRC, many breakthroughs and pioneering works has carried out in computational forefronts. These are the use of the domain-wall fermions, which preserve chiral symmetry, a key symmetry for understanding dynamics of subnuclear elementary particle quark, the three generations of QCD devoted supercomputers and very efficient software library for lattice gauge theories, pioneering works for QCD calculation for Cabibbo-Kobayashi-Maskawa theory, QCD + QED simulation for isospin breaking, novel algorithms for statistical error reduction in general lattice calculation *etc.* The chiral quark simulation has been performed in a uncompromised setup at the physical up, down quark mass, the precision for many basic quantities reached to accuracy of sub-percent, and the group is working for further important and challenging calculations, such as the full and complete calculation of CP violating $K \to \pi\pi$ decay and ε'/ε, or hadronic contributions to muon's anomalous magnetic moment $g-2$.

Recent focus area is stusies of the nucleon's shape, structures, and the motion of quarks and gluon inside nucleon called parton distribution, which provide theoretical guidance to physics for sPHENIX and future Electron Ion Collider (EIC), Hyper Kamiokande, DUNE. Closely related calculation has been carried out for the origin of the current matter rich universe (rather than anti-matter). Towards finite density QCD, they also explored Quantum Computing for field theories. Applications of the Machine Learning (ML) and Artificial Intelligence (AI) for novel and more efficient ways to carry out lattice QCD calculations are among the new topics of the group.

2. Major Research Subjects

(1) Search for new law of physics through tests for Standard Model of particle and nuclear physics, especially in the framework of the Cabibbo-Kobayashi-Maskawa (CKM), hadronic contributions to the muon's anomalous magnetic moment $(g-2)$ for FNAL and J-PARC's experiments, as well as B physics at Belle II and LHCb

(2) Nuclear Physics and dynamics of QCD or related theories, including study for the structures of nucleons related to physics for sPHENIX, Electron Ion Collider (EIC or eRHIC), Hyper Kamiokande, T2K, DUNE, or the matter rich universe

(3) Theoretical and algorithmic development for lattice field theories, QCD machine (co-)design and software development

3. Summary of Research Activity

Research activities during the current report period by RBRC members include various nulcleon formfactor and structure calculations, hadronic contributions to the anomalous magnetic moment $(g-2)_\mu$, kaon and B meson physics, and algorithm & software developments.

In April 2020, $(g-2)_\mu$ experiment collaboration at FNAL carried out a very precise measurement of precession rate of muons under magnetic field to 0.14 parts per million accuracy. This provides a very stringent test of the current understanding of elementary particle physics so called the Standard Model of particle physics. The strong interaction of quark and gluon is described by Quantum Chromo Dyanics (QCD) and is a dominant source of uncertainty in the theoretical prediction of $(g-2)_\mu$. Members of RBRC has been working on the two separate mode of QCD contributions, Hadronic Vacuum Polarization (HVP) and Hadronic Light-by-Light (HLbL). This year, an update of HVP was reported with an improved precision by adding calculation on the finner space-time lattice to remove systematic error due to non-zero lattice spacing. The quantities are not yet the final total conribution for $(g-2)_\mu$ but a large part of QCD contributionfrom intermediate energies scale, roughly 200 MeV–1 GeV. The new results of HVP contribution turned out significantly larger than our previous results and consistent with other lattice QCD calcuation by other groups, which emphasis the importance and difficulty of removing lattice spacing error. No an interesting observation is our new value (and other lattice QCD values) has about $4+\sigma$ tention to the HVP prediction from hadronic cross section in electron-position collision. It is important to note this is still a comparison of the partial HVP contribution from the intemediate energy region, and the final total HVP contribution including other energies as well as the other systematic effects is ongoing to updated with greater precision soon.

This is only a selected research highlight of members of RBRC this year among other various researches: Machine Learning

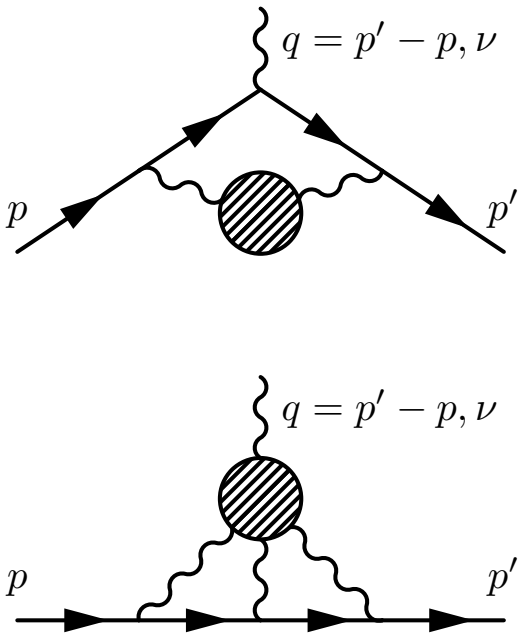

Fig. 1. Feynman diagrams for Lattice QCD computations of Muon's anomalous magnetic moment $(g-2)_\mu$. Hadronic Vaccum Polarization contribution (Left) and Hadronic Light-by-Light contribution (Right).

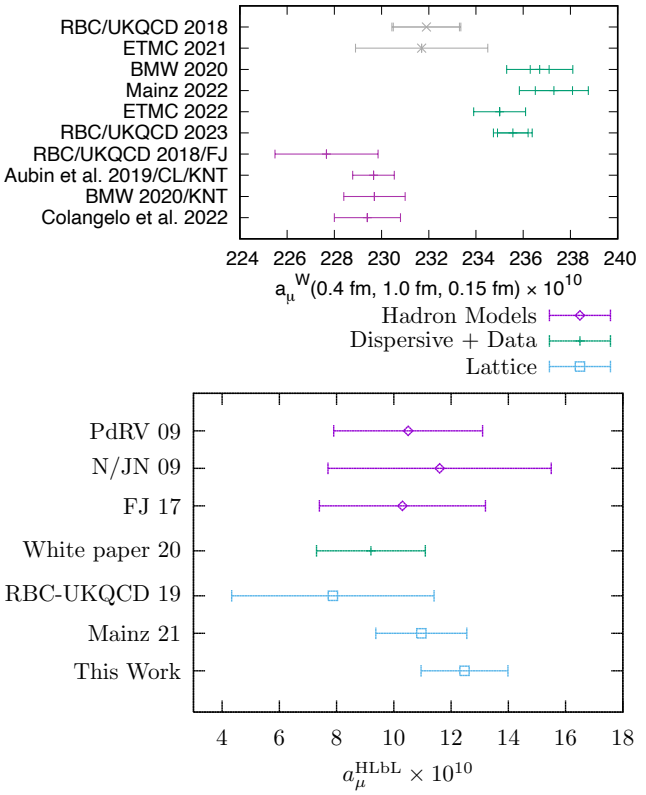

Fig. 2. Current summary of the Hadronic Light-by-Light contribution (HLbL) contribution for Muon's anomalous magnetic moment $(g-2)_\mu$. Above the upper horizontal line shows various Lattice QCD determinations of HVP while the red results from hadronic decay of electron positron scattering (R-ratio), the green bands is the experimental results of $(g-2)_\mu$ showing a 3–4σ discrepancies.

for Lattice QCD ensemble generation, Lattice QCD sampling for non-zero baryon density and sign problem, real-time lattice QCD formulation in Minkowski space-time, solving critical slowing down problem via trivializing maps, lattice QCD+QED and isospin breaking of hadrons and their decays, HLbL for $(g-2)_\mu$, nucleon electric dipole moment and matter-rich universe, nucleon anti-nucleon oscillation, proton decay, CP violating $K \to \pi\pi$ decay and ε'/ε, *etc.*

The RBRC group and its collaborators have emphasized the necessity and importance of precision calculations, which will provide stringent checks for the current understandings of nature, and will have a potential to find physics beyond the current standard model of fundamental physics. We have therefore adopted techniques that aim to control and reduce any systematic errors. This approach has yielded many reliable results, many of basic quantities are now computed within sub-percent accuracies.

The group also delivers several algorithmic breakthroughs, which speed up generic lattice gauge theory computation. These novel technique divides the whole calculation into frequent approximated calculations, and infrequent expensive and accurate calculation using lattice symmetries called All Mode Averaging (AMA), or a compression for memory needs by exploiting the local-coherence of QCD dynamics. Together with another formalism, zMobius fermion, which approximate chiral lattice quark action efficiently, the typical calculation is now improved by a couple of orders of magnitudes, and more than an order of magnitude less memory needs compared to the traditional methods. RBRC group and its collaborators also provide very efficient and generic code optimized to the state-of-arts CPU or GPU, and also improve how to efficiently generate QCD ensemble.

Members

Group Leader

Taku IZUBUCHI

RBRC Researchers

Luchang JIN

Bollweg DENNIS

Special Postdoctoral Researcher

Nobuyuki MATSUMOTO

Visiting Scientists

Thomas BLUM (Univ. of Connecticut)
Hiroshi OKI (Nara Women's Univ.)
Akio TOMIYA (In'l Professional Univ. of Technology in Osaka)

List of Publications & Presentations

Publications

[Original Papers]

T. Blum, P. A. Boyle, M. Bruno, D. Giusti, V. Gülpers, R. C. Hill, T. Izubuchi, Y. C. Jang, L. Jin, and C. Jung *et al.,* arXiv:2301.08696.

T. Blum *et al.* [RBC and UKQCD], "Isospin 0 and 2 two-pion scattering at physical pion mass using all-to-all propagators with periodic boundary conditions in lattice QCD," Phys. Rev. D **107**, 094512 (2023).

J. S. Yoo, Y. Aoki, P. Boyle, T. Izubuchi, A. Soni, and S. Syritsyn, "Proton decay matrix elements on the lattice at physical pion mass," Phys. Rev. D **105**, 074501 (2022).

G. Rendon, T. Izubuchi and Y. Kikuchi, "Effects of cosine tapering window on quantum phase estimation," Phys. Rev. D **106**, 034503 (2022).

B. Chakraborty, M. Honda, T. Izubuchi, Y. Kikuchi, and A. Tomiya, "Classically emulated digital quantum simulation of the Schwinger model with a topological term via adiabatic state preparation," Phys. Rev. D **105**, 094503 (2022).

X. Gao, A. D. Hanlon, J. Holligan, N. Karthik, S. Mukherjee, P. Petreczky, S. Syritsyn, and Y. Zhao, "The Unpolarized Proton PDF at NNLO from Lattice QCD with Physical Quark Masses," arXiv:2212.12569.

X. Gao, A. D. Hanlon, N. Karthik, S. Mukherjee, P. Petreczky, P. Scior, S. Shi, S. Syritsyn, Y. Zhao, and K. Zhou, "Continuum-extrapolated NNLO valence PDF of the pion at the physical point," Phys. Rev. D **106**, 114510 (2022).

X. Gao, A. D. Hanlon, N. Karthik, S. Mukherjee, P. Petreczky, P. Scior, S. Syritsyn, and Y. Zhao, "Pion distribution amplitude at the physical point using the leading-twist expansion of the quasi-distribution-amplitude matrix element," Phys. Rev. D **106**, 074505 (2022).

X. Gao, A. D. Hanlon, S. Mukherjee, P. Petreczky, P. Scior, S. Syritsyn, and Y. Zhao, "Lattice QCD determination of the Bjorken-x dependence of parton distribution functions at next-to-next-to-leading order," Phys. Rev. Lett. **128**, 142003 (2022).

X. Gao, N. Karthik, S. Mukherjee, P. Petreczky, S. Syritsyn, and Y. Zhao, "Pion form factor and charge radius from Lattice QCD at physical point," Phys. Rev. D **104**, 11 (2021).

X. Gao, N. Karthik, S. Mukherjee, P. Petreczky, S. Syritsyn, and Y. Zhao, "Towards studying the structural differences between the pion and its radial excitation," Phys. Rev. D **103**, 094510 (2021).

G. Silvi, S. Paul, C. Alexandrou, S. Krieg, L. Leskovec *et al*., "*P*-wave nucleon-pion scattering amplitude in the Delta(1232) channel from lattice QCD," Phys. Rev. D **103**, 094508 (2021).

M. Yu. Barabanov, M. A. Bedolla, W. K. Brooks, G. D. Cates, C. Chen *et al*., "Diquark correlations in hadron physics: Origin, impact and evidence," Prog. Part. Nucl. Phys. **116**, 103835 (2021).

Y. Hamada and N. Matsumoto, "Energy of the boundary of spacetime," Prog. Theor. Exp. Phys. **2023**, 033B02 (2023).

N. Matsumoto, "Comment on the subtlety of defining a real-time path integral in lattice gauge theories," Prog. Theor. Exp. Phys. **2022**, 093B03 (2022).

X. Y. Tuo, X. Feng, and L. C. Jin, "Lattice QCD calculation of the light sterile neutrino contribution in $0\nu2\beta$ decay," Phys. Rev. D **106**, 074510 (2022).

Y. Fu, X. Feng, L. C. Jin, and C. F. Lu, "Lattice QCD calculation of the two-photon exchange contribution to the muonic-hydrogen lamb shift," Phys. Rev. Lett. **128**, 172002 (2022).

X. Feng, L. Jin, and M. J. Riberdy, "Lattice QCD calculation of the pion mass splitting," Phys. Rev. Lett. **128**, 052003 (2022).

X. Y. Tuo, X. Feng, L. C. Jin, and T. Wang, "Lattice QCD calculation of $K \to \ell\nu\ell\ell' + \ell'$-decay width," Phys. Rev. D **105**, 054518 (2022).

P. X. Ma, X. Feng, M. Gorchtein, L. C. Jin, and C. Y. Seng, "Lattice QCD calculation of the electroweak box diagrams for the kaon semileptonic decays," Phys. Rev. D **103**, 114503 (2021).

[Review Articles]

N. Craig, C. Csáki, A. X. El-Khadra, Z. Bern, R. Boughezal, S. Catterall, Z. Davoudi, A. de Gouvêa, P. Draper, and P. J. Fox *et al.*, "Snowmass Theory Frontier Report," arXiv:2211.05772.

Z. Davoudi, E. T. Neil, C. W. Bauer, T. Bhattacharya, T. Blum, P. Boyle, R. C. Brower, S. Catterall, N. H. Christ, and V. Cirigliano *et al.*, "Report of the snowmass 2021 topical group on lattice gauge theory," arXiv:2209.10758.

A. S. Kronfeld *et al.* [USQCD], "Lattice QCD and particle physics," arXiv:2207.07641.

P. Boyle, D. Bollweg, R. Brower, N. Christ, C. DeTar, R. Edwards, S. Gottlieb, T. Izubuchi, B. Joo, and F. Joswig *et al.* "Lattice QCD and the computational frontier," arXiv:2204.00039.

G. Colangelo, M. Davier, A. X. El-Khadra, M. Hoferichter, C. Lehner, L. Lellouch, T. Mibe, B. L. Roberts, T. Teubner, and H. Wittig *et al.* "Prospects for precise predictions of a_μ in the standard model," arXiv:2203.15810.

T. Blum, P. Boyle, M. Bruno, N. Christ, F. Erben, X. Feng, V. Guelpers, R. Hill, R. Hodgson, and D. Hoying *et al.*, "Discovering new physics in rare kaon decays," arXiv:2203.10998.

R. Alarcon, J. Alexander, V. Anastassopoulos, T. Aoki, R. Baartman, S. Baeßler, L. Bartoszek, D. H. Beck, F. Bedeschi, and R. Berger *et al.* "Electric dipole moments and the search for new physics," arXiv:2203.08103.

D. Bollweg, D. A. Clarke, J. Goswami, O. Kaczmarek, F. Karsch, S. Mukherjee, P. Petreczky, C. Schmidt, and S. Sharma, 'Equation of state and speed of sound of (2+1)-flavor QCD in strangeness-neutral matter at non-vanishing net baryon-number density," arXiv:2212.09043.

[Proceedings]

M. Engelhardt, N. Hasan, T. Izubuchi, C. Kallidonis, S. Krieg, S. Meinel, J. Negele, A. Pochinsky, G. Silvi, and S. Syritsyn, "Transverse momentum-dependent parton distributions for longitudinally polarized nucleons from domain wall fermion calculations at the physical pion mass," PoS **LATTICE2022**, 103 (2023).

P. Boyle, T. Izubuchi, L. Jin, C. Jung, C. Lehner, N. Matsumoto, and A. Tomiya, "Use of Schwinger-Dyson equation in constructing an approximate trivializing map," PoS **LATTICE2022**, 229 (2023).

J. S. Yoo, S. Syritsyn, Y. Aoki, P. Boyle, T. Izubuchi, and A. Soni, PoS **LATTICE2021**, 522 (2022).

J. S. Yoo, S. Syritsyn, Y. Aoki, P. Boyle, T. Izubuchi, and A. Soni, "Proton decay amplitudes with physical chirally-symmetric quarks on a lattice," PoS **PANIC2021**, 443 (2022).

M. Tomii, T. Blum, D. Hoying, T. Izubuchi, L. Jin, C. Jung, and A. Soni, "$K \to \pi\pi$ decay matrix elements at the physical point with periodic boundary conditions," PoS **LATTICE2021**, 394 (2022).

X. Feng, T. Izubuchi, L. Jin, and M. Golterman, "Pion electric polarizabilities from lattice QCD," PoS **LATTICE2021**, 362 (2022).

M. Engelhardt, J. Green, N. Hasan, T. Izubuchi, C. Kallidonis, S. Krieg, S. Liuti, S. Meinel, J. Negele, and A. Pochinsky *et al.,* PoS **LATTICE2021**, 413 (2022).

S. Foreman, T. Izubuchi, L. Jin, X. Y. Jin, J. C. Osborn, and A. Tomiya, "HMC with normalizing flows," PoS **LATTICE2021**, 073 (2022).

M. Fukuma, N. Matsumoto, and Y. Namekawa, "Applying the worldvolume hybrid Monte Carlo method to lattice field theories," PoS **LATTICE2022**, 011 (2023).

M. Fukuma, N. Matsumoto, and Y. Namekawa, "Numerical sign problem and the tempered Lefschetz thimble method," PoS **CORFU2021**, 254 (2022).

M. Fukuma and N. Matsumoto, "Tempered Lefschetz thimble method as a solution to the numerical sign problem," J. Phys. Conf. Ser. **2207**, 012054 (2022).

M. Fukuma and N. Matsumoto, "The basics and applications of the tempered Lefschetz thimble method for the numerical sign problem," PoS **LATTICE2021**, 395 (2022).

M. Fukuma, N. Matsumoto, and Y. Namekawa, "Worldvolume tempered Lefschetz thimble method and its error estimation," PoS **LATTICE2021**, 446 (2022).

P. A. Boyle, D. Bollweg, C. Kelly, and A. Yamaguchi, "Algorithms for domain wall Fermions," PoS **LATTICE2021**, 470 (2022).

Presentations

[International Conferences/Workshops]

S. Syritsyn (invited), "Nucleon electromagnetic form factors at large momentum from lattice QCD," Triangle Nuclear Theory Colloquium at UNC Chapel Hill, November 29, 2022.

S. Syritsyn (invited), "Nucleon electromagnetic form factors at large momentum from lattice QCD," Baryons 2022, Seville, Spain, November 7, 2022.

S. Syritsyn (invited), "Baryon number-violating amplitudes on a lattice with physical chirally-symmetric quarks," 14th Conference on the Intersections of Particle and Nuclear Physics (CIPANP), Orlando, FL, August 31, 2022.

S. Syritsyn (invited), "Nucleon & nuclear structure inputs to beyond-SM searches," SNOWMASS Rare Processes & Precision Frontier, Cincinnati, OH, May 17, 2022.

S. Syritsyn (invited), "Proton decay amplitudes with physical chirally-symmetric quarks," BNL-HET & RBRC Joint Workshop "DWQ@25," December 16, 2021.

S. Syritsyn (invited), "A more perfect universe: Role of lattice QCD in constraining violations of fundamental symmetries," Physics & Astronomy Colloquium, Stony Brook University, November 9, 2021.

L. Jin (Invited), "The hadronic light-by-light scattering contribution to the muon $g-2$," χ QCD annual collaboration meeting, Online, December 17, 2022.

L. Jin (Invited plenary talk), "Muon $g-2$ from lattice QCD," The 13th International Workshop on $e+e^-$ collisions from Phi to Psi, Online, August 17, 2022.

L. Jin (Invited), "Lattice QCD input for the first row CKM unitarity tests," Seattle Snowmass Summer Meeting 2022, Online, July 19, 2022.

L. Jin (Invited), "Combining infinite-volume photons and finite-volume hadronic matrix elements computed on the lattice," QED in Weak Decays, Higgs Centre for Theoretical Physics, JCMB, Online, June 24, 2022.

L. Jin (Invited), "The hadronic light-by-light scattering contribution to the muon $g-2$ (RBC/UKQCD)," SchwingerFest 2022: muon $g-2$, Physics and Astronomy Building, Mani L. Bhaumik Institute, UCLA, June 17, 2022.

L. Jin (Invited), "QCD + QED studies," USQCD All Hands' Meeting 2022, MIT, Online, April 22, 2022.

L. Jin (Invited), "Lattice calculation of the pion mass splitting using the infinite volume reconstruction method," χ QCD annual collaboration meeting, Online, December 19, 2021.

L. Jin, (Invited), "Attice calculation of the pion mass splitting using the infinite volume reconstruction method," BNL-HET & RBRC Joint Workshop "DWQ@25," Online, December 16, 2021.

L. Jin (Invited plenary talk), "Hadronic light-by-light contribution to muon $g-2$," The 10th International Workshop on Chiral Dynamics, Institute of High Energy Physics (IHEP), CAS, Online, November 19, 2021.

L. Jin (Invited), "Lattice calculation of the muon $g-2$," The first annual meeting of lattice QCD in China, Online, November 2, 2021.

L. Jin (Invited), "Lattice QCD input for the first row CKM unitarity tests," Fall Meeting of the Division of Nuclear Physics of the American Physics Society, DNP 2021, Online, October 13, 2021.

L. Jin (Invited), "Lattice QCD results on the hadronic contributions to the muon $g-2$," The XXVIII International Conference on Supersymmetry and Unification of Fundamental Interactions, SUSY 2021, Online, August 23, 2021.

L. Jin, "Pion electric polarizabilities from lattice QCD," LATTICE 2021, MIT, Online, July 29, 2021.

L. Jin (Invited), "Lattice calculation of the hadronic light-by-light contribution to the muon $g-2$ by the RBC-UKQCD collaborations," Muon $g-2$ theory initiative workshop in memoriam of Simon Eidelman, KEK IPNS, High energy physics laboratory in Nagoya University, Online, July 2, 2021.

L. Jin (Invited plenary talk), "Kaon decays from lattice QCD," Flavor Physics and CP violation (FPCP), Online, June 9, 2021.

L. Jin (Invited), "Quark and lepton flavor physics," DOE Virtual Annual Progress Review of USQCD, Online, May 18, 2021.

N. Matsumoto, "Search for an effective change of variable in QCD simulations," DWQ@25, USA (BNL), Online, December 13, 2021.

[Seminars]

N. Matsumoto, "Sign problem and worldvolume tempered Lefschetz thimble method, RIKEN Radiation Laboratory," Wako, Japan (RIKEN), Online, July 14, 2021.

N. Matsumoto, "Worldvolume tempered Lefschetz thimble method as an algorithm towards solving the sign problem," RBRC seminar, USA (BNL), Online, November 18, 2021.

N. Matsumoto, "Comment on the subtlety of defining real-time path integral in lattice gauge theories," Colorado University informal seminar, Colorado, USA, Online, July 21 2022.

N. Matsumoto, "Comment on the subtlety of defining real-time path integral in lattice gauge theories," KEK theory seminar, Tsukuba, Japan, Online, July 12, 2022.

N. Matsumoto, "Comment on the subtlety of defining real-time path integral in lattice gauge theories," Osaka University Particle Physics Group seminar, Osaka, Japan, Online, November 8, 2022.

N. Matsumoto, "Use of Schwinger-Dyson equation in constructing an approximate trivializing map," LATTICE 2022, Bonn, Germany, August 8, 2022.

L. Jin, "Lattice calculations in muon $g-2$," Department of Physics and Astronomy, University of California, Davis, Online, May 3, 2021.

L. Jin, "Lattice calculations in muon $g-2$," Hadron mass and structure forum, Online, April 20, 2021.

L. Jin, "Lattice calculations in muon $g-2$," Institute of Theoretical Physics, Chinese Academy of Sciences, Online, April 15, 2021.

L. Jin, "Muon $g-2$: hadronic light-by-light contribution and lattice QCD," Muon $g-2$ discussion forum, Peking University, Online, April 13, 2021.

Subnuclear System Research Division
RIKEN Facility Office at RAL

1. Abstract

Our core activities are based on the RIKEN-RAL Muon Facility located at the ISIS Neutron & Muon Source at the Rutherford Appleton Laboratory (UK), which provides intense pulsed-muon beams. The RIKEN-RAL Muon Facility is a significant and long-standing collaboration between RIKEN and RAL in muon science–with 2020 being the 30th years of continuous agreements between RIKEN and RAL. The Facility enables muon science throughout Japan and other field—it continues to attract proposals from a wide variety of Japanese universities and institutions (with over 80 groups having now used the facility), and including industrial users such at Toyota, and has been instrumental in establishing scientific links with other Asian universities.

Muons have their own spins with 100% polarization, and can detect local magnetic fields and their fluctuations at muon stopping sites very precisely. The method to study the characteristics of materials by observing time dependent changes of muon spin polarization is called "Muon Spin Rotation, Relaxation and Resonance" (μSR method), and is applied to study electro-magnetic properties of insulating, metallic, magnetic and superconducting systems. Muons reveal static and dynamic properties of the electronic state of materials in the zero-field condition, which is the ideal magnetic condition for research into magnetism. For example, we have carried out μSR investigations on a wide range of materials including frustrated pyrochlore systems, which have variety of exotic ground states of magnetic spins, so the magnetism study of this system using muon is quite unique.

The ultra-cold muon beam can be stopped in thin foil, multi-layered materials and artificial lattices, which enables us to apply the aSR techniques to surface and interface science. The development of an ultra-cold muon beam is also very important as a source of pencil-like small emittance muon beam for muon $g-2$/EDM measurement. We have been developing muonium generators to create more muonium atoms in vacuum even at room temperature to improve beam quality compared with the conventional hot-tungsten muonium generator. We have demonstrated a strong increase in the muonium emission efficiency by fabricating fine laser drill-holes on the surface of silica aerogel. We are also developing a high power Lyman-alpha laser in collaboration with the Advanced Photonics group at RIKEN. The new laser will ionize muoniums 100 times more efficiently for slow muon beam generation.

Over the past 2–3 years, a significant development activity in muon elemental analysis has taken place, proton radius experiments have continued and been developed, and chip irradiation experiments have also continued.

2. Major Research Subjects

(1) Materials science by muon-spin-relaxation method and muon site calculation
(2) Development of elemental analysis using pulsed negative muons
(3) Nuclear and particle physics studies via muonic atoms and ultra-cold muon beam
(4) Other muon applications

3. Summary of Research Activity

(1) Materials science at the RIKEN-RAL muon facility

Muons have their own spins with 100% polarization, and can detect local magnetic fields and their fluctuations at muon stopping sites very precisely. The μSR method is applied to studies of newly fabricated materials. Muons enable us to conduct (1) material studies under external zero-field condition, (2) magnetism studies with samples without nuclear spins, and (3) measurements of muon spin relaxation changes at wide temperature range with same detection sensitivity. The detection time range of local field fluctuations by μSR is 10^{-6} to 10^{-11} second, which is an intermediate region between neutron scattering method (10^{-10}–10^{-12} second) and Nuclear Magnetic Resonance (NMR) (longer than 10^{-6} second). At Port-2 and 4 of the RIKEN-RAL Muon Facility, we have been performing μSR researches on strong correlated-electron systems, organic molecules, energy related materials and biological samples to study electron structures, superconductivity, magnetism, molecular structures and crystal structures.

Among our scientific activities on μSR studies from year up to 2022, following subjects of materiasl sciences are most important achievements at the RIKEN-RAL muon facility:

(1) Quasi magnetic monopole state in the Ru-based pyrochlore systems, $R_2Ru_2O_7$;
(2) Novel superconducting gap structure in the quasi two-dimensional organic superconductor, λ-$(BETS)_2GaCl_4$;
(3) Determination of muon positions estimated from density functional theory (DFT) and dipole-field calculations;
(4) Chemical muonic states in DNA molecules.

Result-1) Quasi magnetic monopole state in pyrochlore systems gave us new interpretations to understand exotic phenomena, like the quantum spin liquid and spin fragmentation states. Result-2) A novel superconducting gap structure in the quasi two-dimensional organic superconductor, λ-$(BETS)_2GaCl_4$. An intermediate one-band superconducting gap-structure was confirmed. Result-3) Well known and deeply investigated La_2CuO_4 has opened a new scheme of the Cu spin. Taking into account quantum effects to expand the Cu-spin orbital and muon positions, we have succeeded to explain newly found muon sites and hyperfine fields at those sites. Result-4) Chemical states of the muon which attaches to DNA molecules were investigated by the avoided level-crossing muon-spin resonance experiments. In conjunction with DFT calculations, we are trying to reveal the electron motion though the DNA molecule.

We have been continuing to develop muon-science activities in Asian countries. We enhanced international collaborations to organize new μSR experimental groups and to develop muon-site calculation groups using computational method. We are creating new collaborations with new teams in different countries and also continuing collaborations in μSR experiments on strongly correlated systems with researchers from Taiwan, Indonesia, China, Thailand and Malaysia including graduate students. We are starting to

collaborate with the new Chinese muon group who are developing the Chinese Muon Facility and trying to develop more muon activities in the Asian area.

(2) Development of elemental analysis using pulsed negative muons

There has been significant development of elemental analysis using negative muons on Port 4 and Port 1 over the past couple of years. Currently, elemental analysis commonly uses X-ray and electron beams, which accurately measure surfaces. However, a significant advantage of muonic X-rays over those of electronic X-rays is their higher energy due to the mass of the muon. These high energy muonic X-rays are emitted from the bulk of the samples without significant photon self-absorption. The penetration depth of the muons can be varied by controlling the muon momentum, providing data from a thin slice of sample at a given depth. This can be over a centimeter in iron, silver and gold or over 4 cm in less dense materials such as carbon.

Some techniques for elemental analysis are destructive or require the material under investigation to undergo significant treatment and some of the techniques are only sensitive to the surface. Therefore, negative muons offer a unique service in which they can measure inside, beyond the surface layer and completely non-destructively.

The areas of science that have used negative muons for elemental analysis have been very diverse. The largest area is the cultural heritage community as the non-destructive ability is particularly important and will become more so. This community have investigated swords from different eras, coins (Roman gold and silver, Islamic silver and from the Tudor Warship Mary Rose), miniature boats from Sardinia, reliefs on Baptist church gate, Bronze Age tools and cannon balls. In addition, energy materials (Li composition for hydrogen storage), bio-materials (search for iron to potentially help understand Alzheimer's), engineering alloys (manufacturing processes for new materials for jet engines), and functional materials (surface effects in piezo electrics) have also been investigated. The study was extended to see the difference by isotopes of silver and lead, which may give hint on the source of the material.

(3) Ultra-cold (low energy) muon beam generation and applications

Positive muon beam with thermal energy has been produced by laser ionization of muonium (bound system of μSR^+ and electron) emitted from a hot tungsten surface with stopping surface muon beam at Port-3. The method generates a positive muon beam with acceleration energy from several 100 eV to several 10 keV, small beam size (a few mm) and good time resolution (less than 8 nsec). By stopping the ultra-cold muon beam in thin foil, multi-layered materials and artificial lattices, we can precisely measure local magnetic field in the materials, and apply the μSR techniques to surface and interface science. In addition, the ultra-cold muon is very important as the source of pencil-like small emittance muon beam for muon $g-2$/EDM measurement. It is essential to increase the slow muon beam production efficiency by 100 times for these applications. There are three key techniques in ultra-cold muon generation: production of thermal muonium, high intensity Lyman-alpha laser and the ultra-cold muon beam line.

A high-power Lyman-alpha laser was developed in collaboration with the Advanced Photonics group at RIKEN. The new laser system is used at J-PARC U-line and, upon completion, will ionize muoniums 100 times more efficiently for slow muon beam generation. In this development, we succeeded to synthesize novel ceramic-based Nd:YGAG and Nd:YSAG crystals, which realized a highly efficient and stable laser system. We are working hard to improve the homogeneity of large size crystals in order to achieve full design power.

We also succeeded in developing an efficient muonium generator, laser ablated silica aerogel, which emits more muoniums into vacuum even at room temperature. Study has been done at TRIUMF utilizing positron tracking method of muon decay position. We demonstrated in 2013 at least 10 times increase of the muonium emission efficiency by fabricating fine laser drill-holes on the surface of silica aerogel. Further study was carried out in 2017 to find the optimum fabrication that will maximize the muonium emission. From the analysis, we found the emission has large positive correlation with the laser ablated area rather than with any other parameters. We also confirmed the muon polarization in vacuum. An alternative detection method for muonium emission using muonium spin rotation, which will be sensitive even to muoniums near the surface, was tested at RIKEN-RAL in 2018 and was found successful. The study was further applied to the measurement of the temperature dependence.

A new ultra-cold muon beam line for muon $g-2$/EDM was constructed based on our various experience. The new beamline has larger aperture for the beam, easier magnetic field monitoring, active field cancelling, and fine beam control for the injection to RFQ accelerator. The beamline is being tested at J-PARC S2 line.

(4) Other fundamental physics studies

We proposed the measurement of the proton radius by using the hyperfine splitting of the muonic hydrogen ground state. This hyperfine splitting is sensitive to the Zemach radius, which is a convolution of charge and magnetic-dipole distributions inside proton. We are planning to re-polarize the muonic hydrogen by a circularly polarized excitation laser (excites one of the $F = 1$ states and regenerates the muon spin polarization), and detect the recovery of the muon decay-asymmetry along the laser.

Preparation using muon beam is in progress. We measured the muon stopping distribution in low-density hydrogen-gas cell, which gave us consistent results with beam simulation. Another key is the lifetime of the upper hyperfine state of the muonic hydrogen that will contribute the polarization. We successfully observed the clear muon spin precession of muonic deuterium atom in 2018 for the first time in the world. The measurement with muonic protium was carried out in 2019 and the data is being analyzed.

(5) Facility operation and refurbishment

The research activity at RIKEN-RAL had severe restriction in FY2021 also since the COVID-19 pandemic continued. It was impossible for users from outside RAL to carry out the experiment. Even though, we managed to carry out several μSR experiments with mailed samples. Since July 2021, RIKEN-RAL muon facility had been undergoing major refurbishment, first time since its operation in 1994. The work coverd many important components, such as the cooling water circuit, vacuum system, radiation shielding, magnet

power supplies and power cables, detectors and beamline control system. Most of the works were completed by December 2022. We had some test beam at the end of December and confirmed that most of the beamline components are working fine. As the ISIS beam delivery in early 2023 was very limited, we are planning the full beam test in middle 2023.

Members

Director
Philip KING

Senior Research Scientist
Isao WATANABE

Contract Researcher
Katsuhiko ISHIDA

List of Publications & Presentations

Publications

[Original Papers]

M. D. Umar, K. Ishida, R. Murayama, D. P. Sari, U. Widyaiswari, M. Fronzi, I. Watanabe, and M. Iwasaki, "Muon-spin motion at the crossover regime between gaussian and lorentzian distribution of magnetic fields," Prog. Theor. Exp. Phys. **2021**, 083101 (2021).

W. N. Zaharim, S. N. A. Ahmad, S. Sulaiman, H. Rozak, D. F. H. Baseri, N. A. M. Rosli, S. S. Mohd-Tajudin, L. S. Ang, and I. Watanabe, "Density functional theory study of 12 mer single-strand guanine oligomer and associated muon hyperfine interaction," ACS Omega **6**, 29641 (2021).

A. Jamaludin, W. N. Zaharim, S. Sulaiman, H. Rozak, A. L. Sin, and I. Watanabe, "Density functional theory investigation of muon hyperfine interaction in guanine-cytosine double-strand DNA," J. Phys. Soc. Jpn. **91**, 024301 (2022).

S. Yoon, W. Lee, S. Lee, J. Park, H. Lee, Y. S. Choi, S. -H. Do, W. -J. Choi, W. -T. Chen, F. Chou, D. I. Gorbunov, Y. Oshima, A. Ali, Y. Singh, A. Berlie, I. Watanabe, and K. -Y. Choi1, "Quantum disordered state in the J_1-J_2 square-lattice antiferromagnet $Sr_2Cu(Te_{0.95}W_{0.05})O_6$," Phys. Rev. Res. **5**, 014411 (2021).

Ce Zhang, T. Hiraki, K. Ishida, S. Kamal, S. Kamioka, T. Mibe, A. Olin, N. Saito, K. Suzuki, S. Uetake, and Y. Mao, "Modeling the diffusion of muonium in silica aerogel and its application to a novel design of multi-layer target for thermal muon generation," Nucl. Instrum. Methods Phys. Res. A **1042**, 167443G (2022).

A. Green, K. Ishida, K. Domoney, T. Agoro, and A. D. Hillier, "Negative muons reveal the economic chaos of Rome's AD 68/9 Civil Wars," Archaeol. Anthropol. Sci. **14**, 165 (2022).

Presentations

[International Conference/Workshop]

K. Ishida on behalf of the J-PARC muon $g-2$/EDM collaboration (E34), "Muon $g-2$/EDM experiment at J-PARC," Fifth Plenary Workshop of the Muon $g-2$ Theory Initiative, UK (The University of Edinburgh), September 5–9, 2022.

[Domestic Conferences/Workshops]

石田勝彦, 「ラザフォードアップルトン研究所ミュオン施設の紹介」, 第 7 回文理融合シンポジウム 量子ビームで歴史を探る—加速器が紡ぐ文理融合の地平—, つくば市 (KEK), 2022 年 11 月 3 日.

石田勝彦, 「ミュオン触媒核融合の利用」, 中間子科学の将来討論会, 和光市 (理研), 2022 年 11 月 9–11 日.

石田勝彦, 「理研 RAL 施設と原子・原子核研究」, 第 13 回 muon 科学と加速器研究研究会, 和光市 (理研), 2023 年 1 月 10–11 日.

Safety Management Group

1. Abstract

The RIKEN Nishina Center for Accelerator-Based Science possesses one of the largest accelerator facilities in the world, which consists of two heavy-ion linear accelerators and five cyclotrons. This is the only site in Japan where uranium ions are accelerated. The center also has electron accelerators of microtron and synchrotron storage ring. Our function is to keep the radiation level in and around the facility below the allowable limit and to keep the exposure of workers as low as reasonably achievable. We are also involved in the safety management of the Radioisotope Center, where many types of experiments are performed with sealed and unsealed radioisotopes.

2. Major Research Subjects

(1) Safety management at radiation facilities of Nishina Center for Accelerator-Based Science
(2) Safety management at Radioisotope Center
(3) Radiation shielding design and development of accelerator safety system
(4) Obtaining permissions for changes accelerators and use of radioisotopes

3. Summary of Research Activity

Our most important task is to keep the personnel exposure as low as reasonably achievable, and to prevent an accident. Therefore, we daily patrol the facility, measure the ambient dose rates, maintain the survey meters, shield doors and facilities of exhaust air and wastewater, replenish the protective supplies, and manage the radioactive waste. Advice, supervision and assistance at major accelerator maintenance works are also our task.

Permissions from Nuclear Regulation Authority of Japan for the Radioisotope Production beamline and additional quantity of unsealed radioisotope astatine-211 was obtained. Safety measures were conducted in the Radioisotope Experimental building owing to the increased use of alpha-emitting nuclides. Measures for the Covid-19 infection in Nishina center were also conducted. A fire drill by a small group of emergency response personnel assuming Saturday, Sunday and nighttime hours were carried out with the general affairs section in RIKEN.

Members

Director
Kanenobu TANAKA

Technical Scientists
Rieko HIGURASHI
Hisao SAKAMOTO
Hiroki Mukai

Expert Technician
Atsuko AKASHIO

Visiting Scientists
Toshiya SANAMI (KEK)
Kenta SUGIHARA (KEK)
Hiroshi YASHIMA (Kyoto Univ.)
Nobuhiro SHIGYO (Kyushu Univ.)
Eunji LEE (KEK)

Administrative Part-time Workers
Kimie IGARASHI
Satomi IIZUKA
Miyabi MURATA
Naoko USUDATE
Tokie KUDO

Temporary Staffing
Ryuji SUZUKI

Assistant
Tomomi OKAYASU

List of Publications & Presentations

Publications

[Original Papers]

K. Sugihara, N. Shigyo, A. Akashio, and K. Tanaka, "Measurement of neutron energy spectra of 345 MeV/nucleon ^{238}U incidence on a copper target," Nucl. Instrum. Methods Phys. Res. B **512**, 102 (2022).

K. Sugihara, N. Shigyo, E. Lee, T. Sanami, and K. Tanaka, "Measurement of thick target neutron yields from 7 MeV/nucleon α incidence on ^{209}Bi," Nucl. Instrum. Methods Phys. Res. B **470**, 15 (2020).

Presentations

[International Conferences/Workshops]

K. Tanaka (plenary), "Resent fire protection status at RIKEN RIBF cyclotron facility," International Technical Safety Forum (ITSF2022), Meyrin, Switzerland, October 24–28, 2022.

K. Sugihara (plenary), N. Shigyo, A. Akashio, and K. Tanaka, "Measurement of neutron production yields of 345 MeV/nucleon ^{238}U + Cu with a time-of-flight method," 15th workshop on Shielding aspects of Accelerators, Tagets, and Irradiation Facilties (SATIF-15), Michigan, USA, September 20–23, 2022.

User Liaison Group

1. Abstract

The User Liaison Group is engaged in activities to promote the efficient and wide-ranging use of the RIBF accelerator facility. The Group has two teams, the RIBF User Liaison Team and the Outreach Team, to carry out these tasks.

The main activities of the RIBF User Liaison Team include i) organizing the International Program Advisory Committees to review scientific experimental proposals to use RIBF, ii) management of beamtime for efficient use of RIBF, iii) acceptance of researchers from outside RIKEN based on the "RIBF Independent User" system established to promote the use of RIBF, and iv) operation of the RIBF Users Office to provide RIBF Independent Users with one-stop processing of various procedures for the use of RIBF.

The Outreach Team has created various information materials, such as pamphlets, posters, and homepages, to introduce the research activities in the RNC. On the homepage, we provide information on usage of the RIBF facility. The team also participate in science introduction events hosted by public institutions. In addition, the Team also takes care of laboratory tours for RIBF visitors from public.

Members

Director

Hideki UENO

Assistants

Yu NAYA
Asako TAKAHASHI
Tomomi OKAYASU

User Liaison Group
RIBF User Liaison Team

1. Abstract

To enhance synergetic common use of the world-class accelerator facility, the Radioisotope Beam Factory (RIBF), it is necessary to promote a broad range of applications and to maximize the facility's importance. The facilitation and promotion of the RIBF are important missions charged to the team. Important operational activities of the team include: i) the organization of international Program Advisory Committee (PAC) meetings to review experimental proposals submitted by RIBF users, ii) RIBF beam-time operation management, and iii) promotion of facility use by hosting outside users through the RIBF Independent Users program, which is a new-user registration program begun in FY2010 at the RIKEN Nishina Center (RNC) to enhance the synergetic common use of the RIBF. The team opened the RIBF Users Office in the RIBF building in 2010, which is the main point of contact for Independent Users and provides a wide range of services and information.

2. Major Research Subjects

(1) Facilitation of the use of the RIBF
(2) Promotion of the RIBF to interested researchers

3. Summary of Research Activity

(1) Facilitation of the use of the RIBF

The RIBF Users Office, formed by the team in 2010, is a point of contact for user registration through the RIBF Independent User program. This activity includes:

- registration of users as RIBF Independent Users,
- registration of radiation workers at the RIKEN Wako Institute,
- provision of an RIBF User Card (a regular entry permit) and an optically stimulated luminescence dosimeter for each RIBF Independent User, and
- provision of safety training for new registrants regarding working around radiation, accelerator use at the RIBF facility, and information security, which must be completed before they begin RIBF research. The RIBF Users Office is also a point of contact for users regarding RIBF beam-time-related paperwork, which includes:
- contact for beam-time scheduling and safety review of experiments by the In-House Safety Committee, and
- maintaining the above information in a beam-time record database.

In addition, the RIBF Users Office assists RIBF Independent Users with matters related to their visit, such as invitation procedures, visa applications, and the reservation of on-campus accommodation.

(2) Promotion of the RIBF to interested researchers

- The team has organized an international PAC for RIBF experiments; it consists of leading scientists worldwide and reviews proposals in the field of nuclear physics (NP) purely on the basis of their scientific merit and feasibility. The team also assists another PAC meeting for material and life sciences (ML) organized by the RNC Advanced Meson Laboratory. The NP PAC meeting is organized once a year regularly, and the ML PAC meetings are organized once or twice a year.
- The team coordinates beam times for PAC-approved experiments and other development activities. It manages the operating schedule of the RIBF accelerator complex according to the decisions arrived at by the RIBF Machine Time Committee.
- To promote research activities at RIBF, proposals for User Liaison and Industrial Cooperation Group symposia/mini-workshops are solicited broadly both inside and outside of the RNC. The RIBF Users Office assists in the related paperwork.
- The team is the point of contact for the RIBF users' association. It arranges meetings at RNC headquarters for the RIBF User Executive Committee of the users' association.
- The Team conducts publicity activities, such as arranging for RIBF tours, development and improvement of the RNC official web site, and delivery of RNC news via email and the web.

Member

Team Leader

Ken-ichiro YONEDA

User Liaison Group
Outreach Team

1. Abstract

The mission of the Outreach Team is to provide various “intangible” technical support for the dissemination of information on the research in the RNC. For instance, the team creates brochures introducing the RNC and the RIBF accelerator facility, posters of symposia and the summer school hosted by the RNC, the center homepage containing information such as details of the RNC and the procedure for the use of the RIBF facility, and images of equipment and facilities available for researchers inside and outside RIKEN, among the others. Furthermore, the team also participates in science introduction events hosted by public institutions.

2. Major Work Contents

The major work contents of the Outreach Team is to promote the publicity of the RNC, through the creation of various materials such as brochures, websites, posters, and videos, among the others. The arrangement of tours of the RIBF facility and the exhibition and introduction of the RIBF facility at science events are also conducted independently or in cooperation with RIKEN Public Relations Office.

3. Summary of Work Activity

The specific work contents performed by the team are as follows:

- [Website] The Team creates/manages the RNC official website (`http://www.nishina.riken.jp`), which introduces the organization and its research activities. This website plays an important role in providing information to researchers who visit the RNC to conduct his/her own research.
- [Pamphlets] The Team has produced various pamphlets introducing the organization of and the studies performed at RNC. The pamphlet named “Your body is made of star scraps” explaining element synthesis in the universe and “Introduction of RIBF Facility” in a cartoon style for children are among them. As a related effort, a notebook for elementary school students featuring RIBF was produced in FY2022. The notebooks will be distributed to elementary school students
- [Posters] Conference/Symposium posters connected with RNC were prepared on the request of organizers. For general purpose, a special poster featuring the nuclear chart has been prepared for distribution. In commemoration of the discovery of nihonium, brochures and posters dedicated to the ceremony were made.
- [RIBF Cyclopedia] In April 2012, the permanent exhibition hall (RIBF Cyclopedia) located at the entrance hall of the RIBF building was set up in cooperation with RIKEN Public Relations Office. Explanatory illustrations on nuclear science, research at RIBF, RIBF history, a 3D nuclear chart built with LEGO blocks, and a 1/6-size GARIS model are displayed to help understanding through visual means. The Team is also working on updating the exhibits.
- [RIBF facility tour] The Team arranges RIBF facility tour for over 2000 visitors per year. The tour is guided by a researcher. Although the number of visitors has not yet reached this level, the number of RIBF tour participants showed a recovery trend in FY2022 as the situation in COVID19 improved.
- [Science event participation] In 2010, 2012, 2013, 2015, and 2016, the Team opened an exhibition booth of RNC to introduce the latest research activities on the occasion of the “Science Agora” organized by Japan Science and Technology Agency (JST). From time to time, the Team was invited to participate in scientific events by MEXT, Wako city, and Nissan global foundation. One attraction targeting children is the hands-on work of assembling “Iron-beads” to create a nuclear chart or a shape of nihonium. For FY2022, the Team did not exhibit at these events, but provided technical assistance to online participants at an event for students held at the RNC.
- [RIKEN Wako Open Campus] In the FY2022 Open Campus, the Team continued to produce all videos to introduce RIBF for online viewing as did last year. The RIBF facility tour was also conducted with a limited number of visitors, with COVID-19 infection control measures in place. Not only the Team, but also almost all members of the User Liaison Group cooperated in the tour event.
- [Yoshio Nishina Memorial Office Unveiling Ceremony] The “Yoshio Nishina Memorial Office Unveiling Ceremony” and the Symposium “Trajectory/Miracle of the RIKEN Yoshio Nishina Laboratory” were held at the RNC on October 28, 2022. The Team has been involved in the preparation of the ceremony from the beginning, producing pamphlets and commemorative items.

In addition to the above-noted work contents, the Team conducts a variety of works, such as taking pictures of meetings organized by RNC, cooperation in the production of a 3D video to explain the accelerators and the research at RIBF, among the others.

Members

Team Leader
Hideki UENO

Technical Staff
Narumasa MIYAUCHI

Special Temporary Research Scientist
Yasushi WATANABE

Office of the Center Director

1. Abstract

This office is in place from JFY2018 to conduct works that the Center Director deems necessary for the operation of the research center and the secretarial work related to the research center in general.

2. Major Work Contents

- Nishina Center Monthly Meeting
  The purpose of the meeting is to share information on activities within the Nishina Center with all of the members. The meeting covers introduction of newcomers, press-released achievements, announcement of events organized by or related to the Nishina Center, safety issues, and others to be informed to all members. The meeting agenda is distributed to all of the members via mailing-list.
- Conference Support
  Assistant staff members support coherently a large-size conference hosted by the Nishina Center.
- Orientation for newcomers to the Nishina Center
  The Orientation is organized once a year to the newcomers to give instructions for emergency response, safety in research, computer and network resources and security, and research misconduct prevention.

3. Summary of Work Activity

- Nishina Center Monthly Meeting
  Noriko Asakawa arranged the agenda and Hidetada Baba supported the on-line video system for the meeting.
  - The 179th, April 13, 2022
    (1) Greetings from the RNC Director to kick off the new fiscal year
    (2) Introduction of newcomers
    (3) Awards
    RIKEN Eiho Award, RIKEN Baiho Award, RIKEN Ohbu Award, PTEP Editors' Choice
    (4) Report from the RNC Director
  - The 180th, May 11, 2022
    (1) Introduction of newcomers
    (2) Award
    Saruhashi Prize
    (3) Report on RIKEN Open Day
    (4) Press release
    Superconducting Ring Cyclotron has been registered in Guinness World Records™!
    "α-Clustering in Atomic Nuclei from First Principles with Statistical Learning and the Hoyle State character"
    "First Application of Mass Measurement with the Rare-RI Ring Reveals the Solar r-Process Abundance Trend at $A = 122$ and $A = 123$"
    (5) Report from the RNC Director
  - The 181st, June 8, 2022
    (1) Introduction of newcomers
    (2) Farewell speech
    (3) Award 2021 Wada Memorial Award
    (4) Nishina Laboratory room reproduction
    Information on related events
    (5) Report on "Physics of RI: Recent progress and perspectives"
    (6) Report from the RNC Director
  - The 182nd, July 13, 2022
    (1) Introduction of newcomers
    (2) Report from the Nishina Center and iTHEMS Promotion Office
    (3) Award
    Friedrich Wilhelm Bessel Research Award
    (4) Press release
    "Observation of a correlated free four-neutron system"
    (5) Diversity promotion activity report
    Website of the Nishina Center Cheering Squad
    (6) Report from the RNC Director
  - The 183rd, September 5, 2022
    (1) Introduction of newcomers
    (2) Report on "Accelerator Kitchen"
    (3) Request for donations for the Yoshio Nishina Memorial Project

(4) Space for external users
(5) Report from the RNC Director

– The 184th, October 12, 2022
(1) Self-introduction by newly appointed personnel
(2) Introduction of newcomer
(3) RIBF Thesis Award
(4) Report from the RNC Director

– The 185th, November 9, 2022
(1) Award
Japanese Society of Crop Science Best Paper Award
(2) Press release
"β-Delayed One and Two Neutron Emission Probabilities South-East of ^{132}Sn and the Odd-Even Systematics in r-Process Nuclide Abundances"
(3) The 19th International Conference on Electromagnetic Isotope Separators and Related Topics (EMIS2022)
(4) Report from the RNC Director

– The 186th, December 9, 2022
(1) Award
The Outstanding Presentation Award presented at the 65th Radiation Chemistry Forum
(2) Press release
"Discovery of ^{39}Na"
(3) Report from the RNC Director
(4) RIKEN Accelerator Progress Report

– The 187th, January 16, 2023
(1) New Year's Greeting from the RNC Director
(2) Press Release
"Study of the N = 32 and N = 34 Shell Gap for Ti and V by the First High-Precision Multireflection Time-of-Flight Mass Measurements at BigRIPS-SLOWRI"
(3) Report from the RNC Director

– The 188th, February 8, 2023
(1) INTT of sPHENIX
(2) Nishina Center Library (archives)
(3) Simplified fire drill on February 21, 2023
(4) Industry Membership to Create the Future with RIKEN
(5) Report from the RNC Director

– The 189th, March 8, 2023
(1) Press release
"Long-Term Density Trend in the Mesosphere and Lower Thermosphere from Occultations of the Crab Nebula with X-Ray Astronomy Satellites"
(2) Report from the RNC Director
(3) Other
(4) Farewell greetings

- Conference Support
No large size conferences hosted by the Nishina Center were organized.
- Orientation for newcomers to the Nishina Center
The Orientation was organized on April 15, 2022.

Members

Director
Motohide YOKOTA

Research Administrator
Narumasa MIYAUCHI

Assistants
Noriko ASAKAWA
Yu NAYA
Asako SAKIHAMA
Karen SAKUMA
Asako TAKAHASHI
Mitsue YAMAMOTO
Izumi YOSHIDA

Partner Institutions

The RIKEN Nishina Center for Accelerator-Based Science (RNC) has collaborated with universities and research institutes since 2008 under the research partnership agreement. This collaboration framework permits an external institute to develop its own projects at the RIKEN Wako Campus in equal partnership with the RNC. At present, two institutes—the Center for Nuclear Study (CNS), the University of Tokyo and the Wako Nuclear Science Center (WNSC), Institute of Particle and Nuclear Studies (IPNS), High Energy Accelerator Research Organization (KEK)—are conducting joint research under the research partnership agreement.

The CNS and RNC signed the research partnership agreement in 2008. Until then, the CNS had collaborated in joint programs with RIKEN under the "Research Collaboration Agreement on Heavy Ion Physics" (collaboration agreement) signed in 1998. The partnership agreement redefines procedures related to the joint programs while keeping the spirit of the collaboration agreement. The joint programs include experimental nuclear-physics activities using CRIB, SHARAQ, OEDO, and GRAPE at the RI Beam Factory (RIBF), accelerator developments, and activities at RHIC PHENIX.

The KEK-WNSC and RNC signed a research partnership agreement on "Low-Energy Unstable Nuclear Beam Science" in 2011. The joint experimental programs are based on the KEK Isotope Separation System (KISS). The KISS has been available for RIBF users since 2015. The research collaboration agreement for the SLOWRI facility and the multi-reflection time-of-flight (MRTOF) mass spectrograph was then signed in 2019, based on which the SLOWRI Joint Operation Committee has been established for the collaborative use and operation of the SLOWRI facility.

Experimental proposals that request the use of the above-noted devices of the CNS and KEK, together with other key devices at the RIBF, are screened by the Program Advisory Committee for Nuclear Physics experiments at the RIBF (NP-PAC). The NP-PAC meetings are co-hosted by the CNS and KEK.

Matters necessary for the smooth promotion of joint research based on the research partner agreement are determined at the Collaboration Liaison Council. More specific matters related to the execution of collaborative research are discussed at the Collaboration Liaison Committee established under the Liaison Council. In order to enhance the effectiveness of coordination and information sharing on joint research programs, the Joint Researchers Meeting was established in 2020 under the Collaboration Liaison Committee.

Several members of both institutes have also been invited to participate as external members in RNC committees related to the operation of the RIBF, such as the Machine-Time Committee and the Safety Review Committee.

The activities of the CNS and KEK are reported in the succeeding pages.

Partner Institution
Center for Nuclear Study, Graduate School of Science
The University of Tokyo

1. Abstract

The Center for Nuclear Study (CNS) aims to elucidate the nature of nuclear system by producing the characteristic states where the Isospin, Spin and Quark degrees of freedom play central roles. These researches in CNS lead to the understanding of the matter based on common natures of many-body systems in various phases. We also aim at elucidating the explosion phenomena and the evolution of the universe by the direct measurements simulating nuclear reactions in the universe. In order to advance the nuclear science with heavy-ion reactions, we develop AVF upgrade, CRIB and SHARAQ facilities in the large-scale accelerators laboratories RIBF. The OEDO facility has been developed as an upgrade of the SHARAQ, where a RF deflector system has been introduced to obtain a good quality of low-energy beam. A new project for fundamental symmetry using heavy RIs has been starting to install new experimental devices in the RIBF. We promote collaboration programs at RIBF as well as RHIC-PHENIX and ALICE-LHC with scientists in the world, and host international meetings and conferences. We also provide educational opportunities to young scientists in the heavy-ion science through the graduate course as a member of the department of physics in the University of Tokyo and through hosting the international summer school.

2. Major Research Subjects

(1) Accelerator Physics
(2) Nuclear Astrophysics
(3) DONUTS/NUSPEQ
(4) Quark physics
(5) Nuclear Theory
(6) OEDO/SHARAQ project
(7) Exotic Nuclear Reaction
(8) Fundamental Physics

3. Summary of Research Activity

(1) Accelerator Physics

One of the major tasks of the accelerator group is the development of ion sources and the optimization of the beam transport system for the experimental devices installed in the E7 experiment room. In 2022, HyperECR ion source was operated for 2,151 hours. A new method for sustainable magnesium beam production was put into practical use for CRIB. The $^{24}Mg^{8+}$ beam was successfully produced for 18 days with four breaks to refill the sample crucible. In a university-industry collaboration, a magnetic design for a new ECR ion source was proposed for industrial applications. For the development of the pepper-pot emittance monitor to diagnose the beam extracted from AVF cyclotron, an optical system with a digital camera was completed. Then, the required angular accuracy was estimated to be less than 0.3 mrad. The beam test for the prototype was planned and the preparation was started.

(2) Nuclear astrophysics

The main activity of the nuclear astrophysics group is to study astrophysical reactions and special nuclear structure, such as clusters, using the low-energy RI beam separator CRIB. In October 2022, a ^{6}He radioactive beam was produced for the second time at CRIB, with imporved beam intensity and purity by introducing wire chambers (MWDC) and a degrader. In Mar 2023, we performed a direct measurement of astrophysical $^{14}O(\alpha, p)$ reaction in an international collaboration with the groups in IBS (Korea), Texas A&M University (US) and others. An active-target system developed in Texas (TexAT) was brought to Japan to perform this measurement with the thick-target method using the ^{14}O radioactive beam at CRIB. This was the first experiment at CRIB with participants from foreign countries after the pandemic.

(3) DONUTS/NUSPEQ

The Low Energy Nuclear Reaction group studies exotic structures in high-isospin and/or high-spin states in nuclei. In the spring of 2022, two nuclear reactions, $^{130}Sn(d, p)$ and $^{56}Ni(d, p)$, SHARAQ18 and 19, respectively, were performed at the OEDO-SHARAQ system in inverse kinematics by employing the surrogate technique, where the decay channels of the unbound states were identified directly from the measurement of reaction residues. Prior to the SHRAQ18, MS22-01 was carried out to establish a new optics for transporting the ion beam with better transmission. In winter 2022, another OEDO experiment, SHARAQ12, for the single particle structure in ^{51}Ca was partially performed. The analyses of the experiments, ImPACT17-02-01, -02, and SHARAQ11, $^{4}He(^{8}He, ^{8}Be)4n$ reaction, are in progress. The analysis of the groundbreaking experiment on the inelastic decay from the isobaric analog resonances is almost finished. The CNS GRAPE (Gamma-Ray detector Array with Position and Energy sensitivity) is a major instrument for high-resolution in-beam gamma-ray spectroscopy. The digital signal processing equipment for the GRAPE is under development.

(4) Quark physics

Main goal of the quark physics group is to understand the properties of hot and dense nuclear matter created by colliding heavy nuclei at relativistic energies. The group has been involved in the PHENIX experiment at Relativistic Heavy Ion Collider (RHIC) at

Brookhaven National Laboratory, and the ALICE experiment at Large Hadron Collider (LHC) at CERN. As for ALICE, the group has involved in the data analyses, which include the measurement of low-mass lepton pairs in Pb-Pb collisions, the measurement of long range two particle correlations in p-Pb collisions, searches for thermal photons in high multiplicity pp collisions. The group has involved in the ALICE-TPC upgrade using a Gas Electron Multiplier (GEM), where the group is very active in the development and benchmarking of the online space-charge distortion corrections using machine learning techniques running on the Graphical Processing Unit (GPU). The group has started simulation studies for the ALICE 3 future upgrade.

(5) Nuclear Theory

The nuclear theory group is conducting large-scale shell-model calculations, having a strong relationship to the project "Program for Promoting Researches on the Supercomputer Fugaku." One of the key achievements in FY2022 is finding the mechanism of the strongly hindered $E0$ transition from the superdeformed 0^+ state to the ground state in ^{40}Ca. We are also performing shell-model calculations for the structure of neutron-rich nuclei in collaboration with experiments carried out in RIBF, RIKEN, focusing on the region around ^{54}Ca. Another important direction of our activity is application to the fundamental physics. In this year, we have found that the nuclear Schiff moment is strongly correlated to nuclear magnetic moments, which enables providing reliable Schiff moments in comparson to existing data.

(6) OEDO/SHARAQ project

The OEDO/SHARAQ group pursues experimental studies with RI beams by using the high-resolution beamline and the SHARAQ spectrometer, and the OEDO for the decelerated RI beams. The uniqueness of the OEDO-SHARAQ system is its versatile performance in low-energy RI production and high-resolution spectroscopy. In FY2022, taking advantage of this feature, two low-energy RI experiments for (d, p)-type surrogate reactions and a high-resolution direct mass measurement for two-proton radioactivity were performed. Through the measurements, we were able to demonstrate a smooth re-arrangement of the beamline and experimental detector setups. In addition, we installed an active stopper detector and γ-ray detectors for the in-flight isomeric tagging of exotic nuclei in the mass measurement program. Data analysis of performed experiments is ongoing. The experimental study of 0^- strength in nuclei using the parity-transfer charge exchange (^{16}O, ^{16}F) is in the final stage. The results of the first and second experiments with the OEDO system for LLFPs will be completed and reported soon.

(7) Exotic Nuclear Reaction

The Exotic Nuclear Reaction group studies various exotic reactions induced by heavy-ion beams. We proceeded with the data reduction of the double charge exchange (^{12}C,^{12}Be) reaction taken in the previous year for a search of double Gamow-Teller resonance.

(8) Fundamental Physics

The development of the quantum sensor to search for a permanent electric dipole moment (EDM) with an optical lattice interferometer is in progress at RIKEN. The RF filter was newly developed and installed to the beam transport system to obtain the secondary beam of the Fr ion with a high purity, which was used to improve the trapping efficiency of the magneto-optical trap. The parameter tuning to get high intensity cold Fr atoms in the MOT is continued. Furthermore, a homemade Yb-doped fiber amplifier (YDFA) is developed, required to generate a deep optical lattice potential that would enable a long interrogation time for the EDM measurement.

Members

Director

Yasuhiro SAKEMI

Scientific Staffs

Yasuhiro SAKEMI (Professor)
Kentaro YAKO (Associate Professor)
Nobuaki IMAI (Associate Professor)
Taku GUNJI (Associate Professor)
Hidetoshi YAMAGUCHI (Lecturer)
Shin'ichiro MICHIMASA (Assistant Professor)
Hiroki NAGAHAMA (Assistant Professor)
Noritaka KITAMURA (Assistant Professor)

Visiting Scientists

Yutaka UTSUNO (Visiting Professor)
Daiki NISHIMURA (Visiting Associate Professor)
Toshitaka KAJINO (Visiting Researcher)
Ikuko HAMAMOTO (Visiting Researcher)
Jongwon HWANG (Visiting Researcher)
Takahide NAKAGAWA (Visiting Researcher)
Susumu SHIMOURA (Visiting Researcher)
Noritaka SHIMIZU (Visiting Researcher)
Shinsuke OTA (Visiting Researcher)
Masanori DOZONO (Visiting Researcher)

Academic Specialist

Reiko KOJIMA

Technical Specialist
Yasuteru KOTAKA

Techinical Assistant
Masayoshi YAGYU

Project Research Associates
Seiya HAYAKAWA
Daiki SEKIHATA
Rin YOKOYAMA

Post Doctoral Associates
Keisuke NAKAMURA
Keita KAMAKURA
Nanru MA
Kota YANASE
Thomas William CHILLERY
Takeshi SAITO

Assistant Teaching Staffs
Yuko SEKIGUCHI
Keita KAWATA
Akane SAKAUE
Shoichiro MASUOKA
Hikari MURAKAMI

Graduate Students
Hideki SHIMIZU
Naoya OZAWA
Shutaro HANAI
Shintaro NAGASE
Ryotaro KOHARA
Jiatai LI
Daisuke UEHARA
Kodai OKAWA
Hitoshi BABA
Mirai FUKASE
Shujiro SINDO

Administration Staffs
Noriko SHIMANE
Ikuko YAMAMOTO
Yukino KISHI
Aki KOTAKA

List of Publications & Presentations

Publications

[Original Papers]

L. Yang, C. J. Lin, H. Yamaguchi, A. M. Moro, N. R. Ma, D. X. Wang, K. J. Cook, M. Mazzocco, P. W. Wen, S. Hayakawa, J. S. Wang, Y. Y. Yang, G. L. Zhang, Z. Huang, A. Inoue, H. M. Jia, D. Kahl, A. Kim, M. S. Kwag, M. L. Commara, G. M. Gu, S. Okamoto, C. Parascandolo, D. Pierroutsakou, H. Shimizu, H. H. Sun, M. L. Wang, F. Yang, and F. P. Zhong, "Breakup of the proton halo nucleus ^{8}B near barrier energies," Nat. Commun. **13**, 7193 (2022).

N. J. Abdulameer *et al.* [PHENIX], "Improving constraints on gluon spin-momentum correlations in transversely polarized protons via midrapidity open-heavy-flavor electrons in $p\uparrow + p$ collisions at $\sqrt{s}$ = 200 GeV," Phys. Rev. D **107**, 052012 (2023).

N. J. Abdulameer *et al.* [PHENIX], "Low-p_T direct-photon production in Au + Au collisions at $\sqrt{s_{NN}}$ = 39 and 62.4 GeV," Phys. Rev. C **107**, 024914 (2023).

N. J. Abdulameer *et al.* [PHENIX], "Measurements of second-harmonic Fourier coefficients from azimuthal anisotropies in $p + p$, $p +$ Au, $d +$ Au, and ^{3}He + Au collisions at $\sqrt{s_{NN}}$ = 200 GeV," Phys. Rev. C **107**, 024907 (2023).

U. Acharya *et al.* [PHENIX], "Study of ϕ-meson production in $p +$ Al, $p +$ Au, $d +$ Au, and ^{3}He + Au collisions at $\sqrt{s_{NN}}$ = 200 GeV," Phys. Rev. C **106**, 014908 (2022).

U. A. Acharya *et al.* [PHENIX], "Measurement of $\psi(2S)$ nuclear modification at backward and forward rapidity in $p + p$, $p +$ Al, and p + Au collisions at $\sqrt{s_{NN}}$ = 200 GeV," Phys. Rev. C **105**, 064912 (2022).

S. Acharya *et al.* [ALICE], "Measurement of anti-^{3}He nuclei absorption in matter and impact on their propagation in the Galaxy," Nat. Phys. **19**, 61 (2023).

S. Acharya *et al.* [ALICE], "Multiplicity dependence of charged-particle jet production in pp collisions at $\sqrt{s}$ = 13 TeV," Eur. Phys. J. C **82**, 514 (2022).

S. Acharya *et al.* [ALICE], "Measurement of beauty production via non-prompt D^0 mesons in Pb–Pb collisions at $\sqrt{s_{NN}}$ = 5.02 TeV," J. High Energy Phys. **12**, 126 (2022).

S. Acharya *et al.* [ALICE], "First study of the two-body scattering involving charm hadrons," Phys. Rev. D **106**, 052010 (2022).

S. Acharya *et al.* [ALICE], "Forward rapidity J/ψ production as a function of charged-particle multiplicity in pp collisions at $\sqrt{s}$ = 5.02 and 13 TeV," J. High Energy Phys. **06**, 015 (2022).

S. Acharya *et al.* [ALICE], "Neutral to charged kaon yield fluctuations in Pb–Pb collisions at $\sqrt{s_{NN}}$ = 2.76 TeV," Phys. Lett. B **832**, 137242 (2022).

U. A. Acharya *et al.* [PHENIX], "Transverse-single-spin asymmetries of charged pions at midrapidity in transversely polarized p + p collisions at $\sqrt{s}$ = 200 GeV," Phys. Rev. D **105**, 032003 (2022).

S. Acharya *et al.* [ALICE], "Production of light (anti)nuclei in pp collisions at $\sqrt{s}$ = 5.02 TeV," Eur. Phys. J. C **82**, 289 (2022).

S. Acharya *et al.* [ALICE], "Observation of a multiplicity dependence in the p_{T}-differential charm baryon-to-meson ratios in proton-proton collisions at $\sqrt{s}$ = 13 TeV," Phys. Lett. B **829**, 137065 (2022).

S. Acharya *et al.* [ALICE], "$\mathrm{K}^0_S\mathrm{K}^0_S$ and $\mathrm{K}^0_S\mathrm{K}^{\pm}$ femtoscopy in pp collisions at s = 5.02 and 13 TeV," Phys. Lett. B **833**, 137335 (2022).

S. Acharya *et al.* [ALICE], "Characterizing the initial conditions of heavy-ion collisions at the LHC with mean transverse momentum and anisotropic flow correlations," Phys. Lett. B **834**, 137393 (2022).

U. A. Acharya *et al.* [PHENIX], "Systematic study of nuclear effects in p + Al, p + Au, d + Au, and ^{3}He + Au collisions at $\sqrt{s_{NN}}$ = 200 GeV using π^0 production," Phys. Rev. C **105**, 064902 (2022).

S. Acharya *et al.* [ALICE], "Investigating charm production and fragmentation via azimuthal correlations of prompt D mesons with charged particles in pp collisions at $\sqrt{s}$ = 13 TeV," Eur. Phys. J. C **82**, 335 (2022).

S. Acharya *et al.* [ALICE], "Measurement of prompt D_s^+-meson production and azimuthal anisotropy in Pb–Pb collisions at $\sqrt{s_{NN}}$ = 5.02 TeV," Phys. Lett. B **827**, 136986 (2022).

S. Acharya *et al.* [ALICE], "Prompt D^0, D^+, and D^{*+} production in Pb–Pb collisions at $\sqrt{s_{NN}}$ = 5.02 TeV," J. High Energy Phys. **01**, 174 (2022).

U. A. Acharya *et al.* [PHENIX], "Transverse single spin asymmetries of forward neutrons in p + p, p + Al and p + Au collisions at $\sqrt{s_{NN}}$ = 200 GeV as a function of transverse and longitudinal momenta," Phys. Rev. D **105**, 032004 (2022).

S. Acharya *et al.* [ALICE], "General balance functions of identified charged hadron pairs of (π, K, p) in Pb–Pb collisions at $\sqrt{s_{NN}}$ = 2.76 TeV," Phys. Lett. B **833**, 137338 (2022).

S. Acharya *et al.* [ALICE], "Measurement of inclusive charged-particle b-jet production in pp and p–Pb collisions at $\sqrt{s_{NN}}$ = 5.02 TeV," J. High Energy Phys. **01**, 178 (2022).

S. Acharya *et al.* [ALICE], "Inclusive quarkonium production in pp collisions at $\sqrt{s}$ = 5.02 TeV," Eur. Phys. J. C **83**, 61 (2023).

S. Acharya *et al.* [ALICE], "Production of light (anti)nuclei in pp collisions at $\sqrt{s}$ = 13 TeV," J. High Energy Phys. **01**, 106 (2022).

S. Acharya *et al.* [ALICE], "Prompt and non-prompt J/ψ production cross sections at midrapidity in proton-proton collisions at $\sqrt{s}$ = 5.02 and 13 TeV," J. High Energy Phys. **03**, 190 (2022).

S. Acharya *et al.* [A Large Ion Collider Experiment and ALICE], "Measurement of the groomed jet radius and momentum splitting fraction in pp and Pb–Pb collisions at $\sqrt{s_{NN}}$ = 5.02 TeV," Phys. Rev. Lett. **128**, 102001 (2022).

S. Acharya *et al.* [ALICE], "Measurements of the groomed and ungroomed jet angularities in pp collisions at $\sqrt{s}$ = 5.02 TeV," J. High Energy Phys. **05**, 061 (2022).

S. Acharya *et al.* [ALICE], "Polarization of Λ and $\bar{\Lambda}$ Hyperons along the Beam Direction in Pb–Pb Collisions at $\sqrt{s_{NN}}$ = 5.02 TeV," Phys. Rev. Lett. **128**, 172005 (2022).

S. Acharya *et al.* [A Large Ion Collider Experiment and ALICE], "Hypertriton Production in p–Pb Collisions at $\sqrt{s_{NN}}$ = 5.02 TeV," Phys. Rev. Lett. **128**, 252003 (2022).

S. Acharya *et al.* [ALICE], "Study of very forward energy and its correlation with particle production at midrapidity in pp and p–Pb collisions at the LHC," J. High Energy Phys. **08**, 086 (2022).

U. A. Acharya *et al.* [PHENIX], "Kinematic dependence of azimuthal anisotropies in p + Au, d + Au, and ^{3}He + Au at $\sqrt{s_{NN}}$ = 200 GeV," Phys. Rev. C **105**, 024901 (2022).

S. Acharya *et al.* [ALICE], "Production of $\mathrm{K}^*(892)^0$ and $\phi(1020)$ in pp and Pb–Pb collisions at $\sqrt{s_{NN}}$ = 5.02 TeV," Phys. Rev. C **106**, 034907 (2022).

S. Acharya *et al.* [ALICE], "Direct observation of the dead-cone effect in quantum chromodynamics," Nature **605**, 440 (2022). [erratum: Nature **607**, E22 (2022)]

S. Acharya *et al.* [ALICE], "Measurement of Prompt D^0, Λ_c^+, and $\Sigma_c^{0,++}(2455)$ Production in Proton–Proton Collisions at $\sqrt{s}$ = 13 TeV," Phys. Rev. Lett. **128**, 012001 (2022).

S. Acharya *et al.* [ALICE], "Charm-quark fragmentation fractions and production cross section at midrapidity in pp collisions at the LHC," Phys. Rev. D **105**, L011103 (2022).

S. Acharya *et al.* [ALICE], "Measurement of $\mathrm{K}^*(892)^{\pm}$ production in inelastic pp collisions at the LHC," Phys. Lett. B **828**, 137013 (2022).

S. Acharya *et al.* [ALICE], "Inclusive, prompt and non-prompt J/ψ production at midrapidity in p-Pb collisions at $\sqrt{s_{NN}}$ = 5.02 TeV," J. High Energy Phys. **06**, 011 (2022).

S. Acharya *et al.* [ALICE], "Investigating the role of strangeness in baryon–antibaryon annihilation at the LHC," Phys. Lett. B **829**, 137060 (2022).

S. Acharya *et al.* [ALICE], "Production of Λ and K_s^0 in jets in p–Pb collisions at $\sqrt{s_{NN}}$ = 5.02 TeV and pp collisions at $\sqrt{s}$ = 7 TeV," Phys. Lett. B **827**, 136984 (2022).

S. Acharya *et al.* [ALICE], "Exploring the NΛ–NΣ coupled system with high precision correlation techniques at the LHC," Phys. Lett. B **833**, 137272 (2022).

S. Acharya *et al.* [ALICE], "Nuclear modification factor of light neutral-meson spectra up to high transverse momentum in p–Pb collisions at $\sqrt{s_{NN}}$ = 8.16 TeV," Phys. Lett. B **827**, 136943 (2022).

T. Otsuka, T. Abe, T. Yoshida, Y. Tsunoda, N. Shimizu, N. Itagaki, Y. Utsuno, J. Vary, P. Maris, and H. Ueno, "α-Clustering in atomic nuclei from first principles with statistical learning and the hoyle state character," Nat. Commun. **13**, 2234 (2022).

E. Ideguchi, T. Kibedi, J. Dowie, H. T. Hoang, Kumar Raju M., G. Lane, L. Bignell, T. K. Eriksen, A. J. Mitchell, A. Akber, B. Combes, B. McCormik, T. Gray, A. Stuchbery, N. Shimizu, and Y. Utsuno, "Electric monopole transition from the superdeformed band in ^{40}Ca," Phys. Rev. Lett. **128**, 252501 (2022).

N. Shimizu and Y. Tsunoda, "SO(3) quadratures in angular-momentum projection," Comput. Phys. Commun. **283**, 108583 (2022).

D. Little, A. D. Ayangeakaa, R. V. F. Janssens, S. Zhu, Y. Tsunoda, T. Otsuka, B. A. Brown, M. P. Carpenter, A. Gade, D. Rhodes, C. R. Hoffman, F. G. Kondev, T. Lauritsen, D. Seweryniak, J. Wu, J. Henderson, C. Y. Wu, P. Chowdhury, P. C. Bender, A. M. Forney, and W. B. Walters, "Multistep Coulomb excitation of ^{64}Ni: Shape coexistence and nature of low-spin excitations," Phys. Rev. C **106**, 044313 (2022).

V. Tripathi, S. Bhattacharya, E. Rubino, C. Benetti, J. F. Perello, S. L. Tabor, S. N. Liddick, P. C. Bender, M. P. Carpenter, J. J. Carroll, A. Chester, C. J. Chiara, K. Childers, B. R. Clark, B. P. Crider, J. T. Harke, B. Longfellow, R. S. Lubna, S. Luitel, T. H. Ogunbeku, A. L. Richard, S. Saha, N. Shimizu, O. A. Shehu, Y. Utsuno, R. Unz, Y. Xiao, S. Yoshida, and Y. Zhu, "β^- decay of exotic P and S isotopes with neutron number near 28," Phys. Rev. C **106**, 064314 (2022).

A. Revel, J. Wu, H. Iwasaki, J. Ash, D. Bazin, B. A. Brown, J. Chen, R. Elder, P. Farris, A. Gade, M. Grinder, N. Kobayashi, J. Li, B. Longfellow, T. Mijatovic, J. Pereira, A. Poves, A. Sanchez, N. Shimizu, M. Spieker, Y. Utsuno, and D. Weisshaar, "Large collectivity in ^{29}Ne at the boundary of the island of inversion," Phys. Lett. B **838**, 137704 (2023).

J. A. Lay, A. Vitturi, L. Fortunato, Y. Tsunoda, T. Togashi, and T. Otsuka, "Two-particle transfer processes as a signature of shape phase transition in Zirconium isotopes," Phys. Lett. B **838**, 137719 (2023).

H. F. Li, S. Naimi, T. M. Sprouse, M. R. Mumpower, Y. Abe, Y. Yamaguchi, D. Nagae, F. Suzaki, M. Wakasugi, H. Arakawa, W. B. Dou, D. Hamakawa, S. Hosoi, Y. Inada, D. Kajiki, T. Kobayashi, M. Sakaue, Y. Yokoda, T. Yamaguchi, R. Kagesawa, D. Kamioka, T. Moriguchi, M. Mukai, A. Ozawa, S. Ota, N. Kitamura, S. Masuoka, S. Michimasa, H. Baba, N. Fukuda, Y. Shimizu, H. Suzuki, H. Takeda, D. S. Ahn, M. Wang, C. Y. Fu, Q. Wang, S. Suzuki, Z. Ge, Yu.A. Litvinov, G. Lorusso, P. M. Walker, Zs. Podolyak, and T. Uesaka, "First application of mass measurements with the Rare-RI Ring Reveals the solar *r*-process abundance trend at $A = 122$ and $A = 123$," Phys. Rev. Lett. **128**, 152701 (2022).

S. Iimura, M. Rosenbusch, A. Takamine, Y. Tsunoda, M. Wada, S. Chen, D. S. Hou, W. Xian, H. Ishiyama, S. Yan, P. Schury, H. Crawford, P. Doornenbal, Y. Hirayama, Y. Ito, S. Kimura, T. Koiwai, T. M. Kojima, H. Koura, J. Lee, J. Liu, S. Michimasa, H. Miyatake, J. Y. Moon, S. Naimi, S. Nishimura, T. Niwase, A. Odahara, T. Otsuka, S. Paschalis, M. Petri, N. Shimizu, T. Sonoda, D. Suzuki, Y. X. Watanabe, K. Wimmer, and H. Wollnik, "Study of the $N = 32$ and $N = 34$ shell gap for Ti and V by the first high-precision multireflection time-of-flight mass measurements at BigRIPS-SLOWRI," Phys. Rev. Lett. **130**, 012501 (2023).

T. Nishi, K Itahashi, D. S. Ahn, G. P. A. Berg, M. Dozono, D. Etoh, H. Fujioka, N. Fukuda, N. Fukunishi, H. Geissel, E. Haettner, T. Hashimoto, R. S. Hayano, S. Hirenzaki, H. Horii, N. Ikeno, N. Inabe, M. Iwasaki, D. Kameda, K. Kisamori, Y. Kiyokawa, T. Kubo, K. Kusaka, M. Matsushita, and piAF Collaboration, "Chiral symmetry restoration at high matter density observed in pionic atoms," Nat. Phys. **19**, 788 (2023).

M. Rosenbusch, M. Wada, S. Chen, A. Takamine, S. Iimura, D. Hou, W. Xian, S. Yan, P. Schury, Y. Hirayama, Y. Ito, H. Ishiyama, S. Kimura, T. Kojima, J. Lee, J. Liu, S. Michimasa, H. Miyatake J. Y. Moon M. Mukai S. Naimi S. Nishimura T. Niwase, T. Sonoda, Y. X. Watanabe, and H. Wollnik "The new MRTOF mass spectrograph following the ZeroDegree spectrometer at RIKEN's RIBF facility," Nucl. Instrum. Methods Phys. Res. A **1047**, 167824 (2023).

D. Piatti, E. Masha, M. Aliotta, J. Balibrea-Correa, F. Barile, D. Bemmerer, A. Best, A. Boeltzig, C. Broggini, C. G. Bruno, A. Caciolli, F. Cavanna, T. Chillery, G. F. Ciani, A. Compagnucci, P. Corvisiero, L. Csedreki, T. Davinson, R. Depalo, A. di Leva, Z. Elekes, F. Ferraro, E. M. Fiore, A. Formicola, Zs. Fülöp, G. Gervino, A. Guglielmetti, C. Gustavino, Gy. Gyürky, G. Imbriani, M. Junker, M. Lugaro, P. Marigo, R. Menegazzo, V. Mossa, F. R. Pantaleo, V. Paticchio, R. Perrino, P. Prati, D. Rapagnani, L. Schiavulli, J. Skowronski, K. Stöckel, O. Straniero, T. Szücs, M. P. Takács, and S. Zavatarelli, "First direct limit on the 334 keV resonance strength in ^{22}Ne$(\alpha,\gamma)^{26}$Mg reaction," Eur. Phys. J. A **58**, 194 (2022).

L. Lalanne, O. Sorlin, A. Poves, M. Assié, F. Hammache, S. Koyama, D. Suzuki, F. Flavigny, V. Girard-Alcindor, A. Lemasson, A. Matta, T. Roger, D. Beaumel, Y. Blumenfeld, B. A. Brown, F. De Oliveira Santos, F. Delaunay, N. de Séréville, S. Franchoo, J. Gibelin, J. Guillot, O. Kamalou, N. Kitamura, V. Lapoux, B. Mauss, P. Morfouace, M. Niikura, J. Pancin, T. Y. Saito, C. Stodel, and J. -C. Thomas, "Structure of ^{36}Ca under the coulomb magnifying glass," Phys. Rev. Lett. **129**, 122501 (2022).

N. Ozawa, H. Nagahama, and Y. Sakemi, "Francium ion source with novel methods of target heating and beam characterization," Rev. Sci. Instrum. **94**, 023306 (2023).

K. S. Tanaka, K. Harada, T. Hayamizu, R. Kita, R. Kono, K. Maruta, H. Nagahama, N. Ozawa, Y. Sakemi, and R. Sugimori, "An accelerator experiment for junior and senior high school students to improve students' involvement in fundamental physics," Phys. Edu. **57**, 045013 (2022).

[Review Articles]

早川勢也, 山口英斉, 梶野敏貴,「ビッグバン元素合成—『トロイの木馬法』で迫る『リチウム問題』」, 日本物理学会誌 **77**, 547 (2022).

N. Shimizu, "Recent Progress of Shell-Model Calculations, Monte Carlo Shell Model, and Quasi-Particle Vacua Shell Model," Physics **4**, 1081 (2022).

Y. Utsuno, "Probing different characteristics of shell evolution driven by central, spin-orbit, and tensor forces," Physics **4**, 185 (2022).

[Proceedings]

X. Yao, M. Kusakabe, T. Kajino, S. Cherubini, Seiya, Hayakawa, amd H. Yamaguchi, "Supernova nucleosynthesis, radioactive nuclear reactions and neutrino-mass hierarchy," EPJ Web Conf. **260**, 01007 (2022).

H. Yamaguchi, S. Hayakawa, N. R. Ma, H. Shimizu, K. Okawa, L. Yang, D. Kahl, M. La Cognata, L. Lamia, K. Abe, O. Beliuskina, S. M. Cha, K. Y. Chae, S. Cherubini, P. Figuera, Z. Ge, M. Gulino, J. Hu, A. Inoue, N. Iwasa, A. Kim, D. Kim, G. Kiss, S. Kubono,

M. La Commara, M. Lattuada, E. J. Lee, J. Y. Moon, S. Palmerini, C. Parascandolo, S. Y. Park, V. H. Phong, D. Pierroutsakou, R. G. Pizzone, G. G. Rapisarda, S. Romano, C. Spitaleri, X. D. Tang, O. Trippella, A. Tumino, N. T. Zhang, Y. H. Lam, A. Heger, A. M. Jacobs, S. W. Xu, S. B. Ma, L. H. Ru, E. Q. Liu, T. Liu, C. B. Hamill, A. St J. Murphy, J. Su, X. Fang, M. S. Kwag, N. N. Duy, N. K. Uyen, D. H. Kim, J. Liang, A. Psaltis, M. Sferrazza, Z. Johnston, and Y. Y. Li, "Experimental studies on astrophysical reactions at the low-energy RI beam separator CRIB," EPJ Web Conf. **260**, 03003 (2022).

J. Hu, H. Yamaguchi, Y. H. Lam, A. Heger, D. Kahl, A. M. Jacobs, Z. Johnston, S. W. Xu, N. T. Zhang, S. B. Ma, L. H. Ru, E. Q. Liu, T. Liu, S. Hayakawa, L. Yang, H. Shimizu, C. B. Hamill, A. St J. Murphy, J. Su, X. Fang, K. Y. Chae, M. S. Kwag, S. M. Cha, Duy, N. N., Uyen, N. K., Kim, D. H., R. G. Pizzone, M. La Cognata, S. Cherubini, S. Romano, A. Tumino, J. Liang, A. Psaltis, M. Sferrazza, D. Kim, Y. Y. Li, and S. Kubono, "First measurement of ^{25}Al + p resonant scattering relevant to the astrophysical reaction ^{22}Mg(α, p)^{25}Al," EPJ Web Conf. **260**, 05001 (2022).

M. L. Sergi, L. Lamia, G. G. Rapisarda, M. Mazzocco, S. Cherubini, G. D'Agata, A. Di Pietro, J. P. Fernandez-Garcia, P. Figuera, M. Fisichella, G. L. Guardo, M. Gulino, S. Hayakawa, M. La Cognata, M. Lattuada, A. A. Oliva, S. Palmerini, R. G. Pizzone, S. M. R. Puglia, S. Romano, R. Spartà, C. Spitaleri, D. Torresi, and A. Tumino, "Trojan Horse Method for n-induced reaction investigations at astrophysical energies," in *Particles and Nuclei International Conference 2021 (PANIC2021)*, Proc. Science, **380**, 342 (2022).

H. Yamaguchi, S. Hayakawa, N. R. Ma, H. Shimizu, K. Okawa, Q. Zhang, L. Yang, D. Kahl, M. La Cognata, L. Lamia, K. Abe, O. Beliuskina, S. M. Cha, K. Y. Chae, S. Cherubini, P. Figuera, Z. Ge, M. Gulino, J. Hu, A. Inoue, N. Iwasa, A. Kim, D. Kim, G. Kiss, S. Kubono, M. La Commara, M. Lattuada, E. J. Lee, J. Y. Moon, S. Palmerini, C. Parascandolo, S. Y. Park, V. H. Phong, D. Pierroutsakou, R. G. Pizzone, G. G. Rapisarda, S. Romano, C. Spitaleri, X. D. Tang, O. Trippella, A. Tumino, N. T. Zhang, Y. H. Lam, A. Heger, A. M. Jacobs, S. W. Xu, S. B. Ma, L. H. Ru, E. Q. Liu, T. Liu, C. B. Hamill, A. St J. Murphy, J. Su, X. Fang, M. S. Kwag, N. N. Duy, N. K. Uyen, D. H. Kim, J. Liang, A. Psaltis, M. Sferrazza, Z. Johnston, and Y. Y. Li, "RIB induced reactions: Studying astrophysical reactions with low-energy RI beam at CRIB," EPJ Web Conf. **275**, 01015 (2023).

K. Okawa, M. Kim, K. Chae, S. Hayakawa, S. Adachi, S. Cha, T. W. Chillery, T. Furuno, G. Gu, S. Hanai, N. Imai, D. Kahl, T. Kawabata, C. Kim, D. Kim, S. Kim, S. Kubono, M. Kwag, J. Li, N. Ma, Shin´ichiro Michimasa, U. N. Kim, D. N. Ngoc, K. Sakanashi, H. Shimizu, O. Sirbu, H. Yamaguchi, R. Yokoyama, and Q. Zhang, "Direct measurement of the ^{26}Si(α, p)^{29}P reaction at CRIB for the nucleosynthesis in the X-ray bursts," EPJ Web Conf. **275**, 02009 (2023).

H. Murakami for the ALICE Collaboration, "Thermal radiation and direct photon production measurements with dielectrons in Pb–Pb and pp collisions," Strangeness in Quark Matter (SQM 2022), June 13–17, 2022, Busan, Korea, EPJ Web Conf. **276**, 06011 (2023).

D. Sekihata for the ALICE Collaboration, "Thermal radiation and direct photon production in Pb–Pb and pp collisions with dielectrons in ALICE," International Conference on High Energy Physics, Bolognia, Italy, July 6–13, 2022, PoS(ICHEP2022)452.

Shutaro Hanai, Shinsuke Ota, Reiko Kojima, Masanori Dozono, Nobuaki. Imai, Shin'ichiro Michimasa, Susumu Shimoura, Juzo Zenihiro, Kento Inaba, and Yuto Hijikata "Development of fast-response tracking detector for high-intensity ion beams,," Radiation Detectors and Their Uses Proceedings of the 36th Workshop on Radiation Detectors and Their Uses in KEK, 2023, pp. 24–34.

S. Motoki, Y. Kazeki, N. Hiroki, O. Naoya, N. Shintaro, N. Teruhito, U. Daisuke, F. Mirai, N. Keisuke, H. Tomohiro, H. Hiromitsu, S. Yasuhiro, and M. Yasuyuki, "Development of neutralization apparatus and francium source for the francium electric dipole moment search," JPS Conf. Proc. **37**, 20605 (2022).

K. Nakamura, S .Nagase, T. Nakashita, T. Hayamizu, T. Aoki, H. Nagahama, N. Ozawa, M. Sato, K. Yamane, M. Fukase, D. Uehara, A. Takamine, and Y. Sakemi, "Development of a laser frequency stabilization and an optical transmission system for the francium electric dipole moment search," J. Phys. Conf. Ser. **2249**, 012010 (2022).

Presentations

[International Conferences/Workshops]

H. Yamaguchi (invited), "RIB induced reactions: Studying astrophysical reactions with low-energy RI beam at CRIB," The 11th European Summer School on Experimental Nuclear Astrophysics (Santa Tecla School, ESSENA 2022), INFN-LNS, Catania, Italy, June 12–19, 2022.

H. Yamaguchi (invited), "New evaluation of ^{22}Mg(α, p) reaction rate and X-ray burst light curve," UKAKUREN-RCNP Conference on AstroNuclear Physics (ANP2022), Osaka University, Toyonaka, Osaka, Japan, July 20–21, 2022.

H. Yamaguchi (invited), "Big-Bang Li problem and nuclear reactions," International Workshop "Origin of Elements and Cosmic Evolution: From Big-Bang to Supernovae and Mergers" (OECE2022), Beihang University, Beijing, China, July 20–22, 2022.

S. Hayakawa (invited), "New measurement of the ^{7}Be + n reactions and its impact on the primordial ^{7}Li abundance," The 16th International Symposium on Origin of Matter and Evolution of Galaxies (OMEG16), Hanoi, Vietnam, October 24–28, 2022.

H. Yamaguchi (invited), "Studies on RI-involving astrophysical reactions at CRIB," ECT* Workshop "Key Reactions in Nuclear Astrophysics," ECT*, Trento, Italy, December 12–16, 2022.

H. Yamaguchi (oral), 「X 線バーストにおける重要不安定核反応の実験的検証/Experimental investigation of relevant unstable-nucleus reactions in X-ray bursts」, RIBF ULIC Mini Workshop-39 星の進化と爆発天体における核反応の物理 (Physics of nuclear reactions in stellar evolution and explosive stellar objects), Wako, Saitama, Japan (RIKEN), February 20–21, 2023.

K. Okawa (poster), "Direct measurement of the ^{26}Si(α, p)^{29}P reaction for the nucleosynthesis in the X-ray bursts," FoPM International Symposium, Hongo Campus (Ito International Research Center), February 6–8, 2023.

S. Hayakawa (oral), "Nuclear astrophysics at the low-energy RI beam separator CRIB," RIBF Users Meeting 2022, Web meeting hosted by RIKEN, Wako, Saitama, Japan, September 7–9, 2022.

T. Gunji (invited) for the ALICE Collaboration, "Recent results from the ALICE experiment at the LHC and its future prospects," The 15th Asia Pacific Physics Conference (APPC15), Online, August 21–26, 2022.

T. Gunji (invited), "Hunting for dark photons," GSI EMMI RRTF, Real and Virtual photon production at ultra-low transverse momentum and low mass at LHC, GSI, August 1–8, 2022.

T. Gunji (invited), "High-energy nuclear physics in Japan and view on EIC," EIC Asia Workshop, RIKEN, March 16–18, 2023.

H. Murakami for the ALICE Collaboration, "Thermal radiation and direct photon production in Pb–Pb and *pp* collisions with dielectrons," Strangeness in Quark Matter (SQM 2022), Busan, Korea & Online, June 13–17, 2022.

D. Sekihata for the ALICE Collaboration, "Thermal radiation and direct photon production in Pb–Pb and *pp* collisions with dielectrons in ALICE," International Conference on High Energy Physics, Bolognia, Italy, July 6–13, 2022.

Y. Utsuno (invited), "Recent findings about shell evolution in the neutron-rich Ca region," RIKEN Workshop on Physics of RI: Recent Progress and Perspectives, Wako, Japan, May 30–June 1, 2022.

Y. Utsuno (invited), "Large-scale shell-model calculations: from low-lying spectra to compound states," A3F-CNS Summer School 2022, Kumagaya, Japan, August 20–24, 2022.

Y. Utsuno (invited), "Overview of shell-model results for the 3rd SEASTAR campaign," REIMEI Workshop on Unveiling nuclear shells and correlations in exotic nuclei through knockout reactions, Darmstadt, Germany, October 10–12, 2022.

K. Yanase (oral), "Theoretical uncertainty on the nuclear Schiff moments of ^{129}Xe and ^{199}Hg," The 14th International Workshop on Fundamental Physics Using Atoms (FPUA2022), Fukuoka, Japan, November 24–25, 2022.

Y. Utsuno (invited), N. Shimizu, and Y. Tsunoda, "Large-scale shell-model approach to nuclear collective motion," 66th DAE Symposium on Nuclear Physics, Guwahati, India, December 1–5, 2022.

K. Yanase (invited), "Shell-model study for the Nuclear Schiff moments of ^{129}Xe and ^{199}Hg," KMI workshop: Searches for Electric Dipole Moments: From Theory to Experiment, Nagoya, Japan, March 2–4, 2023.

Y. Utsuno (invited), "The nuclear shell model," INTPART School 2023, Onna, Japan, February 20–March 7, 2023.

S. Michimasa (invited) "Direct mass measurements around neutron-rich Ca region at SHARAQ," Physics of RI: Recent progress and perspectives RIKEN Nishina Cener, Saitama, Japan, May 30–June 1, 2022.

S. Michimasa (invited) "Present Status of OEDO/FY2020–2022" OEDO/SHARAQ collaboration meeting 2022, Web meeting hosted by CNS, Wako, Saitama, Japan, August 30, 2022.

N. Imai (invited) "SHARAQ18" OEDO/SHARAQ collaboration meeting 2022, Web meeting hosted by CNS, Wako, Saitama, Japan, August 30, 2022.

S. Hanai (invited) "SHARAQ13" OEDO/SHARAQ collaboration meeting 2022, Web meeting hosted by CNS, Wako, Saitama, Japan, August 30, 2022.

S. Michimasa (invited) "OEDO-SHARAQ system: multifaceted performances in low-energy RI production and high-resolution spectroscopy," The 19th International Conference on Electromagnetic Isotope Separators and Related Topics (EMIS XIX), RISP/IBS, Daejeon, Korea, October 3–7, 2022.

S. Michimasa (invited) "Mass measurements of exotic nuclei at OEDO-SHARAQ," The International Symposium on Nuclear Spectroscopy for Extreme Quantum Systems (NUSPEQ2023), Numazu, Sizuoka, Japan, March 7–9, 2023.

T. Chillery (poster) "Treating Radioactive Waste: Measurement of ^{93}Zr + d Reactions at 30 MeV/nucleon," The International Symposium on Nuclear Spectroscopy for Extreme Quantum Systems (NUSPEQ2023), Numazu, Sizuoka, Japan, March 7–9, 2023.

N. Kitamura (poster) "In-beam γ-ray spectroscopy of ^{32}Mg" The International Symposium on Nuclear Spectroscopy for Extreme Quantum Systems (NUSPEQ2023), Numazu, Sizuoka, Japan, March 7–9, 2023.

R. Yokoyama (poster) "New implantation detectors for decay spectroscopy at fragmentation facilities" The International Symposium on Nuclear Spectroscopy for Extreme Quantum Systems (NUSPEQ2023), Numazu, Sizuoka, Japan, March 7–9, 2023.

S. Hanai (poster) "Direct mass measurement of neutron-deficient Fe isotopes" The International Symposium on Nuclear Spectroscopy for Extreme Quantum Systems (NUSPEQ2023), Numazu, Sizuoka, Japan, March 7–9, 2023.

J. Li (poster) "Study of heavy-ion fusion reactions in inverse kinematic systems using low-energy ^{136}Xe beam," The International Symposium on Nuclear Spectroscopy for Extreme Quantum Systems, Numazu, Sizuoka, Japan, March 7–9, 2023.

S. Hanai (invited) "Direct measurement of the masses of Fe isotopes around the proton dripline," RIBF users meeting, Web meeting hosted by RIKEN Nishina Center, Wako, Saitama, Japan, September 22, 2022.

T. Chillery (invited) "Recent Studies on Heavy-Isotope Nucleosynthesis Using (d,p) Transfer Reactions at OEDO-SHARAQ," RIBF users meeting, Web meeting hosted by RIKEN Nishina Center, Wako, Saitama, Japan, September 22, 2022.

J. T. Li (oral), "Study of the fusion reaction in inverse kinematics with the low-energy ^{136}Xe beams," UT-Tsinghua University Joint mini workshop, Tsinghua University, Beijing, China, March 13, 2023.

S. Hanai (poster), "Development of a fast response PPAC for high-intensity heavy-ion beams," The 19th International Conference on Electromagnetic Isotope Separators and Related Topics (EMIS XIX), Daejeon, Korea (RISP/IBS), October 3–7, 2022.

K. Yako (oral), "Double and single charge exchange reactions on ^{48}Ca by ^{12}C beam at 250 A MeV," YKIS2022b, Kyoto, May 23–27, 2022.

A. Sakaue (poster), "The Search for double Gamow-Teller giant resonance at RIBF BigRIPS," Annual meeting of A3 Foresight Program, Nuclear Physics in the 21st century, Osaka, February 13–15, 2023.

A. Sakaue (poster), "The search for double Gamow-Teller giant resonance with the (^{12}C,^{12} Be(0^+_2)) reaction," NUSPEQ2023, Numazu, March 7–9, 2023.

K. Kawata (poster), "The production of high-spin isomers around ^{52}Fe in fragmentation reaction of ^{58}Ni and ^{59}Co beams at 350 MeV/nucleon," NUSPEQ2023, Numazu, March 7–9, 2023.

K. Nakamura (oral), "400-m-Long Polarization-Maintaining Fibers for Magneto-Optical Trapping of francium Atoms," The 15th Pacific

Rim Conference on Lasers and Electro-Optics (CLEO-PR 2022), Online, August 2, 2022.

H. Nagahama (invited), "Searching for the permanent electric dipole moment using laser cooled francium atoms," 6th Workshop on the Physics of fundamental Symmetries and Interactions at low energies and the precision frontier (PSI2022), Switzerland (Paul Scherrer Institute), October 19, 2022.

M. Fukase (invited), "Search for permanent EDM by using Fr atoms," 14th International Workshop on Fundamental Physics Using Atoms (FPUA2022), Fukuoka, Japan (Kyushu University), November 24, 2022.

[Domestic Conferences/Workshops]

鎌倉恵太 (ポスター発表),「14 GHz Hyper ECR イオン源を用いた ECR プラズマの研究」, 第 19 回日本加速器学会年会, オンライン, 2022 年 10 月 18–21 日.

大川皓大 (口頭発表),「X 線バースト中の元素合成における ^{26}Si(α, p)^{29}P 反応の直接測定」, 日本物理学会 2022 年秋季大会, 岡山理科大学, 2022 年 9 月 6–8 日.

S. Hayakawa (oral), "Activity report of CRIB," RIBF Users Meeting 2022, Session 3, オンライン, 2022 年 9 月.

早川勢也 (口頭発表), "Measurement of the ^{7}Be + n reactions by Trojan Horse method updating primordial ^{7}Li abundance," 宇宙核物理の展開 UKAKUREN-RCNP Conference on AstroNuclear Physics (ANP2022), 大阪大学 & オンライン, 2022 年 7 月.

山口英斉 (口頭発表),「軽い原子核の直鎖クラスター状態の実験的検証」, シンポジウム「原子核クラスター物理の新たな進展と展望」, 日本物理学会 2023 年春季大会, オンライン, 2023 年 3 月 25 日.

H. Murakami for the ALICE Collaboration, "Direct photon production in proton-proton collisions at $\sqrt{s}$ = 13 TeV via interanl conversion technique with ALICE," 日本物理学会 2022 年秋季大会, 岡山理科大学, 2022 年 9 月 6–8 日.

関畑大貴,「電磁・ソフトプローブを通した QGP 物理の結果と展望」, 日本物理学会 2023 春季大会, 実験核物理・理論核物理領域合同シンポジウム: 次世代の高エネルギー原子核衝突: 何が理解され, 何を理解すべきか？, オンライン, 2023 年 3 月 22 日.

馬場仁志 for the ALICE Collaboration,「機械学習を用いた, ALICE-TPC 検出器における空間電荷効果の補正」, 日本物理学会 2022 年秋季大会, 岡山理科大学, 2022 年 9 月 6–8 日.

T. Gunji (招待講演), "Future Prospects of Quark Cluster Physics using ultra-relativistic heavy-ions," 第 8 回クラスター階層領域研究会, 大阪大学吹田キャンパス接合科学研究所, 2023 年 2 月 9–11 日.

T. Gunji (招待講演),「LHC-ALICE 実験の新しいデータ収集系」, RCNP 研究会「原子核実験の次世代データ収集システム基盤開発にむけて」, 大阪大学吹田キャンパス, 2022 年 5 月 16–17 日.

T. Gunji (invited),「WG4（オンラインフィルタリング・演算加速器）報告と展望」, 原子核実験の先端データ収集システム—標準化と将来—, 2023 年 3 月 17 日.

T. Gunji (invited),「ALICE 実験における Vertex Trackers」, シリコンプラットフォーム研究会, KEK, 2022 年 8 月 9 日.

宇都野穣 (招待講演),「大規模殻模型計算—現実的な原子核構造を得るには」, 研究会「宇宙核物理の展開」, 豊中市 (大阪大学), 2022 年 7 月 19–21 日.

宇都野穣 (口頭発表), 清水則孝, 井手口栄治, 青井考,「大規模殻模型計算と 3 準位模型による ^{40}Ca の超変形状態からの E0 遷移の理解」, 日本物理学会 2022 年秋季大会, 岡山市 (岡山理科大学), 2022 年 9 月 6–8 日.

柳瀬宏太 (招待講演),「原子核殻模型によるキセノン原子核の核行列要素の理論計算」, 二重ベータ崩壊核行列要素実験理論合同研究会, 吹田市 (大阪大学核物理研究センター), 2022 年 10 月 3–4 日.

柳瀬宏太 (口頭発表), 清水則孝, 角田佑介, 宇都野穣,「モンテカルロ殻模型による N = 82 付近のベータ崩壊半減期の理論計算」, 日本物理学会 2023 年春季大会, オンライン, 2023 年 3 月 22–25 日.

N. Kitamura (招待講演),「高性能波形ディジタイザの需要調査と今後の開発方針」, 原子核実験の先端データ収集システム—標準化と将来—, 大阪大学核物理研究センター, 2023 年 3 月 17 日.

R. Yokoyama (招待講演),「原子核の複数粒子放出過程」, 第四回若手放談会, エキゾチック核物理の未来, 理研神戸・融合連携イノベーション推進棟, 2023 年 3 月 15–17 日.

R. Yokoyama (招待講演),「核破砕・分裂反応式不安定核生成施設における β 核分光のためのシンチレーション検出器」, Scintillator for Medical, Astroparticle and Environmental Radiation Technologies, Tokushima University, December 17–19, 2022.

N. Imai (invited), "Study of the neutron capture rate on the unstable nuclei via the surrogate reactions," Workshop for the nucleosynthesis in the universe from the neutron capture, Tokyo, Japan (University of Tokyo), February 9–10, 2023.

T. Chillery (oral), "Measurement of ^{130}Sn(d,p) Reaction for Neutron-Capture Rate in r-process Nucleosynthesis," JPS Autumn 2022 meeting, Okayama, September 6–8, 2022.

阪上朱音 (口頭発表),「(^{12}C,^{12} Be(0^{+}_{2})) 反応を用いた二重ガモフ・テラー巨大共鳴状態の探索」, 日本物理学会 2022 年秋季大会, 岡山理科大学, 2022 年 9 月 6–8 日.

[Seminars]

S. Hayakawa, C2R2 Seminar "Direct and indirect methods at CRIB for nuclear astrophysical reactions," Online, Organized by CENS, IBS, June 2022.

Y. Utsuno, "Unveiling exotic nuclear structure far from stability," Colloquium at Saha Institute of Nuclear Physics, Kolkota, India, December 7, 2022.

N. Imai, "OEDO beam line at RIBF and Its physics program," Beigjing China (Tsinghua University), March 13, 2023.

N. Imai, "The decelerating and focusing device OEDO in RIBF and the nuclear astrophysics program with the surrogate nuclear reaction," Beijing, China (Chinese Institute of Atomic Energy), March 13, 2023.

N. Imai, "OEDO, the deceleration and focusing element at RIBF, and the physics program using OEDO," Lanzhou, China (Institute of Modern Physics), March 16, 2023.

Awards

S. Hanai, ANPha Award in The International Symposium on Nuclear Spectroscopy for Extreme Quantum Systems (NUSPEQ2023), Numazu, Sizuoka, Japan, March 7–9, 2023.

A. Sakaue, Poster award for young scientists, Annual meeting of A3 Foresight Program, Nuclear Physics in the 21st century, Osaka, February 13–15, 2023.

Outreach Activity

N. Imai “Beyond the nano scale: a femto world consisting of protons and neutrons,” Open campus of the School of Sience, the University of Tokyo, Tokyo, Japan, August 4, 2022.

Partner Institution
Wako Nuclear Science Center, IPNS (Institute of Particle and Nuclear Studies)
KEK (High Energy Accelerator Research Organization)

1. Abstract

The Wako Nuclear Science Center (WNSC) of KEK aims to promote low-energy nuclear physics and nuclear astrophysics research as well as interdisciplinary studies using short-lived radioactive nuclides. WNSC operates the KEK Isotope Separation System (KISS), an electromagnetic isotope separator featuring elemental selectivity from resonance laser ionization in a gas catcher. The KISS facility uniquely provides various neutron-rich isotopes of refractory elements via multinucleon transfer reactions to users from universities. Its provision of nuclei in the vicinity of the neutron magic number $N = 126$ and $N = 152$. Optical and β-γ spectroscopy and mass spectrometry have been applied to these neutron-rich nuclear beams for nuclear structure and nuclear astrophysical studies. The WNSC leads comprehensive mass measurements of all-available nuclides at RIBF using multi-reflection time of flight mass spectrographs (MRTOF-MS). Three MRTOF setups were placed at the GARIS-II, the beam dump of the ZeroDegree spectrometer, and the KISS—the masses of more ore than 400 nuclides, including dozens of first masses. A new uranium isotope, ^{241}U, was discovered at KISS-MRTOF by means of precise mass measurement. An upgrade plan, KISS- II, is being considered a future project of WNSC aiming at the study of the origin of uranium for the first time.

2. Major Research Subjects

(1) Production and manipulation of radioactive isotope beams for nuclear experiments
(2) Explosive nucleosynthesis (*r*- and *rp*-process)
(3) Heavy ion reaction mechanism for producing heavy neutron-rich nuclei
(4) Development of MRTOF mass spectrographs for short-lived nuclei
(5) Comprehensive mass measurements of short-lived nuclei including superheavy elements
(6) Development of KISS-II

3. Summary of Research Activity

The Wako Nuclear Science Center (WNSC) provides low-energy short-lived radioactive ion beams of neutron-rich refractory elements to university researchers using the KEK isotope separator system (KISS). In FY2021, five experiments were executed. Due to the restrictions of COVID-19, only a limited number of foreign collaborators participated in the experiments. Laser spectroscopy of neutron-rich refractory elements, including long-lived isotopes, is uniquely performed using the resonant laser ionization scheme of KISS and the capability of isobaric separation of the MRTOF device.

The team of WNSC leads comprehensive mass measurements of all available nuclides at RIKEN RIBF using multiple MRTOF mass spectrographs. Newly installed beta-ToF detectors to the GARIS-II MRTOF and the ZeroDegree MRTOF setups eliminate background events and allow for the determination of the lifetime of short-lived nuclides.

The WNSC announced two press releases; one is for discovering a new uranium isotope, ^{241}U, the first neutron-rich new uranium isotope in the last 40 years. The other is for the disappearance of a neutron magic number, $N = 34$, for titanium and vanadium isotopes.

The WNSC plans to extend the present KISS facility to investigate the nuclides in the neutron-rich actinides using the multi-nucleon transfer reactions of actinide targets to study the origin of uranium. Some pilot developments are in progress, particularly for a large He gas catcher with a radiofrequency wire curtain device.

Members

Group Leader
Michiharu WADA

Researchers
Yutaka WATANABE
Peter SCHURY
Sunchan JEONG
Yoshikazu HIRAYAMA
Hiroari MIYATAKE
Marco ROSENBUSH
Toshitaka NIWASE
Taiki TANAKA

Visiting Researchers
Hermann WOLLNIK (NMSU)
Andrei ANDREYEV (University of York)
Hiroshi WATANABE (Beihan University)
Dongsheng HOU (IMP)

Assistant
Machiko IZAWA

List of Publications & Presentations

Publications

[Original Papers]

T. Niwase, W. Xian, M. Wada, M. Rosenbusch, S. Chen, A. Takamine, J. Liu, S. Iimura, D. Hou, S. Yan, H. Ishiyama, H. Miyatake, S. Nishimura, D. Kaji, K. Morimoto, Y. Hirayama, Y. X. Watanabe, S. Kimura, P. Schury, and H. Wollnik, "Development of a β-TOF detector: An enhancement of the α-TOF detector for use with β-decaying nuclides," Prog. Theor. Exp. Phys. **2023**, 031H01 (2023).

T. Niwase, Y. X. Watanabe, Y. Hirayama, M. Mukai, P. Schury, A. N. Andreyev, T. Hashimoto, S. Iimura, H. Ishiyama, Y. Ito, S. C. Jeong, D. Kaji, S. Kimura, H. Miyatake, K. Morimoto, J. -Y. Moon, M. Oyaizu, M. Rosenbusch, A. Taniguchi, and M. Wada, "Discovery of new isotope ^{241}U and systematic high-precision atomic mass measurements of neutron-rich Pa-Pu nuclei produced via multinucleon transfer reactions," Phys. Rev. Lett. **130**, 132502-1–6 (2023).

T. Niwase, P. Schury, M. Wada, and SHE-Mass Collaborators, "Accurate event assignment from the decay-correlated mass measurement of the superheavy nuclide ^{257}Db," J. Nucl. Radiochem. Sci. **23**, 1–4 (2023).

M. Rosenbusch, M. Wada, S. Chen, A. Takamine, S. Iimura, D. Hou, W. Xian, S. Yan, P. Schury, Y. Hirayama, Y. Ito, H. Ishiyama, S. Kimura, T. Kojima, J. Lee, J. Liu, S. Michimasa, H. Miyatake, M. Mukai, J. Y. Moon, S. Nishimura, S. Naimi, T. Niwase, T. Sonoda, Y. X. Watanabe, and H. Wollnik, "The new MRTOF mass spectrograph following the ZeroDegree spectrometer at RIKEN's RIBF facility," Nucl. Instrum. Methods Phys. Res. A **1047**, 167824 (2023).

S. Iimura, M. Rosenbusch, A. Takamine, Y. Tsunoda, M. Wada, S. Chen, D. S. Hou, W. Xian, H. Ishiyama, S. Yan, P. Schury, H. Crawford, P. Doornenbal, Y. Hirayama, Y. Ito, S. Kimura, T. Koiwai, T. M. Kojima, H. Koura, J. Lee, J. Liu, S. Michimasa, H. Miyatake, J. Y. Moon, S. Naimi, S. Nishimura, T. Niwase, A. Odahara, T. Otsuka, S. Paschalis, M. Petri, N. Shimizu, T. Sonoda, D. Suzuki, Y. X. Watanabe, K. Wimmer, and H. Wollnik, "Study of the $N = 32$ and $N = 34$ shell gap for Ti and V by the first high-precision multireflection time-of-flight mass measurements at BigRIPS-SLOWRI," Phys. Rev. Lett. **130**, 012501-1–6 (2023).

Y. Hirayama, M. Mukai, Y. X. Watanabe, P. Schury, H. Nakada, J. Y. Moon, T. Hashimoto, S. Iimura, S. C. Jeong, M. Rosenbusch, M. Oyaizu, T. Niwase, M. Tajima, A. Taniguchi, M. Wada, and H. Miyatake, "In-gas-cell laser resonance ionization spectroscopy of ^{200,201}Pt," Phys. Rev. C **106**, 034326-1–11 (2022).

T. Aoki, Y. Hirayama, H. Ishiyama, S. C. Jeong, S. Kimura, Y. Makida, H. Miyatake, M. Mukai, S. Nishimura, K. Nishio, T. Niwase, T. Ogawa, H. Okuno, M. Rosenbusch, P. Schury, Y. Watanabe, and M. Wada, "Design report of the KISS-II facility for exploring the origin of uranium," arXiv:2209.12649.

[Review Article]

和田道治, 「超重元素同位体の精密質量測定」, Isotope News 10 月号 (No.783), 6–10 (2022).

Presentations

[International Conferences/Workshops]

Y. Watanabe (invited), "Spectroscopy of neutron-rich nuclei produced in multinucleon transfer reactions at KISS," Physics with SPIRAL2 Heavy Ion Beams, Caen, France, December 12–16, 2022.

Y. Watanabe (oral), "Experimental studies of neutron-rich nuclei around $N = 126$ and beyond at KEK isotope separation system," 16th International Symposium on Origin of Matter and Evolution of Galaxies (OMEG16), Ha Noi, Viet Nam, October 25–28, 2022.

M. Wada (invited), "Comprehensive mass measurements of short-lived nuclides," 16th International Symposium on Origin of Matter and Evolution of Galaxies (OMEG16), Ha Noi, Viet Nam, October 25–28, 2022.

T. Niwase (poster), "Technique of decay correlated mass measurement via multi-reflection time-of-flight mass spectrograph with an α/β-TOF detector," 19th International Conference on Electromagnetic Isotope Separators and Related Topics (EMIS), Daejeon, Korea, October 3–7, 2022.

M. Rosenbusch (poster), "High-precision MRTOF mass measurements of radioactive isotopes at RIKEN's RIBF facility: Recent projects for ion selection, wideband mass accuracy, and mirror potentials," 19th International Conference on Electromagnetic Isotope Separators and Related Topics (EMIS), Daejeon, Korea, October 3–7, 2022.

P. Schury (invited), "Multi-reflection time-of-flight mass spectroscopy of superheavy nuclides," 19th International Conference on Electromagnetic Isotope Separators and Related Topics (EMIS), Daejeon, Korea, October 3–7, 2022.

M. Rosenbusch (oral), "Exploring exotic nuclei by high-precision MRTOF mass measurements: The new ion catcher and mass spectrograph at RIKEN's RIBF factory," Trapped Charged Particles Conference 2022 (TCP 2022), Glashütten, Germany, September 25–30, 2022.

[Domestic Conferences/Workshops]

向井もも (口頭発表), 「安定イリジウム同位体周辺核の直接質量測定」, 日本物理学会 2023 年春季大会, オンライン, 2023 年 3 月 22–25 日.

M. Rosenbusch (口頭発表), "Recent atomic mass measurements of radioactive species using the new ZD-MRTOF system at BigRIPS/RIKEN," 日本物理学会 2023 年春季大会, オンライン, 2023 年 3 月 22–25 日.

庭瀬暁隆 (口頭発表), 「超重核の直接質量測定」, 日本物理学会 2023 年春季大会, オンライン, 2023 年 3 月 22–25 日.

庭瀬暁隆 (口頭発表), 「超重・超アクチノイド核の精密質量測定」, 2022 重元素化学研究会, あわら市, 2023 年 3 月 20–21 日.

Y. Watanabe (invited), 「中性子過剰アクチノイド実験への展望」, RIBF ULIC ミニワークショップ「理論と実験で拓く中性子過剰核の核分裂」, Wako, Japan, February 16–17, 2023.

平山賀一 (招待講演), 「KISS での核分光研究」, 中世捕獲反応で迫る宇宙の元素合成, 文京区 (東京大学), 2023 年 2 月 9–10 日.

渡邊裕 (口頭発表), 「KISS での核分光研究」, 令和 4 年度専門研究会「短寿命 RI を用いた核分光と核物性研究 IX」, オンライン, 2023 年 1 月 11 日.

M. Rosenbusch (oral), "New nuclear masses, recent and present developments, and future opportunities of the MRTOF-MS at the ZeroDegree spectrometer," RIBF Users Meeting, Online, September 20–22, 2022.

Y. Watanabe (oral), "Present status and future plan of KISS," RIBF Users Meeting, Online, September 20–22, 2022.

T. Niwase (oral), "First direct mass measurement of superheavy nuclide via MRTOF-MS equipped with α-TOF detector," RIBF Users Meeting, Online, September 20–22, 2022.

庭瀬暁隆 (招待講演), 「精密質量と崩壊事象の相関測定法の開拓による超重元素の直接質量測定」, 日本放射化学会第 66 回討論会 (2022), 文京区 (東京大学), 2022 年 9 月 16 日.

庭瀬暁隆 (口頭発表), 「精密質量測定による新同位体 ^{241}U の発見」, 日本物理学会 2022 年秋季大会, 岡山市 (岡山理科大学) & オンライン, 2022 年 9 月 6–9 日.

平山賀一 (口頭発表), 「KISS での低温ヘリウムガスセル開発」, 日本物理学会 2022 年秋季大会, 岡山市 (岡山理科大学) & オンライン, 2022 年 9 月 6–9 日.

M. Rosenbusch (invited), "High-precision mass measurements for astrophysics and nuclear structure studies using the new ZD-MRTOF system," 宇核連-RCNP 研究会「宇宙核物理の展開」, UKAKUREN-RCNP Conference on AstroNuclear Physics (ANP2022), Toyonaka, Japan & Online, July 20–21, 2022.

Y. Watanabe (oral), "Production of neutron-rich nuclei around $N = 126$ and beyond using multinucleon transfer reactions at KISS project," Physics of RI: Recent progress and perspectives, Wako, Japan & Online, May 30–June 1, 2022.

[Seminars]

M. Rosenbusch, "A first review of the SLOWRI-MRTOF mass spectrograph following the ZeroDegree spectrometer at BigRIPS," The 315th RIKEN RIBF Nuclear Physics Seminar, Wako, Japan, February 14, 2023.

M. Wada, "Study of the origins of heavy elements via comprehensive mass measurements of short-lived nuclides/重元素の起源と短寿命核の質量測定," 高エネルギー加速器科学セミナー (2022 High Energy Accelerator Science Seminar), Online, June 8, 2022.

Press Releases

チタン・バナジウム中性子過剰同位体で新魔法数の消失を観測～精密質量測定による原子核構造のより深い理解に期待～, KEK, RIKEN, Osaka University, 2023 年 1 月 6 日, https://www.kek.jp/ja/press/202301061400/.

40 年ぶりに中性子過剰なウラン同位体を新発見～ウランの起源解明に期待～, KEK, RIKEN, 2023 年 3 月 31 日, https://www.kek.jp/ja/press/202304010000/.

Awards

庭瀬暁隆, 「第 17 回（2023 年）日本物理学会実験核物理領域: 若手奨励賞 (Young Scientist Award of the Physical Society of Japan), 第 29 回原子核談話会新人賞」, 2023 年 3 月.

T. Niwase, "RIBF Users Group Thesis Award," September 2022.

庭瀬暁隆, 「日本放射化学会奨励賞」, 2022 年 9 月.

和田道治, 宮武宇也, 「2021 年度高エネルギー加速器科学研究奨励会西川賞」, 2022 年 5 月.

VII. APPENDICES

List of Symposia & Workshops (April 2022—March 2023)

RNC

1	Physics of RI: Recent progress and perspectives https://indico2.riken.jp/event/4120/	online, RIBF2F Large Meeting Room	May 30–Jun. 1
2	Predictions for sPHENIX https://www.bnl.gov/sphenix2022	Online, Brookhaven National Laboratory	July. 20–22
3	RIBF Users Meeting 2021 https://indico2.riken.jp/event/4225/	online	Sep. 20–22
4	International workshop on "hadron physics with kaon beam and related topics" https://kds.kek.jp/event/43204/	online	Oct. 3–4
5	International symposium on clustering as a window on the hierarchical of quantum systems http://be.nucl.ap.titech.ac.jp/cluster/symposium/334/	online, Sendai International Center	Oct. 31–Nov. 3
6	第 5 回「精密武装抗体と機能評価」シンポジウム (Domestic) https://www.adthree.com/event/2022/07/poster.pdf	online	Dec. 16
7	第 10 回 RNC 品種改良ユーザー会 (Domestic) 理研シンポジウム「重イオンビーム育種による持続可能な社会や特産品生産の実現」 https://www.riken.jp/medialibrary/riken/pr/events/symposia/20230119_1/20230119_1_p.pdf	online, Suzuki Umetaro Hall	Jan. 19–20
8	A3 Foresight Annual Meeting 2022 JSPS/NRF/MSFC A3 Foresight Program "Nuclear Physics in the 21st Century"	online, Osaka International Convention Center	Feb. 13–15
9	INTPART School 2023 https://sites.google.com/rcnp.osaka-u.ac.jp/intpart23/home	Kafuu Resort Fuchaku CONDO HOTEL in Okinawa main island	Feb. 20–Mar. 3
10	Nuclear Spectroscopy for Extreme Quantum System (NUSPEQ2023) https://indico2.cns.s.u-tokyo.ac.jp/event/187/overview	Plaza Verde Convention Complex in Numazu	Mar. 7–9
11	2022 年度ビーム物理研究会・若手の会 (Domestic) https://indico2.riken.jp/event/4403/	online, RIBF2F Large Meeting Room	Mar. 8–10
12	第 4 回 RIBF 若手放談会: エキゾチック核物理の将来 (Domestic) https://indico2.riken.jp/event/3968/	online, Integrated Innovation Building	Mar. 15–17
13	EIC Asia Workshop https://indico2.riken.jp/event/4389/	online, Okochi Hall	Mar. 16–18

KEK

1	SSRI-PNS Collaboration meeting 2022 https://indico2.riken.jp/event/4202/timetable/?view=standard_inline_minutes	online	Sep. 1–2

List of Seminars (April 2022—March 2023)

Nuclear Physics Monthly Colloquium

	Not held in 2022		

RIBF Nuclear Physics Seminar

1	Yasuyuki Akiba (RNC)	The Physics at RHIC https://indico2.riken.jp/event/4118/	May 23
2	Newcomers of RNC in FY2022	Newcomers Seminar https://indico2.riken.jp/event/4145/	Jun. 7
3	Tomoya Naito (RIKEN)	Isospin symmetry breaking in nuclear ground state https://indico2.riken.jp/event/4151/	Jun. 22
4	Meytal Duer (TU Darmstadt)	A four-neutron system probed via alpha knockout reaction from ^{8}He https://indico2.riken.jp/event/4167/	Jul. 26
5	Wataru Horiuchi (Osaka Metropolitan U.)	What can we learn from nuclear density profiles? https://indico2.riken.jp/event/4270/	Nov. 7
6	Toshihiko Kawano (Los Alamos National Laboratory)	Recent advances in compound nuclear reaction theory and its applications https://indico2.riken.jp/event/4370/	Jan. 13
7	Gianluca Colò (U. Milan)	A unified framework for nuclear single-particle states and collective vibrations https://indico2.riken.jp/event/4391/	Jan. 17
8	Takuji Tsujimoto (NAOJ)	Galactic chemical evolution identifying core-collapse supernovae as one of the major production sites of r-process elements https://indico2.riken.jp/event/4386/	Jan. 31
9	Marco Rosenbush (KEK)	A first review of the SLOWRI-MRTOF mass spectrograph following the ZeroDegree spectrometer at BigRIPS https://indico2.riken.jp/event/4413/	Feb. 14
10	Masayasu Kamimura (RNC)	Recent developments of muon-catalyzed-fusion study and some theoretical predictions https://indico2.riken.jp/event/4414/	Feb. 28
11	Wen-Chen Chang (Academia Sinica)	Fixed-target charmonium production and pion PDFs https://indico2.riken.jp/event/4438/	Mar. 20
12	Phong Ho Vi (RIKEN)	β-delayed one and two neutron emission probabilities and the nuclide abundances around the second r-process peak https://indico2.riken.jp/event/4445/	Mar. 28
13	Xavier Roca-Maza (U. degli Studi di Milano)	An overview on the nuclear equation of state studied from ground and collective excited state properties of nuclei https://indico2.riken.jp/event/4452/	Apr. 12

RIBF ULIC Symposium/mini-WS

1	Sota Yoshida (Utunomiya U.)	The Physics at RHIC https://indico2.riken.jp/event/4118/	Nov. 29
2	Mini-Workshop	Newcomers Seminar https://indico2.riken.jp/event/4145/	Feb. 16
3	Mini-Workshop	Isospin symmetry breaking in nuclear ground state https://indico2.riken.jp/event/4151/	Feb. 20

Seminar by Each Laboratory

Nuclear Spectroscopy Laboratory

1	Hiroki Yoneda (RIKEN)	Observations of the MeV gamma-ray universe with Compton telescopes (virtual) https://indico2.riken.jp/event/4105/	Apr. 27
2	Kuma Susumu (RIKEN)	Microscopic superfluidity in quantum nanodroplets (virtual) https://indico2.riken.jp/event/4138/	May 27
3	Tomonori Fukuchi (RIKEN)	Measurements of the gamma-ray linear-polarization using the multi-channel detectors (virtual) https://indico2.riken.jp/event/4174/	Aug. 3
4	Yuntao Wu (Chinese Academy of Sciences)	Development of 6Li-loaded Halide Scintillators toward Neutron Detection (virtual) https://indico2.riken.jp/event/4217/	Sep. 2
5	Sohtaro Kanda (KEK)	Study of dynamical processes of muonic atom toward observation of parity nonconservation effects (virtual) https://indico2.riken.jp/event/4267/	Nov. 11

Subnuclear System Research Division

1	Sinya Aoki (Kyoto U.)	NT/RBRC Seminar Conserved non-Noether charge in general relativity: Physical definition vs. Noether's 2nd theorem (virtual)	Apr. 1
2	Katelin Schutz (McGill U.)	High-Energy Physics & RIKEN Theory Seminar Astrophysical handles on searches for new particles (virtual)	Apr. 7
3	Owe Philipsen (Frankfurt U.)	RBRC Seminar The QCD chiral phase transition for different numbers of flavours (virtual)	Apr. 14
4	Hiroyuki Tajima (U. Tokyo)	SNP Seminar Cooper quartet correlations in multi-component fermionic systems (virtual)	Apr. 14
5	Shuai Zhao (Old Dominion U.)	NT/RBRC Seminar One-loop structure of twist-4 PDFs for gluon condensate and topological charge (hybrid)	Apr. 15
6	Adrien Florio (BNL)	RBRC Seminar Dynamics of the O(4) critical point in QCD (hybrid)	Apr. 21
7	Edmond Iancu (Institut de Physique Theorique de Saclay)	NT/RBRC Seminar Probing gluon saturation via diffractive jet production at the EIC (hybrid)	Apr. 22
8	Xiaoxuan Chu (BNL)	RBRC Seminar Probing nonlinear gluon effects by forward di-hadron correlation (hybrid)	Apr. 28
9	Huey-Wen Lin (Michigan State U.)	NT/RBRC Seminar Mapping nucleon parton distributions with lattice QCD (hybrid)	Apr. 29
10	Giuliano Giacalone (U. Heidelberg)	RBRC Seminar Imprints of nucleon structure in high-energy nuclear collisions (virtual)	May 5
11	Felipe Attanasio (U. Heidelberg)	NT/RBRC Seminar QCD equation of state via the complex Langevin method (hybrid)	May 6
12	Alessandro Nada (Turin U.)	RBRC Seminar Stochastic normalizing flows for lattice field theory (virtual)	May 12
13	Xuanbo Tong (Chinese U. Hong Kong)	NT/RBRC Seminar Perturbative calculations of gravitational form factors at large momentum transfer (hybrid)	May 13
14	Jim Talbert (Cambridge U.)	High-Energy Physics & RIKEN Theory Seminar Towards an all-orders flavor formalism in the (geo)SM(EFT) and beyond (hybrid)	May 19
15	Adrian Dumitru (Baruch College)	RBRC Seminar Quark and gluon entanglement in the light-front wave function of the proton at moderate x (hybrid)	May 19

16	Robert Szafron (BNL)	NT/RBRC Seminar Soft-collinear effective field theory for gravity (hybrid)	May 20
17	Mikhail Stephanov (UIC)	RBRC Seminar Predictable randomness of relativistic hydrodynamics (hybrid)	May 26
18	Soeren Schlichting (U. Washington)	NT/RBRC Seminar Non-perturbative determination of the collisional broadening kernel and medium-induced radiation in QCD plasmas (hybrid)	May 27
19	Jessica Howard (UCI)	High-Energy Physics & RIKEN Theory Seminar Dark matter freeze-out during SU(2)_L confinement (hybrid)	Jun. 2
20	Ming Li (North Carolina State U.)	NT/RBRC Seminar Relating gluon bose correlation in nuclear wave function to near side ridge in deep inelastic scattering (hybrid)	Jun. 3
21	Anke Biekoetter (Durham U.)	High-Energy Physics & RIKEN Theory Seminar Standard model effective field theory - indirect constraints on new fundamental physics (hybrid)	Jun. 9
22	KC Kong (U. Kansas)	High-Energy Physics & RIKEN Theory Seminar Double higgs production at the HL-LHC (hybrid)	Jun. 16
23	Tomoya Naito (iTHEMS, RIKEN)	SNP Seminar Isospin symmetry breaking in nuclear ground state (virtual)	Jun. 22
24	Pier Francesco Monni (CERN)	High-Energy Physics & RIKEN Theory Seminar Taming the complex dynamics of scattering events (hybrid)	Jun. 23
25	Kemal Tezgin (U. Connecticut)	RBRC Seminar 3D and 2D distributions of the energy-momentum tensor in a quark model (hybrid)	Jun. 23
26	Alba Soto Ontoso (IPhT)	NT/RBRC Seminar PanScales parton showers for hadron collisions (hybrid)	Jun. 28
27	Tonia Venters (NASA)	High-Energy Physics & RIKEN Theory Seminar Ultra-high energy cosmic rays: exploring the energy frontier by way of the cosmic frontier (hybrid)	Jun. 30
28	Stella Schindler (MIT)	NT/RBRC Seminar Factorization connecting physical and lattice TMDs (hybrid)	Jul. 1
29	Denis Lacroix (U. Paris-Saclay)	SNP Seminar Quantum computing description of atomic nuclei: challenges and opportunities (virtual)	Jul. 5
30	Kim Berghaus (Stony Brook U.)	High-Energy Physics & RIKEN Theory Seminar Warm early dark energy (hybrid)	Jul. 7
31	Chun Shen (Wayne State U.)	RBRC Seminar Longitudinal dynamics and particle production in relativistic nuclear collisions (hybrid)	Jul. 7
32	Julia Gehrlein (BNL)	High-Energy Physics & RIKEN Theory Seminar Quo vadis neutrinoless double beta decay? (hybrid)	Jul. 8
33	Mikko Laine (U. Bern)	NT/RBRC Seminar Heavy quark kinetic equilibration from the lattice (hybrid)	Jul. 8
34	Holmfridur Hannesdottir (IAS)	High-Energy Physics & RIKEN Theory Seminar What is the iε for the S-matrix? (hybrid)	Jul. 14
35	David Frenklakh (Stony Brook U.)	RBRC Seminar Chirality distribution inside baryons in QCD_2 (hybrid)	Jul. 14
36	Zhite Yu (Michigan State U.)	NT/RBRC Seminar Exclusive single-diffractive hard scattering processes for probing the x-dependence of generalized parton distributions (hybrid)	Jul. 15
37	Yair Mulian (Jyvaskyla U.)	NT/RBRC Seminar Next-to-leading order photon+jet production (hybrid)	Jul. 25
38	Myung-Ki Cheoun (Soongsil U.)	SNP Seminar Low Energy Nuclear Reactions for Carbon Isotopes, ^{17}F and ^{17}O (virtual)	Jul. 28

39	Vladi Skokov (BNL)	RBRC Seminar CGC density matrix (hybrid)	Jul. 28
40	Bianka Mecaj (Yale U.)	NT/RBRC Seminar Conformal Colliders meet the LHC (hybrid)	Jul. 29
41	Werner Vogelsang (U. Tubingen)	NT/RBRC Seminar Higher-order QCD corrections to semi-inclusive DIS and fragmentation functions (hybrid)	Aug. 12
42	Krzysztof Kutak (Institute of Nuclear Physics Polish Academy of Sciences)	RBRC Seminar Maximally entangled proton and charged hadron multiplicity in Deep Inelastic Scattering (hybrid)	Aug. 18
43	Akio Tomiya (International Professional U. Technology)	RBRC Seminar T-mu phase diagram using classical-quantum hybrid algorithm (hybrid)	Aug. 25
44	Andrea Shindler (Michigan State U.)	NT/RBRC Seminar Electric dipole moments from lattice QCD (hybrid)	Aug. 26
45	Seth Koren (U. Chicago)	High-Energy Physics & RIKEN Theory Seminar Discrete symmetries, proton stability, and cosmological lithium (hybrid)	Sep. 1
46	Yuki Yokokura (RIKEN)	RBRC Seminar Entropy-area law from interior semi-classical degrees of freedom (hybrid)	Sep. 1
47	Georg Wolschin (Heidelberg U.)	SNP Seminar In-medium bottomonium suppression in p-Pb and Pb-Pb collisions at LHC energies (virtual)	Sep. 2
48	Tomasz Stebel (Jagiellonian)	NT/RBRC Seminar Sampling statistical systems with artificial neural networks (hybrid)	Sep. 2
49	Ian Moult (Yale U.)	High-Energy Physics & RIKEN Theory Seminar Conformal colliders meet the LHC (hybrid)	Sep. 8
50	Lingfeng Li (Brown U.)	High-Energy Physics & RIKEN Theory Seminar Jupiter missions as probes of dark matter (hybrid)	Sep. 15
51	Xiaojun Yao (MIT)	NT/RBRC Seminar Pure quark and gluon observables (hybrid)	Sep. 15
52	Josh Tawabutr (Ohio State U.)	NT/RBRC Seminar Recent developments in small-x helicity evolution (hybrid)	Sep. 16
53	Christopher Monahan (College of William and Mary)	High-Energy Physics & RIKEN Theory Seminar First principles' calculations of the gluon structure of hadrons (hybrid)	Sep. 22
54	Claudio Bonanno (INFN)	NT/RBRC Seminar Large-N SU(N) pure-gauge theories with milder topological freezing via parallel tempering on boundary conditions (hybrid)	Sep. 29
55	Amarjit Soni (BNL)	High-Energy Physics & RIKEN Theory Seminar Flavor anomalies, possible new physics and collider signals (hybrid)	Sep. 30
56	Guillaume Beuf (NCBJ)	NT/RBRC Seminar DIS at NLO in the dipole factorization and mass renormalization on the light-front (hybrid)	Sep. 30
57	Lucas Happ (RIKEN)	SNP Seminar Universality in one-dimensional quantum three-body systems (virtual)	Oct. 3
58	Juan Pedersen (U. Tokyo)	RBRC Seminar Reformulation of anomaly inflow on the lattice and construction of lattice chiral gauge theories (hybrid)	Oct. 6
59	Yang-Ting Chien (Georgia State U.)	NT/RBRC Seminar Probing hadronization with flavor correlations of leading particles in jets (hybrid)	Oct. 7
60	Martha Constantinou (Temple U.)	High-Energy Physics & RIKEN Theory Seminar The structure of the proton from numerical simulations of lattice QCD (hybrid)	Oct. 13

61	Scott Lawrence	RBRC Seminar Probing the hydrodynamics of strongly coupled quantum field theories (hybrid)	Oct. 13
62	Ahmad Jafar Arifi (APCTP)	SNP Seminar Mass spectra and wave functions of mesons in Light-front quark model (virtual)	Oct. 14
63	Savvas Zafeiropoulos (CPT)	NT/RBRC Seminar The extraction of light cone parton distributions from lattice quantum chromodynamics (hybrid)	Oct. 14
64	Dennis Bollweg (BNL)	NT/RBRC Seminar Lattice QCD thermodynamics from cumulants of conserved charge fluctuations (hybrid)	Oct. 20
65	Yuki Fujimoto (U. Washington)	NT/RBRC Seminar Trace anomaly in neutron stars (hybrid)	Oct. 21
66	Cora Dvorkin (Harvard U.)	High-Energy Physics & RIKEN Theory Seminar The universe as a lab for new physics across cosmic times (hybrid)	Oct. 27
67	Waseem Kamleh (U. Adelaide)	RBRC Seminar Emergent phenomena from centre vortices (hybrid)	Oct. 27
68	Matthew Walters (EPFL)	NT/RBRC Seminar Towards a nonperturbative construction of the S-matrix (hybrid)	Oct. 28
69	Anna Suliga (U. California)	High-Energy Physics & RIKEN Theory Seminar Towards probing the diffuse supernova neutrino background in all flavors (hybrid)	Nov. 3
70	Jack Holden (Southampton U.)	RBRC Seminar Partial deconfinement (hybrid)	Nov. 3
71	Abhiram Kaushik (Zagreb U.)	NT/RBRC Seminar Transverse single spin asymmetry at two loops (hybrid)	Nov. 4
72	Friederike Ihssen (ITP Heidelberg)	RBRC Seminar Lee-Yang zeroes from the functional renormalisation group (hybrid)	Nov. 10
73	Koji Miwa Koji Miwa (Tohoku U.)	SNP Seminar Recent progress and future prospects of hyperon nucleon scattering experiment at J-PARC (virtual)	Nov. 15
74	Florian Herren (Fermilab)	High-Energy Physics & RIKEN Theory Seminar A NLL accurate parton shower in sherpa (hybrid)	Nov. 17
75	Sanjin Benic (Zagreb U.)	NT/RBRC Seminar On the odderon mechanism for transverse single spin asymmetry in the Wilczek-Wandzura approximation (hybrid)	Nov. 18
76	Fei Yan (Rutgers U.)	RBRC Seminar Entanglement entropy in (1+1)-d with defects (hybrid)	Dec. 1
77	Fernando Romero-López (MIT)	NT/RBRC Hybrid Seminar Flow-based sampling for lattice field theories (hybrid)	Dec. 2
78	Ilaria Brivio (U. Copenhagen)	High-Energy Physics & RIKEN Theory Seminar The hunt for non-resonant signals of new physics at the LHC (hybrid)	Dec. 8
79	Hersh Singh (U. Washington)	RBRC Seminar From topological theta vacua to asymptotic freedom: Qubit models, sign problems, and anomalies (hybrid)	Dec. 8
80	Simone Rodini (Ecole Polytechnique)	NT/RBRC Hybrid Seminar TMD factorization at next-to-leading power (hybrid)	Dec. 9
81	Jinglun Li (U. Ulm)	SNP Seminar Product spin and binding energy propensities for three-body recombination of ultracold atoms (virtual)	Dec. 15
82	Theodore Jacobson (U. Minnesota)	NT/RBRC Hybrid Seminar 1-form symmetry versus large N QCD (hybrid)	Dec. 16
83	Hai-tao Shu (Regensburg U.)	NT/RBRC Hybrid Seminar Shear viscosity and bulk viscosity from lattice QCD calculation (hybrid)	Jan. 6

84	Stefano Profumo (U. California)	High-Energy Physics & RIKEN Theory Seminar The primordial black holes variations (hybrid)	Jan. 12
85	William Horowitz (U. of Cape Town)	NT/RBRC Hybrid Seminar Small system phenomenology (hybrid)	Jan. 13
86	Cenxi Yuan (IFCEN)	SNP Seminar Configuration-Interaction Shell Model and Its Application in Exotic Nuclei (virtual)	Jan. 16
87	Brenda Frye (U. Arizona)	High-Energy Physics & RIKEN Theory Seminar Unscrambling galaxy cluster fields in the JWST era (hybrid)	Jan. 19
88	Francesco Riva (Geneva U.)	RBRC Seminar Positivity of effective field theories and large-N QCD (hybrid)	Jan. 19
89	Alberto Martin-Caro (IGFAE)	NT/RBRC Hybrid Seminar Skyrmions: from light nuclei to neutron stars (hybrid)	Jan. 20
90	Silvia Ferrario Ravasio (Oxford U.)	High-Energy Physics & RIKEN Theory Seminar Dissecting hadronisation corrections for collider physics (hybrid)	Jan. 26
91	Wenbin Zhao (Harbin U. of Science and Technology)	RBRC Seminar The 3D structure of anisotropic flow in small collision systems at the RHIC and LHC (hybrid)	Jan. 26
92	Gopolang Mohlabeng (U. California)	High-Energy Physics & RIKEN Theory Seminar Terrestrial planet probes for low mass dark matter (hybrid)	Feb. 2
93	Tongyan Lin (U. California)	High-Energy Physics & RIKEN Theory Seminar Dark matter direct detection from single phonons to nuclear recoils (hybrid)	Feb. 9
94	Kazuki Ikeda (Stony Brook U.)	RBRC Seminar Demonstration of quantum energy teleportation by superconducting quantum processors and implications for communications and high energy physics (hybrid)	Feb. 9
95	Marvin Schnubel (Mainz U.)	High-Energy Physics & RIKEN Theory Seminar Flavour probes of axion-like particles (hybrid)	Feb. 10
96	Rajeev Singh (Stony Brook U.)	NT/RBRC Hybrid Seminar Relativistic hydrodynamics with spin for massive spin-1/2 fermions with and without particle collisions (hybrid)	Feb. 10
97	Admir Greljo (Bern U.)	High-Energy Physics & RIKEN Theory Seminar Model building and phenomenology with leptoquarks (hybrid)	Feb. 16
98	Paul Hotzy (Tech. U.)	RBRC Seminar Stabilizing complex Langevin for real-time gauge theories with an anisotropic kernel (online)	Feb. 16
99	Fernando Romero-López (MIT)	NT/RBRC Hybrid Seminar Flow-based sampling for lattice gauge theories (hybrid)	Feb. 17
100	Fangcheng He (Chongqing U. of Education)	RBRC Seminar Charmonium spin decomposition from Lattice QCD (hybrid)	Feb. 23
101	Irene Valenzuela (CERN)	High-Energy Physics & RIKEN Theory Seminar Swampland Constraints and the Dark Dimension (hybrid)	Mar. 2
102	Marton Lajer (BNL)	RBRC Seminar Scattering from energy levels: Truncated Spectrum Approach and Lüscher's method for the φ4 1+1 theory (hybrid)	Mar. 2
103	Jesse Stryker (Maryland U.)	NT/RBRC Hybrid Seminar Loop-string-hadron formulation of an SU(3) gauge theory with dynamical quarks (hybrid)	Mar. 3
104	Masaru Hongo (Niigata U.)	SNP Seminar Effective field theoretical approach to weakly bound Borromean nuclei (virtual)	Mar. 8
105	Shuzhe Shi (Stony Brook U.)	RBRC Seminar Real-time non-perturbative dynamics of jet production in Schwinger model: quantum entanglement and vacuum modification (hybrid)	Mar. 9
106	Daniel Pablos Alfonso (INFN)	NT/RBRC Seminar Looking for evidence of color decoherence in jet observables (hybrid)	Mar. 10

107	Linda Carpenter (Ohio State U.)	High-Energy Physics & RIKEN Theory Seminar LEX-EFT: The light exotics effective field theory (hybrid)	Mar. 16
108	Sipaz Sharma (Bielefeld)	RBRC Seminar Charm fluctuations as a probe for deconfinement from lattice QCD (hybrid)	Mar. 16
109	Niklas Muller (U. Washington)	NT/RBRC Seminar What entanglement structure can tell us about lattice gauge theories (hybrid)	Mar. 17
110	Andrés Luna (Niels Bohr Institute)	High-Energy Physics & RIKEN Theory Seminar Scattering Amplitudes for Spinning Binaries (hybrid)	Mar. 23
111	Hideto En'yo (RIKEN)	Special RBRC Seminar My 40 years of looking up to the world of Nambu (hybrid)	Mar. 23
112	Vladimir Braun (Regensburg U.)	NT/RBRC Seminar Conformal symmetry in strong interactions (hybrid)	Mar. 24
113	Matthew Baumgart (Arizona State U.)	High-Energy Physics & RIKEN Theory Seminar Attacking heavy dark matter on two fronts (hybrid)	Mar. 30

High Energy / Nuclear Theory / RIKEN seminars → https://indico.bnl.gov/category/228/
RBRC Seminar → https://www.bnl.gov/riken/events/

Events (April 2022—March 2023)

RNC

Apr. 23	Wako Open Campus
May 26	The 29th RBRC Management Steering Committee (MSC)
Jul. 22	The 19th Industrial Program Advisory Committee (In-PAC)
Aug. 22–25	The 22nd Program Advisory Committee for Materials and Life Science Researches at RIKEN Nishina Center (ML-PAC)
Oct. 28	Memorial Event for Dr. Yoshio Nishina
Dec. 1–3	The 22nd Program Advisory Committee for Nuclear Physics Experiments at RI Beam Factory (NP-PAC)
Dec. 12–Jan. 6	The 20th Industrial Program Advisory Committee (In-PAC)
Dec. 23–Jan. 10	The 23rd Program Advisory Committee for Materials and Life Science Researches at RIKEN Nishina Center (ML-PAC)

CNS

Aug. 20–24	The 21st CNS International Summer School (A3F-CNSSS22) https://indico2.cns.s.u-tokyo.ac.jp/event/198/

KEK

Sep. 1–2	SSRI-PNS Collaboration meeting 2022 https://indico2.riken.jp/event/4202/timetable/?view=standard_inline_minutes

Press Releases (April 2022–March 2023)

RNC

Apr. 27	α-Clustering in atomic nuclei from first principles with statistical learning and the Hoyle state character https://www.riken.jp/press/2022/20220427_2/index.html	T. Otsuka, T. Abe, Nuclear Spectroscopy Laboratory
Apr. 28	First Application of Mass Measurement with the Rare-RI Ring Reveals the Solar r-Process Abundance Trend at A = 122 and A = 123 https://www.riken.jp/press/2022/20220428_2/index.html	T. Uesaka, S. Naimi, H. Fu Li, Y. Yamaguchi, Spin Isospin Research Laboratory, Rare RI Ring Team
May 25	Variability in the net ecosystem productivity (NEP) of seaweed farms https://www.riken.jp/press/2022/20220525_1/index.html	Y. Sato, Ion Beam Breeding Team
Jun. 23	Observation of a correlated free four-neutron system https://www.riken.jp/press/2022/20220623_1/index.html	H. Otsu, V. Panin, SAMURAI Team, Spin Isospin Laboratory
Sep. 21	Proton Hyperpolarization Relay from Nanocrystals to Liquid Water https://www.riken.jp/press/2022/20220921_2/index.html	T. Uesaka, K. Tateishi, Spin isospin Laboratory
Sep. 28	A CLAVATA3-like gene acts as a gynoecium suppression function in White Campion https://www.riken.jp/press/2022/20220928_1/index.html	T. Abe, Beam Mutagenesis Group
Oct. 19	β-Delayed One and Two Neutron Emission Probabilities South-East of ^{132}Sn and the Odd-Even Systematics in r-Process Nuclide Abundances https://www.riken.jp/press/2022/20221019_1/index.html	V. Ho Phong, S. Nishimura, H. Sakurai, Radioactive Isotope Physics Laboratory
Nov. 17	Discovery of ^{39}Na https://www.riken.jp/press/2022/20221117_3/index.html	T. Kubo, D. S. Ahn, H. Suzuki, Research Instruments Group
Nov. 17	Targeted α-therapy using astatine (^{211}At)-labeled PSMA1, 5, and 6: a preclinical evaluation as a novel compound https://www.riken.jp/press/2022/20221117_2/index.html	H. Haba, Nuclear Chemistry Research Team, RI Application Research Group
Nov. 24	Direct Determination of the Activation Energy for Diffusion of OH Radicals on Water Ice https://www.riken.jp/press/2022/20221124_1/index.html	Y. Nakai, Radioactive Isotope Physics Laboratory
Nov. 25	Polarized x-rays from a magnetar https://www.riken.jp/press/2022/20221125_2/index.html	K. Uchiyama, High Energy Astrophysics Laboratory
Jan. 6	Observation of non-existence of new magic number in titanium and vanadium neutron rich isotopes https://www.riken.jp/press/2023/20230106_2/index.html	H. Ishiyama, SLOWRI Team
Feb. 22	Long-term density trend in the mesosphere and lower thermosphere from occultations of the crab nebula with X-ray astronomy satellites https://www.riken.jp/press/2023/20230222_2/index.html	Y. Motizuki, Astro-Glaciology Research Group
Mar. 2	Singlet fission as a polarized spin generator for dynamic nuclear polarization https://www.riken.jp/press/2023/20230302_1/index.html	T. Uesaka, K. Tateishi, Spin isospin Laboratory
Mar. 27	Chiral symmetry restoration at high matter density observed in pionic atoms https://www.riken.jp/press/2023/20230327_1/index.html	T. Nishi, K. Itahashi, Researcher at the Accelerator Group, Meson Science Laboratory

KEK

Jan. 6	チタン・バナジウム中性子過剰同位体で新魔法数の消失を観測 ～精密質量測定による原子核構造のより深い理解に期待～ https://www.kek.jp/ja/press/202301061400/	KEK, RIKEN, Osaka University
Mar. 31	40 年ぶりに中性子過剰なウラン同位体を新発見 ～ウランの起源解明に期待～ https://www.kek.jp/ja/press/202304010000/	KEK, RIKEN

News (April 2022–March 2023)

RNC

Apr. 22	超伝導リングサイクロトロン、ギネス世界記録™に登録 https://www.riken.jp/pr/news/2022/20220422_2/index.html
May 17	関口仁子客員研究員が猿橋賞を受賞 https://www.riken.jp/pr/news/2022/20220517_2/index.html
Nov. 9	「仁科芳雄記念室お披露目会」およびシンポジウム「理化学研究所仁科研究室のキセキ」を開催 https://www.riken.jp/pr/news/2022/20221109_1/index.html
Mar. 17	理研−RAL 記念式典を開催 https://www.riken.jp/pr/news/2023/20230317_1/index.html
Mar. 13	仁科型電離箱 2 号機の日本天文遺産認定 https://www.riken.jp/pr/news/2023/20230313_2/index.html
Mar. 23	理研栄峰賞、理研梅峰賞の授与 理研栄峰賞：羽場 宏光 「アルファ線核医学治療に向けたアスタチン-211 の大量製造技術の開発」 理研梅峰賞：阿部 喬、大塚 孝治 「炭素-12 原子核のホイル状態における第一原理計算」 山口 由高 「元素起源の謎の解明に向けた世界最速質量測定法確立」 https://www.riken.jp/pr/news/2023/20230323_1/index.html

List of Preprints (April 2022—March 2023)

RIKEN NC-NP

	Not Applicable	

RIKEN NC-AC

	Not Applicable	

RIKEN MP

	Not Applicable	

RIKEN QHP

515	Isospin symmetry breaking in the charge radius difference of mirror nuclei	T. Naito *et al.*
516	Interaction potentials for two-particle states with non-zero total momenta in lattice QCD	Y. Akahoshi and S. Aoki

CNS-REP

101	CNS Annual Report 2021	H. Nagahama

Nishina Center Preprint server (not including Partner Institution) can be found at
http://nishina-preprints.riken.jp/

理化学研究所
埼玉県　和光市　広沢
RIKEN 2023-039
ISSN 0289-842X